

Lecture Notes in Mechanical Engineering

Ravi Pratap Singh

Mohit Tyagi

R. S. Walia

J. Paulo Davim *Editors*

# Advances in Modelling and Optimization of Manufacturing and Industrial Systems


Select Proceedings of CIMS 2021

 Springer

# Lecture Notes in Mechanical Engineering


## Series Editors

Fakher Chaari, National School of Engineers, University of Sfax, Sfax, Tunisia

Francesco Gherardini , Dipartimento di Ingegneria “Enzo Ferrari”, Università di Modena e Reggio Emilia, Modena, Italy

Vitalii Ivanov, Department of Manufacturing Engineering, Machines and Tools, Sumy State University, Sumy, Ukraine

## Editorial Board

Francisco Cavas-Martínez , Departamento de Estructuras, Construcción y Expresión Gráfica Universidad Politécnica de Cartagena, Cartagena, Murcia, Spain

Francesca di Mare, Institute of Energy Technology, Ruhr-Universität Bochum, Bochum, Nordrhein-Westfalen, Germany

Mohamed Haddar, National School of Engineers of Sfax (ENIS), Sfax, Tunisia

Young W. Kwon, Department of Manufacturing Engineering and Aerospace Engineering, Graduate School of Engineering and Applied Science, Monterey, CA, USA

Justyna Trojanowska, Poznan University of Technology, Poznan, Poland

**Lecture Notes in Mechanical Engineering (LNME)** publishes the latest developments in Mechanical Engineering—quickly, informally and with high quality. Original research reported in proceedings and post-proceedings represents the core of LNME. Volumes published in LNME embrace all aspects, subfields and new challenges of mechanical engineering.

To submit a proposal or request further information, please contact the Springer Editor of your location:

**Europe, USA, Africa:** Leontina Di Cecco at [Leontina.dicecco@springer.com](mailto:Leontina.dicecco@springer.com)

**China:** Ella Zhang at [ella.zhang@springer.com](mailto:ella.zhang@springer.com)

**India:** Priya Vyas at [priya.vyas@springer.com](mailto:priya.vyas@springer.com)

**Rest of Asia, Australia, New Zealand:** Swati Meherishi at [swati.meherishi@springer.com](mailto:swati.meherishi@springer.com)

Topics in the series include:

- Engineering Design
- Machinery and Machine Elements
- Mechanical Structures and Stress Analysis
- Automotive Engineering
- Engine Technology
- Aerospace Technology and Astronautics
- Nanotechnology and Microengineering
- Control, Robotics, Mechatronics
- MEMS
- Theoretical and Applied Mechanics
- Dynamical Systems, Control
- Fluid Mechanics
- Engineering Thermodynamics, Heat and Mass Transfer
- Manufacturing
- Precision Engineering, Instrumentation, Measurement
- Materials Engineering
- Tribology and Surface Technology

**Indexed by SCOPUS and EI** Compendex. All books published in the series are submitted for consideration in Web of Science.

To submit a proposal for a monograph, please check our Springer Tracts in Mechanical Engineering at <https://link.springer.com/bookseries/11693>

Ravi Pratap Singh · Mohit Tyagi · R. S. Walia ·  
J. Paulo Davim  
Editors

# Advances in Modelling and Optimization of Manufacturing and Industrial Systems

Select Proceedings of CIMS 2021


 Springer

*Editors*

Ravi Pratap Singh  
Department of Mechanical Engineering  
National Institute of Technology  
Kurukshetra, Haryana, India

Mohit Tyagi  
Department of Mechanical Engineering  
National Institute of Technology  
Kurukshetra, Haryana, India

R. S. Walia  
Department of Production and Industrial  
Engineering  
Punjab Engineering College  
Chandigarh, India

J. Paulo Davim   
Department of Mechanical Engineering  
University of Aveiro  
Aveiro, Portugal

ISSN 2195-4356

ISSN 2195-4364 (electronic)

Lecture Notes in Mechanical Engineering

ISBN 978-981-19-6106-9

ISBN 978-981-19-6107-6 (eBook)

<https://doi.org/10.1007/978-981-19-6107-6>

© The Editor(s) (if applicable) and The Author(s), under exclusive license to Springer Nature Singapore Pte Ltd. 2023

This work is subject to copyright. All rights are solely and exclusively licensed by the Publisher, whether the whole or part of the material is concerned, specifically the rights of translation, reprinting, reuse of illustrations, recitation, broadcasting, reproduction on microfilms or in any other physical way, and transmission or information storage and retrieval, electronic adaptation, computer software, or by similar or dissimilar methodology now known or hereafter developed.

The use of general descriptive names, registered names, trademarks, service marks, etc. in this publication does not imply, even in the absence of a specific statement, that such names are exempt from the relevant protective laws and regulations and therefore free for general use.

The publisher, the authors, and the editors are safe to assume that the advice and information in this book are believed to be true and accurate at the date of publication. Neither the publisher nor the authors or the editors give a warranty, expressed or implied, with respect to the material contained herein or for any errors or omissions that may have been made. The publisher remains neutral with regard to jurisdictional claims in published maps and institutional affiliations.

This Springer imprint is published by the registered company Springer Nature Singapore Pte Ltd. The registered company address is: 152 Beach Road, #21-01/04 Gateway East, Singapore 189721, Singapore

# Preface

This book volume presents select proceedings of the 2nd International Conference on Industrial and Manufacturing Systems (CIMS-2021) and encloses various manuscripts having its roots in the soft computing, modelling and optimization practices attempted for improving the variety of industrial and manufacturing systems. All the manuscripts appended in this volume provide deep insights into its readers about the current scenarios and future advancements through exploring the soft computations, modelling and optimization practices attempted in real-life studies for enhancing the advanced machining methods and performances, industrial operations, processing with hybrid manufacturing techniques, fabrication and developments in micro-machining and its applications, practical issues in supply chain, micro-structure analysis, additive manufacturing processes, reliability and system analysis, material science and metallurgical behaviour analysis, product design and development, etc. The Conference on Industrial and Manufacturing Systems (CIMS) series, from which this special volume has been derived, was started by the Department of Industrial and Production Engineering, Dr. B. R. Ambedkar National Institute of Technology (NIT), Jalandhar, India, in October, 2020. The 1st International Conference CIMS-2020 was organized in association with NIT, Patna; PEC, Chandigarh; MNNIT, Allahabad; and NIT, Delhi, which attracted renowned academicians/researchers, industry representatives and delegates from countries like Canada, UK, Ethiopia, Russia, Malaysia, Brazil, Singapore and India.

The book is a valuable reference for beginners, researchers and professionals interested in the modelling, optimization and soft computing-related aspects of industrial and production engineering and its allied domains. We would like to express our gratitude towards all the authors for contributing their valuable articles for the conference. Furthermore, we would like to acknowledge the reviewers for their painstaking and

time-consuming effort in reviewing manuscripts and providing the throughout evaluations for improving the quality of the manuscripts. We would also like to express our sincere gratitude towards the entire Springer team for the throughout support.

Kurukshetra, India  
Kurukshetra, India  
Chandigarh, India  
Aveiro, Portugal

Ravi Pratap Singh  
Mohit Tyagi  
R. S. Walia  
J. Paulo Davim

# Contents

<b>Revalidation of Components by Implementation of Bar-Coded Route Cards and Enterprise Resource Planning System in Manufacturing Units</b> .....	1
S. Hari, Shanker Krishna, and Rakesh Kumar Vij	
<b>Parametric Study of Process Parameters on Surface Roughness and Dimensional Deviation in Electrical Discharge Machining of Fe-Based SMA</b> .....	9
Ranjit Singh, Ravi Pratap Singh, and Rajeev Trehan	
<b>Analyzing Heat Stress Among Metal Casting Workers Using Selected Thermal Indices: A Pilot Study During Winter Climatic Conditions</b> .....	25
Milap Sharma, N. M. Suri, and Suman Kant	
<b>Prioritizing the Drivers of Green Supply Chain Management Using ISM-Fuzzy-MICMAC Analysis</b> .....	35
Gagandeep, Rahul O. Vaishya, and R. S. Walia	
<b>CRITIC-COPRAS-Based Selection of Commercially Viable Alternative Fuel Passenger Vehicle</b> .....	51
Abhishek Mohata, Nimai Mukhopadhyay, and Vidyapati Kumar	
<b>A Review on Dielectric Issues and Sustainable Alternatives in Electric Discharge Machining</b> .....	71
Saurabh Bhardwaj, C. S. Jawalkar, and Suman Kant	
<b>Numerical Investigation of Mixing Characteristics of a Passive T-Micromixer with a Twisted Outlet Channel</b> .....	85
B. Lohit Nagarjun Reddy and M. Zunaid	
<b>Numerical Investigation of T-Micromixer with Twisted Outlet Channel for Non-newtonian Fluid</b> .....	99
B. Lohit Nagarjun Reddy and M. Zunaid	



<b>To Study the Effect of Electromagnetic Forces on WIRE Electrochemical Discharge Machining</b> .....	109
Yajush Walia and Sarbjit Singh	
<b>Reliability Prediction and Its Simulation for a Friction Stir Processing Tool</b> .....	125
Smriti Mishra, Prashant Bhardwaj, Neha Bhadauria, and Prashant Vashishtha	
<b>Enhancement of Electrochemical Discharge Machining (ECDM) Characteristics with Tool Electrode Rotation</b> .....	135
Viveksheel Rajput, Mudimallana Goud, and Narendra Mohan Suri	
<b>Biomedical Waste Management and Circular Economy Actions in the COVID-19 Pandemic Situation in Jaipur District, India</b> .....	149
Manoj Sharma, Narayan Lal Jain, and Jayant Kishor Purohit	
<b>Atomization Casting of Al–Si Alloys and Their Characterization</b> .....	175
Krishna Vijay, Utkarsh Mishra, and Subodh Kumar Sharma	
<b>Analysing Effects of HVOF Powder Coating on the Tribological Properties of Inconel 800 Under Non-lubricated Conditions</b> .....	183
Sushant Bansal, Ayush Saraf, Ramakant Rana, and Roop Lal	
<b>Use of a Generative Design Approach for UAV Frame Structure Optimization and Additive Manufacturing</b> .....	197
Pratik Yadav, Vinay Yadav, Vishal Francis, and Narendra Kumar	
<b>Study on Welding Parameters in TIG Welding of Incoloy-800: An Investigation with Designed Experiments and ARAS Method</b> .....	209
Ravi Pratap Singh, Ravinder Kataria, Himanshu Bisht, Narendra Kumar, and Mohit Tyagi	
<b>Optimization of Titanium Grade-5 (Ti6Al4V) Alloy on Die Sinking EDM by Using Copper Tungsten Electrode</b> .....	235
Rakesh Kumar Rout, Rajiv Kumar Garg, and Dilbagh Panchal	
<b>A Critical Review on Industry 5.0 and Its Medical Applications</b> .....	251
Shubhangi Chourasia, Ankit Tyagi, Qasim Murtaza, R. S. Walia, and Prince Sharma	
<b>Systematic Review: Implementation of Product Lifecycle Management in Industries</b> .....	263
Harish Vishnu Gunjal and Rajendra M. Belokar	
<b>Optimal Assembly Sequence Planning with Single-Stage Multiple-Component Feasibility: Industry 4.0 Perspective</b> .....	281
Chiranjibi Champatiray, M. V. A. Raju Bahubalendruni, I. Anil Kumar, R. N. Mahapatra, Debasisha Mishra, and B. B. Biswal	

**An Inventory Model for Imperfect Production and Time Sensitive Selling Price** ..... 291  
 Ruchi Sharma and G. S. Buttar

**RIM-Based Performance Evaluation of DLC Coating Under Conflicting Environment** ..... 303  
 Saptarshi Das, Bijan Sarkar, and Vidyapati Kumar

**COMSOL Simulation to Predict the Thickness of Material Removed from Surface During Electropolishing** ..... 321  
 Abhinav Kumar, Manjesh Kumar, H. N. S. Yadav, and Manas Das

**Quality Improvement in Inner Bore Grinding Rejection of Ball Bearing by Using Six-Sigma Methodology** ..... 339  
 Manish Bhargava, Tushar Sharma, Shraddha Arya, and Arindam Sinha

**Achieving Manufacturing Competitiveness Through Six Sigma: A Study on Steel Firms** ..... 363  
 Sudeshna Rath and Rajat Agrawal

**Quality and Efficiency Improvement Through Process FMEA—A Case Study** ..... 375  
 Ramkrishna Bharsakade, Pranav Badgujar, Krishna Malani, Srushti Rithe, and Pranita Salunke

**Study on Mechanical Characteristics of TiB<sub>2</sub>, WC, ZrB<sub>2</sub> and B<sub>4</sub>C Reinforced Al 2XXX, 6XXX and 7XXX Series Alloys—A Systematic Review** ..... 393  
 B. M. Karthik, K. Nithesh, Sathyashankara Sharma, D. Srinivas, and S. Sandeep Nambiar

**Productivity Improvement by Optimizing the Layout and Cycle Time of an MSME** ..... 403  
 Radhika Gupta, Shraddha Sinha, Livea Goyal, Rahul O. Vaishya, and Sidharth Sharma

**Green Manufacturing in Apparel Industry: Future Trends and Scope** ..... 413  
 Ankita S. Pandey and Vasundhara Saluja

**A Critical Review of Fatigue Life Prediction on 316LN SS** ..... 427  
 Raj Kumar, Mohammad Mursaleen, G. A. Harmain, and Ashutosh Kumar

**Weight-Based Object Segregation Using 5 DOF Robotic Arm** ..... 441  
 Awaar Vinay Kumar, Abhignya Rajapu, Kalaka Goutham, Yerravati Shiva Prasad Goud, and Madisetty Anuraag

<b>An Experimental Validation of Thermo-Mechanical Analytical Model in Laser Bending Process</b> .....	455
Utpal Nath and Vinod Yadav	
<b>Heat Transfer Analysis at Mould-Casting Interface for Improving the Casting Process</b> .....	475
Mohammad Asif, Muhammad Muneef Sadiq, and Muhammed Muaz	
<b>Modeling and Analysis of Wire EDM Process Parameters for AZ-31 Alloy Using Response Surface Methodology</b> .....	487
Durgesh Pandey, Rajesh Babbar, Aviral Misra, and R. K. Bansal	
<b>Barriers to Healthcare Waste Management: A QFD Strategy</b> .....	501
Abhishek Raj and Cherian Samuel	
<b>Interference Fringe-Based Metrology for Industrial Applications</b> .....	511
Pavan Kumar Asundi and R. Deepa	
<b>Dimensions of Employee Well-Being at Work: A New Analytic Framework</b> .....	523
Shivangi Singh and Poonam Gautam	
<b>Analysis of Strategies to Tackle the Environmental Impact of the Vaccine Supply Chain: A Fuzzy DEMATEL Approach</b> .....	533
Amit Kumar Yadav and Dinesh Kumar	
<b>Implementation of Total Quality Management in Infrastructure Engineering</b> .....	549
Chidanand Mangrulkar, Tushar Sathe, Suraj Vairagade, Narendra Kumar, and Ravi Pratap Singh	
<b>Analysis of Rear Twist Beam Axle to Evaluate Performance Parameters for Passenger Vehicle Through Reverse Engineering</b> .....	565
Madan Mohan Joshi, Anand Baghel, and Chaitanya Sharma	
<b>Effect of Tool Pin Features on Mechanical Properties of AA7050-T7 Friction Stir Welded Joints</b> .....	581
Anugrah Singh, Vikas Upadhyay, and Joy Prakash Misra	
<b>Damage Detection Using Recurrent Neural Network in Hybrid Composite Beam</b> .....	593
Saritprava Sahoo and Pankaj Charan Jena	
<b>Analysis of the Tribological Behaviours of the Surfaces of Stainless Steel and Inconel 718 Against Each Other Under Non-lubricated Conditions</b> .....	605
Khush Khanna, Sushant Bansal, Roop Lal, and Ramakant Rana	
<b>Interactional Challenges to Effective E-Waste Management of Indian City</b> .....	615
R. S. Gurjar, M. K. Lila, P. Tyagi, and R. P. Verma	

**A Swarm Intelligence and Nearest Neighborhood Approach to Solve an Excess Capacity Vehicle Routing Problem in a FDCG Company** ..... 635  
 T. Srinivas Rao

**Advantages and Applications of Natural Fiber Reinforced Hybrid Polymer Composites in Automobiles: A Literature Review** ..... 645  
 Sarita Choudhary, Jyotirmoy Haloi, Manoj Kumar Sain, and Praveen Saraswat

**Issues and Challenges in Fabrication of Conductive Parts by Additive Manufacturing and Their Applications: A Study** ..... 661  
 Arpit Bajpai and Prashant K. Jain

**Agglomeration of the Various Industry 4.0 Perspectives in the Supply Chain Performance Systems** ..... 673  
 Ram Dayal Pandey, Mohit Tyagi, Narendra Kumar, and R. S. Walia

**Exploration of Circular Economy Enablers Using Fuzzy DEMATEL Approach** ..... 685  
 Shivam Mishra, Mohit Tyagi, Anish Sachdeva, and Ravi Pratap Singh

**Multi-criteria Assembly Line Design and Configuration Using Heuristics—An Automotive Case Study** ..... 703  
 Rajeev Singh Rawat, Anish Sachdeva, Mohit Tyagi, and Dilbagh Panchal

**A Postural Risk Assessment of Manual Dairy Farm Workers Using REBA Technique** ..... 717  
 Umesh Gurnani, Sanjay Kumar Singh, Manoj Kumar Sain, and M. L. Meena

**Feasibility Investigations on the Development of Hybrid Pellet-Based Extruder with Fused Filament Fabrication** ..... 731  
 Yash Soni, Narendra Kumar, Ravi Pratap Singh, and Prashant K. Jain

**Investigations on the Effect of Nanoclay Reinforced ABS/Nylon-Blended Copolymer Filament for Extrusion-Based 3D Printing** ..... 739  
 Vishal Francis, Narendra Kumar, Sonika Sahu, and Ravi Pratap Singh

# About the Editors

**Dr. Ravi Pratap Singh** is presently working as an Assistant Professor in the Department of Mechanical Engineering at National Institute of Technology, Kurukshetra, India. He has received his Doctor of Philosophy (Ph.D.) from National Institute of Technology (NIT) Kurukshetra, India. He is a Life Member of IIIE, India, and SCIEI, Log Angeles, USA. His broad areas of research are advanced manufacturing processes, modelling and optimization methods, advanced engineering materials, etc. He has published over 150 research articles throughout the several SCI/Scopus indexed journals and conferences. He has awarded as Young Scientist in Mechanical Engineering in VIRA-2019 awards, and as Young Faculty in Engineering (Major Area: Mechanical Engineering) in VIFA-2019 awards. Dr. Singh has also awarded as Best Researcher Award in International Scientist Awards on Engineering, Science, and Medicine, New Delhi, India. He has been Awarded Young Engineer Award (Mechanical Engineering) in 37th National Convention on Mechanical Engineering and National Seminar conducted by the Telangana State Center, Khairtabad, Hyderabad under the aegis of Institution of Engineers (India), IEI held during December, 2022. In addition to this, he is also serving as an Ambassador of Bentham Open, Sharjah, UAE as well as a Member of Visor Academic Committee, Singapore. Dr. Singh has also been ranked among the top 2% of Scientists in the world as per the survey conducted by STANFORD University for the year 2021 and 2022.

**Dr. Mohit Tyagi** is currently working an Assistant Professor in the Department of Mechanical Engineering at National Institute of Technology, Kurukshetra, India. He did his Ph.D. from Indian Institute of Technology (IIT) Roorkee in 2015. His research interests include industrial engineering, supply chain management, corporate social responsibilities, system optimization, performance measurement system, data science and fuzzy inference system. He has around 8 years of teaching and research experience. He has over 85 publications in international and national journals.

**Prof. R. S. Walia** is currently working as Professor and Head at Department of Production and Industrial Engineering at Punjab Engineering College (PEC). He pursued his Ph.D. from Indian Institute of Technology (IIT) Roorkee. His research interests are advanced manufacturing processes, production and industrial engineering, human factor engineering and FEM. He has 150 research articles in reputed international journals and various articles in international and national conferences. Dr. Walia is the member of various national and international bodies. He has received a number of prizes and honors. Dr. Walia has coordinated various STC on Advanced Manufacturing processes.

**Prof. J. Paulo Davim** received his Ph.D. in Mechanical Engineering from the University of Porto in 1997, the Aggregate title from the University of Coimbra in 2005, and a D.Sc. from London Metropolitan University in 2013. Currently, he is a professor at the Department of Mechanical Engineering of the University of Aveiro, Portugal. He has over 35 years of teaching and research experience in manufacturing, materials, and mechanical engineering with a special focus on machining and tribology. He has also started taking an interest in management/industrial engineering and higher education for sustainability. He has worked as an evaluator of projects for international research agencies as well as an examiner of Ph.D. thesis for many universities. He is the editor-in-chief of several international journals, guest editor of journals, book editor, book series editor, and scientific advisory for many international journals and conferences. Presently, he is an editorial board member of 30 international journals and serves as reviewer for more than 95 prestigious Web of Science journals. In addition, he has also published, as author and co-author, more than 20 books, 90 book chapters, and 750 articles in journals and for conferences.

# Revalidation of Components by Implementation of Bar-Coded Route Cards and Enterprise Resource Planning System in Manufacturing Units



S. Hari, Shanker Krishna, and Rakesh Kumar Vij

**Abstract** Revalidation is a matter of concern in the manufacturing environment of an organization that manufactures components for aviation, space, oil and gas or defence requirements. As prescribed by Aerospace Standard, AS9100 Revision D, all the components that were checked using out-of-tolerance instruments or gauges have to be rechecked with a new gauge that is within the tolerance limits. This paper presents the significance of implementing an Enterprise Resource Planning (ERP) system in the tool cribs of manufacturing units. The importance of this study lies in the fact that the revalidation process is time-consuming and involves high costs. Hence, it is suggested to carry out the issuance of instruments or tools through an ERP system. In this scheme, the route orders are bar-coded, and the tool is issued on the basis of job order and operation. During the revalidation process, the data of components to be recertified is fetched directly from the ERP system.

**Keywords** Enterprise resource planning (ERP) · Manufacturing environment · Revalidation · Tolerance

## 1 Introduction

The quality requirements in the aerospace, automotive, and petroleum manufacturing sectors are becoming more stringent with advancements in quality management systems. There has been a remarkable rise in the requirement for manufacturing quality, and hence, its integration all over the enterprise is an essential requirement. Implementation of manufacturing quality control ensures the production of components that conform to the industry's expectations and the customers all the time. The process of revalidation is introduced to prevent the entry of faulty components into the system.

---

S. Hari · S. Krishna (✉) · R. K. Vij  
Drilling, Cementing and Stimulation Research Centre, School of Petroleum Technology, Pandit Deendayal Energy University, Knowledge Corridor, Raysan, Gandhinagar, Gujarat 382426, India  
e-mail: [shanker.krishna@spt.pdpu.ac.in](mailto:shanker.krishna@spt.pdpu.ac.in)

Calibration is the relationship between the values of quantities indicated by a measuring instrument represented by a material measure and the values realized by standards under specified conditions [3]. Minor differences in the process output characteristics are termed as tolerances [10]. The values of instrument tolerance depend on the type of industry and location. The tolerance in measurement along with calibration periodicity is specified by the manufacturer during the time of supply. The type of environment, usage and storage are specified by the manufacturer. The frequency of calibration of the equipment is set by the Quality Control Department (QCD) of an organization on the basis of usage, number of parts to be produced and calibration history [1]. The recommendation for calibration interval is not mentioned in a calibration certificate unless the customer agrees to it.

Currently, AS 9100D [15] is an essential certification for maintaining international quality management standards with regard to aviation and defence manufacturing. AS9100D defines a quality management system for aviation, space and defence organizations. The requirement for a quality management system is standardized to such a great extent that it can be used by manufacturing firms all around the world on all platforms of their supply chain. It results in the enhancement of quality and performance. The quality management system is developed primarily for the defence, space and aviation industries. In industries where there is an additional requirement for a quality management system over ISO 9001 [7], AS 9100D standards can be used. As per the guidelines put forth by AS 9100 Revision D, all the components that were checked using out-of-tolerance gauges or equipment have to be rechecked with a new gauge that falls within the tolerance limits.

The organization carries out the validation of any processes for production and service provision wherein the outcome cannot be verified with the help of subsequent monitoring or measurement. In such cases, the deficiencies become apparent only after the product is in use or the service has been delivered. Revalidation is a critical process in an organization that deals with the manufacturing of safety-critical components, which are more often associated with medical equipment [8], aerospace [15] and petroleum industry [9]. During the calibration process, it may be found that some of the instruments or gauges used for manufacturing components are out of tolerance limits. The instruments or gauges that are rejected are removed from the tool cribs. There lies a possibility that the rejected instruments or gauges were used to check components within the previous calibration date. To prevent the entry of faulty components into the system, the process of revalidation is introduced. The process of revalidation is time-consuming and involves high costs. For instance, the revalidation engaged in the alteration of cutting tool geometry to turn a component of an aero-engine would cost approx. €135,000 [11].

## 2 Research Background

In the present-day world, manufacturing companies are being forced to redesign their products and components that encompass these products frequently. Significant



reasons to adopt changes in products, as well as components composed by these products, are listed as follows:

1. Shorter and shorter life cycles of the product [16]
2. Change the requirements of the customer [4]
3. Increasing demands for product optimization [4].

Manufacturing of safety-critical products involves multiple interconnections between the products and the manufacturing methods and a vast extent of complexities. Manufacturing Changes (MC) refer to the alterations in the existing manufacture in order to carry out a change in the component post its entry into the market [12]. Researchers have acknowledged that even though recognizing an appropriate MC in a systematic manner has the potential to minimize the cost and effort involved in the process of revalidation and optimize the economic aspects, it is indeed a scientifically challenging task [2].

The proposed methodology ensures a reduction in cost, effort and time consumption during the process of revalidation. A double verification scheme of the used equipment for inspection in the ERP system is established through this study.

## 3 Research Methods

### 3.1 *Job Order and Job Card*

A job order or work order is prepared by the Methods Engineering Department (MED) of the organization and is used for manufacturing and fabrication. It is generated to initiate the process flow of manufacturing. Generally, the first process is to withdraw the specified material from the store. The bill of materials is included in the job order. The type of raw material, quantity on order, work centres and shops where the process has to be carried out are described in the job order.

A routing card or job card is a document prepared by the MED of the organization. It is a process flow document in which the sequence of operations to be carried out on the raw material is specified. This sequence of operations results in the manufacturing of the final product from the raw material state. The route card is bar-coded by the organization's Scheduling and Progress Department (SPD). When the bar-coded route card is scanned, the details of the route card are fed to the ERP system. An ERP system is an integration of several modules of software and a central database that facilitates efficient, effective and smooth management of resources [5, 13, 17]. It establishes uniformity in the entire organization and ensures that the whole process of business, data sharing, and access to the updated information in real-time settings becomes automated [14]. It improves cross-functional activities in an enterprise [6]. Few gauges within a batch may be identified as out-of-tolerance instruments. A rejection list of instruments and gauges is prepared and forwarded to Detailed Component Inspection Department (DCID). The list of components that

were inspected by the instrument or gauge within the calibration periodicity is then compiled from inspection records and forwarded to the SPD. The document issued by SPD to the manufacturing shops for withdrawal of possibly defective components is called withdrawal routing.

## **4 Result Discussion**

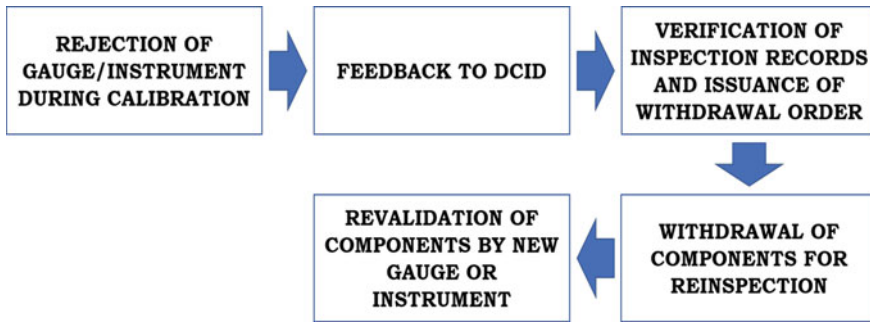
### ***4.1 Conventional Inspection Process Workflow***

The gauges, instruments and several other tools are stored in the tool crib. These instruments or gauges are issued through a tool crib for day-to-day manufacturing activities. The issuance is done based on the operators' request against a tool token. The instrument or gauge is issued from the tool crib to fabricate a component based on the requirement.

The component is fabricated using that gauge or instrument. Inspection of the component is carried out using the same or similar instrument or gauge by the quality assurance personnel. Entry of the instrument or gauge is done in the inspection record and is maintained by the Quality Assurance Department (QAD). The inspection operation is closed in the ERP system once the inspection process is finished.

### ***4.2 Conventional Revalidation Process Workflow***

All gauges, instruments and tools in the tool crib are calibrated by the calibration unit of QAD. All calibration is done in a controlled environment as per the standard norms followed by the organization. If an instrument or gauge is found out of standard limits during the process of calibration, it is rejected. Feedback is sent to the DCID to verify if any component was checked previously with that rejected instrument. All components checked previously with the rejected gauge between the previous calibration date and the next calibration date is traced from the inspection records. A recall notice, with the details of the parts and the work order, is forwarded to the SPD, which prepares the withdrawal route cards for routing back the possibly defective components from the assembly lines and other process shops. The components and the withdrawal route card are received in the DCID from various assembly shops. The components are subjected to reinspection using gauges that are within acceptable limits. Once this is carried out, the components are sent back to the concerned stores or assembly lines. The process workflow is shown in Fig. 1.



**Fig. 1** Process flow chart for revalidation

### ***4.3 Implementation of ERP in Tool Cribs***

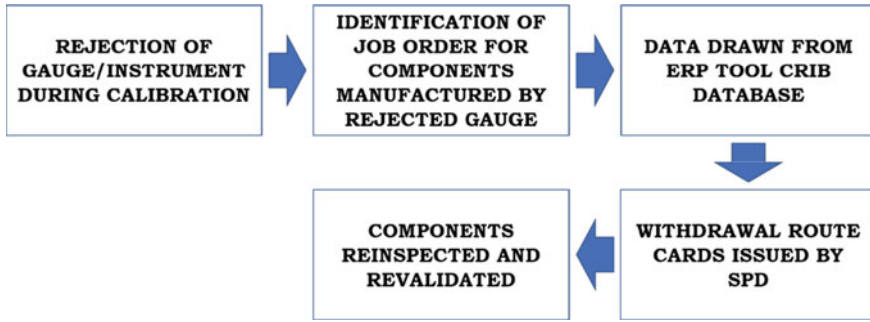
Initially, all the data of instruments, gauge tools and equipment in the tool crib are added as standard parts in the ERP system. A bar-code reader is installed in the tool crib to scan the bar-coded route cards. Each gauge or tool is given a unique Tool Identification Number (TIN). The unique number series is followed to improve traceability among tools that possess the same specification and are large in number. The tool request is made based on a given work order. The bar-coded route cards are scanned at the tool crib. The tool is issued for the assigned work order and operation, and the same is recorded in the ERP system. The details of the route card that contains the operation details and the unique Gauge Identification Number (GIN) are linked and stored in the ERP system. Once this process is completed, the gauge/instrument is issued to the personnel.

### ***4.4 Retrieval of Data from ERP for Revalidation***

A rejection list is received from the calibration unit regarding the rejection of the gauge or tool. The details of the components which were manufactured or inspected by the rejected tool or gauge are obtained from the ERP tool crib database. The job order and the operation for which the tool was used are also obtained.

### ***4.5 Revalidation Workflow After the Implementation of ERP in Tool Cribs***

Job orders in which the rejected tool gauge was used are identified from the ERP system's database. This information is compiled in the form of a document and forwarded to the SPD, which in turn prepares the withdrawal route cards. If the



**Fig. 2** Process flow chart for revalidation after implementation of ERP in tool cribs with bar-coded route cards

component is critical, the part's serial number is also mentioned in the withdrawal routing. The components withdrawn are subjected to reinspection at the DCID and revalidated based on the operation for which the rejected tool was used. The component is checked using the gauges or instruments that are within the tolerance limits. The revised workflow is shown in Fig. 2.

## 5 Conclusion

The salient points of this research article that need to be highlighted are listed below:

1. In conventional revalidation process flow, as mentioned earlier, the list of components that were inspected using the rejected gauge is prepared based on the inspection reports. This list of components is forwarded for withdrawal routing. This process is time-consuming and not completely error free.
2. Upon the implementation of ERP in tool cribs, the tools are issued through ERP for a given operation and job order. Consequently, the process of revalidation becomes much easier for the inspection personnel. The verification has to be carried out only on the basis of the operation for which the rejected gauge was used.
3. The process of revalidation is initiated from the calibration unit as the data of components manufactured by the instrument or gauge is available in the ERP database. The time consumed by the personnel in DCID to check the inspection reports for rejected gauge usage is also avoided.
4. The process improves the traceability of the instruments and gauges along with the components fabricated. The implementation of ERP system in the tool cribs makes the system more effective and efficient.

## References

1. Bare A (2006) Simplified calibration interval analysis (No. WSRC-MS-2006-00099). SRS
2. Bergs T, Hermann L, Rey J, Barth S (2020) Methodology for the identification of alternative manufacturing changes for safety-critical components. *Prod Eng Res Devel* 14(3):297–307
3. Bewoor AK, Kulkarni VA (2009) Metrology and measurement. McGraw-Hill Education
4. ElMaraghy HA (ed) (2008) Changeable and reconfigurable manufacturing systems. Springer Science & Business Media
5. Huang Z, Palvia P (2001) ERP implementation issues in advanced and developing countries. *Bus Process Manage J*
6. Ifinedo P (2006) Extending the Gable et al. enterprise systems success measurement model: a preliminary study. *J Inf Technol Manage* 17(1):14–33
7. International Organization for Standardization (2015) ISO 9001: quality management systems—requirements
8. International Organization for Standardization (2016) ISO 13485: medical devices—quality management systems—requirements for regulatory purposes
9. International Organization for Standardization (2020) ISO 29001: petroleum, petrochemical and natural gas industries—sector specific quality management systems—requirements for product and service supply organizations
10. Jack H (2013) Engineering design, planning, and management. Academic Press
11. Klocke F, Gierlings S, Brockmann M, Sage C, Veselovac D (2010) Adaptive control of manufacturing processes for a new generation of jet engine components. CIRP-ICME Capri
12. Koch J (2017) Manufacturing change management—a process-based approach for the management of manufacturing changes. Doctoral dissertation, Technische Universität München
13. Laudon KC, Laudon JP (2017) Management information systems: managing the digital firm, global edition. Pearson
14. Mahmood F, Khan AZ, Bokhari RH (2019) ERP issues and challenges: a research synthesis. *Kybernetes*
15. SAE Aerospace Standard (2016) AS9100D: quality management systems—requirements for aviation, space, and defense organizations
16. Schuh G, Gartzten T, Basse F, Schrey E (2016) Enabling radical innovation through highly iterative product expedition in ramp up and demonstration factories. *Procedia CIRP* 41:620–625
17. Subramoniam S, Tounsi M, Krishnankutty KV (2009) The role of BPR in the implementation of ERP systems. *Bus Process Manage J*

# Parametric Study of Process Parameters on Surface Roughness and Dimensional Deviation in Electrical Discharge Machining of Fe-Based SMA



Ranjit Singh, Ravi Pratap Singh, and Rajeev Trehan

**Abstract** The need for sophisticated material goods has continuously increased in the contemporary era of research and technology. Precision machining of sophisticated materials has long been a source of worry for scientists and academics. In the commercial and industrial sectors, shape memory alloys are a kind of sophisticated material that is becoming more widely employed as time goes on. It is a highly uncommon and distinct substance with the property of resuming its original shape after being subjected to low exact temperature conditions. Because of its shape-recovery design, it is a valuable metal for large-scale industrial applications due to its high strength and durability. SMAs are also divided into three types: those that are reliant on NiTi, those that are based on Cu, and those that are based on Fe. The Fe-based alloy has a high elasticity and damping coefficient, as well as a broad temperature range. When applying electrical discharge machining on Fe-based SMA, this research aims to examine the effects of pulse-on time, pulse-off time, peak current, and distance voltage on surface roughness and dimensional deviation. 11.26 and 4.18  $\mu\text{m}$  were the highest and lowest levels of surface roughness measured. The dimensional variation ranges from a minimum of 0.02 to a maximum of 0.21 mm. When it comes to surface roughness, the amount of peak current and the timing of the pulse are more important factors. SEM micrographs of the workpiece show the development of microcracks, craters, pockmarks, pores, extruded material, globules of debris, recast layer, macro-ridges, and other features on the surface of the workpiece sample after EDM operations. The variation in the size of the workpiece samples following EDM operations on Fe-based SMA samples was shown in SEM micrographs.

**Keywords** SMA · SME · EDM · SR · DD · Fe-based SMA · Pulse-on time · Peak current · SEM · RL

---

R. Singh · R. P. Singh (✉) · R. Trehan  
Department of Mechanical Engineering, National Institute of Technology, Kurukshetra,  
Haryana 136119, India  
e-mail: [singhrp@nitj.ac.in](mailto:singhrp@nitj.ac.in)

R. Singh  
IPE Department, NIT, Jalandhar, India

## 1 Introduction

The need for smart materials is growing in today's era of technological innovation due to their exceptional and unique characteristics and uses in a broad range of areas, from biomedical to manufacturing. Shape Memory Alloys (SMAs) are a new class of advanced materials that may return to their original shape after being exposed to magnetic and temperature changes [1]. The shape memory effect refers to the process of reverting to its previous form (SME) [2]. Arne Olander was the first to discover SMAs in 1932. SMAs come in three varieties: NiTi, Cu, and Fe based [3–6]. Fe-based SMA is a kind of SMA in which iron is a significant component in comparison with other components. Since Fe-based SMAs may be easily manufactured using liquid or powder metallurgical processes, they are considered low-cost alloys rather than NiTi alloys. An important SMA alloy system with several industrial applications is Fe-based SMA. Using Sato's Fe-30Mn-1Si alloy and the Fe-Mn alloy SME, production costs were lowered. Fe-SMAs, on the other hand, have a large transition hysteresis as well as high stiffness and strength compared to Ni- and Cu-based SMAs. For Fe-16Mn-5Si-10Cr-4Ni-1(V,N) and Fe-17Mn-5Si-10Cr-4Ni-1(V,N), Dong et al. and Leinenbach et al. employed mass fraction to increase SME (V,C). Existing SMEs have prompted widespread interest in the application of these Fe-SMAs in civil engineering sectors such as damping, active control, and pre- or post-stress tensioning of structures, thanks to their high rigidity, high strength, and low production costs. After NiTi and Copper-based SMAs, Iron-based SMAs are the third kind of SMA to be projected. This SMA class has shown to be more cost-effective than the NiTi alloy system because of its low alloy component and simplicity of manufacture. A number of alloys, such as Fe-Pt, Fe-Pd, Fe-Mn-Si, Fe-Al, Fe-Ni-Ti, and Fe-Ni + Co + Ti, are used to make iron-based SMAs, also known as shape memory steels (SMS). SMS can only be economically viable if it is manufactured at the same rate as carbon steel. The use of non-conventional machining processes to machine Fe-based SMA is a concern for the future. Researchers are looking at EDM machining of Fe-based SMA to better understand how various process factors affect machining responses. Fe-based SMA's EDM method is investigated in order to get new machining ideas and help with industrial growth [7–9]. In order to suit the needs of the new industry, non-traditional machining processes develop complicated machining shapes on such specific materials. In EDM, an electric spark is used to remove material from the work surface and obtain the desired form [10–12]. The material is melted and vaporized as a result of the high temperature caused by the electrical discharge at the tool work contact. High precision machining, complicated slice forms, and surface conditions may all benefit from this approach in modern production. All of these processes are based on the EDM system's operating idea, which may be used in a variety of ways. Because of the wide variety of EDM processes [13], it may be used for both small and somewhat large machining areas.

A thermo-erosive method for electrically conductive materials EDM employs pulsed discharges that are spatially and temporally regulated irrespective of their

mechanical, chemical, or thermo-physical features. The EDM technology was introduced in the 1940s [14]. In recent years, EDM has become one of the most popular methods for machining difficult-to-cut components. This machining technology has been used in modern production to help with high-accuracy machining of materials and cutting complicated shapes with maximum surface parameters [15]. It is possible to get a workpiece free of residual tension with EDM since the instrument (electrode) does not come into direct contact with the material being machined when using it. To achieve the required form, EDM manufacturing utilizes an electrical discharge (electrical sparks). Tool erosion unit and die-sinking are other terms for the same process [16–21].

The current research focuses on the impact of process parameters on surface roughness (SR) and dimensional deviation (DD) during EDM machining Fe-based SMA. The surface research investigates the surface characteristics and variation in dimensions of work samples at various process parameters. Pictorial diagrams and figures were used to investigate the differences in SR and DD readings across a wide range of values.

## 2 Materials and Methods

The Fe-based SMA has been chosen for performing experiments. The electrode of copper has been selected as a tool for performing EDM operations. The electrode has diameter of 10 mm. Circular disk with 100 mm diameter and 15 mm height is the shape of the workpiece. The EDM method measures the pulse-on and pulse-off times, peak currents, and gap voltages, among other things. When the process parameters are changed, a response parameter called surface roughness is measured.

Oscar max CNC die-sinking EDM machine was used for the experiments. Pulse-on time, pulse-off time, peak current, and gap voltage are selected as parameters. Surface Roughness (SR) and Dimensional Deviation (DD) have been selected as the responses to examine the impacts of various process factors (DD). EDM die-sinking is seen schematically in Fig. 1.

The range of various selected process parameters has been displayed in Table 1 (Fig. 2).

Table 2 shows the surface roughness for various pulse-on time times in different units of measurement. At pulse times of 30  $\mu\text{s}$  and 400  $\mu\text{s}$ , the lowest and greatest values of surface roughness are 4.18 m and 11.26 m, respectively. Dimensional deviation data are shown in Table 3 for various pulse durations. When the pulse-on time is 30 and 400  $\mu\text{s}$ , DD's lowest and maximum values are 0.02 and 0.21 mm.

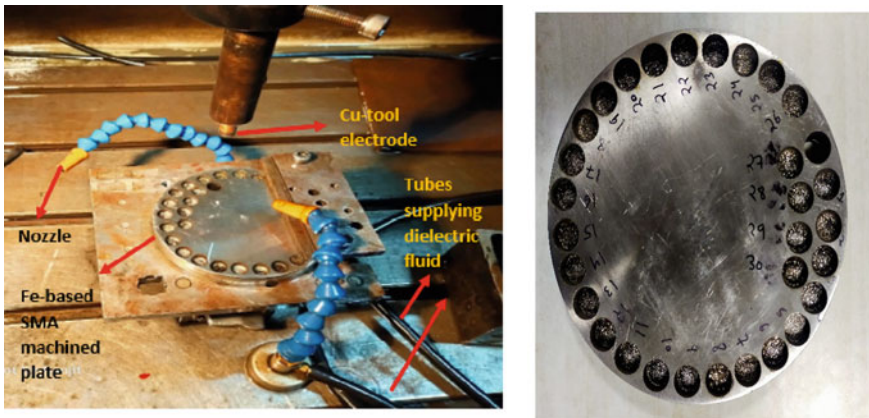




**Fig. 1** Die-sinking EDM setup

**Table 1** Range of process parameters

Process parameters	Range
Pulse-on time ( $T_{on}$ )	30, 45, 60, 90, 120, 150, 250, 300, 400
Pulse-off time ( $T_{off}$ )	20, 45, 60, 90, 120, 200, 250, 300
Peak current ( $I_p$ )	8, 14, 20, 24, 30, 40, 50
Gap voltage ( $G_v$ )	30, 40, 50, 60, 70, 80



**Fig. 2** Fe-based shape memory alloy

At various pulse-off times, the surface roughness values are shown in Table 4. At pulse-off times of 20  $\mu s$  and 60  $\mu s$ , the maximum and minimum values of surface roughness are 9.88 m and 6.21 m, respectively. Different pulse-off times are shown

**Table 2** Surface roughness at various pulse-on time values

S. No	Pulse-on time ( $\mu$ s)	Act. diameter	Actual depth	Time in minutes	Surface roughness ( $\mu$ m)
1	30	10.02	6.81	47.66	4.18
2	45	10.04	6.88	25.66	6.26
3	60	10.05	6.93	20.71	9.72
4	90	10.07	6.97	17	8.85
5	120	10.09	6.99	16.16	8.5
6	150	10.12	7.13	17.13	8.08
7	250	10.16	7.18	16.9	9.5
8	300	10.19	7.22	16.8	9.8
9	400	10.21	7.25	17.43	11.26

**Table 3** Dimensional deviation at different pulse-on time

S. No	Pulse-on time ( $\mu$ s)	Act. diameter (mm)	Actual depth (mm)	Time in minutes	Dimensional deviation (diametral) (mm)
1	30	10.02	6.81	47.66	0.02
2	45	10.04	6.88	25.66	0.04
3	60	10.05	6.93	20.71	0.05
4	90	10.07	6.97	17	0.07
5	120	10.09	6.99	16.16	0.09
6	150	10.12	7.13	17.13	0.12
7	250	10.16	7.18	16.9	0.16
8	300	10.19	7.22	16.8	0.19
9	400	10.21	7.25	17.43	0.21

in Table 5. Maximum and lowest DD at pulse-off times of 20  $\mu$ s and 300  $\mu$ s are 0.15 and 0.02 mm, respectively.

The surface roughness levels at various peak current values are shown in Table 6. At peak currents of 24 A and 50 A, the lowest and greatest values of surface roughness are 7.25 m and 9.2 m, respectively. Table 7 shows the DD values at various peak current levels. At peak currents of 8 A and 50 A, DD's lowest and highest values are 0.02 mm and 0.15 mm, respectively.

At different gap voltages, the surface roughness values are shown in Table 8. At gap voltages of 60 V and 80 V, the maximum and lowest values of surface roughness are 10.77 m and 6.69 m, respectively. At varied gap voltages, the variance in DD values is seen in Table 9. At gap voltages of 30 V and 80 V, the maximum and lowest DD are, respectively, 0.08 and 0.02 mm.

**Table 4** Surface roughness at different range of pulse-off time

S. No	Pulse-off time ( $\mu$ s)	Act. diameter (mm)	Actual depth (mm)	Time in minutes	Surface roughness ( $\mu$ m)
1	20	10.15	7.01	21.43	9.88
2	45	10.12	6.82	16.56	9.79
3	60	10.11	6.32	15.78	6.21
4	90	10.09	6.2	16.53	6.42
5	120	10.07	6.12	18.71	6.65
6	200	10.05	7.05	34.26	6.52
7	250	10.03	6.26	32.91	7.72
8	300	10.02	6.15	35.78	6.61

**Table 5** Dimensional deviation at different pulse-off time

S. No	Pulse-off time ( $\mu$ s)	Act. diameter (mm)	Actual depth (mm)	Time in minutes	Dimensional deviation (diametral) (mm)
1	20	10.15	7.01	21.43	0.15
2	45	10.12	6.82	16.56	0.12
3	60	10.11	6.32	15.78	0.11
4	90	10.09	6.2	16.53	0.09
5	120	10.07	6.12	18.71	0.07
6	200	10.05	7.05	34.26	0.05
7	250	10.03	6.26	32.91	0.03
8	300	10.02	6.15	35.78	0.02

**Table 6** Surface roughness at different values of peak current

S. No	Peak current	Act. diameter	Actual depth	Time in minutes	Surface roughness ( $\mu$ m)
1	8	10.02	7.16	79	9.09
2	14	10.04	7.02	41.9	6.82
3	20	10.05	6.17	22.13	7.19
4	24	10.07	6.12	17.9	7.25
5	30	10.1	6.59	18	7.3
6	40	10.12	6.33	11.26	8.18
7	50	10.15	5.88	9.1	9.2

**Table 7** Dimensional deviation at different peak current values

S. No	Peak current (A)	Act. diameter (mm)	Actual depth (mm)	Time in minutes	Dimensional deviation (diametral) (mm)
1	8	10.02	7.16	79	0.02
2	14	10.04	7.02	41.9	0.04
3	20	10.05	6.17	22.13	0.05
4	24	10.07	6.12	17.9	0.07
5	30	10.1	6.59	18	0.1
6	40	10.12	6.33	11.26	0.12
7	50	10.15	5.88	9.1	0.15

**Table 8** Surface roughness at different gap voltage values

S. No	Gap voltage	Act. diameter	Actual depth	Time in minutes	Surface roughness ( $\mu\text{m}$ )
1	30	10.08	6.54	21.12	9.95
2	40	10.06	6.05	18.03	9.89
3	50	10.04	6.51	22.41	9.8
4	60	10.03	6.04	18.52	10.77
5	70	10.03	6.42	18.14	7.75
6	80	10.02	6.39	21.21	6.69

**Table 9** Dimensional deviation at different gap voltage

S. No	Gap voltage (V)	Act. diameter (mm)	Actual depth (mm)	Time in minutes	Dimensional deviation (diameter) (mm)
1	30	10.08	6.54	21.12	0.08
2	40	10.06	6.05	18.03	0.06
3	50	10.04	6.51	22.41	0.04
4	60	10.03	6.04	18.52	0.03
5	70	10.03	6.42	18.14	0.03
6	80	10.02	6.39	21.21	0.02

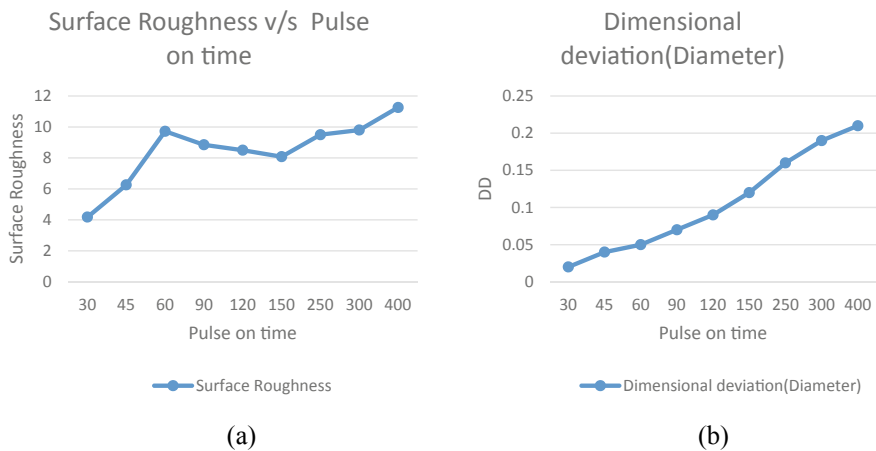
### 3 Results and Discussions

CNC EDM machine setup is used for the tests. Process parameters have been examined while using EDM to process Fe-based SMA. Charts and graphs have been used

to illustrate the results. The graphs represent the relationship between the parameters. The behavior of graph represents the particular parameter effect on SR and DD.

At different pulse-on time values, the SR and DD curves are shown in Fig. 3. The roughness of the surface rises as the pulse-on time increases. Owing to a reduction in the time lag between pulses caused by an increase in pulse-on time, more material is removed from the workpiece due to massive spark generation and high temperature creation. The surface roughness rises as pulse-on time grows because of the substantial material removal. At pulse times of 30  $\mu\text{s}$  and 400  $\mu\text{s}$ , the lowest and greatest values of surface roughness are 4.18 m and 11.26 m, respectively. When pulse-on time grows, DD also increases. The increase in pulse-on time results in a shorter time interval between pulses, which results in more spark creation and a higher temperature, which results in more material removal, which results in an increase in dimensional deviation. When the DD is used, the work material's form deviates from the specified specifications. When the pulse-on time is 30 and 400  $\mu\text{s}$ , DD's lowest and maximum values are 0.02 and 0.21 mm.

Figure 4 depicts how SR and DD behave as the pulse-off time lengthens. Due to an increased pulse-off time, there is a longer time lag between pulses, which results in less sparking. There is less material removal from the workpiece as a result of reduced spark generation. Surface roughness is reduced when less material is removed from the workpiece. At pulse-off times of 20  $\mu\text{s}$  and 60  $\mu\text{s}$ , the maximum and minimum values of surface roughness are 9.88 m and 6.21 m, respectively. The increase in pulse-off time results in a longer time interval between pulses, which reduces the likelihood of a spark forming. Less spark creation means lower temperatures, which means less material loss and, as a consequence, a smaller departure from the original size of the workpiece. The work material's dimensional deviation is reduced when the pulse-off time is prolonged. Maximum and lowest DD at pulse-off times of 20  $\mu\text{s}$  and 300  $\mu\text{s}$  are 0.15 and 0.02 mm, respectively.



**Fig. 3** Effect of pulse-on time on **a** SR and **b** DD

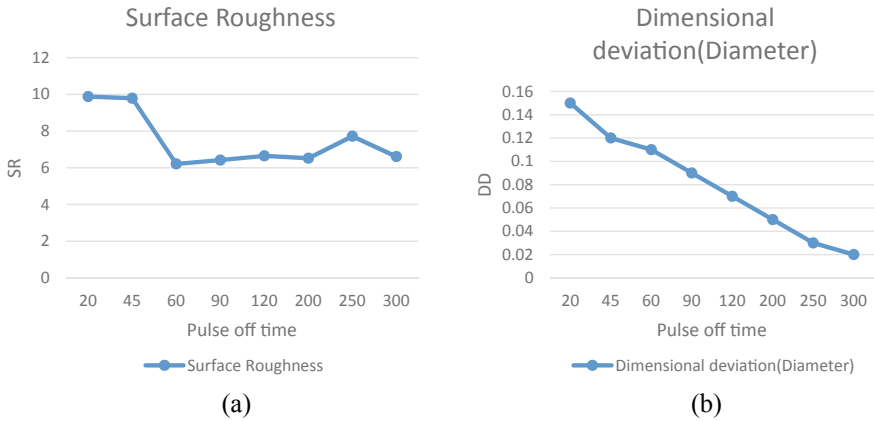


Fig. 4 Effect of pulse-off time on a SR and b DD

Figure 5 depicts the plot of SR and DD with the rise in peak current values. There is rise in surface roughness levels with the increase in peak current. The rise in peak current translates into increased current supply that leads to high temperature which generates significant material removal. The increased MRR turns into higher surface roughness. The lowest and greatest value of surface roughness are 7.25 and 9.2  $\mu\text{m}$  for peak current levels of 24 A and 50 A. The rise in peak current leads to higher current that leads to increased spark generation. Large spark creation translates into more material removal and leads to greater variation in the shape of the workpiece. The lowest and highest values of DD are 0.02 and 0.15 mm at peak current levels, i.e., 8 A and 50 A.

As the gap voltage rises, so does the relationship between SR and DD in Fig. 6. The surface roughness value decreases as the gap voltage increases. More voltage in the gap leads to a longer discharge waiting time, which results in a lower MRR. As a result of the shorter discharge pause caused by the lower gap voltage, more sparks are formed, increasing the temperature, and therefore the MRR. The increase in MRR

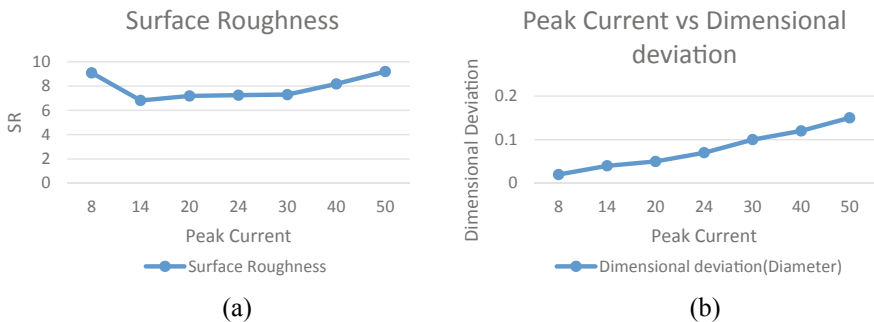
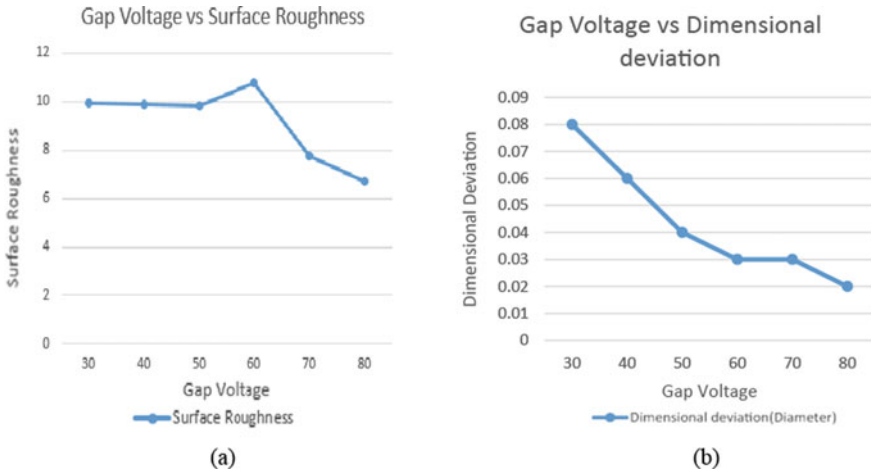


Fig. 5 Effect of peak current on a SR and b DD



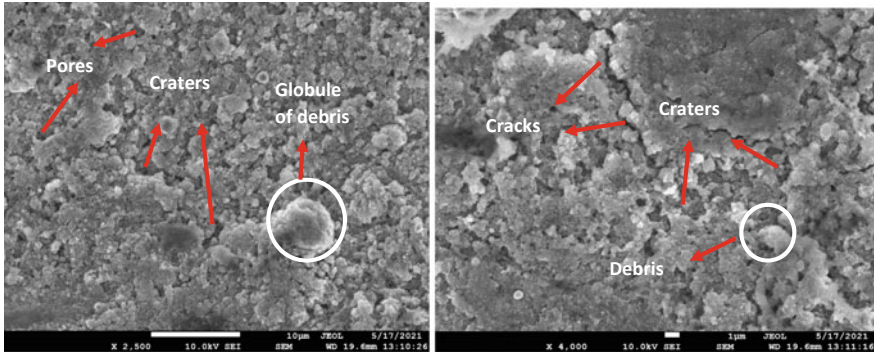
**Fig. 6** Effect of gap voltage on **a** SR and **b** DD

results into more surface roughness of the workpiece. The highest and lowest values of surface roughness are 10.77 and 6.69  $\mu\text{m}$  at gap voltage values of 60 and 80 V. The dimensional deviation decreases with an increase in gap voltage. The extended discharge waiting time improves flushing conditions, which leads to a more stable cut as a result of the increased gap voltage. A more consistent cut has been made. Lower gap voltage settings may reduce discharge waiting time, increasing the amount of sparks produced per unit of time. As a result, the amount of material removed from the workpiece increases, as does the amount of workpiece form deviation. DD values of 0.08 mm and 0.02 mm for gap voltages of 30 V and 80 V, respectively, are the highest and lowest possible.

## 4 Microstructure Characteristics

The present study focuses on assessing the surface integrity and dimensional deviation of the circular cavity imparted on the work surface and tool electrode surface following CNC Die-Sinking EDM machining.  $T_{\text{on}}$  and  $T_{\text{off}}$  durations had a considerable influence on the surface integrity, leading in deep overlapping craters, debris globules, microscopic cracks, and the development of RL, as the results of the experiment shown.

The surface homogeneity of Fe-based SMA was evaluated during the experiment by changing  $G_V$ ,  $I_p$ ,  $T_{\text{off}}$ , and  $T_{\text{on}}$ . EDM is used to verify the metal content of the machined samples before using a scanning electron microscope (SEM). Analyzing the material's surface integrity is done using a scanning electron microscope (SEM). Machined-surface SEM micrographs revealed debris clusters, microcracks, sphere particles, and craters of various sizes. As the pulse rate increased, deep holes appeared



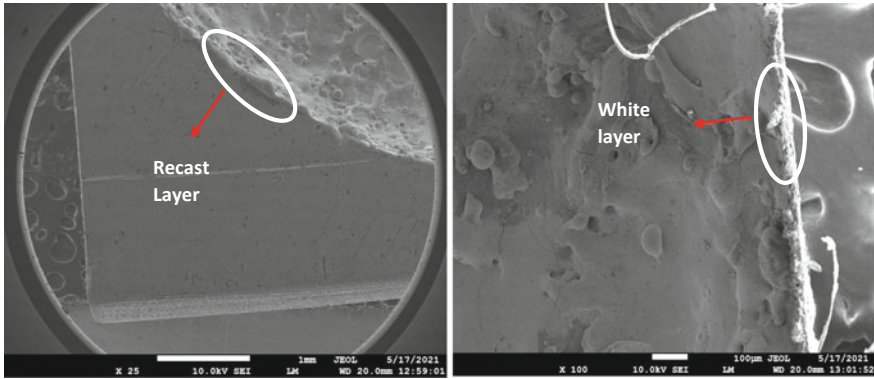
**Fig. 7** SEM micrographs for EDMed Fe-based SMA

on the machined surface [22–31]. Deep and extensive holes in the specimen’s surface were caused by a combination of many electrical discharges, substantial heat transmission, and minimal dissolving or vaporization of work material [32–37]. Some of the discharge-generated fused material was removed by the EDM grease. Work material was found to have an EDMed surface that had a recast layer (RL). Without the use of dielectric fluids, an electric spark-melted material solidifies and deposits on the workpiece’s surface. Various investigations [38–44] have also been reported with the similar findings [45–55], and therefore, the observed theory may be said validated for the elaborated aspects.

Figure 7 shows the SEM machined sample micrographs. It depicts the formation of small cracks, craters, pull-out material, pores, extruded material, pockmarks, and debris globules on the surface of the samples. The surface of the sample is affected by peak current and pulse-on time. The higher the  $T_{on}$ , the more microcraters and debris form on the work sample’s surface.

Figure 8 shows a SEM inspection of the sides and edge sections of machined samples. It depicts the development of a recast layer around the periphery of the machined specimen. Material that has been melted by an electrical spark and re-solidified on the workpiece surface without being cleaned or evacuated with dielectric fluid is referred to as “RL”. The recast layer’s growth on the sample’s edge section is shown in Fig. 8. The SEM micrographs show the development of macro-ridges, pores, spherical debris, and pull-out material on the edge section of the work sample. The re-solidified material has collected on the edge part of the samples, forming a unique layer structure. Its length varies depending on the machining circumstances, ranging from a little to a significant part. The dimensional deviation concept is elaborated with the formation of macro-ridges that represents the deviation in the edge length from actual dimensions.





**Fig. 8** Microstructure images targeted at edge sections of EDMed work sample

## 5 Conclusions

The following interferences are observed after performing the experimentation on Fe-based SMA in CNC EDM machine:

1. Pulse-on time and peak current are two of the most important characteristics that affect surface roughness and dimensional deviation.
2. More frequent and longer pulse-on times result in less time for material to be removed from the workpiece, resulting in larger sparks and greater temperatures. Due to the enormous amount of material removed, the surface roughness rises as the pulse-on time grows. At pulse times of  $30\ \mu\text{s}$  and  $400\ \mu\text{s}$ , the lowest and greatest values of surface roughness are  $4.18\ \mu\text{m}$  and  $11.26\ \mu\text{m}$ , respectively. When the pulse-on time is increased, the time between pulse occurrences is reduced, which causes more spark creation and higher temperatures, which results in greater material removal and an increase in work material dimensional deviation. The work material's shape is altered as a result of the DD's operation. When the pulse-on time is  $30$  and  $400\ \mu\text{s}$ , DD's lowest and maximum values are  $0.02$  and  $0.21\ \text{mm}$ .
3. It takes longer for pulses to occur when pulse-off times are increased; hence, there is less spark creation as a consequence. Material loss from a workpiece is reduced due to reduced spark output, which results in lower temperatures. The roughness of the work surface reduces as less material is removed from it. At pulse-off times of  $20\ \mu\text{s}$  and  $60\ \mu\text{s}$ , the maximum and lowest values of surface roughness are  $9.88\ \mu\text{m}$  and  $6.21\ \mu\text{m}$ , respectively. Spark production is reduced as pulse-off time is increased, as the time gap between pulses is longer. There are fewer sparks, which lowers the temperature, which results in decreased material loss and a smaller workpiece. The dimensional deviation of the work material diminishes as the pulse-off time rises. At pulse-off times of  $20$  and  $300\ \mu\text{s}$ , the DD reaches a high of  $0.15\ \text{mm}$  and a low of  $0.02\ \text{mm}$ .

4. As the peak current increases, so do the surface roughness levels. Peak current increases current supply, leading in high temperatures and severe material loss. The high MRR produces the increased surface roughness. The lowest and greatest value of surface roughness are 7.25 and 9.2  $\mu\text{m}$  for peak current levels of 24 and 50 A. The increase in peak current results in more current, which leads in more spark creation. Large spark generation removes more material and causes the workpiece's form to deviate more. The lowest and highest values of DD are 0.02 and 0.15 mm at peak current levels, i.e., 8 and 50 A.
5. As the gap voltage rises, so does the surface roughness. A lower MRR is the consequence of a longer discharge waiting period, which lowers the temperature. Due to the shorter discharge waiting time caused by the smaller gap voltages, a bigger MRR may be achieved by generating more sparks and increasing temperature formation. Workpiece surface roughness rises as MRR increases. At gap voltages of 60 V and 80 V, the maximum and lowest values of surface roughness are 10.77 m and 6.69 m, respectively. As a consequence, the flushing condition is improved and the cut is more stable with a greater gap voltage. A more consistent cut has been achieved. Increasing the quantity of sparks per unit time is possible by using a machine setting with a lower gap voltage value. Increased material removal and increased variance in the workpiece's shape are the outcome of this method. At a gap voltage of 30 V and 80 V, the maximum and lowest DD are 0.08 mm and 0.02 mm, respectively.
6. Using SEM images, we discovered craters, voids, extruded material, pores, pockmarks, sphere debris, and microcracks. Fractures and craters form as a result of the high amount of heat generated at the tool-to-workpiece contact point. In EDM, the high temperatures cause the workpiece's surface to be worn away. By creating RL edges, re-solidified material on the workpiece's surface may be seen. Images taken with a SEM microscope reveal a white coating, macro-ridges, and pores as well as pullout materials on the edge section of a metal workpiece. With the inclusion of macro-ridges, which illustrate the divergence in edge length from genuine dimensions, the dimensional deviation notion is expanded.

## References

1. Jani JM, Leary M, Subic A, Gibson MA (2014) A review of shape memory alloy research, applications and opportunities. *Mater Design* (1980–2015) 56:1078–1113
2. Sun L, Huang WM, Ding Z, Zhao Y, Wang CC, Purnawali H, Tang C (2012) Stimulus-responsive shape memory materials: a review. *Mater Design* 33:577–640
3. Ölander A (1932) An electrochemical investigation of solid cadmium-gold alloys. *J Amer Chem Soc* 54(10):3819–3833
4. Vernon LB, Vernon HM (1941) US patent and trademark office. Washington DC, pp 234, 993. US Patent No. 2
5. Gao XY, Huang WM (2002) Transformation start stress in non-textured shape memory alloys. *Smart Mater Str* 11(2):256–268
6. El-Feninat F, Laroche G, Fiset M, Mantovani D (2002) Shape memory materials for biomedical applications. *Adv Eng Mat* 4(3):91–104

7. Jani JM, Leary M, Subic A (2014) Shape memory alloys in automotive applications. *Appl Mech Mater* 663:248–253
8. Leo DJ, Weddle C, Naganathan G, Buckley SJ (1998) Vehicular applications of smart material systems. *Int Soc Opt Photonics. Smart Str Mater: Indust Comm Appl Smart Str Tech* 3326:106–116
9. Copaci D, Blanco D, Moreno LE (2019) Flexible shape-memory alloy-based actuator: mechanical design optimization according to application. *Multidisc Digit Publish Inst* 8(3):63
10. Bil C, Massey K, Abdullah EJ (2013) Wing morphing control with shape memory alloy actuators. *J Intel Mater Sys Str* 24(7):879–898
11. Hartl DJ, Lagoudas DC (2007) Aerospace applications of shape memory alloys. *Proc I Mech Eng Part G J Aerosp Eng* 221(4):535–552
12. Van Humbeeck J (1999) Non-medical applications of shape memory alloys. *Mater Sci Eng A* 273:134–148
13. Bisaria H, Shandilya P (2018) Experimental study on response parameters of Ni-rich NiTi shape memory alloy during wire electric discharge machining. *IOP Conf Ser Mater Sci Eng* 330(1):3316–3324
14. Jani JM, Leary M, Subic A (2014) Shape memory alloys in automotive applications. *Trans Tech Publ* 663:248–253
15. Kahn H, Huff MA, Heuer AH (1998) The TiNi shape-memory alloy and its applications for MEMS. *J Micromech Microeng* 8(3):213
16. Sellitto A, Riccio A (2019) Overview and future advanced engineering applications for morphing surfaces by shape memory alloy materials. *Material* 12(5):708
17. Datt M, Singh D (2015) Optimization of WEDM parameters using Taguchi and ANOVA method. *Int J Current Eng Tech* 5(6):3843–3847
18. Singh R, Singla VK (2017) Surface characterization of M42 Hss treated with cryogenic and non-cryogenated brass wire in WEDM process. *IMRF Biann Peer Rev Int Res J* 5:28–32
19. Singh R, Singla VK (2018) Parametric modeling for wire electrical discharge machining of M42 HSS using Untreated and cryogenated treated brass wire by using RSM. *Int J Mech Prod Eng* 5:63–67
20. Pradhan MK, Das R (2011) Recurrent neural network estimation of material removal rate in electrical discharge machining of AISI D2 tool steel. *Proc I Mech E Part B J Eng Manuf* 225(3):414–421
21. Tosun N, Cogun C (2003) Analysis of wire erosion and workpiece surface roughness in wire electrical discharge machining. *Proc I Mech E Part B J Eng Manuf* 217(5):633–642
22. Singh RP, Singhal S (2016) Rotary ultrasonic machining: a review. *Mater Manuf Processes* 31(14):1795–1824
23. Singh RP, Singhal S (2017) Investigation of machining characteristics in rotary ultrasonic machining of alumina ceramic. *Mater Manuf Processes* 32(3):309–326
24. Singh RP, Kumar J, Kataria R, Singhal S (2015) Investigation of the machinability of commercially pure titanium in ultrasonic machining using graph theory and matrix method. *J Eng Res* 3(4):1–20
25. Singh RP, Singhal S (2017) Rotary ultrasonic machining of macor ceramic: an experimental investigation and microstructure analysis. *Mater Manuf Processes* 32(9):927–939
26. Singh RP, Singhal S (2018) Experimental investigation of machining characteristics in rotary ultrasonic machining of quartz ceramic. *Proc Inst Mech Eng Part L: J Mater: Des Appl* 232(10):870–889
27. Singh RP, Singhal S (2018) An experimental study on rotary ultrasonic machining of macor ceramic. *Proc Inst Mech Eng, Part B: J Eng Manuf* 232(7):1221–1234
28. Singh R, Singh RP, Tyagi M, Kataria R (2020) Investigation of dimensional deviation in wire EDM of M42 HSS using cryogenically treated brass wire. *Mater Today: Proc* 25:679–685
29. Singh RP, Kataria R, Kumar J, Verma J (2018) Multi-response optimization of machining characteristics in ultrasonic machining of WC-Co composite through Taguchi method and grey-fuzzy logic. *AIMS Mater Sci* 5(1):75–92

30. Singh RP, Singhal S (2018) Experimental study on rotary ultrasonic machining of alumina ceramic: microstructure analysis and multi-response optimization. *Proc Inst Mech Eng, Part L: J Mater: Des Appl* 232(12):967–986
31. Singh R, Singh RP, Trehan R (2021) State of the art in processing of shape memory alloys with electrical discharge machining: a review. *Proc Inst Mech Eng, Part B: J Eng Manuf* 235(3):333–366
32. Ambade S, Tembhurkar C, Patil AP, Pantawane P, Singh RP (2021) Shielded metal arc welding of AISI 409M ferritic stainless steel: study on mechanical, intergranular corrosion properties and microstructure analysis. *World J Eng*
33. Singh RP, Kataria R, Singhal S (2018) Performance evaluation of macor dental ceramic: an investigation with rotary ultrasonic machining. *Adv Dent Oral Health* 8(2):1–6
34. Singh RP, Tyagi M, Kataria R (2019) Selection of the optimum hole quality conditions in manufacturing environment using MCDM approach: a case study. In: *Operations management and systems engineering*. Springer, Singapore, pp 133–152
35. Kataria R, Singh RP, Kumar J (2016) An experimental study on ultrasonic machining of tungsten carbide-cobalt composite materials. *AIMS Mater Sci* 3(4):1391–1409
36. Singh RP, Kataria R, Singhal S (2019) Decision-making in real-life industrial environment through graph theory approach. In: *Computer architecture in industrial, biomechanical and biomedical engineering*. IntechOpen
37. Haleem A, Javaid M, Singh RP, Suman R (2021) Significant roles of 4D printing using smart materials in the field of manufacturing. *Adv Ind Eng Polym Res*
38. Singh RP, Kataria R, Kumar J (2021) Machining of WC-Co composite using ultrasonic drilling: optimisation and mathematical modelling. *Adv Mater Process Technol* 7(2):317–332
39. Singh RP, Kataria R, Singhal S, Garg RK, Tyagi M (2020) Hole quality measures in rotary ultrasonic drilling of silicon dioxide (SiO<sub>2</sub>): investigation and modeling through designed experiments. *SILICON* 12(11):2587–2600
40. Singh RP, Singhal S (2018) Rotary ultrasonic machining of alumina ceramic: experimental study and optimization of machining responses. *J Eng Res* 6(1)
41. Kumar R, Singh RP, Kataria R (2019) Study on flexural performance of fabricated natural fiber hybrid polypropylene composite: an experimental investigation through designed experiments. *World J Eng*
42. Kumar R, Singh RP, Kataria R (2020) Study on mechanical properties of fabricated hybrid natural fibre polymeric composites. *Int J Mater Prod Technol* 60(1):73–91
43. Singh RP, Singh R, Trehan R, Garg RK, Tyagi M (2021) Investigation into the surface quality in wire-cut EDM of M42 HSS: an experimental study and modeling using RSM. In: *Optimization methods in engineering*. Springer, Singapore, pp 245–256
44. Sharma RC, Dabra V, Singh G, Kumar R, Singh RP, Sharma S (2021) Multi-response optimization while machining of stainless steel 316L using intelligent approach of grey theory and grey-TLBO. *World J Eng*
45. Singh RP, Kumar N, Gupta AK, Painuly M (2021) Investigation into rotary mode ultrasonic drilling of bioceramic: an experimental study with PSO-TLBO based evolutionary optimization. *World J Eng*
46. Butola R, Yuvaraj N, Singh RP, Tyagi L, Khan F (2021) Evaluation of microhardness and wear properties of Al 6063 composite reinforced with yttrium oxide using stir casting process. *World J Eng*
47. Kataria R, Singh RP, Alkawaz MH, Jha K (2021) Optimization and neural modelling of infiltration rate in ultrasonic machining. *OPSEARCH* 1–20
48. Singh R, Singh RP, Trehan R (2021) Parametric investigation of tool wear rate in EDM of Fe-based shape memory alloy: microstructural analysis and optimization using genetic algorithm. *World J Eng*
49. Singh R, Singh RP, Trehan R (2022) Investigation of machining rate and tool wear in processing of Fe-based-SMA through sinking EDM. In: *Proceedings of the international conference on industrial and manufacturing systems (CIMS-2020)*. Springer, Cham, pp 439–451

50. Singh RP, Kataria R, Kumar J, Verma K, Chaudhary B, Singh S (2020) Investigation of process responses in rotary ultrasonic machining of Al/SiC composite through designed experiments. *Mater Today: Proc* 21:2043–2052
51. Singh R, Singh RP, Trehan R (2021) Sustainable engineering approaches used in electrical discharge machining processes: a review. In: *Sustainable environment and infrastructure*, pp 41–50
52. Ranjan S, Singh RP (2021) Investigation of MRR in wire-cut electrical discharge machining of Incoloy-800 using statistical approach. In: *Optimization methods in engineering*. Springer, Singapore, pp 443–457
53. Bisht H, Singh RP, Sharma V (2021) Study of impact strength in TIG welding of Incoloy-800 super alloy: an experimental investigation and optimization. In: *Optimization methods in engineering*. Springer, Singapore, pp 277–289
54. Singh RP, Kataria R, Tiwari AK (2020) Sustainable manufacturing-related aspects in turning operation: a review based study. In: *Manufacturing engineering*. pp 657–667
55. Gupta AK, Singh RP (2022) Application of TLBO to optimize cutting variables for face milling of aluminium alloy Al-8090. In: *Proceedings of the international conference on industrial and manufacturing systems (CIMS-2020)*. Springer, Cham, pp 1–13

# Analyzing Heat Stress Among Metal Casting Workers Using Selected Thermal Indices: A Pilot Study During Winter Climatic Conditions



Milap Sharma, N. M. Suri, and Suman Kant

**Abstract** Excessive hot environments are usually widespread in metal casting industries, where higher ambient temperature and radiant heat exposure could impose subsequent suppression on workers' well-being and negatively impacts the work productivity. The six main agents of thermal stress include four environmental factors (air temperature, radiant temperature, air velocity, and relative humidity) and two personal factors (metabolic rate and clothing worn), which influence the heat exchange mechanism between the worker and its surroundings. The present study aimed to analyze the thermal exposure level in different work sections of the metal casting industry during the winter climatic conditions. Three different widely used thermal indices, i.e., wet bulb globe temperature (WBGT), tropical summer index (TSI), and discomfort index (DI), have been utilized to evaluate the heat stress exposure level under distinct foundry work sections. Further, descriptive and inferential statistics have been used to analyze the evaluated parameters. Results revealed higher thermal exposure levels associated with the furnace and molding work sections as compared to fettling and CNC machining sections. Although, during the selected time period, heat indices were not exceeding the threshold limit values (TLVs) under the respective work sections.

**Keywords** Work environment · Casting workers · Thermal indices · Exposure assessment

## 1 Introduction

Metal casting workers are exposed to harsh work conditions due to the high heat industrial work environment and subjected to intensive physical workload, which imposes significant thermal stress on the workers' health [1]. There are several environmental factors (air temperature, relative humidity, air velocity, and radiation) and

---

M. Sharma (✉) · N. M. Suri · S. Kant

Department of Production and Industrial Engineering, Punjab Engineering College (Deemed to be University), Chandigarh 160012, India

e-mail: [Milapsharma25@gmail.com](mailto:Milapsharma25@gmail.com)

personal factors (clothing worn and muscular activity), which affect the thermal ambience of a person [2]. In foundries, there are various work activities such as high heat furnace work operations, metal pouring and molding tasks, fettling operations, and manual material handling, which require a higher level of physical work activity [3]. A hot work environment imposes thermal stress, which causes thermophysiological effects on the workers' bodies (such as a rise in core body temperature, heart rate, and increased sweating) [1]. India is a diverse country with extreme climatic conditions ranging from tropical and subtropical regions, and there is a huge unorganized sector [4]. Most of India's north and northeast regions are subjected to humid subtropical climates, whereas a humid and hotter tropical climate is found in Southern India. Climatic zones like tropical and subtropical regions with higher air temperature and humidity values may cause greater risks of heat-related illness and safety threats to workers employed in developing countries with low and medium incomes [5, 6]. In developing countries like India, fewer resources are available on the combined effect of workplace heat exposure and climatic conditions [7]. Extreme hot environments are usually widespread in foundries, iron and steel industries, and several other industrial work sectors. A prolonged period of heat exposure with a poor work environment will affect the production level, and at the same time, it will negatively impact the workers' performance [8, 9].

For assessing heat stress, several indices have been developed over the past century, including the environmental factors and personal factors or a combination of both. Heat stress indices can be divided into three different categories, i.e., rational indices (based on the heat exchange equation), empirical indices (relating to objective and subjective strain), and direct indices (involving direct measurements) [10]. The present study research question was to assess whether the foundry indoor industrial heat stress exposure levels exceed the permissible limits/threshold limit values (TLVs) during the winter climatic conditions. So, the present study aimed to assess the environmental parameters followed by evaluating the heat stress exposures levels under distinct foundry work locations during the winter climatic conditions; to have better insights into the indoor workplace heat exposure experienced by the workers engaged in several foundry work activities. Further, descriptive and inferential statistical analysis has also been performed for the evaluated parameters.

## 2 Work Methodology

In the present study, three widely used heat stress indices have been considered to evaluate the heat stress exposure level under indoor industrial work conditions during the last month of the winter season (February 2021) in two different foundry units located in Ambala, India. The environmental measurements were monitored using Kestrel 5400 Heat stress tracker Pro (Nielsen-Kellerman Co.; USA) placed on a tripod at 1.1 m floor surface height as per ISO 7243 standard [11]. The equipment was allowed to stabilize for a minimum of 15 min, after which the monitored readings were considered for evaluation purposes. The environmental variables were



Fig. 1 Monitored work sections (furnace, molding, fettling, and CNC machining)

monitored during the afternoon time period (1:00 PM–3:30 PM) under four different work sections, i.e., fettling, molding, furnace, and CNC machining, as depicted in Fig. 1. From the monitored variables, respective heat stress indices were evaluated to analyze the associated risk exposure levels. Further descriptive and inferential statistics have also been performed on the evaluated variables.

### 2.1 Considered Heat Stress Indices

**Wet bulb globe temperature (WBGT):** WBGT is an empirical index; which is a widely used and validated heat stress index [11], for assessing hot work environments considering the combined effects of air temperature, humidity, air velocity, and radiation by measuring natural wet bulb temperature ( $T_{nw}$ ), dry bulb temperature ( $T_a$ ), and radiant effects using globe temperature ( $T_g$ ) for both indoor and outdoor work conditions.

For indoor work environment;

$$WBGT = 0.7T_{nw} + 0.3T_g \tag{1}$$



For outdoor environment;

$$\text{WBGT} = 0.7T_{\text{nw}} + 0.2T_{\text{g}} + 0.1T_{\text{a}} \quad (2)$$

**Tropical summer index (TSI):** TSI, based on the Indian climatic conditions, gives an equivalent temperature of still air at a constant relative humidity of 50%, which provides a similar thermal sensation experienced by a user as the actual environment under consideration [12]. It is expressed by a mathematical relation as shown in Eq. (3):

$$\text{TSI} = 0.308 * T_{\text{wb}} + 0.745 * T_{\text{g}} - 2.06\sqrt{V_{\text{ar}}} + 0.841 \quad (3)$$

where  $T_{\text{wb}}$  is the wet bulb temperature ( $^{\circ}\text{C}$ ),  $T_{\text{g}}$  is globe temperature ( $^{\circ}\text{C}$ ), and  $V_{\text{ar}}$  is airspeed (m/s).

**Discomfort index (DI):** The development of a direct indices tool called the ‘‘discomfort index’’ based on wet bulb temperature ( $T_{\text{wb}}$ ) and dry bulb temperature ( $T_{\text{db}}$ ) with some correction factor relates to the thermal degree of discomfort perceived by the user in a work environment [13].

$$\text{DI} = 0.5(T_{\text{db}} + T_{\text{wb}}) \quad (4)$$

where  $T_{\text{d}}$  = dry bulb temperature ( $^{\circ}\text{C}$ ) and  $T_{\text{w}}$  = wet bulb temperature ( $^{\circ}\text{C}$ )

### 3 Results and Discussion

#### 3.1 Environmental and Individual Variables

During field visits and manual observations, the clothing insulation values (in ‘‘clo’’; 1 clo equals to  $0.155 \text{ m}^2 \text{ C/W}$ ) varied between 0.7 clo and 0.91 clo (based on the observed clothing worn by employed workers and recommended ISO 9920 standard [14]). Further, ISO 8996 standard provides information about the metabolic rate (in  $\text{W/m}^2$ ) based on the physical work activities [15, 16]. Based on the ISO 8996 guidelines, the metabolic rate for workers employed in a high heat work environment like casting industries was classified as follows; fettling:  $190 \text{ W/m}^2$ , molding:  $165 \text{ W/m}^2$ , furnace work:  $135 \text{ W/m}^2$ , and CNC:  $100 \text{ W/m}^2$ . The monitored environmental variables (relative humidity, dry bulb temperature, globe temperature, wind speed, and natural wet bulb temperature) under different work sections were analyzed using statistical analysis to draw logical conclusions. Tables 1 and 2 depict the descriptive statistics results for the monitored environmental variables. It was observed that furnace and molding sections were exposed to higher ambient temperatures than fettling and CNC machining work sections. At the same time, higher RH values were

**Table 1** Monitored environmental parameters (mean (SD)) in foundry work sections

Parameters	Relative humidity (%)	Air temp. (in Celsius)	Globe temp. (in Celsius)	Air velocity (in m/s)	Natural wet bulb temp. (in Celsius)
<b>Work-section</b>					
Fettling	<b>40.61</b> (1.112)	<b>31.29</b> (0.233)	<b>31.35</b> (0.404)	<b>0.220</b> (0.239)	<b>22.01</b> (0.218)
Furnace	<b>36.40</b> (0.932)	<b>32.89</b> (0.217)	<b>36.28</b> (0.742)	<b>1.615</b> (3.771)	<b>21.25</b> (0.403)
Molding	<b>37.46</b> (0.987)	<b>32.66</b> (0.267)	<b>33.26</b> (0.117)	<b>0.154</b> (0.172)	<b>22.47</b> (0.283)
CNC	<b>40.30</b> (1.437)	<b>30.48</b> (0.869)	<b>30.08</b> (0.521)	<b>0.077</b> (0.129)	<b>21.36</b> (0.402)

The average values of the monitored variables have been presented in bold

**Table 2** Range values for monitored environmental parameters

Parameters	Relative humidity (%)	Air temp. (in Celsius)	Globe temp. (in Celsius)	Air velocity (in m/s)	Natural wet bulb temp. (in Celsius)
<b>Work-section</b>					
Fettling	38.1–42.9	30.7–31.7	30.2–32.1	0.05–1.2	21.6–22.5
Furnace	35.0–39.4	31.4–33.3	33.6–37.3	0.05–29.5	20.5–22.2
Molding	36.2–39.0	32.1–33.1	33.0–33.5	0.05–0.7	21.9–22.9
CNC	38.2–42.5	28.9–31.6	29.5–31.7	0.05–1.0	20.8–22

accountable to the fettling and CNC section compared to the furnace and molding sections. However, the highest values of globe temperature were observed under the furnace work section followed by molding section; due to the radiant heat exposure. Air velocity was found to be higher under the furnace section due to the heavy-duty pedestal fan installed near the furnace zone. The least value of air velocity was observed under the CNC work section. Figure 2 shows the variation among monitored variables (mean values) under the different work sections.

### 3.2 Evaluated Heat Stress Indices

From the analyzed variables, considered heat stress indices (i.e., WBGT, TSI, and DI) were evaluated as given in Tables 3 and 4. Higher values of heat stress indices were observed under the furnace and molding sections as compared to other work sections; with least values accountable to the CNC section. During the selected time period (winter season), fewer variations were observed under the distinct work sections, and also, the indices values were not exceeding the permissible limits. Figure 3 depicts the bar graphs, comparing evaluated heat stress indices mean values under the four distinct work sections.

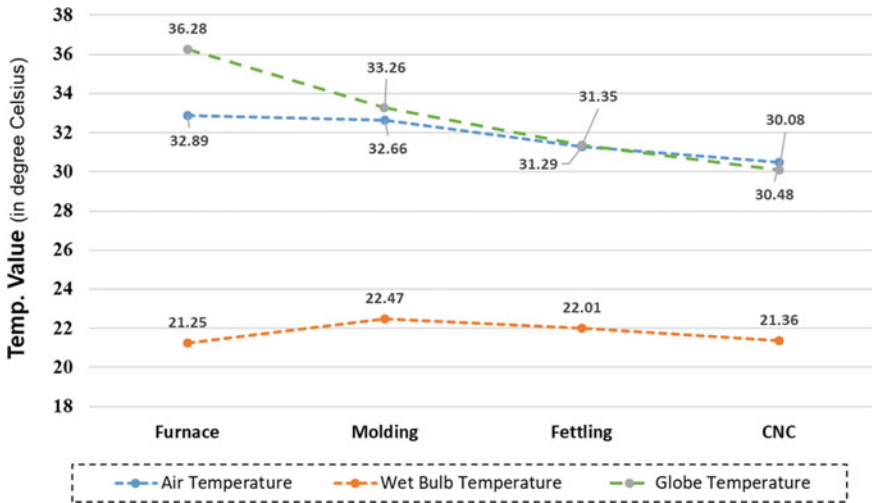


Fig. 2 Environmental parameters mean values under different work sections

Table 3 Evaluated heat stress indices (mean (SD)) (in °C)

Indices →	WBGT	DI	TSI
<b>Work-section ↓</b>			
Fetting	<b>24.81</b> (0.175)	<b>26.65</b> (0.171)	<b>28.02</b> (0.256)
Furnace	<b>25.76</b> (0.360)	<b>26.57</b> (0.245)	<b>30.65</b> (1.482)
Molding	<b>25.70</b> (0.219)	<b>27.56</b> (0.186)	<b>29.65</b> (0.205)
CNC	<b>23.97</b> (0.357)	<b>25.92</b> (0.623)	<b>27.03</b> (0.472)

The average values of the monitored variables have been presented in bold

Table 4 Range values for evaluated heat stress indices (in °C)

Indices →	WBGT	DI	TSI
<b>Work-section ↓</b>			
Fetting	24.45–25.09	26.25–26.95	27.30–28.71
Furnace	25.17–26.36	26.05–27.30	22.45–32.23
Molding	25.29–26.05	27.20–27.80	29.18–30.01
CNC	23.47–24.55	25.10–26.80	25.69–28.34

### 3.3 Scatterplots and Correlation Analysis

Further, Pearson product moment correlation was performed using IBM SPSS 26.0 software package for the evaluated heat stress indices. Highest association was observed among WBGT and TSI ( $r$  – value = 0.861;  $p$ -value < 0.01) followed

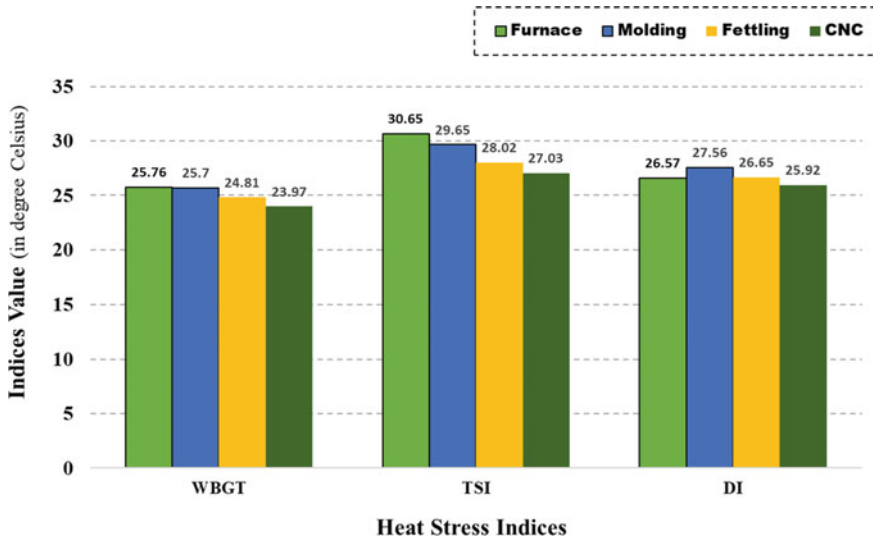


Fig. 3 Evaluated heat stress indices (mean values) under different work sections

Table 5 Correlation analysis for respective heat indices

Bivariate correlation analysis

	WBGT	DI	TSI
WBGT	1	0.751**	0.861**
DI	0.751**	1	0.474**
TSI	0.861**	0.474**	1

\*\*Correlation is significant at the 0.01 level (2-tailed)

by WBGT and DI ( $r$  – value = 0.751;  $p$ -value < 0.01) indices; as given in Table 5. Although, the least association was observed between TSI and DI ( $r$  – value = 0.474) indices. Figure 4 depicts the scatterplots and regression lines for the relationship among respective indices. The results showed a strong relationship between WBGT and TSI ( $R^2$  – value = 0.741) followed by WBGT and DI ( $R^2$  – value = 0.564) indices. However, the least association was observed among TSI and DI ( $R^2$  – value = 0.225) indices.

### 4 Conclusion

Heat stress is often an unacknowledged occupational health hazard, especially in developing countries. In developing countries like India, fewer resources are available on the combined effect of workplace heat exposure and climatic conditions. For

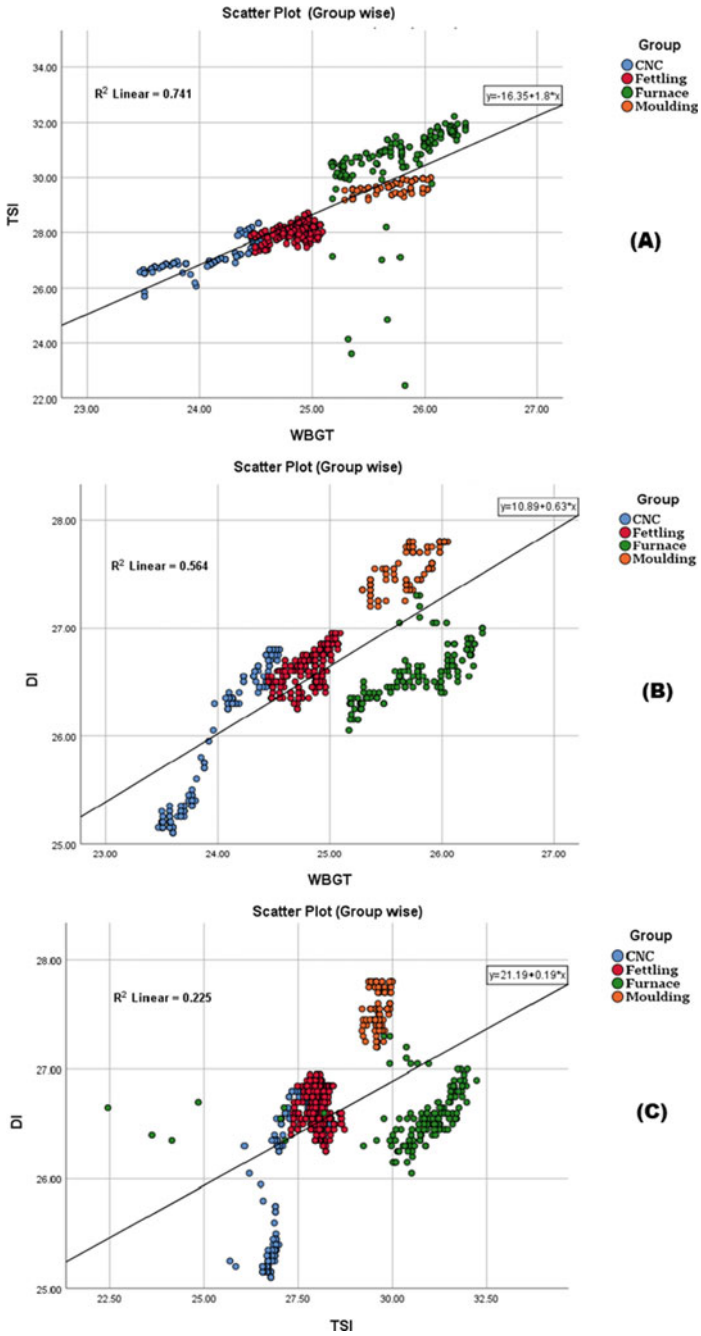


Fig. 4 Scatterplots depicting the relationship between respective indices a TSI versus WBGT, b DI versus WBGT, c DI versus TSI

heat stress assessment, several indices have been developed over the past century, including the environmental factors and personal factors or a combination of both. The present study assessed the heat stress exposures levels under different foundry work sections during the winter climatic season utilizing widely used heat indices. Strong positive association was observed among WBGT and TSI ( $r$  – value = 0.861;  $p$ -value < 0.01) followed by WBGT and DI ( $r$  – value = 0.751) indices. Although, the least association was found for TSI and DI ( $r$  – value = 0.474). Results revealed that the heat stress exposure levels were not exceeding the threshold limit values (TLVs) during the selected climatic condition. However, higher values of globe temperature and heat indices were observed under the furnace and molding sections compared to other work sections, with the least values accountable to the CNC machining section. Although a futuristic study could also be performed, having a comparative analysis of heat stress parameters under the different foundry work sections during the winter and hot summer climatic seasons.

## References

1. Krishnamurthy M, Ramalingam P, Perumal K, Kamalakannan LP, Chinnadurai J, Shanmugam R, Venugopal V (2017) Occupational heat stress impacts on health and productivity in a steel industry in southern India. *Saf Health Work* 8(1):99–104
2. The six basic factors. HSE. Website: <https://www.hse.gov.uk/temperature/thermal/factors.html>. Accessed on 15 Mar 2020
3. Kataria KK, Sharma M, Kant S, Suri NM, Luthra S (2021) Analyzing musculoskeletal risk prevalence among workers in developing countries: an analysis of small-scale cast-iron foundries in India. *Arch Environ Occup Health* 1–18
4. Venugopal V, Chinnadurai JS, Lucas RA, Kjellstrom T (2016) Occupational heat stress profiles in selected workplaces in India. *Int J Environ Res Public Health* 13(1):89
5. Jendritzky G, Tinz B (2009) The thermal environment of the human being on the global scale. *Glob Health Action* 2(1):2005
6. Kjellstrom T (2015) Climate change, direct heat exposure, health and well-being in low and middle-income countries. *Glob Health Action*
7. Kjellstrom T, Holmer I, Lemke B (2009) Workplace heat stress, health and productivity—an increasing challenge for low and middle-income countries during climate change. *Glob Health Action* 2(1):2047
8. Somanathan E, Somanathan R, Sudarshan A, Tewari M (2015) The impact of temperature on productivity and labor supply: evidence from Indian manufacturing. Indian Statistical Institute, New Delhi, India
9. Sharma M, Kataria KK, Suri NM, Kant S (2020) Monitoring respirable dust exposure in fettling work environment of a foundry: a proposed design intervention. *Int J Saf Secur Eng* 10(6):759–767
10. Epstein Y, Moran DS (2006) Thermal comfort and the heat stress indices. *Ind Health* 44(3):388–398
11. International Organization for Standardization (ISO) (2017) ISO 7243, ergonomics of the thermal environment—assessment of heat stress using the WBGT (wet bulb globe temperature) index
12. Sharma MR, Ali S (1986) Tropical summer index—a study of thermal comfort of Indian subjects. *Build Environ* 21(1):11–24
13. Thom EC (1959) The discomfort index. *Weatherwise* 12(2):57–61

14. ISO 9920 (2009) Ergonomics of the thermal environment-Estimation of thermal insulation and water vapor resistance of a clothing ensemble. ISO 9920: 2007, Corrected version 2008-11-01
15. ISO 8996 (2004) Ergonomics of the thermal environment—determination of metabolic rate
16. Sharma M, Alam S, Mohan Suri N, Kant S (2021) Occupational heat stress under high-heat furnace work environments—a comprehensive review on developing countries. *J Therm Eng* 7(14):2068–2092. <https://doi.org/10.18186/thermal.1051603>

# Prioritizing the Drivers of Green Supply Chain Management Using ISM-Fuzzy-MICMAC Analysis



Gagandeep, Rahul O. Vaishya, and R. S. Walia

**Abstract** In present era of globalization, the industrial pollution significantly influences the health of human being. To mitigate the pollution concerns, the industries need to implement the green supply chain management (GSCM). The present research is focused for the identification of key drivers of GSCM in medical industries. Initially, twenty-two drivers were identified by studying available literature and discussed with the supply chain professionals. Accordingly, 5-point Likert scale-based questionnaire is used for collecting the data. Further, ten major drivers were extracted using factor analysis and interpretive structural modeling (ISM) is implemented for study the direct relation between the drivers. To analyze the driving and dependence power of the drivers, fuzzy-MICMAC approach has been used. In this study, ‘government rules and legislation’ was found key driver which was at the base position of ISM model. Furthermore, ‘top management support’ and ‘demand from NGOs’ were recognized as another important drivers that exists on the next level in the ISM model. The findings of the present study help the managerial staff to focus on essential drivers to effective implementation of GSCM.

**Keywords** Interpretive structural modeling (ISM) · Factor analysis (FA) · Drivers · Fuzzy-MICMAC · Green supply chain management (GSCM)

## 1 Introduction

Environment related problems are increasing at alarming rate due the overuse and misuse of natural resources. Due the increasing demand of customers, manufacturing industries focus to satisfy the customers and earning profit without considering the environmental issues. To minimize these problems, organizations need to adopt GSCM [26]. GSCM is notion of introducing environmental thinking into traditional supply chain management [1, 21, 40]. Traditional SCM only focus on economic

---

Gagandeep (✉) · R. O. Vaishya · R. S. Walia

Department of Production and Industrial Engineering, Punjab Engineering College, Chandigarh, India

e-mail: [gagansekh@gmail.com](mailto:gagansekh@gmail.com)



concerns and short relationship with suppliers but on the contrary GSCM is focus on the both economic and environmental concerns and build long-term relationship with suppliers [16, 22, 32]. The concept of GSCM is not novel but there is need to make strategies to adopted GSCM in organizations [24]. There are various factors which encourage the organizations to adopt the green practice within the SCM. These factors are known as drivers of GSCM. The drivers were collected through literature and expert opinions. The goal of present paper to identify essential drivers and prioritize them using ISM-fuzzy-MICMAC analysis. ISM methodology is used to study the inter-relationship across drivers [34]. Further, fuzzy-MICMAC analysis used to inspect dependence or driven and driving power of drivers.

The present study work is organized in five sections as follows comprising introduction. Section 2 discusses the literature review of drivers of GSCM. Methodology is describe in Sect. 3. Results and discussion describe in Sect. 4. At last, Sect. 5 consists of conclusion and future scope.

## 2 Literature Review

GSCM is emerging topic between researchers and practitioners to investigating the drivers of GSCM. A literature was reviewed to investigate enablers and obstacles which influence the GSCM and further segregate into six categories such as internal, external, customers, supplier, competition and market [10]. Diabat and Govindan [11] performed a work in aluminum manufacturing industry for assessment of drivers of GSCM by using ISM-MICMAC approach. This work reveals that ‘government rules and legislation’ and reverse logistics were more important drivers. Walker et al. [45] conduct a survey-based study in public and private sector to identify internal and external drivers and obstacles of GSCM. Study shows that external drivers are more influencing to GSCM. Bhoon and Narwal [6] conducted research work in manufacturing industries in numerous sectors like two-wheelers, four-wheelers and general manufacturing to study the drives of GSCM. A research conducted based on survey in manufacturing industries to investigate crucial drivers and results showed that customers demand, competition and legislative demand as important drivers [5]. Dubey et al. [13] identify and discuss various drivers of GSCM and also said that customer relationship and supplier relationship management are key factors which help to adopt green practices in SCM. A study conducted by Tyagi et al. [42] which identified eleven drivers of GSCM in automotive industries and using ISM-MICMAC analysis to examined interaction among them. Study reveals that legislation and compliance was the key driver. Agi and Nishant [2] explored numerous issues in plastic, petrochemical, mechanical and textiles industries situated in gulf countries and disclose trust and long-term relationship with supplier as crucial factor of GSCM. Singh et al. [39] analyze the drivers of GSCM in fertilizer industry which shown ‘top management commitment’ as most essential driver. Again same study has been performed with twelve drivers to prioritize them by using ISM-MICMAC analysis and get the similar results as previous [38]. Raut et al. [33] examine the drivers in

gas and oil industry and found ‘global climatic pressure and ecological inadequacy of assets’ as critical success factor. Similarly, a research performed in agro-industry using ISM-MICMAC to create a model and recognized ‘the environment management’, ‘competitive pressure’ and ‘regulatory pressure’ as essential enablers [15]. Saeed and Kersten [35] said that legislation assistances to understand about sustainability and motivate the organizations to adopt sustainable practices. Shohan et al. [37] conduct study in chemical industry to develop the model to find influencing factors of GSCM and exposes supplier pressure and willingness toward GSCM were key factor. Thaib [41] analyzes the drivers in an automotive industry in Indonesia are found ‘competitors pressure’ and ‘social responsibility’ as cheering drivers. A study performed in oil and gas industry in iron and found ‘customer satisfaction’ as crucial enabler [29]. Meager et al. [27] explored ‘company culture’ and ‘media focuses’ were crucial drivers to motivate the implementation of GSCM. Lahri [20] was analyze the drivers of GSCM in government, semi-government and private firms using fuzzy analytical hierarchy process. This study reveals that economical design, environmental management and green purchasing were the important drivers.

Plenty of research work on GSCM has been conducted in different fields like chemical industry, gas and oil industry, plastic industry, automotive industries, etc., and there are limited research has been found to prioritize drivers of GSCM in medical field. So present study identifies drivers through literature and with opinions industry experts and assess them using ISM-fuzzy-MICMAC analysis.

### **3 Methodology**

#### ***3.1 Driver’s Identification in GSCM***

To implement GSCM in an organizations, the understanding of the drivers of the GSCM is required which motivates the organizations to adopt GSCM. Initially, going through extensive literature and with expert opinions, twenty-two drivers were found. Further, a questionnaire is prepared based on the drivers for data collection.

#### ***3.2 Factor Analysis***

Factor analysis (FA) is a method which is utilizing for data reduction based on the principal component analysis and offers a close measure of various variables by evaluating the common factors based on the observed correlation [14, 28]. Initially, twenty-two factors were recognized through literature and discussion with expert. Data was collected through a 5-point Likert scale-based questionnaire. A questionnaire was sent to experts who are related to the medical field (doctors, medical industries) and academicians who having knowledge about the green supply chain.

**Table 1** List of drivers

S. No	Extracted drivers	References	Code
1	Eco-friendly design	[11, 20, 33]	DV1
2	Customer awareness	[10, 24, 25, 37]	DV2
3	Brand image	[5, 6, 15, 18, 33, 38]	DV3
4	Reverse logistics	[11, 15, 33, 36]	DV4
5	Top management support	[2, 24, 38, 39]	DV5
6	Economic benefits	[37–39, 47]	DV6
7	Demand from NGOs	[10, 35, 43]	DV7
8	Social responsibility	[10, 35, 41]	DV8
9	Improve quality	[31, 42]	DV9
10	Government rules and legislation	[13, 17, 37, 45]	DV10

Out of one hundred, fifty-two responses were received, which 52% response rate. If the response rate is 30% it may be enough to drive reliability analysis [3, 23]. Collected data is found to be reliable if the Cronbach's alpha coefficient value is between 0.7 and 1 [28]. Cronbach's alpha value for the present analysis is 0.701 which is acceptable and data is to be considered as reliable. Thus, FA is performed to filter the factors by using SPSS-23 software. Then, most important factors/drivers are extracted based on the eigenvalue greater than 1 and factor loadings minimum 0.5 [30] are listed in Table 1. The percentage of total variance explained was found to be 75.236% which is adequate value for factor analysis [8].

### 3.3 ISM Methodology

ISM approach was introduced by Warfield [46] which positions the factors hierarchically associated in the system based on the correlation with other factors. ISM is consisting three words interpretive, structural and modeling. Interpretive means interpret, judge and decide relations among elements. Structural means convert the complicated structure into an easiest one. Modeling means the structure is represented in a specific model of a digraph. In ISM approach, a set of various direct and indirect elements organized into a comprehensive systematic model [4, 19]. Moreover, the model form interprets the structure of a complicated issue in a carefully manner including the graphics and words. However, ISM approach includes limitations as well [7]. There is individual basing of expert who judging the drivers. The relation between the drivers depends upon the expert's knowledge who is dealing with the variables. Further, ISM is not assigning any weight to the drivers.

Various steps include in ISM methodology as following [12, 18, 22, 44]

1. Identify and list the several drivers of GSCM.
2. Create the contextual relationship for each and every pair of drivers recognized in step 1.



**Table 3** Initial reachability matrix

Drivers (DV)	DV1	DV2	DV3	DV4	DV5	DV6	DV7	DV8	DV9	DV10
DV1	1	0	1	1	0	1	0	0	1	0
DV2	1	1	0	1	0	0	0	1	0	0
DV3	1	0	1	0	0	1	0	0	0	0
DV4	1	1	1	1	0	1	0	0	0	0
DV5	1	0	1	1	1	1	1	1	1	0
DV6	0	0	0	0	0	1	0	0	1	0
DV7	1	0	0	1	1	0	1	1	1	0
DV8	1	1	1	1	0	1	0	1	1	0
DV9	0	0	1	0	0	1	0	0	1	0
DV10	1	1	0	1	1	0	1	0	1	1

### 3.3.2 Initial Reachability Matrix

SSIM is transformed into initial reachability matrix using binary system, i.e., 0 and 1 as follows the rules given below:

- When the cell entry  $(a, b)$  is V in SSIM, then change  $(a, b)$  in the initial reachability matrix with 1 and  $(b, a)$  with 0.
- When the cell entry  $(a, b)$  is A in SSIM, then change  $(a, b)$  in the initial reachability matrix with 0 and  $(b, a)$  with 1.
- When the cell entry  $(a, b)$  is X in SSIM, then change  $(a, b)$  in the initial reachability matrix with 1 and  $(b, a)$  with 1.
- When the cell entry  $(a, b)$  is O in SSIM, then change  $(a, b)$  in the initial reachability matrix with 0 and  $(b, a)$  with 0 (Table 3).

### 3.3.3 Final Reachability Matrix

The final reachability matrix is attained from the initial reachability matrix using the transitivity rule as given in Table 4. The transitivity rule said that if driver M is interconnected to driver N and N is interconnected to O, then it is considered that M is interconnected to O. The cell entry which represents the transitivity is indicated with 1\*.

### 3.3.4 Level of Partition

The final reachability matrix was divided into different levels. Begin with the final reachability matrix, 'reachability set' and 'antecedent set' for each factor to be found. The reachability set of the definite driver includes itself along with other drivers that can be influenced by it (row elements). The antecedent set of the definite driver

**Table 4** Final reachability matrix

Drivers (DV)	DV1	DV2	DV3	DV4	DV5	DV6	DV7	DV8	DV9	DV10	Driving power
DV1	1	1*	1	1	0	1	0	0	1	0	6
DV2	1	1	1*	1	0	1*	0	1	1*	0	7
DV3	1	0	1	1*	0	1	0	0	1*	0	5
DV4	1	1	1	1	0	1	0	1*	1*	0	7
DV5	1	1*	1	1	1	1	1	1	1	0	9
DV6	0	0	1*	0	0	1	0	0	1	0	3
DV7	1	1*	1*	1	1	1*	1	1	1	0	9
DV8	1	1	1	1	0	1	0	1	1	0	7
DV9	1*	0	1	0	0	1	0	0	1	0	4
DV10	1	1	1*	1	1	1*	1	1*	1	1	10
Dependence power	9	7	10	8	3	10	3	6	10	1	67

contains itself along with other drivers that can influence it (column elements). The intersection set is obtained for each driver. If the reachability set and intersection set are the similar, then assign level I to these drivers and these are deleted in the next iteration. The following iterations are accomplished with the remaining drivers. The same procedure is followed to find successive levels, and the procedure is continued till the level of each driver will be obtained. The level of partition is given in Table 5.

**Table 5** Level of partition (iteration—I to iteration V)

Driver (DV)	Reachability set	Antecedent set	Intersection set	Levels
DV1	1, 2, 4	1, 2, 4, 5, 7, 8, 10	1, 2, 4	II
DV2	1, 2, 4, 8	1, 2, 4, 5, 7, 8, 10	1, 2, 4, 8	II
DV3	1, 3, 4, 6, 9	1, 2, 3, 4, 5, 6, 7, 8, 9, 10	1, 3, 4, 6, 9	I
DV4	1, 2, 4, 8	1, 2, 4, 5, 7, 8, 10	1, 2, 4, 8	II
DV5	5, 7	5, 7, 10	5, 7	IV
DV6	3, 6, 9	1, 2, 3, 4, 5, 6, 7, 8, 9, 1, 0	3, 6, 9	I
DV7	5, 7	5, 7, 10	5, 7	IV
DV8	8	5, 7, 8, 10	8	III
DV9	1, 3, 6, 9	1, 2, 3, 4, 5, 6, 7, 8, 9, 10	1, 3, 6, 9	I
DV10	10	10	10	V

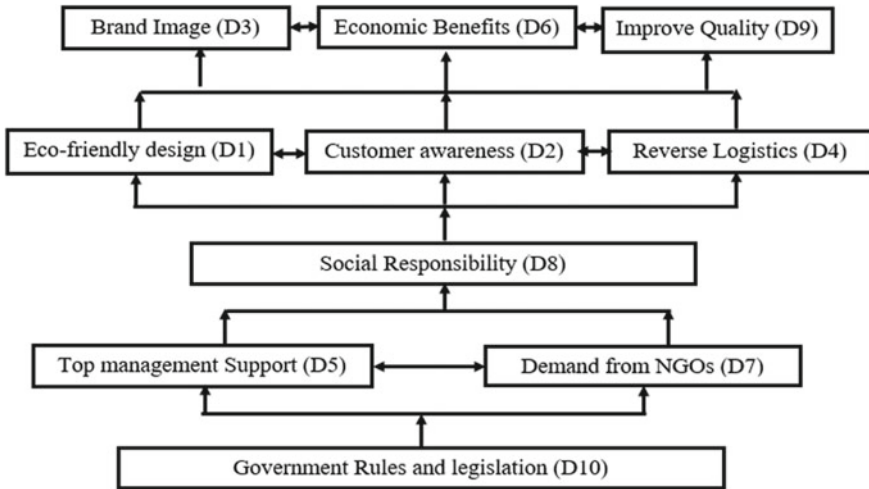


Fig. 1 ISM model of drivers of GSCM

### 3.4 ISM Model Formulation

When all levels are found for drivers of GSCM which showed in level of partition Table 5. By using final reachability matrix and level of partition to develop an ISM model which presented in Fig. 1. This figure depicts the direct relationship between the drivers. The ISM model having five levels as shown.

The model has five levels, where the three drivers—brand image (D3), economic benefits (D6) and improve quality (D9) are found at top level of ISM model. Second level consists three drivers such as eco-friendly design (D1), customer awareness (D2) and reverse logistics (D4).

Social responsibility (D8) is found at the level third in model. On the fourth level driver such as top management support (D5) and demand from NGOs (D7) have found. Driver, government rules and legislation (D10) is found at fifth level of the model at the base position. This is very important driver having strong driving power which drive the whole model.

### 3.5 Fuzzy-MICMAC Analysis

The MICMAC (cross-impact matrix multiplication applied to classification) analysis is method that works on basis of the properties of matrices multiplication [3, 9, 11]. In conventional MICMAC analysis, only binary relationship between the drivers is used but fuzzy-MICMAC analysis increase the sensitivity. This analysis classified the drivers into four clusters based on their driving and dependence power. The steps used for fuzzy-MICMAC analysis are as given.

**Table 6** Binary direct relationship matrix

Drivers	DV1	DV2	DV3	DV4	DV5	DV6	DV7	DV8	DV9	DV10
DV1	0	0	1	1	0	1	0	0	1	0
DV2	1	0	0	1	0	0	0	1	0	0
DV3	1	0	0	0	0	1	0	0	0	0
DV4	1	1	1	0	0	1	0	0	0	0
DV5	1	0	1	1	0	1	1	1	1	0
DV6	0	0	0	0	0	0	0	0	1	0
DV7	1	0	0	1	1	0	0	1	1	0
DV8	1	1	1	1	0	1	0	0	1	0
DV9	0	0	1	0	0	1	0	0	0	0
DV10	1	1	0	1	1	0	1	0	1	0

**Table 7** Possibility values of the reachability

Possibility of reachability	No	Very low	Low	Medium	high	Very high	Complete
Value	0	0.1	0.3	0.5	0.7	0.9	1

### 3.5.1 Binary Direct Relationship Matrix (BDRM)

Initial reachability matrix was converted into BDRM given in Table 6 by changing diagonal elements into 0. The BDRM is shown in Table 7.

### 3.5.2 Fuzzy Direct Relationship Matrix (FDRM)

To upsurge the sensitivity of conventional MICMAC analysis, fuzzy set theory has been used. Here, possibilities values of reachability illustrate in Table 8 has been used to show the relationship between the drivers. To develop the FDRM, the possibilities values were overload in BDRM with help of opinions of the experts of same industry. FDRM given in Table 8.

### 3.5.3 Fuzzy-MICMAC Stabilize Matrix

To construct fuzzy-MICMAC stabilize matrix use FDRM as base matrix. The FDRM shown in Table 8 multiply again and again till the hierarchies of driving and dependence power will stabilize. This multiplication process follows the rules of fuzzy matrix multiplication. Multiplication of two fuzzy matrices are as shown below

$$Z = XY \text{ Max} \{ \min(x_{ij}, y_{ij}) \}$$



**Table 8** Fuzzy direct relationship matrix (FDRM)

Drivers (DV)	DV1	DV2	DV3	DV4	DV5	DV6	DV7	DV8	DV9	DV10
DV1	0	0	0.7	0.9	0	0.5	0	0	0.3	0
DV2	0.7	0	0	0.9	0	0	0	0.9	0	0
DV3	0.5	0	0	0	0	0.7	0	0	0	0
DV4	0.7	0.5	0.9	0	0	0.7	0	0	0	0
DV5	0.7	0	0.7	0.9	0	0.7	0.5	0.5	0.9	0
DV6	0	0	0	0	0	0	0	0	0.5	0
DV7	0.9	0	0	0.7	0.5	0	0	0.7	0.7	0
DV8	0.9	0.9	0.7	0.7	0	0.7	0	0	0.9	0
DV9	0	0	0.3	0	0	0.5	0	0	0	0
DV10	0.9	0.7	0	0.9	0.3	0	0.5	0	0.9	0

where  $X = [x_{ij}]$  and  $Y = [y_{ij}]$  are two fuzzy matrices and product of two fuzzy matrices is also a fuzzy matrix as matrix  $Z$ .

For repeated multiplication, program is written in Python and the fuzzy stabilized matrix obtained after sixth iteration shown in Table 9 and screenshot of program output as shown in Fig. 2.

Driving and dependence diagram has been formed by using fuzzy stabilize matrix based on the driving and driven power as shown in Fig. 3. Driving power is sum of items in row and dependence power or driven power is obtained by summing the items in column in fuzzy stabilize matrix as given in Table 9.

**Table 9** Stabilized fuzzy-MICMAC matrix

Drivers	DV1	DV2	DV3	DV4	DV5	DV6	DV7	DV8	DV9	DV10	Driving power
DV1	0.5	0.5	0.7	0.7	0	0.7	0	0.5	0.5	0	4.1
DV2	0.7	0.5	0.7	0.9	0	0.7	0	0.9	0.5	0	4.9
DV3	0.5	0.5	0.5	0.5	0	0.5	0	0.5	0.5	0	3.5
DV4	0.7	0.5	0.7	0.5	0	0.7	0	0.5	0.5	0	4.1
DV5	0.7	0.5	0.7	0.7	0	0.7	0.5	0.5	0.5	0	4.8
DV6	0.3	0.3	0.3	0.3	0	0.3	0	0	0.5	0	2
DV7	0.7	0.5	0.7	0.7	0.5	0.7	0	0.7	0.5	0	5
DV8	0.9	0.9	0.9	0.7	0	0.7	0	0.5	0.9	0	5.5
DV9	0.3	0.3	0.3	0.3	0	0.5	0	0.3	0.3	0	2.3
DV10	0.7	0.7	0.7	0.7	0.3	0.7	0.5	0.5	0.7	0	5.5
Dependence power	6	5.2	6.2	6	0.8	6.2	1	4.9	5.4	0	41.7

```

Matrix is stabilized on Iteration No. 6

  1  2  3  4  5  6  7  8  9  10  Driving Power
1  0.5 0.5 0.7 0.7 0.0 0.7 0.0 0.5 0.5 0.0  4.1
2  0.7 0.5 0.7 0.9 0.0 0.7 0.0 0.9 0.5 0.0  4.9
3  0.5 0.5 0.5 0.5 0.0 0.5 0.0 0.5 0.5 0.0  3.5
4  0.7 0.5 0.7 0.5 0.0 0.7 0.0 0.5 0.5 0.0  4.1
5  0.7 0.5 0.7 0.7 0.0 0.7 0.5 0.5 0.5 0.0  4.8
6  0.3 0.3 0.3 0.3 0.0 0.3 0.0 0.0 0.5 0.0  2.0
7  0.7 0.5 0.7 0.7 0.5 0.7 0.0 0.7 0.5 0.0  5.0
8  0.9 0.9 0.9 0.7 0.0 0.7 0.0 0.5 0.9 0.0  5.5
9  0.3 0.3 0.3 0.3 0.0 0.5 0.0 0.3 0.3 0.0  2.3
10 0.7 0.7 0.7 0.7 0.3 0.7 0.5 0.5 0.7 0.0  5.5

Dependence Power
[ 6.  5.2 6.2 6.  0.8 6.2 1.  4.9 5.4 0. 41.7]
    
```

Fig. 2 Stabilized matrix in Python program

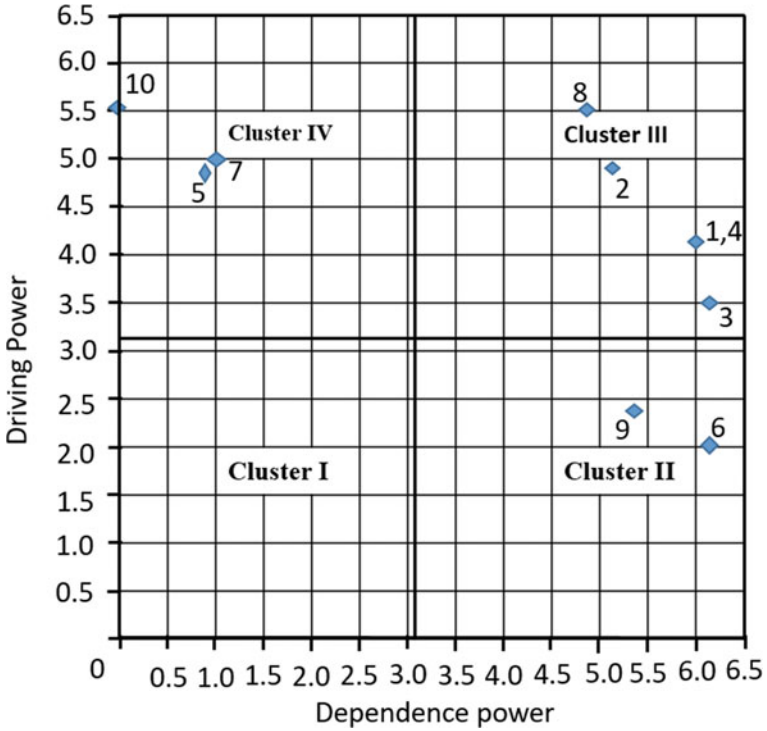


Fig. 3 Driving and dependence diagram

## 4 Result and Discussion

The drivers of GSCM were collected from the literature and with the help of opinions of industry experts and placed into ISM model as given in Fig. 1 to examine the direct relationship among them. By using fuzzy-MICMAC analysis, driving and dependence diagram was presented in Fig. 3 which is used to study the relative importance and interdependencies between the drivers of GSCM. Fuzzy-MICMAC analysis categories the drivers into four clusters as given below.

- Cluster I—Drivers having frail driving and frail driven power fall in this cluster and these driver are called autonomous drivers. In present study, no drivers are found in this cluster this means all consider drivers are significant [7].
- Cluster II—Economic benefits (DV6) and improve quality (DV9) are fall in cluster II. These drivers having tough dependence power and frail driving are known as dependent drivers.
- Cluster III—Drivers belong this cluster having tough driving and tough driven power are known as linkage drivers. Five drivers belong to this cluster such as brand image (DV3), eco-friendly design (DV1), customer awareness (DV2), reverse logistics (DV4) and social responsibility (DV8). These drivers unstable drivers and may affect the implementation of GSCM [12].
- Cluster IV—These drivers having tough driving power and frail driven power and called as independent drivers. Three drivers fall in this cluster such as top management support (DV5), demand from NGOs (DV7) and government rules and legislation (DV10). These are the key drivers having strong driving power, and other dependent drivers are affected by them.

## 5 Conclusion

The implementation of GSCM is required for the industry from environment point of view. To implement GSCM, it necessary to understand about the drivers of GSCM. The aim of present study identifies and analyzes the drivers of GSCM in medical industries. To fulfill the aim of present work, ten drivers were identify from literature and with expert opinions and study the mutual relationship among the drivers by using ISM model. The findings of study of study show that government rules and legislation (DV10) is key driver exists at base position of ISM with high driving power which affects the other drivers for effective execution of GSCM. Further driver, top management support (DV5) and demand from NGOs (DV7) are found essential drivers. Fuzzy-MICMAC performed to examine the driving and dependence power of drivers. Most of drivers were found in cluster III, i.e., linkage cluster. These drivers are more influencing drivers. No drivers were found in autonomous cluster which means all the ten drivers are significant. This study helps the manager to

focus on the various drivers for effective implementation of GSCM. The present work can also be performed in other industries and for the assessment of drivers other methodologies such as fuzzy analytical hierarchy process (FAHP), structural equation modeling (SEM), etc., will be used.

## References

1. Abdul Rehman Khan S (2019) Introductory chapter: introduction of green supply chain management. In: Green practices and strategies in supply chain management. <https://doi.org/10.5772/intechopen.81088>
2. Agi MAN, Nishant R (2017) Understanding influential factors on implementing green supply chain management practices: an interpretive structural modelling analysis. *J Environ Manage* 188:351–363. <https://doi.org/10.1016/j.jenvman.2016.11.081>
3. Ahluwalia S, Singh P, Sharma J (2018) Modelling and analysis of critical factors for phorbol ester degradation in *Jatropha* seed cake using ISM and MICMAC. *Int J Environ Waste Manage* 21(4):287–305. <https://doi.org/10.1504/IJEW.2018.093437>
4. Attri R, Dev N, Sharma V (2013) Interpretive structural modelling (ISM) approach: an overview. *2(2):3–8*
5. Bey N, Hauschild MZ, McAloone TC (2013) Drivers and barriers for implementation of environmental strategies in manufacturing companies. *CIRP Ann Manuf Technol* 62(1):43–46. <https://doi.org/10.1016/j.cirp.2013.03.001>
6. Bhool R, Narwal MS (2013) An analysis of drivers affecting the implementation of green supply chain management for the Indian manufacturing industries. 242–254
7. Bhosale VA, Kant R (2016) An integrated ISM fuzzy MICMAC approach for modelling the supply chain knowledge flow enablers. *Int J Prod Res* 54(24):7374–7399. <https://doi.org/10.1080/00207543.2016.1189102>
8. Biswal JN, Muduli K, Satapathy S (2017) Critical analysis of drivers and barriers of sustainable supply chain management in Indian thermal sector. *Int J Procurement Manage* 10(4):411. <https://doi.org/10.1504/ijpm.2017.10005121>
9. Dewangan DK, Agrawal R, Sharma V (2015) Enablers for competitiveness of Indian manufacturing sector: an ISM-fuzzy MICMAC analysis. *Procedia Soc Behav Sci* 189:416–432. <https://doi.org/10.1016/j.sbspro.2015.03.200>
10. Dhull S, Narwal MS (2016) Drivers and barriers in green supply chain management adaptation: a state-of-art review. *Uncertain Supply Chain Manage* 4(1):61–76. <https://doi.org/10.5267/j.uscm.2015.7.003>
11. Diabat A, Govindan K (2011) An analysis of the drivers affecting the implementation of green supply chain management. *Resour Conserv Recycl* 55(6):659–667. <https://doi.org/10.1016/j.resconrec.2010.12.002>
12. Dube AS, Gawande RR (2016) ISM-fuzzy MICMAC approach for analysis of GSCM enablers. *Int J Logistics Syst Manage* 24(4):426–451. <https://doi.org/10.1504/IJLSM.2016.077281>
13. Dubey R, Gunasekaran A, Papadopoulos T, Childe S (2015) Green supply chain management enablers: mixed methods research. *Sustain Prod Consumption* 1–16. <https://doi.org/10.1016/j.spc.2015.07.001>
14. Fabrigar LR, Wegener DT, Maccallum RC, Strahan EJ (1999) Evaluating the use of exploratory factor analysis in psychological research. *4(3):272–299*
15. Gardas B, Raut R, Jagtap AH, Narkhede B (2019) Exploring the key performance indicators of green supply chain management in agro-industry. *J Model Manag* 14(1):260–283. <https://doi.org/10.1108/JM2-12-2017-0139>
16. Gilbert S (2001) Greening supply chain: enhancing competitiveness through green productivity. Asian Productivity Organization, Taipei, Taiwan (Issue December)

17. Hosseini A (2007) Identification of green management system's factors: a conceptualized model. *Int J Manage Sci Eng Manage* 2(3):221–228. <https://doi.org/10.1080/17509653.2007.10671022>
18. Kannan G, Haq AN, Sasikumar P, Arunachalam S (2008) Analysis and selection of green suppliers using interpretative structural modelling and analytic hierarchy process. 9(2):163–182
19. Kumar D, Jain S, Tyagi M, Kumar P (2018) Quantitative assessment of mutual relationship of issues experienced in greening supply chain using ISM-fuzzy MICMAC approach. *Int J Logistics Syst Manage* 30(2):162–178. <https://doi.org/10.1504/IJLSM.2018.091960>
20. Lahri V (2020) Assessment of critical drivers towards sustainable green supply chain performance management. *Int J Bus Perform Supply Chain Model* 11(3):228–251. <https://doi.org/10.1504/IJBPCSM.2020.110217>
21. Lamba N, Thareja P (2020) Modelling of barriers pertaining to implementation of green supply chain management using ISM approach. *Mater Today: Proc* 43(xxxx):9–16. <https://doi.org/10.1016/j.matpr.2020.09.488>
22. Luthra S, Kumar V, Kumar S, Haleem A (2011) Barriers to implement green supply chain management in automobile industry using interpretive structural modeling technique-an Indian perspective. *J Ind Eng Manage* 4(2):231–257. <https://doi.org/10.3926/jiem.2011.v4n2.p231-257>
23. Malhotra MK, Grover V (1998) An assessment of survey research in POM: from constructs to theory
24. Malviya RK, Kant R (2017) Modeling the enablers of green supply chain management: an integrated ISM—fuzzy MICMAC approach. *Benchmarking* 24(2):536–568. <https://doi.org/10.1108/BIJ-08-2015-0082>
25. Mathiyazhagan K, Datta U, Bhadauria R, Singla A, Krishnamoorthi S (2017) Identification and prioritization of motivational factors for the green supply chain management adoption: case from Indian construction industries. *Opsearch* 55(1):202–219. <https://doi.org/10.1007/s12597-017-0316-7>
26. Mathiyazhagan K, Haq AN, Baxi V (2016) Analysing the barriers for the adoption of green supply chain management—the Indian plastic industry perspective. 8(1):46–65
27. Meager S, Kumar V, Ekren B, Paddeu D (2020) Exploring the drivers and barriers to green supply chain management implementation: a study of independent UK restaurants. *Procedia Manuf* 51(2020):1642–1649. <https://doi.org/10.1016/j.promfg.2020.10.229>
28. Muduli K, Barve A (2013) Empirical investigation of the barriers of green supply chain management (GSCM) implementation in Indian mining industries
29. Narimissa O, Kangarani-Farahani A, Molla-Alizadeh-Zavardehi S (2020) Drivers and barriers for implementation and improvement of sustainable supply chain management. *Sustain Dev* 28(1):247–258. <https://doi.org/10.1002/sd.1998>
30. Oltedal HA, McArthur DP (2011) Reporting practices in merchant shipping, and the identification of influencing factors. *Saf Sci* 49(2):331–338. <https://doi.org/10.1016/j.ssci.2010.09.011>
31. Pil FK, Rothenberg S (2003) Environmental performance as a driver of superior quality 12(3)
32. Rao P, Holt D (2015) Do green supply chains lead to competitiveness and economic performance? *Int J Oper Prod Manage*
33. Raut RD, Narkhede B, Gardas BB (2017) To identify the critical success factors of sustainable supply chain management practices in the context of oil and gas industries: ISM approach. *Renew Sustain Energy Rev* 68:33–47. <https://doi.org/10.1016/j.rser.2016.09.067>
34. Ravi V, Shankar R (2005) Analysis of interactions among the barriers of reverse logistics. *Technol Forecast Soc Chang* 72(8):1011–1029. <https://doi.org/10.1016/j.techfore.2004.07.002>
35. Saeed MA, Kersten W (2019) Drivers of sustainable supply chain management: identification and classification. *Sustainability (Switzerland)* 11(4). <https://doi.org/10.3390/su11041137>
36. Sellitto MA, Bittencourt SA, Reckziegel BI (2015) Evaluating the implementation of GSCM in industrial supply chains: two cases in the automotive industry. pp 1315–1320
37. Shohan S, Ali SM, Kabir G, Ahmed SKK, Suhi SA, Haque T (2019) Green supply chain management in the chemical industry: structural framework of drivers. *Int J Sust Dev World* 26(8):752–768. <https://doi.org/10.1080/13504509.2019.1674406>

38. Singh M, Jawalkar CS, Kant S (2018) Analysis of drivers for green supply chain management adaptation in a fertilizer industry of Punjab (India). *Int J Environ Sci Technol* 16(7):2915–2926. <https://doi.org/10.1007/s13762-018-1759-y>
39. Singh M, Kant S, Jawalkar CS (2017) Development of interpretive structural modeling: an approach for fertilizer industries. *I-Manager's J Mech Eng* 7(2):35. <https://doi.org/10.26634/jme.7.2.13437>
40. Srivastava SK (2007) Green supply-chain management : a state-of-the-art literature review. 9(1):53–80. <https://doi.org/10.1111/j.1468-2370.2007.00202.x>
41. Thaib D (2020) Drivers of the green supply chain initiatives: evidence from Indonesian automotive industry. *Uncertain Supply Chain Manage* 8(1):105–116. <https://doi.org/10.5267/j.uscm.2019.8.002>
42. Tyagi M, Kumar P, Kumar D (2015) Analysis of interactions among the drivers of green supply chain management. *Int J Bus Perform Supply Chain Model* 7(1):92–108. <https://doi.org/10.1504/IJBPSM.2015.068137>
43. Tyagi M, Kumar P, Kumar D (2015) Parametric selection of alternatives to improve performance of green supply chain management system. *Procedia Soc Behav Sci* 189:449–457. <https://doi.org/10.1016/j.sbspro.2015.03.197>
44. Tyagi M, Panchal D, Kumar D, Walia RS (2021) Modeling and analysis of lean manufacturing strategies using ism-fuzzy MICMAC approach. *Oper Res Eng Sci: Theor Appl* 4(1):38–66. <https://doi.org/10.31181/ORESTA2040123T>
45. Walker H, Di Sisto L, McBain D (2008) Drivers and barriers to environmental supply chain management practices: lessons from the public and private sectors. *J Purch Supply Manag* 14(1):69–85. <https://doi.org/10.1016/j.pursup.2008.01.007>
46. Warfield JN (1974) Developing interconnection matrices in structural modeling. *IEEE Trans Syst, Man Cybern SMC-4*(1):81–87. <https://doi.org/10.1109/TSMC.1974.5408524>
47. Zhu Q, Geng Y, Fujita T, Hashimoto S (2010) Green supply chain management in leading manufacturers: case studies in Japanese large companies. *Manag Res Rev* 33(4):380–392. <https://doi.org/10.1108/01409171011030471>

# CRITIC-COPRAS-Based Selection of Commercially Viable Alternative Fuel Passenger Vehicle



Abhishek Mohata, Nimai Mukhopadhyay, and Vidyapati Kumar

**Abstract** The automotive industry has seen a paradigm shift because of e-mobility, which cuts greenhouse gas production and environmental pollution. The selection of the most viable automobile passenger car is a difficult choice in this context due to diverse power sources, technologies, specifications, and prices. In this paper, sixteen alternative vehicles are assessed utilizing an integrated criterion importance through inter-criteria correlation (CRITIC)—complex proportional assessment (COPRAS) technique. CRITIC is the method utilized to achieve weights for selection criteria for vehicles. In contrast, COPRAS is used to classify cars in terms of nine different technical and operational measures that the purchaser examines when it is ready to acquire automobiles, such as fuel efficiency, torque, boot space, top speed, range, the annual cost of fuel, acceleration, cost and kerb weight of their vehicle. The results show that that battery electric vehicle outperforms compressed natural gas. Furthermore, CRITIC-TOPSIS is used to corroborate the findings achieved from CRITIC-COPRAS. In addition, after adjusting the weight of the criterion, a sensitivity analysis is performed to determine model stability.

**Keywords** Car selection · CRITIC · COPRAS · TOPSIS · Sensitivity analysis

## 1 Introduction

The transport industry is a key problem for greenhouse gas emissions such as carbon dioxide and other vehicle pollutants. Under the Paris Agreement (Nov. 2016), which plans to decrease greenhouse gas (GHG) emissions from across the world to 2 °C

---

A. Mohata · N. Mukhopadhyay

Department of Mechanical Engineering, Jalpaiguri Government Engineering College, Jalpaiguri, West Bengal, India

e-mail: [a.mohata15@gmail.com](mailto:a.mohata15@gmail.com)

V. Kumar (✉)

Department of Mechanical Engineering, Indian Institute of Technology Kharagpur, Kharagpur, West Bengal, India

e-mail: [vidyapatikumar.me@kgpian.iitkgp.ac.in](mailto:vidyapatikumar.me@kgpian.iitkgp.ac.in)

throughout this century from pre-industrial levels, while adopting measures to restrict them to 1.5 °C. The issue of global warming can thus be reduced by introducing and promoting alternative fuel automobiles to minimize exhaust gas emissions into the environment. In this perspective, it worthwhile to understand that alternative fuel passenger cars are ones that may be powered partially or entirely by electrically, liquefied petroleum gas (LPG), compressed natural gas (CNG), or a combination of the three [1]. Conventional petrol and diesel-type vehicles are getting replaced due to increased environmental awareness, health issues, and environmental policies. Conventional petrol and diesel automobiles are being superseded by greater awareness of the environment, health hazards, and legislation. A report [2] states that electric vehicle registration has surged by 41% despite a pandemic and over 3 million electric vehicles have been sold worldwide. The worldwide EV turnover in the sustainable development scenario is projected to reach above 230 million except for two/three-wheelers.

## 2 Research Background

This section highlights the prior research work carried out with the selection of commercially viable alternative fuel passenger vehicle. Brey et al. [3] applied data envelopment analysis (DEA)-based preference ranking organization method for enrichment and evaluations (PROMETHEE) method for selection of alternative energy vehicle based on economical, technological, and circumstantial factors. Mohamadabadi et al. [4] developed a multi-criteria evaluation model for ranking different road transportation fuel-based vehicles using the PROMETHEE method. Vahdani et al. [5] utilized the TOPSIS and fuzzy preference selection index (FPSI) technique for the assessment of alternative fuel buses based upon capacity, price, and energy consumption. Tsita and Pilavachi [6] employed AHP to select new-generation vehicles. Biswas and Das [7] employed entropy-based multi-attribute border approximation area comparison (MABAC) method for selecting vehicle and analyzed the criteria such as car cost and fuel economy, tank size, tailpipe emission, as well as volume of the commuter.

Furthermore, Biswas and Das [8] also investigated the commercially available electric vehicle selection problem and employed fuzzy-analytic hierarchy process (F-AHP) and MABAC for considering fuel economy, base model pricing, quick accelerating time, battery range, and top speed as the predominant criteria. So far, a range of methodologies have been used to analyze the new generation of cars, including SECA, MARCOS, MAIRCA, CoCoSo, ARAS, and COPRAS [9]. Based on the observations from the literature review, it can be propounded that the selection of automobiles with alternative fuels has drawn extensive attention of the researchers for several years. Various multi-criteria decision-making methodologies have been successfully deployed such as AHP, DEA, PROMETHEE, TOPSIS, FPSI, SECA, MARCOS, MAIRCA, CoCoSo, ARAS, and COPRAS for the decision-making and



selection of best automobile with alternative fuels problem. The MCDM application has been successfully applied in the past for various applications such as best advanced machining process selection, response optimization, and finding the optimal parametric combinations. This research attempts to include two commonly used MADM techniques, CRITIC and COPRAS, into the assessment and categorization of sixteen ecologically favorable alternative automobiles. CRITIC is a method for calculating weights for automobile preference characteristics, while COPRAS is used to score automobiles based on nine factors, including fuel economy, torque, boot space, top speed, range, annual fuel cost, acceleration, cost, and kerb weight. Afterward, a sensitivity analysis has been conducted to assess the influence of adjusting parameters on the incorporated model's ranking effectiveness. Based on an extensive literature analysis, the following characteristics, as shown in Table 1, have shown to be the most significant in the selection of alternative fuel vehicles.

This work uses four MCDM techniques for ranking purposes, and sensitivity analysis is performed. Furthermore, Spearman's rank correlation coefficient and Kendall's coefficient of concordance are evaluated to obtain more credible findings. The proposed conceptual framework is depicted in Fig. 1. Firstly, an exhaustive literature survey is carried out to determine the criteria for vehicle selection. Nine criteria have been determined: fuel economy, torque, boot space, top speed, range, annual fuel cost, acceleration, vehicle cost, and kerb weight. Following the identification of the requirements, 16 alternative fuel cars are selected and respective technological specifications are obtained from the individual manufacturer's website [25–37], as displayed in Table 2. The whole first decision matrix, which contains the values of the options, is generated in accordance with the evaluation criteria. Weight coefficients of each criterion are calculated by using CRITIC method which is followed by the ranking of the alternatives by COPRAS, EDAS, CoCoSo [38], and TOPSIS [39] methods. To evaluate the robustness of the proposed methodology, Spearman's rank correlation coefficient, Kendall's coefficient of concordance, Borda count, Copeland

**Table 1** Criteria affecting vehicle purchasing decision

Criteria	Code	Unit	Definition	References
Fuel economy	C1	kmpl	Distance traveled by vehicle in 1 L fuel	[10, 11]
Torque	C2	N m	Amount of work that an engine can exert	[ 10, 12–14]
Boot space	C3	L	Space provided in vehicle to keep luggage	[ 11, 15, 16]
Top speed	C4	kmph	Maximum speed	[ 11, 13, 17]
Range	C5	km	Distance that the vehicle can travel with full tank fuel	[ 13, 18–21]
Annual fuel cost	C6	₹	Fuel cost of the vehicle per annum assuming	[ 12, 22, 23]
Acceleration	C7	sec	Time taken for the automobile to propel from 0 to 100 kmph	[ 11, 13, 19]
Vehicle cost	C8	₹	Purchasing cost of the vehicle	[12, 18, 22–24]
Kerb weight	C9	Kg	Vehicle weight without any load	[ 14, 18, 24]

method, and sensitivity analysis have been performed followed by incorporation of the ranks obtained.

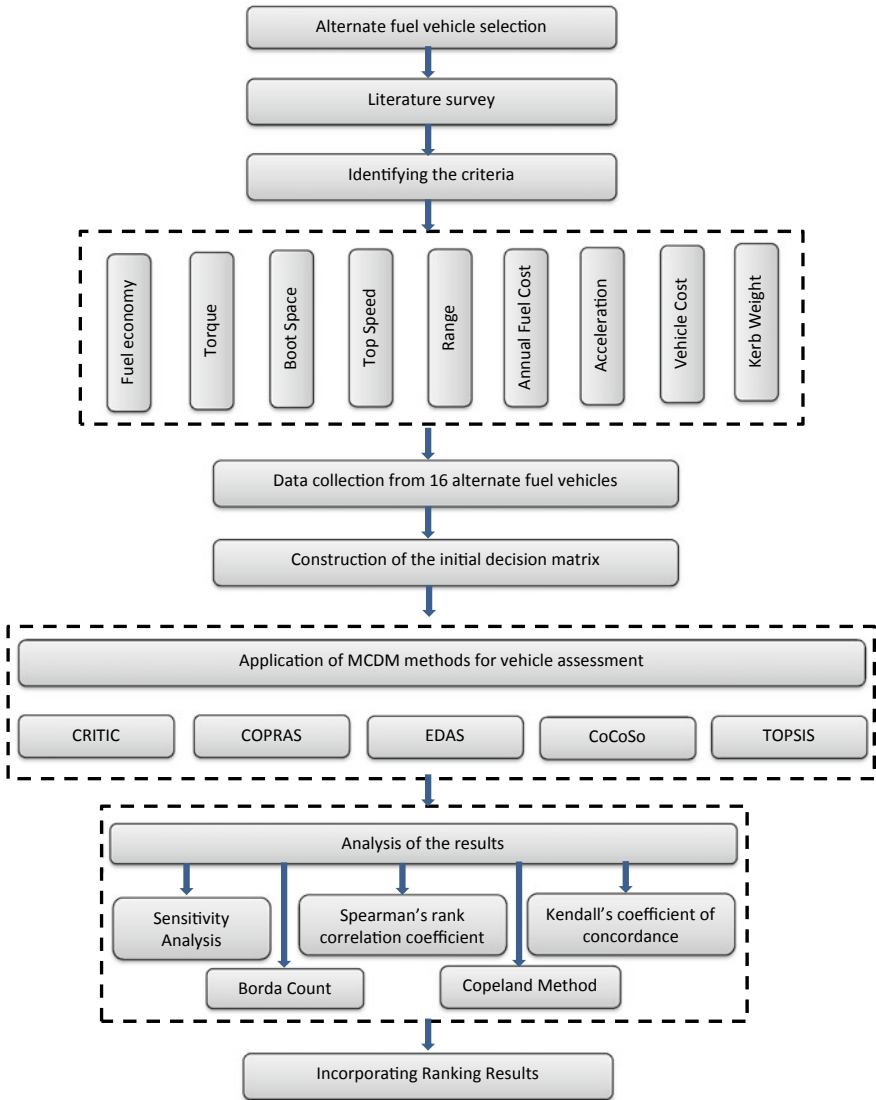


Fig. 1 Research methodology

**Table 2** Decision matrix

Alternate fuel car	Code	Fuel type	C (1)	C (2)	C (3)	C (4)	C (5)	C (6)	C (7)	C (8)	C (9)
Tata Nexon	A1	EV	95.3563	245	350	120	312	19,358.9744	9.3	13.99	1400
Tata Tigor	A2	EV	91.4414	105	255	80	213	20,187.7934	12	9.58	1126
MG ZS	A3	EV	86.9072	353	470	140	419	21,241.0501	8.5	21	1600
Hyundai Kona	A4	EV	69.8019	395	374	165	484	26,446.281	9.7	23.7	1535
Mahindra E Verito	A5	EV	60.9528	91	510	86	140	30,285.7143	8.5	10.15	1265
Maruti Ertiga	A6	CNG	17.5623	122	209	165	312.96	38,343.5583	13	9.14	1235
Maruti Wagon R	A7	CNG	21.899	78	341	152	390.24	30,750.3075	18.6	5.45	910
Maruti Alto 800	A8	CNG	21.2727	60	177	140	379.08	31,655.5872	19	4.43	755
Maruti Celerio	A9	CNG	20.5185	78	235	150	365.64	32,819.1664	15	5.72	920
Maruti Eeco	A10	CNG	14.0606	85	275	130	271.44	47,892.7203	15	5.18	1050
Maruti Spresso	A11	CNG	21.0101	78	270	150	343.2	32,051.2821	16	4.89	850
Maruti Swift Dzire	A12	CNG	17.8788	95	320	80	292.05	37,664.7834	12.6	6.36	1045
Hyundai Aura	A13	CNG	18.8552	95	402	155	364	35,714.2857	19	7.48	1050
Hyundai Santro	A14	CNG	20.5253	85	235	165	365.76	32,808.399	20.39	6	1000
Hyundai Grand i10 Nios	A15	CNG	18.8552	95	260	160	336	35,714.2857	19	6.85	1033
Hyundai Xcent Prime	A16	CNG	16.0741	98	407	80	310.31	41,893.5903	15.35	5.37	1100

### 3 Methodology

#### 3.1 Criteria Importance Through Inter-criteria Correlation (CRITIC) Method

The CRITIC method was proposed by Diakoulaki et al. [40] for the estimation of criteria weights in MCDM problems. It uses correlation analysis to distinguish different criteria [41]. The CRITIC technique includes the following phases:

Step 1 Development of the decision matrix:

$$D = (d_{ij})_{m \times n} = \begin{bmatrix} d_{11} & d_{12} & \cdots & d_{1n} \\ d_{21} & d_{22} & \cdots & d_{2n} \\ \vdots & \vdots & \vdots & \vdots \\ d_{m1} & d_{m2} & \cdots & d_{mn} \end{bmatrix},$$

$$i = 1, 2, \dots, m; \quad j = 1, 2, \dots, n \quad (1)$$

Step 2 Normalization of decision matrix:

$$r_{ij} = \frac{x_{ij} - \max x_{ij}}{\max x_{ij} - \min x_{ij}}, \quad \text{for benefit criteria} \quad (2)$$

$$r_{ij} = \frac{\max x_{ij} - x_{ij}}{\max x_{ij} - \min x_{ij}}, \quad \text{for cost criteria} \quad (3)$$

Step 3 Computation of the criteria standard deviation:

$$\sigma = \sqrt{\frac{\sum_{i=1}^m (r_{ij} - \bar{r}_j)^2}{m}}, \quad (4)$$

where  $\bar{r}_j = \frac{\sum_{i=1}^m r_{ij}}{m}$ .

Step 4 Calculation of symmetric linear correlation matrix:

$$m_{ij} = \frac{\sum_{i=1}^m (r_{ij} - \bar{r}_j)(r_{ik} - \bar{r}_k)}{\sqrt{\sum_{i=1}^m (r_{ij} - \bar{r}_j)^2 \sum_{i=1}^m (r_{ik} - \bar{r}_k)^2}}, \quad (5)$$

Step 5 Calculation of the quantity of information of each criterion:

$$C_j = \sigma \sum_{j=1}^n (1 - m_{ij}), \quad (6)$$

Step 6 Determination of objective weight of a criterion:

$$W_j = \frac{C_j}{\sum_{j=1}^m C_j}, \quad (7)$$

### 3.2 The Complex Proportional Assessment (COPRAS)

COPRAS method chooses the optimal choices among a lot of viable options by regulating a solution with a direct and proportionate ratio to the best possible solution to the ratio with the ideal-worst solution [42].

Step 1 Development of the decision matrix:  $D = (d_{ij})_{m \times n}$

Step 2 Normalization of the decision matrix:

$$X = [x_{ij}]_{m \times n} = \frac{d_{ij}}{\sum_{i=1}^m d_{ij}}, \quad (8)$$

Step 3 Formation of weighted normalized decision matrix:

$$Y = [y_{ij}] = w_j x_{ij}, \quad (9)$$

Step 4 Sum of weighted normalized decision matrix:

$$S_{+i} = \sum_{j=1}^n y_{+ij}, \quad \text{sum of beneficial criteria.} \quad (10)$$

$$S_{-i} = \sum_{j=1}^n y_{-ij}, \quad \text{sum of non - beneficial criteria.} \quad (11)$$

Step 5 Determination of relative significance of alternatives:

$$Q_i = S_{+i} + \frac{S_{-\min} \sum_{i=1}^m S_{-i}}{S_{-i} \sum_{i=1}^m \frac{S_{-\min}}{S_{-i}}}, \quad (12)$$

Step 6 Calculation of the quantitative utility.

$$U_i = \left[ \frac{Q_i}{Q_{\max}} \right] * 100\%, \quad (13)$$

Higher the  $U_i\%$ , better is the alternative.

### 3.3 Evaluation Based on Distance from Average Solution (EDAS)

Step 1 Development of the decision matrix:

$$D = (d_{ij})_{m \times n} \quad (14)$$

Step 2 Determine the average solution:

$$AV_j = \frac{\sum_{i=1}^n X_{ij}}{n} \quad (15)$$

Step 3 Calculate the positive distance from average solution.

$$PDA_{ij} = \frac{\max(0, (X_{ij} - AV_j))}{AV_j}, \text{ for beneficial criteria.} \quad (16)$$

$$PDA_{ij} = \frac{\max(0, (AV_j - X_{ij}))}{AV_j}, \text{ for non - beneficial criteria.} \quad (17)$$

Step 4 Calculate the negative distance from average solution.

$$NDA_{ij} = \frac{\max(0, (AV_j - X_{ij}))}{AV_j}, \text{ for beneficial criteria.} \quad (18)$$

$$NDA_{ij} = \frac{\max(0, (X_{ij} - AV_j))}{AV_j}, \text{ for non - beneficial criteria.} \quad (19)$$

Step 5 Determine the weighted sum of PDA and NDA for all alternatives.

$$SP_i = \sum_{j=1}^m w_j * PDA_{ij}, \quad (20)$$

$$SN_i = \sum_{j=1}^m w_j * NDA_{ij}, \quad (21)$$

Step 6 By normalizing SP and SN

$$NSP_i = \frac{SP_i}{\max(SP_i)}, \quad (22)$$

$$NSN_i = \frac{SN_i}{\max(SN_i)}, \quad (23)$$

Step 7 Calculate the appraisal score.

$$AS = \frac{NSP_i + NSN_i}{2}, \quad (24)$$

Higher the appraisal score, better is the alternative.

### 3.4 Combined Compromised Solution (CoCoSo)

Step 1 Matrix development:  $D = (d_{ij})_{m \times n}$

Step 2 Normalization of the decision matrix

$$Z_{ij} = \frac{x_{ij} - x_{ij}^-}{x_{ij}^+ - x_{ij}^-}, \quad \text{for beneficial criteria.} \quad (25)$$

$$Z_{ij} = \frac{x_{ij}^+ - x_{ij}}{x_{ij}^+ - x_{ij}^-}, \quad \text{for cost criteria.} \quad (26)$$

where  $x_{ij}^+ = \max(x_{ij})$  and  $x_{ij}^- = \min(x_{ij})$

Step 3 Evaluate the values of  $S_i$  and  $P_i$

The  $S_i$  value is determined utilizing grey relational generating methods, whereas the  $P_i$  value is derived using the WASPAS multiplicative property.

$$S_i = \sum_{j=1}^n (w_j Z_{ij}), \quad (27)$$

$$P_i = \sum_{j=1}^n (Z_{ij})^{w_j}, \quad (28)$$

Step 4 Calculation of the appraisal score strategies

$$\xi_{ia} = \frac{P_i + S_i}{\sum_{i=1}^m (P_i + S_i)}, \quad (29)$$

$$\xi_{ib} = \frac{S_i}{\min S_i} + \frac{P_i}{\min P_i}, \quad (30)$$

$$\xi_{ic} = \frac{\lambda(S_i) + (1 - \lambda)(P_i)}{(\lambda \max S_i + (1 - \lambda) \max P_i)} : 0 \leq \lambda \leq 1. \quad (31)$$

In most cases, the value  $\lambda = 0.5$  is used.

Step 5 Estimation of alternative performance scores.

$$\xi_i = (\xi_{ia}\xi_{ib}\xi_{ic})^{\frac{1}{3}} + \frac{1}{3}(\xi_{ia} + \xi_{ib} + \xi_{ic}), \quad (32)$$

Higher the performance score, better is the alternative.

## 4 Application of MCDM Techniques

It is considered that a vehicle runs 20,000 km annually, 1 kg CNG = 1.485 l petrol, 1 l petrol = 9.23 kWh, 1 unit electricity cost = Rs. 10, 1 kg CNG price = Rs. 50 [1, 3, 5]. In the fuel cell EVs, hydrogen gas is converted to fuel cells that do not produce hazardous emissions from the tailpipe. Compared to conventional fuel vehicles, the driving range of these FCEVs is relatively great. In light, medium, and high-duty applications compressed natural gas (CNG), stored in tanks, is employed. Since the power of CNG cars is lower than the petrol or diesel vehicles, the range of CNG vehicles is smaller. Compared to traditional fuels, high mileage and low GHG emission add value to CNG cars. Light cars are outfitted with special systems or bi-fuel systems [1].

### 4.1 Identification of Criteria Weights

The considered alternate fuel vehicles are graded according to the following data C1, C2, ..., C9 out of which the criteria from C1 to C5 are benefit criteria (higher the better) and the remaining are cost criteria (lower the better). The critic method consists of weighing objective criteria by considering the correlation between different data. Furthermore, there is no human intervention in this weighing method, so the bias that may arise due to human intervention is completely eliminated. This results in a more practical method of weighting, what is the rationale behind the CRITIC method's selection. Initially, the decision matrix of Table 2 is first normalized as presented in Table 3 which also shows the value of standard deviation. The inter-criteria correlation coefficient is shown in Table 4, and finally, the weights of the criteria are shown in Table 5.

### 4.2 Ranking of Alternate Fuel Vehicle Using Various MCDM Techniques

Selection of appropriate MCDM technique is of great importance in real-world problems. Using a single MCDM technique may not provide the best result and such a result would be unreliable. This section applies four MCDM techniques COPRAS,



**Table 3** Normalized decision matrix

	C (1)	C (2)	C (3)	C (4)	C (5)	C (6)	C (7)	C (8)	C (9)
A (1)	0.0000	-0.4478	-0.4805	-0.5294	-0.5000	1.0000	0.9327	0.5039	0.2367
A (2)	-0.0482	-0.8657	-0.7658	-1.0000	-0.7878	0.9710	0.7056	0.7327	0.5609
A (3)	-0.1039	-0.1254	-0.1201	-0.2941	-0.1890	0.9340	1.0000	0.1401	0.0000
A (4)	-0.3143	0.0000	-0.4084	0.0000	0.0000	0.7516	0.8991	0.0000	0.0769
A (5)	-0.4232	-0.9075	0.0000	-0.9294	-1.0000	0.6171	1.0000	0.7032	0.3964
A (6)	-0.9569	-0.8149	-0.9039	0.0000	-0.4972	0.3347	0.6215	0.7556	0.4320
A (7)	-0.9036	-0.9463	-0.5075	-0.1529	-0.2726	0.6008	0.1505	0.9471	0.8166
A (8)	-0.9113	-1.0000	-1.0000	-0.2941	-0.3050	0.5691	0.1169	1.0000	1.0000
A (9)	-0.9206	-0.9463	-0.8258	-0.1765	-0.3441	0.5283	0.4533	0.9331	0.8047
A (10)	-1.0000	-0.9254	-0.7057	-0.4118	-0.6179	0.0000	0.4533	0.9611	0.6509
A (11)	-0.9145	-0.9463	-0.7207	-0.1765	-0.4093	0.5552	0.3692	0.9761	0.8876
A (12)	-0.9530	-0.8955	-0.5706	-1.0000	-0.5580	0.3585	0.6552	0.8998	0.6568
A (13)	-0.9410	-0.8955	-0.3243	-0.1176	-0.3488	0.4268	0.1169	0.8417	0.6509
A (14)	-0.9205	-0.9254	-0.8258	0.0000	-0.3437	0.5286	0.0000	0.9185	0.7101
A (15)	-0.9410	-0.8955	-0.7508	-0.0588	-0.4302	0.4268	0.1169	0.8744	0.6710
A (16)	-0.9752	-0.8866	-0.3093	-1.0000	-0.5049	0.2102	0.4239	0.9512	0.5917
$\sigma$	0.3774	0.3052	0.2866	0.3858	0.2340	0.2717	0.3432	0.2991	0.2806

TOPSIS, EDAS, CoCoSo to rank the alternatives. The techniques have been developed and solved by using MS Excel. After evaluating the alternatives using the four above-mentioned MCDM techniques, the results are shown in Table 6.

**Table 4** Inter-criteria correlation coefficient

Criteria	C (1)	C (2)	C (3)	C (4)	C (5)	C (6)	C (7)	C (8)	C (9)
C (1)	1.0000	0.6854	0.4225	-0.2752	-0.0941	0.8648	0.7601	-0.7547	-0.7362
C (2)	0.6854	1.0000	0.4420	0.1746	0.4977	0.5475	0.6535	-0.9742	-0.8827
C (3)	0.4225	0.4420	1.0000	-0.3531	-0.1264	0.2198	0.5396	-0.4956	-0.6083
C (4)	-0.2752	0.1746	-0.3531	1.0000	0.7067	-0.0385	-0.4206	-0.1204	0.0643
C (5)	-0.0941	0.4977	-0.1264	0.7067	1.0000	0.1297	-0.2439	-0.3686	-0.1059
C (6)	0.8648	0.5475	0.2198	-0.0385	0.1297	1.0000	0.4741	-0.6064	-0.4640
C (7)	0.7601	0.6535	0.5396	-0.4206	-0.2439	0.4741	1.0000	-0.7200	-0.8075
C (8)	-0.7547	-0.9742	-0.4956	-0.1204	-0.3686	-0.6064	-0.7200	1.0000	0.9180
C (9)	-0.7362	-0.8827	-0.6083	0.0643	-0.1059	-0.4640	-0.8075	0.9180	1.0000

**Table 5** Final weights

	C (1)	C (2)	C (3)	C (4)	C (5)	C (6)	C (7)	C (8)	C (9)
$C_j$	2.6902	2.0923	2.2815	3.1874	1.7798	1.8676	2.6652	3.3268	2.9805
$W_j$	0.1176	0.0915	0.0998	0.1394	0.0778	0.0817	0.1165	0.1455	0.1303

**Table 6** Alternative ranking sequence using various MCDM techniques

	COPRAS		CoCoSo		EDAS		TOPSIS	
	$U_i$	Rank	$\xi_i$	Rank	$AS_i$	Rank	TOPSIS score	Rank
A1	100.0000	1	1.8947	1	0.6189	1	0.6092	1
A2	94.9462	4	1.6214	10	0.4889	11	0.5669	2
A3	99.0010	2	1.8076	2	0.5313	6	0.5411	3
A4	94.9995	3	1.7741	5	0.5000	8	0.4937	9
A5	89.8218	8	1.5956	11	0.3730	16	0.5235	4
A6	80.1572	16	1.6742	9	0.4871	12	0.4573	16
A7	90.5135	6	1.7745	4	0.6077	2	0.5151	6
A8	89.2853	9	1.4680	14	0.4947	10	0.5037	8
A9	90.0637	7	1.7527	6	0.5760	4	0.5044	7
A10	80.9009	15	1.3846	16	0.3900	15	0.4829	13
A11	92.9493	5	1.7755	3	0.5773	3	0.5171	5
A12	83.3686	12	1.4869	13	0.4315	13	0.4796	15
A13	84.0484	10	1.7248	7	0.5574	5	0.4879	12
A14	83.9237	11	1.5813	12	0.5084	7	0.4923	10
A15	82.2122	13	1.6766	8	0.4996	9	0.4818	14
A16	82.2089	14	1.4623	15	0.4237	14	0.4891	11

### 4.3 Result Discussion

- (a) Spearman’s rank correlation coefficient.
- (b) Kendall’s coefficient of concordance.
- (c) Borda count.
- (d) Copeland method.
- (e) Grade average method.

Spearman’s rank correlation coefficient ranges from  $-1$  to  $+1$ , where the value of  $+1$  shows a perfect correlation between two sets of rankings [29]. Using Eq. (33), the spearman’s rank correlation coefficient result evaluated by comparing the four ranking methods as depicted in Table 7.

$$r_s = 1 - \frac{6 \sum d_i^2}{n(n^2 - 1)}, \tag{33}$$

**Table 7** Spearman's rank correlation coefficient

	COPRAS	CoCoSo	EDAS	TOPSIS
COPRAS	1	0.7510	0.6221	0.8740
CoCoSo	–	1	0.8301	0.5342
EDAS	–	–	1	0.4375
TOPSIS	–	–	–	1

This value of Spearman's rank correlation coefficient ( $r_s$ ) depicts that the four groups of rankings obtained from the applied techniques are closely correlated with each other.

Kendall's coefficient of concordance ranges from 0 to 1, where the value of 1 shows a perfect correlation between two sets of rankings [29]. Using Eqs. (34) and (35), Kendall's coefficient of concordance value obtained by comparing the four ranking methods is **0.755**.

$$S = \sum_{i=1}^n (R_i^2 - \bar{R})^2, \quad (34)$$

$$W = \frac{12S}{m^2(n^3 - n)}, \quad (35)$$

This value of Kendall's coefficient of concordance ( $W$ ) shows that the four sets of rankings obtained from the applied techniques are closely correlated with each other. Borda count, Copeland method, and grade average method have been applied to evaluate the vehicles' final ranking, as shown in Table 8.

Furthermore, a sensitivity analysis was carried out by swapping the criterion weights for both COPRAS and TOPSIS, as the outcomes of any MCDM technique are heavily dependent on the criteria weights. There are nine criteria evaluated, and hence, there are thirty-six potential interchanges ( ${}^9C_2$ ), where nine is the overall number of criteria and two is the number of criteria selected at one time. Figure 2 illustrates all pairs of alternate fuel vehicle priority rankings as well as sensitivity analysis plots for the COPRAS and TOPSIS techniques.

## 5 Conclusion

For numerous years, academics in the field of sustainable development and social demand have attracted great emphasis on selecting automobiles with alternative fuels. It is a particularly tough multi-criteria problem in decision-making when several criteria for different choices in competing environments are taken into account. Researchers should be careful with the ranking results of different ranking techniques since they might lead to different ranks, resulting in different outcomes owing

**Table 8** Final rankings of vehicles

	Borda count		Copeland method				Grade average method	
	Total	Rank	Win	Loss	Final score	Rank	Score	Rank
A1	60	1	60	420	-360	1	1	1
A2	37	7	37	443	-406	7	6.75	7
A3	51	2	51	429	-378	2	3.25	2
A4	39	6	39	441	-402	6	6.25	6
A5	25	9	25	455	-430	9	9.75	9
A6	11	13	11	469	-458	13	13.25	13
A7	46	4	46	434	-388	4	4.5	4
A8	23	11	23	457	-434	11	10.25	11
A9	40	5	40	440	-400	5	6	5
A10	5	16	5	475	-470	16	14.75	16
A11	48	3	48	432	-384	3	4	3
A12	11	13	11	469	-458	13	13.25	13
A13	30	8	30	450	-420	8	8.5	8
A14	24	10	24	456	-432	10	10	10
A15	20	12	20	460	-440	12	11	12
A16	10	15	10	470	-460	15	13.5	15
Total	480							

to differences in the mathematical modeling of various ranking strategies. The decision model based on CRITIC-COPRAS is proposed in this study for the evaluation of the performance of alternative fuel vehicles. The results showed that Tata Nexon (A1) EV fuel is the best choice among six choices, while Maruti Ertiga (A6) CNG fuel is the poorest alternative. The Spearman's and Kendall's performance tests are conducted to govern the degree of concurrence of CRITIC-COPRAS and CRITIC-TOPSIS technique which is found to be satisfactory. The closeness of Spearman's and Kendall's coefficient validates the proposed method. The sensitivity analysis also shows that the ranking of alternative cars for fuel does not change if the criterion weight is modified, indicating the strength of the combined CRITIC-COPRAS decision model. The results obtained from Borda count, Copeland method, and Grade average method is not very surprising. Thus, it can be concluded that applying the CRITIC-COPRAS approach, with a strong mathematical background, can help the concerned decision-makers effectively make the best decision under any conflicting environment.

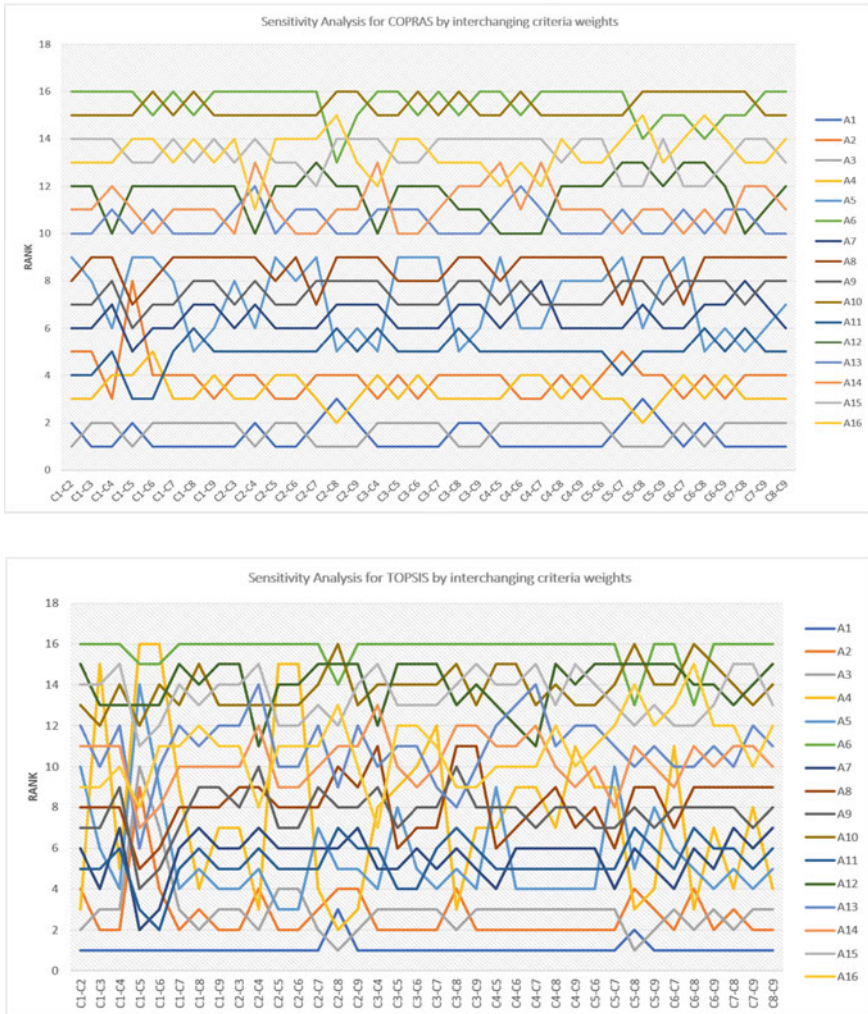


Fig. 2 Sensitivity analysis for COPRAS and TOPSIS

### References

1. Biswas T, Chatterjee P, Choudhuri B (2020) Selection of commercially available alternative passenger vehicle in automotive environment. Oper Res Eng Sci: Theor Appl 3:2620–1747. <https://doi.org/10.31181/oresta200113b>
2. IEA (n.d.) Global EV outlook 2021—analysis. Retrieved 7 May 2021, from <https://www.iea.org/reports/global-ev-outlook-2021>
3. Brey JJ, Contreras I, Carazo AF, Brey R, Hernández-Díaz AG, Castro A (2007) Evaluation of automobiles with alternative fuels utilizing multicriteria techniques. J Power Sources 169(1):213–219. <https://doi.org/10.1016/j.jpowsour.2007.01.052>

4. Safaei Mohamadabadi H, Tichowsky G, Kumar A (2009) Development of a multi-criteria assessment model for ranking of renewable and non-renewable transportation fuel vehicles. *Energy* 34(1):112–125. <https://doi.org/10.1016/j.energy.2008.09.004>
5. Vahdani B, Zandieh M, Tavakkoli-Moghaddam R (2011) Two novel FMCDM methods for alternative-fuel buses selection. *Appl Math Model* 35(3):1396–1412. <https://doi.org/10.1016/j.apm.2010.09.018>
6. Tsita KG, Pilavachi PA (2012) Evaluation of alternative fuels for the Greek road transport sector using the analytic hierarchy process. *Energy Policy* 48:677–686. <https://doi.org/10.1016/j.enpol.2012.05.079>
7. Biswas T, Das M (2018) Selection of hybrid vehicle for green environment using multi-attributive border approximation area comparison method. *Manage Sci Lett* 8(2):121–130
8. Biswas TK, Das MC (2019) Selection of commercially available electric vehicle using fuzzy AHP-MABAC. *J Inst Eng (India): Ser C* 100(3):531–537. <https://doi.org/10.1007/s40032-018-0481-3>
9. Ecer F (2021) A consolidated MCDM framework for performance assessment of battery electric vehicles based on ranking strategies. *Renew Sustain Energy Rev* 143:110916. <https://doi.org/10.1016/j.rser.2021.110916>
10. Bolduc D, Boucher N, Alvarez-Daziano R (2008) Hybrid choice modeling of new technologies for car choice in Canada. Retrieved 8 June 2021, from <https://doi.org/10.3141/2082-08>
11. Sovacool BK, Kester J, Noel L, de Rubens GZ (2018) The demographics of decarbonizing transport: the influence of gender, education, occupation, age, and household size on electric mobility preferences in the Nordic region. *Glob Environ Chang* 52:86–100. <https://doi.org/10.1016/j.gloenvcha.2018.06.008>
12. Aksen J, Mountain DC, Jaccard M (2009) Combining stated and revealed choice research to simulate the neighbor effect: the case of hybrid-electric vehicles. *Resour Energy Econ* 31(3):221–238. <https://doi.org/10.1016/j.reseneeco.2009.02.001>
13. Egbue O, Long S (2012) Barriers to widespread adoption of electric vehicles: an analysis of consumer attitudes and perceptions. *Energy Policy* 48:717–729. <https://doi.org/10.1016/j.enpol.2012.06.009>
14. Ma S-C, Fan Y, Guo J-F, Xu J-H, Zhu J (2019) Analysing online behaviour to determine Chinese consumers' preferences for electric vehicles. *J Clean Prod* 229:244–255. <https://doi.org/10.1016/j.jclepro.2019.04.374>
15. Ali Y, Mehmood B, Huzaifa M, Yasir U, Khan AU (2020) Development of a new hybrid multi criteria decision-making method for a car selection scenario. *Facta Univ, Ser: Mech Eng* 18(3):357–373. <https://doi.org/10.22190/FUME200305031A>
16. Yanmaz O, Turgut Y, Can EN, Kahraman C (2020) Interval-valued Pythagorean fuzzy EDAS method: an application to car selection problem. *J Intell Fuzzy Syst* 38(4):4061–4077. <https://doi.org/10.3233/JIFS-182667>
17. Jensen AF, Cherchi E, Mabit SL (2013) On the stability of preferences and attitudes before and after experiencing an electric vehicle. *Transp Res Part D: Transp Environ* 25:24–32. <https://doi.org/10.1016/j.trd.2013.07.006>
18. Faria R, Moura P, Delgado J, de Almeida AT (2012) A sustainability assessment of electric vehicles as a personal mobility system. *Energy Convers Manage* 61:19–30. <https://doi.org/10.1016/j.enconman.2012.02.023>
19. Skippon S, Garwood M (2011) Responses to battery electric vehicles: UK consumer attitudes and attributions of symbolic meaning following direct experience to reduce psychological distance. *Transp Res Part D: Transp Environ* 16(7):525–531. <https://doi.org/10.1016/j.trd.2011.05.005>
20. Yang S, Deng C, Tang T, Qian Y (2013) Electric vehicle's energy consumption of car-following models. *Nonlinear Dyn* 71(1):323–329. <https://doi.org/10.1007/s11071-012-0663-0>
21. Zhang H, Song X, Xia T, Yuan M, Fan Z, Shibusaki R, Liang Y (2018) Battery electric vehicles in Japan: human mobile behavior based adoption potential analysis and policy target response. *Appl Energy* 220:527–535. <https://doi.org/10.1016/j.apenergy.2018.03.105>

22. Egnér F, Trosvik L (2018) Electric vehicle adoption in Sweden and the impact of local policy instruments. *Energy Policy* 121:584–596. <https://doi.org/10.1016/j.enpol.2018.06.040>
23. Jena R (2020) An empirical case study on Indian consumers' sentiment towards electric vehicles: a big data analytics approach. *Ind Mark Manage* 90:605–616. <https://doi.org/10.1016/j.indmarman.2019.12.012>
24. Weldon P, Morrissey P, O'Mahony M (2018) Long-term cost of ownership comparative analysis between electric vehicles and internal combustion engine vehicles. *Sustain Cities Soc* 39:578–591. <https://doi.org/10.1016/j.scs.2018.02.024>
25. Hyundai Motors (n.d.) Hyundai KONA electric highlights |SUV| Hyundai Motor India. Retrieved 12 Aug 2021, from <https://www.hyundai.com/content/hyundai/in/en/find-a-car/kona-electric/highlights>
26. Mahindra Electric (n.d.) India's biggest brand of electric vehicles. Retrieved 12 Aug 2021, from <https://www.mahindraelectric.com/vehicles/everito/>
27. Maruti Suzuki Alto (n.d.) Alto features, specifications, colours and interior. Retrieved 12 Aug 2021, from [https://www.marutisuzuki.com/alto?form=testdrive&utm\\_source=google&utm\\_medium=cpc&utm\\_campaign=13720054925&utm\\_term=maruti%20alto%20price&utm\\_content=c&gclid=Cj0KCQjw6s2IBhCnARIsAP8RfAgYQUK0uYrd84XfXc90sqmmkb15ESARySL5uUjNbozb1SJuuYRFXIMaAla4EALw\\_wcB](https://www.marutisuzuki.com/alto?form=testdrive&utm_source=google&utm_medium=cpc&utm_campaign=13720054925&utm_term=maruti%20alto%20price&utm_content=c&gclid=Cj0KCQjw6s2IBhCnARIsAP8RfAgYQUK0uYrd84XfXc90sqmmkb15ESARySL5uUjNbozb1SJuuYRFXIMaAla4EALw_wcB)
28. Maruti Suzuki Celerio CNG (n.d.) Celerio CNG mileage, price, specifications, reviews. Retrieved 12 Aug 2021, from [https://www.marutisuzuki.com/cng/celerio?form=testdrive&utm\\_source=google&utm\\_medium=cpc&utm\\_campaign=13799624150&utm\\_term=maruti%20celerio%20cng&utm\\_content=c&gclid=Cj0KCQjw6s2IBhCnARIsAP8RfAgEYARofuFM-YwiJU07wkMqg7R\\_wroc997Jft5ksVJy1yUZ2Rcmw10aAozIEALw\\_wcB](https://www.marutisuzuki.com/cng/celerio?form=testdrive&utm_source=google&utm_medium=cpc&utm_campaign=13799624150&utm_term=maruti%20celerio%20cng&utm_content=c&gclid=Cj0KCQjw6s2IBhCnARIsAP8RfAgEYARofuFM-YwiJU07wkMqg7R_wroc997Jft5ksVJy1yUZ2Rcmw10aAozIEALw_wcB)
29. Athawale VM, Chakraborty S (2011) A comparative study on the ranking performance of some multi-criteria decision-making methods for industrial robot selection. *Int J Ind Eng Comput* 2(4):831–850
30. Maruti Suzuki Dzire Tour S (n.d.) Taxi segment Dzire. Retrieved 12 Aug 2021, from <https://www.marutisuzuki.com/tour/dzire?form=testdrive>
31. Maruti Suzuki Eeco (n.d.) Eeco van features, specification, colours and interior. Retrieved 12 Aug 2021, from [https://www.marutisuzuki.com/eeco?form=testdrive&utm\\_source=google&utm\\_medium=cpc&utm\\_campaign=13868683915&utm\\_term=maruti%20eeco%20cng&utm\\_content=c&gclid=Cj0KCQjw6s2IBhCnARIsAP8RfAi4g3bTxd0d3T9kXsMW3rf7obNDxDwVy0EsJhBoQ2MtnNpLR07cdUaAmOCEALw\\_wcB](https://www.marutisuzuki.com/eeco?form=testdrive&utm_source=google&utm_medium=cpc&utm_campaign=13868683915&utm_term=maruti%20eeco%20cng&utm_content=c&gclid=Cj0KCQjw6s2IBhCnARIsAP8RfAi4g3bTxd0d3T9kXsMW3rf7obNDxDwVy0EsJhBoQ2MtnNpLR07cdUaAmOCEALw_wcB)
32. Maruti Suzuki Ertiga (n.d.) Ertiga features, specifications, colours and interior. Retrieved 12 Aug 2021, from [https://www.marutisuzuki.com/ertiga?form=testdrive&utm\\_source=google&utm\\_medium=cpc&utm\\_campaign=13717491022&utm\\_term=ertiga&utm\\_content=c&gclid=Cj0KCQjw6s2IBhCnARIsAP8RfAgJ5JkWLLFi0\\_ITv2F-TFtMYv7LiLdQuBxpDciqW\\_vSTpdHOEVAKr8aAkXEEALw\\_wcB](https://www.marutisuzuki.com/ertiga?form=testdrive&utm_source=google&utm_medium=cpc&utm_campaign=13717491022&utm_term=ertiga&utm_content=c&gclid=Cj0KCQjw6s2IBhCnARIsAP8RfAgJ5JkWLLFi0_ITv2F-TFtMYv7LiLdQuBxpDciqW_vSTpdHOEVAKr8aAkXEEALw_wcB)
33. Maruti Suzuki S-Presso (n.d.) S-Presso car features, specification, colours and interior. Retrieved 12 Aug 2021, from [https://www.marutisuzuki.com/s-presso?form=testdrive&utm\\_source=google&utm\\_medium=cpc&utm\\_campaign=13800028694&utm\\_term=maruti%20spresso%20cng&utm\\_content=c&gclid=Cj0KCQjw6s2IBhCnARIsAP8RfAjfME4KB0PtH4JF8Kz84nJCAiMANEV3CnU56t53Ds7D3PRfy04QBxoaAkcLEALw\\_wcB](https://www.marutisuzuki.com/s-presso?form=testdrive&utm_source=google&utm_medium=cpc&utm_campaign=13800028694&utm_term=maruti%20spresso%20cng&utm_content=c&gclid=Cj0KCQjw6s2IBhCnARIsAP8RfAjfME4KB0PtH4JF8Kz84nJCAiMANEV3CnU56t53Ds7D3PRfy04QBxoaAkcLEALw_wcB)
34. Maruti Suzuki Wagon R (n.d.) Wagon R features, specifications, colours and interior. Retrieved 12 Aug 2021, from [https://www.marutisuzuki.com/wagonr?form=testdrive&utm\\_source=google&utm\\_medium=cpc&utm\\_campaign=13741156750&utm\\_term=maruti%20wagon%20r%20cng&utm\\_content=c&gclid=Cj0KCQjw6s2IBhCnARIsAP8RfAipKezwU0xk2N2rdWdP2HfMKQzNcFVt6BS4immfDcy9p6CeFBC-KKMaAiCkEALw\\_wcB](https://www.marutisuzuki.com/wagonr?form=testdrive&utm_source=google&utm_medium=cpc&utm_campaign=13741156750&utm_term=maruti%20wagon%20r%20cng&utm_content=c&gclid=Cj0KCQjw6s2IBhCnARIsAP8RfAipKezwU0xk2N2rdWdP2HfMKQzNcFVt6BS4immfDcy9p6CeFBC-KKMaAiCkEALw_wcB)
35. MG ZS EV (n.d.) Latest electric cars|MG Motor India. Retrieved 12 Aug 2021, from <https://www.mgmotor.co.in/vehicles/mgzsev>
36. Tata Nexon EV (2019) India's own electric compact SUV powered by Ziptron. Specifications and features of Tata Nexon EV and Dark Edition. <https://nexonev.tatamotors.com/features/>



37. Tata Motors Limited (n.d.) Towards a cleaner, greener e-mobile tomorrow with delivery of Tata Tigor electric vehicles for EESL. Retrieved 12 Aug 2021, from <https://www.tatamotors.com/blog/corporate/towards-a-cleaner-greener-e-mobile-tomorrow-with-delivery-of-tata-tigor-electric-vehicles-for-eesl/>
38. Kumar V, Kalita K, Chatterjee P, Zavadskas EK, Chakraborty S (2021) A SWARA-CoCoSo-based approach for spray painting robot selection. *Informatica* 1–20. <https://doi.org/10.15388/21-INFOR466>
39. Chakraborty S, Kumar V, Ramakrishnan K (2018) Selection of the all-time best World XI test cricket team using the TOPSIS method. *Decis Sci Lett* 8(1):95–108
40. Diakoulaki D, Mavrotas G, Papayannakis L (1995) Determining objective weights in multiple criteria problems: the critic method. *Comput Oper Res* 22(7):763–770. [https://doi.org/10.1016/0305-0548\(94\)00059-H](https://doi.org/10.1016/0305-0548(94)00059-H)
41. Yilmaz B, Harmancioglu N (2010) Multi-criteria decision making for water resource management: a case study of the Gediz River Basin, Turkey. *Water SA* 36(5), Article 5. <https://doi.org/10.4314/wsa.v36i5.61990>
42. Zavadskas EK, Kaklauskas A, Peldschus F, Turskis Z (2007) Multi-attribute assessment of road design solutions by using the Copras method. *Baltic J Road Bridge Eng* 2(4):195–203

# A Review on Dielectric Issues and Sustainable Alternatives in Electric Discharge Machining



Saurabh Bhardwaj, C. S. Jawalkar, and Suman Kant

**Abstract** Electric discharge machining (EDM) nowadays a major frequently used non-traditional machining processes for machining electrically conductive materials. It can machine even the hardest of known conductive materials; however, this process lacks on the sustainable scale due to its high power consumption, emission of fumes and other harmful waste materials. An operator may develop respiratory problems and skin related infections due to the harmful gaseous emission, odor and chemical nature of dielectrics. Besides this the non-degradable sludge is also a threat to our environment as it can damage our soil and water. In this paper, dielectrics have been studied and reviewed in terms of their developments and alternate. The authors have studied the problems associated with the conventionally used hydrocarbon dielectrics mainly kerosene; power mixed electric discharge machining (PMEDM), a variant of EDM has been studied to understand the effects of adding abrasive powder particles in the dielectrics and its consequences on the improvement of various response parameters along with the environmental effects. Similar kind of study has been performed by using the water-based liquid dielectrics and the gaseous phase dielectrics. Issues related to sustainability and the development in biodegradable dielectrics have also been discussed. Based on these reviews, some future recommendations have been suggested.

**Keywords** Dielectrics · Powder mixing · Health · Biodegradable dielectrics · Sustainable EDM

---

S. Bhardwaj (✉) · C. S. Jawalkar · S. Kant

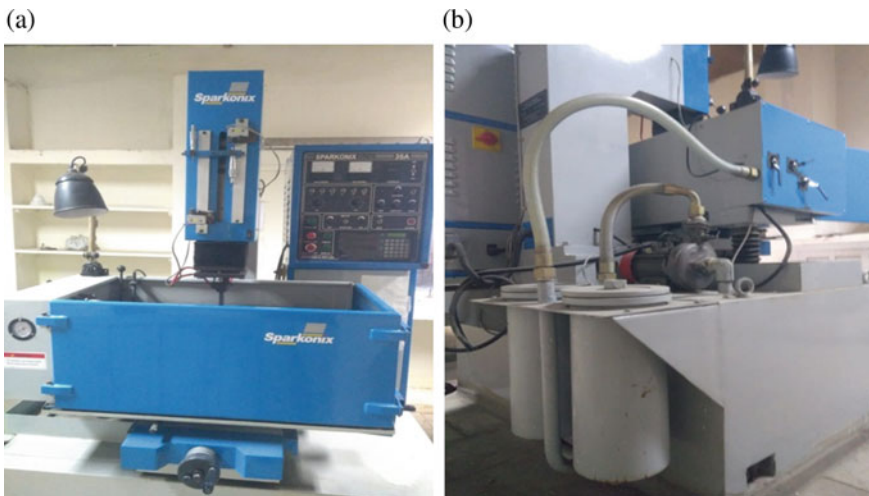
Department of Production and Industrial Engineering, Punjab Engineering College (Deemed to be University), Chandigarh, India

e-mail: [sb05aug@gmail.com](mailto:sb05aug@gmail.com)

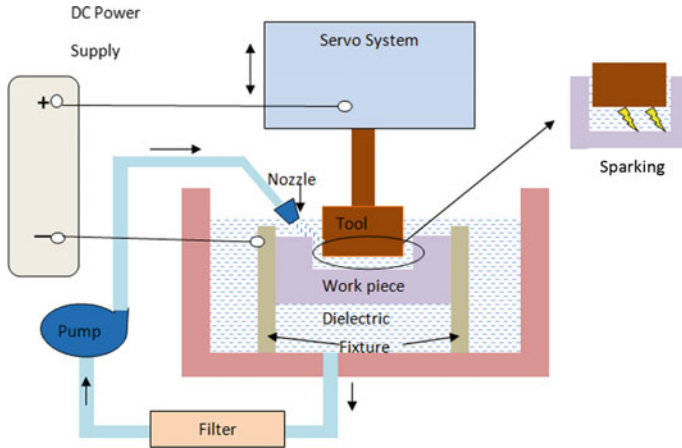
## 1 Introduction

Due to the growing need for different variety and complexity in design of products, the electric discharge machining (EDM) process has been well known as a prominent nontraditional machining process for conductive materials. In the post-World War II era, mass production was strengthened in the field of products having complex features using EDM. Any geometry on an electrically conductive material could be obtained by making its replica on the tool. This feature catered the needs of miniaturization and gradually EDM became a valued machining option in the late twentieth century. An EDM machine set up comprises of mainly the power supply unit, dielectric circulation and filtration arrangement servo system along with “tool” and “workpiece” acting as electrodes. Figure 1a illustrates the overall EDM machine, while Fig. 1b highlights the filtration units for dielectric circulation.

Machining in case of EDM is performed in the submerged region in the vicinity of electrodes. Kerosene is the most preferred dielectric fluid used, owing to its availability and reasonable cost. As the current passage and tool electrode approaches towards the work piece there happens an increase in the electric field intensity which breaks the strength of dielectric and provides a passage for the flow of current between the electrodes. Figure 2 illustrates schematic view of an EDM machine which uses discrete sparks to ionize the dielectric medium followed by generation of extreme high temperature as high as 8000–10,000 K [1] due to the formation of plasma in between the electrode gaps. Spark gets produced at the nearest point in the vicinity of the surfaces of the electrodes and thus being dynamic in nature it changes its spot after each spark which leads to removal of microchips from all the areas uniformly resulting in exact shape as that of tool.



**Fig. 1** a EDM machine. b Filtration units



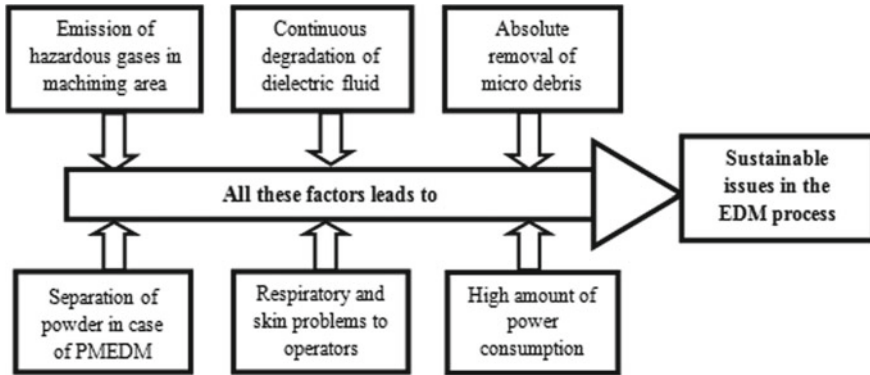
**Fig. 2** Schematic diagram of EDM

EDM is primarily used in the manufacturing of dies, deep cavities, slots, micro-nozzle, micro-pins and machining of aerospace materials. Although it is widely used; yet it is not termed as a sustainable machining process due to the adverse environmental impacts [2]. In EDM, major parameters like pulse on time ( $T_{on}$ ), pulse off time ( $T_{off}$ ), current, workpiece material, tool material, dielectric, flushing mode, flushing pressure, etc., are varied and responses like removal rate of material (MRR), wear rate of tool material (TWR) and surface roughness are among the major outputs.

The emission of hazardous gases mainly takes place in the vicinity of the operator which can cause irritation in eyes, skin itching and respiratory problems; apart from this disposal of the waste dielectric waste also known as dielectric sludge and machined micro-particles is a matter of serious concern. Very high amount of electrical energy is required to operate an EDM machine, while the material removal rate is low, thus it fails to fit in the category of sustainable manufacturing process. The other issues in EDM have been summarized and shown in Fig. 3.

## 2 Dielectrics

In the EDM process, dielectric plays a vital role. It involves flushing of debris; capturing emission vapors, cooling the workpiece and tool used in the spark region, insulating the electrodes (i.e., resistance to the flow of electricity). In order to improve the EDM towards sustainability and green manufacturing; advancement in dielectric material is the need of the hour. In this article, a review on the advancements in the area of dielectric, substitutes of the traditionally used hydrocarbon oil, green manufacturing and sustainability has been done through the available research. The



**Fig. 3** Sustainability issues in EDM

**Table 1** Dielectric properties and purpose

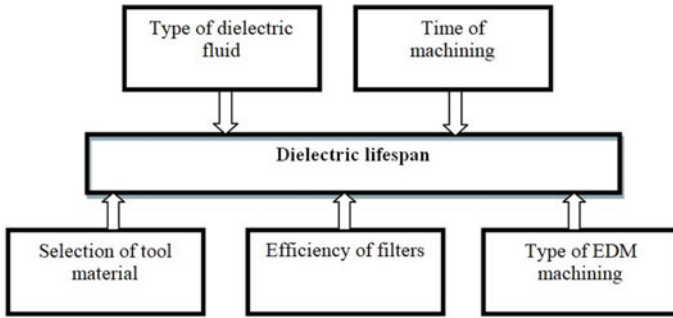
Properties	Magnitude	Purpose
Thermal conductivity	High	Better cooling
Viscosity	Low	Better flow-ability
Density	High	Better flushing
Flash point	High	Prevent fire
Dielectric strength	High	Minimize DC arcing
Biodegradability	High	Environment protection
Toxicity	Low	Operator friendliness
Cost	Low	Economic machining

properties of dielectric fluids keep decreasing with respect to time; with time its color changes, and it develops an unusual odor. Table 1 illustrates the properties of dielectrics along with the purposes for which they are used.

The exact life span of a dielectric cannot be predicted as it depends upon many factors as shown as Fig. 4; however, it is a common practice that hydrocarbon-based dielectrics are generally replaced after 5 years. As the hydrocarbons mixed with debris are hazardous; therefore, their disposal should be done as per the local environmental rules. When the aging filter gets clogged and thousands of conductive debris remains in the dielectric fluid, it ultimately results in longer cycle times and emission of hazardous and bad odor gases.

### 2.1 Powder Mixed in Dielectric

In a quest to enhance the existing process and efficiency variant and hybrid processes are innovated. In a variant process in EDM, very fine metallic powders are poured



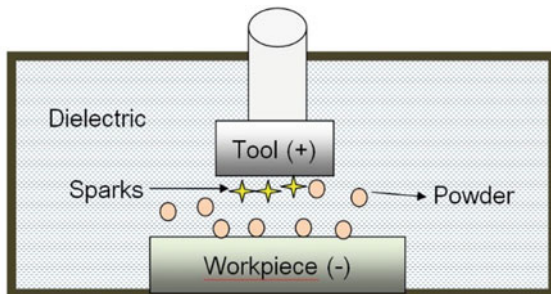
**Fig. 4** Factors affecting the dielectric lifespan

in the dielectric; better known as powder mixed electric discharge machining (PMEDM). Mixing metallic powders in dielectric reduce the insulating strength of the dielectric which ultimately results in better performance of EDM in terms of MRR and surface finish. During machining, these powdered particles get energized and move vigorously in the inter electrode space. The overall effect of plasma formation and the movement of energized abrasive particles results in increased MRR. The working principle of PMEDM is illustrated in Fig. 5. PMEDM can result in mirror like surface finish, hence it is extensively used in machining metal matrix composites (MMCs).

The most important step in PMEDM is the selection of powder material; it must be selected for a particular type of work piece based on properties viz. density, electrical conductivity, thermal conductivity, melting point, specific heat, etc. Table 2 highlights these properties of commonly used powders. The other factors like powder size and concentration also effect the results like MRR, TWR and surface finish.

Jeswani [4] had reported an increase in MRR up to 60% by mixing graphite powder of very fine size (average size  $\approx 10 \mu\text{m}$ ) in dielectric media (kerosene). It was also found that the TWR/MRR ratio reduced by 28%. Koshy et al. [5] have studied the mixing of doping powder elements in the dielectric medium and have concluded that the doping elements can impart certain properties on the workpiece surface. Narumiya [6] have used fine powders of aluminum, silicon and graphite powders and

**Fig. 5** Working principle of PMEDM



**Table 2** Properties of powders materials used with their consequences in PMEDM [3]

Powder material	Density (g/cm <sup>3</sup> )	Thermal conductivity (W cm <sup>-1</sup> °C <sup>-1</sup> )	Electrical conductivity (μ Ω cm <sup>-1</sup> )	Melting point (°C)	Specific heat (Cal g <sup>-1</sup> °C <sup>-1</sup> )	Remarks
Aluminum	2.7	2.38	2.45	660	0.215	Tool wear reduces, mirror surface finish
Chromium	7.16	0.67	12.7	1875	0.11	Machining efficiency increased
Silicon carbide	3.21	1–5	1 * 10 <sup>9</sup>	2975	0.18	Increase in MRR and TWR
Silicon	2.33	1.5	1 * 10 <sup>5</sup>	141	0.17	Reduces surface roughness
Tungsten	19.3	1.673	5.6	341	0.31	Increase in surface micro-hardness
Titanium	4.72	0.22	55	1668	0.125	Lesser number of micro-cracks
Molybdenum disulfide	5.06	0.138	106	1185	0.07	Profile depth and quality improved
Boron carbide	2.52	2.79	5.5 * 10 <sup>4</sup>	2763	–	MRR and machining efficiency increased
Graphite	1.3–1.9	0.25–4.70	500–3000	4550	0.17–0.20	Reduction in TWR
Molybdenum	1.2	1.39	5.27	2610	0.06	–
Alumina	3.98	0.251	103	2072	0.17	Improved topography
Carbon nano-tubes	2	4	50	2800	–	Decreased surface roughness, reduced thickness of recast layer

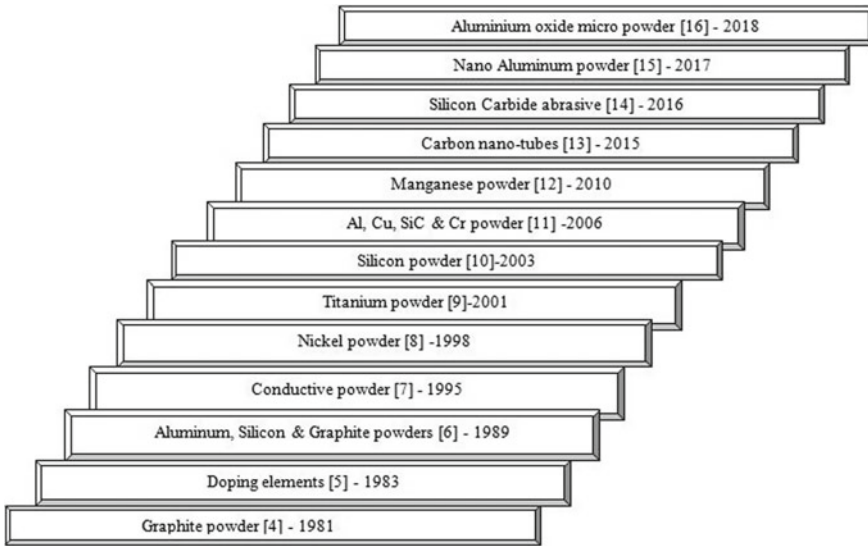
varied its concentration in the range 2–40 g/l. It was found that lower concentration of fine powders of graphite and silicon yielded better surface finish. Ming and He [7] have used copper as tool electrode, high carbon steel as the workpiece and conductive powder was mixed in the dielectric fluid. It was concluded that addition of conductive powders resulted in an increased surface micro-hardness. Uno et al. [8] have added fine nickel powder to the dielectric while machining an alloy surface using EDM. The addition of nickel powder resulted in improved wear resistance properties. Furutani

et al. [9] have studied the effects of addition of titanium powder to kerosene while machining carbon steel workpiece. It was found that a hard layer of titanium carbide was deposited on the workpiece surface. Pecas and Henriques [10] have studied the effects of mixing powder in a dielectric which caused enhanced performance of traditional EDM, it was found that with the addition of silicon powder operating time reduced along with improvement in the surface finish. Kansal et al. [11] have machined Al–10% SiCP metal matrix composite using PMEDM where powders of Al, Cu, SiC and Cr powders were used as additive powders. The response surface methodology (RSM) technique was used to examine the machining responses in terms of MRR and TWR. Kumar and Singh [12] had added manganese powder in dielectric to analyze the amount of material removal. It was found that the surface properties changed and the percentage of manganese and carbon increased which resulted in the increased micro-hardness. Kumar [13] had studied the effects of mixing carbon nanotubes in dielectric fluid to in machining of AISI-D2 steel in order to get mirror like surface finish. Li et al. [14] had used SiC abrasive powder in dielectric along with EDM magnetic stirring for machining titanium alloy workpiece. It was found that the SiC layer so on the improved the hardness. Rani et al. [15] had conducted PMEDM by adding nano Al powder to machine work piece with composition Ti6Al4V using a copper tungsten tool. The results concluded that with increment of nano size powders of aluminum a reduction in micro-cracks which ultimately resulted in increased surface finish was noted. Kumar et al. [16] have observed the effects of adding aluminum oxide ( $Al_2O_3$ ) powder having average diameter below 1 mm in a dielectric used for the machining of an Inconel 825 grade workpiece. It was evident from the experiment finding that the pulse on time, peak current and gap voltage were the significant parameters which affected the MRR and surface roughness. Figure 6 illustrates different powders with their first instance of use in PMEDM.

## 2.2 *Water-Based Dielectrics*

Jewsani [17] had compared the outputs of kerosene and distilled water as dielectric mediums in EDM process. It was found that using distilled water lead to higher MRR and poor accuracy but resulted in better surface finish. Jilani and Pandey [18] have investigated the scope of using water as a dielectric for machining low carbon steel workpiece using brass and copper electrode. In these experiments, the three dielectrics were used (i) distilled water, (ii) tap water and (iii) 25% tap water mixed with 75% distilled water. It was found that MRR rate was best in case of tap water. Koenig and Joerres [19] studied the use of aqueous solution of organic compounds as dielectric medium in case of EDM machining. The results suggested the use of highly concentrated glycerine aqueous solution dielectric as the best one. It was also found that glycerine media had an advantage over the hydrocarbon dielectrics





**Fig. 6** Powders used in PMEDM

while working under high pulse duty factors and long pulse durations. König [20] studied the influence of working medium in case of EDM. It was found that working medium had a significant influence in case of spark machining. Using water as a dielectric resulted in higher thermal stability and higher power input. Yeo and New [21] worked on a parameter namely utility function in order to find the utility value; an outcome of integration of energy, quality, time and mass of different dielectrics. It was found that the value of utility function for de-ionized water was 1.23 and for kerosene it was 1.11. Leao and Pashby [22] have reported that fluids can provide a replacement to hydrocarbon oil, as a dielectric and suggested that oil-based fluids can be replaced by water-based dielectrics in die sink applications. It was also concluded that dielectrics in gaseous phase like oxygen can serve as an alternate. Liu et al. [23] have studied the performance of water in oil emulsion as a dielectric on the basis of orthogonal and additional experiments with single factor. Results revealed that discharge current ( $I$ ) and water content of the emulsion significantly influenced the machining performance of EDM. Also MRR and EWR decreased with the increase in temperature of the emulsion. Pattabhiraman et al. [24] have studied the use of atomized droplets that formed a moving film of dielectric for EDM. The results revealed that for all set of parameters the electrode wear using atomized dielectric was better as compared to dry and wet EDM. Tang and Du [25] have tested tap water in case of Ti–6Al–4V workpiece material as a dielectric fluid because of its safe nature. Experiment results were later compared with those of contrast experiment. The results indicate that the MRR improved from 5.9 to 6.02 mm<sup>3</sup>/min. Paswan et al. [26] have used steam as a dielectric in EDM to machine aluminum-based MMC and compared the result with dielectrics like hydrocarbon oil and kerosene. It

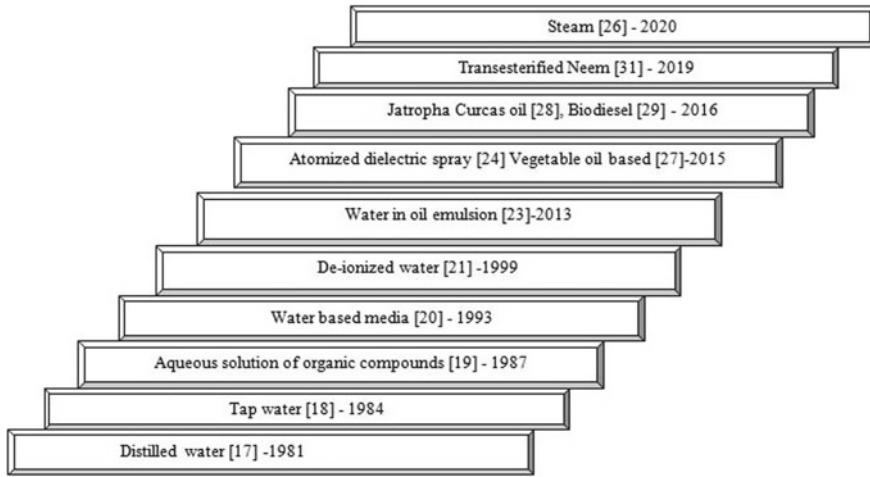
was found that recast layer improved up to 37.15% in structure, morphology, base material bond and thickness. Steam as a dielectric was chosen in order to make the process sustainable and eco-friendly with lesser surface defects in comparison with the hydrocarbon dielectrics which resulted in lower costs of operation.

### **2.3 Biodegradable Dielectrics**

Valaki and Rathoa [27] have studied the operational feasibility of using waste vegetable oil a substitute dielectric medium and compared the outcomes with those of hydrocarbons and kerosene. Experiment results so obtained revealed that these bio-dielectric fluid can be used as a substitute to hydrocarbon oil and synthetic-based dielectrics for EDM. Valaki et al. [28] have investigated the practical feasibility of using “*jatropha curcas*” oil-based bio-dielectric fluid for sustainable EDM and concluded that the response of the parameters were found in good conformance by using regression models. It was suggested that the use of *Jatropha* oil-based bio-dielectric fluids can help to achieve sustainability of EDM process to an extent. Ng et al. [29] have studied the effects of biodiesel as a dielectric in electric discharge micromachining. Canola and sunflower biodiesel were compared against conventional dielectric in terms of MRR and TWR. The experimental results focussed on the fact that both “canola” and “sunflower biodiesels” outperformed the conventional dielectric. Sadagopan and Mouliprasanth [30] have investigated the effect of three different dielectric fluids namely (i) biodiesel, (ii) transformer oil and (iii) kerosene on the responses like MRR, EWR and surface roughness. The machining was performed on a Al 6063 workpiece sample using a die-sinking EDM machine with copper as tool electrode. The result revealed that biodiesel can be used as a dielectric medium in EDM due to increased MRR and lower values of EWR while transformer oil and biodiesel emit smoke in less magnitude. Das et al. [31] have worked on the different sustainability areas of EDM and named transesterified neem; as one of the green dielectrics. The authors have reported that the dielectric “neem” imparts comparatively finer surfaces since the radial craters overlapped repeatedly, and hence, they required lesser time periods for attaining the required material removal. Figure 7 illustrates some alternative dielectric materials, as per their initial usages in EDM process.

## **3 Issues and Their Sustainable Alternatives**

Dahmus and Gutowski [32] have analyzed and revealed that the requirements of energy for material removal were very small as compared to the requirement of total energy in machine operation. Evertz et al. [33] have performed the optimization of EDM primarily in risk reduction assessments. The effects of different parameters have been tested to know their influence on air emissions. Metals and aliphatic



**Fig. 7** Alternate dielectrics used in EDM

compounds showed significant influence for electrodes used as compared to polycyclic aromatic hydrocarbons and volatile organic compounds. Increase in dielectric level above the location of processing resulted in decreased emissions in case of chromium, nickel, BTEX and PAH. With the increase in EDM current air emissions had increased for all the substances that were analyzed. Sivapirakasam et al. [34] have analyzed the aerosol produced during the EDM process and monitored the effects of variation of flushing pressure within the area of breathing zone. The influence of pulse duration, dielectric level and peak current near the spark location were also reported using Taguchi methodology. Peak current and pulse duration were recognized as the most influencing parameters. It was found that spherical shape particulates with average size in the range of 20–29 nm were seen in the morphological studies. Sivapirakasam et al. [35] have developed a combined model of Taguchi with fuzzy TOPSIS methods in order to solve optimization problems having different response parameter in the green manufacturing area. The best machining performance for a green EDM was reported with a peak current value of 4.5 A, pulse duration value of 261  $\mu\text{m}$  along with dielectric level of 40 mm and flushing pressure 0.5  $\text{kg}/\text{cm}^2$ . It was observed that peak current was found out to be the most influential parameter from analysis of the closeness coefficients. Valaki et al. [2] have studied the research work done in EDM process under three sustainability indicators viz. impact on environment, health of operators and operational safety. It was observed that supply mode of dielectric material such as wet/dry/near dry had significant influence on the above sustainability indicators. Jagadish and Ray have combined GRA along with principal component analysis (PCA) method to ultimately optimize the process parameters of the sustainable EDM. Peak current was found out as the most important parameter having 52.87% contribution [2]. Srinivas et al. have suggested the use of alternate green dielectrics along with better environment for operators safety and minimizing

**Table 3** Classification of EDM with respect to the use of alternate dielectrics

EDM type	Wet-EDM	Dry EDM	Near dry EDM	Spray EDM
Alternate dielectrics	Plain water De-ionized water Tap water Distilled water Water in oil emulsion Commercial water-based fluid Transesterified neem Jatropha Curcas Biodiesel	Air Oxygen Argon Helium	Two phase (liquid-gas)	Single phase liquid

environmental degradation effects towards sustainable EDM [36]. Zia et al. [37] have focused on (i) economic, (ii) environmental and (iii) social concerns for EDM process. Issues related to cost, health and environment were discussed extensively; consumption of energy, preparation of electrode and dielectric disposal were found out to be the major concerns. Major health concerns reported were cases of fume inhalation, skin itching and fire threat. Table 3 illustrates the classification of EDM with respect to the use of alternate dielectrics.

Some authors have investigated the feasibility of adding powder in the conventionally used dielectrics like kerosene in order to enhance the MRR and surface finish while machining; however, mixing of powder enhances the emissions of gases. Separation of these powder and debris from the dielectric sludge has been a major concern for the researchers. With the passage of time filter materials gets damaged, hence filtering the powder and debris cannot happen to the full extent; therefore, using the impure dielectric in itself is a danger and in case of its disposal environmental norms should be considered because of its non-biodegradable nature. This has been one of the most important phenomenons where EDM lags behind some other processes in terms of sustainability. With the use of water-based dielectrics, it has been reported that gaseous emissions have reduced. These dielectrics have not been used on all sets of tool and work piece materials; hence, it has not been accepted worldwide as alternate to the conventional hydrocarbon dielectrics. Gaseous, mist and spray form of dielectrics have proved to be environment friendly and needs to be employed in commercial sectors. In order to overcome the shortcomings following improvisations can be applied in the EDM process:

- (i) Filter design should be improved to cope up the wear and tear from the debris and powders mixed in the dielectric sludge.
- (ii) Monitoring dielectric life should be ensured, and it should be instantly replaced as soon as it gets unfit for the environment and operator.
- (iii) Dielectrics having low viscosity should be used as they emit less smoke as compared to the viscous dielectrics.

- (iv) In order to make this process operator friendly, fumes, emissions, odor needs to be minimized or neutralized by developing any possible arrangement or mechanism.
- (v) Combination of tool work piece and dielectrics should be studied, and it should be standardized for commercial use in order to minimize the emissions, wastage, cost and operators health risk.

## 4 Conclusions

The paper discusses on comprehensive review on the recent trends and different types of dielectrics used along with the major findings. Issues in existing dielectrics have been extensively discussed. The PMEDM has been discussed, and the alternative dielectrics have also been classified. The following dielectrics have a promising future:

1. De-ionized water mixed with organic compounds has shown positive results for finishing and roughing operations.
2. Abrasive powders mixed in dielectrics have shown enhanced results in micro-EDM operations.
3. Gaseous dielectrics in micro-EDM have resulted in enhanced MRR.
4. Dielectrics having lower viscosity have resulted in improved machining cycle time.

## References

1. Albinski K, Musiol K, Miernikiewicz A, Labuz S, Malota M (1996) The temperature of a plasma used in electrical discharge machining. *Plasma Sources Sci Technol* 5(4):736
2. Valaki JB, Rathod PP, Khatri BC (2015) Environmental impact, personnel health and operational safety aspects of electric discharge machining: a review. *Proc Inst Mech Eng, Part B: J Eng Manuf* 229(9):1481–1491
3. Joshi AY, Joshi AY (2019) A systematic review on powder mixed electrical discharge machining. *Heliyon* 5(12):e02963
4. Jeswani ML (1981) Effect of the addition of graphite powder to kerosene used as the dielectric fluid in electrical discharge machining. *Wear* 70(2):133–139
5. Koshy G, Philip PK, Geddam A (1983) Hardening of surface layers using electric discharge techniques. In: *Proceedings of the 11th AIMTDR conference*, pp 315–319
6. Narumiya H (1989) EDM by powder suspended working fluid. *ISEM* 9:5
7. Ming QY, He LY (1995) Powder-suspension dielectric fluid for EDM. *J Mater Process Technol* 52(1):44–54
8. Uno Y, Okada A, Yamada T, Hayashi Y, Tabuchi Y (1998) Surface integrity in EDM of aluminum bronze with nickel powder mixed fluid. *J Jpn Soc Electr Mach Eng* 32(70):24–31
9. Furutania K, Saneto A, Takezawa H, Mohri N, Miyake H (2001) Accretion of titanium carbide by electrical discharge machining with powder suspended in working fluid. *Precis Eng* 25(2):138–144

10. Pecas P, Henriques E (2003) Influence of silicon powder-mixed dielectric on conventional electrical discharge machining. *Int J Mach Tools Manuf* 43(14):1465–1471
11. Kansal HK, Singh S, Kumar P (2006) An experimental study of the machining parameters in powder mixed electric discharge machining of Al–10% SiCP metal matrix composites. *Int J Mach Mach Mater* 1(4):396–411
12. Kumar S, Singh R (2010) Investigating surface properties of OHNS die steel after electrical discharge machining with manganese powder mixed in the dielectric. *Int J Adv Manuf Technol* 50(5–8):625–633
13. Kumar H (2015) Development of mirror like surface characteristics using nano powder mixed electric discharge machining (NPMEDM). *Int J Adv Manuf Technol* 76(1–4):105–113
14. Li L, Zhao L, Li ZY, Feng L, Bai X (2017) Surface characteristics of Ti-6Al-4V by SiC abrasive-mixed EDM with magnetic stirring. *Mater Manuf Processes* 32(1):83–86
15. Abdul-Rani AM, Nanimina AM, Ginta TL, Razak MA (2017) Machined surface quality in nano aluminum mixed electrical discharge machining. *Procedia Manufact* 7:510–517
16. Kumar V, Kumar A, Kumar S, Singh NK (2018) Comparative study of powder mixed EDM and conventional EDM using response surface methodology. *Mater Today: Proc* 5(9):18089–18094
17. Jeswani ML (1981) Electrical discharge machining in distilled water. *Wear* 72(1):81–88
18. Jilani ST, Pandey PC (1984) Experimental investigations into the performance of water as dielectric in EDM. *Int J Mach Tool Des Res* 24(1):31–43
19. Koenig W, Joerres L (1987) Aqueous solutions of organic compounds as dielectrics for EDM sinking. *CIRP Ann* 36(1):105–109
20. Konig W (1993) Influence of the working medium on the removal process in EDM sinking. *Asme Ped* 64:649
21. Yeo SH, New AK (1999) A method for green process planning in electric discharge machining. *Int J Adv Manuf Technol* 15(4):287–291
22. Leão FN, Pashby IR (2004) A review on the use of environmentally-friendly dielectric fluids in electrical discharge machining. *J Mater Process Technol* 149(1–3):341–346
23. Liu Y, Zhang Y, Ji R, Cai B, Wang F, Tian X, Dong X (2013) Experimental characterization of sinking electrical discharge machining using water in oil emulsion as dielectric. *Mater Manuf Processes* 28(4):355–363
24. Pattabhiraman A, Marla D, Kapoor SG (2015) Atomized dielectric spray-based electric discharge machining for sustainable manufacturing. *J Micro Nano Manuf* 3(4)
25. Tang L, Du YT (2014) Multi-objective optimization of green electrical discharge machining Ti-6Al-4V in tap water via Grey-Taguchi method. *Mater Manuf Processes* 29(5):507–513
26. Paswan K, Pramanik A, Chattopadhyaya S, Basak AK (2020) A novel approach towards sustainable electrical discharge machining of metal matrix composites (MMCs). *Int J Adv Manuf Technol* 106(3):1477–1486
27. Valaki JB, Rathod PP (2016) Assessment of operational feasibility of waste vegetable oil based bio-dielectric fluid for sustainable electric discharge machining (EDM). *Int J Adv Manuf Technol* 87(5):1509–1518
28. Valaki JB, Rathod PP, Sankhavara CD (2016) Investigations on technical feasibility of *Jatropha curcas* oil based bio dielectric fluid for sustainable electric discharge machining (EDM). *J Manuf Process* 22:151–160
29. Ng PS, Kong SA, Yeo SH (2017) Investigation of biodiesel dielectric in sustainable electrical discharge machining. *Int J Adv Manuf Technol* 90(9):2549–2556
30. Sadagopan P, Mouliprasanth B (2017) Investigation on the influence of different types of dielectrics in electrical discharge machining. *Int J Adv Manuf Technol* 92(1–4):277–291
31. Das S, Paul S, Doloi B (2020) Feasibility investigation of neem oil as a dielectric for electrical discharge machining. *Int J Adv Manuf Technol* 106(3):1179–1189
32. Dahmus JB, Gutowski TG (2004) An environmental analysis of machining. In: *ASME international mechanical engineering congress and exposition*, vol 47136. pp 643–652
33. Evertz S, Dott W, Eisentraeger A (2006) Electrical discharge machining: occupational hygienic characterization using emission-based monitoring. *Int J Hyg Environ Health* 209(5):423–434

34. Sivapirakasam SP, Mathew J, Surianarayanan M (2011) Constituent analysis of aerosol generated from die sinking electrical discharge machining process. *Process Saf Environ Prot* 89(2):141–150
35. Sivapirakasam SP, Mathew J, Surianarayanan M (2011) Multi-attribute decision making for green electrical discharge machining. *Expert Syst Appl* 38(7):8370–8374
36. Viswanth VS, Ramanujam R, Rajyalakshmi G (2018) A review of research scope on sustainable and eco-friendly electrical discharge machining (E-EDM). *Mater Today: Proc* 5(5):12525–12533
37. Zia MK, Pervaiz S, Anwar S, Samad WA (2019) Reviewing sustainability interpretation of electrical discharge machining process using triple bottom line approach. *Int J Precis Eng Manuf-Green Tech* 6(5):931–945

# Numerical Investigation of Mixing Characteristics of a Passive T-Micromixer with a Twisted Outlet Channel



B. Lohit Nagarjun Reddy and M. Zunaid

**Abstract** The present study considers the computational evaluation of the mixing performance of a passive T-micromixer with a twisted outlet channel. The outlet channel is twisted to enhance the mixing performance of the micromixer. For this study, we consider two separate water specimens suitable for simulating the mixing of two miscible liquids of low diffusion coefficients. The results of mixing performance obtained are weighed against a simple T-micromixer with no twists of the same aspect ratio and characteristic dimension. The present study investigates mixing performance for a T-mixer with two twists to the outlet channel with a characteristic dimension of  $133.33\ \mu\text{m}$  for a set of Reynolds numbers (10–266). The twisted T-micromixer has shown an appreciable increase in the mixing index, especially in lower Reynolds numbers.

**Keywords** Micromixer · Computational fluid dynamics · Microchannel · Mixing index

## 1 Introduction

Micromixers are used in the chemical, biological and medical industry extensively for applications in microfluidics systems involving fast chemical reactions, DNA analysis and cell separation [1–8].

The micrometre-scale dimensions of a micromixer mean that laminar flow dominates in these devices. The control of flow characteristics is easy in the laminar flow because it can be predicted with good accuracy. But macroscopic turbulent fluctuations needed for homogeneous mixing are absent [1]. Mixing in micro-channels occurs by molecular diffusion alone. This is a drawback as rapid mixing of two fluid streams becomes difficult.

---

B. Lohit Nagarjun Reddy (✉) · M. Zunaid  
Department of Mechanical Engineering, Delhi Technological University, Delhi, India  
e-mail: [reddy.lohit.97@gmail.com](mailto:reddy.lohit.97@gmail.com)

© The Author(s), under exclusive license to Springer Nature Singapore Pte Ltd. 2023  
R. P. Singh et al. (eds.), *Advances in Modelling and Optimization of Manufacturing and Industrial Systems*, Lecture Notes in Mechanical Engineering,  
[https://doi.org/10.1007/978-981-19-6107-6\\_7](https://doi.org/10.1007/978-981-19-6107-6_7)



The micro-scale mixing systems can be widely categorized into two groups: active and passive [9]. Passive micromixers rely on the energy imparted to the fluid to facilitate their motion, for mixing [10, 11]. Passive micromixers aim to achieve mixing by manipulating the fluid flow with the help of the channel geometry to increase chaos in the fluid flow [12–15]. Active micromixers on the other hand have external sources for providing excitation energy to enhance mixing electric fields, magnetic fields, etc., are suitable excitation agents in active micromixers. Lee et al. [9] discussed the advantages and disadvantages of both groups of micromixers [16]. Passive micromixers are simpler in construction and cheaper to manufacture [17]. But they do not have as good a mixing performance as that of active micromixers for the same dimensions of micromixer [18]. Active micromixers are much more sophisticated and provide better adjustability when it comes to different operating conditions. This due to the fact that the behaviour of the excitation source can be changed at will to suit the flow conditions. Despite the advantages provided by active micromixers, they are less preferred over passive micromixers simply due to their higher cost, complex control systems and difficulty in integration compared to passive micromixers [19, 20].

At the junction of the simple T-micromixer (STM), the flow regime varies depending on the Reynolds number. Engler et al. [21] determined that three flow regimes may occur, namely laminar flow, vortex flow and engulfment flow. In the engulfment regime, the two fluid streams intertwine which rolls up the contact area (which is plane initially), increasing the mixing efficiency, as noted by Bothe et al. [22].

In a simple T-micromixer, Dundi et al. [23] observed that mixing performance can be improved by introducing a swirl component of velocity to the fluid at the inlets. It was also observed that swirls in opposite directions in both the fluids had better mixing than the case when swirling was introduced in the same direction. It can also be observed that the mixing gradient ( $\Delta MI/\Delta x$ ) is higher in the initial span of the channel dropping after a certain distance.

The present study aims to build on these previous studies and observe the results obtained by further alteration to the channel. This alteration is made by providing twists in the outlet channel while retaining a uniform cross-section over the entire span. Jafari et al. [24] studied the performance of twisted micromixers in the liquid–liquid extraction process. But the cross-sectional area of the channel changed with a change in the number of twists because the microchannel was created by physically twisting a circular cross-section microchannel. Twisting resulted in an oval cross-section whose dimensions depended on the number of times it was twisted.

## 2 Methodology

### 2.1 Mathematical Modelling

Two water species are supplied through the two inlets of the micromixer. Water is an incompressible fluid and it obeys Newton's law of viscosity. The model is numerically solved with the help of equations of conservation of mass (the continuity equation) and conservation of momentum (Navier–Stokes's equation).

The mixing process is governed by the following equation:

$$(V \cdot \nabla)c = D\nabla^2c \quad (1)$$

where

- $c$  Concentration
- $D$  Coefficient of diffusion.

The average concentration at any section is given by

$$\bar{c} = \frac{\int c dA}{A} \quad (2)$$

where

- $A$  Area of the section ( $m^2$ ).

The degree of mixing at any section in the micromixer is indicated by the mixing index (MI) which is given as

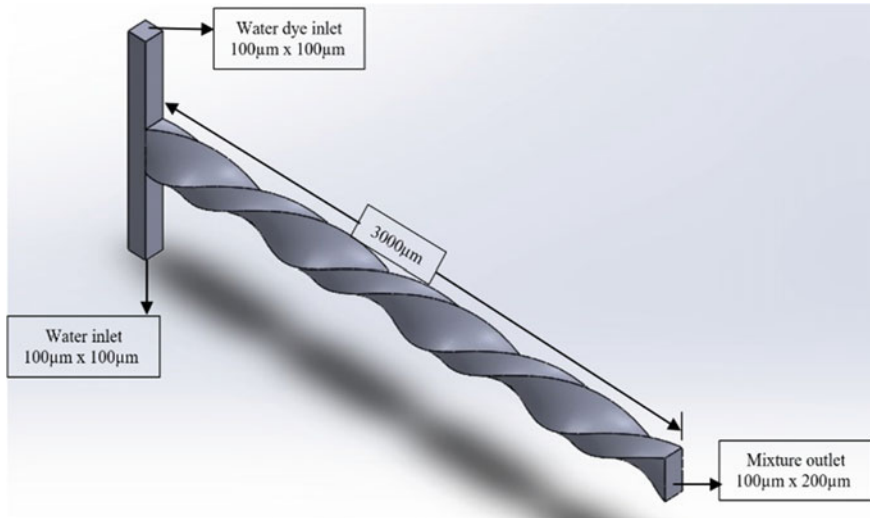
$$MI = 1 - \sqrt{\frac{\int (c - \bar{c})^2 dA}{A \cdot \bar{c}(1 - \bar{c})}} \quad (3)$$

At a certain section in the micromixer, 'MI' of *zero* denotes no mixing whereas 'MI' of *one* denotes complete mixing.

### 2.2 Numerical Modelling

The 3D model of the T-micromixer with twisted outlet channel (TTM) is made on SOLIDWORKS 2020. The governing equations are solved, and the flow is simulated in ANSYS FLUENT 2020.

The micromixer has two inlets with a square cross-section of side  $100 \mu m$ . The outlet channel has a rectangular cross-section with a width and height of  $100 \mu m$



**Fig. 1** Geometry of T-micromixer with twisted outlet channel

and 200  $\mu\text{m}$ , respectively, as shown in Fig. 1. The twists are applied by rotating the exit by  $720^\circ$ . It should be noted the cross-sections of all the sections along the span of the outlet are identical albeit in a different orientation.

For the meshing of the micromixer geometry, hexahedral elements are used as a smaller number of such elements are required to mesh the flow domain as compared to other types of elements. This reduces the computational load. Also, the mesh elements were much more uniform in shape compared to when we use tetrahedral elements. This can be seen in Fig. 2. Hexahedral elements also provided low skewness (maximum skewness = 0.265).

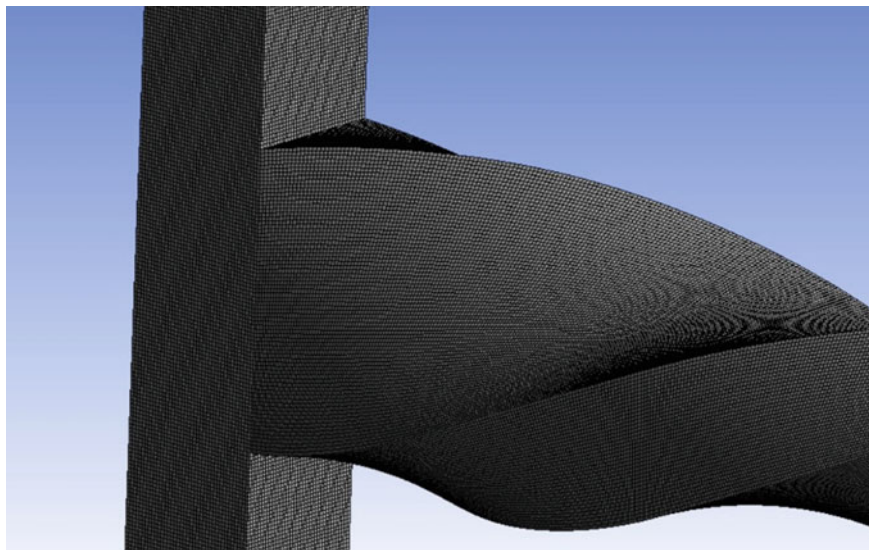
Two species of water ('water' and 'water-dye') are inducted into the micromixer via the two inlets. The concentration at the inlet section for 'water-dye' is taken as 'one' and 'zero' for the inlet section for 'water'.

Properties of liquid water at 20  $^\circ\text{C}$  (Table 1) are considered for this study.

A steady-state laminar flow model along with a species transport model was selected for the study. The residual for continuity is taken as  $10^{-5}$  and  $10^{-4}$  is the residual selected for momentum and species equation (Table 2).

Table 3 indicates the boundary conditions being used for the simulation. The Reynolds number is calculated for the outlet channel.

The solution obtained from the numerical calculation must not be dependent on the number of mesh elements. Therefore, an optimum mesh size is selected to obtain enough mesh elements for which the solution is grid independent. Figure 3 shows the mixing indices for different element count (0.6 million to 7.2 million) for TTM at a Reynolds number of 266. The slope of the curve in Fig. 3 is reducing as we increase the number of elements. Subsequently, we would reach a point where the mixing index would not change with anymore increase in the number of elements.



**Fig. 2** Generated mesh

**Table 1** Properties of water at 20 °C

Coefficient of diffusion (D)	$20 \times 10^{-9} \text{ m}^2/\text{s}$
Coefficient of viscosity ( $\mu$ )	0.001 Pa s
Density of fluid ( $\rho$ )	998.2 kg/m <sup>3</sup>

**Table 2** Solution methods employed

Pressure–velocity coupling	SIMPLEC
Pressure	Standard
Momentum	Second order upwind
Species	Second order upwind

**Table 3** Boundary conditions

S. No	Axial velocity at inlets (m/s)	Reynolds number
1	0.15	20
2	0.45	60
3	0.75	100
4	0.90	120
5	1.32	176
6	1.65	220
7	2.00	266

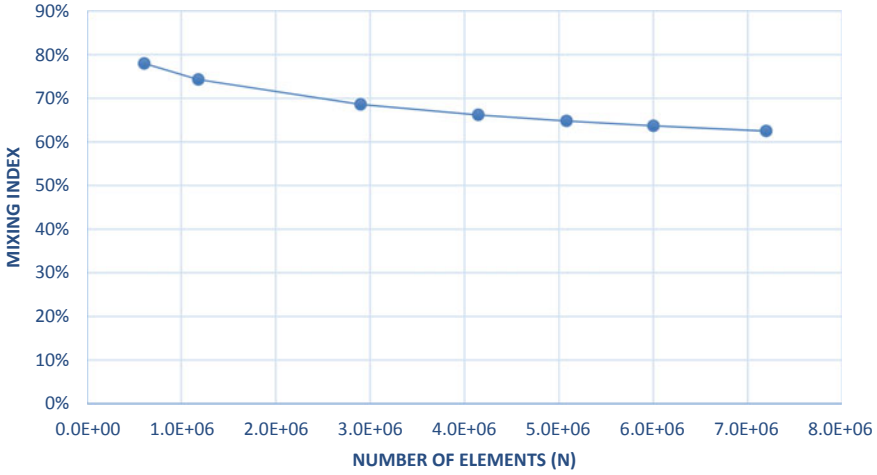


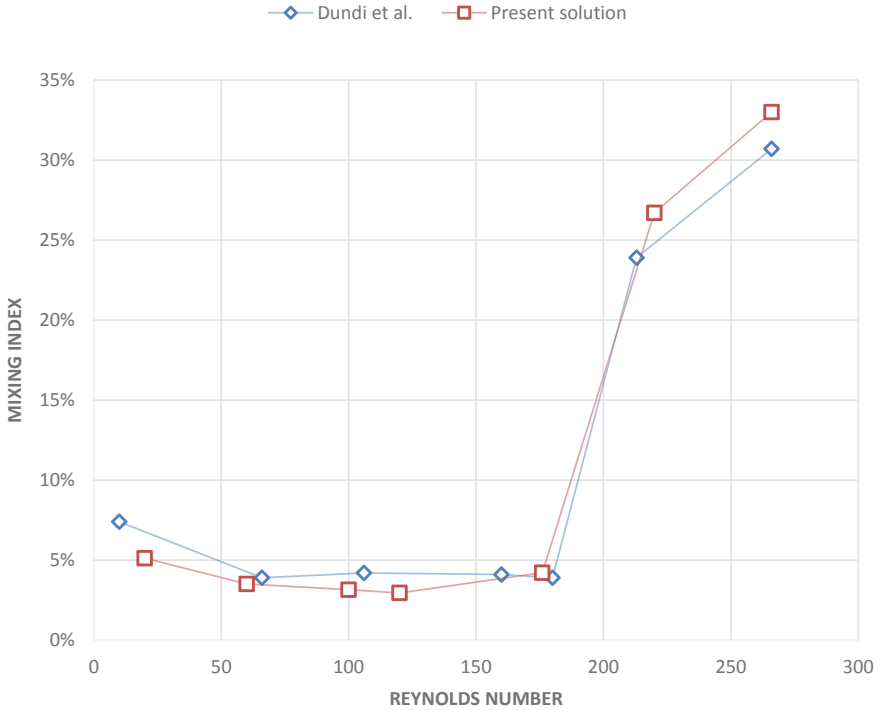
Fig. 3 Plot of mixing index for TTM at RE = 266 at different  $N$  values

At this condition, the solution obtained is said to be grid independent. Increasing the element count further would lead to high computational load while giving negligible improvements. Therefore, we need to select a certain number of elements which is optimized for the available computational power and satisfactory result.

### 3 Result

After carrying out the numerical simulation of TTM to evaluate its mixing performance, it was compared with an STM with the same aspect ratio. The results of the STM were validated with results obtained by Dundi et al. [23]. The comparison between present work and previous literature is shown in Fig. 4. Further, results of MI of STM at Reynolds numbers intermediate to those simulated by Dundi et al. [23] to better analyse its performance relative to TTM.

It can be observed from Table 4 that TTM shows a significant increase in mixing performance compared to STM. This is depicted graphically in Fig. 5. This increase is the greatest at  $Re = 176$ , where the increase in MI is almost 1000%. This can be owed to the fact that MI is nearly constant for low Reynold numbers. In this case for STM, it can be seen that MI increases significantly only for Reynolds numbers above around 176. The increase in MI for fluid flow in TTM can be attributed to two effects imposed on the fluid by the addition of twists. The first effect is the swirl induced in the fluid. Figure 6 shows the swirl velocity imparted to the fluid due to the twists. It can be observed that the magnitude of swirl velocity is greater for fluid that is further away from the centreline of the mixing channel. The mixing is observed to happen well in regions away from the centreline of the mixing channel. This is attributed to



**Fig. 4** Mixing index comparison of current simple T-mixer (STM) with existing literature

the increased swirl in those regions. Because of this swirl velocity imparted the fluid particles, they travel a greater distance while traversing through the outlet channel than that of STM. This is shown in Fig. 7. The second effect is analogous to that observed in 2D fluid analysis for wavy outlet channel conducted by Mondal et al. [5]. We can see this effect manifesting when we observe the surface streamlines longitudinal to the outlet channel as shown in Fig. 8. The MI along the outlet channel at different Reynold’s numbers is shown with the help of Fig. 9.

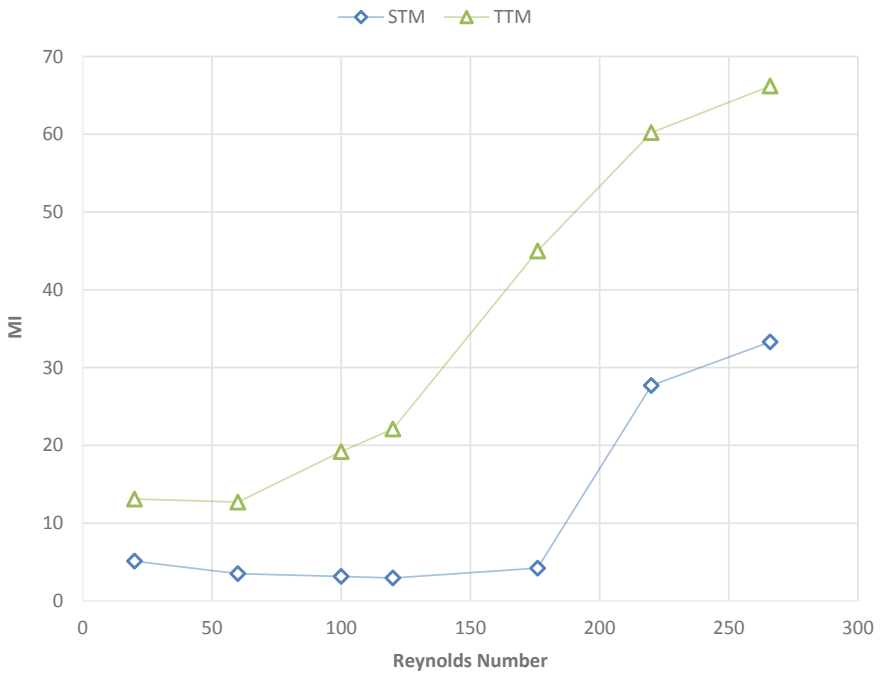
Figure 10 plots the pressure drop ( $\Delta P$ ) for STM and TTM. It can be observed that the increase in pressure drop for TTM is only marginal (13.73% at RE = 266) considering the gain in mixing performance (99.8% gain at RE = 266).

## 4 Conclusions

A study involving computer simulation to propose a new design for a micromixer is presented. A T-mixer with a twisted outlet channel has been investigated. The geometry was created by sweeping the outlet cross-section along a helix. This allowed for the maintenance of a constant area of cross-section along the mixing channel. For

**Table 4** Mixing indices at different Reynolds numbers

Inlet velocity (m/s)	Reynolds number (outlet channel)	Mixing index (MI)	
		Simple T-micromixer (%)	Twisted T-micromixer (%)
0.15	20	5.12	13.1
0.45	60	3.51	12.71
0.75	100	3.15	19.2
0.90	120	2.95	22.1
1.33	176	4.21	45
1.66	220	27.7	60.21
2.00	266	33.3	66.2



**Fig. 5** Comparison of mixing index for TTM and STM for different Reynolds numbers

this study, a helix of an axial length of 3000  $\mu\text{m}$  with two revolutions was selected. A rectangular cross-section of hydraulic diameter of 133.33  $\mu\text{m}$  was chosen for this study and was compared against a simple T-mixer of the same cross-section and axial length. The computational methodology adopted has been validated with results from previous literature. The simulation work done indicates that the application of twisted T-micromixer (TTM), as opposed to simple T-micromixer (STM), provided increased

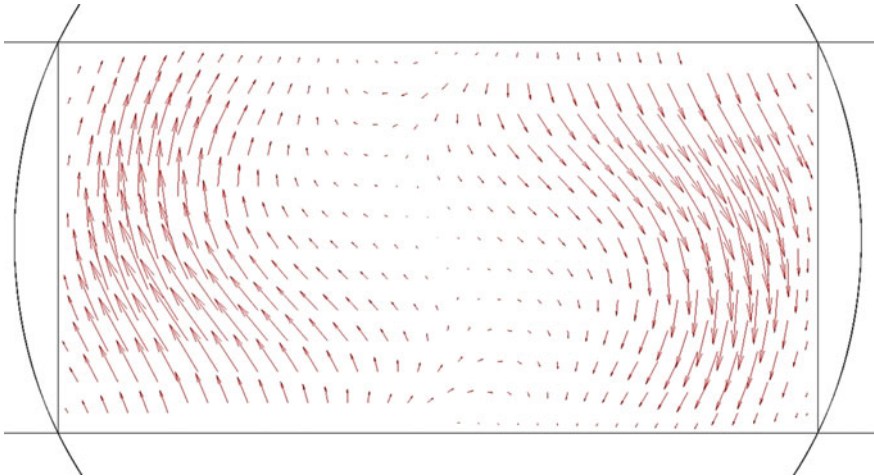


Fig. 6 Swirl velocity vectors at outlet of microchannel

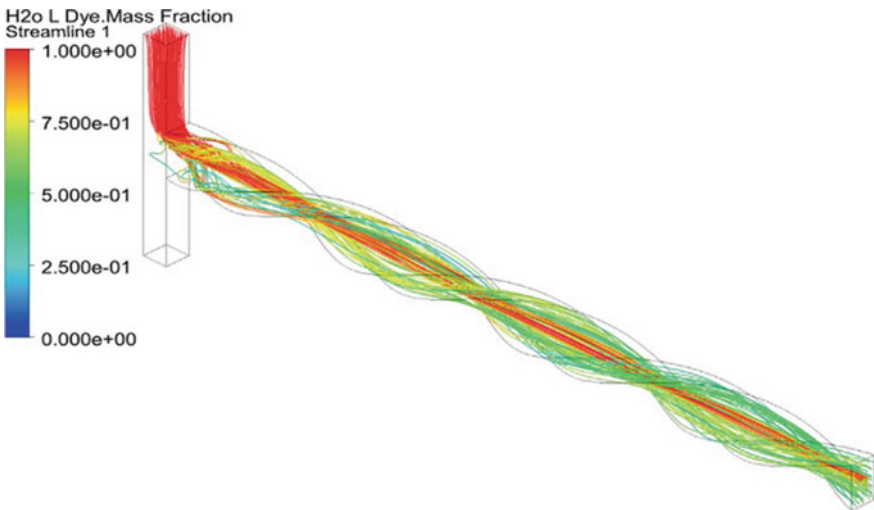
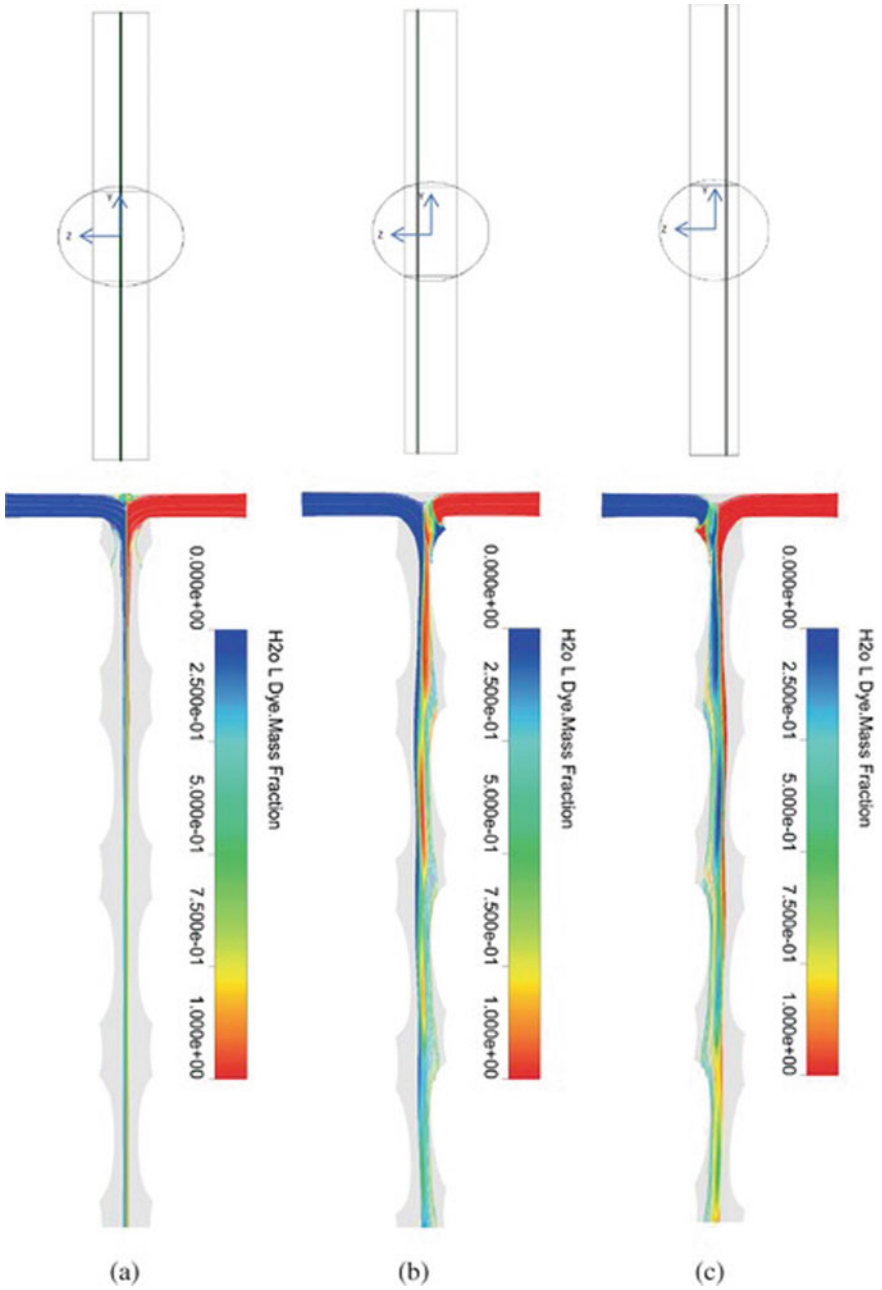


Fig. 7 Streamlines of "water-dye" only. Colour signifies concentration

mixing primarily due to the induction of swirl to the fluid by the twisted geometry. Consequently, there is an increase in the pressure drop along the micromixer although, the increase in mixing index is much more significant compared to the increase in the pressure drop. Using TTM is particularly beneficial at low Reynolds numbers since STM offers significant mixing only after entering the engulfment regime at the junction of the micromixer.





**Fig. 8** Selected planes and their respective surface streamlines alongside them for  $RE = 266$ . **a** Plane 1 ( $Z = 0 \mu\text{m}$ ). **b** Plane 2 ( $Z = 25 \mu\text{m}$ ). **c** Plane 3 ( $Z = -25 \mu\text{m}$ )

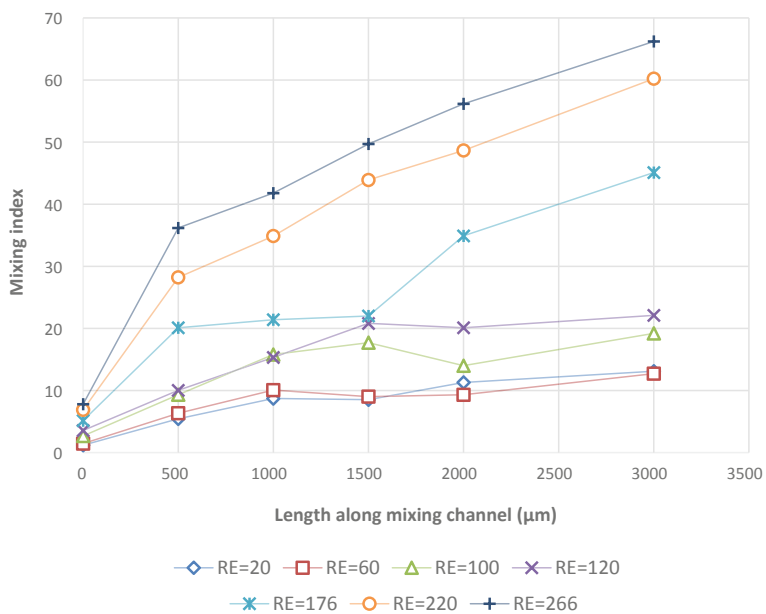


Fig. 9 MI at various sections along the outlet of the channel for TTM

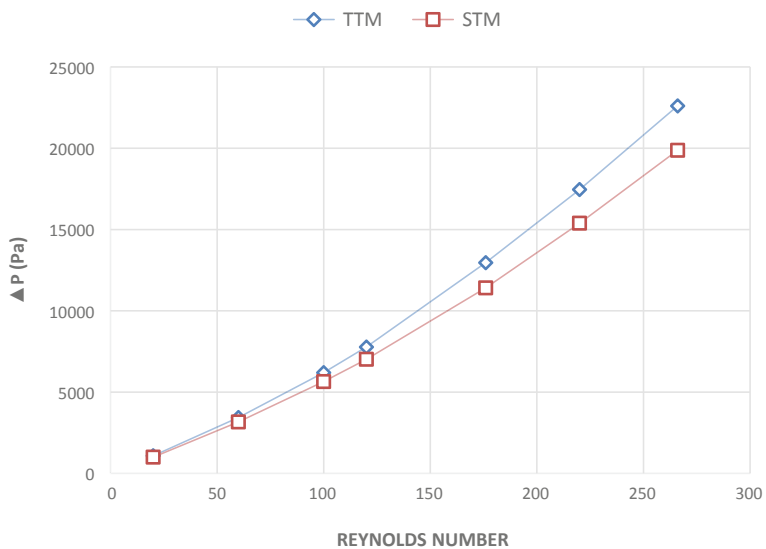


Fig. 10  $\Delta P$  versus RE of STM and TTM

The present work can be extended further by selecting a different number of twists and different aspect ratios for the outlet channel. Their effect on flow at different Reynolds numbers can be studied. This will further strengthen the results presented in this study. Further, study can be done on the mixing characteristic of the new design and its various possible iterations stated above with non-Newtonian fluids which would be much more relevant to the practical applications of the microfluidic device as shown in the work by Tokas et al. [25, 26].

## References

1. Afzal K, Kim KY (2012) Passive split and recombination micromixer with convergent-divergent walls. *Chem Eng J* 203:182–192
2. Afzal K, Kim K (2015) Convergent–divergent micromixer coupled with pulsatile flow. *Sens Actuators B: Chem* 211:198–205
3. Afzal K, Kim KY (2015) Multi-objective optimization of a passive micromixer based on periodic variation of velocity profile. *Chem Eng Commun* 202:322–331
4. Haghghinia A, Movahedirad S (2019) Fluid micro-mixing in passive microchannel: comparison of 2D and 3D numerical simulation. *Int J Heat Mass Transf* 139:907–916
5. Mondal B et al (2019) Numerical study of mixing in wavy micromixers: comparison between racoon and serpentine mixer. *Chem Eng Process: Process Intensification* 136:44–61
6. Bokenkamp D et al (1998) Microfabricated silicon mixers for sub-millisecond quench-flow analysis. *Anal Chem* 70:232–236
7. Cortes-Quiroza CA et al (2017) Effect of channel aspect ratio of 3-D T-mixer on flow patterns and convective mixing for a wide of Reynolds number. *Sens Actuators B: Chem* 12:3263
8. Jeong GS et al (2010) Applications of micromixing technology. *Analyst* 135(3):460–473
9. Lee CY et al (2011) Microfluidic mixing: a review. *Int J Mol Sci*
10. Hossain S et al (2017) A micromixer with two-layer serpentine crossing channels having excellent mixing performance at low Reynolds numbers. *Chem Eng J* 327:268–277
11. Hossain S et al (2010) Numerical study of mixing performance in straight groove micromixer. *Int J Fluid Mach Syst* 227–234
12. Chung CK et al (2010) Design and mixing efficiency of rhombic micromixer with flat angles. *Microsyst Technol* 16(8–9):1595–1600
13. Lob P et al (2004) Steering of liquid mixing speed in interdigital micromixers—from very fast to deliberately mixing. *Chem Eng Technol* 27:340–345
14. Ansari MA, Kim KY (2010) Mixing performance of unbalanced split and recombine micromixers with circular and rhombic sub-channels. *Chem Eng J* 162:760–767
15. Prakash R., Zunaid M, Samsheer (2021) Simulation analysis of mixing quality in T-junction micromixer with bend mixing channel. *Mater Today: Proc*
16. Ward K, Fan ZH (2015) Mixing in microfluidic devices and enhancement methods. *J Micromech Microeng* 25
17. Wang L et al (2013) Numerical and experimental investigation of mixing characteristics in the constructal tree-shaped microchannel. *Int J Heat Mass Transfer* 67:1014–1023
18. Chung K, Shih TR (2008) Effect of geometry on fluid mixing of the rhombic micromixers. *Microfluid Nanofluid* 4:419–425
19. Orsi G et al (2013) Water-ethanol mixing in T-shaped microdevices. *Chem Eng Sci* 95:174–183
20. Hardt S et al (2005) Passive micro-mixers for applications in the microreactor and  $\mu$ TAS fields. *Microfluid Nanofluid* 2:108–118
21. Engler M et al (2004) Numerical and experimental investigations on liquid mixing in static micromixers. *Chem Eng J* 101(1):315–322

22. Bothe D et al (2008) Computation of scales and quality of mixing in a T-shaped microreactor. *Comput Chem Eng* 32(1–2):108–114
23. Dundi TM et al (2019) Numerical evaluation of swirl effect on liquid mixing in a passive T-micromixer. *Aust J Mech Eng*
24. Jafari O et al (2015) Liquid-liquid extraction in twisted micromixers. *Chem Eng Process*
25. Tokas S, Zunaid M, Ansari MA (2021) Numerical investigation of the performance of 3D-helical passive micromixer with Newtonian fluid and non-Newtonian fluid blood. *Asia-Pac J Chem Eng* 16
26. Tokas S, Zunaid M, Ansari MA Non-Newtonian fluid mixing in a three-dimensional spiral passive micromixer. *Mater Today: Proc*

# Numerical Investigation of T-Micromixer with Twisted Outlet Channel for Non-newtonian Fluid



B. Lohit Nagarjun Reddy and M. Zunaid

**Abstract** The current study seeks to add to previous work done to analyse the mixing characteristics of T-micromixers with twisted outlet channel. The non-Newtonian fluid used for this study is blood. The results obtained are compared with those obtained for blood flow in simple T-micromixer. The Carraeu–Yasuda model has been utilised to simulate the viscous behaviour of blood. For this study, the outlet of the T-micromixer has two twists and a characteristic dimension of 133.33  $\mu\text{m}$ . The mixing characteristics have been observed for flow rates ranging from 0.0029 to 0.015 kg/h.

**Keywords** Computational fluid dynamics · Passive micromixer · Mixing performance

## 1 Introduction

The mixing of fluids in the case of channels of micrometre scale is critical. Microchannels are utilised in places like lab-on-chips and micro-total analysis systems. Its application includes sample preparation, biological and chemical synthesis [1–4].

Laminar flow is dominant in the case of fluid flow through microchannels. This means that the system lacks turbulent fluctuations present in macro-scale channels, which help in the homogeneous mixing of two or more fluid streams. Therefore, ensuring that the implemented design of the microchannel is capable of providing sufficient mixing is of utmost importance. Due to the absence of turbulence, mixing is dependent on molecular diffusion only. Molecular diffusion depends on the area of contact between the fluid streams.

---

B. Lohit Nagarjun Reddy (✉) · M. Zunaid  
Department of Mechanical Engineering, Delhi Technological University, Delhi, India  
e-mail: [reddy.lohit.97@gmail.com](mailto:reddy.lohit.97@gmail.com)

© The Author(s), under exclusive license to Springer Nature Singapore Pte Ltd. 2024  
R. P. Singh et al. (eds.), *Advances in Modelling and Optimization of Manufacturing and Industrial Systems*, Lecture Notes in Mechanical Engineering,  
[https://doi.org/10.1007/978-981-19-6107-6\\_8](https://doi.org/10.1007/978-981-19-6107-6_8)

Micromixers can be broadly categorised into active and passive mixers. Active micromixers are primarily reliant on external sources of excitation to facilitate mixing. The source of excitation could be based on magnetic, electric or pressure-related phenomena. One example could be the use of pulsating pressure at the inlet. Another could be providing a vibrating device contained in the channel which would provide the necessary excitation. Passive micromixers on the other hand have to make do with the flow energy imparted to the fluid for adequate mixing. They usually use intricate designs of channels that could potentially generate vortices and increase the area of contact between the two fluid streams which in turn increases the molecular diffusion-based mixing.

Earlier work on examining mixing characteristics of microchannels was based on experimental analysis [5, 6]. With the increasing ability of modern computers to simulate the flow characteristics for such scenarios, work on micromixers has moved towards CFD-based results with experimental observations saved for the validation stage. This has significantly reduced the time and resources required for the tasks.

A popular design for passive micromixer is the T-micromixer which consisted of two inlet channels opposed to each other and a single outlet channel perpendicular to both the inlets. Soleymani et al. [7] concluded in their study of simple T-micromixer that the intensity of the vortices generated is dependent on the geometrical characteristics like aspect ratio and the flow rates. Engler et al. [8] observed the occurrence of three flow regimes in T-micromixer, starting from laminar flow regime at low Reynolds number. With increasing Reynolds number, the flow entered the vortex regime followed by the engulfment regime where significant mixing was achieved. Prakash et al. [9] introduced a bend in the outlet channel of the T-micromixer and found it to give improved mixing performance with a small penalty in the form of increased pressure drop.

Inducing stirring transverse to the flow direction has been found to be an easy method to intensify the mixing process [10]. A micromixer with a wavy structure was an examination by Solehati et al. [11], and it was found that the new structure led to the formation of dean vortices which significantly improved mixing between two fluid streams [12]. Dundi et al. [13] observed that introducing a rotational component of velocity at the inlet led to better mixing performance, and the effect was more pronounced when the direction of the swirl was opposite in the two inlet channels.

Whilst most of the studies focused on the mixing behaviour of Newtonian fluids, most practical applications of micromixers use non-Newtonian fluids like blood. Tokas et al. [14] and Zunaid et al. [15] tested the mixing performance of a modification of T-micromixer in the form of a 3D helical outlet channel and found to gain mixing performance for both Newtonian and non-Newtonian fluids. Numerical simulations are conducted to investigate the mixing performance of non-Newtonian in the proposed T-micromixer with a twisted outlet channel. Jafari et al. [16] tested a T-micromixer whose outlet channel was physically twisted.

## 2 Methodology

### 2.1 Mathematical Modelling

Through the two inlets, two blood species are let in. Blood is non-Newtonian fluid (pseudoplastic fluid). To simulate its viscous behaviour, the Carraeu–Yasuda model is used [17]. The model is numerically solved with the help of equations of conservation of mass and momentum. The shear rate-dependent viscosity according to Carraeu–Yasuda model is given by:

$$\eta(\dot{\gamma}) = \eta_{\infty} + (\eta_0 - \eta_{\infty})[1 + \lambda(\dot{\gamma})^a]^{(n-1)/a} \quad (1)$$

In the above equation,  $n$ ,  $\eta_{\infty}$ ,  $\eta_0$ ,  $a$  and  $\lambda$  are flow index, infinite shear rate viscosity, zero shear viscosity, an empirical constant and characteristic relaxation time, respectively. From the existing work of Abraham et al. [18], the following values— $\dot{\gamma} = 8.2$  s,  $\eta_0 = 0.1600$  Pa s,  $n = 0.2128$ ,  $\eta_{\infty} = 0.0035$  Pa s and  $a = 0.64$  are taken.

The mixing process is governed by the following equation:

$$(V \cdot \nabla)c = D\nabla^2c \quad (2)$$

where  $c$  is the mass fraction of the fluid and  $D$  is the coefficient of diffusion

The efficiency of mixing at a cross-section and is indicated by the mixing index (MI) which is calculated as shown below:

$$MI = 1 - \sqrt{\frac{\int_A (c - \bar{c})^2 dA}{A \cdot \bar{c}(1 - \bar{c})}} \quad (3)$$

In the above equation,  $\bar{c}$  is the average concentration over the entire cross-sectional area, and  $c$  is the concentration of the sample point on the cross-section.

### 2.2 Numerical Modelling

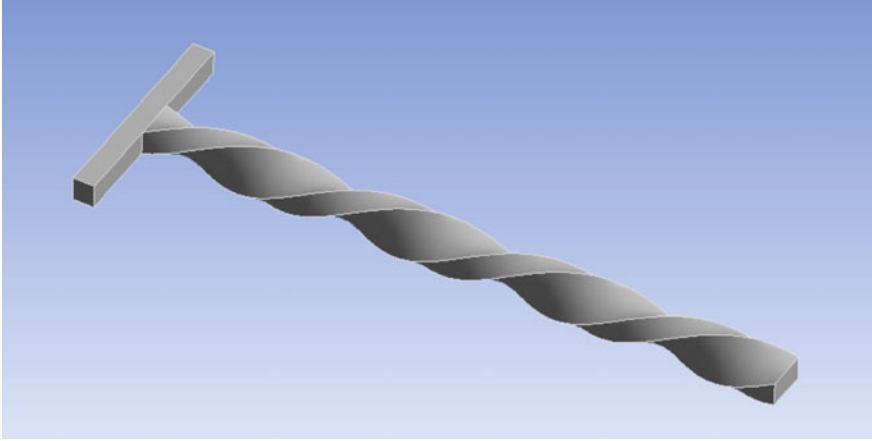
The model of the T-micromixer with the twisted channel was made using SOLIDWORKS 2020. The simulation was performed on ANSYS FLUENT 2020.

The outlet channel has two twists, i.e. the end of the outlet channel has been rotated by  $720^\circ$  with respect to the end connected to the inlets. The inlet channels have a cross-section of  $(100 \mu\text{m} * 100 \mu\text{m})$ , and the outlet channel has a  $(100 \mu\text{m} * 200 \mu\text{m})$ . A channel length of  $3000 \mu\text{m}$  is selected for the outlet channel. The aspect ratio is kept constant along the entire length of the outlet channel as shown in Fig. 1. Hexahedral mesh elements have been used as they create a much more uniform mesh with very

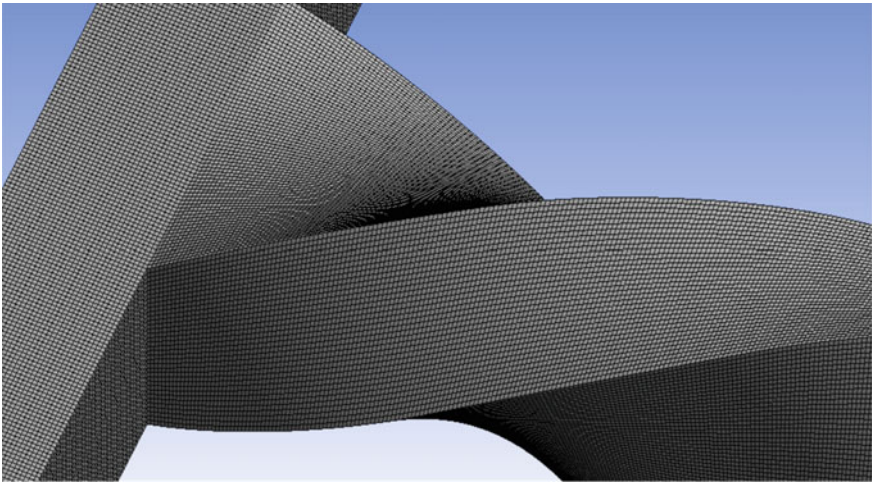
low skewness (maximum skewness = 0.265). Figure 2 shows the mesh created over the flow domain.

Two species of blood, namely “blood” and “blood\_dye” are introduced through the two inlets. The concentration at the inlet of “blood\_dye” is taken as one and that of “blood” is taken as zero.

The residual for solving continuity equation is taken as  $10^{-5}$ , and for momentum and species equation, it is taken as  $10^{-4}$ . The solutions methods employed are indicated in Table 1.



**Fig. 1** Geometry of T-micromixer with a twisted outlet channel



**Fig. 2** Hexahedral mesh at the junction of the micromixer



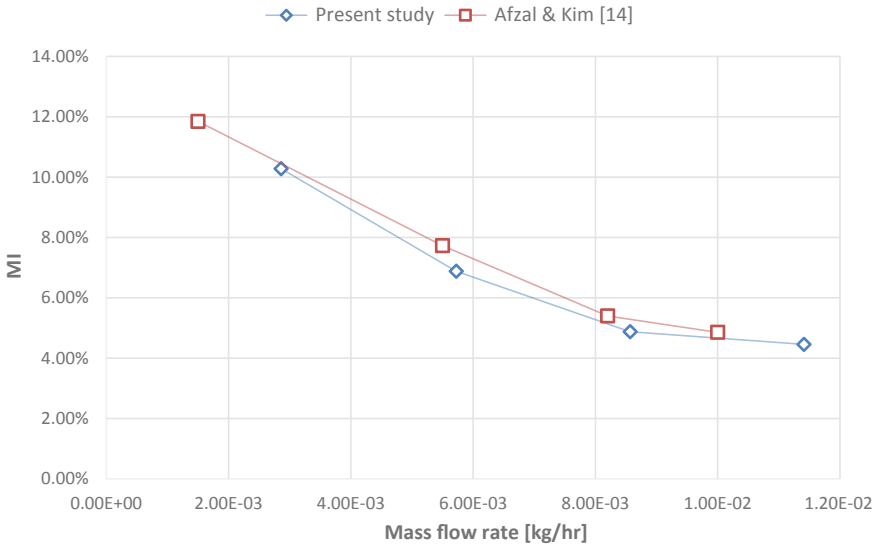
**Table 1** Solution methods employed

Pressure–velocity coupling	SIMPLEC
Pressure	Standard
Momentum	Second-order upwind
Species	Second-order upwind

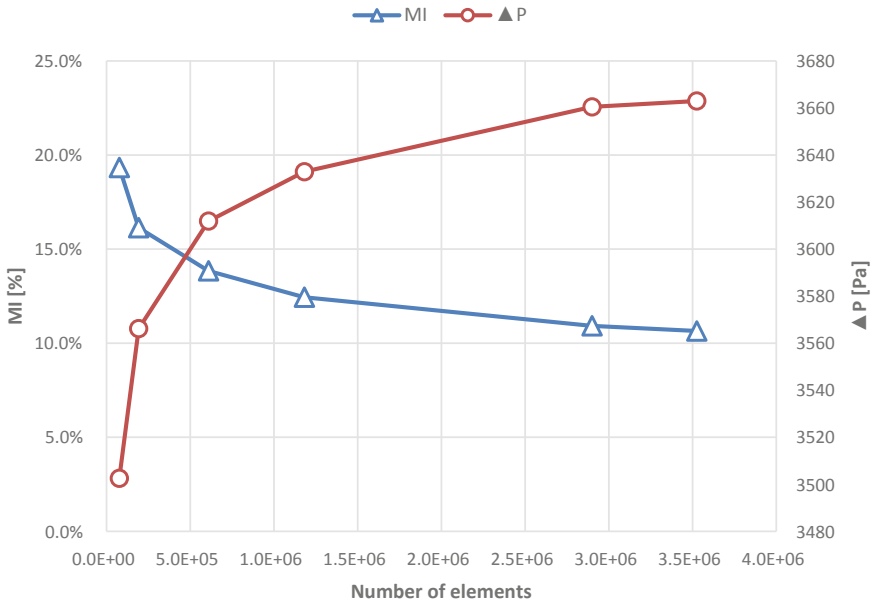
### 2.3 Validation of Computational Approach and Grid Independence

It is critical to make sure that the mathematical model imitates the real-life phenomena with accuracy. Therefore, validation needs to be done. In this case, the validation was performed with previous research of Afzal and Kim [19] which utilised Carraeu–Yasuda model to simulate the viscous behaviour of blood. Figure 3 shows the resemblance between the results of the present study and those of Afzal and Kim [19]. Seeing that the results of the present study closely replicate the results of Afzal and Kim [19], we can conclude that the mathematical model is sufficiently accurate and can be used for the study of T-micromixer with twisted outlet channel.

The computational grid generated must also be optimally refined to give sufficiently accurate results whilst not demanding huge computational resources and time. For that several simulations were run on a single set of boundary conditions with different elements sizes, and the influence of grid size on the MI and pressure drop ( $\Delta P$ ) was evaluated. It can be seen from Fig. 4 that the MI and  $\Delta P$  for element count greater than 3 million showed little variation with further increase in element



**Fig. 3** Comparison of MI of present study and results obtained by Afzal and Kim [19]



**Fig. 4** Grid independence test for T-micromixer with a twisted outlet channel

count. Therefore, an element count of 3.5 million was selected as it was within the bounds of the available computational capabilities, and the results obtained are grid independent. The above-mentioned selection for grid size allows for an element count good enough to provide satisfying results comparable to real-world behaviour whilst also providing the solution within reasonable time frame.

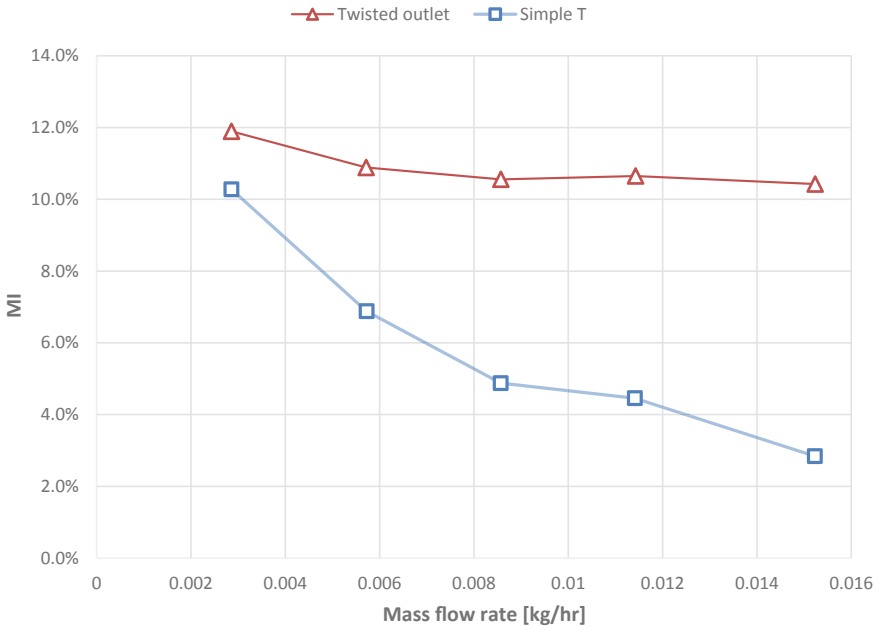
### 3 Results

Table 2 shows the inlet velocities for this study. A “no-slip” boundary condition has been applied to the walls of the micromixer, and a “pressure-outlet” boundary condition has been applied to the outlet of the micromixer. The corresponding mass flow rate of blood for the different inlet velocities has also been indicated in Table 2. Whilst Newtonian fluid flow is characterised using the Reynolds number, the same is not possible in case of non-Newtonian fluids. This is due to the constantly changing value of the viscosity of blood which leads to difficulty in determining the Reynolds number of flow at any particular cross-section. Hence, characterising fluid flow based on the mass flow rate through a certain section proves more useful.

It can be observed from Figs. 5 and 6 whilst the difference in  $\Delta P$  between the twisted outlet micromixer and simple T-micromixer is very small, there is an appreciable increase in MI in the case of twisted outlet micromixer with respect to simple

**Table 2** Inlet conditions studied

S. No	Axial velocity at inlets (m/s)	Mass flow rate (kg/h)
1	0.20	0.0152
2	0.15	0.0114
3	0.1125	0.0086
4	0.075	0.0057
5	0.0375	0.0029

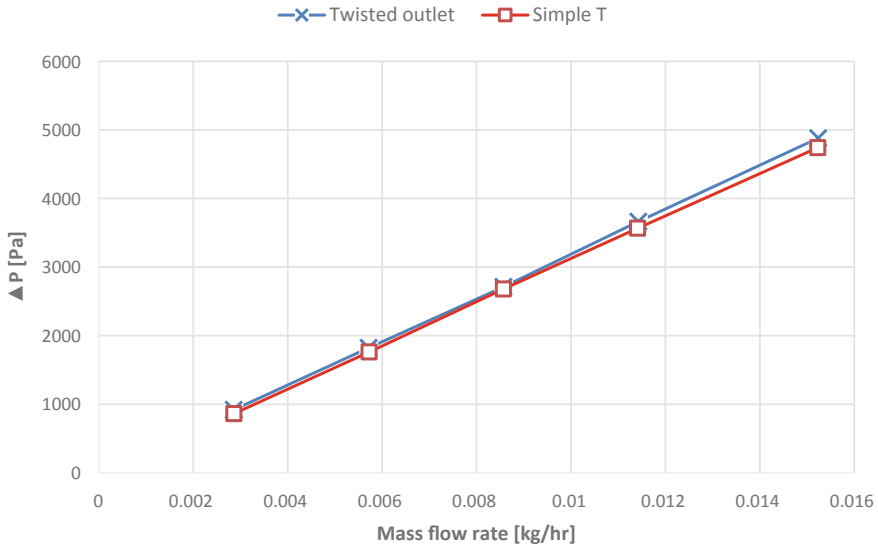


**Fig. 5** MI of T-micromixer with twisted outlet channel for different mass flow rates of blood

T-micromixer. From both Fig. 5 and Table 3, we can see that for the range of mass flow rates selected for our study the MI for twisted outlet micromixer is nearly constant whilst MI of simple T-micromixer is decreasing with an increase in the mass flow rate through the channel.

## 4 Conclusion

A study involving simulation of the behaviour of blood (non-Newtonian fluid) as it flows through a T-micromixer with a twisted outlet channel is presented. The Carraeu–Yasuda model was chosen to simulate the rheological behaviour of blood.



**Fig. 6**  $\Delta P$  for different mass flow rates of blood

**Table 3** Mixing indices at different Reynolds numbers

Mass flow rate (blood) (kg/h)	Mixing index (MI)	
	Simple T-micromixer (%)	Twisted T-micromixer (%)
0.0029	10.28	11.89
0.0057	6.88	10.88
0.0086	4.88	10.56
0.0114	4.46	10.65
0.0152	2.84	10.43

Validation of the selected model was carried out with the help of previous work done by Afzal and Kim [19], Boyd et al. [17]. The results obtained for micromixer with twisted outlet channel were weighed against with conventional T-mixer. It was found that for a minimal penalty in form of increased pressure drop, T-micromixer with twisted outlet channel provided better mixing performance when two bloodstreams were inducted from the two branches of the T-micromixer.

The present study can be extended further by using different non-Newtonian fluid and also by varying the number of twists and the length of the outlet channel. A wider range of mass flow rates may be studied as well.

## References

1. Jeong GS, Chung S, Kim CB, Lee SH (2010) Applications of micromixing technology. *Analyst* 135(3):460–473
2. Lee C, Fu L (2018) Recent advances and applications of micromixers. *Sens Actuators, B Chem* 259:677–702
3. Chew YT, Xia HM, Shu C (2007) Fluid micromixing technology and its applications for biological and chemical processes. In: 3rd Kuala Lumpur international conference on biomedical engineering 15:16–20
4. Nguyen NT, Wu Z (2005) Micromixers—a review. *J Micromech Microeng* 15(2)
5. Bothe D, Stemich C, Warnecke HJ (2006) Fluid mixing in a T-shaped micro-mixer. *Chem Eng Sci* 61(9):2950–2958
6. Bothe D, Stemich C, Warnecke HJ (2008) Computation of scales and quality of mixing in a T-shaped microreactor. *Comput Chem Eng* 32(1–2):108–114
7. Soleymani A, Kolehmainen E, Turunen I (2008) Numerical and experimental investigations of liquid mixing in T-type micromixers. *Chem Eng J* 135(SUPPL. 1)
8. Engler MN et al (2004) Numerical and experimental investigations on liquid mixing in static micromixers. *Chem Eng J* 101(1):315–322
9. Prakash R, Zunaid M, Samsheer (2021) Simulation analysis of mixing quality in T-junction micromixer with bend mixing channel. *Mater Today: Proc* <https://doi.org/10.1016/j.matpr.2021.03.172>
10. Hessel V, Löwe H, Schönfeld F (2005) Micromixers—a review on passive and active mixing principles. *Chem Eng Sci* 60(8–9 SPEC. ISS.):2479–2501
11. Solehati N, Bae J, Sasmito AP (2014) Numerical investigation of mixing performance in microchannel T-junction with wavy structure. *Comput Fluids* 96:10–19
12. Balasubramaniam L, Arayanarakool R, Marshall SD, Li B, Lee PS, Chen PCY (2017) Impact of cross-sectional geometry on mixing performance of spiral microfluidic channels characterized by swirling strength of Dean-vortices. *J Micromech Microeng* 27(9). <https://doi.org/10.1088/1361-6439/aa7fc8>
13. Dundi TM et al (2019) Numerical evaluation of swirl effect on liquid mixing in a passive T-micromixer. *Aust J Mech Eng*. <https://doi.org/10.1080/14484846.2019.1626527>
14. Tokas S, Zunaid M, Ansari MA (2021) Non-Newtonian fluid mixing in a three-dimensional spiral passive micromixer. *Mater Today: Proc*. <https://doi.org/10.1016/j.matpr.2021.03.656>
15. Zunaid M, Tokas S, Ansari MA (2021) Numerical investigation of the performance of 3D-helical passive micromixer with Newtonian fluid and non-Newtonian fluid blood. *Asia-Pac J Chem Eng* 2021(16):e2570. <https://doi.org/10.1002/apj.2570>
16. Jafari O et al (2015) Liquid-liquid extraction in twisted micromixers. *Chem Eng Process* 101:33–40
17. Boyd J, Buick JM, Green S (2007) Analysis of the Casson and Carreau-Yasuda non-Newtonian blood models in steady and oscillatory flows using the lattice Boltzmann method. *Phys Fluids* 19(9). <https://doi.org/10.1063/1.2772250>
18. Abraham F, Behr M, Heinkenschloss M (2005) Shape optimization in steady blood flow: a numerical study of non-Newtonian effects. *Comput Methods Biomech Biomed Eng* 8(2):127–137. <https://doi.org/10.1080/10255840500180799>
19. Afzal A, Kim KY (2014) Flow and mixing analysis of non-Newtonian fluids in straight and serpentine microchannels. *Chem Eng Sci* 116:263–274

# To Study the Effect of Electromagnetic Forces on WIRE Electrochemical Discharge Machining



Yajush Walia and Sarbjit Singh

**Abstract** Some composites with their extraordinary properties are acquiring importance in different industries, i.e., aerospace, defense organization, and many more. The machining of such composites is challenging and sometimes impractical by conventional machining processes. Wire electrochemical discharge machining which is a combined form of wire electric discharge machining and electrochemical machining has the potential to machine non-conducting materials victoriously. In the present study, an electromagnet is used to generate the magnetic lines during the process. The investigation demands an understanding of the removal of material and radial overcut of fabricated WECDM setup for machining of SiC-based PMC. The effect of input parameters (duty cycle, electrolyte concentration, wire feed) was analyzed on the SiC PMC. A comprehensive experimental study was designed and conducted using Taguchi's L9 orthogonal array.

**Keywords** Electromagnet · Electrolyte · Magnetic field intensity · Sparking zone

## 1 Introduction

Advancements in the region of different innovative fields have prompted the utilization of engineering design materials, for example, silicon carbide-based composite, quartz, and so forth machining of these high-level designing materials has been a significant issue for present-day machining ventures as the vast majority of products are non-conducting. The requirement of non-conducting materials in various designing applications has been increasing. Silicon carbide composite has been treated as the reasonable turn-out material for such kinds of use. It was hard to machine SiC composite by customary machining in the light of its non-conductive nature. WECDM process considers a helpful process for slicing non-conducting materials having high resistance.

---

Y. Walia (✉) · S. Singh

Department of Mechanical Engineering, Punjab Engineering College, Chandigarh, India  
e-mail: [yajushwalia@gmail.com](mailto:yajushwalia@gmail.com)

## 2 Research Background

In 1988, it was suggested that the electrolyte co-axial flow instead of perpendicular flow El Hofy and McGeough [1]. In 1991, It was recommended that a plate of graphite instead of a plate of copper as the anode (positive terminal) to prevent electrolyte dissolution of copper Jain et al. [2]. In 1994, appropriate controlling of wire feed rate during slicing of ceramics or carbon fiber epoxy composites with TW-ECSM, this will help in the improvement of quality of machining and thus minimizes the arcing Singh et al. [3]. Bhattacharyya B et al. recommended that as the increase in the machining voltage takes place, increase the machining current also and responsible for the increase in the current density. In 2016, Rattan N et al. worked on the possibilities of employing magnetic field in the TW-ECSM process to improve material removal rate for the impact of electrolytes. In Rattan and Mulik [4] performed TW-ECSM in the presence of magnetic field and reported an improvement in MRR in the range of 9–200% for varying process parameter combinations also reported a reduction in discharge current values in the presence of the magnetic field. They reported that the induced Lorentz force provides motion of ions, which provides magneto hydro-dynamic (MHD) convection. Thus, improved circulation in the narrow gap between tool and workpiece is ensured. The use of tungsten wire till now is very little for this process. In the current research work, a wire (diameter 0.25 mm) has been used to study the effect of using a magnetic field force during WECDM. Magnetic field-assisted WECDM is the latest and inexpensive technique that may be applied for the machining of various non-conducting advanced materials, which cover different kinds of ceramics and composites. The current technique of magnet-assisted WECDM setup is easy, manageable, and needs no significant changes in the TW-ECDM machining setup. The experimentation details of the WECDM are following.

## 3 Inspiration and Problem Formulation

In the current situation, the demand for 3D composites has become very popular due to their good mechanical properties, for example, resistance against impact damage. These refine properties facilitate to enhance their utility in the area of defense, nuclear technology and automobile industries, and many more. For building such micro-level materials of 3D composite, the WECDM played a vital role due to process ability. Moreover, various research has been revealing that using a magnetic field during the process may increase preciseness. Therefore, the problem is formulated and states as “Study the effect of Electromagnetic forces on WIRE Electrochemical Discharge Machining.” Thus, using Taguchi’s L9 orthogonal array, tests were done for micro-slicing of SiC-based [5–8] polymer composites with input process parameters such as electrolyte concentration, duty cycle, and wire feed rate. The radial overcut and

MRR was considered as output quality parameters. Moreover, the experiment has been conducted in the presence and absence of magnetic field lines.

### 4 Fabricated Setup and Electromagnet

The experimental analysis of the non-conductive SiC-based composite material was performed using WECDM-fabricated setup. The machining container was made up of ABS material because of its corrosion resistant. The container model design is firstly made in SOLIDWORKS software; then, fabrication of the container is taking place in a 3D printer. The auxiliary electrode used was a flat rectangular copper plate of size 130 mm × 50 mm × 3 mm was placed in the machining container. This auxiliary copper electrode of a rectangular shape in the machining process was used as an anode. A tungsten wire of a diameter of 250 μm was acted as the cathode in the machining process. Four pulleys were made up of Teflon material which holds the ability of non-conducting and non-reacting. The DC supply can be operated between 0 and 100 V, and the current has a maximum value of 10 A. The negative end of the DC supply is connected with the tool electrode. The positive end of the supply is connected with an auxiliary electrode which is of copper plate material. The supply of electrolyte takes place from a reservoir and through a pump electrolyte is directly supplied to the sparking zone (between wire and workpiece) such that stagnation of debris doesn't occur. During the experiment, the electrolyte used is NaOH because of its highly basic and more dissociation power. In the fabricated setup, an electromagnet was used which has been placed inverted and can be moved vertically upward and downward as per the requirement during the experiment. A digital gauss meter was used to check the magnetic flux intensity of the electromagnet which comes out to be 0.4 T at the tip of it. The electronic control unit circuit was used which provides the DC power supply to the electromagnet having a current value of 1.92 A. A triangular wedge-type shape of mild steel is used over which number of copper coils has been rolled contains several turns approximately equal to 450. Table 1 demonstrates the specification and explanation of electromagnet (Figs. 1 and 2).

As the current is flowing through several coils, then magnetic field lines come perpendicular to the flow of current. It has been observed that as the distance from the tip increases the value magnetic flux intensity decreases. The direction of the magnetic field is based on the right-hand rule which is shown in Fig. 3.

**Table 1** Specification and explanation of electromagnet

Material	Shape	The intensity of the magnetic field	Number of turns of copper coil
Mild steel	Triangular wedge	0.4 T Gauss meter	450 approximate



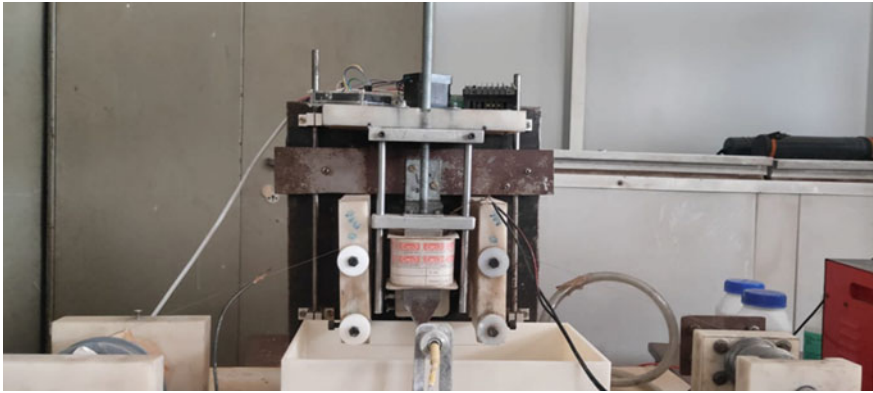


Fig. 1 View of the WECDM process

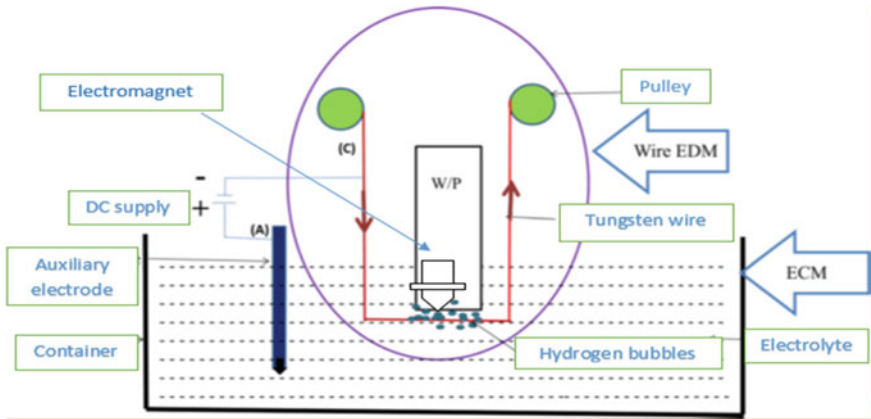


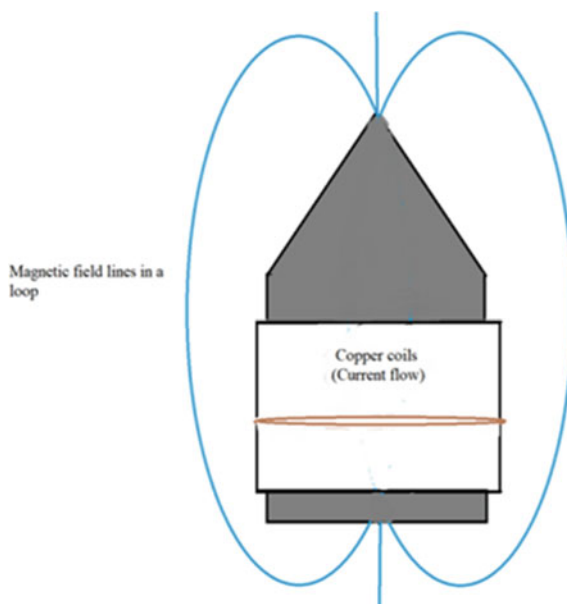
Fig. 2 Schematic representation of the WECDM process

### 5 Input Parameters for Machining

The input parameters and their levels utilized for the machining are shown in Table 2. All the parameters and their ranges were selected based on literature review, constraints in the setup, and pilot experiment (Table 3).

### 6 Experimental Procedure

In the current research, magnetic field lines were given with the assistance of an electromagnet magnet (0.40 T). The various input parameters with their levels have been

**Fig. 3** Direction of the magnetic field**Table 2** Input parameters and their levels

Input parameters	Units	Level 1	Level 2	Level 3
Duty cycle	%	60	70	80
Electrolyte concentration	Molarity	1.5	2	2.5
Wire feed rate	m/min	0.5	0.75	1

**Table 3** Material properties of SiC-based PMC

Workpiece material	Tensile yield (MPa)	Flexural strength (MPa)	Impact strength (J/cm)
PMC	136.49	31.8	7.5

demonstrated in Table 2. SiC-based PMC (Length 114 mm, width 22 mm, thickness 4.7 mm) was taken for the experimentation in the current research. Workpiece consists of properties that include tensile yield (136.49 MPa), flexural strength 31.8 (MPa), and impact strength (7.5 J/cm). These studies were conducted in two stages: Stage I was conducted without the use of a magnet, and stage II was conducted with the use of magnet field lines at the same input parameters with predefined values, as indicated in Table 2. In the beginning, each sample in the experiment was scheduled for a 5-min working period. To find material removal rate, semi-micro analytical balance was used having the least count 0.01 mg. To get accurate weights of the workpiece before and after the machining, every workpiece was sun-dried for 6 h before and after machining. To find radial overcut, Stereo Microscope was used with units set

at micrometers. The ZEISS STEMI305 Stereo Microscope was used for measuring the radial overcut. ZEISS STEMI305 has a magnification range of 8x–40x. From the pilot study on WECDM, it was noticed that the beginning of spark lies in the range of 32–36 V whereas the bubbles start forming at 25 V. The value of voltage remains constant during the experimentation which is 45 V. For wire feed rate which is taken as input parameter, it was observed that the breakdown of wire takes place if the value is less than 0.5 m/min. When the cable feed rate was more than 1 m/min, the spark fluctuation in spark was observed. Consequently, the wire feed rate value is ranging from 0.5 to 1 m/min, chosen to carry out the experimental work. Also, the other input parameters, i.e., duty cycle, electrolyte concentration, with values, were set in the range 60–80% and 1.5–2.5 M, as shown in Table 2. The experiments were carried out by taking NaOH as an electrolyte due to its high dissociation power. The output parameter was concluded as MRR and radial overcut [9–36].

In stage I experiment, parameter like voltage at 45 V and without electromagnetic field. There were three variable input factors varied at three different levels during the experiments. Table 4 shows the values of MRR and ROC obtained using the Taguchi L9 array (three-factor–three-level) as shown in Table 2.

In stage II experiments, parameters like voltage at 45 V, the current value for the electromagnet from the electronic circuit is 1.92 A, were kept constant and in the presence of magnetic field lines. There were three variable input factors varied at three different levels during the experiments. Table 5 shows the values of MRR and ROC obtained using the Taguchi L9 array (three-factor–three-level) as shown in Table 2.

**Table 4** Results for stage I (without electromagnet)

Duty cycle (A)	Electrolyte concentration (molarity) (B)	Wire feed rate (m/min) (C)	Mean MRR (mg/min)	Mean ROC ( $\mu\text{m}$ )	SN ratio for MRR	SN ratio for ROC
60	1.5	0.5	4.2	36.16	12.5062	–31.1646
60	2	0.75	7.43	52.2	17.4198	–34.3401
60	2.5	1	8.32	71.67	18.4025	–37.1067
70	1.5	0.75	12.03	52.8	21.6053	–34.4527
70	2	1	10.01	55	20.0087	–34.8073
70	2.5	0.5	11.33	89.3	21.0846	–39.0170
80	1.5	1	14.83	79.16	23.4228	–37.9701
80	2	0.5	23.43	31.33	27.3954	–29.9192
80	2.5	0.75	28.78	26	29.1818	–28.2995

**Table 5** Results for stage II (with electromagnet)

Duty cycle (A)	Electrolyte concentration (molarity) (B)	Wire feed rate (m/min) (C)	Mean MRR (mg/min)	Mean ROC ( $\mu\text{m}$ )	SN ratio for MRR	SN ratio for ROC
60	1.5	0.5	8.22	25	18.2974	-27.9588
60	2	0.75	9.88	12.4	19.8951	-21.8684
60	2.5	1	11.44	37.33	21.1685	-31.4412
70	1.5	0.75	14.33	17	23.1249	-24.6090
70	2	1	9.03	34.8	19.1133	-30.8316
70	2.5	0.5	12.37	62.83	21.8474	-35.9633
80	1.5	1	16.43	44.67	24.3123	-33.0003
80	2	0.5	25.44	35.16	28.1103	-30.9210
80	2.5	0.75	31.34	21	29.9220	-26.4444

## 7 Result Discussion

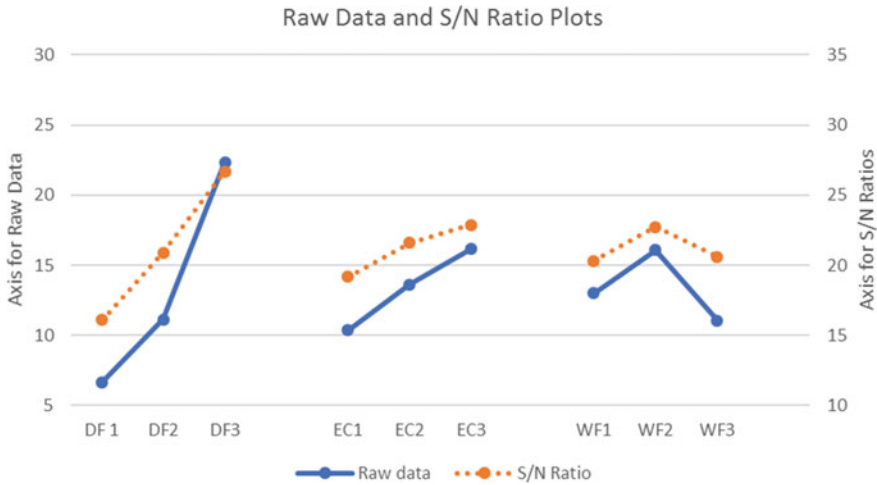
### 7.1 Material Removal Rate (MRR) Effect of Input Parameters for Stage I

The effect of input parameters on MRR is shown in Fig. 4. It has been found that MRR increases remarkably with a rise in the duty cycle. Since the voltage is fixed at 45 V, as the rise in duty cycle takes place from DF1 to DF2, i.e., 60 to 70%, then an increase in MRR is found from 6.657 to 11.123 mg/min., and from DF2 to DF3, i.e., 70 to 80%, the MRR increases as 22.347 mg/min. which is quite significant. 80% of duty cycle shows more contribution of electrode potential for the large time while machining. This causes an increase in the discharge of high thermal energy responsible for the increase in MRR.

MRR increases from 10.360 to 13.623 mg/min as electrolyte concentration increases from EC1 to EC2, i.e., 1.5 to 2 M and at EC3 (2.5 M). A higher concentration of electrolyte increases the available ions inside the electrolyte, which in turn increases the number of ions transported at the machining zone facilitating higher hydrogen bubble formation. Thus, responsible for more MRR.

This has been seen that MRR initially increased as an increase in WFR then demonstrates opposite direction. As the MRR rises from 12.993 to 16.080 mg/min, when an increased in the wire feed rate takes place from WF1 to WF2, i.e., 0.5 to 0.75 m/min.

The further rise in the value of the wire feed rate to WF3, i.e., 1 m/min drops the MRR to 11.053 mg/min. MRR initially rises due to fresh electrolyte available near the machining zone, which produces constant spark responsible for high MRR in the workpiece, i.e., at 1 m/min, MRR decreased because of variation of gas bubbles across the machining area. The fluctuations of hydrogen bubbles lead to a break in



**Fig. 4** Raw data and S/N ratio plots for MRR in stage I

**Table 6** ANOVA for MRR in stage I (without electromagnet)

S. No	Source	Adj SS	DOF	Adj MS	F-value	Contribution (%)
1	Duty factor	392.09	2	196.05	18.27	78.01
2	Electrolyte concentration	50.45	2	25.22	2.35	10.03
3	Wire feed rate	38.56	2	19.28	1.80	7.67
4	Error	21.46	2	10.73		4.27
5	Total	502.56	8			

the spark formation. This fluctuation of sparking creates stagnation of debris across machining zone. This decreases the MRR when the wire feed rate is 1 m/min.

As per the S/N ratio, optimal value for MRR is obtained at duty cycle 80%, electrolyte concentration 2.5 M, wire feed rate 0.75 m/min. A larger value of SN ratio better the quality characteristics since signal dominates more than noise.

Table 6 reveals that the contribution of the duty cycle is significant as compared to other input parameters. The duty cycle contributed 78.01% in MRR whereas the other two contributed 10.03% and 7.67%.

### 7.2 Material Removal Rate (MRR) for Stage II, i.e., in the Presence of Electromagnet Magnet

In the stage II experiment, an increase in MRR from 9.847 to 11.910 mg/min is seen when the duty cycle increased through DF1 to DF2, i.e., from 60 to 70%. From DF2

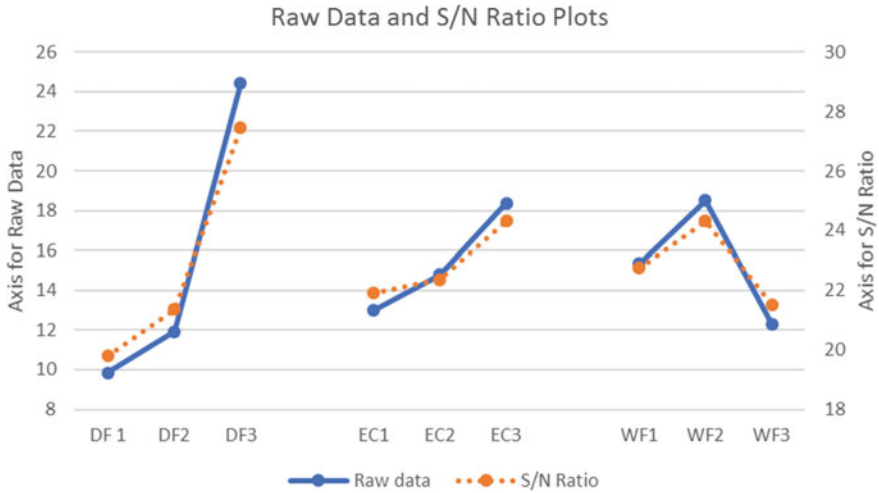


Fig. 5 Raw data and S/N ratio plots for MRR in stage II

to DF3, the MRR rose by 70 to 80%, resulting in a significant increase in MRR to 24.403 mg/min. As a result, when the electrolyte concentration increases from EC1 to EC2, i.e., 1.5 to 2 M, the value of MRR rises from 12.993 to 14.783, and 18.383 mg/min at EC3 (2.5 M).

MRR first rises as the wire feed rate (WFR) increases but eventually reverses direction. For example, when the wire feed rate is increased from WF1 to WF2, i.e., 0.5 to 0.75 m/min, the MRR increased through 15.343–18.517 mg/min (Fig. 5).

The MRR decreases to 12.300 mg/min when the wire feed rate is increased to WF3, which is 1 m/min.

### 7.3 Effect of Input Parameters on Radial Overcut

The effect of machining input factors over radial overcut is shown in Fig. 6. As the duty cycle increases through DF1 to DF2, i.e., 60 to 70%, radial overcut increased from 53.32 to 65.70 μm. Likewise, the additional increased for duty factor of DF3, viz., 80% decreases the radial overcut to 45.50 μm. The increase of duty factor, i.e., for a longer period spark increases radial overcut, but there are two factors on which the output factor depends may decrease the radial overcut at DF3.

Electrolyte concentration, increases from EC1 to EC2, i.e., 1.5 to 2 M there is little decrease in radial overcut which is 56.04–46.15 μm. Further increase in electrolyte concentration increases radial overcut.

The radial overcut decreases from 52.26 to 43.64 μm by increasing WFR through WF1 to WF2, i.e., 0.5–0.75 m/min.; radial overcut found 68.61 at WF3 (Table 7).

The contribution of wire feed rate is more significant for ROC.

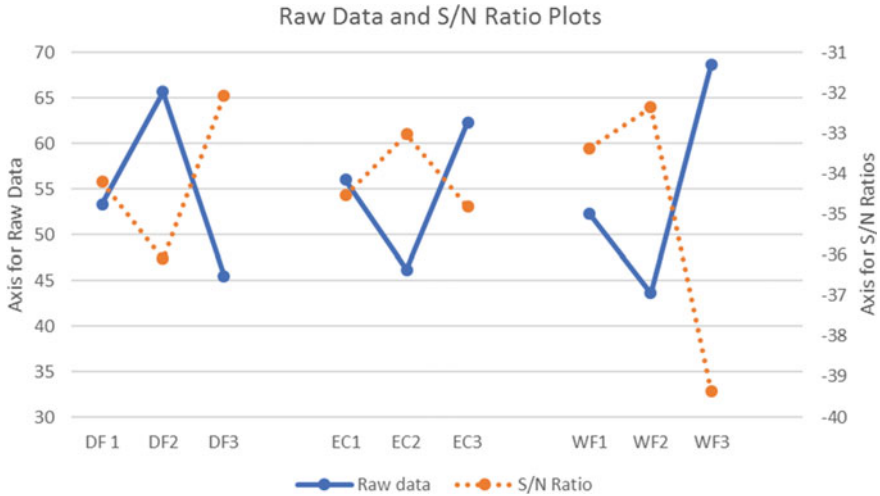


Fig. 6 Raw data and S/N ratio plots for ROC in stage I

Table 7 ANOVA for ROC in stage I

S. No	Source	Adj SS	DOF	Adj MS	F-value	Contribution (%)
1	Duty factor	422.5	2	211.2	1.10	18.42
2	Electrolyte concentration	524.5	2	262.25	1.37	22.87
3	Wire feed rate	965.1	2	482.5	2.53	42.08
4	Error	381.0	2	190.5		16.61
5	Total	2293.1	8			

### 7.4 In the Presence of an Electromagnet, Effect of Input Factors for Radial Overcut

Figure 7 depicts the effect of machining process factors for radial overcut. The radial overcut increases from 24.91 to 38.21 m when the duty cycle increased through DF1 to DF2, i.e., from 60 to 70%. Similarly, increasing the duty factor of DF3 to 80% reduces the radial overcut to 33.61 m.

Electrolyte concentration increases from EC1 to EC2, i.e., 1.5–2 M there is little decrease in radial overcut which is 28.89–27.45 μm. Further increase in electrolyte concentration increases radial overcut.

The radial overcut decreases from 41 to 16.80 μm with increased in WFR through WF1 to WF2, i.e., 0.5–0.75 m/min. At WF3, radial overcut increased to 38.93.

After the experimentation, the result has been calculated using two equipment. To find material removal rate, semi-micro analytical balance was used having the least count 0.01 mg. The ZEISS STEMI305 stereo microscope deployed for measuring radial overcut. From result table, it is noted that as per the S/N ratio, optimal value for

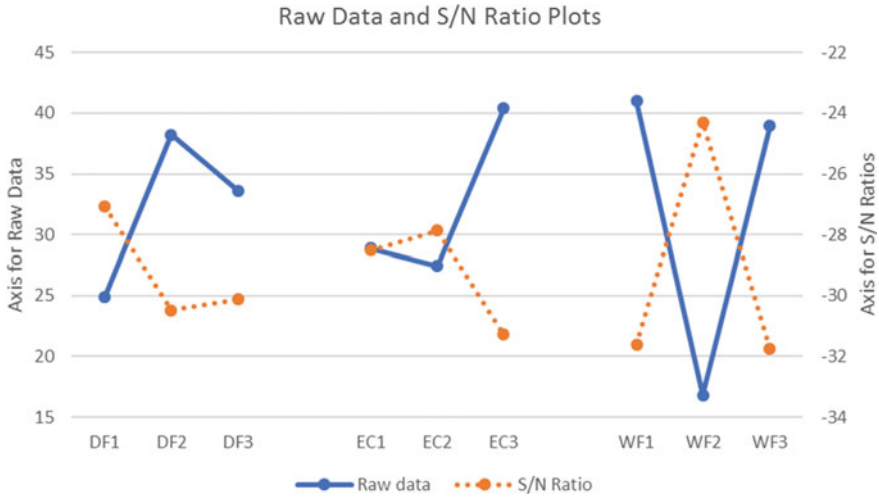


Fig. 7 Raw data and S/N ratio plots for ROC in stage II

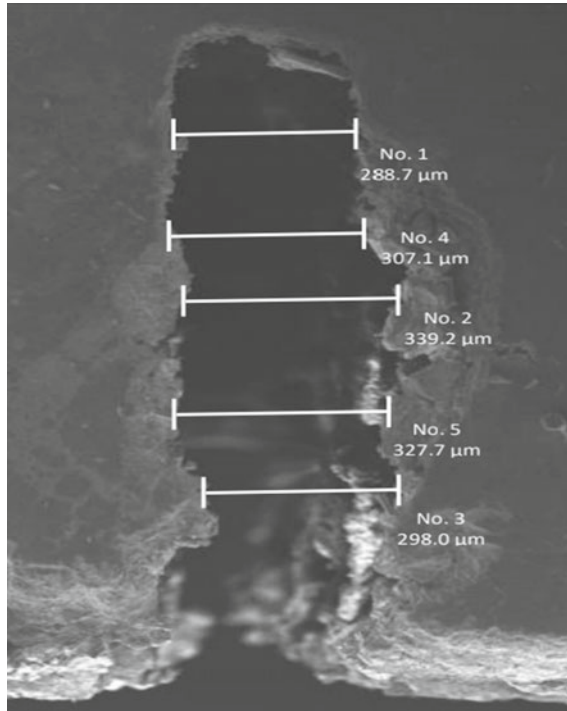
MRR is obtained at duty cycle 80%, electrolyte concentration 2.5 M, wire feed rate 0.75 m/min. A larger value of SN ratio better the quality characteristics since signal dominates more than noise. A comparison in the morphology has been observed between the machining in the absence of an electromagnet and the presence of an electromagnet. It has been also observed that using an electromagnet during machining increases the MRR and reduces the ROC. In Figs. 8 and 9, the morphology of the sample has been machined without of a magnetic field and the presence of a magnetic field.

## 8 Conclusion

### Stage I—Slicing of PMC

1. Slicing of polymer matrix composites was successfully performed keeping process parameters such as voltage at 45 V at a constant value. Duty factor, electrolytic concentrations, and WFR varied through 60–70–80, 1.5–2–2.5 M, and 0.5–0.75–1 m/min, respectively, using Taguchi L9 orthogonal array.
2. Duty factor has a huge significance in stage I for MRR with a contribution of 78.01%. The duty factor is a dominant factor that governs the intensity of the TW-ECDM process. As the duty factor increases, the set voltage is applied for a larger fraction of time that in turn increases the rate of generation of spark which facilitates in slicing of composite. Whereas, for radial overcut, the contribution of wire feed rate is highly significant, i.e., 42.08%.



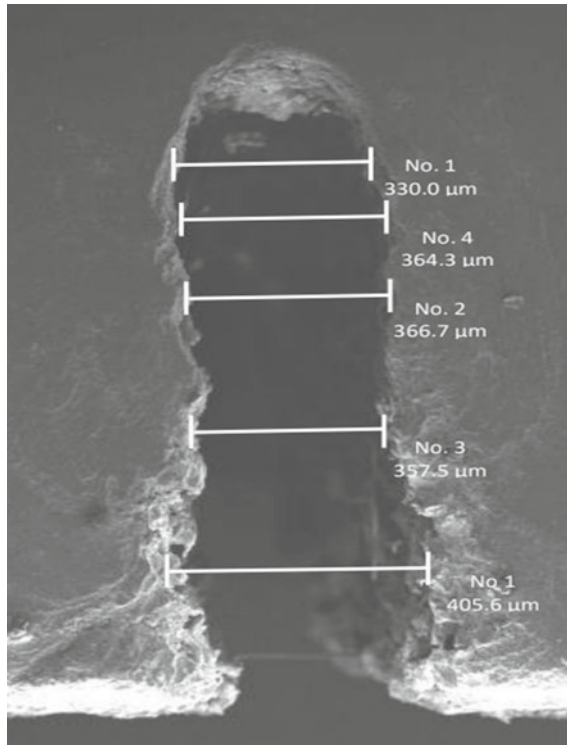


**Fig. 8** SEM of work material machined at the optimal conditions of Taguchi's technique at electrolyte concentration 1.5 M, WFR 0.75 m/min, and DC of 70% (with magnetic field)

3. From Taguchi analysis, the optimal input factors to MRR are duty factor 80, electrolyte concentration 2.5 M, wire feed rate 0.75 m/min, and NaOH as electrolyte.
4. From Taguchi analysis, the optimal input factors to ROC are duty factor 80, electrolyte concentration 2.5 M, wire feed rate m/min 0.75 m/min, and NaOH as electrolyte.
5. ANOVA for MRR in stage I at 95% confidence level reveals that MRR values are enormously affected by duty factor with a contribution of 78.01%. Electrolytic concentrations are the second significant factor with a 10.03% contributions. A third wire feed rate with a contribution of 7.67%.
6. ANOVA for ROC in stage I at 95% confidence level reveals that wire feed rate has a high significance with the contribution of 42.08%, and electrolytic concentrations are the second maximum significant factor by 22.87% contributions whereas duty factor has 18.42% contribution only.

#### **Stage II—Slicing of PMC in the presence of magnetic field**

7. Slicing of polymer matrix composites was successfully performed keeping process parameters such as voltage at 45 V at a constant value and magnetic



**Fig. 9** SEM of work material machined at the optimal condition of Taguchi’s technique at electrolyte concentration 1.5 M, WFR 0.75 m/min, and DC of 70% (without magnetic field)

flux intensity 0.4 T having a current-carrying coil of 1.92 A. Duty factor, electrolytic concentrations, and WFR varied through 60–70–80, 1.5 M–2 M–2.5 M, and 0.5–0.75–1 m/min, respectively, using Taguchi L9 orthogonal array.

8. Magnetic field lines reveal significant change especially in the radial overcut as an output factor that converges the multi-direction spark into a unidirectional spark. Due to which the value of radial overcut decreases. The comparison of experiment with and without magnetic field lines reveal how gradually radial overcut decreases in the presence of the magnetic field.
9. From Taguchi analysis, the optimal input factors to MRR are Duty Factor 80, Electrolyte concentration 2.5 M, and Wire feed rate 0.75 m/min.
10. From Taguchi analysis, the optimal input factors to ROC are duty factor 60, wire feed rate 0.75 m/min, and electrolyte concentration 2 M.
11. ANOVA for MRR at 95% confidence level reveals that MRR values are hugely affected by duty factor with a contribution of 73.77%, and wire feed rate is the second most significant factor with 11.49% contribution.

- ANOVA for ROC at 95% confidence level reveals that ROC values are also dominantly affected by wire feed rate with a huge contribution of 55.76%, and electrolytic concentrations are the second significant factor by a 15.57% contributions.

## 9 Future Scopes

- A study of thermal cracks, surface roughness, and heat-affected zones in TW-ECDM can be done.
- The use of different wires with different surface textures and different materials and their effects on overcut and MRR can be studied in the WECDM process.
- Hybrid forms of TW-ECDM such as LASER-assisted TW-ECDM, ultrasonic vibration-assisted TW-ECDM can be studied.
- Environmental effects of the TW-ECDM, the study of fumes generated during the process, and ways to minimize the harmful effects if any can be studied.
- The effect of SiC particles of various sizes on TW-ECDM output parameters can be studied.
- WECDM assisted with electromagnet has copper wire gets heated up. These copper coil's temperature can be controlled by using dielectric.

## References

- El Hofy H, McGeough JA (1988) Evaluation of an apparatus for electrochemical arc wire-machining. *ASME Trans J Eng Ind* 110(2):119–123
- Jain VK, Sreenivasa Rao P, Choudhary SK, Rajurkar KP (1991) Experimental investigations into traveling wire electrochemical spark machining (TW-ECSM) of composites. *J Eng Ind* 113(1):75–84
- Mitra NS, Doloi B, Bhattacharyya B (2015) Predictive analysis of critical yield during traveling wire electrochemical discharge machining of Hylam based composites. *Adv Produ Eng Manag* 10(2):73
- Rattan N, Mulik RS (2017) Experimental investigations and multiresponse optimization of silicon dioxide (quartz) machining in magnetic field assisted TW-ECSM process. *SILICON* 9(5):663–673
- Mudhukrishnan M, Hariharan P, Palanikumar K (2020) Measurement and analysis of thrust force and delamination in drilling glass fiber reinforced polypropylene composites using different drills. *Measurement* 149:106973
- Peng WY, Liao YS (2004) Study of electrochemical discharge machining technology for slicing non-conductive brittle materials. *J Mater Process Technol* 149(1–3):363–369
- Yang CT, Song SL, Yan BH, Huang FY (2006) Improving machining performance of wire electrochemical discharge machining by adding SiC abrasive to electrolyte. *Int J Mach Tools Manuf* 46(15):2044–2050
- Malik A, Manna A (2016) An experimental investigation on developed WECSM during micro slicing of e-glass fibre epoxy composite. *Int J Adv Manuf Technol* 85(9–12):2097–2106

9. Kumar M, Vaishya RO, Oza AD (2019) Experimental Investigation of wire-electrochemical discharge machining (WECDM) performance characteristics for quartz material. *SILICON* 12:2211–2220
10. Singh T, Dvivedi A, Arya RK (2019) Fabrication of micro-slits using W-ECDM process with textured wire surface: an experimental investigation on kerf overcut reduction and straightness improvement. *Precis Eng* 59:211–223
11. Oza AD, Kumar A, Badheka V (2019) Traveling Wire electrochemical discharge machining (TW-ECDM) of quartz using zinc coated brass wire: investigations on material removal rate and kerf width characteristics. *SILICON* 11:2873–2884
12. Gupta PK, Dvivedi A, Kumar P (2016) Effect of pulse duration on quality characteristics of blind hole drilled in glass by ECDM. *Mater Manuf Process* 31(13):1740–1748
13. Cao XD, Kim BH, Chu CN (2009) Microstructuring of glass with features less than 100  $\mu\text{m}$  by electrochemical discharge machining. *Precis Eng* 33(4):459–465
14. Bhuyan BK, Yadava V (2012) Machining characteristics of borosilicate glass using traveling wire electrochemical spark machining (TW-ECSM) process. In: Proceedings of the national conference on trends and advances in mechanical engineering
15. Singh A, Jawalkar CS, Vaishya R, Sharma AK (2014) A study on wire breakage and parametric efficiency of the wire electrochemical discharge machining process. In: 5th international and 26th all India manufacturing technology, design and research conference (AIMTDR 2014) December 12th–14th, IIT Guwahati, Assam, India
16. Wüthrich R, Fascio V (2005) Machining of nonconducting materials using electrochemical discharge phenomenon-an overview. *Int J Mach Tools Manuf* 45(9):1095–1108
17. Bhuyan BK, Yadava V (2014) Modelling and optimization of travelling wire electro-chemical spark machining process. *Int J Ind Syst Eng* 18:139–158
18. Thakur A, Manna A, Samir S (2019) Multi-response optimization of turning parameters during machining of EN-24 steel with SiC Nano fluids based minimum quantity lubrication. *Silicon* 115
19. Jangra K, Grover S, Aggarwal A (2012) Optimization of multi machining characteristics in WEDM of WC-5.3% co composite using integrated approach of Taguchi, GRA and entropy method. *Front Mech Eng* 7(3):288–299
20. Goud M, Sharma AK, Jawalkar C (2016) A review on material removal mechanism in electrochemical discharge machining (ECDM) and possibilities to enhance the material removal rate. *Precis Eng* 45:1–17
21. Jain VK, Kumar P, Rajurkar KP (1990) Investigation into machining of composites. *Precis Eng* 12(4):227–238
22. Basak I, Ghosh A (1997) A mechanism of material removal in electrochemical discharge machining: a theoretical model and experimental verification. *J Mater Process Technol* 71(3):350–359
23. Nesarikar VV, Jain VK, Choudhury SK (1994) Traveling wire electrochemical spark machining of thick sheets of Kevlar-Epoxy composites. In: Proceedings of sixteenth all India manufacturing technology design and research conference, Bangalore, India. 672677
24. Jain VK, Adhikary S (2008) Mechanism of material removal in electrochemical spark machining of quartz under different polarity conditions. *J Mater Process Technol* 200:460–470
25. Chak SK, Rao PV (2007) Trepanning of Al<sub>2</sub>O<sub>3</sub> by electrochemical discharge machining (ECDM) process using abrasive electrodes with pulsed D.C supply. *Int J Mach Tools Manuf* 47:2061–2070
26. Rttan N, Mulik RS (2018) Experimental set up to improve machining performance of silicon dioxide (quartz) in magnetic field assisted TW-ECSM process. Springer Nature
27. Bhuyan BK, Yadava V (2013) Experimental modeling and multi-objective optimization of traveling wire electro-chemical spark machining (TW-ECSM) process. *J Mech Sci Technol* 27(8):2467–2476
28. Bhuyan BK, Yadava V (2014) Experimental modelling and multi-response optimization of travelling wire electrochemical spark machining of Pyrex glass. *Proc Inst Mech Eng Part B: J Eng Manuf* 228(8):902–916

29. Bhuyan BK, Yadava V (2014) Experimental study of traveling wire electrochemical spark machining of borosilicate glass. *Mater Manuf Processes* 29:298–304
30. Hajian M, Razfar MR, Movahed S (2016) An experimental study on the effect of magnetic field orientations and electrolyte concentrations on ECDM milling performance of glass. *Precis Eng* 45:322–331
31. Elhami S, Razfar MR (2017) Study of the current signal and material removal during ultrasonic-assisted electrochemical discharge machining. *Int J Adv Manuf Technol* 92(5–8):1591–1599
32. Raghuram V, Pramila T, Srinivasa YG, Narayanasamy K (1995) Effect of the circuit parameters on the electrolytes in the electrochemical discharge phenomenon. *J Mater Process Technol* 52:301–318
33. Solaiyappan A, Karuppan S (2015) Investigation of electro-chemical machining characteristics of 20MnCr5 alloy steel using potassium dichromate mixed aqueous NaCl electrolyte and optimization of process parameters. *Proc Inst Mech Eng, Part B: J Eng Manuf* 229(11):1984–1996
34. Kumar M, Vaishya RO, Suri NM et al (2021) An experimental investigation of surface characterization for zirconia ceramic using electrochemical discharge machining process. *Arab J Sci Eng* 46:2269–2281. <https://doi.org/10.1007/s13369-020-05059-4>
35. Oza AD, Kumar A, Badheka V, Arora A, Kumar M, Pruncu CI, Singh T (2021) Improvement of the machining performance of the TW-ECDM process using magnetohydrodynamics (MHD) on quartz material. *Materials* 14(9):2377
36. Kumar M, Satsangi PS (2021) A study on machining performance of wire electric discharge grinding (WEDG) process during machining of tungsten alloy micro-tools. *Sādhanā* 46(2):1–11. <https://doi.org/10.1007/s12046-021-01595-3>
37. Singh M, Singh S (2019) Electro chemical discharge machining: areview on preceding and perspective research. *Proc Inst Mech Eng B J Eng Manuf* 233(5):1425–1449
38. Liu Y, Wei Z, Wang M, Zhang J (2017) Experimental investigation of micro wire electrochemical discharge machining by using a rotating helical tool. *J Manuf Process* 29:265–271
39. Behera BA, Dash BP (2015) Mechanical behavior of 3D woven composites. *Mater Des* 67:261–271

# Reliability Prediction and Its Simulation for a Friction Stir Processing Tool



Smriti Mishra, Prashant Bhardwaj, Neha Bhadauria,  
and Prashant Vashishtha

**Abstract** Reliability estimation plays an important role in planning and implementation of condition-based proactive maintenance program and proposed the method which would help to reduce the losses in productivity. Approximate reliability of any system can be estimated easily with the help of trend exploration method. In this paper, stochastic Markov technique is used to evaluate the reliability of a high-speed steel tool which was used in friction stir processing of an aluminum alloy. This tool was used on the vertical machining center for the friction stir processing at high rotational speed. The probe wear of the tool after every pass over the work-piece was recorded for constant feed, speed, and depth of cut till the failure of the tool. Differential equations are generated based on Markov model for various failure stages and solved using Runge–Kutta method on MATLAB. This result is verified by Monte-Carlo simulation technique.

**Keywords** Reliability · Markov model · Monte-Carlo simulation · Friction stir processing tool · Vertical machining center · Runge–Kutta method

## 1 Introduction

Remaining useful life of any mechanical part involves the time remaining before the machine part need any repair or replacement. Telecommunication network was used

---

S. Mishra (✉) · P. Bhardwaj  
Department of Mechanical Engineering, Manav Rachna University, Faridabad, Haryana, India  
e-mail: [smriti25jss@gmail.com](mailto:smriti25jss@gmail.com)

P. Bhardwaj  
e-mail: [prashant@mru.edu.in](mailto:prashant@mru.edu.in)

N. Bhadauria · P. Vashishtha  
Department of Mechanical Engineering, KIET, Group of Institutions, Ghaziabad, U.P, India  
e-mail: [neha.bhadauria@kiet.edu](mailto:neha.bhadauria@kiet.edu)

P. Vashishtha  
e-mail: [prashant.vashishtha@kiet.edu](mailto:prashant.vashishtha@kiet.edu)

for reliability and availability determination with the help of simulation. Monte-Carlo technique was also used to solve the block layout problem. Efficiency of Monte-Carlo technique could be used to create and solve the approximate material handling cost of the system [4]. RUL estimation is linked with the condition-based maintenance and prognostic health management. Remaining useful life of any system is completely random and based on the information available in the health inspection system [22]. Multistate system reliability was evaluated by considering multiple possible state of the system. This layout allows both system and its component to consider multi-level performance. Multistate reliability system provides more realistic and more genuine representations of reliability [10]. Probabilistic Markovian approach was used for reliability analysis of any BHP redundant system [24]. Multilayer feed forward neural networks, which were based on multi-valued neurons (MLMVN), used to predict the reliability and degradation behavior of the system. Reliability model is formulated in the form of time series to extract complex dynamic pattern to predict long-term system reliability [9]. Markovian approach was also used to evaluate the availability and reliability of the skim milk plant. System was repairable with exponential failure and repair rate. Differential equations were derived from the transition diagram. These differential equations are solved by using normalizing conditions to compute the availability under steady-state condition [1]. Primary purpose of the prognostic and health management of the system is to enhance the reliability, availability, and maintainability of the system. Maintenance cost can also be reduced by estimating the RUL of the system. Author has proposed support vector regression technique and developed the model without considering the failure rate of the system [13]. Yeh et al. [25] considered a production system with association of cost and demand constraint to calculate the reliability and the production rate of the system [25]. A degradation pattern was proposed for RUL estimation of aircraft engine which was based on learning of degradation pattern. Through this paper, author tried to learn the relation which can reflect the degradation pattern by using neural network and learned network [19, 26]. Hidden Markov model can also be used for RUL estimation and parametric estimation of oil industry. This model is used for prediction of the failure time of the lubricating oil with healthy, unhealthy, and failed state three states in HMM. RUL was estimated by mean residual life function and probabilistic conditional reliability function [6, 8, 18]. Sensitivity analysis was done to create the optimal inventory order which can balance the economic condition of the industry during stock-pull and stock-push period [7]. Finite difference technique was also proposed for solving the stochastic partial differential equations of reliability. This method was used to analyze the transition state probability value of the system [11]. Sarouhas in 2019 proposed a method for the estimation of reliability, availability, and maintainability of the milk production layout. Detailed statistics of the failure and repair rates was used to determine the best fitness indexes. Various probabilistic distributions, such as Weibull, exponential, and lognormal, were also evaluated with standard parameters [23]. Polynomial regression in combination with HMM model was also used for the estimation of RUL of a cutting tool. This model was also used for planning autonomous diagnostics and a prognostic of the cutting tool by using a hidden Markovian model [14, 16]. Some analysis have also done to

enhance the failure rate by using the integration of motion time study and quality tools [3]. Sensitivity analysis was also done for the network charts to determine the optimal solution for the reduction of cost as well as time for the same [2]. Simulation model was also used in oil industries for risk assessment process by using Bow-Tie risk model in which system quantifies all the dynamic interaction inside the system and its impact [12]. Age-based preventive maintenance technique was also used for availability prediction of an oil production system along with the principle of Petri nets [20]. A fuzzy Markov model can be also used for risk prediction as well as for reliability prediction of those system whose actual data are not available, i.e., off-shore, aerospace equipments, etc. [21]. Location algorithm-based Markov model can be used for location-based services also which can provide flexibility and convenience for daily life users [17]. From the above-mentioned literature survey, it is clear that various probabilistic and deterministic models such as hidden Markov model, semi-Markov model, and neural network were used for the evaluation of reliability, remaining useful life. In this study, probabilistic approach was used for the estimation of RUL, and reliability of the system and Markovian model with the help of Runge–Kutta mathematical technique was used for the analysis purpose.

## 2 Experimental Setup

In the current study, friction stir processing was performed on Al 8090 workpiece. High-speed steel tool was used for this procedure. Tool was cylindrical in its shape with cylindrical-shaped threaded pin. Hardness of the tool was RC 44. Before starting the processing over the Al 8090, shoulder diameter of the tool was 20 mm; pin diameter was 5 mm, and length of the pin was 3.5 mm. Friction stir processing was performed on the workpiece having length of 200 mm; width was 100 mm, and thickness of the workpiece was 5 mm. For the processing of the alloy, rotational speed of the spindle was taken as 1000 rpm whereas transverse speed was 10 mm/min. Depth of cut on Al 8090 was 3.75 mm. This operation was performed on vertical machining center. A tool room microscope was installed near the spindle of VMC to capture the image of the probe wear of FSP tool. 4 passes were performed over the workpiece for the processing of Al 8090. The wear rate of the tool was recorded after each pass, and the tip wear rate was identified by calibrated digital images. One pass of friction stir processing on the Al 8090 was completed in 20 min. After the fourth pass, tip of the tool deteriorated completely. Total time taken by the process is approximately 80 min as 20 min was taken in single pass of the operation. This time was considered as the failure time of the FSP tool.



### 3 System Description

A probabilistic technique was used to evaluate the reliability of the tool by using the layout given below in which 4 passes of the friction stir processing tool on Al 8090 was shown. An open-series Markov model was used to solve the differential equation of the system. The reliability block diagram used for experimental purpose is shown in Fig. 1.

In this experiment, initial length of the pin was 5 mm. 4 passes was done on the Al workpiece, and the total time taken by the tool on VMC is 80 min, and after the experiment, length of the remaining pin was 1.75 mm. Initially, length of tip of tool was 5 mm. It was found that length of tip was when it fails 1.75 mm. Length was found 3.8 mm at  $t = 15$  min. Length was found 2.9 mm at  $t = 55$  min. It would be the third stage of degradation, and length of the tip was 1.75 mm at  $t = 80$  min. So, time taken in complete machining is 80 min. After 80 minutes of continuous processing tool was failed completely. Reliability of the tool would be evaluated for 80 min. Failure rate for the tool can be calculated by using following equation:

$$\lambda = \frac{1}{nt} \quad (1)$$

where

$n$  number of passes between two consecutive stages.

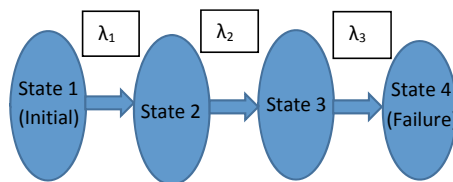
$t$  time taken for a single pass.

$\lambda_1$  (Failure rate between first and second stage) =  $1/15 = 0.067$ .

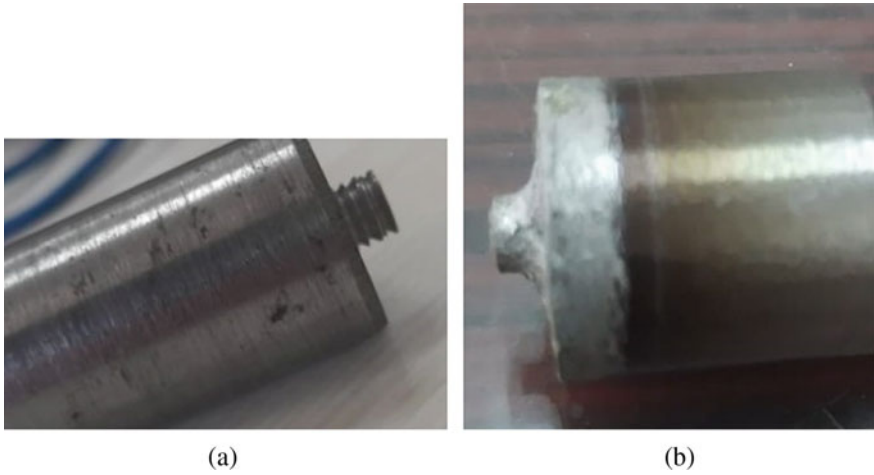
$\lambda_2$  (Failure rate between second and third stage) =  $1/40 = 0.025$ .

$\lambda_3$  (Failure rate between third and fourth stage) =  $1/25 = 0.04$ .

Figure 2 represents the image of the tool before and after failure.



**Fig. 1** Various stages of tool failure



**Fig. 2** a Tool image before failure. b Tool image after failure

**Markovian Approach:** Markov model is a probabilistic model which is used for reliability and availability evaluation for different enumerating system [5]. This model represents the condition of any repairable system from working to failed state by creating its behavior model. The transition model represents the stochastic probabilistic behavior of the system, and different–different mathematical parameters are used to solve the model, and with the help of these parameters, availability can be evaluated. Reliability and availability of complex system can be predicted by generating different transition equations. These equations can be solved by any mathematical model [15].

Probability equations used for reliability evaluation by using Markovian approach are as under:

$$\frac{dy_1}{dt} = -\lambda_1 y_1 \tag{2}$$

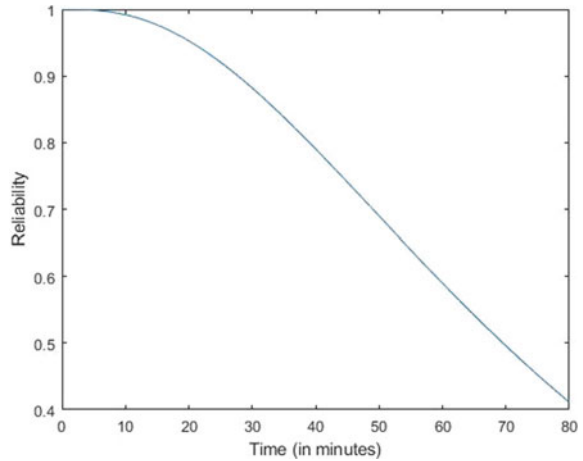
$$\frac{dy_2}{dt} = -\lambda_2 y_2 + \lambda_1 y_1 \tag{3}$$

$$\frac{dy_3}{dt} = -\lambda_3 y_3 + \lambda_2 y_2 \tag{4}$$

$$\frac{dy_4}{dt} = \lambda_3 y_3 \tag{5}$$

Runge–Kutta method was used for reliability evaluation in Matlab by using Markovian approach.

**Fig. 3** Reliability versus time graph in Markov method



## 4 Matlab Program for Markov Method

To evaluate the reliability of the tool for Markovian approach, following program is used:

```
function dydt = rul(t,y)
lmbda1 = 0.067;
lmbda2 = 0.025;
lmbda3 = 0.04;
dydt = [-lmbda1 * y(1);
-lmbda2 * y(2) + lmbda1 * y(1);
-lmbda3 * y(3) + lmbda2 * y(2);
lmbda3 * y(3)];
y0 = [1 0 0 0]
tspan = [0 80]
[t,y] = ode45(@rul,tspan,y0)
R = y(:,1) + y(:,2) + y(:,3)
plot(t,R)
```

It is clear from Fig. 3 that reliability of the system decreases with time.

## 5 Matlab Program for Monte-Carlo Method

To evaluate the reliability of the tool for Monte-Carlo approach, following program is used:

```

function montecarlo()
clc
totalRuns = 0;
totalSuccess = 0;
runs = 500;
matrix = zeros(1,runs);
for i = 1:1:runs
x1 = random('uniform',0,1);
x2 = random('uniform',0,1);
x3 = random('uniform',0,1);
lambda1 = 0.067;
lambda2 = 0.025;
lambda3 = 0.04;
t1 = (-1/lambda1) * log(x1);
t2 = (-1/lambda2) * log(x2);
t3 = (-1/lambda3) * log(x3);
t = t1 + t2 + t3;
if t < 80
success = 0;
else
success = 1;
end
totalRuns = totalRuns + 1;
totalSuccess = totalSuccess + success;
reliability = totalSuccess/totalRuns;
matrix(1,totalRuns) = reliability;
fprintf('Success = %d \n', success,totalRuns);
fprintf('Reliability = %0.15f \n\n\n ',reliability);
end
x = 1:1:runs;
y = matrix(x);
plot(x,y);

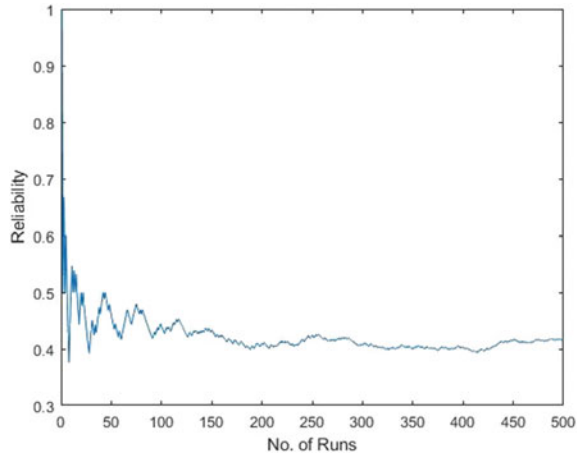
```

After the evaluation from Markov model, it was found that reliability of the system was 42%. And further, the result was validated by using the Monte-Carlo technique, and reliability of the system through Monte-Carlo technique was similar as Markov approach, and it was shown in Fig. 4.

## 6 Conclusion

In the current study, reliability of friction stir processing tool was estimated by Markovian approach in Matlab by using Runge–Kutta method, and further, the result was verified by using Monte-Carlo technique. High-speed steel tool was taken for the

**Fig. 4** Reliability versus no. of runs graph in Monte-Carlo method



data generation, and it was processed on vertical machining center under different time interval with constant speed, feed, and depth of cut. Four-state Markov model was developed for analysis purpose which represents the degradation behavior of the tool. After the evaluation of reliability, remaining useful life of the layout could be predicted. After solving the four-state probabilistic model by Markovian approach, it was found that reliability of the tool was 42%. Monte-Carlo simulation approach was used for the verification of the result obtained from Markovian approach. It can be concluded that after processing of 80 min FSP tool would be fail, and under this condition, reliability of the tool was 42%, and remaining useful life of the tool was 80 min.

## References

1. Aggarwal A, Kumar S, Singh V (2015) Performance modeling of the skim milk powder production system of a dairy plant using RAMD analysis. *Int J Qual Reliab Manage* 32(2):167–181. <https://doi.org/10.1108/IJQRM-01-2014-0007>
2. Aini A, Eshghi K, Salehipour A (2020) A new approach for sensitivity analysis in network flow problems. *Int J Ind Eng* 27(1):72–87
3. Azid IA, Ani MNC, Hamid SAA, Kamaruddin S (2020) Solving production bottleneck through time study analysis and quality tools integration. *Int J Ind Eng* 27(1):13–27
4. Chan WKV, Malmborg CJ (2011) Monte carlo simulation based procedures for solving block layout problems. *Eur J Ind Eng* 5(1):2–21. <https://doi.org/10.1504/EJIE.2011.037223>
5. Chawla R, Kumar G (2013) Condition based maintenance modeling for availability analysis of a repairable mechanical system. *Int J Innovations Eng Technol* 2(2):371–379
6. Chen Z, Li Y, Xia T, Pan E (2019) Hidden Markov model with auto-correlated observations for remaining useful life prediction and optimal maintenance policy. *Reliab Eng Syst Saf* 184:123–136. <https://doi.org/10.1016/j.res.2017.09.002>
7. Cheng YL, Wang WT, Chin W (2018) Optimal production lot sizing when demand is proportional to stock and backorder levels. *Int J Ind Eng* 25(2):137–155

8. Du Y, Wu T, Makis V (2017) Parameter estimation and remaining useful life prediction of lubricating oil with HMM. *Wear* 376–377:1227–1233. <https://doi.org/10.1016/j.wear.2016.11.047>
9. Fink O, Zio E, Weidmann U (2014) Predicting component reliability and level of degradation with complex-valued neural networks. *Reliab Eng Syst Saf* 121:198–206. <https://doi.org/10.1016/j.ress.2013.08.004>
10. Gu Y, Li J (2012) Multi-state system reliability: a new and systematic review. *Procedia Eng* 29:531–536. <https://doi.org/10.1016/j.proeng.2011.12.756>
11. Gupta A, Ram M (2018) Finite difference solution to stochastic partial differential equations in reliability. *Int J Ind Syst Eng* 28(2):166–177. <https://doi.org/10.1504/IJISE.2018.089135>
12. Kbah Z, Erdil NO, Aqlan F (2020) Risk assessment in oil and gas industry using simulation and bow-tie analysis. *Int J Ind Eng* 27(1):110–123
13. Khelif R, Chebel-Morello B, Malinowski S, Laajili E, Fnaiech F, Zerhouni N (2017) Direct remaining useful life estimation based on support vector regression. *IEEE Trans Ind Electron* 64(3):2276–2285. <https://doi.org/10.1109/TIE.2016.2623260>
14. Kumar A, Chinnam RB, Tseng F (2019) An HMM and polynomial regression based approach for remaining useful life and health state estimation of cutting tools. *Comput Ind Eng* 128:1008–1014. <https://doi.org/10.1016/j.cie.2018.05.017>
15. Kumar G, Jain V, Gandhi OP (2014) Steady-state availability analysis of repairable mechanical systems with opportunistic maintenance by using semi-markov process. *Int J Syst Assur Eng Manag* 5(4):664–678. <https://doi.org/10.1007/s13198-014-0231-8>
16. Kumar P, Kumar L, Chaudhari N, Kumar C (2020) Annals of nuclear energy availability analysis of safety-critical and control systems of NPP using stochastic modeling. *Ann Nucl Energy* 147:107657. <https://doi.org/10.1016/j.anucene.2020.107657>
17. Li H, Wang Y, Guo F, Wang J, Wang B, Wu C (2021) Differential privacy location protection method based on the Markov model
18. Li W, Liu T (2019) Time varying and condition adaptive hidden Markov model for tool wear state estimation and remaining useful life prediction in micro-milling. *Mech Syst Signal Process* 131:689–702. <https://doi.org/10.1016/j.ymsp.2019.06.021>
19. Li X, Ding Q, Sun JQ (2018) Remaining useful life estimation in prognostics using deep convolution neural networks. *Reliab Eng Syst Saf* 172:1–11. <https://doi.org/10.1016/j.ress.2017.11.021>
20. Lotovskyi E, Teixeira AP, Soares CG (2020) Maintenance and reliability availability analysis of an offshore oil and gas production system subjected to age-based preventive maintenance by Petri Nets. *Eksplotacja i Niezawodnosc* 22(4):627–637
21. Pang N, Jia P, Liu P, Yin F, Zhou L, Wang L, Yun F (2020) A fuzzy Markov model for risk and reliability prediction of engineering systems: a case study of a subsea wellhead connector. *Appl Sci* 1–24
22. Si XS, Wang W, Hu CH, Zhou DH (2011) Remaining useful life estimation—a review on the statistical data driven approaches. *Eur J Oper Res* 213(1):1–14. <https://doi.org/10.1016/j.ejor.2010.11.018>
23. Tsarouhas P (2019) Evaluation of reliability, availability and maintainability of a milk production line. *Int J Ind Syst Eng* 31(3):324–342. <https://doi.org/10.1504/IJISE.2019.098543>
24. Wang JJ, Fu C, Yang K, Zhang XT, Shi G, Zhai J (2013) Reliability and availability analysis of redundant BCHP (building cooling, heating and power) system. *Energy* 61:531–540. <https://doi.org/10.1016/j.energy.2013.09.018>
25. Yeh CT, Chang PC, Chen CY (2017) Minimal production level and reliability measurement for a maintainable production system under demand and budget constraints. *Eur J Ind Eng* 11(4):526–547. <https://doi.org/10.1504/EJIE.2017.086185>
26. Zhao Z, Liang B, Wang X, Lu W (2017) Remaining useful life prediction of aircraft engine based on degradation pattern learning. *Reliab Eng Syst Saf* 164(457):74–83. <https://doi.org/10.1016/j.ress.2017.02.007>

# Enhancement of Electrochemical Discharge Machining (ECDM) Characteristics with Tool Electrode Rotation



Viveksheel Rajput, Mudimallana Goud, and Narendra Mohan Suri

**Abstract** Electrochemical discharge machining (ECDM) process is a novel process that utilizes the mechanism of thermal melting and chemical dissolution to machine the non-conductive materials. The occurrence of poor micro-hole machining characteristics in gravity-assisted tool feed is one of the challenges in ECDM process. The physical contact of the tool electrode with the work material results in ineffectual electrolyte availability, poor electrolyte flushing and non-uniform sparks. The present study attempts an experimental investigation for enhancing the micro-hole characteristics with the application of tool electrode rotational effect. Material removal rate (MRR), hole circularity (HC), radial overcut (ROC), and heat-affected zone (HAZ) are selected as a response characteristic. The microscopy images emphasized that tool electrode rotation substantially improved the machining characteristic of the micro-holes when compared to characteristic obtained without the tool rotation. Tool electrode rotation helps in replenishment of electrolyte flushing and enables better consistencies of spark distribution. It is concluded that the tool electrode rotation produces micro-holes with better hole circularity compared to stationary tools that produces poor hole circularity. Further, an improvement of 25.21% in MRR and 44.4% in ROC is obtained with the application of tool electrode rotation. The present study successfully describes the enhancement of ECDM characteristics with tool electrode rotation.

**Keywords** ECDM · Tool rotation · Hole circularity · Sparks · Overcut

---

V. Rajput (✉) · M. Goud · N. M. Suri  
Department of Production and Industrial Engineering, Punjab Engineering College, Chandigarh,  
India  
e-mail: [sheelrajput03@gmail.com](mailto:sheelrajput03@gmail.com)

© The Author(s), under exclusive license to Springer Nature Singapore Pte Ltd. 2023  
R. P. Singh et al. (eds.), *Advances in Modelling and Optimization of Manufacturing and Industrial Systems*, Lecture Notes in Mechanical Engineering,  
[https://doi.org/10.1007/978-981-19-6107-6\\_11](https://doi.org/10.1007/978-981-19-6107-6_11)

135

## Nomenclature and Acronyms

### *Notation*

$\mu\text{m}$	Microns
V	Applied voltage unit in volts
wt%	Weight percentage of electrolyte concentration
mg/min	Milligram per minute
wt <sub>b</sub>	Work material weight before machining
wt <sub>a</sub>	Work material weight after machining
$t$	Time
g	Weight unit in grams
$D_{\text{ent}}$	Hole entrance diameter
$d$	Tool diameter

### *Acronyms*

MEMS	Micro-electro-mechanical systems
ECM	Electrochemical machining
EDM	Electric discharge machining
ECDM	Electrochemical discharge machining
MRR	Material removal rate
HAZ	Heat-affected zone
ROC	Radial overcut
HC	Hole circularity
IEG	Inter-electrode gap
NaOH	Sodium hydroxide
3D	Three-dimensional

## 1 Introduction

The sudden increment in the applications of the advanced materials (glass or quartz) with micro-characteristics in industries like aeronautical, bio-medical, and optics prompts the way toward the development of a more sophisticated techniques that can machine these materials. ECDM is known as the recognized process for machining advanced materials with ease by blending the material removal mechanism of electro-discharge machining (EDM) and electrochemical machining (ECM) [2, 14]. The simplified diagram of ECDM process is presented in Fig. 1, consists of tool electrode (cathode) and auxiliary electrode (anode); both are separated by a small distance



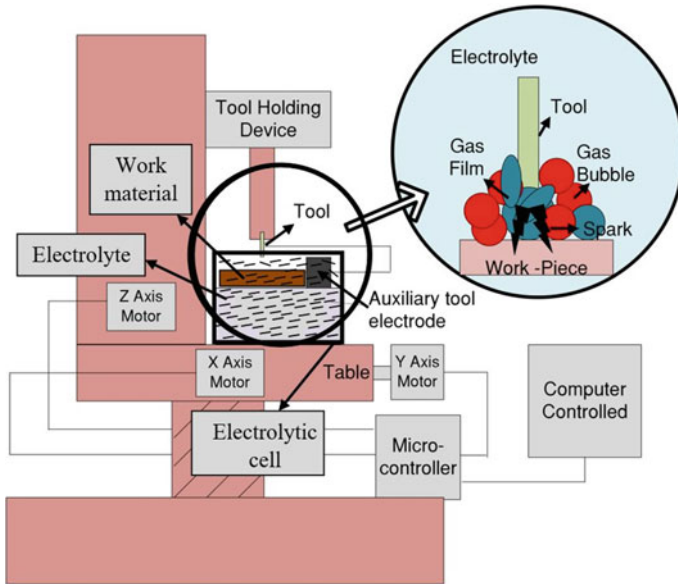


Fig. 1 Schematic diagram of ECDM process

known as inter-electrode gap (IEG). The continuous DC power supply is supplied across the two electrodes in order to ignite the electrochemical reactions. It prompts the generation of hydrogen tiny bubbles at the cathode and oxygen bubbles at the anode. The density of hydrogen bubbles increases with the level increment in applied voltage. Thereafter, the hydrogen bubbles combine physically with each other to form a gas film that isolates the tool electrode. With tool electrode isolation, the flow of the current between the electrodes is ceased. Subsequently, it produces the immense electric field inside the gas film region. Then, a spark is generated from the tool electrode due to the electric breakdown of the gas film. Further, the work material is maintained under the tool electrode, and material is removed due to thermal heating and chemical dissolution.

## 2 Research Background

Kurafuji and Suda [12] were the first who demonstrated the glass material drilling with the help of electrical discharge. Basak and Ghosh [2, 3] demonstrated the mechanism of sparks and material removal mechanism in ECDM process. ECDM exhibits various applications during glass micro-fabrication such as 3D micro-fabrication of glass materials for its utilization in micro-electro-mechanical systems (MEMSs) and other laboratories; and in kitchenware work [27]. They emphasized that critical voltage values are required for spark initiation. From the day of its beginning,

many researchers have been made immense contribution toward the development of ECDM process [6, 9, 16, 25]. The application of gravity tool feed in ECDM successfully machines the non-conductive materials [19]. However, poor circularity and higher thermal cracks may occur in this method due to tool contact [17]. The geometrical characteristics of the micro-holes drilled with ECDM process rely on many input variables such as applied voltage, electrolyte concentration, tool feed method, and others [7]. Any increment in applied voltage and electrolyte concentration enhances the MRR but also increments the tendency of poor hole circularity, high ROC, and cracks [21]. The selection and control of input variables is very critical in enhancing the machining performance [7, 9]. Tool rotation also enhances the MRR, geometrical characteristics, and dimensional accuracies of the micro-holes when compared to ECDM without tool rotation [4, 5]. Tool electrode rotation prevents the occurrence of the sparks at a single point and results in a uniform sparks distribution. Tool electrode rotation assists in preventing the sparks only at a single point and produces uniform sparks distribution [10, 11]. It prevents the occurrence of stray corrosion that may results in better hole circularity. However, many experimental investigations have been made for improving the machining performance of the ECDM process [1, 17]. Fan and Hourng [4] performed a study to explore the tool rotational effect on hole circularity and overcut during micro-hole fabrication process with ECDM. Results indicate that tool rotation produces micro-holes with better circularity, while a deteriorated hole shape is obtained without tool rotation. Lizo et al. (2018) also investigated the influence of tool rotational effect on MRR and radial overcut using graphite powder-mixed electrolyte during glass machining [15]. As a result, micro-holes with reduced overcut were obtained with the application of tool rotation. Huang et al. [8] emphasized that the tool electrode wear significantly reduces with the utilization of the tool electrode rotation. The centrifugal capability of the tool electrode rotation enhances the flushing ability and leads to uniform occurrence of the sparks around the tool surface. Table 1 highlights the critical analysis of the ECDM research findings during machining of glass work material.

## ***2.1 Problem Formulation***

Despite having numerous studies in ECDM using gravity-assisted tool feed method, there are some challenges that need to be explored. The tool permanent contact and its stagnant nature (no rotation) may lead to poor hole circularity and high ROC. Enhancing the geometrical accuracies or micro-hole's circularity is still a challenging task in gravity-assisted tool feed method. Thus, the high chances of hole edge deterioration will remain permanently with this tool feed method if not controlled or improved. The present investigation utilizes the application of tool rotation for improving the geometrical characteristics of the micro-holes.

**Table 1** Critical analysis of the ECDM research findings during the processing of glass work materials

Objective	Inferences	Authors, year
The geometrical characteristics were analyzed during micro-hole fabrication	<ul style="list-style-type: none"> <li>• The obtained characteristics depends upon the input variables used during machining</li> <li>• Higher level of applied voltage produces high thermal cracks and deteriorates the micro-hole edge</li> </ul>	Maillard et al. [13]
To obtain deep micro-holes with high aspect ratio during micro-machining	<ul style="list-style-type: none"> <li>• Tool rotational effect significantly enhances the electrolyte availability and produces better circularity of the micro-holes</li> <li>• Lower level of concentration tends to reduce tapering of the holes and produces high aspect ratio</li> </ul>	Jui et al. [10]
Estimated the material removal rate based on thermal model. Study of machining temperature is performed	<ul style="list-style-type: none"> <li>• The geometry of the machined surface and variables used controls the machining temperature</li> </ul>	Ziki et al. [28]
Evaluate the effect of textured tools on machining characteristics during micro-channeling operation	<ul style="list-style-type: none"> <li>• A stable gas film is obtained with textured tools because of the availability of the micro-cavities</li> <li>• A significant improvement in MRR, overcut, and machining depth is observed with the application of textured tools</li> </ul>	Singh and Dvivedi [23]
A pressured tool feeding system is developed for effective machining gap to improve machining depth	<ul style="list-style-type: none"> <li>• The developed system successfully results in effective machining gap that causes constant availability of the electrolyte underneath the tool during the machining process</li> <li>• Improved machining depth is obtained with this method</li> </ul>	Singh and Dvivedi [24]
Investigated the effect of mixed electrolytes on machining characteristics	<ul style="list-style-type: none"> <li>• The surface characteristics of the machined micro-channels increase with the increased etching action of the mixed electrolytes</li> </ul>	Sabahi and Razfar [22]
The effect of tool surface roughness on gas film is evaluated	<ul style="list-style-type: none"> <li>• Tool material alters the tool wettability property that further gives variable gas film thickness. As a result, variable machining characteristics are obtained. Tungsten carbide tool produces better machining results compared to stainless steel and tungsten tool</li> </ul>	Yang et al. [26]

(continued)

**Table 1** (continued)

Objective	Inferences	Authors, year
Multi-response optimization of the input variables using gray relational analysis (GRA)	<ul style="list-style-type: none"> <li>GRA techniques can be successfully utilized for optimizing the parameters that behave differently. Feed rate was identified as the most dominant input variables among the other variables</li> </ul>	Goud and Sharma [6]
Investigate the different tool shapes on machining characteristics during micro-drilling with ECDM process	<ul style="list-style-type: none"> <li>Tool shape effects the gas film stability and flow of electrolyte during the machining process</li> <li>Pointed tool results in high MRR, while cylindrical tool results in better circularity</li> </ul>	Rajput et al. [18]
Investigate the surfactant mixed electrolyte in ECDM process	<ul style="list-style-type: none"> <li>Improves the etching action and results in better surface characteristics</li> </ul>	Rajput et al. [17]

### 3 Research Methods

The experiments are performed on a developed gravity feed experimental setup integrated to vertical milling machine as shown in Fig. 2, to study the tool rotational effect on machining characteristics by comparing it with the machining characteristics obtained without tool rotation. The work material under study is soda lime glass for evaluating the geometrical characteristics of the micro-holes. The cylindrical shape tool electrode is utilized and made up of stainless steel having 1 mm diameter. Table 2 presents the input variables and other machining conditions used in the present study. The machined micro-holes are analyzed with the help of stereo microscope (make: Carl Zeiss and model: Stemi-305 Trino) from the top view side. The input variables considered in this study are applied voltage (V) and electrolyte concentration (wt%), while MRR, HC, ROC, and HAZ are selected as a response characteristic.

### 4 Results and Discussions

The comparison of machining characteristics obtained with and without tool rotation is carried out to analyze the tool rotational effect during micro-hole drilling in ECDM. The responses considered are MRR, HC, ROC, and HAZ.

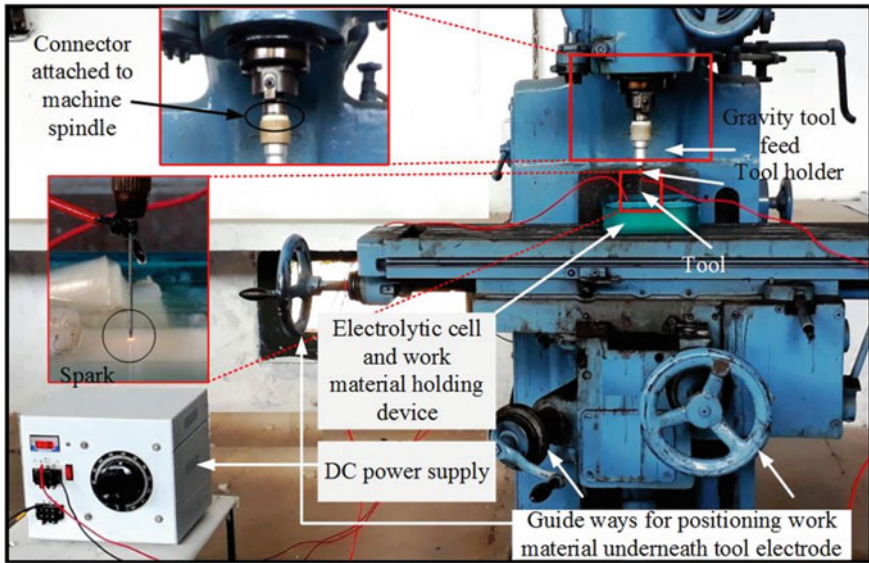


Fig. 2 Developed gravity feed-assisted ECDCM setup [18]

Table 2 Machining conditions used in present investigation

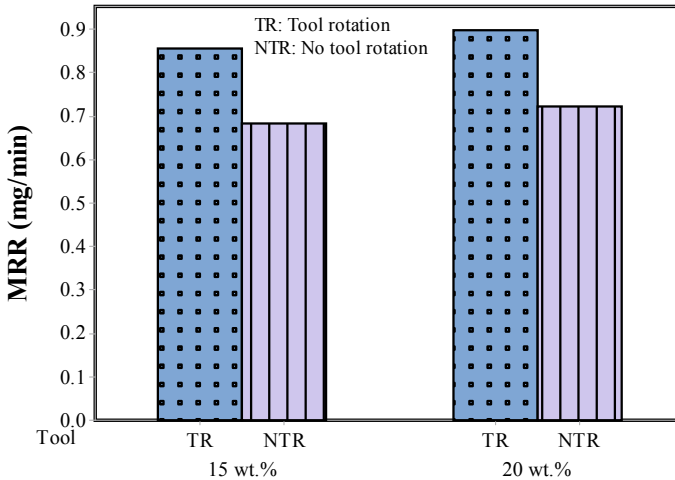
Variable	Value	Variable	Value
Electrolyte concentration	15–20 wt%	Electrolyte level	1 mm
Applied voltage	35 V	Electrolyte	NaOH
Tool rotation	355 rpm	Inter-electrode gap	35 m
Tool material	SS ( $\Phi = 1000 \mu\text{m}$ )	Machining time	2 min

### 4.1 Effect of Tool Rotation on MRR

The material removal rate is measured as the weight difference in the work material before and after micro-hole drilling divided by the total machining time ( $t$ ) as given in Eq. 1, where  $w_{t_b}$  is weight before machining and  $w_{t_a}$  is weight after machining.

$$\text{MRR} = ((w_{t_b} - w_{t_a})/t) \tag{1}$$

Figure 3 presents the plot of MRR obtained at different electrolyte concentrations with and without tool rotation. It is observed that MRR improves with the application of tool rotation since a more uniform sparks distribution is obtained in the machining zone. A more efficient occurrence of the sparks takes place at the cylindrical tool rim. Additionally, an improved circulation of electrolyte and sludge removal takes place with the help of rotation. It is also reported that more uniform etching action takes place with the help of tool rotation. Moreover, it is observed that MRR increments

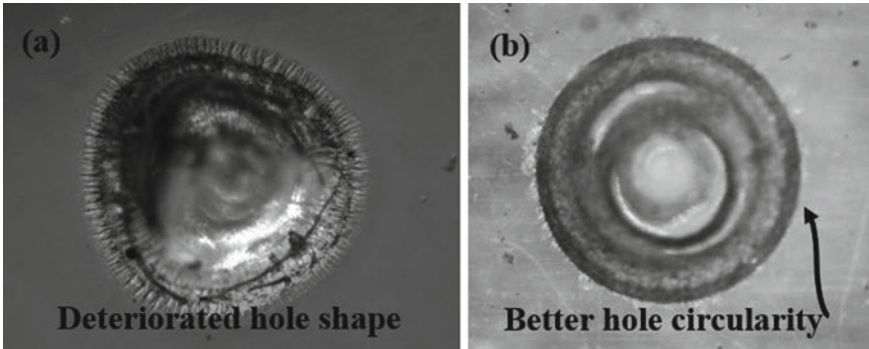


**Fig. 3** Plot of MRR with 'tool rotation' and 'no tool rotation' at 35 V

with the level increment of electrolyte concentration from 15 to 20 wt% due to the increment in electrolyte's electrical conductivity. With any increment in electrolyte conductivity, there is an increment in the generation of the hydrogen and oxygen bubbles inside the electrolyte. It results in the rapid generation of the gas film around the tool electrode surface. Hence, a high intensity of sparks is observed with the increment in electrolyte concentration [20]. As a result, increment in MRR is noticed.

#### ***4.2 Effect of Tool Rotation on Hole Circularity***

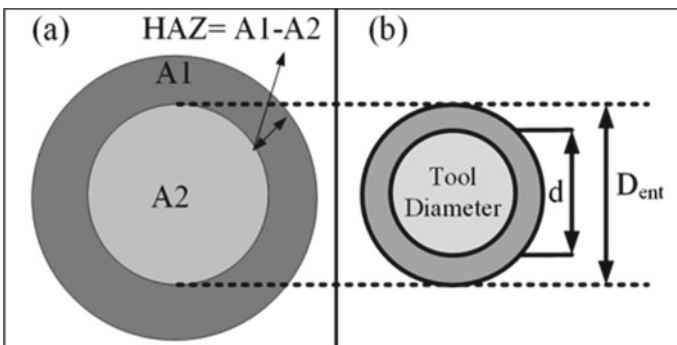
It is observed that tool rotation produces better hole circularity since it prevents the spark to occur only at a single point. Figure 4 presents the microscopy images of the micro-holes obtained with and without tool rotation. A much improvement in hole circularity is clearly seen with the utilization of tool rotation (Fig. 4b) compared to micro-hole obtained without tool rotation (Fig. 4a). The reason for better circularity is seen as the better replenishment of the electrolyte underneath the tool electrode or in the machining zone due to the rotational effect. As a result, a uniform distribution of the sparks is obtained. Thus, a better thermal heating effect is seen in the machining zone. Additionally, the tool rotational effect induces better removal of the sludge from the machining zone. It helps in retaining the fresh electrolyte in the machining zone.



**Fig. 4** Microscopy images showing hole circularity at 15 wt% and 35 V. **a** No tool rotation. **b** Tool rotation

### 4.3 Effect of Tool Rotation on ROC

ROC is defined as the extra material removed from the micro-hole edges compared to the utilized tool diameter as shown in Fig. 5b. The occurrence of side sparks or stray sparking generally results into the removal of the material in an inconsistent way. It causes high ROC. Figure 6 exhibits that the ROC of the micro-hole reduces significantly with the application of tool rotation because of prevention of side and stray sparking from the tool. A uniform material removal is observed all around the micro-hole edges that produces better circularity and better ROC as shown in Figs. 4, 6 and 7. Moreover, it is noticed that with the level increment in electrolyte concentration, there is an increment in the ROC values since high spark intensity is observed from the sides of the tool. It leads to the increment in ROC at higher level of electrolyte concentration.



**Fig. 5** Simplified diagram for calculating. **a** HAZ. **b** ROC Rajput et al. [19]

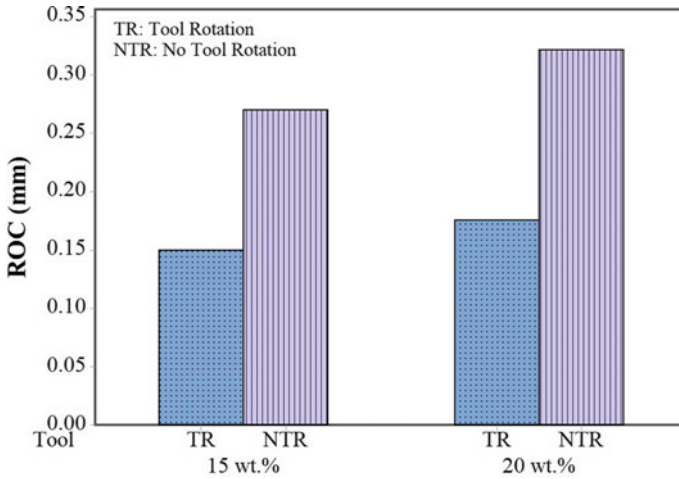


Fig. 6 Plot of ROC with ‘tool rotation’ and ‘no tool rotation’ at 35 V

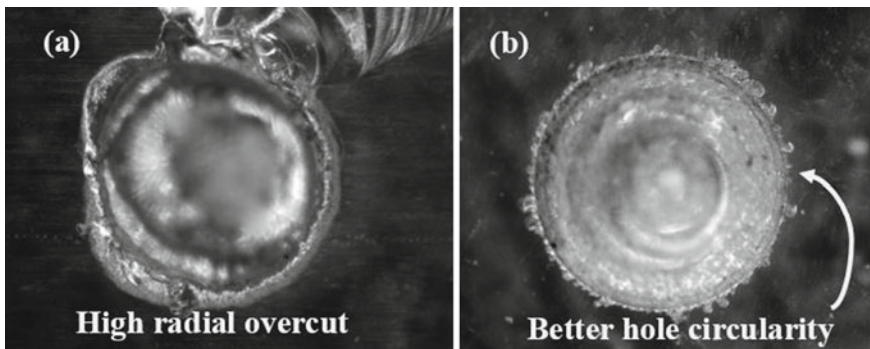


Fig. 7 Microscopy images of micro-hole exhibits ROC at 15 wt% and 35 V. a No tool rotation. b Tool rotation

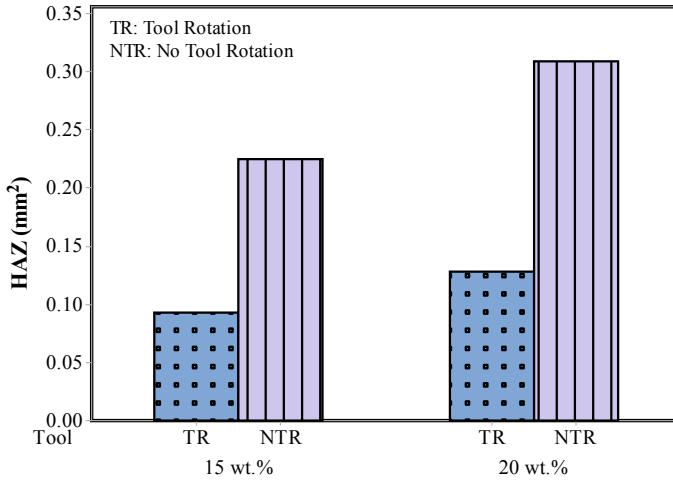
#### 4.4 Effect of Tool Rotation on HAZ

HAZ happens due to the transference of the thermal energy within the work material and is calculated as the difference between the area (A1) and micro-hole area (A2) as shown in Fig. 5a.

$$HAZ = A1 - A2 \tag{2}$$

The plot of HAZ with and without tool rotation is given in Fig. 8. It is observed that tool rotational effect significantly reduces the occurrence of HAZ because of uniform spark consistencies at the cylindrical rim of the tool. The microscopy images of the





**Fig. 8** Plot of HAZ with ‘tool rotation’ and ‘no tool rotation’ at 35 V

micro-holes clearly indicate that HAZ is rarely occurred in a reduced manner with the application of tool rotation (Figs. 4b and 7b) when compared to the micro-holes obtained without the application of the tool rotation. Moreover, a further increment in HAZ with the increment in concentration is noticed because of increment in thermal energy on the top surface of the work material. Increment in electrolyte concentration displays similar concept of increment in generation of the bubbles inside electrolytes due to incremented electrical conductivity. Hence, higher spark’s frequencies occurred which resulted into a higher HAZ.

#### 4.5 Effect of Increase in Tool Rotation on Machining Characteristics

It is observed that tool rotation enhances the machining characteristics or geometrical characteristics during micro-hole drilling with gravity-assisted tool feed ECDM process. The effect of increment in tool rotation is investigated by increasing the tool rotation at three different levels (355,560 and 900 rpm). The levels of tool rotation are selected based on available rotations of the vertical milling machine. Figure 9 presents the MRR and ROC of the micro-hole obtained at three different levels of tool rotation where level 1 is 355 rpm, level 2 is 560 rpm, and level 3 is 900 rpm, respectively. It is observed that increment in tool rotation enhances the geometrical characteristics of the micro-hole characteristics that may be due to increment in spark consistencies and fast replenishment of the electrolyte. However, there may also be chances that micro-hole characteristics may deteriorate at very high tool rotation owing to tool electrode contact with the work material.

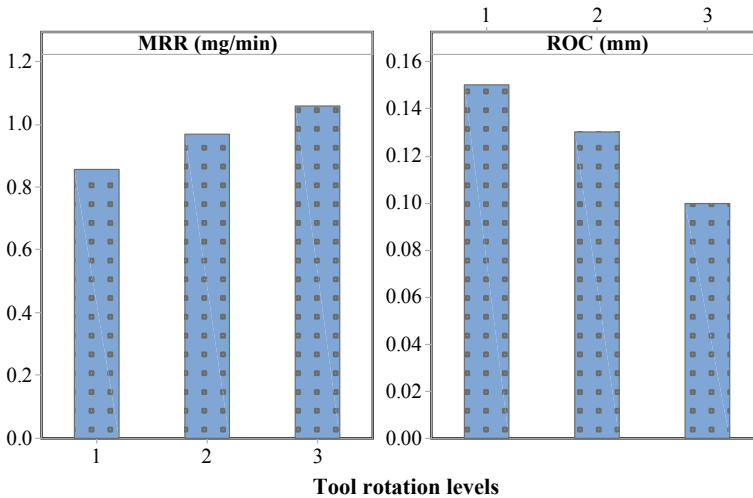


Fig. 9 Plot of MRR and ROC at different tool rotations at 15 wt% and 35 V

## 5 Conclusions and Future Scope

The present study evaluates the effect of tool rotation on machining characteristics of the micro-hole by comparing it with the characteristics obtained without tool rotation. The effect of increment in tool rotation is also observed of machining characteristics. The major conclusions withdrawn from the study are given herewith:

- Tool rotation enhances the machining characteristics of the micro-holes obtained with gravity-assisted tool feed ECDM process.
- Tool rotation produces better spark consistencies by preventing the spark to occur only at one point. A better replenishment of the fresh electrolyte is available in the machining zone. It maintains the better consistencies of the sparks and thermal heating in the machining zone.
- A significant improvement in MRR, ROC, HC, and HAZ is observed with the utilization of tool rotation in gravity-assisted tool feed ECDM process. An improvement of 25.21% in MRR and 44.4% in ROC is obtained with the application of tool electrode rotation.
- An increment in tool rotation further enhances the geometrical characteristics owing to more enhanced sparks distribution in the machining zone.

The future work can be extended by using tool rotation with constant tool feed method. The investigation on the effect of input variables such as applied voltage and electrolyte concentration on machining characteristics should be carried out. An increment in the tool rotation up to very high level may deteriorate the micro-hole characteristics. Thus, an optimization of input variables can be performed to obtain the range of input variables for better machining characteristics of the micro-holes.

## References

1. Antil P (2020) Modelling and multi-objective optimization during ECDM of silicon carbide reinforced epoxy composites. *SILICON* 12:275–288. <https://doi.org/10.1007/s12633-019-00122-8>
2. Basak I, Ghosh A (1997) Mechanism of material removal in electrochemical discharge machining a theoretical model and experimental verification. *J Mater Process Technol* 71:350–359. [https://doi.org/10.1016/S0924-0136\(97\)00097-6](https://doi.org/10.1016/S0924-0136(97)00097-6)
3. Basak I, Ghosh A (1996) Mechanism of spark generation during electrochemical discharge machining a theoretical model and experimental verification. *J Mater Process Technol* 62:46–53. [https://doi.org/10.1016/0924-0136\(95\)02202-3](https://doi.org/10.1016/0924-0136(95)02202-3)
4. Fan ZW, Hourng LW (2011) Electrochemical micro-drilling of deep holes by rotational cathode tools. *Int J Adv Manuf Technol* 52:555–563. <https://doi.org/10.1007/s00170-010-2744-x>
5. Gautam N, Jain VK (1998) Experimental investigations into ECSD process using various tool kinematics. *Int J Mach Tool Manuf* 38:15–27. [https://doi.org/10.1016/S0890-6955\(98\)00034-0](https://doi.org/10.1016/S0890-6955(98)00034-0)
6. Goud MM, Sharma AK (2017) On performance studies during micromachining of quartz glass using electrochemical discharge machining. *J Mech Sci Technol* 31:1365–1372. <https://doi.org/10.1007/s12206-017-0236>
7. Goud MM, Sharma AK, Jawalkar CS (2016) A review on material removal mechanism in electrochemical discharge machining ECDM and possibilities to enhance the material removal rate. *Precis Eng* 45:1–17. <https://doi.org/10.1016/j.precisioneng.2016.01.007>
8. Huang SF, Liu Y, Li J et al (2014) Electrochemical discharge machining micro-hole in stainless steel with tool electrode high-speed rotating. *Mater Manuf Process* 29. <https://doi.org/10.1080/10426914.2014.901523>
9. Jain VK, Dixit PM, Pandey PM (1999) On the analysis of the electrochemical spark machining process. *Int J Mach Tools Manuf* 39:165–186
10. Jui SK, Kamaraj AB, Sundaram MM (2013) High aspect ratio micromachining of glass by electrochemical discharge machining ECDM. *J Manuf Process* 15:460–466. <https://doi.org/10.1016/j.jmapro.2013.05.006>
11. Kumar S, Divedi A (2018) On effect of tool rotation on performance of rotary tool micro-ultrasonic machining. *Mater Manuf Process* 34(5):475–486. <https://doi.org/10.1080/10426914.2018.1512130>
12. Kurafuji H, Suda K (1968) Electrical discharge drilling of glass. *Ann CIRP* 16:415–419
13. Maillard P, Despont B, Bleuler H et al (2007) Geometrical characterization of micro-holes drilled in glass by gravity-feed with spark assisted chemical engraving SACE. *J Micromech Microeng* 17:1343–1349. <https://doi.org/10.1088/0960-1317/17/7/017>
14. Nesarikar VV, Jain VK, Choudhury SK (1994) Traveling wire electrochemical spark machining of thick sheets of Kevlar-Epoxy composites. In: Proceedings of the 16th all India manufacturing, technology, design and research (AIMTDR 1994) conference. Central Machine Tool Institute, Bangalore, India, pp 672–677
15. Paul L, Antony D (2018) Effect of tool diameter in ECDM process with powder mixed electrolyte. *IOP Conf Ser: Mater Sci Eng* 396:012070. <https://doi.org/10.1088/1757-899X/396/1/012070>
16. Rajput VS, Goud MM, Suri NM (2020a) Review-electrochemical discharge machining: gas film electrochemical aspects, stability parameters, and research work. *J Electrochem Soc* 168(1). <https://doi.org/10.1149/1945-7111/abd516>
17. Rajput VS, Goud MM, Suri NM (2020b) Performance analysis of ECDM process using surfactant mixed electrolyte. In: Sharma V, Dixit U, Sørby K, Bhardwaj A, Trehan R (eds) *Manufacturing engineering. Lecture notes on multidisciplinary industrial engineering*. Springer, Singapore. [https://doi.org/10.1007/978-981-15-4619-8\\_22](https://doi.org/10.1007/978-981-15-4619-8_22)
18. Rajput V, Goud MM, Suri NM (2020c) Numerical and experimental investigations to analyze the micro-hole drilling process in spark-assisted chemical engraving (SACE). *SN Appl Sci* 2:1525. <https://doi.org/10.1007/s42452-020-03311-y>

19. Rajput VS, Pundir SS, Goud MM, Suri NM (2021a) Multi-response optimization of ECDM parameters for silica (quartz) using grey relational analysis. *SILICON* 13:1619–1640. <https://doi.org/10.1007/s12633-020-00538-7>
20. Rajput VS, Goud MM, Suri NM (2021b) Three-dimensional finite element modeling and response surface based multi-response optimization during silica drilling with closed-loop ECDM. *Silicon*. <https://doi.org/10.1007/s12633-020-00867-7>
21. Rajput VS, Goud MM, Suri NM (2021c) Performance analysis of closed-loop electrochemical discharge machining (CLECDM) during micro-drilling and response surface methodology based multi-response parametric optimisation. *Adv Mater Process Technol*. <https://doi.org/10.1080/2374068X.2020.1860494>
22. Sabahi N, Razfar MR (2018) Investigating the effect of mixed alkaline electrolyte (NaOH + KOH) on the improvement of machining efficiency in 2D electrochemical discharge machining (ECDM). *Int J Adv Manuf Technol* 95:643–657. <https://doi.org/10.1007/s00170-017-1210-4>
23. Singh T, Dvivedi A (2018a) On performance evaluation of textured tools during micro-channeling with ECDM. *J Manuf Process* 32:699–713. <https://doi.org/10.1016/j.jmapro.2018.03.033>
24. Singh T, Dvivedi A (2018b) On pressurized feeding approach for effective control on working gap in ECDM. *Mater Manuf Processes* 33:462–473. <https://doi.org/10.1080/10426914.2017.1339319>
25. Wuthrich R, Hof LA, Lal A, Fujisaki K, Bleuler H, Mandin PH, Picard H (2005) Physical principles and miniaturization of spark assisted chemical engraving (SACE). *J Micromech Microeng* 15:S268–S275
26. Yang CK, Cheng CP, Mai C et al (2010) Effect of surface roughness of tool electrode materials in ECDM performance. *Int J Mach Tool Manu* 50:1088–1096. <https://doi.org/10.1016/j.ijmachtools.2010.08.006>
27. Zheng ZP, Cheng WH, Huang FY et al (2007) 3D microstructuring of Pyrex glass using the electrochemical discharge machining process. *J Micromech Microeng* 17:960–966. <https://doi.org/10.1088/0960-1317/17/5/016>
28. Ziki JDA, Hof LA, Wuthrich R (2015) The machining temperature during spark assisted chemical engraving of glass. *Manuf Lett* 3:9–13. <https://doi.org/10.1016/j.mfglet.2014.11.003>

# Biomedical Waste Management and Circular Economy Actions in the COVID-19 Pandemic Situation in Jaipur District, India



Manoj Sharma, Narayan Lal Jain, and Jayant Kishor Purohit

**Abstract** Circular economy is gaining popularity across the world, but its implementation in Jaipur District, as in other developing nations, is lacking. The Covid-19 epidemic has resulted in massive volumes of hazardous trash that require specific handling. The goal of this study was to evaluate CE and waste management efforts in Jaipur District, India during the Covid-19 epidemic. Two quarantine healthcare centers in Jaipur District were used as case studies, with data collected using quantitative and qualitative approaches and evaluated to establish the problems of hazardous waste management in Jaipur District. A total of 220 questionnaires were sent to the employees, with 216 (98.18%) of them being returned. There were 118 males (55%) and 98 women (45%) among the respondents, who worked in a variety of fields, including health workers ( $n = 108$ ; 50%), maintenance personnel ( $n = 62$ ; 28.7%), and cleaners/waste handlers ( $n = 46$ ; 21.29%). The majority of the participants (94.44%) said Covid-19 wastes should be separated, whereas 116 people (53.7%) thought managing personal protective equipment during a pandemic was reasonable. According to the findings, training and retraining of personnel on hazardous waste management at the examined healthcare institutions is critical to the implementation and enforcement of national policies for solid waste management. Rajasthan's government must dispose of biological waste in one step, straight out of town, rather than in two steps, first in Jhalana, Jaipur, and then in Jamdoli, Jaipur.

**Keywords** Circular economy (CE) · Covid-19 · Solid waste · Isolation center · Solid waste management (SWM) · Hazardous waste management

---

M. Sharma (✉) · N. L. Jain  
Department of Mechanical Engineering, Poornima University, Jaipur, Rajasthan 303905, India  
e-mail: [64manoj@gmail.com](mailto:64manoj@gmail.com)

N. L. Jain  
e-mail: [narayanjain.c@rediffmail.com](mailto:narayanjain.c@rediffmail.com)

J. K. Purohit  
Department of Mechanical Engineering, Banasthali University, Tonk, Rajasthan 304022, India  
e-mail: [jkp.mnit@gmail.com](mailto:jkp.mnit@gmail.com)

## 1 Introduction

Yuan [1] gives the proposed concept of a circular economy (CE) in China and formally accepted in 2002 by the central government of China. Feng [2] gave the core of CE is the circular (closed) flow of materials and the use of raw materials and energy through multiple phases. The “3R” principles—reduction, reuse, and recycling of materials and energy—are often cited to describe the three possible approaches in practice.

In the linear economy of manufacturing, work is based on the take, make, and dispose principle in Jaipur as well as India due to a lack of legislative act or enforcement for solid waste management (SWM) [3]. By the use of special attention and effective techniques of management, medical wastes can reduce. Hazardous waste management minimizes harmful effects on the human health and environment through use of proper techniques of treatment, storage, handling, transportation, and disposal [4].

In Jaipur district, solid waste is disposed by transportation in two stages by mini truck first to JHALANA which is located in city near K.V. 3 School and Malaviya National Institute of Technology (MNIT) where population is too high [5]. After that solid waste is collected again in trucks and discharged in open dumps which are located at near JAMDOLI, Jaipur. This place is located outside of Jaipur city where humans are minimal.

According to 2011 census, the population of Jaipur district is 66.3 lakhs, and area is 11,152 km<sup>2</sup>. Based on population, output of solid waste in this district is 11.16 lakhs tons per annum. This model has suggested that Jaipur district will be produced solid waste 18.16 lakhs tons per annum by the year of 2030. So, if the SWM will not follow by this district, then it will increase day by day. Solid waste management is a public health service which controls the waste, recycle and reuse it. Poor waste management systems linked with a hot climate increase the environmental problems and health problems [6].

As of now, open-dump frameworks are among the significant dangers to well-being and ecological feel, while they additionally debase regular assets and increment the danger of fire episodes, contamination of waterways and underground offices by leachate, and other grave medical problems [7, 8]. Disease transmission, fire danger, odor pollution, atmospheric and water pollution, esthetic pollution, and economic losses are some of the most prevalent concerns connected with poor solid waste management [9]. Through anaerobic decomposition, open-dump systems have significantly contributed to climate change, resulting in methane emissions and negatively harming human quality of life. The fact that SWM is accompanied by a public health emergency, such as the Corona virus disease 2019 (Covid-19) pandemic, emphasizes the necessity of these services to the authorities even more [10, 11].

Covid-19 is a disease caused by a novel corona virus strain that has never been detected in humans before, and it was designated a worldwide pandemic in February 2020, immediately caused monumental challenges. The effect of Covid-19 is spread over in Jaipur as well as India. The Indian government is attempting to protect its citizens from the Corona virus by issuing SOPs for lockdown to all states and offering services such as home isolation, testing, and treatment, as well as establishing Covid-19 centers. But, the Government of Rajasthan in Jaipur city is not focused on producing hazardous waste materials and their management during lockdown.

Hospitals, healthcare institutions, and individuals have been creating more waste than normal in response to the Covid-19 pandemic, including masks, gloves, and other protective equipment that may be contaminated with the virus [7]. Infected medical wastes may be subjected to uncontrolled disposal, increasing public health concerns, while their open burning or uncontrolled cremation may result in the release of different poisons. While SWM is an essential sanitary barrier for disease control, it is not without flaws [7]. Uncollected solid waste is a major source of disease transmission in cities.

Following the emergence and spread of Covid-19 over the last several months, critical observations have revealed that the SWM situation in Jaipur City in terms of collection, recycling, and disposal has usually gotten hazardous for waste handlers [12]. There have been no recommendations or warnings released about the management of municipal solid trash originating from the Covid-19 lockdown and limitations, as well as Covid-19 wastes, which may escape the essential protocols in private and government hospitals in the treatment of such wastes. Covid-19 wastes should be monitored by developed nations, who should optimize current waste management methods while minimizing possible long-term environmental effects [7]. However, irregular clearance of Covid-19 medical wastes at multiple hospitals in Jaipur constitutes a serious threat to the spread of the Covid-19 viral infection, which has been linked to the virus's resurgence in and around hospitals during the current pandemic owing to ineffective management.

In this aspect, waste management standards have been weak and obsolete, and trash storage and collection procedures have been mainly ineffective throughout the current epidemic, with no accurate recording of waste creation rates or waste composition. When toxic and hazardous wastes are dumped indiscriminately, municipal wastes are mixed up with them, resulting in an inefficient economy. To close the loop in a circular economy, it is necessary to recycle waste resources. Furthermore, waste energy recovery is critical for establishing a proper and safe waste management system. Waste disposal should be phased out as much as possible, and if it is unavoidable, it should be handled efficiently to ensure that it is safe for human health and the environment [13].

During the Covid-19 epidemic, Fig. 1 shows unsegregated solid wastes in a hospital environment.



**Fig. 1** Unsegregated solid waste disposal during Covid-19 pandemic in SMS Hospital, Jaipur

Because of reasons such as the lack of a regulatory framework to govern dangerous waste management practices and the insufficiency of the current infrastructure to adequately handle the volume and types of generated trash, Jaipur is becoming increasingly concerned about the circular economy [14]. The lack of implementation of existing laws and legislations, the need to upgrade obsolete legal instruments, insufficient budgetary provisions and funding mechanisms, and poor monitoring and evaluation mechanisms to guide environmentally safe SWM practices are all contributing to the country's main issue with SWM [15].

The executive, legislature, and judiciary at the federal, state, and local government levels are all involved in Jaipur SWM policy. The policy covers the major sources of solid waste in Jaipur, ensuring that trash is segregated, collected, transported, stored, treated, and disposed of in accordance with legal requirements to preserve the environment and human health.

The policy document was to be followed in terms of compliance and enforcement by the Federal Government of Jaipur's 5R hierarchy for SWM (reduces, repair, reuse, recycle, and recover). Environmental standards are protected; rules and legislation are enforced; international treaties are followed, and standards are adhered to. As a result, Jaipur must transition to a more circular economy by mainstreaming its concepts and practices into local, in each ward road maps for a long-term transition from a linear to a circular economy, which appears to be critical at this time.

In several parts of life, Jaipur implements circularity, such as micro-level engagement in home trash reduction and reuse techniques, as well as the usage of informal marketplaces as garbage scavengers, merchants, and recyclers [14].

Covid-19 is a novel virus that has been labeled a pandemic by the World Health Organization (WHO). As a result, hazardous waste management requires specific attention and measures. In order to evaluate circularity and management activities during the epidemic in Jaipur City, this study was performed to address human issues, quantified with numbers using surveys, and evaluated using statistical tools.



## 2 Materials and Methods

This study was conducted in 2021 at the Swai Maan Singh Hospital (S.M.S.) and Rajasthan University of Health Science Hospital (RUHS), which are primarily two large Covid centers in Jaipur as the Covid-19 isolation facilities in Jaipur, Rajasthan State, India, with a focus on the recognition of the challenges in the management of such a waste category. Data were collected using quantitative and qualitative approaches, as well as a checklist [15]. In line with Creswell 2009, questionnaires were sent to healthcare professionals, maintenance workers, and cleaners/waste handlers at health institutions. Covid-19 healthcare wastes (identification, characterization, and segregation in healthcare facilities), emergency preparedness and response, safety, health, and the environment were all covered in the checklist. Field observations and key informant interviews were used to achieve the qualitative approach.

Data on the management and disposal of Covid-19 wastes, perceptions of medical wastes during the Covid-19 pandemic, and other technical questions were collected using a series of semi-structured questionnaires. The distribution of the study instrument was done using simple random sampling among hospital employees (medical and healthcare professionals) and maintenance staff (ward attendants, cleaners, waste handlers, incinerator operators, and cleaning supervisors).

A total of 220 questionnaires were distributed, with 160 being provided at the SMS and 56 being distributed in the RUHS. There were 216 surveys returned in all.

## 3 Statistical Analysis

Data from the examined Covid-19 isolation facilities were cleaned, edited, and frequency tables were created in SPSS version to illustrate the findings.

## 4 Result and Discussion

Jaipur City, Rajasthan State Covid-19 Centers and Infectious Waste Management.

Table 1 shows the total bed availability in hospitals in Jaipur district during Covid-19 in year 2021.

Table 2 shows the bio-data of the respondents: 120 of 216 (55.55%) were aged between 18 and 40 years of age while 96 of 216 (44.44%) were aged between 41 and 65 years. 118 of 216 (55%) were male, while 98 of 216 (45%) were female.

**Table 1** Total no. of beds available in Jaipur city during Covid-19 period, 2021

District	Total hospitals in Jaipur city—126			General beds			Oxygen beds			ICU beds without ventilator			ICU beds with ventilator		
	T	O	A	T	O	A	T	O	A	T	O	A	T	O	A
Jaipur	2815	93	2722	3178	44	3134	924	16	908	629	76	553			

*Note* The above information is courtesy Medical & Health Department Government of Rajasthan

*Source* <https://Covidinfo.rajasthan.gov.in/Covid-19hospital-wisebedposition-wholeRajasthan.aspx>

**Table 2** Bio-data

Characteristics		N	%
Age of respondents (year)	18–40	120	55.55
	41–65	96	44.44
Gender	Male	118	55
	Female	98	45

**Table 3** Status of cases of COVID in Rajasthan till 31.05.2021

State/UTS	Total cases	Active	Discharged	Deaths	Active ratio	Discharge ratio	Death ratio
Jaipur	1,84,653	37	1,82,861	1754	0.02%	99.03%	0.95%

*Note* The above information is courtesy Medical & Health Department Government of Rajasthan

Table 3 shows the status of cases of Covid in Jaipur as 31.05.2021.

Table 4 included technical questions about respondents' discipline, solid waste rating prior to Covid-19, attention paid to the disposal and management of personal protective equipment (PPE) during and prior to Covid-19, separation of Covid-19 hazardous waste from other solid wastes, extent of PPE use during the pandemic, and whether PPE was purchased from personal purse.

Table 5 No of beds available in Jaipur district, Rajasthan, India during Covid-19 (attached at last).

The number of the confirmed cases increased to 184,653 with 182,861 discharged patients and 1754 deaths as of May 31st, 2021.

The infected patients in Jaipur are confined at the RUHS Hospital isolation unit in Jaipur, the state capital. The S.M.S, on the other hand, is the state's largest government hospital, and it sees suspected cases that are later verified at the diagnostic facility. Various steps have been put in place by the state to limit the epidemic and manage its extremely contagious medical waste.

The present investigation found that both study sites had double-chambered storage facilities for processing hazardous trash. As a result, all trash coming from the hospital must be burned openly by waste managers. Furthermore, neither of the research sites separates trash; thus, all of the waste generated by the isolation centers is regarded as infectious waste and sent to the dump yard.

## 5 Conclusion

During the present pandemic in Jaipur District, Rajasthan State, India, this study intended to analyze the circular economy and problems in the management of Covid-19 wastes at two important locations. According to the findings, there are significant

**Table 4** Included technical questions

Characteristics	Number	Percentage
<i>Discipline</i>		
Healthcare worker (doctors, nurses, etc.)	108	50
Cleaner/waste handler	62	28.7
Maintenance staff	46	21.29
<i>Prior to Covid-19, solid waste was rated</i>		
Poor	63	29.16
Good	135	62.5
Very good	15	6.94
Excellent	3	1.38
<i>Is the appropriate attention being paid to the disposal and management of PPE at this time?</i>		
Yes	205	94.9
No	11	5.09
<i>Before Covid-19, how would you evaluate the disposal and management of personal protective equipment (PPE)?</i>		
Poor	57	26.38
Good	128	59.25
Very good	29	13.42
Excellent	2	0.92
<i>Should Covid-19 wastes be segregated from other solid wastes, in your opinion?</i>		
Yes	204	94.44
No	12	5.55
<i>Do you utilize more personal protective equipment (PPE) during Covid-19 than before the pandemic?</i>		
Yes	205	94.9
No	11	5.09
<i>Do you purchase personal protective equipment with your own funds?</i>		
Yes	49	22.68
No	167	77.31
<i>How would you rate the Covid-19 disposal and management of expired PPE?</i>		
Poor	27	12.5
Good	116	53.7
Very good	58	26.85
Excellent	15	6.94
<i>Is it possible to prevent the spread of Covid-19 using present waste management practices?</i>		

(continued)

**Table 4** (continued)

Characteristics	Number	Percentage
Yes	170	78.7
No	46	21.29
<i>Do you think you are paying more attention to how you dispose of your worn PPE today than you were before Covid-19?</i>		
Yes	208	96.29
No	8	3.7
<i>Is it possible to dispose of Covid-19 wastes in separate trash bins?</i>		
Yes	118	54.62
No	98	45.37
<i>Is it possible for Covid-19 to spread through solid waste?</i>		
Yes	200	92.59
No	16	7.4
<i>How often does your company's solid trash be hauled away to be disposed of?</i>		
Daily	152	70.37
Twice daily	56	25.92
Every two days	6	2.77
More than two days	2	0.92

flaws in the handling of hazardous wastes. The two regions employ linear economy and use double-chambered storage facilities for final waste disposal.

The majority of respondents (59.25%) rated the management of used Covid-19 PPE as good, 94.9% agreed to more used PPE during the pandemic than before; some (22.68%) use their own money to provide PPE for their own safety; 78.7% believe current waste management practices are effective in preventing Covid-19 spread, and the majority (96.29%) pay more attention during the pandemic than before. The respondents in this survey appear to be aware of the hazards that may arise from improper waste management; nonetheless, healthcare providers must do more in terms of providing sufficient PPE and trash management. Government of Rajasthan has to dispose the biomedical waste in one step directly out of city instead of two steps in Jhalana, Jaipur, and then to out of city Jamdoli, Jaipur.

**Table 5** No of beds available in Jaipur district, Rajasthan, India, during Covid-19 as on 31.05.2021

S. No		District		Hospital name		General beds			Oxygen beds			ICU beds without ventilator			ICU beds with ventilator			Hospital helpline No	Dist. control room No
						T	O	A	T	O	A	T	O	A	T	O	A		
				Total	2815	93	2722	3178	44	3134	924	16	908	629	76	553			
1	Jaipur			AARYA Hospital JLN MARG	0	0	0	0	0	0	0	0	0	0	0	0	NA	0141-2605858	
2	Jaipur			APEX Hospitals Pvt Ltd	18	0	18	20	0	20	20	0	20	10	0	10	8306177764	0141-2605858	
3	Jaipur			Aanch Hospital	0	0	0	17	0	17	11	0	11	4	0	4	8949192003	0141-2605858	
4	Jaipur			Advanced Neurology and Superspeciality Hospital	0	0	0	13	0	13	4	0	4	3	0	3	0141-2724258	0141-2605858	
5	Jaipur			Amer Medical and Research Hospital, Mansarovar	3	0	3	36	0	36	11	0	11	10	0	10	8000126320	0141-2605858	
6	Jaipur			Asian Cancer Hospital	0	0	0	20	0	20	0	0	0	0	0	0	9413849602	0141-2605858	
7	Jaipur			Asopa Hospital	0	0	0	7	0	7	7	0	7	1	0	1	0141-2246161	0141-2605858	
8	Jaipur			Asthma Bhawan	0	0	0	35	0	35	7	0	7	0	0	0	8302199357	0141-2605858	

(continued)

Table 5 (continued)

Beds availability in hospitals in Jaipur District, Rajasthan, India																
S. No	District	Hospital name	General beds			Oxygen beds			ICU beds without ventilator			ICU beds with ventilator			Hospital helpline No	Dist. control room No
			T	O	A	T	O	A	T	O	A	T	O	A		
		Total	2815	93	2722	3178	44	3134	924	16	908	629	76	553		
9	Jaipur	Avani Maternity and General Hospital, 22 Godam	10	0	10	20	0	20	6	0	6	0	0	0	NA	0141-2605858
10	Jaipur	B.L. Choudray Hospital Kalwad road Jhotwara	22	1	21	20	0	20	4	0	4	4	0	4	9571178373	0141-2605858
11	Jaipur	BDM Kotputli	70	1	69	30	2	28	0	0	0	0	0	0	9116534500	0141-2605858
12	Jaipur	Balaji Soni Hospital, Bagru	32	0	32	14	0	14	4	0	4	0	0	0	NA	0141-2605858
13	Jaipur	Bhagwan Mahaveer Cancer Hospital	28	1	27	10	0	10	0	0	0	2	0	2	0141-2700107	0141-2605858
14	Jaipur	Bhandhari Hospital and Research Center, Jaipur	7	0	7	36	0	36	7	0	7	7	0	7	8003295163	0141-2605858
15	Jaipur	C K Birla Hospital	0	0	0	6	0	6	12	1	11	1	0	1	9549022994	0141-2605858

(continued)

**Table 5** (continued)

Beds availability in hospitals in Jaipur District, Rajasthan, India																
S. No	District	Hospital name	General beds			Oxygen beds			ICU beds without ventilator			ICU beds with ventilator			Hospital helpline No	Dist. control room No
			T	O	A	T	O	A	T	O	A	T	O	A		
		Total	2815	93	2722	3178	44	3134	924	16	908	629	76	553		
16	Jaipur	CHC AMER	1	0	1	5	0	5	0	0	0	0	0	0	NA	0141-2605858
17	Jaipur	CHC Bassi	20	0	20	10	0	10	0	0	0	0	0	0	1429294213	0141-2605858
18	Jaipur	CHC Bichoon	50	0	50	18	0	18	0	0	0	0	0	0	9079116498	0141-2605858
19	Jaipur	CHC JALSU	10	1	9	9	0	9	0	0	0	0	0	0	9024354599	0141-2605858
20	Jaipur	CHC JAMWA RAMGARH	10	0	10	10	0	10	0	0	0	0	0	0	9829320343	0141-2605858
21	Jaipur	CHC Jobner	10	0	10	10	0	10	0	0	0	0	0	0	01425-254220	0141-2605858
22	Jaipur	CHC Kothkhawada	10	0	10	10	0	10	0	0	0	0	0	0	9829208032	0141-2605858
23	Jaipur	CHC NARHEDA	20	0	20	20	1	19	0	0	0	0	0	0	9530178090	0141-2605858
24	Jaipur	CHC PAWTA	5	0	5	5	0	5	0	0	0	0	0	0	NA	0141-2605858
25	Jaipur	CHC Phagi	50	0	50	10	0	10	1	0	1	0	0	0	8824266929	0141-2605858
26	Jaipur	CHC Phulera	5	0	5	5	0	5	0	0	0	0	0	0	NA	0141-2605858
27	Jaipur	CHC Renwal	0	0	0	10	0	10	0	0	0	0	0	0	01424-226104	0141-2605858
28	Jaipur	CHC SAMOD	20	0	20	13	0	13	17	0	17	0	0	0	8947947969	0141-2605858
29	Jaipur	CHC SHAHPURA	18	0	18	18	4	14	0	0	0	0	0	0	9116152442	0141-2605858
30	Jaipur	CHC SIRSI	9	0	9	6	0	6	0	0	0	0	0	0	NA	0141-2605858

(continued)



**Table 5** (continued)

Beds availability in hospitals in Jaipur District, Rajasthan, India																
S. No	District	Hospital name	General beds			Oxygen beds			ICU beds without ventilator			ICU beds with ventilator			Hospital helpline No	Dist. control room No
			T	O	A	T	O	A	T	O	A	T	O	A		
		Total	2815	93	2722	3178	44	3134	924	16	908	629	76	553		
31	Jaipur	CHC Sambhar	15	0	15	10	0	10	0	0	0	0	0	0	1425229412	0141-2605858
32	Jaipur	CHC Tunga	6	0	6	4	0	4	0	0	0	0	0	0	7374004599	0141-2605858
33	Jaipur	CHC VIRAT NAGAR	10	0	10	5	0	5	0	0	0	0	0	0	01422-243531	0141-2605858
34	Jaipur	CKS Hospitals	5	0	5	10	0	10	10	0	10	10	0	10	7230001367	0141-2605858
35	Jaipur	Cradle Children Hospital Vaisali Nagar	0	0	0	6	0	6	6	0	6	2	0	2	0141-6761628	0141-2605858
36	Jaipur	Chirayu Hospital, Jaipur	0	0	0	57	0	57	19	0	19	9	0	9	7230025066	0141-2605858
37	Jaipur	Covid Care Center, Radha Soami Satsang Beas, Bilwa	0	0	0	0	0	0	0	0	0	0	0	0	7023557768	0141-2605858
38	Jaipur	Criticonix Khandaka Hospital	0	0	0	15	0	15	7	0	7	3	0	3	9928180283	0141-2605858
39	Jaipur	Deshbandhu Ent Hospital	10	0	10	10	0	10	8	2	6	0	0	0	0141 4024043	0141-2605858
40	Jaipur	Danashivam Hospital, Jaipur	8	0	8	16	0	16	7	0	7	1	0	1	0141-223220	0141-2605858

(continued)

Table 5 (continued)

Beds availability in hospitals in Jaipur District, Rajasthan, India																
S. No	District	Hospital name	General beds			Oxygen beds			ICU beds without ventilator			ICU beds with ventilator			Hospital helpline No	Dist. control room No
			T	O	A	T	O	A	T	O	A	T	O	A		
		Total	2815	93	2722	3178	44	3134	924	16	908	629	76	553		
41	Jaipur	Deep Hospital and Research Center, Jaipur	12	0	12	28	0	28	12	0	12	4	0	4	0141-2466330	0141-2605858
42	Jaipur	Dhanwantri Hospital and Research Center, Jaipur	0	0	0	10	0	10	12	0	12	8	0	8	6375285763	0141-2605858
43	Jaipur	ESIC Model Hospital, Jaipur	140	0	140	60	0	60	0	0	0	0	0	0	1412228038	0141-2605858
44	Jaipur	Eternal Hospital, Jaipur	5	0	5	63	0	63	41	0	41	4	0	4	0141-5174000, 2774000, 9549651555	0141-2605858
45	Jaipur	Fortis Hospital	0	0	0	91	0	91	30	1	29	4	0	4	9602541710	0141-2605858
46	Jaipur	GP Shekhawati Hospital	0	0	0	42	0	42	22	0	22	6	0	6	+91 7728-852929	0141-2605858
47	Jaipur	Gupta Chest and General Hospital Kalwad Road Hospital Kalwad Road	30	0	30	26	0	26	5	0	5	2	0	2	NA	0141-2605858
48	Jaipur	HCG Cancer Hospital	0	0	0	30	0	30	0	0	0	0	0	0	NA	0141-2605858

(continued)

**Table 5** (continued)

Beds availability in hospitals in Jaipur District, Rajasthan, India																
S. No	District	Hospital name	General beds			Oxygen beds			ICU beds without ventilator			ICU beds with ventilator			Hospital helpline No	Dist. control room No
			T	O	A	T	O	A	T	O	A	T	O	A		
		Total	2815	93	2722	3178	44	3134	924	16	908	629	76	553		
49	Jaipur	Heart and General Hospital	5	0	5	15	0	15	15	2	13	5	0	5	9352238111	0141-2605858
50	Jaipur	Imperial Hospital and Research Center	0	0	0	5	0	5	0	0	0	3	0	3	9549006777	0141-2605858
51	Jaipur	Indus Hospital	38	0	38	50	0	50	4	0	4	8	0	8	9680030356	0141-2605858
52	Jaipur	Jain ENT Hospital	3	3	0	0	0	0	0	0	0	0	0	0	NA	0141-2605858
53	Jaipur	Jeevan Raksha Multi Speciality Hospital Khatipura Road	30	1	29	35	0	35	5	0	5	3	0	3	01416655892, 9001969740	0141-2605858
54	Jaipur	Jaipur Durbeen Hospital Sodala	15	8	7	25	0	25	4	0	4	0	0	0	9829043953	0141-2605858
55	Jaipur	Jaipur National University Institute for Medical Sciences and Research Center Jaipur	320	0	320	22	0	22	30	0	30	28	0	28	0141 7199012	0141-2605858

(continued)

**Table 5** (continued)

Beds availability in hospitals in Jaipur District, Rajasthan, India																
S. No	District	Hospital name	General beds			Oxygen beds			ICU beds without ventilator			ICU beds with ventilator			Hospital helpline No	Dist. control room No
			T	O	A	T	O	A	T	O	A	T	O	A		
		Total	2815	93	2722	3178	44	3134	924	16	908	629	76	553		
56	Jaipur	Jaipuria hospital	206	43	163	50	0	50	3	3	0	21	0	21	1412553358	0141-2605858
57	Jaipur	Jan Kalyan Hospital Chomu	0	0	0	0	0	0	0	0	0	0	0	0	NA	0141-2605858
58	Jaipur	Jeevan Rekha Hospital	0	0	0	25	0	25	6	0	6	3	0	3	0141-5155050	0141-2605858
59	Jaipur	Jyoti Nursing Home Jaipur	10	0	10	30	0	30	3	0	3	2	0	2	9314404024	0141-2605858
60	Jaipur	K.R.M Hospital	15	0	15	40	0	40	9	0	9	2	0	2	9166212336	0141-2605858
61	Jaipur	Khandaka Hospital	6	0	6	8	0	8	3	0	3	3	0	3	NA	0141-2605858
62	Jaipur	Khandelwal Heart Institute Vichyadhar Nagar	0	0	0	7	0	7	2	0	2	1	0	1	7737014388	0141-2605858
63	Jaipur	Krishiv Hospital Vaishali	0	0	0	22	0	22	15	0	15	13	2	11	9251023775, 8980829090	0141-2605858
64	Jaipur	M.J.F. Hospital Chomu	10	0	10	10	0	10	5	0	5	5	0	5	9829269004	0141-2605858

(continued)

Table 5 (continued)

Beds availability in hospitals in Jaipur District, Rajasthan, India																
S. No	District	Hospital name	General beds			Oxygen beds			ICU beds without ventilator			ICU beds with ventilator			Hospital helpline No	Dist. control room No
			T	O	A	T	O	A	T	O	A	T	O	A		
		Total	2815	93	2722	3178	44	3134	924	16	908	629	76	553		
65	Jaipur	Manas Hospital Heerapura Road	0	0	0	0	0	0	0	0	0	0	0	0	8104040163	0141-2605858
66	Jaipur	Mexwell Multispeciality and General Hospital Peetal Factory	0	0	0	0	0	0	0	0	0	0	0	0	NA	0141-2605858
67	Jaipur	Maharaj Vinayak General Hospital	23	0	23	15	0	15	12	0	12	4	0	4	9785400723, 8875484888, 8209112988	0141-2605858
68	Jaipur	Maharaja Agarsen Hospital	0	0	0	0	0	0	11	0	11	7	1	6	9784837830	0141-2605858
69	Jaipur	Mahatma Gandhi Hospital Jaipur	0	0	0	350	0	350	50	0	50	80	2	78	8306998891	0141-2605858
70	Jaipur	Mahila Chikitsalaya Sangneri Gate	20	20	0	20	0	20	10	0	10	10	0	10	0141-2617824	0141-2605858
71	Jaipur	Manipal Hospitals Jaipur	10	0	10	50	0	50	15	3	12	15	3	12	8003898907	0141-2605858

(continued)

Table 5 (continued)

Beds availability in hospitals in Jaipur District, Rajasthan, India																
S. No	District	Hospital name	General beds			Oxygen beds			ICU beds without ventilator			ICU beds with ventilator			Hospital helpline No	Dist. control room No
			T	O	A	T	O	A	T	O	A	T	O	A		
		Total	2815	93	2722	3178	44	3134	924	16	908	629	76	553		
72	Jaipur	Manjeet Institute of Critical care Viddhyadhar Nagar	0	0	0	20	5	15	20	2	18	0	0	0	9251101110	0141-2605858
73	Jaipur	Marudhar Hospital	5	0	5	2	0	2	2	0	2	1	0	1	0141-2356944, 7221000123	0141-2605858
74	Jaipur	Maxwell Hospital	23	0	23	23	0	23	7	0	7	7	0	7	0141-2283683	0141-2605858
75	Jaipur	Metro MAS Hospital Jaipur	18	0	18	18	0	18	7	0	7	3	0	3	7665009641	0141-2605858
76	Jaipur	Metro city Hospital, Jhotwara	5	0	5	14	0	14	9	0	9	1	0	1	9667059913	0141-2605858
77	Jaipur	Military Hospital	12	0	12	101	0	101	0	0	0	7	0	7	8890014418	0141-2605858
78	Jaipur	Monica hospital	6	0	6	12	0	12	6	0	6	1	0	1	9352790668	0141-2605858
79	Jaipur	Monilek Hospital	45	0	45	45	0	45	4	0	4	7	0	7	8949379459, 7221000123	0141-2605858
80	Jaipur	NIMS Hospital Jaipur	140	0	140	25	1	24	30	0	30	55	0	55	9784717000	0141-2605858

(continued)

**Table 5** (continued)

Beds availability in hospitals in Jaipur District, Rajasthan, India																
S. No	District	Hospital name	General beds			Oxygen beds			ICU beds without ventilator			ICU beds with ventilator			Hospital helpline No	Dist. control room No
			T	O	A	T	O	A	T	O	A	T	O	A		
		Total	2815	93	2722	3178	44	3134	924	16	908	629	76	553		
81	Jaipur	Narayana Multispeciality Hospital, Jaipur	2	0	2	4	0	4	2	0	2	2	0	2	01417122200, 8696950077	0141-2605858
82	Jaipur	Om Hospital and Trauma Center	10	0	10	15	0	15	22	0	22	3	0	3	9950370110/8764011010	0141-2605858
83	Jaipur	Pink Vinayak Hospital Dulesvar Gardan	25	0	25	25	0	25	5	0	5	3	0	3	7206623053	0141-2605858
84	Jaipur	Pooja hospital	0	0	0	4	0	4	5	2	3	5	1	4	9694000116	0141-2605858
85	Jaipur	R.N. Multi Speciality Hospital Nirman Nagar	6	0	6	13	0	13	2	0	2	1	0	1	NA	0141-2605858
86	Jaipur	RAJ Khurana Memorial Adrash Nagar	10	0	10	10	0	10	8	0	8	0	0	0	+91 8104655745	0141-2605858
87	Jaipur	RKB Maxima Hospital	0	0	0	38	0	38	0	0	0	0	0	0	8000654909	0141-2605858
88	Jaipur	RUHS Hospital	628	3	625	442	23	419	39	0	39	125	39	86	NA	0141-2605858
89	Jaipur	Radha Hospital	12	0	12	14	0	14	3	0	3	1	0	1	9782910099	0141-2605858

(continued)

**Table 5** (continued)

Beds availability in hospitals in Jaipur District, Rajasthan, India																
S. No	District	Hospital name	General beds			Oxygen beds			ICU beds without ventilator			ICU beds with ventilator			Hospital helpline No	Dist. control room No
			T	O	A	T	O	A	T	O	A	T	O	A		
		Total	2815	93	2722	3178	44	3134	924	16	908	629	76	553		
90	Jaipur	Raj ENT Hospital Jaipur	0	0	0	0	0	0	0	0	0	0	0	0	NA	0141-2605858
91	Jaipur	Rajasthan Hospital	0	0	0	30	0	30	61	0	61	6	0	6	8696666417	0141-2605858
92	Jaipur	Raksha Hospital Jhotwara	5	0	5	15	0	15	6	0	6	0	0	0	7976196121	0141-2605858
93	Jaipur	Railway Hospital	60	0	60	30	0	30	5	0	5	5	0	5	1412222573	0141-2605858
94	Jaipur	Ramanji Hospital	28	3	25	13	0	13	8	0	8	1	0	1	1412973926	0141-2605858
95	Jaipur	Regen hospital	15	0	15	35	0	35	21	0	21	5	0	5	91168 89911	0141-2605858
96	Jaipur	Rungta	0	0	0	61	0	61	7	0	7	15	0	15	0141-4039999	0141-2605858
97	Jaipur	S.K.G Hospital and Research Center Vidhydhar Nagar	5	0	5	5	0	5	4	0	4	1	0	1	9672064954	0141-2605858
98	Jaipur	S.R.K. Hospital Lalkothi	6	0	6	15	0	15	10	0	10	1	0	1	1414922333	0141-2605858

(continued)



Table 5 (continued)

Beds availability in hospitals in Jaipur District, Rajasthan, India																
S. No	District	Hospital name	General beds			Oxygen beds			ICU beds without ventilator			ICU beds with ventilator			Hospital helpline No	Dist. control room No
			T	O	A	T	O	A	T	O	A	T	O	A		
		Total	2815	93	2722	3178	44	3134	924	16	908	629	76	553		
99	Jaipur	S.R.K. Hospital Lalkothi	0	0	0	0	0	0	0	0	0	0	0	0	NA	0141-2605858
100	Jaipur	Sadhna Hospital Khatipura Road	14	0	14	6	0	6	6	0	6	1	0	1	NA	0141-2605858
101	Jaipur	SDH Dudu	5	0	5	0	0	0	0	0	0	0	0	0	1428277233	0141-2605858
102	Jaipur	SDM Hospital	52	0	52	20	2	18	2	0	2	2	1	1	रवि कपूर/9929607050	0141-2605858
103	Jaipur	Shanti Hospital Balaji Vihar, Niwaru Road	5	0	5	3	0	3	2	0	2	0	0	0	NA	0141-2605858
104	Jaipur	Shree Nidan Hosp Ajmer Road	14	4	10	5	0	5	2	0	2	2	0	2	NA	0141-2605858
105	Jaipur	SMS Medical College Jaipur	0	0	0	50	0	50	0	0	0	35	27	8	1412569898	0141-2605858
106	Jaipur	Saket Hospital (A Unit of Saket Medicare and Research Center Pvt Ltd)	12	0	12	46	0	46	16	0	16	6	0	6	0141-2785075	0141-2605858

(continued)

Table 5 (continued)

Beds availability in hospitals in Jaipur District, Rajasthan, India																
S. No	District	Hospital name	General beds			Oxygen beds			ICU beds without ventilator			ICU beds with ventilator			Hospital helpline No	Dist. control room No
			T	O	A	T	O	A	T	O	A	T	O	A		
		Total	2815	93	2722	3178	44	3134	924	16	908	629	76	553		
107	Jaipur	Sardar Singh Memorial Hospital	10	0	10	10	0	10	0	0	0	0	0	0	8003077223	0141-2605858
108	Jaipur	Satellite Chaksu	20	0	20	5	0	5	0	0	0	0	0	0	820984387	0141-2605858
109	Jaipur	Satellite Sanganer	10	0	10	7	0	7	0	0	0	0	0	0	1412723273	0141-2605858
110	Jaipur	Sevyan Hospital civil line	4	0	4	8	0	8	0	0	0	0	0	0	8003214000	0141-2605858
111	Jaipur	Sewaytan Hospital Sodala	20	0	20	6	0	6	12	0	12	2	0	2	2943142	0141-2605858
112	Jaipur	Shalby hospital	0	0	0	70	0	70	0	0	0	0	0	0	7947080307	0141-2605858
113	Jaipur	Shiv Adarsh Hospital Bindayka	3	0	3	15	0	15	5	0	5	2	0	2	9887151962	0141-2605858
114	Jaipur	Shiv Dhara Chomu	15	0	15	10	0	10	5	0	5	0	0	0	8739879000	0141-2605858
115	Jaipur	Shiv Trident Hospital Vaisali Nagar	17	4	13	17	4	13	12	0	12	1	0	1	8619217018	0141-2605858

(continued)

**Table 5** (continued)

Beds availability in hospitals in Jaipur District, Rajasthan, India																
S. No	District	Hospital name	General beds			Oxygen beds			ICU beds without ventilator			ICU beds with ventilator			Hospital helpline No	Dist. control room No
			T	O	A	T	O	A	T	O	A	T	O	A		
		Total	2815	93	2722	3178	44	3134	924	16	908	629	76	553		
116	Jaipur	Shree Ambe Hospital Newaru Road	14	0	14	0	0	0	11	0	11	1	0	1	9462354194	0141-2605858
117	Jaipur	Siddham ENT Hospital	5	0	5	9	0	9	3	0	3	2	0	2	7742110099	0141-2605858
118	Jaipur	Sir Chotu Ram Hospital, Vaushali Nagar	0	0	0	0	0	0	0	0	0	0	0	0	9413790790	0141-2605858
119	Jaipur	Somani Hospital	7	0	7	7	0	7	7	0	7	0	0	0	NA	0141-2605858
120	Jaipur	Soni Hospital	10	0	10	41	0	41	7	0	7	1	0	1	9001669977	0141-2605858
121	Jaipur	Sparsh Hospital	10	0	10	30	0	30	17	0	17	3	0	3	7732909036	0141-2605858
122	Jaipur	Star Women and General Hospital	70	0	70	15	0	15	0	0	0	0	0	0	8239252272	0141-2605858
123	Jaipur	Tagore hospital	28	0	28	25	0	25	5	0	5	2	0	2	9610488880	0141-2605858
124	Jaipur	Unique Sangeeta Vaushali	10	0	10	15	1	14	8	0	8	2	0	2	9511858425	0141-2605858
125	Jaipur	Urmil hospital	0	0	0	20	1	19	8	0	8	2	0	2	7221072260	0141-2605858

(continued)

**Table 5** (continued)

Beds availability in hospitals in Jaipur District, Rajasthan, India																
S. No	District	Hospital name	General beds			Oxygen beds			ICU beds without ventilator			ICU beds with ventilator			Hospital helpline No	Dist. control room No
			T	O	A	T	O	A	T	O	A	T	O	A		
		Total	2815	93	2722	3178	44	3134	924	16	908	629	76	553		
126	Jaipur	Vedanta Superspeciality Hospital	14	0	14	4	0	4	11	0	11	1	0	1	9358845571	0141-2605858

*Note* The above information is courtesy Medical & Health Department Government of Rajasthan  
*Source* <https://Covidinfo.rajasthan.gov.in/Covid-19hospital-wisebedposition-wholeRajasthan.aspx>

## References

1. Yuan Z, Bi J, Moriguichi Y (2006) The circular economy: A new development strategy in China. *J Ind Ecol* 10(1–2):4–8
2. Feng Z (2004) Circular economy overview. People's Publishing House, Beijing, China, pp 18–25
3. Sharma M, Jain NL, Purohit JK. A Review of Circular Economy in Manufacturing Sector
4. Olukanni DO, Mokuolu OA, Lasode OA, Ahoje MA, Ojowuro OM (2019) Circular economy: Nigeria perspective. Springer, pp 279–297
5. Sharma M, Purohit JK (2019) Indicators for sustainable manufacturing for industries—a review. In: International conference on recent trends and innovation in engineering
6. Mokuolu OA, Akindele RS, Olawumi HO (2016) Development of improved solid hospital waste management practices in a Nigerian Tertiary Hospital. *Niger J Technol* 35(3):674–680
7. Nzeadibe TC, Ejike-Alieji AU (2020) Solid waste management during Covid-19 pandemic: policy gaps and prospects for inclusive waste governance in Nigeria. *Local Environ* 25(7):527–535
8. Oruonye ED, Ahmed AY (2020) Covid-19 and challenges of management of infectious medical waste in Nigeria: a case of Taraba State. *Int J Waste Resour* 10(3):381–385
9. Onoh RC, Adeke AS, Umeokonkwo CD, Ekwedigwe KC, Agboeze J, Ogah EO (2019) Knowledge and practices of health-care waste management among health workers in Lassa
10. Sharma M, Purohit JK (2020) Achieving sustainable mass customization capabilities—a review *UGC CARE* 10(6):299–304
11. Hantoko D, Li X, Pariatamby A, Yoshikawa K, Horttanainen M, Yan M (2021) Challenges and practices on waste management and disposal during COVID-19 pandemic. *J Environ Manage* 286:112140
12. Ezirim I, Agbo F (2018) Role of national policy in improving health care waste management in Nigeria. *J Health Pollu* 8(19)
13. Chidiebere OA, Abubakar M, Shabako JG (2018) municipal solid waste management in African cities: a case study of Lagos State, Nigeria. *Malays J Civ Eng* 30(1)
14. Sumathi VR, Natesan U, Sarkar C (2008) GIS-based approach for optimized siting of municipal solid waste landfill. *Waste Manage* 28(11):2146–2160
15. Creswell JW (2009) Research design: qualitative and mixed methods approaches, 3rd edn

# Atomization Casting of Al–Si Alloys and Their Characterization



Krishna Vijay, Utkarsh Mishra, and Subodh Kumar Sharma

**Abstract** Atomization casting provides the low-cost casting process with better attributes and performance. It acts as a major competitor for existing technologies, such as normal casting and powder casting route. The economy benefit in this process is derived from a step integrated operation of converting superheated molten alloy directly into a semi-finished product. Atomization casting converts a molten stream into a spray of droplets by high pressure gas atomization. The grain refinement is occurred in Al-6%Si and Al-12%Si atomization cast alloys.

**Keywords** Atomization casting · Mechanical property · Convergent divergent nozzle

## 1 Introduction

Aluminum alloys are widely used due to its light weight property and good response to various finishing process. It is widely used in automobile and aerospace.

Silicon provides the improved wear resistance to its alloys [1]. Al–Si alloys are widely used in various application such as in connecting rods, cylinder sleeve, piston rings, lightweight optics, etc., due to its attractive properties. Hypereutectic Al–Si alloys produced by conventional method have large grain growth is found [2] because of slow cooling, which create the difficulty in the machining of the material. In case of rheocasting, some grain refinement occurs in Al–Si alloys as compared to that of conventional casting [3].

---

K. Vijay (✉) · U. Mishra · S. K. Sharma  
KIET Group of Institutions, Ghaziabad, India  
e-mail: [krishna.ojha@kiet.edu](mailto:krishna.ojha@kiet.edu)

© The Author(s), under exclusive license to Springer Nature Singapore Pte Ltd. 2023  
R. P. Singh et al. (eds.), *Advances in Modelling and Optimization of Manufacturing and Industrial Systems*, Lecture Notes in Mechanical Engineering,  
[https://doi.org/10.1007/978-981-19-6107-6\\_13](https://doi.org/10.1007/978-981-19-6107-6_13)

175

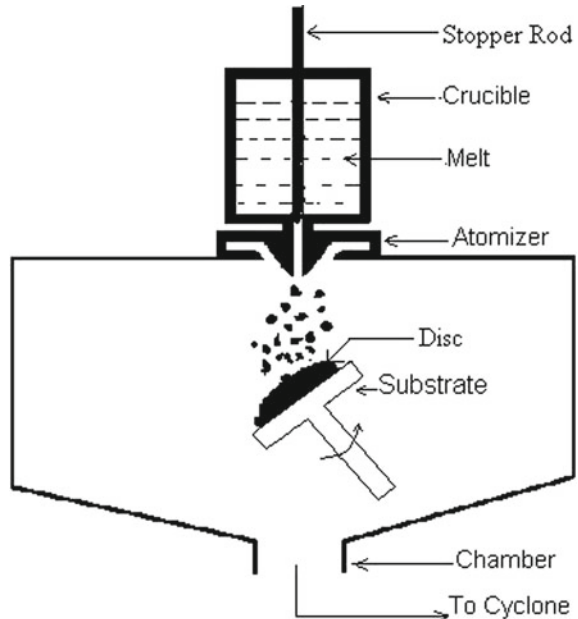
These droplets produced in atomization cool rapidly in flight and arrive at the preform with sufficient liquid content to spread on the preform surface to form a dense surface layer with a very fine and uniform microstructure [4].

## 2 Experimental

### 2.1 Setup

The setup (schematic) of atomization casting is described in Fig. 1. The picture of atomization casting is shown in Fig. 2. The photograph of rotating and tilting substrate is described in Fig. 3. The nozzle is placed on the top of the setup, and the resistance heating furnace is put above the nozzle. The alloy was heated to melt in the crucible. A stopper rod was placed to prevent the melt flow through the delivery tube before passing gas from the atomizer. The stopper rod was removed after the gas flow in atomizer to start the atomization of molten metal. The atomized droplets were collected over the copper disk of thickness 7 mm and diameter 190 mm which could be inclined at desired angle and could also be rotated at varying r.p.m.

**Fig. 1** Schematic arrangement of atomization casting



**Fig. 2** Photograph of atomization casting setup



## 2.2 *Microstructure*

Approximately on Kg of alloy is taken for preparation of atomization cast sample. The alloy were heated to 200 °C above its liquidus temperature. The melting point of different composition of Al–Si alloys can be obtained from the phase diagram of Al–Si alloy. Nitrogen gas was supplied for atomization. The deposition was carried out for Al-6%Si, Al-12%Si and a nitrogen gas pressure of 7 kg/cm<sup>2</sup>. The preforms were made for 400 mm distance of substrate from atomizer.

Samples from the different parts of cast deposits were cut for its microstructural figure. These samples were prepared using technique mentioned elsewhere [2].

## 2.3 *Hardness*

Brinell hardness number of these samples were measured using Brinell hardness testing machine at 15.625 kg load for Al-6%Si and Al-12%Si. The indentation at five places were taken, and the value is averaged to get a final reading of hardness.



**Fig. 3** Photograph of substrate which can be rotated or inclined

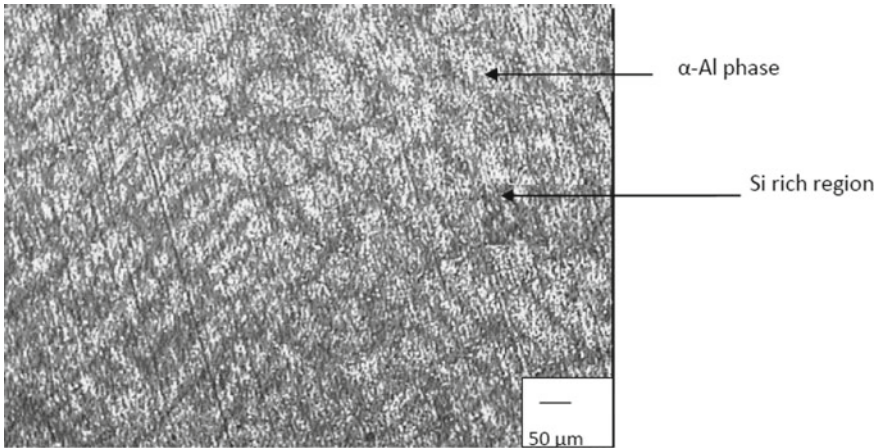


## 2.4 Tensile Properties

Tensile properties were measured by universal testing machine. Tensile testing specimen were taken from the central region of the preform.

## 3 Result and Discussion

The photograph of microstructure of ingot metallurgy cast Al-6%Si is shown in Fig. 4. The microstructural feature of as cast Al-6%Si shows the fine eutectic ferrous silicon particles along the grain boundaries. The grains are found to have dendritic structure. The length is around 40–60  $\mu\text{m}$  and width is around 5–10  $\mu\text{m}$ . The atomization cast microstructure of Al-6%Si is shown in Fig. 5. Figure 5a and b show microstructure at central and peripheral regions, respectively. Grains are finer at the peripheral region. It shows uniform equiaxed grains of Al-6%Si. The silicon is uniformly distributed throughout the casting. The size of grains is 3–8  $\mu\text{m}$ .



**Fig. 4** Microstructure of I/M cast Al-6%Si

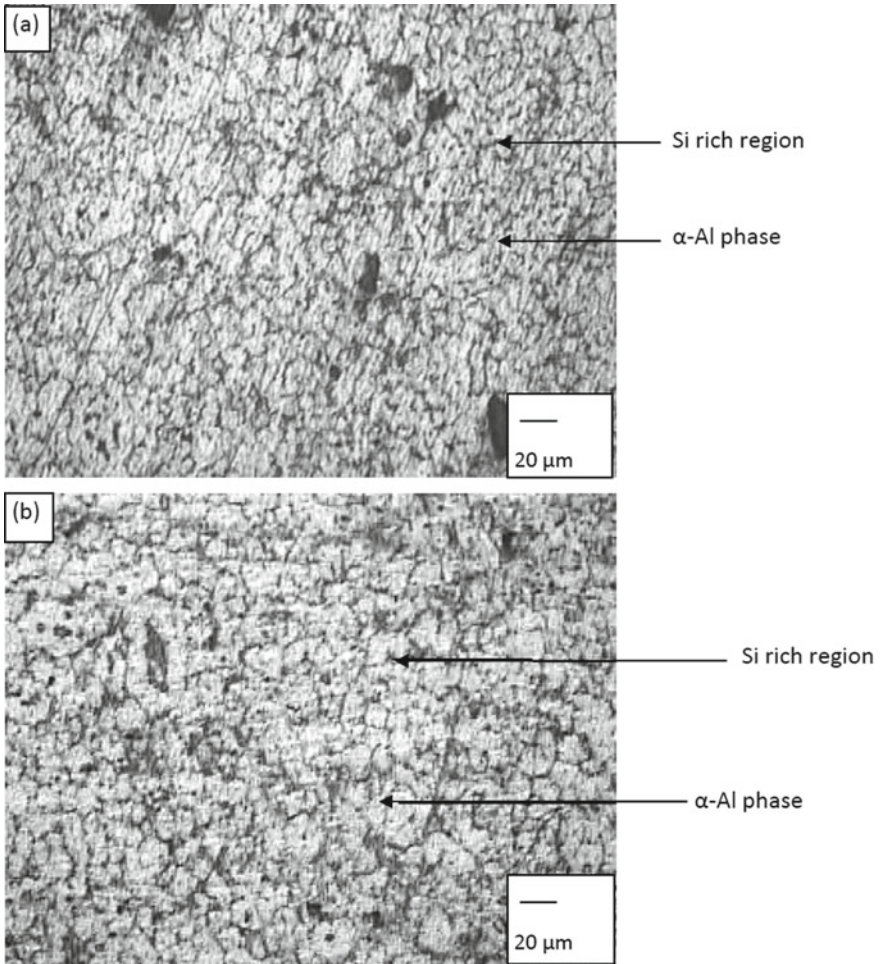
Figure 6 shows the microstructure of I/M cast Al-12%Si alloy. The optical microscopy shows the Si particle,  $\alpha$ -Al and needle shape eutectic Si. The optical microscopy of spray cast sample shows uniform variation of silicon in eutectic phase throughout the casting as shown in Fig. 7. This shows the uniform distribution of eutectic silicon in the matrix. The EPMA results of spray formed Al-12%Si shows that the percentage of Si in Si-rich phase is  $\sim 85.4\%$  Si and percentage of Al in  $\alpha$ -Al is 90.2%. The size of eutectic silicon is 3–8  $\mu\text{m}$ . The equiaxed grains are obtained in spray casting.

Hardness of spray deposit was studied as a function of % Si. The Brinell hardness number is higher for atomization cast Al–Si alloys than that of I/M cast Al–Si alloys and hardness increases with the increase in percentage of Si. The minimum and maximum Brinell hardness number is 56.8 and 70 for 6% Si 12% Si, respectively as compared to I/M cast samples (51 and 65 for I/M cast samples).

The yield strength of spray deposit was studied as a function of % Si. For example, the yield strength of Al-6Si alloy for spray cast and I/M cast are 44.15 and 40.97 MPa, respectively. And for Al-12Si it is 65 MPa and 73 MPa, respectively, for I/M cast and atomization cast alloys. The yield strength increases with the increase in Si content.

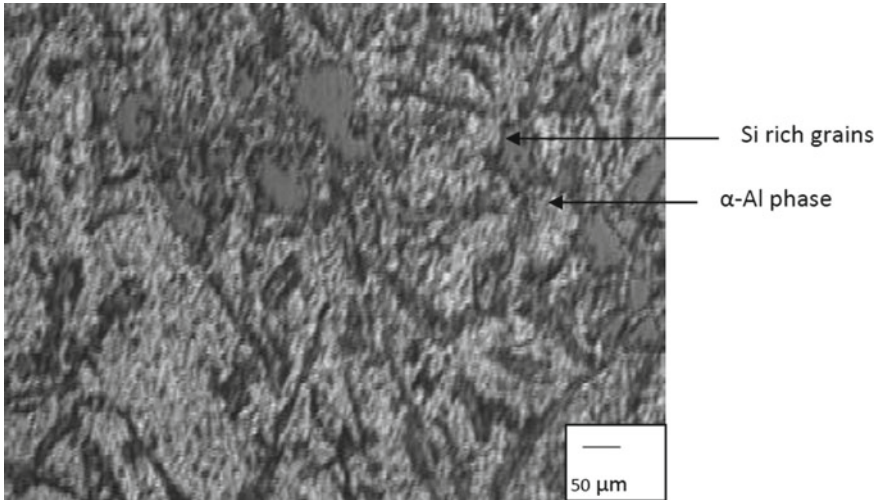
## 4 Conclusion

Grain refinement occurs in the atomization cast Al–Si alloys in contrast to that of ingot metallurgy cast alloys. The uniform distribution of secondary phase is observed in atomization casting. The grain refinement is more at periphery than that of central region.

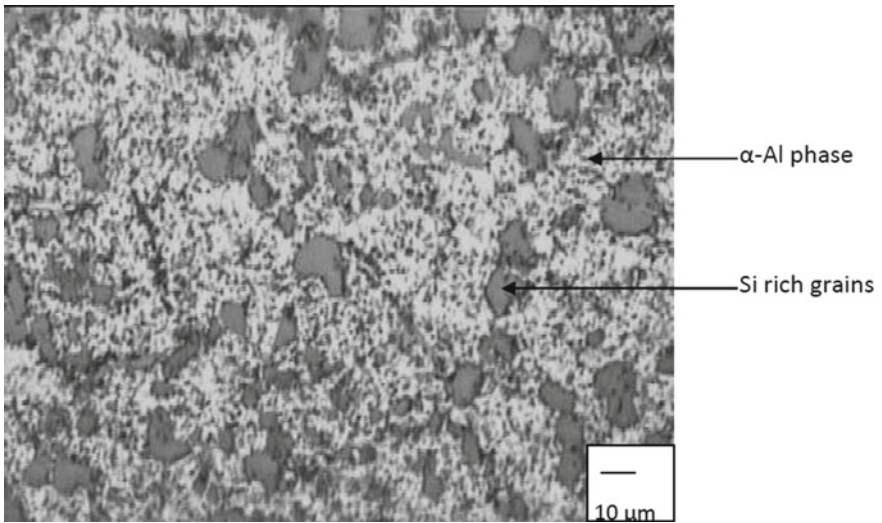


**Fig. 5** **a** Microstructure of atomization-deposited Al-6%Si at central region and **b** at peripheral region of preform showing grain refinement by atomization casting

The hardness of atomization cast Al-Si alloys is comparably good than that of ingot metallurgy cast alloys is observed.



**Fig. 6** Microstructure of I/M cast Al-12%Si showing needle shape of Si-rich grains



**Fig. 7** Microstructure of atomization-deposited Al-12%Si showing grain refinement of Si-rich grains

## References

1. Tenekdjiev N, Gruzleski JE (1990) Hypereutectic aluminium-silicon casting alloys-a review. *Cast Metals* 3(2):96-105
2. Wiess JC, Loper R (1987) Primary silicon in hypereutectic aluminum-silicon alloy. *AFS Trans* 32:5162

3. Dey AK, Poddar P, Singh KK, Sahoo KL (2006) Mechanical and wear properties of rheocast and conventional gravity die cast A356 alloy. *Mater Sci Eng, A* 435–436(5):521–529
4. See JB, Johnston GH (1978) Interaction between nitrogen jets and liquid lead and tin stream. *Powder Tech* 21–5:119–133

# Analysing Effects of HVOF Powder Coating on the Tribological Properties of Inconel 800 Under Non-lubricated Conditions



Sushant Bansal, Ayush Saraf, Ramakant Rana, and Roop Lal

**Abstract** The objective that this paper holds is of analysing the significant effects of coating on Inconel 800 specimen used as the material of the piston ring and being worked at under non-lubricated conditions. The sole aim of the paper is to carry out such experiments which helps in studying the tribological behavioural dynamics of the working on the interface of the HVOF powder-coated Inconel 800 piston ring material and the SS 304 metal as the cylinder material. With the working parameters already defined for the working of the experiment, such as the track distance travelled, the load applied and the sliding velocity over the whole period of wear for different diameters of specimen used, the values of wear, coefficient of friction and the variation in temperature, throughout the experimental duration will be measured. The pin and disc interface will be provided with no lubrication, and the experiment will be run under non-lubricated working condition. The pre-testing and post-experiment testing of the specimen pins, the plate and the powder for coating will also be done so as to analyse the material composition properties using the help of EDAX before and after the undergoing of the experimental process as well as after the spray coating process is done upon the specimen pins, hardness testing of the specimens will also be performed in order to know material's hardness. This study solely helps in a much clearer and supportive understanding of the prospect of the surface coating processes on the surface, which leads to a systematic reduction in the friction and also the enhances the wear resistance of the IC engines' interface taken into consideration.

**Keywords** Inconel · Tribology · Wear · Coating

---

S. Bansal · A. Saraf · R. Rana  
Maharaja Agrasen Institute of Technology, Delhi 110086, India

R. Lal (✉)  
Delhi Technological University, Delhi 110042, India  
e-mail: [rooplal@dtu.ac.in](mailto:rooplal@dtu.ac.in)

© The Author(s), under exclusive license to Springer Nature Singapore Pte Ltd. 2023  
R. P. Singh et al. (eds.), *Advances in Modelling and Optimization of Manufacturing and Industrial Systems*, Lecture Notes in Mechanical Engineering,  
[https://doi.org/10.1007/978-981-19-6107-6\\_14](https://doi.org/10.1007/978-981-19-6107-6_14)

183

## 1 Introduction

The objective that this paper caters to ID to provide an experimental analysis of the notable effects on the surface of the specimen material, i.e. Inconel 800 by various tests. As of now, not many credible researches have been done for observing the variations in the tribological properties of the aforementioned material while observing its working with respect to another material such as SS 304 or any other [1–4].

The linear reciprocating setup is considered to study and observe the effects of the material specimens in contact. The pin represents the piston ring material, whereas the plate represents the wall linings of the engine cylinder. The experiment help determines and calculate the expected improvement in the wear results, so as to observe an increment in the levels of efficiency of the engine cylinder's piston ring materials.

Wear measurements were taken into account, and the analysis was done for the cylinder and piston ring representing material specimen during their constant interaction with each other, when the automotive engine was operated under artificially created dusty environmental conditions [5–9]. Tests were conducted on linear reciprocating test rig with boundary-lubricated cast iron materials and the values of specific wear rates were observed.

### Brief Overview of Reciprocating Type Tribometer Setup

Reciprocating type wear test setup or reciprocating Tribometer is used for measurement of wear and frictional properties of a material. This type of test differs from PIN-ON-DISC setup mainly due to differences in the type of relative motion which the materials undergo with respect to each other [10–12]. Reciprocating type Tribometer uses reciprocating motion either between the cylindrical pin and square plates or ball on plate depending upon the type and motion required, i.e. sliding-type reciprocation or rolling-type reciprocation.

### HVOF Coating

High Velocity Oxygen Fuel Coating machine or HVOF is a thermal-based spray coating machine that utilizes heat in form of flames or any other heat source to form a coating of any material or a mixture of materials in powder form upon the final workpiece which is to be coated [13–15].

The basic principle of the functioning of an HVOF machine is based on the basic thermal spraying process which is explained below:

The HVOF process uses high velocity gas by burning of combustion product in the combustion chamber, this high velocity gas is used to coat the base material with supersonic speed and with very high striking energy for producing a very high dense surface quality of the coating upon the base material at relatively low temperatures as compared to other techniques [14–17]. The particles of the coating powder and the substrate (One which is being coated) form a bond between each other which may be adhesive, due to adherence, any chemical reaction, due to diffusion, or it may also

be a partial fusion between the two surfaces. This bonding of the coating particles and the substrate leads to the formation of a coating that is relatively uniform and is continuous [16–22].

## 2 Methodology

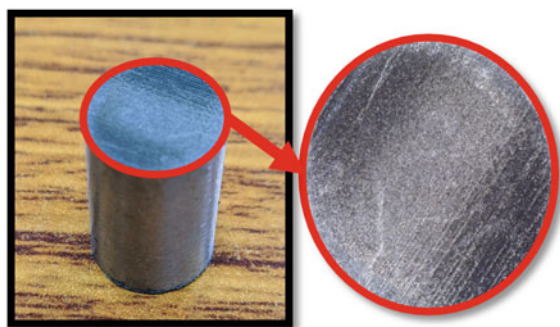
### 2.1 Specimen Preparation Pin and Selection

Inconel alloy 800 is an amalgamation of three metals, namely Chromium, Iron and Nickel. This alloy has the capability of maintaining the stability and also of keeping up its austenitic structure despite experiencing prolonged exposures to high temperatures [23, 24]. Amongst many other characteristics, a namely few of the alloy are good strength, and high resistance to oxidizing, reducing and aqueous environments (Fig. 1).

The dimension of Inconel alloy 800 used for the experiment was 10 mm in diameter and 50 mm in length.

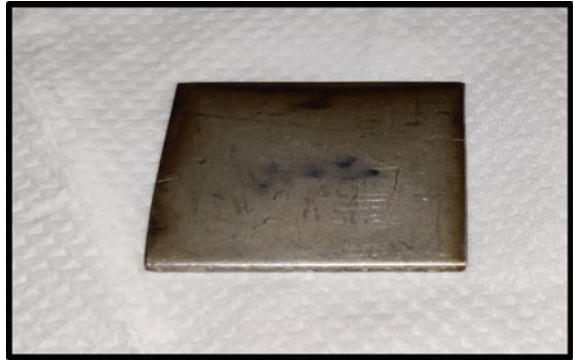
- An uncut rod of Inconel 800 material was selected and acquired as the specimen for the pins. Following this, the Wire Electrical Discharge Machining process was employed upon them to have the pins machined as per the desired and required dimensions. Pins were then collected back after the machining process with dimensions 10 mm in diameter and 50 mm in length. These pins were then subjected to the Surface Grinding finishing process to obtain a clean and smooth surface. The final specimen resulted from the before mentioned processes in conjunction were the Inconel 800 pins, uncoated.
- Similarly, the pins were cut and prepared for the coated specimens' preparation. These pins were then subjected to Sandblasting process to obtain a clear and smooth finished surface. This provided us with the specimen pins now ready for the application of the HVOF coating process upon them. Selected coating powders were thermally sprayed upon the surface of the specimen pins via the

**Fig. 1** Uncoated pin before the experiment





**Fig. 2** Plate specimen before the experimentation



High Velocity Oxy-Fuel process, leading to the surface of the pins getting coated by them. The final specimen resulted from the before mentioned processes in conjunction were the Inconel 800 pins, coated.

## 2.2 Specimen Preparation Plate

This grade of stainless steel belongs to the 300 series of the stainless steel and the austenitic class similar to the 200 series and primarily has the inclusion of a higher content of Nickel added to its alloy than the 200 series [25–28]. The material has high corrosion resistance and a high tensile strength as well (Fig. 2).

The dimension of the plate used for the experiment on the linear reciprocating Tribometer was 40 mm \* 40 mm.

- An AISI 304 grade stainless steel plate was selected and acquired as the material for the specimen of the plate against which the Inconel 800 pins were to be tested. Following this, the Wire Electrical Discharge Machining process was employed upon it to have the plates machined as per the required dimensions, i.e. 40 mm in breadth and 40 mm in length. The plates were then subjected to the Surface Grinding finishing process to obtain a clean and smooth surface.

## 2.3 EDAX Test for Specimens

- (1) The following are the graph and table of composition of **Inconel 800** metal specimen, obtained as a result of the EDAX test (Fig. 3; Table 1).
- (2) Similarly, following are the graph and table of composition of **SS 304** metal specimen, obtained as a result of the EDAX test (Fig. 4; Table 2).

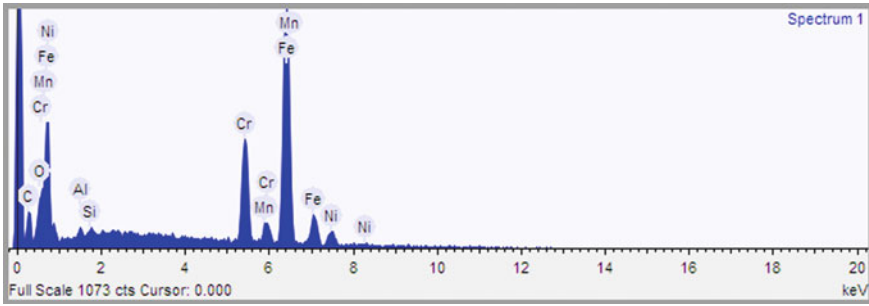


Fig. 3 EDAX graph for Inconel 800

Table 1 EDAX test of Inconel 800

Element	Weight %
Carbon	0.747
Aluminium	0.234
Silicon	0.481
Chromium	18.36
Manganese	0.566
Iron	40.98
Nickel	34.41
Titanium	0.381
Molybdenum	3.84

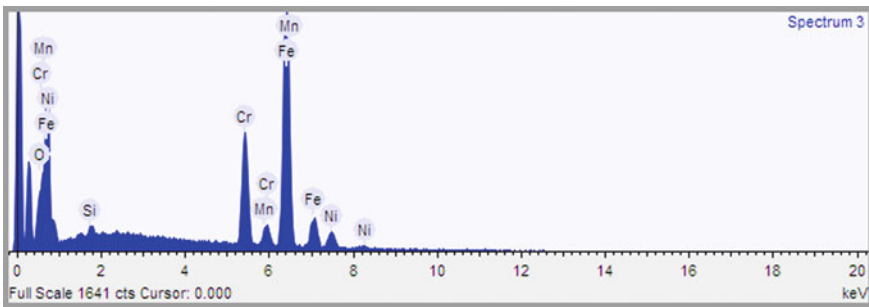


Fig. 4 EDAX graph for SS 304

### 2.4 Powder Selection

It is an extremely hard refractory ceramic material, like tungsten carbide and has one the highest melting and boiling point of a naturally occurring metal which allows it to withstand temperatures as high as up to 3000 °C without any substantial changes

**Table 2** EDAX test of SS 304

Element	Weight %
Oxygen	1.704
Silicon	0.721
Chromium	18.515
Manganese	2.011
Iron	69.133
Nickel	7.914

**Fig. 5** Titanium carbide powder

to its properties; Titanium Carbide Nanoparticles are very hard that makes it an attractive substance for coating [27–32]. It is also resistant to wear over long periods of time ensuring longer life for the material (Fig. 5).

## 2.5 Coating Process Using HVOF

HVOF coating process begins with the introduction of the material selected for the coating application in powder state along with a High Velocity Oxy-Fuel such as Hydrogen and Oxygen into the combustion chamber [33–36]. An ignition source is introduced into the chamber which results in the combustion of the Oxygen and Oxy-Fuel, and the resultant gas along with the powder mixture is sprayed upon the surface of the specimen via a nozzle at high speed and pressure. Since the temperature of the resultant gas is very high, it results in the powder mixture melting and achieving either a melted or partially melted state (Figs. 6 and 7).



Fig. 6 HVOF coating setup in precision manufacturing lab, DTU

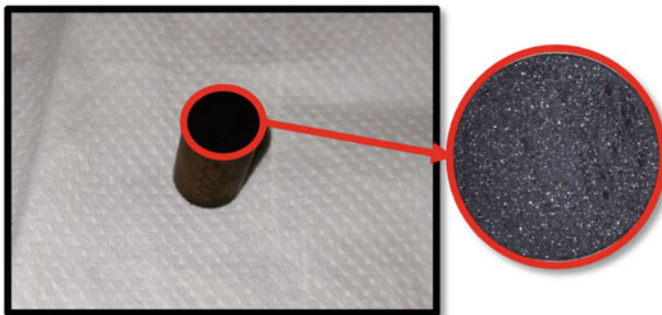


Fig. 7 Coated pin before the experimentation

### 3 Experimentation

#### 3.1 Design of Experiment (DOE)

##### 3.1.1 Design Using Taguchi Method

Taguchi design is the use of statistical methods developed and employed to improve the quality of the product. A planned set of experiments in which various parameters of interest selected, varying over a specified range, is the optimum process to obtain data sets of desired results as close to accuracy as possible. Since the number of experiments and resources required are prohibitively large, Taguchi design eliminates this by using only a subset of the complete set of experiments as it tests selected

parameter pairs in combinations which allows us to gain the same necessary results and lets us know which factors are affecting the quality of the product the most [37, 38].

It employs outer array/orthogonal array experiments, which simulate the random environment in which the product would function and allows the analysis of different chosen parameters by providing their respective impact on the mean and variance of the process performance along with the optimum settings of control parameters that are to be dictated.

### 3.1.2 Selection of Orthogonal Array

The purpose of the orthogonal arrays is to provide with a set of minimum experiments as well as Signal-to-Noise ratios (S/N). These are the log functions of the desired output, and they serve as the working objective functions for the optimization and also help in data analysis and prediction of optimum results.

The selection of orthogonal arrays is dependent upon the number of independent design variables and levels as each array is meant for only specific value of them. In this experiment, we chose 4 different independent variables: load, distance, frequency and stroke with each variable having 3 set values. And the corresponding array for experimenting with 4 independent variables with 3 set values each is the L9 array, which is the one used for this experiment. It was assumed that there was no interaction between any two factors (Table 3).

**Table 3** Experiment design matrix

Experiment number	Independent variables		
	Load (N)	Distance (m)	Frequency (Hz)
1	10	50	20
2	10	100	25
3	10	150	30
4	20	50	30
5	20	100	20
6	20	150	25
7	30	50	25
8	30	100	30
9	30	150	20

### 3.2 Linear Tribology Test

For emulation of cylinder-piston interface and evaluating the property such as wear resistance for different material interfaces, tribological test was performed. Pin-On-Disc Setup provided us with a continuous reciprocating type contact motion between the pin and plate contact which coincides with the application of this interface as a piston and cylinder form when used in automobiles. It provided us with an accurate and effective way to produce results which were as close to being real as possible.

Bolting of disc onto the setup ensured secure operation of setup during the experimentation. Tribometer was used with a normal load range of 5–50 N, frequency range of 1–50 Hz and stroke range of 1–20 mm.

The experiments were performed for a constant temperature and by varying the other parameters individually for a set of iterations in the following ranges:

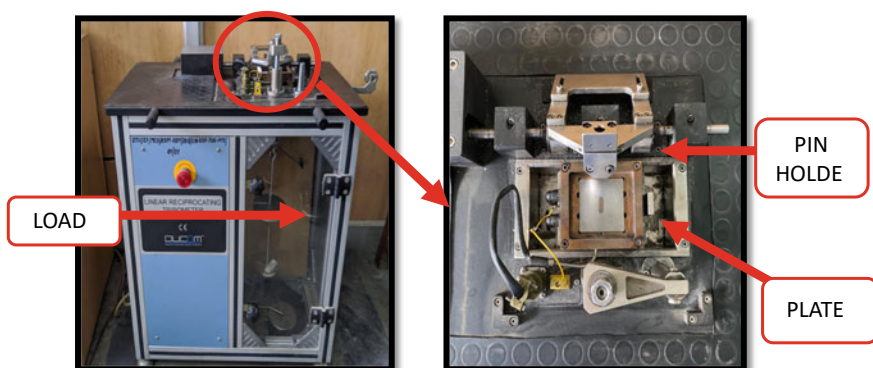
Frequency: 20–30 Hz.

Load: 10–30 N.

Distance: 50–150 m.

The experimental process involved is explained below in brief:

- (1) The material whose wear resistance is to be checked is set up as a cylindrical pin which is the reciprocating part of this setup, and the material which is to be used to calibrate the wear resistance of the pin is used as a square shape plate.
- (2) A specific load is applied onto the pin and temperature is set for defining constant conditions for the testing of wear.
- (3) The pin is then set in reciprocating motion at a constant frequency, and the measurement of coefficient of friction and amount of wear on the pin is known (Figs. 8 and 9).



**Fig. 8** Linear reciprocating type Tribometer

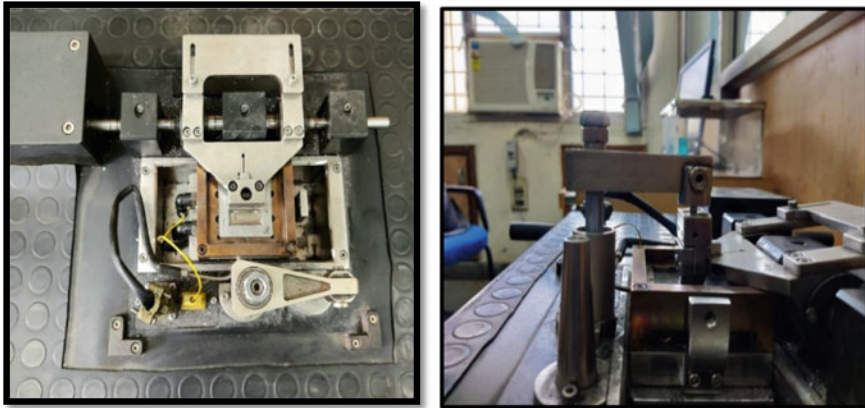


Fig. 9 Top and side view of linear reciprocating Tribometer

## 4 Results and Discussion

### 4.1 Specific Wear Rate

Shown above are the enlarged microscopic images of the contact surfaces of the uncoated as well as coated pin surfaces along with that of the plate (Figs. 10, 11, 12 and 13).

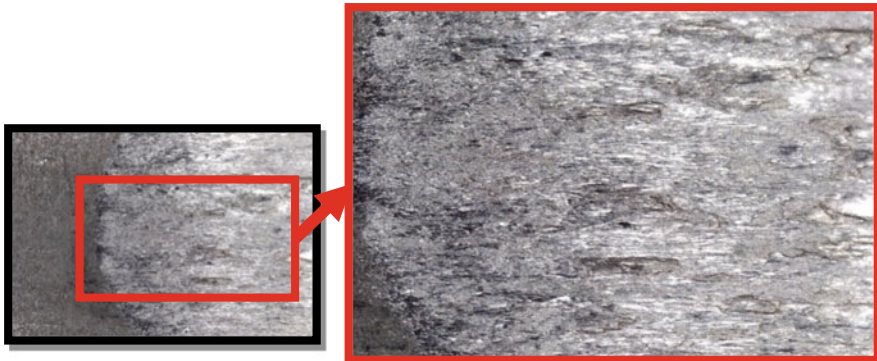
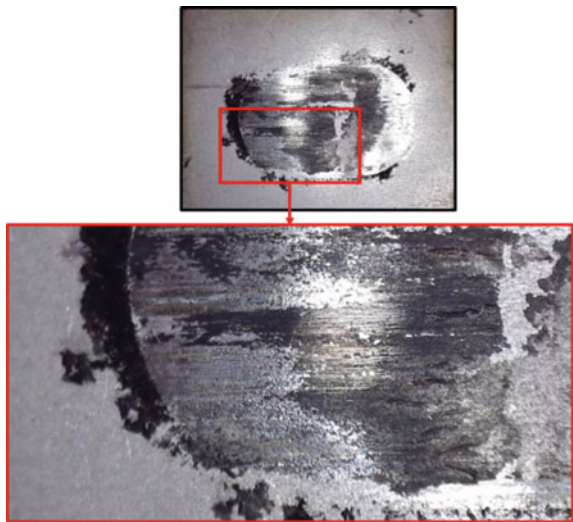


Fig. 10 Enlarged microscopic images of AISI 304 after wear



**Fig. 11** Enlarged microscopic images of worn-out uncoated Inconel 800 pin

**Fig. 12** Enlarged microscopic image of wear on plate due to coated pin



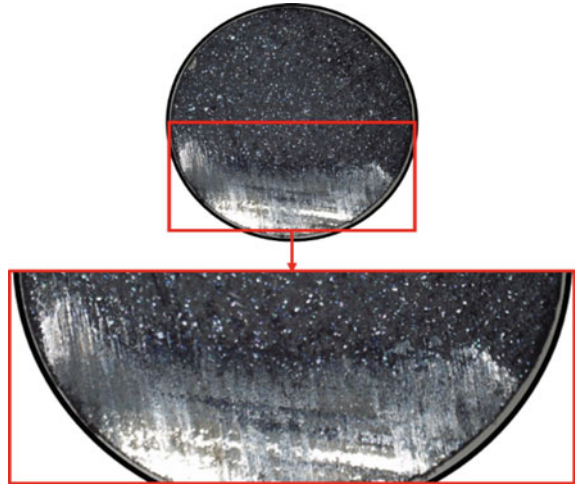
## 5 Conclusion

The present investigation has been carried out to analyse and investigate the impact of HVOF coating on tribological behaviour of pins of Inconel metal to find the variation between the metal's tribological properties under both, coated and uncoated conditions. Also, to find conditions for better wear properties and appropriate coefficient of friction, while conducting the tribological testing on the linear reciprocating Tribometer. From this study, following conclusions can be obtained:

- (i) EDAX testing was done in order to determine the compositions of both, the pin and the plate metal specimens.



**Fig. 13** Enlarged microscopic image of wear on coated pin



- (ii) The values of specific wear for all iterations reveal better wear resistant surface of the HVOF coated pins in comparison with the uncoated pins.
- (iii) Microscopic examination of the surfaces of the pins, after the experimentation, shows that the amount of metal removed was more in uncoated surface.

## References

1. Sun W, Tan AWY, King DJY, Khun NW, Bhowmik A, Marinescu I, Liu E (2020) Tribological behavior of cold sprayed Inconel 718 coatings at room and elevated temperatures. *Surf Coat Technol* 385:125386
2. Kaleli H (2016) New universal Tribometer as pin or ball-on-disc and reciprocating pin-on-plate types. *Tribol Ind* 38(2)
3. Chaudhari R, Ingle A, Kalita K (2017) Tribological investigation of effect of grain size in 304 austenitic stainless steel. *Trans Indian Inst Met* 70(9):2399–2405
4. Nascimento FC, Foerster CE, Silva SLRD, Lepiński CM, Siqueira CJDM, Alves Junior C (2009) A comparative study of mechanical and tribological properties of AISI-304 and AISI-316 submitted to glow discharge nitriding. *Mater Res* 12:173–180
5. Birol Y (2010) High temperature sliding wear behaviour of Inconel 617 and Stellite 6 alloys. *Wear* 269(9–10):664–671
6. Ahmadi A, Sadeghi F, Shaffer S (2018) In-situ friction and fretting wear measurements of Inconel 617 at elevated temperatures. *Wear* 410:110–118
7. Rahman MS, Ding J, Beheshti A, Zhang X, Polycarpou AA (2019) Helium tribology of Inconel 617 at elevated temperatures up to 950 °C: parametric study. *Nucl Sci Eng*
8. Debbarma D (2020) The study of wear behaviour of the Inconel 800 material in dry and solid lubricated condition. *Mater Today Proc*
9. Pauly V, Kern J, Clark M, Grierson DS, Sridharan K (2021) Wear performance of Incoloy 800HT and Inconel 617 in various surface conditions for high-temperature gas-cooled reactor components. *Tribol Int* 154:106715

10. Wang Y, Zhao S, Jia Z, Ji J, Liu D, Guo T, Ding Y (2020) Study on friction and wear behavior of Inconel 625 superalloy during hot extrusion. *Advances in materials science and engineering*, 2020
11. Cho TY, Yoon JH, Kim KS, Park BK, Youn SJ, Back NK, Chun HG (2006) Wear behaviors of HVOF spray coating of Co-alloy T800. *J Korean Cryst Growth Cryst Technol* 16(3):121–126
12. Singh R, Sachan D, Verma R, Goel S, Jayaganthan R, Kumar A (2018) Mechanical behavior of 304 austenitic stainless steel processed by cryogenic rolling. *Mater Today Proc* 5(9):16880–16886
13. Lata GS, Rana R, Lal R (2021) A statistical approach for overcut and burr minimization during drilling of stir-casted MgO reinforced aluminium composite, pp 269–283. [https://doi.org/10.1007/978-981-15-8542-5\\_23](https://doi.org/10.1007/978-981-15-8542-5_23)
14. Thakur RR (2021) Traffic noise modelling considering traffic compositions at roundabouts, pp 657–672. [https://doi.org/10.1007/978-981-15-8542-5\\_57](https://doi.org/10.1007/978-981-15-8542-5_57)
15. Singh D, Lata S, Rana R (2018) Reverse engineered structure of tool post aiding tool tip alignment with work center. *Mater Today Proc* 5:6433–6443. <https://doi.org/10.1016/j.matpr.2017.12.256>
16. Jain S, Aggarwal V, Tyagi M, Walia RS, Rana R (2016) Development of aluminium matrix composite using coconut husk ash reinforcement. In: *International conference on latest developments in materials, manufacturing and quality control (MMQC-2016)*, pp 12–13
17. Raheja K, Jain A, Sharma C, Rana R, Lal R (2021) Comparative study of tribological parameters of 3D printed ABS and PLA materials, pp 95–108. [https://doi.org/10.1007/978-981-15-8542-5\\_9](https://doi.org/10.1007/978-981-15-8542-5_9)
18. Kaplish A, Choubey A, Rana R (2016) Design and kinematic modelling of slave manipulator for remote medical diagnosis. In: *International conference on advanced production and industrial engineering*, pp 9–10
19. Khanna R, Maheswari R, Modi A, Tyagi S, Rana TR (2017) A review on recent research development on electric discharge machining (EDM). *Int J Adv Res Innov* 5:444–445
20. Kumar R, Rana R, Lata S, Kumar Sonkar R, Kumar A, Pawar S, Lal R (2015) Optimization of process parameters on over-cut in drilling of Al-B4C MMC. *Int J Mod Eng Res* 5(6):24–30
21. Lata S, Gupta A, Jain A, Kumar S, Srivastava A, Rana R, Lal R (2016) A review on experimental investigation of machining parameters during CNC machining of OHNS. *Int J Eng Res Appl* 6:63–71
22. Chaudhary MK, Pathak A, Goyal R, Rana R, Sharma VK (2021) Fabrication of aluminium 6082–B4C–aloe vera metal matrix composite with ultrasonic machine using mechanical stirrer, pp. 221–229. [https://doi.org/10.1007/978-981-15-8542-5\\_19](https://doi.org/10.1007/978-981-15-8542-5_19)
23. Rana R, Murtaza Q, Walia RS (2020) GA based optimization of tri-biological behaviour of diamond coated tungsten carbide. *World J Eng* 17:335–346. <https://doi.org/10.1108/WJE-08-2019-0220>
24. Rana R, Murtaza Q, Walia RS (2020) Optimization using genetic algorithm of tribological behaviour of WC tool material. *Ind J Eng Mater Sci* 27:889–896
25. Rana R, Walia RS, Murtaza Q (2021) Characterization and parametric optimization of performance parameters of dlc-coated tungsten carbide (Wc) tool using topsis. *Coatings* 11. <https://doi.org/10.3390/coatings11070760>
26. Rana R, Walia RS, Lata S (2018) Development and investigation of hybrid electric discharge machining electrode process. *Mater Today Proc* 5:3936–3942. <https://doi.org/10.1016/j.matpr.2017.11.650>
27. Ramakant R, Adarsh M, Kochhar A, Wadhwa S, Daiya SK, Taliyan S, Lal R (2015) An overview on process parameters improvement in wire electrical discharge machining. *Int J Mod Eng Res* 5(4):22–27
28. Ramakant R, Walia RS, Manik S (2016) Effect of friction coefficient on En-31 with different pin materials using pin-on-disc apparatus. In: *International conference on recent advances in mechanical engineering (RAME-2016)*, pp 619–624
29. Ramakant R, Walia RS, Qasim M, Mohit T (2016) Parametric optimization of hybrid electrode EDM process. In: *TORONTO'2016 AESATEMA international conference "advances and trends in engineering materials and their applications*, pp 151–162

30. Rana R (2016) Development of hybrid EDM electrode for improving surface morphology (Doctoral dissertation)
31. Rana R, Rajput K, Saini R, Lal R (2014) Optimization of tool wear: a review. *Int J Mod Eng Res* 4(11):35–42
32. Rana S, Kumar S, Rana R, Optimization of temperature variations on steel grade EN-18 using pin-on-disc method. *Int J Adv Prod Ind Eng* 171:21–26
33. Roop L, Ramakant R (2015) A textbook of engineering drawing, 1st edn. IK International Publishing House Pvt.
34. Bansal S, Saraf A, Rana R, Lal R (2021) Effect of picosecond laser texture surface on tribological properties on high-chromium steel under non-lubricated conditions, pp 257–267. [https://doi.org/10.1007/978-981-15-8542-5\\_22](https://doi.org/10.1007/978-981-15-8542-5_22)
35. Lata S, Pandey A, Labhansh, Sharma A, Meena K, Rana R, Lal R (2018) An experimental study and analysis of the mechanical properties of titanium dioxide reinforced aluminum (AA 5051) composite. *Mater Today Proc* 5:6090–6097. <https://doi.org/10.1016/j.matpr.2017.12.214>
36. Lata S, Rana R (2018) Hitesh, investigation of chip-tool interface temperature: effect of machining parameters and tool material on ferrous and non-ferrous metal. *Mater Today Proc* 5:4250–4257. <https://doi.org/10.1016/j.matpr.2017.11.689>
37. Upadhyaya S, Raj D, Gupta K, Saini RC, Rana R, Lal R (2020) Designing and analyzing the brake master cylinder for an ATV vehicle. *Int J Adv Prod Ind Eng* 5. <https://doi.org/10.35121/ijapie202001143>
38. Singla M, Rana R, Lata S (2016) Microstructure and mechanical properties of aluminium based metal matrix composite—a review. In: International conference on advanced production and industrial engineering, pp 9–10)

# Use of a Generative Design Approach for UAV Frame Structure Optimization and Additive Manufacturing



Pratik Yadav, Vinay Yadav, Vishal Francis, and Narendra Kumar

**Abstract** Additive manufacturing (AM) has changed the way products are designed and manufactured by providing enormous design freedom. AM is suitable for manufacturing of complex geometries in less span of time. By democratizing design and manufacturing, AM has assisted the growth of the maker movement. In recent years, generative approaches have become increasingly popular in a variety of technological domains. The present research focuses on design and analysis of UAV frame structure using generative design methodology. The work presented discusses the overall procedural steps for design and analysis using Fusion 360.

**Keywords** Drones · Optimization · Additive manufacturing · Generative design

## 1 Introduction

In contrast to subtractive manufacturing approaches, such as traditional machining, additive manufacturing builds a part in layer-by-layer fashion. Additive manufacturing is utilized for manufacturing of end-use parts by various industries. The technology works on the principle of layer manufacturing. There are various AM processes which can be classified based on the form of material which AM systems can process.

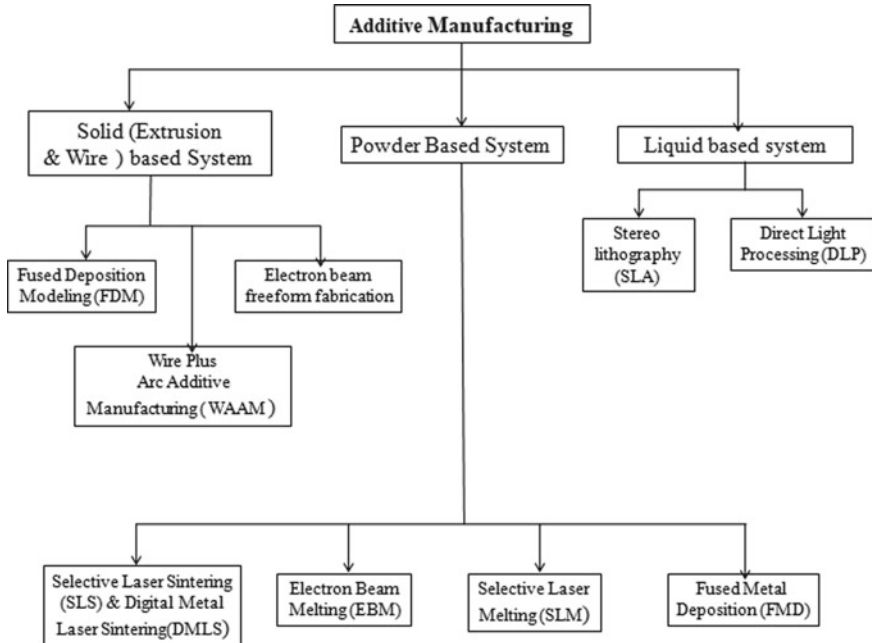
---

P. Yadav · V. Yadav · V. Francis (✉)  
Lovely Professional University, Phagwara, Punjab, India  
e-mail: [vishal.24813@lpu.co.in](mailto:vishal.24813@lpu.co.in)

N. Kumar  
Dr. B. R. Ambedkar National Institute of Technology, Jalandhar, India

© The Author(s), under exclusive license to Springer Nature Singapore Pte Ltd. 2023  
R. P. Singh et al. (eds.), *Advances in Modelling and Optimization of Manufacturing and Industrial Systems*, Lecture Notes in Mechanical Engineering,  
[https://doi.org/10.1007/978-981-19-6107-6\\_15](https://doi.org/10.1007/978-981-19-6107-6_15)

197



**Fig. 1** Classification of additive manufacturing [1]

Figure 1 shows the classification of AM processes. Some of the different types of process are explained in short as follows:

(1) **Binder jetting**

This method involves depositing successive layers of powder mixture and a liquid binder as an adhesive using a 3D printing style head that moves on the  $x$ ,  $y$ , and  $z$  axes.

(2) **Directed energy deposition**

A wide variety of materials, including ceramics, metals, and plastics, can be utilized for direct energy deposition additive manufacturing. As a bed moves up, a laser, electric arc, or electron beam gun positioned on an arm melts wire, filament feedstock, or powder.

(3) **Material Extrusion**

Spun plastics are either projected or pulled via a heated nozzle positioned on a moving arm in this popular AM method. As the nozzle travels laterally and the bed moves up, melted material is built layer by layer. Temperature range or chemical adhesive is used to keep the layers together.

(4) **Powder bed fusion**

Direct metal laser melting (DMLM), direct metal laser sintering (DMLS), electron beam melting (EBM), selective laser sintering (SLS), and selective heat sintering are all examples of powder bed fusion procedures (SHS). Fine layers

of material are melted or partially melted using electron beams, lasers, or heated print heads, and the superfluous powder is blown to pieces.

(5) **Sheet Lamination**

Laminated object manufacturing (LOM) and ultrasonic additive manufacturing (UAM) are the two types of sheet lamination methods. The employment of alternate layers of paper and glue in laminated object production is ideal for making things with visual or aesthetic appeal. Ultrasonic welding (UAM) is a low-energy, low-temperature procedure that can be used to connect small metal sheets. It can be utilized with a variety of metals, including aluminum, stainless steel, and titanium [1].

### 1.1 Digital Flow Work of Additive Manufacturing

Figure 2 is the complete process followed in additive manufacturing. Following are some steps used in this workflow which are explained.

#### CAD Preparation

The first step is to create a CAD model which resembles the part to be manufactured. The CAD model can be prepared in any CAD packages, and it may also be prepared with reverse engineering equipment.

#### STL Format Conversion

STL file format is used by most of the AM system. The CAD file is converted to STL format. This file describes the original CAD model's exterior enclosed surfaces and serves as the foundation for calculating the slices.

#### Data Preparation

The STL file is corrected for any error, and the model is oriented and sliced to generate the codes.

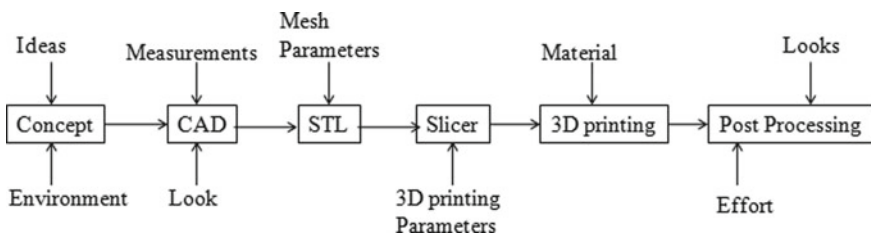


Fig. 2 Digital workflow of additive manufacturing [1]

## **Machine Setup**

Prior to beginning the setup, the AM machine must be correctly set up. Such characteristics might include material restrictions, energy supply, layer thickness, and timings, among others.

## **Build**

The part is fired, and the fabrication process is initiated. At this moment, only a cursory examination of the machine is required to confirm that no problems have occurred, such as material shortages, power outages, or software malfunctions.

## **Removal**

Once the part is completed, it needs to be removed from the machine. Proper care has to be given while removal of complicated structures.

## **Post-processing**

Parts that have been extracted from the system may require extra cleaning before they can be used. Parts may be weak or contain supportive features that must be eliminated at this stage. As a result, time and careful, expert physical manipulation are frequently required [2].

## ***1.2 Important Parameters to Be Considered for AM***

The important parameters to be considered while manufacturing with AM are listed below:

- (1) **Cost:** Due to the use of technology like lasers, they might be more expensive than others.
- (2) **Material:** Certain devices can only handle few materials, but others can handle a variety of materials, including hybrids.
- (3) **Maintenance:** Because some equipment is more complicated than others, they will require different maintenance.
- (4) **Speed:** AM machines are faster compared to many other technologies.
- (5) **Versatility:** Some machines feature complicated setup options that can be used to optimize part quality against other factors such as production speed. Other machines have fewer setup options, making them easier to operate but possibly less adaptable.
- (6) **Layer thickness:** Due to material processing factors, some devices have a layer thickness constraint. The construction speed would be slowed if these layers were thinner.
- (7) **Accuracy** is influenced by in-plane resolution in addition to layer thickness. This can have an impact on a part's minimum particle size and plate thickness [2].

## 2 Generative Design

Designers of complicated artifacts, such as buildings or products, must consider a variety of options. Currently, the majority of this research is done with pencil and paper during the conceptual stage of design. At this point of the design process, CAD is rarely employed. In its current form, it is mostly an implementation tool, but it is also becoming more of an analysis tool, and it is most beneficial at the end of the design phase [3–6]. This is a big part of what generative design is all about. Though it is still relatively unknown among engineers, generative design is on the verge of becoming mainstream in architecture. It has been accepted by some of the world’s most prestigious architecture firms. Most architecture programmers now include it, especially at the master’s level. Within CAD environments, architects may now explore thousands of design options thanks to generative design. Considering the absence of a defined description and formal procedures for execution, architects and design scholars now realize its importance. A specific application of generative design on top of history-based customizable CAD systems is proposed in this research (Fig. 3).

The primary motivations for using generative design (GD) technologies in design are to employ computing performance to assist human designers and (or) to automate portions of the design process. Aside from attaining efficiency (many design instances in a limited amount of time), cost reduction (reduced time and labor), optimization, correctness, consistency, and other goals, one of the key aims is to explore a broader design space and assist design creation [3, 7–13].

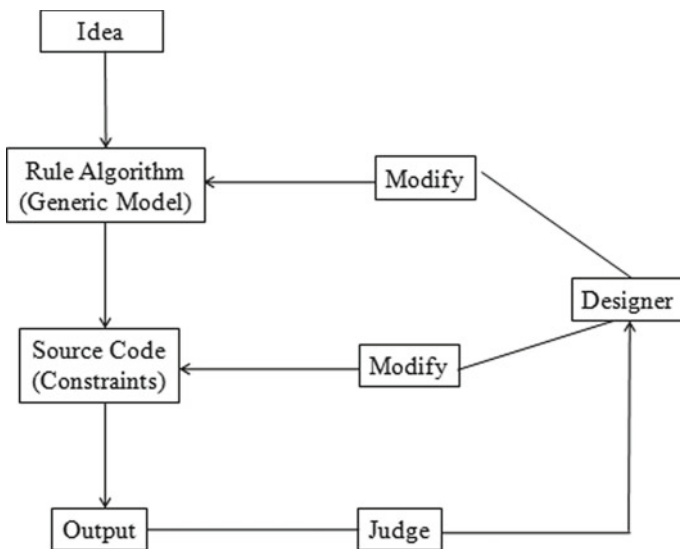
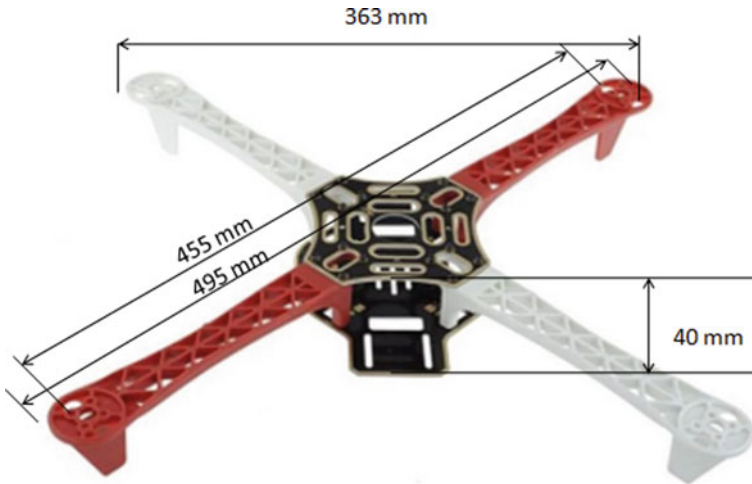


Fig. 3 Generative design flow work [3]





**Fig. 4** Dimensions of the structure for the case study [17]

### 3 Case Study

The frame structure of a quadcopter was selected as the case study due to importance of its design optimization [14, 15] (refer Fig. 1).

The base and the arms are the two elements of the body frame. Two identical portions make up the upper and lower foundation frames [16–18] (Fig. 4).

### 4 Generative Design Analysis

Define, Generate, and Explore are the three key stages in the generative design process. Define essentially means finding the flaws or issues that must be addressed in order to solve the situation. The computer analyzes the user's design and limitations and explores alternative options. When the computer and the user talk and make decisions, this is referred to as the explore process. As previously stated, generative architecture makes use of AI technologies (Fig. 5).

Table 1 shows the comparison of parameters between the proposed design and DJIF450. After many iterations, unconventional designs were generated, four of which were considered to be the most appropriate and relevant based on our needs (Fig. 6).

The generative design can create complex design solutions since the methodology adopts removing the material from block maintaining the design's singularity. The preserved geometries like holes are left vacant. The design is rejected if it does not fit the required objective. The selected designs are shown in Fig. 7.

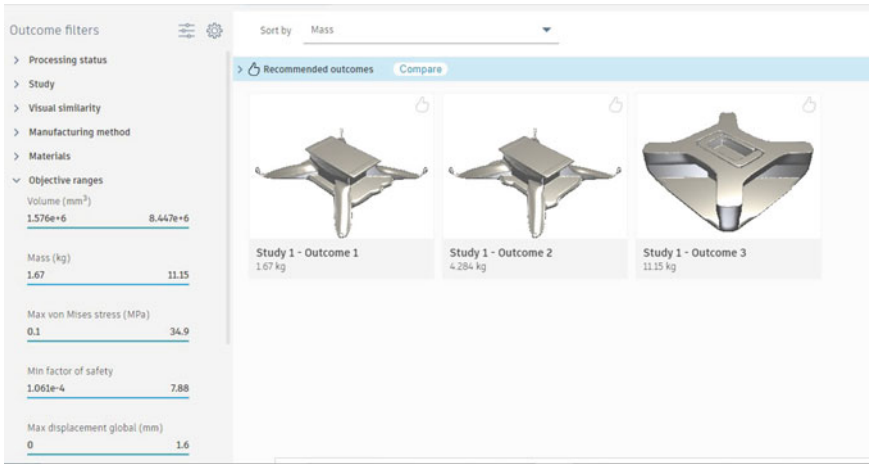


Fig. 5 Software outputs of design

Table 1 Parameters of compared frames

Parameter	1st structure	2nd structure	3rd structure
Mass of frame (g)	287	329	372
Minimum factor of safety	18.5	3.21	3.301
Manufacturing method	Additive manufacturing	Additive manufacturing	Additive manufacturing
Volume (mm <sup>3</sup> )	271,150	310,444	
Max Von Mises stress	1.1	6.2	21.33
Material used	ABS plastic	ABS plastic	Polyamide nylon
Max displacement global (mm)	0.15	0.82	4.016

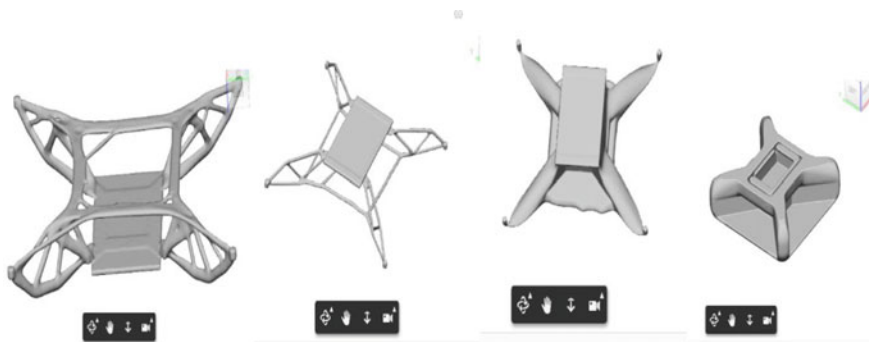


Fig. 6 Few design iterations

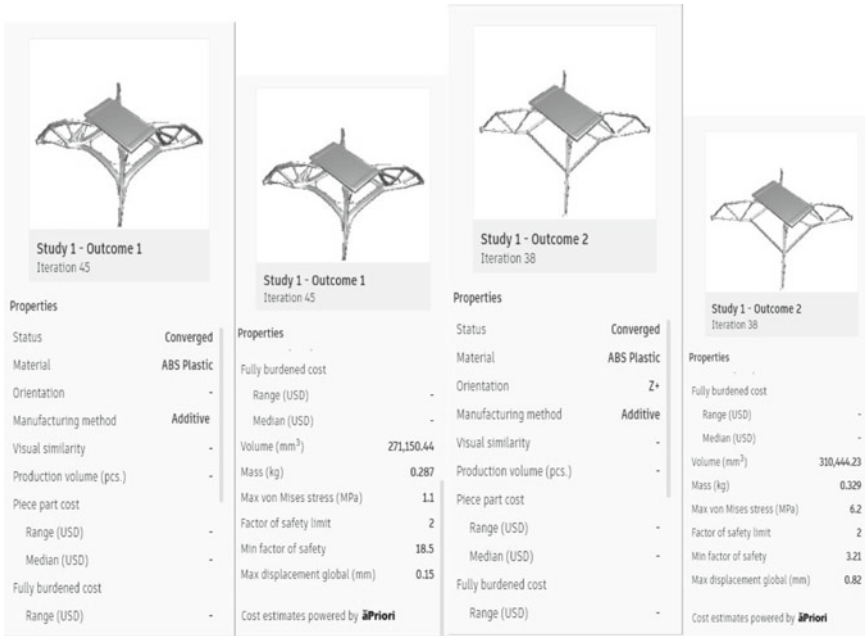


Fig. 7 Outcomes of various frames/structures

The selected drone frame (Fig. 8) utilizing the generative approach seems better regard to the weight and load bearing capacity. Figures 9, 10 and 11 show the analysis of stress, preserved geometry, and obstacle of selected design. Compared to base structure (case study), generative design drones had a lower likelihood and probability of failure on the basis of data and material parameters. In Fig. 9, the stress value is around 11 times that of frame 1, indicating resistance is higher than that of a regularly constructed drone frame.

## 5 Conclusion

Generative design is a sophisticated method for design generation that generates multiple solutions for most engineering challenges, mimicking the natural world’s evolutionary history. As a result of these computational processes, several astonishing and diverse structures with an organic nature are generated. Using two generatively produced drone frames, a full comparison between traditional and generative design methodologies is made. It was found that the design proposed is better, and generative design methodology can serve as a potential candidate for designing of components.

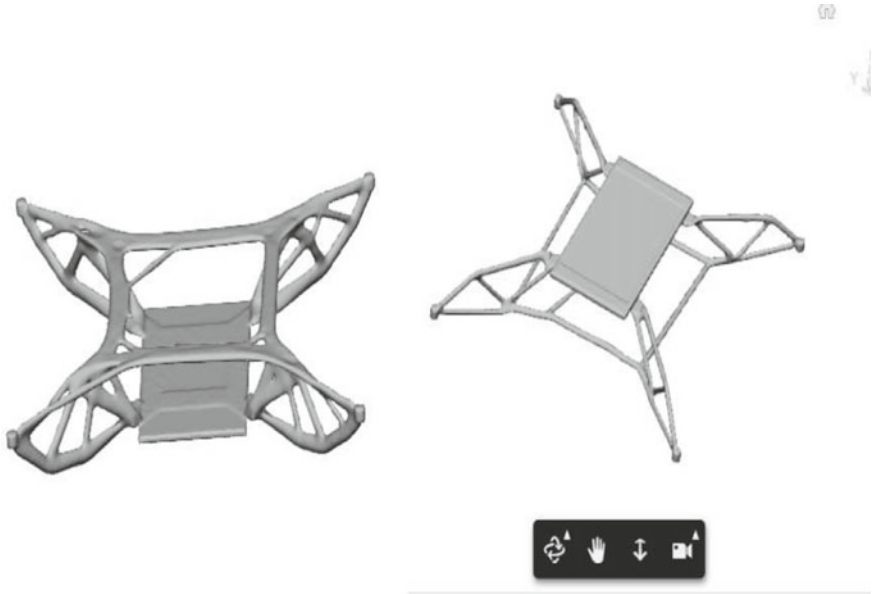


Fig. 8 The selected design

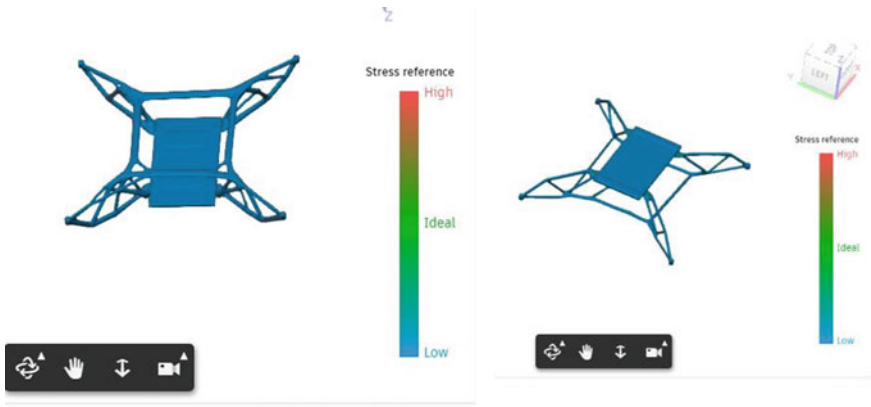


Fig. 9 Stress evaluation of frames

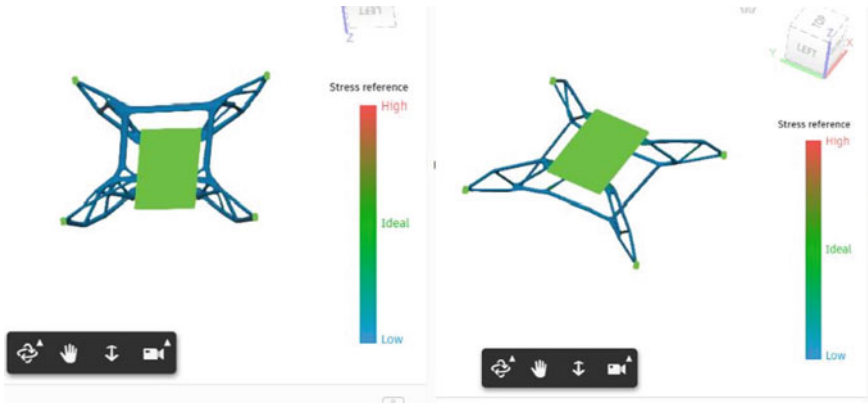


Fig. 10 Preserved geometry analysis



Fig. 11 Analysis of obstacle geometry

## References

1. Joshi S, Sheikh A (2015) 3D printing in aerospace and its long-term sustainability. *Virtual Phys Prototyping* 10:1–11. <https://doi.org/10.1080/17452759.2015.1111519>
2. Gibson I et al (2015) *Additive manufacturing technologies*. Springer Science, Business Media New York. [https://doi.org/10.1007/978-1-4939-2113-3\\_19](https://doi.org/10.1007/978-1-4939-2113-3_19)
3. Krish S (2011) A practical generative design method. *Comput Aided Des* 43(1):88–100
4. Buelow PV 2002, Using evolutionary algorithms to aid architects 315-336
5. McKnight M (2017) What is generative design? How is it being put to use? Why is it such a game-changer? 2 176–181 in *KNE Eng*
6. Wu J, Qian X, Wang M (2019) Advances in generative design. 116 102733 *Computer-aided design*
7. Doraiswamy H, Ferreira N, Lage M, Vo H, Wilson L, Werner H, Park M, Silva C (2015) A topology-based catalog exploration framework for finding view-enhanced tower designs

- 34:1–13
8. Janssen P, A generative evolutionary design method published in 2006. *Dig Creativity* 17(49):49–63
  9. Sosnovik I, Oseledets I (2019) Neural networks for topology optimization 34:215–223
  10. Sun H, Ma L (2020) Generative Design Using Reinforcement Learning Exploration Approaches Learning in Structural Topology Optimization Using Density 4:10
  11. Oh S et al (2019) Deep generative design: integration of topology optimization and generative models. *J Mech Des* 141:1
  12. Yi J, Zeng T, Rong J (2014) Topology optimization for continua considering global displacement constraint. *Strojniski Vestnik*. 60:43–50
  13. Aman B (2020) Generative design for improved performance, weight loss, and industrial implications
  14. Shah MKN, Dutt MBJ, Modh H (2014) Quadrotor—an unmanned aerial vehicle 1299–1303. *Int J Eng Develop Res*
  15. Mahen MA, Anirudh S, Naik A, Chethana HD, Shashank AC (2014) Amphibious quadcopter design and development. *Int J Mech Prod Eng* 2(7):30–34
  16. Optimization of quadcopter frame using generative design and comparison with DJI F450 drone frame. *Res IOP Conf Series Mater*. <https://doi.org/10.1088/1757-899X/1012/1/012019>
  17. Singh R, Kumar R, Mishra A, Agarwal A (2020) Structural analysis of quadcopter frame. *Mater Today: Proc* 22:3320–3329
  18. Md. Ahmed, Mohd. Zafar, Mohanta J (2020) Modeling and analysis of quadcopter F450 frame 196–201

# Study on Welding Parameters in TIG Welding of Incoloy-800: An Investigation with Designed Experiments and ARAS Method



Ravi Pratap Singh, Ravinder Kataria, Himanshu Bisht, Narendra Kumar, and Mohit Tyagi

**Abstract** In the intended research, an effort was made to combine Incoloy-800 using TIG welding. Various welding factors like as current, speed, and gas flow rate are tested to see what influence they have on the output reactions such as tensile strength, length, and impact toughness. For single-response optimization, Taguchi Technique is used; for multi-response optimization, ARAS approach is used. For example, at 120 A, 6 mm/s and 10Lpm, the observed result is 303.57 MPa, which is 3.87% lower than the projected value in tensile strength when using the same single-response optimization. There is a 4.66% discrepancy between the observed and projected impact toughness of 55.96 J and the best welding current of 120 A; the best welding speed of 10 mm/s; and the best gas flow of 18Lpm. The measured elongation is 1.62 mm, with a 3.57% deviation from the predicted value, and the optimized parameters are welding current (WC) 120 A, welding speed (WS) 8 mm/s, and gas flow rate (GFR) 14 Lpm. To optimize impact toughness and tensile strength, ARAS uses multi-response optimization techniques. ARAS Utility Grade is 0.6641, which is 4.53% lower than the predicted value for the optimal input process parameters of 120 A welding current, 6 mm/s welding speed, and 10Lpm gas flow rate.

**Keywords** TIG · ARAS · Taguchi · Incoloy-800 · Welding speed

---

R. P. Singh (✉) · H. Bisht · N. Kumar · M. Tyagi  
Department of Mechanical Engineering, National Institute of Technology, Kurukshetra, Haryana, India  
e-mail: [singhrp@nitj.ac.in](mailto:singhrp@nitj.ac.in)

R. Kataria  
National Institute of Fashion Technology, Srinagar, Jammu & Kashmir, India

N. Kumar  
IPE Department, NIT, Jalandhar, India

## 1 Introduction

Iron, nickel, and cobalt, or a combination of iron, cobalt, and nickel, are all common building blocks for superalloys, which may also include alloying metals including molybdenum, cobalt, tungsten, chromium, iron, aluminum, zirconium, niobium, titanium, and tantalum. Because of their outstanding qualities, superalloys are often used in industry. In addition to providing remarkable toughness and creep resistance, superalloys also provide enhanced strength at elevated temperatures and good corrosion resistance and oxidation. At least half of the nickel in Ni-based superalloys comes from nickel, which is also a substantial component of Ni-Fe base alloys. To increase surface stability, more alloying elements such as aluminum and chromium are added [1–3]. Ni-based superalloys typically include between 5 and 15% Co, 10 to 20% Cr, 8% Ti and Al combined, and modest amounts of additional additives such as molybdenum, tungsten, mg, zr, and nb in order to enhance their properties. Formed nickel-based superalloys often have an Al/Ti ratio of 8–10%, a Cr/Co ratio of 5–15%, and trace amounts of boron, magnesium, zirconium, and carbon in small amounts. Additional materials include molybdenum, tungsten, and niobium. The use of chromium and aluminum is also important to maintain the surface's stability. Inconel-718 is the most common commercially available superalloy, consisting of up to 45% of forged nickel-based alloy production and 25% of cast nickel-based alloys. The present study centered on the investigation of process parameters for the tool wear rate (TWR) while machining Cu-based SMA, i.e., Cu-Zn-Ni, at the EDM. This article introduced and assessed the pilot analysis. The chemistry of TWR was investigated, as well as the variations in drug removal when testing on various criteria. To highlight the changes in TWR, picture representations were presented. Because of their exceptional characteristics, connecting these created superalloys has long thought to be a challenge. As a consequence, the TIG welding process has been recognized as a suitable solution for combining these superalloys while still giving typical advantages. There are several types of welds, but one of the most common is TIG (also known as Gas Tungsten Arc welding), which uses tungsten electrodes to fuse metals together. Protecting weld pools from air contamination is commonly done using shielding gases like argon and helium.

Shielding gas flow affects the output of MIG welding and laser-arc hybrid welding on 6N01 aluminum, according to Yang et al. [4]. MIG welding process stability is reduced when the shielding gas flow rate is increased. A broader weld bead width and a brighter look of the weld bead were noticed with a high shielding gas flow rate. It was discovered via computational fluid dynamic (CFD) study that increasing the advance gas flow rate minimizes weld oxidation and expands the region of high argon concentration. Wei et al. [5] used high-speed double wire MIG welding on A7N01-T4 aluminum alloy. The fusion zone showed a dendritic pattern of equiaxed grains at a welding speed of 1200 mm/min, whereas the weld zone displayed a fine crystal structure of equiaxed grains. Elongated columnar structure was found in the weld zone near to the fusion zone, whereas coarse microstructure was found in the HAZ. Araujo et al. [6] examined laser welding of Inconel-718, a nickel-based superalloy. At



1300 °C, it was discovered that significant and persistent liquation occurred at grain boundaries. The grain size grew as the overheating duration increased, resulting in a decrease in the extent of the grain border. Srirangan and Paulraj [7] used Taguchi gray relation analysis on Incoloy-800HT superalloy for TIG welding process parameter optimization. All of these variables were used to control the weld process. The experiments focused on determining the material's impact toughness, yield strength, and ultimate tensile strength (UTS). A number of optimization-based studies on TIG welding procedures using current and old methodologies have been noted in the prior literature [8–17]. Variety of different experimentation and the parallel optimization have been undertaken by the several investigators for attempting upon the modeling and optimization of the joining and machining perspectives of the advanced material [18–27]. These further optimizations and modeling-based studies have enabled the applicability and wide acceptability of these advanced methods for their exploration into the real-life exposure for industrial solicitations [28–35].

An emphasis on TIG welding for joining Incoloy-800 was necessary in light of what has been said so far. Tests are done to examine whether welding factors like gas flow rate, speed, and current have an influence on weld characteristics such as elongation and toughness. Taguchi's Technique is used for single-response optimization, whereas the Additive Ratio Assessment (ARAS) approach is used for multi-response optimization.

## 2 Materials and Methods

To weld Incoloy-800 plates with dimensions of 100 × 50 × 5 mm, direct current straight polarity (DCSP) or direct current electrode negative (DCEN) welding may be used (DCEN). Welding speed (WS), gas flow rate (GFR), and welding current (WC) were the three parameters that needed to be provided. As a noise-shielding welding gas, argon was used. The lower and maximum limits of the input process parameters were determined via a series of pilot studies. Studies were conducted using Taguchi L9 orthogonal arrays. Strength, elongation, and impact toughness of different weld reactions were examined under varied input process circumstances. The chemical makeup of Incoloy-800 is shown in Table 1. Table 2 displays the various control variables employed in the investigation and the amounts at which they were used in the current study.

**Table 1** Chemical composition of Incoloy-800

Fe	Cr	Ni	C	Mn	Si	Cu	Al	Ti	S
39.5 min	19–23	30–35	0.10 max	1.50 max	1.00 max	0.075 max	0.15–0.60	0.15–0.60	0.015 max

**Table 2** Factors and levels

Factor	Unit	Level 1	Level 2	Level 2
Welding current (WC)	A	100	120	140
Gas flow rate (GFR)	L/min	10	14	18
Welding speed (WS)	mm/s	6	8	10

The experiment table’s layout is shown in Table 3. Using the Taguchi Method, the experiment table is designed, which is subsequently built. On the basis of this newly created table, more tests are carried out. In order to avoid distortion during the welding process, the metals that will be joined together by TIG welding must first be held together using adhesive. Samples for tensile strength and impact toughness testing are cut from the welded plates and tested in the laboratory. The work material following the TIG welding process is shown in Fig. 1.

**Table 3** Design of experiment table with parameter levels

S.No.	Welding current (WC)	Welding speed (WS)	Gas flow rate (GFR)
1	1	1	1
2	1	2	2
3	1	3	3
4	2	1	2
5	2	2	3
6	2	3	1
7	3	1	3
8	3	2	1
9	3	3	2



**Fig. 1** Incoloy-800 plates after TIG welding



**Fig. 2** Tensile testing setup

### ***Tensile Testing***

A tensile test, often known as a tension test, falls under the category of destructive testing and is one of the most frequent and essential form of mechanical testing (Fig. 2).

In most cases, tensile tests are carried out using electromechanical or universal testing machines. They are straightforward to carry out and are completely standardized. Specimens for the tensile test are cut in accordance with ASTM E-8 specifications. As shown in Fig. 3, the ASTM E-8 tensile testing standard is employed in the industry [36–41]. TIG welding was used to create the samples in Fig. 4, which were then cut out for tensile testing.

### ***Impact Toughness Testing***

In order to determine the amount of energy a material absorbs during a fracture, the Charpy test is used. In order to perform the impact toughness test, we used welded samples of 20,050 mm to cut a 20,010 mm-long starting sample. The impact toughness test was then carried out on this specimen. Afterward, final impact toughness samples measuring 5510 mm were cut from the sample. Samples for the impact toughness test were cut from a parting wheel using a diamond blade. Figure 5 depicts the samples that were prepared for the impact testing. The specimen for the toughness or impact test is cut out according to the ASTM A370 subsize (55 mm × 10 mm × 5 mm) standard.

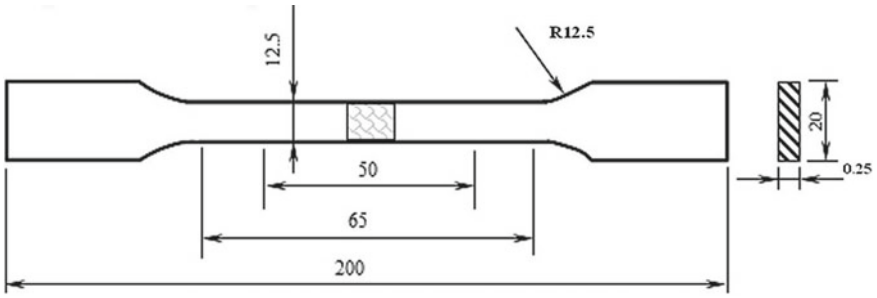


Fig. 3 ASTM E-8 standard



Fig. 4 Samples for tensile test

### 3 Results and Discussions

On Incoloy-800, researchers are experimenting with the effects of welding process factors like as welding speed (WS), gas flow rate (GFR), and welding current (WC) on output parameters such as impact toughness. In order to determine the optimum potential TIG welding combination for the superalloy Incoloy-800, an experiment was conducted. For a variety of process settings, Table 4 shows the mean and S/N ratios for output response tensile strength.

**Fig. 5** Samples for impact test



**Table 4** Mean and S/N ratios for tensile strength

S.No.	Welding current (WC) (A)	Welding speed (WS) (mm/s)	Gas flow rate (GFR) (Lpm)	Tensile strength (Mpa) (means)	Tensile strength (S/N ratio)
1	100	6	10	417.913	52.4198
2	100	8	14	199.500	45.9804
3	100	10	18	164.050	44.2681
4	120	6	14	331.675	49.6543
5	120	8	18	404.462	52.1320
6	120	10	10	359.250	51.0952
7	140	6	18	425.450	52.5748
8	140	8	10	460.250	53.2346
9	140	10	14	181.925	45.1214

The accompanying table does not provide any light on the underlying factors that led to the change. Using the ANOVA (Analysis of Variance) method, this information may be gathered. Analysis of variance (ANOVA) is a mathematical method for comparing the means of different groups in a sample.

Tables 5 and 6 show the results of the Analysis of Variance for the Means and the S/N ratio, respectively. Table 5: The tables also reveal which control factor is statistically significant and which control factor is not statistically significant. While all of the control parameters, except for welding current, have a statistically significant influence on the output response Tensile strength, Table 5 demonstrates that all of them have a statistically significant effect.

There is a normal probability plot for Means and S/N ratios in Figs. 6 and 7, as well as a normal probability plot for the S/N ratio for TIG-welded Incoloy-800 weld joints. The normal probability plot shows how closely our data resembles the distribution of probability in the normal distribution. As the data approaches a straight line, there is a greater likelihood that the data will conform to the conventional normal distribution.

**Table 5** Analysis of variance for means for tensile strength

Source	DF	Seq SS	Adj SS	Adj MS	F	P
WC	2	20,134	20,134.3	10,067.1	51.25	0.019*
WS	2	40,209	40,208.7	20,104.3	102.34	0.010*
GFR	2	45,895	45,895.0	22,947.5	116.82	0.008*
Residual error	2	393	392.9	196.4		
Total	8	106,631				
R <sup>2</sup>	0.9963		R <sup>2</sup> (adjusted)		0.9853	

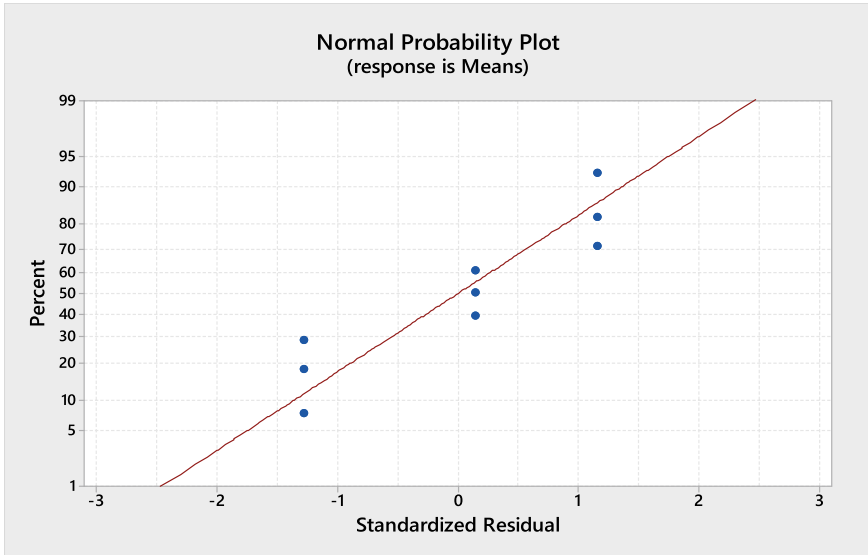
\*Significant

**Table 6** Analysis of variance for S/N ratios for tensile strength

Source	DF	Seq SS	Adj SS	Adj MS	F	P
WC	2	19.598	19.598	9.7991	14.06	0.066**
WS	2	36.613	36.613	18.3065	26.26	0.037*
GFR	2	42.642	42.642	21.3211	30.59	0.032*
Residual error	2	1.394	1.394	0.6971		
Total	8	100.248				
R <sup>2</sup>	0.9861		R <sup>2</sup> (adjusted)		0.9444	

\*Significant

\*\*Not Significant



**Fig. 6** Normal probability plot (means) for Tensile strength

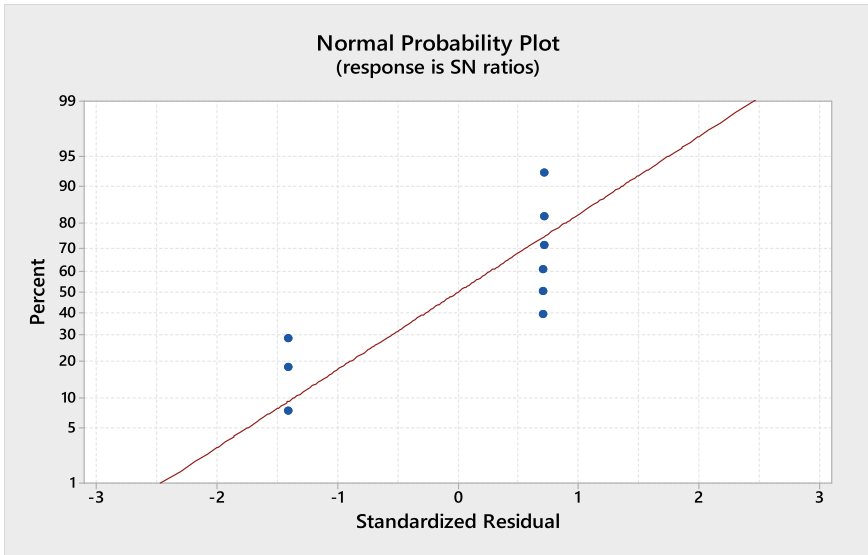


Fig. 7 Normal probability plot (S/N ratios) for tensile strength

Figures 8 and 9 provide plots of the Mean and S/N ratios for Incoloy-800 TIG-welded plate tensile strength. The charts show that tensile strength rises with welding current and ultimately falls. Because greater tensile strength is needed, the choice bigger which is better in the signal to noise ratio is selected.

**Effects of Variable Process Parameters on Tensile Strength of Incoloy-800**

Increasing the welding current causes the tensile property to increase initially before decreasing. When the welding current is raised to a certain level, ductility increases, resulting in this behavior. Greater welding current causes grain expansion, which causes grains to become stress free (from fine grains to coarse grains, then columnar grains, and eventually equiaxed stress-free grains) and elongated, resulting in increased ductility. Tensile strength improves as ductility increases, but it begins to decline at a certain point.

TIG welding requires careful manipulation of the tungsten electrode and filler material. Controlling the welding speed is thus critical. The change in tensile characteristics with increasing welding speed is equivalent to the variation in welding current. It grows initially and then declines. At low speeds, heat buildup rises, which assists in grain expansion and, as a result, enhances ductility. The reason for the improvement in tensile strength is due to the higher ductility. Argon is a gas that acts as a shielding agent. Argon, being a noble gas that does not react, offers shielding to the weld zone and protects it from ambient pollution. The higher the gas flow rate, the better the welding joint. A better weld junction equals a better plate fusion. As the flow rate of gas rises, the tensile strength of a material also increases. At various levels of input process parameters, the mean and S/N ratios of the impact toughness

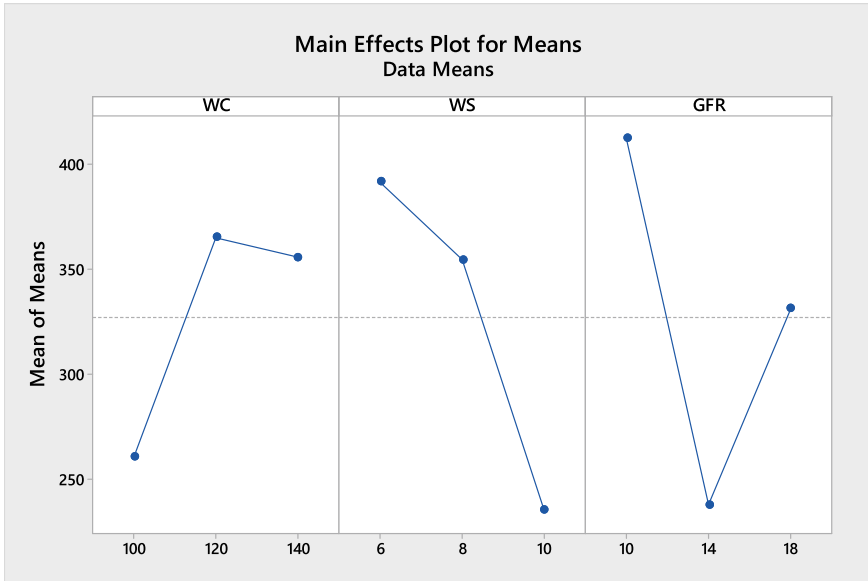


Fig. 8 Main effects plot for means for tensile strength

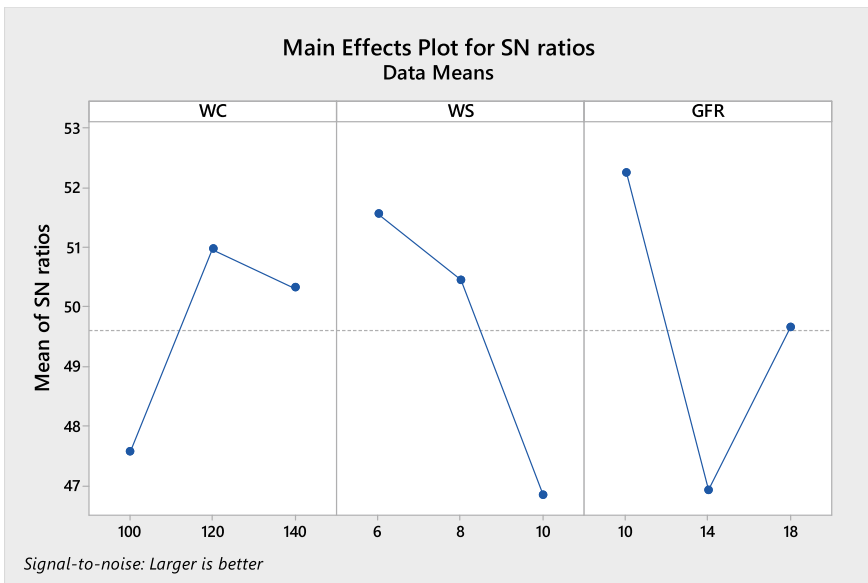


Fig. 9 Main effects plot for S/N ratios for tensile strength



of Incoloy-800 superalloy are presented in Table 7. Tables 8 and 9 provide the S/N ratio and the analysis of variance for the mean values. The tables show which control elements are most important and which ones are not very important. When it comes to welding current, Tables 8 and 9 place it above welding speed and gas flow rate.

Normal probability charts for Mean and SN output response ratios and impact toughness of TIG-welded Incoloy-800 weld joints can be shown in Figs. 10 and 11. With the help of this graph, we can see how closely our data resembles the expected distribution. For Impact Toughness, Figs. 12 and 13 show the Means Main Effects plot and the S/N ratio. In the graphs, you can see how changes in process variables affect the material’s hardness. As the speed of the welding process increases, so does the material’s toughness.

**Effects of Studied Process Parameters on Impact Toughness of Incoloy-800**

The impact toughness of Incoloy-800 rises initially and subsequently diminishes as welding current values increase. The finer structure of the material transforms to coarse structure as the welding current increases, reducing its impact toughness.

**Table 7** Mean and S/N ratios for impact toughness

S.No.	Welding Current (WC) (A)	Welding Speed (WS) (mm/s)	Gas Flow Rate (GFR) (Lpm)	Impact toughness (J) (Means)	Impact toughness (S/N Ratio)
1	100	6	10	40.30	32.0636
2	100	8	14	47.85	33.5969
3	100	10	18	46.50	33.2620
4	120	6	14	56.90	34.9890
5	120	8	18	63.80	36.0030
6	120	10	10	60.50	35.6334
7	140	6	18	43.35	32.7321
8	140	8	10	37.15	31.3907
9	140	10	14	43.40	32.6916

**Table 8** Analysis of variance for means for impact toughness

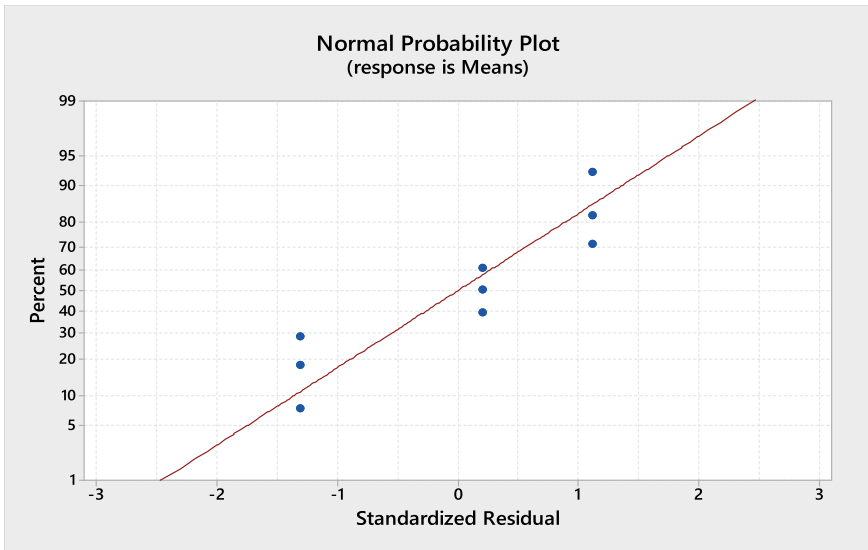
Source	DF	Seq SS	Adj SS	Adj MS	F	P
WC	2	618.42	618.42	309.209	29.25	0.033*
WS	2	18.63	18.63	9.314	0.88	0.532**
GFR	2	42.31	42.31	21.154	2.00	0.333**
Residual error	2	21.14	21.14	10.570		
Total	8	700.49				
R <sup>2</sup>	0.9698		R <sup>2</sup> (adjusted)		0.8793	

\* Significant  
 \*\* Not significant

**Table 9** Analysis of variance for SN ratios for impact toughness

Source	DF	Seq SS	Adj SS	Adj MS	F	P
WC	2	17.7815	17.7815	8.8908	19.80	0.048*
WS	2	0.5619	0.5619	0.2809	0.63	0.615**
GFR	2	1.5309	1.5309	0.7654	1.70	0.370**
Residual error	2	0.8981	0.8981	0.4491		
Total	8	20.7724				
R <sup>2</sup>	0.9568		R <sup>2</sup> (adjusted)		0.8271	

\*Significant  
 \*\*Not significant



**Fig. 10** Normal probability plot (means) for impact toughness

Increases in welding speed contribute to increases in impact toughness because when speed is low, heat build-up is greater, resulting in coarse grain structure, and coarse grains have less strength than finer grains.

Increasing the flow of shielding gas results in better and more stable welding because the weld zone is protected from air contamination, resulting in greater impact toughness. Table 10 displays the mean and standard deviation for elongation of TIG-welded Incoloy-800 plates in the present study. Tables 11 and 12 demonstrate the Analysis of Variance for SN ratios and Means for output response elongation under various process parameters. It also shows which control factors are important and which are not. In the Analysis of Variance for Means, weld current is shown to be a major control factor.

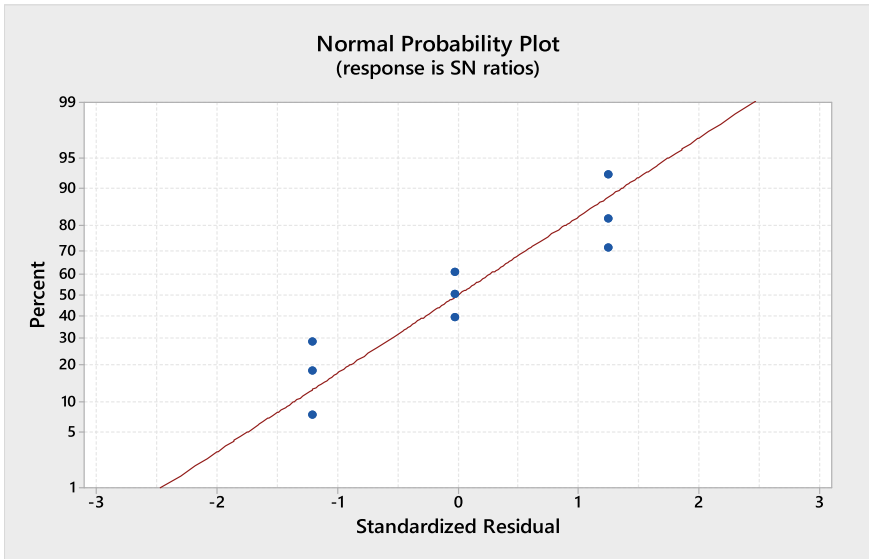
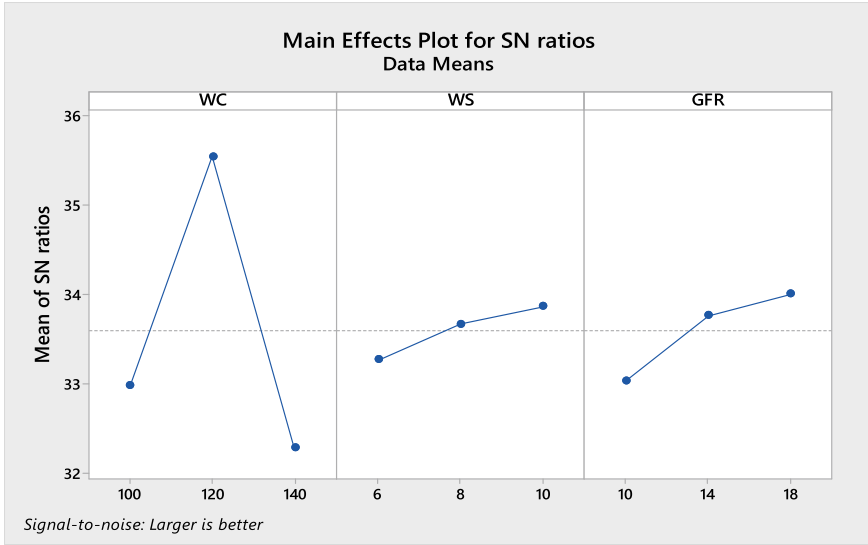


Fig. 11 Normal probability plot (S/N ratio) for impact toughness



Fig. 12 Main effects plot for means for impact toughness



**Fig. 13** Main effects plot for S/N ratios for impact toughness

**Table 10** Mean and S/N ratios for elongation

S.No.	Welding current (WC) (A)	Welding speed (WS) (mm/s)	Gas flow rate (GFR) (Lpm)	Elongation (mm) (Means)	Elongation (S/N ratio)
1	100	6	10	1.34	17.9048
2	100	8	14	1.175	26.1083
3	100	10	18	0.93	36.9897
4	120	6	14	1.585	19.4885
5	120	8	18	1.74	24.9485
6	120	10	10	1.79	16.1618
7	140	6	18	2.04	21.4267
8	140	8	10	1.99	24.9485
9	140	10	14	1.895	33.4679

Weld joints made of Incoloy-800 and TIG welded in this study are shown in Figs. 14 and 15 as normal probability graphs for the SN ratio and mean output response elongation, respectively. The normal probability plot is showing how closely the data matches a normal distribution (see below). Figures 16 and 17 show the S/N ratio and Means Main Effects plot for Elongation. Elongation fluctuates depending on various process factors, as seen in the graphs.

**Table 11** Analysis of variance for means for elongation

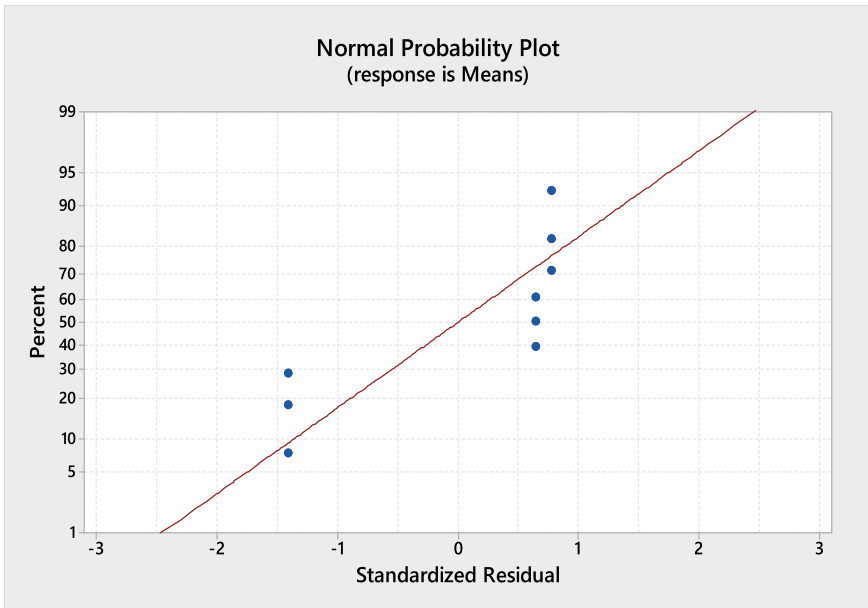
Source	DF	Seq SS	Adj SS	Adj MS	F	P
WC	2	1.06616	1.06616	0.53308	20.34	0.047*
WS	2	0.02336	0.02336	0.01168	0.45	0.692**
GFR	2	0.04304	0.04304	0.02152	0.82	0.549**
Residual error	2	0.05242	0.05242	0.02621		
Total	8	1.18497				
R <sup>2</sup>	0.9558		R <sup>2</sup> (adjusted)		0.8230	

\*Significant  
 \*\*Not significant

**Table 12** Analysis of variance for SN ratios for elongation

Source	DF	Seq SS	Adj SS	Adj MS	F	P
WC	2	87.56	87.56	43.78	1.58	0.388**
WS	2	131.20	131.20	65.60	2.36	0.297**
GFR	2	112.60	112.60	56.30	2.03	0.330**
Residual error	2	55.53	55.53	27.77		
Total	8	386.89				
R <sup>2</sup>	0.8565		R <sup>2</sup> (adjusted)		0.4259	

\*\*Not significant



**Fig. 14** Normal probability plot (means) for elongation

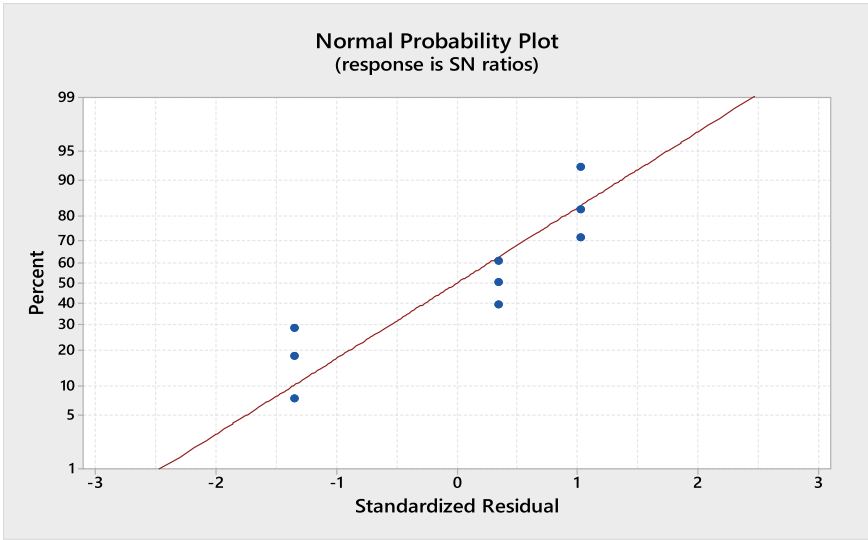


Fig. 15 Normal probability plot (S/N ratio) for elongation



Fig. 16 Main effects plot for means for elongation

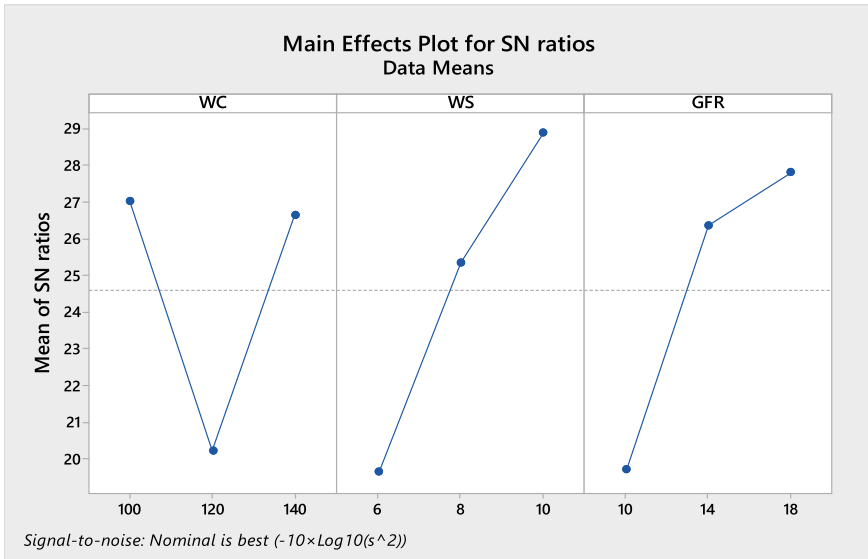


Fig. 17 Main effect plot for S/N ratios for elongation

**Effects of Variable Process Parameters on Elongation of Incoloy-800**

Increased welding current causes grain development. Grain growth causes a rise in ductility. Increased ductility leads to increased elongation. However, there will be no extension beyond a certain point, and the specimen will break. Increased welding speed results in less heat accumulation, which results in finer grains and more brittleness, i.e., very little elongation, but at low speeds, heat accumulation rises and finer structure transforms to coarse, which enhances elongation. This control factor has no influence on the elongation of the material. With a rise in gas flow rate, the welding joint improves and hence has a high strength.

**Single-Response Optimization using Taguchi Method**

**Tensile Strength (A2 B1 C1)**

Different TIG welding process parameters were used to test Incoloy-800’s tensile strength. Welding current (WC), welding speed (WS), and gas flow rate (GFR) were employed as input process parameters. The goal of the optimization procedure is to raise the tensile strength of the final product. At optimal settings, the welding current was 120 A; the welding speed was 6 mm/s; and the gas flow rate was 10 Lpm (A2 B1 C1) (Table 13).

**Impact toughness (A2 B3 C3)**

The impact toughness of Incoloy-800 was studied at different process parameter values in order to establish the ideal value of input process parameters for impact

**Table 13** Tensile strength at optimized values

Optimized values	Predicted value (MPa)	Observed value (MPa)	Percentage (%) error
A2 B1 C1	315.80	303.57	3.87

**Table 14** Impact toughness at optimized values

Optimized values	Predicted value (J)	Observed value (J)	Percentage (%) error
A2 B3 C3	58.70	55.96	4.66

toughness. Input process parameters included welding current (WC), welding speed (WS), and gas flow rate (GFR). Optimum impact toughness is the goal of the optimization approach. The ideal welding parameters were found to be 120 A welding current, 10 mm/s welding speed, and 18 Lpm gas flow (A2 B3 C3) (Table 14).

**Elongation (A2 B2 C2)**

Tests were conducted on Incoloy-800’s elongation at different process parameter values in order to establish the most effective elongation input parameters. These parameters were utilized as inputs for the WC, WS, and GFR. By optimizing, we want to keep it at its nominal levels at all times. The welding current was 120 A, the welding speed was 8 mm/s, and the gas flow rate was 14Lpm when the process parameters were optimized (A2 B2 C2). Table 15 displays the anticipated value at the optimal level of input process parameters as well as the actual value at this level, as well as the percentage error involved.

**Multi Response Optimization Using Additive Ratio Assessment (ARAS) Method**

The ARAS approach is based on measured capacity and the utility idea. The stages involved in implementing the ARAS approach are listed below.

1. For advantageous characteristics;

$$r_{jy} = [x_{jy} - \min.(x_{jy})]/[\max.(x_{jy}) - \min.(x_{jy})] \quad (j = 1, 2, 3, \dots, m; y = 1, 2, 3, \dots, p) \tag{1}$$

For non-advantageous characteristics, the normalization process is of two stages. Perform primarily the reciprocal of individual condition with respect to involved substitutes as:

$$x_{jy}^* = \frac{1}{x_{jy}} \tag{2}$$

**Table 15** Elongation at optimized values

Optimized values	Predicted value (mm)	Observed value (mm)	Percentage (%) error
A2 B2 C2	1.68	1.62	3.57



and then compute the further values as:

$$R = [r_{jy}]_{m \times n} = \frac{x_{jy}^*}{\sum_{j=1}^m x_{jy}^*} \tag{3}$$

2. The weighted standardized matrix ( $D$ ), as defined by:

$$D = [f_{jy}]_{m \times n} = r_{jy} \times w_y \tag{4}$$

3. The ideal function ( $S_j$ ) for the  $j$ th substitution is computed. The higher the  $S_j$  score, the better the substitution.

$$S_j = \sum_{y=1}^p f_{jy} \tag{5}$$

4. Calculate the utility grade ( $U_j$ ) of each substitution. It is determined by a comparison of the alternatives with the most effective option ( $S_o$ ). The reasoning used to calculate the value of  $U_j$  is as follows:

$$U_j = \frac{S_j}{S_o} \tag{6}$$

The best option is the one with the highest utility score among the alternatives.

**Normalized Matrix for Raw Data**

It was necessary to normalize raw data in order to remove undesired characteristics from the case study as specified in Eqs. (2) and (3). Table 16 shows the normalized response data.

**Table 16** Normalized matrix for response data

S.No.	WC	WS	GFR	Tensile strength	Impact toughness	Normalized IT	Normalized TS
1	1	1	1	40.30	417.913	0.11819887	0.857066172
2	1	2	2	47.85	199.5	0.40150094	0.119682647
3	1	3	3	46.50	164.05	0.35084428	0
4	2	1	2	56.90	331.675	0.74108818	0.565918298
5	2	2	3	63.80	404.462	1	0.811654288
6	2	3	1	60.50	359.25	0.87617261	0.65901418
7	3	1	3	43.35	425.45	0.2326454	0.882511816
8	3	2	1	37.15	460.25	0	1
9	3	3	2	43.40	181.925	0.23452158	0.060347738

**Weighted Normalized Matrix**

Tensile strength and impact toughness are the two output responses examined in this scenario. There is a 0.5 weighting assigned to each response, which means that all of the attributes are equal in importance. Using equation, the weighted normalized matrix is then generated (4). Under different input process settings, Table 17 displays a weighted standardized matrix for responsiveness, tensile strength, and impact toughness.

**Computation for the Optimality Function (Ideal Function and Utility Grade)**

Weighed tensile strength and impact toughness values are combined to provide the best performance. There is a significant difference between the lowest and highest computed values for experimental runs nine and five, respectively. The higher the optimum function score, the better the substitution. The estimated values of Ideal function and Utility Grade are shown in Table 18.

**Table 17** Weighted standardized matrix for response data

S.No.	WC	WS	GFR	Tensile strength	Impact toughness	Weighted IT	Weighted TS
1	1	1	1	40.30	417.913	0.0590994	0.42853309
2	1	2	2	47.85	199.5	0.2007505	0.05984132
3	1	3	3	46.50	164.05	0.1754221	0
4	2	1	2	56.90	331.675	0.3705441	0.28295915
5	2	2	3	63.80	404.462	0.5	0.40582714
6	2	3	1	60.50	359.25	0.4380863	0.32950709
7	3	1	3	43.35	425.45	0.1163227	0.44125591
8	3	2	1	37.15	460.25	0	0.5
9	3	3	2	43.40	181.925	0.1172608	0.03017387

**Table 18** Calculated values of ideal function and utility grade

Exp. runs	Ideal function ( $S_j$ )	Utility grade ( $U_j$ )
1	0.487633	0.538300
2	0.260592	0.287700
3	0.175422	0.193700
4	0.653503	0.721500
5	<b>0.905827</b>	1.000000
6	0.767593	0.847400
7	0.557579	0.615600
8	0.500000	0.552000
9	<b>0.147435</b>	0.162800

The bold data denotes reflecting the highest and lowest values of the ideal function

**Table 19** ARAS utility grade

WC	WS	GFR	ARAS grade
100	6	10	0.53834
100	8	14	0.28769
100	10	18	0.19367
120	6	14	0.72147
120	8	18	1.00000
120	10	10	0.84742
140	6	18	0.61556
140	8	10	0.55200
140	10	14	0.16277

**Table 20** Analysis of variance of means for utility grade

Source	DF	Seq SS	Adj SS	Adj MS	F	P
WC	2	0.44783	0.44783	0.22392	29.29	0.033*
WS	2	0.09517	0.09517	0.04758	6.22	0.138**
GFR	2	0.11213	0.11213	0.05607	7.33	0.120**
Residual error	2	0.01529	0.01529	0.00765		
Total	8	0.67042				
R <sup>2</sup>	0.9772		R <sup>2</sup> (adjusted)		0.9088	

\*Significant

\*\*Not significant

The estimated values  $U_j$  are clearly between 0 and 1. The computed values may be sorted in ascending order, which is the desired precedence order. The utility function values may be used to calculate the complicated relative efficiency of the viable option (Tables 19 and 20).

The ARAS Utility Grade function’s Means and S/N ratios are shown in Figs. 18 and 19, respectively. This phenomenon has been shown to be true when the welding current is increased and subsequently decreased. As the welding speed rises, it decreases. The gas flow rate begins to decrease and then begins to increase again (Table 21).

According to the ARAS Method, the ideal welding configuration is A2 B1 C1, i.e., 120 A welding current (WC), 6 mm/s welding speed (WS), and 10 Lpm gas flow rate (GFR) (multi-response optimization technique). Observed results deviate by 4.53% from expected values after further testing at the optimal setting.

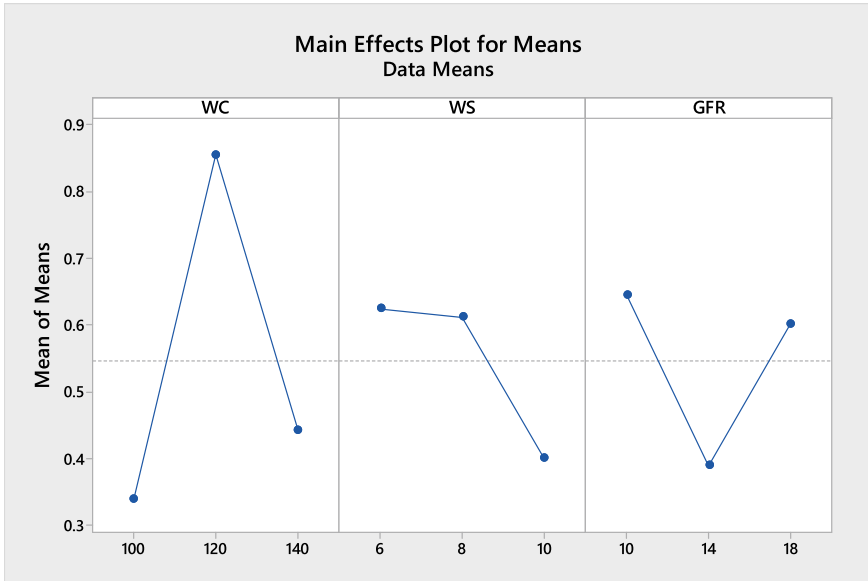


Fig. 18 Main effects plot for means

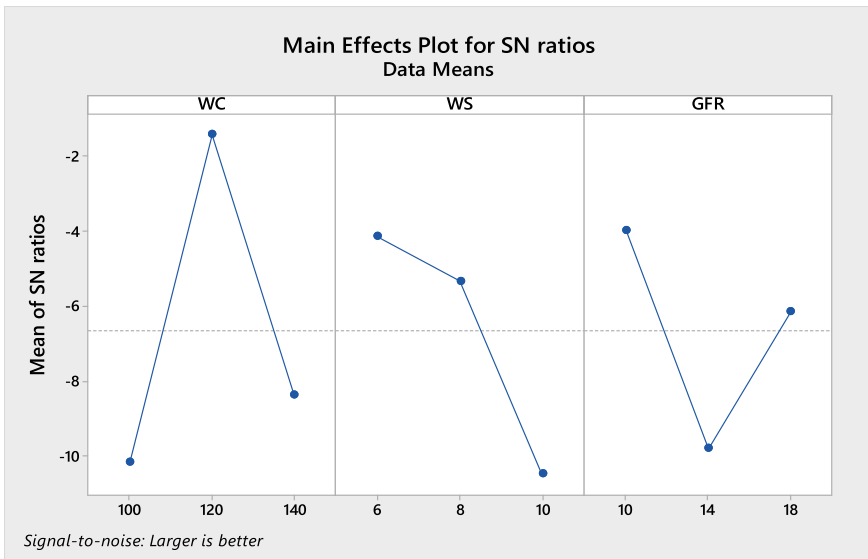


Fig. 19 Main effect plot for SN ratios

Table 21 Validation of multi-response optimization settings

Optimized values	Predicted value	Observed value	Percentage (%) error
A2 B1 C1	0.6957	0.6641	4.53

## 4 Conclusions

The following interferences are observed after performing the experimental investigation:

1. Tensile strength improves initially and then drops as the welding current increases. Increasing welding current up to a certain level causes ductility to rise. Stress-free and long-grain welds are the consequence of higher welding current's effect on grain formation.
2. The impact toughness of Incoloy-800 rises initially and subsequently diminishes as welding current values increase. The finer structure of the material transforms to coarse structure as the welding current increases, reducing its impact toughness. Increased welding current causes grain development. Grain growth causes a rise in ductility. Increased ductility leads to increased elongation. However, there will be no extension beyond a certain point, and the specimen will break.
3. The change in tensile characteristics with increasing welding speed is equivalent to the variation in welding current. It grows initially and then declines. At low speeds, heat buildup rises, which aids in grain expansion and, as a result, enhances ductility. The reason for the improvement in tensile strength is due to the higher ductility. Increases in welding speed contribute to increases in impact toughness because when speed is low, heat buildup is greater, resulting in coarse grain structure, and coarse grains have less strength than finer grains.
4. Increased welding speed results in less heat accumulation, which results in finer grains and more brittleness, i.e., very little elongation, but at low speeds, heat accumulation rises and finer structure transforms to coarse, which enhances elongation.
5. Gas shields the weld zone and prevents contamination from the environment. The higher the gas flow rate, the better the welding joint. When a result, as the gas flow rate rises, so does the tensile strength. Increasing the flow of shielding gas results in better and more stable welding because the weld zone is protected from air contamination, resulting in greater impact toughness.

## References

1. Thellaputta GR, Chandra PS, Rao CSP (2017) Machinability of nickel based superalloys: a review. *Mater Today Proc*
2. Shang SL, Kim DE, Zacherl CL, Wang Y, Du Y, Liu ZK (2012) Effects of alloying elements and temperature on the elastic properties of dilute Ni-base superalloys from first-principles calculations. *J Appl Phys*
3. Choudhury I, El-Baradie M (2002) Machinability of nickel-base super alloys: a general review. *J Mater Process Technol* 77:278–284. [https://doi.org/10.1016/s0924-0136\(97\)00429-9](https://doi.org/10.1016/s0924-0136(97)00429-9)
4. Yang X, Chen H, Zhu Z, Cai C, Zhang C (2019) Effect of shielding gas flow on welding process of laser-arc hybrid welding and MIG welding. *J Manuf Process*. <https://doi.org/10.1016/j.jmpro.2019.01.045>

5. Wei Z, Xu R, Li H, Hou Y, Guo X (2019) Investigation on double wire metal inert gas welding of A7N01-T4 aluminum alloy in high-speed welding. *High Temp Mater Process*. <https://doi.org/10.1515/htmp-2018-0073>
6. Araujo LS, De Melo CH, Gonçalves RP, De Vasconcelos Varela A, De Almeida LH (2019) The effect of a very high overheating on the microstructural degradation of superalloy 718. *J Mater Res Technol*. <https://doi.org/10.1016/j.jmrt.2018.03.006>
7. Srirangan AK, Paulraj S (2016) Multi-response optimization of process parameters for TIG welding of Incoloy 800HT by Taguchi grey relational analysis. *Eng Sci Technol Int J* 19:811–817. <https://doi.org/10.1016/j.jestch.2015.10.003>
8. Singh RP, Singhal S (2016) Rotary ultrasonic machining: a review. *Mater Manuf Process* 31(14):1795–1824
9. Singh RP, Singhal S (2017) Investigation of machining characteristics in rotary ultrasonic machining of alumina ceramic. *Mater Manuf Process* 32(3):309–326
10. Singh RP, Kumar J, Kataria R, Singhal S (2015) Investigation of the machinability of commercially pure titanium in ultrasonic machining using graph theory and matrix method. *J Eng Res* 3(4):1–20
11. Singh RP, Singhal S (2017) Rotary ultrasonic machining of Macor ceramic: an experimental investigation and microstructure analysis. *Mater Manuf Process* 32(9):927–939
12. Singh RP, Singhal S (2018) Experimental investigation of machining characteristics in rotary ultrasonic machining of quartz ceramic. *Proceedings of the Institution of Mechanical Engineers, Part L: Journal of Materials: Design and Applications* 232(10):870–889
13. Singh RP, Singhal S (2018) An experimental study on rotary ultrasonic machining of macor ceramic. *Proceedings of the Institution of Mechanical Engineers, Part B: Journal of Engineering Manufacture* 232(7):1221–1234
14. Singh R, Singh RP, Tyagi M, Kataria R (2020) Investigation of dimensional deviation in wire EDM of M42 HSS using cryogenically treated brass wire. *Mater Today Proc* 25:679–685
15. Singh RP, Kataria R, Kumar J, Verma J (2018) Multi-response optimization of machining characteristics in ultrasonic machining of WC-Co composite through Taguchi method and grey-fuzzy logic. *AIMS Mater Sci* 5(1):75–92
16. Singh RP, Singhal S (2018) Experimental study on rotary ultrasonic machining of alumina ceramic: microstructure analysis and multi-response optimization. *Proceedings of the Institution of Mechanical Engineers, Part L: Journal of Materials: Design and Applications* 232(12):967–986
17. Singh R, Singh RP, Trehan R (2021) State of the art in processing of shape memory alloys with electrical discharge machining: a review. *Proceedings of the Institution of Mechanical Engineers, Part B: Journal of Engineering Manufacture* 235(3):333–366
18. Ambade S, Tembhurkar C, Patil AP, Pantawane P, Singh RP (2021) Shielded metal arc welding of AISI 409M ferritic stainless steel: study on mechanical, intergranular corrosion properties and microstructure analysis. *World J Eng*
19. Singh RP, Kataria R, Singhal S (2018) Performance evaluation of macor dental ceramic: an investigation with rotary ultrasonic machining. *Adv Dent Oral Health* 8(2):1–6
20. Singh RP, Tyagi M, Kataria R (2019) Selection of the optimum hole quality conditions in manufacturing environment using MCDM approach: a case study. In: *Operations management and systems engineering*. Springer, Singapore, pp 133–152
21. Kataria R, Singh RP, Kumar J (2016) An experimental study on ultrasonic machining of tungsten carbide-cobalt composite materials. *AIMS Mater Sci* 3(4):1391–1409
22. Singh RP, Kataria R, Singhal S (2019) Decision-making in real-life industrial environment through graph theory approach. In: *Computer architecture in industrial, biomechanical and biomedical engineering*. IntechOpen
23. Haleem A, Javaid M, Singh RP, Suman R (2021) Significant roles of 4D printing using smart materials in the field of manufacturing. *Adv Ind Eng Polym Res*
24. Singh RP, Kataria R, Kumar J (2021) Machining of WC-Co composite using ultrasonic drilling: optimisation and mathematical modelling. *Adv Mater Process Technol* 7(2):317–332

25. Singh RP, Kataria R, Singhal S, Garg RK, Tyagi M (2020) Hole quality measures in rotary ultrasonic drilling of silicon dioxide ( $\text{SiO}_2$ ): investigation and modeling through designed experiments. *SILICON* 12(11):2587–2600
26. Singh RP, Singhal S (2018) Rotary ultrasonic machining of alumina ceramic: experimental study and optimization of machining responses. *J Eng Res* 6(1)
27. Kumar R, Singh RP, Kataria R (2019) Study on flexural performance of fabricated natural fiber hybrid polypropylene composite: an experimental investigation through designed experiments. *World J Eng*
28. Kumar R, Singh RP, Kataria R (2020) Study on mechanical properties of fabricated hybrid natural fibre polymeric composites. *Int J Mater Prod Technol* 60(1):73–91
29. Singh RP, Singh R, Trehan R, Garg RK, Tyagi M (2021) Investigation into the surface quality in wire-cut EDM of M42 HSS: an experimental study and modeling using RSM. In: *Optimization methods in engineering*. Springer, Singapore, pp 245–256
30. Sharma RC, Dabra V, Singh G, Kumar R, Singh RP, Sharma S (2021) Multi-response optimization while machining of stainless steel 316L using intelligent approach of grey theory and grey-TLBO. *World J Eng*
31. Singh RP, Kumar N, Gupta AK, Painuly M (2021) Investigation into rotary mode ultrasonic drilling of bioceramic: an experimental study with PSO-TLBO based evolutionary optimization. *World J Eng*
32. Butola R, Yuvaraj N, Singh RP, Tyagi L, Khan F (2021) Evaluation of microhardness and wear properties of Al 6063 composite reinforced with yttrium oxide using stir casting process. *World J Eng*
33. Kataria R, Singh RP, Alkawaz MH, Jha K (2021) Optimization and neural modelling of infiltration rate in ultrasonic machining. *OPSEARCH*, 1–20
34. Singh R, Singh RP, Trehan R (2021) Parametric investigation of tool wear rate in EDM of Fe-based shape memory alloy: microstructural analysis and optimization using genetic algorithm. *World J Eng*
35. Singh R, Singh RP, Trehan R (2022) Investigation of machining rate and tool wear in processing of Fe-based-SMA through sinking EDM. In: *Proceedings of the international conference on industrial and manufacturing systems (CIMS-2020)*. Springer, Cham, pp 439–451
36. Singh RP, Kataria R, Kumar J, Verma K, Chaudhary B, Singh S (2020) Investigation of process responses in rotary ultrasonic machining of Al/SiC composite through designed experiments. *Mater Today Proc* 21:2043–2052
37. Singh R, Singh RP, Trehan R (2021) Sustainable engineering approaches used in electrical discharge machining processes: a review. *Sustain Environ Infrastruct* 41–50
38. Ranjan S, Singh RP (2021) Investigation of MRR in wire-cut electrical discharge machining of Incoloy-800 using statistical approach. In: *Optimization methods in engineering*. Springer, Singapore, pp 443–457
39. Bisht H, Singh RP, Sharma V (2021) Study of impact strength in TIG welding of Incoloy-800 super alloy: an experimental investigation and optimization. In: *Optimization methods in engineering*. Springer, Singapore, pp 277–289
40. Singh RP, Kataria R, Tiwari AK (2020) Sustainable manufacturing-related aspects in turning operation: a review based study. *Manuf Eng* 657–667
41. Gupta AK, Singh RP (2022) Application of TLBO to optimize cutting variables for face milling of aluminium alloy Al-8090. In: *Proceedings of the international conference on industrial and manufacturing systems (CIMS-2020)*. Springer, Cham, pp 1–13

# Optimization of Titanium Grade-5 (Ti6Al4V) Alloy on Die Sinking EDM by Using Copper Tungsten Electrode



Rakesh Kumar Rout, Rajiv Kumar Garg, and Dilbagh Panchal

**Abstract** Die sinking EDM of Ti6Al4V has been carried out with copper tungsten electrode. The Input current ( $I_p$ ), Pulse on Time ( $T_{on}$ ) and Spark Gap Voltage ( $S_v$ ) have been taken as the input factors. The MRR, EWR, and Ra have been optimized. The Response Surface Methodology (Box-Bhenken Design) has been used as DOE for analysis and optimization. The three levels of input factors has been taken as per DOE, Input current ( $I_p$ ), Pulse on Time ( $T_{on}$ ), Spark Gap Voltage ( $S_v$ ), and the levels were taken on which, machining has been performed, i.e., 10 A, 15 A, 20 A, 100  $\mu$ s, 150  $\mu$ s, 200  $\mu$ s, 15 V, 20 V, and 25 V. The analysis of variance has been performed for MRR, EWR, and Ra by RSM, Quadratic equations for model analysis and 3D surface models have been optimized by RSM.

**Keywords** EDM ·  $I_p$  ·  $T_{on}$  ·  $S_v$  · RSM · DOE · BBD

## 1 Introduction

Die-sinking EDM is an unconventional machining methods that has been broadly used in modern manufacturing industries. In EDM, a pulsed voltage has flanked by the electrode and the workpiece, generating a plasma channel due to dielectric fluid. Extremely high temperature ranging from 6000 to 12,000 K, has been generated locally resulting removal of materials from the workpiece [1–4]. The fundamental achievement of EDM has its ability to machine any complex geometry at high dimensional precision. Due to the exceptional qualities of titanium and its alloys it has been employed in diversity of high-end applications in the field of aerospace, biomedical, and automotive industries. The exceptional strength, low weight, great corrosion resistance, low wear rate, high fatigue property, and high biocompatibility are the primary advantages of titanium alloys [5–12]. Despite it has been categorized as less machinability material due to its intrinsic features of inadequate thermal conductivity

---

R. K. Rout · R. K. Garg (✉) · D. Panchal

Department of Industrial and Production Engineering, Dr. B R Ambedkar National Institute of Technology, Jalandhar, India

e-mail: [gargrk@nitj.ac.in](mailto:gargrk@nitj.ac.in)



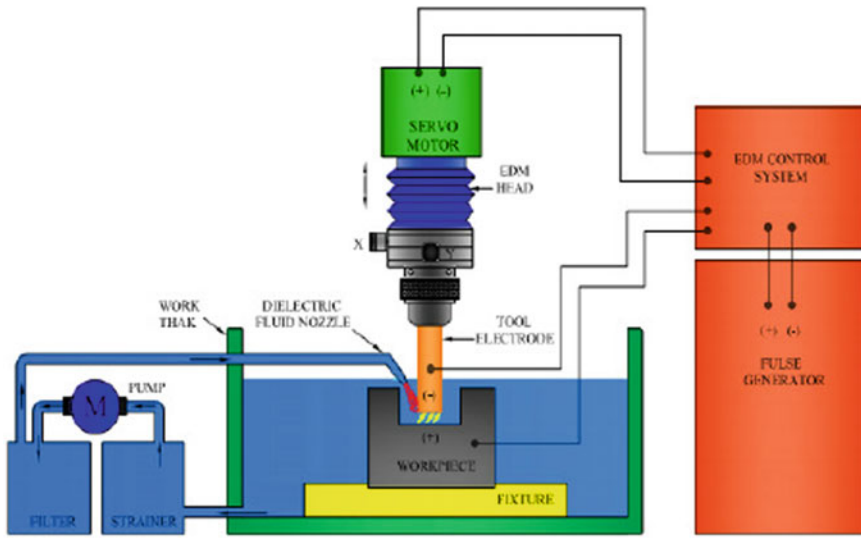


Fig. 1 Die-sinking EDM

and elevated chemical sensitivity. Because of the aforesaid reasons, titanium alloy (Ti6Al4V) has been machined by using die-sinking EDM is an enormous concern, and as a result substantial research is being conducted with the goal of optimizing the process. Many researches had already tried to establish  $I_p$ ,  $T_{on}$ , and  $D_f$  machining parameters to MRR, TWR, and Ra. The schematic diagram (Fig. 1) represents the machining process of die-sinking EDM [13–19].

## 2 Literature Analysis

EDM of alumina for analysis of MRR and Ra has been carried out by using RSM.  $I_p$ ,  $T_{on}$ , and  $S_v$  have been taken as input factors to complete the experiment [1]. The investigational study has been performed on Ti6Al4V ELI at high accuracy EDM with graphite electrode has been conducted.  $I_p$  and  $T_{on}$  have been taken as input factors ranging from 25 to 65 A and 25 to 200  $\mu$ s correspondingly. Tool material removal rate (TMRR), MRR, tool wear ratio (TWR), and surface roughness are the corresponding responses for measuring machining effectiveness [4]. Furthermore, optical microscope and SEM has been used to examine the machined surfaces in order to study their surface features as well as their cross sections in order to determine the AWLT and HAZ thickness [2, 3]. An ANOVA was used to determine how process parameters affect the machining output for the aforementioned performance metrics. The optimizing of Al-TiC has been performed with a copper hollow tube electrode for finding process parameters of EDM. Experiment has been carried out and the

findings were statistically analyzed by using RSM. For determination of wear ratio between electrode and workpiece,  $I_p$ ,  $T_{on}$ , and  $P_f$  have been taken as input factors for process parameters [4]. Finally, the optimal values for these variables have been established where  $T_{on}$  ranged from 50 to 600  $\mu\text{s}$  and  $P_f$  ranged from 3 to 9  $\text{kgf}/\text{cm}^2$ . With the help of design of experiments, a set of five experiments has been carried out to replace a 20-set of trials. The set of five reflects the cumulative effect on the input factors. The MINITAB 17 has been used to conduct the wear ratio and RSM has been taken as design of experiment (DOE) [4]. The composites of Al-TiC have been machined by EDM with  $I_p$ ,  $T_{on}$ , and  $P_f$  as input factors for finding the significant value by using RSM. 15 A, 600  $\mu\text{s}$ , and 6  $\text{kgf}/\text{cm}^2$  have been found the best settings for machining TiC reinforced aluminum composites [4]. A silicon–titanium nitride ceramic composite has been machined by EDM with copper electrode. The  $I_p$ ,  $S_v$ ,  $T_{on}$ , and  $T_{off}$  has been taken as the input factors and MRR, EWR has been optimized by using RSM (Box Behnken Design) for output responses. The analysis of variance has been performed and  $I_p$  has been found as a significant input factor for MRR and EWR [5, 6]. Differences in  $T_{off}$  had no effect on the responses. When  $I_p$  and  $T_{on}$  were larger the material abrasion loss has been found more and when the  $S_v$  and  $I_p$  were low, the EWR has been found lesser. Optimum value of machining factor has been calculated.  $I_p$ ,  $S_v$ ,  $T_{on}$ , and  $T_{off}$ , as well as the products  $I_p^2$  and  $S_v^2$  have the positive influence on EWR. At 4 A, 6  $\mu\text{s}$ , 10  $\mu\text{s}$ , and 40 V EWR has been found lesser. About 46.73% of  $S_v$  and 41.21% of  $I_p$  have a significant impact on the electrode abrasion rate [5, 7]. The Ti-6246 has been machined by utilizing an EDM with a graphite electrode and EDM oil as dielectric fluid.  $I_p$ ,  $T_{on}$ , and  $T_{off}$  has been chosen as process variables. The experiment has been designed as per RSM Box-Behnken Design approach [8]. The optimization process has been carried out by using a desirability technique [9]. 4.5 A, 50.07  $\mu\text{s}$ , and 100  $\mu\text{s}$  have been taken as input factors, respectively. Surface roughness of 0.99 mm has been considered as best response value [20–26].

### 3 Research Methods

The machining of Titanium Grade-5 (Ti6Al4V) has been carried out by using copper tungsten electrode. The input parameters are  $I_p$ ,  $T_{on}$ , and  $S_v$ . MRR, TWR and surface roughness has been considered as responses. RSM (Box-Behnken Design) has been taken as an optimization method. Material removal rate and tool removal rate has been measured before and after machining by scientific digital weight measuring instrument and surface roughness has been measured by using surfaceness tester. Analysis of variance and 3D surface modeling for MRR, TWR, and surface roughness has been performed by using RSM (BBD). The input parameters and levels are responsible for responses. Table 1 is showing the selected parameters and their working units.

**Table 1** Parameters and their units

Name	Units	Low	High
Input current ( $I_p$ )	A	10	20
Pulse on time ( $T_{on}$ )	$\mu s$	100	200
Spark gap voltage ( $S_v$ )	V	15	25

## 4 Result and Discussion

The Ti6Al4V has been machined by copper tungsten electrode, and the data which has been collected during machining operation with respect to input parameters has been tabulated for analysis and optimization (Table 2).

$$MRR = \frac{W_{bm} - W_{am}}{t} \text{ g/min}$$

$$TWR = \frac{T_{bm} - T_{am}}{t} \text{ g/min}$$

where

$W_{bm}$  and  $W_{am}$  Weight of workpiece pre and post machining  
 $T_{bm}$  and  $T_{am}$  Weight of electrode pre and post machining  
 $t$  time.

### 4.1 Work Material (Ti6Al4V) Machined by Copper Tungsten Electrode

#### 4.1.1 Responce1: MRR Graphical Columns

The graphical column represents the MRR values depending upon the input parameters in each run (Fig. 2).

#### 4.1.2 ANOVA for MRR

The  $F$ -value 9.94 makes the model significant and  $p$ -value 0.33% represents the more of  $F$  value due to noise.

Coefficient of factor indicates the change in responses per change in input factors. Here, the VIF value is 1. More than 1 in VIF value indicates multi co linearity in model (Tables 3 and 4).

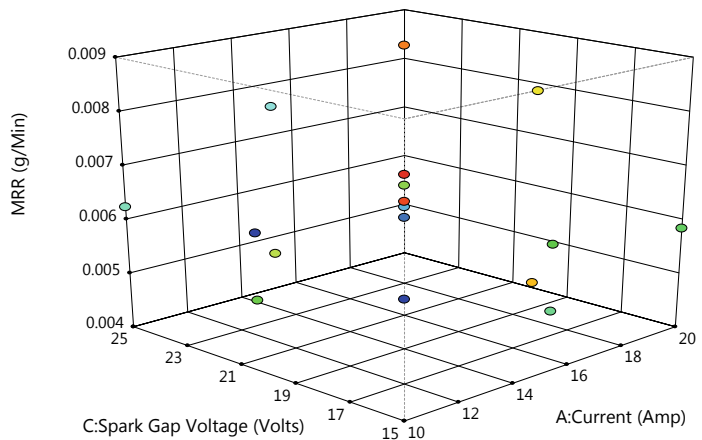
**Table 2** Design matrix for experiments

Std	Run	Factor1 input current ( $I_p$ )	Factor2 pulse on time ( $T_{on}$ )	Factor3 spark gap voltage ( $S_v$ )	MRR (g/min)	TWR (g/min)	Ra ( $\mu\text{m}$ )
5	1	10	150	15	0.0061	0.0042	1.884
1	2	10	100	20	0.0065	0.0043	1.884
15	3	15	150	20	0.0061	0.0043	1.886
17	4	15	150	20	0.0063	0.0049	1.873
12	5	15	200	25	0.0076	0.0057	1.776
7	6	10	150	25	0.0063	0.0047	1.749
9	7	15	100	15	0.0051	0.0031	1.874
6	8	20	150	15	0.0059	0.0033	1.868
10	9	15	200	15	0.0063	0.0049	1.992
3	10	10	200	20	0.0053	0.0041	1.863
13	11	15	150	20	0.0067	0.0037	1.835
11	12	15	100	25	0.0047	0.0042	1.878
4	13	20	200	20	0.0079	0.0061	1.843
2	14	20	100	20	0.0041	0.0038	1.866
8	15	20	150	25	0.0083	0.0059	1.856
16	16	15	150	20	0.0064	0.0041	1.876
14	17	15	150	20	0.0069	0.0045	1.876

Correlation: 0.000

Color points by

Run



**Fig. 2** MRR graphical data

**Table 3** Response ANOVA table for MRR

Source	Squares total	$D_f$	Square average/mean	$F$ -value	$p$ -value	
Model	0.0000	9	1.945E-06	9.94	0.0031	Significant
A-current	5.000E-07	1	5.000E-07	2.55	0.1541	
B-pulse on time	5.611E-06	1	5.611E-06	28.66	0.0011	
C-spark gap voltage	1.531E-06	1	1.531E-06	7.82	0.0267	
AB	6.250E-06	1	6.250E-06	31.92	0.0008	
AC	1.210E-06	1	1.210E-06	6.18	0.0418	
BC	7.225E-07	1	7.225E-07	3.69	0.0962	
A <sup>2</sup>	4.003E-08	1	4.003E-08	0.2044	0.6648	
B <sup>2</sup>	1.658E-06	1	1.658E-06	8.47	0.0227	
C <sup>2</sup>	2.213E-08	1	2.213E-08	0.1130	0.7466	
Residual	1.370E-06	7	1.958E-07			
Lack of fit	9.625E-07	3	3.208E-07	3.15	0.1486	Not significant
Error	4.080E-07	4	1.020E-07			
Cor total	0.0000	16				

**Table 4** Response table for coded factors coefficients

Factor	Estimate coefficient	$D_f$	Error standard	95% CI (low)	95% CI (high)	Fit variance
Intercept	0.0065	1	0.0002	0.0060	0.0069	
A-current	0.0003	1	0.0002	-0.0001	0.0006	1.0000
B-pulse on time	0.0008	1	0.0002	0.0005	0.0012	1.0000
C-spark gap voltage	0.0004	1	0.0002	0.0001	0.0008	1.0000
AB	0.0012	1	0.0002	0.0007	0.0018	1.0000
AC	0.0006	1	0.0002	0.0000	0.0011	1.0000
BC	0.0004	1	0.0002	-0.0001	0.0009	1.0000
A <sup>2</sup>	0.0001	1	0.0002	-0.0004	0.0006	1.01
B <sup>2</sup>	-0.0006	1	0.0002	-0.0011	-0.0001	1.01
C <sup>2</sup>	0.0001	1	0.0002	-0.0004	0.0006	1.01

### 4.1.3 Quadratic Equation for MRR

$$\begin{aligned}
 \text{MRR} = & 0.020808 - 0.001257 * I_p - 0.000017 * T_{\text{on}} - 0.000613 * S_v \\
 & + 5.0000E - 06 * I_p * T_{\text{on}} + 0.000022 * I_p * S_v + 1.70000E \\
 & \text{quad} - 06 * T_{\text{on}} * S_v + 3.90000E - 06 * I_p^2 - 2.51000E - 07 * T_{\text{on}}^2 \\
 & + 2.90000E - 06 + S_v^2.
 \end{aligned}$$

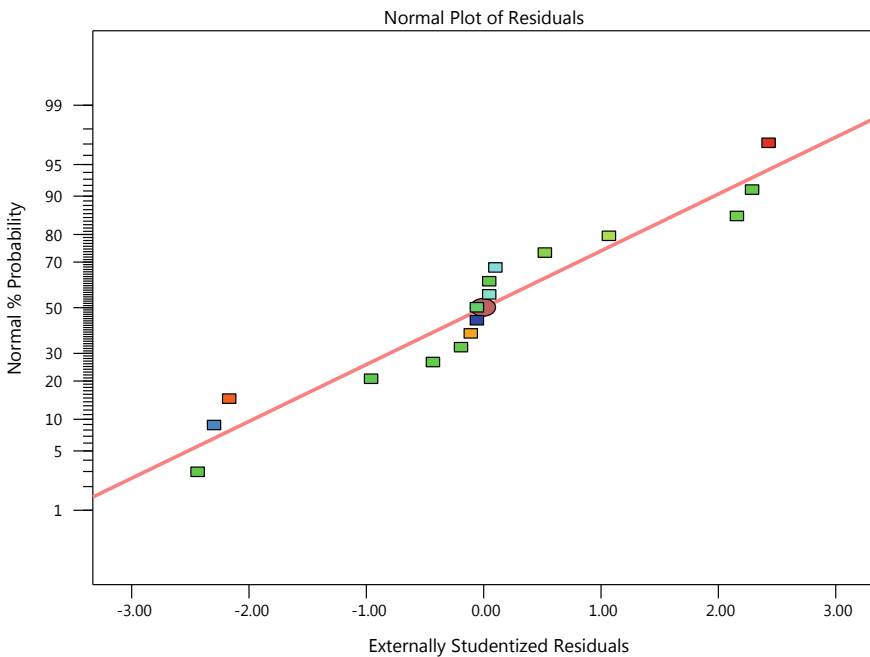
The Normal versus Residual plot for MRR has been represented here (Fig. 3).

The plot represents the Actual versus predicted values of MRR (as shown in Fig. 4).

The 3D surface diagram represents that at high  $T_{\text{on}}$  and high  $I_p$ , MRR has been found more. At high  $I_p$  and low  $T_{\text{on}}$  MRR has been found less (as explored in Fig. 5).

Here, 3D surface diagram represents that at high voltage and high current MRR is more (as shown in Fig. 6).

The 3D surface diagram represents that at high voltage and high spark gap voltage MRR is more (as shown in Fig. 7).



**Fig. 3** Normal versus residual plot for MRR

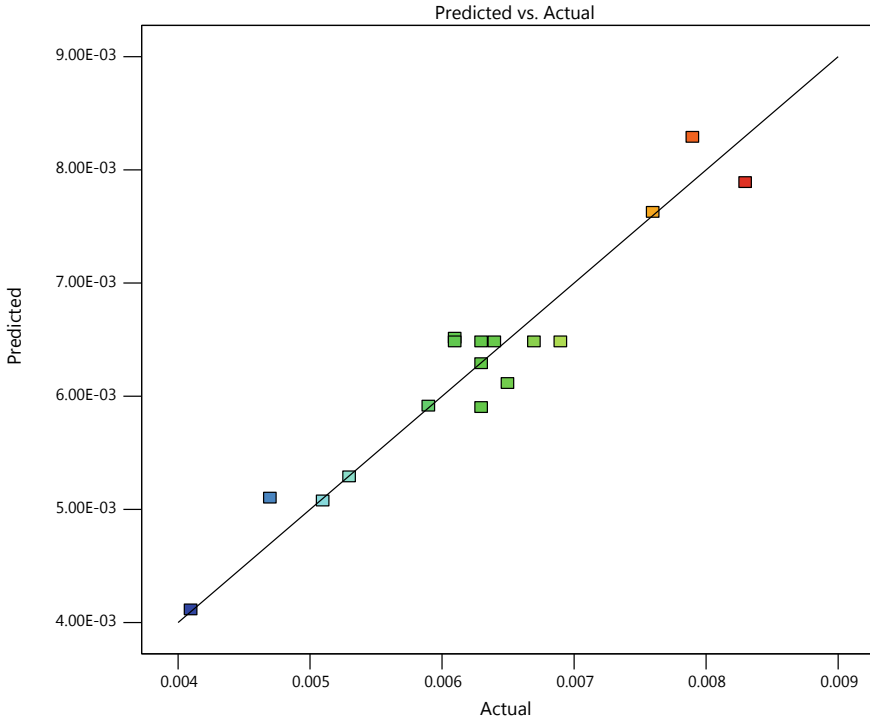


Fig. 4 Actual versus predicted plot for MRR

#### 4.1.4 Response: TWR Graphical Columns

The Graphical column represents the values of TWR with respect to input factors for run (Fig. 8).

#### 4.1.5 ANOVA for TWR

$F$ -value 5.84 makes the model significant and  $p$ -value 1.49% more of  $F$ -value. Lack of Fit 0.9 makes the model not significant and has 51% chance of making the Lack of Fit significant (as detailed in Table 5).

#### 4.1.6 Coefficients in Terms of Coded Factors

The coefficient factor indicates the chance of variance of responses per change in unit factors. The VIF value is 1, VIF value more than 1 makes the model multi co linearity (as shown in Table 6).

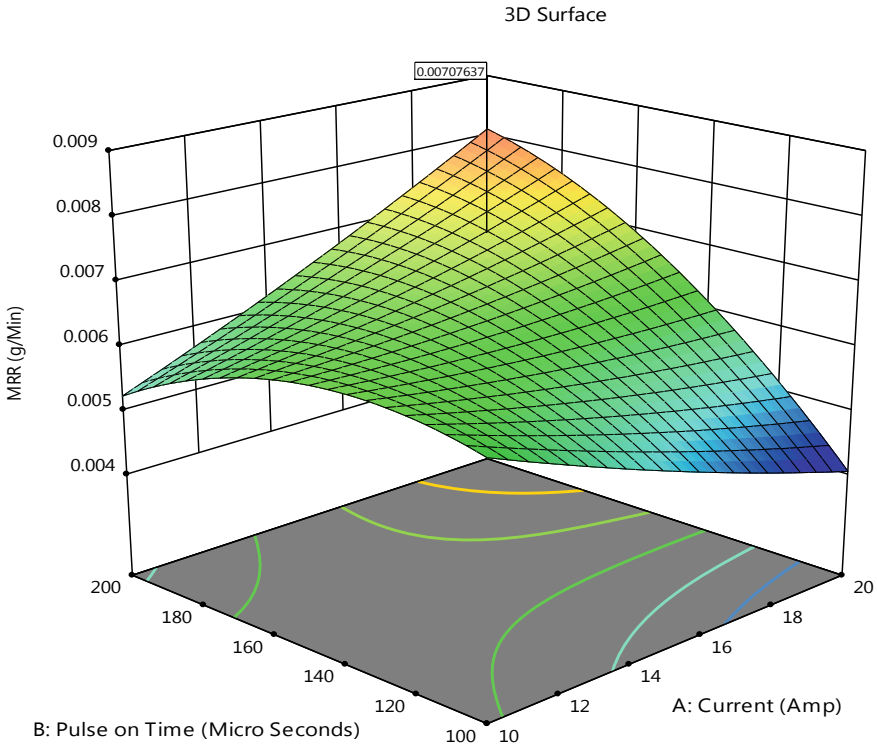


Fig. 5 3D plot of responses selected

### 4.1.7 Quadratic Equation for TWR

$$\begin{aligned}
 \text{TWR} = & 0.013600 - 0.000945 * I_p - 0.000032 * T_{\text{on}} - 0.000245 * S_v \\
 & + 2.50000E - 06 * I_p * T_{\text{on}} + 0.000021 * I_p * S_v \\
 & - 3.00000E - 07 * T_{\text{on}} * S_v + 6.50000E - 06 * I_p^2 + 4.50000E \\
 & - 08 * T_{\text{on}}^2 + 2.50000E - 06 * S_v^2.
 \end{aligned}$$

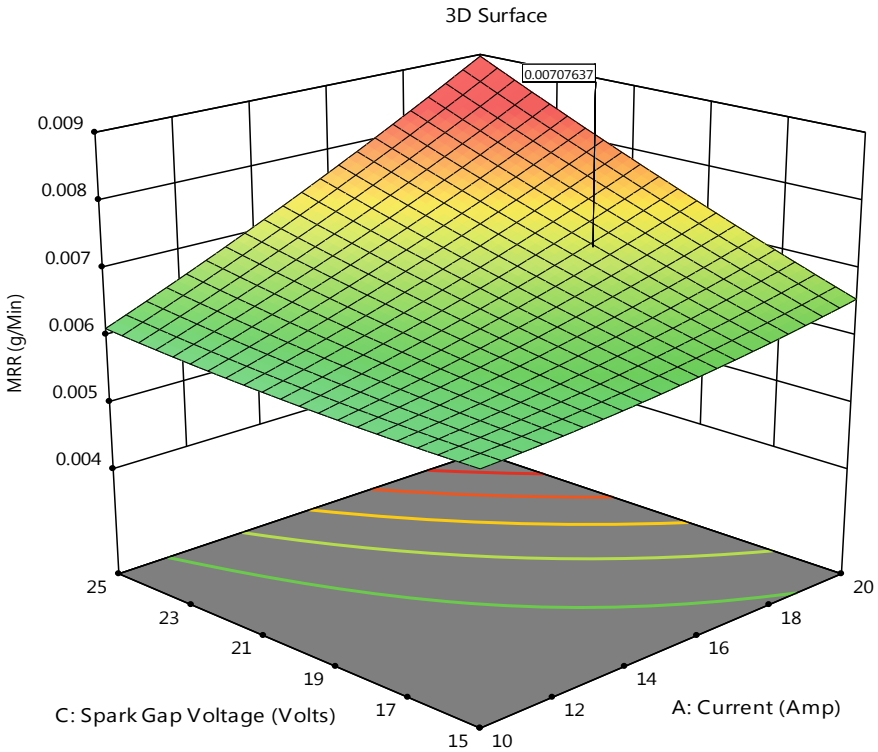
The plot represents the Normal versus residual values of TWR depending upon the input parameters.

The above diagram represents the predicted versus actual values of TWR (as reflected in Fig. 9).

The 3D surface model represents that at high current and high voltage the TWR is maximum. And at low current and low voltage, the TWR is minimum (as reflected in Figs. 10 and 11).

Here, the above 3D surface model represents that at high  $S_v$  and high  $T_{\text{on}}$ , electrode wear has been found maximum. And at less  $S_v$  and  $T_{\text{on}}$ , the electrode wear has been found minimum (as reflected in Fig. 12).





**Fig. 6** 3D plot for current and spark gap voltage

## 5 Conclusion

The following conclusions can be drawn;

1. Input current  $I_p$ , Spark Gap Voltage  $S_v$  has significant influence on both MRR and TWR. At 15 A, 150  $\mu$ s and 20 V the Maximum MRR has been found. At 20 A, 100  $\mu$ s and 20 V the MRR has been found less.
2. At 20 A, 200  $\mu$ s and 20 V the TWR has been found maximum. At 15 A, 100  $\mu$ s and 15 V the TWR has been found less.
3. AT 10 A, 150  $\mu$ s and 25 V the Surface Roughness value is less.  $T_{on}$  has a significant influence on Ra value. Lesser pulse on time has been observed batter at high current and voltage.

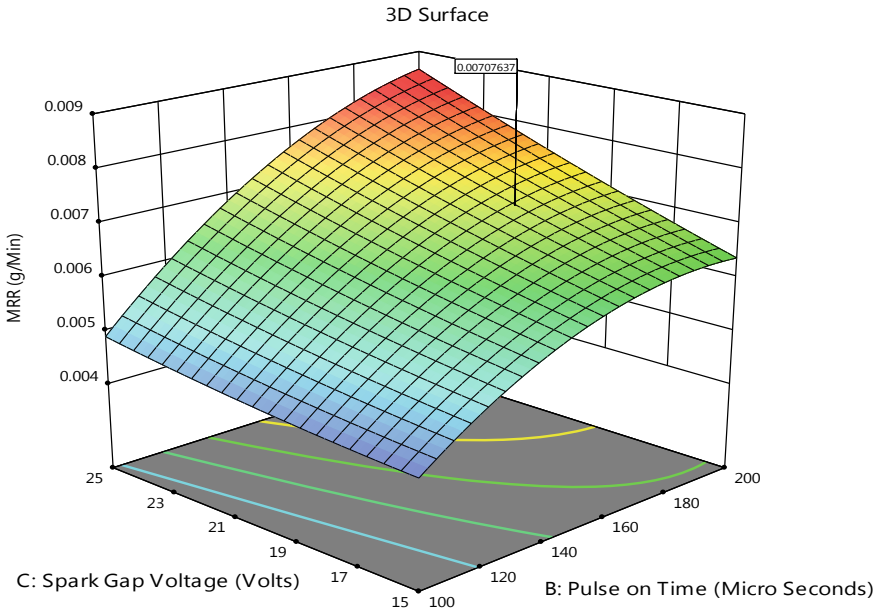


Fig. 7 Plot for pulse on time and gap voltage for MRR

Correlation: 0.000  
Color points by  
Run  
1

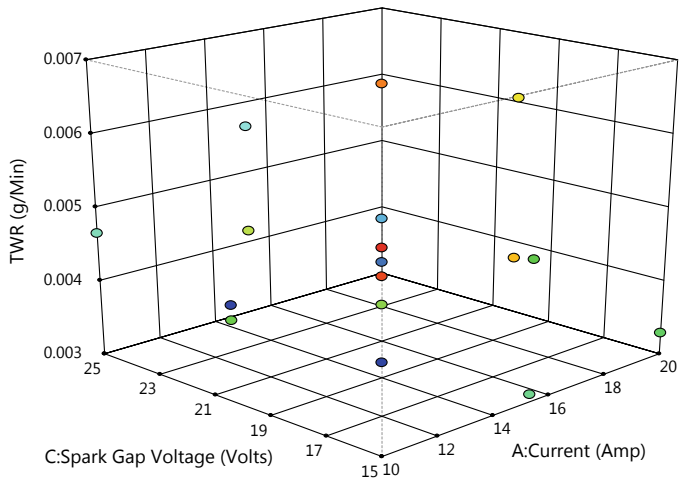


Fig. 8 Graphical columns for TWR

**Table 5** Response ANOVA table for TWR

Source	Squares total	$D_f$	Square average/mean	$F$ -value	$p$ -value	
Model	0.0000	9	1.118E-06	5.84	0.0149	Significant
A-current	4.050E-07	1	4.050E-07	2.12	0.1891	
B-pulse on time	3.645E-06	1	3.645E-06	19.04	0.0033	
C-spark gap voltage	3.125E-06	1	3.125E-06	16.32	0.0049	
AB	1.562E-06	1	1.562E-06	8.16	0.0244	
AC	1.103E-06	1	1.103E-06	5.76	0.0475	
BC	2.250E-08	1	2.250E-08	0.1175	0.7418	
A <sup>2</sup>	1.112E-07	1	1.112E-07	0.5808	0.4709	
B <sup>2</sup>	5.329E-08	1	5.329E-08	0.2784	0.6141	
C <sup>2</sup>	1.645E-08	1	1.645E-08	0.0859	0.7779	
Residual	1.340E-06	7	1.914E-07			
Lack of fit	5.400E-07	3	1.800E-07	0.9000	0.5151	Not significant
Error	8.000E-07	4	2.000E-07			
Cor total	0.0000	16				

**Table 6** Coded factors coefficients

Factor	Estimate coefficient	$D_f$	Error standard	95% CI (low)	95% CI (high)	Fit variance
Intercept	0.0043	1	0.0002	0.0038	0.0048	
A-current	0.0002	1	0.0002	-0.0001	0.0006	1.0000
B-pulse on time	0.0007	1	0.0002	0.0003	0.0010	1.0000
C-spark gap voltage	0.0006	1	0.0002	0.0003	0.0010	1.0000
AB	0.0006	1	0.0002	0.0001	0.0011	1.0000
AC	0.0005	1	0.0002	7.708E-06	0.0010	1.0000
BC	-0.0001	1	0.0002	-0.0006	0.0004	1.0000
A <sup>2</sup>	0.0002	1	0.0002	-0.0003	0.0007	1.01
B <sup>2</sup>	0.0001	1	0.0002	-0.0004	0.0006	1.01
C <sup>2</sup>	0.0001	1	0.0002	-0.0004	0.0006	1.01

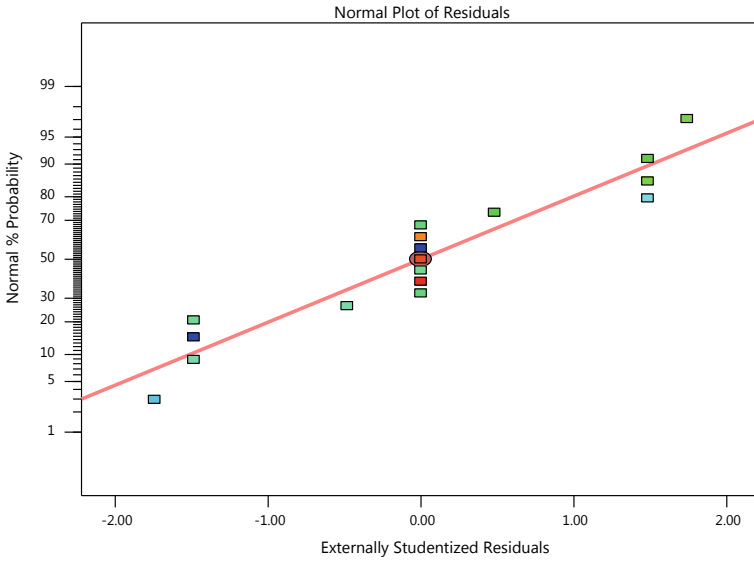


Fig. 9 Predicted versus actual values of TWR

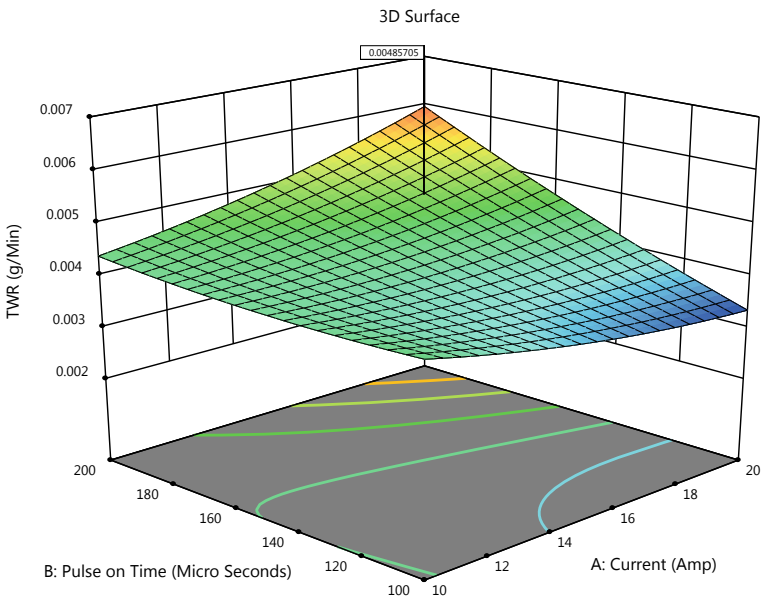


Fig. 10 3D plot for TWR

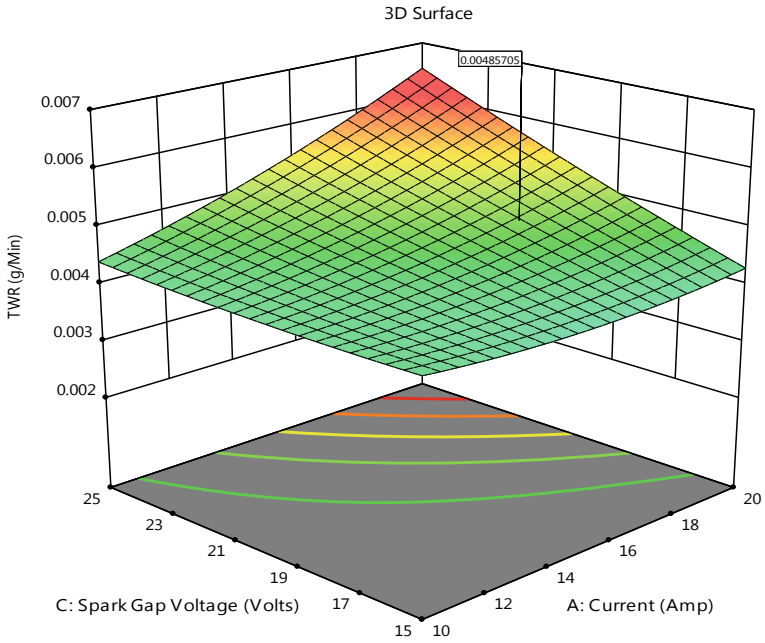


Fig. 11 Current versus gap voltage graph for TWR

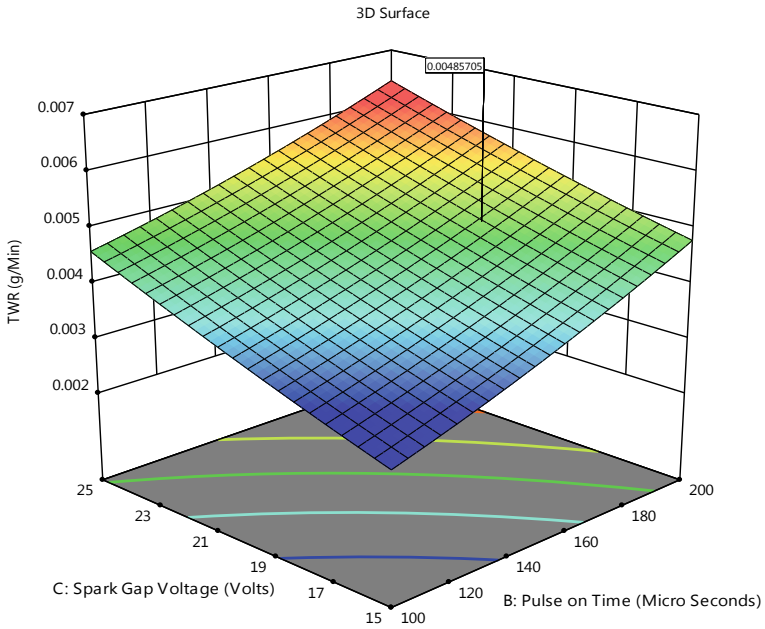


Fig. 12 Pulse on time and gap voltage for TWR

## References

- Jain N (2018) Effect of Al<sub>2</sub>O<sub>3</sub> powder in deionized water on metal removal rate during electro discharge machining of H11 die steel effect of Al<sub>2</sub>O<sub>3</sub> powder in deionized water on metal removal rate during electro discharge machining of H11 die steel, no. October, 2018. <https://doi.org/10.1088/1757-899X/402/1/012012>
- Tialv G, Suresh S, Jamil MA, Sulaiman S, Shokor MRM (2016) Optimization of electrode material for EDM die-sinking of titanium alloy grade 5—Ti6Al4V. <https://doi.org/10.18517/ijaseit.6.4.902>
- Ali MY, Moudood MA, Maleque MA, Hazza M, Adesta EYT (2017) Electro-discharge machining of alumina: investigation of material removal rate and surface roughness. *J Mech Eng Sci* 11(4):3015–3026. <https://doi.org/10.15282/jmes.11.4.2017.5.0271>
- Zhong C, Liu J, Zhao T, Schopphoven T, Fu J (2020) Applied sciences laser metal deposition of Ti6Al4V—a brief review, pp 1–12. <https://doi.org/10.3390/app10030764>
- Analysis and evaluation of MRR, Ra and HAZ
- Singh H, Garg R (2009) Effects of process parameters on material removal rate in WEDM, vol 32, no 1, pp 70–74
- Edm HP (2021) A comprehensive study on processing Ti–6Al–4V ELI with. *Materials* (Basel), pp 1–17
- Ojha K, Garg RK, Singh KK (2011) Parametric optimization of PMEDM process using chromium powder mixed dielectric and triangular shape electrodes, vol 10, no 11, pp 1087–1102
- Singh N (2016) Optimization of process parameters in die sinking EDM—a review, vol 2, no 11, pp 808–813
- Pugazhenthir R, Sreeram D, Scaria CT, Anbuezhayan G, Nanthakumar P (2020) Effect of process parameters on machining of Al-TiC metal matrix composites using RSM. *Mater Today Proc* 46(xxxx):3282–3287. <https://doi.org/10.1016/j.matpr.2020.11.357>
- Singh N, Bhatia OS (2016) Analysis of the influence of EDM parameters on material removal rate of low alloy steel and electrode wear of copper electrode, vol 3, no 6, pp 2322–2330
- Kumar H, Garg RK (2010) Analysis and evaluation of heat affected zones in electric discharge machining of EN-31 die steel, vol 17, no. April, pp 91–98
- Kumar SR, Srinivasan VP, Balamurugan S, Krishnaa SD, Gokul V, Anudeep S (2020) Materials today : proceedings optimization of machine machining parameters in EDM of silicon nitride-titanium nitride based on RSM. *Mater Today Proc*, no. xxxx. <https://doi.org/10.1016/j.matpr.2020.05.429>
- Bypass GTR, Bypass GTR, A review of tool electrode designs for sinking EDM process 2 different aspects of electrode design, pp 25–30
- Thakur A, Rao PS, Khan MY (2020) Materials today : proceedings study and optimization of surface roughness parameter during electrical discharge machining of titanium alloy (Ti-6246). *Mater Today Proc*, no. xxxx. <https://doi.org/10.1016/j.matpr.2020.10.785>
- Garg RK, Singh K (2010) MRR improvement in sinking electrical discharge machining: a review MRR improvement in sinking electrical discharge machining: a review. <https://doi.org/10.4236/jmmce.2010.98051>
- 6 Karmiris-Obratański\_2021\_IOP\_Conf.\_Ser.\_Mater.\_Sci.\_Eng.\_1037\_012003.pdf
- Cooperative C, Box PO, Vic H (2009) Numerical and experimental investigation of the heat-affected zone in a laser-assisted machining of Ti-6Al-4V alloy process Nancy Yang a , Milan Brandt and Shoujin Sun, pp 143–146. <https://doi.org/10.4028/www.scientific.net/MSF.618-619.143>
- Bilal A, Perveen A, Talamona D, Jahan MP (2021) Understanding material removal mechanism and effects of machining parameters during EDM of zirconia-toughened alumina ceramic
- Reddy RV, Reddy UR, Sagar KR, RRP, Optimization of die sink EDM process parameters using Taguchi method with copper Tungsten electrode, vol IX, no V, pp 3228–3236
- Jeevamar J, Ramabalan S, Sivashanmugam N (2018) A review on die sinking EDM process parameters

22. Pontevedra V et al (2018) ScienceDirect ScienceDirect ScienceDirect ScienceDirect 2nd international conference on materials manufacturing and design engineering a perspective on shaping of advanced ceramics by electro discharge a perspective on shaping of advanced ceramics by electro discharge machining costing models for capacity optimization between used capacity. Proc Manuf, vol 20, pp 65–72. <https://doi.org/10.1016/j.promfg.2018.02.009>
23. Mayor H (2019) Director speech on 8th ASAIS 2019
24. Access O (2013) Electrical discharge machining ( EDM ) of Inconel 718 by using copper electrode at higher peak current and pulse duration electrical discharge machining (EDM ) of Inconel 718 by using copper electrode at higher peak current and pulse duration. <https://doi.org/10.1088/1757-899X/50/1/012062>
25. Majhi SK, Soni H (2013) Optimization of EDM parameters using integrated approach of RSM, GRA and entropy method optimization of EDM parameters using integrated approach of
26. Srivastava S, Garg RK, Author's personal copy process parameter optimization of gas metal arc welding on IS: 2062 mild steel using response surface methodology

# A Critical Review on Industry 5.0 and Its Medical Applications



Shubhangi Chourasia, Ankit Tyagi, Qasim Murtaza, R. S. Walia,  
and Prince Sharma

**Abstract** In the modern era, academicians, industrialists, and researchers are more concerned about Industry 4.0 as it is on the verge to get obsolete, which led to the development of Industry 5.0. Many modernists have discussed the fifth revolution concept and its applications in various fields such as manufacturing, health care system, and hospitality. The idea of Industry 5.0 is entirely based on human–robot co-working and bio-economy based on intelligent manufacturing systems and digital technologies. The present paper initially provides a brief overview role and components of Industry 5.0 in medical applications. Then the article briefly discussed the application of Industry 5.0 and the benefits and limitations of Industry 5.0.

**Keywords** Industry 5.0 · Human–robot · Digital innovation · Artificial intelligence

## 1 Introduction

Advanced additive manufacturing technologies have many possibilities and capabilities in the design of freedom. However, in the daily routine work of the designer, adopting a strategy for components or parts is not essential and straightforward

---

S. Chourasia · A. Tyagi (✉)

Department of Mechanical Engineering, SGT University, Haryana, India

e-mail: [tyagiankit10506@yahoo.com](mailto:tyagiankit10506@yahoo.com)

Q. Murtaza

Department of Mechanical Engineering, Delhi Technological University, Delhi, India

R. S. Walia

Department of Production and Industrial Engineering, PEC, Chandigarh, India

P. Sharma

Department of Design, ISGEC, Hitachi Zosenn Limited, Gujarat, India



to examine the all-mechanical properties of materials along with their characteristics according to the applications. The redesigning of components is based on additive processes rather than subtractive processes [1]. In the present scenarios, customers' expectations are changing rigorously, and they want the personalization of the goods, which would contain unique and distinctive properties and devouring human touch. This mindset of customers can only be attained when industries will adopt the dynamic concept of Industry 5.0. The innovative idea of Industry 5.0 is to work from the concept of mass customization to mass personalization. According to this concept, products and services are provided to customers as per their requirements, that is why the manufacturing industries, as well as medical health care systems, are moving ahead for implementation of Industry 5.0, which is enabled latest technologies like machine learning, IoT, IOS, AI, and cloud computing.

The term Industry 5.0 is coined in 2015 and is also known as the "fifth industrial revolution of India," which is visualized to have an enormous scope in sustainable civil society, medical health care system, manufacturing, and daily human life [2]. In the fifth industrial revolution (I 5.0), a particular focus is kept on the personalized need and requirements of the customer. Formerly, the fourth industrial revolution (I 4.0) was embedded with mass customization of products and services, which was not sufficient. In industrial revolution 5.0, human to machines refers to significant interaction to make work easy, improved, and faster with the enabling of software and use of high tech technologies such as machine learning, algorithms, special software's which are connected to the web to bring changes in old system [3]. There is massive involvement of automated and semi-automated robots to perform the welding, loading, unloading in manufacturing areas, and as surgical assistants during the surgery to examine the patients in rural area locations by providing them telepresence in the health care system and touring manufacturing facilities [4].

## ***1.1 Need of the Study***

In the modern era, academicians, industrialists, and researchers are more concerned about Industry 4.0 as it is on the verge to get obsolete, which led to the development of Industry 5.0. Advanced additive manufacturing technologies have many possibilities and capabilities in the design of freedom. However, in the daily routine work of the designer, adopting a strategy for components or parts is not essential and straightforward to examine the all-mechanical properties of materials, their characteristics according to the applications. The concept of Industry 5.0 is entirely based on human-robot co-working and bio-economy based on intelligent manufacturing systems and digital technologies. So, there is a need to identify and explore Industry 5.0 and its medical and health care application.

## 1.2 Research Questions

The present research addresses the following questions:

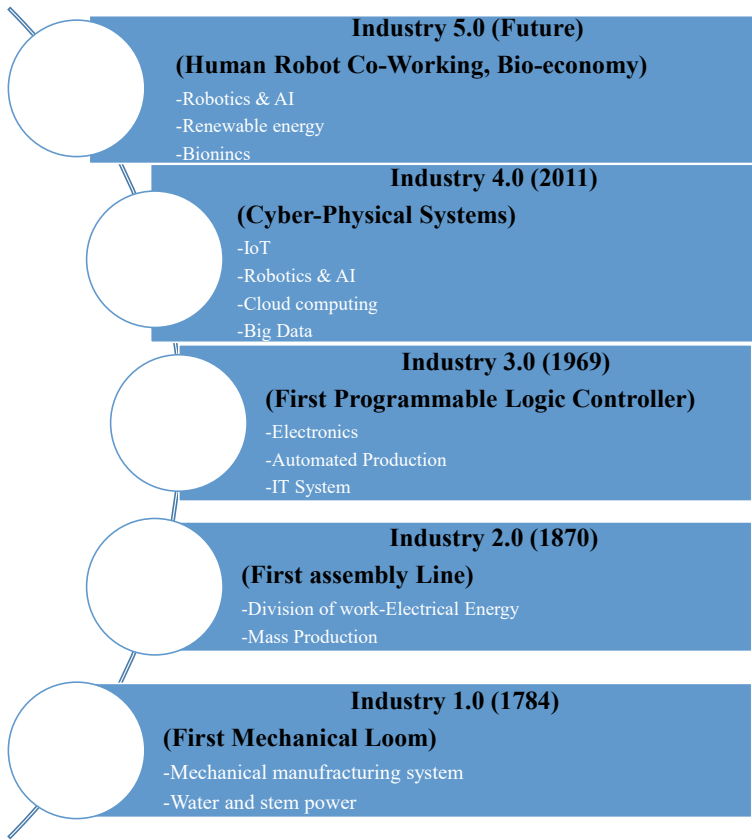
1. To study the role and components of Industry 5.0 in medical applications.
2. Provides brief discussion about the application of Industry 5.0.
3. To introduce the future scope along with benefits and limitations of Industry 5.0.

## 2 Literature Review

The machines and humans are interlinked with each other to get improve productivity as well as human efficiency. Figure 1 shows the transformation journey of the industrial revolution first to the industrial revolution 5. Figure 1 shows various industrial revolutions from the 1800 years to future predictions. It is a matter to notice that the time between reach the first industrial revolution to third industrial was 100 years. In contrast, it took almost only forty years to touch the fourth revolution from the third industrial revolution. After seeing the progress of industrial revolutions in the graph's timeline, it is easy to predict that to reach the mount of the fifth revolution, and industries will take less time than before [5].

Industry 5.0 came with steam and waterpower utilization, and Industry 2.0 announced the concept of mass production in manufacturing which assisted the water-produced power; the 3rd industrial revolution brought significant advancements in digital and electronic devices. The fourth industrial revolution is connected to the world with artificial intelligence, clouding system, the Internet of Things, and other technologies. In contrast, the fifth revolution helps connect industries with intelligent systems such as IoT, AI, and cybersystems to achieve widespread automation. The sole aim of this revolution is to improve and enhance the overalls efficiency of the production system with the help of robots. In Industry 5.0, humans and machines are in a convergence relationship where the imagination of humans toward the work is converted into the task with the aid of robots [6–8]. The robots perform the work that human desire. Presently, two unique visions arise from Industry 5.0. The first vision is the co-working of humans and robots. In this current vision, humans and robots work together when and where possible. The human performs the creative tasks, and the rest work will complete by the robots. The following vision of Industry 5.0 is centered on the bio-economy [9]. In bio-economy, biological resources are practices for industrial drives, which will help attain stability between the capital economy, industry, and ecosystem/ecology. Table 1 depicts the explicit comparison between visions of Industry 4.0 and Industry 5.0.

Industry 5.0 is an emerging field nowadays, which provides a human and machine-friendly environment to industries enabled with many high techs technologies such as multi-agent systems, artificial intelligence, IoT, and digital environment. In contrast, different features of Industry 5.0 are depicted in Fig. 2.



**Fig. 1** Journey of industry revolution [5]

### 3 Application of Industry 5.0

#### 3.1 Industry 5.0 in the Medical Field

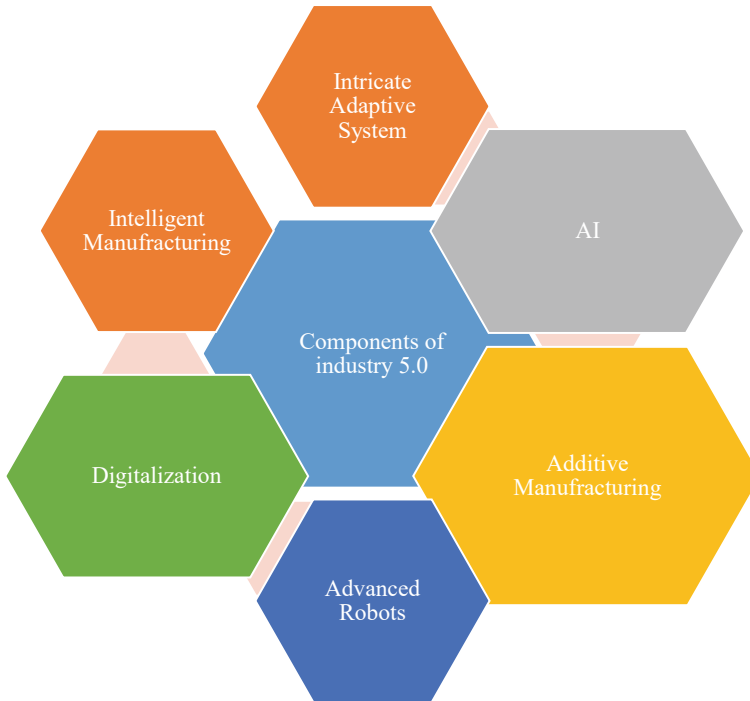
In today's time, every patient wants personalization in medical services, such as blood measuring portable machines, sugar level measuring devices, and other body parts measuring parameters that fill their requirements. The emerging high-tech technologies provide real-time data of patients to doctors. All the relevant data of individual patients are recorded and set into discrete medical records, which helps data/facts mining for single patients and patients. All these are intelligent devices based on machine learning, IoT, and AI interconnected among themselves and provide accurate information to doctor then. The only doctor can give the proper treatment as per the need of the specific patient. Industry 5.0 uses much software to monitor health and daily lifestyles. Artificial intelligence is introduced in Industry 5.0, which is

**Table 1** A brief comparison between the Industry 4.0 and Industry 5.0 vision 1st and 2nd [5]

S.No.	Agendas	Industry 4.0	Industry 5.0 in 1st vision	Industry 5.0 in 2nd vision
1	Motivation	Based on smart manufacturing	Co-working of humans and robots together	Moved to bio-economy
2	Technologies	Artificial intelligence (AI) Cloud computing Robotics engineering and AI Big data	Collaboration of humans and robots with use of renewable resources	Electrical power used as resources and renewable power sources
3	Aim	Based on mass production	Based on intelligent production for society	Based on sustainability models
4	Research areas	Based on business administration Organizational research Innovation in ideas Process improvement	Smart working environment Based on business administration Organizational research Innovation in ideas Process improvement	Based on waste prevention, agriculture, and biology Based on business administration Organizational research Innovation in ideas Process improvement

entirely a life changer tool in human life and teaches how the human body reacts in any situation. It opens the door of opportunities to the medical health care system and mechanizes the manufacturing system [10]. Industry 5.0 provides digital data and big data networking by balancing innovation and providing the pertinent health information and vital records of patients.

This revolution uses robots and support to human-co-robots working culture to enhance the correctness and quality of work that human wants. This collective work of robots and humans is used to attain exclusive surgeries in the health care system. Thus, doctors or surgeons can adore the advantages of this innovative technology. The work with robots is an automation practice that also has some hazardous effects on the workers who work on the shop floor [11]. The sole aim of Industry 5.0 is to develop an intelligent medical system with actual-time abilities. At the time of pandemic (COVID-19), these software-enabled expertise technologies can deliver an outskirts vigilance structure in the medical health care system. By using these technologies, one can trail and easily predict the presence of the COVID-19 virus and store a considerable amount of patients’ informative data, which helps save time. A cost occurs during the treatment process. These technologies employ to evaluate the causes of diseases and their chances of improvements where data related to patients are stored in categories wise like demographic location-wise, age-wise, and gender-wise [8, 12–14]. Industry 5.0 is a powerful tool that furnishes an intelligent resolution for critical and intricate problems during the treatments. With these technologies,



**Fig. 2** Various unique components of Industry 5.0 [3]

the health care system or organization can build a good hospital structure and make human life easy by making minor failures in the operation process [15–17].

### **3.2 Industry 5.0 in the Hospitality Field**

The Internet of the system (IOS), human-cyber-physical (HCP), and Internet of Things (IoT) are the essential elements of Industry 5.0 [18]. The HCP system is connected with humans, AI, and the high-speed Internet of organization [19]. A good number of sensors show their significant role in the human-cyber-physical system. The touch sensor, light sensor, and others are primarily employed in the human-cyber-physical system to achieve various organization functions [20]. Human beings are served by the practice of HCPS and AI [21]. The role of HCPS in the hotel industry comprises enhancing edibles care by using sensors via scanning process for dangerous diseases and measuring the cleanness and bloom of products, and applying the bar code or labels to understand the location from where food comes [22]. In IoT, the system is connected with calculating devices such as computers and transferred the data via Internet networks with or without human–human and

**Table 2** Application of Industry 5.0

S.No.	Area of application	Issues	Solutions	Sources
1	Manufacturing	Mass personalization in automotive manufacturing industries	AI and alliance with communication technologies and human smartness is the right path to get the fixed target	[26]
2	Health care	Medical services costs are too high for caring the older people and dealing with social security	Older adults can be cured by the practice of AI and robots in the surveillance of nurses and doctors	[27]
3	Fintech	The bank’s financial services of cash transactions are indigent and slow due to hooch pouch methodology in overpopulated countries	Blockchain technology is the solution to this issue for transactions and can promote cashless payments	[28]
4	Infrastructure	Scarcity skilled labor in developing countries during the fast growth in infrastructure	Use of robots, 3D printers, ICT, human intelligence, AI for doing the inspection, construction, and detection of areas requiring repair with the help of sensors and robots	[28]

human–computer working [18]. Throughout the pandemic time of COVID-19, the IoT properly controlled and synchronized the various electronic and smart devices of visitors during post and pre checkout without direct person-to-person contact [23]. In COVID-19 pandemic, the hospitality industries use IoT by enabling phone enabled on and off light, door closing and opening sensors, smart thermostat, etc. [24]. Industry 5.0 is working on the principle of providing the personalized services rather than customized services. The idea of Industry 5.0 is well suited for the congeniality, catering, and tourism industry since every guest wishes to have customized services. Hotel owners and staff have to deliver these for customer satisfaction [25]. Table 2 shows the area of application with related issues and solutions of Industry 5.0.

#### 4 The Benefit of Industry 5.0 in the Medical Health Care System

The worldwide fifth industrial revolution is identified as Industry 5.0. Industry 5.0 entails the new innovative and generative high-tech smart technologies associated

wirelessly and can be employed to enrich the man-free system (automation) in manufacturing and health systems (Robot-based surgery). Industry 5.0 is the dawn in all the manufacturing, healthcare, IT sectors, etc. This is the combination of advanced technologies where virtuous collaborations among the human and machine can be performed. The idea of Industry 5.0 is flourishing with the concept of intelligent technologies and state-of-the-art technologies. It is the power complete tool for achieving sustainable, safeguarding products, and effective services [29–31]. Industry 5.0 has also provided assistance in the manufacturing and medical fields with excellent collaboration among the medical surgeon and patient by using various automated technologies such as robots for surgery purposes and many more. Industry 4.0 is based on the customization of products or services, whereas Industry 5.0 focuses on personalized customer demands. Digital data and various high-tech software are employed to create the digital factories in Industry 4.0, whereas in Industry 5.0, IoT, AI, cloud technologies, etc., are used to construct the intelligent industries. Industry 5.0 has brought storm in technologies with the application of highly advanced intelligent technologies in the medical health care system where the interconnect web linkage is used to fill the numerous essential services in the medical system in the COVID-19 time [32–34]. The technologies used in Industry 5.0 will help to fulfill to store real-time data of patients during the medical examination of their body in the clouds and save the time of patients and doctors efficiently. Cloud computing technologies are an essential part of Industry 5.0 like the others because it is an intelligent technology used to interchange valuable data with a concerned system such as COVID-19. With the application of this cloud platform, a medical warrior can easily envisage the signs of the patient who is suffered from COVID-19 [35–37]. The sensitive data of patients can quickly be accumulated, and the take appropriate monitoring of health care system in Industry 5.0. Nowadays, the medical system uses additive manufacturing technologies to develop personalized body parts of the patient, such as artificial liver, kidney, and ortho prosthesis utilizing digital numerical data. Synthetic biology helps make the biological parts; systems redesign the system by using digital data encoded onto the components of synthetic DNA [38].

## **5 Limitations of Industry 5.0 in the Medical Health Care System**

Industry 5.0 technologies are an advanced tool, which can bring a huge revolution in the field of health care as well as manufacturing systems due to their versatile approach. To implement these technologies such as IoT, AI, IOS, and cloud computing. Highly trained workforce is required to note accurate data of patients and feed to the system. This transformation offers personalized health care services and convinces and eminence life to the patient in the health care system. However, the higher cost is one of the major limitations to the implementation of these technologies. Due to some human cum technical reasons, these intelligent technologies

do not provide accurate, precise, and trustworthy outcomes that may cause a great challenge to clinical staff. Therefore, good runs or trials must be required before executing these technologies in clinical and manufacturing systems because the affinity with the present gadgets or devices is essential for the commercialization purpose. Virtual consultations via the Practo application and Google glasses are used for consultation purposes by few clinical doctors [39]. Additionally, The IoE, big data, AI machine learning, and intelligent algorithm provide accurate digital data to doctors for appropriate diagnosis. Doctors can easily diagnose outskirt patients through internet-connected gadgets. Industry 5.0 has great capability to deliver all the digital information for fabricating the human prosthesis, implants, devices, and tools and simultaneously observe all the human body or health actions with the help of software [39].

## 6 Conclusion and Future Scope

In the modern era, academicians, industrialists, and researchers are more concerned about Industry 4.0 as it is on the verge to get obsolete, which led to the development of Industry 5.0. Many modernistic, has created a discussion over the fifth revolution concept and its applications in various fields such as manufacturing, health care system, and hospitality. The concept of Industry 5.0 is entirely based on human-robot co-working and bio-economy based on intelligent manufacturing systems and digital technologies. In the shadow of Industry 5.0, all advanced machines and high-tech technologies are involving; doctors, researchers, and professionals who are moving one step ahead to take all the supercritical challenges such as teaching, development, surgery with the help of robots, implants by use of machines and medication. The implementation of Industry 5.0 in the field of medicine could be helped the medical warrior and patients improve the health care system and help doctors provide healthier and efficient care.

Industry 5.0 has a remarkable ability in manufacturing, medical care system, and many more. It has excellent propensity in the technologies, which can create a bridge between humans and machines to enhance the full competency of the working system. In the future, all the necessary actions such as surgery, cancer treatment, injections, and other medical processes will be handle by Industry 5.0, while doctors/clinical staff/nurses would be fixing another level of jobs. All the patients and customers are digitally supported by Industry 5.0, where all the follow-up, monotonous work is performed by them [39].



## References

1. Lettori J (2020) Additive manufacturing adoption in product design: an overview from literature and industry, ScienceDirect. Available online at [www.sciencedirect.com](http://www.sciencedirect.com). Proc Manuf 51:655–662, The Authors. Published by Elsevier Ltd.
2. Rada M (2015) Industry 5.0—from virtual to physical. <https://www.linkedin.com/pulse/industry-50-from-virtual-physical-Michael-rada>
3. Haleem A, Javaid M (2019) Industry 5.0 and its applications in orthopedic. J Clin Orthop Trauma 10:807e80
4. Sethi C, Telepresence robots take over. The American Society of Mechanical Engineers
5. Demir KA (2019) Industry 5.0 and human-robot co-working. ScienceDirect Available online at [www.sciencedirect.com](http://www.sciencedirect.com). Proc Comput Sci 158:688–695
6. Xu LD (2020a) Industry 4.0—frontiers of the fourth industrial revolution. Syst Res Behav Sci 37(4):531–534
7. Xu LD (2020b) The contribution of systems science to Industry 4.0. Syst Res Behav Sci 37(4):618–631
8. Haleem A, Javaid M (2019) Additive manufacturing applications in industry 4.0: a review. J Ind Integr Manag 4(4):1930001
9. Demir KA, Cicibaş H (2018) The next industrial revolution: industry 5.0 and discussions on industry 4.0. Industry 4.0 from the management information systems perspectives. Peter Lang Publishing House
10. Kowalkiewicz M (2017) Health 5.0: the emergence of digital wellness. Chair in digital economy. <https://medium.com/qut-cde/health-5-0-the-emergence-of-digital-wellness-b21fdff635b9>
11. Rossi B (2018) Manufacturing gets personal in industry 5.0. Raconteur. <https://www.raconteur.net/technology/manufacturing-gets-personal-industry-5-0>
12. Ozdemir V, Hekim N (2018) Birth of industry 5.0: making sense of big data with artificial intelligence, “the internet of things,” and next-generation technology policy. Omics J Integr Biol 22(1):65–76
13. Nahavandi S (2019) Industry 5.0—a human-centric solution. Sustainability 11(16):4371
14. Abeler J, Bäcker M, Buermeyer U, Zillesen H (2020) COVID-19 contact tracing and data protection can go together. JMIR Mhealth Uhealth 8(4):e19359
15. Kim JH (2017) A review of cyber-physical system research relevant to the emerging IT trends: industry 4.0, IoT, big data, and cloud computing. J Ind Integr Manag 2(3):1750011
16. Chen H (2017) Theoretical foundations for cyber-physical systems: a literature review. J Ind Integr Manag 2(3):1750013
17. Zhang C, Chen Y (2020) A review of research relevant to the emerging industry trends: industry 4.0, IoT, BlockChain, and business analytics. J Ind Integr Manag 5(1):165–180
18. Alcácer V, Cruz-Machado V (2019) Scanning the industry 4.0: a literature review on technologies for manufacturing systems. Eng Sci Technol Int J (June 1). <https://doi.org/10.1016/j.jestch.2019.01.006>
19. Pathak P, Pal PR, Shrivastava M, Ora P (2019) Fifth revolution: applied AI & human intelligence with cyber-physical systems. Int J Eng Adv Technol 8(3):23–27
20. Hermann M, Pentek T, Otto B (2016) Design principles for industry 4.0 scenarios. In: 49th Hawaii international conference on system sciences (HICSS). Koloa, HI, pp 3928–3937. <https://doi.org/10.1109/HICSS.2016.488>
21. Gurkaynak G, Yilmaz I, Haksever G (2016) Stifling artificial intelligence: human perils. Comput Law Secur Rep 32(5):749–758. <https://doi.org/10.1016/j.clsr.2016.05.003>
22. Iqbal J, Khan ZH, Khalid A (2017) Prospects of robotics in the food industry. Food Sci Technol 37(2):159–165. <https://doi.org/10.1590/1678-457x.14616>
23. Mogelonsky L (2020) Why Hoteliers should make guestroom IoT a top priority (after COVID safety measures). <https://hoteltechnologynews.com/2020/07/why-hoteliers-should-make-guestroom-iot-a-top-priority-after-covid-safety-measures/>

24. Nadkarni S, Kriechbaumer F, Rothenberger M, Christodoulidou N (2019) The path to the hotel of things: internet of things and big data converging in hospitality. *J Hosp Tour Technol* 11(1):93–107. <https://doi.org/10.1108/JHTT-12-2018-0120>
25. Shamim S, Cang S, Yu H, Li Y (2017) Examining the feasibilities of Industry 4.0 for the hospitality sector with the lens of management practice. *Energies* 10(4). <https://doi.org/10.3390/en10040499>
26. Jarrahi MH (2018) Artificial intelligence and the future of work: human-AI symbiosis in organizational decision making. *Business Horizons*
27. Yao B, Zhou Z, Wang L, Xu W, Yan J, Liu Q (2018) A function block-based cyber-physical production system for physical human-robot interaction. *J Manuf Syst*
28. Pathak P, Pal PR, Shrivastava M, Priyanka O (2019) Fifth revolution: applied AI & human intelligence with cyber-physical systems. *Int J Eng Adv Technol (IJEAT)* 8(3). ISSN: 2249-8958
29. Allam Z, Dey G, Jones DS (2020) Artificial intelligence (AI) provided early detection of the coronavirus (COVID-19) in China and will influence future Urban health policy internationally. *AI* 1(2):156–165
30. Sachsenmeier P (2016) Industry 5.0—the relevance and implications of bionics and synthetic biology. *Engineering* 2(2):225–229
31. Chauhan V, Galwankar S, Arquilla B, Garg M, Di Somma S, El- A, Stawicki SP (2020) Novel coronavirus (COVID-19): leveraging telemedicine to optimise care while minimising exposures and viral transmission. *J Emerg Trauma Shock* 13(1):20
32. Roy S, Menapace W, Oei S, Luijten B, Fini E, Saltori C, Peschiera E (2020) Deep learning for classification and localisation of COVID-19 markers in point-of-care lung ultrasound. *IEEE Trans Med Imaging* 39(8):2676–2687
33. Javaid M, Haleem A (2019) 4D printing applications in the medical field: a brief review. *Clin Epidemiol Glob Health* 7(3):317–321
34. Aslam F, Aimin W, Li M, Ur Rehman K (2020) Innovation in the era of IoT and industry 5.0: absolute innovation management (AIM) framework. *Information* 11(2):124
35. Gorodetsky V, Larukhin V, Skobelev P (2019) Conceptual model of digital platform for enterprises of industry 5.0. In: *International symposium on intelligent and distributed computing*. Springer, Cham, pp 35–40
36. Javaid M, Haleem A (2020) Critical components of Industry 5.0 towards a successful adoption in the field of manufacturing. *J Ind Integr Manag*. <https://doi.org/10.1142/S2424862220500141>
37. Castka P, Searcy C, Fischer S (2020) Technology-enhanced auditing in voluntary sustainability standards: the impact of COVID-19. *Sustainability* 12(11):4740
38. Sachsenmeier P (2016) Industry 5.0—the relevance and implications of bionics and synthetic biology. *Engineering* 2:225–229. <https://doi.org/10.1016/J.ENG.2016.02.015>
39. Javaid M et al, Industry 5.0: potential applications in COVID-19. *J Ind Integr Manag*. <https://doi.org/10.1142/S2424862220500220>

# Systematic Review: Implementation of Product Lifecycle Management in Industries



Harish Vishnu Gunjal and Rajendra M. Belokar

**Abstract** In the era of Industry 4.0, global industries are moving from traditional approach of manufacturing to digitalisation to improve the productivity. To achieve the efficient productivity, best tool observed is product lifecycle management (PLM). PLM is a concept which manage and integrate information related to a product complete lifecycle from design, development, manufacturing, material requirement, vendors, customer feedback, recycle, etc. This paper reviews five case studies—foundry, power transformer, fashion, automotive and aerospace industry who implement PLM, which will answer the three questions—(1) Why PLM implementation is needed in industry? (2) How to implement PLM in industry? (3) What are the benefits of PLM implementation? A generalised overview of PLM implementation procedure is answered. Comparison of conventional technology and PLM technology is explained through changes experienced by five industries. Conclusion provides the benefits to industry after PLM implementation. Future research is needed over the PLM implementation according to Industry 4.0.

**Keywords** PLM · Software · Implementation · SME · Industry 4.0 · Industries

## 1 Introduction

In present scenario, competition between industries increases due to Industry 4.0 all over the globe. In order to increase production capability, the highly competitive manufacturing industry is undergoing a paradigm change towards smart manufacturing through data-based digitalisation [1–3]. Artificial intelligence (AI), big data, cloud computing, and the Internet of Things (IoT), amongst other advances in information technology, have enabled the digitisation of the manufacturing business

---

H. V. Gunjal · R. M. Belokar (✉)

Department of Production and Industrial Engineering, Punjab Engineering College (Deemed to be University), Chandigarh, India  
e-mail: [rmbelokar@pec.edu.in](mailto:rmbelokar@pec.edu.in)

H. V. Gunjal

e-mail: [gunjalharish007@gmail.com](mailto:gunjalharish007@gmail.com)

[4, 5]. A new concept called sustainability arises due to shortage of resources and global warming effects over mother earth, so industries are also trying to produce eco-friendly products or less environmental affected products. Industries are moving from traditional approach to modern approach. Because the traditional approach is not fulfilling the complete demands of customers within time and quantity to stay in competition. This does not mean that industries with traditional approach unable to fight, just they need to update their processes to achieve customer needs and stay in competition. In 2020, rise of pandemic COVID-19 disturbs the processes of manufacturing industries. Many industries which were operating through traditional processes collapsed and industries with modern approach just survived. According to literature review, it is observed that the concept that will help industries to change and upgrade their process to cope up in the global competition is product lifecycle management.

PLM is a concept which manage and integrates all the data of product from its birth to death. Nowadays, as recycling concept is growing rapidly, so concept of PLM changed as, which manage data of product from cradle to cradle. Similar to human lifecycle which has five stages- Birth, growth, maturity, decline and death. The lifecycle of product consists of four stages- Introduction, growth, maturity and decline, shown in Fig. 1. Introduction describes the launch of a product, growth describes its expansion due to rising demand, maturity describes its development in response to client feedback, and decline describes its demise as a result of the entry of new products with improved specifications into the market. The management of all the data related to each stage are managed properly to improve the processes. PLM enables an organisation to cut costs at practically every point of the lifecycle, lowering overall costs and expanding product offers. PLM adoption necessitates significant intra-and inter-organisational changes, as well as changes in processes and culture. Adoption can be either in premises or cloud basis. This encompasses a number of different functional areas. Engineering data management (EDM), product data management (PDM), computer integrated manufacturing (CIM), sales and service, and disposal and recycling, as well as various domains of knowledge or enterprise software systems like materials resource planning (MRP), enterprise resource planning (ERP), customer relationship management (CRM), and supply chain management (SCM) [6].

Data comprises product production procedures, product design, product development, product manufacturing processes, cost, inspection, customer feedback, and amongst other things. All parties (vendors, design engineers, production engineers, etc.) have access to the data. The PLM system coordinates the production process in all product-related information and processes using database technology and an Intranet or Internet network [8]. One should not get confuse with PLM and PLM software; PLM software supports processes within PLM. Examples of PLM modules are product data management (PDM), CAD/CAM, project management, workflow management, production planning, etc. [9] as shown in Fig. 2.

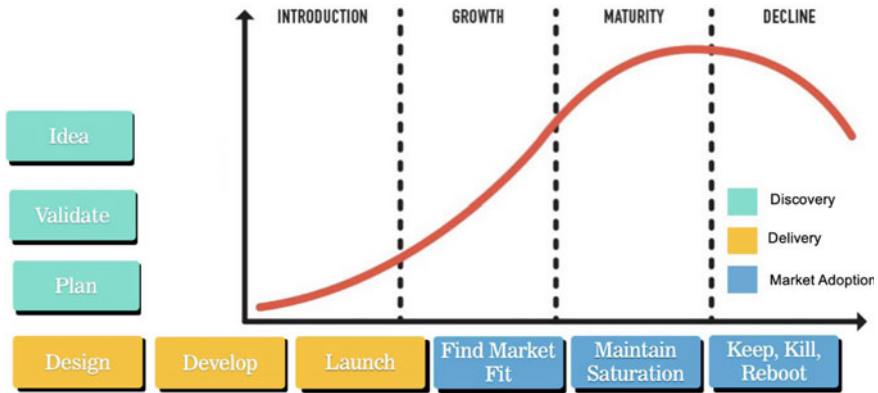
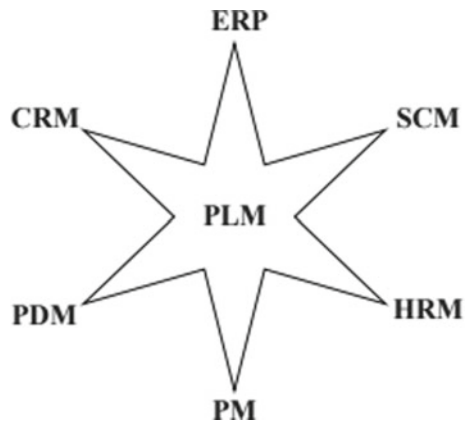


Fig. 1 Stages of product lifecycle [7]

Fig. 2 PLM modules [10]



### 1.1 Historical Development of PLM

Otto Klepper proposed a product lifecycle model in 1931, stating that products should go through three stages: pioneering, competitive, and retentive. Jones, who worked for Booz, Allen and Hamilton in 1957, proposed that most products have a five-stage lifecycle: introduction, growth, maturity, saturation, and decline. PLM was first used in 1985 by American Motors Corporation, which was attempting to speed up the manufacturing of the Jeep Grand Cherokee [<https://www.concurrent-engineering.co.uk>] [11] (Fig. 3).

The origins of PLM may be traced back to the computer-aided design (CAD) tools that first appeared in the manufacturing industry in the 1980s [13]. Product data Management was used to meet the need of disseminating product data (developed through electronic versions) to globally scattered teams and supply chain partners (PDM). Simultaneously, new technology tools for managing and supporting

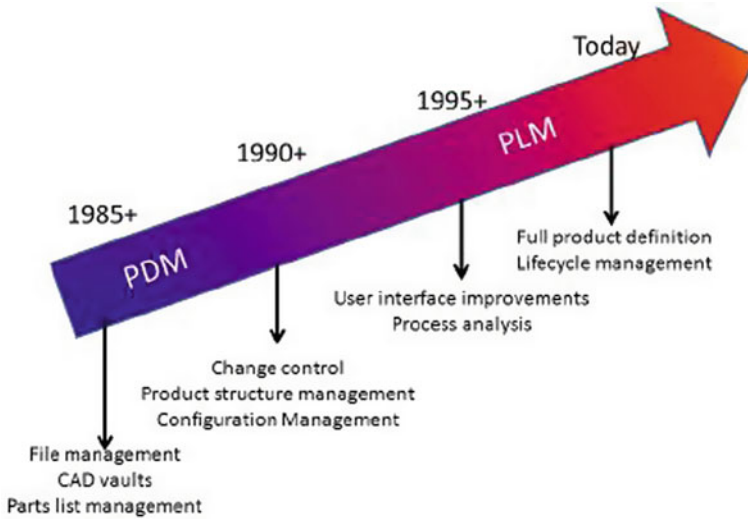


Fig. 3 History of PLM [12]

operations, such as enterprise resource planning (ERP) and customer relationship management (CRM), were launched (CRM). Unlike other software, PLM is based on the notion of knowledge connectedness [13], with PLM systems serving as a foundation for other applications via integration and interfaces. After 2000, a new generation of PLM software emerged, PLM 3.0. PLM 3.0 is a new evolution that puts more of an emphasis on product launches. It has more features throughout the lifecycle, such as requirements management and innovation, and it also has better linkages with downstream productions (processes that occur after the production process like marketing, sales, packaging, shipping, invoicing, etc.). (<https://www.oracle.com/scm/product-lifecycle-management/what-is-plm/>) [14]. After digital transformation, Cloud systems, Industry 4.0 there were modification in PLM due to which PLM 4.0 is formed where new processes and practices will yield a more collaborative effort between design, manufacturing, supply chain and customer.

PLM implementation is based on different strategies which depends on the problems like unable to meet customer demands, lead time, poor inventory control, lack of communication between employees, vendors, suppliers, owners, customer, etc. Different strategies are as follows

- Increased customer involvement
- Customisation of products
- Highest functionality products and services
- Most robust products or services
- Best processes
- Lowest cost competitor
- Value adding life cycle

- Fastest time to market
- Standard product and services
- Widest range of products and services
- Longest life product
- Environmentally friendly product.

The various strategies listed above should be chosen based on the issues facing industry. An example shows that the ideal method to use is “fastest time to market” if any industry wishes to execute operations like information sharing, upgrading of information, simulation, etc. more quickly. This tactic will assist the sector in speeding up the process times and enabling early product availability.

In this paper, five case studies of PLM implementation in **Foundry, a SME of impeller manufacture, a company that produces power transformers, Fashion Industry, Aerospace industry and Automotive Industry** were analyzed. According to study, need of PLM, how to implement PLM and Benefits after PLM implementation has been explained. So, research method has explained in Sect. 2. In Sect. 2.1.1, five case studies are explained—why these industries required the PLM tool and how they implement PLM in respective industries. In addition, generalized and simple framework of PLM adoption has provided. Benefits of PLM implementation in respective industries are explained through results and discussion. In Sect. 3 conclusion of paper and future scope of PLM has explained.

## 2 Methodology

We analyzed five case studies of different domain industries who implement PLM and do systematic literature review to establish a map of PLM implementation process in Industry. To get to know more about challenges in industry during PLM implementation, we studied the papers in references of case studies. After study, we decide to answer three questions in this paper

1. Why there is a need to implement PLM in industry?
2. How to implement PLM in industry?
3. What are the benefits of PLM implementation to industry?

Regarding the procedure to implement PLM tool in industries, generalised framework provided in simple terms, so through understanding it, PLM can be implemented in every industry whether it is SME or multinational. In results and discussion, we decided to compare the conventional technology and PLM technology, after implementing PLM in industry provided in case studies, what changes observed by industries are specified. In conclusion and future scope section, what are the difficulties faced by industries while implementing PLM and gaps in the procedure are explained. What areas should need to improve are discussed in future scope. Selection criteria of papers is as follows in Table 1.

**Table 1** Selection criteria of papers

Searching index	Specific content
Database	Elsevier, Emerald, Journals
Article types	Scientific article
Search string	“Product lifecycle management” or “implementation” or “industries” or “case studies” or “production process” or “framework”
Search period	January 2003 to December 2021
Screening procedure	Case studies are selected of different industries through detailed reading of complete papers, chapters
Classification	Papers selected according to the journals and information presented

## 2.1 *Need and Implementation of PLM*

Many new companies/organisations are forming in the market as a result of the current industrial world and the “Make in India” programme. Everyone is attempting to meet increasing client demands on schedule while still maximising profitability. Many SMEs have been harmed or destroyed as a result of the COVID-19 outbreak. The workload of the design department has increased in recent years, resulting in an added duty of managing information generated and used by designers [8]. Many industries face issues such as worldwide competitiveness, rising labour prices, expanding product complexity, and properly managing a company’s data, to name a few [15]. According to case studies, challenges faced by industries which explain the need of PLM and how they implement PLM in their industry is explained in Table 2.

### 2.1.1 Case Studies

#### 1. Foundry Industry

A small foundry in Belgaum foundry cluster in India, which manufacture impeller casting. It supplies the products to original equipment manufacturers (OEMs) located at 8 km from foundry. PLM has been implemented in OEMs and achieved increase in productivity, improvement in product quality, and speed up delivery. Its supplier foundry still working without PLM.

**Need**—The foundry industry is facing problems to meet the rising customer demands due to market fluctuations, poor inventory control, lack of material availability at the machine, etc. The need for PLM implementation in industry grows as a result.

**Implementation**—According to the problems faced by foundry, they decided to implement PLM strategies

- shorter time to market
- automation
- best process
- minimisation of production cost.



**Table 2** Need and implementation of industries

Industries	Need of PLM	Implementation of PLM
Foundry	<ul style="list-style-type: none"> <li>• Increase in demands</li> <li>• Difficulty to meet 3M resources</li> <li>• Poor control of inventory</li> </ul>	<ul style="list-style-type: none"> <li>• Qualitative assessment of manufacturing activities</li> <li>• Selection of strategies according to need</li> <li>• Use of digital manufacturing</li> <li>• Increase interaction through PLM Teamcenter</li> <li>• User logins created</li> </ul>
Power transformer	<ul style="list-style-type: none"> <li>• Increased frequency of information exchange</li> <li>• Errors in documents and information</li> <li>• Poor management process</li> </ul>	<ul style="list-style-type: none"> <li>• Identification of problems</li> <li>• Steering committee formed with members of all departments</li> <li>• Dividing work in three phases—preparation, test, production</li> <li>• Workshops for understanding of new concept</li> <li>• Selection of proper software solution</li> <li>• Implementation works according to subassemblies to main assemblies</li> </ul>
Aerospace	<ul style="list-style-type: none"> <li>• Less quality of products</li> <li>• innovation</li> <li>• Collaboration within departments</li> <li>• Security of information</li> <li>• More paper work to store information</li> </ul>	<ul style="list-style-type: none"> <li>• Finding strategy depending on problems</li> <li>• Selection of PLM software solution</li> <li>• Collaboration</li> <li>• Documentation</li> <li>• Customisation</li> </ul>
Fashion	<ul style="list-style-type: none"> <li>• Increased demands of customer</li> <li>• Difficult to manage large number of stocks keeping units (SKUs)</li> <li>• Complex supply chains</li> <li>• Communication gaps between customer and company</li> </ul>	<ul style="list-style-type: none"> <li>• Analysis of different process involved in product lifecycle</li> <li>• Splitting in activities</li> <li>• Mapping with business process model and notation (BPMN)</li> <li>• Use of Agile approach</li> <li>• Final testing and training</li> </ul>
Automotive	<ul style="list-style-type: none"> <li>• Missing of product features required for product development</li> <li>• Poor connection between departments</li> <li>• Less efficient project management</li> <li>• Lack of interaction between customer and industry over requirements</li> </ul>	<ul style="list-style-type: none"> <li>• Understanding and mapping customer requirements</li> <li>• Focussed on translating requirements into product feature</li> <li>• Selecting best PLM solutions</li> <li>• Testing and validation</li> <li>• Final handover to production and departments all over the information</li> </ul>

Strategies were decided after planning and discussion with management members of foundry. Qualitative assessment was done on manufacturing of impeller casting. Healthy services and digital manufacturing concept have been introduced. Healthy practices include use of PLM tool (Teamcenter) for timely interaction between users, CAD software, structural analysis and simulation of casting process, evaluation of man–machine hours, online monitoring of resources and accounting. In Teamcenter, user logins were designed to handle duties and ensure proper contact between users and customers. To produce the intricate pattern of casting, digital manufacturing incorporates the use of a rapid prototyping (RP) machine with a fused deposition model (FDM). Part is designed and real-time analysis is performed online using CAD software, by converting CAD file into STL file (which represents a 3D surface to an assembly of planar triangles), RP machine receives the file and pre-processing of part is performed in INSIGHT programme (User-interface of RP machine), and part is fabricate on machine within the time and quantity of material required by software, material used for fabrication—ABS-M30.

## 2. Power Transformer

**Need**—An investigation into the ongoing implementation of PLM in the power transformer manufacturing business. The power transformer business has a long history of using 2D and 3D CAD tools to produce computer models. However, demand has increased over time, resulting in an increase in information flow in the design office and an increase in the workload on the design team. Additional tasks in the administration of documents generated by designers at work must be performed by the designed team. In design and other areas, the frequency of information interchange has been raised. Verification and change in documentation processes are required in such an environment to reduce errors. To address the aforementioned difficulties, management made the strategic choice to install a well-designed and efficient PLM platform.

**Implementation**—Firstly, management formed a team of members from design office, company’s IT department, Planning and organisation department, software vendor, university, etc. Team responsibility is to perform the PLM implementation properly according to planning. Team divides there work into three phases—

1. Preparation
2. Testing
3. Production phase.

In the preparation stage, PLM software supporting the industry-available CAD software was chosen (for example-Windchill PLM software solution is supported to the creo software). A number of workshops were held in the sector to help employees in understanding the PLM system. In order to continuously test the PLM tool on routine activities to guarantee that the process was operating properly, a small group of designers was assembled throughout the testing phase. In the production phase, component production has begun in accordance with the flow of the part modules—core, tank, and receiver.

### 3. Aerospace Industry

**Need**—After studying various articles and papers, it has found that in three main areas PLM is needed are

- To secure the product information and compliance of information technology
- Maintaining the product information and definition throughout its lifecycle
- Business process management and work with a different type of data and sharing.

Improvement needed in engineering approach due to traditional approach which results in lot of negative impacts, lack of information sharing, less productive environment, zero collaboration, and lack of communication.

**Implementation**—Study and planning has been done to identify the problems and, on that basis, strategies selected to improve the areas of industries

- Time to market
- Managing risks and reducing development cost
- Security.

Collaboration is an Internet-based computational architecture that allows departments or geographically based regions to share information and data throughout the product lifecycle in order to make better decisions in a collaborative setting. The design phase is the most important in the aerospace industry. Data is exchanged, and product information is allocated using [standard for sharing of product model data (STEP)]. To preserve data security, only critical people are allowed access to aerospace data through PLM implementation. Documentation is done with the help of software such as MS Office, which eliminates the need for paper. The following are three types of software services offered to clients in order to improve customer interaction.

- The industry as a service (IaaS)
- Platform as a service (PaaS)
- Software as a service (SaaS).

Customisation needed to modify the PLM solution according to increase in workload over staff of respective departments.

### 4. Fashion Industry

**Need**—In recent years, fashion industries have observed wide transformation in some cases

1. Due to increase in demand at faster rate, life of product getting shorter.
2. Fashion industries have managed a very large number of stocks keeping units (SKUs) due to combinatorial explosion of variants.
3. The supply chain networks become highly complex due outsourcing non-core activities by industries in global scenario.
4. Need of more efficient processes, eliminating activities without added value.

**Implementation**—Framework proposed for effective implementation of PLM in fashion industry based on four phases

1. Identification of business issues and needs
2. Model process and data
3. Identification of PLM business objects
4. Scenario analysis to select PLM solution, with detailed implementation and tests need before actual work.

In supply chains macro-process includes—design, prototyping, sampling and engineering, sourcing, production and order and retail. Interviews provide the needs related to each activity which helps to map the user's needs. Business process model and notation (BPMN) standard used to carry out first stage. In second stage, quality function deployment approach tool is used to identify main PLM functionalities that meet the customer needs. In third stage, PLM detailed designed which provides review and validation of deployment, implementation includes functions release by sprint were get approved and processes further for testing phase. In final stage, final test and training-key users conduct an integration and system test.

#### 5. **Automotive Industry**

A study was performed on automotive industry having employees more than 2500 and very active in developing new products.

**Need**—The industry now functions in a semi-automated mode, in which particular programmes are utilised to optimise processes, such as CAD for design and CAPP for process planning, but information flow across departments is not automated. During the research, it was discovered that data for the development of needed product features was absent. As a result, a platform is necessary to construct and validate information flow from beginning to finish, allowing the industry to not only solve current issues but also to build more efficient systems for providing the proper product.

**Implementation**—To understand the implementation of PLM in industry, first investigation of the different departments (marketing and application engineering, product design, process engineering, programme management, and production engineering) performed. A theoretical framework for PLM implementation was designed with five phases

1. Requirement management—understanding and mapping customer requirements
2. Collaboration—Focussed on translating requirement into product features
3. Integration—Selecting best process for manufacturing
4. Efficiency—Validating process and production steps
5. Knowledge management—Final handover to production with all necessary information.

Architectural framework proposed

1. Leverage data exchange technology—This system deal with various types of data formats and reports to be available for design and analysis purposes.
2. Utilise workflow capabilities—Define the sequence of activities to completely automate the business processes.

### 2.1.2 Software Solution

PLM as a concept is managing all the products data from its introduction to decline, which is accompanied with the help of installation the PLM software. It observed that there is need to have CAD software when industry install PLM software, because to define the specification and make documentation of product its model is required which is build on CAD software. It will be easy to work when both CAD software and PLM software are taken from same vendors, like NX CAD and Teamcenter are of Siemens. PLM software provides user all the data including parts, subassemblies of parts, bill of materials, production process involved in product life, documents regarding product, customer requirements, etc., at one place, which make users to find any data at any time.

Because it provides a digital basis and enterprise product record for a holistic product development and supply chain strategy, modern PLM software is fast rising and becoming increasingly vital for company transformation. When industry processes are matched with the latest PLM software on a single platform, it unifies the product value chain with integrated business planning and supply chain execution, allowing for faster innovations and better product design, manufacturing, maintenance, and support [14] (Table 3).

In five case studies, industries used PLM software as follows (Table 4).

**Table 3** List of vendors of PLM software and application to industries

PLM software	Vendor	Industries
Accolade	Sopheon	SME
Agile advantage	Oracle/Agile	SME
Aras innovator	Aras Corp	SME
Arena PLM	Arena Solutions	SME
Enovia Matrix One	Dassault Systems	Medium-large
Enovia SmarTeam	Dassault Systems	SME
BPMplus	Ingennus	SME
ProductCenter	SofTech	SME
SAP PLM	SAP	Medium-large
TeamcenterEngg	Siemens PLM	Medium-large
TeamcenterExpress	Siemens PLM	SME
Think PLM	Think3	SME
Windchill	PTC	Medium-large
Windchill On-Demand	PTC	SME

**Table 4** List of PLM software and vendors of Industries

Industry	PLM software	Vendors
Foundry	Teamcenter	Siemens
Power transformer	Windchill	PTC
Aerospace	Arena PLM	Arena Solutions
Fashion	Agile advantage	Oracle/Agile
Automotive	Think PLM	Think 3

## 2.2 Generalised Procedure of PLM Implementation

PLM implementation in any industry is difficult and complex process. It requires both time and money to be invest while implementing. But, the advantages observed after implementing PLM were recover three to four times of money invested. According to case studies, we decided to provide a generalised map of PLM implementation in large and SMEs industries. It will provide basic idea, how to implement PLM in any industries/organisation. Implementation of PLM provided is a simple form which helps user to understand easily and can be implemented in any industry. It is observed that complete implementation of PLM in industry will be costlier process, so for SMEs it will not be affordable. SMEs can implement some part of PLM in major departments for improvement in certain areas of product lifecycle. There will be four stages of PLM implementation.

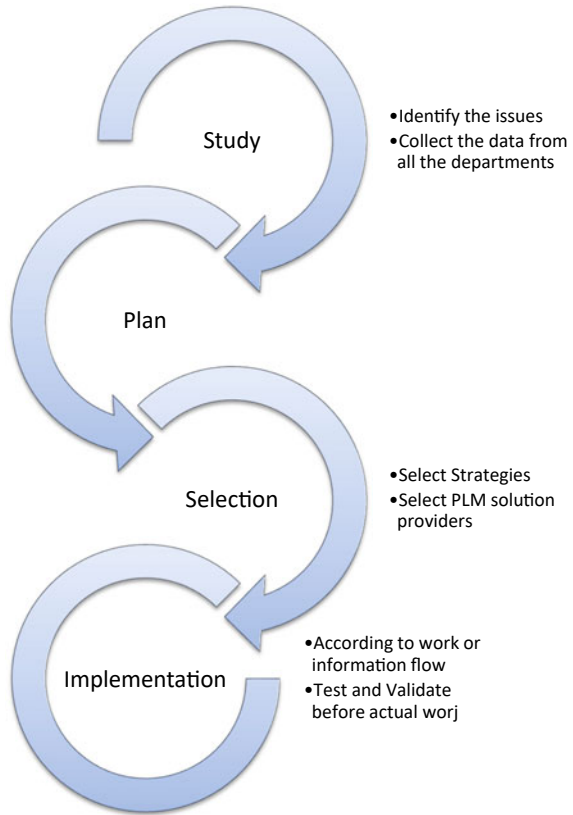
### 2.2.1 Study

Assign a project team with specialised members of all departments in industry. Identify the gaps in process flow of industries, problems and challenges facing in industries, what type of failures and reasons behind failures. Collect all the information regarding size of data internal and external to company that we have to integrate in PLM. Data includes the hard documents, CAD designs, Bill of material, product information, manufacturing processes, etc. Study of all these factors will help to define goals of PLM implementation. Must do detailed analysis of production processes involved in product lifecycle. Identify the customer needs and evaluate market demands. SMEs should select the areas properly because PLM process is costly and time-consuming. So, step by step upgradation within industry should be done (Fig. 4).

### 2.2.2 Plan

Define the goals according to the collected data. Make a flowchart of how should the data or information flow within the company. Knowledge of PLM system should be provided to employees through workshop. Through workshop target particular

**Fig. 4** Overview of PLM implementation process



groups within company to gather information about processes and workplaces [9] (for large enterprises). There are number of strategies of PLM can adopted by SMEs such as customisation of product, highest functionality products and services, value adding life cycle, lowest cost competitor, and fastest time to market [8]. Well, these strategies depend on market situation and available resources. For example, fastest time to market requires immediate commencement of projects, sharing of information, simulation rather than trial and error and reusing for continuous improvement [15].

### 2.2.3 Selection

In market, there are many PLM software vendors available. The purpose of PLM software vendors is to transform all the information related to product lifecycle into tangible or virtual knowledge [15]. PLM software selection can be done through presently in use CAD software vendors such as Creo CAD—Windchill PLM of PTC, NX CAD—Teamcenter PLM of Siemens and through identification of their

needs (if someone don't know how to identify needs, then assessing to PLM solutions is good way to select PLM software).

#### **2.2.4 Implementation**

The implementation of PLM should be done in accordance with the product building modules. Product modules in the power transformer industry, for example, are core, tank, equipment, cover, and conservator [8]. Implementation can also be done according to the flow of information within company. All the data gathered by groups and individuals should cater into PLM software. Install the software in company. But, after installing, user feedback is necessary. To maintain the security of data and designs of product, user login credentials must be generated.

Testing and validation required on regular daily basis before hand overing the PLM system to the industry users. Training and workshops should be arranged to provide the information and knowledge to industry users for proper functioning of process.

### ***2.3 Results and Discussion for Benefits of PLM***

According to the literature and case studies, we find out the benefits of PLM implementation. In the need, we specify the challenges face by industries before PLM implementation in SMEs and large enterprises. During implementation, industries face difficulties of load of work over employees, time and money consumption, but after implementing they observed very good results. Table 5 defines the benefits of PLM implementation from the case studies and advantages of PLM technology over conventional technology.

Implementation of PLM provided enormous benefits to industry, and the cost of installation is very high. Overview of generalised procedure to be follow during PLM implementation is provided. Studies shown that during implementation, customisation is required such as in power transformer industry scripts have to create to read the product number in drawing by Creo, when information is transfer between Windchill and Creo. These customisations increase the cost of implementation, so special care should take to avoid customisation or replace it with new solution. It is advisable to SMEs strategies discussed in plan should follow during PLM implementation. Special care should be taken if PLM solution is based on the wed and open-source technologies because frequent changes in web technologies may affect the performance of PLM software. PLM implementation achieved paper free usage which helps industries to as sustainable development by reducing cutting of trees required for paper.



**Table 5** Benefits and comparison of conventional and PLM technology

Industry and characteristics	Conventional technology	PLM technology
<i>Foundry</i>		
• Reduction in lead time	– 4 h to place the order in person	– 10 min to place order through mail
• Easy generation of model	– 5 h 2D drawing in paper	– 1 h using CAD tool in PLM
• Proper utilisation of organisational resources	– 4 h to define a project and discussion	– Through online discussion
• Structural analysis and check	– Time required based on experience	– Using analysis tool within PLM
• Improved quality	– Good	– Very good
<i>Power transformer</i>		
• Reduction in design cycle time	– Take more time	– Reduced by 40%
• Increase in overall product quality	– More number of design errors	– Less design errors
<i>Aerospace industry</i>		
• Collaboration between departments	– Less communication	– Improve communication
• Amount of paperwork	– Too much	– Make paper free with digital tools
• Security	– Chances of data leakage	– Highly secured data within the industry
<i>Fashion industry</i>		
• Easy to reuse designs	– Designs on paper difficult to find	– Designs in PLM are easily accessible at any time
• Decrease Communication gap	– Data has to shared separately to vendors, employees, managers	– Data is accessible to everyone
• Data security	– Less safe	– Everyone has provided login and password
<i>Automotive industry</i>		
• Automation	– Semi automated	– Complete automated
• Product features for product development	– Missing	– Easily available
• Use of designs	– Difficult to search for reuse	– Easily available

### 3 Conclusion

On the basis of literature and case studies analysis we conclude that, PLM implementation will provide benefits to the industry which are working on conventional technologies. PLM helps industries to compete in global market, improve product

quality, and meet customer demands on time. Most important benefit of PLM implementation in the era in which sustainability and recycling of product is old designs are easily accessible to everyone and easy to modify. It also reduces the paper work, which reduces cutting of trees. PLM implementation can be done in every department from design of product to dispatching to the customer. To implement PLM in SMEs, case study of foundry is good reference. Due to Industrial fourth revolution or Industry 4.0, need of PLM implementation has been increased. Generalised framework has been provided so that SMEs as well as multinational companies in either manufacturing sector or services sector can follow the steps which are explained.

But, there some gaps identified during the study

1. Adopting PLM in industry is very complex process. It consumes time as well as money.
2. Common people don't know the PLM, hence while implementing PLM there is a need of train the PLM to the workers of industry.
3. Due to Industry 4.0, global industries are moving towards digitalisation to stay in competition and in PLM paper are replaced by online documents, manual work is replaced by automation, which arises new problem of unemployment at the worker's stage.
4. Complete adoption of PLM for small scale industries will be costly process.

As observed benefits of PLM implementation, which helps industries to stay in competition in the situations like COVID-19 pandemic, future demands will be going to increase the PLM implementation. PLM implementation can never be complete in any industries, it is ongoing process with customisation of services. In this paper, only focused is on implementing PLM manufacturing industry, there is a need to have study in services provider industry.

**Acknowledgements** We thank to Siemen Centre at Punjab Engineering College, Chandigarh to provide practical experience of PLM software-Teamcenter.

## References

1. Papetti A, Gregori F, Pandolfi M, Peruzzini M, Germani M (2020) A method to improve workers' well-being toward human-centered connected factories. *J Comput Design Eng* 7(5):630–643
2. Uhlemann THJ, Schock C, Lehmann C, Freiburger S, Steinhilper R (2017) The digital twin: demonstrating the potential of real time data acquisition in production systems. *Proc Manuf* 9:113–120
3. Scafa M, Marconi M, Germani M (2020) A critical review of symbiosis approaches in the context of Industry 4.0. *J Comput Design Eng* 7(3):269–278
4. Qi Q, Tao F (2018) Digital twin and big data towards smart manufacturing and Industry 4.0: 360-degree comparison. *IEEE Access* 6:3585–3593
5. Tao F, Qi Q (2017) New IT driven service-oriented smart manufacturing: framework and characteristics. *IEEE Trans Syst Man Cybern Syst* 49(1):81–91

6. Abramovici M (2007) Future trends in product lifecycle management (PLM). In: The future of product development. Springer, Berlin, Heidelberg, pp 665–674
7. <https://productcoalition.com/product-lifecycle-and-the-product-management-process-f7447943981d>
8. Bojcetic N, Salopek D, Marjanovic D (2015) PLM implementation: case study. In: International conference on engineering design, ICED15
9. Koomen B (2018) PLM in SME, what are we missing? An alternative view on PLM implementation for SME. IFIP Int Fed Inform Process IFIP AICT 540:681–691
10. Kulkarni K, Kulkarni VN, Gaitonde VN, Kotturshettar BB (2021) State of the art review on implementation of product lifecycle management in manufacturing and service industries. AIP Conf Proc 2316:030012
11. <https://www.concurrent-engineering.co.uk/Blog/bid/100180/A-Brief-History-of-Product-Lifecycle-Management>
12. [https://www.researchgate.net/figure/Misleading-development-from-PDM-to-PLM-4\\_fig5\\_261142355](https://www.researchgate.net/figure/Misleading-development-from-PDM-to-PLM-4_fig5_261142355)
13. Jo C (2019) From PLM 1.0 to PLM 2.0: the evolving role of product lifecycle management (PLM) in the textile and apparel industries. J Fashion Mark Manag An Int J 1361–2026
14. <https://www.oracle.com/scm/product-lifecycle-management/what-is-plm/>
15. Patil R, Mohan Kumar S, Abhilash E (2012) Tools and strategies for product life cycle management—a case study in foundry. Int J Adv Res Technol 1(3). ISSN 2278-7763

# Optimal Assembly Sequence Planning with Single-Stage Multiple-Component Feasibility: Industry 4.0 Perspective



Chiranjibi Champatiray, M. V. A. Raju Bahubalendruni, I. Anil Kumar, R. N. Mahapatra, Debasisha Mishra, and B. B. Biswal

**Abstract** The recent advances in manufacturing technologies give product design engineers the flexibility to model complex and intricate geometries, reducing the part count. It's easier to assemble and less expensive when a product's parts count is reduced, but creating a feasible assembly sequence for a revised product with different topologies requires careful consideration of many heuristics and attributes during the manufacturing process. This research proposed a novel assembly sequence planning (ASP) method for a given product, rapidly generating the feasible plan with minimum assembly levels. This method considers the possibility of assembling multiple parts at a single stage through various feasible directions, which promises reduced assembly time. The proposed method is tested on a fictitious product, and the solution is found to be more efficient than that obtained by current prominent methods.

**Keywords** Assembly sequence planning (ASP) · Maximum liaison count · Multi-component feasibility · Multi-stage

## 1 Introduction

With advanced communication technologies for manufacturing applications, Industry 4.0 promotes automation and collaborative working culture [21]. Companies in the product manufacturing industries compete with one another to get their product into the market as quickly as possible. With the use of an appropriate assembly

---

C. Champatiray (✉) · R. N. Mahapatra · B. B. Biswal  
Department of Mechanical Engineering, National Institute of Technology Meghalaya, Shillong, Meghalaya, India  
e-mail: [chiranjibi@nitm.ac.in](mailto:chiranjibi@nitm.ac.in)

M. V. A. Raju Bahubalendruni · I. Anil Kumar  
Department of Mechanical Engineering, National Institute of Technology Puducherry, Puducherry, India

D. Mishra  
Department of Strategic Management, Indian Institute of Management Shillong, Shillong, Meghalaya, India

© The Author(s), under exclusive license to Springer Nature Singapore Pte Ltd. 2023  
R. P. Singh et al. (eds.), *Advances in Modelling and Optimization of Manufacturing and Industrial Systems*, Lecture Notes in Mechanical Engineering,  
[https://doi.org/10.1007/978-981-19-6107-6\\_20](https://doi.org/10.1007/978-981-19-6107-6_20)

281

sequence, there is significant potential for time and cost savings during the assembly sequence [9, 10]. A large number of computational complexities and assembly heuristic considerations are involved in determining a feasible assembly sequence for a new product configuration [7, 18]. Several assemblies impose constraints on the data that must be considered in order to ensure that an assembly sequence is practical [4, 10–13]. The assembly constraints data provides information about the surface contact between the mating parts in the assembled state of the product and the geometrical feasibility of an assembly operation in a specified direction [6, 16, 22]. Several researchers have developed computer-aided methods to extract the assembly surface contacts through application program interfaces by performing the contact analysis [4, 6]. The Geometrical feasibility of appending a part to its assembled product in the presence of other primary parts can be verified through assembly interference relations with part moments; computer-aided programs have already been proposed to extract such relations along principal orthogonal axes and oblique orientations [6, 16, 28]. Stability is one assembly valuable attribute for finding possible sub-assemblies [7]. Several researchers tried to find out feasible assembly sequences using the assembly constraints with the help of computational methods with assembly heuristics [1, 14, 15, 27]. These methods are highly time-consuming and cannot be implemented for large products with a more significant number of parts [2, 3, 19, 26]. These methods can often find a feasible solution rather than an optimal solution [27, 29–31]. Searching techniques and optimization algorithms are so helpful in finding an optimal assembly sequence from a vast set of initial assembly space. Teaching learning-based optimization (TLBO), advanced immune optimization (AIO), simulated annealing optimization (SAO), and particle swarm optimization (PSO) algorithms are effective in finding an optimal feasible assembly sequence for a given product. However, the computational time was high for larger products [12, 13, 17, 20, 24]. Few researchers try parallel ASP to find stable sub-assemblies during the ASP [5, 14, 23].

However, the preceding methods take into account one component at a single-stage assembly operation in a specific direction and consume a significant amount of assembly time. To address the issues, a single-stage multi-component assembly (SSMCA) in multiple feasible directions has been proposed.

## 2 Research Methods

A list of valid assumptions is considered in the current ASP approach for simplification.

1. All the components in the product are rigid; no change in size and shape is permitted during the assembly operation.
2. The stability of the component in the assembly is not considered.
3. The connectors (nuts and bolts, pins, and screws) are considered primary parts.

4. The assembly process is considered the reverse of disassembly sequence planning to ease the geometrical feasibility testing.

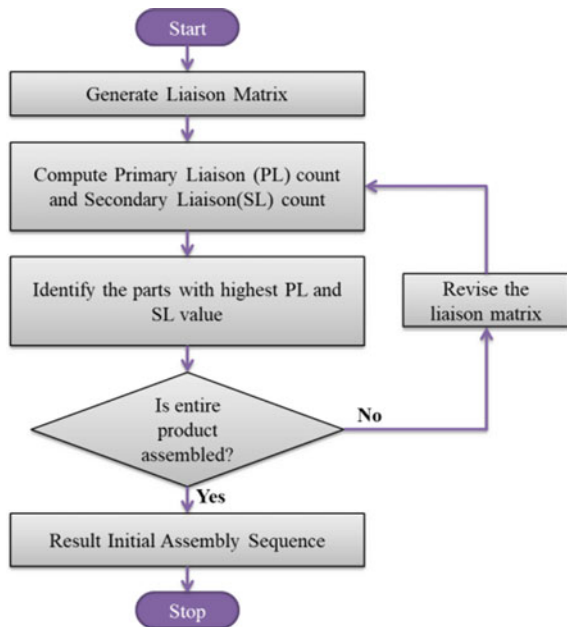
### 2.1 Initial Assembly Sequence Planning

The proposed method is divided into two phases. First, the product’s liaison information is used to determine the most interior part of being placed based on the concept of maximum liaison count. Second, once a part is assembled, the corresponding row and columns are deleted to create an updated liaison matrix based on the concept of geometric feasibility. The process is repeated till all the parts in the product are assembled. Figure 1 depicts a detailed procedure for generating the initial assembly sequence (IAS) plan. The proposed method is demonstrated by a 7-part hypothetic assembly model, as shown in Fig. 2.

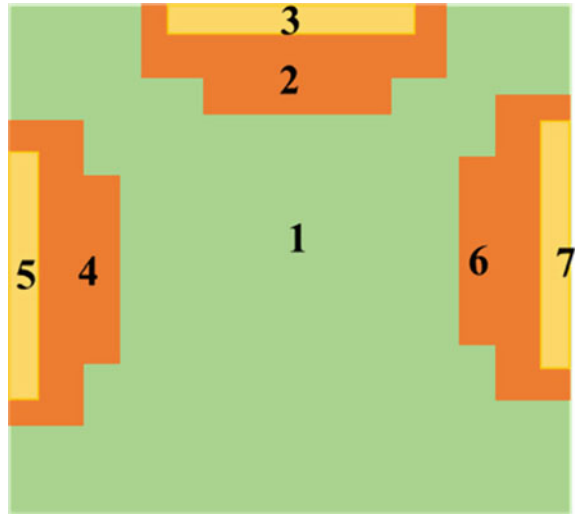
Table 1 shows the liaison matrix for the product, which includes the primary liaison (PL) count and secondary liaison (SL) count. Equations (1) and (2) can be used to calculate the PL and SL counts.

$$PL(i) = \sum_{j=1}^n l(i, j) \tag{1}$$

**Fig. 1** Initial assembly sequence (IAS) plan generation method



**Fig. 2** An assembled product for implementation



**Table 1** 1st level configurations with PL and SL values

	1	2	3	4	5	6	7	PL	SL
1	0	1	0	1	0	1	0	3	6
2	1	0	1	0	0	0	0	2	4
3	0	1	0	0	0	0	0	1	2
4	1	0	0	0	1	0	0	2	4
5	0	0	0	1	0	0	0	1	2
6	1	0	0	0	0	0	1	2	4
7	0	0	0	0	0	1	0	1	2

$$SL(i) = \sum_{j=1}^n \sum_{k=1}^n l(j, k) \quad l(i, j) = 1 \tag{2}$$

**2.1.1 Procedure to Generate Initial Assembly Sequence**

The IAS is generated using the maximum liaison count concept, which means that the part with the highest PL or SL value is chosen first. From Table 1, it can be seen that part 1 has the maximum PL value, and it has maximum liaisons with other parts of the assembly so that it can be identified as the base part or starting position of the IAS. To obtain the updated liaison matrix in IAS, the corresponding row and column of part 1 are removed. The next position in the IAS after position 1 (part-1) could be

**Table 2** 2nd level configurations with PL and SL values

	2	3	4	5	6	7	PL	SL
2	0	1	0	0	0	0	1	1
3	1	0	0	0	0	0	1	1
4	0	0	0	1	0	0	1	1
5	0	0	1	0	0	0	1	1
6	0	0	0	0	0	1	1	1
7	0	0	0	0	1	0	1	1

2 or 3 or 4 or 5 or 6 or 7, so the 2nd position in the IAS can be determined using the maximum liaison count (PL and SL) concept.

Table 2 shows the updated liaison matrix with PL and SL values, where part-2, 3, 4, 5, 6, and 7 have the same PL values and must be compared to their respective SL values and the respective SL values are the same as well. The first part needs to be selected in this scenario, i.e., part-2 is selected as the IAS’s second position.

Similarly, the next positions of IAS can be determined by using the preceding procedure, the IAS can be deduced as 1–2–4–6–3–5–7. The initial assembly sequence is further sent for sequence edition based on the geometric feasibility.

### 2.2 Sequence Editing for Geometric Feasibility

Geometric feasibility describes the possibility of appending a part in the presence of other parts in a specific direction. Suppose a part-*i* can be assembled in the presence of part-*j* in a specific direction, then part-*i* is feasible to disassemble from the assembled state in the opposite direction. Numerous methods exist for generating a geometric feasibility matrix for a given product. These methods typically involve assembly snapping and contact analysis between the parts [6, 8, 25, 28].

The IAS was validated in this section through the use of a sequence editing technique. Figure 3 depicts a flowchart of the procedure for editing sequences for geometric feasibility. The following steps provide more information on the procedure.

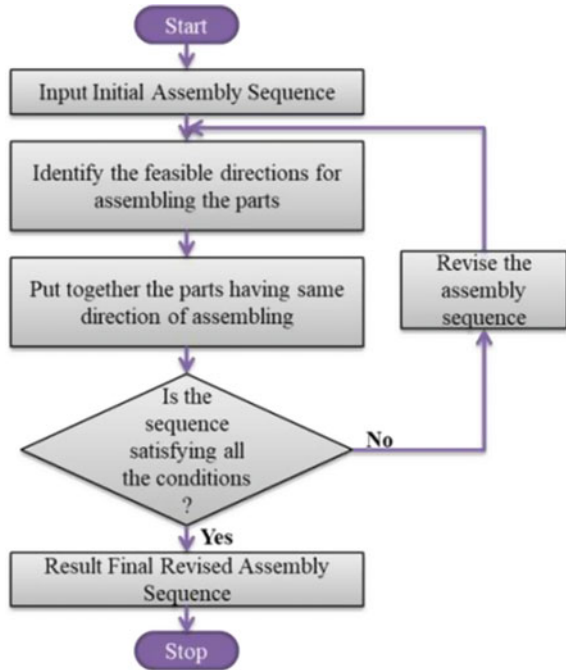
Step 1:

The preliminary sequence is 1–2–4–6–3–5–7, as 1 is the base part; the other parts will be assembled after part-1. The geometrical feasibility must be considered to arrive at the following feasible positions.

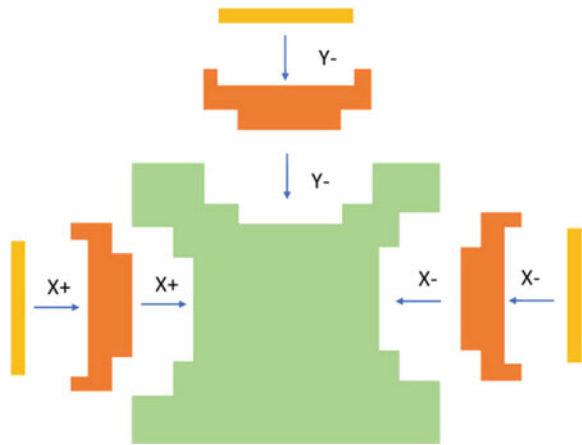
Figure 4 shows the parts and their feasible assembly direction that helps revise the IAS. As shown in Table 3, part-2, 4, 6, 3, 5, 7 can be assembled in the –*Y*, +*X*, –*X*, –*Y*, +*X*, and –*X*-direction, respectively. As a result, the positions of parts 4 and 3 are swapped to make the sequence more geometrically feasible, and then the sequence is revised to 1–2–3–6–4–5–7.



**Fig. 3** Flow diagram of the sequence editing method



**Fig. 4** Exploded view of the assembly model with feasible directions



**Table 3** Parts and their feasible directions

Parts	2	4	6	3	5	7
Directions	-Y	+X	-X	-Y	+X	-X

**Table 4** IAS and FAS representation

IAS	1-2-4-6-3-5-7
FAS	1-2-3-4-5-6-7

**Step 2:**

The input sequence for this step is 1-2-3-6-4-5-7. Because positions 2 and 3 have the same direction, the sequence correction begins at entry position 5. Position 4 (part-6) can be assembled in the -X direction (refer Table 3) and part-4 in +X direction. So, positions 5 and 7 need to be interchanged, and write the corrected sequence as 1-2-3-6-7-5-4.

**Step 3:**

The input of this step is 1-2-3-6-7-5-4, and from the sequence editing concept, the revised sequence can be written as 1-2-3-6-7-4-5 by interchanging positions 6 and 7.

Following the proposed sequence editing rule, the final assembly sequence (FAS) can be written as 1-2-3-6-7-4-5 for simplicity, interchanging between part-4 and part-6, part-5, and part-7 can be done, and rewriting the FAS as 1-2-3-4-5-6-7.

Table 4 shows how the IAS got revised after implementing the sequence editing rule and how geometric feasibility influences the IAS.

### 3 Results and Discussions

The applicability of the proposed model is verified by a hypothetical product depicted in Fig. 2. And, a feasible assembly sequence is generated. Recent methods were thoroughly examined and compared to the proposed method. The obtained results and comparative assessment are shown in Table 5.

According to Table 5, the concatenation method has 6 assembly levels, and the sub-assembly identification method has 4 assembly levels. So, it is evident that the proposed method can generate a feasible assembly sequence with a minimum number of assembly levels (two numbers) by considering multiple parts/subassemblies at a single stage along with multiple directions.

### 4 Conclusion

This article aims to generate an optimal assembly sequence using a novel SSMCA approach that offers parallel assembly operations to speed up the process by reducing the number of assembly levels and comparing the results to current methods.

**Table 5** Comparative assessment

Method adopted/reference	Assembly sequence with geometric feasibility							No. of assembly levels
Concatenation method [3]	1←	2←	4←	6←	3←	5←	7	6
		Y−	X+	X−	Y−	X+	X−	
		L <sub>1</sub>	L <sub>2</sub>	L <sub>3</sub>	L <sub>4</sub>	L <sub>5</sub>	L <sub>6</sub>	
Sub-assembly identification method [19]	1←		(2-3)←		(4-5)←		(6-7)	4
			Y−		X+		X−	
			L <sub>2</sub>		L <sub>3</sub>		L <sub>4</sub>	
	*L <sub>1</sub> for sub-assembly generation							
Proposed method			1←	Y−	2←	3		2
				X+	4←	5		
				X−	6←	7		
			L <sub>2</sub>		L <sub>1</sub>			

The procedure is presented on a hypothetical model, which can be extended to more extensive products with large parts to test the application in real-life industrial problems in an automated way.

### References

1. Abbas A, Maire F, Shirazi S, Dayoub F, Eich M (2018) A dynamic planner for object assembly tasks based on learning the spatial relationships of its parts from a single demonstration. In: Australasian joint conference on artificial intelligence, pp 759–765
2. Bahubalendruni MR, Biswal BB (2016) A review on assembly sequence generation and its automation. Proc Inst Mech Eng C J Mech Eng Sci 230(5):824–838
3. Bahubalendruni MR, Biswal BB (2017) A novel concatenation method for generating optimal robotic assembly sequences. Proc Inst Mech Eng C J Mech Eng Sci 231(10):1966–1977
4. Bahubalendruni MVAR, Biswal BB, Deepak BBVL (2017) Computer aided assembly attributes retrieval methods for automated assembly sequence generation. World Acad Sci Eng Technol Int J Mech Aerosp Ind Mechatron Manuf Eng 11(4):759–767
5. Bahubalendruni MR (2018) An efficient method for exploded view generation through assembly coherence data and precedence relations. World J Eng 15(2):248–253
6. Bahubalendruni MVA, Biswal BB (2014) An algorithm to test feasibility predicate for robotic assemblies. Trends Mech Eng Technol 4(2):11–16
7. Bahubalendruni MV, Biswal BB (2016) Computer aid for stability testing between parts towards automatic assembly sequence generation. J Comput Technol Appl 7(1):22–26
8. Bahubalendruni MR, Biswal BB (2014) Computer aid for automatic liaisons extraction from cad based robotic assembly. In: 2014 IEEE 8th international conference on intelligent systems and control (ISCO), pp 42–45
9. Bahubalendruni MR, Biswal BB, Upadhyaya V (2014) Assembly sequence generation and automation. In: International conference on design, manufacturing and mechatronics, vol 2014, pp 185–192

10. Bahubalendruni MVA, Biswal BB, Khanolkar GR (2015) A review on graphical assembly sequence representation methods and their advancements. *J Mechatron Autom* 1(2):16–26
11. Bahubalendruni MR, Biswal BB, Kumar M, Nayak R (2015) Influence of assembly predicate consideration on optimal assembly sequence generation. *Assem Autom* 35(4):309–316
12. Bahubalendruni MR, Biswal BB, Kumar M, Deepak BBVL (2016) A note on mechanical feasibility predicate for robotic assembly sequence generation. In: *CAD/CAM, robotics and factories of the future*, pp 397–404
13. Bahubalendruni MR, Deepak BBVL, Biswal BB (2016) An advanced immune based strategy to obtain an optimal feasible assembly sequence. *Assem Autom* 36(2):127–137
14. Bahubalendruni MR, Gulivindala AK, Varupala SP, Palavalasa DK (2019) Optimal assembly sequence generation through computational approach. *Sādhanā* 44(8):1–9
15. Bahubalendruni MR, Sudhakar U, Lakshmi KV (2019) Subassembly detection and optimal assembly sequence generation through elephant search algorithm. *Int J Math Eng Manag Sci* 4(4):998–1007
16. Bahubalendruni MVA, Biswal BB, BB, V. (2015) Optimal robotic assembly sequence generation using particle swarm optimization. *J Autom Control Eng* 4(2):89–95
17. Murali GB, Deepak BBVL, Bahubalendruni MR, Biswal BB (2017) Optimal assembly sequence planning towards design for assembly using simulated annealing technique. In: *International conference on research into design*, pp 397–407
18. Deepak BBVL, Bala Murali G, Bahubalendruni MR, Biswal BB (2019) Assembly sequence planning using soft computing methods: a review. *Proc Inst Mech Eng Part E J Process Mech Eng* 233(3):653–683
19. Gulivindala AK, Bahubalendruni MR, Varupala SVP, Sankaranarayananasamy K (2020) A heuristic method with a novel stability concept to perform parallel assembly sequence planning by subassembly detection. *Assem Autom* 40(5):779–787
20. Gunji AB, Deepak BBBVL, Bahubalendruni CR, Biswal DBB (2018) An optimal robotic assembly sequence planning by assembly subsets detection method using teaching learning-based optimization algorithm. *IEEE Trans Autom Sci Eng* 15(3):1369–1385
21. Inkulu AK, Bahubalendruni MR, Dara A, Sankaranarayana Samy K (2021) Challenges and opportunities in human robot collaboration context of Industry 4.0-a state of the art review. In: *Industrial Robot: the international journal of robotics research and application*
22. Kumar GA, Bahubalendruni MR, Prasad VV, Ashok D, Sankaranarayanasamy K (2021) A novel geometric feasibility method to perform assembly sequence planning through oblique orientations. *Eng Sci Technol Int J*
23. Murali GB, Deepak BBVL, Raju MVA, Biswal BB (2019) Optimal robotic assembly sequence planning using stability graph through stable assembly subset identification. *Proc Inst Mech Eng C J Mech Eng Sci* 233(15):5410–5430
24. Nayak R, Bahubalendruni MR, Biswal BB, Kumar M (2015) Comparison of liaison concatenation method with simulated annealing for assembly sequence generation problems. In: *2015 1st international conference on next generation computing technologies (NGCT)*, pp 531–535
25. Bahubalendruni MR, Biswal BB (2015) An intelligent method to test feasibility predicate for robotic assembly sequence generation. In: *Intelligent computing, communication and devices*, pp 277–283
26. Bahubalendruni MR, Biswal BB (2016) Liaison concatenation—a method to obtain feasible assembly sequences from 3D-CAD product. *Sadhana* 41(1):67–74
27. Tariqi K, Kiyokawa T, Nagatani T, Takamatsu J, Ogasawara T (2021) Generating complex assembly sequences from 3D CAD models considering insertion relations. *Adv Robot* 35(6):337–348
28. Varupala SSV, Gulivindala AK, Bahubalendruni MVAR (2021) An efficient geometrical feasibility testing method for exploded view generation to perform assembly sequence planning. *Curr Adv Mech Eng* 963–973
29. Yang H, Chen J, Wang C, Cui J, Wei W (2020) Intelligent planning of product assembly sequences based on spatio-temporal semantic knowledge. *Assembly Autom* 40(5)

30. Yang Y, Yang M, Shu L, Li S, Liu Z (2020) A novel parallel assembly sequence planning method for complex products based on psobc. *Math Prob Eng*
31. Zhou Z, Ji L, Xiong R, Wang Y (2020) A spatial information inference method for programming by demonstration of assembly tasks by integrating visual observation with CAD model. *Assem Autom* 40(5):689–701

# An Inventory Model for Imperfect Production and Time Sensitive Selling Price



Ruchi Sharma and G. S. Buttar

**Abstract** In this article, an inventory model for a production unit with an uneven production rate and time sensitive selling cost has been considered. The considered production inventory model is accepted to make perfect items at commencement of production but owing to various factors, it starts producing defective items after some time and it increases exponentially by time, i.e., the uneven production rate has been considered. The demand is considered to be time dependent. Initially for a definite time, production rate is considered as constant, but eventually, due to different factors, production starts decreasing. Thus, the efficiency ( $E$ ) of these units must be improved to get extra production which can sustain the production competence. In view of this fact, inverse efficiency  $\lambda$  is introduced in production rate. Using concepts of differential calculus, expected maximum profit has been determined. The purpose of the current investigation is to find the perfect arrangement for a production policy that increases the total benefit subject to certain limitations. Results are examined by means of a mathematical example to support the theory.

**Keywords** Inventory optimization · Imperfect production · Mathematical modeling · Time sensitive selling price

## 1 Introduction

In manufacturing and trade activity, the inventory issues are usual components. In any manufacture inventory structure, vulnerabilities are generally associated with demand, crude materials availability, different relevant expenses, and life of the manufacturing amenities, appliance fixes and repairs time. At the point when these vulnerabilities are not important then, using old style “Economic Order Quantity” (EOQ) or “Economic Production Quantity” (EPQ) modeling, we can assessed these vulnerabilities.

---

R. Sharma (✉) · G. S. Buttar  
Department of Mathematics, Chandigarh University, Gharuan, Mohali, India  
e-mail: [ruchi.r1066@cumail.in](mailto:ruchi.r1066@cumail.in)

At the beginning when production is going on in a manufacturing plant, production rate remain practically consistent up to certain time. Since all elements related with manufacturing are afresh, for example, all equipments are in good conditions, all workers are physically and mentally sound. At first up to definite time, production rate remains constant. But after a short time, owing to different factors, production will reduce. Thus, the efficiency ( $E$ ) of these units must be improved to get extra production which can sustain the production competence. In view of this fact, inverse efficiency  $\lambda$  is introduced in production rate. Manufacture capacity of the manufacturing plants might suffer owing to these and shortcomings of skilled or unskilled manpower. Commonly, the manufacturing unit is considered as flexible to deliver in accordance with the demand.

## 2 Research Background

The purpose of this study is to find the expected optimum manufacturing time with the final goal of decreasing the overall cost per unit time. A lot of work has been done related to these issues and offered solutions accordingly. Teng and Chang [1] considered EPQ model of deteriorating item with cost and inventory. Hou [2] considered a model of inflation with shortages, stock dependent demand. Sana et al. [3] considered an EPQ model having trended demand with shortages and deterioration. Chakraborty et al. [4] considered an EPQ with machine collapse and corrosion. They considered precautionary and remedial maintenance, all together. An imperfect multi-product manufacturing system with uneven demand is investigated. The study proposes an optimal production policy to reduce the failure rate and energy consumption of the production system with an additional development cost Singh and Jain [5] considered an EPQ model with inflation and supplier credits. Sana [6] considered a model to evaluate the rate and consistency of product to maximize the profit. Chakraborty and Giri [7] proposed a model for vendor and buyer supply chain coordination and developed a screening after each replenishment to optimize the cost. Wang et al. [8] developed an EOQ model to optimize the function with defective quality stuff, and decision variables depend upon time interval. Li et al. [9] considered for random demand and remanufacturing yields to optimize the model. Marchi et al. [10] considered the learning outcome in power efficiency in manufacturing units. Thus, they projected a lot-sizing problem to demonstrate the relations between knowledge in production and energy competence directly and indirectly and also a suitable decision about the lot size quantity. Shamayleh et al. [11] proposed a replacement approach for retailers who is facing a time-varying demand for cold stored products. Jawa and Singh [12] took an EPQ model to analyze the conservation innovation sway with machine failure by accepting multivariate interest rate with firm and fluffy circumstance. Pousoltan et al. [13] suggested an EPQ model by taking stochastic machine failure and fix time with stochastic crumbling items and they all talked about the complete expense correlation for various uptime. Be that as it may, potential connections between request parcel and quality are not examined in

these investigations. Genuine frameworks for stock or creation control unavoidably view that as, for different reasons; got request parts incorporate deficient things. The standard reasons are defects underway, harm on the way, or both. Such faulty things will influence accessible stock levels, making deficiencies and requiring changes to the recurrence of orders.

### 3 Assumptions Made for Proposed Model

To show the planned model the accompanying assumptions have been utilized:

- (i) The demand is time subordinate and is given by  $\alpha + \beta t$ ,  $0 < \beta < 1$ , where  $\beta$  signifies the shape parameter and is a proportion of responsiveness of demand and  $\alpha$  means the scale parameter.
- (ii)  $S$ : total set up cost,
- (iii) P.R.: production rate per unit time,
- (iv)  $I$ : inventory of the production,
- (v)  $T$ : total selling period,
- (vi) S.P.: producer selling cost per product,
- (vii)  $\lambda$ : inverse efficiency (choice variable),
- (viii)  $K$ : total production cost,
- (ix)  $h$ : holding cost per unit product per unit time,
- (x)  $R$ : total revenue,
- (xi)  $E$ : efficiency cost,
- (xii)  $H$ : total holding cost,
- (xiii) T.P.: total profit,
- (xiv)  $C_e$ : rate of efficiency cost,
- (xv)  $t_1$ : time period of constant production,
- (xvi)  $t_2$ : total production period,
- (xvii)  $Q_1$ : inventory level at time  $t_1$ ,
- (xviii)  $Q_2$ : inventory level at time  $t_2$ ,

To satisfy the clients' demand during the selling time frame  $T$ , a few efficiencies ( $E$ ) of various factors in the framework must be expanded for additional manufacturing. Considering this reality in the manufacture inventory framework, production rate, PR, taken as a component of another variable  $\lambda$  identified as inverse efficiency, is planned as follows:

$$\begin{aligned}
 \text{PR} &= p, & 0 \leq t \leq t_1 \\
 \text{PR} &= pe^{(-\lambda(t-t_1))} & t_1 \leq t \leq t_2 \\
 \text{where } \lambda &= \frac{1}{E}
 \end{aligned}$$



The production will be halted after a specific time  $t_2$  so that the framework gives the ideal benefit fulfilling the clients' all out demand.

Our objective is to find time at which producer stop the production to get the maximum profit. However, after certain time, the quality of the items will be perished progressively regarding time up to the finish of production because of hardware flaw, absence of experts or the quality people for continual working, and so forth. In this way the selling cost S.P. of a thing has been assumed the premise of production time, as per the accompanying:

$$\begin{aligned} \text{S.P.} &= C \quad 0 \leq t \leq t_1 \\ \text{S.P.} &= Cx \quad t_1 \leq t \leq t_2, \quad 0 < x < 1 \end{aligned}$$

### 4 Formulation of Mathematical Model for Proposed Inventory System

Initially system produces perfect item, i.e., from time  $t = 0$  to  $t = t_1$ . Production rate  $P$  remains constant. At  $t = t_1$  inventory level is  $Q_1$ . After time  $t_1$  manufacture rate decreases exponentially and manufacturing stops at time  $t = t_2$ . Inventory built up through the period  $[0, t_2]$  to satisfy the demand. For the period of the period  $[t_2, T]$  stock slowly decreases and it depletes at the end of period  $t = T$ . Let  $I$  be stock level at the time  $t$ , then differential equation of  $I$  is (Fig. 1).

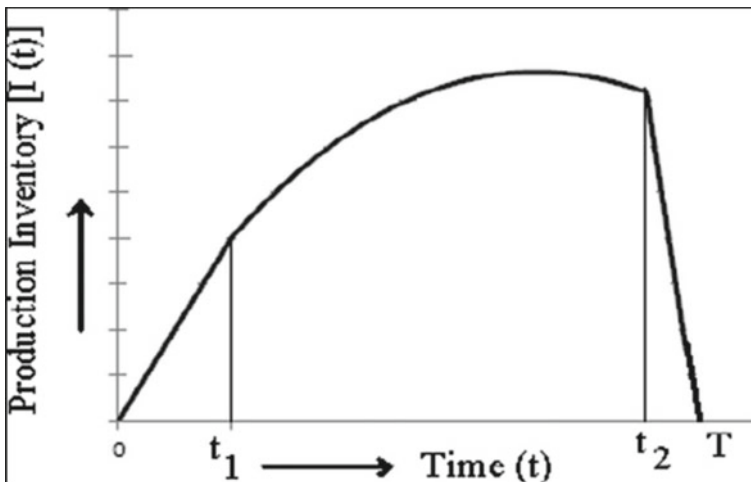


Fig. 1 Graphical illustration of planned model

$$\frac{dI}{dt} = P - (\alpha + \beta t), \quad 0 \leq t \leq t_1 \tag{1}$$

$$\frac{dI}{dt} = P e^{-\lambda(t-t_1)} - (\alpha + \beta t), \quad t_1 \leq t \leq t_2 \tag{2}$$

$$\frac{dI}{dt} = -(\alpha + \beta t), \quad t_2 \leq t \leq T \tag{3}$$

Using the boundary condition

$$I(0) = 0, I(t_1) = Q_1, I(t_2) = Q_2, I(T) = 0 \tag{4}$$

Integration of the differential Eq. (1) for the interval  $[0, t]$  yields

$$\int_0^t dI = \int_0^t [P - (\alpha + \beta t)] dt$$

or  $I(t) - I(0) = (P - \alpha)t - \frac{\beta t^2}{2}$

with boundary condition  $I(t_1) = Q_1$ , we have,

$$Q_1 = (P - \alpha)t_1 - \frac{\beta t_1^2}{2} \tag{5}$$

Again, integration of the differential Eq. (2) for the interval  $[t_1, t]$  yields

$$\int_{t_1}^t dI = \int_{t_1}^t [P e^{-\lambda(t-t_1)} - (\alpha + \beta t)] dt$$

$$I(t) - I(t_1) = \left[ \frac{-P e^{-\lambda(t-t_1)}}{\lambda} - \alpha t - \frac{\beta t^2}{2} \right]_{t_1}^t$$

Using the boundary condition  $I(t_1) = Q_1$  and  $I(t_2) = Q_2$

$$Q_2 = Q_1 - \frac{P e^{\lambda t_1} (e^{-\lambda t_2} - e^{-\lambda t_1})}{\lambda} - \alpha(t_2 - t_1) - \frac{\beta(t_2^2 - t_1^2)}{2} \tag{6}$$

Also, performing integration of the differential Eq. (3) for the interval  $[t_2, t]$ , it is obtained that

$$\int_{t_2}^t dI = \int_{t_2}^t -(\alpha + \beta t) dt$$

$$\text{or } I(t) - I(t_2) = -\alpha(t - t_2) - \frac{\beta(t_2^2 - t_1^2)}{2}$$

Using boundary condition  $I(T) = 0$  we have

$$Q_2 - \alpha(T - t_2) - \frac{\beta(T^2 - t_2^2)}{2} = 0 \tag{7}$$

Using Eqs. (3), (4), and (5) the time  $t_2$  at which productions stop, is obtained as follows

$$t_2 = t_1 - \frac{\ln \left[ 1 + \lambda t_1 - \frac{\lambda(\alpha T + \frac{\beta T^2}{2})}{P} \right]}{\lambda} \tag{8}$$

Now the various costs related with the planned inventory method are production cost ( $K$ ), setup cost ( $S$ ), holding cost ( $H$ ), and efficiency cost ( $E$ ).

The expressions for these costs are obtained as follows:

Total holding cost “ $H$ ”:

$$\begin{aligned} H &= h \int_0^T I dt \\ &= h \left[ \frac{(P - \alpha)t_1^2}{2} - \frac{\beta t_1^3}{6} + Q_1(t_2 - t_1) + \frac{P(e^{-\lambda(t_2-t_1)} - 1)}{\lambda^2} + \frac{P(t_2 - t_1)}{\lambda} \right. \\ &\quad - \frac{\alpha(t_2^2 - t_1^2)}{2} - \frac{\beta(t_2^3 - t_1^3)}{6} + \alpha t_1(t_2 - t_1) + \frac{\beta t_1^2(t_2 - t_1)}{2} + Q_2(T - t_2) \\ &\quad \left. - \frac{\alpha(T^2 - t_2^2)}{2} + \alpha t_2(T - t_2) - \frac{\beta(T^3 - t_2^3)}{6} + \frac{\beta t_2^2(T - t_2)}{2} \right] \tag{9} \end{aligned}$$

And the efficiency cost “ $E$ ” is obtained as:

$$E = c_e \int_{t_1}^{t_2} P e^{-\lambda(t-t_1)} dt = \frac{c_e P (1 - e^{-\lambda(t_2-t_1)})}{\lambda} \tag{10}$$

Now total Revenue “ $R$ ” obtained by selling all items to the customers at the rate of “ $p$ ” per item is given by

$$R = \int_0^{t_1} P c dt + \int_{t_1}^{t_2} P x e^{-\lambda(t-t_1)} dt = P c t_1 - \frac{P x c (e^{-\lambda(t_2-t_1)} - 1)}{\lambda} \tag{11}$$

Therefore, total profit satisfying in the production inventory system is given by

$$\begin{aligned}
 TP(\lambda, t_2) &= R - K - S - H - E \\
 TP(\lambda, t_2) &= Pct_1 - \frac{Pxc(e^{-\lambda(t_2-t_1)} - 1)}{\lambda} - K - S - h \left[ \frac{(P - \alpha)t_1^2}{2} - \frac{\beta t_1^3}{6} \right. \\
 &+ Q_1(t_2 - t_1) + \frac{P(e^{-\lambda(t_2-t_1)} - 1)}{\lambda^2} + \frac{P(t_2 - t_1)}{\lambda} - \frac{\alpha(t_2^2 - t_1^2)}{2} \\
 &- \frac{\beta(t_2^3 - t_1^3)}{6} + \alpha t_1(t_2 - t_1) + \frac{\beta t_1^2(t_2 - t_1)}{2} + Q_2(T - t_2) \\
 &- \left. \frac{\alpha(T^2 - t_2^2)}{2} + \alpha t_2(T - t_2) - \frac{\beta(T^3 - t_2^3)}{6} + \frac{\beta t_2^2(T - t_2)}{2} \right] \\
 &- \frac{c_e P(1 - e^{-\lambda(t_2-t_1)})}{\lambda} \tag{12}
 \end{aligned}$$

This equation represents the required deterministic profit function for time dependent demand.

### 5 Procedure for Optimal Result

Our purpose is to establish the optimal value of  $t_2$ , so that total profit (TP) can be maximized. The basic condition for TP to be maximum is  $\frac{d(TP)}{dt_2} = 0$  and  $\frac{d^2TP}{dt_2^2} < 0$

$$\text{Now } \frac{d^2TP}{dt_2^2} = \frac{d^2R}{dt_2^2} - \frac{d^2K}{dt_2^2} - \frac{d^2S}{dt_2^2} - \frac{d^2H}{dt_2^2} - \frac{d^2E}{dt_2^2}$$

$$\text{Since } \frac{dt_1}{dt_2} = 1 + \frac{1 - \left(\frac{\alpha + \beta T}{P}\right) \frac{dT}{dt_2}}{\lambda t_1 - \frac{\lambda(\alpha T + \frac{\beta T^2}{2})}{P}}$$

$$\text{Therefore } \frac{d^2R}{dt_2^2} = \frac{d^2K}{dt_2^2} = \frac{d^2S}{dt_2^2} = 0$$

$$\text{This gives } \frac{d^2TP}{dt_2^2} = -\frac{d^2H}{dt_2^2} - \frac{d^2E}{dt_2^2}$$

This has a negative value. Hence  $\frac{d^2TP}{dt_2^2} < 0$ .

## 6 Numerical Example

During the time (3 months) of harvesting season, people groups have a lot of cash and after that their income steadily diminishes. Based on this data organization has chosen to fix a consistent and high selling cost during the interim 3 months and afterward selling cost is decreased to 50%.

Here,

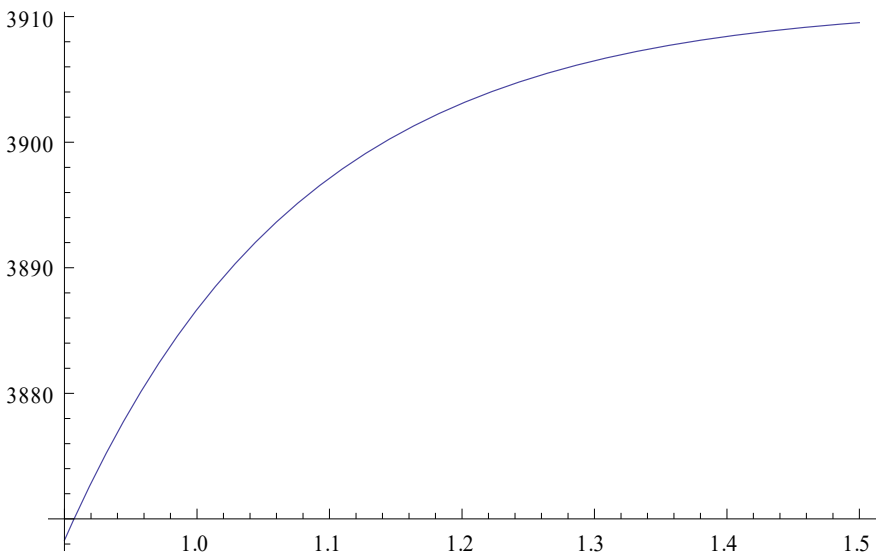
$$p = 200; \alpha = 20; t_1 = 0.4; C = 40; h = 1; C_e = 2; S = 90; X = 0.5.$$

Table 1 depicts the effect of responsiveness of demand on total production period, total selling period, inverse efficiency, and total profit.

Figure 2 shows the variation in revenue  $R$  ( $Y$ -axis) with change in production time  $t_2$  ( $X$ -axis) (when the production stops).

**Table 1** Effect of  $\beta$  on  $t_2$ ,  $T$ ,  $\lambda$ , and T.P.

$\beta$	0.2	0.4	0.6	0.8
$t_2$	0.933199	0.9786	1.0247	1.0718
$T$	8.933199	8.98	9.025	9.0718
$\lambda$	5.6264	5.1849	4.8023	4.4656
T.P.	1408.9211	1193.6542	1097.6440	1002.3530



**Fig. 2** Variation in  $R$  with  $t_2$

Figure 3 shows the variation of total production period with respect to responsiveness of demand. The total production period increases with increase in responsiveness of demand.

Figure 4 shows the variation of total selling period and inverse efficiency with respect to responsiveness of demand. The total selling period also increases with increase in responsiveness of demand, whereas the inverse efficiency decreases.

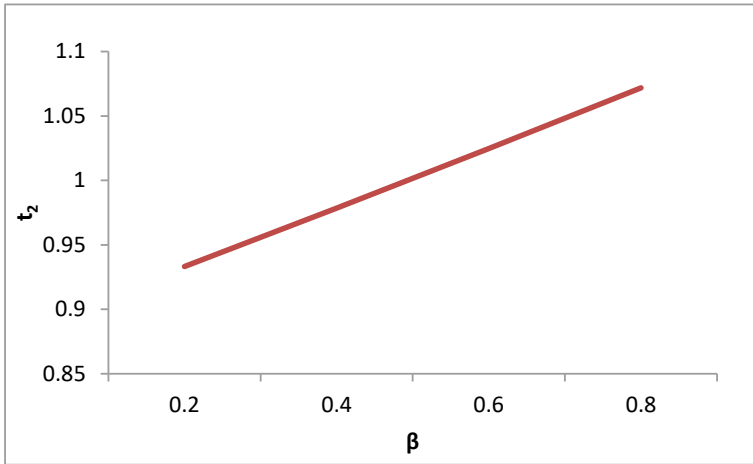


Fig. 3 Effect of responsiveness of demand on total production period

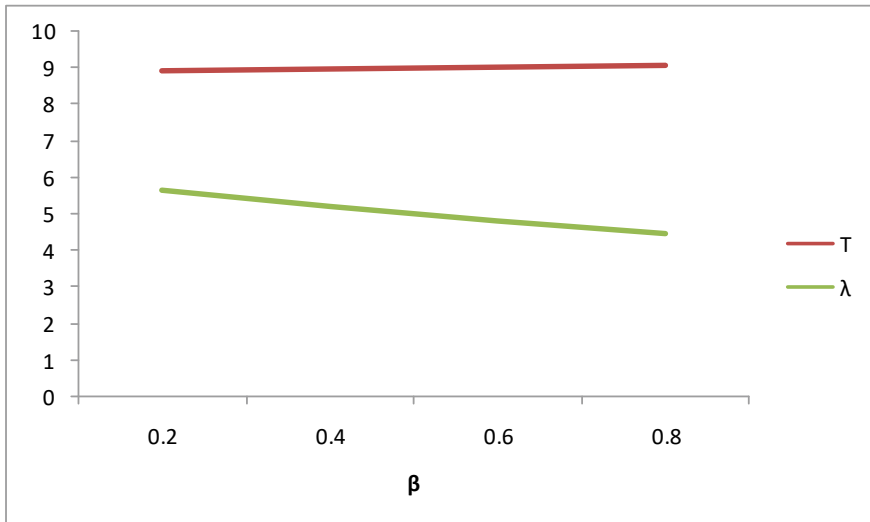
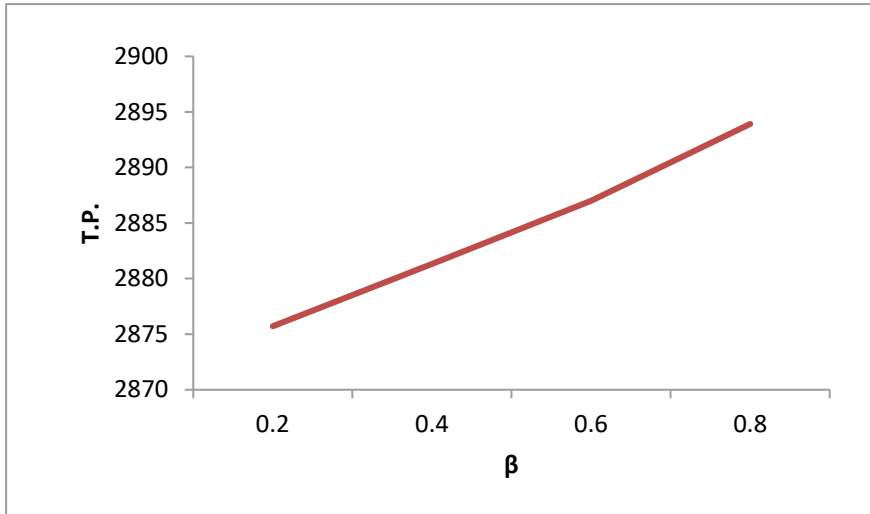


Fig. 4 Effect of responsiveness of demand on total selling period and inverse efficiency



**Fig. 5** Effect of responsiveness of demand on total profit

Figure 5 shows the increase in total profit with respect to responsiveness of demand. It can be seen from the graph that total profit increases with increase in responsiveness of demand.

## 7 Observations

- As responsiveness of demand,  $\beta$ , increases, inventory level increases, and the time at which the production stops also increases.
- The higher value of responsiveness of demand,  $\beta$ , leads to a decrease in inverse efficiency, i.e., efficiency increases.
- As responsiveness of demand,  $\beta$ , increases, total profit also increases.

## 8 Conclusion

During the time (3 months) of harvesting people groups have a lot of cash and after that their income steadily diminishes. Based on this data organization has preferred to stick to a consistent and elevated selling cost (40\$) through the interim 3 months and afterward selling cost is lowered to 50%. At the beginning of production all machinery and other associated assets for manufacturing are in good condition, henceforth organization considers delivering the things at the rate 200 every 3 months and past time interim of 3 months there may be deficiency in the machine differently,

so manufacturing by machines will be diminished exponentially. In the event that such circumstance emerges, at that point to satisfy the clients' complete demand organization wants to expand production by augmenting the effectiveness of the machine. Henceforth, under these conditions the normal most extreme benefit from the trade judgment the ideal productivity of the machine and ideal time up to which production proceeds was calculated by taking a particular case.

The following are the finding of the case discussed:

1. The organization is selling its products in accordance with customer demand as well as their pocket.
2. By applying the extra efficiency, the organization is getting profit even if their production is exponentially decreasing.
3. Their work is going on in all the seasons.

## References

1. Teng JT, Chang CT (2005) Economic production quantity models for deteriorating items with price-and stock-dependent demand. *Comput Oper Res* 32(2):297–308
2. Hou KL (2006) An inventory model for deteriorating items with stock-dependent consumption rate and shortages under inflation and time discounting. *Eur J Oper Res* 168(2):463–474
3. Sana SS, Goyal SK, Chaudhuri K (2007) An imperfect production process in a volume flexible inventory model. *Int J Prod Econ* 105(2):548–559
4. Chakraborty T, Giri BC, Chaudhuri KS (2008) Production lot sizing with process deterioration and machine breakdown. *Eur J Oper Res* 185(2):606–618
5. Singh SR, Jain R (2009) On reserve money for an EOQ model in an inflationary environment under supplier credits. *Opsearch* 46(3):303–320
6. Sana SS (2010) A production–inventory model in an imperfect production process. *Eur J Oper Res* 200(2):451–464
7. Chakraborty A, Giri B (2011) Supply chain coordination for a deteriorating product under stock-dependent consumption rate and unreliable production process. *Int J Ind Eng Comput* 2(2):263–272
8. Wang WT, Wee HM, Cheng YL, Wen CL, Cárdenas-Barrón LE (2015) EOQ model for imperfect quality items with partial backorders and screening constraint. *Eur J Ind Eng* 9(6):744–773
9. Li X, Li Y, Cai X (2015) Remanufacturing and pricing decisions with random yield and random demand. *Comput Oper Res* 54:195–203
10. Marchi B, Zanoni S, Jaber MY (2019) Economic production quantity model with learning in production, quality, reliability and energy efficiency. *Comput Ind Eng* 129:502–511
11. Shamayleh A, Hariga M, As'ad R, Diabat A (2019) Economic and environmental models for cold products with time varying demand. *J Cleaner Prod* 212:847–863
12. Jawla P, Singh SR (2020) A production reliable model for imperfect items with random machine breakdown under learning and forgetting. In: *Optimization and inventory management*. Springer, Singapore, pp 93–117
13. Poursoltan L, Seyedhosseini SM, Jabbarzadeh A (2020) An extension to the economic production quantity problem with deteriorating products considering random machine breakdown and stochastic repair time. *Int J Eng* 33(8):1567–1578



# RIM-Based Performance Evaluation of DLC Coating Under Conflicting Environment



Saptarshi Das, Bijan Sarkar, and Vidyapati Kumar

**Abstract** A coating is a layer of materials that shields a vital machine component from wear and tear or a severe impact. As a consequence, selecting the right coating material extends the life of machine components. The coating, which has diamond-like and amorphous features in nature, has several uses in aerospace, automotive, electronics, and other industries. In this work, a research study is undertaken to choose the suitable diamond-like carbon (DLC) coating material on steel utilizing the novel Reference ideal method (RIM). Six criteria were selected based on their mechanical and tribological qualities, and a ranking was performed to determine the utmost suitable alternative. The sensitivity analysis was carried out in the later phase to see how the outcomes changed when subjected to different variations. Following the investigation, it was discovered that ZR-DLC-H coating is the best alternative available and should be used in the industrial surroundings. Furthermore, the analysis outlined in this article will help the process engineer throughout the selection process in the future.

**Keywords** Coating selection · Diamond-like carbon (DLC) · Reference ideal method · Sensitivity analysis

## 1 Introduction

Effective material selection for every operation is currently a hard job for any industry since it is the basis of engineering design [1]. Because of resource constraints, material selection is critical, requiring the use of effective selection methods while

---

S. Das · B. Sarkar

Department of Production Engineering, Jadavpur University, Kolkata, West Bengal, India  
e-mail: [saptarshidas1989@gmail.com](mailto:saptarshidas1989@gmail.com)

*Present Address:*

V. Kumar (✉)

Department of Mechanical Engineering, Indian Institute of Technology, Kharagpur, West Bengal, India

e-mail: [vidyapatikumar.me@kgpian.iitkgp.ac.in](mailto:vidyapatikumar.me@kgpian.iitkgp.ac.in)

focusing on required procedures, range of applications, and other scientific and economic factors [3]. In these situations, multi-criteria decision making (MCDM) is a useful method for determining the suitable materials from the different options by taking into account several factors.

The primary goal of this article is to investigate the most superior coating materials from different alternatives. A coating is a layer of material that is usually applied to the surface of a base material in order to enhance the mechanical and tribological characteristics of the surface [4]. It adds oxidation, corrosion resistance, wear resistance, and thermal insulation to the base metal [6]. When selecting among a variety of coating materials, the decision maker must evaluate factors such as Mechanical, Thermal, Chemical, Environmental, and cost [18].

Because of the adoption of various clean and green manufacturing concepts, the use of lubricant has been drastically reduced, and the new trend in the manufacturing sector is to adapt solid lubricant coatings, which allow the contacting surfaces to graze against each other with reduced friction and wear. In this situation, diamond-like carbon coating (DLC) is a dominating competitor in the area of solid lubricant coatings [22]. Diamond-like carbon coatings have minimal friction, high wear resistance, and high hardness. In mechanical engineering, reduced friction is linked with lower energy loss, greater dependability, and better wear resistance [21]. It outperforms traditional nitride coatings such as TiN, CrN, and others due to its reduced friction and better wear resistance. Because of its excellent tribological characteristics, it is useful in a variety of sectors such as automobiles, aerospace, textiles, and mechanical equipment [26, 28].

The basic criteria, which have to take into consideration during the selection of most desirable coating materials are Hardness ( $H$ ), Young's Modulus ( $E$ ), Critical load ( $N$ ), Co-efficient of friction ( $\mu$ ),  $H/E$  ratio,  $H^3/E^2$  ratio. In actual practice  $H/E$  ratio is the indices of plastic deformation and  $H^3/E^2$  ratio indicate wear resistance [8].

In this paper, the most effective finding has been done through the application of MCDM technique. During material selection, the DM employs a variety of MCDM methods. In this study, a common method known as the Reference Ideal Method (RIM) was used for calculation, and sensitivity analysis was also performed to determine the superiority of one criterion over the others.

## 2 Literature Review

The MCDM application has been successfully applied in the past for various applications such as best advanced machining process selection, response optimization, and finding the optimal parametric combinations. Anojkumar et al. [1] conducted a comparison of MCDM techniques for pipe material selection in the sugar sector. FAHP-TOPSIS, FAHP-VIKOR, FAHP-ELECTRE, and FAHP-PROMTHEE were used to choose the best option among the different materials. Girubha and Vinodh [14] used fuzzy VIKOR in conjunction with environmental impact analysis to choose

a material for an automobile component. Using the MCDM method, Çalışkan [6] selected boron-based tribological hard coatings. For selecting the optimum coating material for cutting tools, the EXPROM2, TOPSIS, and VIKOR techniques are employed. Prasad et al. [27] used the Fuzzy AHP-TOPSIS technique to choose a coating material for a magnesium alloy. Athanasopoulos et al. [2] presented a fuzzy logic and MCDM-based decision support system for coating material selection. Chauhan and Vaish [11] used multi-criteria decision making to specify hard coating material selection. To choose hard coating materials, material selection charts (Ashby method) were utilized. Pathan et al. [25] use the MCDM method to choose a coating material for AISI 4140 steel. In MCDM, Cables et al. [4] developed the Reference ideal method (RIM). In this article, the notion of “ideal solution” is given as a potential alternative. For addressing machining problems, Sofuoğlu [31] proposed the Hybridizing Taguchi Algorithm with Reference Ideal Method. During the weight calculation of the criterion, Hafezalkotob and Hafezalkotob [15] has establish an extended MULTIMOORA method based on Shannon entropy concept in order to tackle materials selection process. Entropy concept has been considered for assigning relative importance to decision making attributes. Likewise, Delgado and Reyes [12] has been chosen entropy method for assigning weights of the criterion while selecting best alternative plants as food for livestock. For conducting the sensitivity analysis Li et al. [22] assess the water quality using TOPSIS method. The sensitivity of TOPSIS to the parameter weights was discussed in detail. The MCDM application has been successfully applied in the past for various applications such as best advanced machining process selection [8, 9, 18, 30], response optimization [7, 17, 19], and finding the optimal parametric combinations.

Following a study of previous studies, a novel strategy with the application of the Reference ideal technique in the area of coating material selection with the assistance of expert opinion is suggested in this article. Six options from the realm of diamond-like carbon coating on steel as a base metal have been considered. Shannon’s Entropy technique was used to determine the relative weightage of the criterion. Following the completion of the computation, a sensitivity analysis was performed to determine the relative significance of each option in relation to others.

### 3 Methodology

#### 3.1 *Shannon Entropy Method for Weight Calculation of Each Criterion*

This is a very effective mathematical model for calculating weightage of alternatives of an MCDM problem. It has an application on numerous fields. The concept of Shannon entropy used to measure the contrast among criteria, which is used for decision making. The steps associated with this method are shown below.

**Step 1:** Normalization of Decision Matrix  $Z = \{x_{ij}; i = 1, 2, \dots, m; j = 1, 2, \dots, n\}$  for each criterion  $C_j$ . The normalized values  $p_{ij}$  can be evaluated as

$$p_{ij} = \frac{x_{ij}}{\sum_{i=1}^m x_{ij}} \quad (1)$$

**Step 2:** Calculation of Entropy value  $H_j$  for each criterion  $C_j$ .

$$H_j = -k \sum_{i=1}^m p_{ij} \ln p_{ij} \quad (2)$$

where  $k = 1/\ln(m)$

**Step 3:** Evaluation of degree of divergence,  $d_j$  of each criterion  $C_j$

$$d_j = 1 - H_j \quad (3)$$

**Step 4:** Calculation of weight,  $w_j$  of each criterion

$$w_j = \frac{d_j}{\sum_{j=1}^n d_j} \quad (4)$$

### 3.2 Reference Ideal Method (RIM)

This method was proposed by Cables Pérez and other associates [4, 5]. This method, criterion for DM established the reference point for accessing the attribute of each alternative. However, this is not necessary for each criterion to be associated with the same field or belongs to same range. The steps associated with the Reference ideal method (RIM) are:

**Step 1:** Prescribe the work context. It identifies the following aspects for each criterion.

- The range,  $t_j$
- The reference ideal  $s_j$
- The weightage with respect to each criterion,  $w_j$ . This can be evaluated using Shannon's Entropy method.

**Step 2:** Construction of decision matrix,  $X$ .

$$X = \begin{bmatrix} x_{11} & x_{12} & \dots & x_{1n} \\ x_{21} & x_{22} & \dots & x_{2n} \\ \vdots & \vdots & & \vdots \\ x_{m1} & x_{m2} & \dots & x_{mn} \end{bmatrix},$$

$i = 1, 2, 3 \dots m(\text{Alternatives}); j = 1, 2, 3 \dots n(\text{Criteria})$  (5)

**Step 3:** Normalization of the decision matrix  $X$  with reference ideal, where the basic equation used to evaluate the normalized value of each element of decision matrix using Range and reference ideal are as follows:

$$f(x, [A, B], [C, D]) = \begin{bmatrix} 1 & \text{When, } x \in [C, D] \\ 1 - \frac{d \min(x, [C, D])}{|A - C|} & \text{When, } x \in [A, C] \text{ and } A \neq C \\ 1 - \frac{d \min(x, [C, D])}{|D - B|} & \text{When, } x \in [D, B] \text{ and } D \neq B \end{bmatrix} \quad (6)$$

where

$[A, B]$  Indicate the entire range which belongs to the universe of discourse

$[C, D]$  Indicate the Reference ideal

$$x \in [A, B]$$

$[C, D] \subset [A, B]$  these two conditions must be satisfied.

**Step 4:** To find out the weighted normalized decision matrix,  $Y$ . It can be constructed by multiplying it with the calculated weightage. In this presentation, the weightage has been done by Shannon Entropy method.

$$[Y = X \times W] \quad (7)$$

**Step 5:** Calculation of variation of normalized reference ideal for each alternative:

- For positive reference ideal,

$$I_i^+ = \sqrt{\sum_{j=1}^n (y_{ij}' - w_j)^2} \quad (8)$$

- For negative reference ideal,

$$I_i^- = \sqrt{\sum_{j=1}^n (y_{ij}')^2} \quad (9)$$

where  $i = 1, 2, 3 \dots m$  (Alternatives);  $j = 1, 2, 3 \dots n$  (Criteria)

$y_{ij}$ : Weighted normalized matrix values

$w_j$ : Weight values

**Step 6:** Find out relative index of each alternative  $A$  through expression

$$R_i = \frac{I_i^-}{I_i^+ + I_i^-} \quad (10)$$

where  $0 < R_i < 1$ ;  $i = 1, 2 \dots m$

**Step 7:** Rank the alternatives on the basis of relative index.

After performing the MCDM calculation the sensitivity analysis has to be performed and we can find the variation of criterion against each alternative while changing the assign weightage of the criteria. It is discussed in detail at result and discussion. Moreover, in industrial application this research work will be a beneficial for selection of tribological coating materials (Fig. 1).

## 4 Case Studies

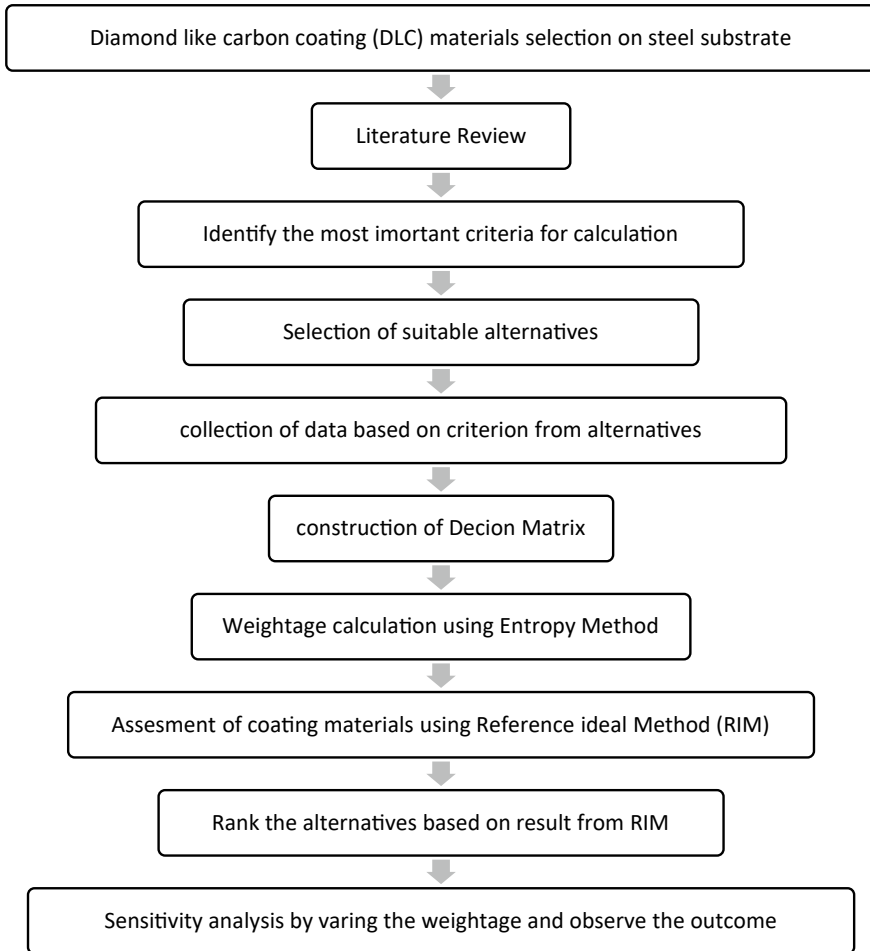
After going through a number of previous research [10, 12–16, 20, 23, 24, 29] the factors which are most effective in order to differentiate the DLC coating are, Hardness ( $H$ ), Young's Modulus ( $E$ ), Critical load ( $N$ ), Co-efficient of friction ( $\mu$ ),  $H/E$  ratio,  $H^3/E^2$  ratio. Out of the six criterion, co-efficient of friction is the tribological factor, and rest of those are Mechanical criteria. The criterion except co-efficient of friction is favorable criterion, i.e., more the value will give better result. Six numbers of alternatives have been taken for the case study namely, DLC-H, ZR-DLC, ZR-DLC-H, Ti-DLC, Si-DLC, and W-DLC [32–36]. And based on reference papers, the decision matrix has been constructed as below (Table 1).

The results obtain from the calculation of the research work has shown below. Weightage of the criterion obtain from the Entropy method has shown below (Table 2).

After the estimation of the weightage, the steps associated with the RIM has been adopted as shown from Eqs. 5 to 10. But before the adaptation of those steps, the ranges and reference ideal values of different criterion have to be identified. In this regard, the values have been chosen with the help of the expert from industry and academic background. The values of the ranges and the reference ideals of the selected criterion tabulated below (Table 3).

While conducting the calculation using the RIM method, the normalized decision matrix was formed using the Step 3 of the RIM analysis which is tabulated below (Table 4).

After getting the values of normalized decision matrix, the weighted normalized form has been evaluated by following the step 4 and after that step 5 and step 6 are



**Fig. 1** Research methodology

**Table 1** Decision matrix

Alternatives	Criteria					
	$E$ (GPA) (+)	$H$ (GPA) (+)	$H/E$ (+)	$H^3/E^2$ (+)	Critical load ( $N$ ) (+)	Co-efficient of friction ( $\mu$ ) (-)
DLC-H	89	10.1	0.113	0.130	22	0.20
ZR-DLC	102	8.8	0.086	0.066	42	0.10
ZR-DLC-H	116	13.3	0.115	0.175	35	0.06
Ti-DLC	106	12.9	0.122	0.191	28	0.25
Si-DLC	175	20	0.145	0.420	50	0.05
W-DLC	120	12	0.100	0.120	26	0.30

**Table 2** Weightage of the criterion

Criteria	$E$ (GPA) ( $w_1$ )	$H$ (GPA) ( $w_2$ )	$H/E$ ( $w_3$ )	$H^3/E^2$ ( $w_4$ )	Critical load ( $w_5$ )	Co-efficient of friction ( $w_6$ )
Weightage	0.128512	0.136391	0.119764	0.230086	0.139526	0.245721

**Table 3** Ranges and reference ideals of the criterion

Criteria	Range	Reference ideal
$E$ (GPA)	62–213	150–170
$H$ (GPA)	7–30	18–22
$H/E$	0.032–0.484	0.075–0.20
$H^3/E^2$	0.0075–7.02	0.01–0.5
Crit. load	20–50	30–35
Co eff of friction	0.02–0.4	0.05–0.15

**Table 4** Normalized decision matrix

Alternatives	Criteria					
	$E$ (GPA)	$H$ (GPA)	$H/E$	$H^3/E^2$	Critical load (N)	Co-efficient of friction ( $\mu$ )
DLC-H	0.307	0.273	1	1	0.2	0.8
ZR-DLC	0.455	0.182	1	1	0.533	1
ZR-DLC-H	0.613	0.545	1	1	1	1
Ti-DLC	0.5	0.545	1	1	0.8	0.6
Si-DLC	0.884	1	1	1	0	1
W-DLC	0.659	0.454	1	1	0.6	0.4

evaluated in order to find out the relative index of all alternatives. The results are shown in Table 5.

Finally, the rank of the alternatives has been given based on the relative index score. From the above case studies, it is clearly seen that the “ZR-DLC-H” has qualified with the top score and shown its dominance over the other alternatives (Fig. 2; Table 6).

**Table 5** Alternative wise relative index values

Alternatives	DLC-H	ZR-DLC	ZR-DLC-H	Ti-DLC	Si-DLC	W-DLC
Relative index score	0.64700444	0.71596	0.833659014	0.710675	0.739802	0.631561



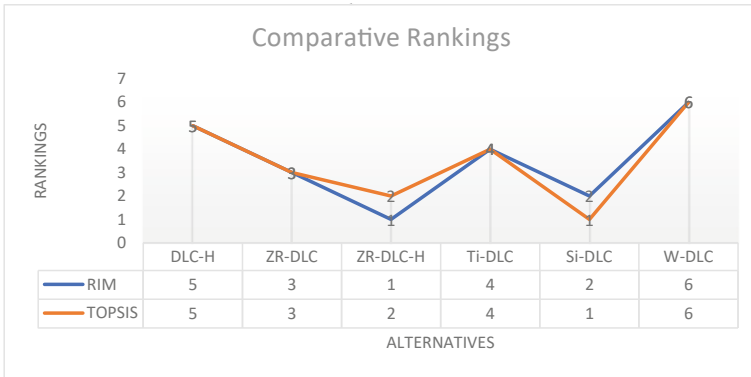


Fig. 2 Comparative rankings of various MCDM techniques

Table 6 Ranks of the alternatives

Alternatives	DLC-H	ZR-DLC	ZR-DLC-H	Ti-DLC	Si-DLC	W-DLC
RIM score	5	3	1	4	2	6
TOPSIS score [8]	5	3	2	4	1	6

### 5 Result and Discussion

The sensitivity analysis has been performed once the findings have been calculated. In this study, the analysis was performed by varying the weights of the criterion and observing the feedback of the outcome as the weights were changed. Suppose one weightage of a criterion change from  $w_p$  to  $w_p^*$  where  $w = 1, 2, \dots n$ .  $w_p^* = \gamma_p w_p$ , where  $\gamma_p$  known as initial variation ratio. But one thing we should notice that the sum of weight of all the criterion under an alternative should be equal to 1. Due to change of weight of one criterion will affect the remaining criterion. From the above conclusion, the new weight of each criterion can be represented as:

$$w'_1 = \frac{w_1}{w_1 + w_2 + \dots w_p^* + \dots w_n} = \frac{w_1}{1 + (\gamma_p - 1)w_p}$$

$$w'_2 = \frac{w_2}{w_1 + w_2 + \dots w_p^* + \dots w_n} = \frac{w_2}{1 + (\gamma_p - 1)w_p}$$

$$\vdots$$

$$w'_p = \frac{w_p^*}{w_1 + w_2 + \dots w_p^* + \dots w_n} = \frac{\gamma_p w_p}{1 + (\gamma_p - 1)w_p}$$

$$\vdots$$

$$w'_n = \frac{w_n}{w_1 + w_2 + \dots w_p^* + \dots w_n} = \frac{w_n}{1 + (\gamma_p - 1)w_p} \tag{11}$$

Values of  $\gamma_p$  can be obtained by:

$$\gamma_p = \frac{\beta_p - \beta_p w_p}{1 - \beta_p w_p} \tag{12}$$

The term  $\frac{w'_p}{w_p}$  can be represented by  $\beta_p$  which is known as unitary variation ratio. These values are generally designed according to the number of results the user want to calculate. Any change associated with the  $\beta_p$  value will change the weightage of a certain criteria. And due to that it will affect the other criterion, which can be calculate using Eq. 11. The change associated with the weightage will influence the entire MCDM method as the weightage normalized matrix will be shifted from its initial value. Finally, it will influence the overall rankings of the alternatives due to change of relative index values. In the case studies the unitary variation ratio is taken in ten intervals, e.g., 0.1, 0.3, 0.5, 0.7, 0.9, 1.1, 1.3, 1.5, 1.7, and 1.9. Now from Table 2, we have taken the weightage of hardness values to observe the effect of change on the other criterion while varying the unitary variation ratio. The details values of weightage of all other criterion, corresponding to hardness criterion with respect to each value of unitary ratio are shown in Table 7.

After calculating the weightage of the criterion, the RIM analysis conducted further in order to calculate relative index of each alternative while varying the unitary variation ratio and tabulated in Table 8.

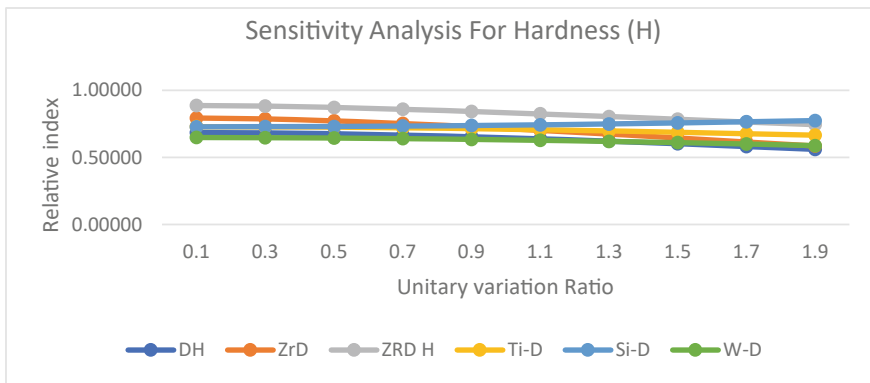
The Relative index Versus Unitary variation ratio graph was produced based on the sensitivity analysis to examine the change of the relative index of the alternatives when the weightage of the criteria was modified. The sensitivity analysis graph based on hardness criterion has been shown in Fig. 3.

**Table 7** Weightage values of other criterion with respect to Hardness criterion

$\beta_2$	$\gamma_2$	$w_2^*$	$w_1'$	$w_2'$	$w_3'$	$w_4'$	$w_5'$	$w_6'$
0.1	0.0875551	0.011942	0.146779	0.013639	0.136787	0.26279	0.159358	0.280647
0.3	0.270136	0.036844	0.14272	0.040917	0.133004	0.255523	0.154951	0.272886
0.5	0.4634068	0.063204	0.138661	0.068195	0.129221	0.248255	0.150544	0.265124
0.7	0.6683348	0.091155	0.134601	0.095473	0.125438	0.240987	0.146137	0.257363
0.9	0.8860072	0.120843	0.130542	0.122752	0.121655	0.23372	0.14173	0.249601
1.1	1.1176512	0.152437	0.126483	0.15003	0.117872	0.226452	0.137323	0.24184
1.3	1.3646565	0.186126	0.122424	0.177308	0.11409	0.219185	0.132915	0.234079
1.5	1.6286035	0.222126	0.118364	0.204586	0.110307	0.211917	0.128508	0.226317
1.7	1.9112972	0.260683	0.114305	0.231864	0.106524	0.20465	0.124101	0.218556
1.9	2.2148082	0.302079	0.110246	0.259142	0.102741	0.197382	0.119694	0.210795

**Table 8** Relative index values of each alternative based on hardness criterion

Unitary variation ratio	Alternatives					
	DLC-H	ZR-DLC	ZR-DLC-H	Ti-DLC	Si-DLC	W-DLC
0.1	0.68507	0.79355	0.88672	0.72902	0.72776	0.64835
0.3	0.68217	0.78659	0.88195	0.72766	0.72861	0.64714
0.5	0.67609	0.77276	0.87249	0.72481	0.73043	0.64455
0.7	0.66676	0.75311	0.85906	0.72035	0.73332	0.64049
0.9	0.65430	0.72912	0.84266	0.71428	0.73734	0.63491
1.1	0.63906	0.70224	0.82426	0.70670	0.74255	0.62785
1.3	0.62149	0.67365	0.80464	0.69778	0.74894	0.61941
1.5	0.60211	0.64422	0.78442	0.68778	0.75643	0.60978
1.7	0.58145	0.61456	0.76408	0.67699	0.76494	0.59922
1.9	0.56000	0.58511	0.74399	0.66573	0.77433	0.58799



**Fig. 3** Sensitivity analysis for hardness (*H*)

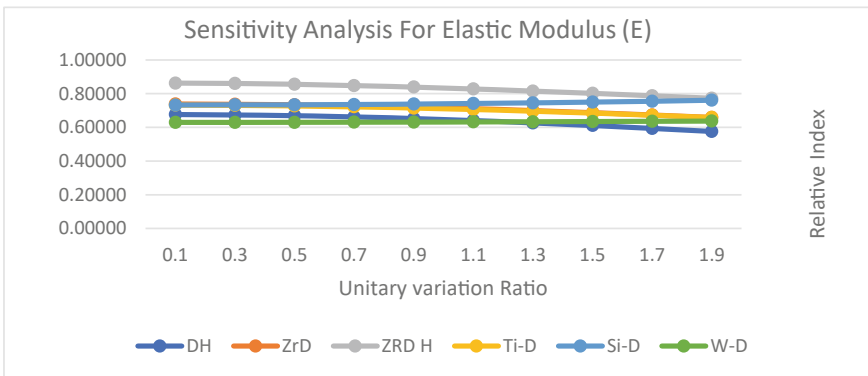
Similarly, the relative index values are provided in Table 9, and Fig. 4 illustrates the graph plot of the remaining criteria while conducting the sensitivity analysis (Figs. 5, 6, 7 and 8; Tables 10, 11, 12 and 13).

## 6 Conclusion

With the growth of industrialization, the major purpose of each component’s design is to reduce wear and friction between mating components in order to extend the component’s lifespan. Coating, as a consequence, is a crucial treatment. This article focused on a coating (DLC) with several industrial uses. RIM is a selection process that assists in selecting the best solutions according on the designer’s preferences. To

**Table 9** Relative index values of each alternative based on young modulus criterion

Unitary variation ratio	Alternatives					
	DLC-H	ZR-DLC	ZR-DLC-H	Ti-DLC	Si-DLC	W-DLC
0.1	0.67629	0.73879	0.86266	0.73217	0.73275	0.62957
0.3	0.67409	0.73709	0.86035	0.73057	0.73325	0.62971
0.5	0.66949	0.73353	0.85558	0.72719	0.73430	0.63001
0.7	0.66235	0.72798	0.84841	0.72196	0.73599	0.63049
0.9	0.65272	0.72045	0.83905	0.71488	0.73835	0.63116
1.1	0.64074	0.71102	0.82786	0.70606	0.74144	0.63202
1.3	0.62668	0.69988	0.81527	0.69572	0.74526	0.63307
1.5	0.61090	0.68729	0.80168	0.68413	0.74982	0.63430
1.7	0.59378	0.67354	0.78750	0.67162	0.75509	0.63569
1.9	0.57570	0.65896	0.77306	0.65851	0.76101	0.63721



**Fig. 4** Sensitivity analysis for young modulus (*E*)

choose the most desired material, the designer or experts must provide the range and reference ideal values based on their specifications. The results of this investigation reveal that Si-DLC beats all other alternative coatings. Except for Hardness, the relative index did not change much throughout the calculation. Although the SI-DLC is one of the most reliable techniques, TOPSIS ranks it as one of the alternatives. However, when the values are evaluated using RIM, the ZR-DLC-H comes in first position based on the range of reference ideal values provided by the experts. Furthermore, this strategy is a little bit customer-focused. Sensitivity analysis demonstrates that the ZR-DLC-H outperforms the others. As a consequence, it can be concluded that this decision making process is beneficial to enterprises in order to choose the best and most sought resources.

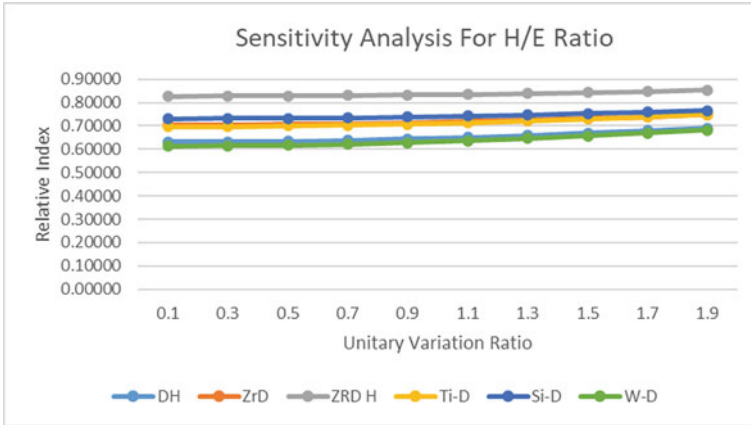


Fig. 5 Sensitivity analysis for  $H/E$  ratio

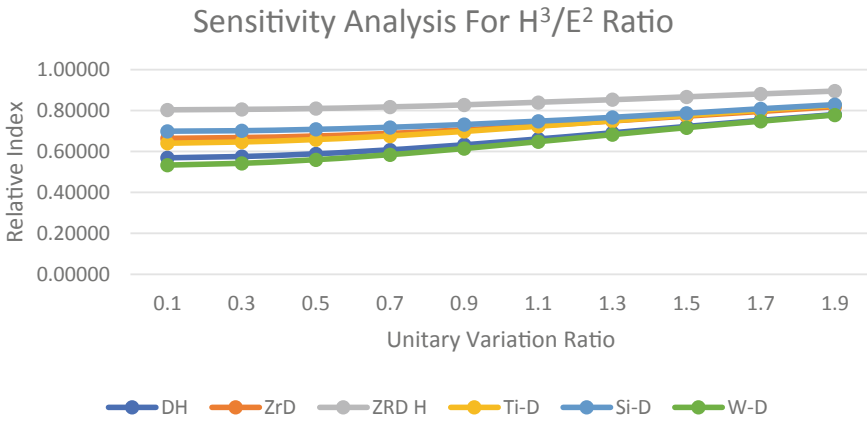


Fig. 6 Sensitivity analysis for  $H^3/E^2$  ratio

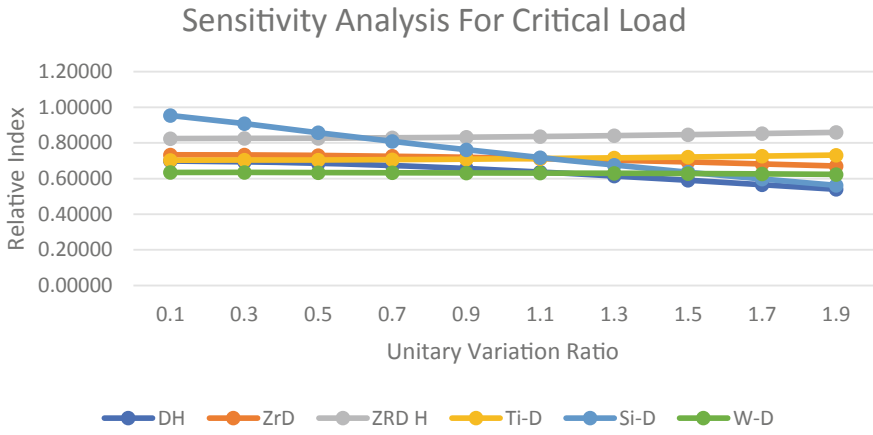


Fig. 7 Sensitivity analysis for critical load ( $N$ )

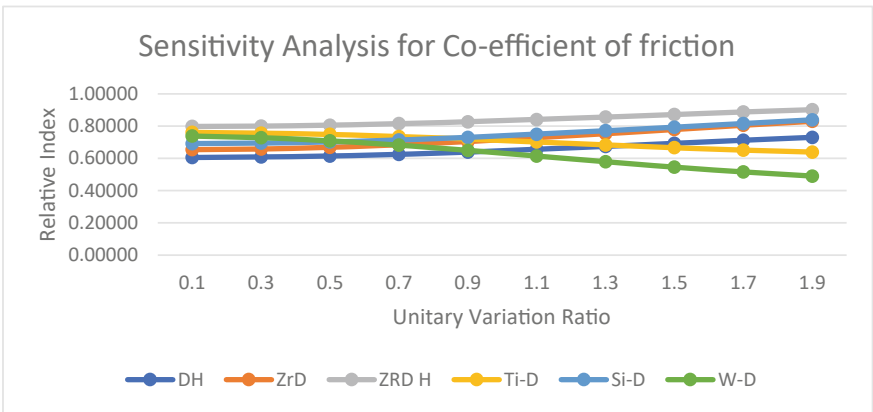


Fig. 8 Sensitivity analysis for co-efficient of friction ( $\mu$ )

**Table 10** Relative index values of each alternative based on  $H/E$  ratio

Unitary variation ratio	Alternatives					
	DLC-H	ZR-DLC	ZR-DLC-H	Ti-DLC	Si-DLC	W-DLC
0.1	0.63097	0.70470	0.82705	0.69639	0.73069	0.61248
0.3	0.63214	0.70551	0.82752	0.69743	0.73134	0.61389
0.5	0.63461	0.70722	0.82853	0.69963	0.73272	0.61684
0.7	0.63847	0.70993	0.83011	0.70308	0.73490	0.62146
0.9	0.64379	0.71368	0.83232	0.70782	0.73794	0.62777
1.1	0.65058	0.71851	0.83516	0.71385	0.74189	0.63576
1.3	0.65878	0.72441	0.83865	0.72110	0.74674	0.64530
1.5	0.66828	0.73133	0.84276	0.72949	0.75248	0.65624
1.7	0.67893	0.73921	0.84744	0.73884	0.75908	0.66836
1.9	0.69056	0.74792	0.85264	0.74901	0.76645	0.68142

**Table 11** Relative index values of each alternative based on  $H^3/E^2$  ratio

Unitary variation ratio	Alternatives					
	DLC-H	ZR-DLC	ZR-DLC-H	Ti-DLC	Si-DLC	W-DLC
0.1	0.56933	0.66435	0.80387	0.64061	0.69937	0.53374
0.3	0.57546	0.66814	0.80601	0.64621	0.70221	0.54205
0.5	0.58845	0.67633	0.81066	0.65805	0.70844	0.55926
0.7	0.60806	0.68913	0.81800	0.67581	0.71835	0.58434
0.9	0.63305	0.70614	0.82789	0.69824	0.73185	0.61498
1.1	0.66162	0.72647	0.83987	0.72361	0.74844	0.64858
1.3	0.69194	0.74896	0.85327	0.75021	0.76734	0.68297
1.5	0.72255	0.77246	0.86738	0.77670	0.78764	0.71662
1.7	0.75239	0.79602	0.88159	0.80217	0.80848	0.74864
1.9	0.78084	0.81895	0.89541	0.82612	0.82916	0.77859

**Table 12** Relative index values of each alternative based on critical load (*N*)

Unitary variation ratio	Alternatives					
	DLC-H	ZR-DLC	ZR-DLC-H	Ti-DLC	Si-DLC	W-DLC
0.1	0.69856	0.73353	0.82447	0.70289	0.95398	0.63440
0.3	0.69447	0.73226	0.82512	0.70345	0.90797	0.63420
0.5	0.68600	0.72955	0.82652	0.70463	0.85763	0.63377
0.7	0.67323	0.72530	0.82872	0.70650	0.80879	0.63309
0.9	0.65658	0.71946	0.83179	0.70910	0.76221	0.63214
1.1	0.63672	0.71208	0.83574	0.71243	0.71797	0.63092
1.3	0.61443	0.70328	0.84054	0.71648	0.67597	0.62944
1.5	0.59045	0.69327	0.84613	0.72116	0.63610	0.62772
1.7	0.56543	0.68229	0.85241	0.72637	0.59820	0.62581
1.9	0.53993	0.67064	0.85926	0.73199	0.56214	0.62376

**Table 13** Relative index values of each alternative based on co-efficient of friction ( $\mu$ )

Unitary variation ratio	Alternatives					
	DLC-H	ZR-DLC	ZR-DLC-H	Ti-DLC	Si-DLC	W-DLC
0.1	0.60551	0.65406	0.79811	0.76114	0.69174	0.73842
0.3	0.60842	0.65870	0.80070	0.75710	0.69516	0.72891
0.5	0.61483	0.66872	0.80634	0.74852	0.70266	0.70950
0.7	0.62505	0.68422	0.81518	0.73563	0.71452	0.68188
0.9	0.63891	0.70446	0.82691	0.71949	0.73050	0.64901
1.1	0.65572	0.72812	0.84085	0.70163	0.74981	0.61389
1.3	0.67444	0.75367	0.85609	0.68361	0.77137	0.57899
1.5	0.69386	0.77975	0.87177	0.66672	0.79404	0.54608
1.7	0.71284	0.80534	0.88720	0.65177	0.81684	0.51629
1.9	0.73049	0.82977	0.90192	0.63914	0.83905	0.49028

## References

1. Anojkumar L, Ilangkumaran M, Sasirekha V (2014) Comparative analysis of MCDM methods for pipe material selection in sugar industry. *Expert Syst Appl* 41(6):2964–2980
2. Athanasopoulos G, Riba CR, Athanasopoulou C (2009) A decision support system for coating selection based on fuzzy logic and multi-criteria decision making. *Expert Syst Appl* 36(8):10848–10853
3. Athawale VM, Kumar R, Chakraborty S (2011) Decision making for material selection using the UTA method. *Int J Adv Manuf Technol* 57(1):11–22
4. Cables EH, Lamata MT, Verdegay JL (2019) Ideal reference method with linguistic labels: a comparison with LTOPSIS. In: *Uncertainty management with fuzzy and rough sets*. Springer, Cham, pp 115–126
5. Cables E, Lamata MT, Verdegay JL (2018) FRIM—fuzzy reference ideal method in multi-criteria decision making. In: *Soft computing applications for group decision-making and*



- consensus modeling. Springer, Cham, pp 305–317
6. Çalışkan H (2013) Selection of boron based tribological hard coatings using multi-criteria decision-making methods. *Mater Des* 50:742–749
  7. Chakraborty S, Das PP, Kumar V (2017) A grey fuzzy logic approach for cotton fibre selection. *J Inst Eng (India): Series E* 98(1):1–9
  8. Chakraborty S, Kumar V, Ramakrishnan K (2018) Selection of the all-time best World XI test cricket team using the TOPSIS method. *Decision Sci Lett* 8(1):95–108
  9. Chakraborty S, Das PP, Kumar V (2018b) Application of grey-fuzzy logic technique for parametric optimization of non-traditional machining processes. *Grey Syst* 8(1):46–68
  10. Chakraborty S, Kumar V (2021) Development of an intelligent decision model for non-traditional machining processes. *Decision Making Appl Manag Eng* 4(1):194–214
  11. Chauhan A, Vaish R (2013) Hard coating material selection using multi-criteria decision making. *Mater Des* 44:240–245
  12. Delgado A, Reyes EC (2016) Applying Shannon entropy to select alternative plants as food for livestock: a case study in Ecuador. In: *IEEE CACIDI 2016-IEEE conference on computer sciences*. IEEE, pp 1–5
  13. Field SK, Jarratt M, Teer DG (2004) Tribological properties of graphite-like and diamond-like carbon coatings. *Tribol Int* 37(11–12):949–956
  14. Girubha RJ, Vinodh S (2012) Application of fuzzy VIKOR and environmental impact analysis for material selection of an automotive component. *Mater Des* 37:478–486
  15. Hafezalkotob A, Hafezalkotob A (2016) Extended MULTIMOORA method based on Shannon entropy weight for materials selection. *Journal of Industrial Engineering International* 12(1):1–13
  16. Hainsworth SV, Uhure NJ (2007) Diamond like carbon coatings for tribology: production techniques, characterisation methods and applications. *Int Mater Rev* 52(3):153–174
  17. Kumar V, Chakraborty S (2022) Analysis of the surface roughness characteristics of EDMed components using GRA method. In: *Proceedings of the international conference on industrial and manufacturing systems (CIMS-2020)*. Springer, Cham, pp 461–478
  18. Kumar V, Das PP, Chakraborty S (2020) Grey-fuzzy method-based parametric analysis of abrasive water jet machining on GFRP composites. *Sādhanā* 45(1):1–18
  19. Kumar V, Diyaley S, Chakraborty S (2020) Teaching-learning-based parametric optimization of an electrical discharge machining process. *Facta Universitatis Series Mech Eng* 18(2):281–300
  20. Kumar V, Kalita K, Chatterjee P, Zavadskas EK, Chakraborty S (2021) A SWARA-CoCoSo-based approach for spray painting robot selection. *Informatica* 1–20
  21. Lotfi FH, Fallahnejad R (2010) Imprecise Shannon's entropy and multi attribute decision making. *Entropy* 12(1):53–62
  22. Li P, Qian H, Wu J, Chen J (2013) Sensitivity analysis of TOPSIS method in water quality assessment: I. Sensitivity to the parameter weights. *Environ Monitoring Assessment* 185(3):2453–2461
  23. Mousavi-Nasab SH, Sotoudeh-Anvari A (2017) A comprehensive MCDM-based approach using TOPSIS, COPRAS and DEA as an auxiliary tool for material selection problems. *Mater Des* 121:237–253
  24. Ni W, Cheng YT, Lukitsch MJ, Weiner AM, Lev LC, Grummon DS (2004) Effects of the ratio of hardness to Young's modulus on the friction and wear behavior of bilayer coatings. *Appl Phys Lett* 85(18):4028–4030
  25. Pahan F, Dambhare S, Mali A, Nawale S (2018) Implementation of multi-criteria decision making for selection of coating material on AISI 4140 steel. *Int Res J Eng Technol* 5(12):1514–1517
  26. Prakash C, Kumar V, Mistri A, Uppal AS, Babbar A, Pathri BP, Mago J, Sharma A, Singh S, Wu LY, Zheng HY (2021) Investigation of functionally graded adherents on failure of socket joint of FRP composite tubes. *Materials* 14(21):1–13
  27. Prasad RV, Rajesh R, Thirumalaikumarasamy D (2020) Selection of coating material for magnesium alloy using fuzzy AHP-TOPSIS. *Sādhanā* 45(1):1–20

28. Sánchez-Lozano JM, Rodríguez ON (2020) Application of fuzzy reference ideal method (FRIM) to the military advanced training aircraft selection. *Appl Soft Comput* 88:106061
29. Sedlaček M, Podgornik B, Vižintin J (2008) Tribological properties of DLC coatings and comparison with test results: development of a database. *Mater Charact* 59(2):151–161
30. Sharma A, Kumar V, Babbar A, Dhawan V, Kotecha K, Prakash C (2021) Experimental investigation and optimization of electric discharge machining process parameters using grey-fuzzy-based hybrid techniques. *Materials* 14(19):1–21
31. Sofuoğlu MA (2017) Hybridizing Taguchi algorithm with reference ideal method to solve machining problems. *Int J Intell Syst Appl Eng* 5(2):64–69
32. Van der Kolk GJ (2008) Wear resistance of amorphous DLC and metal containing DLC in industrial applications. In: *Tribology of diamond-like carbon films*. Springer, Boston, MA, pp 484–493
33. Veverkova J, Hainsworth SV (2008) Effect of temperature and counterface on the tribological performance of W-DLC on a steel substrate. *Wear* 264(7–8):518–525
34. Vitu T, Escudeiro A, Polcar T, Cavaleiro A (2014) Sliding properties of Zr-DLC coatings: the effect of tribolayer formation. *Surf Coat Technol* 258:734–745
35. Voevodin AA, Rebbholz C, Matthews A (1995) Comparative tribology studies of hard ceramic and composite metal-DLC coatings in sliding friction conditions. *Tribol Trans* 38(4):829–836
36. Voevodin AA, Zabinski JS (1998) Superhard, functionally gradient, nanolayered and nanocomposite diamond-like carbon coatings for wear protection. *Diam Relat Mater* 7(2–5):463–467

# COMSOL Simulation to Predict the Thickness of Material Removed from Surface During Electropolishing



Abhinav Kumar, Manjesh Kumar, H. N. S. Yadav, and Manas Das

**Abstract** Electropolishing (EP) is a non-traditional polishing method which is governed by Faraday's law of electrolysis. An experimental setup is design and developed to perform the EP of maraging steel. EP removes some layers of material from the surface to achieve a mirror finish polish surface. In this paper, a simulation of 2D model is developed to predict the thickness of material removed from the work-piece surface during EP to achieve mirror like surface finish. A finite element-based COMSOL software is used to design the model for EP. A comparative analysis of thickness removal from experiment and simulation is done. The measured thickness of material removed is 13.16  $\mu\text{m}$  and 14.51  $\mu\text{m}$  from experiment and simulation, respectively. The surface roughness, Ra is also measured and it is 0.276  $\mu\text{m}$  before EP, which reduces to 0.107  $\mu\text{m}$  after EP, an improvement of about 61% is observed.

**Keywords** Electropolishing · Thickness removal · Surface roughness · Polarization curve · COMSOL

## 1 Introduction

Electropolishing (EP) is finishing process which removes material from the surface and reduces the surface roughness. In EP, removal of metal takes place in the form of ions by ions from the surface [1]. It is a non-conventional process and the fundamental principal behind electropolishing is Faraday's law of electrolysis [2]. The metallic surface which had to electropolished is dipped into the electrolyte along with the tool and connected to the positive and negative terminal of power supply, respectively. Generally, strong acid such as phosphoric acid, sulphuric and their mixture is used as electrolyte [3]. Metal which is to be is electropolished is made anode and appropriate tool is selected to make it as cathode, such that it will be inert during EP. Researchers have utilized several tool such as copper [4], titanium mesh [5] and

---

A. Kumar (✉) · M. Kumar · H. N. S. Yadav · M. Das  
Department of Mechanical Engineering, Indian Institute of Technology Guwahati, Guwahati,  
India  
e-mail: [kumar176103020@iitg.ac.in](mailto:kumar176103020@iitg.ac.in)

© The Author(s), under exclusive license to Springer Nature Singapore Pte Ltd. 2023  
R. P. Singh et al. (eds.), *Advances in Modelling and Optimization of Manufacturing and Industrial Systems*, Lecture Notes in Mechanical Engineering,  
[https://doi.org/10.1007/978-981-19-6107-6\\_23](https://doi.org/10.1007/978-981-19-6107-6_23)

321

graphite [6]. The foremost function of the tool is to complete the circuit, i.e. it should be conducting and it should not chemically react with the electrolyte. During EP, a viscous film layer of vary thickness is formed at the anode surface due to dissolution and limits mass transport due to resistance property. The viscous layer formed has maximum thickness over the micro-depression and minimum thickness over the micro-projection. As thickness of viscous layer is minimum over micro-projection hence its provide minimum electrical resistance which result greater metal removal rate compare to micro-depression area hence, creates a polishing effect which leads to uniform surface after electropolishing [7]. The polarized surface is formed during EP due to evaluation of gas which form passive oxide film on the surface result in increase in corrosion resistance and biocompatibility [8]. Łyczkowska-Widłak et al. [9] had reviewed the electrochemical polishing (ECP) of austenitic stainless steel. Studied has been carried on different mechanism, parameters, electrolyte solution and the results. ECP is capable of improving the surface finish, chemical composition, surface gloss and corrosion resistant. Two layers namely, viscous and oxide layer are formed over the anode surface. These layers limit the migration of hydrated ions and diffusion of water particles in the electric field. Also discussed the effect of aqueous and organic solvent in ECP. It also reduces the adhesion of bacteria and blood cells, which increases the durability and usability.

Any polishing technique either conventional or non-conventional, some thickness of the material is removed from the surface to achieve polished surface. Han and Fang [1] had briefly describe about the fundamental aspects of EP. It was mentioned that as polishing time increases, more material is removed from the surface which leads to dimensional inaccuracies and results in poor surface finish. Tyagi et al. [10] had utilized EP for the roughness reduction of steel manufactured by additive method. It was observed that more than 200  $\mu\text{m}$  thick material had to remove from the top surface to get a good polished surface of 0.091  $\mu\text{m}$ . As polishing time increases, the rate of decrease of surface roughness is high, however this rate decreases after sometime, although material removal continues [11].

The selection of parameters for EP is very significant for the better surface finish. The initial surface roughness directly influences the EP and affects the polishing time [1]. Lee [7] has investigated the characteristics of electropolishing of tube made of stainless steel (STS316L). The parameters investigated were current density, temperature, machining time, electrode gap and initial surface roughness of workpiece. A current density–voltage curve was drawn to find the electropolishing range. A copper rod was used as cathode and place inside the hollow steel tube. The electrolyte consists of 50% (vol.) phosphoric acid, 20% (vol.) sulphuric acid and 30% (vol.) distilled water. They concluded that current density is the most influencing parameter for electropolishing. Surface roughness of the surface increases with increase in polishing time. An electrode gap of 1 mm and temperature of 65 °C gave best result of 0.59  $\mu\text{m}$   $R_{\text{max}}$ . The acidic electrolytes are harmful and proper care has to be taken whilst handling, however acidic medium gives better polishing effect than the salt solution [12]. More smooth and reflective surface for acidic electrolyte. Higher current density is required for basic electrolyte than the acidic electrolyte [13].

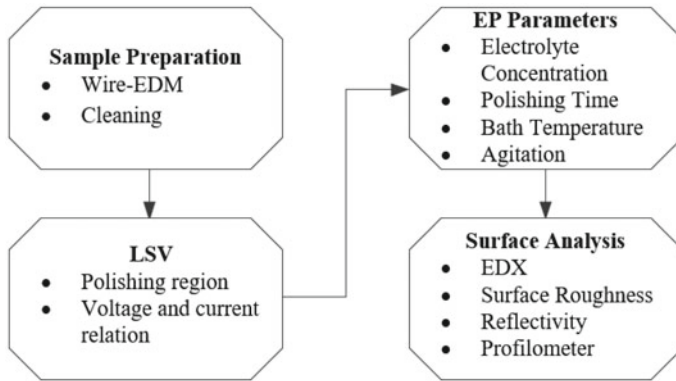
Higher the concentration of the acid in the electrolyte, thicker will be the viscous layer. It will obstruct the escape of gas bubbles and higher limiting current is required to passive layer to perform the EP. Viscous layer thickness reduces on increasing the stirrer speed [13]. Electrolyte temperature plays a crucial role in EP as increase in temperature increases the rate of material dissolution as current density increases. However, higher the temperature of the electrolyte, more electrolyte will convert into vapour, which is harmful to the environment as well as operator. Another important parameter is the polishing time. More material is dissolved on increasing the polishing time.

With the help of numerical modelling, it will be easier to predict the dissolution and the amount the material dissolve. Ma et al. [14] had formulated a model to determine the thickness of material dissolve. The formulated model was the function of the polishing time, applied voltage and the gap between the electrodes. Taylor et al. [15] had investigated the formation of passive layer and its stability during EP by numerical modelling. Various parameters of EP have been considered and its effect on uniformity of passive layer.

In this paper, EP of maraging steel is performed with ortho-phosphoric acid (64%), sulphuric acid (34%) and hydrochloric acid (2%) as an electrolyte. Linear sweep voltammetry is performed to find the constant current zone suitable for EP. Energy dispersive X-ray spectroscopy (EDX) has been done to analyse the elemental composition before and after EP. Surface profilometer is used to measure the thickness of material remove from the surface after EP. A 2D simulation model is developed to predict the thickness of material remove and compare it with the experimental results. With the help of non-contact surface analyser, surface roughness,  $R_a$  (average surface roughness) is measured before and after EP. The effect of EP on surface reflectance has also been analysed.

## 2 Experimental Procedure of EP

The sample preparation is the pre-requisite for starting of electropolishing. In the present investigation, maraging steel is considered as the workpiece over which EP has to be performed. A sample size of 25 mm × 10 mm × 3 mm has been cut with the help of wire-EDM. After wire-EDM, several dirt's and stains stick to the sample. The cut sample has been de-ionized by placing into the ultrasonicator for 15 min. Finally, it is cleaned with acetone to remove the dirt's. Before EP, the surface must be clean. Now, the main requirement for EP to take place is to find the polishing region. The polishing region can be found through polarization curve also known as linear sweep voltammetry (LSV). Different combination of metal and the electrolyte exhibit different polarization curve. Therefore, polarization curve should be drawn initially for every metal with a particular electrolyte combination to find the constant current region suitable for EP. From the preliminary experiments, EP parameters like electrolyte concentration, polishing time, electrolyte temperature and agitation have been selected for the investigation. Post analysis of EP surface



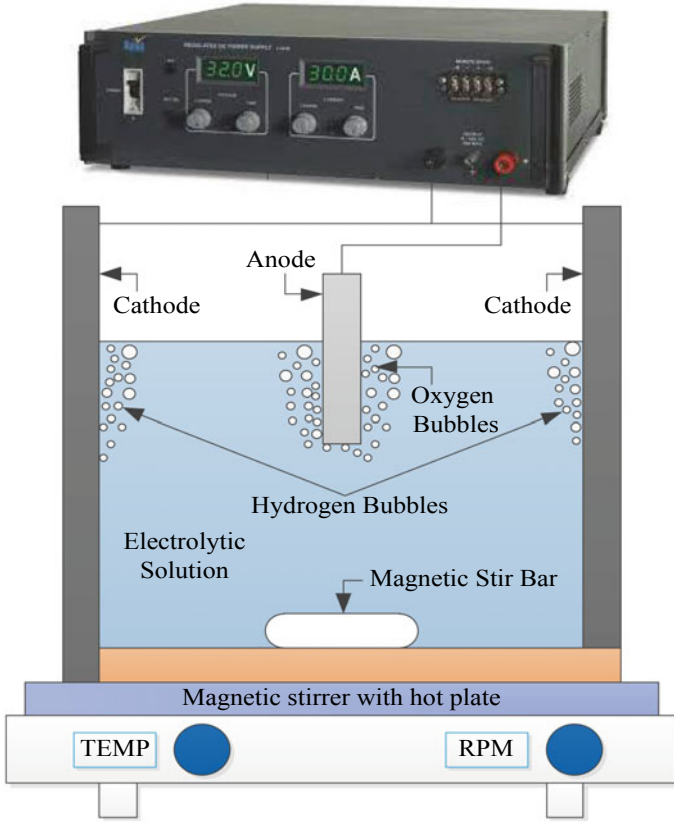
**Fig. 1** Flow chart of EP process

has been performed by utilizing EDX, which tells about the elemental composition before and after EP; reflectance, which tells about the surface reflectiveness before and after EP; roughness, which tells about the surface roughness before and after EP and profilometer, which tells about the thickness of material removed from the surface after EP. The complete analysis of EP has been presented as a flow chart and the same is shown in the Fig. 1.

The schematic setup for electropolishing has been shown in Fig. 2. It consists of an electrolytic cell in which the workpiece (maraging steel), which has to be electropolished, is connected to positive terminal of power supply and the tool (graphite) is connected to the negative terminal of power supply (make-Aplab). The rating of the power supply is 60 V and 30 A. Both the tool and workpiece are dipped into the electrolyte. The workpiece is dipped half and another half is covered such that it will not participate in EP. On the application of potential difference between the electrodes, hydrogen and oxygen gas bubbles are formed during EP which has to be removed from the electrode surface for continuous EP. A magnetic stirrer with hot plate (make-Tarson) has been used to heat the electrolyte and with the help of magnetic bid, circulation is provided in the electrolyte to easily remove the gas evolved during EP.

The parameters at which experiments are performed are presented in Table 1. It consists of volumetric ratio of different electrolyte utilized for the EP of maraging steel. As graphite sheets are inert and does not participate during EP, it is selected as a tool material. The selection of input voltage was determined from the polarization curve. The selection of polishing time and speed of magnetic stirrer was selected from preliminary experiments. All the experiments were performed at room temperature.

EP takes place during the constant current density when the electrodes are dipped in the electrolyte after applying the potential. To determine the EP zone, linear sweep voltammetry has to be performed which consists of three electrodes namely, the reference electrode (Ag/AgCl), the working electrode (maraging steel) and the counter electrode (platinum wire). The potential is sweep from 4.5 to 0 V with a scan rate



**Fig. 2** Schematic of EP setup

**Table 1** Parameters for EP

Parameters	Value or range
Electrolyte	Ortho-phosphoric acid (64%), sulphuric acid (34%) and hydrochloric acid (2%)
Electrolyte temperature	Room temperature
Workpiece material	Maraging steel 300
Tool material	Graphite sheet
Input voltage	2 V
Electrolyte conductivity	30–60 mS/cm
Polishing time	6 min
Magnetic stirrer	400 rpm

of 10 mV/s at room temperature with the help of the potentiostat (make-Gamry). The potential must be sweep from positive values towards the cathodic direction to obtain reproducible measurements and to avoid the pitting of electrode surface [16].

To analyse the elemental composition of the surface before and after EP, Energy Dispersive X-Ray Spectroscopy (EDX) has been done (make-Sigma, Zeiss). The height difference between the surfaces before and after EP is measured with the help of stylus surface profilometer (make-Dektak150). An optical non-contact surface analyser (make-Taylor Hobson) is used to measure the surface roughness before and after EP. The surface reflectance before and after EP has also measured to find the effect of EP on reflectivity of the surface using UV spectrometer (make-Lambda 950).

### 3 Modelling of EP Process

To analyse the thickness of material removed from the surface during EP, a model has been developed in the XY plane in COMSOL<sup>®</sup> Multiphysics software, which works on finite element. The electrochemistry module consists of primary current distribution in COMSOL, which is governed by Faraday's law of electrolysis is the best suited for application [17].

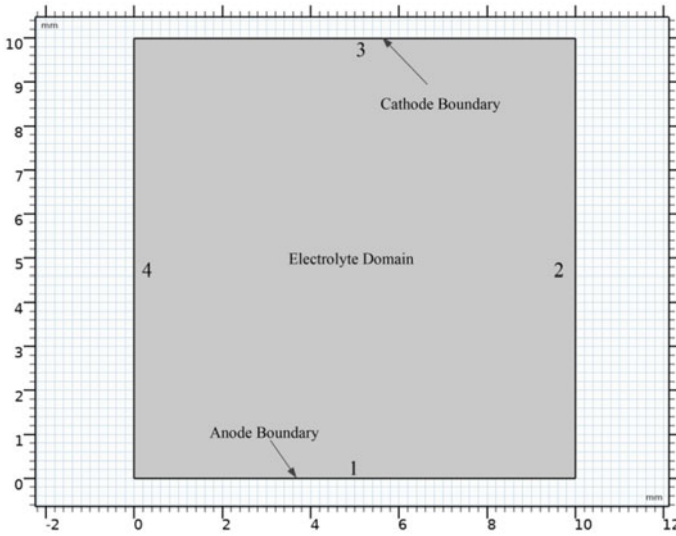
A 2-dimensional investigation was selected for solving the boundary condition and consumes less time also. As the material is removed from the anode surface, it was selected as the deformed geometry. As the EP is an anodic dissolution process, the workpiece undergoes anodic dissolution and the tool acts as cathode. Certain assumptions are considered whilst performing EP simulation [15].

- The time-dependent concentration term is zero.
- The temperature is constant which implies that the electrolyte properties remain unaltered.
- The dissolution occurs only at the anode.
- Bubble formation and sludge generation are assumed to have negligible effect.
- Efficiency of current is assumed to be 100%.

The 2D geometry of EP model has been shown in Fig. 3. It consists of one electrolyte domain with four boundaries. The tool is facing towards the workpiece which has to be electropolished. The interelectrode gap (IEG) between the electrodes is 10 mm.

As shown in Fig. 3, anode boundary (workpiece surface) and cathode boundary (tool surface) are denoted by 1 and 3, respectively. Boundaries 2 and 4 acts as insulation as they do not participate in EP. In EMM, workpiece undergoes anodic dissolution process, material from the workpiece surface will dissolve potential difference is applied. For the simulation, the boundary conditions have been applied to the surfaces as shown in Table 2.





**Fig. 3** 2D Geometry of the EP model

**Table 2** Electric current boundary condition

Boundary condition	Boundary	Property
Electrical insulation	2, 4	$\frac{d\varphi}{dn} = 0$
Electrical potential	Workpiece surface (1)	$\varphi = 2\text{ V}$
Ground	Tool surface (3)	$\varphi = 0$

Where  $\varphi$  is the potential applied to the electrode surfaces and  $d\varphi/dn$  is the potential gradient applied to the boundary normal to the tool and the workpiece

The potential applied to anode surface and the cathode surfaces are 2 V and 0 V, respectively. The dissolving species like the density ( $\rho$ ) and molecular weight ( $M$ ) has been applied to the anode as it will undergo anodic dissolution. All the boundaries are arrested except the anode. So, all the surfaces have non-deforming boundary and for the anode have the deforming electrode surface [18]. Primary current distribution has been assigned to the domain which is governed by Ohm’s law.

The boundaries of the domain will undergo deformation as described in Table 3. The workpiece surface will be polished and the surface will deform by anodic dissolution. The tool surface remains intact at its place, thus no movement of tool is provided in  $x$  as well as  $y$ -direction. During EP, the normal boundaries (2, 4) should not have any velocity in  $x$ -direction.

**Table 3** Deformable mesh boundary conditions

Boundary condition	Boundary	Property
Prescribed normal mesh velocity	Workpiece surface (1)	$V_n = -K J_n$
Prescribed mesh displacement	Tool surface (2)	$dx = 0; dy = 0$
Prescribed mesh velocity	2, 4	$V_x = 0$

Where  $K = \eta M / \rho z F$ ,  $\eta$  is the efficiency of current,  $F$  is Faraday's electrolysis constant and  $M$ ,  $z$  and  $\rho$  is atomic mass, valence and the density of the dissolving species,  $J_n$  is the normal current density and  $V_n$  is the linear material removal rate

## 4 Results and Discussion

In this section, the results obtained from experiments and simulations are presented. The parameter is the same for experiments as well as for simulations and the same is presented in Table 1. A brief discussion has been performed before and after EP and linear material removed has been compared with the experimental results with the simulation results.

### 4.1 Electrochemical Analysis

Linear sweep voltammetry (LSV) has been utilized to find the maraging steel polarization behaviour for the selected electrolyte and the same is shown in Fig. 4. It consists of three electrodes system to determine the region of EP. The LSV is done at room temperature by changing the potential from 4.5 V to 0 V with 10 mV/s as the scan rate. The polarization curve is obtained for the electrolyte which consists of Ortho-phosphoric acid (64%), Sulphuric acid (34%) and Hydrochloric acid (2%). It consists of three regions. The region from 0 to 0.38 V is the active region (I) in which increase in potential increases current. In this region, etching takes place and material starts to dissolve with pits marks over the surface. The region from 0.38 to 2.05 V is the passive region (II), in which current is stable with respect to increase in voltage. After this, the current increases quickly in the transpassive region (III). As per literatures, EP occurs only in passive region [19]. Based on the curve Fig. 4, the activation potential ( $E_a$ ) was 0.2 V, the passivation potential ( $E_p$ ) was 0.38 V and the breakdown potential ( $E_b$ ) was 2.05 V. The region (I) between potential  $E_a$  to  $E_p$  represent active region. In this region the sample will be etched and the surface could not be smoothed. When potential is between  $E_p$  and  $E_b$ , it is termed as passive region (II) and a viscous layer is formed on the sample surface which is made up metal ions. For electropolishing, 2 V is preferred. The region beyond  $E_b$  is called transpassive layer. A serrated current curve is observed in this region which results in non-uniform dissolution of the sample surface due to huge amount of gas bubbles formation.

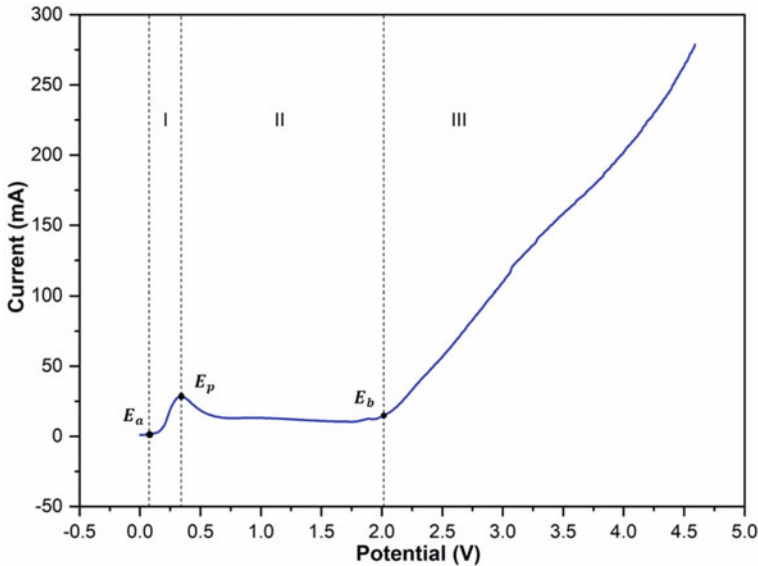


Fig. 4 Polarization curve of Maraging steel

## 4.2 Effect of EP on Elemental Composition

In order to understand the effect of EP on elemental composition, EDX have been performed for the maraging steel before and after EP. The sample after cutting in the desired shape by wire-EDM, cleaned and then EDX has been performed and the same is shown in Fig. 5. It can be inferred from Fig. 5 that iron (Fe), nickel (Ni), cobalt (Co) and molybdenum (Mo) are the major constituents of maraging steel with fine traces of titanium (Ti), oxygen (O) and aluminium (Al). As the percentage of oxygen is very less, it is very prone to corrosion.

The cleaned sample have been electropolished and EDX is performed to investigate the change occurred in the elemental composition and the same is presented in Fig. 6. It can be inferred from Fig. 6 that after EP, there are slight changes in the composition of Fe, Ni and O<sub>2</sub>. After EP, concentration of O<sub>2</sub> increases, there is a possibility that oxide layer has been formed which increases corrosion resistant [4, 8]. Oxygen may have formed the oxide layer with the Ni which acts as corrosion inhibitor.

## 4.3 Effect of EP on Surface Reflectance

In order to understand the effect of EP on surface reflectance, the samples before and after EP has been studied under the UV spectrometer. Initially, a silver sample

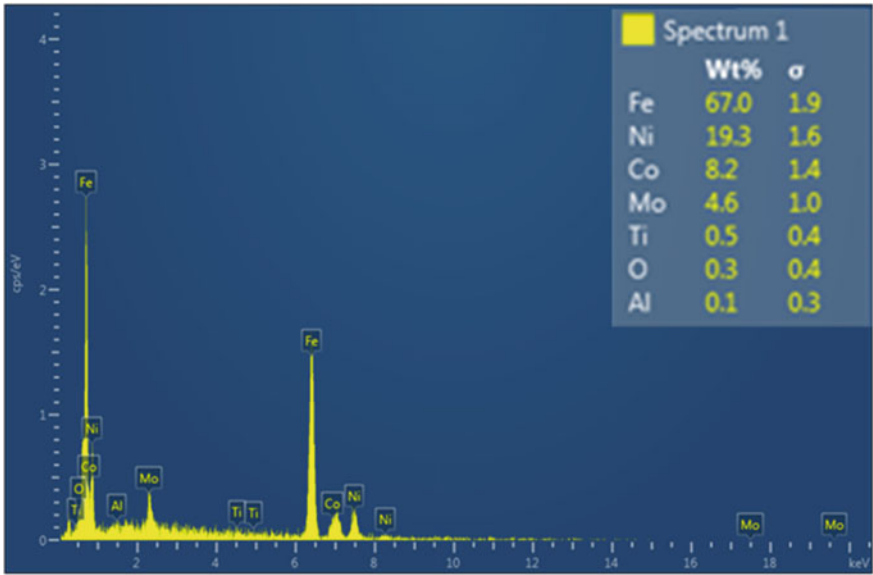


Fig. 5 Elemental composition before EP

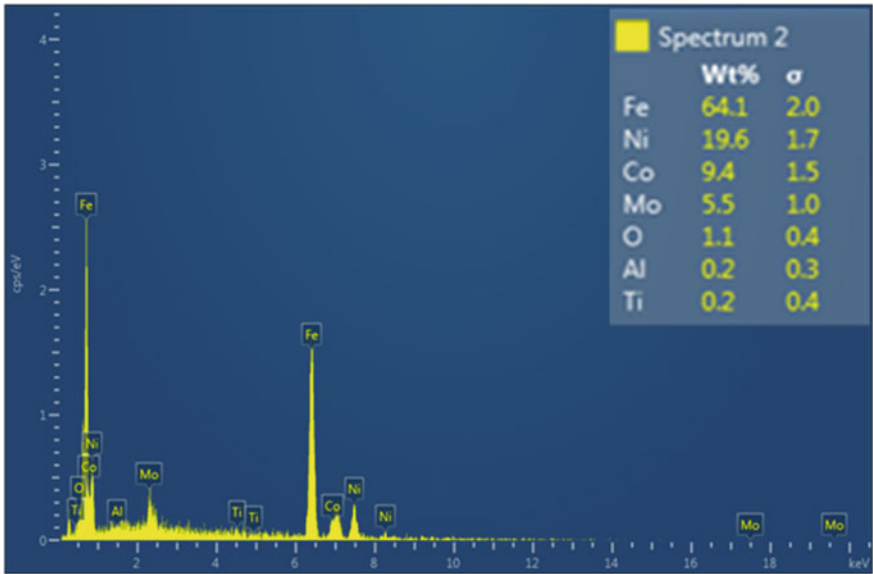
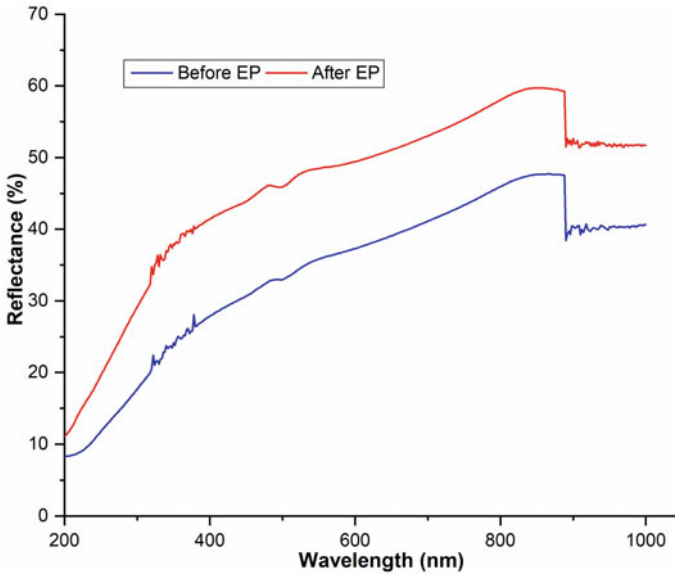


Fig. 6 Elemental composition after EP



**Fig. 7** Surface reflectance before and after EP

with mirror finish is tested for reflectance by varying the wavelength of light from 1000 to 200 nm and the data is recorded. With reference to the above reflectance, the reflectance of sample before and after EP has been presented in Fig. 7.

The base material (before EP) is kept in the spectrometer and the wavelength is varied to observe its reflectance. The maximum reflectance of  $\sim 45\%$  is observed. The sample after EP yields a maximum reflectance of  $\sim 60\%$ , an improvement of 33.33% is observed. The removal of layer from the top surface after EP may be the possible reason for the improvement in surface reflectance. High reflective surface finds application in radiation sensitive area and helps to minimize the increase of surface temperature [10].

#### 4.4 Effect of EP on Surface Roughness

The polishing time is very crucial factor for the EP as polishing time increases, more amount of material undergoes anodic dissolution and it also enhances surface finish [20]. However, the improvement of surface roughness is negligible after certain polishing time as all the protrusions are dissolved and came to the level of valley. In can be inferred from Fig. 8 that initially the surface roughness of the base material is  $0.276 \mu\text{m}$  and with increase in polishing time, the surface roughness decreases. However, after 300 s of polishing time, improvement of surface roughness is very less. Thus, the polishing time of 360 s was considered for the present investigation.

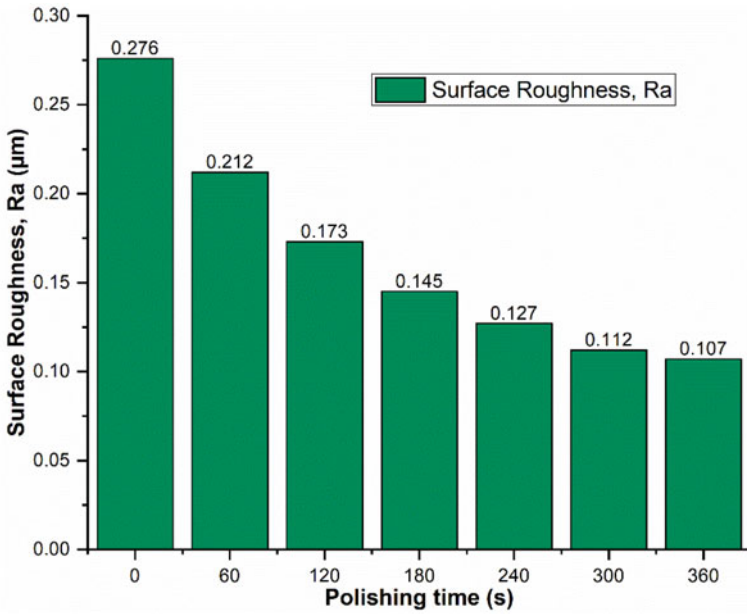


Fig. 8 Effect of polishing time on surface roughness

The 2D surface roughness profile of the maraging steel before EP and after EP has been analysed and the same is shown in Fig. 9. Before EP, the Ra value is 0.276 µm, which reduces to 0.107 µm, an improvement of about 61% is observed. EP reduces the undulation in the surface by creating a viscous layer over the surface, thus an improvement of surface roughness is observed [10]. It can be inferred from Fig. 9 that before EP (blue colour line), the undulation in the surface is quite large. However, after EP (red colour line), the undulation in the surface is very small, which describes that EP minimizes the surface roughness.

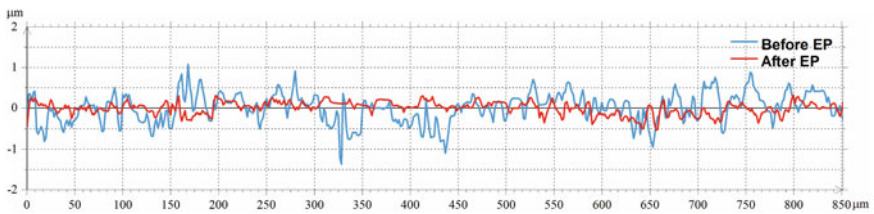
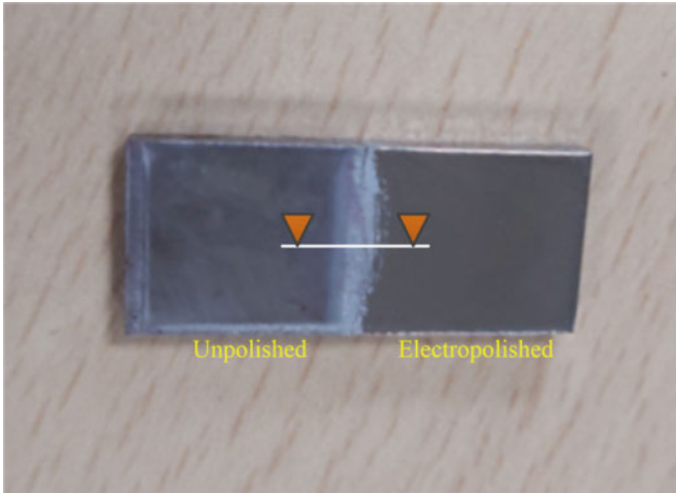


Fig. 9 Surface roughness profile before and after EP



**Fig. 10** Image with white colour line from unpolished to electropolished region

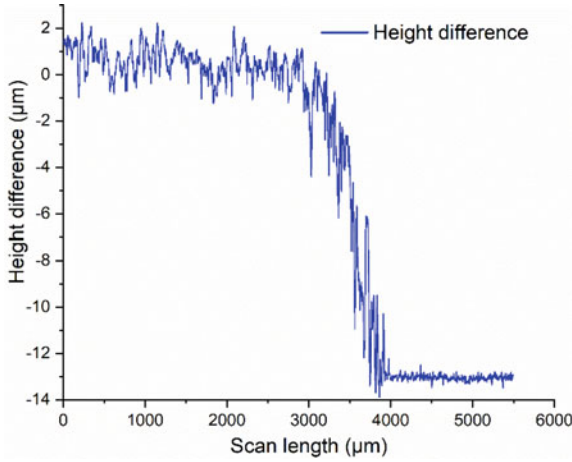
#### ***4.5 Thickness of Material Removed During EP***

The maraging steel is electropolished and it is tried to find the thickness of the material removed from the surface after EP. An optical microscopic image is considered which clearly distinguish between the unpolished and electropolished surface as shown in Fig. 10. With the help of surface profilometer, the stylus is moved from the unpolished surface to the electropolished surface as shown by white colour line in Fig. 10. Electropolished surface is very smooth and possess more reflectance property.

With the help of a stylus profilometer, it was tried to find the height difference between the unpolished and electropolished region. As the probe is very sensitive, as it glides over the sample, the unpolished surface is rough and the electropolished surface is smooth as shown in Fig. 11. The total distance travel by the stylus is 5500  $\mu\text{m}$  and it travel along the white line as shown in Fig. 10. The height difference obtained between the unpolished and electropolished surface is 13.16  $\mu\text{m}$ .

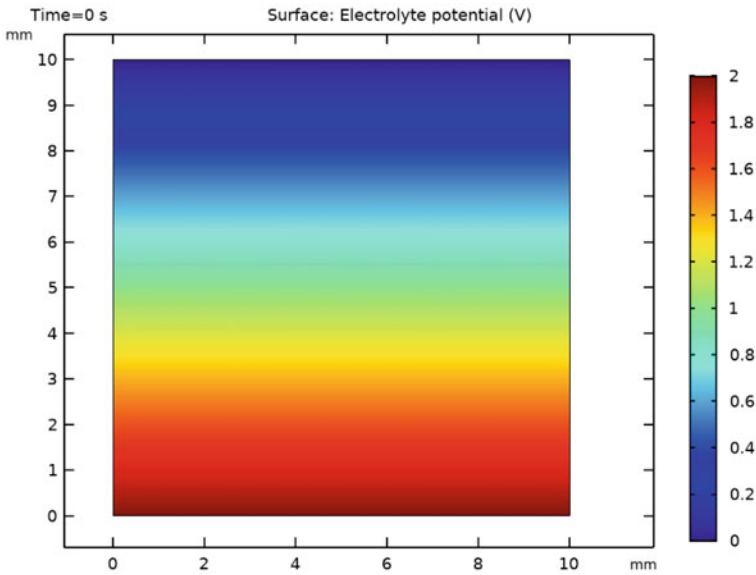
#### ***4.6 Numerical Modelling of Material Removal in EP***

COMSOL multiphysics simulation is performed to analyse the behaviour of maraging steel in the electrolyte [Ortho-phosphoric acid (64%), Sulphuric acid (34%) and Hydrochloric acid (2%)]. Primary current distribution is applied in the electrolyte domain between the tool and the workpiece. The same parameters as in experimental analysis are taken to compare the results between them. The potential distribution between the electrodes can be seen in Fig. 12 as the workpiece to be electropolished



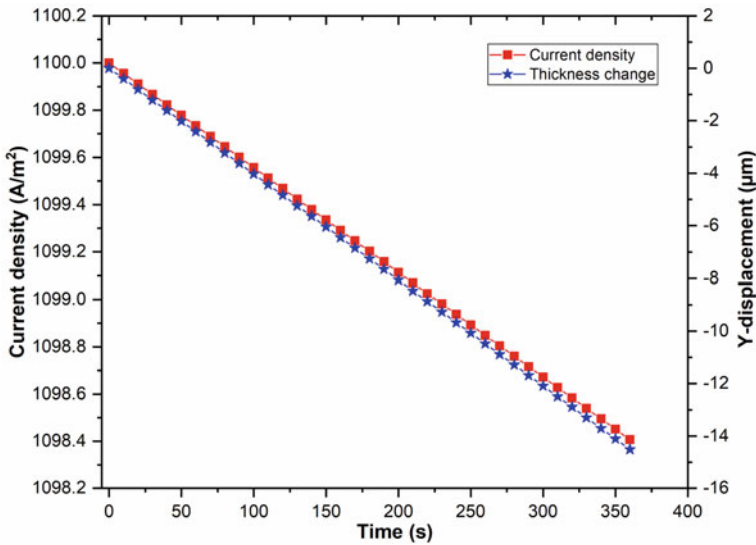
**Fig. 11** Height difference profile along the white colour line

is given the positive potential (2 V) and the tool is connected to the ground (0 V) (For geometry, refer Fig. 3). The potential distribution between the electrodes is uniform as it varies from anode to the cathode. The boundary conditions for the electrodes are presented in Tables 2 and 3. The material removed from the surface works on Faraday’s law of electrolysis.



**Fig. 12** Potential distribution between the anode and cathode





**Fig. 13** Current distribution and thickness change from 0 to 360 s

The anode undergoes anodic dissolution and the material from the surface removes till the EP takes place. The amount of current density generated is the influencing factor for material removal. For EP to take place, the current density should be maintained constant [1]. From the simulation results, the current density varies from 1100 to 1098.4 A/m<sup>2</sup> over a period of time from 0 to 360 s as shown in Fig. 13 (black colour line with square symbol). The change in current density is negligible and can be considered constant.

From Table 3, the material removes or thickness change from the surface is calculated and plotted in Fig. 13 (blue colour line with star symbol). The material removal is the function of current density. As the current density is almost constant, the thickness change will be linear and increases with polishing time. The final thickness change obtained after EP from simulation for 6 min is 14.51 μm. The thickness change is almost linear with respect to time for a constant current density [21].

## 5 Conclusions

Analysis to predict the thickness of material removed from the surface during EP has been done with the help of COMSOL<sup>®</sup> Multiphysics software. The various conclusions can be derived with the help of 2D model. Experiments are also performed to validate the model.

1. Polarization curve has been plotted using three electrode systems to find the EP zone (constant current region) for the specific material corresponding to an electrolyte.
2. EDX analysis has been performed to investigate the surface elemental composition before and after EP. It is found that the concentration of O<sub>2</sub> increases after EP, an oxide layer has been formed which increases corrosion resistant.
3. Effect of EP on the surface reflectance has been analysed. An improvement of 33.33% in surface reflectance has been observed after EP as surface gets smoother after EP.
4. 2D surface roughness profile before and after EP has been analysed. An improvement of around 61% is observed with mirror finish. During EP, a viscous layer is formed over the surface which creates a polishing effect and reduces the surface undulation.
5. An experimental setup is designed to perform the EP of maraging steel with the Ortho-phosphoric acid (64%), Sulphuric acid (34%) and Hydrochloric acid (2%) as an electrolyte for 6 min. The thickness of material removed from the surface is calculated using surface profilometer is 13.16 μm.
6. COMSOL<sup>®</sup> Multiphysics simulation is performed to predict the thickness of the material removed from the surface during EP. The predicted thickness of the material removed is 14.51 μm, with an error of 10.3% from the experimental value. Several assumptions are considered during simulation which may be the reason for the error.

## References

1. Han W, Fang F (2019) Fundamental aspects and recent developments in electropolishing. *Int J Mach Tools Manuf* 139(April):1–23. <https://doi.org/10.1016/j.ijmactools.2019.01.001>
2. Kumar A, Das M (2021) Multiphysics simulation and experimental investigation of micro-tool fabricated by EMM. *Mater Manuf Process* 36(13):1489–1500. <https://doi.org/10.1080/10426914.2021.1905837>
3. Landolt D (1987) Fundamental aspects of electropolishing. *Electrochim Acta* 32(1):1–11. [https://doi.org/10.1016/0013-4686\(87\)87001-9](https://doi.org/10.1016/0013-4686(87)87001-9)
4. Han W, Fang F (2019) Electropolishing of 316L stainless steel using sulfuric acid-free electrolyte. *J Manuf Sci Eng* 141(10). <https://doi.org/10.1115/1.4044518>
5. Han W, Fang F (2020) Investigation of electrochemical properties of electropolishing Co–Cr dental alloy. *J Appl Electrochem* 50(3):367–381. <https://doi.org/10.1007/s10800-019-01390-3>
6. Pendyala P, Bobji MS, Madras G (2014) Evolution of surface roughness during electropolishing. *Tribol Lett* 55(1):93–101. <https://doi.org/10.1007/s11249-014-0336-x>
7. Lee ES (2000) Machining characteristics of the electropolishing of stainless steel (STS316L). *Int J Adv Manuf Technol* 16(8):591–599. <https://doi.org/10.1007/s001700070049>
8. Habibzadeh S, Li L, Shum-Tim D, Davis EC, Omanovic S (2014) Electrochemical polishing as a 316L stainless steel surface treatment method: Towards the improvement of biocompatibility. *Corros Sci* 87:89–100. <https://doi.org/10.1016/j.corsci.2014.06.010>
9. Łyczkowska-Wiślak E, Lochyński P, Nawrat G (2020) Electrochemical polishing of austenitic stainless steels. *Materials (Basel)* 13(11):2557. <https://doi.org/10.3390/ma13112557>

10. Tyagi P et al (2020) Roughness reduction of additively manufactured steel by electropolishing. *Int J Adv Manuf Technol* 106(3–4):1337–1344. <https://doi.org/10.1007/s00170-019-04720-z>
11. Yang G, Wang B, Tawfiq K, Wei H, Zhou S, Chen G (2017) Electropolishing of surfaces: theory and applications. *Surf Eng* 33(2):149–166. <https://doi.org/10.1080/02670844.2016.1198452>
12. Ramasawmy H, Blunt L, Rajurkar KP (2005) Investigation of the relationship between the white layer thickness and 3D surface texture parameters in the die sinking EDM process. *Precis Eng* 29(4):479–490. <https://doi.org/10.1016/j.precisioneng.2005.02.001>
13. Han W, Fang F (2020) Eco-friendly NaCl-based electrolyte for electropolishing 316L stainless steel. *J Manuf Process* 58(October):1257–1269. <https://doi.org/10.1016/j.jmapro.2020.09.036>
14. Ma N, Xu W, Wang X, Tao B (2010) Pulse electrochemical finishing: modeling and experiment. *J Mater Process Technol* 210(6–7):852–857. <https://doi.org/10.1016/j.jmatprotec.2010.01.016>
15. Tailor PB, Agrawal A, Joshi SS (2015) Numerical modeling of passive layer formation and stabilization in electrochemical polishing process. *J Manuf Process* 18:107–116. <https://doi.org/10.1016/j.jmapro.2015.02.001>
16. Piotrowski D, Madore O, Landolt C (1998) The mechanism of electropolishing of titanium in methanol-sulfuric acid electrolytes. *J Electrochem Soc* 145(7):2362
17. Dickinson EJJ, Ekström H, Fontes E (2014) COMSOL Multiphysics®: finite element software for electrochemical analysis. A mini-review. *Electrochem Commun* 40:71–74. <https://doi.org/10.1016/j.elecom.2013.12.020>
18. Kumar A, Singh A, Yadav HNS, Kumar M, Das M (2021) 3D simulation of machining parameters of electrochemical micromachining for stainless steel (316L). *Mater Today Proc* 45(6):4565–4570. <https://doi.org/10.1016/j.matpr.2021.01.005>
19. Wang K, Yan Y, Zhou P, Zhang C, Kang R, Guo D (2020) Preparation of flat and smooth copper surface by jet electrochemical machining and electrochemical polishing. *J Electrochem Soc* 167(16):163501. <https://doi.org/10.1149/1945-7111/abcbb2>
20. Hou Y, Li R, Liang J, Su P, Ju P (2018) Electropolishing of Al and Al alloys in AlCl<sub>3</sub>/trimethylamine hydrochloride ionic liquid. *Surf Coatings Technol* 335:72–79. <https://doi.org/10.1016/J.SURFCOAT.2017.12.028>
21. Urlea V, Brailovski V (2017) Electropolishing and electropolishing-related allowances for powder bed selectively laser-melted Ti-6Al-4V alloy components. *J Mater Process Technol* 242:1–11. <https://doi.org/10.1016/J.JMATPROTEC.2016.11.014>

# Quality Improvement in Inner Bore Grinding Rejection of Ball Bearing by Using Six-Sigma Methodology



Manish Bhargava, Tushar Sharma , Shraddha Arya, and Arindam Sinha

**Abstract** The purpose of this research paper is to present the importance of six-sigma methodology to improve the quality of ball bearing, which deals with significant factors identification and reduction in ‘inner bore grinding rejection’ of ball bearing. Six-Sigma approach works through several phases, which are Define, Measure, Analyze, Improve, and Control (DMAIC). The rejection in inner Bore grinding process has directly affected the production and manufacturing of ball bearing and it is not good for any ball bearing industry. The rejection in inner bore grinding majorly depend on various factors like damage faced, Large Bore and small Track, wearing on diamond point, improper Diamond center height, unskilled operators, sudden power failures, etc. The use of DMAIC method in ball bearing grinding operations reflects several factors such are decrease of tools costs, meager quality, and product scrap in bore grinding process. In addition, Six-Sigma is also used to deliver quantifiable pointers and satisfactory data for logical analysis for improvement. There is prospect of application of various Six-Sigma tools such are alleged process scoping, pareto diagrams, cause and effect matrix, and analysis of variation and ability studies. This study mainly described the affecting factors and the improvement done in inner bore grinding rejection of ball bearings by using the Six-Sigma methodology.

**Keywords** Bore grinding rejection · Cause and effect diagram · DMAIC · Six-sigma methodology · Quality improvement

---

M. Bhargava · A. Sinha (✉)

Department of Mechanical Engineering, National Institute of Technology, Agartala, India  
e-mail: [arin.sinha619@gmail.com](mailto:arin.sinha619@gmail.com)

T. Sharma (✉)

Department of Mechanical Engineering, JIT College (Rajasthan Technical University), Jaipur, Rajasthan, India  
e-mail: [tushar.lakshya@gmail.com](mailto:tushar.lakshya@gmail.com)

S. Arya (✉)

Department of Mechanical Engineering, Jagannath University, Jaipur, Rajasthan, India  
e-mail: [shraddha.jpr@gmail.com](mailto:shraddha.jpr@gmail.com)

## 1 Introduction

Six-Sigma is a developing method to quality assurance with prominence on incessant quality developments. In the manufacturing process of ball bearing, it is common to have unwanted scrap in manufacturing process, if unwanted scrap starts to exceed in any industry then the demand and production rate also got affected, and therefore it becomes difficult to survive in the market. This situation was recognized through a survey, conducted to understand the problems faced by the ball bearing industries, as referred to us by a ball bearing industry itself.

The results of the survey revealed that the rejection of bore grinding might be due to several reasons like Damage face, Large Bore, and small track. It is also reliant on the operations of grinding machine and grinding tool.

The rejection rate of inner bore grinding can be reduced by improving in the quality of the Bore grinding process. Therefore, by the optimization of different process parameters, the significant factors are identified and improved the inner bore grinding rejection, while at the same time, increased the overall quality level, which ultimately contributed to the overall success and profitability of the business [1, 2].

## 2 Methodology

The DMAIC methodology uses a process-step structure, hence, in this research study it is used for quality improvement as well as reduction in inner bore grinding rejection. This methodology mainly consists of five phases, which are:

- 2.1. Define Phase
- 2.2. Measure Phase
- 2.3. Analyze Phase
- 2.4. Improve Phase
- 2.5. Control Phase.

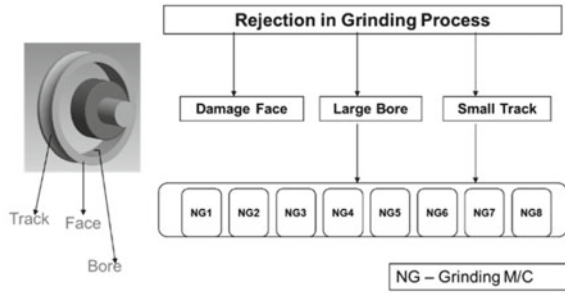
These all five phases make a cyclic process involving the tools. Together these are implemented as a quality improvement process.

### 2.1 *Define Phase*

The main objective of this phase is to define the problem and its effects in the various parts of the ball bearing. Here the main aim is to identify the rejection rate in grinding process and to decrease the quantity of unwanted scrap. To achieve this aim, Problem Statement, Project Scoping, and Objective statement are required.

In the beginning of this phase, Problem Statement is prepared to identify the problematic areas. The main problem was generation of unwanted scrap by bore grinding rejection in the ball bearing.

Fig. 1 Scoping tree



- Business Problem: Rejection ppm is high in all Bore Grinding Machines and it can directly affect the annual cost and profits.
- Critical X: Degraded Quality and it can directly affect the Market goodwill.
- Where and Who can suffered: Bore Grinding Machines and Manufacturing division can be suffered.

After problem statement, Scoping is defined. All process phases are separated and show the suitable action plan for diminishing inconsistency within the process as well as decrease of production time of preparation; this is Project Scoping [2].

Also, ‘Process Map’ and ‘Cause and Effect’ diagram is defined.

Process FMEA is directed and created on found effects, required movements and tools for process analysis are nominated [3].

The rejection in grinding process in scoping tree is shown in Fig. 1.

From this process of Scoping, problematic areas are identified. Now by the usage of Pareto Analysis the individual values like Bore, Face, and Track are represented in descending order by bars. These same values are represented through line chart as well. Also, major characteristics, NG-1 to NG-8 (Grinding machines) and the cumulative total are represented by the line.

The Bore Size, which is contributing 89.2% in 2016–17, is shown in the Pareto analysis (Problematic Product Part and Problematic Process) Figs. 2 and 3. As per the previous year data, the scoping output of Pareto analysis (Problematic Parameter) is identified (Figs. 4 and 5).

Here the NG-5 Grinding machine is recognized as a problematic Process and the overall Grinding Scrap with 3P scoping is defined as:

- Problematic Product: Inner Race
- Problematic Process: Bore Grinding
- Problematic Parameter: Bore Size.

As per the Pareto Analysis the data of overall inner Bore Scrap of NG-5 line in 2015–16, are shown in Fig. 6.

As per the Graph 1, the Average NG PPM of last one year is 2914 PPM, minimum NG PPM is 2026 PPM, as achieved. Here entitlement at the rate of 70% is 622 PPM and the Target is 2292 PPM. The targeted Projected Annual Saving on NG-5 Line

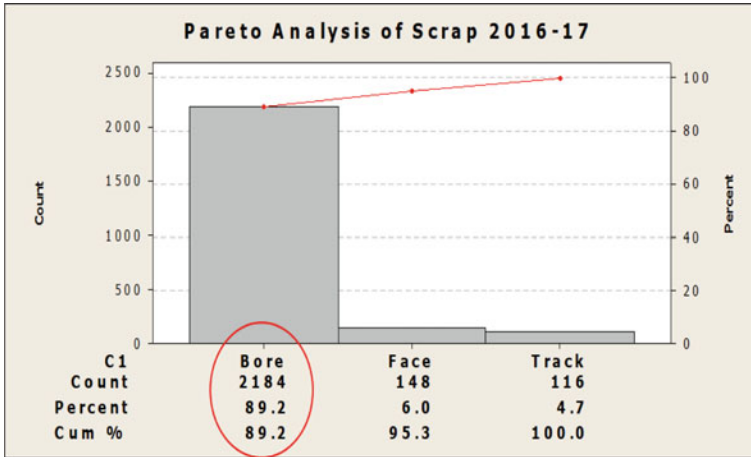


Fig. 2 Pareto chart of bore scrap rate (2016–17)

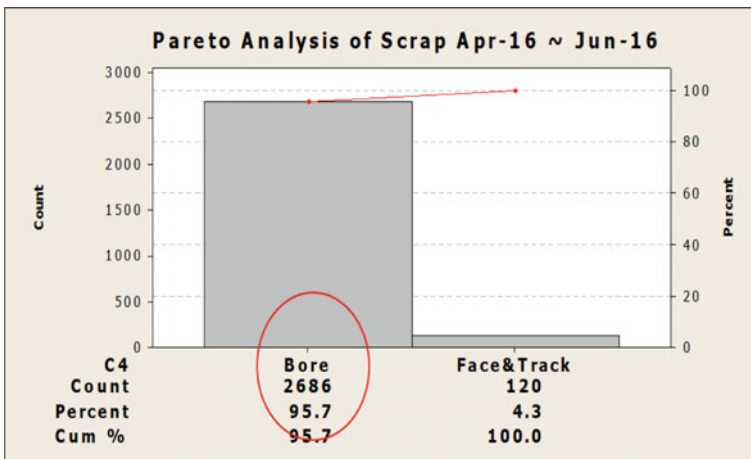


Fig. 3 Pareto chart of bore scrap rate (April 16–June 16)

can be around Rs. 83,970/- and projected saving on other lines target can be achieved approximately Rs. 503,820/-.

Therefore, the outcome of this phase is ‘Reducing inner Bore grinding rejection from 2914 PPM (Base Line) to 2292 PPM (Target Line) on NG-5 Line’, which was the main objective of this research.

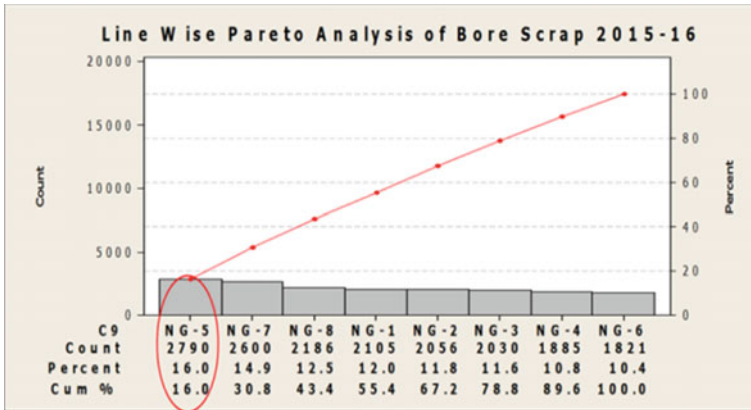


Fig. 4 Line wise Pareto chart of bore scrap (2015–16)

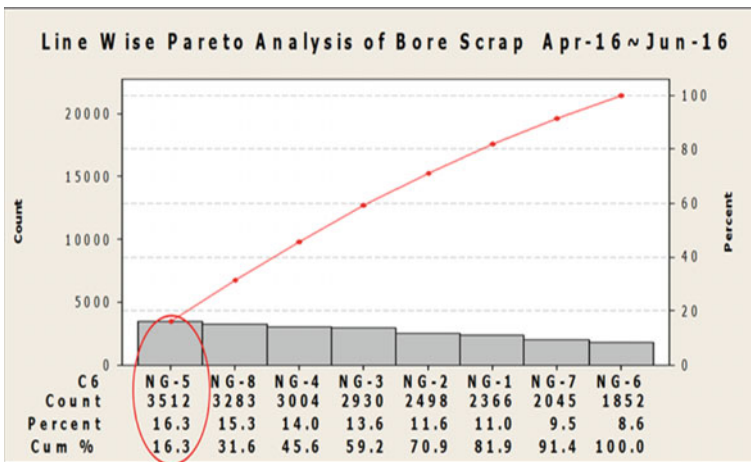


Fig. 5 Line wise Pareto chart of bore scrap (April 2015–June 2016)

## 2.2 Measure Phase

In this phase, the overall process or performance and categorization of data was already available for the research. As well as various factors and parameters were defined, which affected the process of bore grinding.

Measure phase usually involves utilization of graphical tools to show the present status and comparison of the data. Once the objective of the projects identified, the various factors will be listed which affect the inner Bore Grinding rejection. Constructed on Pareto chart, molded team made decision to analyze the bore grinding process by the flow chart diagram, input output sheet and to make improvements



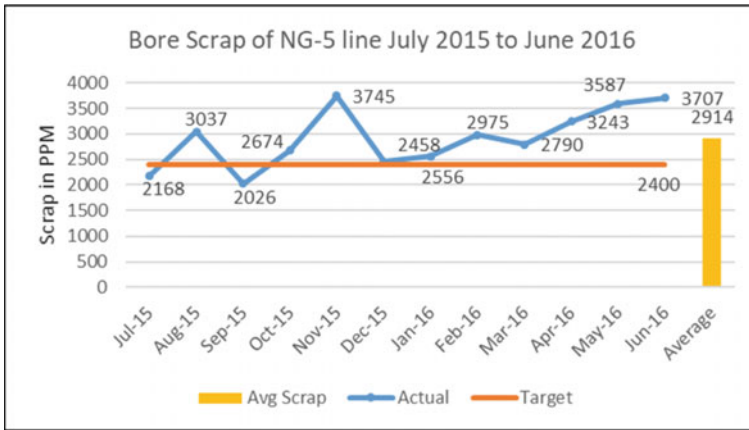


Fig. 6 Average bore scrap of NG-5 line (2015–16)

within grinding operator and some factors like Heavy vibration (Jerk) found in slide and play in Oscillation due to Bearing worn out. Hence, concluded that quality upgrading and decrease of quality factors within process are attainable [4].

These important improvements were proficient by:

- Wheel head slide open and repaired
- Wheel head oscillation Bearing changed
- Minimizing or eliminating scrap.

This was also observed that the process capability of Heat Treated Race and Bore size is less than 1.33, but the process capability of track Grinding is greater than value of 1.33. It means that the problem is with heat-treated race and bore size, and not with the track grinding.

Analysis of Variance (ANOVA) is a statistical method used to test differences between two or more means. It may seem odd that the technique is called ‘Analysis of Variance’ [2, 4]. As you will see, the name is appropriate because inferences about means are made by analyzing variance.

Hereby the (ANOVA R&R assessment) Repeatability and Reproducibility Assessment of track size checking gauge is 15.25%, in Process (IP) Bore Checking Gauge 13.09% and Bore Checking Gauge 20.70%, means all are in controlled range. Now, the different factors, which were depicted by the cause and effect diagram, were compared with the input output sheet, to pick three common factors, which are also marked in the following diagram [2] (Fig. 7).

The three common factors are: diamond change schedule method, vibration level and power failure. These are the main root causes behind the inner bore rejection of ball bearing.

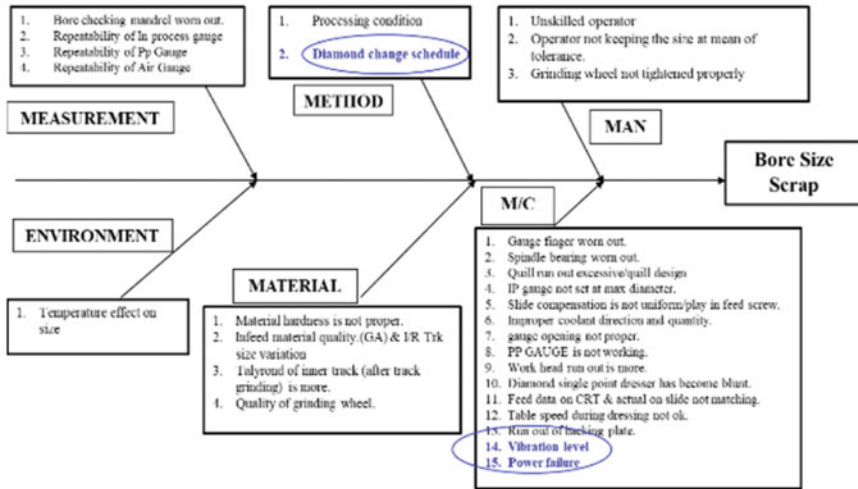


Fig. 7 Cause and effect diagram

### 2.3 Analyze Phase

In this phase, analysis of the current performance is conducted to isolate the problem. Through this analysis (both statistical and qualitative), test hypotheses about the root cause of the problem begins to formulate and hence, PFMEA for the deburring process was made. PFMEA sheet is shown in Table 2 in Annexure 1.

After the PFMEA process, seven main factors are identified. These seven factors and the tools to be used for improvement process are defined in Table 1 [1, 5].

According to the above table, analysis of seven factors is to be done systematically. Here ‘C’ stands for Countable data and ‘D’ stands for discrete data. It indicated 1, 2, 6, and 7 factors as significant and 3, 4, 5 factors as insignificant, which means that the considerable factors for improvement are 1, 2, 6, and 7.

The Tool analysis of significant factors is shown below:

1. Wearing of Diamond Point: The Fig. 2.6: Box Plot, show the after and before the Diamond Change effect and Fig. 2.7 show the Interval plot after and before the diamond change.

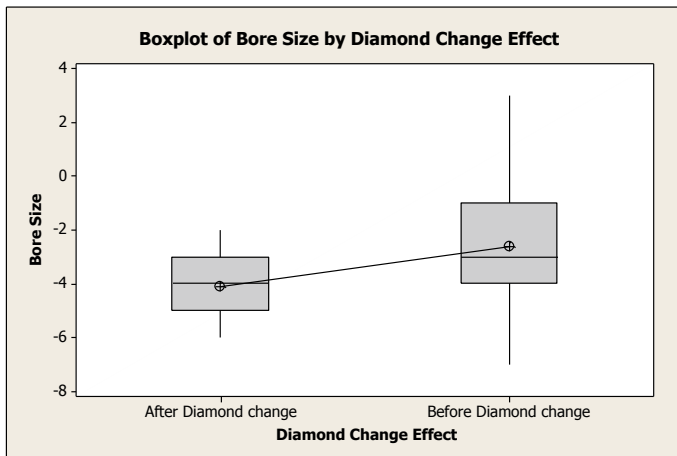
Figures 8 and 9, show the outcome as the difference between position of diamond change, after and before change in bore size.

The *T* Test/CI and One-way ANOVA are shown in Figs. 10 and 11. Here the *P*-value (statistical significance of the difference) is makeable. And Test for Equal Variance is shown in Fig. 2.10.

The outcome of Figs. 10 and 11, the *P*-value is found to be 0.00, but in the correct form, the *P*-value should always be less than 0.05. Therefore, it becomes a significant factor for improvement.

**Table 1** Application of various tools

S.No.	Factor (X)	Data type	Output (Y)	Data type	Tools to be used
1	Wearing of diamond point (diamond change effect)	D	Bore scrap	C	Box plot
					Interval plot
					Two sample <i>T</i> test
					One-way ANOVA
					Test for equal variance
2	Diamond center height	C	Bore scrap	C	Fitted line plot
					Regression analysis
3	Grinding allowance	C	Bore scrap	C	Fitted line plot
					Regression analysis
4	Track size	C	Bore scrap	C	Fitted line plot
					Regression analysis
5	Improper wheel size	C	Bore scrap	C	Fitted line plot
					Regression analysis
6	Low skilled operator	D	Bore scrap	C	Box plot
					Interval plot
					One-way ANOVA
					Test for equal variance
7	Sudden power failure	D	Bore scrap	C	Box plot
					Interval plot
					Two sample <i>T</i> test
					One-way ANOVA
					Test for equal variance



**Fig. 8** Box plot of bore size by diamond change effect

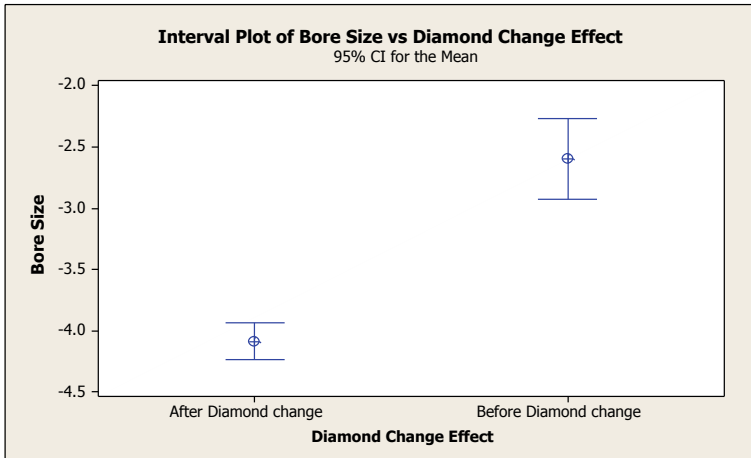


Fig. 9 Interval plot between bore size and diamond change effect

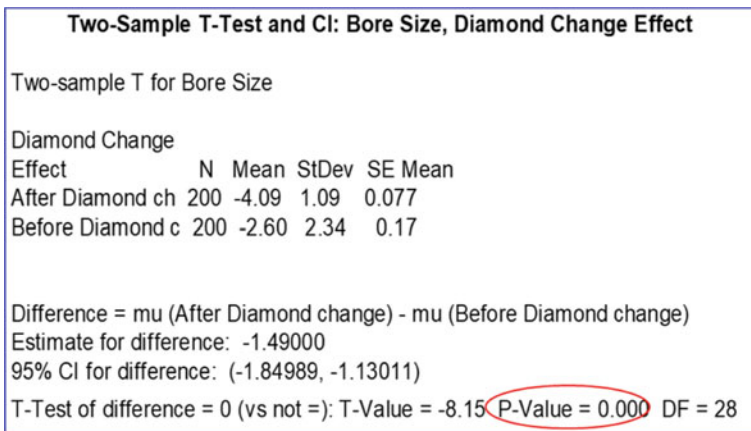


Fig. 10 T Test between bore size and diamond change effect

After the test of equal variance for bore size, the outcome is same as above applied tools. *P*-value is found to be 0.00, which means it is a validation of significance factor.

2. Diamond center Height: Figs. 12 and 13 show the fitted line plot for number of dressing and total feed, the regression analysis of total feed versus number of dressing is shown by Fig. 15.

As per Figs. 13 and 14, we established that the feed is decreasing with respect to number of dressing and it is indicative that diamond center height is not correct (Fig. 15).

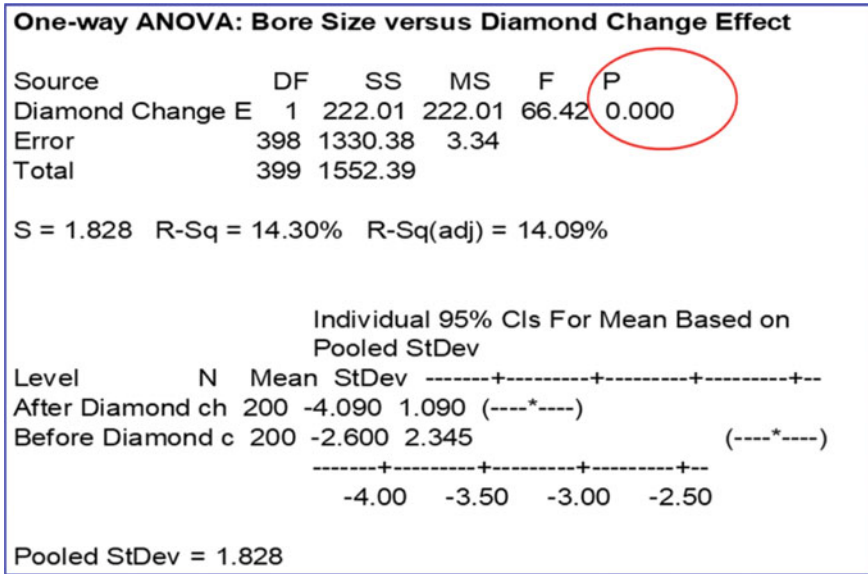


Fig. 11 One way ANOVA between bore size and diamond change effect

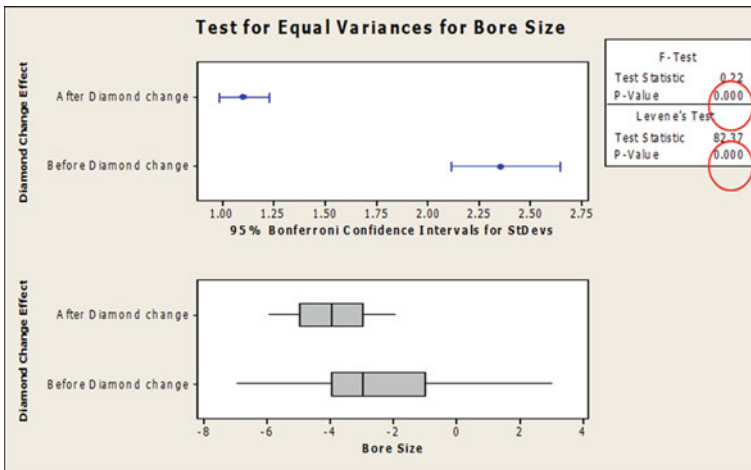


Fig. 12 Test for equal variances for bore size

The regression analysis between the total feed and number of dressing depicted the outcome as the *P*-value 0.00, which means the factor is considered for improvement.

Similarly, the other five factors are analytically processed and following results are achieved:

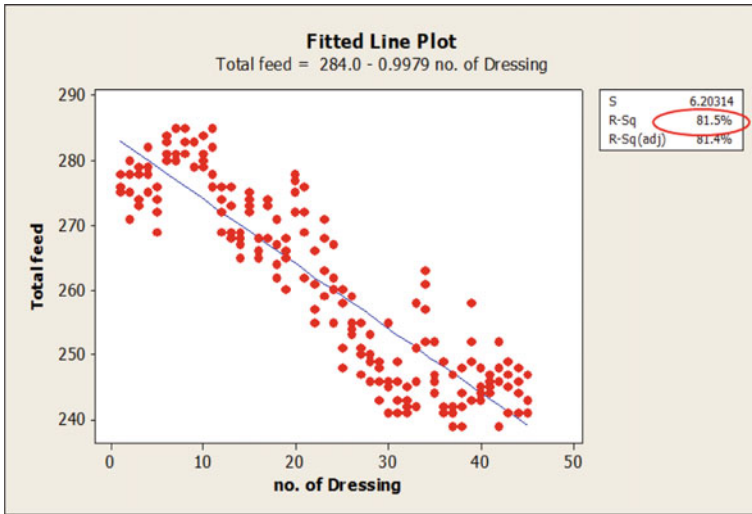


Fig. 13 Fitted line plot between total feed and numbers of feed

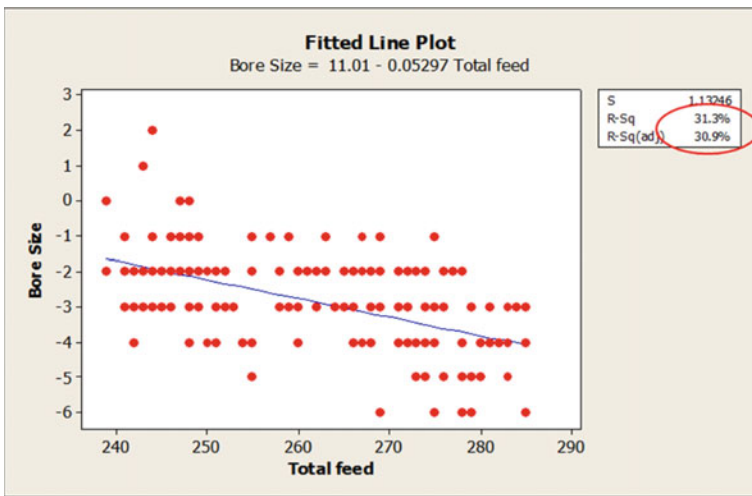


Fig. 14 Fitted plot between bore size and total feed

1. Grinding Allowance, *P*-value is 0.207 (insignificant)
2. Track Size, *P*-value is 0.357 (insignificant)
3. Improper Wheel size, *P*-value is 0.217 (insignificant)
4. Skill of Operators, *P*-Value is 0.00 (Significant)
5. Sudden power failure, Before power cut Air pressure is between 4 to 4.5 kg/cm<sup>2</sup> and After power cut Air pressure is between 2 to 2.5 kg/cm<sup>2</sup>, *P*-Value is 0.00 (Significant).

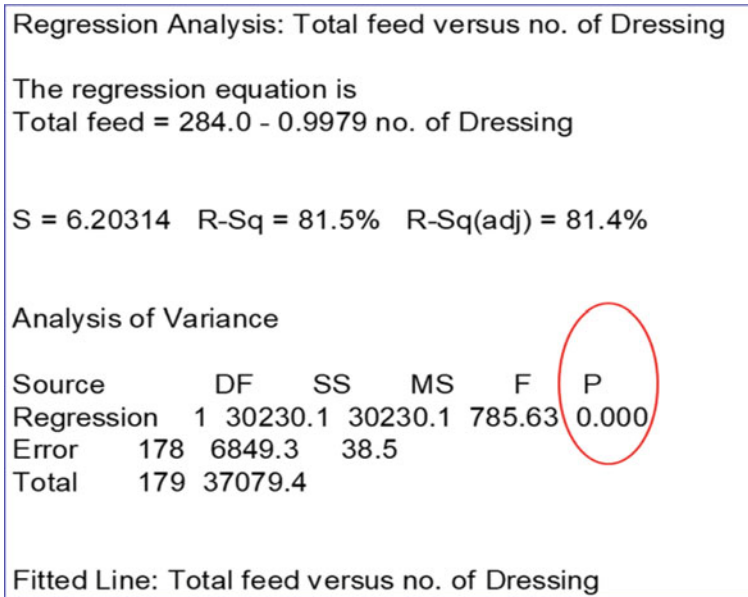


Fig. 15 Regression analysis between total feed and number of dressing

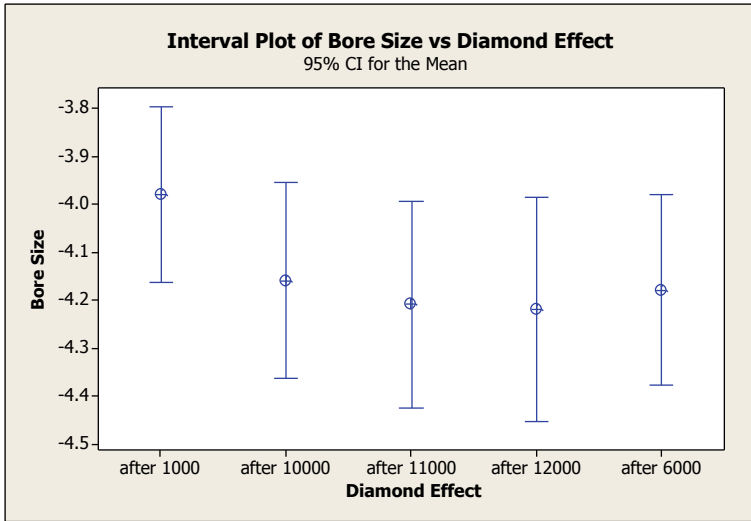
The Inference of Hypothesis testing has to be done by using different tools. Identified significant and insignificant factors and the root cause of the problem, which affected the inner bore grinding are shown in Table 3 in **Annexure 2**.

As per the analysis of tools' application, the outcome of analyze phase has identified the four main factors for improvement, which are following:

1. Wearing of Diamond point (Diamond Change effect)
2. Diamond Center Height
3. Low Skilled Operator
4. Sudden Power Failure.

## 2.4 Improvement Phase

In improvement Phase, problem is improved by selecting a solution. Based on the identified root cause in the prior step, the cause with an improvement could be directly addressed. Complete followed devising sitting, decision was made that tool adjustment is desirable to reduce the root causes of the issue and to avoid the scrap presence. Alteration is useful and noteworthy results are obtained, primarily in scrap and tool exhausting. Obtained results lead the way to make some amendments in the operations to avoid or decrease impact of material scrap and automatically decrease scrap expenses.



**Fig. 16** Interval plot of bore size vs diamond effect

After appropriate tool construction, several improvements were done with process competence study and measurement system study (Gage R&R analyses), Shown in Table 2.4. Therefore, counteractive actions were taken for significant factors.

- (i) Wearing of Diamond Point (Diamond Change effect), Interval plot of bore size versus Diamond effect is shown in Fig. 16 and Test for equal variance for bore size in Fig. 17.

After the applied immediate actions for improvement the result of Interval plot and test of equal variance tools, the *P*-value 0.101 is marked, means it is improved.

- (ii) Diamond Center Height, fitted line plot between total feed and number of dressing or Regression analysis, shown in Figs. 18 and 19.

Similarly, the result of fitted line plot and Regression analysis, the *P*-value 0.110 is marked means it is improved by proper height setting of diamond.

Operator’s Skill, Boxplot between bore Size and Operator Name or Test for equal variances for bore size, shown in Figs. 20 and 21.

The outcome of box plot and test for equal variance, the *P*-value 0.822 is marked means it is improved by the proper training and Education given to operators to check size as per control plan and adjust the size to run mean of the tolerance.

Sudden Power failure, Boxplot between Bore Size and Before-After power cut or Test for equal Variance for bore size shown in Figs. 22 and 23.

The outcome of box plot and test for equal variance, the *P*-value 0.766 is marked means it is improved by the interlocking of power cut. Therefore, the following data



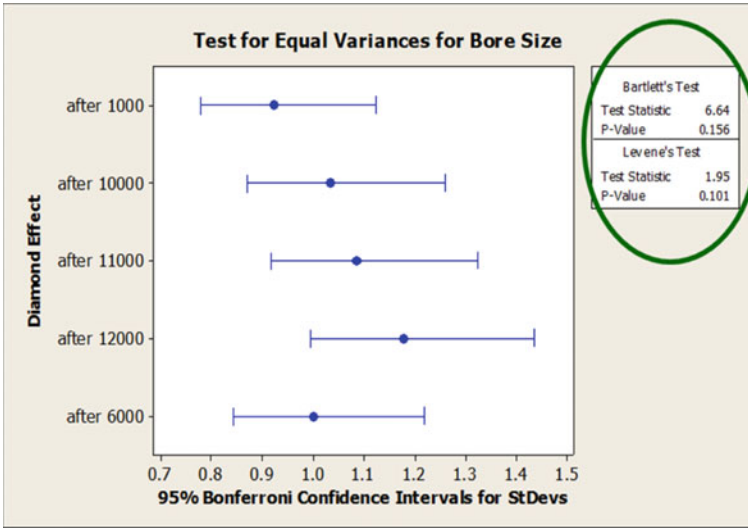


Fig. 17 Test for equal variances for bore size

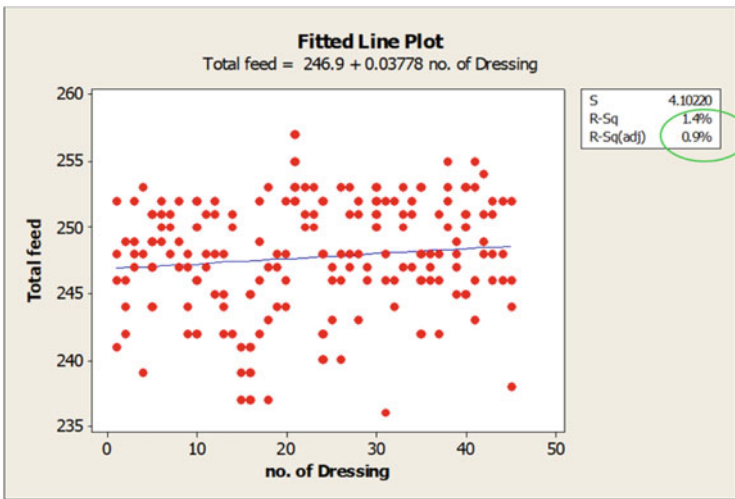


Fig. 18 Fitted line plot for feed

table defines the action taken with the help of tools for the improvement of significant factors Data summary is shown in Table 4 in Annexure 3.

The Annexure also shows the main factors, which affect the performance of ball bearing. After using different tools, the optimizing result had to be identified and action was to be taken for improvement.

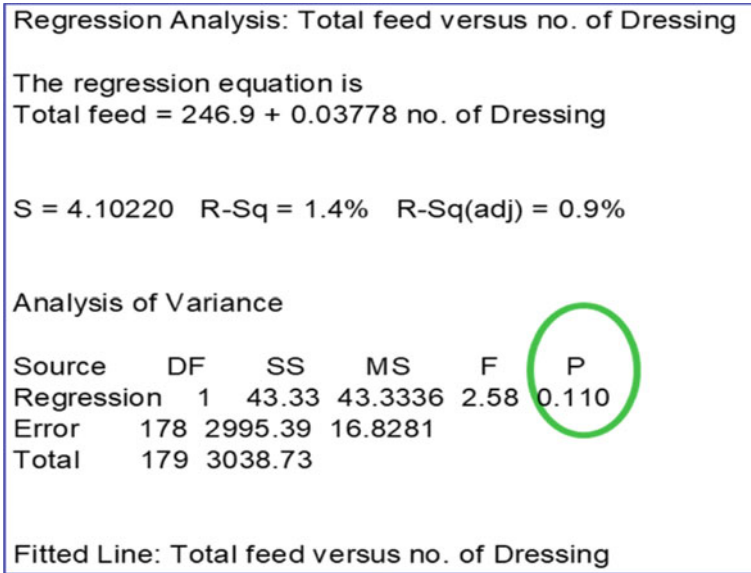


Fig. 19 Total feed vs no. of dressing plot

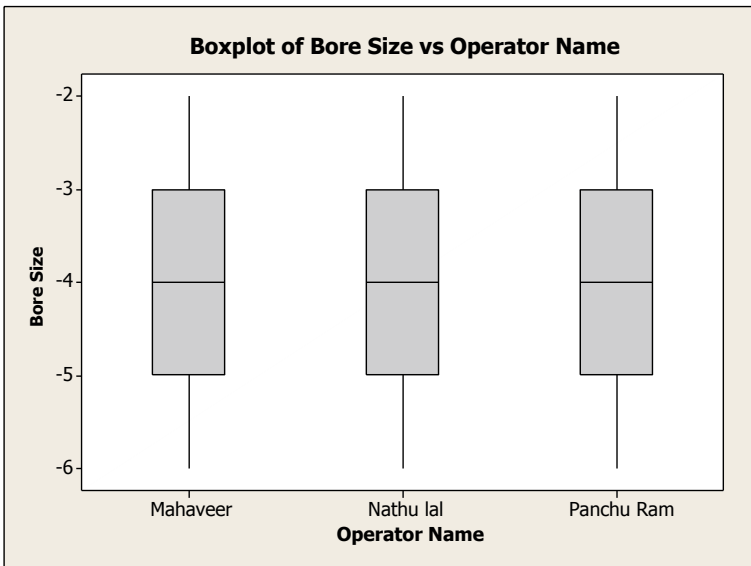


Fig. 20 Box plot of bore size vs operator name

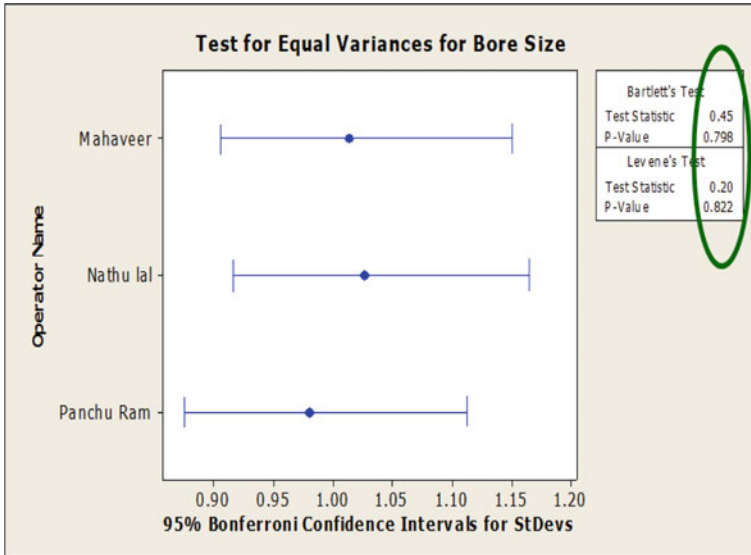


Fig. 21 Equal variances of bore size

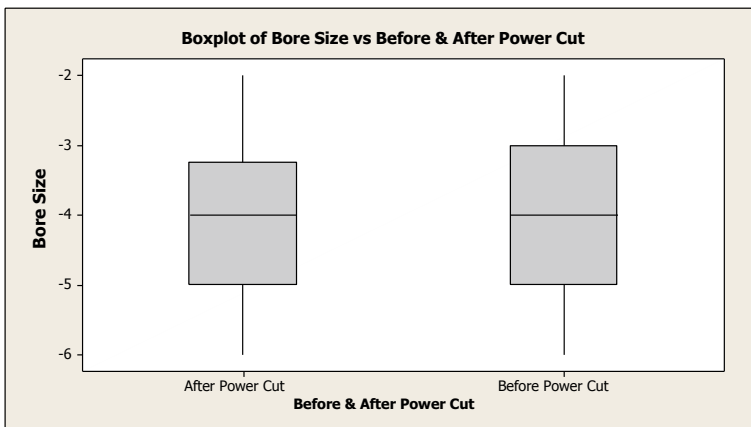


Fig. 22 Box plot of bore size before and after power cut

### 2.5 Control Phase

Control phase is about to maintain the changes made in the improve phase, to guarantee continued and justifiable success. A Control chart can be useful during the control stage to appraise the consistency of the enhancements over time by being allocated as a guide to continue monitoring the process and provide a comeback plan for each of the measures being supervised in case the process becomes unbalanced.

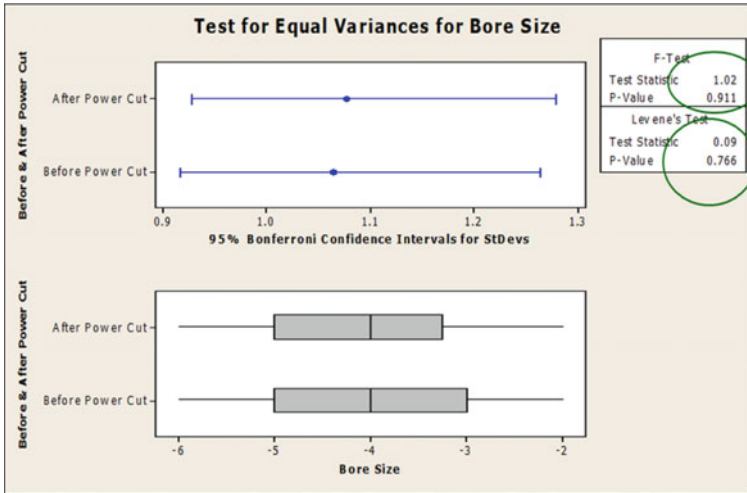


Fig. 23 Equal variances of bore size

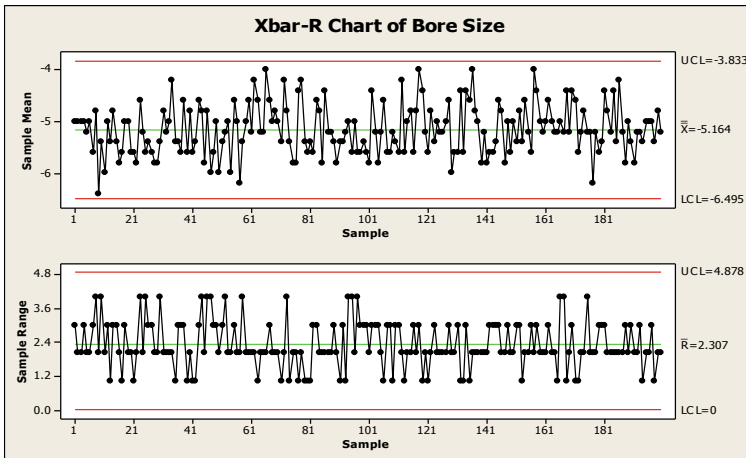
Control action Taken:

- Wheel head slide repaired
- Wheel head oscillation Bearing changed
- Table slide interlocking provided If sudden power failure
- Diamond changing instruction and schedule provided on M/c
- A OPL is provided for diamond height setting to reduce total feed variation
- Chiller for Coolant provided for Grinding for temperature.
- Result monitoring through X Bar R chart
- In feed material quality improved by regular feedback and interaction
- Training and Education given the operators
- Height setting of diamond
- To run M/c mid of the tolerance of Specification
- To check parameter as per control plan.

In this final phase of DMAIC methodology, a control plan is established to confirm that processes and products reliably meet requirements of industry and customers, and to check how external clamping system make an impact on quality production level.

### 3 Result and Conclusion

A Phase Summary is defined here in the form of Define, Measure, Analyze, Improve, and Control (DMAIC) methodology to show the process of reducing the Inner Bore grinding rejection from 2914 to 2292 PPM on NG-5 Line, Shown in Fig. 26.



**Fig. 24** X bar- R chart of bore size

However, after experiments and graphical representation in Pareto chart and regression analysis (MINITAB), the result shows that the all four significant factors are improved. After taking corrective actions, the rejections were within acceptable limit. Figures 24 and Fig. 25 show the X-bar R chart Data and process capability of Bore Size. No. 5 Grinding Machine NG-5 Line, Bore Grinding machine shows the result.

As per above mentioned Data, the Result is found as: the Process is under control and the value of Process compatibility and Process performance ( $Cpk \& Ppk$ )  $> 1.33$ . Also, Ppk has improved from 0.85 to 1.60.

This quality development project based on Six-Sigma methodology delivers adjacent associate with all phases of process while Six-Sigma tools enable correct decisions and the most noteworthy developments.

As we will see that after conducting the DMAIC method, major 4 factors have been improved. Hence, Overall Inner Grinding Scrap, which is 2806 ppm against target of 2400 ppm, is achieved as depicted in Annexure 4 Fig. 26.

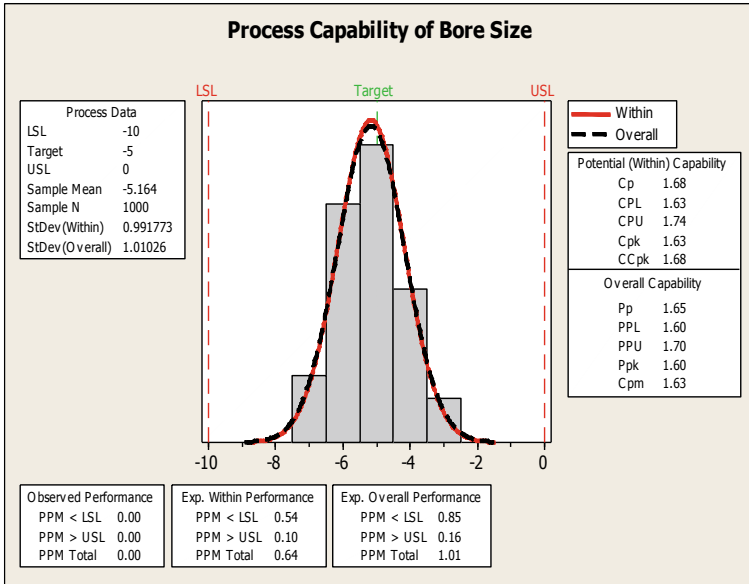


Fig. 25 Process capability of bore size

## Annexure and Supportive Tables

### Annexure 1

**Table 2** Process failure mode analysis (PFMEA) Shee

Process function	Potential failure mode	Potential effects of failure	SEV	Potential causes/mechanisms of failure	OCC	Current process controls	DET	RPN
The highest value process step from the C&E matrix	In what ways might the process potentially fail to meet the process requirements and/or design intent?	What is the effect of each failure mode on the outputs and/or customer requirements? The customer could be the next operation, subsequent operations, another division or the end user	How SAVERE is the effect to the customer?	How can the failure occur? Describe in terms of something the can be corrected or controlled, Be specific. Try identified the causes that directly impact failure mode, i.e., root causes	How often dose the causes of failure mode occur?	What are the existing controls and procedures (in section and test) that either prevent failure mode from occurring or detect the failure should it occur? Should include an SOP number	How well can you detect Cause of FM?	SEV X OCC X DET
Dressing	Uneven or improper dressing	Defect in bore size	7	Due to wearing of diamond point	9	No frequency mentioned	8	504
	Wheel size after dressing not as per set data	Defect in bore size	5	Total feed variation from start to end of the wheel (due to diamond center height high or low during spindle/diamond dresser setting during mount	7	Setting approval check sheet	5	175

(continued)

Table 2 (continued)

Process function	Potential failure mode	Potential effects of failure	SEV	Potential causes/mechanisms of failure	OCC	Current process controls	DET	RPN
Finish grinding and Sp. out	Improper cutting of material in grinding	Defect in bore size	3	Due to variation in input material (grinding allowance)	9	Receiving inspection and in process checking	6	162
	Difference in position of inner race on shoe	Defect in bore size	4	Due to variation in track size from I/R Trk grinding M/C	7	Setting approval check sheet and in process checking at previous station	6	168
	Wheel acting hard during grinding	Defect in bore size	7	Due to improper wheel wear size	8	Automatic control/processing condition	6	336
Workman	Wrong feeding/control size	Defect in bore size	7	Due to unawareness/indiscipline	8	Skill sheet	7	392
Power	Sudden power failure	Defect in bore size	3	Due to low air pressure	9	No interlocking	7	189



## Annexure 2

**Table 3** Hypothesis verification with conclusion

S.No.	Factor (X)	Verify hypothesis	Remark		Conclusion
1.	Wearing of diamond point (diamond change effect)	Box plot	Significant		Yes, it is root cause
		Interval plot	Significant		
		Two sample <i>T</i> test	Significant	<i>P</i> -value 0.00	
		One-way ANOVA	Significant	<i>P</i> -value 0.00	
		Test for equal variance	Significant	<i>P</i> -value 0.00	
2.	Diamond center height	Fitted line plot	Significant	$R^2 = 81.5$	Yes, it is root cause
		Regression analysis	Significant	<i>P</i> -value 0.00	
3.	Grinding allowance	Fitted line plot	Insignificant	$R^2 = 0.8$	No, it is not root cause
		Regression analysis	Insignificant	<i>P</i> -value 0.207	
4.	Track size	Fitted line plot	Insignificant	$R^2 = 0.4$	No, it is not root cause
		Regression analysis	Insignificant	<i>P</i> -value 0.357	
5.	Improper wheel size	Fitted line plot	Insignificant	$R^2 = 0.52$	No, it is not root cause
		Regression analysis	Insignificant	<i>P</i> -value 0.217	
6.	Low skilled operator	Box plot	Significant		Yes, it is root cause
		Interval plot	Significant		
		One-way ANOVA	Significant	<i>P</i> -value 0.00	
		Test for equal variance	Significant	<i>P</i> -value 0.00	
7.	Sudden power failure	Box plot	Significant		Yes, it is root cause
		Interval plot	Significant		
		Two sample <i>T</i> test	Significant	<i>P</i> -value 0.00	
		One-way ANOVA	Significant	<i>P</i> -value 0.00	
		Test for equal variance	Significant	<i>P</i> -value 0.00	

## Annexure 3



### Annexure 4

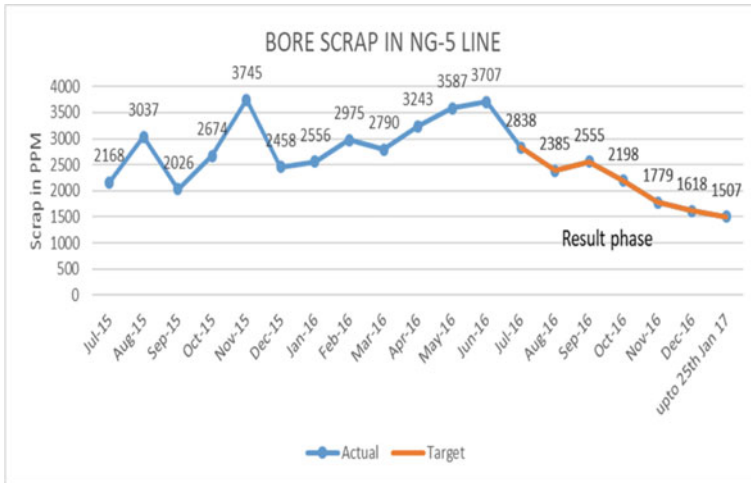


Fig. 26 Bore scrap in NG-5 line

### References

1. Tennakoon BMMM, Palawatta TMB (2015) A case study on application of DMAIC to improve delivery efficiency. In: Proceedings of 12th international conference on business management, 7th and 8th December 2015, Colombo, Sri Lanka
2. Modi VKK (2016) Review paper: quality improvement through six-sigma DMAIC methodology in plastic injection moulding. *Int J Innov Res Sci Eng Technol* 5(12)
3. Sindha N, Suthar K (2017) Review on implementation of six-sigma DMAIC methodology in manufacturing industries. *IJSTE Int J Sci Technol Eng* 3(08). ISSN: (Online): 2349-784X
4. Tripathi S, Jain S (2017) Study of the product failure modes and effects analysis (PFMEA) on welding process—a implementation paper. *Int J Innov Res Sci Eng Technol* 6(5)
5. Bambharoliya SH, Thakkar HR (2015) Reducing rejection rate in small scale machining unit using 7 quality control tools—a review. *IJEDR* 3(4). ISSN: 2321-9939

# Achieving Manufacturing Competitiveness Through Six Sigma: A Study on Steel Firms



Sudeshna Rath and Rajat Agrawal

**Abstract** This study investigates that Six Sigma has potential feasibility to be instrumental in enhancing the manufacturing competitiveness of the Indian steel industries. The research paper has been categorized into three sections, viz: identification of the competitive priorities from the relevant studies, surveying Six Sigma users and non-users of Indian steel industries employing a 5-point Likert scale, data analysis of the steel industries. One-way multivariate analysis of variance (MANOVA) was used for statistical data analysis. A conceptual framework was built on previous literature, demonstrating the five drivers of manufacturing competitiveness, namely, quality, cost, delivery, flexibility, and innovation. In conclusion, all five hypotheses were supported with significant results. However, the cost priority showed to be the least depending on the manufacturing competitiveness. On the scales of competitiveness, the Six Sigma users had relatively higher mean scores than the non-users.

**Keywords** Six Sigma · Manufacturing competitiveness · Competitive priorities · Multivariate analysis of variance (MANOVA) · Steel industries

## 1 Introduction

It is worth noting that operations strategy definitions are characterized by content and process frameworks. Performance factors and decision areas define the content framework. Continuous improvement [2] is a comprehensive procedure centered on step-by-step transformation which incorporates the whole organization. This improvement is a basic, low-cost strategy that is now commonly recognized as one among the most successful methods to augment competitive advantage [14, 17]. However, there are challenges in properly adopting this notion in businesses that piques people's interest in adopting the DMAIC methodology to achieve process improvement and enhance performance [1].

---

S. Rath · R. Agrawal (✉)

Department of Management Studies, Indian Institute of Technology Roorkee, Roorkee, India  
e-mail: [rajat@ms.iitr.ac.in](mailto:rajat@ms.iitr.ac.in)

The models which enhance manufacturing competitiveness by curtailing defects, also stimulate value addition and contribute to competitive advantage of companies. DMAIC is a method that may help organizations improve their performance when adequately implemented. A few of the performance consequences include improved quality, shorter cycle times, and creating value for stakeholders across the organization [6]. As a result of this affirmation, the following research questionnaire was developed: *What is the linkage between Six Sigma implementation and drivers of manufacturing competitiveness in the steel industry?*

### ***1.1 Motivation for Performing Six Sigma***

William Smith recommended a systematic approach of Six Sigma named (DMAIC: Define, Measure, Analyze, Improve, and Control) for improving product quality. According to Schroeder et al. [16], because of global competition and evolving technologies, the Indian steel industry is pressured to maintain its competitiveness in international markets. Today, Six Sigma is a fundamental component of business success since it aids in the improvement of processes and services and reduces the variation of business processes to increase manufacturing competitiveness.

The novelty of this study is that it evaluates the impact of Six Sigma implementation on the manufacturing competitiveness that considers the firms' strategic competitive priorities in Indian steel industries. This industry was chosen for a variety of reasons. The expansion of India's iron ore and steel sector is one of its most significant industries, as it helps build its economy. Iron and steel are two of the essential components needed for the country's infrastructural development. Steel consumption is also used as a gauge of economic growth.

### ***1.2 Manufacturing Competitiveness***

The concept of manufacturing competitiveness started from the concept of manufacturing strategy as proposed by Skinner [19]. Various companies like Toyota followed this concept for its competitive advantage. Following more than three decades of relevant research development according to Skinner [20], short delivery cycles, flexibility in variations in volume, improved quality and reliability of products, the potential to develop new goods efficiently and cheap cost are all standard competitive metrics for manufacturing strategy. The debate over manufacturing competitiveness originated with Porter's defining work on manufacturing competitiveness in 1996, "who defined manufacturing competitiveness as a link between the manufacturing of goods including upgradation of quality and improved services in order that a company's products and services can compete in the international market". Manufacturing competitiveness is an essential factor in the Indian economy, as it helps to boost Gross Domestic Product [3].

### 1.3 Concept of Competitive Priorities

In order to harmonize precisely the manufacturing approach with the business design, it is crucial to define the priorities of manufacturing competitiveness for each product or types of goods concerning the market. The competitive approach sets the path for all priorities, preparation of a blueprint, purposeful resolution and implementations, all necessary for a successful firm. The primary goal is to introduce a manufacturing strategy to complement competitive strategy to obtain the best possible production capabilities [9].

Leong et al. [11] discovered a distinction between complementing models: the content model and the process model of the operation approach studies. The content model for manufacturing approach describes the importance of the competing priorities developed on goals of business or corporate unit. The model for process depicts the creation, implementation, and evaluation of an operation approach. Different topologies, such as those of Hill [10], Leong et al. [11], Slack [21], are presented in the literature for this paradigm. Most of these frameworks provide the variables and logic needed to develop an operations strategy, but they do not detail how the process is implemented. Authors adopted these five competitive priorities (quality, cost, delivery, flexibility, and innovation) from various researchers which can be defined as follows:

Competitive priorities	Description	Supporting literature for measurement scales
Quality	Manufacturing of highly efficient or superior quality goods	Hayes and Wheelwright [9], Skinner [19], Hill [10], Dangayach and Deshmukh [4]
Cost	Low-cost manufacturing and product distribution	
Delivery	Observe delivery deadlines	
Flexibility	Respond quickly to modifications in product mix and production, adjustments in design, material variations, and sequence modifications	
Innovation	New products and procedures are being introduced	

## 2 Conceptual Framework and Hypothesis Development

According to Dangayach and Deshmukh [4], cost, quality, delivery, and flexibility help a business strive toward attaining competitiveness. Therefore, companies should implement techno-managerial techniques such as Six Sigma, automation, just-in-time (JIT), benchmarking, total quality management, as well as human resource

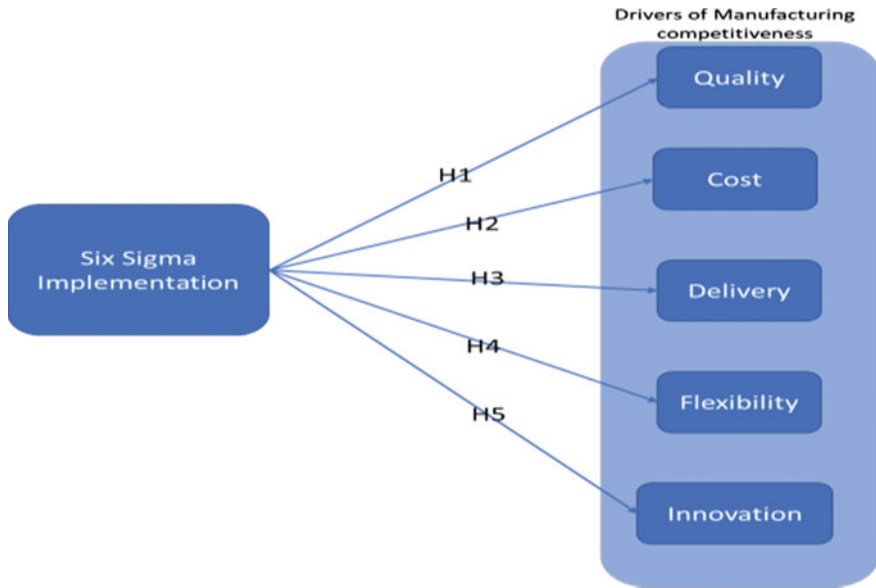


Fig. 1 Conceptual model of six sigma theory

strategies such as employee training and empowerment. As derived from the literature review, a conceptual framework is created and presented in Fig. 1, incorporating improvement models like Six Sigma and manufacturing strategy defined by manufacturing priorities.

### 3 Building and Validating the Research Tool

This research aims to figure out how steel industries may better use their resources with Six Sigma adoption by increasing their performance and focusing on competitive priorities. The study investigates a relation between Six Sigma adoption and specific aspects of manufacturing competitiveness in India’s steel industry. Then we set out to see any significant differences between the users and non-users of Six Sigma. The general hypothesis being considered as follows:

*H1: There is significant evidence that quality is an important driver of manufacturing competitiveness in the Six Sigma users as compared to Non-six Sigma users.*

*H2: There is significant evidence that cost is an important driver of manufacturing competitiveness in the Six Sigma users as compared to Non-six Sigma users.*

*H3: There is significant evidence that flexibility is an important driver of manufacturing competitiveness in the Six Sigma users as compared to Non-six Sigma users.*

*H4: There is significant evidence that delivery is an important driver of manufacturing competitiveness in the Six Sigma users as compared to Non-six Sigma users.*

*H5: There is significant evidence that innovation is an important driver of manufacturing competitiveness in the Six Sigma users as compared to Non-six Sigma users.*

## **4 Methodology**

When exploring a relationship between two variables, explanatory research is utilized. A survey-based technique was used to gather information from companies. For the purpose of analyzing data, statistical methodologies were applied to analyze the data statistically with the help of the software IBM SPSS. The relationship between the implementation of Six Sigma and the drivers of manufacturing competitiveness was investigated using a multivariate analysis of variance (MANOVA). It is worth noting that MANOVA needs the independent variable to be a categorical variable with two options, i.e., Six Sigma users and non-users. On a five-point Likert scale, executives were asked for assessing the severity of the different drivers of the manufacturing competitiveness (dependent variable) for their organization (1—low priority, 5—high priority) in this study.

## **5 Results and Discussion**

### ***5.1 Sample Demographics***

An online questionnaire was sent to all possible steel manufacturers in India. There was a geographical delimitation criterion that the steel companies were selected for the questionnaire. As a result, respondents (operation and quality managers) possessed the essential knowledge to complete the survey. Some firms refused to



**Table 1** Statistical summary and construct reliability

S.No.	Variables	Mean	SD	Number of items	Cronbach alpha
1	Quality	36.05	9.15	9	0.9
2	Cost	23.96	5.968	7	0.93
3	Delivery	34.5	5.874	6	0.85
4	Flexibility	39.55	9.93	11	0.88
5	Innovation	17.06	5.05	5	0.8

participate, claiming a busy schedule and the need to keep the required data secret as justifications. One hundred six responses were received over two months, despite repeated reminders, phone calls, and emails. However, it is also expected that more responses will come in the future as this research is still ongoing. These 106 responses so far have been received that were efficient to develop an intermediate understanding of this study. Out of them, 32 were found to be Six Sigma non-users, and 74 were found to be Six Sigma users.

## 5.2 Testing for Reliability

The scales are checked for internal consistency and reliability using inter-item analysis. Cronbach's coefficient alpha is computed for all scales, common for empirical research in operations management [5]. Statistical summary is addressed in Table 1. The Cronbach's alpha coefficients were in the range 0.80–0.93 for each construct. These values are found to be exceeding the value 0.5 which is the minimum requisite for an exploratory study like the present one [12].

## 5.3 Testing for Normality Assumption

The MANOVA is based on a multivariate normal distribution in terms of normality. According to Hair et al. [7], skewness and kurtosis were used to check whether the values are less than 1. It was found that all of the variables are within the normal range.

## 5.4 MANOVA Analysis

The results of the multivariate tests that are run within MANOVA are presented below.

**Table 2** Box’s test

Box’s test of equality of covariance matrices <sup>a</sup>	
Box’s M	56.892
<i>F</i>	1.846
df1	28
Sig	0.004

Tests the null hypothesis that the observed covariance matrices of the dependent variables are equal across groups

<sup>a</sup>Design: Intercept + Six Sigma

### 5.4.1 Box’s Test

A Box’s test determines any violations of variance–covariance homogeneity, with a significant threshold of significance above 0.001 [13]. Table 2 demonstrates the Box’s test results.

Box’s test of the equality of covariance matrices assumption is shown in the output. Because this statistic is significant ( $p = 0.004$ ; higher than 0.001), the covariance matrices are nearly similar, as expected.

### 5.4.2 Levene’s Test

Furthermore, Levene’s test specifies any violation of the test of equality of variance made for any dependent variable. The significance level must be greater than 0.05, which means that if it is less than 0.05, the dependent driver is not regarded statistically significant and should not be used to assess the represented category appropriately as shown in Table 3, all dependent variables except cost and delivery had 0.004 and 0.019. This indicates that cost and delivery will be retained in the analysis despite heteroscedasticity [7].

**Table 3** Results of Levene’s test

Levene’s test of equality of error variances <sup>a</sup>				
	<i>F</i>	df1	df2	Sig
Quality	0.304	1	104	0.582
Cost	8.497	1	104	0.004
Delivery	5.711	1	104	0.019
Flexibility	0.011	1	104	0.918
Innovation	0.868	1	104	0.354

Tests the null hypothesis that the error variance of the dependent variable is equal across groups

<sup>a</sup>Design: Intercept + Six Sigma

### 5.4.3 Wilks' Lambda

Wilks' Lambda is suggested for looking for significant differences between sets of dependent variables in a linear arrangement. If the significance of Wilks' Lambda is less than 0.05, one can conclude that dependent variables have variance between them within the group SPS:refid:bib13[13]. The significant level of the test concerning the categorical independent variable Six Sigma is 0, which is less than 0.05, as shown in Table 4. As a result, it is possible to conclude that there is a difference in the data collected from the respondents, who are users and non-users of Six Sigma.

### 5.4.4 Between-Subjects Effects

The between-subjects effects test determines if all dependent variables or only part of them distinguish between the two independent categories. Because the between-subjects effects tests reveal five different univariate ANOVAs that were concluded as a step-down analysis after the MANOVA, the significance level is suggested to be adjusted accordingly using the Bonferroni adjustment [13]. The revised alpha level is adjusted from 0.05 to  $(0.05/5 = 0.01)$  0.01 using the Bonferroni technique of alpha. As seen in Table 5, quality, cost, delivery, flexibility, and innovation fall below the new alpha level and, as a result, are considered significant for the analysis. The Partial Eta Square (PES) states that which dependent variable is most dependent on the independent variable which matters in answering the research question. When looking at the PES of each dependent variable, Quality shows a PES of 0.892, or 89.2%, cost shows 0.605 or 60.5%, delivery shows 0.789 or 78.9%, flexibility 0.794 or 79.4% and innovation 0.680 or 68.0%. Consequently, it is reasonable to infer that the strongest relationship between Six Sigma adoption and one of the dependent factors was in the area of quality.

### 5.4.5 Hypothesis Testing

A multivariate analysis of variance found that each of the five dependent variables had a significant main impact for Six Sigma adoption, Wilks'  $\lambda = 0.102$ ,  $F(5, 100) = 176.154$ ,  $p < 0.001$ , PES = 0.914. The power to identify the effect was 1.00, indicating that the ability to detect dependent variables' variances using Six Sigma as the independent variable is confirmed.

As a result of the overall significance of the test, the univariate main effects for each of the dependent variables were investigated [8]. The estimated marginal means of each dependent variable, along with the results based on the two category independent variables, are shown in Fig. 2. As already discussed, the findings show that the relationship between Six Sigma adoption and all the drivers of manufacturing competitiveness was found significant that as a result, develops support for H1 (hypothesis 1): (PES = 0.892,  $p < 0.01$ ), H2 (PES = 0.605,  $p < 0.01$ ), H3 (PES = 0.789,  $p < 0.01$ ) H4 (PES = 0.794,  $p < 0.01$ ), and H5 (PES = 0.680,  $p < 0.01$ ).

**Table 4** Wilks' lambda

Multivariate tests <sup>a</sup>										
Effect	Value	F	Hypothesis df	Error df	Sig.	Partial eta squared	Noncent parameter	Observed power <sup>c</sup>		
Six sigma	0.898	176.152 <sup>b</sup>	5.000	100.000	0.000	0.898	880.769	1.000		
	0.102	176.152 <sup>b</sup>	5.000	100.000	0.000	0.898	880.769	1.000		
	8.808	176.152 <sup>b</sup>	5.000	100.000	0.000	0.898	880.769	1.000		
	8.808	176.152 <sup>b</sup>	5.000	100.000	0.000	0.898	880.769	1.000		

<sup>a</sup>Design: Intercept + Six Sigma

<sup>b</sup>Exact statistic

<sup>c</sup>Computed using alpha = 0.05

**Table 5** Results of between-subjects effects

Tests of between-subjects effects		Type III sum of squares	Df	Mean square	F	Significance	Partial eta squared	Noncent. parameter	Observed power <sup>a</sup>
Six sigma	Quality	7840.336	1	7840.336	857.924	0.000	0.892	857.924	1.000
	Cost	2261.974	1	2261.974	159.178	0.000	0.605	159.178	1.000
	Delivery	2858.007	1	2858.007	388.361	0.000	0.789	388.361	1.000
	Flexibility	8219.491	1	8219.491	400.055	0.000	0.794	400.055	1.000
	Innovation	1823.120	1	1823.120	220.845	0.000	0.680	220.845	1.000

<sup>a</sup>Computed using alpha = 0.05

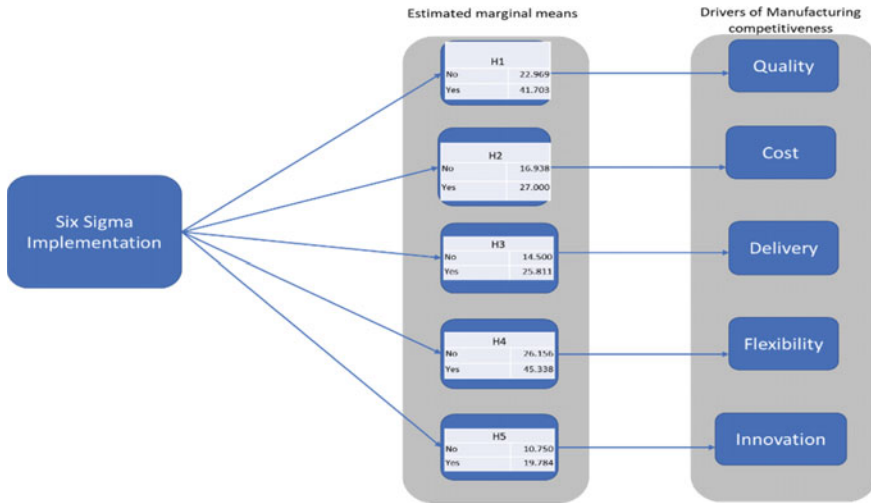


Fig. 2 Hypothesis testing

## 6 Conclusion

To determine whether Six Sigma implementation improves competitiveness, MANOVA was used to evaluate the significance of the relationship of manufacturing competitiveness between Six Sigma users and non-users. The dimensions of competitiveness in the Indian steel sector were identified in this study. It can be concluded that companies that employ Six Sigma outperform their competitors on various priorities, such as quality, flexibility, and delivery. Eventually, flexibility was observed to be the main dominating driver for competitive priorities with high averages. These findings corroborate other research, e.g., Porter [15]; Swamidass and Newell [22], Ward et al. [23], which conclude that insisting on flexibility, delivery performance, and quality is a prudent approach.

These findings are based on survey respondents’ perceptions. One other important point is that the application of Six Sigma allows for attaining a more excellent range of competitive priorities and another benefit of cost reduction is that it also helps the company to be more cost-effective, more consistent, have superior quality, and be able to provide better customer service [1].

## References

1. Antony J (2011) Six sigma vs. lean: some perspectives from leading academics and practitioners. *Int J Prod Perform Manag* 60(2):185–190. <https://doi.org/10.1108/17410401111101494>

2. Caffyn S (1999) Development of a continuous improvement self-assessment tool. *Int J Oper Prod Manag* 19(11):1138–1153. <https://doi.org/10.1108/01443579910291050>
3. Chandra P, Sastry T (1998) Competitiveness of Indian manufacturing. *Vikalpa: J Decis Makers* 23:25–36
4. Dangayach GS, Deshmukh SG (2003) Evidence of manufacturing strategies in Indian industry: a survey. *Int J Prod Econ* 83(3):279–298. [https://doi.org/10.1016/S0925-5273\(02\)00372-9](https://doi.org/10.1016/S0925-5273(02)00372-9)
5. Flynn BB, Sakakibara S, Schroeder RG, Bates KA, Flynn EJ (1990) Empirical research methods in operations management. *J Oper Manag* 9(2):250–284. [https://doi.org/10.1016/0272-6963\(90\)90098-X](https://doi.org/10.1016/0272-6963(90)90098-X)
6. George M (2002) *Lean six sigma—combining six sigma quality with lean speed*. McGraw-Hill
7. Hair JF, Black WC, Babin BJ, Anderson RE (2014) *Multivariate data analysis*, 7th edn. Pearson Education Limited
8. Hair JJ, Wolfinbarger MC, Money AH, Samouel P, Page MJ (2011) *Essentials of business research methods*, 2nd edn. Sharpe Inc., M.E
9. Hayes R, Wheelwright S (1984) *Restoring our competitive edge: competing through manufacturing*. Wiley
10. Hill TJ (1983) Manufacturing strategic role. *J Oper Res Soc* 34(9):853–860. <https://doi.org/10.1057/jors.1983.182>
11. Leong GK, Snyder DL, Ward PT (1990) Research in the process and content of manufacturing strategy. *Omega* 18(2):109–122. [https://doi.org/10.1016/0305-0483\(90\)90058-H](https://doi.org/10.1016/0305-0483(90)90058-H)
12. Nunnally JC (1978) *Psychometric theory*. McGraw-Hill, New York
13. Pallant J (2010) *SPSS survival manual*, 4th edn. McGraw-Hill Education
14. Petterson J (2009) Defining lean production: some conceptual and practical issues. *TQM J* 21(2):127–142. <https://doi.org/10.1108/17542730910938137>
15. Porter ME (1980) *Competitive strategy*. Free Press
16. Schroeder RG, Linderman K, Liedtke C, Choo AS (2008) Six sigma: definition and underlying theory\*. *J Oper Manag* 26(4):536–554. <https://doi.org/10.1016/j.jom.2007.06.007>
17. Shah R, Ward PT (2007) Defining and developing measures of lean production. *J Oper Manag* 25(4):785–805. <https://doi.org/10.1016/j.jom.2007.01.019>
18. Hung S-C, Hung S-W, Lin M-J (2014) Are alliances a panacea for SMEs? The achievement of competitive priorities and firm performance. *Total Qual Manag Bus Excellence*. <https://doi.org/10.1080/14783363.2014.927133>
19. Skinner W (1969) Manufacturing—missing link in corporate strategy. *Harvard Bus Rev* 46(3)
20. Skinner W (1996) Manufacturing strategy on the “S” curve. *Prod Oper Manag* 5(1):3–14. <https://doi.org/10.1111/j.1937-5956.1996.tb00381.x>
21. Slack N (1991) *The manufacturing advantage*. Mercury Books
22. Swamidass PM, Newell WT (1987) Manufacturing strategy, environmental uncertainty, and performance: a path analytic model. *Manage Sci* 33(4):509–524. <https://doi.org/10.1287/mnsc.33.4.509>
23. Ward PT, Duray R, Keong Leong GK, Sum C (1995) Business environment, operations strategy, and performance: an empirical study of Singapore manufacturers. *J Oper Manag* 13(2):99–115. [https://doi.org/10.1016/0272-6963\(95\)00021-J](https://doi.org/10.1016/0272-6963(95)00021-J)

# Quality and Efficiency Improvement Through Process FMEA—A Case Study



Ramkrishna Bharsakade, Pranav Badgujar, Krishna Malani, Srushti Rithe, and Pranita Salunke

**Abstract** A failure mode and effect analysis (FMEA) helps to identify potential failure modes which can occur in any industry. These failures can lead to major quality defects in the product. In this study, we used a process FMEA approach in a maize flake producing company to enhance the quality and efficiency of the process. A field study approach was used to understand the process, potential failure modes present, and its causes in the process. We developed an FMEA model to evaluate the impact of these failure modes on the process. According to the effects of the potential failure mode on the process and product, a severity ranking was assigned to the respective potential failure mode. Using this severity ranking, detectability in the company and occurrences of the failure modes, a risk priority number (RPN) was assigned to these failure modes. By prioritizing the failure modes, some corrective actions were suggested to the company. These actions reduced the occurrences of the failure modes leading to a reduction in the RPN associated with the potential failure modes. These RPN reductions led to enhance the quality of product and overall increment in productivity and efficiency of the process.

**Keywords** Food industry · Failure mode and effect analysis (FMEA) · Risk priority number (RPN) · Potential failure mode · Quality enhancement

---

R. Bharsakade · P. Badgujar (✉) · K. Malani · S. Rithe · P. Salunke  
Department of Industrial and Production Engineering, Vishwakarma Institute of Technology,  
Pune, India  
e-mail: [pranav.badgujar18@vit.edu](mailto:pranav.badgujar18@vit.edu)

© The Author(s), under exclusive license to Springer Nature Singapore Pte Ltd. 2023  
R. P. Singh et al. (eds.), *Advances in Modelling and Optimization of Manufacturing and Industrial Systems*, Lecture Notes in Mechanical Engineering,  
[https://doi.org/10.1007/978-981-19-6107-6\\_26](https://doi.org/10.1007/978-981-19-6107-6_26)

375



# 1 Introduction

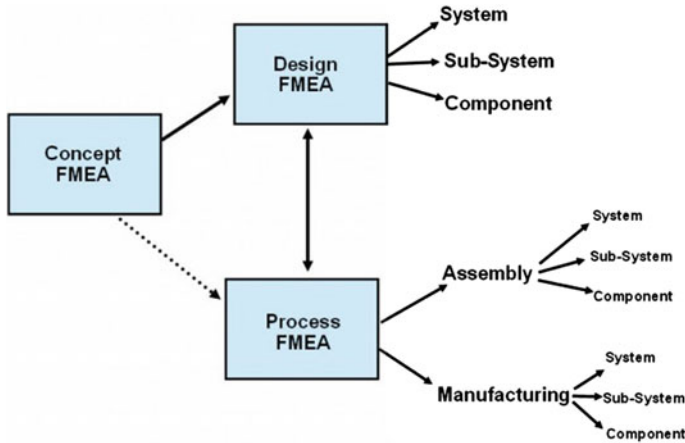
In any industry, a small failure or problem in a product or process may lead to a large impact on the process, surrounding workplace, people working in the process, or people consuming the product. This failure sometimes may be fatal and may incur huge costs for the industry. An Failure Mode and Effect Analysis (FMEA) is a method that identifies the problems and prevents the problems before they occur. Preventing defects and enhancing safety which increases the value of the product ultimately increasing customer satisfaction are the main objectives of FMEA.

In 1949, U.S. Army developed the FMEA system and implemented it for the first time. Later, Apollo's space program executed it to temperate the risk [10]. The aerospace industry in 1950 developed the FMEA technique because of the increasing awareness paid to safety and the necessity to forbid predictable accidents [9]. In manufacturing processes, it was set as a key tool to augment quality and efficiency [10]. Later, the FMEA technique was used as a quality improvement tool by the automotive industry [7]. In 1977, Ford Motors, introduced FMEA in the Research and Development (R&D) to identify the problems during the early stage. In 1984, they introduced the handbook on FMEA to encourage this method. Later, the American automobile manufacturers also introduced this FMEA technique into the management of suppliers [10].

In this paper, a study of FMEA analysis was conducted in a maize flake producing company. It is a small-scale producing unit. The company produces only maize flakes with some variations in quality. The major quality variations are in the thickness of maize flakes. The main objectives of the study were to analyze the Failure modes and their effects on the processes carried in the company, calculate the risk associated with the failure modes and suggest some methods to reduce the risk associated with the failure modes.

## 1.1 Failure Mode and Effect Analysis (FMEA)

FMEA is a proactive analysis tool. It defines and identifies known potential failures and problems from the system, design, process, or service and also helps to eliminate them [6]. The motive of FMEA is to examine the characteristics of a design relative to the planned manufacturing process which helps to ensure that the resultant product meets customer needs and expectations [11]. The FMEA team includes members from different departments who are highly skilled and are knowledgeable about their processes or departments. The departments included in the team may be Research & Development, design, operations, production, maintenance, and procurement.



**Fig. 1** FMEA types. *Source* Rana and Belokar [11]

In the FMEA process, various numerical values are considered for various failure causes using severity, occurrence, and detection ratings. An increase in effect on failure mode results in an increase in its rating [2]. A number is given to assigning the priority to the failure modes analyzed. This number is known as risk priority number (RPN) and is calculated by taking the product of severity, occurrence, and detectability ratings. This number ranges from 1 to 1000 for each failure mode.

*Types of FMEA:*

FMEA is broadly classified into two major types which are Design or Product FMEA, also known as DFMEA, and Process FMEA, also known as PFMEA. Figure 1 shows the types of FMEA.

1. *Design/Product FMEA*

The purpose of a product or design FMEA is to understand problems with the product that have effects such as safety hazards, product malfunctions, or a shortened product life [7]. Design FMEA helps to eliminate the effects and helps in selecting the optimal design variant. It plays an important role to develop a documentary base that reduces risks associated with faulty products to support future designs [11]. Design FMEA can be carried out on products that are in the preliminary design stage or final design stage or Prototype or products that are already in the production stage.

2. *Process FMEA*

The purpose of process FMEA is to find out the potential failure modes of manufacturing or assembly processes at the operation, subsystem, or system level. It also helps to get rid of the process failures which could lead to the separation of defective products as early as possible, and it also avoids using unacceptable methods as part of the processes [11]. People, materials, equipment, methods, and environment are the five elements that should be thought of while

conducting a process FMEA [7]. Process FMEA can also be used to develop future processes and validation programs.

### *Steps of FMEA:*

All Product/Design and Process FMEA follow these ten steps [7]:

- Step 1. Examine the process or product of the company.
- Step 2. Identify potential failure modes through brainstorming sessions.
- Step 3. Identify effects of potential failure modes.
- Step 4. Understand each effect and allocate its severity.
- Step 5. Understand each failure mode and allocate its occurrences.
- Step 6. Allocate ranking for detection of each failure mode.
- Step 7. Determine the risk priority number for each failure mode and/or effect.
- Step 8. Rank each failure mode according to the RPN value to take further action.
- Step 9. Take some measures to terminate or decrease failure modes.
- Step 10. Determine the resulting RPN after taking measures.

## **2 Literature Review**

Parsana and Patel [10] used the process of FMEA in a manufacturing process of a cylinder head to improve the reliability of subsystems in their paper. Various causes of failure modes that are possible and the effects on them with their prevention are also discussed by the authors. As per the authors, these preventions will decrease the loss of money, time, and quality of the industry. Baghele et al. [2] in their paper applied the FMEA technique for litter picker machine in the design and development phase. A holistic thinking approach was applied by authors to break down the whole system into sub-assembly and parts.

Kulkarni and Shrivastava [6] in their paper used FMEA as a tool to enhance the process capability of the system by adopting innovative technologies and integrating them with operational aspects. Their study focused on improving machine reliability and enhancing the safety of CNC grinding machine. Shinde et al. [13] in their study also used the FMEA to increase the process capability in a bush manufacturing process. Their study focused on improving the performance and reliability of the system.

Souza and Álvares [14] used FMEA and fault tree analysis (FTA) as tools to study failures in the oil circulation system of the combined bearing of a hydraulic Kaplan turbine used in a hydraulic plant. In their study, they performed a comparison between the above two tools to implement a structured predictive maintenance plant. Arabian-Hoseynabadi et al. [1] used proprietary software in their study to understand the reliability of wind turbines using the FMEA method.

Capunzo et al. [4] applied this FMEA technique in a clinical laboratory. Also, Burgmeier [3] applied the FMEA technique to eliminate the process errors in a transfusion Laboratory/Blood Bank. This showed that the FMEA technique can be applied in a clinical laboratory, even if of small dimensions [4]. McNally et al. [8]

applied FMEA in an Australian hospital to identify deficiencies in the ward stock system which were used to store bulk drug packs that lead to medication errors. After knowing the deficiencies in the system, they proposed an alternative drug distribution system.

Rana and Belokar [11] used the process FMEA in improving a welding process. The authors detected the failure modes and suggested some preventive action in their study. Namdari et al. [9] used the FMEA technique in their paper to optimize fuel consumption in tillage. They identified that plowing speed, soil moisture content and plowing depth were the important factors that affected the fuel consumption in tillage. Scipioni et al. [12] in their paper applied a design FMEA in a food company to assure product quality and improve the performance of the production cycle.

Tanik [15] in his paper used systematic quality control tools to improve the order handling process in food package production and to strengthen the supply chain in the food industry. Teng et al. [16] in their paper aimed to implement FMEA in a collaborative supply chain environment. They illustrated a Microsoft Excel tool to determine sampling size, reliability, and confidence level for tests in design verification and control plan as a part of the integrated FMEA process. To select new suppliers from a supply chain risk perspective, Chen and Wu [5] proposed a modified FMEA in their paper. They applied the analytical hierarchy process method to find out the weight of each criterion and sub-criterion which are used for supplier selection.

### 3 Methodology

A process FMEA was carried out in the company. The authors followed a standard stepwise approach to conducting a process FMEA in the company. Below mentioned is the stepwise approach carried out by the authors in the company.

#### Step 1. Examine the process or product of the company

Many visits were conducted by authors to know and understand the process of the company. The process started with cleaning maize grains where the maize grains, i.e., the raw material are cleaned in a cleaning machine. After cleaning, the maize grains were polished. During the polishing of maize grains, the upper coating of maize is removed by the polishing machine.

Once the grains were polished, they were sorted in a sorting machine. During this process, the polished grains are sorted according to the standard size required. If the grains are not of standard size, they were rejected for the further process and were separately packed. The final polished grains with standard size were stored in a silo. The polished grains are then boiled in a cooker where steam, water, and some ingredients are also added. The steam is generated through an automated boiler. Once the grains are perfectly boiled, they are rolled on a large conveyor belt for cooling purposes.

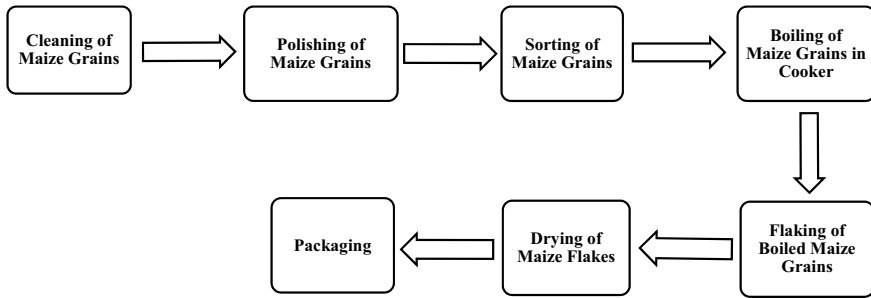


Fig. 2 Process chart of company

The boiled maize grains are then poured into a flaking machine where the boiled grains are flaked to a certain thickness. After flaking, these maize flakes are then dried in a drying machine. In this machine, the maize flakes which have high moisture content in them were dried to a certain temperature where the desired moisture is kept. And finally, the ready maize flakes are packed. Figure 2 shows the process chart of the company.

Step 2. **Identify potential failure modes through brainstorming sessions**

Once the processes of the company were known and understood by authors, brainstorming sessions were carried out between authors, company owner, company manager, and some workers to jot down the possible failure modes for the processes in the company. The failure modes identified are shown below—

• Improper cleaning	• Excess cooking	• Less flaked
• Excess polishing	• Less cooking	• Less dried
• Less polishing	• Excess flaked	• Excess dried
• Improper sorting		

Step 3. **Identify effects of potential failure modes**

Each failure mode was further discussed in detail with the company. All the possible scenarios that can take place for the respective failure modes were also discussed with the company. After a lot of discussions, the possible effects were listed next to the failure mode.

Step 4. **Understand each effect and allocate its severity**

Each failure mode can have various effects and these effects can be of various severity levels that can have an impact on various aspects of a company. Considering this, the authors gave each effect its severity ranking. The severity of each potential failure was given by considering its potential effect on the product and further processes. The severity of each failure mode was different according to each member. Considering this, the average was taken of the severity given by all the members. To assign

the severity of potential effect due to potential failure all members were given a table of severity for reference. The table provided for reference is shown in Table 1.

**Step 5. Understand each failure mode and allocate its occurrences**

An occurrence table for potential failure mode was provided to the company. The company manager and workers of the team referred to the table and discussed the occurrences of the failure modes. After a lot of discussions, the occurrences of each failure mode were listed. The table provided to the company for reference is shown in Table 2.

**Step 6. Allocate ranking for detection of each failure mode**

The authors discussed the current control system for each possible failure mode with the company. After understanding the detection system at each process stage, the authors referred to the table and assigned the detection ranking to each failure mode. The table referred to, is given in Table 3.

**Step 7. Determine the risk priority number for each failure mode and/or effect**

The rating of severity, occurrence, and detectability of each failure mode was listed, the Risk Priority Number (RPN) for each potential failure mode was calculated by the authors. The RPN is calculated by—

$$\text{RPN} = \text{Severity Rating} \times \text{Occurrence Rating} \times \text{Detectability Rating}$$

The smallest RPN calculated was 60 for failure mode in the cleaning and sorting process. The largest RPN calculated was 392 for failure mode in the cooking process.

**Step 8. Rank each failure mode according to RPN value to take further actions**

A Pareto diagram for the potential failure modes was created by the authors. The authors decided to work on any failure mode that had an RPN of 100 or higher. With the criteria of RPN 100 or more, seven failure modes were needed to be taken into consideration (Fig. 3).

**Step 9. Take some measure to terminate or decrease failure modes**

The prioritized failure modes were discussed with the company to determine the action which could be taken to reduce or eliminate the risk. After a lot of discussions, some actions were suggested to the company which can be implemented to reduce the occurrences of the potential failure modes which in turn will reduce the risk associated with the respective failure mode.

**Step 10. Determine the resulting RPN after taking measures**

There was a discussion between the authors and the company to address the results of the corrective actions. The company was pleased with the results as the occurrences of prioritized failure mode were reduced. The new occurrences of prioritized failure modes were listed by authors and the risk priority number associated with the failure mode was calculated.

**Table 1** Severity evaluation criteria

Effect	Customer effect	Manufacturing/assembly effect	Ranking
Harmful with no warning	Extreme high severity which affects the safety of operations with no warning	Or may risk the life of the operator with no warning	10
Harmful with some warning	Extreme high severity which affects the safety of operations with some warnings	Or may risk the life of operator with some warnings	9
Very high	Product is waste and of no use	Or hundred percent of product may have to be discarded, or the product needs to be repaired which will require at least 1 h time	8
High	Product cannot be operated at its maximum performance level High level of dissatisfaction	Or product may have to be sorted and a portion which is less than hundred percent have to be discarded, or product needs to be repaired which will require more than 1/2-h time	7
Moderate	Product can be operated at low performance level Moderate level of dissatisfaction	Or a portion of the product which is less than hundred percent may have to be discarded with no sorting, or product needs to be repaired which will require at least 1/2-h time	6
Low	Product can be operated at moderate performance level	Or hundred percent of product may have to be repaired or reworked with no product being discarded	5
Very low	Product does not comply with standards. More than 3/4th of customers notices the defect	Or the product may have to be sorted, with no product being discarded, and a portion which is less than hundred percent have to be reworked	4
Minor	Product does not comply with standards. Around 1/2 of customers notice the defect	Or a portion which is less than hundred percent of the product may have to be reworked, with no product being discarded	3
Very minor	Product does not comply with standards. Less than 1/4 of customers notice the defect	Or a portion which is less than hundred percent of the product may have to be reworked, with no product being discarded	2

(continued)

**Table 1** (continued)

Effect	Customer effect	Manufacturing/assembly effect	Ranking
None	Effect is not detectable	Or minor trouble to operation or operator, or no effect	1

Source McDermott et al. [7]

**Table 2** Occurrence evaluation criteria

Possibility of failure	Occurrence of failure (considering per 1000)	Rank
Very high	More than 10%	10
High	Around 5%	9
	Around 2%	8
	Around 1%	7
Moderate	Around 0.2%	6
	Around 0.05%	5
	Around 0.01%	4
Low	Around 0.001%	3
	Less than 0.0001%	2
Very Low	Using preventive control failure will be eliminated	1

Source McDermott et al. [7]

## 4 Results and Discussion

After calculating the RPN of current failure modes, the failure modes with RPN of 100 or more were taken as a priority. Some suggestions were suggested for the prioritized failure modes. The suggestions suggested are—Analyzing the size of grains before processing, checking the moisture content at different stages, and having standard size markings on machines. The suggestions suggested are listed in the FMEA sheet shown in Table 4.

By implementing these suggestions, the occurrences associated with the potential failure modes are reduced and this will result in a reduction of risk associated with the failure modes. The new RPN’s for the potential failure mode were calculated and there was a reduction of 38%, on average. The percent reduction in each failure mode is shown in Table 5. The comparison between old RPN and new RPN is shown in below bar chart in Fig. 4.

The recommended suggestions not just reduce the occurrences but increases the overall productivity of the company. This will happen because the occurrences of the failure modes have reduced, and this reduction reduces the time, which was earlier wasted on rework, and there is a reduction in wastage of maize grains which used to break in the polishing stage. There is also a reduction of excess boiled or less boiled maize grains, reduction in excess flaking or less flaking of maize grains, and excess



**Table 3** Detection evaluation criteria

Possibility of detection	Opportunity for detection	Likelihood of detection by process control	Rank
Almost impossible	Chances for detection is none	No system to detect or check problem	10
Very remote	Possibility of detection at any stage is none	Detection of problem is difficult and can be achieved through random checks only	9
Remote	Detection of problem after processing	Visual detection of problem after processing	8
Very low	Detection of problem at origin	Visual detection of problem while processing or by using attribute gaging after processing	7
Low	Detection of problem after processing	Variable gaging and attribute gauging used to detect problem after processing or while processing, respectively	6
Moderate	Detection of problem at origin	Variable gaging detection by operator or automatic control detection (light, buzzer, etc.) which will signal operator	5
Moderately high	Detection of problem after processing	Automatic control detection after processing which will detect defective part and stop it from further processing	4
High	Detection of problem at origin	Automatic control detection while processing which will detect defective part and stop it from further processing	3
Very high	Detection of problem is certain	Automatic control detection while processing which will detect defective part and discard it	2
Almost certain	Detection not applicable; error prevention	Defective parts cannot be made because item has been error-proofed by process/product design	1

Source McDermott et al. [7]

drying and less drying of maize flakes. These reductions of all types of wastes in the company increase its productivity. As there is a reduction in rework, and also an increment in productivity, this will result in a reduction of the lead time of a product, which ultimately increases customer satisfaction, and will add value to the product.

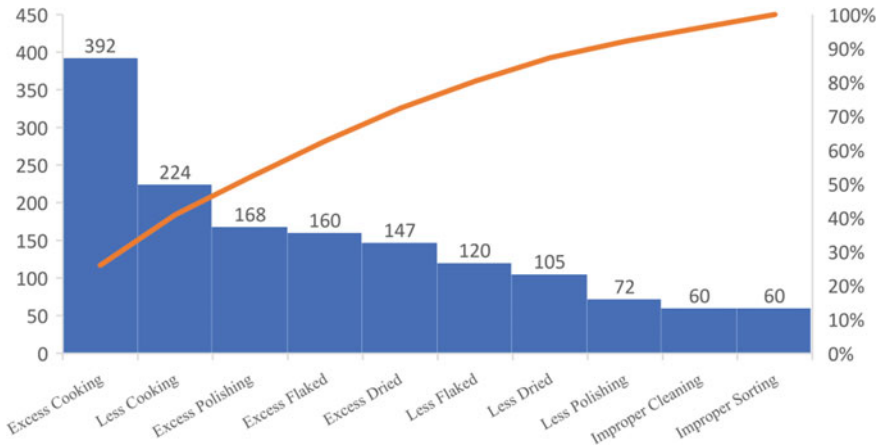


Fig. 3 Pareto analysis of potential failure modes

## 5 Conclusion

From the study, we can understand that the failure modes like excess cooking, less cooking, excess flaking, less flaking, excess drying, and less drying can lead to major quality defects which leads to rejection from the customers. By using FMEA, we can analyze the severity of these failure modes and take corrective actions for them. These actions will reduce failure modes and enhance the quality of the product which will help in building a good image of the company. From the study, we understand that FMEA helps us to identify the weak points in the processes and take actions accordingly. By taking action, the risk associated with it can be reduced and the processes can be improved. This leads to promising results which shows that FMEA will help to identify and improve further weak points. A successful process FMEA leads to increment of productivity of the company. The calculated RPN helps us to identify which potential failure mode needs more attention as compared to other potential failure modes. In this study, the highest RPN calculated came out to be of failure mode associated with excess boiling of maize grain. This failure mode may result in major quality defects in the product which will lead to rejection in the product. FMEA helped to identify and prioritize this risk and was reduced by taking corrective actions. This shows that FMEA is a simple but important tool for quality improvement.

**Table 4** Process FMEA sheet

Process failure mode and effect analysis														
Part/product: Maize Flakes					Key contact person: ***									
Customer name (if any): ***					Key contact: ***									
Other details: –					Core team: ***									
Process	Potential failure mode	Potential effect	Sev	Potential causes of failure	Occ	Current controls, prevention	Current controls detection	Det	RPN	Recommended action	Sev	Occ	Det	RPN
Cleaning	Some unwanted material not getting cleaned	Will make disturbances in polishing stage	2	Excess vibration of machine	3	None	None	10	60	None	2	3	10	60
Polishing	Excess polishing of maize grains leading to breaking of grains	Grains will break into small pieces	7	Excess pressure by roll	3	None	Visual inspection post-processing	8	168	Analyzing the size of maize grains by taking some samples and adjusting the position of the roller accordingly	7	2	8	112
	Grains getting less polished than the desired quality	Grains will not cook properly due to their coating	3	Pressure by roll less than required	3	Checking the position of roll	Visual	8	72	None	3	3	8	72

(continued)

**Table 4** (continued)

Process failure mode and effect analysis														
Part/product: Maize Flakes					Key contact person: ***									
Customer name (if any): ***					Key contact: ***									
Other details: –					Core team: ***									
Process	Potential failure mode	Potential effect	Sev	Potential causes of failure	Occ	Current controls, prevention	Current controls detection	Det	RPN	Recommended action	Sev	Occ	Det	RPN
Sorting	Maize grains not getting properly sorted according to their size	Some broken pieces of maize grains will enter in the further process leading to quality issues	3	Slackness in belt leading to lower rpm of machine and grains not getting sorted according to the requirement	2	None	None	10	60	None	3	2	10	60
Cooking	Excess cooking of maize grains	The Color of maize grains gets darker and maize grains get excess flaked further	7	Supply of steam more than required	7	None	Visual inspection post-processing	8	392	Checking the moisture content in maize grains and if it is more than required then reducing the supply of steam for process	7	3	8	168

(continued)

**Table 4** (continued)

Process failure mode and effect analysis														
Part/product: Maize Flakes						Key contact person: ***								
Customer name (if any): ***						Key contact: ***								
Other details: –						Core team: ***								
Process	Potential failure mode	Potential effect	Sev	Potential causes of failure	Occ	Current controls, prevention	Current controls detection	Det	RPN	Recommended action	Sev	Occ	Det	RPN
	Grains getting cooked less than the desired quality	Grains will not get flaked properly	7	Supply of steam less than required	4	None	Visual inspection post-processing	8	224	Checking the moisture content in maize grains and if, it is less than required then increasing the supply of steam for process	7	3	8	168
Flaking	Maize grains getting excess flaked than the required size	It will lead to the breaking of maize grain after drying	5	The gap between two rollers much more than required	4	Adjusting the roller size post-inspection	Visual inspection post-processing	8	160	Having standard size markings of maize flakes and tolerance limit on adjustment screw of machine	5	2	8	80

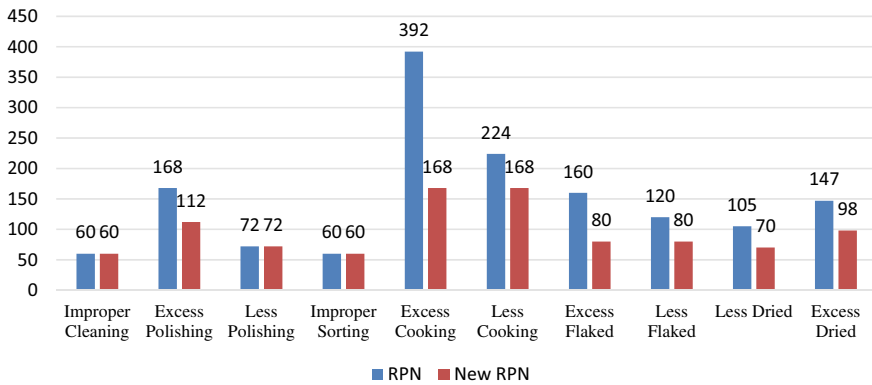
(continued)

**Table 4** (continued)

Process failure mode and effect analysis														
Part/product: Maize Flakes					Key contact person: ***									
Customer name (if any): ***					Key contact: ***									
Other details: –					Core team: ***									
Process	Potential failure mode	Potential effect	Sev	Potential causes of failure	Occ	Current controls, prevention	Current controls detection	Det	RPN	Recommended action	Sev	Occ	Det	RPN
	Maize grains getting less flaked than the required size	Maize flakes will not dry properly	5	The gap between two rollers much less than required	3	Adjusting the roller size post-inspection	Visual inspection post-processing	8	120	Having standard size markings of maize flakes and tolerance limit on adjustment screw of machine	5	2	8	80
Drying	Maize grains getting less dried than the required quality	There will be more moisture in maize flakes leading to quality issues	5	The speed of conveyors less than required	3	Adjusting the speed of dryer post-inspection	Visual inspection post-processing	7	105	Checking the moisture content in maize flakes and accordingly setting the speed of conveyor in the dryer	5	2	7	70
	Maize grains getting excess dried than the required quality	It will lead to the breaking of maize grain while packaging	7	The speed of conveyors more than required	3	Adjusting the speed of dryer post-inspection	Visual inspection post-processing	7	147	Checking the moisture content in maize flakes and accordingly setting the speed of conveyor in the dryer	7	2	7	98

**Table 5** Percentage reduction of RPN

Failure mode	Old RPN	New RPN	Percentage reduction (%)
Improper cleaning	60	60	0.00
Excess polishing	168	112	33.33
Less polishing	72	72	0.00
Improper sorting	60	60	0.00
Excess cooking	392	168	57.14
Less cooking	224	168	25.00
Excess flaked	160	80	50.00
Less flaked	120	80	33.33
Less dried	105	70	33.33
Excess dried	147	98	33.33



**Fig. 4** Comparison between old and new RPN

## References

1. Arabian-Hoseynabadi H, Oraee H, Tavner PJ (2010) Failure modes and effects analysis (FMEA) for wind turbines. *Int J Electr Power Energy Syst* 32(7):817–824
2. Baghele P, Londhe N, Rode B, Bharsakade R, Kuber S, Kotwal G (2020) Failure modes and effects analysis (FMEA) for litter picking machine. In: *Proceedings of the 2020 international conference on industry 4.0 technology (I4Tech)*, Pune, India, pp 55–60
3. Burgmeier J (2002) Failure mode and effect analysis: an application in reducing risk in blood transfusion. *Jt Comm J Qual Improv* 28(6):331–339
4. Capunzo M, Cavallo P, Boccia G, Brunetti L, Pizzuti S (2004) A FMEA clinical laboratory case study: how to make problems and improvements measurable. *Clin Leadersh Manag Rev* 8(1):37–41
5. Chen PS, Wu MT (2013) A modified failure mode and effects analysis method for supplier selection problems in the supply chain risk environment: a case study. *Comput Ind Eng* 66(4):634–642
6. Kulkarni P, Shrivastava R (2013) Failure mode effect analysis: process capability enhancement—a case study. *Int J Eng Res Technol* 2(4):1859–1868

7. McDermott R, Mikulak R, Beauregard M (2008) *The basics of FMEA*, 2nd edn. CRC Press, Florida
8. McNally K, Page M, Sunderland B (1997) Failure-mode and effects analysis in improving a drug distribution system. *Am J Health Syst Pharm* 54(2):171–177
9. Namdari M, Sh, Rafiee, Jafari A (2011) Using the FMEA method to optimize fuel consumption in tillage by Moldboard Plow 1 introduction. *Int J Appl Eng Res* 1(4):734–742
10. Parsana T, Patel M (2014) A case study: a process FMEA tool to enhance quality and efficiency of manufacturing industry. *Bonfring Int J Ind Eng Manag Sci* 4(3):145–152
11. Rana S, Belokar R (2017) Quality improvement using FMEA: a short review. *Int Res J Eng Technol* 04(06):263–267
12. Scipioni A, Saccarola G, Centazzo A, Arena F (2002) FMEA methodology design, implementation and integration with HACCP system in a food company. *Food Control* 13(8):495–501
13. Shinde R, Shrivastava R, Morey R (2015) Failure mode effect analysis-case study for bush manufacturing process. *Int J Sci Eng Appl Sci (IJSEAS)* 1(4):2395–3470
14. Souza R, Álvares A (2008) FMEA and FTA analysis for application of the reliability-centered maintenance methodology: case study on hydraulic turbines. *ABCM Symp Series Mechatron* 3:803–812
15. Tanik M (2010) Improving “order handling” process by using QFD and FMEA methodologies: a case study. *Int J Q Reliab Manag* 27(4):404–423
16. Teng SG, Ho SM, Shumar D, Liu PC (2006) Implementing FMEA in a collaborative supply chain environment. *Int J Qual Reliab Manag* 23(2):179–196



# Study on Mechanical Characteristics of TiB<sub>2</sub>, WC, ZrB<sub>2</sub> and B<sub>4</sub>C Reinforced Al 2XXX, 6XXX and 7XXX Series Alloys—A Systematic Review



B. M. Karthik, K. Nithesh, Sathyashankara Sharma, D. Srinivas, and S. Sandeep Nambiar

**Abstract** The effect of heat treatment and various reinforcement additions on aluminium alloys is discussed in this article. Metal matrix composites are now widely employed in aerospace and automotive applications. Composites utilization has been rapidly increasing because of their notable properties, viz. improved strength and impact resistance. The current review work, on the other hand, collects the possibility of using different reinforcements in bare with or without hybridization. Data assessment with property analysis will pave the path for future hybridization research endeavours. The purpose of this article is to collect data on aluminium matrix composites with TiB<sub>2</sub>, WC, ZrB<sub>2</sub> and B<sub>4</sub>C reinforcements and provide collective information regarding prospective improvements that might be made based on the data.

**Keywords** Aluminium matrix composites (AMCs) · Titanium diboride (TiB<sub>2</sub>) · Tungsten carbide (WC) · Boron carbide (B<sub>4</sub>C) · Zirconium diboride (ZrB<sub>2</sub>)

## 1 Introduction

Composites typically constitute more than one dissimilar material (with different chemical or physical properties) that, when combined, have traits more desirable than the individual materials by themselves [1–3]. The components do not fully blend or lose their assets; they come together and contribute valuable traits to improve the resulting product. Composites are designed to provide benefits such as higher strength, stiffness, corrosion resistance and improved fatigue properties [4].

---

B. M. Karthik · K. Nithesh (✉) · S. Sharma · D. Srinivas · S. S. Nambiar  
Department of Mechanical and Manufacturing Engineering, Manipal Institute of Technology,  
Manipal Academy of Higher Education, Manipal, Karnataka, India  
e-mail: [nithesh.nithesh@learner.manipal.edu](mailto:nithesh.nithesh@learner.manipal.edu)

© The Author(s), under exclusive license to Springer Nature Singapore Pte Ltd. 2023  
R. P. Singh et al. (eds.), *Advances in Modelling and Optimization of Manufacturing and Industrial Systems*, Lecture Notes in Mechanical Engineering,  
[https://doi.org/10.1007/978-981-19-6107-6\\_27](https://doi.org/10.1007/978-981-19-6107-6_27)

393

The primary classifications of the constituent materials of a composite are recognized as: matrix and reinforcement. Matrix phase embeds and surrounds the reinforcements by maintaining their relative locations and supporting the reinforcement. The reinforcement itself provides a superior level of support and stiffness to the composite [5]. The reinforcement, according to their structure, may be classified as continuous or discontinuous type. Monomolecular fibres such as SiC or carbon fibres fall under continuous reinforcement. Discontinuous reinforcement may be isotropic; they can be constructed using standard metalworking methods, such as forging, rolling and extrusion [6].

Depending on the material type of matrix, composites are broadly of three types: polymer matrix composites (PMC), metal matrix composites (MMC) and ceramic matrix composites (CMC). Out of these, due to their low cost and varied range of properties, metal matrix composites are increasingly getting more attention [7]. Metal matrix composites are composites where matrix is compulsorily a metal, whereas reinforcement may be another metal, ceramic or even an organic compound in dispersion. They are majorly used for prototyping of the commercial airliners, space shuttles, bicycles, automobiles, electronic substrates and even articles like golf clubs [8]. MMCs are favoured based on their greater properties of specific strength and specific modulus. Further, they possess thermal conductivity, stiffness and low coefficient of thermal expansion and, in some cases, better wear resistance. MMCs may consist of particles, layers or fibres as their enhancing reinforcements [9].

In a category of MMCs, AMCs are considered to have high performance, especially light-weight aluminium-based material composites. These days, AMCs are getting widely accepted for automobile, aerospace and several industrial applications owing to their critical properties such as strength, low density and improved wear resistance in contrast to other available MMCs [10].

Various grades of aluminium are used in the production of AMCs depending on their usage and application. Aluminium has several alloys ranging from 1xxx to 8xxx. 1xxx is classified as pure aluminium of 99% or higher with excellent workability qualities. The heat treatable alloys comprise 2xxx, 6xxx and 7xxx series with primary alloying elements as copper, silicon + magnesium and zinc, respectively. Non-heat treatable alloys comprise 3xxx, 4xxx and 5xxx series that possess increased metal strength [11]. Composites that are aluminium based are very frequently used and extensive research had been conducted to explore the possibility of tribomechanical usage [12].

Different heat treatment results in a change in the microstructure of alloy. Grain size changes according to the heat treatment process applied. In AMCs, the change in grain size determines the mechanical properties. This study tells us about the effect of mechanical properties on the addition of ceramic reinforcements such as  $TiB_2$ , WC,  $ZrB_2$  and  $B_4C$  to aluminium matrix in varying proportions. Each reinforcement imparts characteristic properties that amend the properties of the base alloy accordingly.

## 2 Reinforcements

### 2.1 Titanium Diboride (TiB<sub>2</sub>)

Titanium diboride is a favourable reinforcement as it has high values of hardness and stiffness coupled with good electrical and thermal conductivity. When paired with aluminium matrix to form a composite, it does not react and thus avoids brittle reaction products [13]. As a ceramic TiB<sub>2</sub> displays high melting point (2790 °C), remarkable wear resistance and superior strength to density ratio [14]. This makes the TiB<sub>2</sub> an appreciable supplement for the cutting tool and thus, it finds applications in seals and wear parts. It is also used in high-temperature structural components [15].

The microstructures of AMCs reinforced with TiB<sub>2</sub> portray uniform distribution of particles with interface and strong bonding with matrix. TiB<sub>2</sub> particles formed in situ display various geometries of cubic, spherical and hexagonal structures [16].

When Al 7075 is reinforced with TiB<sub>2</sub> in 4, 8, 12 wt% (via in situ) gradually, the density rises with increase of reinforcement. Tensile strength also shows an increasing trend with addition of reinforcement. Microhardness also shows improvement with a maximum of 42.4% compared to base alloy on addition of 12 wt% of TiB<sub>2</sub> [17]. Another study conducted for Al 6061 shows similar tendencies in mechanical properties upon adding TiB<sub>2</sub> in 4, 8 and 12 wt%. Tensile strength shows a steady increasing pattern on raising TiB<sub>2</sub> content, so does the hardness, measured by Rockwell hardness test. The wear behaviour noted indicates that higher number of TiB<sub>2</sub> particles will improve the wear resistance of the composite [18]. In Al 2021, tensile strength improves to 135 MPa at 10 wt% TiB<sub>2</sub> addition when compared to as cast samples. However, at 10 wt% TiB<sub>2</sub> addition, the hardness value increases to 189 HV [19]. Another investigation on stir casted Al 7075 with reinforcement taken in 4, 6 and 8 wt% reaffirms the increase of hardness with more amount of TiB<sub>2</sub> particles. In this case, maximum hardness was achieved at 8 wt%. The wear rate is also the least at 8 wt%, consistent with previous results [20]. In a study, base alloy Al 6063 and its composite with TiB<sub>2</sub> reinforcement was compared, and results show a spike in the mechanical properties by 21% increase in microhardness, 65% increase in elasticity modulus and 47% increase in ultimate tensile strength (UTS), respectively. Ductility denoted by elongation percentage increased significantly by 368% [21]. When TiB<sub>2</sub> is varied in 5 and 10 wt% in Al 6063, the density increased linearly. The hardness results show consistent improvement as well [8]. An experiment was carried out to see the effect of wt% of TiB<sub>2</sub> on Al 6061 matrix. Results showed a linear rise in the hardness and density of the composite at 5 and 10 wt%. Similar trend remains noticed in hybrid Al 6061 composite reinforced with SiC/TiB<sub>2</sub>, hardness was increased for 5 wt% (SiC + TiB<sub>2</sub>) as compared to 3 wt% SiC+2 wt% TiB<sub>2</sub> [22]. With the increase in the wt% of TiB<sub>2</sub>, it shows that the bonding between the particles and matrix increases [23].

## 2.2 Tungsten Carbide (WC)

Tungsten carbide is a fine dark powder used in making protective coatings, as an abrasive material, cutting tool and other industrial applications. The density and stiffness are high, nearly double that of steel. The hardness of WC is also impressive, comparable to corundum [24]. Moreover, tungsten carbide is a high strength of material which is considered to be tough and rigid. The compressive strength is virtually greater than all forged, melted or cast metals and alloys, making it a desirable reinforcement for metal matrices. Several studies observe that varying the per cent of tungsten carbide reinforcement in Al matrix alters mechanical properties of composite sample. One study on Al 6061 shows that when the wt% of WC was raised from 0 to 4% in steps of 1%, the tensile strength is enhanced by 3% along with 55% increase in UTS [25]. Another study gave matching results for these parameters up to 3 wt% and beyond 3 wt% WC tensile strength decreased because of improper bonding between matrix and reinforcement [26]. In another study, hybrid Al 7075 composite with tungsten carbide (2, 4, 6, 8 and 10 wt%) + molybdenum disulphide ( $\text{MoS}_2$ ) (4 wt%) as reinforcements was fabricated using stir casting process. Addition of WC up to 6 wt% enhanced the hardness. Further increase in wt% of WC showed a decreasing trend. The tensile strength showed a rise with higher wt% of WC, though a declining trend in hardness is observed at 8 and 10 wt% of WC and 4 wt%  $\text{MoS}_2$  [24]. Composite samples of Al 6082 with WC (2, 4, 6, 8 and 10 wt%) was fabricated by stir casting. A reduction in density of composites is observed with increase in WC. Mean decrease in density is 1.15% per 2% increase of WC by weight [27]. When compared to the base alloy, the density of the composites (10 wt% of WC) is reduced to a maximum of 5.88%, and strength increases with higher WC up to 8 wt% and then a decline on further addition of WC. The UTS rose by 16% and yield strength increased up to 22% related to the base alloy [27]. When WC is stir casted to Al 2024, microhardness and wear property of the material showed an increasing trend with addition of reinforcements from 0 to 5 wt% [28]. One study revealed that on adding WC to Al 6061 mechanical properties like wear resistance, tensile strength and hardness improved. Results obtained were greatest at 3 wt% of WC addition. Ductility of the composite was however compromised with the reinforcement addition [29]. When compared to Al 6061 base alloy, the elongation of Al 6061-WC composite material increased. It is evident that composite material shows higher brittleness with increase in the filler (WC). This shows that the matrix experiences ductility due to influence of reinforcement material. So, ductility drops by about 100% when WC content increased from 0 to 4 wt%, as the material gets harder, ductility is lost, and we know that at 4 wt% of WC, the composite becomes extremely hard thus its loses its ductility entirely [30]. This also states that as the material becomes harder, it becomes less tensile but can bear compressive loadings. At 4 wt% of WC, the composite loses its ductility almost entirely, but it becomes excellent under compression.

### 2.3 Zirconium Boride (ZrB<sub>2</sub>)

Zirconium boride (ZrB<sub>2</sub>) has high electrical conductivity [31], high melting point and high hardness versus molten iron and slags. Several industrial sectors, including as foundry and refractory industries, use this as a desirable material for high-temperature applications. Metal matrix can be fabricated by various means like hot pressing. It has been found that hot pressing without a protective atmosphere leads to the production of heavy composite material with good physical properties and mechanical properties [32]. Another way is powder metallurgy which is combined with microwave sintering which gives high-density composites at low temperature [33]. Spark plasma sintering is another means to produce composite. This ensures a uniform distribution of ZrB<sub>2</sub> in aluminium matrix. When compared to microwave, spark plasma produces composites of higher density [34]. Strength of composite material increases with addition of reinforcement material. When Al 2618 was reinforced with ZrB<sub>2</sub> along with Si<sub>3</sub>N<sub>4</sub> and AlN, it was found that micro-Vickers hardness, tensile strength and ultimate strength were improved and the wear rate decreased [31]. Further addition of Al<sub>2</sub>O<sub>3</sub> + ZrB<sub>2</sub> + TiB<sub>2</sub> reinforcement, increases the hardness of pure aluminium considerably. It was found that the stiffness of composites exceeds the hardness of non-reinforced composites by more than 63% [32]. In AA 6061 + ZrB<sub>2</sub> + SiC hybrid composite, an increase in the percentage of ZrB<sub>2</sub> shows a significant increase in tensile strength, along with yield strength and UTS, but it was found that any further increase in the percentage of SiC results in a decrease in the tensile strength, but leads to an increase in the microhardness [35]. When microwave sintering was applied to Al-ZrB<sub>2</sub> composites high density was obtained at low temperature. Bending strength and microhardness were 340 MPa and 56 VHN, respectively [33]. In another study, it was found that sample X-Al 6061+10%Al-10%Zr and 30%Al-3%B when compared sample Y-Al 6061+20%Al-10%Zr and 60%Al-3%B has larger grain size, but sample Y has a greater microhardness, yield strength and UTS [36]. As the wt% of ZrB<sub>2</sub> increases from 0 to 10, the UTS reportedly increases by 31.77% [37]. The grain size reduces in presence of ZrB<sub>2</sub>. When ZrB<sub>2</sub> in situ with AA 5052 is developed, there is again significant impact in the mechanical properties like UTS and yield strength up to 9 vol% reinforcement addition. The ductility was also increased compared to base alloy [38]. Another important characteristic of the addition of ZrB<sub>2</sub> is the reduction in the elongation of the matrix [35, 37]. The elongation reduces by 38.82% as ZrB<sub>2</sub> increase from 0 to 10 wt% [37].

### 2.4 Boron Carbide (B<sub>4</sub>C)

B<sub>4</sub>C is a by-product of the reaction involving metal borides. It is an extremely hard B<sub>4</sub>C ionic material which finds application in bulletproof vests [39], armoured tank engine sabotage powders as well as in industrial application. B<sub>4</sub>C is the hardest known material after cubic boron nitride and diamond. The material can be classified

as robust, having excellent chemical and thermal stability and is very hard with low density. The specific gravity is low with high elastic modulus and excellent neutron absorption chemical and thermal stability [40]. Given these mentioned properties, Al–B<sub>4</sub>C systems have been widely used as cermet and armour materials, which have a significant industrial investment as high-strength applications. Boron carbide possesses the stability of ionizing radiation [41]. The composites are fabricated by various means, some by addition of SiC, Al<sub>2</sub>O<sub>3</sub>, glass fibres, B<sub>4</sub>C using stir casting method [40] and some by extrusion process [42]. It has been found that the liquid metallurgy route was the most suitable route for the fabrication of Al–B<sub>4</sub>C composites because of its affordability and flexibility when compared to stir casting [43], but the stir casting process ensures homogeneous distribution [40]. It also ensures strong bond with the metal matrix [42]. Fabrication at higher temperatures like 900 °C causes agglomeration of reinforcement due to change in viscosity. Agglomeration also takes place when small-sized reinforcement is added in higher quantity which leads to a drop in mechanical properties of AMC [42]. The physical properties of metal increase with addition of reinforcement, particularly B<sub>4</sub>C and SiC. It was found that addition of B<sub>4</sub>C increased the mechanical properties of the composites, i.e. increase in compressive strength, hardness, elastic modulus and young's modulus [44]. Stir cast Al 6061 reinforced with the constant percentage of B<sub>4</sub>C and different percentage of SiC hybrid composites was fabricated. Better tribological properties were identified at 10 wt% SiC and 3 wt% B<sub>4</sub>C [45]. Varied percentage of reinforcement material brings insignificant effect on mechanical properties of the composite. Three samples with varied percentage of alumina (2 and 3 wt%) and B<sub>4</sub>C (2 and 3 wt%) with Al base alloy was casted. It was found that 3 wt% alumina + 2 wt% B<sub>4</sub>C reinforcement addition (sample 1) showed higher tensile strength than 2 wt% alumina + 3 wt% B<sub>4</sub>C (sample 2) composite. The impact value of sample 1 was found to be higher than base alloy but lower than sample 2, and the BHN of sample 1 is lower than sample 2 but higher than base alloy [41]. Studies show that the size of reinforcement also plays an important role in determining the properties of AMC [46]. Micro-Vickers hardness value varies with the size of B<sub>4</sub>C added [3]. Micro-Vickers hardness value shows that the maximum hardness was for the particle size of 350 μm but the tensile strength was found to be maximum for particle size of 105 μm of B<sub>4</sub>C powder [46].

### 3 Conclusion

The addition of reinforcements such as TiB<sub>2</sub>, WC, ZrB<sub>2</sub>, and B<sub>4</sub>C to Al 6061 enhanced its mechanical characteristics to a considerable extent. Better results were obtained with 12 wt% TiB<sub>2</sub>, 3 wt% WC, 10 wt% ZrB<sub>2</sub>, and 3 wt% B<sub>4</sub>C. The addition of reinforcements such as TiB<sub>2</sub> and WC to Al 7075 significantly improved its mechanical properties. Better results were achieved with 12 wt. % TiB<sub>2</sub> and 10 wt% WC. Similarly, reinforcements enhanced mechanical properties in 2xxx series of Al alloys. Performance of TiB<sub>2</sub>, WC and ZrB<sub>2</sub> was enhanced by 10%, 5% and 8%,

respectively. Stir casting process has been proven to be more efficient and cost-effective method of casting AMCs. Hybrid composites showed superior mechanical properties when compared to MMCs.

## References

1. Hashin Z (1983) Analysis of composite materials-A survey
2. Hahn HT, Tsai SW (1980) Introduction to composite materials, CRC Press
3. Teti R (2002) Machining of composite materials. *CIRP Ann* 51(2):611–634
4. Cantwell WJ, Morton J (1991) The impact resistance of composite materials-a review. *Composites* 22(5):347–362
5. Dawoud MM, Saleh HM (2018) Introductory chapter: background on composite materials. In: *Characterizations of some composite materials*. IntechOpen
6. Jagadish BS (2015) Synthesis and characterisation of aluminium 2024 and graphene metal matrix composites by powder metallurgy means. *SSRG Int J Mech Eng* 2(7):13–17
7. Rosso M (2006) Ceramic and metal matrix composites: routes and properties. *J Mater Proc Technol* 175(1–3):364–375
8. Krishnamurthy K, Venkatesh J (2013) Study on machining parameters of TiB<sub>2</sub> reinforced aluminium 6063 composites. *Int J Sci Res Publ* 3(4):130–137
9. Sharma R, Jhap S, Kakkar K, Kamboj A, Sharma P (2017) A review of the aluminium metal matrix composite and its properties. *Int Res J Eng Technol* 4(02)
10. Vamsikrishna B, Charankumar RG, Ramakrishna G, Venkatsurya ARB (2015) Fabrication of hybrid aluminium composite using stir casting method. *Int J Appl Eng Res* 10(65)
11. Ng CH, Yahaya SNM, Majid AAA (2017) Reviews on aluminium alloy series and its applications. *Acad J Sci Res* 5(12):708–716
12. Venci A, Rac A, Bobic I (2004) Tribological behaviour of Al-based MMCs and their application in automotive industry. *Tribol Ind* 26(3–4):31–38
13. Meseguer-Valdenebro JL, Portoles A, Oñoro J (2017) Numerical study of TTP curves upon welding of 6063-T5 aluminium alloy and optimization of welding process parameters by Taguchi's method
14. Munro RG (2000) Material properties of titanium diboride. *J Res Nat Inst Stand Technol* 105(5):709
15. Liu B, Wei W, Gan Y, Duan C, Cui H (2020) Preparation, mechanical properties and microstructure of TiB<sub>2</sub> based ceramic cutting tool material toughened by TiC whisker. *Int J Refract Metal Hard Mater* 93:105–372
16. Xi L, Wang P, Prashanth KG, Li H, Prykhodko HV, Scudino S, Kaban I (2019) Effect of TiB<sub>2</sub> particles on microstructure and crystallographic texture of Al-12Si fabricated by selective laser melting. *J Alloy Compd* 786:551–556
17. Ramesh M, Jafrey DD, Ravichandran M (2019) investigation on mechanical properties and wear behaviour of titanium diboride reinforced composites. *FME Transactions* 47(4):873–879
18. Venkatachalam S, Baskaran S, Karthik RS, Raj DBTG, Kumar TR (2019) Titanium diboride reinforced aluminium composite as a robust material for automobile applications. *AIP Conf Proc* 2128(1):020010
19. Siva MM, Rajesh R, Pugazhendhi S, Sivapragash M, Neelajaran RR (2016) analysis of microstructural, corrosion and mechanical properties of aluminium titanium diboride particles (Al–TiB<sub>2</sub>) reinforced metal matrix composites (MMCs). *Indian J Sci Technol* 9(43)
20. Pradeep P, Kumar PSR, Jayabal S (2017) Characterization of particulate-reinforced aluminium 7075/TiB<sub>2</sub> composites. *Int J Civil Eng Technol* 8(9):178–190
21. Ramesh CS, Ahamed A, Channabasappa BH, Keshavamurthy R (2010) Development of Al 6063-TiB<sub>2</sub> in situ composites. *Mater Des* 31(4):2230–2236

22. Lawrance CA, Prabhu PS (2014) Production and characterization of Al 6061-TiB<sub>2</sub> in-situ metal matrix composite. *Int Adv Res J Sci Eng Technol* 1(3):156–158
23. Poria S, Sahoo P, Sutradhar G (2016) Tribological characterization of stir-cast aluminium-TiB<sub>2</sub> metal matrix composites. *SILICON* 8(4):591–599
24. Anish A, Kumar MA (2018) Characterization of aluminium matrix reinforced with tungsten carbide and molybdenum disulphide hybrid composite. *IOP Conf Ser Mater Sci Eng* 402(1):012006
25. Abhijith R, Harish TM (2016) Fabrication and analysis of Al2024 and WC MMC by in-situ method. *Int J Eng Tech Res* 5:400–407
26. Hima Gireesh C, Durga Prasad KG, Ramji K (2018) experimental investigation on mechanical properties of an Al6061 hybrid metal matrix composite. *J Compos Sci* 2(3):49
27. Kumar KR, Kiran K, Sreebalaji VS (2017) Micro structural characteristics and mechanical behaviour of aluminium matrix composites reinforced with titanium carbide. *J Alloy Compd* 723:795–801
28. Punith Gowda K, Prakash JN, Gowda S, Satish Babu B (2015) Effect of particulate reinforcement on the mechanical properties of Al2024-WC MMCs. *J Miner Mater Charact Eng* 3(6):469–476
29. Veeresh Kumar G, Pramod R, Shivakumar Gouda P, Rao C (2019) Effect of tungsten carbide reinforcement on the aluminium 6061 alloy. *J Test Eval* 47(4):2613–2629
30. Swamy ARK, Ramesha A, Kumar GV, Prakash JN (2011) Effect of particulate reinforcements on the mechanical properties of Al6061-WC and Al6061-Gr MMCs. *J Miner Mater Charact Eng* 10(12):1141
31. Kumar NM, Kumaran SS, Kumaraswamidhas LA (2015) An investigation of mechanical properties and material removal rate, tool wear rate in EDM machining process of Al2618 alloy reinforced with Si<sub>3</sub>N<sub>4</sub>, AlN and ZrB<sub>2</sub> composites. *J Alloy Compd* 650:318–327
32. Farhadinia F, Sedghi A, Nooghani MT (2017) Properties of an Al/(Al<sub>2</sub>O<sub>3</sub> + TiB<sub>2</sub> + ZrB<sub>2</sub>) hybrid composite manufactured by powder metallurgy and hot pressing. *J Appl Mech Tech Phys* 58(3):454–460
33. Ghasali E, Yazdani-Rad R, Rahbari A, Ebadzadeh T (2016) Microwave sintering of aluminium-ZrB<sub>2</sub> composite: focusing on microstructure and mechanical properties. *Mater Res* 19(4):765–769
34. Ghasali E, Pakseresht A, Safari-Kooshali F, Agheli M, Ebadzadeh T (2015) Investigation on microstructure and mechanical behavior of Al-ZrB<sub>2</sub> composite prepared by microwave and spark plasma sintering. *Mater Sci Eng A* 627:27–30
35. Ruban SR, Wins KLD, Selvam JDR, Richard AA (2016) Effect of dry sliding wear behaviour of AA6061/ZrB<sub>2</sub>/SiC hybrid composite. *Int J Veh Struct Syst* 8(2):108
36. Kumar RV, Keshavamurthy R, Perugu CS (2016) Microstructure and mechanical behaviour of Al6061-ZrB<sub>2</sub> in-situ metal matrix composites. *Mater Sci Eng* 149(1):012–062
37. Dinaharan I, Murugan N, Parameswaran S (2011) Influence of in situ formed ZrB<sub>2</sub> particles on microstructure and mechanical properties of AA6061 metal matrix composites. *Mater Sci Eng, A* 528(18):5733–5740
38. Kumar N, Gautam RK, Mohan S (2015) In-situ development of ZrB<sub>2</sub> particles and their effect on microstructure and mechanical properties of AA5052 metal-matrix composites. *Mater Des* 80:129–136
39. Kishore NV, Rao DKV (2016) Mechanical properties in MMC of aluminium alloy (A356/LM25) matrix and boron carbide (B<sub>4</sub>C) reinforcement. *Int J Eng Res Technol* 5(02):683–689
40. Mahesh VP, Nair PS, Rajan TPD, Pai BC, Hubli RC (2011) Processing of surface- treated boron carbide-reinforced aluminium matrix composites by liquid-metal stir-casting technique. *J Compos Mater* 45(23):2371–2378
41. Ramnath BV, Elanchezian C, Jaivignesh M, Rajesh S, Parswajinan C, Ghias ASA (2014) Evaluation of mechanical properties of aluminium alloy-alumina-boron carbide metal matrix composites. *Mater Des* 58:332–338



42. Manjunatha B, Niranjana HB, Satyanarayana KG (2015) Effect of mechanical and thermal loading on boron carbide particles reinforced Al-6061 alloy. *Mater Sci Eng A* 632:147–155
43. Kumar A, Rai RN (2018) Fabrication, microstructure and mechanical properties of boron carbide (B<sub>4</sub>Cp) reinforced aluminium metal matrix composite-a review. *IOP Conf Ser Mater Sci Eng* 377:012092
44. Nanjan S, Janakiram GM (2019) Characteristics of A6061/(Glass Fibre + Al<sub>2</sub>O<sub>3</sub> + SiC + B<sub>4</sub>C) reinforced hybrid composite prepared through stir casting. *Adv Mater Sci Eng*
45. Uvaraja VC, Natarajan N (2012) Tribological characterization of stir-cast hybrid composite aluminium 6061 reinforced with sic and B<sub>4</sub>C particulates. *Eur J Sci Res* 76(4):539–552
46. Gopal Krishna UB, Sreenivas Rao KV, Vasudeva B (2013) Effect of boron carbide reinforcement on aluminium matrix composites. *Int J Metall Mater Sci Eng* 3:41–48

# Productivity Improvement by Optimizing the Layout and Cycle Time of an MSME



Radhika Gupta, Shraddha Sinha, Livea Goyal, Rahul O. Vaishya,  
and Sidharth Sharma

**Abstract** This paper named “Productivity Improvement by Optimizing the Layout and Cycle Time of an MSME” is aimed at identifying some major issues regarding the current layout of the screw manufacturing company part of production industry and develop an effective layout design to improve the production performance of enterprise. Facility planning is very important in the manufacturing process due to many reasons like their impact on achieving an effective product flow. Correct analysis of plant layout design can be used to improve the production performance, such as reducing the bottleneck rate, minimizing material handling costs, and reducing idle time, improve the efficiency and utilization of labor, equipment and space. String diagram is applied to the initial industrial layout planning to map out the path of the material movement, and to the scale, drawing of the plant was done using SolidWorks. Afterward, a new layout was designed to minimize the movement of materials and reduce the cycle time of the process. The research solves these problems by designing the factory layout, thereby increasing productivity and increasing product output in a shorter cycle time.

**Keywords** Facility layout · Cycle time · String diagram · Material handling · Layout optimization

---

R Gupta and S Sinha are contributed equally.

---

R. Gupta (✉) · S. Sinha · L. Goyal · R. O. Vaishya  
Department of Production and Industrial Engineering, Punjab Engineering College (Deemed to be University), Sector-12, Chandigarh 160012, India  
e-mail: [gradhika500@gmail.com](mailto:gradhika500@gmail.com)

S. Sharma  
Intelligent Machines and Communication System, CSIR-Central Scientific Instruments Organisation, Sector-30 C, Chandigarh 160030, India  
e-mail: [sharmasidharth055@gmail.com](mailto:sharmasidharth055@gmail.com)

© The Author(s), under exclusive license to Springer Nature Singapore Pte Ltd. 2023  
R. P. Singh et al. (eds.), *Advances in Modelling and Optimization of Manufacturing and Industrial Systems*, Lecture Notes in Mechanical Engineering,  
[https://doi.org/10.1007/978-981-19-6107-6\\_28](https://doi.org/10.1007/978-981-19-6107-6_28)

## 1 Introduction

Many forms of studies have been carried out in the field of facility design. Efficient facility planning can substantially reduce a company's operating costs by 10–30%. Proper analysis of the design of the facility layout may result in improved production line efficiency. This can be achieved by increasing the capacity of a bottleneck, lowering material handling costs, reducing idle time, and making better use of labor, equipment, and space [1]. The potential production scheme must be dynamically reconfigurable for personalized development of small batch goods with quick turn-around times in the cost-effective manner [2]. A crucial element in retaining productivity in the manufacturing market environment is the ability to reconfigure an existing production structure [3]. Taha et al. indicated that managers would search for innovative approaches to facility planning in order to be effective in today's dynamic manufacturing climate [4]. According to Balakrishnan et al. in the United States, it has been reported that over \$250 billion is spent annually on preparing and re-planning facilities. In addition, between 20 and 50% of the overall production costs are related to material handling, and efficient planning of facilities will minimize these costs by 10–30%. Many studies have been conducted in the field of facility design. There are some difficulties and limitations in finding the best design for the layout [3]. Facility planning deals with the design, configuration, and accommodation of a system or enterprise's people, machines, and activities within a physical spatial environment [5]. The three main styles of layout are product layout, process layout, and group layout in production systems, which are further classified into flow line, cell, and middle [6]. According to Tompkins, the differentiation is focused on device features such as output volume and product variation between these types of layouts [7]. Huang states that in order to reduce overall production time, optimize organizational and arrangement flexibility, maximize work-in process (WIP) turnover, and maximize factory productivity in compliance with production schedules, he notes that facility layout design determines how to organize, locate, and distribute the equipment and support services in a manufacturing facility [8]. Zuhdi et al. imply that to produce new goods, manufacturing firms need to be knowledge intensive and highly innovative. Upgrading the process and embracing information technology are also the task of small and medium enterprises in order to stay competitive. A crucial task that can influence the economic aspect of the business is the decision-making to either update the particular process or reconfigure the whole system as a response to consumer demand [9]. According to Reith et al. the simulation process is favored because of the ability to capture the complex system's dynamics. The validation of the design or redesign of a complex manufacturing system prior to implementation is an important feature of simulation in the age of lean manufacturing [10]. The paper presented a comprehensive description of plant layout and identified efficient use of labor, ease of manufacturing and maintenance, improved production, versatility in manufacturing, efficient use of workers, machinery, materials and equipment, as well as reducing injuries, hazards, and cost of inventory handling as some of the advantages of well-designed plant layout [11]. Product development cycle time has

become a strategic competitive tool for an organization and a priority for product development management analysis [12]. Reducing the duration of the product development cycle and hence the time for a new product to be launched will produce relative benefits in terms of market share, profit, and long-term competitive advantage [13–15]. Quick cycle times can lead to errors due, for example, to a lack of data. The production can also be carried out in such hurry that the item has not been properly debugged [16]. In addition, compressing cycle time could lead to the wrong technology being chosen [17].

## 2 Research Gaps

- Existing layout was inefficient because layout optimizing techniques were not used.
- The equipment/processes were not used to their full capacity because cycle time of the processes was high as layout optimization was not done.

## 3 Methodology

In this research paper, we studied the plant layout of a screw manufacturing company part of production industry to identify the shortcoming of the existing plant layout. After that the mapping of all the machines placed was done to scale using Solid-Works, and this was done using advanced manufacturing methods. A new layout was designed to minimize the material movement and increase the productivity of the company's plant. In the new layout, we propose to use the group layout type in which we group the same item being manufactured together, and all these groups are in the sequence of production. In this, the cycle time of various activities was also calculated to identify the bottleneck activity. For this, we used string diagram to map out the movement of materials in the factory and then reduced the movement and increased the efficiency of the system. Initially, the cycle time was more because the full capacity of all the machines couldn't be utilized due to the bottleneck activity, i.e., polishing. Then, we proposed a solution to reduce the cycle time of the entire process.

## 4 Objectives

- Comparison of existing and proposed layout
- Increase efficiency of the process
- Calculation of time study, identification of bottleneck, and finding solution to the same.

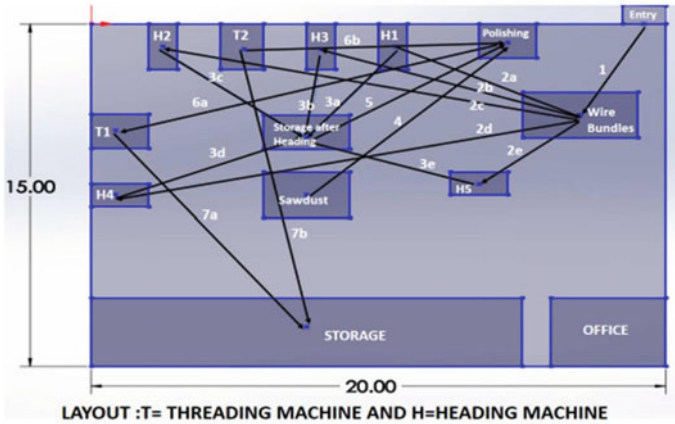


Fig. 1 Sequence wise process in the existing layout

### 5 Existing Layout

The heading machine produces 100 pieces/min per machine. There are 5 heading machines. So, 25,500 pieces are produced in 51 min. The polishing machine produces 450 pieces/min per machine. There is 1 polishing machine only. The machine works for 40 min. So, 18,000 pieces are produced in 40, 11 min for segregation of saw dust from screws. So, the process time of polishing screws is 51 min. The threading machine produces 300 pieces/min per machine. There are 2 threading machines. So, every 51 min materials are transferred from polishing to threading machine. It has a capacity of making 30,600 pieces in 51 min, but since only 18,000 pieces come from polishing machine, it takes 30 min to complete that batch. From this, we concur that polishing process is the bottleneck. The process time is 155 min. In 155 min, 18,000 pieces are made. So, for 1 screw is 0.516–0.52 s. Therefore, the cycle time to produce 1 screw is 0.52 s (Fig. 1 and Table 1).

### 6 Proposed Changes

- The capacity of 5 heading machines and 2 threading machines is not fully utilized because of the bottleneck activity—polishing.
- Purchase another polishing machine to match up with the production by heading and threading machine.
- Redesigning the layout to reduce material movement distance as well as time.

**Table 1** Cycle time of the existing layout

S. No.	Process	Basic time (mins)	Allowances (10%)	Standard time (mins)
1	Movement of wire bundles and sawdust from entry to storage	–	–	–
2	Movement of wire bundle from storage to heading m/c	0.31	0.03	0.33
3	Fixing and setting up the machine	15	1.5	16.5
4	Heading process + Setting up polishing machine	50	–	50
5	Movement from heading machine to storage	0.17	0.02	0.19
6	Movement from storage to rolling machine of screws	0.24	0.02	0.26
7	Rolling process (polishing)	40	–	40
8	Segregation of sawdust and screws	10	1	11
9	Movement from rolling to threading machine of screws	0.70	0.07	0.77
10	Setting of threading machine	5	0.5	5.5
11	Threading process	30	–	30
12	Movement from threading machine to storage	0.35	0.04	0.39
13	Movement of screws for hardening and tempering to other plant	–	–	–

## 7 Proposed Layout

The heading machine produces 100 pieces/min per machine. There are 5 heading machines. So, 25,500 pieces are produced in 51 min. The polishing machine produces 450 pieces/min per machine. Now, there are 2 polishing machines. They work for 40 min, so 36,000 pieces in 40 min. 11 min for segregation of saw dust from screws. So, the process time of polishing screws is 51 min. The threading machine produces 300 pieces/min per machine. There are 2 threading machines. So, every 51 min

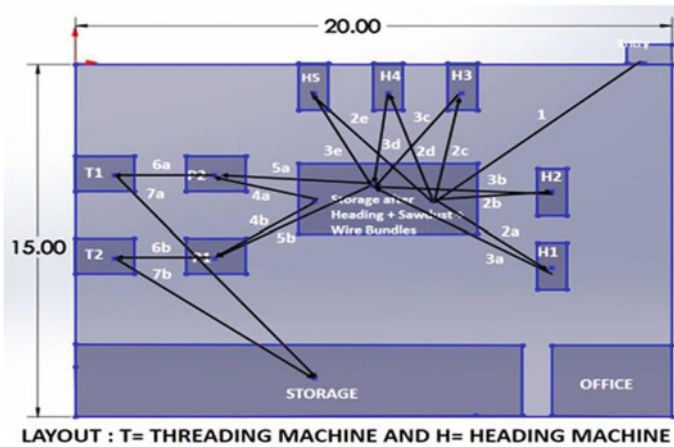


Fig. 2 Sequence-wise process in the proposed layout

Table 2 Comparison of distance of various stations using string diagram

From-to string	Distance traveled in meters (before)	Distance traveled in meters (after)
Entry-01	4.57	9.19
01-02	52.64	24.56
02-03	28.80	26.19
04-05	9.69	7.64
05-06	8.16	11.45
06-07	27.11	6.74
07-Storage	19.35	19.35

materials are transferred from polishing to threading machine. It has a capacity of making 30,600 pieces in 51 min, but since only 25,500 pieces come from polishing machine, it takes 30 min to complete that batch. The process time is 149 min. In 149 min, 25,500 pieces are made. So, for 1 screw is 0.35–0.4 s. Therefore, the cycle time to produce 1 screw is 0.4 s (Fig. 2, Tables 2 and 3).

## 8 Expenditure Comparison

In this section, we compared the monthly expenditure of the company for the existing layout and the proposed layout.

In this, we proposed to change the plant layout and add a polishing machine. So,

**Table 3** Cycle time of the proposed layout

S. No.	Process	Basic Time (mins)	Allowances (10%)	Standard Time (mins)
1	Movement of wire bundles and sawdust from entry to storage	–	–	–
2	Movement of wire bundle from storage to heading machine	0.14	0.01	0.15
3	Fixing and setting up the machine	15	1.5	16.5
4	Heading process + Setting up polishing machine (10 mins)	50	–	50
5	Movement from heading machine to storage	0.15	0.02	0.17
6	Movement from heading to rolling machine of screws	0.17	0.02	0.19
7	Rolling process (polishing)	40	–	40
8	Segregation of sawdust and screws + Setting of threading machine (5.5 min)	10	1	11
9	Movement from rolling to threading machine of screws	0.10	0.01	0.11
10	Threading process	30	–	30
11	Movement from threading machine to storage	0.30	0.03	0.33
12	Movement of screws for hardening and tempering to other plant	–	–	–

- Cost of the machine = Rs. 3,60,000
- Cost of layout change (electrical wiring change + cranes + setup charges) = Rs. 40,000
- Total business loan = Rs. 4,00,000
- Business loan interest = 11.2%



**Table 4** Monthly expenditure comparison

Expenses	Before	After
Screws produced in one day	2,11,764	2,80,000
Weight of one screw	0.002 kg	0.002 kg
Cost of screws	Rs. 115/kg	Rs. 115/kg
Cost of raw material	Rs. 55/kg	Rs. 55/kg
Cost of sawdust, coolant	$(300 * 3 * 30 + 20 * 80 * 30)$ = Rs. 75,000	$(600 * 3 * 30 + 26 * 80 * 30)$ = Rs. 1,16,400
Water charges (200L/day, Rs 0.015/L)	Rs. 90	Rs. 112
Transportation (Distance 46 km)	Rs. 9660 (Rs. 7/km)	Rs. 12,420 (Rs 9/km)
Hardening and tempering	Rs. 1,27,050	Rs. 1,68,000
Electroplating (Rs 9/kg)	Rs. 1,14,360	Rs. 1,51,200
Packaging cost (Rs 6/kg)	Rs. 76,230	Rs. 1,00,800
Cost of raw material in one month	Rs. 6,98,822	Rs. 9,24,000
Labor cost per month	Rs. 74,000	Rs. 96,000
Electricity cost per month	Rs. 55,000	Rs. 60,000
Rent	Rs. 60,000	Rs. 60,000
Overhead expense (Labor + Electricity + Rent + 10%)	Rs. 2,07,900	Rs. 2,37,600
Total expense	Rs. 13,09,112	Rs. 17,19,269
Revenue generation in one month	Rs. 14,61,172	Rs. 19,32,000
Profit	Rs. 1,52,060	Rs. 2,12,731
Profit percentage (%)	10.40	11.01

- Loan tenure = 5 years
- EMI = Rs. 8737
- Break even time =  $2,12,731/5,24,214 = 2.46-2.5$  years
- ROI = 40.65% (Table 4).

## 9 Profit Calculations

By layout change and addition of one polishing machine, the number of screws manufactured per day has increased.

**Productivity increased** =  $(\text{Change in production of screws}/\text{Original production of screws}) * 100 = (2,80,000 - 2,11,764)/2,11,764 * 100 = 32.22\%$ .

By layout change, the material movement had reduced which is calculated by change in the length of string.

- Length of string in the initial layout = 150.32 m
- Length of string in the proposed layout = 105 m
- **Efficiency increased** in the material movement =  $(45.32/150) * 100 = 30.21\%$ .

#### **Profit calculation**

- Profit by the company before = 10.40%
- Profit by the company after layout change = **11.01%**
- The process time enhanced by =  $(155-149)/155 * 100 = 3.8\%$ .

## **10 Conclusion**

This research paper has provided information about plant layout for improvement of efficiency as well as to meet customer demands. To adopt a good layout for long-term success, analysis of operations required should be done properly. The most important thing to be addressed during designing the layout is as follows: how flexible should the plant layout be in order to adjust to future changes in production which was kept in mind while designing the new layout. As market requirements are changing with time and competition is increasing, to meet these requirements, production should be increased; cycle time should be reduced, and thus, cost of manufacturing will automatically decrease. This paper focused on minimizing the total distance for movement of material by redesigning the plant layout, and thus, the increase in the efficiency of material movement was by 30.21%. Using this concept, the cycle time of the entire process was also reduced by 3.8%. The profit of the company also increased from 10.40 to 11.01%. So, by implementing the changes mentioned above, the productivity and efficiency of the manufacturing unit increased significantly.

## **References**

1. Barnwal S, Dharmadhikari P (2016) Optimization of plant layout using SLP method. *Int J Innov Res Sci Eng Technol* 5(3)
2. McLean C, Kibira D (2002) Virtual reality simulation of a mechanical assembly production line proceeding of the winter simulation conference, p 1130–1137
3. Balakrishnan J, Cheng CH (2007) Multi-period planning and uncertainty issues in cellular manufacturing: a review and future directions. *Eur J Oper Res* ed 177: 281–309
4. Taha Z, Tahriri F (2008) A classification of different type of facility layout design. In: *Proceeding of Asia Pacific conference on management of technology and technology entrepreneurship*, p 1–5
5. Garcia AD, Smith MG (2008) Facility planning and design. In: Pearson international ed, Prentice Hall, New York
6. Askin RG, Standridge CR (1993) Modeling and analysis of manufacturing systems, Wiley, New York

7. Tompkins JA (2003) Facilities planning, John Willey and Son, New York
8. Huang H (2003) Facility layout using layout modules: Ph.D. Thesis, The Ohio State University
9. Zuhdi A, Taha Z (2008) Simulation model of assembly system design. In: Proceeding Asia Pacific conference on management of technology and technology entrepreneurship
10. Reith D, Gerlach S (1996) Planning and controlling of flexible assembly systems for automotive industry. In: Proceeding of the IEEE international symposium on computer-aided control system design, dearborn, p 15–18
11. Plant layouts' analysis and design, department of industrial/production engineering, Nnamdi Azikiwe University, P.M.B. 5025 Awka, Anambra State, Nigeria
12. McDonough EF III, Spital FC (1984) Quick response new product development. *Harvard Bus Rev Sep-Oct* 52–58
13. Ali A, Krapfel R, LaBahn D (1995) Product innovativeness and entry strategy: impact on cycle time and break-even time. *J Prod Innov Manage* 12:54–69
14. Lieberman MB, Montgomery DB (1988) First mover advantages. *Strateg Manage J* 9(summer special issue):41–58
15. Sanchez R (1995) Strategic flexibility in product competition. *Strateg Manage J* 16(summer special issue):135–159
16. Clark KB, Fujimoto T (1991) *Product Development Performance*: Cambridge. Harvard Business School Press, MA
17. Krubasik EG (1988) Customize your product development. *Harvard Bus Rev Nov-Dec* 46–52

# Green Manufacturing in Apparel Industry: Future Trends and Scope



Ankita S. Pandey and Vasundhara Saluja

**Abstract** Humans have been exploiting the environmental resources as much as the environment today stands in crisis. There has become an urgent need of aligning profits with peace and prosperity of people and planet. In the race of economic growth and development, the disparity between social, economic and environment has aroused. The impact of Covid-19 pandemic further has highlighted the sustainable growth to be considered for a better future. Also, viewing the United Nations Sustainable Development Goals, there needs to be responsible consumption and production. Sustainability is the greatest challenge faced by the apparel industry. The industry, running on the adrenaline of glamor, pricing and pace, has recently realized that the old systems and processes cannot sustain, but there are not enough new systems and processes to replace. We are facing redundancies in an empty-handed way. Green manufacturing is an inevitable future. The paper explores key aspects of green manufacturing from apparel industries perspective, noting down the innovation and entrepreneurial solutions to the problems, identifying gaps and future scope.

**Keywords** Sustainable development goals · Green manufacturing · Apparel industry · Sustainability · Eco-friendly circular design

## 1 Introduction

The world is heading toward unprecedented economic growth, the growth which is adversely affecting the people and the planet. In a call to action, the United Nations has set up Sustainable Development Goals in favor of the prosperity of people and the planet. The 17 SDGs are integrated—they recognize that action in one area will

---

A. S. Pandey · V. Saluja (✉)

Department of Art and Design, Sharda School of Design, Architecture and Planning, Sharda University, Gautam Buddh Nagar, Uttar Pradesh, India  
e-mail: [vasundhara.saluja@sharda.ac.in](mailto:vasundhara.saluja@sharda.ac.in)

affect outcomes in others, and that development must balance social, economic and environmental sustainability. It is expected by all Nations to harmonize these goals. The goals focuses on (i) No Poverty, (ii) Zero Hunger, (iii) Good Health and Well-Being, (iv) Quality Education, (iv) Gender Equality, (v) Clean Water and Sanitation, (vi) Affordable and Clean Energy, (vii) Decent Work and Economic Growth, (viii) Industry, Innovation and Economic Growth, (ix) Reduced Inequalities, (x) Sustainable Cities and Communities, (xi) Responsible Consumption and Production, (xii) Climate Action, (xiii) Life below Water, (xiv) Life on land, (xv) Peace, justice and Strong Institutions, (xvi) Partnerships for the goals, (xvii) Affordable and Clean energy. UNDP aims to bring these from paper to practice [16]. There needs to be an integration to achieve this goal, this research is majorly led by the goal toward “Responsible Consumption and Production.”

The apparel industry today is the world’s second largest polluting industry; based on statistics and data available, wearing clothes has become a trend, and we are buying clothes more than ever what our elders used to wear. This trend of frequent buying has become popular in recent times; it is impacting the environment. The broad understanding of the term “Green manufacturing” is based on the definition given by the Green Manufacturing Expo 2008 held at New York city, “sustainable manufacturing is the creation of manufactured products that uses processes to conserve energy and natural resources, are non-polluting, are economically sound, and safe for communities, employees and consumers”. As established in the introduction, there are pressing concerns about environmental pollution. Also, taken up by the 12th UNDP, toward reducing ecological footprint by changing the way, we produce goods [16]. Producing goods through better means including efficient management of natural using circular manufacturing processes, eco-friendly raw material and waste management systems. These are continuous areas of research and innovation in the apparel industry. The apparel manufacturers are increasingly required to consider the complete product life cycle starting from raw materials to waste disposal from the circular design and ecological design perspectives. Highly Complicated are the already complex human-centered and human-managed systems, processes and outcomes. According to Elkington, “successful companies will have little option but to get involved in this rapidly emerging area” of taking care of sustainability in their business. Thus, the concept of sustainable development has emerged in manufacturing since the late 1990s and has focused on increasing competitiveness by improving environmental and social performance in an economic way (Fig. 1).

## 2 Research Background

In this century, population and resource management has become the biggest challenge. Environment is at stake with the growth all around. Global economy is proceeding at a rapid rate due to increased consumerism. As published by renowned



Fig. 1 Impact of apparel industry [5]

research organization EMarketer, the retail sales worldwide including both offline and online sales are growing enormously each year. The increased needs and wants of the consumers seem to be a lucrative opportunity for the producers and retailers. This economic growth sets a very positive mood, but the same is at the altar of environmental abyss, leading to overuse of resources, undermining the entire ecosystem. These practices have become a part of modern lifestyle to its core. It leads both producers and consumers to regard more and more products as little more than commodities that can be discarded relatively quickly rather than items that embody valuable energy and materials and that should be well maintained and designed for long life spans.

Organizations all over the world are trying to make efforts to create a balance between production, consumerism and environment. ISO has set up criteria for an environmental management system and the organizations can be certified to. It maps out a framework that a company or organization can follow to set up an effective

environmental management system. For the world which continues to face environmental challenges, ISO is supporting the organizations reducing the environmental impact. Achieving accredited certification to ISO 14001 certainly delivers commercial value to an organization, including reduced greenhouse gas emissions and streamlined waste management, as well as providing a better handle on business risk and competitive advantage. So, it is commercially good for business as well as helping the environment. Environmental challenges need strategizing at each level [10]. Businesses are aligning themselves with these rising needs to benefit all stakeholders. In concurrence with the increased consumption which is essential for economy and people both, there is an awareness toward the concept of sustainability. “People all over the worlds have realized the importance of sustainability be it on consumer end or producer end both.”

Fashion has been widely assessed as the second most polluting industry in the world. According to UNCTAD, some 93 billion cubic meters of water—enough to meet the needs of five million people—is used by the fashion industry annually, and around half a million tons of microfiber, which is the equivalent of 3 million barrels of oil, is now being dumped into the ocean every year. As for carbon emissions, the industry is responsible for more than all international flights and maritime shipping combined [17]. Fashion is style, trend and is evolving, which means that it impacts the environment rigorously, it needs deep strategizing at different levels. Fast fashion is an essential concept in the fashion industry which is in unanimity to sustainability. These are two very different concepts to its core, wherein fashion is heading toward consumerism and sustainability stands for conscious consumption. The supply chain of this industry is massive and to control each component is difficult. Hence, to align fashion with sustainability needs to be thought over from a vast perspective where the strategies are framed and implemented from inception.

### **3 Research Methods**

The approach for this is through qualitative methods of research. It was much needed to collect accurate insights, as it aims to understand the path for the apparel industry in achieving sustainable development goals. The research will be exploratory in nature which includes a lot of desk research and literature review to develop an understanding of sustainability and complicated processes involved in the manufacturing of apparel and textiles. Apart from collecting the data about the concepts and processes, there are in-depth case studies conducted for different brands trying to align themselves with sustainability. The data will be collected through various journals, reports and Web sites. The case study aims at gaining concrete, contextual information about the way brands have been trying to achieve sustainability, the way they are aligning the processes and taking steps in this direction.

## 4 Case Studies

### 4.1 Eco-friendly Raw Materials

Looking at the global fiber market overview, we found that in 2018–19, polyester fiber had the largest global market share of a whopping 57.7%, followed by cotton 25.7%. The third most preferred fiber group is that of man-made cellulose fibers such as Viscose, Lyocell, Cupro, Modal and Acetate, with a total global market share of 6.4%, further followed by plant-based fibers, such as hemp, jute and linen, with a market share of about 6% [12, 13]. Apparel manufacturers are increasingly adopting sustainably grown and produced fibers and fabrics, with cotton experiencing maximum positive development. Recycling, organic farming and man-made cellulose fibers are expected to see fastest market adoption. Some of the sustainable fibers and fabrics which are commonly in use in the global market are organic cotton, recycled polyester, Lyocell, Cupro, hemp, linen, Ramie, bamboo and recycled wool. Some of the newer textile innovations are focusing on extracting fiber from orange, pineapple and banana. In this section of the paper, we have studied the recent market trends and adoption of sustainable fibers by the apparel industry.

Organic cotton is grown without using chemical fertilizers and pesticides and therefore without adding toxic material to soil. When compared to chemical cotton, the water consumption is similar but without negative health and environmental impact. The yield per hectare of organic cotton is similar to chemically produced cotton with no difference in the properties of the fiber [12].

The organic cotton myth has broken dramatically in both the agricultural and apparel manufacturing sectors. This can be attributed to the sustained efforts by government and non-government organizations. Organic cotton production increased 31% in 2018/19 when compared to 2017–2018. India fuels this growth by adding fiber volume by 37,138 MT in the year 2018/19 and contributing 51% to the total production of organic cotton [15], p. 4 (Fig. 2).

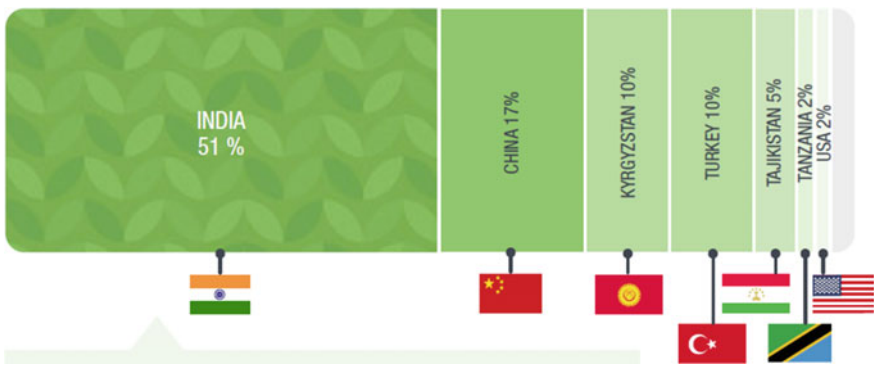


Fig. 2 Organic cotton production share in 2018–19 [12, 13]



Increased organic cotton fiber production has become the decisive factor for brands across the world, in adopting organic cotton in place of chemical cotton. Brands like Patagonia, Veja and Nudie Jeans have shifted to organic cotton for 100% production. Eileen Fisher, Levi Strauss and Co, HandM, Timberland, Decathlon, Outerknown, etc., had committed to shift to 100% organic cotton or recycled cotton by 2020. Target and Bestseller, on the other hand, have committed to shift to sustainably sourced cotton by 2022 and 2025, respectively [15], p. 17. The apparel industry is adopting the route of standardization and certification to ensure and communicate authenticity of the organic cotton source. Global Organic Textile Standard (GOTS), Organic Content Standard (OCS) and Better Cotton Initiative (BCI) are the leading certifications ensuring environmental and social sustainability. The logos are included as pictures below.

Recycled polyester is made using plastic bottles, ocean waste, polyester textiles, etc.; market share of recycled polyester has increased from 9% in 2009 to 14% in 2019 mostly sourced from plastic bottle recycling and not textile-to-textile recycling. The prominent standards used for recycled polyester are the Global Recycled Standard (GRS), Ocean Bound Plastic Certification, the Recycled Claim Standard (RCS) and the SCS Recycled Content Standard. ([13], pp. 61–66) There is an urgent need to off-set the negative environmental impact of polyester at a greater speed. Brands like Patagonia are acting as trail-blazers in such initiatives followed by commitments of HandM, Adidas, IKEA and Inditex to replace all virgin polyester with recycled polyester.

Lyocell fabric is also called Tencel; its global production was 415.6 kg tons in 2018, which has been forecasted to double in 10 years. It is a compostable and biodegradable fiber made of wood cellulose. 100% Lyocell products take approximately 2 months to decompose and can contribute to the renewal of resources in a much shorter span of time, especially when compared to polyester. (Lenzing AG, n.d.)

Hemp, linen, flax are all fibers with several similarities and a sustainable alternative to cotton. All these fibers are plant based. In recent studies of hemp, post-legalizing the production of hemp plants in countries such as the United States, hemp has been rated as the most sustainable and economical alternative to cotton. linen, Ramie and flax are fibers with similar properties and source as that of hemp. This group of fibers are being commonly blended with cotton to give smoother and more sustainable finish to the fabric.

## ***4.2 Circular Design and Production Processes***

The principle of circular design is based upon the idea of designing out waste (CircuLab, n.d.). “The future of design is circular,” as described by CircuLab, an international community focused on making circular design a reality through partnership, upskilling and research (CircuLab, n.d.). Industrial or commodity design must reinvent itself to design for the urgent ecological and societal needs of the present and

the future, following the principles of circular design, where the central idea is reduction and management of waste through design, manufacturing and retail processes. Thus, changing the linear industrial process to a multi-loop circular process, with considerations for industrial waste, retail waste and consumer waste. Resulting to creation of need for multiple loops life cycle design approach. Brands, such as Nike, Patagonia and Mud Jeans, have created self-regulating targets such as in the case of Nike—“zero carbon and zero waste” and are driving the initiative by defining long-term targets and short-to-medium-term milestones. Nike’s sustainability initiatives are motivated with the mission to protect sports in the future. Realizing that there will be no sport if there is no climate. The brand’s research linking climatic temperature with athletic performance is further fueling the initiatives. Their sustainability targets have been divided into two dimensions—sustainable material and innovation, circular design methods (Nike, n.d.). Both the areas are currently at different research and development stages in the apparel industry.

Industrial design historically has been short sighted and ended up creating unmanageable quantities of waste and wasteful consumption of resources. This has further been manifested in the apparel industry to dangerous levels making it one of the highest polluting industries of the world (Marina Qutab, n.d.). The sustainable innovations have accelerated in the last two decades, but have been largely limited to textile manufacturing. With innovations focusing on fiber, textile processes, such as dyeing and printing, this has created a singular outcome, by providing apparel manufacturers the opportunity to create eco-friendly products, which are not sustainable. Interesting to note here are the key findings of Business for Social Responsibilities (BSR) report “Apparel Industry Life Cycle Carbon Mapping”—laundering is the largest contributor to a garment’s life cycle GHG footprint followed by raw materials.

Figure 3 presents how design can interact with the complete life cycle of garments which can broadly be divided into 5 stages—design, production, distribution, use and end-of-life. Looking for raw material intake from all the stages to minimize consumption of resources not limited to raw materials. Designing for durability and innovating with repair and recycle techniques. Extending itself from product design to service design while creating aspirational sustainable stories to influence mindset shift in consumers.

The key circular garment and textile design strategies that can be adopted to increase life of garment and raw materials are listed below:



Fig. 3 GOTS, OCS and BCI certification logos [3, 7, 12, 13]

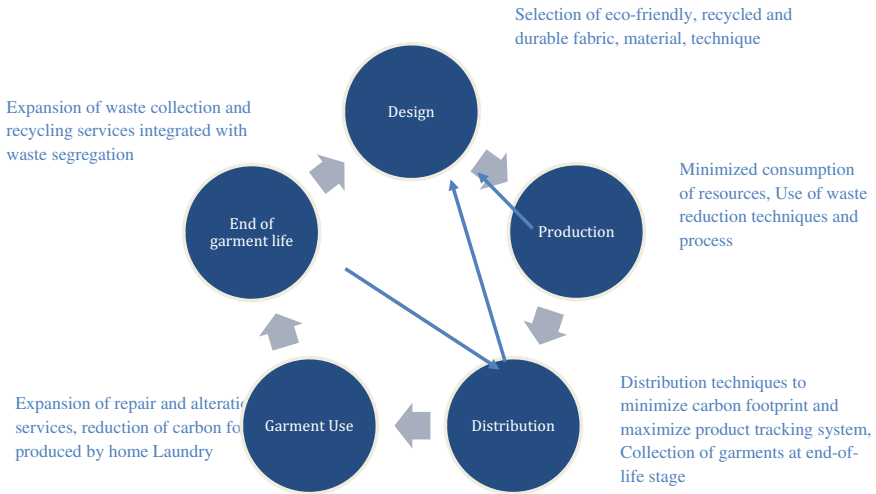
1. Designing and producing durable and recyclable garments.
2. Designing garments using 2D and 3D digital tools [11]. The new age technology companies are creating efficient and easy to use 3D design tools. The two most used tools in the Indian apparel manufacturing industry are “Clo3D” and “Tuka3D.” These software create virtual true-to-life garments minimizing the sampling waste.
3. Increasing brand commitment to design and produce garments using recycled materials, such as recycled cotton, recycled polyester, recycled man-made cellulose fibers. Brands such as Patagonia, Quicksilver, Batoko and Ecoalf have led the initiative of recycling ocean waste into garment production through multi-company collaborations [9].
4. Increasing market share of chemical and biological recycling methods [13], p. 63.
5. Increasing market share of textile–textile recycling vis-a-vis plastic bottle recycling.
6. Use of “closed-loop fiber–fiber technology” to ensure raw material does not enter the waste loop [8] p. 158.
7. Increased use of zero-waste pattern making.
8. Focus on waste collection and segregation. Brand MUD jeans has made a trailblazing contribution to green manufacturing by creating a renting service along with garments. Also by creating a recycling unit along with a garment manufacturing facility.

The Indian perspective of adopting circular economy that will include circular design and green manufacturing is predicted to be positive, with projected annual benefits of ₹40 lakh crore in 2050 compared with the current linear development path [6].

An important case to be considered here is that of Arvind Ltd., who has adopted judicial water consumption and water recycling policies. Some of these policies include—efficient treatment and recycling mechanisms, identification and plugging of leaks in pipes and processes, conservation projects and monitoring of water use [2]. Figure 4 reports the outcome of these policies, showing a steady increase in the use of recycled water.

### **4.3 Waste Management**

Excessive waste generation is one of the biggest challenges faced by the apparel industry with approximately 48 million MT garments disposed annually. Out of this, 35 million mt is post-consumer waste, and 1 million MT is retailer overstock [13], p. 92. In the production stage on an average, 15% of the textile raw material is wasted at the cut-make stage itself [11]. Some of the key waste reduction methods that have been discussed in this section of the article are—zero-waste garment construction, closed-loop production systems and life cycle assessment technology.



**Fig. 4** Circular design and manufacturing process and systems

Zero-waste garment construction techniques focus on the pre-consumer waste in garment manufacturing processes. Some of the techniques that can enable effective implementation of this policy are:

- Use of creative pattern making by making the reduction of textile waste a priority and starting point of the design process, instead of a preconceived look. The shape and form of the garment is driven by fabric width. Figure 5 below is an example of a zero-waste garment and its pattern.

TOTAL WATER TREATED & REUSED IN PROCESS					In '000 m <sup>3</sup>
Units	FY 14-15	FY 15-16	FY 16-17	FY 17-18	FY 18-19
Woven Knits (Santej)	5,036	5,550	4,294	4,569	5,198
Denim (Naroda)	2,852	99	270	129	106
Garments Export Division	114	2,781	2,465	2,161	1,950
Volles	55	33	242	462	463
<b>Total</b>	<b>5,205</b>	<b>5,682</b>	<b>4,806</b>	<b>5,160</b>	<b>5,767</b>

\* Note: Yarns business include - Arvind cotspin & Arvind Intex. Arvind Intex uses only purchased electricity and hence no direct energy consumption.

**Fig. 5** Report of water recycling initiatives by Arvind Ltd. [2]



**Fig. 6** Design by timo rissanen [11], pp. 31–32

- Use of digital design tools to reduce the prototype process. Prototype development or sample development process in garment manufacturing is a time- and resources-consuming process. It often involves considerable cost with low production order conversion. Digital design and presentation tools, such as Adobe creative Suite, CorelDRAW and TUKA CAD, have been in use since early 2010's and have simplified the design and development. In the last few years, several virtual and 3D tools have also been developed and are gaining popularity, such as TUKA CAD 3D and CLO 3D. These tools, when combined with Adobe creative Suite, are offering designers a portfolio of tools, where they can develop prints, patterns, construction techniques, and fit as well (Fig. 6).

The second waste management approach that we have examined in this paper is closed-loop supply chain system. This is a supply chain system that will completely reuse, recycle or compost all materials. Or alternatively, the brands and garment manufacturers will also be responsible for the disposal of the garment, at the end of its life. These systems can be developed in broadly two categories—pre-consumer and post-consumer waste.

Pre-consumer supply chain system—in this model—the three important stakeholders will be design, production and supply chain with continuous tracking and reporting of waste produced during the manufacturing stage. The waste which needs to be considered will range from raw material to natural resources such as water.

- Design team will adapt the waste into its design and modulate the design process method accordingly using the zero-waste design approach.

- Production team has to ensure continuous tracking and sharing of raw material waste and build lean systems based on recycling and reuse of textile waste and other raw material waste.
- Recycling units to recycle textile waste or water waste have to become an integral part of the manufacturing vertical in addition to traditional verticals such as laundry and packaging; one such case of Arvind Ltd.'s water recycling initiative has been covered under circular design and production methods in the paper. Another case is that of Liva Reviva fabric, by Birla Cellulose, is a man-made cellulosic fiber made using 80% wood pulp and 20% pre-consumer fabric waste [4].

Aditya Birla group, a leading textile and garment manufacturer of India, has developed close partnerships and waste management policies, such as “Solid and Hazardous waste management policy” and “Zero Waste to Landfill program” across its retail factories and warehouses. [1].

Post-consumer supply chain system works toward applying the circular principle by changing the take-make-waste pattern to take-make-waste-take pattern. Under this model, all the 5 major stages of a garment's life cycle are re-routed to design and manufacturing systems. The distributor's role expands into collecting the garment and packaging waste from consumers and sending it back to (a) manufacturer (b) recycler to build up a green network.

LCA or life assessment is a smart technology which is used in helping to assess environmental impacts of any product, i.e., from the raw material stage to the final stage (disposal). However performing life cycle assessment is a challenging process and there are always some errors, as smart technologies usually depend on reliable input data derived from representative sampling. It is a complex process and therefore usually ends in trial and error and is clearly not flawless. However, the evolution of this tool has been immense and is sustainable as well. The most common in today's world is the environmental-life cycle assessment (E-LCA) which mainly measures the inputs and outputs of various activities like energy and carbon footprint. Although the LCA has become a trend which is being incorporated by some governments across the world, as a steady tool and the requirement of precision and other factors, especially with the ever-changing uniqueness of the environment. Life cycle assessment needs to be looked at from a consumer and producer perspective as well, the basis of which is circular economy, in order to avoid both pre-consumer waste and post-consumer waste. Wherein both the parties should take the responsibility of durability, reparability, re-usability and recyclability of the product. Life cycle assessment systems need technology support and also shift in the value systems, meaning both regulatory as well as self-regulatory.

## 5 Findings

Indian garment manufacturing needs to focus on the aspects of waste management, conscious consumption, conscious production, sustainable supply chain systems and ethical practices. In all these areas, we have identified there are innovation and innovative entrepreneurial gaps. The most successful initiatives out of all that have been discussed in the paper are organic cotton farming, Arvind Ltd. and Aditya Birla Groups waste management and recycling initiatives.

Fiber and fabrics have the largest share in the list of raw materials in the apparel industry. There are also several common myths around the use of eco-friendly material, such as all natural fibers are eco-friendly and all synthetic fibers are not. Whereas, eco-friendly material in context with green manufacturing is a material that is either biodegradable or extracted from waste material, as well as is not over-consumed and is easily recyclable. So, one can conclude that over use of cotton, which contributes majorly in increased use of harmful pesticides and insecticides, is biodegradable but not eco-friendly. We can also say that recycled polyester, though synthetic, helps in making the process circular and hence is eco-friendly.

A green manufacturer should ensure that any one fiber is not overused, or the fabric is not made using complex fiber blends. Some of the key indicators while choosing the raw material in a responsible way are as follows: low water consumption, low energy needs, chemical control, no soil erosion, biodegradable and recycled material (Sustain Your Style, n.d.). The same indicators are applicable to all the raw materials such as buttons, zippers, threads, fusible, interlinings or decorative material such as sequins, beads, tapes, laces and ribbons. Some examples of recently introduced sustainable trims are—NATULON® Chemically Recycled Zipper, Plant-based zippers, Eco-friendly Finish (Snap Fastener Finishing Technology), ECO-DYE® (Waterless Zipper Dyeing Technology) (YKK fastening, n.d.). The eco-friendly material segment of the paper showcases that the fruits of sustainability initiatives in the areas of fibers and fabrics have now reached the commercial application stage not just in luxury fashion but also everyday clothing items. The apparel trims industry also is supported with new research and new products in the area of sustainability though they are still limited to luxury and premium price segments of apparel goods due to supply and demand matrix.

On the other hand, circularity or circular design is still in the research and innovation stage. Few brands such as Patagonia or Mud Jeans have been at the fore-front of the initiative and have developed successful models rooted on robust and largely independent retail and marketing formats. They have successfully established a connection with the consumer and are leading the path toward the future. The drawback of these existing successful models is that they are dependent on creating their own independent retail channels as the traditional retail channels do not support the needs of circularity. Hence, limiting the circular design process to large manufacturers and leaving the small to medium sized business units out of the loop.

Examples of efficient waste management systems in apparel manufacturing are limited to large manufacturers following green compliances. The industry on the

other hand is made up of innumerable sizes of manufacturing companies as well as craft and unorganized sector. These largely are non-compliant or unaccountable. Both the compliant and non-compliant contribute significantly in the waste creation. Product design in the apparel industry traditionally focuses on functionality, esthetics, trends and pricing, ignoring the process and product life cycle completely. Adding to this challenge, mapping life cycle assessment of apparel products is complex due to its largely unaccountable and varied use at the consumer level. Hence, there is a need for more multi-scale, easy to adopt and affordable life cycle assessment systems that can be adopted by all types of manufacturers.

## 6 Challenges and Future Scope

As evident by the finding, green manufacturing in the apparel industry is a fairly new concept with shallow penetration. It is largely a work-in-progress, and philosophically, the journey toward sustainability has just started. This creates a high tension and friction scenario as the ecological and societal needs are urgent but not being efficiently catered to. Due to research, skill, innovation and awareness gaps.

Few opportunities that the paper has identified for future research and entrepreneurial initiatives are pointed below:

1. Green manufacturing will affect the industry in the long run; these are not short-term oriented goals.
2. Green manufacturing needs to be supported by “Green Design Thinking” to bridge the gap between consumers and manufacturers. The definition and framework of “Green Design Thinking” itself is under consideration and needs research, studies and academic focus.
3. Building and adapting textile-to-textile recycling technology is also an area that seems to be completely ignored by textile engineers in India.
4. Recycling networks are the need of the hour, to ensure that recycling is a commercially viable option for smaller manufacturers.
5. The concern of “Sustainability” is not understood by all; this needs to be addressed and created awareness about.
6. There are lot of small-scale industries all over the world, wherein aligning the processes to SDGs is a scope for innovation.

## References

1. Aditya Birla Group (2019) Building Sustainable Businesses Fit For a Sustainable World. Aditya Birla Sustain. <https://sustainability.adityabirla.com/group-sustainable-business-report/Group-Sustainable-Business-report.pdf>. Retrieved 19 Jan 2022
2. Arvind Ltd (2019) Cultivate. Arvind. <https://www.arvind.com/pdf/ArvindSR.pdf>. Retrieved 19 Jan 2022



3. Better Cotton Initiative (2021) who-we-are/our-manifesto/. better cotton. <https://bettercotton.org/who-we-are/our-manifesto/>
4. Birla Cellulose. (2020). *Liva Reviva*. Birla Cellulose. <https://www.birlacellulose.com/liva-reviva.php>
5. Charpail M (n.d.) Fashion and Environment—SustainYourStyle. Sustain Your Style. <https://www.sustainyourstyle.org/en/whats-wrong-with-the-fashion-industry>. Retrieved 19 Jan 2022
6. Climate Works Foundation and United Nations Conference on Trade and Development (2016) Circular economy in India: Rethinking growth for long-term prosperity. Ellen MacArthur Foundation. December 5. <https://ellenmacarthurfoundation.org/circular-economy-in-india>. Retrieved 19 Jan 2022
7. Global Organic Textile Standard (2021) The Standard. global-standard. <https://global-standard.org/the-standard>
8. Gwilt A (2020) *A Practical Guide to Sustainable Fashion*. Bloomsbury Publishing
9. Henderson E (2020) 9 Best brands turning recycled plastic bottles into clothes. Independent. September 8. <https://www.independent.co.uk/extras/indybest/fashion-beauty/best-brands-turning-recycled-plastic-bottles-into-clothes-a8774446.html>
10. ISO (2015) Achieving environmental focus with ISO 14001:2015. ISO. November 3. <https://www.iso.org/2015/11/Ref2013.html>. Retrieved 18 Jan 2022
11. McQuillan H, Rissanen T (2015) *Zero Waste Fashion Design*. Bloomsbury Publishing
12. Textile Exchange (2017) What You Wear Matters! Quick Guide to Organic Cotton. [www.textileexchange.org](http://www.textileexchange.org). June 23. <https://textileexchange.org/quick-guide-to-organic-cotton/>. Retrieved 17 Jan 2022
13. Textile Exchange (2021) Organic-content-standard. Text Exch Stand. <https://textileexchange.org/standards/organic-content-standard/>
14. Textile Exchange (2021) *Textile-Exchange\_Preferred-Fiber-Material-Market-Report\_2020*
15. *Textile-Exchange\_Organic-Cotton-Market-Report\_2020* (2020)
16. UNDP (n.d.) Sustainable Development Goals. United Nations Development Programme. <https://www.undp.org/sustainable-development-goals>. Retrieved 19 Jan 2022
17. Villemain C (2019) UN launches drive to highlight environmental cost of staying fashionable. UN News, March 25. <https://news.un.org/en/story/2019/03/1035161>. Retrieved 18 Jan 2022

# A Critical Review of Fatigue Life Prediction on 316LN SS



Raj Kumar, Mohammad Mursaleen, G. A. Harmain, and Ashutosh Kumar

**Abstract** Fatigue failure is referred to the slow deterioration process of structures that are subjected to cyclic loading, including the structural elements of nuclear power plants, aircraft, railways, and rotating machinery. During their operating life, high-temperature components resist three major damaging phenomena: creep, fatigue, creep-fatigue interaction (CFI), and oxidation. Temperatures, strain amplitude, strain rates, hold period effect on fatigue, creep-fatigue interaction, and fatigue crack growth (FCG) for 316LN stainless steel (SS) are presented, and dynamic strain aging (DSA) role is discussed in the article. The fatigue life (FL) increases with nitrogen content (NC), and reduction in the stress precipitation and stress relaxation (SR) due to changes in dislocation structure are given in detail. Fatigue life decrease with increasing hold time is also presented.

**Keywords** 316LN Stainless steel · FCG · Low-cycle fatigue · DSA

## 1 Introduction

316LN stainless steel is selected for its high-temperature (HT) service conditions as it shows good weldability, intergranular stress corrosion and chloride-induced crack, adaptability with sodium coolants, and corrosive environments [2, 3, 67, 75]. It has been extensively used in nuclear power plants, thermal power plants, and aircraft components that operate at elevated temperature [33, 43, 73]. High nitrogen content (0.22%) enhances elevated temperature creep resistance, fatigue, and fracture strength [13, 31, 60]. During thermomechanical processes, 316LN SS experiences several metallurgical changes including flow instabilities, work hardening, dynamic recovery, and dynamic recrystallization [51]. Dynamic recrystallization nucleation produces in subgrain growth and grain boundary projecting mechanism [71]. Mechanical strength of 316LN SS decreases with increasing temperature. The

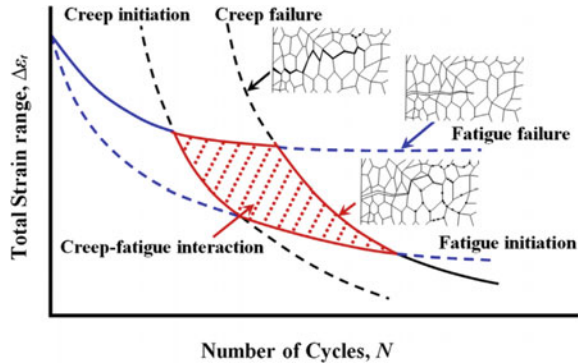
---

R. Kumar · M. Mursaleen (✉) · G. A. Harmain · A. Kumar  
Mechanical Engineering Department, National Institute of Technology Srinagar, Srinagar,  
J&K 190006, India  
e-mail: [mursaleen@nitsri.net](mailto:mursaleen@nitsri.net)

© The Author(s), under exclusive license to Springer Nature Singapore Pte Ltd. 2023  
R. P. Singh et al. (eds.), *Advances in Modelling and Optimization of Manufacturing and Industrial Systems*, Lecture Notes in Mechanical Engineering,  
[https://doi.org/10.1007/978-981-19-6107-6\\_30](https://doi.org/10.1007/978-981-19-6107-6_30)

427

**Fig. 1** Schematic diagram of CFI and failure modes due to fatigue and CFI [73]



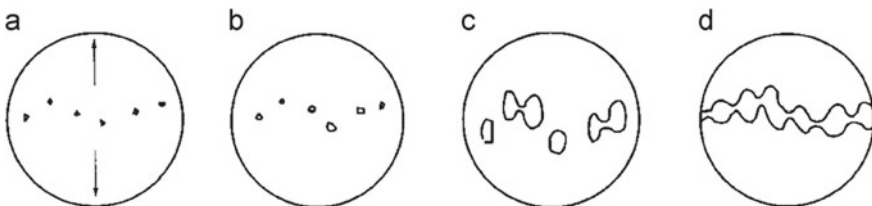
strain-induced martensite increases the fracture stress during the impact test [72]. Under high-temperature start–stop conditions, temperature and load vary with time, resulting in a combination of creep and fatigue deformation [29, 32, 37, 61]. Due to cavitation damage, creep damage can occur during the holding period and is usually manifested as a creep cavity at the grain inner edge [74]. While in creep-fatigue interactions, strong cavitation damage is observed in this material, and fatigue crack damage develops on the surface. When this interaction occurs, the failure mode is mixed (transgranular as well as intergranular), as shown in Fig. 1 [16, 48]. Elastic–plastic fracture mechanics (EPFM) is a tool for determining the leak before break (LBB) of pressurized piping systems and estimating the service life of reactor vessels [30].

## 2 Research Background

Structural components which are subjected to cyclic loading such as elements of nuclear power plants, aircraft, and rotating machinery, fatigue life assessment study were presented by [23]. There are three stages: initiation of cracks, development of short crack to long crack, and ultimately fracture of the component [68]. The Paris rule is generally accepted as a useful method for measuring fatigue crack extension rate with a stress intensity factor [20, 63]. Modeling and simulating the fatigue crack extension mechanism of various structural components is of utmost importance to ensure safety and reliability under different loading conditions [17, 21]. An enormous number of numerical techniques have evolved to simulate the crack extension problem [26, 27] and fatigue [24] like as the finite element method (FEM), boundary element method (BEM), and an extended finite element method (XFEM) [13]. XFEM is an effective numerical technique for simulating various discontinuities, such as cracks, contact [34, 36] inclusions [35], and cavity without the need for a finite element mesh to correspond to these discontinuities [13, 25].

Samuel et al. [52], studied the tensile work hardening behavior of 316LN SS at different temperatures and strain rates. It has been observed that the tensile properties of the material are changed at intermediate temperatures due to dynamic stress aging. Experimental results show that the load-deformation curves were smooth at ambient and HT, whereas at a medium temperature, the irregular flow was obtained. Srinivasan et al. [66], investigated the LCF and CFI behavior of 316LN SS under different experimental condition such as various deformation behavior on this material reported based on several mechanisms including DSA under stress, creep, oxidation, and sub-structural recovery. Using the data generated in that study, an artificial neural network (ANN) model enabled life prediction model under LCF and CFI conditions.

Kim et al. [28], conducted LCF and CF tests for two materials (316L and 316LN SS) with continuous cycling and 10-min hold period at temperature 600 K in air. It was noticed that the addition of nitrogen increased FL, CF life, and saturation stress. It is reported that the fracture mode in the fatigue test was transgranular and for the CF test was intergranular. In addition, the dislocation structure for 316L was cellular and planar for 316LN in the fatigue, creep-fatigue test. Precipitation of carbides at grain boundaries has been reported in CF tests, and it has been suggested that these precipitation can be avoided with addition of nitrogen. Roy et al. [49] examined the LCF tests of 316LN SS at room temperature with the range of strain amplitude ( $\pm 0.3$  to  $\pm 1.0\%$ ) and strain rate ( $3 \times 10^{-3} \text{ s}^{-1}$ ). The material exhibited non-masing behavior at higher strain rates and masing behavior at lower strain rates. It has been reported that FL decreases with increasing stress amplitude, and the hysteresis loop behavior was in good agreement with the test results. Babu et al. [3], conducted FCG test on 316LN SS at room temperature; the nitrogen percentage was varied through 0.8, 0.14, and 0.22 wt%. In this study, the direct current potential drop (DCPD) technique was used to estimate FCG, and the compliance technique was used to estimate the crack closure. It was observed that the threshold stress intensity factor ( $\Delta K_{th}$ ) and effective threshold stress intensity factor  $\Delta K_{eff,th}$  were different for various nitrogen contents. Also, the fracture surface roughness parameter was used to quantify the slip irreversibility model. The cracks are often formed by the microcavity nucleating, growing, and converging, as shown in Fig. 2 [75].



**Fig. 2** Crack formation involves **a** cavity nucleation, **b** cavity growth, **c** cavity polymerization, and **d** fracture [75]

### 3 Factors Affecting Mechanical Properties of 316LN SS

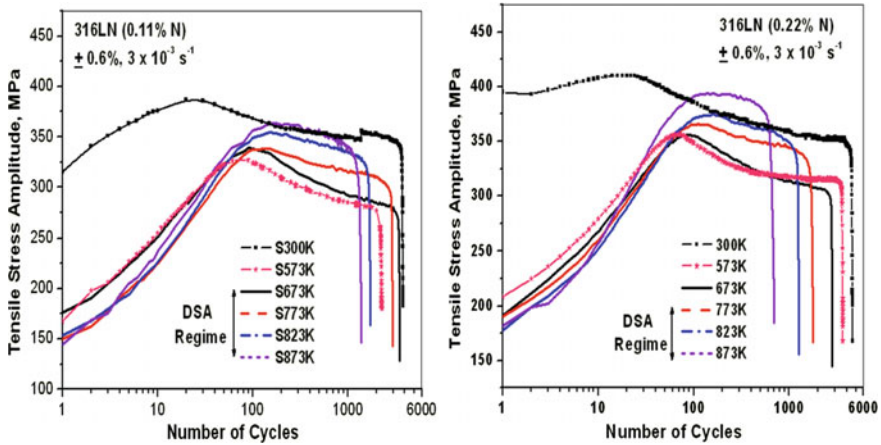
The effect of temperature and strain rate, hold period, nitrogen content, and dynamic strain aging on deformation behavior of 316LN SS has been discussed in this study.

#### 3.1 Effect of Temperature and Strain Rate

The load-deformation curve is smooth at room and elevated temperature although irregular flow curves were obtained at intermediate temperatures. The sufficient plastic stress-strain data for 316LN SS are best expressed in terms of Ludwigson relation at ambient temperature [8, 72]. Several flow parameters observed in the Ludwigson-Voce equation varies with deformation rate and temperature [8]. The decrease in FL with an increase in the temperature range (673–873 K) is ascribed to detrimental effects of DSA, and beyond 873 K, the FL was affected by oxidation [56, 64]. This material exhibited a higher ratio of normalized stress with increasing temperature (573–873 K) and also observed irregular fluctuation in tensile properties due to DSA at a medium temperature and a normal behavior at elevated temperatures [66]. Isothermal cycling at the HT of thermomechanical fatigue yielded lower endurance than in-phase and out-of-phase cycling [44]. The ratcheting strain increases with an increase in temperature, and fatigue life decreased because of higher plastic deformation [58].

In the load-deformation curve, irregular flow/twitching at the mean temperature is observed, related to the attractive interaction between the solute and the mobile dislocation throughout deformation, known as DSA [45, 52, 56]. DSA temperature regime is sensitive to nitrogen percentage, with temperatures ranging from 673 to 873 K (Fig. 3a) for nitrogen percentage less than 0.11 wt% and from 773 to 873 K (Fig. 3b) for nitrogen percentage greater than 0.11 wt% [45]. The direction of generating a set of non-cellular displacements increased with increasing DSA. 316LN SS is available in two irregular flow temperature regimes, such as the relatively low temperature (523–598 K) and the high temperature (673–923 K) [8].

A low-cycle fatigue test was conducted for short cycles, and no evidence of dynamic precipitation in the temperature range associated with rapid cycle hardening. That study explicitly ruled out a precipitation effect in the rapid hardening of 316LN SS. The fatigue strength decreased by increasing the temperature and decreasing the strain rate from  $3 \times 10^{-2}$  to  $3 \times 10^{-5} \text{ s}^{-1}$  [66]. At all strain rates of 773 and 823 K, DSA played a vital role in fatigue deformation and fracture. In tensile tests at 873 K, DSA has been reported to result in a decrease in service life and increased fatigue strength. DSA has been described to cause hardening at an earlier fatigue life stage, and nitrogen retarded influence of DSA [28]. Samantaray et al. [50] This article has reported the influence of strain rate, deformation, working environment (temperature), and method of loading on tensile behavior of 316LN,



**Fig. 3** Cyclic stress response (CSR) curves of 316LN SS alloyed with different nitrogen contents [45]

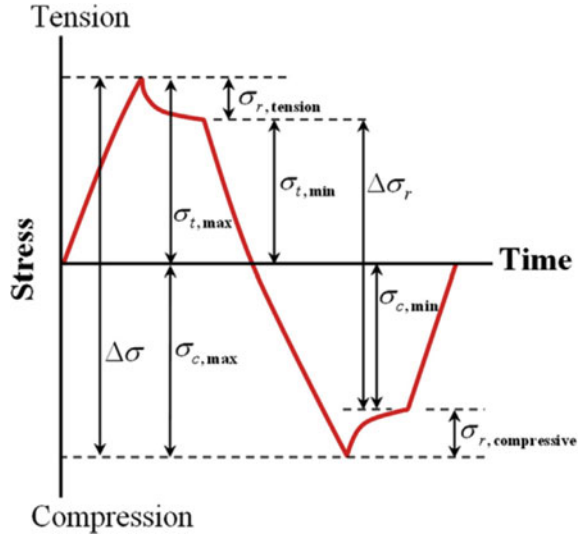
and a correlation between deformation and microstructural features has been established. The higher temperature regime of 316LN SS serrated flow conflicts with the temperature range (773–973 K) in which precipitation of chromium carbide has been observed. In the low-temperature range (523–623 K), the diffusion of interstitial solutes to displacements is responsible for serrated flow. The mechanism accountable for the serrated yielding in the HT range (973–923 K) is an alternative solute like Cr [54].

### 3.2 Effect of Hold Period

The SR behavior in the cyclic regime at half-life was presented by the CFI, which introduced hold time at the peak tensile strain or peak compression strain as shown in Fig. 4 [73].

CFI tests have been conducted at 873 K to estimate the impact of the hold period (1–90 min). It has been reported that there was a reduction in fatigue resistance with an increase in hold time. CFI is caused by a flaw in the grain boundary that leads to creep in the intergranular cavity, which can lead to intergranular gaps and cracks that coincide with fatigue cracking and constitute the most common cause of premature failure [66]. It has been found that SR varies with nitrogen content and saturating stress during the hold time [6, 40]. In CF experiments, the creep deformation occurring during the hold period has been evaluated to play a vital role in nucleation and growth of voids indicating the occurrence of an intergranular failure mode attributed to gap nucleation at the grain boundary [28].

**Fig. 4** In hold-time tests, different stress values were found [73]



The occurrence of creep during hold time results in the reduction of cyclic stress to attain a given strain in creep-fatigue tests [61]. Declaring that 316LN stainless steel has a high DSA in the temperature range (573–923 K), cyclic hardening behavior develops. However, the planar dislocation structure deteriorates, and the dislocation density decreases during the hold time; the resistance to dislocation motion decreases [10, 28]. In CF tests, at a constant temperature and plastic strain range, FL is found to be reduced, while the tensile hold time is increased [39]. Sarkar et al. [57], Conducted creep-fatigue interaction experiment at elevated temperature (650 °C) for 316LN SS where selected loading parameter is below endurance strength with high load ratio. They reported that small load amplitude shows substantial CFI which indicates the influence of stress amplitude on the failure mechanism of material at higher temperatures.

### 3.3 Effect of Nitrogen Content and Dynamic Strain Aging

Nitrogen has been reported to affect fatigue and creep properties at HT by modifying metallurgical factors like dislocation, precipitation, and DSA. With the addition of nitrogen percentage, the dislocation structure is changed from unitary to planar in the fatigue and CF tests [40]. The temperature and time for carbide precipitation have been reported to increase by the addition of nitrogen [41]. The integrated effect of precipitation strengthening by excellent carbides and substantial solution strengthening by nitrogen in 316LN SS resulted in increased creep rupture life and decreased creep life [38]. High-temperature LCF life increased with the adding nitrogen because it produced planar slip and restrained DSA [28, 29, 43, 65].

The fatigue strength at 300 and 77 K increases with the addition of nitrogen [70]. The creep and tensile endurance of 316LN SS was reported to improve significantly by enhancing the nitrogen percentage [37, 44] and also improving fracture toughness at cryogenic temperatures [31]. Surface and internal creep damage decreased with an increase in nitrogen percentage [13]. The steady-state creep rate, the region of intragranular cracks, and surface cracks reduced with an increase in nitrogen percentage [62]. The addition of nitrogen to 316LN SS improved corrosion resistance by preventing pitting, intergranular corrosion, sensitization, corrosion fatigue, and stress corrosion cracking [18]. Two typical manifestations of dynamic strain aging have elastic shakedown and strain burst [55]. The cyclic stress response of 316LN steel is observed to show initial hardening, softening, saturation, and eventual fracture over a long period [45, 49]. Addition nitrogen in austenitic stainless steels (304LN and 316LN SS) shows a beneficial effect on flow strength via strain hardening characteristics which can be attributed to bulk material strengthening and inclination toward planar slip hence, trim downs the susceptibility to dynamic recovery [42].

The effect of nitrogen on the CSR was observed in the LCF test with a strain amplitude of 0.6% and an ambient temperature of 300 K. The degree of softening increased by increasing the nitrogen percentage, especially for 0.14 and 0.22% at 300 K [47]. The CSR with a strain amplitude of  $\pm 0.6\%$  develops into a plastic deformation greater than the strain amplitude of  $\pm 0.4\%$  [59]. The CSR increased with decreasing strain rate as depicted in Fig. 5 which shows variation of half-life tensile stress amplitude (HLSA) with respect to nitrogen percentage at different strain rates of  $3 \times 10^{-5} \text{ s}^{-1}$  and  $3 \times 10^{-4} \text{ s}^{-1}$  and temperatures [43]. The CSR of 316LN SS under high-temperature fatigue loading is influenced by multiple factors such as dislocation–dislocation and interaction, DSA, recovery process, and creep [12, 32]. Dynamic strain aging (DSA) is based on time and temperature phenomena. When DSA reduces ductility, it may affect crack propagation at high temperatures, as seen in Fig. 6 [29]. The activation energy of  $200 \text{ kJ mol}^{-1}$  was attained in temperature range (673–873 K), which encourages the opinion that the diffusion of exchange elements such as Cr to dislocation was produced by the DSA [65]. In LCF experiments, it is also significant that nitrogen percentage greater than 0.07 wt% results in substantially larger cyclic tensile stresses [29]. Ganesan et al. [11], studied the deformation behavior of 316LN SS at high temperature and constant load (creep) for varying nitrogen percentage at 650 °C and reported that material creep resistance increases with increasing nitrogen percentage (0.07–0.22%) while creep ductility decreases. Increasing nitrogen percentage increases the tendency of intergranular deformation, while in the case of low nitrogen it shows both transgranular as well as intergranular cracking. Fatigue crack propagation at elevated temperature is governed by intergranular mode, due to the synergetic effect of DSA and oxidation, while in absence of oxidation, fatigue damage will transgranular [76].

The influence of nitrogen percentage in 316LN on LCF life can be obtained only when the time-dependent effects are minimum and the failure mode is typically transgranular, as shown in Fig. 7, [43].



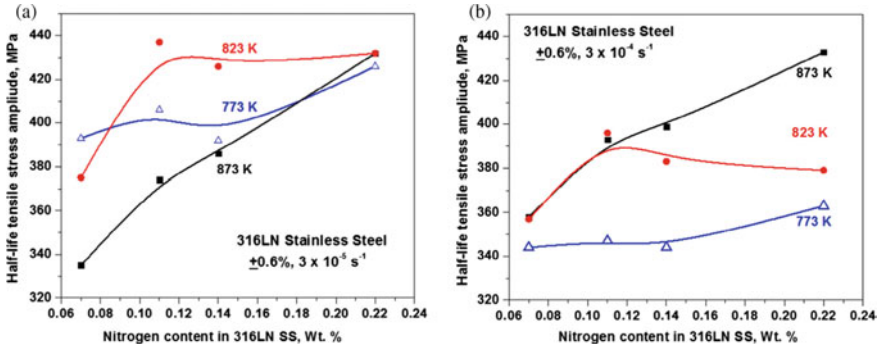


Fig. 5 Effect of temperature on 316 LN with two strain rates and variation in nitrogen content [43]

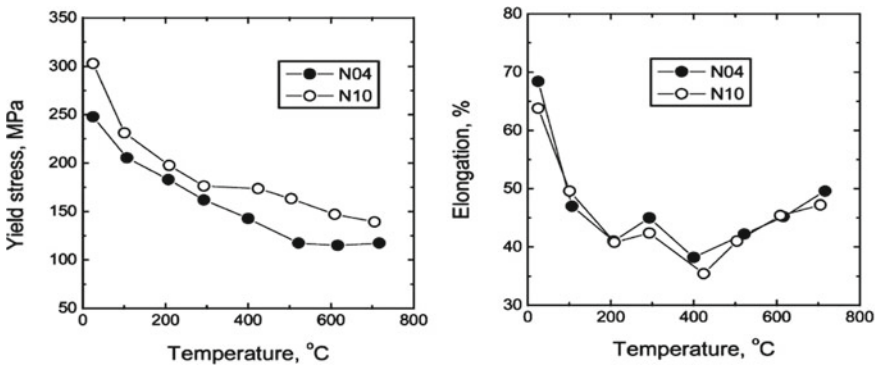
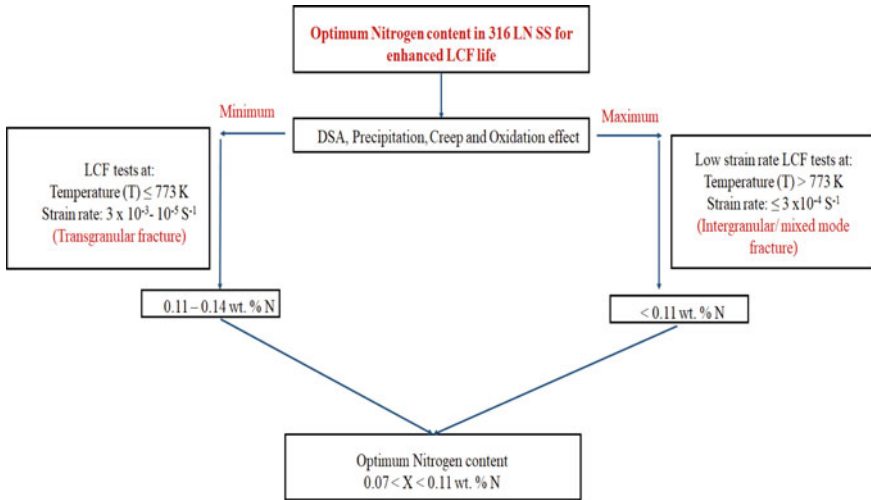


Fig. 6 Effect of temperatures on yield stress and elongation for 316LN SS [29]

The flow stress rises with reducing deformation rate but increases with increasing temperature [46, 65]. It was observed that for 0.14% N steel, the strain increased by 0.4% with increasing temperature (773–873 K), and the strain amplitude was 0.6%, showing DSA. The initial cyclic hardening of 773 and 300 K, with a deformation magnitude of 0.6%, occurred during DSA. In the stress–strain hysteresis loop, 0.07 and 0.22% N of the steel at all stress amplitudes of 873 and 823 K were irregular flow, independent of the nitrogen. A continuous cyclic decrease in the degree of stress drop associated with tensile results was observed over the half-life period [46]. The influence of nitrogen on FL was observed at 773 and 873 K with strain amplitudes between 0.25 and 1.0%. It was also observed that the fatigue life increases or decreases with changing nitrogen content or becomes saturated with temperature and amplitude of applied strain at 0.14% N [47]. Reddy et al. [47], conducted LCF tests with a strain amplitude of 0.25% and at temperatures 773 and 873 K. It has been reported that the cyclic strain is influenced by DSA and secondary cyclic hardening (SCH) for 0.14% N steel. DSA is exhibited as a general increase in stress response with increasing temperature except at 873 K, whereas SCH is observed throughout



**Fig. 7** Increased LCF life for 316LN SS with optimum nitrogen percentage is due to time-dependent processes

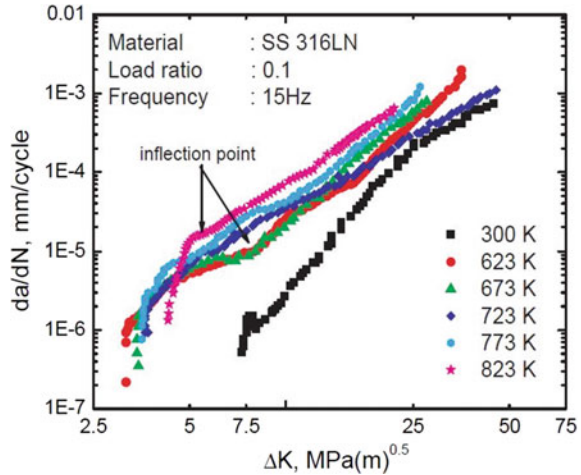
the full temperature range from 773 K to 873 K with different amounts of hardening (during SCH) at each temperature. During SCH, increasing the nitrogen content and decreasing the temperature can increase the degree of hardening. At 773 K, DSA and SCH develop matrix hardening, and the life of LCF falls with increasing nitrogen content due to the rapid propagation of cracks during matrix.

Hardening [45, 47]. In LCF tests with a strain amplitude of  $\pm 0.4\%$  and a temperature of 873 K, 316LN SS displayed constant CSR from the initial cycle until it reached a near-saturated state before a rapid decrease in stress (GV and GA 2018). In the high-temperature regime, deformation rates of the load-deformation curves and temperature-dependent fragmentation flow dissipation occur. [69] In a research paper, the effect of sub-creep temperature on dynamic strain aging which influence the hardening behavior was analyzed. 316LN SS, DSA exists between 523 and 923 K; the material tends to have minimal ductility, and it has been observed that fracture resistance diminishes with rising temperature [9].

### 3.4 Effect of Temperature on Fatigue Crack Growth

The FCG experiments were conducted at temperatures from 300, 573, and 823 K in the air using the  $\Delta K$  decreasing mode under a constant  $R$  of 0.1 at a loading frequency of 15 Hz as shown in Fig. 8. The online crack length was estimated with the help of the direct current potential drop (DCPD) method [4]. The 0.22% N steel exhibited a larger FCG rate and lower threshold stress intensity factor ( $\Delta K_{th}$ ) in the Paris regime than the 0.14% N steel. The FCG results with crack closure correction,

**Fig. 8** Effect of various temperatures on the FCG behavior of SS316LN [4]



FCG resistance of 0.14% N steel is better than the other two 0.08 and 0.22% N steel in Paris and threshold regimes [3, 60]. Nitrogen is useful to the LCF resistance while the high slip planarity and decrease in stacking fault energy (SFE), which produces a high tendency to slip reversibility and reduces the cyclic strain localization [32, 44]. The 316LN SS will damage by creating stacking fault rings during the comparable stress that leads to a significant level of nearly 600 MPa due to several encouraging measures including radiance, raising strain, and diminishing test temperature [7]. A complex microstructural phenomenon governs the initiation of intragranular cracks during the LCF test [62]. Plastic deformation induces an effect on fatigue crack propagation was reported in [19].

While in the case of various loading patterns, loading patterns are associated with crack tip stress–strain behavior which controls the fatigue crack propagation rate [22]. The anisotropic behavior of SS 316LN at this microscopic level has been shown to perform an essential role in the development of fatigue cracks. Fatigue cracking depends on 316LN stainless steel's graininess for surface cracks without damages and existing cracks [9, 63]. (Zhang et al. [76]) found that the environmental-aided effect on FCG rate was equivalent to the  $K$  value and that under the same  $K$  and rise time situations, the increase in FCG rate in HT water became more evident as the load ratio ( $R$ ) value raised. The influence of grain boundary atmosphere distribution and grain size on corrosion fatigue analysis of 316LN SS in borated and lithiated HT water was examined by [14]. The grain boundary engineering method, rather than increasing the fraction of low-coincidence site lattice boundaries, was found to improve FL due to grain refining. The 316LN SS undergoes significant hardening under both cold and hot conditions. The plastic deformation of 316LN SS was formulated and depends on various processing parameters like deformation amplitude, deformation rate, temperature, and load type [50]. Samuel et al. [53], In this article, effect of varying load ratios on fatigue crack threshold has been reported and found that threshold stress intensity factor has an inverse relation with load ratio. The hardness

value of 316LN stainless steel increases with increasing deformation rate, reaching a maximum amount of 350 HV at a maximum applied deformation rate of  $3 \times 10^{-3} \text{s}^{-1}$  [1]. The growth rate of fatigue cracking decreases with an increasing load angle. Using different ranges of stress intensity factors, FCG rate  $da/dn$  of mode-I is lower than that of the mixed mode [5].

## 4 Conclusion

The interaction between creep-fatigue and fatigue has been studied in this review. In the secondary cyclic hardening process, hardening is increased by increasing the nitrogen content and with the decrease in temperature. Dynamic strain aging is a time and temperature-dependent phenomenon, so yield strength increases with decreasing deformation rate or increasing temperature. Adding nitrogen increases the life of the high-temperature low-cycle fatigue as it creates glide and preserves dynamic strain aging. With increased hold duration, fatigue life decreases.

## References

1. Acharya S et al (2019) Effect of high strain rate deformation on the properties of SS304L and SS316LN Alloys. *Mech Mater* 136:103073
2. Babu MN et al (2010) On the anomalous temperature dependency of fatigue crack growth of SS 316(N) weld. *Mater Sci Eng A* 527(20):5122–5129
3. Babu MN et al. (2013) Fatigue crack growth behavior of 316LN stainless steel with different nitrogen contents. *Proc Eng* 55:716–21
4. Babu MN, Sasikala G (2020) Effect of temperature on the fatigue crack growth behaviour of SS316L (N). *Int J Fatigue* 140:105815
5. Babu MN, Venugopal S, Sasikala G (2014) Evaluation of fatigue crack growth behaviour of SS 316 LN steel under mixed mode loading (Mode I and II). *Proc Eng* 86:639–644
6. Brinkman CR (1985) High-temperature time-dependent fatigue behaviour of several engineering structural alloys. *Int Met Rev* 30(1):235–258
7. Byun TS, Lee EH, Hunn JD (2003) Plastic deformation in 316LN stainless steel-characterization of deformation microstructures. *J Nucl Mater* 321(1):29–39
8. Choudhary BK, Isaac Samuel E, Bhanu Sankara Rao K, Mannan SL (2001) Tensile stress-strain and work hardening behaviour of 316ln austenitic stainless steel. *Mater Sci Technol* 17(2):223–231
9. Dutt BS et al (2014) Effect of nitrogen addition and test temperatures on elastic-plastic fracture toughness of SS 316 LN. *Proc Eng* 86:302–307
10. Fan Y-N, Shi H-J, Tokuda K (2015) A generalized hysteresis energy method for fatigue and creep-fatigue life prediction of 316L (N). *Mater Sci Eng A* 625:205–212
11. Ganesan V et al. (2022) Role of nitrogen content on interrelationship between creep deformation and damage behaviour of 316LN SS. *Trans Indian National Acad Eng* 1–9
12. Ganesan V, Mathew MD, Parameswaran P, Laha K (2013) Effect of nitrogen on evolution of dislocation substructure in 316LN SS during creep. *Proc Eng* 55:36–40
13. Ganesan V, Mathew MD, Parameswaran P, Bhanu Sankara K, Rao. (2010) Creep strengthening of low carbon grade type 316LN stainless steel by nitrogen. *Trans Indian Inst Met* 63(2):417–421

14. Gao J, Tan J, Wu X, Xia S (2019) Effect of grain boundary engineering on corrosion fatigue behavior of 316LN stainless steel in borated and lithiated high-temperature water. *Corros Sci.* <https://doi.org/10.1016/j.corsci.2019.01.036>
15. GV, Prasad Reddy, and Harmain GA. (2018) Simulation of low cycle fatigue stress-strain response in 316LN stainless steel using non-linear isotropic kinematic hardening model—a comparison of different approaches. *Fatigue Fract Eng Mater Struct* 41(2):336–347
16. Hales R (1980) A quantitative metallographic assessment of structural degradation of type 316 stainless steel during creep-fatigue. *Fatigue Fract Eng Mater Struct* 3(4):339–356
17. Jameel A, Harmain GA (2016) Modeling and numerical simulation of fatigue crack growth in cracked specimens containing material discontinuities. *Strength Mater* 48(2):294–307
18. Jayakumar T et al (2013) Nitrogen enhanced 316LN austenitic stainless steel for sodium cooled fast reactors. *Trans Tech Publ, In Advanced Materials Research*, pp 670–680
19. Kant C, Harmain GA (2021a) An investigation of constant amplitude loaded fatigue crack propagation of virgin and pre-strained aluminium alloy. In: International conference on advanced manufacturing and materials processing (CAMMP 2021), Bentham Science Publishers, Jaipur
20. Kant C, Harmain GA (2021b) An investigation of fatigue crack closure on 304LSS and 7020-T7 aluminium alloy. In: International conference on progressive research in industrial and mechanical engineering (PRIME-2021), Patna
21. Kant C, Harmain GA (2021c) Fatigue life prediction under interspersed overload in constant amplitude. In: 9th International conference on fracture fatigue and wear (FFW 2021) (Lecture notes in mechanical engineering), Springer, Ghent, Belgium
22. Kant C, Harmain GA (2021) Analysis of single overload effect on fatigue crack propagation using modified virtual crack annealing model. In: International conference on mechanical engineering
23. Kant C, Harmain GA (2021d) A model based study of fatigue life prediction for multifarious loadings. *Key Eng Mater* 882:296–327. <https://www.scientific.net/KEM.882.296>
24. Kanth SA, Harmain GA, Jameel A (2021) Investigation of fatigue crack growth in engineering components containing different types of material irregularities by XFEM. *Mech Adv Mater Struct* 1–39. <https://doi.org/10.1080/15376494.2021.1907003>
25. Kanth SA, Harmain GA, Jameel A (2018) Modeling of nonlinear crack growth in steel and aluminum alloys by the element free Galerkin method. *Mater Today Proc* 5(9):18805–18814
26. Kanth SA, Lone AS, Harmain GA, Jameel A (2019) Elasto plastic crack growth by XFEM: a review. *Mater Today Proc* 18:3472–3481. <https://doi.org/10.1016/j.matpr.2019.07.275>
27. Kanth SA, Lone AS, Harmain GA, Jameel A (2019b) Modeling of embedded and edge cracks in steel alloys by XFEM. *Mater Today Proc* 26(xxxx):814–18. <https://doi.org/10.1016/j.matpr.2019.12.423>
28. Kim DW, Chang J-H, Ryu W-S (2008) Evaluation of the creep-fatigue damage mechanism of type 316L and type 316LN stainless steel. *Int J Press Vessels Pip* 85(6):378–384
29. Kim DW, Kim WG, Ryu W-S (2003) Role of dynamic strain aging on low cycle fatigue and crack propagation of type 316L (N) stainless steel. *Int J Fatigue* 25(9–11):1203–1207
30. Krishnan SA et al (2015) Coupled FEM and experimental analysis to characterize initial crack growth regime in AISI 316L (N) stainless steel. *Int J Struct Integrity* 6:390–401
31. Kumar JG et al (2010) High temperature design curves for high nitrogen grades of 316LN stainless steel. *Nucl Eng Des* 240(6):1363–1370
32. Li B et al (2020) Cyclic deformation and cracking behavior of 316LN stainless steel under thermomechanical and isothermal fatigue loadings. *Mater Sci Eng A* 773:138866
33. Li B et al. (2021) Cyclic deformation behavior and dynamic strain aging of 316LN stainless steel under low cycle fatigue loadings at 550 °C. *Mater Sci Eng A* 818(November 2020):141411. <https://doi.org/10.1016/j.msea.2021.141411>
34. Lone AS, Jameel A, Harmain GA (2018) A coupled finite element-element free Galerkin approach for modeling frictional contact in engineering components. *Mater Today Proc* 5(9):18745–18754. <https://doi.org/10.1016/j.matpr.2018.06.221>
35. Lone AS, Kanth SA, Harmain GA, Jameel A (2019) XFEM Modeling of frictional contact between elliptical inclusions and solid bodies. *Mater Today Proc* 26(xxxx): 819–24. <https://doi.org/10.1016/j.matpr.2019.12.424>

36. Lone AS, Kanth SA, Jameel A, Harmain GA (2019) A state of art review on the modeling of contact type nonlinearities by extended finite element method. *Mater Today Proc* 18:3462–3471. <https://doi.org/10.1016/j.matpr.2019.07.274>
37. Mathew MD, Laha K, Sandhya R (2013) Creep and low cycle fatigue behaviour of fast reactor structural materials. *Proc Eng* 55:17–26
38. Mathew MD, Sasikala G, Bhanu Sankara Rao K, Mannan SL (1991) Influence of carbon and nitrogen on the creep properties of type 316 stainless steel at 873 K. *Mater Sci Eng A* 148(2):253–260
39. Nam SW et al (1996) The normalized coffin-manson plot in terms of a new damage function based on grain boundary cavitation under creep-fatigue condition. *Metall Mater Trans A* 27(5):1273–1281
40. Nilsson JO (1988) Effect of nitrogen on creep-fatigue interaction in austenitic stainless steels at 600 °C. In: *Low cycle fatigue*, ASTM International
41. Oh YJ, Ryu WS, Hong JH (1997) The effect of nitrogen on the grain boundary precipitation and sensitization of Type 316 L stainless steels. *J Korean Inst Met Mater (South Korea)* 35(8):942–50
42. Palaparti DP, Rao V, Ganesan JC, Prasad Reddy GV (2021) Tensile flow analysis of austenitic type 316LN stainless steel: effect of nitrogen content. *J Mater Eng Perform* 30(3):2074–2082. <https://doi.org/10.1007/s11665-021-05484-y>
43. Reddy GV, Prasad RK et al (2015) Effect of strain rate on low cycle fatigue of 316LN stainless steel with varying nitrogen content: part-I cyclic deformation behavior. *Int J Fatigue* 81:299–308
44. Reddy GV, Prasad AN et al (2015) Thermomechanical and isothermal fatigue behavior of 316LN stainless steel with varying nitrogen content. *Metall Mater Trans A* 46(2):695–707
45. Reddy GV, Prasad RS, Bhanu Sankara Rao K, Sankaran S (2010) Influence of nitrogen alloying on dynamic strain ageing regimes in low cycle fatigue of AISI 316LN stainless steel. *Proc Eng* 2(1):2181–2188
46. Reddy GV, Prasad RS, Sankaran S, Mathew MD (2014) Low cycle fatigue behavior of 316LN stainless steel alloyed with varying nitrogen content part I: cyclic deformation behavior. *Metall and Mater Trans A* 45(11):5044–5056
47. Reddy GV, Prasad RS, Sankaran S, Mathew MD (2014) Low cycle fatigue behavior of 316LN stainless steel alloyed with varying nitrogen content part II: fatigue life and fracture behavior. *Metall Mater Trans A* 45(11):5057–5067
48. Rodriguez P, Bhanu Sankara K, Rao. (1993) Nucleation and growth of cracks and cavities under creep-fatigue interaction. *Prog Mater Sci* 37(5):403–480
49. Roy SC, Sunil Goyal R, Sandhya, and S K Ray. (2013) Analysis of hysteresis loops of 316L (N) stainless steel under low cycle fatigue loading conditions. *Proc Eng* 55:165–170
50. Samantaray D et al (2017) Plastic deformation of SS 316LN: thermo-mechanical and microstructural aspects. *Proc Eng* 207:1785–1790
51. Samantaray D, Mandal S, Phaniraj C, Bhaduri AK (2011) Flow behavior and microstructural evolution during hot deformation of AISI type 316 L (N) austenitic stainless steel. *Mater Sci Eng A* 528(29–30):8565–8572
52. Samuel EI, Choudhary BK, Bhanu Sankara K, Rao (2002) Influence of temperature and strain rate on tensile work hardening behaviour of Type 316 LN austenitic stainless steel. *Scripta Mater* 46(7):507–512
53. Samuel KG, Sasikala G, Ray SK (2011) On R ratio dependence of threshold stress intensity factor range for fatigue crack growth in type 316(N) stainless steel weld. *Mater Sci Technol* 27(1):371–376
54. Samuel KG, Mannan SL, Rodriguez P (1988) Serrated yielding in AISI 316 stainless steel. *Acta Metall* 36(8):2323–2327
55. Sarkar A, Nagesha A, Parameswaran P et al (2013) Influence of dynamic strain aging on the deformation behavior during ratcheting of a 316LN stainless steel. *Mater Sci Eng A* 564:359–368
56. Sarkar A et al (2018) Manifestations of dynamic strain aging under low and high cycle fatigue in a type 316LN stainless steel. *Mater High Temp* 35(6):523–528

57. Sarkar A, Dash MK, Nagesha A (2021) Mechanism of HCF-creep interaction in a Type 316LN stainless steel. *Mater Sci Eng A* 825(July):141841. <https://doi.org/10.1016/j.msea.2021.141841>
58. Sarkar A, Nagesha A, Sandhya R, Mathew MD (2013) Effect of Temperature on ratcheting behaviour of 316LN SS. *Proc Eng* 55:650–654
59. Sarkar A, Nagesha A, Sandhya R, Mathew MD (2015) A perspective on fatigue damage by decoupling LCF and HCF loads in a type 316LN stainless steel. *High Temp Mater Process (London)* 34(5):435–439
60. Sasikala G, Babu MN, Dutt BS, Venugopal S (2013) Characterisation of fatigue crack growth and fracture behaviour of SS 316L (N) base and weld materials. *Trans Tech Publ, In Advanced Materials Research*, pp 449–459
61. Sauzay M et al (2004) Creep-fatigue behaviour of an AISI stainless steel at 550 °C. *Nucl Eng Des* 232(3):219–236
62. Schwartz J, Fandeur O, Rey C (2010) Modelling of Low Cycle Fatigue Initiation of 316LN Based on crystalline plasticity and geometrically necessary dislocations. *Trans Tech Publ, In Materials Science Forum*, pp 1137–1142
63. Sistaninia M, Niffenegger M (2015) Fatigue crack initiation and crystallographic growth in 316L stainless steel. *Int J Fatigue* 70:163–170
64. Srinivasan VS et al (1991) Effects of temperature on the low cycle fatigue behaviour of nitrogen alloyed type 316L stainless steel. *Int J Fatigue* 13(6):471–478
65. Srinivasan VS et al (1999) High temperature time-dependent low cycle fatigue behaviour of a type 316L (N) stainless steel. *Int J Fatigue* 21(1):11–21
66. Srinivasan VS et al (2003) Low cycle fatigue and creep-fatigue interaction behavior of 316L (N) stainless steel and life prediction by artificial neural network approach. *Int J Fatigue* 25(12):1327–1338
67. Suresh Kumar T, Nagesha A, Mariappan K, Dash MK (2021) Deformation and failure behaviour of 316 LN austenitic stainless steel weld joint under thermomechanical low cycle fatigue in as-welded and thermally aged conditions. *Int J Fatigue* 149(January):106269. <https://doi.org/10.1016/j.ijfatigue.2021.106269>
68. Taylor D, Knott JF (1981) Fatigue crack propagation behaviour of short cracks; the effect of microstructure. *Fatigue Fract Eng Mater Struct* 4(2):147–155
69. Valsan M, Nagesha A (2010) Low cycle fatigue and creep-fatigue interaction behaviour of 316L(N) stainless steel and its welds. *Trans Indian Inst Met* 63(2–3):209–215
70. Vogt JB et al (1991) Low-temperature fatigue of 316L and 316LN austenitic stainless steels. *Metall Trans A* 22(10):2385–2392
71. Wang S, Zhang M, Wu H, Yang B (2016) Study on the dynamic recrystallization model and mechanism of nuclear grade 316LN austenitic stainless steel. *Mater Charact* 118:92–101
72. Wang S, Yang K, Shan Y, Li L (2008) Plastic deformation and fracture behaviors of nitrogen-alloyed austenitic stainless steels. *Mater Sci Eng A* 490(1–2):95–104
73. Yan X-l, Zhang X-C, Shan-tung T, Mannan S-L (2015) International journal of pressure vessels and piping review of creep e fatigue endurance and life prediction of 316 stainless steels. *Int J Press Vessels Pip* 126–127:17–28
74. Zhang X, Shan-Tung T, Xuan F (2014) Creep–fatigue endurance of 304 stainless steels. *Theoret Appl Fract Mech* 71:51–66
75. Zhang X, Zhang Y, Li Y, Liu J (2013) Cracking initiation mechanism of 316LN stainless steel in the process of the hot deformation. *Mater Sci Eng, A* 559:301–306
76. Zheng Y et al. (2022) Multiaxial low cycle fatigue behavior and life prediction method of 316LN stainless steel at 550 °C. *Int J Fatigue* 156(October 2021): 106637. <https://doi.org/10.1016/j.ijfatigue.2021.106637>

# Weight-Based Object Segregation Using 5 DOF Robotic Arm



Awaar Vinay Kumar, Abhignya Rajapu, Kalaka Goutham,  
Yerravati Shiva Prasad Goud, and Madisetty Anuraag

**Abstract** In the forthcoming industrial revolution 5.0 and the present industrial revolution 4.0, robotic arms play an integral role in automating the manufacturing industry; hence, it is critical that these robotic arms have the most robust features. Hence, arms with features like weight-based object segregation using high-precision load cells can be game changing in industries with injection molding where inline weight measurement of materials can save a lot of time and resources. Hence, in this paper, we proposed an android app-controlled Bluetooth-enabled robotic arm with a high-precision weight monitoring sensor module, which depicts the weight of the object it picks and displays it on the serial monitor as it picks. The arm takes the input from a graphical user interface developed on the mobile. The android app provides user interface for controlling and configuring this robot arm as well as executing commands such as picking, grasping, and homogeneous grasping. The robotic arm has 5° of freedom which means that it has the capability to move at 5 different joints which get their ability to move from 6 servo motors. The robotic arm can easily pick and place small to medium-sized objects using the 2-finger gripper and simultaneously weigh the picked object.

**Keywords** 5 Degrees of freedom robotic arm · Load cell · Hx711 load cell module · Hc-05 Bluetooth module · Weight-based segregation · SG90 servo motor · MG996R servo motor

## 1 Introduction

Robots are capable of amazing feats of strength, speed, and seemingly intelligent decisions; however, this last ability is entirely dependent upon the continuing development of machine intelligence and logical routines [1]. Our future is closely bound with robotics as it is becoming an intrinsic part of human race. International Federation of Robotics (IFR) defines a service robot as a robot which operates semi-

---

A. Vinay Kumar (✉) · A. Rajapu · K. Goutham · Y. S. P. Goud · M. Anuraag  
Department of Electrical and Electronics Engineering, GRIET, Hyderabad, India  
e-mail: [vinaykumar.a@griet.ac.in](mailto:vinaykumar.a@griet.ac.in)

© The Author(s), under exclusive license to Springer Nature Singapore Pte Ltd. 2023  
R. P. Singh et al. (eds.), *Advances in Modelling and Optimization of Manufacturing and Industrial Systems*, Lecture Notes in Mechanical Engineering,  
[https://doi.org/10.1007/978-981-19-6107-6\\_31](https://doi.org/10.1007/978-981-19-6107-6_31)

441



or fully autonomously to perform services useful to the well-being of humans and equipment, excluding manufacturing operations [2]. The new advancements in the field of robotics are giving us an unprecedented definition of what robots can do.

In effect, robotic arms are emerging in automobile and manufacturing industries automating the process and thus streamlining it. There are many companies offering robotic arm models but teaching how to operate and change the functionality or position of the robotic arm to a factory worker who is a layman can become a painstakingly arduous task. Thus, in this paper, we proposed an android app-enabled IoT-based robotic arm with weight-based object segregation. That even a layman can control with their fingertips. Though there are papers on robotic arm and Bluetooth-enabled robotic arms, our attempt in this paper is to develop an android app-enabled Bluetooth-controlled robotic arm with a weight-based object segregation.

The weight detecting sensor decoupled with the robotic arm will detect and display the weight of the object picked up by the robotic arm; this feature can help the manufacturing and packing industries where sometime the robotic arm can pick up weight exceeding its limit and can lead to malfunction or breaking of the robotic arm; this can also help in packaging of manufacturing industry where the weight of the product needs to be measured and segregated before packing it.

The robotic arm system is designed by using components and hardware with embedded software to provide an android app-controlled robotic arm, based on Bluetooth technology, has been proposed in this paper to automate the manufacturing industry. The mass of the object is calculated using a custom-build 50-kg load sensor module and is then exhibited on serial monitor in real time along with the tag number so that it can be logged and tracked accordingly; the objects picked up by the robotic arm can then be segregated based on their weight.

## 2 Literature Review

In the past, some researcher's proposed various means of designing building and controlling a robot arm for instance, a previous project on autonomous robot navigation using radio frequency [3]. The robot was prepared mechanically to be suitable for this RF to work. In a later published work, researchers Kurt E. Clothier and Ying Shang proposed A Geometric Approach for Robotic Arm Kinematics with Hardware Design, Electrical Design, and Implementation [4] where they initiated a dimensional perspective to the robotic arm.

With time, there have been multiple papers published on the robotic arm which also include "Robotic Arm Control using Bluetooth Device" with an android application [5] in which they put forward a mechanism to control the robotic arm using a Bluetooth module, which is close to our project in terms implementation. What we are proposing in this paper is a more efficient and robust variant of the robotic arm that can revolutionize the manufacturing industry.



**Fig. 1** 3D model of a robotic arm

### **3 Methodology**

#### **3D Modeling Analysis of the Robotic Arm**

The robotic arm was designed using SolidWorks software; the arm includes 5 axis for the movement of different joints the first 3 axis which are the elbow, shoulder, and the waist are equipped with MG996R servos and the other 2 axis joints which are the wrist pitch and the wrist roll are equipped with SG 90 servos (Fig. 1).

The gripper which is used for the pick and place function is also equipped with a SG90 servo. The parts of the arm were 3D printed and assembled using 2 and 4-mm screws.

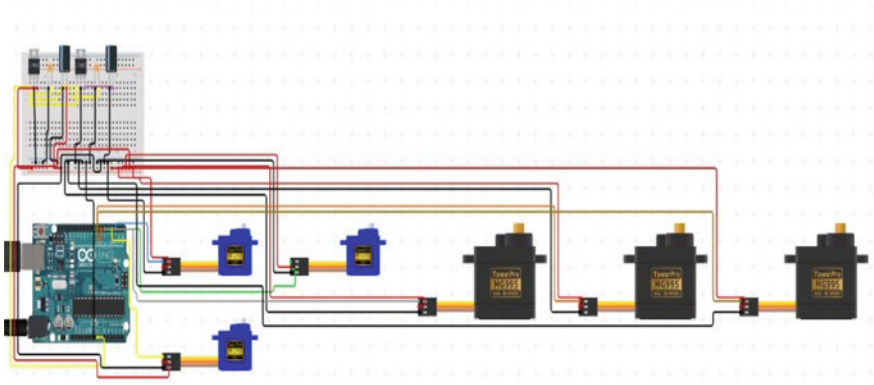
### **4 Electrical Circuit Analysis**

#### **4.1 Robotic Arm Circuit Analysis**

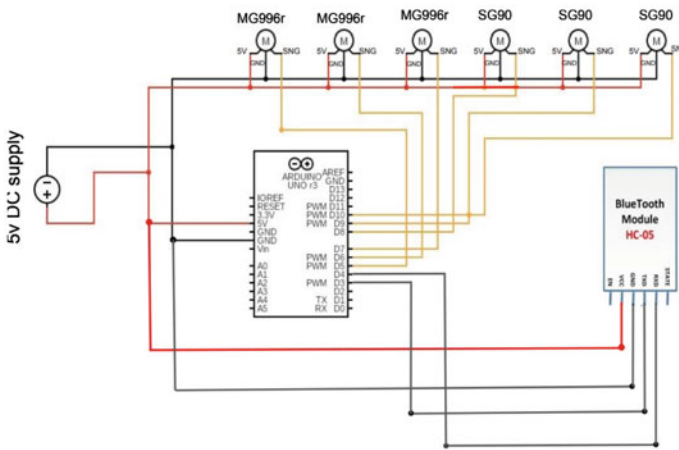
For the circuit of the robotic arm, we are using the Arduino Uno and the HC-05 module for the communication; we are using the servos SG90 and MG996R as actuators; servo motor is one of the DC-type motors with feedback that used in many applications that required controlling the system in up–down direction. Servos are extremely useful in robotics [6]. As we can see that the 6 digital pins of the Arduino

are attached to 6 servo motors. Also, we need an ambient power source of voltage: 5 V and current: 2 Amp to power the servos as the power from the Arduino isn't sufficient to move the servos.

The power pins of all the servos are connected in parallel with the power pin of the Arduino and the power pin of the external 5 V power source. The ground pins of all the servos are also connected in parallel with ground of the Arduino and the external power source. In the Arduino, digital pins 3, 4 act as the TX and RX pins appropriately (Fig. 2).



(a)



(b)

Fig. 2 a Circuit diagram b schematic of the circuit

## 4.2 Load Cell Module Circuit Analysis

For the circuit of the load, we are using 1 Arduino, 1 HX711 module, and two 50-kg load cells are present. First, we need to connect the positive and negative strain which are the opposite black and white wires. The resistance between the positive and the negative strain wires must be maintained at  $1\text{ K}\Omega$ , so by using a multi-meter, the resistance between the set of 2 wires is steadied. The resistance between the corresponding two red wires should also be maintained at about  $1\text{ k}\Omega$ .

In the two pairs of black–white wires, one is connected to the E + pin of the HX711 module, and the other goes is given to the E-pin of the module. The E + and E– wires from the load cell are the power wires. The red wires are connected to the A+ and A– pins of the HX711 module which act as the measurement input pins. By connecting the DT and SCK pins to digital pins 4 and 5, VCC to 5 V, GND to ground of Arduino, the circuit of the weight sensor is done (Fig. 3).

The 2-load cell weight sensor circuit is coupled to the bottom of the robotic arm so that it computes the weight of the objects which are picked by the arm. As the load cell will give the output in microvolts and ARDUINO is not capable of reading these values, therefore, amplification is required. The best solution is to use HX711 amplifier which is a 24-bit analog to digital amplifier [7]. While calculating the weight of the object, we have calibrated the sensor in such a way that it considers the weight of the robotic arm as tare and displays the value.

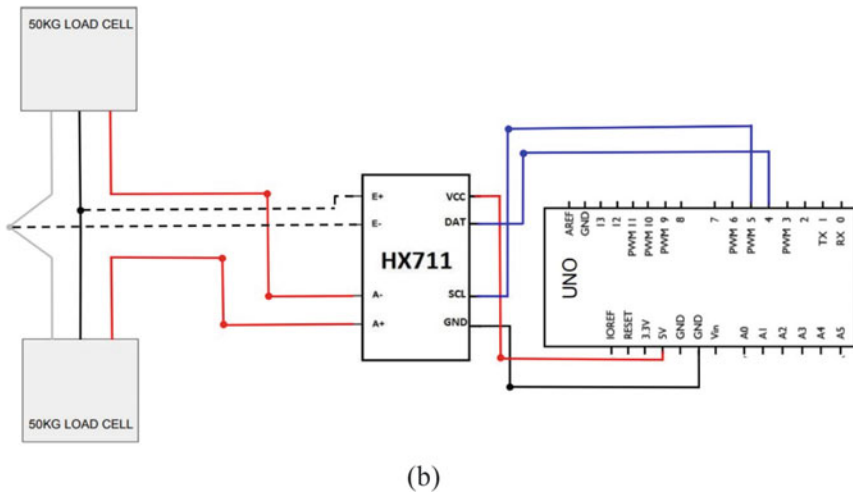
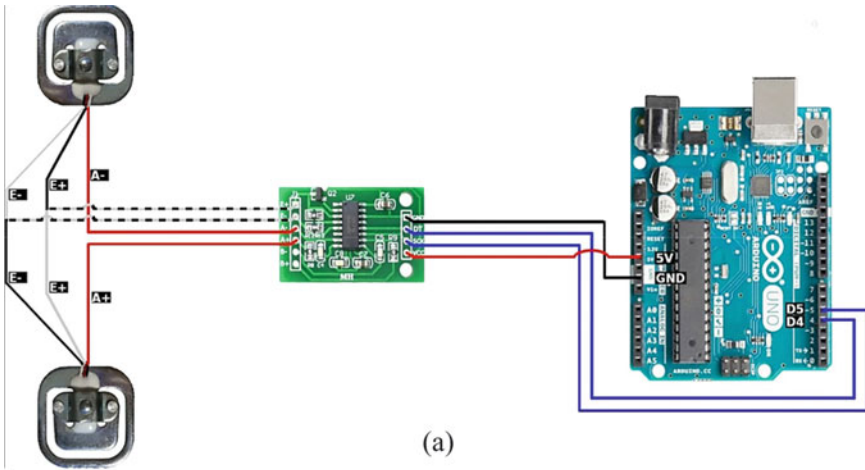
## 5 Graphical User Interface Analysis

MIT app inventor is a drag-and-drop interface visual programming tool that allows everyone for designing and building fully functional mobile apps for android. App inventor advocates a new era of personal mobile computing in which people are enabled to design, create, and employ personally relevant and meaningful mobile technology solutions for a variety of context in their daily lives, in endlessly unique situations [8].

The input to the servos is given through the app via the Bluetooth module; the app was built using the MIT app inventor and interface of which can be seen in the image. Each axis servo has a separate control to it on the app's display along with it the arm speed can also be controlled through the app.

We have used an android application which is designed using the MIT application inventor to control and operate the robotic arm in various modes of speeds and angles. This robotic arm is mainly controlled using the android device and with the help of the Bluetooth module which is present in the internal circuit of the robotic arm. By viewing at the site of the android application and the Bluetooth module, it can be known which sort of data is actually fleeting to the Arduino (Fig. 4).

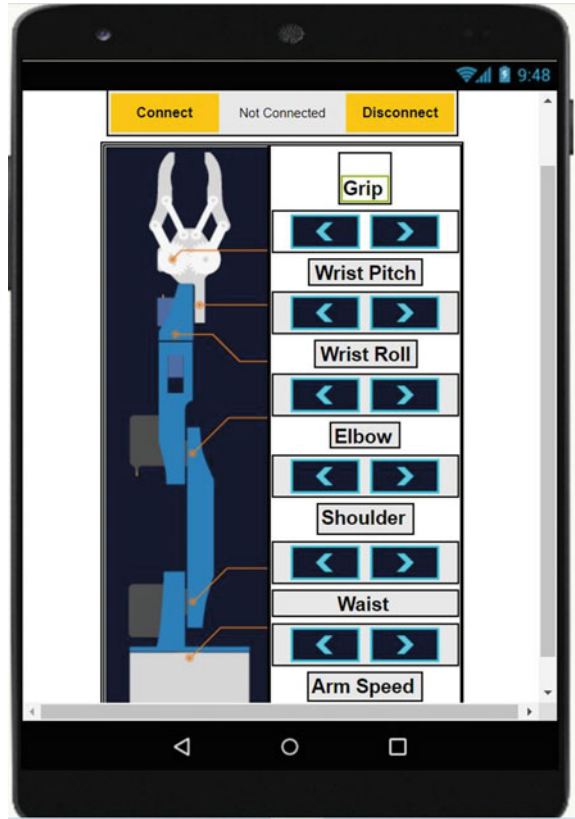
When seen at the android application interface at the beginning, there are two buttons for the connecting the smartphone to the HC-05 Bluetooth module via the



**Fig. 3** a Load cell circuit model, b load cell module circuit schematic

created android application. Next, on the left side, there is an image preview of the robotic arm that shows all the different joints in the robotic arm. Then, on the opposite to this robotic arm preview, there is a slider tab for the easy controlling and moving of the servos and one more slider for the various speed controlling. When it comes to the controlling and operation of the robotic arm for moving the joints, there are different options, and they are grip control, wrist pitch control, wrist roll control, elbow control, shoulder control, and the waist control and finally the arm speed control. By changing the values of these operating parameters, we can operate the robotic arm in a very efficient and a precise manner.

**Fig. 4** Android app interface



The slider tabs have a variant starting, low and high value that takes care of the robotic arm joints. The robotic arm can be controlled to run inevitably through three buttons at the conclusion of the android application’s interface: SAVE, RUN, and RESET. There is also an option which is the label that demonstrates the total number of steps that we have come up to present stage. At the right side of the application interface, there is a disconnect button to disconnect the connection with the Bluetooth module. The Bluetooth module and the smartphone can be completely disconnected with this button easily.

The design of the interface, buttons, and the all sliders in the android application are possible only with the blocks that are built behind the application. There are different blocks for each specified option and feature in the android application.

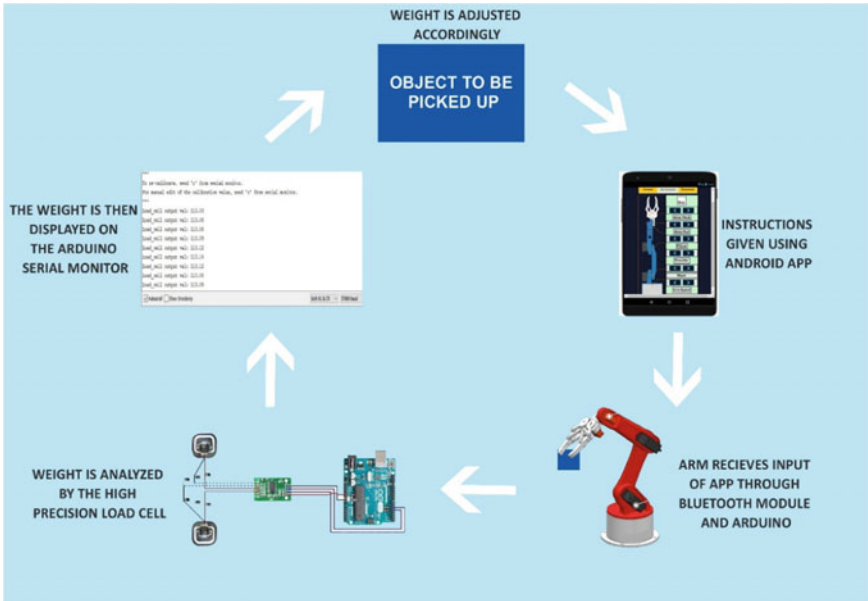


Fig. 5 Process chart of the weight-based segregation using 5 DOF robotic arm

## 6 Mechanism of the IoT-Based Robotic Arm with Weight-Based Segregation

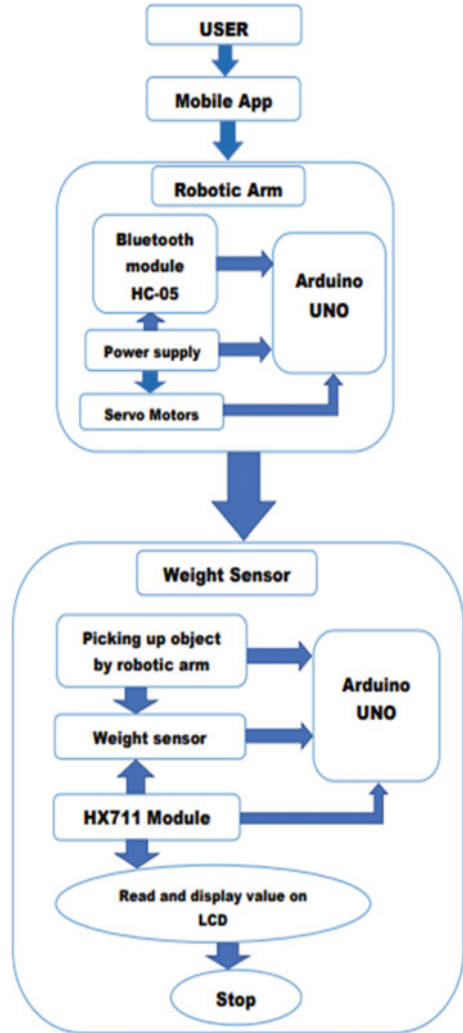
The user gives the input to the robotic arm through the app input is transmitted to the Hc-05 Bluetooth module via Arduino Uno; the Bluetooth module further transmits it to the servos placed in the robotic arm to perform a certain function in this case which is to pick or place an object of interest. The process of sending requests and receiving a response of sensed data using the Bluetooth HC-05 module also starts from the initialization of Arduino pin, status, baud rate, and SD card chip [9] (Figs. 5 and 6).

Once the object is picked up, the weight of the object is calibrated by the load cells; since they are force transducers, they convert the weight or pressure or force into electrical; this conversion and transmission to the serial monitor is done by HX711 module and Arduino. On the serial monitor screen, the values are displayed along with the time stamp.

## 7 Simulation Results

As we can infer from the image, the weight of the object can be seen displayed on the screen at different time stamps. From these time stamps, we can also calculate

**Fig. 6** Flowchart of the working of the robotic arm with load cell module



the weight of the object as the arm is moving, while different objects are being lifted by the arm.

The weight of the robotic arm is considered as tare in order to avoid the arm’s weight to interrupt with the picked-up object’s weight tare basically which means that the sensor is calibrated in such a way that it doesn’t consider the weight of the robotic arm in the process of lifting the object irrelevant to the angle or position in which the object is being lifted.

As we can see from Fig. 7, we can infer that no object is being picked up by the arm; hence, the value being displayed on the serial monitor is close to zero from which we can also conclude that the weight of the arm is being considered as tare,



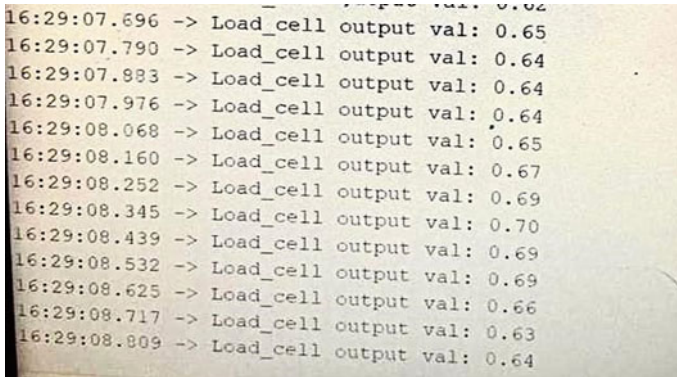


Fig. 7 Weight displayed on the serial monitor when there is no load

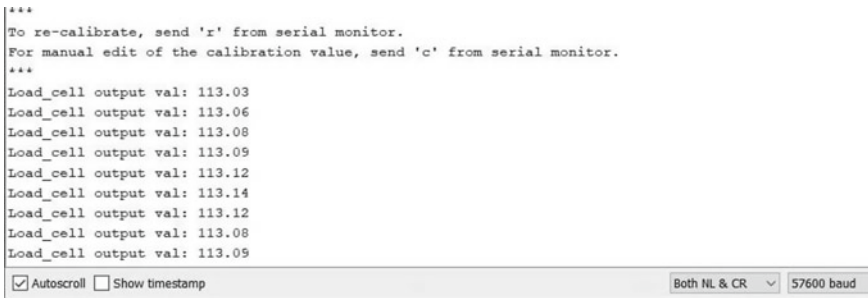


Fig. 8 Weight displayed on the serial monitor when there is load

whereas in Fig. 8, we can see that there is a difference in the value being displayed on the monitor which means that the arm is holding an object.

This result can be useful in segregating the objects based on their weight, and to monitor the load, the arm is being administered so that if we place a larger load which can result in the damage of the servos we can be intimated, this method is also being researched for the use in injection mold-based product manufacturing where the weight of the object to be measured is very important to maintain the precision in molding and weight of the whole product.

## 8 Result

In this way, we have implemented an IoT-based robotic arm with weight-based segregation controlled wirelessly by a graphical user interface. Therefore, the robotic arm is successfully connected with the smart device and with the Bluetooth module, and this total setup was further ordered to perform the segregation based on the parameter

“WEIGHT.” We can see that load cell is working as per the given instructions. It is given the task of displaying the weight quantity of the load, the robotic arm picks. And then, we can see that the robotic arm places the object at the specified place without any deviation.

We can see that the robotic arm accepts all the commands that the user passes through the android application. The load cell performs and fulfills all the tasks entrusted to it without hesitation. At the next step, the load cell’s readings are mirrored on the serial monitor. By all these tasks and after the appropriate testing of the load cell and weight sensor, it can be stated that the weight-based segregation using the IoT-based robotic arm is carried out precisely. As a sign of result, we have administered various commands to the arm by picking and placing different objects and monitoring and segregating the load being apportioned to the arm.

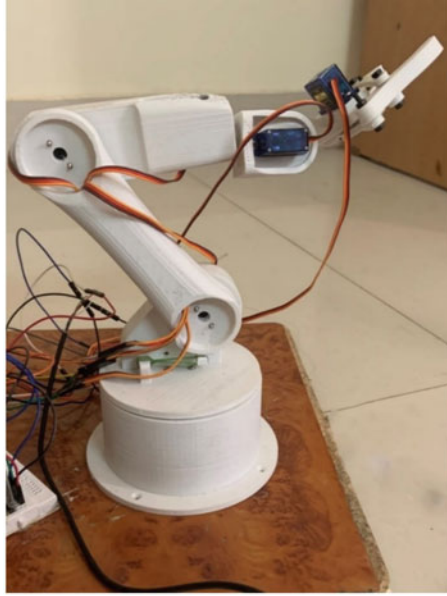
This method helps immensely in inline weight measurement without the need of picking up weighing and placing the object on the conveyor line every time and eliminated the need of weighing each object separately after production. Inline weighing can act as a hundred percent parts check because on the basis of weight plastic processors are able to ascertain if the sprues (a channel through which metal or plastic is poured into a mold) are cut clean or whether excessive or insufficient injection has been done.

And after we have performed the weight segregation with the help of the robotic arm and the load cell sensor by taking numerous loads with variant weights, and it can be depicted and leading to the necessary result that the robot is working efficiently by weighing all the different loads given to precisely and by also helping us determine missing parts in two identical objects with the help of weight. The results can be illustrated shown in Fig. 9.

## 9 Conclusion

In the present scenario, robotic arms are taking over the work load of humans simplifying and automating various processes. Although, significant development in this field is necessary. From their inception, amount of human error and involvement has significantly reduced.

The purpose of our project is to provide control of 5 axis moving robot arm design and this robot arm with a suitable microcontroller and Bluetooth module with an android application which can also monitor the load and segregate objects based on their weight. And this cutting-edge technology is really helpful in industries with injection molding where the component weight demonstrates the quality of the component and also the process consistency, and with aid of weight-based segregation, the NOK or not okay parts can be easily separated from the good ones. The necessary theoretical and practical information for this purpose has been obtained, and the necessary infrastructure has been established for the project.



(a)



(b)

**Fig. 9** **a** Final resulting product of robotic arm with load cell module, **b** final resulting product of robotic arm with load cell module lifting a load

**Acknowledgements** This paper and the research behind it would not have been possible without the exceptional support of our professor and mentor, **Shri.A.Vinay Kumar**. His knowledge and exacting attention to detail have been a great deal of inspiration for all of us.

We also would like to thank the organizers and jury of CIMS 2021 in helping us present our paper and giving us their valuable insights in improving the efficacy of the paper.

## References

1. Kemp CC, Edsinger A, Torres-Jara E (2007) Challenges for robot manipulation in human environments [grand challenges of robotics]. *IEEE Robot Autom Mag* 14(1):20–29
2. Luo RC, Su KL (2003) A multi agent multi sensor based real-time sensory control system for intelligent security robot. In: *IEEE international conference on robotics and automation*, vol 2, pp 2394–2399
3. Tan MC (2005) Autonomous robot navigation using radio frequency. Bachelor Project. Thesis. University Teknologi Malaysia, Skudai
4. Clothier KE, Shang YA Geometric approach for robotic arm kinematics with hardware design, electrical design, and implementation. *Hindawi Publishing Corporation J Robot* 2010:10. Article ID 984823
5. Alagappan MP, Varsha NS Robotic arm control using bluetooth device with an android application. *Int J Eng Res Technol (IJERT) IJERT*. [www.ijert.org](http://www.ijert.org) NCACCT'14 Conference Proceedings
6. Firoozian R (2008) *Servo motors and industrial control theory*, Springer; 1st ed, Dec 8
7. Das S, Karmakar A, Das P, Koley B (2019) Manufacture of electronic weighing machine using load cell. *IOSR J Electr Electron Eng (IOSR-JEEE)* 14(4):32–37, e-ISSN: 2278-1676, p-ISSN: 2320-3331
8. Pokress SC, Veiga JJD MIT App inventor enabling personal mobile computing
9. Faiqurahman M, Novitasari DA, Sari Z (2019) Universitas Muhammadiyah Malang QoS analysis of kinematic effects for bluetooth HC-05 and NRF24L01 communication modules on WBAN system. *KINETIK* 4(2):187–196

# An Experimental Validation of Thermo-Mechanical Analytical Model in Laser Bending Process



Utpal Nath and Vinod Yadav

**Abstract** The present study presents a coupled thermo-mechanical analytical model to find out the temperature field and bend angle during laser line heating. In-house experiments were performed considering Al 6061-T6 aluminum alloy sheets to validate the proposed model. The results of parametric study are presented to see the influence of laser power intensity and scanning speed on the temperature distribution and bend angle. Further, the effect of convective heat transfer coefficients on the temperature distribution is studied at different cooling arrangements on the irradiated and bottom surfaces of the sheet. The measured experimental results show an averaged error of 8.3% with the analytically predicted bend angles. Hence, the proposed model can be useful to the dedicated laser-based manufacturing industries for the quick estimation of temperature and bend angle.

**Keywords** Laser material processing · Gaussian heat flux · Integral transform technique · Temperature distribution · Bend angle

## 1 Introduction

Laser bending of metallic sheets is one of the promising techniques among manufacturing processes that is attained by irradiating its surface with a defocused laser source. Recently, laser bending has drawn great attention from various researchers. As a newly developed approach, laser bending has provided significant progress in the automotive, aircraft, marine, and electronic sectors, where it offers rapid processing and fabrication of intricate shapes that previously relied on expensive conventional techniques. Laser bending has numerous merits over the conventional forming techniques, for example high design flexibility, minimal heat-affected zone, no spring-back and formability in inaccessible areas [18]. Dixit et al. [3] presented a

---

U. Nath · V. Yadav (✉)

Department of Mechanical Engineering, Maulana Azad National Institute of Technology Bhopal, Madhya Pradesh, Bhopal 462003, India

e-mail: [vyadav@manit.ac.in](mailto:vyadav@manit.ac.in)

detailed review on the present scenario of the laser forming systems. The basic understanding of the mechanism and main parameters associated with the laser bending process considering different materials had been explored with various analytical and experimental studies. Kalvettukaran et al. [7] optimized the laser processing factors, namely laser beam radius, laser power, laser beam moving speed, and workpiece thickness based on the temperature measurement.

A number of researchers have been proposed mathematical model of laser bending process for estimating the bending angle and temperature distribution. Temperature and thermal stress propagation during laser heating of a material is the prime concern of research to get the desired bend angle in laser bending because the distortion of the workpiece mainly relies on the temperature field. Cheng and Lin [2] proposed an exact solution to assess the temperature distribution in the finite plate considering a Gaussian heat flux. They compared the different heat sources, e.g., point, uniform, and Gaussian, to analyze the temperature profiles and found that the Gaussian heat source depicts the realistic results in the laser heating of metallic sheets. They performed a detailed parametric study to assess the thermal history in the laser-heated sheet. Shi et al. [24] presented a simplified analytical solution to estimate the temperature distributions in the laser bending process. They reported that the sequential thermo-mechanical analyses can be performed to assess the bend angle precisely. Khan and Yilbas [9] carried out semi-analytical modeling to find out the radial and hoop stresses in the laser bent sheet. In their study, the temperature distribution is calculated by analytical solution, and the deformation analysis is carried out using a numerical approach. They found that the distribution of the temperature field was influenced by laser scanning speed, which further changed the stress field in the workpiece material. Kyrsanidi et al. [10] compared the bending angle considering at different scan speeds of sheets made of steel D36 and 1430 using an analytical model and finite element method (FEM) using Gaussian heat source. The FEM model is based on the temperature-dependent material properties. It was noticed that the bend angle is more pronounced at low scanning speed at different laser beam power. Mishra and Dixit [16] presented a series solution to assess the temperature distribution along the workpiece thickness during laser line heating. Shen et al. [23] analyzed the temperature distribution at different locations along the thickness of the sheet by employing the analytical solution. They emphasized that the temperature data across the workpiece thickness of the bended sheet is needed to accurately determine the bend angle. The authors reported that the model is promising to assess the deformation under different well-known bending mechanism as compared to the experimental results. Shi et al. [25] presented a mathematical model based on the temperature gradient mechanism (TGM) in which temperature field and distortion of the sheet were predicted assuming both convective and radiation boundary conditions. They used a one-dimensional heat conduction model to examine the variation of temperature in the thickness direction. It was noticed that under the considered process conditions of TGM, the sheet bends about both longitudinal and transverse directions. Kyrsanidi et al. [11] assessed the mechanism of laser bending using both numerical and experimental approaches by introducing temperature-dependent material properties. To observe the characteristic of the bending, steel alloys with 4 and

6 mm in thickness were considered and developed a three-dimensional numerical scheme based on a FE model. In order to examine the bend angle of laminated plate by applying the laser heat source, [15] proposed a TGM-based analytical model. They observed that trend of the bend angle with changing the laser power and scan speed is in line with the existing published results. Lambiase and Ilio [13] presented analytical solution for the prediction of temperature field and bend angle during the laser forming considering different materials. Eideh et al. [4] provided a simplified analytical solution to assess the bend angle in laser bending of steel metal sheets based on elastic–plastic bending analysis. Further, they also proposed an inverse technique on the basis of temperature measurement for estimating the yield stress of the sheet. Mulay et al. [17] developed a strain energy-based mathematical model for evaluating the bending angle in a single laser scan.

Over the last few decades, many researchers studied the temperature distribution and bend angle by numerical simulations as well as experiments. Roohi et al. [20] analyzed the influence of laser parameters, viz. beam power intensity, scanning speed, number of scans, and workpiece thickness on the final bend angle of aluminum alloy sheet. The results obtained from the experiments showed an ideal range of input laser parameters for the required bend angle of the sheet material. Zhang et al. [26] also investigated the bending phenomena of DP 980 steel foils (1.4 mm thick), taking laser power, line energies, no of passes, and direction of laser scans as process variables for high-quality forming operations. The authors revealed that the deformation behavior of formed geometry increases linearly with the increase of line energy. Hu et al. [5] conducted various experimental tests and numerical simulations to study the mechanism of laser bending on geometrically scaled aluminum and steel sheets. Numerical simulations based on the FEM were conducted in ANSYS to predict the nature of the bending phenomenon. Experiments of laser bending were performed using an Nd-YAG laser system by varying the component thickness and validated with the developed FEA module, which exhibits the significance of considering the size effects. Hu et al. [6] provided an experimental study to investigate the physics behind the laser forming by introducing the edge effects. Kant and Joshi [8] performed various experimental tests and FEM simulations to examine the optimum laser process conditions for larger bending angles with negligible edge effect in laser-heated slab. Shen et al. [22] developed a thermo-mechanical FEM numerical model to analyze the temperature distribution and bend angle with moving boundary conditions and suggested the possibility of utilizing forced cooling systems in a single laser scan. It is evident from results that the arrangement of forced cooling can drastically reduce the maximum temperature as compared to natural cooling, which further increased the bend angle of the sheet. Labeas [12] developed a three-dimensional FEM model to estimate both temperature distribution and bend angle considering a single or multi-pass moving heat source. The authors also carried out a number of experimental trials on aluminum thin sheets to validate the simulated FEM results.

In this work, a simplified thermo-mechanical model is employed for finding out the temperature distribution and bend angle during laser bending process. The model comprises two modules—thermal module and deformation module. The thermal

modules use the integral transform method to solve the governing heat transfer equation, whereas the deformation module is relying on the strain energy theory. The proposed analytical model incorporates the effect of workpiece geometry, the laser-irradiated path, convective heat transfer coefficients at the bottom and top surfaces, and the laser parameters associated with the single pass of heating source. To include the aforementioned laser process parameters together is the novelty of this work. It is evident from past literature that the existing thermo-mechanical numerical models required a considerable amount of computational time, even with powerful workstations. Thus, an attempt is made to develop an analytical solution that requires insignificant computational time in an ordinary computer. The efficacy of the developed model is verified by performing a set of in-house experiments under different process conditions. Further, the thermal stress, thermal strain, and stored strain energy in the sheet surface are evaluated based on the obtained temperature distribution.

## 2 Analytical Model

In this section, an analytical model is proposed to analyze the temperature field and bend angle in the laser bending. Section 2.1 presents the series solution to estimate the temperature distribution in a laser-heated sheet considering a single pass of laser heat source. Section 2.2 derived the closed-form expression to calculate the bend angle.

### 2.1 *Estimation of Temperature Distribution*

During laser bending, the laser source irradiates along with the pre-set locations of the sheet surface that causes thermal expansion in the irradiated zone. The expansion due to the temperature variations across the workpiece thickness is countered by the surrounding material. The mechanism of laser bending is a complicated phenomenon [4]. Following assumptions are considered to develop the analytical model: (i) The worksheet is free of gravitational force, (ii) the laser-scanned region does not undergo any phase transition, (iii) creep strains are negligible, (iv) surface melting is not considered, and (v) plastic deformation in the laser heating line of metallic substrate is neglected. Figure 1 shows a schematic arrangement of the laser bending process. A moving laser heat source traverses the material surface at specified scan speed in the predefined direction.

In order to simplify the mathematical model, the one-dimensional heat transfer is considered. Figure 2 shows the one-dimensional heat source. Consider a one-dimensional plate with convective boundary conditions subjected with an instantaneous heat source at  $z = b$  for time  $t = \tau$ , as shown in Fig. 2.

Following governing heat transfer equation is solved for obtaining the temperature field:



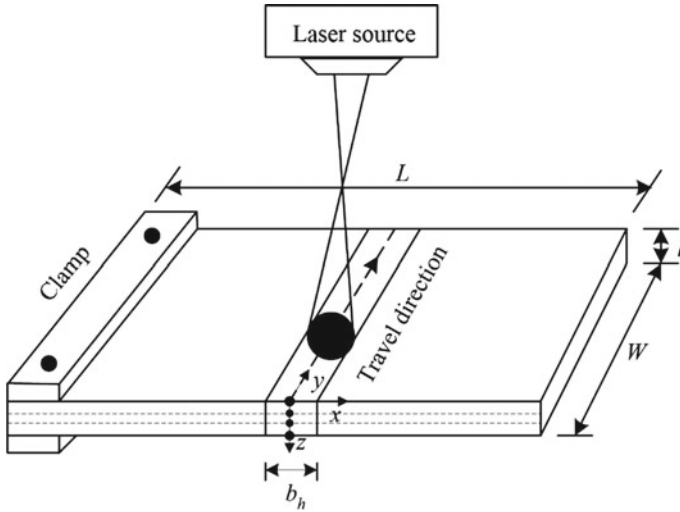


Fig. 1 general schematic representation of laser bending

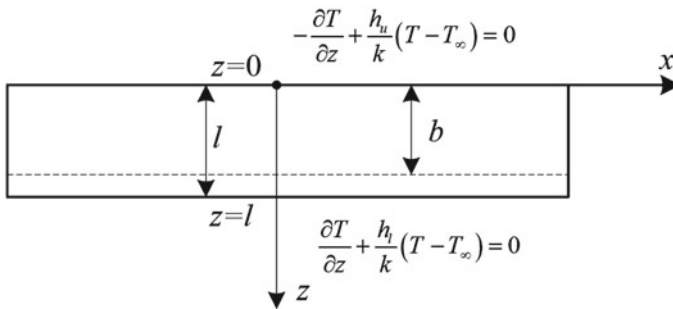


Fig. 2 1D plate subjected with instantaneous heat source

$$\frac{\partial^2 T}{\partial z^2} + \frac{q}{k} \delta(z - b) \delta(t - \tau) - \frac{1}{\alpha} \frac{\partial T}{\partial t} = 0 \tag{1}$$

Where  $q$  is the heat input per unit area,  $k$  is the thermal conductivity,  $b$  is the instantaneous distance along the thickness direction,  $\delta$  is the Dirac delta function,  $\tau$  is the instantaneous time,  $t$  is the time,  $T$  is the temperature, and  $\alpha$  is the thermal diffusivity of the material. The thermal diffusivity is defined as

$$\alpha = \frac{k}{\rho c_p} \tag{2}$$

where  $\rho$  is the material density and  $c_p$  is the specific heat of the material. The boundary and initial conditions are considered as

$$-\frac{\partial T}{\partial z} + \frac{h_u}{k}(T - T_\infty) = 0 \quad \text{at, } z = 0 \tag{3}$$

$$\frac{\partial T}{\partial z} + \frac{h_l}{k}(T - T_\infty) = 0 \quad \text{at, } z = l \tag{4}$$

$$T = T_\infty, \quad t = 0 \tag{5}$$

where  $h_l$  and  $h_u$  are the heat transfer coefficients (HTC) at the bottom and top surfaces of the workpiece, respectively. Equations (1–5) are solved using integral transform technique [19, 21]. The following expression provides the temperature distribution in  $z$ -direction of the sheet:

$$T = T_\infty + \frac{2q}{\rho c} \sum_{m=1}^{\infty} \exp\{-\alpha\beta_m^2(t - \tau)\} \frac{(\beta_m \cos \beta_m z + \frac{h_u}{k} \sin \beta_m z)(\beta_m \cos \beta_m b + \frac{h_u}{k} \sin \beta_m b)}{\left[ \left\{ \beta_m^2 + \left(\frac{h_u}{k}\right)^2 \right\} \left\{ l + \frac{\frac{h_l}{k}}{\beta_m^2 + \left(\frac{h_l}{k}\right)^2} \right\} + \frac{h_u}{k} \right]} \tag{6}$$

where  $\beta_m$  is the positive roots which is defined by following transcendental equation:

$$\left\{ \beta_m^2 - \left(\frac{h_u}{k}\right) \left(\frac{h_l}{k}\right) \right\} \sin(\beta_m l) - \left\{ \beta_m \left(\frac{h_u}{k} + \frac{h_l}{k}\right) \right\} \cos(\beta_m l) = 0 \tag{7}$$

In this work, the moving laser beam is assumed to be circular with the Gaussian heat source distribution [8].

$$q = \frac{\eta P}{\pi r^2} \exp\left\{-\frac{(x^2 + y^2)}{r^2}\right\} \tag{8}$$

where  $\eta$ ,  $P$ , and  $r$  are the absorption coefficient of the material, the beam power intensity, and the laser beam radius, respectively.

Substituting Eq. (8) into Eq. (6) and utilizing the Green function theorem, the following series solution of three-dimensional transient temperature distribution is obtained as [1]:

$$T = T_\infty + \frac{2\eta P}{\pi \rho c_p} \int_0^t \frac{1}{4\alpha(t - \tau) + r^2} \exp\left\{-\frac{x^2 + (y - v(t - \tau))^2}{4\alpha(t - \tau) + r^2}\right\} \sum_{m=1}^{\infty} \frac{\beta_m (\beta_m \cos \beta_m z + \frac{h_u}{k} \sin \beta_m z)}{\left[ \left\{ \beta_m^2 + \left(\frac{h_u}{k}\right)^2 \right\} \left( l + \frac{\frac{h_l}{k}}{\beta_m^2 + \left(\frac{h_l}{k}\right)^2} \right) + \frac{h_u}{k} \right]} \{\exp(-\alpha\beta_m^2(t - \tau))\} d\tau \tag{9}$$

Where  $v$  is the travel speed of the heating source in m/s. Appendix provides the detailed derivation of Eq. (9).

## 2.2 Estimation of Bending Angle

In order to evaluate the equivalent thermal strains and stresses induced during laser heating, the mean temperature is calculated as follows [4, 17]:

$$T_m = \frac{\sum_{i=1}^n T}{n} \quad (10)$$

where  $n$  defines the number of locations to measure the temperature along with the sheet thickness. In this work, a total of four locations are taken into account to estimate the mean temperature, as shown in Fig. 1. The expression of the thermal strain and stresses can be written as

$$\varepsilon_{t_{\text{avg}}} = \alpha_{\text{th}}(T_m - T_{\infty}) \quad (11)$$

and

$$\sigma_{t_{\text{avg}}} = \alpha_{\text{th}} E (T_m - T_{\infty}) \quad (12)$$

where  $E$  and  $\alpha_{\text{th}}$  represent Young's modulus and thermal expansion coefficient of the workpiece. Thus, the strain energy of the laser-heated sheet due to induced thermal strain and stress can be expressed as

$$U_{\sigma-\varepsilon_{\text{avg}}} = \frac{1}{2} \sigma_{t_{\text{avg}}} \varepsilon_{t_{\text{avg}}} V_h \quad (13)$$

where  $V_h$  is the volume of the irradiated zone for unit width and can be given by

$$V_h = b_h l \quad (14)$$

where  $b_h$  is the heated length of laser beam and  $l$  is the workpiece thickness. The strain energy stored by means of reactive bending moment is calculated as

$$U_{\text{BM}} = \frac{1}{2} M \theta \quad (15)$$

where  $M$  is given by

$$M = \frac{EI}{b_h} \theta \quad (16)$$

where  $\theta$  and  $I$  are the bend angle and the second moment of inertia, respectively. By equating the Eqs. (13) and (15), the expression of bend angle is obtained as

$$\theta = \sqrt{\frac{\sigma_{t_{avg}} \varepsilon_{t_{avg}} b_h^2 l}{EI}}. \quad (17)$$

### 3 Determination of Temperature Field and Bending Angle by FEM

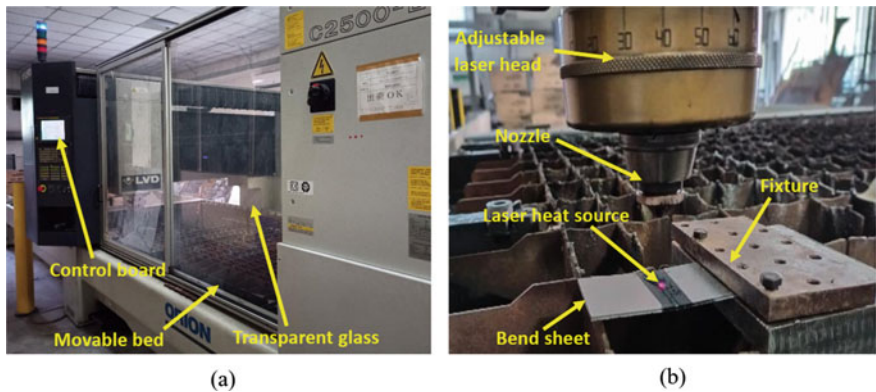
The three-dimensional numerical solutions based on FE model are carried out to compare the temperature distribution profiles with time of the proposed analytical model. In lieu of experimentally measured temperature distribution with time, a FEM result is considered as the virtual experiments for the laser bending process. However, the bend angle is measured experimentally. The experimental procedure is explained in the next section.

A FE-based numerical model was developed using commercial software Abaqus 6.10 to obtain the temperature history as well as the bend angle during the single pass of laser heat source. Following assumptions are considered to simulate the laser bending process: the sheet is assumed to be flat and free from the residual stresses. The heat source is modeled by a Gaussian distribution. The von Mises yield criteria is employed in order to evaluate the plastic deformation. The HTC of  $20 \text{ W/m}^2\text{-}^\circ\text{C}$  has been taken for the natural convection. During simulations, one edge of the sheet parallel to the predefined laser line is clamped, which was fully constrained in terms of both displacements and rotations. The details of the FEM simulation procedure are explained in [18].

### 4 Experimental Study

In the present study, experiments on single scan laser bending of Al6061-T6 aluminum alloy strips were conducted to better understand the laser bending process. A continuous-wave LVD Orion 3015 2.5 kW CNC operated  $\text{CO}_2$  laser machine was used to perform the experimental tests. The experiments were carried out at the IIT Guwahati, and the experimental test setup is shown in Fig. 3. The samples of Al6061-T6 aluminum alloy were cut into the required dimension of  $(100 \times 50 \times 1.5) \text{ mm}^3$ . Before the laser line heating, the predefined laser scan path on the metal surface was coated with black spray paint, ensuring the uniform absorption along the predefined traveling path. The coated sheets are allowed to air-dry at ambient temperature for about half an hour. The coated test specimen was clamped at one end using a fixture over the movable laser bed, as shown in Fig. 3b. A defocus laser

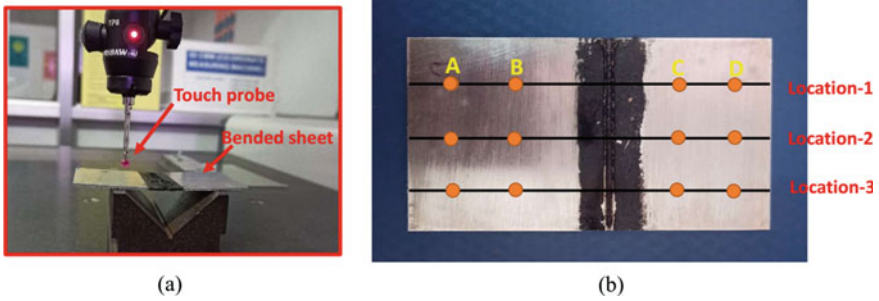
beam of spot size 3.87 mm was moved along the predefined locations of the metallic substrate. The coating of the sheet is damaged due to the heating of the moving laser source. After the laser line heating, the test samples are allowed to cool at normal room temperature. Table 1 depicts the set of experimental tests which was conducted by taking the different combinations of laser power and scan speed from different parameter levels. Figure 4 shows the photograph of the CMM for measuring the obtain bend angle. For the same process condition, the experiment was performed twice, and the average of generated bend angles (measured at different locations as shown in Fig. 4b) was taken as the experimental result. After completing the laser line heating, the bending angle was calculated at three different locations along the sample width using M/s. Accurate making coordinate measuring machine (CMM), and the average of three readings was taken as the final result of bend angle. The touch probe was moved along all three-axis to obtain the data points on both sides of the scanned path. Figure 5 shows some laser bended workpieces obtained during the laser line heating at different process conditions.



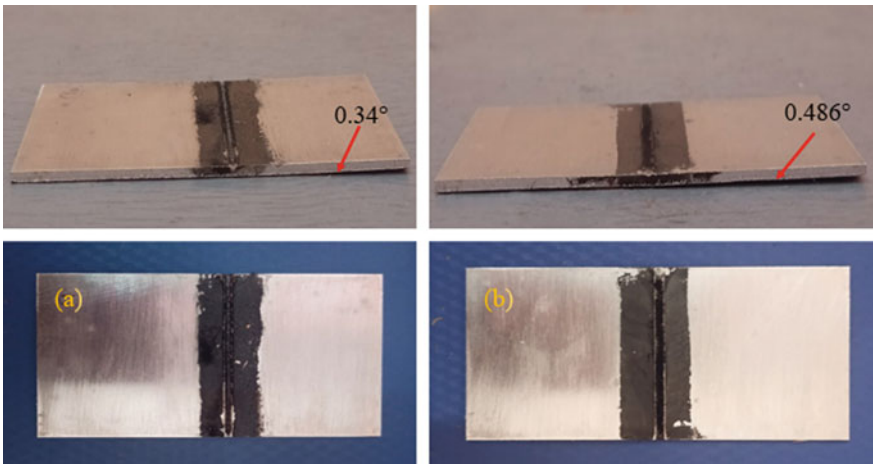
**Fig. 3** Photograph of the experimental setup **a** CO<sub>2</sub> laser machine and **b** fixture to bend the sheet by applying laser heat source

**Table 1** Different laser parameters used for the tests considering single laser pass

Laser bending parameters	Unit	Ranges
Laser beam power, $P$	W	450, 500, 550, 600, 700
Scan speed, $v$	mm/min	1000, 1250, 1500, 2000, 2500
Beam diameter, $D$	mm	3.87
Sheet thickness, $l$	mm	1.5



**Fig. 4** Photograph of **a** CMM to calculate the bend angle of laser bended specimen and **b** measurement locations of bend angle along the length of the workpiece



**Fig. 5** Laser bent workpieces with single laser scan. **a**  $P = 500$  W,  $V = 2000$  mm/min, and  $D = 3.87$  mm; **b**  $P = 600$  W,  $V = 1500$  mm/min, and  $D = 3.87$  mm

## 5 Results and Discussion

The proposed analytical solution is compared by estimating the temperature and deformation field at different laser process parameters for a single pass with the results available in the literature followed by the in-house experimental results. After validating the analytical model, a parametric study is also presented.

## 5.1 Comparison of Analytical Solution with the Existing Literatures

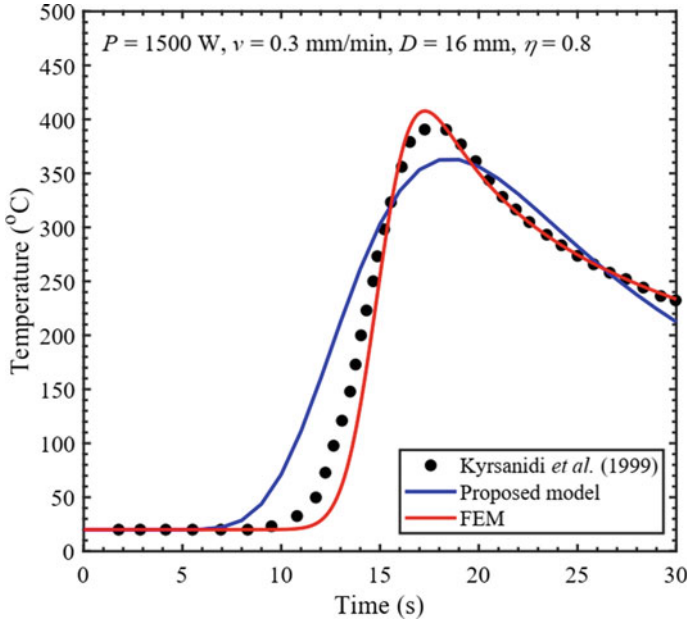
The transient temperature profile and the bend angle estimated with the analytical model are validated with the results [11, 18]. Kyrsanidi et al. [11] performed the experiments on D36 shipbuilding steel having the dimensions  $(300 \times 150 \times 6) \text{ mm}^3$ . The following laser process parameters are considered:  $P = 1500 \text{ W}$ ,  $D = 16 \text{ mm}$ ,  $v = 5 \text{ mm/s}$ ,  $\eta = 0.8$ ,  $k = 35.1 \text{ W/m}^\circ\text{C}$ ,  $h_u = h_l = 20 \text{ W/m}^2\text{-}^\circ\text{C}$ ,  $\rho = 7860 \text{ kg/m}^3$ ,  $c_p = 427 \text{ J/kg-}^\circ\text{C}$ ,  $E = 210 \text{ GPa}$ , and  $\alpha_{\text{th}} = 12 \times 10^{-6}/^\circ\text{C}$ . Figure 6 compares the proposed model with the FEM simulations and experimental results of [11]. It is found that the variation of the temperature distribution is similar to that obtained by FEM and experimental study. Due to consideration of the semi-infinite plate, the prediction of maximum temperature from the proposed analytical solution deviates from FEM results [11]. Results show that the maximum deviation in the temperature rise is approximately less than 10% while comparing with the results [11]. Hence, the proposed analytical model provides an excellent estimation of the temperature field for a finite thickness plate. In addition that, it is found that the proposed model provides the bending angle with an accuracy of 76.5% and 80% while comparing the results reported by [11] and FEM, respectively (Fig. 7). Thus, the proposed analytical model is validated and can be used to obtain the bending angles for a different set of workpiece materials as well.

Further assessing the proposed model with the different classes of workpiece material, the results reported by [23, 4] are taken as a benchmark. The dimension of the workpiece made by AISI 1010 was considered as  $(80 \times 80 \times 2.3) \text{ mm}^3$ . The laser power was varied between 800 and 1300 W and the beam travel speed between 40 and 65 mm/s. The radius of the laser beam was 2 mm, and the absorption coefficient is 0.8. Figure 8 compares the bend angle obtained from the analytical model with the experimental [23] and analytical results [4]. Results show that the analytical model predicts the bending angle with an accuracy of 93.6% and 81.29% while comparing with published [23] and [4] results, respectively.

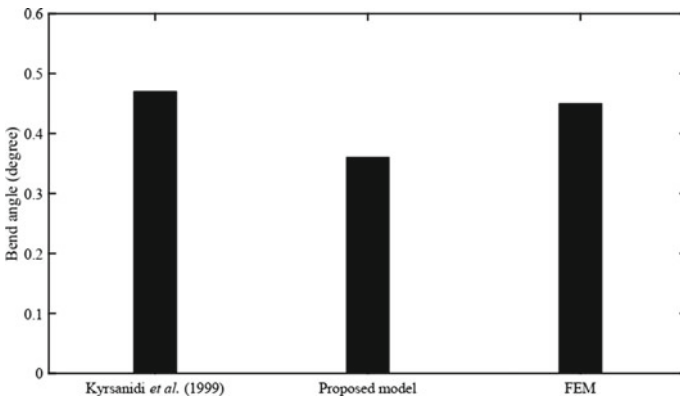
## 5.2 Comparison of Analytical Solution with Experiment

In this subsection, the bend angles given by analytical model are compared with that given by the experimental tests. The detail of the experimental procedure is described in Sect. 4. Each experiment was performed with two replicates. The properties of the Al 6061-T6 aluminum alloy is taken from [20]. The absorption coefficient of the workpiece is assumed to be 0.65.

Table 2 shows the percentage deviation between the proposed model and experimentally measured bend angles at different sets of process conditions. It is observed that the maximum deviation is 16.31% at corresponding the process parameters of Case 10. By comparing the proposed model with the experimental results, it is



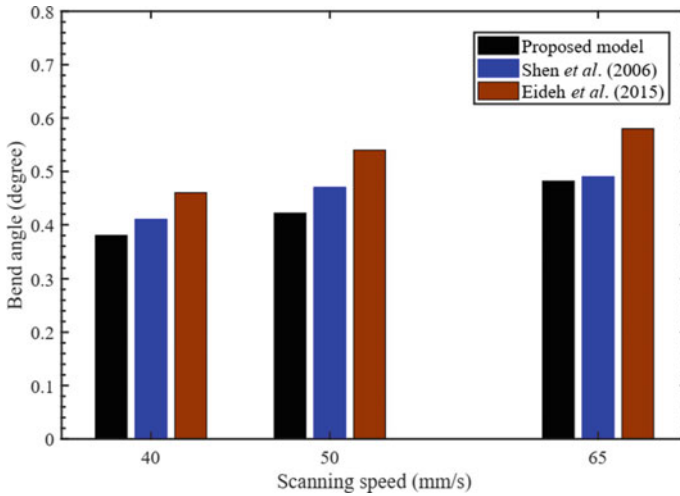
**Fig. 6** Comparison of transient temperature distribution obtained from proposed analytical model with FEM simulation and experimental results of [11] at the mid-point of bottom surface



**Fig. 7** Evaluation of bend angle obtained from proposed analytical model with [11] and FEM

observed that the average error of bend angles is less than 10%. Thus, the proposed model is validated. Further, it is found that the bend angle is increased with increasing the laser beam power keeping scanning speed constant. With an increase in the laser power, the magnitude of input energy into the metallic sheet has increased, resulting in higher plastic deformation. Similarly, the effect of scan speed on the bend angle is also analyzed. As expected, an increase in scan speed results in a decrease in bending





**Fig. 8** Evaluation of bend angle obtained from proposed analytical model with [23] and [4] at the mid-point of bottom surface

angle. It is because of the fact that the interaction span between the laser heat source and sheet surface is reduced. Thus, the energy input per unit length decreases, which results reduction in the magnitude of final bend angle.

**Table 2** Experimental and analytical bend angle

Case	Parameter			Bend angle (°)				Error (%)
	P (W)	v (mm/min)	D (mm)	Experiment			Proposed model	
				Trial 1	Trial 2	Averaged		
1	450	1500	20	0.31	0.33	0.32	0.343	7.18
2	500	1500	20	0.37	0.398	0.384	0.418	8.13
3	550	1500	20	0.425	0.445	0.435	0.46	5.74
4	600	1500	20	0.472	0.5	0.486	0.506	4.12
5	700	1500	20	0.521	0.551	0.536	0.587	9.51
6	500	1000	20	0.41	0.436	0.423	0.434	2.6
7	500	1250	20	0.384	0.416	0.4	0.423	5.75
8	500	1500	20	0.37	0.398	0.384	0.418	8.85
9	500	2000	20	0.33	0.35	0.34	0.39	14.71
10	500	2500	20	0.318	0.332	0.325	0.378	16.31

### 5.3 Parametric Study Using the Proposed Temperature Model

For determining the relationships between the bending angle and different laser parameters, it is essential to first analyze the influence of different processing parameters on the temperature profile during laser bending. The effect of processing factors, viz. beam input power, scanning speed, and HTC on the temperature distribution of laser-formed sheets is investigated in this section. The related change in induced thermal stain and stress and its effect on the stored strain energy in the workpiece is also discussed. Figure 9 depicts the variation of temperature with time at three different laser powers keeping constant scan speed  $v$  is 1500 mm/min. This study shows that the magnitude of temperature at the mid-point of the bottom surface increases with increasing the laser power intensity. This is due to the increase in the laser input energy per unit area at the heated zone. Figure 10 shows the temperature distribution for various scan speeds keeping constant  $P$  is 500 W. It is seen that the magnitude of temperature rise decreases with increasing scan speed. It is because the interaction span between the laser source and the sheet surface is reduced.

To investigate the influence of HTC on the temperature distribution, four different cooling conditions are considered as natural cooling on both top and bottom surfaces (*Case 1*); natural cooling on the top surface, and forced cooling on the bottom surface (*Case 2*); natural cooling on the bottom surface and forced cooling on the top surface (*Case 3*); and forced cooling on both top and bottom surfaces (*Case 4*). The similar cooling conditions are analyzed by Shen et al. [22] using FEM simulations. Figure 11 depicts the temperature distribution with time at the mid-point of the bottom surface

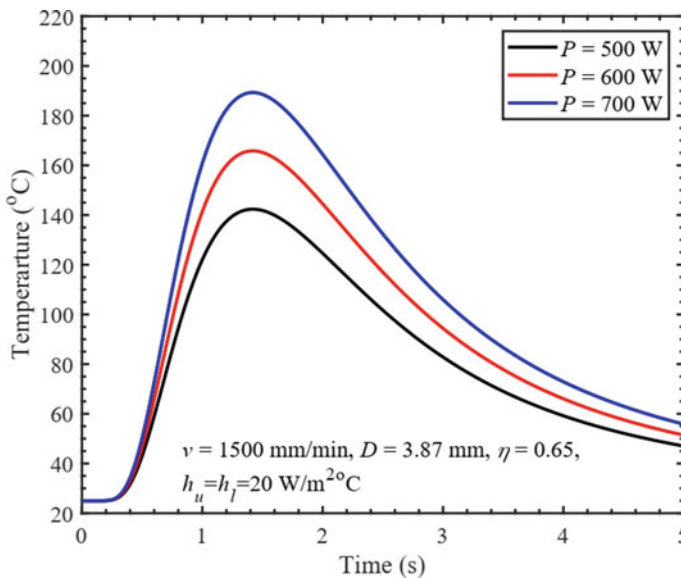
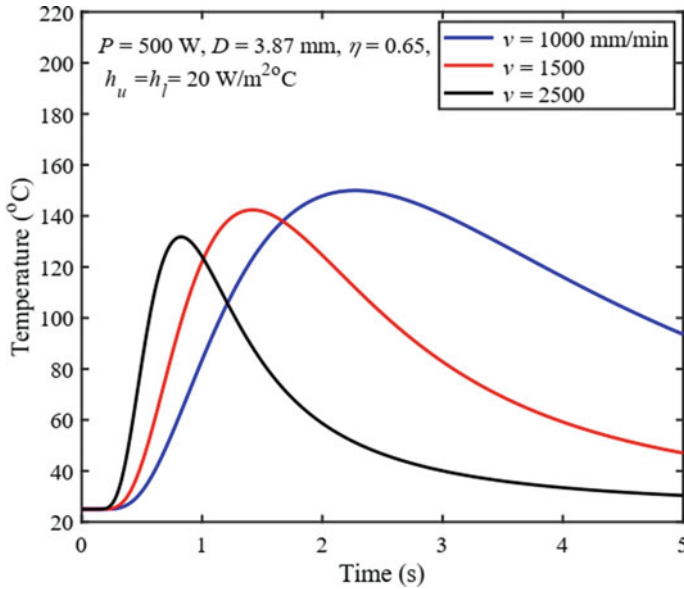


Fig. 9 Effect of laser input power on the surface temperature distribution

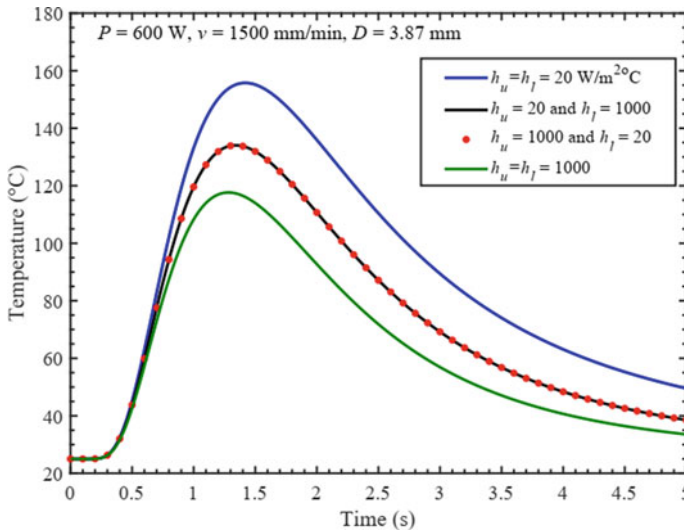


**Fig. 10** Effect of scan speed on the surface temperature distribution

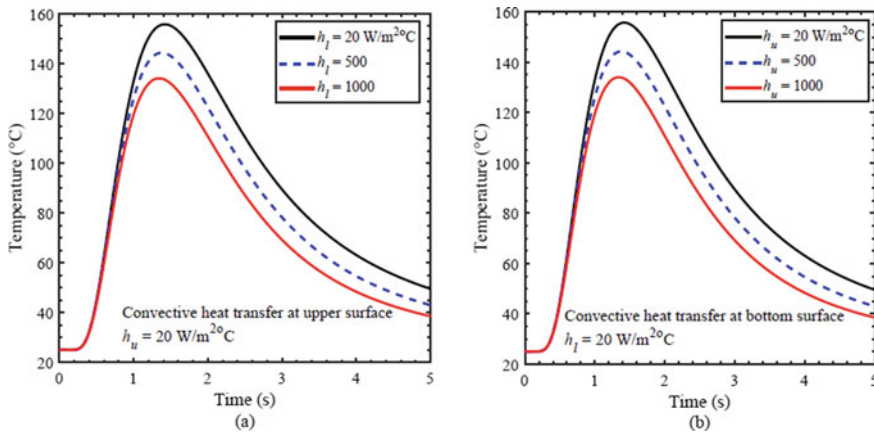
for all the cases. The laser process parameters are considered, such as the laser input power is 600 W, the scan speed is 1500 mm/min, and the spot size is 3.87 mm. The convective HTC for air and water are assumed to be 20 and 1000 W/m<sup>2</sup> K, respectively, as depicted in Fig. 11. The values of convective heat transfer coefficients are taken from [14]. It is observed that the temperature profile for forced cooling conditions is lower as compared to natural cooling. It is due to the effect of water cooling, which is characterized by a HTC almost 50 times more than calm air media. Comparing all four cooling conditions, cooling on both top and surfaces with the forced cooling results in the lowest, while the rest two forced cooling conditions have almost the same temperature profile. These results are also in line with the results of FEM simulations [22]. This observation is further explored here by varying the convective HTC at the top and bottom surfaces of the workpiece (Fig. 12).

### 5.4 Estimation of Strain Energy at Different Laser Bending Process Parameters

The strain energy is calculated at different laser beam power and scanning speed keeping constant other laser process parameters. It is observed that the temperature fields differ with the different laser bending process conditions. Therefore, the strain energy stored in the laser-heated sheets is varied. Hence, the strain energy is calculated at different laser process parameters and tabulated in Table 3. The results depicted



**Fig. 11** Effect of convective HTC at top and bottom surfaces on the transient surface temperature distribution



**Fig. 12** Comparison of the surface temperature distribution at different cooling conditions in laser forming

in Table 3 show that the thermal stress (average stress) increases linearly with the increased laser power at a constant scan speed, which further increases the induced strain energy in the workpiece. On the one hand, an increase in scan speed decreases the thermal stress at constant beam power intensity and, furthermore, decreases the stored strain energy and results in the reduction of worksheet bending.

**Table 3** Variations of stress–strain and strain energy in laser-formed Al 6061-T6 aluminum sheet

Case	$P$ (W)	$v$ (mm/min)	Average stress (MPa)	Average strain	Strain energy (N-mm)
1	450	1500	176.5	0.002563	1.32
2	500	1500	198	0.002873	1.65
3	550	1500	219.1	0.00318	2.02
4	600	1500	238	0.003457	2.39
5	700	1500	280.9	0.00407	3.32
6	500	1000	209	0.003027	1.84
7	500	1250	203.3	0.00294	1.74
8	500	1500	198	0.002874	1.65
9	500	2000	189.5	0.002749	1.51
10	500	2500	181.7	0.002637	1.39

## 6 Conclusions

In this chapter, a coupled thermo-mechanical analytical model is developed to calculate the temperature history and bend angle of the sheet during laser bending process. The estimation of temperature distribution solution is derived by using integral transform technique. The temperature distribution is taken as the input to find the bend angle using the strain energy approach. The proposed model is validated by performing the in-house experiments at different laser power intensity and scan speed. The averaged error between results predicted by analytical model and experimental results is found to be less than 10%. Hence, the proposed analytical model may be useful to assess the temperature distribution and bend angle precisely.

**Acknowledgements** Authors gratefully acknowledge the CO<sub>2</sub> laser machine and computational facilities made available by IIT Guwahati and NIT Jalandhar to perform the experimental work and simulations. The research initiation grant provided by MANIT Bhopal, Madhya Pradesh, India (letter no. Dean (R and C) 19/1055 Dated 17/09/2019) is also gratefully acknowledged.

## Appendix

### Derivation of Eq. (9) by Utilizing the Green Function Theorem [1]

Green function for  $x$ - $y$  plane of order infinity for a heating source at  $x'$ - $y'$  plane, one can write as

$$G(x, y, x', y'|t, \tau) = \frac{1}{4\pi\alpha(t - \tau)} e^{-R^2/4\alpha(t-\tau)} \tag{18}$$

where

$$R = (x - x')^2 + (y - y')^2 \tag{19}$$

Equation (6) can be written in the form of Green function for  $z$ -direction only with the given heat source at  $b = 0$  as follows:

$$G(z|t, \tau) = 2 \sum_{m=1}^{\infty} e^{-\alpha\beta_m^2(t-\tau)} \frac{\beta_m \left( \beta_m \cos \beta_m z + \left(\frac{h_u}{k}\right) \sin \beta_m z \right)}{\left[ \left( \beta_m^2 + \left(\frac{h_u}{k}\right)^2 \right) \left( l + \frac{\left(\frac{h_l}{k}\right)}{\beta_m^2 + \left(\frac{h_l}{k}\right)^2} \right) + \left(\frac{h_u}{k}\right) \right]} \tag{20}$$

Utilizing Eqs. (18) and (20), Green function of temperature distribution relation for three-dimensional case considering the convective heat transfer losses ( $h_l$  and  $h_u$ ) at  $z = 0$  and  $l$  obtains

$$G(x, y, z|t, \tau) = \frac{1}{4\pi\alpha(t - \tau)} e^{-R^2/4\alpha(t-\tau)} 2 \sum_{m=1}^{\infty} e^{-\alpha\beta_m^2(t-\tau)} \frac{\beta_m \left( \beta_m \cos \beta_m z + \left(\frac{h_u}{k}\right) \sin \beta_m z \right)}{\left[ \left( \beta_m^2 + \left(\frac{h_u}{k}\right)^2 \right) \left( l + \frac{\left(\frac{h_l}{k}\right)}{\beta_m^2 + \left(\frac{h_l}{k}\right)^2} \right) + \left(\frac{h_u}{k}\right) \right]} \tag{21}$$

The expression for temperature field can be derived as [25]

$$T - T_{\infty} = \frac{q}{2\pi\alpha(t - \tau)} e^{-R^2/4\alpha(t-\tau)} \sum_{m=1}^{\infty} e^{-\alpha\beta_m^2(t-\tau)} \frac{\beta_m \left( \beta_m \cos \beta_m z + \left(\frac{h_u}{k}\right) \sin \beta_m z \right)}{\left[ \left( \beta_m^2 + \left(\frac{h_u}{k}\right)^2 \right) \left( l + \frac{\left(\frac{h_l}{k}\right)}{\beta_m^2 + \left(\frac{h_l}{k}\right)^2} \right) + \left(\frac{h_u}{k}\right) \right]} \tag{22}$$

Substituting Eq. (8) into Eq. (22), the solution of the transient heat transfer equation with laser heating source can be evaluated from the superposition of heat transfer equation for the instantaneous heat source over the distributed zone. The heat transfer equation is solved primarily in the fixed coordinates then integrated with respect to time. The superposition can be written as follows:

$$T - T_{\infty} = \int_{-\infty}^{\infty} \int_{-\infty}^{\infty} \int_0^t \frac{q'(x', y')}{2\pi\alpha(t - \tau)} e^{-R^2/4\alpha(t-\tau)} \sum_{m=1}^{\infty} e^{-\alpha\beta_m^2(t-\tau)} \frac{\beta_m \left( \beta_m \cos \beta_m z + \left(\frac{h_u}{k}\right) \sin \beta_m z \right)}{\left[ \left( \beta_m^2 + \left(\frac{h_u}{k}\right)^2 \right) \left( l + \frac{\left(\frac{h_l}{k}\right)}{\beta_m^2 + \left(\frac{h_l}{k}\right)^2} \right) + \left(\frac{h_u}{k}\right) \right]} dx' dy' d\tau \tag{23}$$

Integrating Eq. (23) with respect to space variables  $x$ ,  $y$  and instantaneous time  $\tau$ , the final expression of temperature distribution given by Eq. (9) is obtained.

## References

1. Carslaw HS, Jaeger JC (1959) *Conduction of heat in solids*. Clarendon, Oxford
2. Cheng PJ, Lin SC (2001) An analytical model to estimate angle formed by laser. *J Mater Process Technol* 108(3):314–319
3. Dixit US, Joshi SN, Kant R (2015) Laser forming systems: a review. *Int J Mech Manuf Syst* 8(3–4):160–205
4. Eideh A, Dixit US, Echempati R (2015) A simple analytical model of laser bending process. In: *Lasers based manufacturing*, Springer, New Delhi, pp 1–15
5. Hu Z, Labudovic M, Wang H, Kovacevic R (2001) Computer simulation and experimental investigation of sheet metal bending using laser beam scanning. *Int J Mach Tools Manuf* 41(4):589–607
6. Hu J, Xu H, Dang D (2013) Modeling and reducing edge effects in laser bending. *J Mater Process Technol* 213(11):1989–1996
7. Kalvettukaran P, Das S, Marimuthu S, Misra D (2017) Numerical methods for the selection of process parameters for laser processing of materials. *Lasers Eng* 38:1–23
8. Kant R, Joshi SN (2016) Thermo-mechanical studies on bending mechanism, bend angle and edge effect during multi-scan laser bending of magnesium M1A alloy sheets. *J Manuf Process* 23:135–148
9. Khan OU, Yilbas BS (2004) Laser heating of sheet metal and thermal stress development. *J Mater Process Technol* 155:2045–2050
10. Kyrsanidi AK, Kermanidis TB, Pantelakis SG (2000) An analytical model for the prediction of distortions caused by the laser forming process. *J Mater Process Technol* 104(1–2):94–102
11. Kyrsanidi AK, Kermanidis TB, Pantelakis SG (1999) Numerical and experimental investigation of the laser forming process. *J Mater Process Technol* 87(1–3):281–290
12. Labeas GN (2008) Development of a local three-dimensional numerical simulation model for the laser forming process of aluminium components. *J Mater Process Technol* 207(1–3):248–257
13. Lambiase F, Di Ilio A (2013) A closed-form solution for thermal and deformation fields in laser bending process of different materials. *Int J Adv Manuf Technol* 69(1–4):849–861
14. Lambiase F, Di Ilio A, Paoletti A (2013) An experimental investigation on passive water cooling in laser forming process. *Int J Adv Manuf Technol* 64(5):829–840
15. Li Z, Wang X (2019) Analytical model for estimating bending angle in laser bending of 304 stainless steel/Q235 carbon steel laminated plate. *J Laser Appl* 31(4):042012
16. Mishra A, Dixit US (2013) Determination of thermal diffusivity of the material, absorptivity of the material and laser beam radius during laser forming by inverse heat transfer. *J Mach Forming Technol* 5(3/4):207
17. Mulay S, Paliwal V, Babu NR (2020) Analytical model for prediction of bend angle in laser forming of sheets. *Int J Adv Manuf Technol* 109(3):699–715
18. Nath U, Yadav V, Purohit R (2021) Finite element analysis of AM30 magnesium alloy sheet in the laser bending process. *Adv Mater Process Technol* 1–13
19. Özışık MN (1989) *Boundary value problems of heat conduction*, Courier Corporation
20. Roohi AH, Moslemi Naeini H, Hoseinpour Gollo M (2017) An experimental investigation of parameters effect on laser forming of Al6061-T6 sheets. In: *Proceedings of the institution of mechanical engineers, Part L. J Mater Design Appl* 231(5):433–442
21. Sahu P (2015) Estimation of temperature distribution in laser line heating. MTech thesis, IIT Guwahati

22. Shen H, Hu J, Yao ZQ (2011) Cooling effects in laser forming. In: *Materials science forum*, vol 663. Trans Tech Publications Ltd, pp 58–63
23. Shen H, Shi Y, Yao Z, Hu J (2006) An analytical model for estimating deformation in laser forming. *Comput Mater Sci* 37(4):593–598
24. Shi Y, Shen H, Yao Z, Hu J (2007) An analytical model based on the similarity in temperature distributions in laser forming. *Opt Lasers Eng* 45(1):83–87
25. Shi Y, Shen H, Yao Z, Hu J (2007) Temperature gradient mechanism in laser forming of thin plates. *Opt Laser Technol* 39(4):858–863
26. Zhang YJ, Kim JB, Song JH, Lee GA, Lee HJ, Lee NK (2015) FEM analysis for laser bending process of DP980 steel sheet. *Int J Precis Eng Manuf* 16(2):315–321



# Heat Transfer Analysis at Mould-Casting Interface for Improving the Casting Process



Mohammad Asif, Muhammad Muneef Sadiq, and Muhammed Muaz

**Abstract** The interfacial heat transfer coefficient (IHTC) formed at the casting-mould interface is an important parameter to affect the quality of cast product. Hence, the present study aims to perform the heat transfer analysis on the interface of mould and casting. The effect of pouring temperature and the properties of the cast metal were investigated by evaluating interfacial heat flux and interfacial heat transfer coefficient (IHTC) using transient temperatures inside the mould and casting. During the experiments, transient temperatures inside the mould and casting are recorded. Effects of pouring temperature, casting material and mould material on the transient heat flux and IHTC are also studied. From the results, both interfacial heat flux and interfacial heat transfer coefficient are found to be increasing with increase in pouring temperature keeping all other parameters constant. At same pouring temperature, interfacial heat flux is found to be independent of casting material, whilst IHTC is found to be dependent on the properties of casting material. Peak value of IHTC is found to be much higher in case of zinc metal casting as compared to aluminium metal casting. Novel and physically based analytical interpretation of the results is provided. The results will be useful for metal forming industries to develop better castings at lower costs.

**Keywords** Interfacial heat transfer coefficient · Metal casting · Permanent mould · Inverse method · Interfacial heat flux

## 1 Introduction

A sudden change in the temperature is observed at the interface of a hot and a cold contacting body. It is due to resistance to heat transfer between the contacting surfaces known as thermal contact resistance. Its reciprocal is called interfacial heat transfer coefficient (IHTC). IHTC is an important parameter in modelling and designing of casting operation. For the casting, the thermal contact resistances, found at the

---

M. Asif (✉) · M. M. Sadiq · M. Muaz  
Department of Mechanical Engineering, Aligarh Muslim University, AMU, Aligarh, India  
e-mail: [masif@zhcet.ac.in](mailto:masif@zhcet.ac.in)

© The Author(s), under exclusive license to Springer Nature Singapore Pte Ltd. 2023  
R. P. Singh et al. (eds.), *Advances in Modelling and Optimization of Manufacturing and Industrial Systems*, Lecture Notes in Mechanical Engineering,  
[https://doi.org/10.1007/978-981-19-6107-6\\_33](https://doi.org/10.1007/978-981-19-6107-6_33)

475

casting and mould interface, have been considered amongst the crucial factors to control the mechanical and physical properties of the final castings [1]. Casting involves (a) pouring of molten metal into a mould cavity, (b) allowing it to solidify and (c) removing the part from the mould. As the molten metal starts solidifying, it shrinks, and a gap is formed between the casting and inner wall of the mould which is occupied by the metal oxide gases released during solidification of the molten metal. This gap results in an additional thermal resistance which leads to a considerable temperature gradient between the mould wall and casting. Rate of heat transfer through the mould-casting interface is a function of this temperature gradient and (IHTC) at the interface. Quality of casting products depends on the rate of heat transfer through the mould-casting interface during solidification and cooling of the casting materials. Microstructure of casting products and its mechanical properties depend upon the solidifying and cooling process of the casting. Further, casting defects such as hot spots can also be avoided by proper cooling practices. Therefore, accurate knowledge of interfacial heat transfer coefficient (IHTC) at the mould-casting interface is necessary in design of casting process [2]. In casting, it depends on various factors such as mould/die material casting material, initial temperature of the mould, pouring temperature of the molten metal, coating material and its thickness at the inner wall of the mould, pressure at the interface, ambient condition and types of casting method. Interfacial heat transfer has been an important area of research in past few decades [3–6].

Interfacial or surface heat flux and interfacial heat transfer coefficient are two important parameters for the study of systems involving heat transfer [7]. Prabhu et al. [8] performed experiments to analyse heat flux at the die-casting interface. Castings of lead, zinc and aluminium metal were cast in three different moulds made up of steel and graphite. Inverse method was used to obtain the interfacial heat flux during solidification of the casting. Surface temperatures and IHTC have been evaluated. Correlations of maximum value of heat flux with thermal diffusivities and transient heat flux with time were formulated. Kim et al. [9] performed experiments to evaluate interfacial heat transfer coefficient at the die-casting interface. Cylindrical copper die was used to cast aluminium castings during the experiments. Temperature data with time at the casting surface and inside the die were used as an input to solve inverse problem. Interfacial heat transfer coefficient was analysed during different phases of the casting material such as liquid phase, solid phase and during solidification. Effects of ceramic and carbon coatings at the die surface and superheating of casting material on the IHTC were also analysed. Peak values of IHTC were found maximum when no coating was applied and minimum for carbon coating. Oliveira et al. [10] applied the non-linear inverse heat transfer method to estimate heat transfer coefficient at interface of the metal and sand mould. Experiments have been performed on plate shape castings with varying thicknesses for aluminium alloys. The IHTC was observed to depend on the casting material. Bohacek et al. [6] estimated the heat transfer coefficient at the cast-mould interface using the air gap thickness which was calculated by applying a plane stress model. Model was applied for different coating thicknesses, rotation rates and temperatures of solidus. Oliveira et al. [11] applied the Levenberg–Marquardt technique to estimate the thermal contact resistance at

metal–mould interface, hence to find out the interfacial heat transfer coefficient. The finite volume method was utilized to solve for the cooling process of an alloy casting in a mould. Heat dissipation in only one side of the mould has been considered so as to ensure uphill and unidirectional solidification. Vishweshwaran et al. [12] numerically investigated a one-dimensional transient heat conduction model at the metal–mould interface in order to find out the interfacial heat transfer coefficient during horizontal directional solidification of Sn–5-wt% Pb alloy. The unknown IHTC was estimated using an inverse method of particle swarm optimization along with Bayesian framework. Aksoy and Koru [1] estimated the interfacial heat transfer coefficient and heat flux at the interface of casting mould. They worked on the pressure casting of cylindrical mould made of AlSi8Cu3Fe aluminium alloy. IHTC and heat flux were determined by using experimentally measured temperatures. Further, machine learning algorithms were utilized in order to determine IHTC. ANNR algorithm has been observed as the most accurate model. Natsume et al. [13] carried out experiments on unidirectional castings of Al-1mass% Si alloy and acquired the cooling curves during solidification. The time-dependent heat transfer coefficient was determined to evaluate the suitability of the method for real experimental data. Jayakrishna et al. [14] established an inverse heat transfer model based on Salp swarm optimization algorithm for the estimation of heat flux at the hot faces of a mould in thin slab continuous casting. A funnel-shaped mould was assumed having complex arrangement of cooling slots. The estimated heat flux profile was utilized to observe the fluid flow and thermal characteristics of the solidifying steel strand inside the mould. Stieven et al. [15] developed two numerical models to estimate the IHTC in directional solidification. The models were based on thermal resistance and thermal gradient formulation at the interface of metal–mould. In the literatures, it was found that experiments for the study of heat flux at mould-casting interface with copper die were generally performed which is costly [7]. Mild steel might be a good alternative to serve as die material. Further, study using mild steel die with zinc as casting material was not properly performed. In addition, it has been noted that heat transfer analysis at the interface of aluminium casting and mild steel die has not been performed. Therefore, in the present work, the objective was to study interfacial heat transfer at the mould-casting interface for different mould and casting materials for various parameters. Further, experiments were performed using indigenously fabricated experimental setup. The experimental results were first used to estimate the interfacial heat flux and interfacial heat transfer coefficient at the mould-casting interface. Finally, the effect of different pouring temperature on the interfacial heat flux and interfacial heat transfer coefficient was studied. Hence, heat transfer experiments were performed by taking pure aluminium and zinc as casting materials, whilst mild steel was taken as die material. The heat transfer analysis performed in study might be useful for metal forming industries to develop better castings at lower costs.

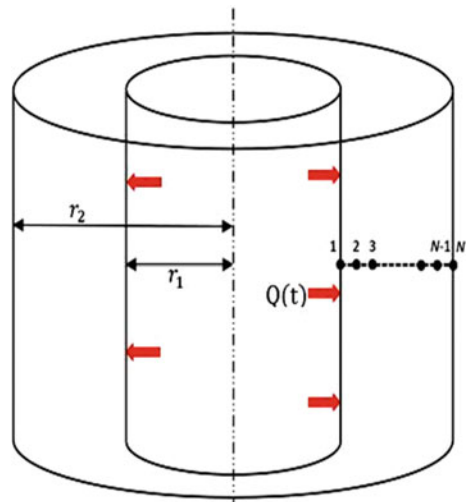
## 2 Materials and Method

### 2.1 Numerical Methodology

Transient heat flux is estimated numerically by using inverse heat conduction method. A hollow cylindrical die is considered whose top and bottom surfaces are insulated. When the casting material is poured into the die, a transient heat flux will be subjected at the inner curved surface of the cylinder, as shown in Fig. 1. Here, heat transfer is assumed to be in radial direction only through the cylinder wall to atmosphere and assumed to be neglected in all other directions. Conjugate gradient method with adjoint problem has been employed to solve the inverse heat conduction problem for the estimation of unknown transient heat flux at the die-casting interface. In the inverse problem, thermophysical properties of the die, casting, boundary conditions and transient temperature data in the die and casting at different radial locations have been provided as an input to estimate the unknown heat flux with time. The transient temperature distribution in the wall has been provided for various die and casting materials. The steps involved in conjugate gradient method are direct problem, inverse problem, sensitivity problem, adjoint problem, gradient equation, iterative procedure, stopping criterion, computational algorithm [16]. The implicit form of finite difference method has been used for discretizing the intermediate boundary value problems as it is unconditionally stable and fast convergent. All the problems have been programmed with MATLAB.

Mathematically, the one-dimensional heat conduction problem considered is given as:

**Fig. 1** Geometry of the die and computational grid formation



$$Q(t) = -K \frac{\partial T}{\partial r}, \quad \text{at } r = r_1, \quad t > 0 \quad (1)$$

$$\frac{\partial^2 T}{\partial r^2} + \frac{1}{r} \frac{\partial T}{\partial r} = \frac{1}{\alpha} \frac{\partial T}{\partial t}, \quad \text{at } r_1 < r < r_2, \quad t > 0 \quad (2)$$

$$-K \frac{\partial T}{\partial r} = h_\infty (T_N - T_\infty), \quad \text{at } r = r_2, \quad t > 0 \quad (3)$$

$$T_o = T_{\text{initial}}, \quad \text{at } r_1 \geq r \leq r_2, \quad t = 0 \quad (4)$$

The solution of the inverse problem is done in such a way that the following objective function is minimized:

$$S[Q(t)] = \int_0^{t_f} \left[ \sum_{i=2}^{N_1-1} (T_i - Y_i)^2 \right] dt \quad (5)$$

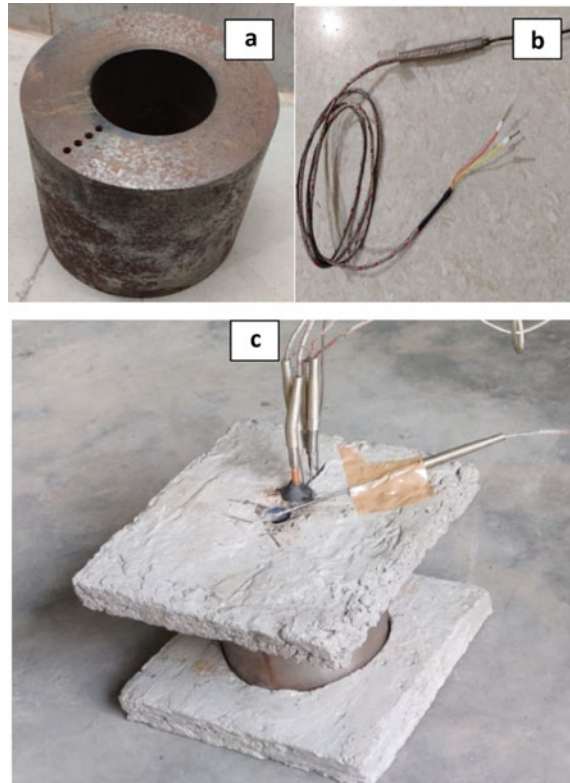
where  $T_i$  is the temperatures estimated by the inverse problem and  $Y_i$  is the measured temperatures.

## 2.2 Experimental Methodology

Casting experiments are performed using permanent moulds/dies of cylindrical shape. Temperature history inside the die wall at radial locations and inside the casting material near the surface is recorded. These temperature data are given as input to the inverse method, and heat flux at the die-casting interface and transient temperature at the inner die surface are estimated. Using the heat flux and interface temperatures, thermal contact conductance during solidification of the casting is calculated. The die used in the experiments is made up of mild steel (Thermal conductivity = 54 W/mK, thermal diffusivity =  $1.48 \times 10^{-5}$  m<sup>2</sup>/s) in the form of a hollow cylinder having outer diameter of 100 mm, inner diameter of 50 mm and height of 100 mm. Four blind holes of 3 mm diameter have been created on the top side of the die and 40 mm in depth at four different radial locations 5 mm (centre to centre) apart from each other, as shown in Fig. 2a.

Due to cylindrical shape of the die and symmetrical heat flux condition, heat transfer can take place in radial and axial directions. Since we are considering one-dimensional radial heat transfer, we have to inhibit the heat transfer in axial direction. For this purpose, the insulating covers at the top and bottom of the die have been provided. The insulating covers are made up of concrete material having thermal conductivity much less than the die metals. Further, small holes are provided at the top plate for inserting thermocouples and to release the trapped air during casting. Six mineral-insulated Chromel–Alumel (*K*-Type) very fine thermocouples of 0.1 mm

**Fig. 2** a Casting die, b K-type thermocouple, c experimental setup

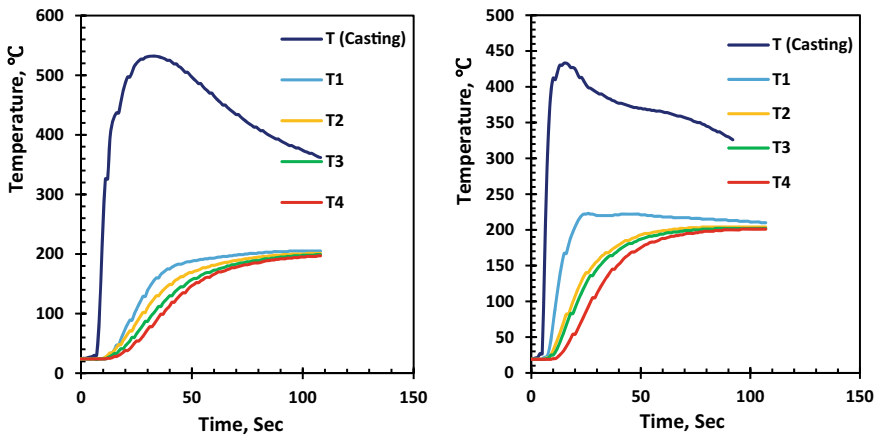


diameter covered in a SS probe of 40 mm length and 1.5 mm diameter (Fig. 2b) are used to measure the temperatures. These thermocouples are having range of 200–1260 °C with accuracy  $\pm 1.1$  °C or  $\pm 0.4\%$ . All the thermocouples are connected to the temperature data logger. The temperature data logger indicates temperatures in the real time as well as save these temperatures with time in a data storage device. The temperature data logger can have a resolution of 1 °C.

A coal-based pit furnace has been used to melt the casting material. The pit furnace can melt maximum of 20-kg metal at a time. It is fitted with an electric blower. Figure 2c shows the actual pictorial view of the combined setup which shows the metallic die with top and bottom insulation slabs and all the thermocouples placed in die and in casting gap. Pouring temperature is an important parameter in order to produce defect-free sound castings. For each set of material, experiments are performed for three different pouring temperatures. Two materials, namely aluminium and zinc, are taken for producing castings. Both the materials are selected because of their applications in casting, low melting point and easy availability and wide industrial application.

Casting experiments are performed in order to study the interfacial heat transfer at the casting-mould interface. Initially, experimental setup is assembled as shown in Fig. 2c by placing the die between top and bottom insulating plates. Then, the thermocouples are fixed at the required locations at which temperature has to be recorded. Four thermocouples are inserted inside the holes drilled for them in the die wall. One thermocouple is placed very close to the die wall at the same depth at which thermocouples in the die wall are inserted. In order to prevent this thermocouple from getting stuck inside the solidifying casting, a copper sleeve is used to protect it. A thermocouple is placed on the hole through which molten metal is poured in order to measure the pouring temperature of the molten metal. All the thermocouples are connected to data logger in order to record the transient temperatures. Simultaneously, casting material is melted inside the furnace and then superheated up to the desired pouring temperature. Once the molten metal reached the desired temperature, it is poured inside the mould, and temperatures are recorded through the data logger. The temperatures are recorded until the temperatures inside the die reach the steady-state conditions. Typical temperature versus time curves for aluminium and zinc casting materials are shown in Fig. 3a and b, respectively.

In these curves, T (casting) refers to the temperature of casting near the interface. T1, T2, T3 and T4 are the temperatures inside the mould wall with T1 being closest to the interface. It can be noticed from these curves that as the molten metal is poured into the mould, the mould temperatures closest to the interface (T1) increase more rapidly to a maximum temperature. After the occurrence of a peak, these temperatures decrease at a slower rate and become nearly constant after a short period of time. For example, in Fig. 3b, temperature T1 inside the mould increases rapidly as the molten zinc is poured into the mild steel mould. It reaches a peak value of 222 °C in 24 s and then decreases slowly to a value of 210 °C and then become nearly constant. Temperatures at other locations (T2, T3 and T4) inside the mould increase rapidly at



**Fig. 3** a Transient temperature data of thermocouples for aluminium casting, b Transient temperature data of thermocouples for zinc casting

the initial stage when the molten metal is poured. Then, these temperatures increase at a slow rate and become approximately constant after a period of time.

Temperature inside the casting near the mould-casting interface,  $T$  (casting), initially rises very fast to a peak value and then decreases at a relatively slower rate to the freezing point of the casting metal. After the solidification of the casting near the interface is completed, the temperature of the casting decreases at a nearly constant rate which is much lower as compared to the liquid state of the casting. Initially, the temperatures may be lower than the expected values due to the delayed response of the thermocouples. Further, the temperatures can be found lower due to the thermal contact resistance at the interface of thermocouples and mould/casting materials.

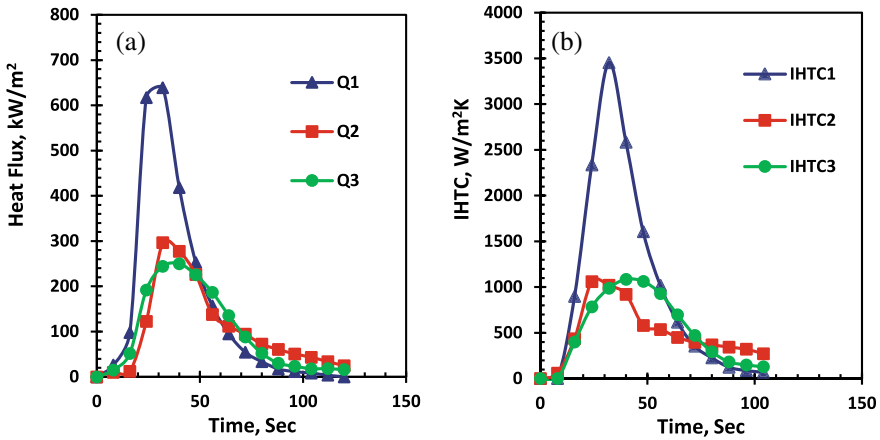
### 3 Results and Discussion

#### 3.1 Zinc Casting in Mild Steel Mould

Castings of zinc metal have been produced inside mild steel mould for three different pouring temperatures. Variation of heat flux with time, for these castings, is shown in Fig. 4a. Q1, Q2 and Q3 are transient heat flux estimated at the mould-casting interface for pouring temperatures 750 °C, 550 °C and 500 °C, respectively. At all the three pouring temperatures, heat flux is increasing rapidly as soon as the molten metal is poured into the casting. It is reaching the peak values for Q1 and Q2 in nearly 32 s. Peak value of Q3 is taking a little longer and occurring in 40 s. Peak value of heat flux for Q1 (639.09 kW/m<sup>2</sup>) is much greater than peak values for Q2 (296.40 kW/m<sup>2</sup>) and Q3 (249.85 kW/m<sup>2</sup>). The occurrence of peak heat flux can be associated with the formation of thin shell of solidified metal at the interface and/or completion of filling of mould with molten metal [10]. After attaining the peak values, the heat flux starts decreasing. As the solidification propagates, slopes of all the three curves decrease. After the completion of solidification, the heat flux at the interface decreases due to shrinkage of casting and expansion of mould which is result of heat transfer from casting to the mould. Heat flux values for Q1 become miniscule after 88 s, whilst values of Q2 and Q3 take longer time of nearly 120 s. It is evident from the figure that the maximum value of heat flux is increasing with increasing the value of pouring temperature.

Variation of interfacial heat transfer coefficient with time is shown in Fig. 4. IHTC1, IHTC2 and IHTC3 are interfacial heat transfer coefficients at the mould-casting interface for pouring temperatures 750 °C, 550 °C and 500 °C, respectively. IHTC has been calculated using estimated transient heat flux and temperature gradient at the interface. The IHTC curves thus obtained are somewhat similar to the heat flux curves. Peak values of IHTC are increasing with increase in pouring temperature as well. Values of IHTC in all the curves increase rapidly to a maximum value and then decrease to a negligible value at a comparatively slower rate. Peak



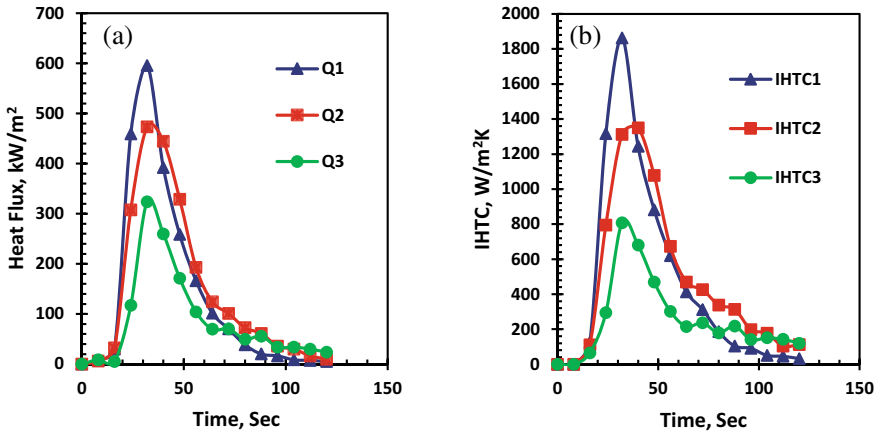


**Fig. 4** a Variation of heat flux with time for three different pouring temperatures for zinc casting, b variation of IHTC with time for three different pouring temperatures for zinc casting

value of IHTC1 (3453.98 W/m<sup>2</sup>K) is much higher than the peak values of IHTC2 (1060.86 W/m<sup>2</sup>K) and IHTC3 (1085.70 W/m<sup>2</sup>K). Curve for IHTC2 and its peak value is not as expected. It can be due to the delayed response of the thermocouple used to measure the interface temperature of casting and/or experimental error induced in the temperature measurements. Curve for IHTC3 increases to a maximum value of 1085.70 W/m<sup>2</sup>K in initial 40 s and then decreases for nearly 60 s to reach its minimum value. After 56 s, values of IHTC1 and IHTC3 are comparable and their curves have similar slopes.

### 3.2 Aluminium Casting in Mild Steel Mould

Castings of aluminium metal have been produced inside mild steel mould for three different pouring temperatures. Variations of heat flux with time, for these castings, are shown in Fig. 5a. Q1, Q2 and Q3 are transient heat flux estimated at the mould-casting interface for pouring temperatures 730 °C, 710 °C and 670 °C, respectively. As the molten metal is poured into the mould cavity, heat flux increases suddenly and reaches a maximum value in 32 s for all the pouring temperatures. It can be easily observed that maximum value of heat flux is increasing with increase in the pouring temperature. Peak values for Q1, Q2 and Q3 are 595.37 kW/m<sup>2</sup>, 473.22 kW/m<sup>2</sup> and 323.72 kW/m<sup>2</sup>, respectively. Then, the values of heat flux keep decreasing throughout the considered time span. Values of heat flux for Q1 become negligible in 104 s, whilst for Q2 and Q3, it took nearly 120 s. It can be observed that area under the curve for Q3 is much less as compared to Q1 and Q2. It is because the molten metal is poured nearly at melting point in case of Q3, whilst in case of Q1 and Q2, it is superheated to a higher temperature.



**Fig. 5** **a** Variation of heat flux with time for three different pouring temperatures for aluminium casting, **b** Variation of IHTC with time for three different pouring temperatures for aluminium casting

Variation of interfacial heat transfer coefficient with time is shown in Fig. 5b. IHTC1, IHTC2 and IHTC3 are interfacial heat transfer coefficients at the mould-casting interface for pouring temperatures 730 °C, 710 °C, and 670 °C, respectively. As the molten metal is poured into the mould cavity, IHTC values for all the pouring temperatures increase rapidly to a peak value. Maximum values occur in 32 s for IHTC1 and IHTC3 curves which are same as in case of heat flux curves. Whilst a peak shift is observed in case of IHTC2 curve as it took 40 s to reach its maximum value. Peak values of IHTC1, IHTC2 and IHTC3 are 1862.55 W/m<sup>2</sup>K, 1349.96 W/m<sup>2</sup>K and 807.21 W/m<sup>2</sup>K, respectively. Hence, peak values of IHTC are also increasing with increase in pouring temperature. After attaining peak values, IHTC decreases continuously throughout the time span considered. Values of IHTC1 diminish a bit earlier as compared to the values of IHTC2 and IHTC3.

## 4 Conclusion

The analysis of interfacial heat transfer at the mould-casting interface has been done in this work by taking pure aluminium and zinc as casting materials whilst mild steel as die material. Conclusions on the basis of this study are as follows:

- Interfacial heat flux and interfacial heat transfer coefficient depend on pouring temperature of molten metal and mould material.
- Both heat flux and IHTC tend to increase with increase in the pouring temperature.
- Interfacial heat transfer coefficient depends upon properties of casting material.

- Maximum value of IHTC for zinc casting is found to be much more than aluminium casting for same mould material.
- Mild steel can be used as a good alternative to serve as die material. It will be useful for metal forming industries to develop better castings at lower costs.

## References

1. Aksoy B, Koru M (2020) Estimation of casting mold interfacial heat transfer coefficient in pressure die casting process by artificial intelligence methods. *Arab J Sci Eng* 45:8969–8980
2. Rajaraman R, Gowsalya L, Velraj R (2018) Interfacial heat transfer coefficient estimation during solidification of rectangular aluminum alloy casting using two different inverse methods. *Front Heat Mass Transf* 11(23):1–8
3. Prabhu K, Ashish AA (2002) Inverse modeling of heat transfer with application to solidification and quenching. *Mater Manuf Process* 17:469–481
4. Mirbagheri S (2006) Modelling of metal–mold interface resistance in the A356 aluminium alloy casting process. *Commun Numer Methods Eng* 23:295–312
5. Hamasaiid A, Dour G, Loulou T, Dargusch MS (2010) A predictive model for the evolution of the thermal conductance at the casting–die interfaces in high pressure die casting. *Int J Therm Sci* 49(2):365–372
6. Bohacek J, Kharicha A, Ludwig A, Wu M, Karimi-Sibaki E (2018) Heat transfer coefficient at cast-mold interface during centrifugal casting: calculation of air gap. *Metal Mater Trans B* 49:1421–1433
7. Wang F, Ma Q, Meng W, Han Z (2017) Experimental study on the heat transfer behavior and contact pressure at the casting–mold interface in squeeze casting of aluminum alloy. *Int J Heat Mass Transf* 112:1032–1043
8. Prabhu K, Mounesh H, Mahadeva S, Ashish A (2003) Casting/mould interfacial heat transfer during solidification in graphite, steel and graphite lined steel molds. *Int J Cast Met Res* 15:565–571
9. Kim HS, Cho IS, Shin JS, Lee SM, Moon BM (2005) Solidification parameters dependent on interfacial heat transfer coefficient between aluminum casting and copper mold. *ISIJ Int* 45(2):192–198
10. Zhang A, Liang S, Xiong S (2017) Determination of the interfacial heat transfer coefficient at the metal-sand mold interface in low pressure sand casting. *Exp Thermal Fluid Sci* 88:472–482
11. Oliveira EP, Stieven GM, Lins EF, Jerson RPV (2019) An inverse approach for the interfacial heat transfer parameters in alloys solidification. *Appl Therm Eng* 155:365–372
12. Vishweshwara PS, Gnanasekaran N, Arun M (2019) Inverse estimation of interfacial heat transfer coefficient: during the solidification of Sn-5wt%Pb alloy using evolutionary algorithm. In: *Advances in materials and metallurgy. Lecture notes in mechanical engineering*, Springer, Singapore
13. Natsume Y, Oka Y, Ogawa J, Ohno M (2020) Estimation of time-dependent heat transfer coefficient in unidirectional casting using a numerical model coupled with solidification analysis and data assimilation. *Int J Heat Mass Transf* 150:119222
14. Jayakrishna P, Vaka AS, Chakraborty S, Ganguly S, Talukdar P (2021) Interfacial heat flux estimation in a funnel-shaped mould and analysis of solidification characteristics in thin slab continuous casting. *ASME J Heat Transf* 143(12):122401
15. Stieven GM, Soares DR, Oliveira EP, Lins EF (2021) Interfacial heat transfer coefficient in unidirectional permanent mold casting: modeling and inverse estimation. *Int J Heat Mass Transf* 166:120765
16. Ozisik MN, Orlande HRB (2000) *Inverse heat transfer: fundamentals and applications* (1st ed.), CRC Press, New York (NY)

# Modeling and Analysis of Wire EDM Process Parameters for AZ-31 Alloy Using Response Surface Methodology



Durgesh Pandey, Rajesh Babbar, Aviral Misra, and R. K. Bansal

**Abstract** Magnesium alloys are some of the recently developed biomaterials that have a number of beneficial properties including biocompatibility, biodegradability, and mechanical properties that are comparable to that of bone. The poor corrosion resistance of magnesium alloys is sometimes beneficial in terms to avoid the second surgery to remove the implant. This paper focuses on the machining characteristics of the wire EDM process for AZ-31 alloy. The input process parameters selected based on past literature are pulse-on duration, servo voltage, wire tension, and wire feed rate, whereas the output response is kerf width. The experiments are designed based on central composite design (CCD) of response surface methodology. To determine the critical process parameters, ANOVA analysis has also been conducted. Experimental results indicate that with the increase in pulse-on duration and servo voltage, kerf width of AZ-31 alloy always increases, whereas the kerf width for AZ-31 alloy always decreases with an increase in wire feed rate and wire tension.

**Keywords** AZ-31 · Kerf width · Wire EDM · RSM

## 1 Introduction

Medical application like orthopedic implants requires a biocompatible and biodegradable material. Materials such as titanium alloys and magnesium alloys are popular these days. Magnesium has a principal advantage as it has a strength modulus comparable to that of the human bone, which minimizes the stress shielding effect [1]. The human body has a natural regeneration ability to form fresh tissues, and the biodegradable magnesium alloy implant can dissolve with the formation of new fresh natural bone tissues. As a result, a second surgery to remove temporary or permanent implants can be avoided [2]. The part fabrication using biomaterials, such as magnesium alloys for biomedical applications, is extremely challenging by

---

D. Pandey · R. Babbar · A. Misra (✉) · R. K. Bansal  
Department of Industrial and Production Engineering, Dr. B. R. Ambedkar N.I.T Jalandhar,  
Jalandhar, India  
e-mail: [mishraa@nitj.ac.in](mailto:mishraa@nitj.ac.in)

© The Author(s), under exclusive license to Springer Nature Singapore Pte Ltd. 2023  
R. P. Singh et al. (eds.), *Advances in Modelling and Optimization of Manufacturing and Industrial Systems*, Lecture Notes in Mechanical Engineering,  
[https://doi.org/10.1007/978-981-19-6107-6\\_34](https://doi.org/10.1007/978-981-19-6107-6_34)

487

using traditional methods of manufacturing, particularly for the part having intricate shapes and requires high-dimensional accuracy [3]. Magnesium alloy is the mixture of magnesium with other alloying elements such as aluminum, zinc, manganese, and silicon (denoted by  $A$ ,  $Z$ ,  $M$ , and  $S$ , respectively). AZ-31 magnesium alloy has the composition of aluminum (3%) and zinc (1%). Wire EDM is a non-conventional machining technique that can be used for machining of a variety of materials including titanium, magnesium alloy having intricate shapes and are difficult to machine with conventional methods [4]. A fine surface finish, high-dimensional accuracy, and stress-free surface could be obtained by using wire EDM [5].

In the past, attempts have been made to study the machining characteristics of wire EDM considering the output response such as surface roughness ( $R_a$ ) of the machined part, material removal rate (MRR), cutting speed, and kerf width. Chaudhary et al. [6] had studied the effect of mechanical wire tension on  $R_a$ , kerf width, MRR, and hardness of recast layer using AISI 404 stainless steel as workpiece. Pulse-on duration, pulse-off duration, and current were fixed input parameters. It has been observed that  $R_a$  value decreases with increase in wire mechanical tension, and wire mechanical tension has almost no considerable influence on the MRR and recast layer hardness. Sharma et al. [7] had conducted experiments on high-strength low alloy steel (HSLA) on wire EDM using RSM to optimize output response such as MRR and  $R_a$ . Experimental results indicate MRR, and  $R_a$  increases with increase in  $T_{on}$  and peak current and decreases with increase in  $T_{off}$  and servo voltage. Alias et al. [8] had studied the effect of three different machine feed rates (2, 4 and 6 mm/min) on output responses such as kerf width, MRR, and  $R_a$ , while current, wire feed rate, wire tension, and voltage were kept constant taking Ti-6Al-4 V as workpiece. It has been found that the increase in machine feed rate leads to decrease in kerf width. Pulse-on time and open-circuit voltage were found to be the most influencing parameters on MRR and kerf width. Experimental results also indicate lower  $R_a$  value obtained with lower machine feed rate, and  $R_a$  was mostly affected by wire tension and spark gap voltage. Klocke et al. [9] had studied the surface quality of slots produced by wire EDM vs broaching operation for Inconel 718 superalloy using different wire electrode materials such as standard brass wire (BS), coated high-speed wire electrode (TPX), and prototype wire (AG). Experimental results indicate BS wire electrode had the best mean  $R_a = 0.61$  value, and a practically layer-free surface was obtained in terms of the recast layer. Tosun [10] had investigated the influence of cutting parameters on the size of the crater (depth and diameter) on the electrode wire.  $T_{on}$ , open-circuit voltage (OCV), wire feed rate, and dielectric cleansing pressure were used as input cutting parameters. Tool electrode and work material were made brass wire ( $\phi$  0.25 mm) and AISI 4140, respectively. Experimental results indicate that increases in  $T_{on}$ , open-circuit voltage (OCV), and wire feed rate result in a rise in crater size, but increases in dielectric flushing pressure result in a reduction in crater size on wire electrode. Khan et al. [11] had conducted experiments on WEDM taking cryogenic treated Ti-6Al-4 V as workpiece. In their investigation,  $T_{on}$ ,  $T_{off}$ , wire feed rate, flushing pressure, wire tension, peak current, and spark gap voltage have been taken as input variable and  $R_a$  was taken as output response. The cryogenic treatment of Ti-6AL-4 V has been done in a liquid nitrogen environment for 24 h. Pulse-on

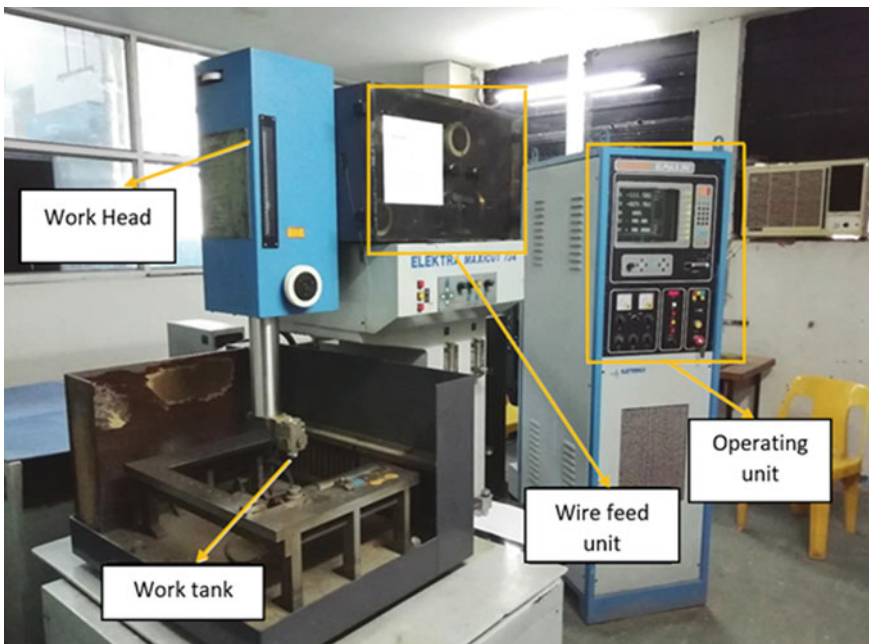
time, peak current, and servo voltage were found to be main significant input parameter. Ramamurthy et al. [12] had conducted experiments on Ti-6Al-4 V workpiece by using WEDM. Different wire electrodes such as zinc-coated, brass, and diffused brass wire have been chosen for the experiments. Experimental results indicate that a diffused brass wire tool electrode can produce a minimum  $R_a$  with minimum kerf width than the zinc-coated wire and brass wire electrode due to its lower flush ability. Razak et al. [13] had conducted experiments on wire EDM taking magnesium AZ-31 alloy as workpiece. It has been found that the  $T_{on}$  was the most significant input variable that affects  $R_a$ . Experimental results indicate peak current, 80 V, 16  $\mu$ -sec  $T_{on}$ , and 512  $\mu$ -sec  $T_{off}$  were the best EDM conditions. Tosun et al. [14] investigated the effect of process parameters on wire wear, size of craters erosion on the wire, and  $R_a$  taking brass wire as electrode, and AISI 4140 steel as workpiece. It was found that the increase in  $T_{on}$  and OCV increases the wire wear rate, and increase in wire feed rate and dielectric flushing pressure decreases the wire wear rate. Nain et al. [15] had examined the effect of process parameters on  $R_a$  and the effect of recast layer by using the fuzzy and BP-ANN model, and  $T_{on}$  was found to be most influencing parameter followed by wire tension and servo voltage. Mandal et al. [16] had investigated the effect of process parameters on surface integrity for Al 6061 alloy and kerf width. Average value of kerf width along with the cutting length has been taken in study.  $T_{on}$  and servo voltage were found to be the most influencing parameters followed by  $T_{off}$  and wire tension. With increase in  $T_{on}$  and servo voltage, the kerf width also increases. Prasad et al. [4] had investigated the wire EDM process parameters on output response as  $R_a$  and MRR taking Ti-6Al-4 V as workpiece. Author concludes that  $T_{on}$  and peak current ( $I_p$ ) were the most significant parameters for MRR and  $R_a$ , whereas servo voltage and  $T_{off}$  were less effective parameters. The literature survey suggested that very few attempts are made to examine the machining characteristics of wire EDM on magnesium alloy AZ-31. Hence, in the present work, attempt has been made to analyze the machining characteristics of wire EDM for AZ-31 alloy. The part accuracy is considered as major machining characteristics; thus, kerf width is taken as output machining response. The input processes parameters selected are pulse-on duration, wire feed rate, servo voltage, and wire mechanical tension that are varied during the experimentations, and all other parameters are kept constant. An ANOVA analysis was performed of the experimental data to estimate the percentage contribution of the variable process parameters. A statistical model is formulated from the experimental data, and surface plot is observed for the interaction between the process parameters.

## 2 Experimentations

The experiments were carried out on “Electronica Elektra Maxi cut 734” wire EDM machine setup. The wire EDM machine consists of several parts such as work head, operating unit, wire feed unit, and work tank. The photograph of the experimental setup is shown in Fig. 1. The magnesium alloy AZ-31 plate of dimension 100 ×

50 × 6 mm<sup>3</sup> was used as the workpiece material. The chemical composition of the AZ-31 plate is given in Table 1. A brass wire of diameter 0.25 mm was used as a tool electrode. Deionized water was used as the dielectric fluid. It was continuously circulated through the machining region to eliminate debris generated during erosion and also offer adequate cooling to the wire electrode and workpiece. The magnesium alloy AZ-31 workpiece was mounted on the wire EDM machine, and a 15 mm straight cut has been made sample to measure the kerf width. An optical microscope (LEICA DM 2700 M) is used to measure the kerf width.

The machining characteristics of wire EDM is affected by the process parameters like pulse-off duration, pulse-on duration, servo voltage, peak current, wire feed rate, wire mechanical tension, flushing pressure, and material of the tool wire electrodes. However, depending on the capabilities and configuration of the wire cut EDM machine, pulse-on duration, wire feed rate, servo voltage, and wire tension have been selected as input variable process parameters, whereas other machining parameters like peak current, pulse-off duration, dielectric fluid pressure, and distance between the upper nozzle and lower flushing nozzle were kept constant, and their magnitude



**Fig. 1** Machine setup for experimentation

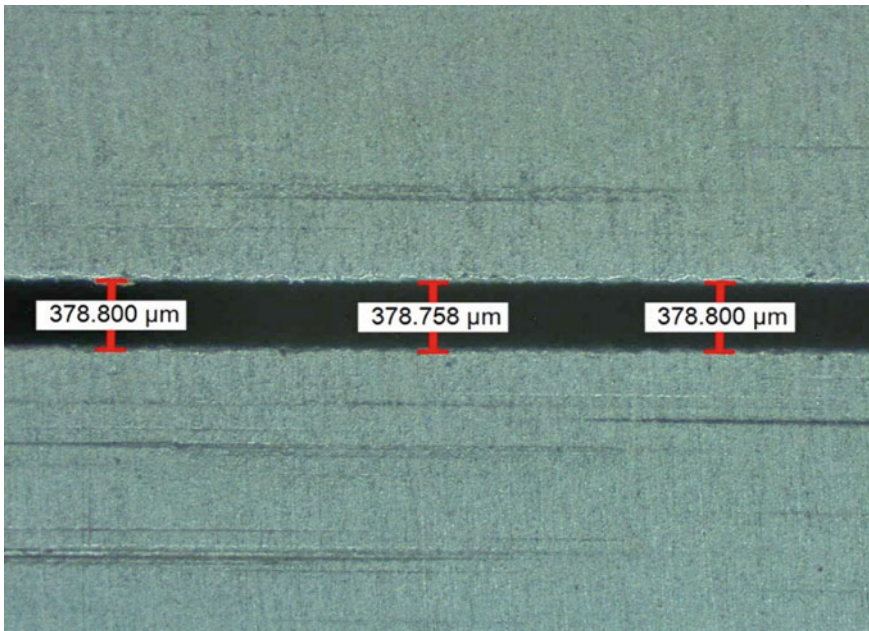
**Table 1** Chemical composition of AZ-31 alloys

Element	Mg	Al	Zn	Fe
Content (%)	95.82	2.80	1.36	0.02

**Table 2** Input variables and their ranges

S. No.	Input variables	Level I	Level II	Level III	Level IV	Level V
1	Pulse-on duration ( $T_{on}$ ) in $\mu s$	2	4	6	8	10
2	Wire feed rate (WFR) in m/min	1	2	3	4	5
3	Servo voltage (SV) in volt	40	50	60	70	80
4	Wire tension (WT) in gm	200	400	600	800	1000

is 1 Amp, 8  $\mu$ -sec, 10 kg/cm<sup>2</sup>, and 25 mm, respectively. Output response was taken as kerf width. The experiments were designed using response surface methodology (RSM) since the number of experiments required reduced substantially compared to a full factorial design [17]. Based on central composite design (CCD), 31 sets of experiments had been designed. The input process parameters and their levels for experimentation are given in Table 2. For each experiment number, three repetitions are made to do away with any experimental bias. For each set of experiment, three 15 mm straight cuts at three different locations were made and an optical microscope (LEICA DM 2700 M) was used to measure the kerf width. The optical microscopic image of kerf width of magnesium alloy for experiment no. 8 is shown in Fig. 2. The average of three values of kerf width was considered as an output response for each set of experiment.



**Fig. 2** Optical microscopic image of kerf width of magnesium alloy (experiment no. 8)



### 2.1 Response Surface Methodology (RSM)

The best method to discover the best-fitted model which has several independent variables affect the response variable is to use response surface methodology (RSM). The empirical model, as given in Eq. (1), may be used to predict the relation between the output response and its independent input variables. Surface plots may be used to visualize the response for any output response ( $\varphi$ ).

$$\varphi = \psi(y_1, y_2, y_3, \dots, \dots, y_i, \dots, \dots, y_k) \tag{1}$$

where  $\varphi$  represents the system’s output response,  $\psi$  represents the response function,  $y_i$  represents the independent parameter, and  $k$  represents the number of controllable parameters.

As indicated in Eq. (2), the response surface for the two-degree mathematical model is made up of nonlinear, linear, and two-factor interaction terms of  $y_i$ ’s parameters.

$$\varphi = d_o + \sum_{i=1}^k d_i y_i + \sum_{i=1}^k d_{ii} y_i^2 + \sum_{i=1}^{k-1} \sum_{i+1}^k d_{ij} y_i y_j + \beta \tag{2}$$

where  $d_o$  is a constant term,  $d_i$ ,  $d_{ii}$ , and  $d_{ij}$  are the coefficients of the regression, and  $\beta$  is the random error.

A RSM with an axial or star point, in addition to the three-level components, is known as a central composite design (CCD). The axial or star point ( $\alpha$ ) raises the number of levels to five, allowing the experimental design to be more flexible. It also makes precise predictions of the linear and quadratic interaction effects of the process parameters.

The total number of experiments for a given factor ( $k$ ) is given by Eq. (3)

$$N = 2^k + 2 * k + n_c \tag{3}$$

Here,  $N$  is the total experiments,  $k$  is the total number of factors in the experiments, and  $n_c$  is the total number of center points in the experimentation. To find the value of the axial point, we need to find the value of  $\alpha$  as given by Eq. (4)

$$\alpha = 2^{(k/4)} \tag{4}$$

In the present experimentation work, for four factors and seven center points, the total number of experimental runs is computed as  $= 2^4 + 2 * 4 + 7 = 31$ .

The experimental design with output response as kerf width is given in Table 3.

**Table 3** Experimental design and results

Exp. no.	Pulse-on duration $T_{on}$ ( $\mu s$ )	Wire feed rate (WFR) (m/min)	Servo voltage (SV) (volt)	Wire tension (WT) (gm)	Kerf width ( $\mu m$ )
1	6	3	40	600	332
2	8	2	70	400	398
3	8	4	50	800	344
4	8	4	70	400	404
5	8	4	50	400	355
6	10	3	60	600	382
7	6	3	80	600	398
8	6	1	60	600	378
9	6	3	60	600	382
10	6	3	60	600	376
11	6	3	60	600	375
12	6	5	60	600	361
13	8	2	50	800	365
14	8	2	50	400	359
15	6	3	60	600	370
16	6	3	60	200	374
17	4	4	50	400	332
18	2	3	60	600	350
19	4	2	50	800	351
20	8	4	70	800	380
21	6	3	60	600	367
22	6	3	60	1000	351
23	6	3	60	600	371
24	4	4	50	800	317
25	6	3	60	600	366
26	4	2	70	800	383
27	4	2	70	400	386
28	8	2	70	800	387
29	4	4	70	800	362
30	4	4	70	400	387
31	4	2	50	400	355

### 3 Results and Discussion

In order to analyze the results for the experimental observation, an analysis of variance (ANOVA) technique was used. Thereafter, to obtain a multivariable regression equation, regression analysis was performed. The developed model was verified by comparing the  $p$ -value (at 95% confidence interval) for the adequacy of the model. ANOVA is a statistical analysis tool for obtaining the contribution of process parameters on output responses. To assess the significance of created regression model, lack of fit, model terms, and coefficients, an ANOVA test has been conducted and the results are given in Table 4. The F-value of the model is found to be 43.11 indicating that the F values are statistically significant and that the data fits into them adequately. For further investigation, the lack of fit must be insignificant. The  $p$ -value for lack of fit is 0.8986 indicating that the lack of fit is not significant. The significant term that affects the kerf width of AZ-31 was found to be servo voltage (SV), pulse-on duration ( $T_{on}$ ), wire tension (WT), and wire feed rate (WFR). Furthermore, the interaction between the parameters is found significant for ( $T_{on}$ )  $\times$  (WFR), (WFR)  $\times$  (SV), (WT)  $\times$  (SV), and (WFR)  $\times$  (WT). In Table 4, Adeq Precision is a measure of the signal-to-noise ratio which comes out to 27.3546, which is greater than 4, which indicates the model fitted significantly. The coefficient of variation (C.V.) represents the variation in the data, which comes out to be 1.21%.

Furthermore, a statistical model is developed using regression analysis, and the regression equation developed for predicting and analyzing the effect of process parameters on kerf width is given by Eq. (5).

$$\begin{aligned}
 \text{Kerf width} = & 174.1 + 5.98(T_{on}) - 22.75(\text{WFR}) + 3.81(\text{SV}) + 0.1683(\text{WT}) \\
 & - 0.368(T_{on} \times T_{on}) - 0.597(\text{WFR} \times \text{WFR}) \\
 & - 0.01722(\text{SV} \times \text{SV}) - 0.000059(\text{WT} \times \text{WT}) \\
 & + 1.594(T_{on} \times \text{WFR}) - 0.0531(T_{on} \times \text{SV}) \\
 & + 0.00109(T_{on} \times \text{WT}) + 0.381(\text{WFR} \times \text{SV}) \\
 & - 0.01969(\text{WFR} \times \text{WT}) - 0.001219(\text{SV} \times \text{WT}) \quad (5)
 \end{aligned}$$

The main effect plot for kerf width as a response is obtained as shown in Fig. 3. It is observed from the main effect plot that with an increase in  $T_{on}$ , kerf width of magnesium alloy increases. This is due to the reason that with an increase in  $T_{on}$ , discharge energy increases that leads to more ionization in the working gap which increases the number of electrons that impacts the workpiece surface leading to a generation of greater kerf width. It is also observed that with an increase in wire feed rate, the kerf width of magnesium alloy shows a decreasing trend. This is due to the reason that with increasing wire feed rate, the amplitude of wire vibration in the direction perpendicular to the cutting motion decreases, so kerf width decreases. With an increase in servo voltage, the kerf width of magnesium alloy increases. This is due to the reason that with an increase in servo voltage, the specific discharge energy increases and the material removal takes place with higher crater depth, so kerf width

**Table 4** ANOVA table for kerf width of AZ-31 magnesium alloy

Source	Sum of squares	Degree of freedom	Mean square	F-value	P-value	
Model	12,031.81	14	859.41	43.11	< 0.0001	Significant
$T_{on}$	1395.38	1	1395.38	70.00	< 0.0001	
WFR	782.04	1	782.04	39.23	< 0.0001	
SV	8103.37	1	8103.37	406.48	< 0.0001	
WT	737.04	1	737.04	36.97	< 0.0001	
$T_{on} \times$ WFR	162.56	1	162.56	8.15	0.0114	
$T_{on} \times$ SV	18.06	1	18.06	0.9061	0.3553	
$T_{on} \times$ WT	3.06	1	3.06	0.1536	0.7003	
WFR $\times$ SV	232.56	1	232.56	11.67	0.0035	
WFR $\times$ WT	248.06	1	248.06	12.44	0.0028	
SV $\times$ WT	95.06	1	95.06	4.77	0.0442	
$T_{on} \times T_{on}$	61.94	1	61.94	3.11	0.0970	
WFR $\times$ WFR	10.18	1	10.18	1.5108	0.4851	
SV $\times$ SV	84.77	1	84.77	4.25	0.0492	
WT $\times$ WT	157.48	1	157.48	7.90	0.0126	
Residual	318.96	16	19.94			
Lack of fit	129.25	10	12.93	0.4088	0.8986	Not significant
Pure error	189.71	6	31.62			
Core. total	12,350.77	30				
<i>Fit statistics</i>						
Std. dev	4.46	$R^2$	0.9742			
Mean	367.68	Adjusted $R^2$	0.9516			
C.V. %	1.21	Predicted $R^2$	0.9188			
Adeq precision						27.3546

increases. From Fig. 3, it was also observed that an increase in wire tension kerf width of magnesium alloy shows a decreasing trend. The reason for the behavior is due to fact that increased tension in the wire electrode reduces mechanical vibrations in the wire. So, the amplitude of wire vibration in the direction perpendicular to the cutting motion decreases with increases in wire tension; hence, kerf width decreases.

Figure 4 shows the percentage contribution of the significant process parameters on the kerf width of AZ-31. The most contributing factor in regression model is servo voltage (65.61%), followed by pulse-on duration (11.3%), wire feed rate (6.33%), wire tension (5.967%), interaction term of wire feed rate and wire tension (2%), interaction term of wire feed and servo voltage (1.88%), error (1.54%), square of

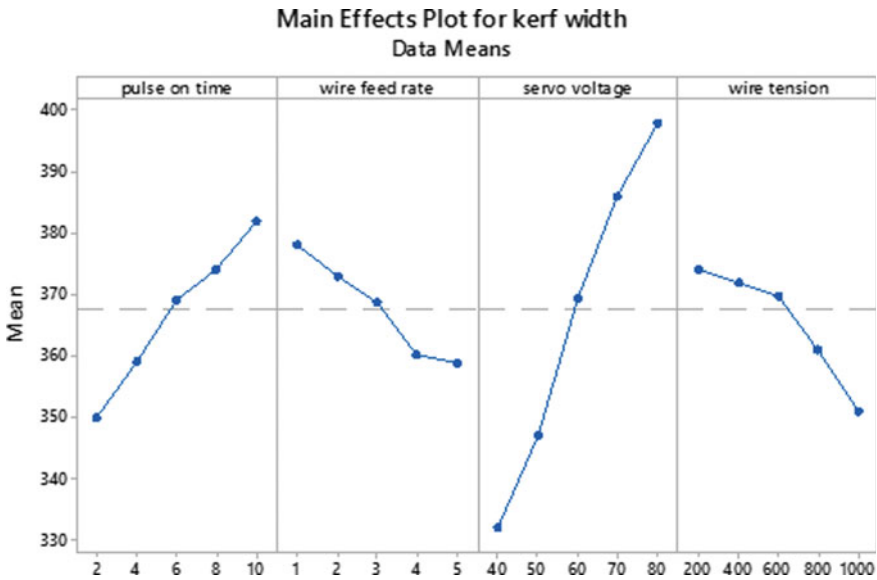


Fig. 3 Main effect plot of process parameters for kerf width

wire tension (1.27%), interaction term of servo voltage and wire tension (0.769%), and square of wire tension (0.6863%).

Figure 5 illustrates the surface plot for the significant interaction terms. Figure 5a shows that the minimum value of the kerf width is obtained for a low pulse-on duration and increased wire feed rate. An increase in pulse-on duration and the

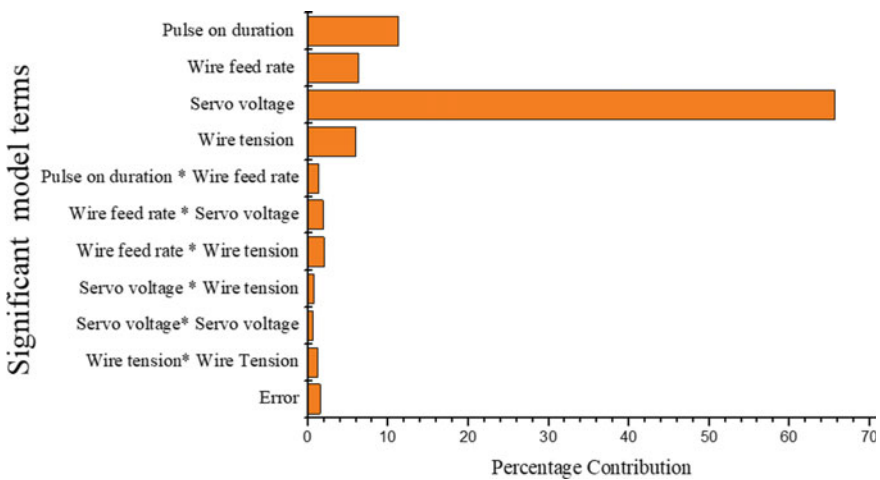


Fig. 4 Bar graph of percentage contribution of significant model term for kerf width

decreased pulse-on time can increase the kerf width to a certain extent, and thereafter, it becomes constant. The surface plot as shown in Fig. 5b illustrates that a low servo voltage and a high feed rate are required to achieve a low value of the kerf width. The wire tension reduces the vibration; hence, an increased wire tension and a low servo voltage will provide a low kerf width or an increased accuracy of cut as shown in Fig. 5c. Figure 5d illustrates that a high wire tension and a high wire feed rate provide a more accurate cut. But, an increased wire tension leads to frequent wire breakage, and an increased wire feed rate increases the cost of machining. Hence, a thoughtful selection of parameters is required during the machining of AZ-31 alloy using wire EDM.

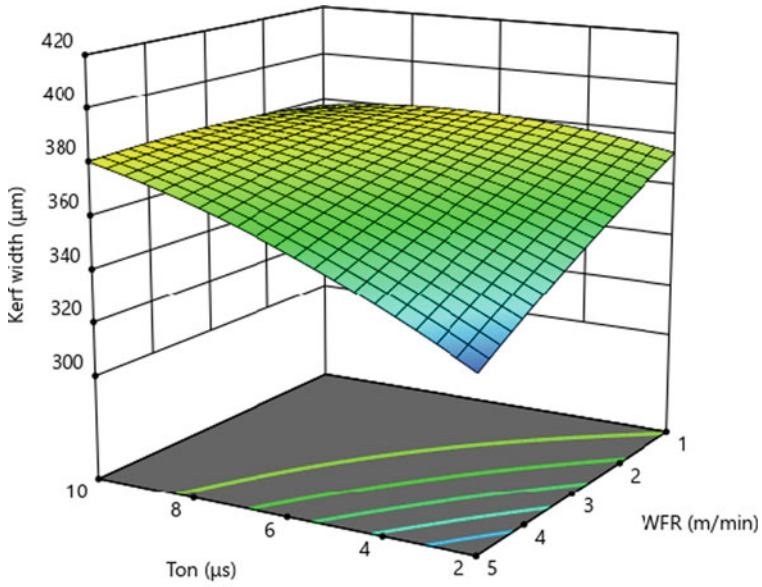
## 4 Future Scope of Research

- In the present investigation, only four process parameters, i.e., pulse-on duration, servo voltage, wire feed rate, and wire mechanical tension on kerf width were studied. Some other process parameters like pulse-off duration, peak current, flushing pressure, etc., could also be considered to investigate the effect of input process parameters.
- Similar kinds of investigations could also be made to investigate some other machining responses like micro hardness, heat affected zone, surface roughness, recast layer thickness, etc. Further, similar kinds of investigations could also be made on different biomaterials like titanium, magnesium alloys, etc.

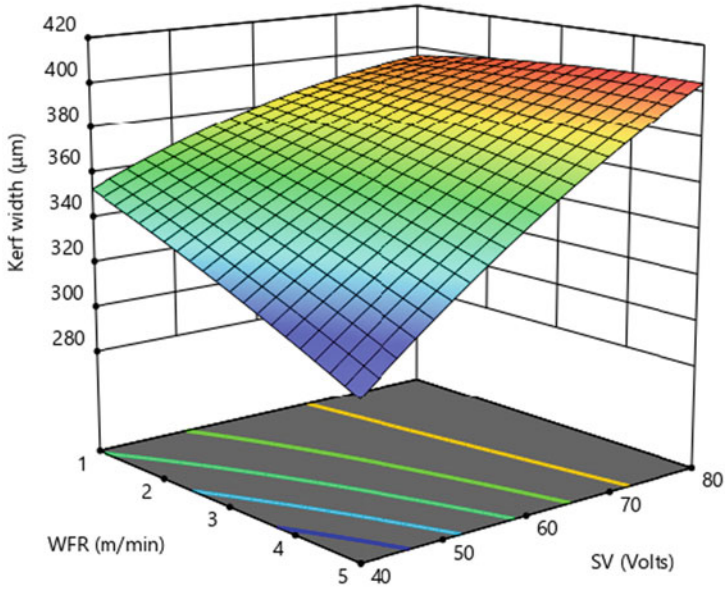
## 5 Conclusions

In this paper, experiments have been carried out to identify the effect of process parameters such as  $T_{on}$ , SV, WFR, and WT on kerf width for AZ-31 alloy. Experimental results were statistically analyzed to find out the significant factors affecting kerf width. Based on the present work, the following conclusions are drawn:

- Kerf width for AZ-31 alloy always increases with an increase in  $T_{on}$  and SV, whereas it decreases with an increase in WFR and WT.
- The developed regression model indicates that SV was the most influencing parameter followed by  $T_{on}$ , WFR, and WT.
- The developed regression model is used to draw the surface plots for the interaction between the process parameters, and considering the production time and cost, a judicious selection of process parameters can be made.

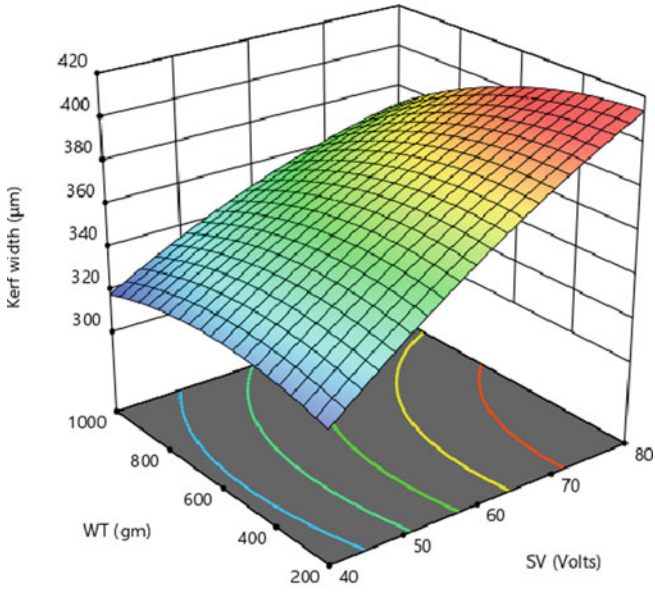


a)

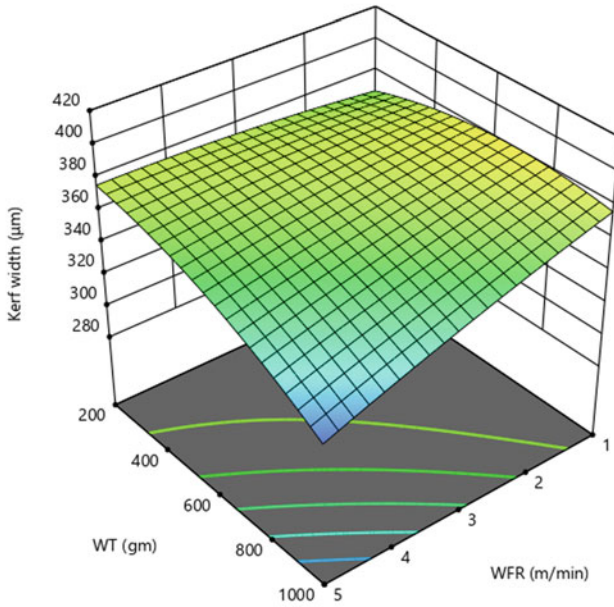


b)

**Fig. 5** 3-Dimensional surface plot of kerf width for **a** pulse-on duration ( $T_{on}$ ) and wire feed rate, **b** wire feed rate and servo voltage, **c** wire tension and servo voltage, and **d** wire tension and wire feed rate



c)



d)

Fig. 5 (continued)



## References

1. Karunakaran R, Ortgies S, Tamayol A, Bobaru F, Sealy MP (2020) Additive manufacturing of magnesium alloys. *Bioact Mater* 5(1):44–54
2. Kamrani S, Fleck C (2019) Biodegradable magnesium alloys as temporary orthopaedic implants: a review. *Biomaterials* 32(2):185–193
3. Serge A, Walton D (1992) Machining of composite materials II. *Compos Manuf* 2(2):85–94
4. Prasad AVSR, Ramji K, Datta GL (2014) An experimental study of wire EDM on Ti-6Al-4V alloy. *Procedia Mater Sci* 5:2567–2576
5. Sathish T, Mohanavel V, Ansari K, Saravanan R (2021) Synthesis and characterization of mechanical properties and wire cut EDM process parameters analysis in AZ61 magnesium alloy+ B4C+ SiC
6. Chaudhary T, Siddiquee AN, Chanda AK (2019) Effect of wire tension on different output responses during wire electric discharge machining on AISI 304 stainless steel. *Def Technol* 15(4):541–544
7. Sharma N, Khanna R, Gupta R (2013) Multi quality characteristics of WEDM process parameters with RSM. *Procedia Eng* 64:710–719
8. Alias A, Abdullah B, Abbas NM (2012) Influence of machine feed rate in WEDM of Titanium Ti-6Al-4V with constant current (6A) using brass wire. *Procedia Eng* 41:1806–1811
9. Klocke F, Welling D, Klink A, Veselovac D, Nöthe T, Perez R (2014) Evaluation of advanced wire-EDM capabilities for the manufacture of fir tree slots in inconel 718. *Procedia CIRP* 14:430–435
10. Tosun N (2003) The effect of the cutting parameters on performance of WEDM. *KSME Int J* 17(6):816–824
11. Khan B, Davis R, Singh A (2019) Effect of input variables and cryogenic treatment in wire electric discharge machining of Ti-6Al-4V alloy for biomedical applications. *Mater Today Proc* 27:2503–2507
12. Ramamurthy A, Sivaramakrishnan R, Muthuramalingam T, Venugopal S (2015) Performance analysis of wire electrodes on machining Ti-6Al-4V alloy using electrical discharge machining process. *Mach Sci Technol* 19(4):577–592
13. Razak MA, Abdul-Rani AM, Rao TVVLN, Pedapati SR, Kamal S (2016) Electrical discharge machining on biodegradable AZ31 magnesium alloy using Taguchi method. *Procedia Eng.* 148:916–922
14. Tosun N, Cogun C (2003) Analysis of wire erosion and workpiece surface roughness in wire electrical discharge machining. *Proc Inst Mech Eng Part B J Eng Manuf* 217(5):633–642
15. Nain SS, Sihag P, Luthra S (2018) Performance evaluation of fuzzy-logic and BP-ANN methods for WEDM of aeronautics super alloy. *MethodsX* 5:890–908
16. Mandal K, Sarkar S, Mitra S, Bose D (2019) *Innovation in materials science and engineering*. Springer, Singapore
17. Montgomery DC (2013) *Design and analysis of experiments*, 8th edn., vol 48, no. 1. Wiley

# Barriers to Healthcare Waste Management: A QFD Strategy



Abhishek Raj and Cherian Samuel

**Abstract** One of the most critical aspects of sustainability is healthcare waste management. Waste increases at a high rate as the population and healthcare services grow. As a result, proper healthcare waste treatment is increasingly vital for the environment's and people's safety. Healthcare waste management (HCWM) necessitates efficient waste collection and segregation for proper disposal. The article outlines a method for identifying the concerns and challenges that the healthcare industry has regarding the treatment and management of healthcare waste. A survey was conducted, and quality function deployment was used to analyze the results. The research reveals various elements that impact the healthcare waste management. This study will produce a report that will assist stakeholders in implementing healthcare waste management.

**Keywords** Healthcare waste management · QFD · India

## 1 Introduction

As we all know, healthcare waste is a rapidly expanding waste in the world. Healthcare waste is being driven by several pandemics and a growing number of hospitals. The proper handling of healthcare waste necessitates cost-effective, ecologically benign methods. The most important aspect of hospital waste management is collection and segregation. Because many healthcare wastes are nonhazardous, adequate segregation is required to save high treatment costs. Healthcare waste is a problem in both developing and rich countries. Following a literature review, it was determined that healthcare waste management is a critical issue for all sorts of countries and that its disposal is a complex undertaking. Healthcare waste management is difficult for healthcare companies.

---

A. Raj (✉) · C. Samuel

Mechanical Engineering Department, IIT Varanasi (Banaras Hindu University), Varanasi, India  
e-mail: [abhishekraj.rs.mec17@itbhu.ac.in](mailto:abhishekraj.rs.mec17@itbhu.ac.in)

However, a detailed study on HCWM obstacles is sparse for underdeveloped countries like India. Various constraints and problems that are roadblocks to adopting proper healthcare waste management are identified in this research. Using the two parameters, a QFD analysis was performed to identify the significant flaws in the supply chain structure. The parameters that will assist the authorities in efficiently implementing the law have also been prioritized in the analysis. The best way for converting customer requirements into a technological design that enhances healthcare waste management service quality and meets customers want to use quality function deployment (QFD) [1, 2].

## 2 Research Background

### 2.1 Healthcare Waste

Every country's healthcare waste management is constantly a hot topic of discussion. Even though it is a critical issue, it receives little attention in some countries. There are severe concerns with the lack of waste management methods, transparent regulations, proper knowledge and awareness, strict regulation, and sufficient finances [3]. International trade agreements must increase economic gains, but they are not as beneficial in terms of health [4]. In India, garbage creation ranges from 0.5 to 2 kg per bed and per day, with a total of 0.33 million tons per year, this is a massive amount of rubbish that must be managed carefully [5]. There are about six lakh hospital beds, twenty-three thousand Health Centers, and registered nursing homes in India. Many health centers are involved in every part of metropolitan and semi-urban areas, and some hospitals and dispensaries are not registered [6]. An increase in population also contributes to a higher likelihood of disease outbreaks. Open dumping and poorly built landfills are the most common disposal and treatment methods employed in underdeveloped countries, posing health and societal risks. The lack of consciousness and general alertness is a severe obstacle [7].

### 2.2 HCWM in Various Countries

Since the first act was passed, China has paid less attention to waste management act 380. The centralization of trash removal is required under this act [8]. Proper segregation of waste is unavoidable, and if there is a failure in parting, it will be highlighted by the healthcare waste pointers [9]. If workers are not adequately trained, they will not see the importance of the exercise code, and there will always be a risk of death to workers, patients, and others [10]. Jakarta, one of Indonesia's capitals, suffers from the NIMBY (Not in My Backyard). By 2020, most existing and potential landfill sites will be complete [11].

A study on healthcare waste management was conducted in Ghanaian hospitals. The findings show that healthcare personnel in private hospitals are more knowledgeable about healthcare waste and disposal materials than those in government and semi-government hospitals (Stephen et al. 2020). This research presents a set of indicators for evaluating HCWM in developing cities. The proposed indicator can be used by government agencies and hospitals to examine the HCWM system and identify common roadblocks (Navarro et al. 2020). Many countries have previously enacted rigorous restrictions regarding the disposal of medical waste. However, there are still several obstacles and issues that prevent the proper disposal of healthcare waste. Hospital employees must also receive proper training and be aware of their surroundings. India is classified as a developing country. Due to unequal resource allocation, poor infrastructure, and high healthcare costs, there is inequality in access to healthcare services in India. Because safe disposal of healthcare waste is a difficult task, healthcare waste management has gotten a lot of attention since the Biomedical Waste Management and Handling Rules were implemented in 1998. In India, garbage creation ranges from 0.5 to 2 kg per bed and per day, with a total of 0.33 million tons per year; this is a massive amount of rubbish that must be managed carefully (Patil et al. 2001). There are about six lakh hospital beds, twenty-three thousand Health Centers, and registered nursing homes in India. Many hospitals and dispensaries are unregistered, and health clinics can be found in every corner of urban and semi-urban areas [6]. An increase in population also contributes to a higher likelihood of disease outbreaks. The barriers were identified using a literature study of publications published in various journals over the previous years and expert opinion. Only articles that have been peer-reviewed have been targeted.

### 3 Research Methods

Quality Function Deployment (QFD) is a tool used in Total Quality Management (TQM) to develop customers' demands and expectations systematically. Mitsubishi developed QFD for shipbuilding requirements in the late 1960s and early 1970s. QFD is a method for translating a customer's voice into technical needs in an organized manner. The QFD process is driven by the "voice of the customer"; hence, the process starts with recording the "voice of the customer." The quality department is not the only place where QFD is used. It is a handy tool for everyone (Fig. 1).

### 4 Application of Research Methods

The HOQ matrix is used to apply QFD in this investigation.

"What's" is presented by HOQ as client feedback, while "How's" is presented as technical requirements for "What's" (Fig. 2).

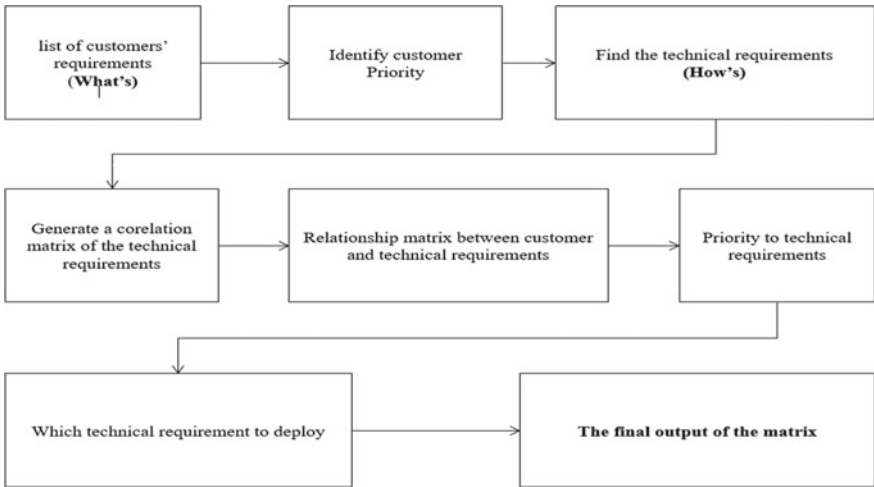


Fig. 1 Flow chart of QFD

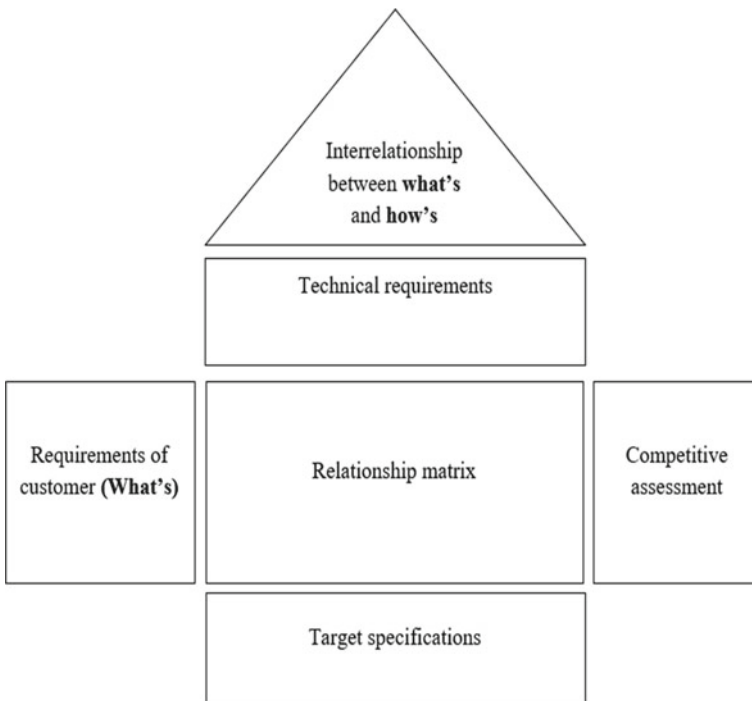


Fig. 2 HOQ. Source Akao [12]

The steps to use the HOQ tool are as follows.

- Compile a list of consumers’ spoken and unspoken wants (What’s)
- Determine which customers are the most important.
- Determine the technical specifications (How’s).
- Create a matrix of correlations.
- Create a matrix of relationships.
- Prioritize the technological specifications.
- Determine which technological requirement should be implemented.

The application of QFD in the healthcare waste management sector is performed for the first time, as far as we know. This study found customers’ requirements by using the QFD technique.

**Step 1: Make the set of customer requirements (What’s)**

In this step, the customer requirements, known as the “voice of the customers,” are identified and defined as the “what’s” in the HOQ matrix. 4 experts participated, including two from Government hospitals and two from private hospitals. All of the experts have more than 20 years of experience in the healthcare sector. To identify the customers’ requirements and improve the quality of healthcare waste management services, this group will help. For further information, the group was contacted through phone and email.

**Step 2: Find customer priority**

The customers were asked to fill the questionnaire using a standard five-point Likert scale with five assigned as the Highest Priority and one as the lowest priority. Customer priority will be placed on the right-hand side of the customer requirements (Table 1).

**Table 1** Customer Priority List

User’s need (what’s)	User importance (1–5; 5 = highest importance)
Easy segregation and collection of waste	5
Low disposal cost of waste	5
No harmful effects of waste	4
Recycling of waste	2
Neat and clean hospital	4
Awareness of employees regarding healthcare waste	3
Less quantity of waste	3

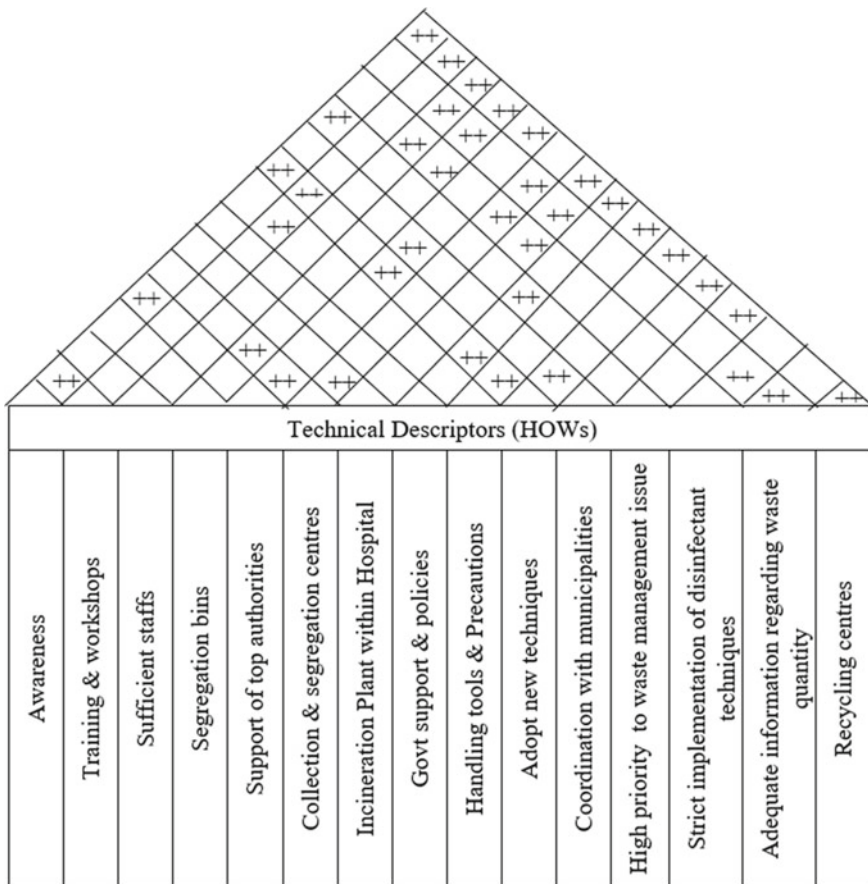
**Step 3: Find the technical requirements (How's)**

The technical requirements are assigned at the top of the HOQ, known as the “How's” of the HOQ [2]. ISM is used to find the technical requirements. “How's” describes how the organization will meet the customer requirements.

**Step 4: Generate a correlation matrix of the technical requirements**

By using the symbols: ++ for (strong positive); + for (positive); -- for (strong negative); and - for (negative) [2]. It represents those technical requirements that have a significant impact on the result (Fig. 3).

**Step 5: Generation of a relationship matrix**



**Fig. 3** Correlation matrix

This step will find how the how's are related to what's. The symbols which are used in this study are:  $\odot = 9$  (strong relation);  $O = 3$  (medium relation);  $\Delta = 1$  (weak relations); and if there is no relationship, we will use blank cells for that.

Step 6: Give priority to the technical requirements

The relative priority of the technical requirements is found through the technical priority matrix.

Step 7: Find which technical requirement to deploy

Using this step, the organization can find the strategic goals by considering the requirements.

## 5 Results

The design requirements are identified using these barriers. A five-point Likert scale was used to determine the priority of each criterion among customers. The interrelationships between technical and customer needs were mapped out in a correlation matrix. Implementing QFD allows for the selection of key activities to meet the needs of the healthcare waste management sector, and it tends to improve residents' quality of life. The healthcare sector requires continuous improvement since it improves internal and external elements.

## 6 Discussion

Presently, healthcare waste management is one of the most complex issues. So, proper implementation of waste management is necessary to make the atmosphere less polluted. During this study, many barriers were identified. These barriers are the main obstacles in implementing healthcare waste management. Top authorities must be supportive, and there must be some good policies of the government which promote proper management of healthcare waste. There must be some training and awareness programs organized at the hospital level to enhance the knowledge of workers and staff. Healthcare waste management must be on the priority list of all the hospitals so that enough numbers of employees must be assigned for the management of waste correctly. This study gives a unique insight into healthcare waste management service quality. QFD is a modified approach that can be used to enhance service quality. This study proposes new ideas for determining which aspects have the most impact on customer satisfaction. There are certain drawbacks to this study. These impediments have essential repercussions for persons and society. Hence, their removal is required to implement healthcare waste management properly. These hurdles must aid lawmakers, and hospital administrators in developing



policies that benefit persons and society. The barriers to the healthcare waste management sector, which we identified, are the leading barriers supported by various studies (Ranjan et al. 2020) [5, 6]. The barriers to implementing healthcare waste management in India are similar to that of most other developing nations, identified by several research [3, 10].

## 7 Conclusions

Government support and policies, awareness, training and workshops, high importance to waste management, and assistance of top authorities are all design needs with higher weights than others, as shown in Fig. 4. Because these issues have a significant impact on people and society, proper implementation of healthcare waste management necessitates consideration. These elements must be relevant to politicians and hospital administrators for policies beneficial to people and society. Our research is timely and has practical ramifications, according to us.

This research provides a unique perspective on the quality of healthcare waste management services. QFD is a modified strategy that can improve the quality of service. This study proposes a new way of determining which aspects have the most impact on customer happiness. In the future, QFD can be combined with other approaches such as AHP to solve data structures and perform requirement prioritizing.

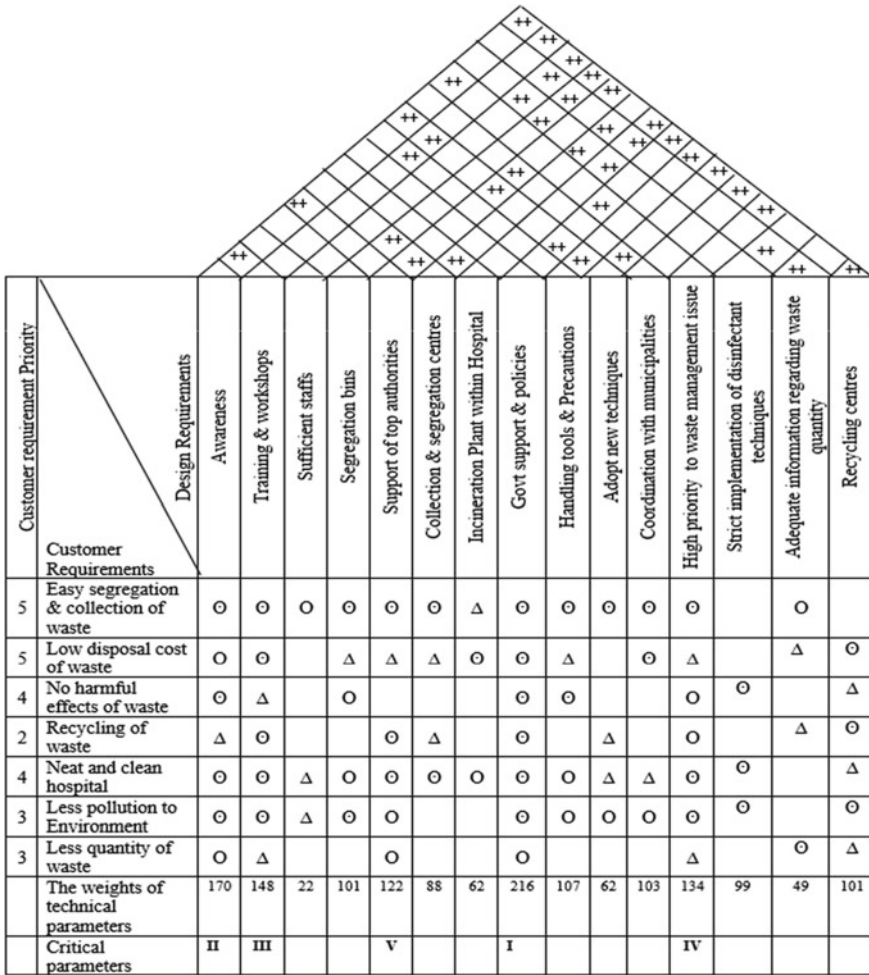


Fig. 4 House of quality

References

1. Cauchick Miguel PA (2005) Evidence of QFD best practices for product development: a multiple case study. *Int J Qual Reliab Manage* 22(1):72–82
2. Hussain M, Tsironis L, Ajmal MM (2011) A QFD strategy for improving customer satisfaction: case study of telecom companies of Pakistan. *Asian J Qual* 12(3):282–295
3. Khan BA, Cheng L, Khan AA, Ahmed H (2019) Healthcare waste management in Asian developing countries: a mini review. *Waste Manage Res* 37(9):863–875
4. Birnbaum D (2016) Have international trade agreements been good for your health? *Int J Health Gov* 21(2):47–50
5. Patil AD, Shekdar AV (2001) Healthcare waste management in India. *J Environ Manage* 63(2):211–220

6. Swain S, Muduli K, Biswal JN, Tripathy S, Panda TK (2017) Evaluation of barriers of health care waste management in India—a gray relational analysis approach. In: Satapathy SC, Bhateja V, Udgata SK, Pattnaik PK (eds) Proceedings of the 5th international conference on frontiers in intelligent computing: theory and applications. Springer, Singapore, pp 181–188
7. Mmereki D, Baldwin A, Li B, Liu M (2017) Healthcare waste management in Botswana: storage, collection, treatment and disposal system. *J Mater Cycles Waste Manage* 19(1):351–365
8. Yong Z, Gang X, Guanxing W, Tao Z, Dawei J (2009) Medical waste management in China: a case study of Nanjing. *Waste Manage* 29(4):1376–1382
9. Delmonico DVDG, Santos HHD, Pinheiro MA, de Castro R, de Souza RM (2018) Waste management barriers in developing country hospitals: case study and AHP analysis. *Waste Manage Res* 36(1):48–58
10. Mbongwe B, Mmereki BT, Magashula A (2008) Healthcare waste management: current practices in selected healthcare facilities, Botswana. *Waste Manage* 28(1):226–233
11. Chaerul M, Tanaka M, Shekdar AV (2008) A system dynamics approach for hospital waste management. *Waste Manage* 28(2):442–449
12. Akao Y (1990) History of quality function deployment in Japan. In: *The best on quality: targets, improvement, systems*, pp 183–196
13. Sharma HB, Vanapalli KR, Cheela VS, Ranjan VP, Jaglan AK, Dubey B, ... Bhattacharya J (2020) Challenges, opportunities, and innovations for effective solid waste management during and post COVID-19 pandemic. *Resour conserv recycl* 162:105052
14. Ferronato N, Ragazzi M, Torrez Elias MS, Gorrity Portillo MA, Guisbert Lizarazu EG, Torretta V (2020) Application of healthcare waste indicators for assessing infectious waste management in Bolivia. *Waste Manage Res* 38(1):4–18
15. Odonkor ST, Mahami T (2020) Healthcare waste management in Ghanaian hospitals: Associated public health and environmental challenges. *Waste Manage Res* 38(8):831–839

# Interference Fringe-Based Metrology for Industrial Applications



Pavan Kumar Asundi and R. Deepa

**Abstract** Optical 3D scanners have become widely used metrological tool for rapidly capturing dense 3D models of objects. The contact-based measurement techniques offer high accuracy but are hindered by the operational speed and ease of operation. The optic-based metrology, a non-contact approach, is an alternative which would offer reliable accuracy with high data acquisition rate. Interference property of light is one of the tools extensively used in optic-based metrology to derive measurements. In interference-based optical metrology, the resultant fringes which are a band of light intensity are analyzed by an optical transfer function which yields the 2D and 3D data. An extension of fringe frequency principle is digital fringe projection technique where fringes are digitally generated and illuminated on the component and the deformed fringes are analyzed by transfer functions to draw the 3D measurements. This article would brief sinusoidal fringe-based measurement techniques.

**Keywords** Optical metrology · Interference fringe · Digital fringe projection · Triangulation

## 1 Introduction

In conventional contact-based metrology, the duration for the scan of component is high and portability of equipments is a tedious task. The optic-based measurements, a non-contact technique, provide ease of operation and mobility. Optic-based metrology is an application of geometric and wave nature of light.

The fringes, the resultant of wave nature of the light, are formed by superposition of waves. Correlating the intensity of the fringe pattern, measurements can be derived. The fringes are resultant of either by interference or by the diffraction phenomena [1, 2]. In this article, measurement based on fringes obtained from interference phenomena is viewed.

---

P. K. Asundi (✉) · R. Deepa  
Central Manufacturing Technology Institute, Bengaluru, India  
e-mail: [pavankumar.svm@gmail.com](mailto:pavankumar.svm@gmail.com)

The conventional interferometer is employed for determination of surface topography, optical flatness, refractive index and dimension measurements. The analysis of the fringe pattern by path difference and phase shift analogies derives the dimensional data.

The 3D topographic measurements can be obtained by the fringes' interference principle and the spatial domain analysis. Fringes carry information about the object's depth, which can be retrieved through phase shifting algorithm and the point spread function. These techniques are employed by few devices like vertical scanning interferometer, phase shift interferometer, etc. [3–5].

The interferometer for topographic measurement relies on the wave properties of light. During the measurement iterations, interferometer separates the source light into two independent paths, one of which falls on reference surface and the other on the object surface. The separated light beam is recombined and is directed to a digital camera which captures the intensity pattern (fringe pattern). The intensity pattern is highly sensitive to the differences in path lengths of reference arm and measurement arm. Efficient comparison of the fringe pattern of object surface with the reference surface retrieves the nanometer resolutions [6–9].

Measurement based on interferometry is sought only for components having a reflective surface and are of dimensions in few millimeters. The digital fringe projection technique, which involves digitally generated fringe pattern, caters to components with non-reflective surface with higher dimensions [4, 10].

In digital fringe projection (DFP), sinusoidal fringe pattern of desired frequency and bandwidth are generated and impinged on the component to derive the measurements. The DFP system consists of projector to project the desired pattern, camera to capture the fringe pattern and the PC for the computation [10].

Section 2 discusses about the 2D measurements derived from interference fringes, and Sect. 3 describes about the 3D profile measurement techniques involving the principle of interference and spatial fringe analysis. Section 4 describes about the DFP technique, and Sect. 5 draws the conclusion.

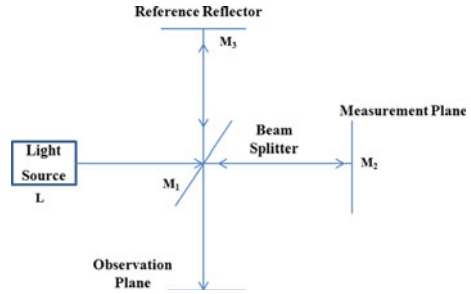
## 2 2D Measurements

In this section principle of interference, 2D measurements and form analysis by fringes are discussed.

### 2.1 *Linear Measurements*

Michelson employed the principle of interference to measure the distance between the sun and the earth and employed the same to measure the object dimension [1]. The construction of Michelson interferometer is described in Fig. 1.

**Fig. 1** Michelson interferometer



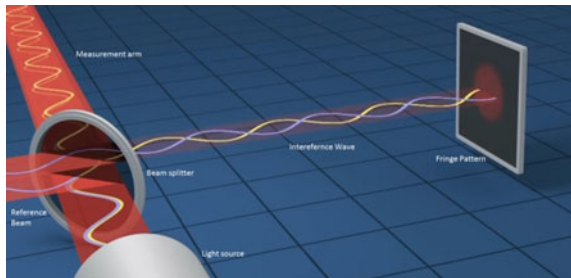
The Michelson interferometer setup consists of a light source  $L$  and a beam splitter  $M1$  which is a semi-silvered glass plate. The reference reflector  $M3$  is perfect reflecting mirror placed at a known distance. Measurement plane  $M2$  consists of plane mirror placed normal to light source, at the unknown distance, whose distance to be found out. At the observation plane, generated fringe patterns are analyzed. Light from the source gets split at beam splitter  $M1$ , where splitter partially reflects beam toward  $M3$  and transmits the rest toward measurement plane  $M2$ , which is placed normal to the beam splitter. The  $M1$  recombines the reflected rays from  $M2$  and  $M3$  and directs the resultant wave to observation plane. The resultant fringes seen at observation plane are generated by the superposition of light waves at  $M1$ . When the path difference of light waves is in even harmonics, constructive interference occurs. When the path difference of light waves is in odd harmonics, destructive interference occurs. These alternative harmonics generate bright and dark band of fringes as shown in Fig. 2. Figures 3 and 4 describe the path difference variation on intensity of the fringe pattern.

Michelson working module is based on the amplitude division of wavefronts, which would measure small wavefront deformations with a high accuracy, in the order

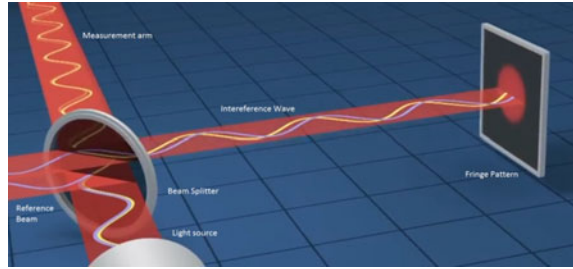
**Fig. 2** Fringe pattern



**Fig. 3** Resultant intensity due to odd harmonic



**Fig. 4** Resultant intensity due to even harmonic



of a fraction of the wavelength. For linear measurements of optics using Michelson setup, the fringe patterns are first observed at reference state. The test object, whose dimension to be measured, is introduced in the measurement arm, and the deflection in the fringe pattern is observed. To counter the fringe deflections and to obtain the fringe pattern similar at reference state, the reference plane is translated. The displaced units are noted, and the dimension is determined using Eq. (1) [6, 9].

$$\text{Length} = (\text{Displacement of Reference plane}) / (\text{Refractive Index of object}) \quad (1)$$

The Michelson setup can measure only one dimension of a component at a given instance.

The accuracy of an interferometer depends on factors, such as the optical quality of the components, the measuring methods, the light source properties and external factors, such as ambient lighting and mechanical vibrations.

## 2.2 Form Analysis

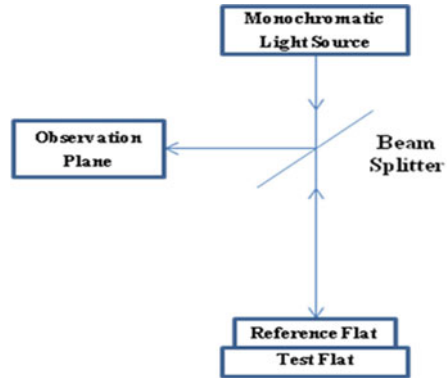
To check the optical flatness and to analyze topographic form, Fizeau interferometer is preferred as the fringes obtained in this setup are of equal thickness, equal inclination and uniform intensity distribution [7]. Fizeau setup is as shown in Fig. 5.

Fizeau setup is equipped with a collimated monochromatic light source which provides normal incidence. Fringes obtained in this setup are centered normally at observation plane, which is the reason for equal inclination. Since the optical paths of reference and observation plane are comparable, deviation in fringe intensity is easily noticeable.

An optical flat is an ideal reference with flat reflecting surface, made of quartz or pyrex which produces plane wavefront at optimized wavelength [11, 12]. Fizeau setup employs a reference flat, as the interference fringe makes it possible to accurately compare the flatness of test object with reference optical flat.

The optical flatness is dimensionless, but inferred with respect to the operating wavelength. Numerical value of optical flatness is calculated using Eq. (2) [4, 11].

**Fig. 5** Construction of Fizeau interferometer



$$\text{Optical Flatness} = (k * \lambda)/(2dt) \tag{2}$$

where

$k$  is the fringe deviation,

$d$  is the distance between the two fringe,

$\lambda$  is the operating wavelength,

$t$  is the thickness of object.

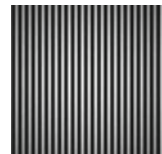
Roughness  $R_a$  can be measured by accessing the fringe intensity described by Eq. (3) [7].

$$R_a = \lambda/(4\pi) * \sqrt{(\ln((\text{Max} + \text{Min})/(\text{Max} - \text{Min})))} \tag{3}$$

Max and Min correspond to maximum and minimum fringe intensities.

Another advantage of Fizeau setup is Fizeau fringe depicts variation based on the topographic changes of the optics, and hence, it is employed to check the concave/convex feature or any surface deformation present in the optics. If the workpiece is flat and parallel to the base plate, the fringe pattern will be uniform, parallel and equally spaced as shown in Fig. 6. When the workpiece is flat with non-uniform thickness, fringes with irregular pattern will be obtained as shown in Fig. 7. When the test piece has concave or convex surfaces, the fringes project the same deformations as the test surface as shown in Fig. 8.

**Fig. 6** Fringe pattern of uniform flat test optic

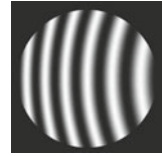




**Fig. 7** Fringe pattern of non-uniform flat test optic



**Fig. 8** Fringe pattern of convex surfaces



Fizeau interferometer is sensitive to multiple reflections; hence, stray reflection needs to be addressed for accurate results.

### 3 3D Measurements

Conventional technique to get 3D profile of the micro-structures and tools such as MEMS and micro-mirrors is by stylus profiler or by scanning probe microscopy, which involves physical contact of the probing with the component. These techniques are time consuming, and there are probabilities of component damage during the measurement process. In non-contact approach, accurate 3D profile of the components is realized by the combination of interference principle and the spatial domain transforms [8]. The sinusoidal fringes carry surface deformation information. The surface information is retrieved by subjecting the fringes to point spread function. Fourier analysis of point spread function and optical transfer function derives the phase information by the spatial analysis of the frequency to the surface variation. The depth information is retrieved from the phase relations depicted by Eq. (4).

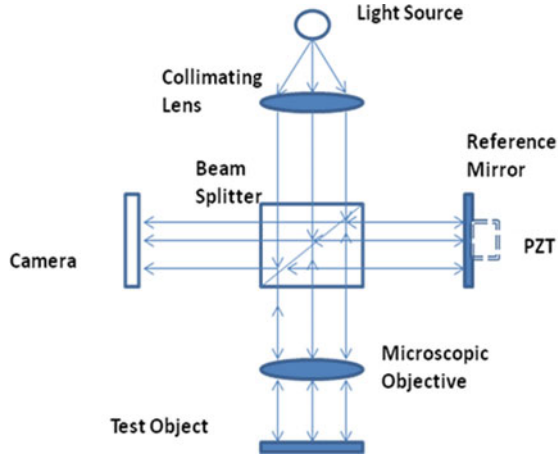
$$\text{Depth} = \lambda / (4\pi) * \text{Phase} \quad (4)$$

where

$\lambda$  is the fringe wavelength.

To derive the phase information, fringe must be of good contrast and be clearly distinguishable between sharp and blurred regions. Highly distinguishable fringes can be obtained by minimizing the stray reflection [9]. Phase shift interferometer and vertical scan interferometer are the two major derivatives of these combinations.

**Fig. 9** Phase shift interferometer



### 3.1 Phase Shift Interferometer

The phase shift interferometer (PSI) uses laser, which offers long coherence length; hence, with ease high contrast fringe patterns are obtained. Figure 9 depicts the PSI.

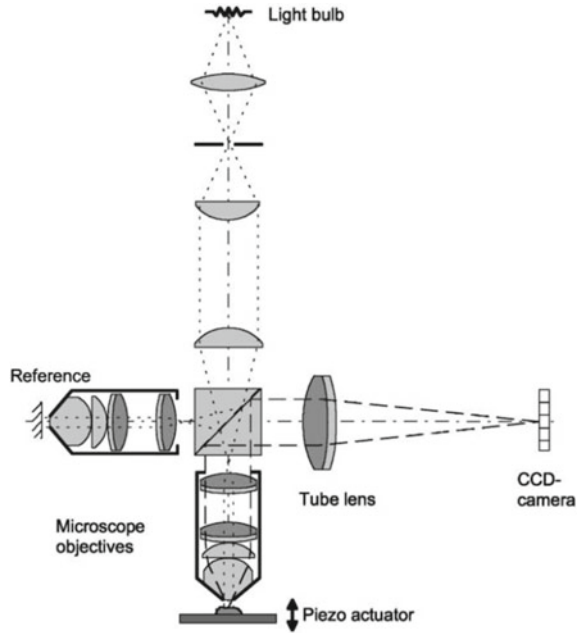
The PSI has conventional Twyman–Green interferometric setup, with the microscopic objective to achieve higher resolution and magnification. PSI reference plane is driven by piezo-electric transducer, which aids the mechanical motion of reference to achieve the desired path length to get high contrast fringes. It is embedded with high-resolution camera to capture the interferogram.

In PSI, sequence of images with controlled phase shifts of fringes is captured. The phase shift is introduced by movement of reference plane. In general, for ease of analysis, phase shift of  $\pi/2$  is introduced between successive images, which is implied by moving reference mirror by  $\lambda/8$ . The interferogram is processed using phase shifting or Fourier transform technique. The calculated phases are between  $-\pi$  and  $+\pi$ . In order to obtain the actual phases, which are directly related to the profile of the measured surface, a phase unwrapping technique is to be carried out [8, 9]. The 3D data is retrieved from the relation described by Eq. (4). PSI is suitable for components with smooth surface and has topographic transitions greater than quarter wavelength.

### 3.2 White Light Interferometer

White light interferometer (WLI) works based on coherence scanning interferometry (CSI), which considers the changes in the intensity of the fringes, obtained by superposition of multiple wavelengths. Figure 10 depicts WLI construction which has Twyman–Green setup. The illumination is sourced with incoherent high intensity

**Fig. 10** White light interferometer [5]



light. It has micro-objectives for better magnification and resolution and camera to capture the interferogram. To adjust the desired path difference, the setup is aided with piezo-actuator, which accelerates vertical displacement [5].

The resultant fringes in the CSI are formed due to the incoherent superposition of varied frequencies. WLI with low coherence light source works based on this principle. The variation in fringe frequency is due to the vertical position offset of the microscopic object and the component, hence also termed as vertical scan interferometer. The WLI offers low coherence length; hence, focus of fringe can be done at ease. The noise due to spurious interference fringes is avoided because of the low coherence length, and interference can be obtained only when the path length is within a few microns or less, thereby reducing the multiple reflections and the diffraction losses. This makes the WLI immune to ambient lighting. If spurious reflections are present, they do not form the fringe patterns due to mismatch coherence length, hence less prone to noise [3, 8]. During the scan process, intensities of fringes with coherent wavelength combine at plane of observation. From the intensity correlation and point spread function, 3D depth data is derived.

One of the hindrances of WLI is the restricted field of view, usually in few millimeters, i.e., due to choice of optics. The vertical size of the test object is restricted, and also if the lateral size increases, the number of images to be stitched also increases, resulting in hampered depth information [5]. Advantage of WLI over PSI is the parallel phase shift is encoded simultaneously on spatial position in single interferogram, whereas in case of PSI interferograms are captured sequentially [4]. Since WLI has short coherence length of source light, this evades the shading problem and

makes it suitable for analysis of surfaces with deep structural variations less than quarter wavelength [4, 5, 8].

## 4 Digital Fringe Projection

Interferometer has limitation with respect to the surface reflectivity and the dimensions. To retrieve the measurement quality at resolution of interferometer, digital fringe projection (DFP) technique is evolved, where sinusoidal fringes of desired frequencies are generated digitally and impinged on the test object. DFP technique is conglomerate of principle of sinusoidal fringes and the computer vision.

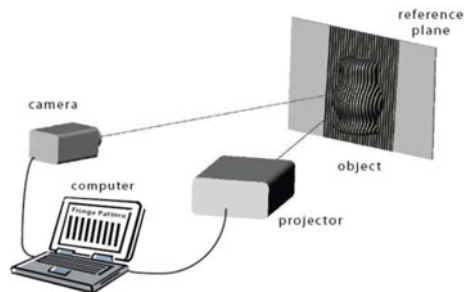
The generated fringes are projected on the surface of the object under a certain angle of incidence. The deformed pattern is observed in different orientation. The observed fringes are spatially analyzed to derive the 3D profile measurements. The DFP utilizes the spatial properties of fringes and the triangulation principle [10, 13]. The fringe projection system consists of a projector to project the pattern of desired utility on the test object, a camera to capture the fringe patterns and a computer to carry out the fringe analysis. Figure 11 depicts the fringe projection system.

Measurement through fringe projection techniques involves the following:

- Projection of a sinusoidal fringe pattern on the object.
- Recording the interferogram, obtained by the object's surface variation.
- Calculation of the phase modulation by fringe analysis techniques to obtain the phase maps.
- Unwrap the phase maps to get continuous phase distribution, proportional to the object height variations.
- Calibrate the system for mapping the unwrapped phase values to 3D coordinates.

The digital fringe patterns may be either binary coded, gray coded or color coded, whereas the conventional interference fringe pattern is sinusoidal. Since the pattern is coded, correspondences between image points and points of the projected pattern can be easily found. The decoded points can be triangulated, and 3D information is retrieved [14]. The maximum number of patterns that can be projected is the

**Fig. 11** Fringe projection system [10]



resolution in pixels of the projector device. The projector projects the fringe pattern sequentially on the object, and the camera captures these patterns. The captured images are analyzed in frequency domain to obtain the wrapped phase maps. The wrapped phase maps are discontinuous as it is generated by the arctan function; thus, unwrapping is carried out by comparing the phase at neighboring pixels to determine the fringe order and then adding or subtracting  $2\pi$  to get the continuous phase maps [15, 16]. The continuous phase maps are obtained either by spatial or by temporal unwrapping techniques. The spatial method unwraps by comparing the neighboring phase values and thus does not provide absolute phase value. Spatial unwrapping is prone to noise and surface reflectivity errors, and it is suitable for static projections on uniform surface. Temporal phase unwrap is suitable for dynamic scenarios for varied textures as it acquires information at a differential time scenarios resulting in absolute fringe order and absolute unwrapped phase maps [14]. In temporal unwrap method, multiple images with varied pattern sequences are captured and processed to derive the phase values. For high-speed measurements, the number of pattern sequences must be restricted [16, 17]. Once the phase values are retrieved, corresponding projector coordinate with respect to the camera is determined. The stereo calibration is carried out to obtain the 3D point cloud of the test object.

Care must be taken during the capturing of the fringe images as the presence of shadows or non-uniform reflectivity of the object surface results in the fringe discontinuities which would make the phase unwrapping difficult. The angle between the camera axis and the projector axis also plays a vital role. As the angle of triangulation increases, the depth information retrieved is more accurate. At larger angles, the pattern sequence on the object will not be uniformly projected, as the projector will be having a shallow angle with the object plane resulting in wider pattern on the lateral end of the object [15]. DFP has been extensively used in industry for solid modeling, fast prototyping, quality control and deformation analysis as it is a non-contact measuring with high spatial resolution measurement capability.

## 5 Conclusion

Interferometry is a choice for ultra-high precision measurements for the nano-level resolution. Interferometric approach is sought for objects which have reflective surfaces and dimensions up to 1000 mm.

To test the optics and measure its optical characteristics such as aberrations, flatness, circularity and radius of curvature, Fizeau interferometer setup is preferred. Mirror, glass plate and lens are few objects which are tested using Fizeau setup. PSI is used for analysis of test object with uniform topographical feature. Characteristics such as form, roughness, radius of curvature, eccentricity of silicon wafers, thin transparent films and micro-mirrors are inspected using the PSI. For object with varied topography, WLI is apt, as it is equipped with short coherence length. To obtain the 3D profiles of the MEMS devices, WLI is preferred. WLI is used in micro-lens fabrication to characterize the focal length, surface roughness and optical aberrations, as

its response is quick to sporadic variations. Semiconductor chips, micro-needle and micro-tool analysis and strain and form analysis of micro-structures are carried out using WLI. Typical object size under WLI inspection would be less than 50 mm. The DFP technique is preferred for measurement of macro-components. Performance of DFP in ambient light is better compared to conventional interferometric setup. DFP can be employed for reverse engineering. Realization of DFP is more economic and convenient. The DFP system cannot be implemented on dark objects or on highly reflective objects. DFP offers a decent accuracy at sub-micron level and is suitable when the objects have higher dimensions.

**Acknowledgements** This research was funded by Department of Science and Technology, Govt. of India, under the Advanced Manufacturing Technology (AMT) Program.

**Funding** This research was funded by Department of Science and Technology, Govt. of India, under the Advanced Manufacturing Technology (AMT) Program. The grant number is DST/TDT/AMT/2017/42(G).

## References

1. Dyson J (1970) Interferometry as a measuring tool. The Machinery Publishing Co. Ltd.
2. Hariharan P (2007) Basics of interferometry, 2nd edn. Academi Press
3. Wyant JC (2002) White light interferometry. Optical Sciences Center, University of Arizona
4. Huntley JM (1998) Automated fringe pattern analysis in experimental: a review. Loughborough University, Leicestershire
5. Windecker R, Fleischer M, Korner K, Tiziani HJ (2001) Testing microdevice with fringe projection and white light interferometry. Opt Lasers Eng. Elsevier Science Ltd.
6. Malacara D (2007) Optical shop testing, 3rd edn. Wiley
7. Gasvik KJ (2002) Optical metrology, 3rd edn. Wiley
8. Leach R (2011) Optical measurement of surface topography. Springer
9. Mitsuya Y, Chihara K, Yoshioka M (1999) Novel measurements of flying weight and attitudes using michelson laser interferometry. IEEE Trans Magn 35
10. Gorthi SS, Rastogi P (2009) Fringe projection techniques: whither we are? Opt Lasers Eng
11. Moona G, Sharma R, Kiran U, Chaudhary KP (2014) Evaluation of measurement uncertainty for absolute flatness measurement by using Fizeau interferometer with phase-shifting capability. J Metrol Soc India
12. Lewis A (1994) Measurement of length, surface form and thermal expansion coefficient of length bars up to 1.5 m using multiple wavelength phase stepping interferometry, Meas Sci Technol. IOP Publishing Ltd.
13. Zhang S (2018) Absolute phase retrieval methods for digital fringe projection profilometry: a review. Opt Lasers Eng 107. Elsevier Ltd.
14. Salvi J, Fernandez S, Pribanic T, Llado X (2010) A state of the art in structured light patterns for surface profilometry, Pattern Recognition 43. Elsevier Ltd.
15. Burke J, Bothe T, Osten W, Hess C (2002) Reverse engineering by fringe projection. Proc SPIE Digit Libr 4778
16. Srinivasan V, Liu HC, Halioua M (1984) Automated phase measuring profilometry of 3D diffuse objects. Appl Opt 23. Optical Society of America
17. Salvi J, Pages J, Batlle J (2003) Pattern codification strategies in structured light systems. Pattern Recognition. Elsevier Science Ltd.

# Dimensions of Employee Well-Being at Work: A New Analytic Framework



Shivangi Singh and Poonam Gautam

**Abstract** The conception of employee well-being has attracted increasing interest in recent years. The study discussed dimensions of employee well-being such as physical, social, and psychological dimensions. The purpose of this study is to understand the critical nature of employee well-being, an often-overlooked aspect of human resource management. The paper attempted to identify the relationship between physical, social, psychological, and employee well-being. Further, it also aims to identify the impact of gender on employee well-being. The findings of the study indicated that there is a significant difference on the basis of gender on perceived employee well-being. The physical, psychological, and social well-being are affecting the well-being of employees. The study suggested placing more emphasis on the aspect of social well-being.

**Keywords** Employee well-being · Physical well-being · Psychological well-being · Social well-being · Textile industry · Human resource management

## 1 Introduction

The conception of employee well-being has attracted increasing interest in recent years [20, 5]. The researchers have argued that having a healthy workforce can be good for businesses [4]. As a result, understanding the dynamics of employee well-being at work is very important in learning about the different domains that have an impact on how well people are able to do their jobs.

Employees are the valuable assets of any organisation without whom, there can be buildings standing all alone. The term employee well-being has attracted attention from both corporate and academic fraternities. Hence, it became the need of the hour in today's dynamic environment. It has become an important concern for the benefit of organisations and society. Employee well-being has been demonstrated to have a number of positive effects on firms, including performance, productivity,

---

S. Singh (✉) · P. Gautam  
University School of Management, Kurukshetra University, Thanesar, Haryana, India  
e-mail: [shivangis.mgmt18@kuk.ac.in](mailto:shivangis.mgmt18@kuk.ac.in)

© The Author(s), under exclusive license to Springer Nature Singapore Pte Ltd. 2023  
R. P. Singh et al. (eds.), *Advances in Modelling and Optimization of Manufacturing and Industrial Systems*, Lecture Notes in Mechanical Engineering,  
[https://doi.org/10.1007/978-981-19-6107-6\\_37](https://doi.org/10.1007/978-981-19-6107-6_37)

523

turnover, and indirect costs [6, 10, 21]. Numerous scholars recognise the critical nature of employee well-being and undertake research beginning with a definition of employee well-being. According to Currie [5], employee well-being has defined as the combination of a person's contentment, physical health, and mental well-being. Grant et al. [9] defined three dimensions to describe well-being by analysing different study results from psychologists and sociologists, these include psychological, physical, and social well-being. The psychological components encompass "satisfaction, self-respect, personal growth, purpose in life, environmental mastery, and autonomy". The physical dimensions include "nourishment, shelter, health care, clothing, and mobility", to name a few. These include being part of the community, being accepted in public, being social, making a contribution to society, and being part of a social group [10]. Unfortunately, human resource management (HRM) usually does not pay much attention to the well-being of employees [15]. According to [9], firms choose to devote more resources to improving employee well-being because individuals, especially managers, believe in the "happy-productive worker hypothesis", which asserted that employees who are happier will be productive than those who are not [8].

## 2 Review of Literature

Grant et al. [9] classified employee well-being into physical, psychological, and social well-being.

### Psychological Well-being

Psychological well-being is a mental state where people experience happiness and satisfaction with their own lives. It is about how people interpret and add some meaning to their lives. Job satisfaction refers to the extent to which employees feel satisfied with their job. Psychological well-being encompasses good mental health, peace of mind, happiness, sorrow, and job satisfaction. Employees experiencing a high level of psychological well-being are found to be associated with a high level of income, good relationships with others, peace of mind, better employee performance, and productivity at work.

Cartwright and Cooper [2] found two important aspects of psychological well-being. The first one is about employees experiencing a feeling of happiness and positive emotions at work called Hedonic well-being, which is also known as subjective well-being [7]. Hedonic well-being also has been categorised into two components namely affective and cognitive components [16]. Bandyopadhyay and Srivastava [1] identified psychological well-being as an important factor determining the behaviour and decision-making ability of employees in organisations. To sum up, Hedonic well-being is represented by the presence of positive and negative emotions at work. The second one refers to the extent of attaining some purpose and meaning in life called eudaimonic well-being. Ryff et al. [18] talked about eudaimonic well-being in terms of six things: "self-acceptance, personal growth, autonomy, purpose in life, positive



relationships with other people, and environmental mastery”. Self-acceptance refers to the extent where people are aware of their own strengths, weaknesses, talents, abilities, and skills. In other words, it is an individual’s own satisfaction with one self-indicating positive outlook towards their life by accepting both strengths and weaknesses. Personal growth involves realising one’s own potential, bringing change and improvement in their own behaviour resulting in the personal development of an individual. Autonomy is the capability to make decisions on their own. Purpose in life means deriving some meaning to life. Environmental mastery means how capable an individual is, in handling the critical situation and meeting the growing demands of the environment.

### Social Well-being

The concept of social well-being was introduced by Keyes in 1998. Social well-being refers to the feeling of sense of belongingness, good relationship with others, love, and affection for each other. Maslow in his paper “A Theory of Human Motivation” in 1943 identified five basic needs of motivation at the workplace. In his five hierarchy of need theory of motivation, physiological well-being bestows physical well-being comprising of need for food, clothing, and shelter, on the other hand, social needs set forth social well-being encompass the need for belonging, love, affection, and friendship. Maslow placed social needs above physiological and safety needs. He argued humans always have a thirst for friendship, love, affection, and belongingness to others. If this need is unmet, then one cannot move upward to self-esteem and self-actualisation needs, respectively. Keyes [11] defined “social well-being as the appraisal of one’s circumstance and functioning in society”.

There are five dimensions of social well-being, “social integration, social acceptance, social contribution, social coherence, and social actualisation”. Social integration is the context in which an individual identifies himself/herself with society and feels connected with communities. Social acceptance refers to gaining acceptance of oneself by others in society. Humans are social animals who urge social acceptance by other people. Employees who have accepted their strengths and weaknesses tend to be healthy. Social contribution is the combination of one’s self-efficacy and social responsibility. It refers to the extent where people live and evaluate contributions made by them in society. In particular, it is a step towards the upliftment of society, therefore striking to maintain the balance. Social actualisation can be termed as realising the potential of society to flourish through its people and institutions. Social coherence is the perceived behaviour of an individual to analyse the things happening in the world. In nutshell, Healthy people identify themselves with society, and they tend to socialise, assess their contribution, and are very much concerned about happenings around the world [11].

### Physical Well-being

Physical well-being is analogous to physical health and mental health [13, 14]. Physical well-being refers to the state of being physically and mentally fit to perform the task. McCloughen et al. [13] defined physical well-being as “happiness, contentment, or confidence with general physical health”. It is firmly believed that employees

suffering from bad physical and mental health tend to affect employment. This could result in a loss of earnings and employee productivity reducing the consumption of healthy food. There can be various reasons responsible for bad physical and mental health including occupational stress, improper sleep, smoking habits, alcohol, unhealthy diet, and depression [14]. Therefore, people with good health are most likely to experience better emotional well-being at work. On physical well-being, several studies have been done relating it with different aspects. For example, [19] produced empirical evidence discussing the strong relationship and beneficial effects of optimism with physical well-being. Optimism refers to the positive state of mind, attitude, and outlook towards life. Optimism was found to be a protective factor influencing the physical well-being of employees by maintaining a healthy lifestyle. This is the reason why it is found to be a positive correlate of physical well-being in several studies [3]. Thus, people with optimistic attitudes toward life are likely to be high at physical well-being at work. In contrast, McKee-Ryan et al. [12] does a meta-review of studies related to psychological and physical well-being. They categorised physical well-being into two parts, subjective health such as alcohol consumption and objective physical health. The study found that growing rate of unemployment causes severe effect on psychological and physical well-being.

Objectives of the study

1. To examine the impact of gender on employee's well-being.
2. To examine the relationship between employee well-being, physical well-being, social well-being, and psychological well-being.
3. To examine the impact of psychological, social, and physical well-being on employee's overall well-being working in the textile sector.

### 3 Material and Methods

This study aims to examine the role of gender in influencing employee well-being and also attempted to analyse the impact of physical, social, and psychological well-being on employee's overall well-being at work on textile employees in Ludhiana. The data has been collected from medium and small organisations. The present study is based on primary data, and the research is descriptive in nature. The employees working in Ludhiana Textile organisations were the population for the study. Employees who were present at the time of the survey were included in the study. 254 workers (139 males, 115 females) were surveyed from the Ludhiana Industrial Textile hub.

#### Instruments

The data was collected through structured administered questionnaires from previous studies. For this purpose, employee well-being was measured through Juniper (20) instrument, and physical well-being and social well-being were measured using the Wellbeing Assessment Tool of Mckinsey Health Centre at the University of Illinois on a 5-point Likert scale (1—Strongly Disagree to 5—Strongly Agree); and Carol and Ryff 18 items measures were used comprising six dimensions (“autonomy”,

“environmental mastery”, “self-acceptance”, “purpose in life”, personal growth”, “positive relations with others”) on 5-point Likert scale from strongly disagree to strongly agree.

## 4 Results and Discussion

### Descriptive Statistics

The descriptive statistics and Cronbach’s alpha values are depicted in Table 1. The mean value of physical well-being is 39.1 indicating employees were physically fit and healthy. The mean value of social well-being (40.4) indicates that whenever employees will find better, they will develop congenial relations with their colleagues and managers. On the other hand, the mean value of psychological well-being (24.9) indicates that employees were happy and satisfied with their work. Similarly, the mean value of employee well-being (31.7) indicates that employees will perform activities for the organisation whether it adds value directly or indirectly.

The Cronbach’s alpha values of physical well-being (0.803), social well-being (0.630), psychological well-being (0.507), and employee well-being (0.603) are above 0.5 indicating that the sample is a true representative of the population.

*H<sub>01</sub>: There is a significant relationship between gender and employee well-being.*

As gender was selected to be an aspect associated with employee well-being, Independent-samples *t* test was used to test whether there is a mean-level difference in perceived employee well-being between male and female employees.

Table 2 displays the result of the *t* test and Levene’s test for equality of variance, where a significant difference in the variance of two groups (male and female), i.e. *p* value—0.000 is found to be less than 0.05. Thus, an alternative hypothesis is accepted.

The results indicated that male employees are more satisfied with employee well-being practices than female employees.

*H<sub>02</sub>: There is a significant relationship between employee wellbeing, physical wellbeing, social wellbeing, and psychological wellbeing.*

**Table 1** Mean, standard deviation, and reliabilities

Variable	Mean	SD	Cronbach’s alpha
Physical well-being	39.1	3.98	0.803
Social well-being	40.4	2.67	0.630
Psychological well-being	24.9	3.22	0.507
Employee well-being	31.7	3.47	0.603

Source Primary data

**Table 2** *t* Test result, test of homogeneity of variances and mean across gender

Gender	Mean	Levene’s test for equality of variances	<i>t</i> test for equality of means					
			<i>F</i>	Sig.	<i>T</i>	Df	Sig. (2-tailed)	Mean diff
Male	3.28	1.695	0.194	5.507	252	0.000	2.28	0.414
Female	3.05							

*Correlation*

The correlation was employed to examine the correlation between employee well-being (EW), physical well-being (PW), social well-being (SW), and psychological well-being (PSW).

*H<sub>02</sub>: There is a significant relationship between employee wellbeing, physical wellbeing, social wellbeing, and psychological wellbeing.*

The results shown in Table 3 indicated the relationship between employee well-being, physical well-being (0.496), social well-being (0.177), and psychological well-being (0.334) is positively correlated and significant. The relationship between physical well-being and social well-being (0.691) is positively correlated and significant. On the other hand, the physical well-being and psychological well-being are negatively correlated and insignificant at 0.672. Social well-being and psychological well-being are negatively correlated but significant at 0.001.

*Stepwise Multiple Regression*

The stepwise multiple regression was employed to find out the impact of physical well-being, social well-being, and psychological well-being on employee well-being. On the basis of objectives, the following hypothesis has been framed.

*H<sub>03</sub>: Physical Wellbeing is positively related to Employee Wellbeing*

As shown in Table 4, the value of *R*<sup>2</sup> is 0.246 indicating 24.6% of the variation in employee well-being is explained by physical well-being; on the other hand, *F* value (*F* = 82.110) at which sig. value is 0.000 less than 0.005 indicating physical well-being is predicting employee well-being.

**Table 3** Correlation matrix

Variable name	EW	PW	SW
Physical well-being	0.496**		
Social well-being	0.177**	0.691**	
Psychological well-being	0.334**	- 0.027	- 0.206**

Source Primary data

EW Employee well-being; PW Physical well-being; SW Social well-being

\*\*Correlation is significant at the *p* < 0.01

**Table 4** Multiple regression (physical well-being and employee well-being)

Model summary				ANOVA		
<i>R</i>	<i>R</i> <sup>2</sup>	Adjusted <i>R</i> <sup>2</sup>	Std. errors of the estimate	<i>F</i>	Sig. <i>F</i>	
0.496 <sup>a</sup>	0.246	0.243	3.02065	82.110	0.000 <sup>b</sup>	
<i>Source</i> Primary data						
Unstandardised coefficients			Standardised coefficients		<i>T</i>	Sig
Model	<i>B</i>	Std. error	Beta			
(Constant)	14.847	1.879			7.901	0.000
Physical well-being	0.432	0.048	0.496		9.061	0.000

<sup>a</sup>Predictors: (constant), physical well-being

<sup>b</sup>Dependent variable: employee well-being

As shown in Table 4, under coefficients, Employee well-being = 14.847 + 0.432 (physical well-being) which indicates physical well-being is positively related to employee well-being. The research results revealed physical well-being was found to be significant and positively related to employee well-being. Thus, an alternative hypothesis is accepted. Employees were completely involved in physical activities such as brisk walking, maintained desirable weight, were involved in exercises, and were free from diseases. They are able to make prompt decisions, satisfied with their job, and increased involvement in work.

*H<sub>04</sub>: Social Wellbeing is positively related to Employee Wellbeing.*

As shown in Table 5, the value of *R*<sup>2</sup> is 0.031 indicating 3.1% of the variation in employee well-being is explained by social well-being. The *F* value (*F* = 8.139) at sig. value 0.005 less than 0.05 indicating social well-being is predicting employee well-being.

As shown in Table 5, under unstandardised coefficients, employee well-being = 22.518 + 0.229 (social well-being) which indicates social well-being is positively related to employee well-being. The research results revealed social well-being was found to be significant and have a positive impact on employee well-being. As a

**Table 5** Multiple regression (social well-being and employee well-being)

Model summary				ANOVA <sup>b</sup>		
<i>R</i>	<i>R</i> <sup>2</sup>	Adjusted <i>R</i> <sup>2</sup>	Std. errors of the estimate	<i>F</i>	Sig. <i>F</i>	
0.177 <sup>a</sup>	0.031	0.027	3.42328	8.139	0.005 <sup>b</sup>	
Unstandardised coefficients			Standardised coefficients		<i>T</i>	Sig
Model	<i>B</i>	Std. error	Beta			
(Constant)	22.518	3.256			6.915	0.000
Social well-being	0.229	0.080	0.177		2.853	0.005 <sup>b</sup>

<sup>a</sup>Predictors: (constant), social well-being

<sup>b</sup>Dependent variable: employee well-being

**Table 6** Multiple regression (psychological well-being and employee well-being)

Model summary				ANOVA <sup>b</sup>	
<i>R</i>	<i>R</i> <sup>2</sup>	Adjusted <i>R</i> <sup>2</sup>	Std. errors of the estimate	<i>F</i>	Sig. <i>F</i>
0.334 <sup>a</sup>	0.112	0.108	3.27838	31.641	0.000 <sup>b</sup>
Unstandardised coefficients			Standardised coefficients	<i>T</i>	Sig
Model	<i>B</i>	Std. error	Beta		
(Constant)	0.360	0.064		14.165	0.000
EE	0.335	0.077	0.334	5.625	0.000

<sup>a</sup>Predictors: (constant), psychological well-being

<sup>b</sup>Dependent variable: employee well-being

result, the alternative hypothesis is accepted. Employees have good and trustable relations with their family, friends and colleagues. A person’s overall health is greatly influenced by their sense of social well-being.

*H<sub>05</sub>: Psychological Wellbeing is positively related to Employee Wellbeing.*

As shown in Table 6, the value of *R*<sup>2</sup> is 0.112 indicating 11% of the variation in employee well-being is explained by psychological well-being. The *F* value (*F* = 31.641) at sig. value 0.000 less than 0.05 indicating psychological well-being is predicting employee well-being.

As shown in Table 6, in unstandardised coefficients, the value of employee well-being = 0.360 + 0.335 (psychological well-being) indicates there is a positive relationship between psychological well-being and employee well-being. The results revealed psychological well-being was found to be significant and have a positive impact on employee well-being. Thus, an alternative hypothesis is accepted. The results indicated that employees scored high on the aspect of personal growth and environmental mastery dimensions of psychological well-being.

## 5 Conclusion

In nutshell, the present study examined the impact of physical, social, and psychological well-being on employee well-being. Human resource managers in firms frequently overlook these important factors of employee well-being [15]. The conception of well-being should be particularly promoted in textile organisations in order to offer a better life to employees.

Therefore, the relationship between employee well-being, physical well-being, social well-being, and psychological well-being are positively correlated and significant. The results revealed that overall physical well-being and psychological well-being are able to predict the well-being of employees. Moreover, only 3% of the variation in employee well-being is explained by social well-being which is very

low. One cause for this could be a lack of adequate measurement of the aforementioned characteristics or of social well-being. Furthermore, this means that there must be more things in life that are linked to social well-being. The study also suggested placing emphasis on developing positive relations with others, attaining some purpose in life, and realising their own potentialities.

## 6 Limitations

The study has some limitations. According to some researchers, employee well-being has a number of significant effects on an organisation's performance [6, 10, 21]. The authors do not investigate how employee well-being affects an organisation's performance. In the future, a combination of qualitative and quantitative research methods should be used to explore other aspects of employee well-being and its dimensions.

## 7 Managerial Implications

Our research results can be used both for theoretical and practical purposes. Managers can encourage the overall development of the textile sector workforce by promoting the well-being of all employees at the middle and lower level. The implications for management include those healthy relationships that may be established in the organisations through fostering support, building trust, and involving employees [17]. This is likely to be facilitated by managers' effective application of human resource management strategies, which foster positive attitudes and behaviours that create a positive work environment.

## References

1. Bandyopadhyay G, Srivastava KBL (2017) Determinants of psychological well-being and its impact on mental health and employee engagement. *Indian J Health Well Being* 8(4):250–257
2. Cartwright S, Cooper C (2014) Towards organizational health: stress, positive organizational behavior, employee well-being. In: Bauer GF, Hämmig O (eds) Springer, pp 29–42. [https://doi.org/10.1007/978-94-007-5640-3\\_3](https://doi.org/10.1007/978-94-007-5640-3_3)
3. Conversano C, Rotondo A, Lensi E, Della Vista O, Arpone F, Reda MA (2010) Optimism and its impact on mental and physical well-being. *Clin Pract Epidemiol Mental Health CP EMH* 6:25–29. <https://doi.org/10.2174/1745017901006010025>
4. Cooper C, Robertson I (2001) Well-being in organizations: a reader for students and practitioners. Wiley. <https://www.wiley.com/en-us/Well+Being+in+Organizations%3A+A+Reader+for+Students+and+Practitioners-p-9780471495581>
5. Currie J (2001) Early childhood education programs. *J Econ Perspec* 15(2):213–238

6. Danna K, Griffin R (1999) Health and well-being in the workplace: a review and synthesis of the literature. *J Manage* 25:357–384. <https://doi.org/10.1177/014920639902500305>
7. Diener E (2000) Subjective well-being: the science of happiness and a proposal for a national index. *Am Psychol* 55(1):34–43. <https://doi.org/10.1037/0003-066X.55.1.34>
8. Fisher C (2014) Conceptualizing and measuring wellbeing at work, pp 1–25. <https://doi.org/10.1002/9781118539415.wbwell018>
9. Grant A, Christianson M, Price R (2007) Happiness, health, or relationships? Managerial practices and employee well-being tradeoffs. *Acad Manag Perspect* 21:51–63. <https://doi.org/10.5465/AMP.2007.26421238>
10. Keyes CLM, Hysom SJ, Lupo KL (2000) The positive organization: leadership legitimacy, employee well-being, and the bottom line. *Psychol Manag J* 4(2):143–153. <https://doi.org/10.1037/h0095888>
11. Keyes CLM (1998) Social well-being. *Soc Psychol Quart* 61:121–140
12. McKee-Ryan F, Song Z, Wanberg C, Kinicki A (2005) Psychological and physical well-being during unemployment: a meta-analytic study. *J Appl Psychol* 90:53–76. <https://doi.org/10.1037/0021-9010.90.1.53>
13. Mccloughen A, Foster K, Huws-Thomas M, Delgado C (2012) Physical health and wellbeing of emerging and young adults with mental illness: an integrative review of international literature. *Int J Ment Health Nurs* 21:274–288. <https://doi.org/10.1111/j.1447-0349.2011.00796.x>
14. Ohrnberger J, Fichera E, Sutton M (2017) The relationship between physical and mental health: a mediation analysis. *Soc Sci Med* 1982(195):42–49. <https://doi.org/10.1016/j.socscimed.2017.11.008>
15. Renee Baptiste N (2008) Tightening the link between employee wellbeing at work and performance: a new dimension for HRM. *Manag Decis* 46(2):284–309. <https://doi.org/10.1108/00251740810854168>
16. Robertson I, Flint-Taylor J (2009) Leadership, psychological well-being, and organizational outcomes. In: *The oxford handbook of organizational well being*. <https://doi.org/10.1093/oxfordhb/9780199211913.003.0008>
17. Rogers RW (1995) The psychological contract of trust: part I. *Executive Dev* 8(1):15–19
18. Ryff CD, Singer BH, Dienberg Love G (2004) Positive health: connecting well-being with biology. *Philos Trans R Soc B Biol Sci* 359(1449):1383–1394. <https://doi.org/10.1098/rstb.2004.1521>
19. Scheier MF, Carver CS (1992) Effects of optimism on psychological and physical well-being: theoretical overview and empirical update. *Cogn Ther Res* 16(2):201–228. <https://doi.org/10.1007/BF01173489>
20. Warr P (2002) The study of well-being, behaviour and attitudes. In: *Psychology at work*, 5th edn. Penguin Press, pp 1–25
21. Wright T, Cropanzano R, Bonett D (2007) The moderating role of employee well being on the relationship between job satisfaction and job performance. *J Occup Health Psychol* 12:93–104. <https://doi.org/10.1037/1076-8998.12.2.93>



# Analysis of Strategies to Tackle the Environmental Impact of the Vaccine Supply Chain: A Fuzzy DEMATEL Approach



Amit Kumar Yadav and Dinesh Kumar

**Abstract** To combat the COVID-19 pandemic, the scientific community has progressed from discovering antivirals to the large-scale production of vaccines. Mass vaccination programs to curb the COVID-19 pandemic started in many parts of the world at the beginning of 2021. Mass vaccination aims to exit from health emergencies by vaccinating all the population with the required dose in the shortest possible time. The production rate has been boosted, and many new production facilities have been opened to fulfill worldwide demand. The objective of the vaccination program is to maximize the medical benefit with the lowest cost and equitable distribution of vaccines worldwide. However, the environmental impact of this long-run immunization program has received very little attention. This study explores the environmental impact of the vaccine supply chain (VSC) and analyzes the mitigation strategies to minimize it without affecting the medical, economic, and social benefits of vaccination. The fuzzy DEMATEL technique has been used to prioritize the mitigation techniques and find cause and effect relations among them. The finding of studies shows that the “optimal vial design” is most important, and “vaccine awareness and education” is the most impactful strategy to tackle the environmental impact of VSC.

**Keywords** COVID-19 · Vaccine wastage · Vaccine supply chain · Environmental impact · Sustainability · Fuzzy DEMATEL

---

A. K. Yadav (✉) · D. Kumar  
Mechanical and Industrial Engineering Department, Indian Institute of Technology Roorkee,  
Roorkee 247667, India  
e-mail: [ayadav2@me.iitr.ac.in](mailto:ayadav2@me.iitr.ac.in)

A. K. Yadav  
Jindal Global Business School, O.P. Jindal Global University, Sonapat 131001, India

© The Author(s), under exclusive license to Springer Nature Singapore Pte Ltd. 2023  
R. P. Singh et al. (eds.), *Advances in Modelling and Optimization of Manufacturing and Industrial Systems*, Lecture Notes in Mechanical Engineering,  
[https://doi.org/10.1007/978-981-19-6107-6\\_38](https://doi.org/10.1007/978-981-19-6107-6_38)

533

## 1 Introduction

The unprecedented event of the COVID-19 pandemic created great havoc on human life, resulting in strict lockdown measures worldwide. Normalcy has returned to various regions of the world following a nearly year-long lockdown, all thanks to vaccines. The end of COVID-19 is in sight, with billions of people now vaccinated. In the last one year, vaccine production has been unparalleled, and almost 5 billion doses were administered in different parts of the world as of mid-September 2021 [28]. While this is an incredible success for humanity, it is not so for the earth because the need to distribute vaccines has taken precedence over sustainability considerations due to the severity of the pandemic. This disadvantage arises from the fact that vaccine-related energy consumption was not optimized throughout vaccine development-distribution [15], and the vaccination wastages are not disposed of properly at the end of life. The vaccination rollout produces massive amounts of trash, which is exacerbated by the fact that most vaccines require two doses, resulting in double the waste [24]. When compared to the medical and economic issues created by the pandemic, the ecological impact of immunization appears to be a minor issue [17].

Vaccines, being biopharmaceutical product, requires stringent temperature control from their inception to final delivery. The vaccine's storage and transportation related emissions are some of the most significant environmental concerns. The vaccines are kept at low and ultra-low temperatures (specified by manufacturers); thus, their distribution requires cold chain logistics. The giant freezers that keep vaccines cool to the trucks and planes of cold chain logistics, as well as the millions of trash vials and syringes at the immunization sites, are detrimental to the environment and pose the risk of climate change [11].

Many of the vaccines approved for COVID-19 require deep freezers for their storage. The quantity of vaccines required to immunize the whole population requires a large number of cold storage for a very long time, and it will add huge pressure to climate change. The environmental imbalance caused by vaccines' packaging, warehousing, and deep freezing has resulted in a considerable surge in CO<sub>2</sub> greenhouse emissions [22]. Vaccines from Pfizer-BioNTech are needed to be stored at temperatures between  $-80$  and  $-60^{\circ}\text{C}$  [1]. Companies have been employing hydrofluorocarbons (HFCs) based refrigeration units to store and transfer vaccines at this temperature. Unfortunately, HFCs have a 23,000-fold larger global warming effect than CO<sub>2</sub> [24]. Even in this grave scenario, when priorities have shifted dramatically in the fight for the survival of the population, the environmental impact should not be overlooked [15].

The vaccine waste created due to improper handling and quality failure during storage and transportation along with open vial waste at vaccination sites, are significant concerns globally. It slows down the vaccination rate and also poses environmental and health-related risks. The point of delivery of vaccine or vaccination site

contributes waste such as disinfectants, protective equipment of workers, packaging materials, syringes, needles, vials, and single-use plastic equipment [13]. The proper disposal of biohazardous and infectious vaccine waste is critical for a sustainable vaccine supply chain. The infectious medical waste produced at the vaccination sites is potentially dangerous because they have high pathogenicity (ability to cause disease) and may be resistant to treatment [5]. Waste treatment and management of vaccine waste collection, treatment, recycling, and energy recovery seem to be more difficult during the mass vaccination process for COVID-19. In today's healthcare environment, employees, patients, and the community must all be educated on how to manage infectious waste. The administration and policymakers should be aware of the consequence of managing hazardous infectious waste and emissions related to cold chain logistics and make strategies accordingly to minimize the environmental impact of energy, materials, and process used in vaccination programs.

The analysis of mitigation strategies to control the environmental impact plays a critical role in the selection of these strategies. This study explores the strategies to tackle the environmental impact of the vaccine supply chain with the following objectives.

1. Identification of strategies for minimization of environmental impact of vaccination.
2. Prioritization of environmental impact mitigation strategies.
3. Establishment of cause effect among these mitigation strategies.

The mitigation strategies are identified from the literature and finalized with the help of expert interviews and field visits. A multicriteria decision-making (MCDM) method has been used to prioritize the strategies and establish cause-effect relationships among them.

## 2 Literature Review

Vaccination is used as one of the most feasible preventive measures for the control of infectious diseases. In the past, several infectious diseases were either eliminated or successfully controlled with vaccines. Many countries run regular vaccination programs for infants and pregnant ladies to prevent existing infectious diseases [7]. The successful delivery of vaccine within stipulated time requires a vaccine supply chain (VSC) with optimal cost and minimum impact to the environment. Vaccines and associated products are produced, manufactured, procured, disseminated, and disposed of at their own risk to the environment. The VSC impacts the environment in two ways: i) the infectious medical wastes of vaccine waste and other immunization-associated waste at the point of delivery, ii) the CO<sub>2</sub> emission due to cold-chain logistics.

Excessive waste in vaccinations is a major issue around the world. Overordering, moving products to locations, where they can't be adequately stored or used, and accepting products with insufficient remaining shelf life are all major causes. Work

on product optimization can assist in strengthening logistics systems and, as a result, reduce the amount of trash that needs to be disposed of by boosting capacity for right quantification, redistribution, and proper acceptance procedures [27]. Schiffing and Breen [23] reported that vaccine waste ranges from 0.3 to 30% during mass vaccination in different parts of the world. The major cause of vaccine waste is failure to maintain the required temperature conditioning, vaccine expiration, vial breakage, and open vial waste due to poor crowd management at vaccination sites [25]. Several studies show how the vial size and effective crowd management can reduce open vial waste [2, 12, 14]. Babanyara [4] study explored the environmental and human health effects of hazardous medical waste, including infectious wastes from immunization. The vaccine waste, along with other solid waste generated during immunization, requires standard guidelines to dispose of so that its impact on human health and the environment can be minimized [19, 26].

Zaffran et al. [29] study was one of the initial studies which considered the environmental impact of energy, material, and process used in VSC. They also highlighted that more research and development are required for technical advancement to minimize the ecological impact of vaccination. Lloyd et al. [18] presented a method for increasing the energy efficiency of vaccine and temperature-sensitive medicine distribution that was tested in Tunisia's Kasserine region. In the previous studies, the major impact of vaccination was related to the vaccine waste and medical waste produced at immunization sites, but mass vaccination for COVID-19 raised several other challenges to the environment, including energy efficiency and CO<sub>2</sub> emission.

The urgency of large-scale vaccination efforts against COVID-19, a tremendous and unprecedented race in industrial production, resulted in a huge amount of raw material and energy requirement and a significant increase in the production of glass, needles, plastic, and rubber for syringes and vials [21]. Also, maintaining the cold chain logistics throughout the supply chain requires a massive amount of energy and uses highly detrimental HFCs in case of ultra-low temperature requirements [11]. Jiang et al. [15] gave perspective about the energy and environmental impact of COVID-19 vaccination and concluded that the UN sustainable goal couldn't be achieved with unsustainable vaccine management. Phadke et al. [21] study shows how sustainable packaging and prefilled syringes can save a considerable amount of vaccine waste and also states that recycling needles and plastic can reduce material wastage. Klemeš et al. [16] gave the details of energy estimates in the life cycle of a vaccine and suggested that the environmental impact must be minimized even during emergencies to avoid risk of climate change. Kurzweil et al. [17] estimated the environmental impact of mRNA vaccines based on their CO<sub>2</sub> equivalent with their different storage strategies, cooling technology, logistics route, and vaccination sites. This study also observed that air freight, road transportation, and last-mile delivery emit roughly 19 times as much carbon dioxide as ultra-deep freeze technologies, dry ice manufacture, glass, and medical polymers for packaging. Santos et al. [22] compared the ideal storage of different COVID-19 vaccines approved by WHO with their thermal load for cooling as well as the type of refrigerant fluid used in freezers. This study also developed an index to measure the energy efficiency and environmental impact of different vaccines. Hasija et al. [13] study assessed

the different type of vaccine-related waste and its potential impact on environment based on the proportion of population vaccinated. The study also discussed the several medical waste treatment techniques based on the microfiber generated during their disposal.

The literature review of the vaccine supply chain waste management and its environmental impact shows that there are few studies that consider the environmental impacts of the vaccine supply chain, but there is almost no study that analyzes the mitigation strategy to tackle the environmental impact of VSC.

### 3 Methodology

This section of the study gives a brief overview of the methodology used to identify and analyze the mitigation strategies of the environmental impact of VSC. The mitigation strategies have been identified with the help of literature review, field survey, and experts. The literature related to vaccine wastage, vaccine waste management, and environmental impact of vaccination/immunization is explored, which shows the impact of vaccine-related wastes on the environment and suggestions/strategies to reduce it. Field survey of different vaccine warehouses, mass immunization sites, and hospitals of North India was conducted to assess the energy requirement in storing and shipping of vaccines as well as vaccine and solid waste produced at the different nodes of VSC. A total of four experts were contacted, a senior doctor of community healthcare, a pharmacist involved in cold chain logistics, a senior professor having expertise in the green supply chain, and a consultant of the medical waste management agency: all having sound expertise in their respective fields. Several strategies were identified from the literature review and field visit, but eight strategies were finalized after several rounds of discussion with the expert. The finalized strategies with their brief description are given in Table 1. After the finalization of mitigation strategies, the fuzzy DEMATEL technique is used to prioritize and find the cause-effect relationship among the strategies.

#### 3.1 Fuzzy DEMATEL

The DEMATEL approach was first suggested by the Battelle Memorial Institute Geneva Research Center [10]. DEMATEL is an approach for decision-making that analyzes interrelationships and finds the influence of significant factors in the form of a cause and effect diagram, i.e., digraph [6]. In this study, fuzzy is integrated with the standard DEMATEL technique to model the ambiguity of expert's opinion and allows a more accurate decision-making process.

**Table 1** Strategies to tackle environmental challenges of VSC

Code	Strategies	Description	References
TV	Thermostable vaccines	Vaccine than can be stored at normal temperature for longer durations	[29]
NR	Use of natural refrigerants	Natural refrigerants have a lesser impact on environment compared to HFCs	[16]
LM	Innovations for last-mile delivery	Cool box and other technique to keep vaccines at a lower temperature for remote vaccination centers	Expert opinion
IT	Installation of IoT devices	To monitor the temperature of vaccines throughout SC and avoid wastage	Expert opinion
OV	Optimal vials	Vial size to be optimized for minimum open vial waste	[3, 12, 14]
RR	Recycle and reuse	Reuse of packaging materials and recycling of the vials, syringes, and needles	[15, 21]
WM	Selection of waste management techniques	Proper segregation and disposal techniques which minimizes the CO2 emission and other environmental impact	[13, 15, 16, 21]
VA	Vaccine awareness	Educating masses for safe and responsible vaccination	[8]

### 3.1.1 Fuzzy Set Theory

The fuzzy set concept was given by Zadeh 1965, with the purpose of measuring uncertainty. The fuzzy sets use number ranges between 0 and 1 to measure uncertainty. Linguistic scales are used to assess the degree of uncertainty in a given circumstance. The triangular fuzzy numbers (TFN) were introduced, as shown in Fig. 1, and the membership function ( $x$ ) is defined as follows:

$$\mu(x) = \begin{cases} \frac{x-l}{m-l}, & x \in [l, m] \\ \frac{x-u}{m-u}, & x \in [m, u] \\ 0, & \text{otherwise} \end{cases}$$

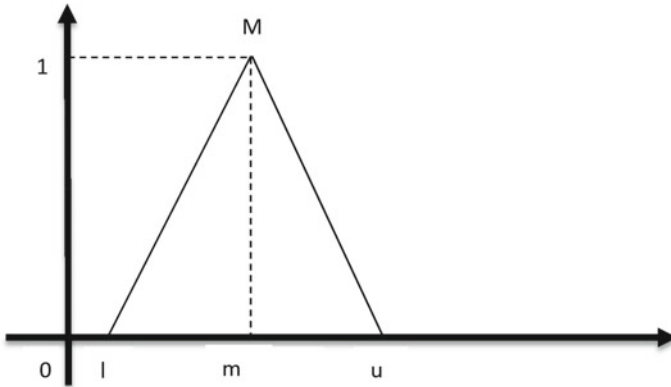


Fig. 1 Triangular fuzzy number

### 3.1.2 Steps of Fuzzy DEMTEL

#### Step 1: Fuzzy initial direct relation matrix

$$\tilde{B}_{ijk} = (\tilde{b}_{ijk})_{n \times n} = \begin{pmatrix} 0 & \tilde{b}_{12k} & \tilde{b}_{12k} \\ \tilde{b}_{21k} & 0 & \tilde{b}_{2nk} \\ \cdot & & \cdot \\ \cdot & & \cdot \\ \cdot & & \cdot \\ \tilde{b}_{n1k} & \tilde{b}_{n2k} & 0 \end{pmatrix} \quad (1)$$

The Eq. (1) shows the influence of factor *i* on factor *j* based on the linguistic variable and their triangular fuzzy numbers given in Table 2. Where  $\tilde{b}_{ijk} = (l_{ijk}, m_{ijk}, u_{ijk})$ , *i* and *j* denote pairwise values of each element, and *k* shows the number of experts.

The fuzzy initial direct relation matrix is obtained by aggregating all the *K* fuzzy matrices of Eq. (1) as,

**Table 2** Linguistic variables to triangular fuzzy number conversion [9]

Linguistic variables	TFN
No influence (NO)	(0.0, 0.0, 0.25)
Very low influence (VL)	(0.0, 0.25, 0.5)
Low influence (L)	(0.25, 0.5, 0.75)
High influence (H)	(0.5, 0.75, 0.1)
Very high influence (VH)	(0.75, 1, 1)

$$\tilde{Y} = \begin{bmatrix} 0 & \tilde{y}_{12} & \tilde{y}_{1n} \\ \tilde{y}_{21} & 0 & \tilde{y}_{2n} \\ \cdot & & \cdot \\ \cdot & & \cdot \\ \cdot & & \cdot \\ \tilde{y}_{n1} & \tilde{y}_{n2} & 0 \end{bmatrix} \tag{2}$$

$$\tilde{y}_{ij} = (l_{ij}, m_{ij}, u_{ij}) = \left[ \min(l_{ijk}), \frac{1}{k} \sum_k \max(u_{ijk}) \right], (k = 1, 2 \dots K) \tag{3}$$

**Step 2: Normalized Fuzzy matrix**

$$\text{If, } \tilde{M} = \begin{bmatrix} \tilde{p}_{11} & \tilde{p}_{12} & \tilde{p}_{1n} \\ \tilde{p}_{21} & \tilde{p}_{22} & \tilde{p}_{2n} \\ \cdot & & \cdot \\ \cdot & & \cdot \\ \cdot & & \cdot \\ \tilde{p}_{n1} & \tilde{p}_{n2} & \tilde{p}_{33} \end{bmatrix} \tag{4}$$

where matrix  $\tilde{M}$  is normalized fuzzy direct matrix produced with the help of Eqs. (5) and (6)

$$\tilde{M} = (\tilde{p}_{ij}) = \frac{\tilde{y}_{ij}}{r} = \frac{l_{ij}}{r}, \frac{m_{ij}}{r}, \frac{u_{ij}}{r} \tag{5}$$

$$r = \max \left( \max_{1 \leq i \leq n} \left( \sum_{j=1}^n u_{ij} \right), \max_{1 \leq j \leq n} \left( \sum_{i=1}^n u_{ij} \right) \right) \tag{6}$$

**Step 3: Total Fuzzy relation matrix**

Total fuzzy relation matrix  $\tilde{T}$  is developed by adding all direct and indirect effects of factors by Eq. (7),

$$\tilde{T} = \lim_{k \rightarrow \infty} (\tilde{M}^1 + \tilde{M}^2 + \dots \dots \tilde{M}^k) = \tilde{M} \times (I - \tilde{M})^{-1} \tag{7}$$

**Step 4: Defuzzification of Total Fuzzy relation matrix**

The total fuzzy matrix  $\tilde{T}$  calculated by Eq. (7) is defuzzified using Eq. (8) and got the crisp total relation matrix  $T = (t_{ij})$

$$(t_{ij}) = \frac{l''_{ij} + 4m''_{ij} + u''_{ij}}{6} \tag{8}$$



**Step 5: Calculating prominence ( $R + C$ ) and relation ( $R - C$ )**

$$R = \left[ \sum_{j=1}^n t_{ij} \right]_{n \times 1} \tag{9}$$

$$C = \left[ \sum_{i=1}^n t_{ij} \right]_{1 \times n} \tag{10}$$

The ( $R + C$ ) shows the amount of influence of each factor and ( $R - C$ ) values divides the attributes into cause-effect groups.

**4 Application of the Proposed Methodology**

The above-mentioned fuzzy DEMATEL methodology is used to prioritize the strategies to tackle the environmental impact of VSC. The experts’ initial direct relation matrix was in linguistic form, and these matrices were converted to fuzzy direct relation matrices using Table 2. Equation (3) combined the initial fuzzy direct matrices into a single aggregated fuzzy matrix, which is shown in Table 3. After aggregating the individual matrices, Eqs. (5) and (6) are used to create the normalized fuzzy direct matrix, which is shown in Table 4. With the help of Eq. (7), the total fuzzy relation matrix is computed using the approach described in Step 3. The total fuzzy relation matrix is defuzzified for further calculation using Eq. (8) and given in Table 5 as defuzzified total relation matrix.

**5 Result and Discussion**

The result of the proposed methodology is given in Table 6. The ( $R_i + C_i$ ) value shows the total influence of a criteria/technique, both in terms of receiving and dispatching over each other. The ranking of importance is based on the ( $R_i + C_i$ ) value. The importance of mitigation strategies is in the order of  $OV > LM > WM > TV > VA > IT > RR > NR$ . The “Optimal vial design (OV)” is weighted highest among all, followed by the innovations in last-mile delivery (LM). The high importance of the vial design may be due to the excessive open vial wastage during mass vaccination, which leads to the generation of a huge amount of hazardous waste on a daily basis [20]. Innovation in last-mile delivery is the next ranked important strategy which is also related to vaccine wastage at remote vaccination centers due to the lack of low-temperature storage for an extended time. The geographic and demographic distribution of north India, which includes the hilly area as well as the deserts, requires customized last-mile delivery techniques to reach all populations

**Table 3** Fuzzy aggregate direct relation matrix

	TV	NR	LM	IT	OV	RR	WM	VA
TV	(0,0,0)	(0.75,1,1)	(0.5,0.92,1)	(0,0.17,0.75)	(0.25,0.67,1)	(0,0.25,0.75)	(0,0.42,1)	(0,0.17,0.75)
NR	(0,0.25,0.75)	(0,0,0)	(0.25,0.67,1)	(0,0.08,0.5)	(0.5,0.75,1)	(0,0,0.25)	(0.25,0.58,1)	(0,0,0.25)
LM	(0,0.33,1)	(0,0.17,0.75)	(0,0,0)	(0,0.5,1)	(0.25,0.58,1)	(0,0.42,1)	(0,0.42,1)	(0,0.17,0.5)
IT	(0,0.25,0.75)	(0,0.33,0.75)	(0.5,0.75,1)	(0,0,0)	(0.5,0.75,1)	(0,0.25,0.75)	(0.5,0.75,1)	(0,0.33,0.75)
OV	(0.25,0.58,1)	(0,0.33,0.75)	(0.5,0.83,1)	(0,0.08,0.5)	(0,0,0)	(0,0.33,0.75)	(0,0.58,1)	(0,0,0.25)
RR	(0,0.25,0)	(0,0,0.25)	(0,0.17,0.5)	(0,0,0.25)	(0,0.17,0.5)	(0,0,0.75)	(0.75,1,1)	(0,0.25,0.75)
WM	(0,0.25,0)	(0,0,0.25)	(0,0,0.25)	(0,0,0.25)	(0,0.17,0.5)	(0.75,1,1)	(0,0,0)	(0.25,0.5,0.75)
VA	(0,0.17,0.75)	(0,0.33,0.75)	(0,0.25,0.75)	(0,0.5,1)	(0.5,0.83,1)	(0.75,1,1)	(0.75,1,1)	(0,0,0)

**Table 4** Normalized fuzzy matrix

	TV	NR	LM	IT	OV	RR	WM	VA
TV	(0,0,0)	(0,0,0,12)	(0,0,12,0,16)	(0,12,0,16,0,16)	(0,16,0,16,0,08)	(0,16,0,08,0,15)	(0,08,0,15,0,16)	(0,15,0,16,0)
NR	(0,0,04,0,12)	(0,04,0,12,0)	(0,12,0,0)	(0,0,0)	(0,0,0,04)	(0,0,04,0,11)	(0,04,0,11,0,16)	(0,11,0,16,0)
LM	(0,0,05,0,16)	(0,05,0,16,0)	(0,16,0,0,03)	(0,0,03,0,12)	(0,03,0,12,0)	(0,12,0,0)	(0,0,0)	(0,0,0)
IT	(0,0,04,0,12)	(0,04,0,12,0)	(0,12,0,0,05)	(0,0,05,0,12)	(0,05,0,12,0,08)	(0,12,0,08,0,12)	(0,08,0,12,0,16)	(0,12,0,16,0)
OV	(0,04,0,09,0,16)	(0,09,0,16,0)	(0,16,0,0,05)	(0,0,05,0,12)	(0,05,0,12,0,08)	(0,12,0,08,0,13)	(0,08,0,13,0,16)	(0,13,0,16,0)
RR	(0,0,0,04)	(0,0,04,0)	(0,04,0,0)	(0,0,0,04)	(0,0,04,0)	(0,04,0,0,03)	(0,0,03,0,08)	(0,03,0,08,0)
WM	(0,0,0,04)	(0,0,04,0)	(0,04,0,0)	(0,0,0,04)	(0,0,04,0)	(0,04,0,0)	(0,0,0,04)	(0,0,0,04,0)
VA	(0,0,03,0,12)	(0,03,0,12,0)	(0,12,0,0,05)	(0,0,05,0,12)	(0,05,0,12,0)	(0,12,0,0,04)	(0,0,04,0,12)	(0,04,0,12,0)

**Table 5** Defuzzified total relation matrix

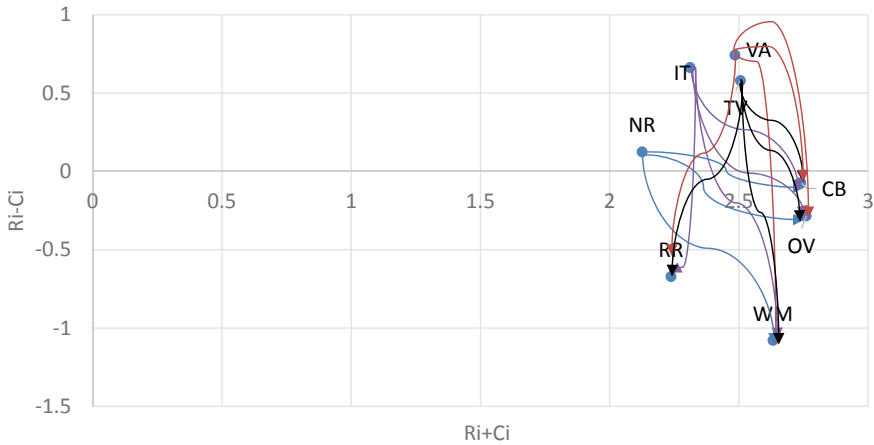
	TV	NR	LM	IT	OV	RR	WM	VA	$R_i$	$C_i$
TV	0.1083	0.2451	0.2685	0.1266	0.2478	0.1812	0.2406	0.1245	1.5426	0.9634
NR	0.127	0.0781	0.201	0.0904	0.2195	0.1163	0.2156	0.0771	1.1249	1.0006
LM	0.1555	0.1314	0.1271	0.1572	0.2211	0.1954	0.2278	0.118	1.3334	1.4063
IT	0.1462	0.1491	0.2421	0.088	0.2518	0.1867	0.2808	0.1424	1.487	0.8242
OV	0.1744	0.1387	0.231	0.0967	0.1207	0.1681	0.2231	0.0853	1.238	1.5226
RR	0.0586	0.0556	0.0903	0.054	0.1006	0.0892	0.2351	0.0994	0.7828	1.4549
WM	0.0552	0.0534	0.0677	0.0515	0.0991	0.2222	0.102	0.1256	0.7766	1.8556
VA	0.1382	0.1494	0.1787	0.1598	0.262	0.2959	0.3307	0.0988	1.6135	0.8712

with minimum wastage and emission. Zaffran et al. [29] also emphasize on innovation in last-mile delivery for environmentally sustainable VSC. The selection of the best waste management technique is also important to reduce the environmental impact of the waste generated during the vaccination. The emission and microfiber created during the disposal process also contribute to significant pollution. The use of thermostable vaccines is the next ranked strategy that will significantly reduce the load of the low and ultra-low freezer in VSC. This will also reduce the vaccine wastages due to temperature variances related issues during storage and shipment. These outcomes also indicate that reducing vaccine wastage is more important in the current scenario than other environmental impacts due to the huge amount of vaccine waste is producing daily due to mass vaccination of COVID-19.

The  $(R_i - C_i)$  value of Table 6 shows the impact of mitigation strategies, and the strategies are ranked in order of their impact as  $VA < IT < TV < NR < LM < OV < RR < WM$ . The “vaccine awareness and education” (VA) gained the most impact, followed by the “Installation of IoT” and other connected devices (IT) to monitor the temperature and other energy-related information. The high impact value of VA may be because awareness and education regarding the responsible use of the vaccine have multifold benefits. The aware beneficiary will demand a greener supply chain

**Table 6** Fuzzy DEMATEL results

Strategy	$(R_i + C_i)$	Importance	$(R_i - C_i)$	Impact	Identity
TV	2.505972	4	0.579176	3	Cause
NR	2.125552	8	0.124275	4	Cause
LM	2.739749	2	- 0.07287	5	Effect
IT	2.311215	6	0.662845	2	Cause
OV	2.760608	1	- 0.28456	6	Effect
RR	2.237654	7	- 0.67212	7	Effect
WM	2.632141	3	- 1.07904	8	Effect
VA	2.484645	5	0.742298	1	Cause



**Fig. 2** Cause and effect digraph

and participate in the proper disposal of waste, resulting in a more sustainable VSC. The IoT and other connected devices will help monitor the VSC energy requirement at each node and avoid storage wastage due to temperature leakage. The use of “Thermostable vaccine” and use of “Natural refrigerants” are other strategies that have a higher impact.

Table 6 also divides the strategies into cause -and effect types. The factor with positive ( $R_i - C_i$ ) values come in cause group and the factors with negative ( $R_i - C_i$ ) values come in effect group. Figure 2 shows cause-effect digraph in which thermostable vaccines, use of natural refrigerants, installation of IoT devices, and vaccine awareness come in the cause group, and they are influencing the other strategies. These strategies should be implemented first, and they will influence the other strategies of the effect group.

## 6 Conclusion

Mass vaccination programs worldwide gave a ray of hope with the pandemic struggle, but it will not save the earth from climate change. Thus, the environmental impact of mass vaccination programs must be minimized. This study analyzes the key strategies to tackle the environmental impacts of VSC by using the fuzzy DEMATEL approach. Total eight strategies were finalized with the help of a literature review and experts’ opinions. The fuzzy technique is used with DEMATEL to model the cause-effect relationship along with the ambiguity of human judgment. The “Optimal vial design (OV)” became the most important strategy, and “vaccine awareness and education” (VA) has the highest impact value. The inclusion of these studies will enhance the environmental sustainability of VSC.

The study was conducted during the initial phase of mass vaccination against COVID-19 with a limited number of experts in Northern India. As mass vaccination programs in different parts of the world advance, additional environmental concerns will emerge. Empirical studies with more experts and innovative mitigation strategies may be another extension of such research.

## References

1. Administration overview for Pfizer-BioNTech COVID-19 vaccine | CDC (2021). Retrieved from <https://www.cdc.gov/vaccines/covid-19/info-by-product/pfizer/index.html>. Accessed 29 Aug 2021
2. Assi TM, Brown ST, Djibo A, Norman BA, Rajgopal J, Welling JS, Chen SI et al. (2011) Impact of changing the measles vaccine vial size on Niger's vaccine supply chain: a computational model. <https://doi.org/10.1186/1471-2458-11-425>
3. Azadi Z, Gangammanavar H, Eksioglu S (2020) Developing childhood vaccine administration and inventory replenishment policies that minimize open vial wastage. *Ann Oper Res* 292(1):215–247
4. Babanyara Y (2013) Poor medical waste management (MWM) practices and its risks to human health and the environment: a literature review. *Int J Environ Health Sci Eng* 11(7):1–8
5. Babanyara YY (2015) Poor medical waste management (MWM) practices and its risks to human health and the environment: a literature review environmental pollution view project medical waste management view project. Retrieved from <https://www.researchgate.net/publication/285242270>. Accessed 18 Oct 2019
6. Biswas B, Gupta R (2019) Analysis of barriers to implement blockchain in industry and service sectors. *Comput Ind Eng* 136:225–241. Elsevier Ltd.
7. Chandra D, Kumar D (2018) A fuzzy MICMAC analysis for improving supply chain performance of basic vaccines in developing countries. *Expert Rev Vaccines* 17(3):263–281. Taylor & Francis
8. Chandra D, Vipin B, Kumar D (2021) A fuzzy multi-criteria framework to identify barriers and enablers of the next-generation vaccine supply chain. *International J Prod Perform Manage*. <https://doi.org/10.1108/IJPPM-08-2020-0419>
9. Chirra S, Kumar D (2018) Evaluation of Supply Chain Flexibility in Automobile Industry with Fuzzy DEMATEL Approach. *Glob J Flex Syst Manage* 19(4):305–319. Global Institute of Flexible Systems Management
10. Gabus A, Fontela E (1972) World problems, an invitation to further thought within the framework of DEMATEL. Undefined
11. Guillot L (2021) The environmental impact of mass coronavirus vaccinations. *Politico*
12. Haidari LA, Wahl B, Brown ST, Privor-Dumm L, Wallman-Stokes C, Gorham K, Connor DL et al. (2015) One size does not fit all: the impact of primary vaccine container size on vaccine distribution and delivery. *Vaccine* 33(28):3242–3247. Elsevier
13. Hasija V, Patial S, Raizada P, Thakur S, Singh P, Hussain CM (2021) The environmental impact of mass coronavirus vaccinations: a point of view on huge COVID-19 vaccine waste across the globe during ongoing vaccine campaigns. *Sci Total Environ* 151881. Elsevier
14. Heaton A, Krudwig K, Lorenson T, Burgess C, Cunningham A, Steinglass R (2017) Doses per vaccine vial container: an understated and underestimated driver of performance that needs more evidence. *Vaccine*, The Author(s)
15. Jiang P, Klemeš JJ, Fan YV, Fu X, Tan RR, You S, Foley AM (2021) Energy, environmental, economic and social equity (4E) pressures of COVID-19 vaccination mismanagement: a global perspective. *Energy* 235:121315. Pergamon

16. Klemeš JJ, Jiang P, Fan YV, Bokhari A, Wang XC (2021) COVID-19 pandemics stage II—energy and environmental impacts of vaccination. *Renew Sustain Energy Rev* 150:111400. Pergamon
17. Kurzweil P, Müller A, Wahler S (2021) The ecological footprint of covid-19 mrna vaccines: estimating greenhouse gas emissions in germany. *Int J Environ Res Public Health* 18(14).<https://doi.org/10.3390/ijerph18147425>
18. Lloyd J, McCarney S, Ouhichi R, Lydon P, Zaffran M (2015) Optimizing energy for a ‘green’ vaccine supply chain. *Vaccine* 33(7):908–913. Elsevier Ltd.
19. Oke IA (2008) Management of immunization solid wastes in Kano State, Nigeria. *Waste Manage* 28(12):2512–2521. Pergamon
20. Oo AN, Thekkur P, Thar AMC, Htet KKK, Lin HH (2020) Small session size and big vial size: operational research assessing open vial vaccine wastage at the service delivery points in the mandalay region of myanmar during 2018. *Trop Med Infect Dis* 5(2):60. Multidisciplinary Digital Publishing Institute
21. Phadke R, dos Santos Costa AC, Dapke K, Ghosh S, Ahmad S, Tsagkaris C, Raiya S et al. (2021) Eco-friendly vaccination: tackling an unforeseen adverse effect. *J Clim Change Health* 1:100005. Elsevier
22. Santos AF, Gaspar PD, de Souza HJL (2021) Refrigeration of COVID-19 vaccines: ideal storage characteristics, energy efficiency and environmental impacts of various vaccine options. *Energies* 14(7). <https://doi.org/10.3390/en14071849>
23. Schiffing S, Breen L (2021) COVID vaccine: some waste is normal—but here’s how it is being kept to a minimum. Conversation Trust. Retrieved from <https://theconversation.com/covid-vaccine-some-waste-is-normal-but-heres-how-it-is-being-kept-to-a-minimum-152772>. Accessed 16 Jan 2022
24. Valeviciute S (2021) The environmental impact of mass vaccination. *Climate, Features*
25. Wallace AS, Willis F, Nwaze E, Dieng B, Sipilanyambe N, Daniels D, Abanida E et al. (2017) Vaccine wastage in Nigeria: an assessment of wastage rates and related vaccinator knowledge, attitudes and practices. *Vaccine*. <https://doi.org/10.1016/j.vaccine.2017.09.082>
26. Wanyoike S, Ramirez Gonzalez A, Dolan SB, Garon J, Laroche Veira C, Hampton LM, Chang Blanc D et al. (2017) Disposing of excess vaccines after the withdrawal of oral polio vaccine. *J Infect Dis* 202(1):216
27. WHO (2011) Developing a vision for immunization supply systems in 2020: landscape analysis summaries. pp 1–45
28. World Health Organization (2021) Bangladesh: WHO coronavirus disease (COVID-19) dashboard with vaccination data | WHO coronavirus (COVID-19) dashboard With vaccination data. World Health Organization
29. Zaffran M, Vandelaer J, Kristensen D, Melgaard B, Yadav P, Antwi-Agyei KO, Lasher H (2013) The imperative for stronger vaccine supply and logistics systems. *Vaccine* 31(SUPL2):B73–B80. Elsevier Ltd.

# Implementation of Total Quality Management in Infrastructure Engineering



Chidanand Mangrulkar, Tushar Sathe, Suraj Vairagade, Narendra Kumar, and Ravi Pratap Singh

**Abstract** The quality and manufacturing process go hand in hand for any production unit. The potential growth of the industry depends upon the overall quality of its product in the market. Due to globalization, numerous firms are established for the fabrication and production of commercial goods. The total quality management (TQM) is the new concept incorporated to boost the productivity of the firm with the different quality check levels introduced at the different stages of production. In case of infrastructure engineering, quality check is the most critical aspect as the products are to be utilized for public transport/use. In the present study, the implementation of total quality management (TQM) for infrastructure engineering such as electric tower fabrication in the transmission system is discussed. The quality check at each level of fabrication is studied for maintaining the overall quality of the products at the field site. This paper discusses the TQM concepts and practices adopted in the field of infrastructure engineering. The study is carried out using questionnaire survey conducted in Wardha region and also using physical interviews with managers and engineers at all levels and then subsequent analysis was done for its effective implementation.

---

C. Mangrulkar (✉)

Department of Mechanical Engineering, B.M.S. College of Engineering, Bull Temple Road, Bengaluru, India  
e-mail: [cmangrulkar@gmail.com](mailto:cmangrulkar@gmail.com)

T. Sathe

Department of Production Engineering, Veermata Jijabai Technological Institute (VJTI), Mumbai, India

S. Vairagade

Department of Mechanical Engineering, Bajaj Institute of Technology, Wardha, Maharashtra, India

S. Vairagade · N. Kumar · R. P. Singh

Department of Industrial and Production Engineering, Dr. B. R. Ambedkar National Institute of Technology Jalandhar, Jalandhar, India

R. P. Singh

Department of Mechanical Engineering, National Institute of Technology, Kurukshetra, India

© The Author(s), under exclusive license to Springer Nature Singapore Pte Ltd. 2023

549

R. P. Singh et al. (eds.), *Advances in Modelling and Optimization of Manufacturing and Industrial Systems*, Lecture Notes in Mechanical Engineering,

[https://doi.org/10.1007/978-981-19-6107-6\\_39](https://doi.org/10.1007/978-981-19-6107-6_39)

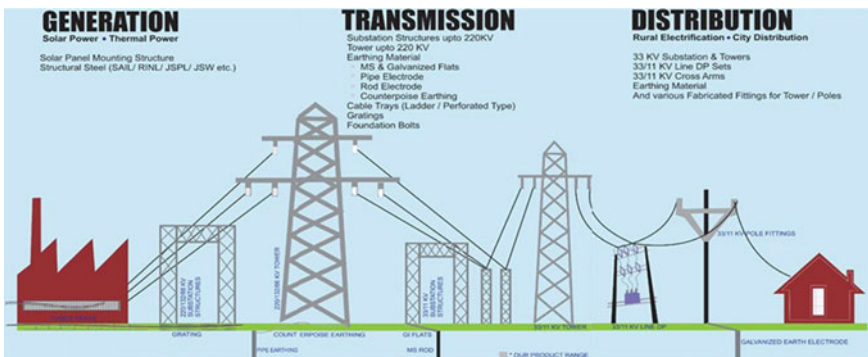


**Keywords** Transmission line · Towers · Angles · Plates · Galvanizing · Flange thickness · Hardness

## 1 Introduction

The overall growth and development of the nation resemble the growth in infrastructure engineering. The infrastructure engineering contributes significant amount to the country’s gross domestic product (GDP). The rapid growth in infrastructure engineering is seen after World War-II. Infrastructure engineering leads to the construction of high-speed expressway, bridges, dam, which will improve the standard of living with comfort for the common man. In energy sector, the consistent growth is observed since last two decades due to the ever-increasing energy demand of the country with the increase in the per capita income. The rise is significant sine year 2000, however dependency on the conventional fuel is also reduced. In case of the energy sector, infrastructure engineering is related to the construction of energy station, sub-station, along with uniform power transmission line and grids. The transmission line usually has the voltage ratings of 220 and 400 kV for the transmission purpose, later gets step down at the sub-station. The transmission system provides the linkage between the power generation system and distribution system, hence maintaining the desired standards of the quality level is essential. The present study is related to the total quality management in the infrastructure engineering pertaining to the transmission system [1]. The fabrication process which includes the machining operations along with the galvanization operation which includes surface coating are the two major procedureds in production process. The generalized layout of the transmission line is as shown in Fig. 1.

The transmission system can be further sub-categorized in fabrication and design layout. In the present study, the total quality management associated with the fabrication process of the transmission tower is focused [2]. The fabrication process involves selection of the suitable grade of steel for the production unit till dispatch of the final



**Fig. 1** The generalized layout of the power distribution system from generation to consumer

sub-components to the desired site of the transmission system. The detail quality check in all the processes is discussed in the subsequent chapters.

## 2 Need of Total Quality Management

After World War-II, W. Edwards introduced the concept of total quality management (TQM) in order to rebuild the shattered Japanese economy. The TQM primarily focused on continuous quality improvement in the areas of product, service, consumer and business relationship. The concept of TQM though introduced in the late 1950s became more popular in 1980s due to the rapid industrialization. It is a method in which all the stakeholders involved actively to improve the overall quality of goods and services. According to ISO, total quality management is defined as management approach of an organization centered on quality, based on participation of all its members and aiming at long term benefits to all members of the organization and society. In infrastructure engineering, the product cycle starts with the procurement of the raw material, pre-processing, processing, post-processing, along with packing, dispatch and erection/assembly of the sub-components at the site. Hence, maintaining the desired level of quality in each processing unit is utmost important for maintaining the overall quality of product. In the present work, the total quality management for the infrastructure engineering related to the fabrication of the transmission tower is performed at the various level to get at insight for the overall quality of the plant [3].

The quality check is performed at each level from the selection of raw material to erection of tower at the site location. The TQM involves the four-level quality check model, which is as follows;

- Level 1. Inspection
- Level 2. Quality control
- Level 3. Quality assurance
- Level 4. Total quality management.

The above four levels of quality check are performed at different level in case of infrastructure engineering which is incorporated in the subsequent sections.

## 3 Quality Check for the Raw Materials

### 3.1 *Material Yard*

Once the order is received from the particular firm for the establishment of the transmission line between the source and final sub-station, the total number of electric tower and grade of tower is finalized from the design and planning department. The steel requirement for the fabrication of the power transmission tower is L-section

channel. The material requirement is usually mild steel and high tensile steel. Each tower is made up of series of mild steel and high tensile steel angles in order to provide the required strength and flexibility under different loading conditions.

There are two types of elementary check for estimating the different grades of steel. Both the processes are primary processes followed by the chemical testing in each case. The color coding and embossing method is usually used at the primary stage [4].

**Color coding:** The use of different colors is used to identify the different grade of steel. In general, the extreme edges of the flanges are painted with different colors to identify the steel grade. In case of high tensile steel, red color is used to paint the side flange, while in case of mild steel, a green or yellow color is used. As it is the basic identification process, hence cannot be applied to the angle after cutting from the material end.

**Material embossing:** The mild steel and high tension steel is identified with the suitable embossing on the inner surface of the angle flanges. The mild steel is embossed with “MS” while the high tensile steel is with “HT” symbols to identify the basic grades of steel. The different embossing is at the regular interval for the entire length of the angle, hence it is relatively easy to identify the steel grades.

**Material testing:** The material testing is followed by the elementary primary check for the steel grades. The steel plates and angles are cut on CNC cutting machines for the desired length and dimensions. The raw material in the form of angles and plates are usually bundled in the order of 10 and final stack for each angle dimension and plate is made arranged for the material testing. The generalized check is performed for the physical dimension of the angle and plate before the actual material testing.

**Mechanical testing:** The mechanical properties are the vital aspects for any angle and plate. The entire strength of the angle depends upon the mechanical properties of raw material. The raw material in the form of angle and plate is usually cold-rolled with relatively low variation in mechanical properties. The material testing involves yield strength, impact strength along with hardness measurement for the selected steel grade. As, all the above mechanical testing processes are destructive in nature, as the material gets damaged in the testing procedure. In all the processes, the standard specimen of  $10 \times 10$  mm is selected for the different mechanical testing. In every lot size the first, twenty-fifth, and last piece are selected for the mechanical testing. In case of yield strength, universal testing machine (UTM) is used, while for the impact testing Izod chary test is performed with the same sample configuration. The hardness of the material is identified with Rockwell hardness testing machine. Mechanical testing is the first quality check process before the start of the actual fabrication of the angles and plates. Figure 2 indicates the various mechanical testing equipment's.

**Chemical testing:** After the primary check for the physical strength of the material, the chemical analysis is performed for the determination of chemical content in ferrous and non-ferrous materials. The spectrometer is used for determination of such type



**Fig. 2** Various mechanical testing machines—universal testing machine, Izod-Charpy machine, and Rockwell hardness testing machine

chemical composition. The optical and mass spectrometers are most commonly used for the chemical composition analysis. The sample size for the chemical test is similar to that of the mechanical test, as the metal is to be cut from the same lot size. Figure 3 illustrates spectroscope for chemical testing of angles and plates.

The percentage of carbon, manganese, and nickel determines the strength and the suitable grade of the steel. As both mechanical and chemical quality check process is destructive in nature, the implementation of the total quality management is not possible. Both mechanical and chemical testing procedure are under level 1 and 2 characteristics of quality check, as limiting value of quality is specified by the user. After the above quality check, the material is ready for the fabrication process such as drilling, bending, and notching.



**Fig. 3** Spectroscope for chemical composition

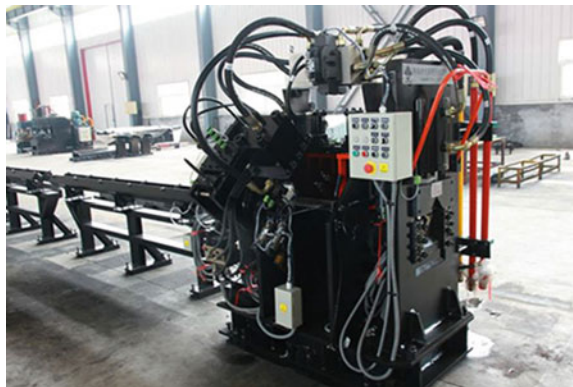
### 3.2 Production Process

The fabrication process is the actual production process in which various manufacturing processes are used to machine the raw material by several material removal processes. The transmission tower is a truss element containing several members, carrying different loads. These different elements are interconnected at the ends with other members. Hence, the machining process is primarily carried out at the end of the members for the joining process. The various machining processes are as follows;

1. **Angle cutting:** The angle cutting is the basic cutting operation involving cutting the angle into the required length as per the job card supplied from the planning department. The measuring tape is usually used to check and verify the length of the angle after the cutting operation. As no other operations are performed in cutting, the quality check is performed for every fifteenth element in cutting operation, to verify the length of angle.
2. **Punching:** The operation of generating the holes of the desired dimension on the metal blank is termed as punching. The punching operation is performed up to flange thickness of 8 mm. The punching is performed either by manual punching with help of flywheel or by computerized numeric control (CNC) machine. In case of CNC machine, the machine is programmed with the g-code for the exact location and size of the hole to be punched in the angle. The CNC machine can even punch the flange with thickness up to 10 mm. The punching operations is most time-consuming operations as usually each member contains 16–20 holes on both sides for the firm joint with other members. The CNC enabled punching machine is as shown in Fig. 4.

The quality check in case of punching operations is performed with the use of different Go, and No-go gages for the different hole size. In case of the punch pitch, vernier calipers are used to estimate the intermediate distance. In case of lot size of 100, after the first every, third, seventh, fifteenth, twenty-fifth, fiftieth, and seventy-fifth element is used verify the quality check as per the desired standard. In the present operation quality check of level 1, 2 and 3 are performed.

**Fig. 4** CNC machine for punching operations



3. **Drilling:** The primary difference between the punching and the drilling operations is the flange thickness. The drilling operations are preferred only if the flange thickness is more than 10–12 mm. The radial drilling machines are used to drill the flange with a higher flange thickness. The holes are usually of the order of 1 inch due to the higher flange thickness. The drilling is performed with smaller drill size and drilled with one size smaller than the actual hole size. The superfinishing operations are performed to patch the hole with the exact size in order to achieve the interference fit. As the angles are of higher section,  $150 \times 150 \times 15$ , the 100% quality check is performed with the help of various gages and vernier calipers simultaneously along with the drilling operations. Figures 5 and 6 illustrates the radial drilling machine and angle notching machine used for the machining of raw materials.
4. **Notching:** As the angles are interconnected to the number of members at different angles, the side flanges are protruding outward. The outward projections can



**Fig. 5** Radial drilling machine



**Fig. 6** Angle notching machine

cause injury to the servicemen in field while fitting nut bolts at the project site. In order to prevent such type of unwanted projections, the side flanges are cut at a suitable angle to trim the sharp edges. The edges are selected in such a way that the strength of the material will remain the same. The side fillet is the most common operations performed in case of notching machine. The angle is clamped at the desired angle with the appropriate feed, in order to cut the side angle. The notching machine is operated with the help of hydraulic pressure ranging from 50 to 150 bars. As the degree of freedom of the angle is restricted, before the notching operation, desired cut is achieved. The quality check with the right angle scale and linear scale are used to check the level of sidecut. Apart from the first check, fifth, seventh, and fifteenth piece is used for quality check. Every fiftieth and seventy-fifth piece is used for the quality check in the standard operation line, even after the side clamps are fixed for constraining the degree of freedom of the angle [5].

5. Hot and cold bending: The angle cross-section reduces from the base of the structure towards the apex. Hence, in any tower, angles of various sections are used from bottom to top. Due to the formation of apex, some members of the angles are required to bend at a suitable angle for the stability of the structure. In order to achieve the above requirement, hot and cold bending operations are

performed. The angle of bending determines the mode of bending in an angle. If the bending angle is up to 50, then cold bending operations are preferred, above which hot bending operations are performed. The operations performed at a temperature below the recrystallization temperature of metal are termed as cold bending, while above which is hot bending operations. The oil-fired furnace is used with light diesel oil (LDO) as the fuel for raising the temperature of the angle. The hydraulic press operates from 10 to 200 bars for bending the angle at the desired angular inclination. The angular scales are available to verify the degree of bending. As operating pressure may vary in each case, 100% inspection for each member is used in bending operations. The air gap between the angular scale and the bent angle indicates the amount of tolerance than the actual bending inclination. The bending angle also changes as the temperature of the angle decreases from higher temperature to the room temperature.

6. Grinding: The grinding is the finishing operation with the least material removal rate. During the entire process of fabrication, the raw material is subjected to burr formation in cutting, punching, and notching operations. So, grinding operation is performed to remove only the sharp metal burr formed during an earlier machining operation. The rate of material removal is very low owing to the finishing operation. The quality check procedure for the grinding operations is not fixed as in case of other machining operations. The visual inspection with touch is performed at the sharp edge of the flange to verify that the metal burr is removed completely [6].

The above processes are carried out in the production unit, and the finished product after operations are dispatched as the raw material for the galvanizing unit, which is discussed in the next section.

## 4 Quality Check for Galvanizing Unit

As the material is ferrous in nature, it is subjected to oxide formation and corrosion. In order to prevent the base metal from corrosion, galvanizing method is adopted. The galvanizing is the process of coating thin layer of material over the angle so that corrosion and oxide formations are prevented. Such methods are used to increase the overall life span of the product. Apart from the galvanizing, painting can be used as an alternative method to prevent oxide formation over the material surface [7].

### 4.1 Degreasing

During the machining operations, various oil/grease is applied on the angle flange through the tool. The oil gets stick to the metal surface over the period of time which performing different machining operations. In degreasing unit the angles are



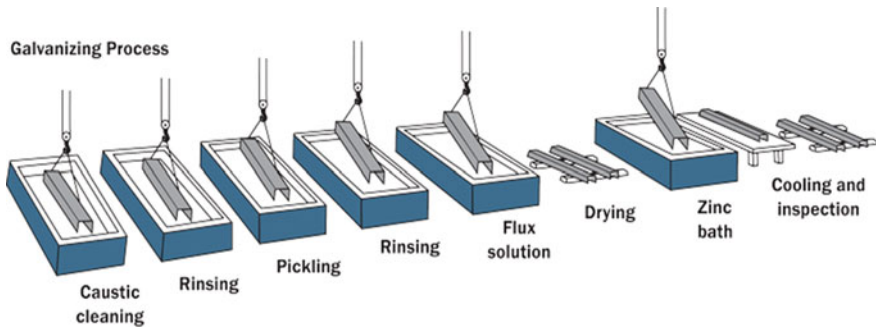
thoroughly cleaned so as to remove dust/dirt and oil marks from the flange surface before the galvanizing operations. A hot alkali solution, mild acidic bath, or biological cleaning bath removes organic contaminants such as dirt, paint markings, grease, and oil from the metal surface. Epoxies, vinyl, asphalt, or welding slag, which cannot be removed by degreasing, must be removed before galvanizing by grit blasting, sand blasting, or other mechanical means. The angles are bundled in the stack of 10/25/50/100 depending upon the dimension of the flange. To prevent the surface contact, metal chain is used in each stack row of the angles and inserted into the water tank. As it is the pre-processing operation, only visualization check process is followed in washing unit. After removal of the angles, the stack is held inclined to drain out all the water from the stack before the next operation.

## **4.2 Pickling Tank**

After the initial cleaning, the angle stack is inserted into the pickling tank containing the solution of dilute hydrochloric acid (HCl) with water. The dilute hydrochloric acid (HCl) is commercially purchased which is further diluted with distilled water. The dilute hydrochloric acid (HCl) with water performed the task of metal removal in minute quantity along the sides of the punched holes after the punching operations. The minute metal particles do usually stick to the side of the holes after the punching operations. These particles if not removed may generate the unwanted obstacle in the nut bolt fitting assembly. The duration of insertion of the angle stack within the pickling tank depends upon the flange dimension and concentration of the solution. In normal case, 3–4 pickling tanks with different concentration of dilute hydrochloric acid (HCl) with water is used for different angle dimensions. The concentration of the pickling tank is charged up after the series on insertion. The normal insertion time in the pickling tank is 5–10 min. After the removal from the pickling tank, the stack is now ready for the actual galvanizing process. As an alternative to or in conjunction with pickling, this step can also be accomplished using abrasive cleaning or air blasting sand, metallic shot, or grit onto the steel [8]. The various series of pre-processing and galvanizing operations is depicted in Fig. 7.

## **4.3 Galvanizing Unit**

The use of zinc is best suitable to prevent the oxide formation over the metal surface. The process of application of a thin layer of zinc coating over the angled surface is termed as hot-dip galvanization. The zinc bricks used for the galvanizing process contains purity level of 99.995% with the melting temperature around 450 °C. The angle stack after the pickling process is inserted into the hot bath of zinc to coat the layer of zinc over the angle and plates for the higher durability in all seasons. The zinc bricks are commercially purchased and top-up the concentration of the bath



**Fig. 7** Galvanizing process for angles and plates

after every five insertions. The average thickness of the zinc coating varies from 85 to 150 microns. The lower zinc coating will develop the inferior quality of the finished product, while the higher zinc coating will lead to the loss of capital. The elcometer is used to estimate the average thickness of zinc over the entire length of the channel. The average duration of insertion varies from 5 to 15 min along with the thickness of the flange. Excess zinc is removed by draining, vibrating, and/or centrifuging. The metallurgical reaction will continue after withdrawal from the bath, as long as the article remains near bath temperature. The angles are cooled either by immersion in a passivation solution or water or by being left in open air [9].

#### **4.4 Inspection**

The last stage of the process, is inspection which is simple and quick. The two properties of the hot-dip galvanized coating carefully examined are coating thickness and coating appearance. A very precise determination as to the quality of the galvanized coating can be accomplished through a visual inspection of the material because zinc will not react with unclean steel. A variety of simple physical and laboratory tests may also be performed to determine thickness, uniformity, adherence, and appearance to ensure the coating is in compliance with specification requirements. The products with lower surface coating can be further dipped to increase the thickness of zinc. During inspection, cooling of product also takes place with either natural or forced convection. The overall quality of the product can be checked after the galvanizing process [10].

The galvanizing process is concluded with the cooling of the angles and plates under natural convection followed by stacking as per the job order. The plates and angles are stack with the batch size of 10/50/100 and deliver it to the dispatch section for final delivery.

## 5 Implementation of Total Quality Management

Total quality management is defined as a customer-oriented process and aims for the uninterrupted improvement of business procedures. It certifies that all necessary works are toward the common goals of improving product quality or service quality, as well as enhancing the production process. In case of infrastructure engineering, the total quality management can be implemented at a various level such as:

### 5.1 *Commitment from the Management*

- **Plan:** Planning is the most critical aspect of any production firm. In case of infrastructure engineering, planning of raw material requirement as per the purchase order need to be planned carefully considering the reserve stock and inventory.
- **Do:** The management must motivate the employee by conducting a non-technical workshop for work ethics, leadership, etc.
- **Check:** The management must do the continuous check and planning activities are promptly followed by all the shop in charge and employees.
- **Act:** The management must act after attaining the check and feedback about the planning activities performed prior to the actual production. The act may be in terms of potential increment to the employee with due reward in position.

### 5.2 *Employee Empowerment*

- **Training:** The professional training is to be conducted for all the staff and employee as per their work schedule and workplace in the industry. This will enhance their decision-making capacity with improved productivity.
- **Excellence team:** The team formation in each of the production unit must be excellent with a good combination of the highly skilled, semi skilled and unskilled workforce. This will ensure smooth functioning of all the sections in production unit.
- **Measurement and recognition:** The measurement and recognition is an important aspect as it ensures the tolerance band for the unacceptable products. This will ensure that proper rework on the “rejected” products can be made “acceptable” with proper re-machining of the products. This will boost the productivity of the firm.
- **Suggestion scheme:** The proper suggestion scheme is to be implemented from the employee/ staff members/workers once proper training and measurement techniques are implemented. The appropriate modification in the action plan can be implemented accordingly [11].

### 5.3 *Continuous Improvement*

- Systematic measurement: For continuous quality improvement, systematic measurement of errors is essential. The systematic measurement deals with the exact reason for deviation in the quality from the desired level of satisfaction.
- Cross-functional process management: The proper action plan is to be work out with suitable measures to eliminate or reduce the factors causing the variation in the quality level at the different section of the production unit.
- Attain, maintain, and improve standards: With the slight improvement in the quality of the product after the cross functioning, new height in the quality and reduction of rejected products can be achieved with the reduction in the tolerance limit in the machining of products. With the continuous improvement in the standards, the total quality management can be converted into the six-sigma approach, due to very few rejected components.

### 5.4 *Customer Focus*

- Partnership with suppliers: In case of unforeseen circumstances, the partnership with multiple suppliers and vendors is essential to reduce the burden on the sole supplies.
- Service relationship with internal customers: The internal customers can be benefited by conducting a training program for staff members and employees. This will ensure strong bond among different department which will boost the quality and productivity of organization.
- Customer-driven standards: As the customer is the driving force in the current century, the standard set by the customer must be adopted for market acceptability of the product. Customer can also be included in the in-house training program for the vital suggestions [12].

## 6 **Benefits of Total Quality Management**

The management aimed at achieving the objectives of the organization in most effective and cost-effective manner. Furthermore, management primarily focused on satisfying the needs and expectation of the customers, who is considered as the king in the present market scenario [13, 14]. The way of managing the organization to achieve excellent results in terms of productivity, market hold, and profit is defined as total quality management. In other words, it can be quoted as:

Total—every single aspect.

Quality—degree of excellence.

Management—process of governing, organizing, planning and guiding towards attainment of pre-define goals.

A series of in-house training programs are required for the successful implementation of total quality management. Initially, such in-house workshops may affect the productivity of the firm for the short span of time, but eventually boosts the production in long run, once the employee realize the importance [15, 16]. However, due to such on-going in-house and on-site training program with consistent incremental changes in the operation process, some of the employee who prefer existing process may develop a negative feeling of losing the job, due to inferior performance. The strong support to employee and full dedication from the management is essential for the successful implementation of Total Quality Management [17].

## 7 Conclusion

In the case of infrastructure engineering, the overall quality of the product can be enhanced by improving the quality of the machining so as to produce the superior quality of semi-finished goods. The total quality management can be implemented by carefully analyzing the factors causing error in the fabrication of the angles and plates [18]. The suitable measures in design and fabrication methods must be adopted to reduce the error that yields to the faulty products. Although 100% inspection is not possible in case of the mass production, inspection policy designed by statistical arrangement can reduce the number of faulty products. However, 100% inspection of the products will consume significantly higher time that will reduce the overall productivity of the firm. In addition, as per the requirement 100% inspection can be carried out for the limited batch of products for the short duration. Once desired standards are achieved, the inspection time is reduced in statistical way to boost productivity [19]. The new way of random inspection can be implemented on trial basis for the limited period to estimate the overall quality and production rate. In case of the random inspection, the exact root cause of the error determination will be difficult to examine. In short, the implementation of total quality management will involve participation of all the stakeholders from raw material supplier to the final customers [20]. After the adoption of the total quality management in small steps, the inventory and the maintenance cost of the firm will also reduce due to the efficient planning of the firm [21]. The overall profitability of the vendors will also increase due to effective training and planning. Lastly, the implementation of total quality management is ever-improving process with proper feedback, check, and modification as and when required [22–24].

## References

1. Albermani FGA, Kitipornchai S (2003) Numerical simulation of structural behaviour of transmission towers. *Thin-Walled Struct* 41(2–3):167–177. [https://doi.org/10.1016/S0263-8231\(02\)00085-X](https://doi.org/10.1016/S0263-8231(02)00085-X)
2. Knight BGMS (1993) Material testing tension tests were conducted on three pieces taken from the main mem-. 119(3):698–712
3. Prasad Rao N, Knight GMS, Lakshmanan N, Iyer NR (2010) Investigation of transmission line tower failures. *Eng Fail Anal* 17(5):1127–1141. <https://doi.org/10.1016/j.engfailanal.2010.01.008>
4. Roy S, Fang SJ, Rossow EC (1984) Secondary stresses on transmission tower structures. *J Energy Eng* 110(2):157–172. [https://doi.org/10.1061/\(ASCE\)0733-9402\(1984\)110:2\(157\)](https://doi.org/10.1061/(ASCE)0733-9402(1984)110:2(157))
5. Li M, Yang J, Li Z (2011) Latest developments of materials used in transmission tower structure. *Adv Mater Res* 250–253:4038–4041. <https://doi.org/10.4028/www.scientific.net/AMR.250-253.4038>
6. Fei Q, Zhou H, Han X, Wang J (2012) Structural health monitoring oriented stability and dynamic analysis of a long-span transmission tower-line system. *Eng Fail Anal* 20:80–87. <https://doi.org/10.1016/j.engfailanal.2011.11.001>
7. Shibli SMA, Meena BN, Remya R (2015) A review on recent approaches in the field of hot dip zinc galvanizing process. *Surf Coat Technol* 262:210–215. <https://doi.org/10.1016/j.surfcoat.2014.12.054>
8. He B, Zhao M, Feng W, Xiu Y, Wang Y, Feng L, Wang C (2019) A method for analyzing the stability of the tower-line system under strong winds. *Adv Eng Softw* 127:1–7. <https://doi.org/10.1016/j.advengsoft.2018.10.004>
9. Yin T, Lam HF, Chow HM, Zhu HP (2009) Dynamic reduction-based structural damage detection of transmission tower utilizing ambient vibration data. *Eng Struct* 31(9):2009–2019. <https://doi.org/10.1016/j.engstruct.2009.03.004>
10. Akamphon S, Sukkasi S, Boonyongmaneerat Y (2012) Reduction of zinc consumption with enhanced corrosion protection in hot-dip galvanized coatings: a process-based cost analysis. *Resour Conserv Recycl* 58:1–7. <https://doi.org/10.1016/j.resconrec.2011.10.001>
11. Lin WE, Savory E, McIntyre RP, Vandelaar CS, King JPC (2012) The response of an overhead electrical power transmission line to two types of wind forcing. *J Wind Eng Ind Aerodyn* 100(1):58–69
12. Malik MZ, Banerjee R, Ahmad SA (2018) A review paper on implementation of total quality management (TQM) in construction industry. *Int J Recent Sci Res* 9(5):26515–26517. <https://doi.org/10.24327/ijrsr.2018.0905.2074>
13. Horstmann D (1956) The influence of impurities in iron on attack by molten zinc. In: *Proceedings of the fourth international conference on hot dip galvanizing*
14. Arditi D, Gunaydin HM (1997) Total quality management in the construction process. *Int J Proj Manage* 15(4):235–243. Elsevier Science Ltd. and IPMA
15. American Society of Civil Engineers (ASCE) (2010) Guidelines for electrical transmission line structural loading, 3rd edn. In: *ASCE manuals and reports on engineering practice, vol 74*. Reston, VA
16. Darwish MM, El Damatty AA, Hangan H (2010) Dynamic characteristics of transmission line conductors and behaviour under turbulent downburst loading. *Wind Struct* 13(4):327–346
17. Ueda S, Taguchi O, Iijima Y, Takahashi G, Yamaguchi K (2008) Growth kinetics of intermediate phase layers in an early stage of hot dip galvanizing at 450 °C. *J Mater Sci* 43:5666–5668
18. Wang J, Zhang Z (2015) Review on the impact of typhoon on the transmission line and the measures of anti-typhoon. *Mod Ind Econ Inform* 5(20):67–68
19. Hossein K, Marjan P, Jorrit A et al (2016) Influence of partial undergrounding on the transient stability of EHV power transmission systems. *Electr Power Syst Res* 131:126–138
20. Mahadevan S, Raghothamachar P (2000) Adaptive simulation for system reliability analysis of large structure. *Comput Struct* 77(6):725–734

21. Rao NP, Knight GMS, Mohan SJ et al (2012) Studies on failure of transmission line towers in testing. *Eng Struct* 35:55–70
22. Shi H, Salim H (2015) Geometric nonlinear static and dynamic analysis of guyed towers using fully nonlinear element formulations. *Eng Struct* 99:492–501
23. Belloli M, Melzi S, Negrini S et al (2010) Numerical analysis of the dynamic response of a 5-conductor expanded bundle subjected to turbulent wind. *IEEE Trans Power Deliv* 25(4):3105–3112
24. An Y, Pandey MD (2005) A comparison of methods of extreme wind speed estimation. *J Wind Eng Ind Aerodyn* 93(7):535–45. GB50545 (2010) Code for design of 110 kV–750 kV overhead transmission lines. Beijing

# Analysis of Rear Twist Beam Axle to Evaluate Performance Parameters for Passenger Vehicle Through Reverse Engineering



Madan Mohan Joshi, Anand Baghel, and Chaitanya Sharma

**Abstract** The chapter discusses, the concept and key design factors of Rear Twist Beam axle (RTB) and deals with the analysis of existing RTB axle (tubular cross beam) through reverse engineering and to propose an alternate concept i.e. new design, to achieve similar or better performance characteristics. The prime goal is to achieve reduction in complexity without compromising the product performance characteristics: stiffness and compliance. Proposed model G exhibits higher roll stiffness characteristics and lower camber compliance than the tubular cross beam profile.

**Keywords** Compliance · Rear twist beam axle · Reverse engineering · Stiffness

## 1 Introduction

In rear twist beam, the two trailing arms are interconnected with the cross member; the cross member is positioned toward the vehicle front direction. The connection of a RTB to vehicle body is done by two bushings. During parallel wheel travel, the RTB motion causes marginal variations in track, toe, and camber, behaving similarly to a rigid axle. However, during an opposite wheel travel, the behavior is similar to an independent suspension system [1].

Therefore, the rear twist beam suspension is best known semi-independent suspension axle. Apart from the spring seats, dampers, or end plates in some cases, the rear twist beam axle has the following distinctive parts shown in Fig. 1, that define the particular properties of the concept [2]:

---

M. M. Joshi · A. Baghel

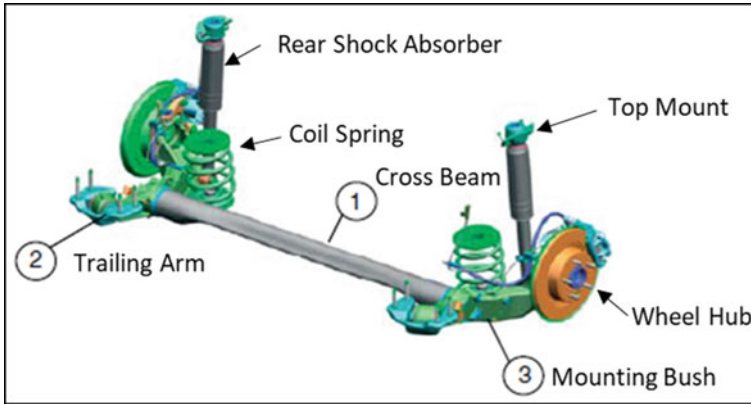
Automobile Engineering Department, RJIT BSF Academy, Tekanpur, India

C. Sharma (✉)

Department of Mechanical Engineering, BIT, Sindri, Dhanbad, Jharkhand, India

e-mail: [cs.me@bitsindri.ac.in](mailto:cs.me@bitsindri.ac.in)





**Fig. 1** Key elements of the rear twist beam axle

1. Cross beam
2. Left and right trailing arms
3. Front mounting bushing or, the “A-bushing”.

During driving, the moments and forces applied to tire and wheel are taken by RTB. The construction of RTB permits noise isolation and fine tuning of both, ride quality and handling performance. Each component of RTB serve several functions, not like multilink suspension links where every link has distinct purpose and controlling load directions. The following section briefly describes geometrical features and function of cross beam and trailing arm of RTB.

### ***1.1 Cross Beam***

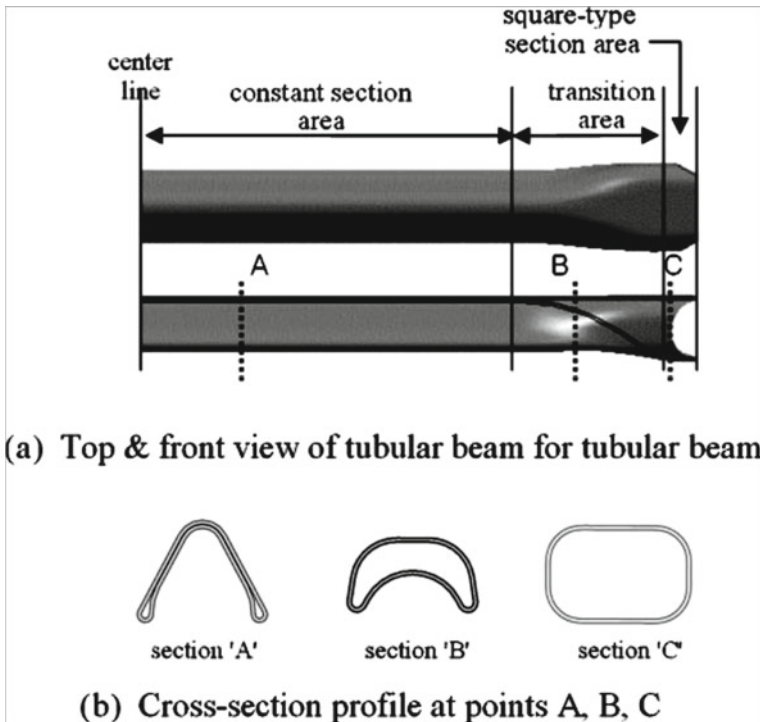
Cross beam provides distinct functional characteristics of RTB [3]. Classically, there are two categories of cross beam:

- (a) V- or U-shaped open section cross beam formed by stamping process of steel sheet, and
- (b) a hollow closed-section tubular cross beam formed by pressing a steel pipe;

The tubular cross beam is well known and can supplant numerous parts such as, stabilizer bar and gussets. It has three different zones:

- (i) a constant cross-section area or region (at center),
- (ii) followed by transition zone (significant for stamping process),
- (iii) and interface zone, to ensure the required structural characteristics, limiting weldment stresses. Details of cross beam section are shown in Fig. 2.

A lot of design variables need to be calculated during preliminary design phase, this is regardless of the relatively simple structure of a cross beam. For example, to



**Fig. 2** Cross section of cross beams

anticipate the impact of various design variables on performance of cross beam an ADAMS analysis is utilized [4, 5] along with different Finite Element (FE) codes [6] for making an allowance for studying the temporary deformation. Ansys software was used to design, and analyze the adequacy and performance of each designed component/system of battery powered environmental friendly Eco-Kart with a top speed of 40 km per hour [7].

In any case, such analysis software furnishes equivalent outcomes with test information [7, 8] the entire interaction is tedious, including the pre and post processing of cross beam model. Likewise, it requires master abilities and comprehension. Hence, a substitute effective method is required to obtain fast results, particularly during preliminary design phase. Sugiura et al. [9], indigenously developed a worksheet in MS Excel to determine reduced stiffness matrix from cross beam cross section and afterward the toe and camber properties to be determined. Lyu et al. [10], portrayed the cross member similar to the linkage of a lumped mass associated by nonlinear twisting torsional springs that can be solved by non-linear analysis. Satchell [11], postulated that the performance of cross beam in roll motion and semi trailing arm in kinematic motion is comparable. This postulation permits to anticipate the stiffness and compliance of RTB.

For V-shape cross beam, Kang [8] suggested, as there is no analytical equation available to compute torsional stiffness of V shape cross beam and also the rubber bushing stiffness is not considered, therefore, FE software is required to compute the torsional stiffness. Silveira et al [12], assessed the effect of cross beam on the kinematic behavior of the rear twist beam axle by moving the cross beam to different orientations and different positions along the trailing arm, as they can influence the vehicle behavior while cornering. Evaluating the factor of cross beam position, it is analyzed that closer the cross beam to mounting bush of the trailing arm, the smaller is the variation of both camber and convergence. Though, these findings are preliminary results, and needs further evaluation considering various parameters that can influence cross beam: open and closed profile cross beam with variable profile along the length, situation of symmetrical loading etc.

## ***1.2 Trailing Arms***

The rear trailing arms are connected to both the wheel carriers and are interconnected to one another by a cross beam in a rigid manner forming “H-Shape” geometry.

Satchell [11] postulated, Trailing arms need to be strong enough to withstand torsion & bending. It must support the weight of the vehicle through shock absorbers mounted on it as well as the tension and compression forces generated between the rear wheels and the chassis. It creates a strong reinforcement by connecting the axle to the frame, stabilizing it against the longitudinal forces and keeping the rear wheels on their correct axis. Since the axle moves up and down, the trailing arm also needs to be hinged where it is connected to the chassis. This hinged, point of connection between the trailing arm and the frame is where the rear trailing arm bushings are located. The rear trailing arm bushings cushion and soften the movement of the rear suspension while keeping the rear wheels on their correct axis.

### **1.2.1 Advantages of Rear Twist Beam Axle Over Independent Suspension**

- (1) Simple design and minimal expense arrangement.
- (2) When compared to other suspension, RTB has Only 2 mounting bushes having reduced wear and tear.
- (3) Simple in construction.
- (4) Flawless compact packaging.
- (5) Durable and optimal weight.

### 1.2.2 Disadvantages of Rear Twist Beam Axle Over Independent Suspension

- (1) Difficult to adjust (tune) roll stiffness.
- (2) Camber compliance may be high.
- (3) Camber characteristics are very limited.
- (4) Basic toe vs lateral force characteristic is over steer.
- (5) Due to long welds, it is prone to fatigue failures. Need a lot of development for weldments to improve fatigue behaviour.
- (6) Cross beam geometry need to be precisely optimized to make sufficient package room for exhaust and so on.
- (7) Wheel alignment geometry is factory set and usually not adjustable. Deviation of geometry from specifications/tolerances may result uneven tire wear or a bent axle or compromised mounting points.

## 2 Interaction Between Design variables and Axle Properties

In the previous few years, extensive researches have addressed the concept of structural requirements (parameters), key design factors (performance) of rear twist beam axles.

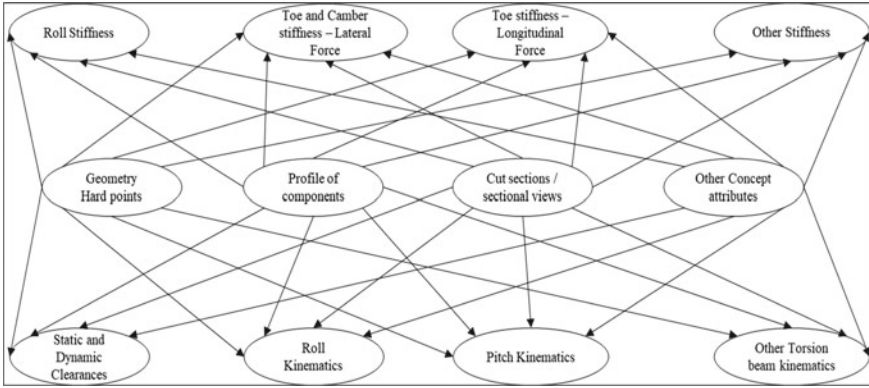
A number of researchers have conducted a range of analysis on this subject. Bastow et al. [13] found that on comparison to other types of suspension systems, RTB axles have a lot of benefits: optimal weight, ideal cost, and compact packaging. The performance parameters of RTB are stiffness characteristics, kinematics and compliances as well as durability. As shown in Fig. 3, these parameters are determined by design variables such as hard points, shape and the cross-section size of components as well as the proper material selection. All performance parameters are simultaneously influenced by design variables. Because of large number of variables, the interaction between variable and properties is extremely complex, enables infinite concept potentials simultaneously.

On the contrary, the product optimization becomes challenging. The minor iteration or revision of one input may affect another input. That is the critical test for designing RTB's [14].

Cross beam or torsion beam profile is the main part of the twist beam which outlines the complete roll stiffness, compliances and weight. Therefore, cross beam profile need to be observed first to accomplish efficiency on a twist beam suspension (Table 1).





This chapter presents the design of new RTB to achieve:

- (1) Similar or better performance characteristics.
- (2) Reduction in complexity without compromising the product performance characteristics such as stiffness and compliance.



**Fig. 3** Complex interactions between concept variables and axle properties

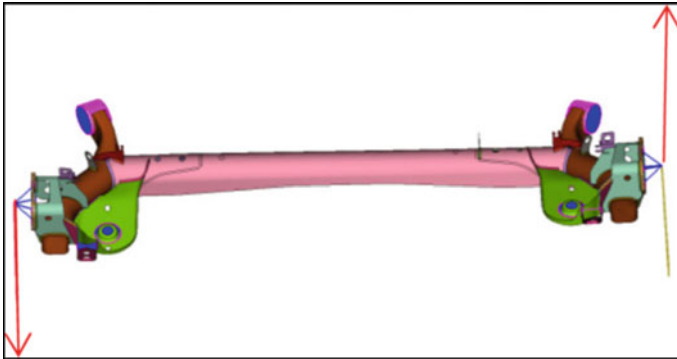
**Table 1** The crossbeam profile classification

Cross beam profile type	Profile Image
U-shaped open section	
Open section with stabilizer bar	
Tubular profile	
Omega Profile	

(3) Simple design and construction.

### 2.1 Performance Characteristics

To address the concept development of new RTB, following product performance characteristics were chosen as targets: such as stiffness and compliance. Definitions of some of the terms are given below:



**Fig. 4** Roll stiffness calculation

### 2.1.1 Roll Stiffness

The resistance offered by twist beam against the twisting moment is called as roll stiffness. To calculate the roll stiffness, application of a fix displacement on the wheel center, in anti-phase “z” direction and then calculating the reaction force and roll angle (Fig. 4) [15].

$$\text{Roll Stiffness(Nm/deg)} = F * T / \theta$$

where

$F$  = Reaction Force at Wheel Center (N)

$T$  = Track width of the Twist beam (m)

$\theta$  = Roll Angle (°).

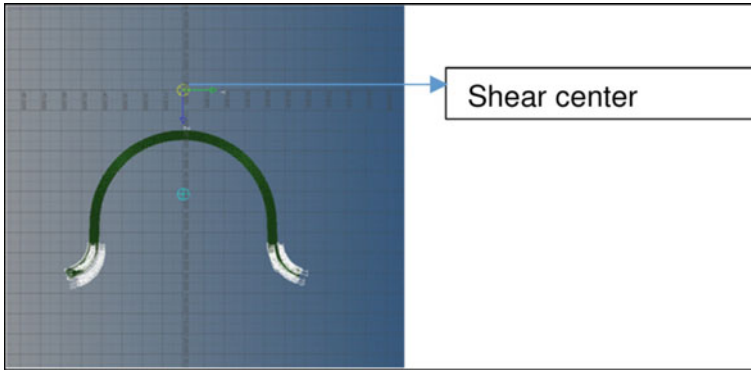
### 2.1.2 Camber Compliance

Camber compliance is the rotation of the end plate around X axis when load applied at tire contact point in opposite directions.

### 2.1.3 Shear Centre

Shear center is the point on the beam cross section (or outside the beam cross section), where if any load is applied and produce beam bending without torsion or twisting. Loads applied anywhere other than the shear center will produce both bending (moment) and twisting (torsion).

The kinematic behavior of RTB, is influenced by the shear center. Shear center has a direct correlation to the roll steer of the vehicle. Reference Fig. 5 [15].



**Fig. 5** Shear center

Shear center of rear twist beam profile plays an important role for defining the twist beam axle roll center, suspension roll is not produced when a lateral force is applied in sprung mass at roll center point.

Vehicle's roll axis can be derived when roll centers of both front and rear suspensions are linked by a straight line, resulting the influence on vehicle's roll angle during cornering. While calculating the roll center, by keeping an account of axle flexibility, and done through trajectory of center of a tire contact patch in opposite wheel travel [16].

The point in the transverse vertical plane through any pair of wheel centers at which lateral forces may be applied to the sprung mass without producing suspension roll [17]. Subsequently, it's height may be termed as "the height from hypothetical point on the ground at which the normal vector for the curve of the tire contact intersects at the center of the vehicle" [18].

Leal [19], reported that in today's competitive and cost sensitive environment, rear twist beam is the simplest design considering manufacturing process, representing acceptable results when applied in small passenger cars. Even though the twist beam suspension is widely used globally, there are very few studies related to this topic. Most important component of rear twist beam axle is the cross beam.

Elements such as polar moment of inertia, neutral axis position, and moment of inertia may vary the performance behavior of suspension. The shape and geometry of the cross beam controls the parameters such as convergence and camber, vertical reaction wheels, and radius of turn.

U, V, and C reversed are the most common profile of cross beam. Predominantly, these are used because of ease of manufacturing (forming, welding, and assembly), and roll stiffness principally governed by sheet thickness of cross beam. Finite element analysis of RTB reduces cost, time, and results in rapid development [12].

At present a lot of simulation software are available in market, to simulate high nonlinearity events, quasi-static, or dynamic events. This is all possible due to the development of multi-processor PCs that allows to perform high-complexity simulations. Finite element method has been widely used during virtual design stages, to have good correlations with experimental results [20].

The key outcomes of research background are stated under:

1. Main structural requirements (parameters) of RTB depends on selection of cross beam and trailing arm section types and sizes.
2. The key design factors of cross beam are [21]
  - i. Cross beam orientation
  - ii. Cross beam section thickness
  - iii. Cross beam vertical position
  - iv. Cross beam longitudinal position.
3. The trailing arm type and cross-section definition is critical and it should be strong enough to withstand torsion and bending.

## ***2.2 Evaluation of Cross Beam Profiles***

In Table 2, “+” sign denotes higher value compared to base, while “-” sign denotes lower value compared to base. From the above evaluation, open section with stabilizer bar fits screening criteria but compromises with shear center criteria.

A lot of compromises need to be done for achieving designed performance requirements, therefore, evaluation of a new cross beam is necessary, which should meet all requirements equal or better than the existing beam. Design is established by optimizing the cross section, thickness and shape of the cross beam profile or trim line.



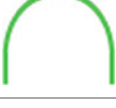

## **3 Design Process**

Different cross beam profiles were evaluated to the current tubular design of cross beam rear twist beam axle. The current design of RTB was reverse engineered and analyzed using FEA for stiffness and compliance, i.e., roll stiffness, camber compliance, and shear center.

During the proposal of alternate concept (new design) the boundary conditions and load cases are kept same for having comparable results (Fig. 6).



**Table 2** Evaluation of cross beam profiles

Torsion profile type	Profile Image	Roll stiffness (kNm/deg)	Camber compliance (deg/KN)	Shear center height	Remarks
Tubular profile		base	base	base	Base for comparison
U-shaped open section		---	-	-	Low roll stiffness
Open section with stabilizer bar		base	base	-	Fits screening criteria low shear center
Omega profile		-	-	++	Low roll stiffness and high shear center

### 4 Case Study

Before reaching to final design proposal, a detailed study of stiffness and compliance characteristics is done, a design named as model G was recommended among the various proposals. Model G design uses the cross sectional property of the tubular cross beam profile for the performance characteristics, i.e., roll stiffness and shear center adjustment (Fig. 7).

The shape of the cross beam profile trim line when viewed from front or back is not a straight line but it varies as one goes closer to the center of the cross beam. Furthermore, the cross beam shape is not uniform; cross beam profile at center is in ‘V’ shape and at the ends of ‘U’ shape. Figure below shows the new design concept (Fig. 8).

Key characteristics of the new design concept of cross beam profile, is the use of trim line for achieving the stiffness rather than the reducing the thickness of the material.

It can be observed that for a given roll stiffness, model G profile provides better utilization of material and cross beam with variable open cross-section profile shape in different sections with stabilizer bar provides less compliances compared to tubular cross beam.

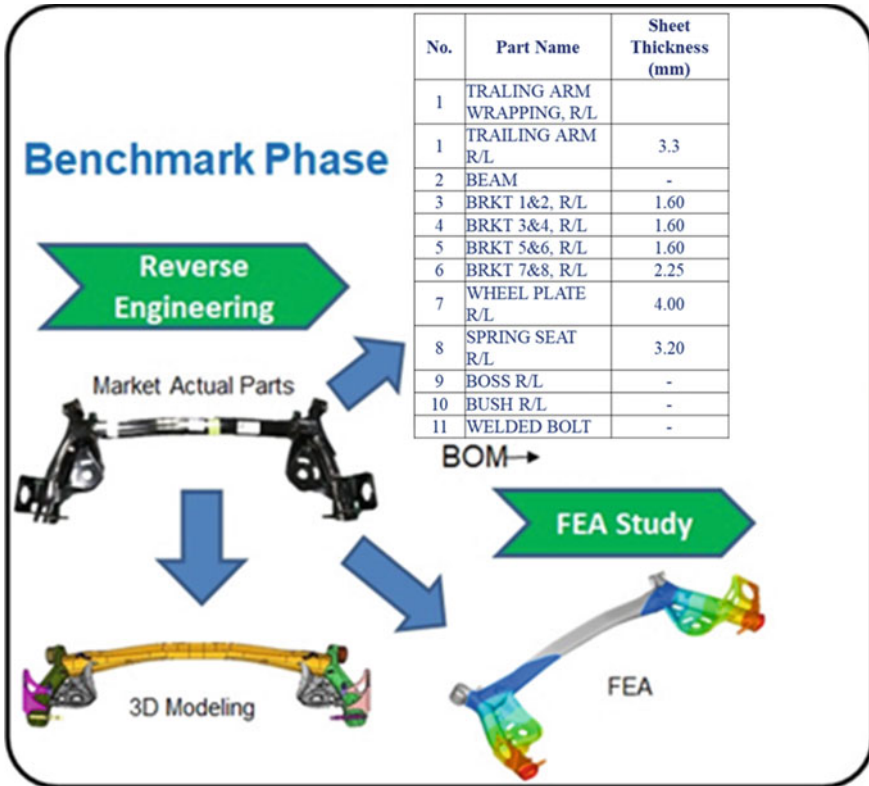


Fig. 6 Schematic approach for research methods

### 4.1 Comparison of Model G Cross Beam with Other Profiles

Table 2 is updated as Table 3: Model G is compared to other cross beam profiles (Table 4).

From above result tables, it is noted that:

- (1) The roll stiffness characteristics of Model G is higher than tubular profile and,
- (2) The camber compliance is lower than the than the tubular cross beam profile.

Thus, Model G meets the screening criteria as well achieved better performance characteristics.

Durability is a critical attribute of rear twist beam axle. It should be performed to ensure that there is no significant durability issue in the proposed design component.

This can be done by using similar approach of comparing the benchmark model against the new proposed design. Both the designs need to subjected to same durability conditions in CAE and compared against.

Based on durability results, weight or manufacturing process optimization can be done for new proposed design.

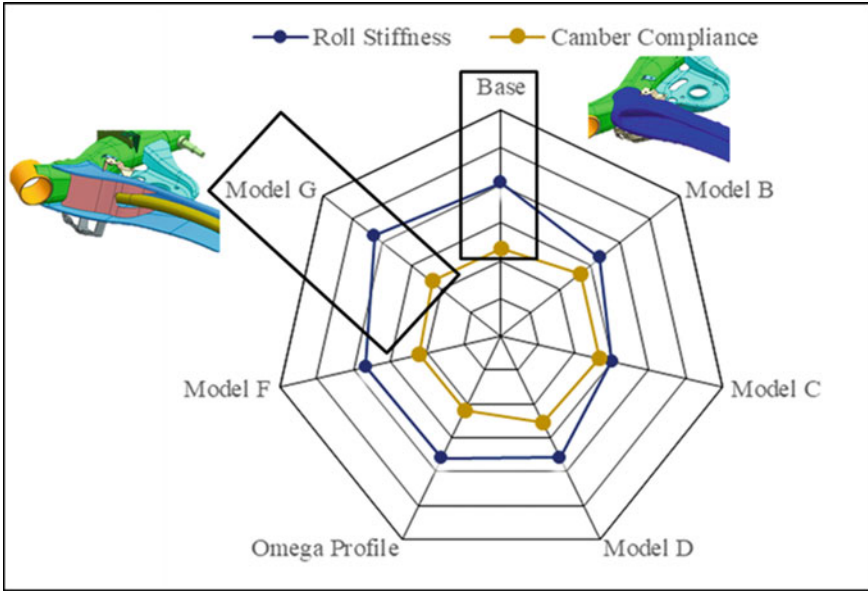


Fig. 7 Comparison of new design cross beam profile for roll stiffness and camber compliance

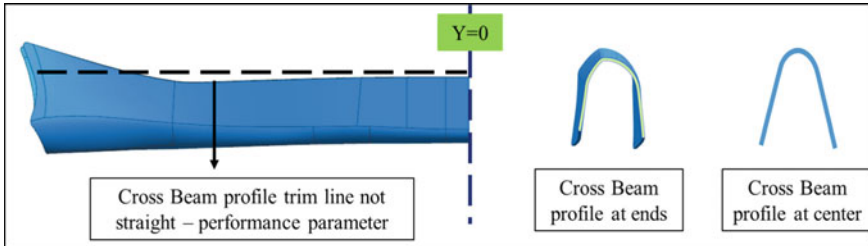






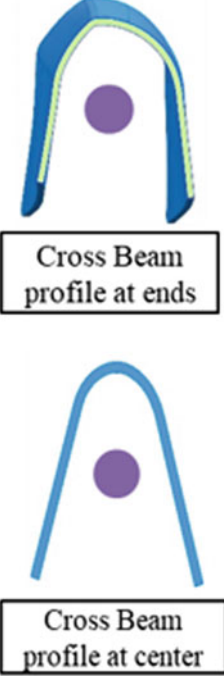
Fig. 8 Model G cross beam profile

## 5 Conclusion

Reverse engineering along with FEM is suitable technique to analyze available cross beam profiles. A lot of iterations are needed for achieving the performance requirements. The proposed design Model G met all requirements equal or better than the existing rear twist beam axle.

- (1) The new design is established by optimizing the cross section, thickness and shape of the cross beam profile or trim line.
- (2) U-Type cross beam with flanges is easier to tune compared to tubular cross beam.
- (3) Tube type cross beam has variable sections and difficult to tune.
- (4) U-Type cross beam with flanges is having ease in manufacturing, less complex.

**Table 3** Complete table with addition of Model G

Torsion profile type	Profile Image	Roll stiffness (kNm/deg)	Camber compliance (deg/KN)	Shear center height	Remarks
Tubular profile		Base	Base	Base	Base for comparison
U shaped open section		---	-	-	Low roll stiffness
Open section with stabilizer bar		+	base	-	Fits screening criteria low shear center
Omega profile		-	-	++	Low roll stiffness and high shear center
Model G	 <p>Cross Beam profile at ends</p> <p>Cross Beam profile at center</p>	++	-	base	Lower camber compliance higher roll stiffness

**Table 4** Result summary

Performance characteristics	Tubular profile	Model G
Roll stiffness (kNm/deg)	0.45	0.52
Camber compliance (deg/kN)	0.17	0.16

## References

1. Heiβing B, Ersoy M (2011) Chassis handbook: fundamentals, driving dynamics, components, mechatronics, perspectives. Springer
2. Held V, Hiemenz R (2014) Adam Opel AG, Rüsselsheim. Wiley, Germany. Encyclopedia of automotive engineering
3. Mun K-J, Kim T-J, Kim Y-S (2010) Analysis of the roll properties of a tubular-type torsion beam suspension. Proc Inst Mech Eng Part D: J Autom Eng 224:1–13
4. Kim S, Lee S, Jung H, Lee C (2002) Kinemastatic analysis of torsion beam suspension with varying cross section and location of the beam. In: Proceedings of the transactions of the Korean society of automotive engineers conference, May, pp 813–818 (Korean Society of Automotive Engineers, Seoul)
5. Marsh AJ, Wolperding K, Wille HC (1996) Simulation of the twist beam rear suspension system using flexible bodies in ADAMS. In: Proceedings of the 11th European ADAMS user conference, Frankfurt, Germany, Nov19–20, p 15
6. Fichera G, Lacagnina M, Petrone F (2004) Modelling of torsion beam rear suspension by using multibody method. Multibody SysDyn 12:303–316
7. Sharma C et al (2014) Design and fabrication of environment-friendly kart. Int J Eng Res Appl. Special Issue: 338–342
8. Kang J (2004) Kinematic analysis of torsion beam rear suspension. Trans Korean Soc Autom Eng 12(5):146–153
9. Sugiura H, Mizutani Y, Nishigaki H (2002) First order analysis for automotive suspension design. R&D Rev Toyota CRDL 37(1):25–30
10. Lyu N, Park J, Urabe H, Tokunaga H, Saitou K (2006) Design of automotive torsion beam suspension using lumped-compliance linkage model. In: Proceedings of the asme international mechanical engineering congress and exposition, Chicago, Illinois, USA, Nov 5–10, vol 119, Part A, paper IMECE2006-15436, pp 219–228
11. Satchell TL (1981) The design of trailing twist axles. SAE paper 810420
12. Silveira ME, Passos FM, Dares JA (2008) Simulação numérica do teste de impacto por trenó de tanques de combustíveis utilizando formulações implícitas e explícitas. In: VIII Simpósio de Mecânica Computacional—SIMMEC, Belo Horizonte
13. Bastow D, Howard G, Whitehead JP (2004) Car suspension and handling. SAE International, Warrendale, USA
14. Fang XF, Tan K (2018) Analytical modelling of twist beam axles. Int J Veh Syst Model Test 13(1):1–25
15. Seth M, Glorer J, Schellhaas R (2017) Design of a new weight and cost efficient torsion profile for twist beam suspension. SAE Technical Paper 2017-01-149
16. Morales E (2016) Study of different twist-beam axle configurations in elasto-kinematics and handling behaviour of a vehicle. Society of Automotive Engineers Technical Paper 2016–36–0184. <https://doi.org/10.4271/2016-36-0184>
17. Gillespie TD (1992) Fundamentals of vehicle dynamics. Society of Automotive Engineers, New York
18. Reimpell R, Stoll H (1996) The automotive chassis: engineering principles. Society of automotive engineers, New York
19. Leal V (2007) Estudo Cinemático de Suspensões Veiculares do Tipo Eixo de Torção. Dissertação de Mestrado. PUCMinas, Belo Horizont

20. Holdmann P, Köhn P, Möller B (1998) Suspension kinematics and compliance - measuring and simulation. Society of Automotive Engineers, 980897
21. Hamed B, Webb J (2007) The new twist beam axle design for a passenger vehicle. SAE Technical Paper 2007-01-0863
22. Vasconcelos L, Silveira M, Christoforo A (2012) Evaluation of the torsion beam of a twist-beam suspension by numerical simulation. SAE Technical Paper 2012-36-0483

# Effect of Tool Pin Features on Mechanical Properties of AA7050-T7 Friction Stir Welded Joints



Anugrah Singh, Vikas Upadhyay, and Joy Prakash Misra

**Abstract** The joint quality and efficiency in friction stir welding extensively rely on tool geometry, including tool shoulder and pin features. Present research effort aimed to investigate the effect of threaded cylindrical and combined semi-cylindrical pin cross-section (each half of different diameters) features with swept ratios (SR) of 1.01, 1.18, and 1.38, respectively, on AA7050-T7 butt-weld joint quality. Joint quality was scrutinized through tensile testing, microhardness measurements, and fractography. Impressive tensile properties were detected for the tool with 1.01 SR value. Highest average microhardness value was evaluated for weld nugget using FSW tool having 1.38 SR value followed by SR values of 1.01 and 1.18. The fracture location of tensile specimens was witnessed at the nugget zone (NZ) for defecting welds using tool pins having 1.18 and 1.38 SR values. Besides, fractured surfaces were examined through a scanning electron microscope (SEM) to evaluate the experimental outcome critically.

**Keywords** Friction stir welding · Pin feature · Swept ratio · Mechanical properties and fractography

## 1 Introduction

High strength 7xxx-series aluminum alloys exhibit low density, better tensile strength, good impact strength, and significant corrosion resistance properties [1]. Among various 7xxx-series alloys, commercially available AA7050 exhibits better toughness, good corrosion resistance, and less quench sensitive than AA7075; thus it found applications in fuselage frames, bulkheads, and wing skin applications [2]. The AA7050 is extensively used in the T7 (overaged) condition [3]. 7xxx-series alloys

---

A. Singh (✉) · V. Upadhyay

Department of Mechanical Engineering, National Institute of Technology Patna, Patna, India

e-mail: [anugrahs.phd16.me@nitp.ac.in](mailto:anugrahs.phd16.me@nitp.ac.in)

J. P. Misra

Department of Mechanical Engineering, Indian Institute of Technology (BHU), Varanasi, India

© The Author(s), under exclusive license to Springer Nature Singapore Pte Ltd. 2023

581

R. P. Singh et al. (eds.), *Advances in Modelling and Optimization of Manufacturing*

*and Industrial Systems*, Lecture Notes in Mechanical Engineering,

[https://doi.org/10.1007/978-981-19-6107-6\\_41](https://doi.org/10.1007/978-981-19-6107-6_41)

are particularly not fusion weldable due to porosity formation, brittle solidification products, and crack sensitivity in the joint region that significantly deteriorates the weld properties [4, 5]. For joining these high-strength aluminum alloys, friction stir welding (FSW) is an environmental-friendly, high potential and proven technique [6]. The FSW process generally results in significant weld profile development with better joint surface quality as compared to conventional fusion welding process [7].

During FSW, the movement of non-consumable tool generates frictional heat on abutting plate faces. Thus, the plasticized material flows under almost hydrostatic conditions around the tool pin as well as between the tool shoulder and work-piece top surface [8]. Apart from other process parameters, tool design affects the plastic flow and heat generation within the weld region which significantly affects mechanical properties and defect formation [9, 10]. The tool design also affects axial, longitudinal, and lateral forces acting on tool surfaces [11, 12]. An efficient tool design promotes a more significant plastic flow, lowers defect density, and enhances mechanical properties of the FSW joint [13]. The FSW defects formation such as voids, tunnels, kissing bond, nugget collapse, excessive flash, surface grooves, surface galling, lack of fusion, and lack of penetration are directly concerned to a list of welding parameters that includes tool design features, rotational speed (RS), welding speed (WS), plunge depth, tool tilt angle, and axial load [14]. The formation of defects in friction stir welded joints such as voids, pinholes, tunnel, a zigzag line, cracks, piping defect, and flash are caused by improper material flow and insufficient material consolidation in weld nugget [15, 16]. Trimble et al. [17] emphasized new tool feature development as the most critical FSW research area. The same lowers the force required to stir the material, reduces cost-relevant energy, and advantageously permits high WS with lower thermal cycles. The FSW tool imparts a vital role during the solid-state welding process and needs to be regularly updated for improved process and quality efficiency [18]. In general, FSW tool designs needs to be regularly updated on trial and error basis for adequate FSW joint properties.

The tool pin profile is the most crucial factor in determining weld geometry, stirring action, relocation of stirred materials, localized heating, and defect generation [15, 19, 20]. Thomas et al. [21] reviewed that cylindrical threaded tool pin was adequate for butt welding for 12 mm thick aluminum alloy plates. Upon employing cylindrical threaded pin feature, Alvarez et al. [22] reported formation of defects in weld nugget as the entrapped material within the thread feature hinders the cavity filling process. To assure better material intermixing, a greater path for material flow may be generated by a suitable tool with a higher SR value that requires reducing the tool pin static volume. The tool pin shape may comprise different forms or features (i.e. flutes, flats, and steps) in place of typically employed cylindrical threaded tools [23, 24]. Among these, flat face tool pins (such as square and triangle) were sometimes eccentricity associated with permitting in-compressed material flow around the tool pin [18, 19].

During FSW of AA7075-T6, Azimzadegan and Serajzadeh [25] noted tunnel or wormhole defects due to velocity field discontinuities around the FSW tool while a sound weld was produced at an optimum parameter combination of 1300 rpm RS and 40 mm/min WS. Bisadi et al. [26] investigated the effect of square, triangle and



**Table 1** Elemental composition and mechanical properties of AA7050

Materials	Elemental composition (wt%)											Mechanical properties		
	Si	Cu	Mg	Zn	Mn	Fe	Ti	Zr	Cr	Sc	Al	UTS (MPa)	El (%)	Hardness (HV)
AA7050	0.1	2.1	2.0	6.0	0.1	0.03	0.12	0.13	0.04	0.07	Bal	521.67	18.5	155

cylindrical tool pin shape with 6° concave shoulder feature during plunge stage in FSW of AA7075 at fixed process parameter combination of 1100 rpm RS, 0.1 mm/s plunge speed and 4° tool tilt angle. It was reported that friction was most influential factor in determining temperature around the pin compared to plastic deformation. The material transfer behavior of the thermo-mechanical affected zone (TMAZ) during AA7075-T6 FSW process was studied by Ji et al. [27]. The maximum material transfer displacement occurred in the middle of weld cross-section toward the retreating side. However, the tendency related to the displacement of material transfer decreases with increasing RS and decreasing WS.

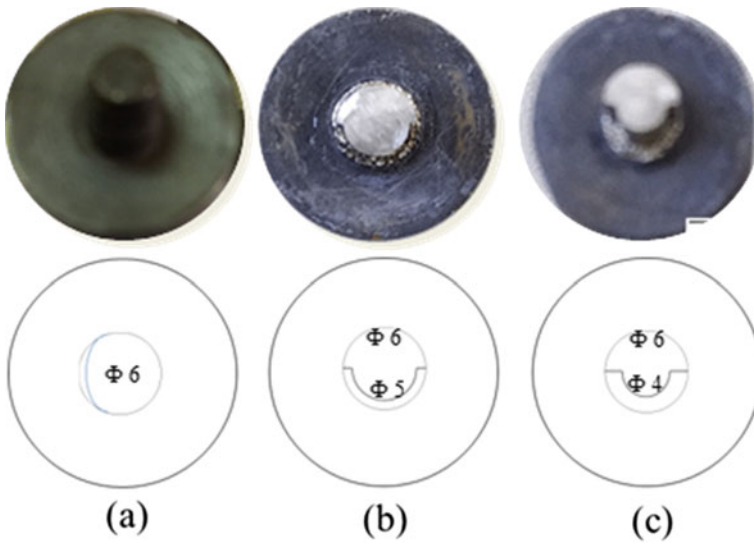
Through extensive literature review, it was observed that only a few literature reported on effect of tool pin features during FSW of 7xxx series aluminum alloys. The present work focuses the effect of tool pin features on mechanical properties of friction stir welds of AA7050-T7.

## 2 Experimental Methods

Aluminum alloy 7050-T7 plates of 6.35 mm thickness were friction stir welded in rectangular butt-joint configuration ( $145 \times 100 \times 6.35 \text{ mm}^3$ ). The elemental composition and mechanical properties (such as ultimate tensile strength, UTS; percentage elongation; and hardness) of AA7050-T7 were enlisted in Table 1.

Three FSW tools with different pin features were shaped from 20 mm diameter H13 grade steel rod with 6° concave shoulder feature of diameter 18 mm. The right hand cylindrical threaded pin profile (M6  $\times$  1) with 6 mm diameter swept volume was designated as Tool 1. Two new FSW tool pins with combined cross-sections of two semi-cylinder having different diameters were shaped by electric discharge machining and designated as Tool 2 (Combined semi-cylindrical cross-section with each half diameter of 6 mm and 5 mm) and Tool 3 (Combined semi-cylindrical cross-section with each half diameters of 6 mm and 4 mm). The fabricated tools were then heat treated to improve their hardness, as shown in Fig. 1.

As there is no such pulsating action for cylindrical threaded and newly designed tool pin profiles, FSW tools were compared through SR value. The SR value of FSW tools was evaluated for the pin height of 6 mm, Table 2.

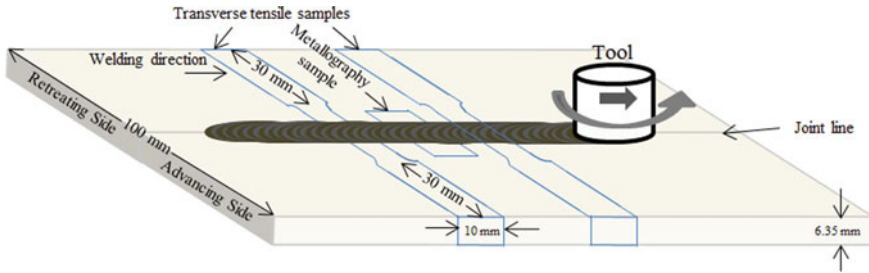


**Fig. 1** FSW tools with different pin cross-sections: **a** Tool 1, **b** Tool 2, and **c** Tool 3

**Table 2** SR ratio of different FSW tools

FSW tools	Dynamic volume	Static volume	SR (ratio of dynamic to static volume)	Dynamic orbit
Tool 1	169.65	167.18	1.01	
Tool 2	169.65	143.73	1.18	
Tool 3	169.65	122.52	1.38	

FSW of AA7050-T7 was performed at fixed welding parameters with 0° tool tilt angle, WS of 120 mm/min and RS of 1200 rpm on vertical CNC (computer numerical control) milling machine (Make: Manford VL760 model). The tool was traversed perpendicular to rolling direction of the parent material. Transverse tensile (ASTME8 M-13 standard) and metallographic samples were sectioned from each weld through a wire-electric discharge machine (Fig. 2). The tensile testing was performed on a universal testing machine (Make: Tinius Olsen H50KS model) with 1 mm/min cross-head speed. Metallographic samples were prepared through standard polishing procedure. Polished samples were then etched with Kellers’ reagent (a solution of 3 ml nitric acid, 6 ml hydrochloric acid, 6 ml hydrofluoric acid, and 190 ml distilled water) for 50 s. Hardness of the joint region was recorded along the mid-thickness line of polished surface with 1 mm gap between two successive indents by diamond



**Fig. 2** Schematic representation of friction stir weld and testing sample

indenter on a microhardness tester instrument (Make: UHL VMHT model) operated at 100 gf applied load for 30 s dwell time.




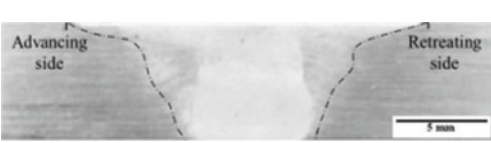

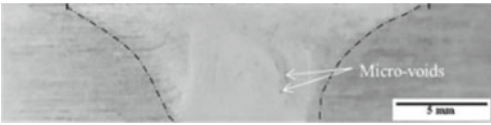
### 3 Results and Discussions

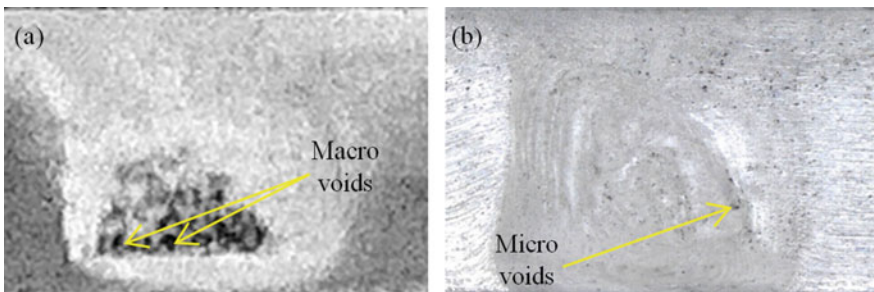
The visuals of weld top surface and transverse cross sections for joints fabricated using different FSW tools were enlisted in Table 3. FSW joints fabricated from Tool 1 has smooth top surface finish as compared to welds made by Tool 2 and Tool 3. However, large amount of flash was generated during FSW by Tool 2 than others. This new tool design induces high deformation that causes most materials to flow out and insufficient material stirred at the bottom part. It was previously reported that weld quality relies on the deformation ability and material around the FSW tool [28]. Although, a small amount of flash was observed on the weld top surface during FSW by Tool 3.

The transverse weld cross-section comprises distinct metallographic regions based on heat generation and material flow during the FSW process; thus, the shape and size of the weld nugget changed with increasing SR ratio. In NZ, the pin-driven zone shape strongly depends on pin geometry [29]. Through macrostructure, a wide shoulder affected region was observed in Tool 3 weld than others. The decrement in pin tip surface area overall through the pin lateral surface area causes increased contact surface area of shoulder to the weldments that reflect as wide shoulder interacted part in transverse weld cross-section [26].

The defect-free weld was obtained in FSW using a threaded tool pin. FSW with Tool 3 resulted in micro-void on the weld transverse cross section, whereas FSW with Tool 2 resulted in macrovoids caused by improper mixing of material at the weld bottom part (Fig. 3). The insufficient availability of material at the bottom side during weld fabrication with Tool 2 caused the coalescence of macro-voids. It was observed that defect size in friction stir welds gets reduced by increasing tool interference with the weldments due to better interaction. Additionally, the adequate flow path is provided due to higher swept-to-static volume ratio [19].

**Table 3** a Photograph of weld top surface. b Photograph of weld transverse cross-sections

(a)	
Weld fabricated with	Weld joints
Tool 1 (SR = 1.01)	
Tool 2 (SR = 1.18)	
Tool 3 (SR = 1.38)	
(b)	
Weld fabricated with	Macrostructure
Tool 1 (SR = 1.01)	
Tool 2 (SR = 1.18)	
Tool 3 (SR = 1.38)	



**Fig. 3** Enlarged view of weld defects with: **a** Tool 2 and **b** Tool 3

### 3.1 Tensile Properties

The variation in tensile properties for welds using different tool pin profiles was shown in Fig. 4. The highest UTS value was obtained as 405 MPa for weld joint using Tool 1 followed by 299 MPa for Tool 3, and 276.5 MPa for Tool 2. Also, the highest elongation value of 8.81% was evaluated for weld joint using Tool 1, followed by 6.05% in the case of Tool 3 and 5.77% for Tool 2. It was observed that tensile properties decrease with increasing SR value from 1.01 to 1.18 due to improper mixing of materials causing macro defects in weld nugget produced by Tool 2. However, a further increase in SR value from 1.18 to 1.38 shows a marginal increment in tensile properties due to a low tendency for defect formation. FSW tool with high eccentricity or SR value produces more effective stirring or mixing action and significantly reduces voids formation [19, 24]. Overall, a decreasing-increasing trend was observed in tensile properties of AA7050-T7 friction stir welds using different tool pin features with increasing SR value from 1.01 to 1.38.

The highest joint strength and elongation efficiency were evaluated as 77.63% and 47.62%, respectively, for FSW joint using Tool 1. Moreover, the joint strength and elongation efficiency of Tool 3 weld samples were calculated as 57.32% and 32.70%, respectively. The lowest joint strength and elongation efficiencies were 53% and 31.19%, respectively, for welded joint using Tool 2. The joint efficiency of 50% was obtained through fusion welding of AA7075-T6 [16]. Thus, the newly introduced design tool pin feature shows a marginal advantage over the fusion welding process and maybe modified further for better results.

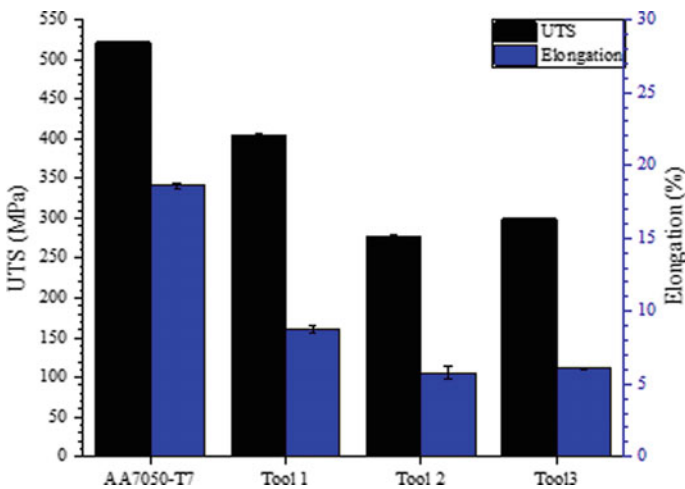


Fig. 4 Variation in tensile properties of welded joint by different FSW tools

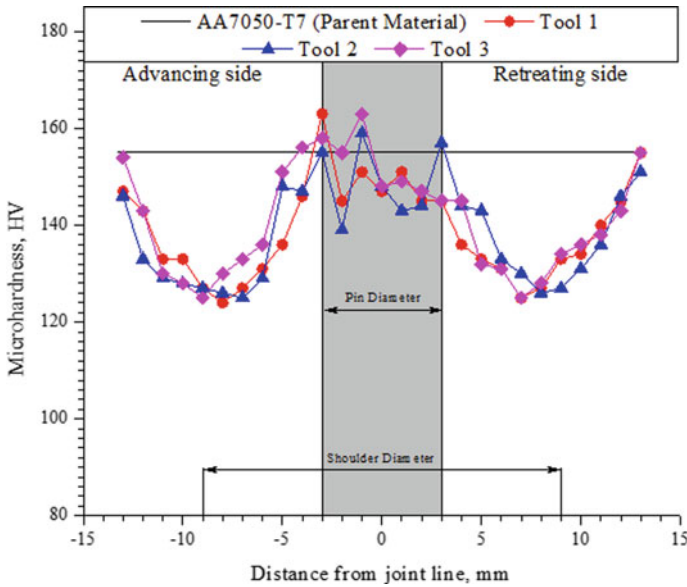


Fig. 5 Variation in vickers microhardness in the welded joint using different tool pin profiles

### 3.2 Microhardness

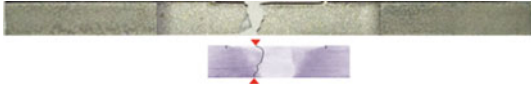
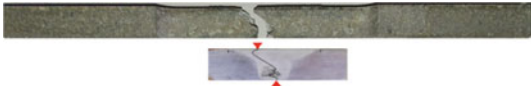
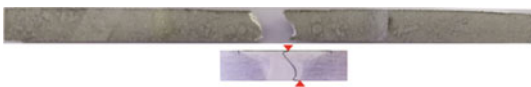
Microhardness variation at different locations across the mid-thickness line of the welded region using different tool pin profiles was plotted and shown in Fig. 5.

The W-shaped microhardness profile was observed for all welds as the minimum hardness value lies between the hardness of NZ and unaffected parent material with the lower respective value. Highest average microhardness value of 152.14 HV was evaluated for welded region produced by Tool 3, having a higher SR value followed by 149.57 HV for Tool 1 and 149.29 HV for Tool 2. Thus, a lower average microhardness value was noted for developed weld regions of FSW joints in comparative to 155 HV hardness of base metal. For increased SR value from 1.18 to 1.38, better intermixing materials with a few micro defects in NZ reflect a higher average microhardness value. A similar observation was obtained for friction stir welds fabricated using tool having higher SR values as they exhibit higher nugget microhardness values [19].

### 3.3 Fractography

In tested tensile samples, fracture locations were measured along the mid-thickness line from the joint center (intersection of joint line and mid-thickness line) of fractured samples and are presented in Table 4. The defect-free transverse tensile specimens of

**Table 4** Fracture position in FSW welded tensile specimen

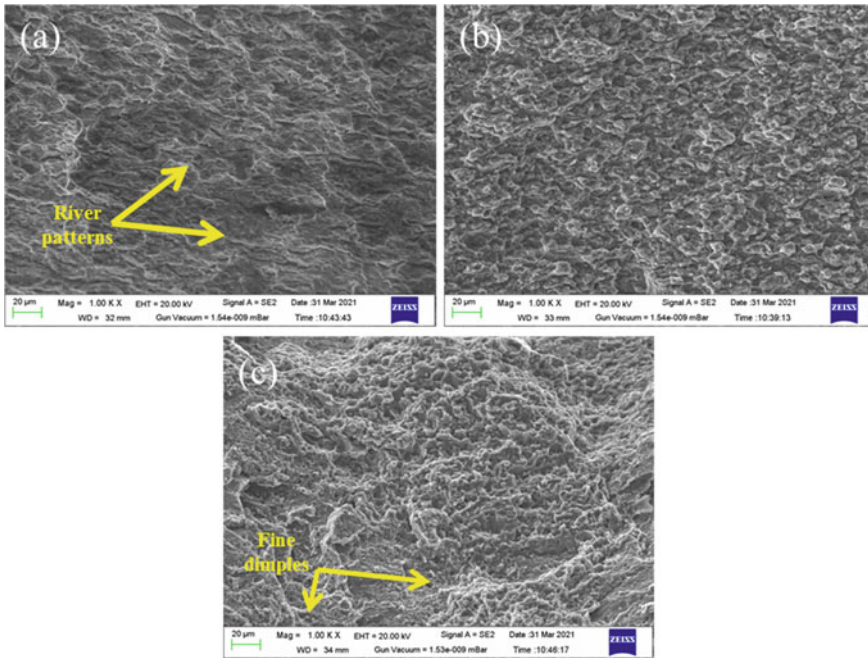
Samples welded with	Tensile tested specimens		Fracture	
	Advancing side	Retreating side	Location (mm)	Zone
Tool 1 (SR = 1.01)			3.42	NZ-TMAZ
Tool 2 (SR = 1.18)			Defect	NZ
Tool 3 (SR = 1.38)			Defect	NZ

weld using Tool 1 were fractured at 3.42 mm toward the advancing side due to hard second phase particles that were most favorable for crack initiation. However, the tensile specimens of defected weld samples fabricated with Tool 2 and Tool 3 were fractured with zigzag patterns originating from defect location. The welded tensile samples of Tool 3 showing micro defects get fractured from retreating side unlike others.

SEM images of fractured surface reveal the presence of fine microscopic voids with torn edges for Tool 3 welds, while transgranular brittle behavior with erratic fracture section was observed for Tool 2 weld (Fig. 6b, c). The presence of torn edges with fine dimples on exposed fracture surface reflects more ductile behavior for FSW joint due to capability to sustain tensile load after micro-void coalescence starts [30]. However, mixed river patterns with fine dimples were observed for Tool 1 fabricated weld joint (Fig. 6a).

## 4 Conclusion

In this work, a comparative analysis was carried out for a similar FSW of AA7050-T7 using three different tool pin features at fixed welding parameters. With increased SR value, the broadest joint area was observed for Tool 3 than others due to strong stirring and high frictional heat generation. The highest joint strength and elongation efficiency were evaluated for the FSW joint using Tool 1 (SR-1.01), followed by Tool 3 (SR-1.38) and Tool 2 (SR-1.18). Meanwhile, the highest average microhardness value of 152.14 HV was evaluated for the Tool 3 welded region, followed by 149.57



**Fig. 6** SEM fractography of fractured surfaces for welds fabricated by: **a** Tool 1, **b** Tool 2, and **c** Tool 3

HV in the case of Tool 1 and 149.29 HV for Tool 2 weld joint region. Compared to weld using Tool 2, the increased UTS, elongation, and average microhardness value for weld of Tool 3 with fewer defects emphasized that further design modifications may result in improved and significant weld joint properties.

**Acknowledgements** The authors thankfully acknowledge the Science and Engineering Research Board, India, for the support to carry out this research work through Grant No. ECR/2016/001738.

## References

1. Buchibabu V, Reddy GM, De A (2017) Probing torque, traverse force and tool durability in friction stir welding of aluminium alloys. *J Mater Process Technol* 241:86–92
2. Dursun T, Soutis C (2014) Recent developments in advanced aircraft aluminium alloys. *Mater Des* 56:862–871
3. Canaday CT, Moore MA, Tang W, Reynolds AP (2013) Through thickness property variations in a thick plate AA7050 friction stir welded joint. *Mater Sci Eng A* 559:678–682
4. Sivaraj P, Kanagarajan D, Balasubramanian V (2014) Fatigue crack growth behaviour of friction stir welded AA7075-T651 aluminium alloy joints. *Trans Nonferrous Met Soc China* 24:2459–2467



5. Su JQ, Nelson TW, Mishra R, Mahoney M (2003) Microstructural investigation of friction stir welded 7050–T651 aluminium. *Acta Mater* 51:713–729
6. Kumar K, Kailas SV (2008) The role of friction stir welding tool on material flow and weld formation. *Mater Sci Eng, A* 485:367–374
7. Cam G, Mistikoglu S (2014) Recent developments in friction stir welding of Al-alloys. *J Mater Eng Perform* 23(6):1936–1953
8. Thomas WM, Nicholas ED (1997) Friction stir welding for the transportation industries. *Mater Des* 18(4–6):269–273
9. Mugada KK, Adepu K (2018) Influence of ridges shoulder with polygonal pins on material flow and friction stir weld characteristics of 6082 aluminum alloy. *J Manuf Process* 32:625–634
10. Wang G, Zhao Y, Hao Y (2018) Friction stir welding of high-strength aerospace aluminum alloy and application in rocket tank manufacturing. *J Mater Sci Technol* 34(1):73–91
11. Arora KS, Pandey S, Schaper M, Kumar R (2010) Effect of process parameters on friction stir welding of aluminum alloy 2219–T87. *Int J Adv Manuf Technol* 50(9):941–952
12. Rai R, De A, Bhadeshia HKDH, DebRoy T (2011) Friction stir welding tools. *Sci Technol Weld Joining* 16(4):325–342
13. Ghiasvand A, Hassanifard S, Jalilian MM, Kheradmandan H (2021) Investigation of tool offset on mechanical properties of dissimilar AA6061-T6 and AA7075-T6 joint in parallel FSW process. *Weld World* 65(3):441–450
14. Qian J, Li J, Sun F, Xiong J, Zhang F, Lin X (2013) An analytical model to optimize rotation speed and travel speed of friction stir welding for defect-free joints. *Scripta Mater* 68:175–178
15. Dawood HI, Mohammed KS, Rahmat A, Uday MB (2015) Effect of small tool pin profiles on microstructures and mechanical properties of 6061 aluminum alloy by friction stir welding. *Trans Nonferrous Met Soc China* 25(9):2856–2865
16. Lotfi AH, Nourouzi S (2014) Predictions of the optimized friction stir welding process parameters for joining AA7075-T6 aluminum alloy using preheating system. *Int J Adv Manuf Technol* 73(9–12):1717–1737
17. Trimble D, Donnell GEO, Monaghan J (2015) Characterisation of tool shape and rotational speed for increased speed during friction stir welding of AA2024-T3. *J Manuf Process* 17:141–150
18. Essa ARS, Ahmed MMZ, Mohamed AKYA, El-Nikhaily AE (2016) An analytical model of heat generation for eccentric cylindrical pin in friction stir welding. *J Mater Res Technol* 5(3):234–240
19. Elangovan K, Balasubramanian V, Valliappan M (2008) Effect of tool pin profile and tool rotational speed on mechanical properties of friction stir welded AA6061 aluminium alloy. *Mater Manuf Processes* 23(3):251–260
20. Krasnowski K, Sędek P, Lomozik M, Pietras A (2011) Impact of selected FSW process parameters on mechanical properties of 6082–t6 aluminium alloy butt joints. *Arch Metall Mater* 56:965–965
21. Thomas WM, Johnson KI, Wiesner CS (2003) Friction stir welding—recent developments in tool and process technologies. *Adv Eng Mater* 5(7):485–490
22. Alvarez P, Janeiro G, Da Silva AAM, Aldanondo E, Echeverría A (2010) Material flow and mixing patterns during dissimilar FSW. *Sci Technol Weld Joining* 15(8):648–653
23. Gibson BT, Lammlein DH, Parter TJ, Longhurst WR, Cox CD, Ballun MC, Dharmaraj KJ, Cook GE, Strauss AM (2014) Friction stir welding: Process, automation, and control. *J Manuf Process* 16:56–73
24. Zhang YN, Cao X, Larose S, Wanjara P (2012) Review of tools for friction stir welding and processing. *Can Metall Q* 51(3):250–261
25. Azimzadegan T, Serajzadeh S (2010) An investigation into microstructures and mechanical properties of AA7075-T6 during friction stir welding at relatively high rotational speeds. *J Mater Eng Perform* 19(9):1256–1263
26. Bisadi H, Rasaei S, Farahmand M (2014) Effects of pin shape on the tool plunge stage in friction stir welding. *Trans Indian Inst Met* 67(6):989–995

27. Ji SD, Jin YY, Yue YM, Gao SS, Huang YX, Wang L (2013) Effect of temperature on material transfer behavior at different stages of friction stir welded 7075-T6 aluminum alloy. *J Mater Sci Technol* 29(10):955–960
28. Fu RD, Sun RC, Zhang FC, Liu HJ (2012) Improvement of formation quality for friction stir welded joints. *Weld J* 91:169–173
29. Radisavljevic IZ, Zivkovic AB, Grabulov VK, Radovic NA (2015) Influence of pin geometry on mechanical and structural properties of butt friction stir welded 2024-T351 aluminum alloy. *Hem Ind* 69(3):323–330
30. Gupta RK, Das H, Pal TK (2012) Influence of processing parameters on induced energy, mechanical and corrosion properties of FSW butt joint of 7475 AA. *J Mater Eng Perform* 21(8):1645–1654

# Damage Detection Using Recurrent Neural Network in Hybrid Composite Beam



Saritprava Sahoo and Pankaj Charan Jena

**Abstract** Structure health condition monitoring is better controlled by using the vibrational characteristic of damage detection; this is a quiet smart technique. In the present research, an inverse technique based on Recurrent Neural Networks (RNNs) has been presented for damage detection. Estimation of the crack location and depth in a graphene fiber reinforced polymer (GFRP) cantilever composite beam structure is formulated as a development of the problem; the optimum location and depth are found by reducing the objective function. The crack is determined by the implementation of the Recurrent Neural Network (RNN). The natural frequencies of a damaged beam are determined analytically using the finite element method (FEM). The optimization algorithm is programmed in MATLAB. The approach reduces the variations between the actual and predicted frequencies to determine the location and severity of the cracked GFRP cantilever beam. The method is verified using finite element analysis (FEA) measured data on a GFRP cantilever composite beam under consideration. The Fourier transform is used to develop frequency accuracy. The results show better accuracy in the projected technique.

**Keywords** Crack detection · Vibration analysis · GFRP · FEM. RNN

## 1 Introduction

Composite materials are becoming more prevalent in the aerospace industry due to their various advantages, such as their high strength, lightweight, and mechanical flexibility. The goal of this field is to develop effective methods and techniques that can detect and locate the location and severity of structural damage caused by vibration. Various studies have been performed in order to find a way to identify the damage caused by a structure. The objective of these investigations is to find a way to prevent or minimize the damage. A smart method for monitoring a structure's

---

S. Sahoo · P. C. Jena (✉)

Department of Production Engineering, VSS University of Technology, Burla, Odisha 768018, India

e-mail: [pcjena\\_pe@vssut.ac.in](mailto:pcjena_pe@vssut.ac.in)

condition is the use of the vibration signature. This method is usually used to detect damage caused by a moving component. In this paper, damage detection through Recurrent Neural Networks (RNN) has been proposed.

The early detection of structural cracks is very important to maintain the stability and dynamic behavior of the structures. In the past, the use of artificial neural networks for fault analysis has been widely used. The researchers analyzed various variable factors that affect the strength of a composite structure with an edge crack [1]. They developed a technique for identifying damage by implementing the process of factors associated with the natural frequency of the beam structure [2]. Using variations in natural frequencies and amplitudes of frequency response functions, they developed a damage detection technique for structural components [3]. They have investigated the impact of free vibration on the dynamic properties of epoxy-glass composite beams, and various crack locations and depths may affect the natural curvature of the beam [4, 5]. It has been shown that Elman's recurrent neural network can identify problems in nuclear power plants and rotating machine structures, according to Seker et al. [6]. Malhi and Gao employed recurrent neural networks to predict machine monitoring conditions [7]. Lee et al. developed a neural network technique for damage diagnosis in a bridge structure based on modal characteristics and taking baseline finite element model errors into consideration [8]. Yeung and Smith created a bridge-like structural damage detection method based on neural network ideas for pattern identification of the vibration signature and simulated real damage and then evaluating the *structural* response to conditions of moving traffic [9]. Bu et al. developed an innovative idea for calculating the bridge position based on a traversing vehicle's behavior. Elman's recurrent neural network has been applied in several comparative experimental studies by Hu and Balasubramaniam [10]. Ekici et al. employed Elman's recurrent network (ERN) to determine the location of a transmission line fault [11]. To identify structural damage in a bridge structure, the artificial neural network approach was used [12, 13]. Coban presented a new context layer for recurrent neural networks based on an Adaptive Learning rate algorithm [14]. Using the function of frequency response, they developed an artificial neural network-based approach for identifying damage in a structure [15]. Kourehli presented a technique to estimate the damage caused by an ANN and its location [16].

Many works on the subject of damage locations in geometric structures are based on the concept of ANN. However, the effects of non-homogeneity on the composite materials are still being studied. Most damage detection techniques involve the use of measures of structural responses to predict damage. Using RNN concepts to identify damage in structural dynamics concerns is rare in the literature. RNNs are superior to ANNs in terms of their ability to provide explicit model memory and to identify inter-tended dependencies. In this paper, the RNN technique is presented as a reversed approach for identifying the locations and determining the severity of cracks by dynamic excitation of the beam. ANSYS 14.0 is used to find the three relative natural frequencies for GFRP cantilever cracked beams with different crack parameters with 20 samples. The input relative natural frequency in RNN using MATLAB 2016a code-language to find the crack locations and depth is optimized.

## 2 The Basic Form of RNN

An RNN is an improved type of artificial neural network that consists of three multiple layers: input, hidden, and output. There are two differences, hence, as compared to the traditional networks: (i) The RNN nodes in the same hidden layer are connected. (ii) The present inputs of the hidden layer include both the present outputs of the input layer and the previous outputs of the hidden layer [17]. The fundamental architecture of RNN is shown in Fig. 1. This structure allows an RNN to study the temporal dynamic behavior of a time series. It can also be used to model the patterns of the current step.

Calculating Formula for Current State

$$h_t = f(h_{t-1}, x_t) \tag{1}$$

Formula for Activation Function (tanh)

$$h_t = \tanh(W_{hh}h_{t-1} + W_{xh}x_t) \tag{2}$$

Output calculation formula

$$y_t = W_{hy}h_t \tag{3}$$

- $h_t$  The current state
- $h_{t-1}$  The Previous state
- $x_t$  The Input state
- $W_{hh}$  The weight of a recurrent neuron
- $W_{xh}$  Weight at the input neuron
- $y_t$  The Output
- $W_{hy}$  The weight at the output layer

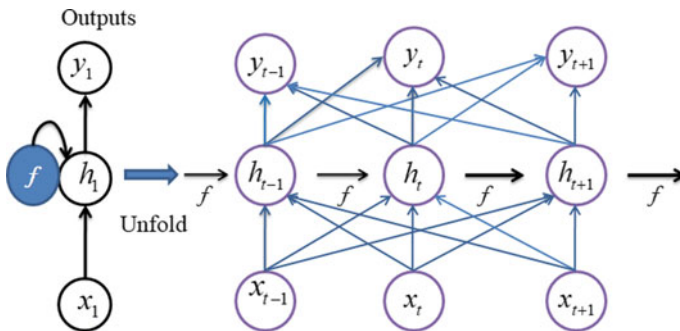


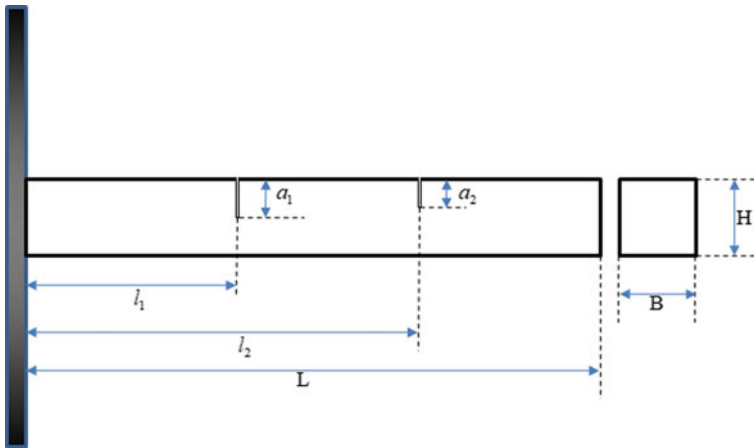
Fig. 1 Architecture of recurrent neural network

### 3 The Finite Element Technique (ANSYS)

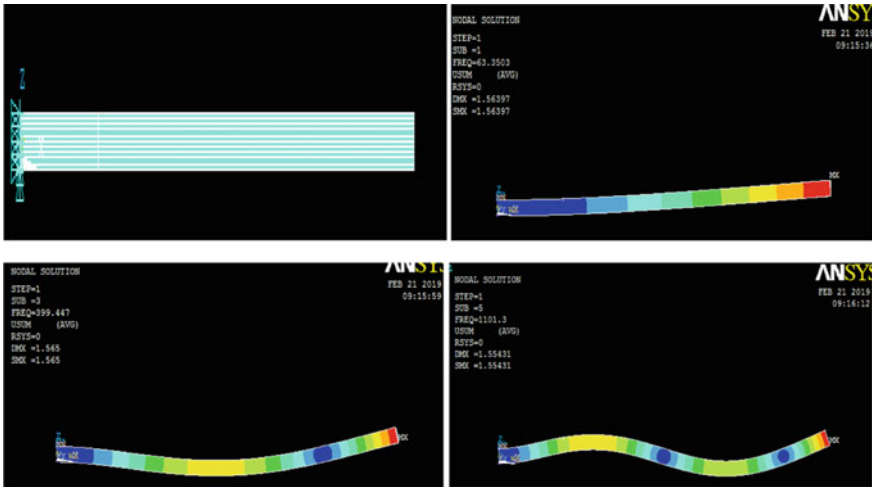
The present study used ANSYS 14.0 to determine the natural frequencies and mode shapes of a GFRP beam. E-glass fiber is employed as reinforcement, while epoxy resins are used as bases in the fabrication of the beam [18]. Table 1 provides a list of the material properties. The finite element technique (FET) is implemented with ANSYS 14.0 to analyze the natural frequencies and mode shapes of a fiber reinforced polymer composite beam in the present research work. A beam with a dimension of  $600 \times 50 \times 6$  mm, as shown in Fig. 2. For modal analysis, 8 nodded solid brick 185 components are used to represent the structure. It is designed to use a total of twelve layers of reinforcement. Different cracks are located at various depths (i) are developed in various locations (ii) and the cantilever beam end condition, the modal parameters are analyzed. Figure 3 presents the FEA beam model and the first three mode-shapes of an un-cracked beam [19]. Figure 3b–d presents the first three mode shapes of an unbroken beam, whereas the first three natural frequencies of a cracked beam, as shown in Table 2.

**Table 1** Epoxy and glass fiber have mechanical properties [18]

Properties	Glass fiber	Epoxy
Elasticity modulus (GPa)	80	2.4
Shear modulus (GPa)	3	0.895
Density ( $\text{kg/m}^3$ )	2600	1350
Poisson ratio	0.32	0.34



**Fig. 2** Double cracked FRP cantilever beam



**Fig. 3** ANSYS results. **a** layered beam, **b** first mode-shape **c** second mode-shape, **d** third mode-shape [18]

**Table 2** The results of finite element analysis (FEA) on a cracked beam

Data No.	rfnf	rsnf	rtnf	$l_1$	$l_2$	$a_1$	$a_2$
1	0.847555	0.850021	0.849465	0.166	0.333	0.3	0.2
2	0.843949	0.844243	0.845923	0.166	0.416	0.1	0.2
3	0.837189	0.833774	0.839686	0.166	0.416	0.2	0.4
4	0.82612	0.817505	0.830215	0.166	0.416	0.4	0.3
5	0.808251	0.793369	0.816817	0.166	0.5	0.1	0.4
6	0.847555	0.850021	0.849465	0.166	0.5	0.4	0.1
7	0.835227	0.844136	0.843536	0.166	0.5	0.4	0.4
8	0.828678	0.833625	0.837453	0.166	0.5	0.5	0.4
9	0.817928	0.817292	0.82829	0.166	0.66	0.1	0.2
10	0.800575	0.793049	0.8152	0.166	0.66	0.5	0.4
11	0.82262	0.849744	0.842381	0.333	0.66	0.2	0.2
12	0.819319	0.843923	0.839147	0.333	0.66	0.2	0.3
13	0.813129	0.833348	0.833449	0.333	0.66	0.4	0.1
14	0.802988	0.816908	0.824748	0.333	0.66	0.5	0.1
15	0.78655	0.792431	0.812274	0.416	0.66	0.1	0.1
16	0.847555	0.850021	0.849465	0.416	0.66	0.2	0.3
17	0.843949	0.844243	0.845923	0.416	0.66	0.2	0.4
18	0.837189	0.833774	0.839686	0.416	0.66	0.3	0.4
19	0.82612	0.817505	0.830215	0.5	0.66	0.1	0.3
20	0.808251	0.793369	0.816817	0.5	0.66	0.2	0.3

## 4 Result

The prevention of cracks in structures is essential in order to prevent a dangerous failure or accident. The presence of multiple cracks increases the chance of early breakdown of the structures. In order to avoid structural failures, it is critical that they are diagnosed and treated. In this article, the data is trained into the recurrent neural network, and the outputs are obtained as a result. ANSYS 14.0 is used to determine the first three non-dimensional natural frequencies of a GFRP cantilever cracked beam for different crack locations and depths. The MATLAB R2016a software tool that uses multi-layer direction has been developed for a recurrent neural network with a multi-hidden layer back propagation method used to predict the crack location and depth. The first, second, and third relative natural frequencies are denoted by the abbreviations *rfnf*, *rsnf*, and *rtnf*, respectively. Using Tables 3 and 4, it was observed that there was very less difference between the analysis and the RNN outputs in terms of the position and severity of the double cracks in the GFRP cantilever beam. These are obtained from Eq. 4.

$$rnf = \frac{w_{nc}}{w_{unc}} \quad (4)$$

where  $w_{unc}$  and  $w_{nc}$  denote the first three natural frequencies of cracked and uncracked composite beams, respectively. The input parameters are the first three relative natural frequencies are (*rfnf*, *rsnf*, and *rtnf*); the output parameters are relative length ( $l_1$  and  $l_2$ ) and relative depth ( $a_1$  and  $a_2$ ).

The performance function is the mean square error (MSE), and the activation function ( $\tanh$ ). Table 1 provides the input parameters required for data testing. The recurrent neural network is trained using the data from Table 1, and the outputs are predicted based on the testing data. Comparison of crack locations ( $l_1$ ,  $l_2$ ) and crack depth ( $a_1$ ,  $a_2$ ) of FEA and RNN results as shown in Tables 3 and 4. In this article, the first three relative natural frequencies are taken from the GFRP cracked cantilever beam. Equation (5) is used to determine the absolute error (AE) (Fig. 4).

$$AE = \frac{[\text{FEA result} - \text{RNN result}]}{\text{FEA result}} \quad (5)$$

The Fig. 5a, b indicate that the projected curve is in excellent agreement with the observed curve. Figure 5a, b also confirm the result of Table 3.

Figure 6 shows the regression analysis of RNN training, validation, and test data, which indicates good agreement with a minimum error (less than 2%) to the FEA results.



**Table 3** Error calculation of crack locations ( $l_1, l_2$ )

Data. No.	$l_1$ (FEA)	$l_1$ (RNN)	Error	$l_2$ (FEA)	$l_2$ (RNN)	Error
1	0.166	0.17003	- 0.0243	0.333	0.32751	0.01647
2	0.166	0.16606	- 0.0004	0.333	0.34292	- 0.0298
3	0.166	0.16421	0.01079	0.333	0.33938	- 0.0192
4	0.166	0.16892	- 0.0176	0.333	0.33173	0.00381
5	0.166	0.1731	- 0.0428	0.416	0.40603	0.02397
6	0.166	0.15874	0.04373	0.416	0.41607	- 0.0002
7	0.166	0.16692	- 0.0055	0.416	0.41211	0.00935
8	0.166	0.16368	0.01395	0.416	0.41435	0.00396
9	0.166	0.16895	- 0.0178	0.5	0.49455	0.01089
10	0.166	0.15575	0.06178	0.5	0.50925	- 0.0185
11	0.166	0.1635	0.01506	0.5	0.4945	0.011
12	0.166	0.15996	0.0364	0.66	0.65511	0.00741
13	0.166	0.1582	0.04701	0.66	0.67124	- 0.017
14	0.166	0.16011	0.03548	0.66	0.66818	- 0.0124
15	0.333	0.33593	- 0.0088	0.66	0.66323	- 0.0049
16	0.333	0.33664	- 0.0109	0.66	0.66195	- 0.003
17	0.333	0.33712	- 0.0124	0.66	0.66121	- 0.0018
18	0.333	0.34071	- 0.0232	0.66	0.65545	0.00689
19	0.333	0.33444	- 0.0043	0.66	0.66185	- 0.0028
20	0.333	0.34249	- 0.0285	0.66	0.65766	0.00355

## 5 Conclusion

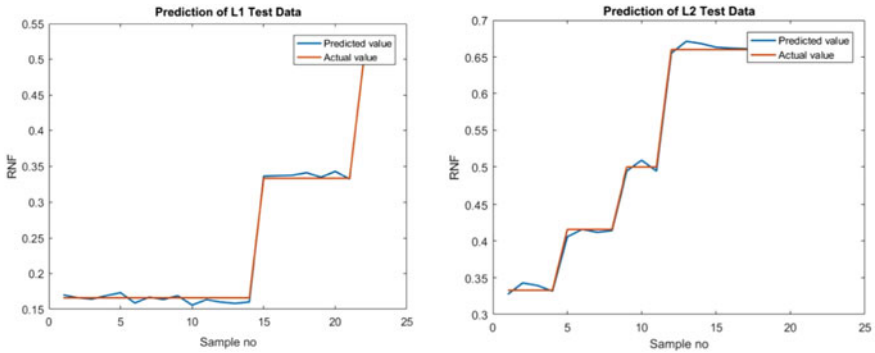
The natural frequency of a cracked beam is determined using the Euler’s equation and its natural shapes and mode are obtained at different crack locations. The finite element analysis results are compared with the results obtained from the recurrent neural network algorithm. The natural frequencies of the cracked beams are trained in the Feed-Forward Neural Network. Figure 4a, b, it can be shown that there is a high correlation between the predicted curve and the actual curve.

- In Table 4, it can be observed that there is a maximum error percentage of less than 2% between the actual (FEA) and predicted (RNN) results, which proves that the RNN is well-suited to predicting the crack parameters of an FRP cantilever cracked beam.
- The average error percentage between the FEA and ANN outputs is for depth  $a_1 = 2.7803e-04$  and  $a_2 = 7.8924e-07$ , and for crack location is  $l_1 = 2.7803e-04$  and  $l_2 = 3.4277e-05$ .

The crack location and crack depth parameters are calculated through RNN and ANSYS. This research concludes the following:

**Table 4** Calculation of crack depth ( $a_1, a_2$ ) error

Data. No.	$a_1$ (FEA)	$a_1$ (RNN)	Error	$a_2$ (FEA)	$a_2$ (RNN)	Error
1	0.1	0.12694	- 0.2694	0.3	0.30051	- 0.0017
2	0.2	0.19354	0.03228	0.1	0.10033	- 0.0033
3	0.2	0.20061	- 0.003	0.5	0.50051	- 0.001
4	0.3	0.29864	0.00453	0.2	0.1998	0.001
5	0.1	0.09028	0.09719	0.5	0.49862	0.00277
6	0.4	0.41702	- 0.0426	0.3	0.30031	- 0.001
7	0.4	0.39702	0.00744	0.5	0.49994	0.00012
8	0.5	0.49506	0.00987	0.2	0.20101	- 0.0051
9	0.2	0.18975	0.05127	0.2	0.1999	0.00052
10	0.3	0.2853	0.04901	0.1	0.09959	0.00408
11	0.3	0.31395	- 0.0465	0.3	0.29951	0.00162
12	0.1	0.135	- 0.35	0.2	0.19872	0.0064
13	0.2	0.16722	0.1639	0.3	0.29987	0.00042
14	0.3	0.29219	0.02603	0.4	0.40262	- 0.0066
15	0.1	0.06923	0.30773	0.3	0.30125	- 0.0042
16	0.2	0.17972	0.10141	0.3	0.30063	- 0.0021
17	0.3	0.28752	0.04159	0.2	0.19973	0.00135
18	0.4	0.41057	- 0.0264	0.3	0.29992	0.00025
19	0.4	0.41181	- 0.0295	0.5	0.49941	0.00118
20	0.5	0.50328	- 0.0066	0.3	0.2998	0.00065



**Fig. 4** Comparison of crack locations ( $l_1, l_2$ ) test data

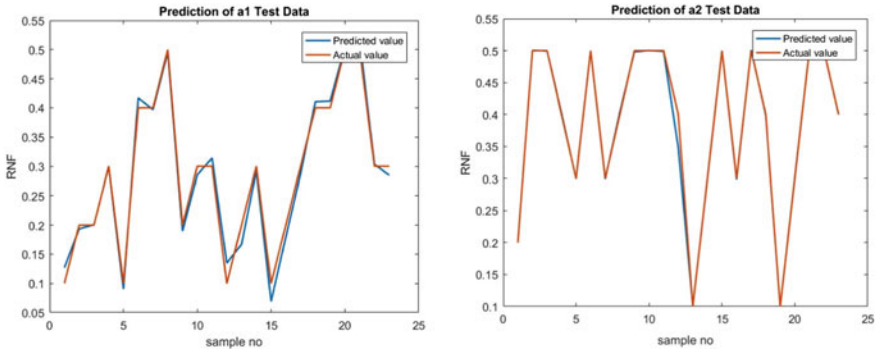


Fig. 5 Comparison of crack depth ( $a_1, a_2$ ) test data

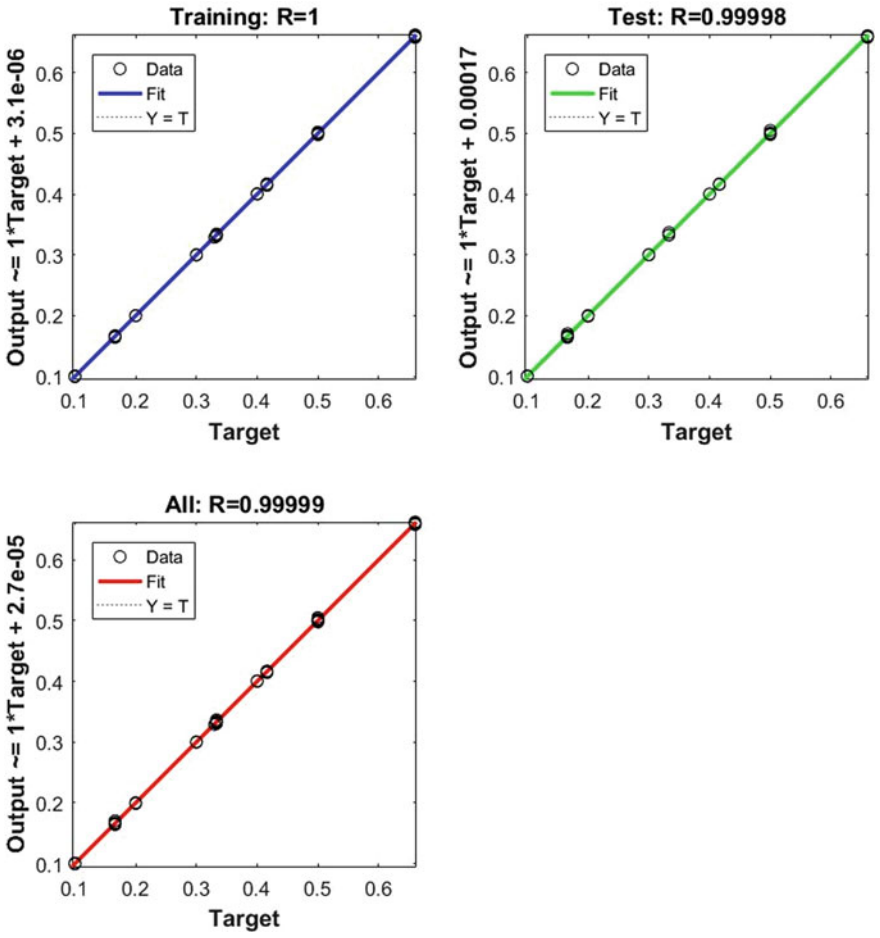


Fig. 6 The regression analysis

- The maximum error percentage between the RNN and FEA results is less than 2%, as shown in the FEA results, indicating that the data is in excellent agreement with each other.
- RNN should be used to identify defects in machine components and predict damage in metallic and composite structures.

**Acknowledgements** The authors do hereby acknowledge the facilities and supports of Veer Surendra Sai University of Technology, Department of Production Engineering, Burla, for carrying out this research work. Authors have not received any funding from any agencies to carry out this work.

**Declaration of Competing Interest** The authors declare that have no know competing financial interests or personal relationships that could have appeared to influence the work reported in this paper.

## References

1. Krawczuk M, Ostachowicz W (1995) Modeling and vibration analysis of a cantilever composite beam with a transverse open crack. *J Sound Vib* 183(1):69–89
2. Dems K, Mróz Z (2001) Identification of damage in beam and plate structures using parameter dependent frequency changes. *Eng Comput* 18(1/2):96–120
3. Owolabi GM, Swamidas ASJ, Seshadri R (2003) Crack detection in beams using changes in frequencies and amplitudes of frequency response functions. *J Sound Vib* 265:1–22
4. Jena PC, Parhi DR, Pohit G (2012) Faults detection of a single cracked beam by theoretical and experimental analysis using vibration signatures. *IOSR J Mech Civil Eng (IOSR-JMCE)* 4(3):01–18
5. Jena PC, Parhi DR, Pohit G (2014) Theoretical, numerical (FEM) and experimental analysis of composite cracked beams of different boundary conditions using vibration mode shape curvatures. *Int J Eng Technol* 6:509–518
6. Seker S, Ayaz E, Turkcan E (2003) Elman's recurrent neural network applications to condition monitoring in nuclear power plant and rotating machinery. *Eng Appl Artif Intell* 16:647–656
7. Malhi A, Gao XR, (2004) Recurrent neural networks for long-term prediction in machine condition monitoring. *IMTC 2004, Como, Italy*
8. Lee JJ, Lee JW, Yi JH, Yun BC, Jung YH (2005) Neural networks-based damage detection for bridges considering errors in baseline finite element models. *J Sound Vib* 280:555–578
9. Yeung TW, Smith WJ (2005) Damage detection in bridges using neural networks for pattern recognition of vibration signatures. *27(5):685–698*
10. Hu X, Balasubramaniam P (2008) Case studies for applications of Elman recurrent neural networks. *Recurrent Neural Netw* 357–378. InTech Publications, Shanghai, China
11. Ekici S, Yildirim S, Poyraz M (2009) A transmission line fault locator based on Elman recurrent networks. *Appl Soft Comput* 9:341–347
12. Gonz'alez-P'erez C, Vald'es-Gonz'alez J (2011) Identification of structural damage in a vehicular bridge using artificial neural networks. *Struct Health Monit* 10(1):33–48
13. Aydin K, Kisi O (2015) Damage diagnosis in beamlike structures by artificial neural networks. *J Civil Eng Manage* 21(5):591–604
14. Coban R (2013) A context layered locally recurrent neural network for dynamic system identification. *Eng Appl Artif Intell* 26:241–250
15. Bandara RP, Chan THT, Thambiratnam DP (2014) Structural damage detection method using frequency response functions. *Struct Health Monit* 13(4):418–429

16. Kourehli SS (2015) Damage assessment in structures using incomplete modal data and artificial neural network. *Int J Struct Stab Dyn* 15(6):1450087
17. Su B, Lu S (2017) Accurate recognition of words in scenes without character segmentation using recurrent neural network. *Pattern Recogn* 63:397–405
18. Sahoo S, Jena PC (2021) Preparation and characterization of hybrid laminated composite beams. *Adv Mater Proc Technol* <https://doi.org/10.1080/2374068X.2021.1953924>
19. Sahoo S, Jena PC (2021) Analysis of GFRP cracked cantilever beam using artificial neural network. *Mater Today: Proc* 44:1788–1793

# Analysis of the Tribological Behaviours of the Surfaces of Stainless Steel and Inconel 718 Against Each Other Under Non-lubricated Conditions



Khush Khanna, Sushant Bansal, Roop Lal, and Ramakant Rana

**Abstract** This paper entirely focuses on obtaining the experimental analytical result of the tribological behaviour of the surface of the test specimens, of the materials chosen, i.e. Inconel 718 and stainless steel, which were in continuous contact throughout the sliding motion. Inconel 718 is a nickel–chromium–molybdenum alloy that is highly corrosion resistant. It also exhibits high yield strength, tensile strength, and creep resistance. It is used in various places ranging from aerospace to nuclear reactors and gas turbines. In this paper, we perform tribological testing on Inconel 718 by using a pin-on-disc method. Inconel 718 pins are used along with a stainless steel disc. L8 orthogonal array was used for setting up the experimentation parameters.

**Keywords** Inconel 718 · Tribology · Wear · Dry sliding

## 1 Introduction

Inconel is a nickel–chromium-based super-4 alloy that offers high corrosion resistance. It can retain strength at high temperatures and is resistant to creep, therefore it is suitable for use in high temperature and pressure environments [1–4]. It is used in gas turbine blades, seals and turbocharger rotors and seals, it also finds applications in heat exchanger tubings, etc.

Inconel 718 is an alloy in the Inconel family and it also goes by its common trade names like Nicrofer 5219, Superimphy 718, Haynes 718, etc. [5–9].

Inconel 718 contains 50–55% Ni, 17–21% Cr, 2.8–0.3% Mo, 4.75–5.5% Nb&Ta, < 1% Co and a few other elements in small quantities. It balances the rest with Fe. Inconel 718 is age-hardened and is therefore machined by an aggressive slow cut using a hard tool, with minimal number of passes [8–13].

---

K. Khanna · S. Bansal · R. Rana

Department of Mechanical and Automation Engineering, Maharaja Agrasen Institute of Technology, Delhi 110086, India

R. Lal (✉)

Department of Mechanical Engineering, Delhi Technological University, Delhi 110042, India  
e-mail: [rooplal@dtu.ac.in](mailto:rooplal@dtu.ac.in)

There has been some work conducted in improving the tribological properties of Inconel 718 already. Xiao et al. [4] used graphene nanopellets to create an Inconel graphene composite. Selective layer melting was used to create the composites and it was found that at 1% Graphene Nanopellets, the coefficient of friction decreases by 22.4% and decreases the wear rate by 66.8%. Wan et al. [3] performed plasma nitriding of Inconel 718 at different temperatures, different treatment times, and different compositions of N<sub>2</sub> and H<sub>2</sub>. They found that the coefficient of friction can reduce about 3.7 times, but there is a formation of surface cracks which can lead to detachment of sliding layer after prolonged sliding use. Sun et al. [5] used cold sprayed Inconel 718 coatings in an attempt to enhance tribological properties and found that wear rate decreases at high temperatures due to a glaze layer being formed which acts a protection. It was also found that the coefficient of friction decreases at high temperatures because the breakage of oxides provided a debris that acted as a lubricant thereby reducing friction. Kurzynowski et al. [1] studied the wear behaviour of Inconel 718 laser surface alloyed with Rhenium at 14% and 28%. It was found that alloying with 28% rhenium gives 82% less sliding wear rate. The surface in contact at the time of sliding against each other have different outcomes on the material pertaining to the physical conditions such as the lubrication at the area of contact. So, not having any lubrication will have quite varying results too which are taken into consideration here [14–19].

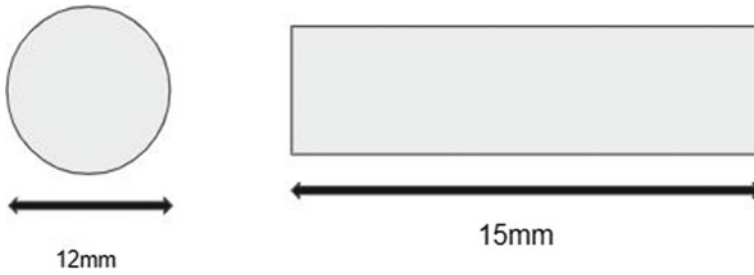
## 2 Materials and Specimen Preparation

### 2.1 Disc

A stainless steel disc of Diameter 10 cm and thickness 1 cm was prepared by the process of by the process of WEDM. After the plated of required dimensions were cut, circular grooves were made by drilling in it [18–23]. On obtaining the required specimen the surface was smoothened out using a surface grinder.

### 2.2 Pins

The pins were prepared from a cylindrical rod of the selected material, i.e. INCONEL 718. The specimens were made in a cylindrical shape, by the process of WEDM having a diameter of 12 mm and height being 15 mm. The pin surface, which was to be used as the contact surface, was then smoothed by the process of surface grinding [24, 25] (Fig. 1).



**Fig. 1** The pin specimen

### 3 Experimentation

#### 3.1 Selection of Orthogonal Arrays

The purpose of the Orthogonal arrays are to provide with a set of minimum experiments as well as Signal-to-Noise ratios (S/N). These are the log functions of the desired output, and they serve as the working objective functions for the optimization, and also help in data analysis, and prediction of optimum results [25–31].

The selection of orthogonal arrays is dependent upon the number of independent design variables and levels as each array is meant for only specific value of them. In this experiment, we chose 3 different independent variables; Load, distance, and speed with each variable having 2 set values. And the corresponding array for experimenting with 3 independent variables with 2 set values each is the L8 array, which is the one used for this experiment. It was assumed that there was no interaction between any two factors (Table 1).

**Table 1** Design of experiments

Experiment number	Independent variables		
	Load (N)	Distance (m)	Speed
1	20	100	0.5
2	20	200	0.5
3	20	100	1
4	20	200	1
5	30	100	0.5
6	30	200	0.5
7	30	100	1
8	30	200	1

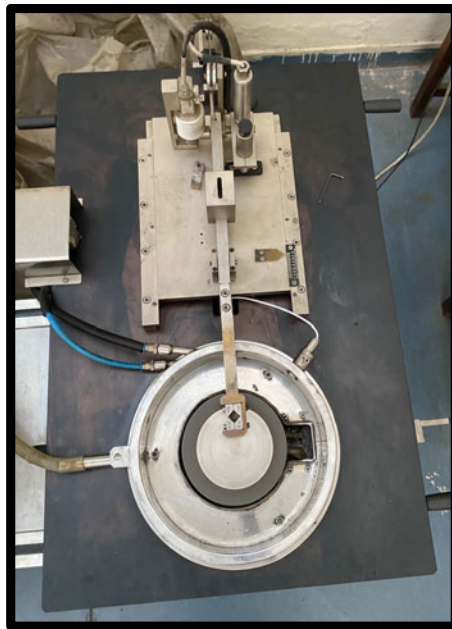


### 3.2 Tribological Testing

Tribological testing is a way to quantify the wear resistance and coefficient of friction. It usually involves simulating the sliding of a pair under the applied load to get a reading of the wear characteristics [31–33].

A pin-on-disc setup was chosen for this experiment. This consists of a disc that is mounted on the Tribometer setup and is rotated continuously on varying the speed by the help of input parameters. The machine also has a lever that extends over the disc and holds our specimen pin via a clamp. A load is hung on a rope that passes through the lever and over a pulley. This load pushes the pin down on the disc with the desired force which is also modified per experimental iteration as the input varying parameter [34–37].

The setup consisted of the Inconel pin mounted on a clamp kept perpendicular to the rotating disc. The pin is pressed against the disc with a certain pressure, and the wear resistance and coefficient of friction are found on the evaluation of wear. For the experimentation, different input parameters are varied to obtain varying outputs as results which are mainly obtained as the COF and wear of the specimen surface. The testing was carried out in a non-lubricated environment [36–39] (Fig. 2).



**Fig. 2** Top view of the setup

## 4 Results

Throughout the duration of the test the pin-on-disc interface was to be subjected to continuous sliding motion relative to each other this motion is the type of motion which in the chosen application, i.e. the IC Engine Piston Cylinder interface constitutes for the most part apart from very few percentages of lateral motion possibilities due to any error and wear that may occur during the usage of the part. Since this motion is of most importance to use, usage of pin-on-disc setup was most appropriate.

### 4.1 *Coefficient of Friction*

The laws of friction have established that whenever two surfaces are in contact with each other and experience some form of relative motion between them there is generation of some force which acts along the axis of relative motion between them this force is known as frictional force and acts in the direction which is opposite to that of the body motion. The frictional force is guided by two factors which are coefficient of friction, and the normal force or load which is applied between the two surfaces. The former is a material surface property and hence is governed by various factors such as temperature variation and abrasive nature of surface of specimens and other surface properties such as roughness of the surface, the value of COF for different materials varies due to above mentioned factors and hence is different for different material specifications. During the tribological experiment the coefficient of friction was observed at each point and a graph representing the variation of these values was plotted for both specimens has been plotted below, it was observed that the Coefficient of Friction (COF) for the material chosen, i.e. Inconel 718 for the experimentation was 1.333816. This value is mean COF value of all the iterations which were observed in experiment since there was variation in values of COF at during the experimental stage mainly due to the continuous change in surface properties of both stainless steel and Inconel 718 due to change in wear as the experiment proceeded which led to creation of abrasives and other surface topography changes which influence COF Values.

### 4.2 *Wear*

Due to this continuous sliding motion both the pin and disc experienced wear and absence of any kind of lubricant led to more amount of wear if compared to experiments performed under lubrication. In this experiment the test was performed under constant pressure which was applied using the normal load, equal to 20 and 30 N which provided us with constant pressure at the pin and disc interface, further during the experimentation the wear on the specimen pin was observed and it was concluded

that the pin experienced an almost continuous wear for the complete period of the experiment, just the initial seconds being the ones having a higher value on all iterations, though. The mean wear of all the iterations came out to be of 70.91145  $\mu\text{m}$  (Figs. 3 and 4).

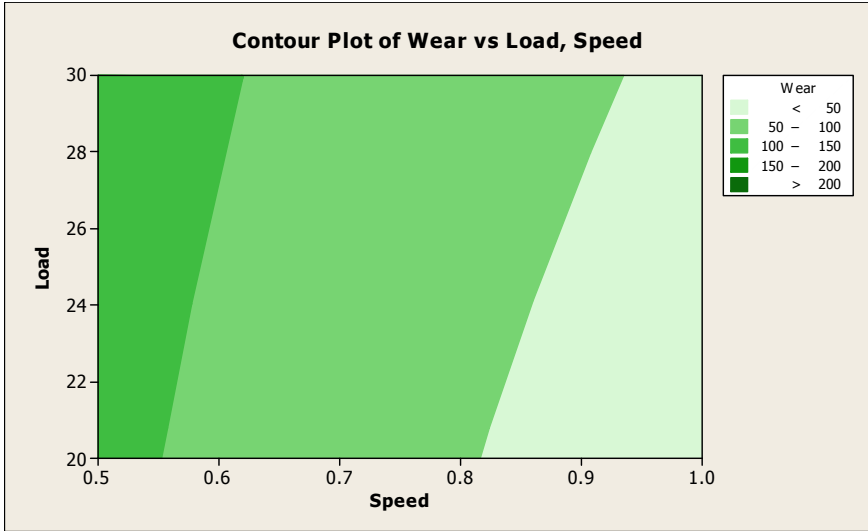


Fig. 3 Graph plot of wear versus load and speed

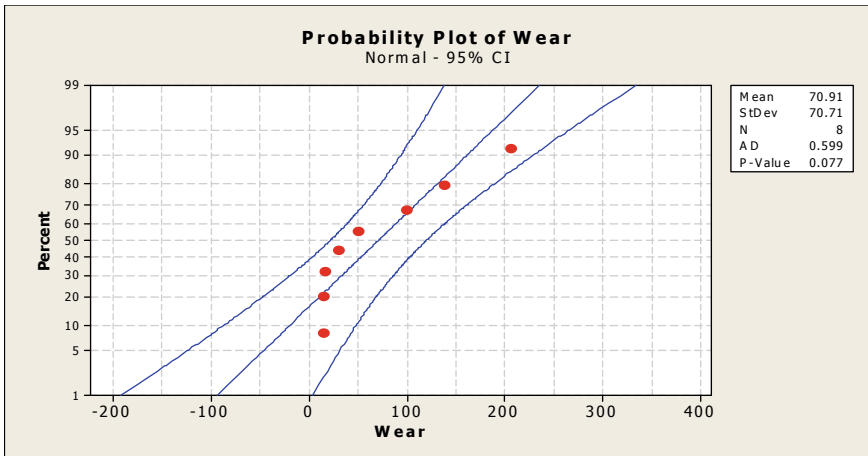


Fig. 4 Probability plot of wear

## 5 Conclusion

The tribological behaviour of silver steel was studied and observed with the help of experimental investigation via the use of pin-on-disc Tribometer setup. The pin was made of material required to be simulated as that of the piston ring, whilst the disc material stainless steel to simulate the inner piston cylinder. The usage of a pin-on-disc type Tribometer was made to simulate the experiment as per real conditions and in order to determine results in the form of wear and Coefficient of Friction (COF).

From the conduction of the above experiments following observations were made:

- (1) The wear of all the iterations were almost the same. With the ones with the heavier loads being slightly higher than the ones with the lesser load.
- (2) The COF values of all the iterations were nearly the same and therefore the Mean Value Obtained was 1.333816.
- (3) The results of wear were quite less despite the surface contact having no lubrication at all highlighting the properties of the selected metals.

## References

1. Kurzynowski T, Smolina I, Kobiela K, Kuźnicka B, Chlebus E (2017) Wear and corrosion behavior of Inconel 718 laser surface alloyed with rhenium. *Mater Des* 132:349–359
2. Wos S, Koszela W, Pawlus P, Drabik J, Rogos E (2018) Effects of surface texturing and kind of lubricant on the coefficient of friction at ambient and elevated temperatures. *Tribol Int* 117:174–179
3. Wan Y, Xiong DS (2008) The effect of laser surface texturing on frictional performance of face seal. *J Mater Process Technol* 197(1–3):96–100
4. Xiao WH, Lu SQ, Wang YC, Jing SHI (2018) Mechanical and tribological behaviors of graphene/Inconel 718 composites. *Trans Nonferrous Met Soc China* 28(10):1958–1969
5. Sun W, Tan AWY, King DJY, Khun NW, Bhowmik A, Marinescu I, Liu E (2020) Tribological behavior of cold sprayed Inconel 718 coatings at room and elevated temperatures. *Surf Coat Technol* 385:125386
6. Rahman M, Seah WKH, Teo TT (1997) The machinability of Inconel 718. *J Mater Process Technol* 63(1–3):199–204
7. Kaleli H (2016) New universal tribometer as pin or ball-on-disc and reciprocating pin-on-plate types. *Tribol Ind* 38(2)
8. Chaudhari R, Ingle A, Kalita K (2017) Tribological investigation of effect of grain size in 304 Austenitic stainless steel. *Trans Indian Inst Met* 70(9):2399–2405
9. Birol Y (2010) High temperature sliding wear behaviour of Inconel 617 and Stellite 6 alloys. *Wear* 269(9–10):664–671
10. Ahmadi A, Sadeghi F, Shaffer S (2018) In-situ friction and fretting wear measurements of Inconel 617 at elevated temperatures. *Wear* 410:110–118
11. Debbarma D (2020) The study of wear behaviour of the Inconel 800 material in dry and solid lubricated condition. *Mater Today: Proc*
12. Pauly V, Kern J, Clark M, Grierson DS, Sridharan K (2021) Wear Performance of incoloy 800HT and inconel 617 in various surface conditions for high-temperature gas-cooled reactor components. *Tribol Int* 154:106715
13. Wang Y, Zhao S, Jia Z, Ji J, Liu D, Guo T, Ding Y (2020) Study on friction and wear behavior of inconel 625 superalloy during hot extrusion. *Adv Mater Sci Eng*

14. Singh R, Sachan D, Verma R, Goel S, Jayaganthan R, Kumar A (2018) Mechanical behavior of 304 Austenitic stainless steel processed by cryogenic rolling. *Mater Today: Proc* 5(9):16880–16886
15. Gupta A, Lata S, Rana R, Lal R (2021) A statistical approach for overcut and burr minimization during drilling of stir-casted MgO reinforced aluminium composite. In: *Advances in manufacturing and industrial engineering*, pp 269–283. [https://doi.org/10.1007/978-981-15-8542-5\\_23](https://doi.org/10.1007/978-981-15-8542-5_23)
16. Thakur A, Rana R (2021) Traffic noise modelling considering traffic compositions at roundabouts. In: *Advances in manufacturing and industrial engineering*, pp. 657–672. [https://doi.org/10.1007/978-981-15-8542-5\\_57](https://doi.org/10.1007/978-981-15-8542-5_57).
17. Singh D, Lata S, Rana R (2018) Reverse engineered structure of tool post aiding tool tip alignment with work center. *Mater Today Proc* 5:6433–6443. <https://doi.org/10.1016/j.matpr.2017.12.256>
18. Jain S, Aggarwal V, Tyagi M, Walia RS, Rana R (2016) Development of aluminium matrix composite using coconut husk ash reinforcement. In: *International conference on latest developments in materials, manufacturing and quality control (MMQC-2016)*, pp 12–13
19. Raheja K, Jain A, Sharma C, Rana R, Lal R (2021) Comparative study of tribological parameters of 3D printed ABS and PLA materials. In: *Advances in manufacturing and industrial engineering*, pp 95–108. [https://doi.org/10.1007/978-981-15-8542-5\\_9](https://doi.org/10.1007/978-981-15-8542-5_9)
20. Kaplish A, Choubey A, Rana R (2016) Design and kinematic modelling of slave manipulator for remote medical diagnosis. In: *International conference on advanced production and industrial engineering*, pp 9–10
21. Khanna R, Maheswari R, Modi A, Tyagi S, Rana TR (2017) A review on recent research development on electric discharge machining (EDM). *Int J Adv Res Innov* 5:444–445
22. Kumar R, Rana R, Lata S, Kumar Sonkar R, Kumar A, Pawar S, Lal R (2015) Optimization of process parameters on Over-Cut in drilling of Al-B4C MMC. *Int J Mod Eng Res* 5(6):24–30
23. Lata S, Gupta A, Jain A, Kumar S, Srivastava A, Rana R, Lal R (2016) A Review on experimental investigation of machining parameters during CNC machining of OHNS. *Int J Eng Res Appl* 6:63–71
24. Chaudhary MK, Pathak A, Goyal R, Rana R, Sharma VK (2021) Fabrication of aluminium 6082–B4C–Aloe vera metal matrix composite with ultrasonic machine using mechanical stirrer. In: *Advances in manufacturing and industrial engineering*, pp 221–229. [https://doi.org/10.1007/978-981-15-8542-5\\_19](https://doi.org/10.1007/978-981-15-8542-5_19)
25. Rana R, Murtaza Q, Walia RS (2020) GA based optimization of tri-biological behaviour of diamond coated tungsten carbide. *World J Eng* 17:335–346. <https://doi.org/10.1108/WJE-08-2019-0220>
26. Rana R, Murtaza Q, Walia RS (2020) Optimization using genetic algorithm of tribological behaviour of wc tool material, *Indian. J Eng Mater Sci* 27:889–896
27. Rana R, Walia RS, Murtaza Q (2021) Characterization and parametric optimization of performance parameters of dlc-coated tungsten carbide (Wc) tool using topsis. *Coatings* 11. <https://doi.org/10.3390/coatings11070760>.
28. Rana R, Walia RS, Lata S (2018) Development and investigation of hybrid electric discharge machining electrode process. *Mater Today Proc* 5:3936–3942. <https://doi.org/10.1016/j.matpr.2017.11.650>
29. Ramakant R, Adarsh M, Kochhar A, Wadhwa S, Daiya SK, Taliyan S, Lal R (2015) An overview on process parameters improvement in wire electrical discharge machining. *Int J Mod Eng Res* 5(4):22–27
30. Ramakant R, Walia RS, Manik S (2016) Effect of friction coefficient on En-31 with different pin materials using pin-on-disc apparatus. In: *International conference on recent advances in mechanical engineering (RAME-2016)*, pp 619–624
31. Ramakant R, Walia RS, Qasim M, Mohit T (2016) Parametric optimization of hybrid electrode EDM process. In: *TORONTO 2016 AESATEMA international conference “advances and trends in engineering materials and their applications*, pp 151–162

32. Rana R (2016) Development of hybrid EDM electrode for improving surface morphology (Doctoral dissertation)
33. Rana R, Rajput K, Saini R, Lal R (2014) Optimization of tool wear: a review. *Int J Mod Eng Res* 4(11):35–42
34. Rana S, Kumar S, Rana R (2018) Optimization of temperature variations on steel grade EN-18 using pin-on-disc method. *Int J Adv Prod Ind Eng Delta* 171:21–26
35. Roop L, Ramakant R (2015) A textbook of engineering drawing, 1st edn. IK International Publishing House Pvt.
36. Bansal S, Saraf A, Rana R, Lal R (2021) Effect of picosecond laser texture surface on tribological properties on high-chromium steel under non-lubricated conditions. In: *Advances in manufacturing and industrial engineering*, pp 257–267. [https://doi.org/10.1007/978-981-15-8542-5\\_22](https://doi.org/10.1007/978-981-15-8542-5_22)
37. Lata S, Pandey A, Labhansh, Sharma A, Meena K, Rana R, Lal R (2018) An experimental study and analysis of the mechanical properties of titanium dioxide reinforced aluminum (AA 5051) composite. *Mater Today Proc* 5:6090–6097. <https://doi.org/10.1016/j.matpr.2017.12.214>
38. Lata S, Rana R (2018) Hitesh, investigation of chip-tool interface temperature: effect of machining parameters and tool material on ferrous and non-ferrous metal. *Mater Today Proc* 5:4250–4257. <https://doi.org/10.1016/j.matpr.2017.11.689>
39. Singla M, Rana R, Lata S (2016) Microstructure and mechanical properties of aluminium based metal matrix composite—a review. In: *International conference on advanced production and industrial engineering*, pp 9–10

# Interactional Challenges to Effective E-Waste Management of Indian City



R. S. Gurjar, M. K. Lila, P. Tyagi, and R. P. Verma

**Abstract** In spite of the initial e-waste regulations entering into force in India in 2011 and also being modified in 2016, it is approximated that some 90–95% of e-waste is handled in the casual market in and unorganized manner. The current medal fabrication for different event in Tokyo Olympics also changed the vision of the people about e-waste. The present manuscript provides an overview of the awareness and management of e-waste in the capital of Rajasthan as a part of study. Different articles have been reviewed and analysed in the domain of e-waste management and a detailed insight about the current scenario, effects and possible solution are provided in terms of better management of e-waste.

**Keywords** E-waste · Source · Current scenario · Hazardous elements · Disposal

## 1 Introduction

It is widely agreed that the Asia Pacific region is among the world's most populous and fastest growing and in world India soon get top of this rank. Due to this huge population, it will be biggest market for all manufacturing companies larger purchasing power create large amount of waste production. It is the goal of this research to examine critically the existing strategies and practises used by the major

---

R. S. Gurjar

Department of Automation, Banasthali University, Jaipur, Rajasthan, India

M. K. Lila (✉)

Department of Mechanical Engineering, Graphic Era Hill University, Dehradun, India

e-mail: [manish.lila@gmail.com](mailto:manish.lila@gmail.com)

P. Tyagi

Department of Physical Sciences, Banasthali University, Jaipur, Rajasthan, India

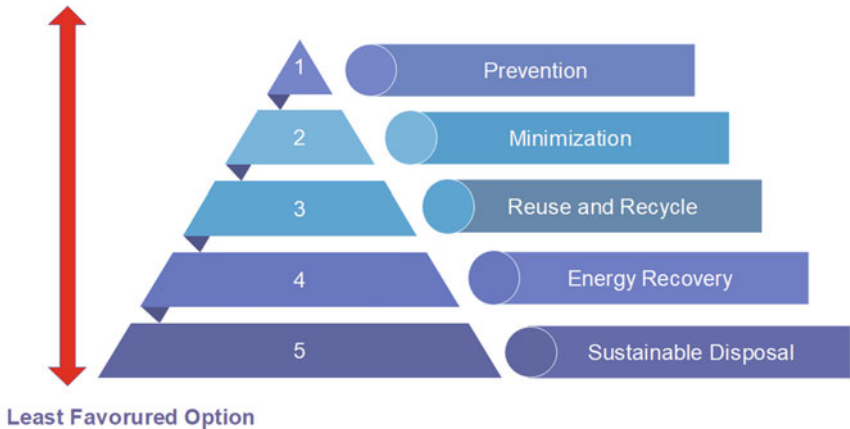
R. P. Verma

Department of Mechanical Engineering, Graphic Era Deemed to be University, Dehradun, India

electronic waste generating countries such as China, USA, Japan, India and may more, have to manage and regulate electronic waste in order to reduce the harm that inappropriate recycling and disposal practises have to the humans and other living organisms. Disposed of digital waste is the fastest expanding stream of waste in developed nations electronic devices are altering the lives of individuals almost everywhere—beginning with the method we operate, raise kids, maintaining touch with others or individual amusements. Not shocking, the electronic devices sector is the fastest expanding production market. Customers are attracted to the most recent cellular telephones, laptop computers, a/c unit and also customer electronic devices. The obsolescence of these items causes a special frame of mind where customers liked to change the items instead fix and also recycle Fig. 1 shows the best possible ways for the every kind of waste whether it belongs to solid waste or electronically generated waste.

The fast obsolescence is additionally as a result of the quick progressing innovation however on the other hand it is clear that the get rid of concept returns financial advantages to business. Following this twenty-first century transformation, this discard concept makes certain to harm the high quality of our lives as well as the generations ahead. The issue of digital waste, or e-waste, needs worldwide activity [1]. Digital waste (e-waste) describes broken down digital gadgets that are no more helpful for the objectives they were meant for. The interpretation consist of that usage electrical power however have actually reached their end-of-life. Various other parts of e-waste such as power line, below assemblages and also consumables that become part of digital items at the time of discarding them belong to the waste. The meaning

**Most Favoured Option**



**Fig. 1** Preference for minimization of waste



of e-waste consists of digital items that are not indulged however discarded by their proprietors.

Digital waste is not simply waste in the genuine feeling, yet a fantastic business chance for those taken part in the marketing and also recycling of the waste. Because of this, huge inflow of Digital waste right into establishing nations has actually happened because of weak regulative criteria as well as bad enforcement of ecological legislations when it involves removal and also handling of important steels such as silver, gold and also iron from e-waste. Personation of this e-waste creek is of important significance for creating a pocket friendly as well as additionally environmental pleasurable recycling system. E-waste is identified by the government of India under the broad programme of infected products [2]. Within e-waste, there are numerous teams such as significant in addition to little residence gadgets, electrical as well as likewise electronic toys in addition to displaying devices, gadgets, computer system systems as well as likewise pertinent gadgets and more which includes steel as well as likewise non-metals, alloys along with materials such as some precious metal [3]. Correct e-waste recycling is really vital for the lasting growth of a creating nation, due to the fact that it is straight gotten in touch with ecological issues because of visibility of a big unapproved market [4]. A range of heavy metals consisting of various unsafe compounds exist in e-waste which triggers ecological and also well-ness dangers, if these materials are not taken care of effectively. Casual recycling triggers negative impacts on the work participated in it, which has actually come to be a significant concern [5]. In this context, the ecological authorities in India are currently paying significant interest on establishing an approach for quitting the casual field as a result, the purpose of this mini-review post is to existing the brief summary on e-waste administration in India.

Generally waste content change according to area, region but overall content is shown in diagram.

## 2 Source of E-Waste Generations

The yearly e-waste amount created nearly 1641KT. Whilst according to an earlier record [6]. The highest degree of e-waste is produced in the state of Mumbai (Maharashtra), followed with by other states. Furthermore, about 71% are produced from different public, private sector includes various economics zone and also just 16% comes from private families. E-waste consists of range of digital and also electric home appliances, such as computer, cell phone and also their related devices. The optimum e-waste element contains home appliances (43%), adhered to by details and also interaction innovation (35%), customer electronic devices (15%) and also others (11%). This waste is made up of Iron as well as steel (51%), plastics (22%), non-ferrous steels (14%) and also various other elements (17%). Other than iron such as steels and copper, Al and also rare-earth elements such as gold, palladium as well

**Table 1** Policies and methods for e-waste in India and other countries

Norms	India	European union	USA
Govt. rules	E-waste (Management) rules, 2016	Cost waste electrical and electronic equipment (WEEE) directive 2012/19/ EU and Restriction of hazardous substances directive (RoHS) 2011/65/EU	Resource conservation and recovery act (RCRA), 1976 environmental protection agency (EPA) cathode ray tube rules
Recycling approach	Mechanical technology (including manual dismantling)	Advance version of mechanical and smelter technology	Advanced mechanical technology pyro metallurgical and hydrometallurgical technology has been applied to a smaller scale
Recycling Rate	Overall: 30% [8] Paper: 30–50% Plastic 50–70% Others 40% [9, 10]	Overall: 40% [11]	Overall: 32% [12]

as platinum [7]. Table 1 provide a brief overview of policies on e-waste adapted in India, European countries and United States.

### 3 Current E-Waste Scenerio

#### 3.1 Worldwide Scenario

Worldwide amount of e-waste produced before 2015 was near about 42.3 Mt. Driven by the nationwide legislations for e-waste monitoring, around 6.5 Mt was reported as officially dealt with via take-back systems. In 28 European Union states, around 0.7 Mt of e-waste was tossed right into the waste containers. The quantity of e-waste that is included containers is unidentified for various other areas. Nonetheless there is a space in between e-waste created, formally gathered and also those in waste containers. Most notably, main information for the transboundary activity of e-waste are unidentified. The majority of the e-waste (i.e. 16 Mt) was produced in Asia. This quantity of e-waste is 3.7 kg/inhabitant. Europe has actually created 15.6 kg/inhabitant, the greatest per citizen e-waste amount worldwide. Figure 2 provide the current and expected e-waste generation in upcoming years with current CAGR.

The entire African continent created 2.1 MT. The American subcontinent created 12.2 Mt in complete out of which 8.2 MT are generated in United States and Canada,

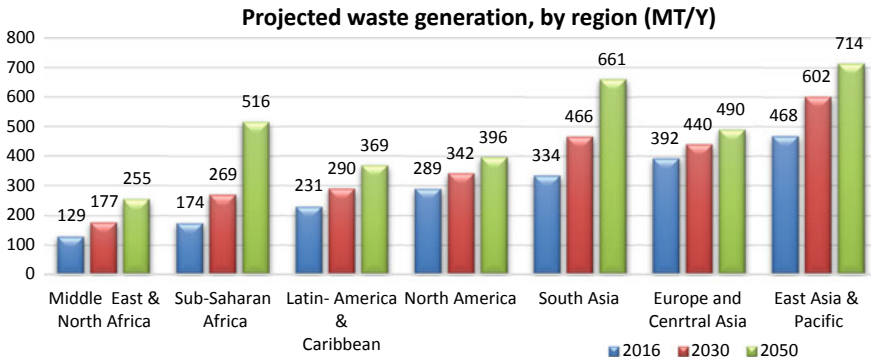


Fig. 2 Current and projected e-waste generation, by region [13]

2.01 MT from Central as well as 2.7 MT from South America which stands for 12.2 kg/inhabitant. [14]. The quantity is expanded to 50 MT in 2018, with a CAGR of 6% [15].

### 3.2 Scenario in Indian Context

A variety of looks into have really recommended that the e-waste stream gives relating to 1000 numerous threats to human health as well as likewise eco-friendly premium, therefore making its management a challenge or problem in numerous areas [16] (Table 2).

The e-waste supply based upon the obsolescence price and also set up base in India for 2005 has 150 K tonnes [17, 18]. E-waste is becoming a severe public health problem as well as different kind of serious ecological problem in India. As population increase which creates greater than 2 million tonnes of e-waste each year [19].

India rates 3rd placement in greatest e-waste generation amongst worldwide. The nation has actually created 1.7 Mt in outright amounts for the year 2014. Major 64 cities create more than 60% of the complete e-waste created in India. Ten states create 70% of the overall e-waste. Maharashtra places comes on top of the list followed by Tamil Nādu and Delhi. Amongst leading 10 cities creating e-waste, Mumbai places initial adhered to by other cities. Greater than 95% of India’s e-waste is refined by waste pickers, famously referred to as ‘kabadiwalas’ or ‘raddiwala’. They are main back bone of Indian recycling mission. This casual network of employees is accountable for the collection, taking down as well as reusing of such e-waste as well as runs outside controlled or official business systems, usually unlawfully. There are 2 tiny e-waste taking apart centres are working in Bangalore as well as Chennai. There is no huge range arranged e-waste reusing centre in the country as well as the whole recycling exists in messy market. There is an absence of genuine as well

**Table 2** State-wise number of authorized dismantler/recycler and processing capacity in India (As on 16.03.2020)

States	Authorized dismantler/recycler	Capacity (MTPA)
Andhra Pradesh	1	480
Chhattisgarh	1	600
Gujarat	16	49,053
Goa	1	103
Haryana	28	87,378
Himachal Pradesh	1	1000
Jammu and Kashmir	1	165
Karnataka	71	52,722
Maharashtra	75	78,179
Madhya Pradesh	2	9600
Odisha	3	3680
Punjab	3	4850
Rajasthan	26	90,769
Tamil Nadu	24	97,271
Telangana	11	41,493
Uttar Pradesh	41	243,627
Uttarakhand	4	19,250
West Bengal	3	1860
India (Total)	312	782,080

as detailed information on e-waste schedule for residential generation and also the numerous data related to e-waste now accumulating in country by state and centre pollution control boards.

### 3.3 *E-Waste Scenario in Context of Jaipur*

This study was carried out in the Jaipur city (Rajasthan), INDIA, relevant with families' devices' usually existing in our residence. Jaipur is the Funding city of Rajasthan State; its complete location is 467 km<sup>2</sup>, as well as the populace, is 30.73 lakh with a 10% drifting populace as well as having 91 wards, with a yearly budget of 941 Cr well as 75° 37 min eastern longitude to 76 levels 57 min—Eastern longitude. The Nahargarh hillsides border the city in the north and Jhalana in the east, which belongs to the Aravalli hillsides varieties environment [20, 21].

Jaipur lies in the semi-Arid Area of India. It has been identified by heat, reduced rains, and also moderate wintertime. The mean temperature level of Jaipur is 36 °C, differing from 18 °C in wintertime (January) to 40 °C in summertime (June). Hence,

January and also June are the chilliest and also best months [22]. Jaipur is found on  $26^{\circ}55'$  north latitude and also  $75^{\circ}49'$  eastern longitude. Its community limit expands from  $26^{\circ} 46$  min north latitude to  $27^{\circ} 01$  min north latitude. The population of Jaipur increasing with the rate of 2.54 on average, which also shows how the population growth effect the waste generation [23]. The rate of waste generation last two years in Jaipur is shown in Table 3.

More than 303 Authorized districts wise, more than 30% of these centres are present in Jaipur. These centres are mostly run or maintained by some multinational companies, and few are independent setups. Ninety-three owners run these 303 centres. They are operating it in a different area of the state [26].

**Table 3** Collection of e-waste in Jaipur in last 2 years [24, 25]

S. No.	Classification	2018–19	2019–20
1	Refurbished product related to CPU, mobile phone, monitor, CRT, Networking related item	318.441	1964.554
2	Ferrous material	2131.666	6525.925
3	Non-ferrous material	707.251	1215.26
4	Plastic	2708.504	4996.363
5	Glass/laminated glass	351.556	226.047
6	PCB	540.556	324.472
7	Lead battery scrap	14.316	17.164
8	Li battery	0.001	0.075
9	Chip IC processor etc.	2.059	3.843
10	Paper/paper board/paper packing material	10.592	21.095
11	Wooden items	2.117	2.383
12	Stone	90.28	115.823
13	PU foam	50.325	72.852
14	Other packing material	1.157	4.395
15	Toner powder	0.058	0.128
16	Mixed metal scrap	42.36	668.301
17	Rubber scrap	27.676	35.025
18	Process waste, oil	0.641	2.954
	Total	6999.556	16,196.659

## 4 Problems Associated with E-Waste

### 4.1 *Drastic Increment in E-Waste Collection*

Item obsolescence is coming to be extra fast given that the rate of technology as well as the dynamism of item production/advertising and marketing has actually led to a brief lifetime (less than 2 years) for several computer system items. Brief item life expectancy paired with rapid boost at a typical 15% annually will certainly cause increasing of the quantity of e-waste over the following 5–6 years.

### 4.2 *Toxic Components and Health Impacts*

E-waste can be considered as a complete package of the different poisonous components inside it in their parts such as Pb, Cd, Hg, polychlorinated bi-phenyls (PCBs) and so on, which are called for to be managed securely. The reusing techniques were discovered irregular in casual industries causing unrestrained launch of hazardous products right into the atmosphere as a result of inappropriate handling of such products. There is little policy in the casual market to secure the health and wellness of those that take care of e-waste. Employees are badly secured in an atmosphere where e-waste from COMPUTER displays, PCBs, CDs, motherboards, wires, printer toner cartridges are melted outdoors as well as launch lead as well as mercury contaminants right into the air. Rautela et al. [27] A lot of these employee's experience eye irritability, breathing troubles and also continuous frustrations. Some important work health and wellness concerns are inadequate functioning area, bad lights and also air flow, stressing the eyes as well as breathing contaminated air, resting confined on the ground for lengthy hrs, breathing in hazardous fumes, direct exposure of body components to fire, acid as well as various other chemicals as well as absence of tidy alcohol consumption water as well as bathrooms. The very best instance is the community of Guiyu in south-east China. Given that 1995, the typically rice-growing area of Guiyu has actually developed into an extensive casual e-waste reusing centre, possibly the biggest on the planet. Scientist observed numerous health and wellness impacts in connection with the primary recycling methods [28]. Chemicals in e-waste products can collect in water, dirt, as well as bordering plant life. Poisonous as well as genotoxic degrees can generate negative environmental as well as human wellness results [29, 30].

Harmful heavy metals such as As, Cd, Hg, Pb from e-waste are recognized to create cancer cells [31, 32] In human lymphocytes, dirt and also plant examples from e-waste unloading and also refining websites caused substantial concentration-dependent boosts in DNA damages compared to the adverse control [33]. Table 4 shows the toxic materials present in e-waste and their effect on human body.

**Table 4** Toxic materials present in e-waste and their effect [34–36]

S. No.	Toxic material	Body part/cell	Effect	Reference
1	Pb	Human cord blood leukocytes	Maternal exposure associated with global hypomethylation	[37]
2	Hg	Polar bear brain	Brain Hg associated with brain genomic DNA hypomethylation	[38]
3	Cd	Cd-transformed prostate epithelial cells	Genomic hypermethylation, hypermethylation in RASSF1A and p16 gene. The pattern of genomic DNA hypermethylation together with up-regulation of DNMT3b may provide a unique set of biomarkers to specifically identify cadmium-induced human prostate cancers	[39–42]
		Rat liver cells	Initial DNA hypomethylation, subsequent DNA hypermethylation after prolonged exposure	
		Human embryo lung fibroblast cells	DNA hypermethylation	
		Human lung cancer	Hypermethylation in p16 gene	
4	Cr	Human lung A549 cells	Increased global histone H3 lysine 9 (H3K9) and H3K4 di- and trimethylation, decreased H3K27 trimethylation and histone H3arginine 2 (H3R2) dimethylation	[43]
		Human cord blood leukocytes	Hypermethylation of ACLS3 gene promoter region	
5	PAHs	Neonatal rat hippocampal neurons	Global DNA hypomethylation	[44]
6	PBDEs	DNA	In vitro exposure to certain nickel or arsenic compounds induces changes in both DNA methylation patterns, as well as, in the levels of posttranslational modifications of histone tails	[45]
7	As	Include in Food chain due soil fouling may cause tumour and other similar disease	The concentration of heavy metals (Cd, Hg, As, Pb and Cr) in soil, water and sediment	[15]

### ***4.3 Lack of Recycling Facilities***

Regardless of the development in the official taking apart and also reusing industry (in regards to the variety of such centres), the real waste refined in the official market still continues to be really reduced. Unscientific proof suggests that the majority of these official centres are running well listed below their accepted abilities due to their lack of ability to resource sufficient waste. It has actually been developed that e-waste, in the lack of correct disposal method also identify junk suppliers, which are additional pressed right into scrap dealer's supply chain. Existing eco-audio reusing facilities in position is not geared up to take care of the boosting quantities of e-waste. The significant taking down procedures are happening in an unsecure/Unhygienic place converted into huge industry which is an unsafe fashion. The capacity of boosted e-waste as well as absence of sufficient reusing centres have actually brought in the interest of a variety of recyclers worldwide, revealing rate of interest to begin reusing centre in India.

The absence of understanding relating to e-waste as well as expenses of returning the end-of-life devices to official collection centres are lowering the determination of family and also institutional customers to return their waste to official industry. Most notably, the casual field, via the ease of house collection as well as financial rewards (even if small), makes it a lot more appealing for customers to return their waste, about the official market, which is yet to purchase durable systems of collection and also handling. The casual e-waste industry supplies resources to countless individuals, usually coming from one of the most marginalized teams; on the other hand, the field's waste administration methods position significant ecological as well as carcinogen to the employees themselves in addition to the bigger public. This provides a possible ethical problem for public law and also continual success of any type of e-waste monitoring system will certainly rest on our capacity to fix this issue.

### ***4.4 Impact on Environment***

E-waste consists of heavy metals, consistent natural toxins, fire resistant's as well as various other possibly unsafe materials. These contaminants can trigger threats to the atmosphere otherwise handled correctly. Throughout reusing and also product recuperation 3 major teams important are launched in to the atmosphere which requires high top priority focus as they are extremely unsafe in nature. The very first team is the initial components of devices such as lead and also mercury, 2nd team such as cyanide, included throughout some healing procedures as well as 3rd team which are created throughout reusing procedures such as dioxins as well as furans. If incorrectly taken care of, such materials might present considerable human and also ecological health and wellness dangers. The list below sorts of exhausts or results reveals the visibility of poisonous compounds in e-waste handling as well as administration, and leachates from disposing tasks contaminate the dirt and also water sources, crude as



well as great particle issue from taking down, base and also fly ashes from shedding tasks, fumes from mercury amalgamate, de soldering as well as various other burning tasks, wastewater from taking down as well as shredding centres and also effluents from cyanide leaching and also various other seeping tasks. Incorrect splitting or burning of published circuit card (PCBs) as well as changes might bring about the launch of mercury, cadmium and also beryllium which are very hazardous to human wellness. An additional unsafe procedure is the recycling of elements including harmful substances such as halogenated chlorides as well as bromides made use of as fire-resistants in plastic, which create relentless dioxins and also furans on burning at reduced temperature levels. A research study on melting published circuitry boards in India revealed disconcerting focus of dioxins in the environments of open burning areas getting to 30 times the Swiss assistance degree. Around 70% of the heavy metals specifically mercury and also cadmium, in landfills originated from digital waste. Customer electronic devices is the source for the existence of regarding 40% of the lead in garbage dumps. These contaminants can trigger mental retardation, allergies and also cancer cells. The extremely spread reusing devices throughout India, causes troubles such as discharges of dioxins as well as heavy metals like lead, cadmium, mercury in air, unplanned unloading of invested liquids as well as chemicals hence polluting dirt, groundwater contamination via leachate, land dental filling of non-recyclables.

## 5 Treatment and Disposal

The existence of harmful aspects in e-waste provides the possibility of raising the strength of their discharge in setting because of land filling up and also incineration. The possible therapy disposal alternatives based upon the make-up are:

- Land filling
- Incineration
- Acid bath
- Biological method.

### 5.1 Land Filling

The deterioration procedures of e-waste in landfills are really made complex and also run over a large time period. Presently it is not feasible to evaluate ecological effects from e-waste in it, but it has complying with factors:

- Landfills have mixes of with different type of waste streams;
- Releasing of various type of toxins from landfills;
- It also contaminates ground water resource.
- Also release harmful gases during it degradation.



**Fig. 3** Land filling done mainly by the municipal due to an low cost disposal methods

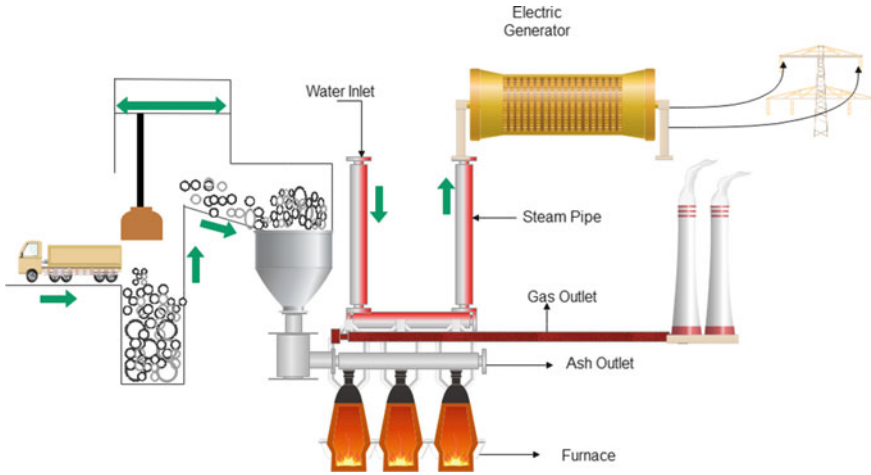
Amongst the research studies on garbage dumps records that the ecological threats from land dental filling of e-waste could not be ignored since the problems in a land fill website are various from a soil, especially worrying the sleeping habits of steels (Fig. 3).

Furthermore, it is recognized that cadmium as well as mercury are produced in scattered kind or using the land fill gas burning plant. Although the threats cannot be measured as well as mapped back to e- waste, land dental filling does not seem an eco-audio therapy approach for compounds, which are unstable as well as not naturally decompose. Consequently, of the facility product mix in e-waste, it is not feasible to leave out ecological (long-lasting) threats also in safe land dental filling.

## 5.2 Incineration

Incineration likewise consists of pyrolysis; materials created throughout incineration are most likely to be a lot more harmful than its normal type, pyrolysis home heating the compound in the lack of oxygen, right here the burning does not happen however the materials are transformed to fumes, oils as well as charcoal. Nevertheless, in gasification minimal air is offered to transform the materials right into fume, ash as well as tar (Fig. 4).

Incineration is a typically utilized approach of the dispersal of e-waste in African subcontinent and India its neighbouring countries. When heating up the plastic or PVC motherboard it launches sensual fume includes Polycyclic aromatics (PCA), polychlorinated dibenzo-para-dioxins (PCDDs) and also polychlorinated dibenzofurans (PCDFs) which are recognized health hazards as well as gases such as carbon monoxide gas, sulphur dioxide, nitrogen oxides. Smoke likewise includes small



**Fig. 4** Incineration disposal methods

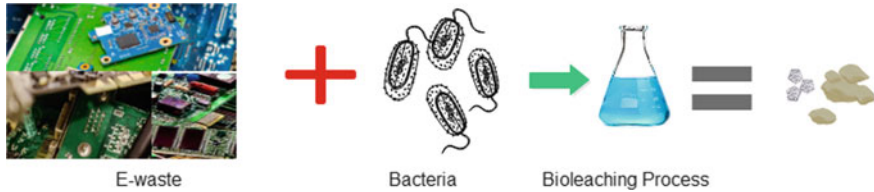
amounts of oxides of complying with heavy metal deposits antimony, lead, thallium, arsenic, copper, manganese, mercury as well as nickel, pointer wound up in the ashes.

### 5.3 Acid Bath

Acid bathroom technique is made use of to remove Copper, right here the circuit card is immersed in to Sulfuric acid for concerning 10–15 h to liquefy metal such as Copper after that remedy is steamed, precipitated Copper Sulphate is taken as well as continuing to be service is included with scratched fragments, ultimately Copper spots are gotten rid of. Acid bathrooms additionally utilized to liquefy the lead and also in the removal of Silver and gold.

### 5.4 Biological Method

Metal extraction by biological procedures has become different innovation today specifically in steels like Au and Cu. Metallic ores and e-wastes are being processed by microorganisms in this promising new technology. Bio metallurgical procedures which transform metal right into soluble salts in liquid media from ores/ concentrates/wastes. Bio metallurgy is a total mixing of biotechnology as well as metallurgy. Clinically, the two methods by which ore is bioleached are known as direct and indirect bio-oxidation, respectively. Most researchers have recognized the indirect



**Fig. 5** Bioleaching disposal methods

bio-oxidation mechanism. Some researcher shows that the physicochemical procedure which fall in a branch of hydrometallurgy that entails using bacteria to create chemical oxidants to carry out this procedure, we make use of in the recovery of metals from such waste, Microorganisms for example *Acidithiobacillus ferrooxidans*, *Leptospirillum ferrooxidans*, *Acidithiobacillus thiooxidans* [46]. It has been a recognized procedure for the removal of metals consisting of different material [47] (Fig. 5).

Bioleaching is an approach checked for the healing of several base as well as rare-earth elements. There are 2 seeping systems for boosting the launch price of steels. To start with, bacteria can straight oxidize minerals as well as solubilize steels in a straight activity system, [48, 49].

## 6 Administrative Methods

The plan will deal with all problems varying from manufacturing to last disposal, consisting of eco-audio modern technology for the recycling of digital waste. Rules to regulate both lawful as well as unlawful exports and also imports of e-wastes have to be clear in the plan. Loophole openings in the fundamental lawful structure job likewise to be dealt with to avoid or lower the transboundary motion of e-waste from established to establishing nations. The disposal of e-wastes in community landfills have to be banned in the policies purely. Proprietors as well as generators of e-wastes must be urged to effectively reuse their wastes by supplying economic motivations. Manufactures of items need to be made monetarily, literally as well as lawfully in charge of their items. Plan has to focus administration of limited compounds with understanding amongst manufacturers and also produces in the brand-new item advancement. Ecological risk labelling of items to produce understanding amongst the public need to additionally to be covered in the plan. A full nationwide degree supply, which cover all area of cities and all the fields need to be started. A model which is very popular now days is joint venture of government and private sector in e-waste administration. It needs to be established. Expanded manufacturer duty is an environmental policy strategy in which a manufacturer's duty for an item is included the blog post customer phase of the item's life process, including its last disposal All suppliers of digital tools will supply take-back and also monitoring solutions for

their items at stage of rejection. The used or rejected E-item ought to after that be sent for reusing or reuse, either in a different reusing department at the production device or in a typical centre. Collection systems are to be developed via collection facilities to make sure correct collection as well as transport straight to the reusing system. Recyclers that are having permission for dealing with, handling, repair, as well as reusing conference eco-audio administration standards must just be allowed.

The e-waste administration in the future depends not just on the efficiency of plan degree campaigns from the federal government, efficiency in reusing solutions, however additionally on the mind-set of customers. Absence of understanding amongst the citizens to set apart e-waste from local waste is boosting the size of e-waste issue in India. Area involvement has to be started in order to comprehend the vital function of produces and also bulk customers in e-waste monitoring. Recognition increasing programmes as well as tasks on concerns associated with the eco-audio administration, health and wellness elements of e-wastes might be performed in order to motivate far better monitoring methods amongst various target teams. Customers to be enlightened to purchase just required items that use arising innovations such as use lead-free, halogen-free items to be recognized with eco-labelling. ESM of e-wastes can be well arranged with an assistance of technological standards which focus on far better collection, reusing as well as disposal choices.

## 7 Suggestions

Over 75% of electronic devices are kept in storage as a result of their ignorance about their proper care and management [50]. In many homes, businesses, and warehouses, these electronic wastes are left unmanaged and intermingled with household garbage, which are then deposited in landfills. Implementable management measures are required to deal with this. E-waste management needs to begin at the source of generation in the workplace. This can be accomplished through waste reduction and environmentally friendly product design. In order to reduce industrial waste, it is necessary to do.

- Keeping track of inventory
- Modification of the manufacturing process,
- Reducing the volume,
- Reuse and recycling
- The design of environmentally friendly products
- Putting Together a Stable System for Handling Electronic Waste
- Put an end to the export of foreign e-waste.
- Educating the general public.

## 8 Conclusions

Governments, particularly in poorer nations, face a substantial environmental burden as a result of the tremendous growth in electronic items and e-waste over the previous decade or so. The ineffectiveness of India's old e-waste management rules is a sign of the difficulties the country faces. Weak regulation and enforcement, as well as low public knowledge, are all cited in this article as problems facing India's informal sector for recycling and proper disposal method opt for such waste. Every stakeholder should be involved in the development of a future electronic waste management system. Casual enthusiasts and anthropologists are still obtaining the significant quantity of e-waste disposed and gathered. If these stars are bypassed by brand-new official systems for e-waste monitoring, there is a danger that more recent official drivers merely will not have the ability to obtain accessibility to the e-waste stream Casual collection networks are much more efficient than official ones, whilst official therapy procedures could recuperate even more sources from the e-waste. By bringing formal and informal sector with each other, the collection as well as end-processing performance of the e-waste worth chain can be taken full advantage of, whilst work can be ensured with the growth of brand-new comprehensive company versions. Comprehensive company designs incorporating the official and casual permit greater effectiveness not just for product healing however likewise generate conformity, depend on amongst the worth chain stars as well as openness in the waste monitoring circumstance Government must focus on this sector for regular earning like other sector, but due to lack of government scheme, funding and any proper training to the people who involve in this work. Major waste collection is done by the private sector. The person doing this collection are sometime minors and mostly do not have any kind of training of handling such type of waste, they don't use any protective gears while dealing treatment process. Government must initiate some public private partnership for the proper e-waste management, time to time there must be updating in rule and regulation related with e-waste collection and handling those NGO's working in this area must create some awareness related with handling and proper disposal of such waste with help of small video, street play, information brochure, etc. Those manufacturing unit involving in production of such good must launch some scheme regarding collection of old waste. If any company provide some rebate on new product by collection old one then this process will create a cycle of Reuse-Recycle-Reduce. The present post sums up the situation of e-waste generation in India and in various other nations. Interpretation, product make-up, existing disposal approaches, harmful nature of e-waste is likewise provided to comprehend the dangerous nature of e-waste in the form of heavy metals and halogenated substances. Incorrect handling and administration of these waste throughout recycling and various other end-of-life therapy choices appears to have prospective threats to both human health and wellness and the setting. The absence of public recognition concerning the disposal of digital items as well as insufficiency of plans to take care of the problems connected to E-waste boost the issue in India. There is no big range arranged E-waste reusing centre in India and most of the reusing exists in

messy industry. Furthermore, the administration techniques are usually badly developed as well as have a great deal of wellness and ecological concerns. There exists an immediate demand for a thorough analysis of the present and future situation consisting of metrology, characterization, existing disposal techniques, ecological effects and work carcinogen. E-waste collection, transport, therapy, storage space, healing as well as disposal, require to be developed, at nationwide and/or local degrees for the ecologically audio administration of e-wastes.

## References

1. U.N.E. Programme, Sustainable innovation and technology transfer industrial sector studies: Recycling-From E-waste to resources (2009)
2. Borthakur A, Govind M (2017) Emerging trends in consumers' E-waste disposal behaviour and awareness: a worldwide overview with special focus on India. *Resour Conserv Recycl* 117:102–113
3. Awasthi AK, Li J (2017) Management of electrical and electronic waste: a comparative evaluation of China and India. *Renew Sustain Energy Rev* 76:434–447
4. Awasthi AK, Zeng X, Li J (2016) Environmental pollution of electronic waste recycling in India: a critical review. *Environ Pollut* 211:259–270
5. StEP solving the E-waste Problem-StEP Initiative. <https://www.step-initiative.org/>. Accessed 20 Aug 2021
6. [https://rajyasabha.nic.in/rsnew/publication\\_electronic/publication\\_electronic.asp](https://rajyasabha.nic.in/rsnew/publication_electronic/publication_electronic.asp) Accessed 20 Aug 2021
7. Awasthi AK, Wang M, Wang Z, Awasthi MK, Li J (2018) E-waste management in India: a mini-review. *Waste Manage Res* 36(5):408–414
8. Why India Needs A Plastic Recycling Revolution. <https://www.outlookindia.com/website/story/society-news-why-india-needs-a-plastic-recycling-revolution/386902>. Accessed 20 Aug 2021
9. Nandy B, Sharma G, Garg S, Kumari S, George T, Sunanda Y, Sinha B (2015) Recovery of consumer waste in India—a mass flow analysis for paper, plastic and glass and the contribution of households and the informal sector. *Resour Conserv Recycl* 101:167–181
10. India's growth story—Recycling today. <https://www.recyclingtoday.com/article/indias-recycling-growth-story/>. Accessed 20 Aug 2021
11. Waste recycling—European environment agency. <https://www.eea.europa.eu/data-and-maps/indicators/waste-recycling-1/assessment-1>. Accessed 20 Aug 2021
12. National overview: facts and figures on materials, wastes and recycling|US EPA. <https://www.epa.gov/facts-and-figures-about-materials-waste-and-recycling/national-overview-facts-and-figures-materials>. Accessed 20 Aug 2021
13. Trends in Solid Waste Management. [https://datatopics.worldbank.org/what-a-waste/trends\\_in\\_solid\\_waste\\_management.html](https://datatopics.worldbank.org/what-a-waste/trends_in_solid_waste_management.html). Accessed 14 Aug 2021
14. Koli SK, Hussain A (2018) Status of electronic waste management in India, in book. *Adv Treat Tech Indust Waste Water*, IGI Global USA, 238–250
15. Houessionon MGK, Ouendo ED, Bouland C, Takyi SA, Kedote NM, Fayomi B, Fobil JN, Basu N (2021) Environmental heavy metal contamination from electronic waste (E-waste) recycling activities worldwide: a systematic review from 2005 to 2017. *Int J Environ Res Public Health* 18(7):3517
16. Dashboard|Greene. <https://greene.gov.in/dashboard/>. Accessed 20 Aug 2021
17. Fakhredin F, Huisman J (2013) Analyzing end of life LCD TV WEEE flows in Europe. In: *Conference on EcoDesign*

18. Turaga RMR, Bhaskar K, Sinha S, Hinchliffe D, Hemkhaus M, Arora R, Chatterjee S, Khatriwal Ds, Radulovic V, Singhal P, Sharma H (2019) E-Waste Management in India: Issues and Strategies, *Vikalpa J Decis Makers* 44(3):127–162
19. Generating Green Shoots of Opportunities from E-waste-CII Blog. <https://www.ciiblog.in/generating-green-shots-of-opportunities-from-e-waste/> Accessed 20 Aug 2021
20. Jaipur District. <https://www.veethi.com/places/rajasthan-jaipur-district-506-5.htm>. Accessed 14 Aug 2021
21. Home. <https://office.incometaxindia.gov.in/jaipur/Pages/default.aspx>. Accessed 14 Aug 2021
22. Jaipur Nagar Nigam (Greater). <http://jaipurmc.org/presentation/aboutmcjaipur/cityprofile.aspx>. Accessed 14 Aug 2021
23. Jaipur, India Metro Area Population 1950–2021|MacroTrends. <https://www.macrotrends.net/cities/21280/jaipur/population> Accessed 16 Aug 2021
24. Rajasthan State Pollution Control Board Dep. <https://environment.rajasthan.gov.in/content/environment/en/rajasthan-state-pollution-control-board.html>. Accessed 20 Aug 2021
25. E-Waste Management. [https://environment.rajasthan.gov.in/content/environment/en/rajasthan-state-pollution-control-board/information/WasteManagement/E-Waste\\_Management.html](https://environment.rajasthan.gov.in/content/environment/en/rajasthan-state-pollution-control-board/information/WasteManagement/E-Waste_Management.html). Accessed 20 Aug 2021
26. Dismantlers/Re-Furbishers/Recyclers. [https://environment.rajasthan.gov.in/content/environment/en/rajasthan-state-pollution-control-board/information/WasteManagement/E-Waste\\_Management/DISMANTLERS-REFURBISHERS-RECYCLERS.html](https://environment.rajasthan.gov.in/content/environment/en/rajasthan-state-pollution-control-board/information/WasteManagement/E-Waste_Management/DISMANTLERS-REFURBISHERS-RECYCLERS.html). Accessed 20 Aug 2021
27. Rautela R, Arya S, Vishwakarma S, Lee J, Kim KH, Kumar S (2021) E-waste management and its effects on the environment and human health. *Sci Total Environ* 773:145623
28. Chen A, Dietrich KN, Huo A, Ho SM (2011) Developmental neurotoxicants in e-waste: an emerging health concern. *Environ Health Perspect* 119(4):431–438
29. Wang J, Chen S, Zheng X, Gonzales L, Ohura T, Mai B, Simonich SLM (2012) Inhalation cancer risk associated with exposure to complex polycyclic aromatic hydrocarbon mixtures in an electronic waste and urban area in South China. *Environ Sci Technol* 46(17):9745–9752
30. Bandowe BAM, Nkansah MA (2016) Occurrence, distribution and health risk from polycyclic aromatic compounds (PAHs, oxygenated-PAHs and azaarenes) in street dust from a major West African Metropolis. *Sci Total Environ* 553:439–449
31. Martin AK, Mack DG, Falta MT, Mroz MM, Newman LS, Maier LA, Fontenot AP (2011) Beryllium-specific CD4 + T cells in blood as a biomarker of disease progression. *J Allergy Clin Immunol* 128(5):1100–1106
32. Abakay A, Gokalp O, Abakay O, Evliyaoglu O, Sezgi C, Palanci Y, Ekici F, Karakus A, Tanrikulu AC, Ayhan M (2012) Relationships between respiratory function disorders and serum copper levels in copper mineworkers. *Biol Trace Elem Res* 145(2):151–157
33. Alabi OA, Bakare AA, Xu X, Li B, Zhanfg Y, Huo X (2012) Comparative evaluation of environmental contamination and DNA damage induced by electronic-waste in Nigeria and China. *Sci Total Environ* 423:62–72
34. Awasthi AK, Zeng A, Li J (2016) Relationship between e-waste recycling and human health risk in India: a critical review. *Environ Sci Pollut Res* 23(12):11509–11532
35. Benbrahim-Tallaa L, Waterland RA, Dill AL, Webber MM, Waalkes MP (2007) Tumor suppressor gene inactivation during cadmium-induced malignant transformation of human prostate cells correlates with overexpression of de Novo DNA methyltransferase. *Environ Health Perspect* 115(10):1454–1459
36. Axelrad DA, Bellinger DC, Ryan LM, Woodruff TJ (2007) Dose-response relationship of prenatal mercury exposure and IQ: an integrative analysis of epidemiologic data. *Environ Health Perspect* 115(4):609–615
37. Pilsner JR, Hu H, Ettinger A, Sanchez BN, Wright RO, Cantonwine D, Lazarus A, Lamadrid-Figueroa H, Mercedo-Garcia A, Tellez-Rojo MM, Hernandez-Avila MM (2009) Influence of prenatal lead exposure on genomic methylation of cord blood DNA. *Environ Health Perspect* 117(9):1466–1471



38. Pilsner JR, Lazarus AL, Nam D, Letcher RJ, Sonne C, Dietz R, Basu N (2010) Mercury-associated DNA hypomethylation in polar bear brains via the luminometric methylation assay: a sensitive method to study epigenetics in wildlife. *Mol Ecol* 19(2):307–314
39. Benbrahim-Tallaa L, Waterland RA, Dill AL, Webber MM, Waalkes MP (2007) Tumor suppressor gene inactivation during cadmium-induced malignant transformation of human prostate cells correlates with overexpression of de Novo DNA. *Environ Health Perspect* 115(10):1454–1459
40. Takiguchi M, Achanzar WE, Qu W, Li G, Waalkes MP (2003) Effects of cadmium on DNA-(Cytosine-5) methyltransferase activity and DNA methylation status during cadmium-induced cellular transformation. *Exp Cell Res* 286(2):355–365
41. Jiang G, Xu L, Song S, Zhu C, Wu Q, Zhang L, Wu L (2008) Effects of long-term low-dose cadmium exposure on genomic DNA methylation in human embryo lung fibroblast cells. *Toxicology* 244(1):49–55
42. Kondo K, Takahashi Y, Hirose Y, Nagao T, Tsuyuguchi M, Hashimoto M, Ochiai A, Monden Y, Tangoku A (2006) The reduced expression and aberrant methylation of p16INK4a in chromate workers with lung cancer. *Lung Cancer* 53(3):295–302
43. Sun H, Zhou X, Chen H, Li Q, Costa M (2009) Modulation of histone methylation and MLH1 gene silencing by hexavalent chromium. *Toxicol Appl Pharmacol* 237(3):258–266
44. Chen J, Liufu C, Sun W, Sun X, Chen D (2009) Assessment of the neurotoxic mechanisms of decabrominated diphenyl ether (PBDE-209) in primary cultured neonatal rat hippocampal neurons includes alterations in second messenger signaling and oxidative stress. *Toxicol Lett* 192(3):431–439
45. Rabbani M, Heidari R, Farrokhi-Asl H, Rahimi N (2018) Using metaheuristic algorithms to solve a multi-objective industrial hazardous waste location-routing problem considering incompatible waste types. *J Clean Prod* 170:227–241
46. Eriüst C, Akcil A, Gahan CS, Tuncuk A, Devci H (2013) Biohydrometallurgy of secondary metal resources: a potential alternative approach for metal recovery. *J Chem Technol Biotechnol* 88(12):2115–2132
47. Watling HR (2014) Review of biohydrometallurgical metals extraction from polymetallic mineral resources. *Minerals* 5(1):1–60
48. Suzuki I (2001) Microbial leaching of metals from sulfide minerals. *Biotechnol Adv* 19(2):119–132
49. Kiddee P, Pradhan JK, Mandal S, Biswas JK, Sarkar B (2020) An overview of treatment technologies of E-waste. *Handb Electron Waste Manage Int Best Practices Case Stud* 1–18
50. Dwivedi M, Mittal RK (2010) Future trends in computer waste generation in India. *Waste Manage* 30:2265–2277

# A Swarm Intelligence and Nearest Neighborhood Approach to Solve an Excess Capacity Vehicle Routing Problem in a FDCG Company



T. Srinivas Rao

**Abstract** The paper has been modeled as the traveling sales man problem with ant colony algorithm and nearest neighborhood algorithm and compared their effectiveness. There is an evergreen demand for Fast delivery goods in the consumer segment. The challenge lies in the efficient delivery of goods to the customer in the quickest possible time. Both cost and time bound dispatch of materials are the most important variables dealing with the FDCG. The basis of vehicle routing algorithm is that the routes are covered in an optimal manner such that each city is visited only once meeting the capacity constraints. Often there are situations when the load of the manufacturer exceeds the capacity. Wherever there is an excess load an another vehicle is routed to collect the material, the distance covered may not be same and the path traced is different. We have implemented the vehicle routed algorithm using ant colony to trace out a new shortened path.

**Keywords** FDCG · Algorithm · Vehicle routing · Capacity constraint

## 1 Introduction

The Ant colony optimization is best suitable for solving difficult optimization problems such as vehicle routing problems, though we do not get the exact solution but approximate solutions can be achieved. The ACO uses an artificial ant as the basis for searching the good solutions, they are also called as software agents for a vehicle routing problem. On a selected tour the ACO obtains the best path which is the shortest distance taken to cover the entire tour. The solutions are built incrementally on the graph with the help of artificial ants or software agents. The ants use pheromone to track the tour path and the ACO follows random process of development for the development of solutions. Pheromone is a chemical substance secreted by the natural ants in order to find the shortest distance for reaching the food destinations [1].

---

T. Srinivas Rao (✉)

Department of Mechanical Engineering, Amrita School of Engineering, Amrita Vishwa Vidyapeetham, Bengaluru, India  
e-mail: [t\\_srinivas@blr.amrita.edu](mailto:t_srinivas@blr.amrita.edu)

Vehicle routing problem (VRP) can be best solved using ant colony optimization. The VRP is characterized by a set of cities and its location. In the VRP the rule is that the vehicle visits each location only once and reaches the destination in a closed loop manner. The objective of VRP is to find the optimized travel path which minimizes both cost and distance in reaching the final destination, thus it determines the shortest distance from the origin to the final destination without violating the VRP rule [2].

In the VRP (TSP) graph the touring cities are represented by the vertices of the graph which are also called as construction graph. While applying VRP we can reach back to the starting point by randomly starting from any city. The traversing path of the various cities is mapped on the graph in which edge length represents the distance between the cities. The pheromone values are computed and the shortest destination is mapped on the graph. Pheromone is an important feature which is updated during the successive iterations of the ACO till the optimized path is reached.

The ACO follows a standard procedure in which the ants are placed in each city and the movement of ants from one place to another is determined probabilistically. The formula for determining the pheromone content is done probabilistic. The distance traveled by the species is memorized by the algorithm and it is determined by the pheromone content and no ant visits the city twice. The pheromone content is updated once the ant visits all the cities.

## 2 Research Background

Routing Problem of vehicle (RPV) is an optimization problem where materials are commuted in one travel mode to different geographical nodes [3]. there are markable improvements have been noticed. Routing Problem which have capacity as the one of the constraint (CVRP) is one of the premiere vehicle routing problem [4].

We can solve the capacitated routing problems with combinatorial optimization algorithms, these algorithms give fast and approximate solution which are near to the true value also they guarantee less complexity, good accuracy and efficient with low running time [5]. The solutions provided by different algorithms are inadequate [6]. There are certain often used algorithms such as Wright and Clarke Savings code [7], Sweeping code [8], Fisher and Jaikumar discusses about the aggregate algorithm [9] and routing algorithm discussed in Holmes and Parker algorithm [10]. In the present work evolutionary colony algorithm is being used to solve a typical vehicle routing problem for a FDCG company [2]. A brief summary about the evolutionary codes is being explained in the subsequent section. Papers from [11–17, 20] are exclusively on traveling sales man problem which are modeled by various algorithms. Paper [11] discusses about the application and comparative efficiencies of various algorithms. Paper [12] by Vamsikrishna discusses and solves transportation problem using genetic algorithm, which can be a good option to solve the current paper with genetic algorithm and compare efficiencies. Paper [13] by Vamsikrishna introduces concept of six sigma concepts in optimization which can be a breakthrough technique in applying to the current model. Dispatching rule [14] for dynamic job shop

scheduling is a good technique in adopting to the current problem. Thennarasu et al. [15] discusses about multi criterion decision making problem in make span problems. Sathish kumar et al. [16] presents a supply chain model using particle swarm approach. A case study on productivity improvements [17] by Dr. Saleshya has been discussed in great depth.

Development and selection of hybrid **Research Methods**

Most Combinatorial optimization problems are difficult to solve and the solutions are NP (Non deterministic polynomial time) hard therefore we adopt Ant colony algorithm to solve NP hard problems which is a meta heuristic algorithm and it also solves quadratic assignment and vehicle routing problems [1, 18]. A near optimal solution can be obtained using ant colony algorithms for various combinatorial problems like vehicle routing. The graph changes dynamically in real time when we use ant colony algorithm as compared to evolutionary algorithm and other algorithms. Urban transportation and network routing are the domain areas where ant colony algorithms are applied extensively.

The artificial ants are the basis on which the ACO algorithm works. It is a probabilistic algorithm. As the probability for a particular city is more than the ant moves to that city from its current destination. The methodology and modality of rules are given below:

- (1) No two cities should be visited at a time.
- (2) A distant city will never be chosen. The probability to choose the same will be less.
- (3) The probabilistic formulae in ant colony algorithm determines the pheromone content which guides the evolutionary swarms to commute from one node to another. Higher the pheromone content of the ants greater the probability for the ant to move from one city to another.
- (4) There is a higher probability of more pheromone content as the optimized path is computed. In real life the swarm lays a chemical substance on the path it traverses. There is an evaporation of pheromone trail after each iteration.

The behavior of ant gives birth to the optimization process of ant colony. Whenever a food destination is reached the ants cooperate and communicate to the other ants through the presence of pheromone content secreted by the visiting ants. This complex phenomenon results into the derivation of shortest path of food destination. The pheromone acts like a communication system for the other swarms to follow. As the ant secretes more chemical more ants will follow. In each city an artificial ant is randomly placed so that during there is a movement of ant from one city to another.

For the swarms to travel from one place (*i*) to another place (*j*) there is a stochastic formulae devised by Dorigo which is stated as follows.

$$\delta_k(i, j) = \begin{cases} \frac{\mu_{ij}^\alpha \times Y_{ij}^\beta}{\sum g \in J_k^j} & \\ 0 & \end{cases} \tag{1}$$

where:

- $\delta_k(i, j)$  represents the ant  $k$ 's probability to visit the routes.
- $g \in J_k^j$  represents the range of places not traveled by swarm  $k$  in place  $i$ .
- $\alpha$  highlights the value of chemical pheromone trails.
- $\beta$  denotes the relative value of distance between the places.

The availability of chemical trail that a chosen path is how close the route is represented by the stochastic Eq. 1. We can determine larger weights by tweaking with the  $\alpha$  and  $\beta$  parameters. We can calculate the pheromone evaporation at the edges as more and more ants visit the designated route. A mathematical expression represented by Dorigo is used to calculate the pheromone content.

These are the steps of the algorithm:

1. The tour can be started randomly from any city and it can be chosen as an arbitrary vertex which can be set as current vertex.
2. Determine the shortest edge to connect the nearest vertex which is not visited and it will be treated as the current vertex
3. We can set current vertex as  $V$ .
4. The city visited is denoted as  $V$ .
5. The program can be terminated when all the vertices are visited.
6. Go to step 2.

All the visited cities which are the vertices is the output of the algorithm.

The quantity of pheromone laid by each ant  $k$  is represented by  $Art * j. (t)$  on each edge  $(i, j)$  which was used, once the tour has been completed, the value  $Art * (i)$  indicates the performance of the ant. The artificial deposition of pheromone is indicated by iteration  $t$ , swarm  $k$  lays  $Art ^ (t)$  on endpoint  $(I, j)$ :

$$\begin{aligned}
 Art * j &= \frac{T}{K^L} (t) \text{ if } (i, j) \in K^t (t) \\
 Art * j &= 0 \text{ otherwise}
 \end{aligned}
 \tag{2}$$

The value  $K^t(i)$  is the swarm movement done by swarm  $k$  during iteration  $i$ ,  $K^L(t)$  is the tour length, and  $T$  is a value which should be equal to the optimal tour length.

Its quick to implement the nearest neighbor algorithm as it is easy and fast to execute, but due to its grabbing nature sometimes it misses the routes which are shorter.

**Update rule of Pheromone:** In the swarm system all the swarms are allowed to deposit the chemical substance called pheromone once they complete their travels. The swarms which complete the best travel is allowed to deposit the chemical substance called pheromone along all its branches. The swarms are therefore allowed to search near the paths of the tour. The formulae for updating the tour is given by:

$$\mu_{ij}(t) \leftarrow (1 - \text{rho}) \cdot \mu_{ij}(t) + \text{rho} \cdot \Delta\mu_{ij}(t)
 \tag{3}$$

where  $i, j$  are the nodes belonging to  $T+$ , which is the best tour since the inception of the trial,  $\rho$  is the factor governing the decay of the chemical substance.

$$\Delta\mu_{ij}(t) = \frac{1}{Q} + \tag{4}$$

where  $Q+$  is the length of the tour  $T+$ . from this update we understand that the procedure allows the global updates of the best tour. New solutions emerge due to local updates of pheromone.

**Updates of local pheromone trail:** The local update is represented as follows, once the swarms is in the node  $h$ . the update of the chemical substance called pheromone takes place as follows.

$$\mu_{ij}(t) \leftarrow (1 - \rho) \cdot \mu_{ij}(t) + \rho \cdot \mu_o \tag{5}$$

The value of  $\mu_o$  occupies the pheromone trials initial value and it is found experimentally that by setting  $\mu_o = (n \cdot Q_{nn})^{-1}$  where  $n$  represents the no of nodes or cities and the length of the travel is represented by  $Q_{nn}$ .

### 3 Result Discussion

We have tested the data of an FMSCG company dealing in groceries and vegetables and the data for the vehicle movement is shown in the Table 1 [11, 19]. Using this data in Table 1 we have implemented the swarm colony algorithm using MATLAB version 2019. The various distances of the depots are recorded in terms of latitude and longitude in and around Bangalore city.

**Table 1** Distances in latitude and longitude for the several depots and customers

Depot No.	X-Co-ordinate	Y-Co-ordinate
1	45	68
2	45	70
3	42	66
4	42	68
5	42	65
6	40	69
7	40	66
8	38	68
9	38	70
10	35	66

### 4 Conclusion

With an increase in the complexities of real industrial systems, maintenance decision making has become a challenge for maintenance managers. In the present study, the authors have used an integrated MCDM framework for the selection of an optimal maintenance strategy for ASU of a urea fertilizer industry.

The nearest neighbor algorithm due to its greedy nature is quick and easy to implement but sometimes it misses shorter routes as a result of which the code is executed fast. The tour is near optimal if the first few stages and last few stages are comparable to tour length, if the length of the tour is greater than more optimal routes are available.

The nearest neighbor algorithm performs better than ant colony algorithm. The results of NN algorithm select the best route covering a distance of 261 units for a demand of 50 Customers is optimally selected for the best route as shown in Fig. 2. It is still possible to improve the route by manually adjusting the graph. The ant colony performs better for 200 ants but it covers distance of 284 units only as shown in Fig. 1. We have solved one more solution for customers were excess loads are there, it is represented by Fig. 3. Here the number of destinations are small so the ant colony computes the shortest routes for these destinations as represented (Figs. 4; Table 2).

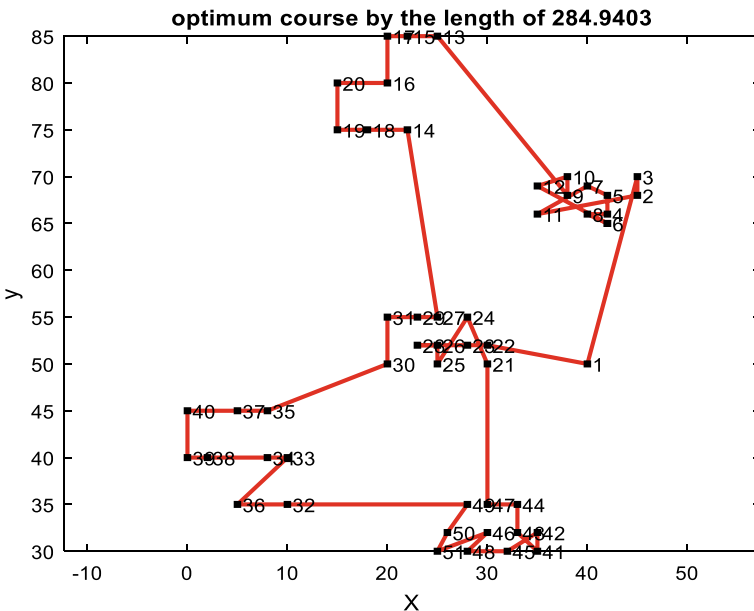


Fig. 1 Results of TSP using swarm for 200 ants

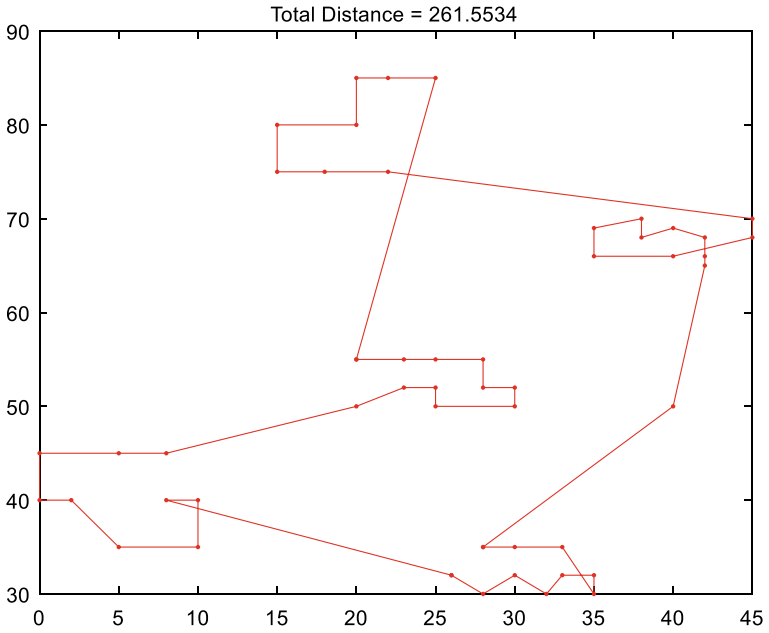


Fig. 2 Results of TSP using NN algorithm

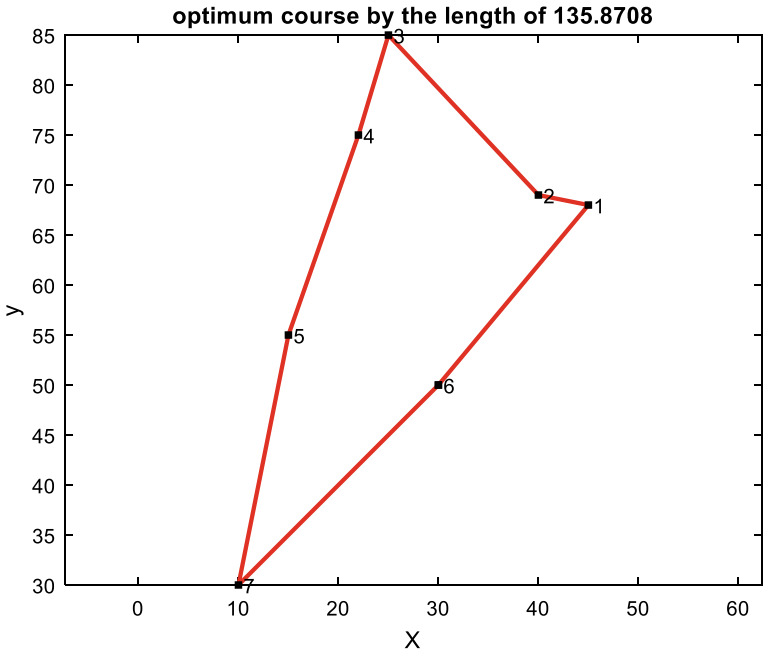


Fig. 3 Results of TSP using swarm algorithm for short loads



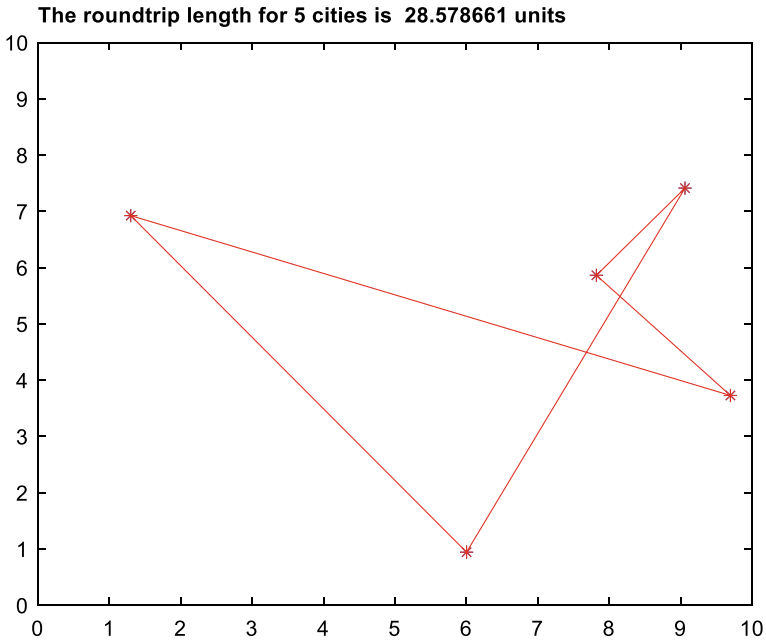


Fig. 4 Results of TSP using swarm algorithm for short loads (Not optimum)

Table 2 Swarm and NN algorithm results

Depos	Swarm colony	Nearest neighbor
50	285 Units	261 Units

### References

1. Dorigo G, Gambardella LM (1997) Learning approach to the traveling salesman problem. *IEEE Trans Evol Comput* 1(1):214
2. Xin MA (2010) Vehicle routing problem with time windows based on improved ant colony algorithm. *Int Conf Inf Technol Comput Sci*
3. Abdulkader MMS, Yuvraj Gajpal TYE (2015) Hybridized ant colony algorithm for the multi compartment vehicle routing problem. *Appl Soft Comput* 37:196–203
4. Christofides N (1976) The vehicle routing problem. *RAIRO Oper Res* 10:55–70
5. Vidal T, Crainic TG, Michel Gendreau CP (2013) Heuristics for multi-attribute vehicle routing problems: a survey and synthesis. *Eur J Oper Res* 231:1–21
6. Laporte G (1991) The vehicle routing problem: An overview of exact and approximate algorithms. *Eur J Oper Res* 59:345–358
7. Clarke G, Wright JW (1964) Scheduling of vehicles from a central depot to a number of delivery points. *Oper Res* 12:568–581
8. Gillett B, Miller L (1974) A heuristic algorithm for the vehicle-dispatch problem. *Oper Res* 22:340–349
9. Fisher ML, Jaikumar R (1981) A generalized assignment heuristic for vehicle routing. *Networks* 11:109–124
10. Holmes RA, Parker RG (1976) A vehicle scheduling procedure based upon savings and a solution perturbation scheme. *Oper Res Q* 27:83–92. <https://doi.org/10.2307/3009212>

11. Divya Sharma SG, Tatavarthy SR (2019) Development of optimized solution for a generic disaster management problem through construction of responsive supply chain a review. In: Published by AIP conference proceedings, vol 2148. p 030049. <https://doi.org/10.1063/1.5123971>
12. Vamsikrishna A, Raj V, Divya Sharma SG (2021) Cost optimization for transportation using linear programming. In: Jha K, Gulati P, Tripathi UK (eds) Recent advances in sustainable technologies (Lecture notes in mechanical engineering). Springer, Singapore. [https://doi.org/10.1007/978-981-16-0976-3\\_2](https://doi.org/10.1007/978-981-16-0976-3_2)
13. Vamsikrishna A, Shruti M, Divya Sharma SG (2021) Six sigma in piston manufacturing. In: Phanden RK, Mathiyazhagan K, Kumar R, Paulo Davim J (eds) Advances in industrial and production engineering (Lecture notes in mechanical engineering). Springer, Singapore. [https://doi.org/10.1007/978-981-33-4320-7\\_52](https://doi.org/10.1007/978-981-33-4320-7_52)
14. Thenarasu M, Ramesh Kumar K, Anbuudayasankar SP, Arjunbarath G, Ashok P (2020) Development and selection of hybrid dispatching rule for dynamic job shop scheduling using multi-criteria decision making analysis (MCDMA). *Int J Qual Res* 14(2):487–504
15. Thenarasu M, Ramesh Kumar K, Anbuudayasankar SP (2019) Multi-criteria decision making approach for minimizing makespan in a large scale press-shop. *Int J Indus Eng Theory Appl Pract* 26(6):962–985
16. Sathish Kumar VR, Anbuudayasankar SP, Ramesh Kumar K (2017) Optimizing Bi-objective, multi-echelon supply chain model using particle swarm intelligence algorithm. In: *IConAmma 2017*
17. Chandran A, Saleeshya PG (2020) Productivity improvement through lean initiatives-a service sector case study. *Int J Bus Innov Res* 22(2)
18. Srinivas Rao T (2018) An evaluation of ACO and GA TSP in a supply chain network. Published in *Mater Today Proc* 5:25350–25357. Srinivas Rao T (2017) A comparative evaluation of GA and SA Tsp in a supply chain network. Published in *Mater Today Proc* 4:2263–2268
19. Srinivas Rao T (2019) An ant colony and simulated annealing algorithm with excess load VRP in a FMCG company. In: Published in IOP conference series material science and engineering, vol 577. IOP Publishing, p 012191. <https://doi.org/10.1088/1757-899X/577/1/012191>
20. Taillard E, Badeau P, Gendreau M, Guertin F, Potvin J-Y (1997) A tabu search heuristic for the vehicle routing problem with soft time wind. *Transp Sci* 31:170–186

# Advantages and Applications of Natural Fiber Reinforced Hybrid Polymer Composites in Automobiles: A Literature Review



Sarita Choudhary, Jyotirmoy Haloi, Manoj Kumar Sain,  
and Praveen Saraswat

**Abstract** Composite materials have been identified as the most promising and popular material due to their wide applications and unique properties. Natural or synthetic fiber reinforced composites are gaining traction due to increasing market demand for materials having high specific strength for customized purposes. Due to the fact that the performance of composite materials is largely determined by their constituent materials and manufacturing procedures, it is needed to investigate the mechanical and tribological properties of various fibers available worldwide. There is a need also to investigate the classification of natural fibers with their fabrication in order to determine the material's optimal characteristic for the intended use. The aim of this work is to deliver a state of art summary of hybrid fiber reinforced polymer composites, their broad range of properties, usefulness, classification, and numerous fiber composite manufacturing procedures for key applications. Due to their superior performance in a wide diversity of applications, fiber reinforced composite materials have emerged as a viable alternative to solo metals or alloys. Hybridization has the potential to significantly enhance the mechanical characteristics of uni-fiber reinforced polymer composites.

**Keywords** Composite materials · Hybridization · Fiber reinforced polymer · Literature review

## 1 Introduction

Rapid expansion in market demand and manufacturing has resulted in material advancements in terms of mechanical properties such as density, strength, toughness, and cost-effectiveness, all of which lead to increased sustainability [1], Sherif

---

S. Choudhary (✉) · J. Haloi  
Department of Mechanical Engineering, University of Engineering & Management, Jaipur, India  
e-mail: [saritachoudhary02@gmail.com](mailto:saritachoudhary02@gmail.com)

M. K. Sain · P. Saraswat  
Department of Mechanical Engineering, Swami Keshvanand Institute of Technology,  
Management & Gramothan, Jaipur, India

© The Author(s), under exclusive license to Springer Nature Singapore Pte Ltd. 2023  
R. P. Singh et al. (eds.), *Advances in Modelling and Optimization of Manufacturing and Industrial Systems*, Lecture Notes in Mechanical Engineering,  
[https://doi.org/10.1007/978-981-19-6107-6\\_46](https://doi.org/10.1007/978-981-19-6107-6_46)

et al. [2, 3]. Natural fiber reinforced polymer composite materials have gained popularity in recent years as a result of their ease of fabrication, low density, biocompatibility, low thermal conductivity, renewability, low toxicity, and combustibility, as well as their low production cost. Due to their enhanced qualities, composite materials have the potential to be used in a wide variety of applications [4, 5]. On the other hand, forecasting the thermal and mechanical properties of fiber reinforced polymer hybrid composites is a difficult problem for present modeling techniques, necessitating a complete understanding of simulation analysis for such materials. Composite materials are composed of at least two constituents: matrix and reinforcement. Natural and synthetic fibers have found significant applications in a variety of fields, including construction, mechanical engineering, automobile manufacturing, aircraft, biomedicine, and maritime [6], Movahedi et al. [7, 8]. Despite these advantages, natural fibers have a number of disadvantages, including a high capacity for moisture absorption and a low impact strength. The hybridization technique can be used to circumvent these limits. By incorporating additional fibers into a polymer matrix alongside a single fiber, composites were developed. Hybrid natural composites are more sophisticated than typical fiber-supported composites and offer a greater variety of application options. Earlier research on natural–synthetic fiber hybrid composites focused on reducing the amount of synthetic fibers used.

## 2 Background of Natural Fibers

Natural fibers are having irregular cross sections, which distinguishes their structures from conventional or man-made fibers like carbon fibers, glass fibers, etc. Based on their origin, these fibers can be categorized as vegetable/plant fibers, animal or protein fibers and mineral fibers [9]. Natural fibers are classified in Fig. 1.

Animal fibers are mostly composed of protein, whereas mineral fibers are comprised of the asbestos group of minerals. Nowadays, these fibers are avoided due to the health risks linked with them and are banned in a number of nations [12]. Plant fibers have a better stiffness and strength than animal fibers, which are more commonly available. Natural fibers such as jute, banana, coconut shell, bamboo, cotton, coir, pineapple, husk, sisal, and ramie are abundant in India, making them ideal for the development of natural fiber-based composites with the primary goal of exploring value-added application possibilities. Natural fibers play a critical role in determining current ecological and biological challenges [13]. Natural fibers, particularly hemp, sisal, flax, and jute, have reasonably strong mechanical qualities and comparable with glass fiber in terms of specific mechanical and physical properties [14]. Natural fibers are good thermal and acoustic insulators due to their low-density structure. They also have a low bulk density [15]. Interestingly, different types of plentiful natural fibers have been shown to provide effective and durable reinforcement in thermoset and thermoplastic matrices.

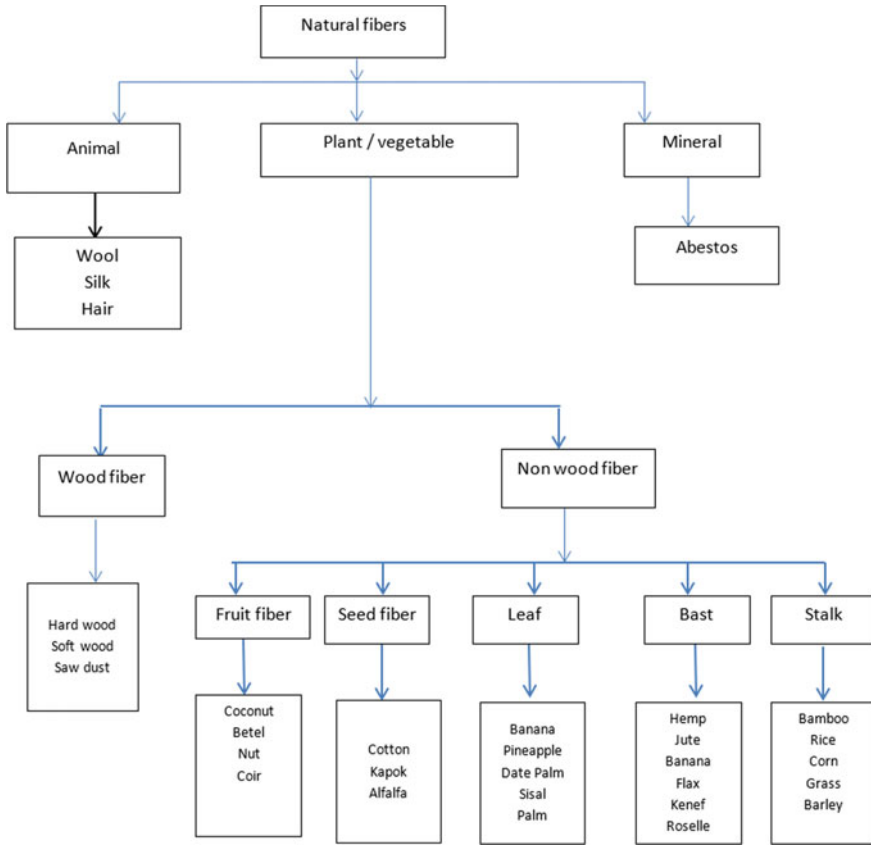


Fig. 1 Classification of natural fibers [10, 11]

### 3 Methodology for Bibliometric Analysis

Bibliometric analysis considers the study of papers and other publications via the application of statistical tools. This technique is widely used to conduct a quantitative assessment of a certain scientific field’s current trends [16].

This study used bibliometric analysis, which involved examining the bibliographic characteristics of journal articles published between 2010 and 2021. The data on natural fibers’ advancement in the automotive industry was collected from Scopus database. Only journal articles were included in this study and the search was narrowed to 189 items after applying exclusions.

The trend of articles published on the use of natural and sustainable fiber reinforced composites in automotive sector in last decade are depicted in Fig. 2. Substantially good research growth can be observed from the figure.

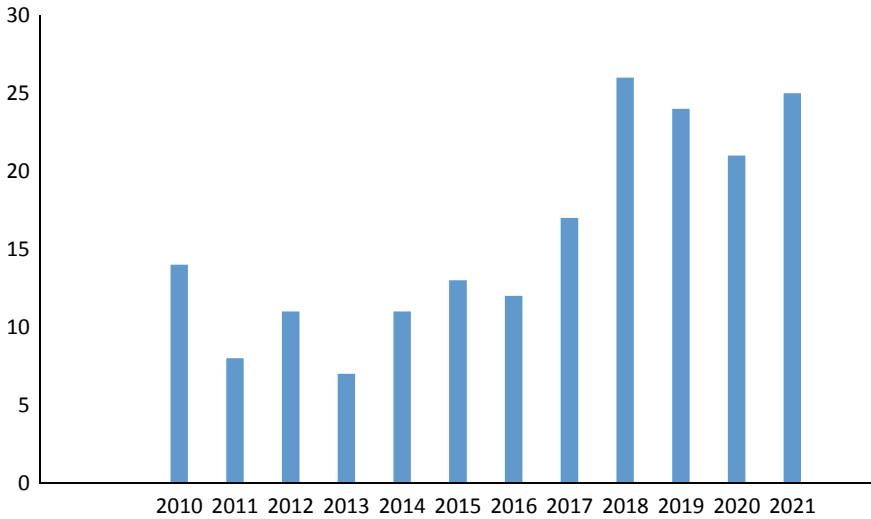


Fig. 2 Publication trend in last decade

The journals published maximum research articles on the use of natural and sustainable fiber composites in automotive sector are depicted in Fig. 3. Revista Materia, journal of cleaner production, journal of material research and technology and polymers are the leading journal in the field.

Country-wise publication trend depicted in Fig. 4 shows that India is leading country followed by Brazil in the natural and sustainable fiber composite research. France, USA, and China also have the significant publications in this field.

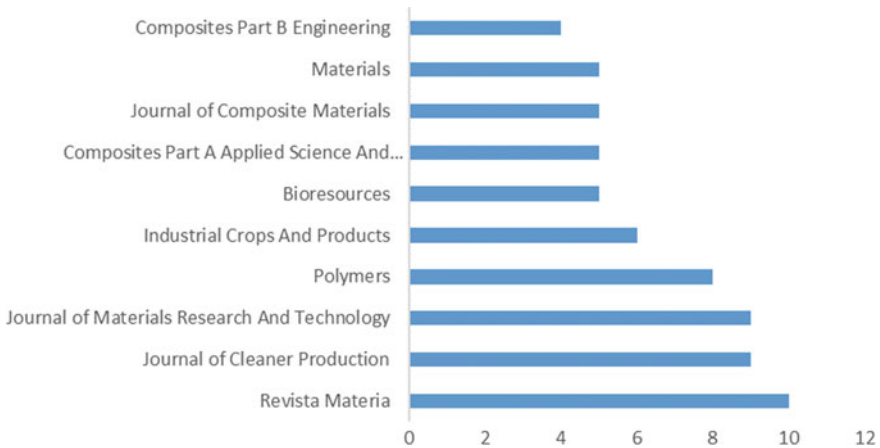


Fig. 3 Leading journals in the field of natural and sustainable fiber composites

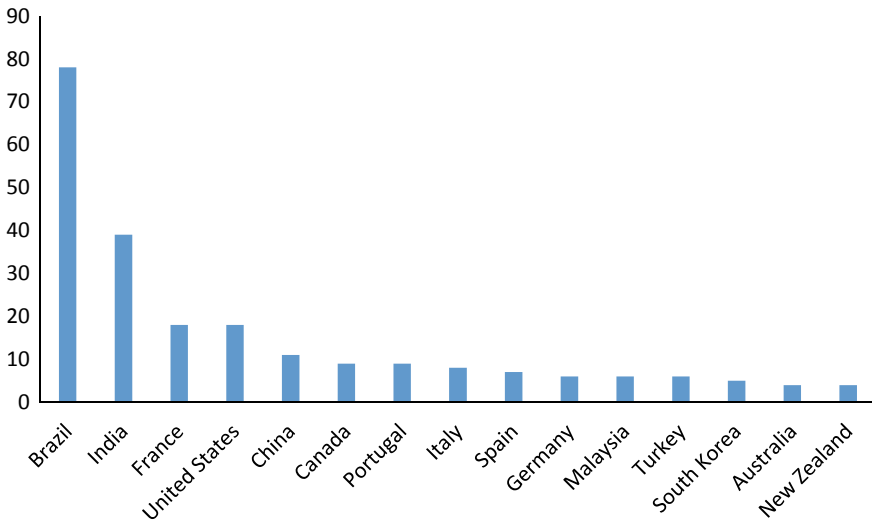


Fig. 4 Country-wise publication trend

## 4 Literature Review Findings

This section summarizes key findings from various authors' studies on composite materials. Devaraju [17] investigated the effect of fiber loading on the mechanical characteristics of epoxy-based sisal and banana Fiber composites manufactured by hand layup. Tensile strength of composites containing 35% banana fibers was found to be greater than that of other compositions. Additionally, the impact resistance of banana and sisal Fibers in a 20:20 ratio was found to be greater than that of other compositions, and a 20:15 ratio of banana and sisal Fibers gives increased hardness. Athijayamani et al. [18] investigated the possibility of replacing glass fiber reinforced composites with natural Fiber. The experiment was conducted on a hybrid natural fiber composed of short roselle and sisal and discovered that increasing the fiber length and composition boosts tensile strength but decreases impact strength. Tensile and flexural strengths are proportional to the proportion of roselle and sisal fiber hybrid reinforcement, whereas impact strength is proportional to the proportion of sisal fiber. Natural fibers, according to [19], are less expensive, lighter in weight, environment friendly, recyclable, and readily available. These fibers can be employed as reinforcement in polymer matrixes in a variety of configurations, including random orientation, uni-directional orientation, bi-directional orientation, and woven mat pattern. Compression molding and hand layup processes are frequently employed in manufacturing. Due to its comparable mechanical properties and inexpensive cost, natural fiber can be utilized in place of synthetic Fiber. Hybridization of fibers can be used to improve the mechanical properties of single fiber reinforced polymer composites. Additionally, the hybridization process helps in overcoming the constraints of

single fiber. Natural Fibers, according to [20], are biodegradable and environmentally friendly, however synthetic fibers provide more rigidity. Hybrid fiber reinforced composites combine the advantages of natural and synthetic fibers. Composite materials are manufactured in a variety of ways depending on the material chosen, and their effectiveness is determined by the volume and type of matrix and fiber material used. Composite materials are employed in a variety of applications including mechanical, automotive, aerospace, marine, and construction. Shireesha et al. [21] investigated the mechanical properties of natural fiber composite materials such as tensile strength, flexural strength, impact strength, hardness, and surface morphology. Natural Fibers were discovered to be less expensive, more readily available, lighter in weight, recyclable, biodegradable, and harmless in nature than synthetic Fibers. Tensile and impact strengths rose with Fiber loading, whereas flexural strengths climbed to a certain point and then began to decline. Surface treatment was found to improve matrix-fiber bonding and strength. Hybridization of Fibers enhanced mechanical qualities while reducing reliance on synthetic Fibers. Yadav et al. [22] investigated the preparation, characterization, and finite element analysis of epoxy composites based on sugarcane dry leaves at six volume percentages. The study discovered that at an 8 vol% percentage, the mechanical properties of the composite were superior to those of pure epoxy samples. A micromechanical model based on numerical homogenization anticipated an increase in the Young's modulus of composites of up to 10.33%. Stress research found that reinforced composites exhibit up to a 167% increase in Von Mises stress and a 3.5% reduction in deformation when compared to pure epoxy. Ku et al. [23] proved that natural fibers are cost-effective, recyclable, lightweight, and environmentally friendly reinforcing materials with high tensile qualities that may be used in place of traditional fibers such as glass and carbon fiber. However, natural fiber's primary disadvantage is its weak adherence to matrix resin, which can be enhanced through physical and chemical modification. According to this study, mathematical modeling is also an excellent method for predicting the tensile properties of natural fiber reinforced composites composed of plant and animal Fibers. According to [24], natural fiber reinforced polymer composites have gained popularity in recent years in car manufacturing due to their light weight, cost-effectiveness, design flexibility, and eco-friendliness. According to the study, hybridizing natural fibers with a little proportion of synthetic Fiber improves their qualities and overcomes their inherent constraints such as low durability, low modulus, and hydrophilicity. Thus, the enhanced end-of-life disposal and reduction in weight of automobile components pave the way for improving automotive fuel economy and lowering the engine emissions. This trend will continue with increased research on the sustainability of natural fiber reinforced composites in automotive applications (Tables 1, 2 and 3).

Bolcu and Stănescu [28] investigated the mechanical characteristics of composite materials composed of three separate hybrid resins generated from Dammar and two distinct types of flax fabric. According to the study, as Dammar's volume ratio increases, yield strength and modulus of elasticity fall while elongation increases. Elastic modulus, yield strength, and elongation all decrease when the Dammar volume ratio in composite increases. The vibration dampening capabilities of these



**Table 1** Applications of natural fiber used in automobile applications [19, 25]

Fiber (type of fiber)	Country	Application
Abaca fiber (leaf)	Bolivia, Malaysia, Philippines, Uganda	Seat backs, spare tire cover, underbody panels
Bamboo (stem)	China, India	Floor mats
Banana (stem)	China, Japan	Ceiling liner
Coir (fruit)	India, Malaysia, Sri Lanka, Philippines,	Bumpers, interiors, door panels,
Cotton (stem)	West and central Africa, China USA, India, Mexico,	Acoustic insulator, ceiling liner
Flax (stem)	Canada, China, India	Door panels, shelves
Hemp (stem)	China, India, Yugoslavia,	Door panel
Jute (stem)	Ghana, Tanzania,	Door panels and dashboard
Kenaf (stem)	South Africa, Togo	Door panel, other interior trim
Sisal (stem)	Antiqua, Bahamas, East Africa, Kenya, Tanzania, India	Glove box, door panels
Coconut	India, Indonesia, Philippines	Loadfloor, seat bottoms, back cushion
Corn	Argentina, Brazil, China, United States	Air conditioning vent, instrument panel, floor mats

composite materials have been demonstrated to be quite good. Composite materials can be employed in aeronautics (fuselage elements, flaps), automotive (bodywork parts such as wings, doors), civil and industrial engineering due to these qualities.

Ali [42] employed the Analytical Hierarchical Process (AHP) to pick materials, replacing the traditional materials selection system with software tools. The decision to optimize materials was challenging, since it entails a diverse range of materials and a variety of influencing criteria. Sensitivity analysis of the results enhances the level of confidence even more. The achieved result emphasizes environmental issues while simultaneously meeting mechanical, physical, and cost standards. The eco-friendly and biodegradable materials selected reduce the need on conventional petroleum-based products while simultaneously increasing passenger safety. Additionally, these materials meet the standards for product development set forth by industries. As a result, the natural fiber reinforced composite material used for this project is suitable for use in the construction of vehicle components. Balasubramanian and colleagues investigated the mechanical properties of hybrid natural fiber composites (2020).The composites were made by hand laying technique using hybrid of banana, jute and glass fibers. Various mechanical tests including tensile, flexural, impact, double shear, and interlamination, were conducted on the hybrid fiber composites and compared with single jute and banana fiber composites. The ultimate tensile strength, percentage elongation, flexural strength, and impact resistance of hybrid composites were all shown to be greater. Additionally, hybridization improved interlamination. To forecast the presence of voids, flaws, crack propagation, and resin dispersion, SEM pictures of specimens were analyzed morphologically. Singh

**Table 2** Compositions and applications of natural fiber reinforced polymer composites in various automobile parts [26, 27]

Composite	Manufacture (model)	Application
Zytel/castor	Fiat Alfa romeo 500 Panda Punto	Fuel line
Polyurethane/kenaf Polyurethane/soy Polyurethane/wheat straw Polyurethane/coconut	Ford Fiesta Edge Fusion Flex Focus BEW	Interior door panel Headline Console door Interior storage bins Luggage-compartment and speakers
Polyester/cotton/kenaf	GMC Terrain	Acoustic insulators
Polyethylene/bamboo/corn	Lexus CT200h	Floor mats
Polyurethane/soy	Lincoln MKZ	Console door
Polylactic acid/corn	Mazda 5 hydrogen	Console, seat fabric
Polyethylene/abaca/banana/Flax Polyethylene/flax	Mercedes Benz A class Benz C class	Seatbacks, panels
Sorona/Corn	Nissan Leaf	Floor mats
Sorona/Corn Zytel Kenaf/strach Sorona/corn	Toyota Pruis Camry Ranum SAI	Floor mats, sun visor, pillar garnish
Polyurethane/flax/sisal	Volkswagen Audi A2	Interior door panel

et al. [29] investigated epoxy-based natural fiber composites (sisal, jute, and banana). This research sought to ascertain the effect of chemical treatment on the mechanical properties of natural fiber composites. The surface was treated with 5% NaOH to improve its mechanical properties. Although surface treatment increased tensile and flexural strengths, and alkali surface treatment increased tensile strengths by up to 50%, untreated jute fiber-based composites had the best impact strength. The tensile strength of jute-based composites was the highest of the three natural fiber treated and untreated composites. These composites find application in a wide number of fields, including automotive components, electrical assemblies, and construction. Agunsoye et al. [43] examined the mechanical and morphological properties of a polyethylene composite reinforced with coconut shell natural fibers. Tensile and yield strengths

**Table 3** Key findings of existing literature review

Reference	Natural fiber	Key findings
[17]	Sisal fiber, banana fiber	The study concluded that an equal mixture of banana and sisal (BS) fibers have superior mechanical qualities
[18]	Roselle fiber, sisal fiber	According to the study, increasing fiber content and length improves tensile and flexural strength but decreases impact strength
[19]	Sisal, jute with glass fiber, banana with glass fiber	The hybridization procedure improved the mechanical characteristics of single fiber reinforced polymer composites. Additionally, the hybridization procedure alleviates the limitations of single fiber
[28]	Dammar, cotton, flax	The research found that composite materials possess a variety of qualities that enable them to be employed in a variety of applications including aeronautics (fuselage elements, flaps), automotive (bodywork parts such as wings, doors), civil and industrial engineering
[29]	Jute, banana, sisal	The study demonstrated that a 5% NaOH surface treatment improves mechanical characteristics. Surface treatment improves tensile and flexural strength, and alkali surface treatment increases tensile strength by up to 50%
[30]	Abaca fiber	The results indicated that the surface roughness of abaca fiber is lowest when left untreated and increases to a maximum when treated with 5% NaOH. By removing hydroxyl, abaca fibers become substantially more hydrophobic, resulting in decreased water absorption

(continued)

**Table 3** (continued)

Reference	Natural fiber	Key findings
Yu et. al. [31]	Short bamboo fiber	The redesigned mechanical tester's functionality and reliability are demonstrated through mechanical characterization of bamboo fibers at constant and varied moisture content
Giorcellia et. al. [32]	Biochar and biochar heat treated	The study concluded that ultimate strength and young modulus are is maximum for Tensile toughness reached its maximum capacity at 1% of biochar, whereas tensile toughness reached its maximum capacity at 2% of biochar. Additionally, it was shown that adding a little amount of biochar improves mechanical characteristics
[33]	Flax, sisal, aloevera	Project showed that hybrid natural composites have excellent mechanical characteristics
[34]	Bamboo and sisal fiber	Mechanical properties of hybrid fiber composite vary with fiber orientation and found that 0° fiber orientations exhibit maximum tensile, compressive and flexural strength
[35]	Jute fiber	Experimented found that five layer of composite glass-jute (longitudinal direction)-areca sheath (transverse direction)-jute (longitudinal direction)-glass shown better flexural, tensile and shear behavior than pure jute and glass fiber
[36]	Flax fiber	The study concludes that the fiber orientation affects the various energies that influence the cutting behavior and chip production of the polymer composites

(continued)

decreased as the volume percent of coconut shell increased, while modulus of elasticity decreased to 5% initially and later increased to 25%. The inclusion of coconut shell volume increased the hardness. Porosity diminishes as the number of coconut shell particles increases. These characteristics make them ideal for automotive interior components. Sinha et al. [30] conducted an experimental investigation on the

**Table 3** (continued)

Reference	Natural fiber	Key findings
Zeeshan et al. [37]	Flax/waste cotton	Glass, flax and waste cotton are better combination than glass and waste cotton for 10% of waste cotton. Impact strength are improved but flexural strength and moisture sensitivity are decrease with waste cotton content
Lokesh et al. [38]	Bamboo fiber	It can be seen that NaOH treated fibers influenced extremely the mechanical properties of the epoxy-based hybrid composites
[39]	Jute, pineapple leaf fiber	Hybrid composite of jute and pineapple leaf with polyester gives better tensile, flexural strength than epoxy resin. Mechanical properties improve with increase in fiber loading from 0.18 to 0.42 by fraction
[40]	Sisal and jute	Experimental result shows that 20% sisal and 20% jute with epoxy resin treated with NaOH increase 25% flexural strength
[41]	Jute	Natural hybrid fiber with glass fiber composites gives higher hardness and impact strength. These composites can be used in bumper, front end modules and interior structure of automotives

effect of alkali treatment on abaca Fiber and discovered that the composite's performance is dependent on the interfacial bonding between the matrix and reinforcing agent. The surface roughness of abaca Fiber is minimal when left untreated and increases to a maximum of 5% NaOH. Alkali treatment reduces the surface finish of the abaca Fiber by removing the hydroxyl layer (OH<sup>-</sup>), non-cellulosic components, and wax. By removing hydroxyl, abaca Fibers become considerably more hydrophobic, resulting in decreased water absorption.

Ramnath et al. [44] studied the mechanical characteristics of hybrid natural fiber reinforced composites. The composites were constructed utilizing the hand lay method and reinforced with banana, jute, and glass fiber. We evaluated the mechanical properties of hybrid fiber composites to those of jute and banana reinforced GFRP composites. Ultimate tensile strength, percentage elongation, flexural strength and impact resistance were found to be higher in case of hybrid fiber composites. Hybridizing also improve the inter de-lamination. To predict the voids, defects, crack propagation and resin distribution morphological analysis was done by SEM images of specimens and this is also used for better understanding of the composites.

Cinelli et al. [45] investigated hybrid composite laminates composed of PVA and lignocellulose filler derived from sugarcane bagasse, apple, and orange waste, with glycerol serving as a plasticizer. They evaluated hybrid composites mechanically, respirometrically, and through simulation. We discovered that the elongation at break, ultimate tensile strength, and Young's modulus all changed with fiber type and plasticizer agent. The addition of starch to the formulation decreased the mechanical characteristics significantly, while increasing the rate of deterioration and lowering the cost of the finished product.

Reddy et al. [39] investigated a hybrid composite matrix made of polyester and epoxy resin and reinforced with a blend of natural jute and pineapple leaf fibers as well as synthetic glass fiber. The study's findings indicate that such composite materials have a wide range of uses, including car components, electrical packages, and construction.

Khandai et al. [46] studied epoxy resin composites reinforced with a blend of flax, kenaf, glass, and carbon fibers with a 1:10 hardener (Triethylene tetra amine). Glass and carbon fiber composites were shown to have a higher hardness than natural fiber composites. In comparison to natural fiber, carbon fiber has a high flexural strength and modulus value (kenaf and flax). Additionally, it was discovered that glass fiber was more robust than natural fibers. The specific wear rate of glass fiber composites was found to be the highest, while that of kenaf fiber composites was found to be the lowest. Carbon fiber has a natural frequency that is 28.9% greater than kenaf fiber.

Khandai et al. [46] investigated epoxy resin composites reinforced with a 1:10 blend of flax, kenaf, glass, and carbon fibers (Triethylene tetra amine). The hardness of glass and carbon fiber composites was found to be greater than that of natural fiber composites. Carbon fiber, in comparison to natural fiber, has a high flexural strength and modulus value (kenaf and flax). Additionally, glass fiber was discovered to be more strong than natural fibers. The highest specific wear rate was seen for glass fiber composites, whereas the lowest was observed for kenaf fiber composites. Carbon fiber has a 28.9% higher natural frequency than kenaf fiber.

In 2011, Ku et al. examined the influence of ramie fiber loading on the mechanical characteristics of epoxy-based composites. SEM and FTIR analysis were used to determine the morphological properties and functional groups of raw and treated fiber. They concluded that increasing the amount of fiber in composites increases their mechanical properties. Composites containing 30% ramie fiber performed the best, and increasing the fiber content to 40% resulted in a significant decrease in mechanical properties due to fiber clustering, which resulted in poor adhesion and stress transfer. SEM investigation of the surface revealed that the primary failure modes were fiber pull-out, fiber fracture, matrix rupture, and debonding.

#### ***4.1 Application of Natural Fiber in Automobile***

Natural composites are the recent trends in the automotive sector because they physical and bio characteristics and emerge as an alternative of conventional fibers. Natural fibers are light in weight, therefore using it in automobile parts to reduce

the weight of the parts, lowering the vehicle's fuel consumption and lowering CO<sub>2</sub> emissions. Many automobile manufacturers, including top branded companies, have incorporated natural fiber components in their vehicles.

Natural fibers are most frequently used in exterior and interior part material. Although Toyota has employed natural fibers in its outside tire covers and radiator end tanks.

## 5 Conclusion and Future Scope

The careful analysis of the literature demonstrates that composites reinforced with natural fibers are more environmentally friendly and sustainable than composites reinforced with synthetic fibers. Due to a variety of increased features and characteristics, natural fiber composites are a superior solution for automotive applications. As evidenced from the literature, some top automotive manufacturers have already begun using natural fiber composites, a trend that can be accelerated further with enough study in this subject. Furthermore, the literature indicates that the disadvantages of natural fiber reinforcement can be overcome through the hybridization of natural and synthetic fibers. Numerous studies demonstrating the numerous applications of natural fiber reinforced polymer composites in automotive components have laid the groundwork for future study in the field of hybrid natural reinforced polymer composites.

The present study concludes the following points:

1. The newly applications of natural fiber reinforced composite materials exceed conventional materials from industrial to aerospace to consumer goods.
2. The hybrid composites can be used to minimize the energy consumption of interior panels, armrest, headliners, packaging trays, back part of seats, control panels, and dashboards in the car sector. The recent study shown that these hybrid composites exhibit superior thermal insulation properties. As a result, these composites may also be advised for use in panels, door shutters and frames, roofing sheets, partition walls, window frames, and insulation sheets to provide excellent thermal and acoustic insulation in buildings.
3. Natural fibers are reinforced in a variety of ways in polymer matrixes, including arbitrarily oriented, uni-directional, bi-directional, and knit mat topologies. These composites can be made in a variety of ways and with a range of fiber weights or volume fractions. Hand layup and compression molding are two of the most common manufacturing processes.

## References

1. Yashas Gowda TG, Sanjay MR, Subrahmanya Bhat K, Madhu P, Senthamaraikannan P, Yogesha B (2018) Polymer matrix-natural fiber composites: an overview. *Cogent Eng* 5(1):1446667
2. Sherif G, Chukov D, Tcherdyntsev V, Torokhov V (2019) Effect of formation route on the mechanical properties of the polyethersulfone composites reinforced with glass fibers. *Polymers* 11(8):1364

3. Sherif G, Chukov D, Tcherdyntsev V, Torokhov V (2019) Effect of formation route on the mechanical properties of the polyethersulfone composites reinforced with glass fibers. *Polymers* 11(8):1364
4. Chukov D, Nematulloev S, Zadorozhnyy M, Tcherdyntsev V, Stepashkin A, Zherebtsov D (2019) Structure, mechanical and thermal properties of polyphenylene sulfide and polysulfone impregnated carbon fiber composites. *Polymers* 11(4):684
5. Linul E, Lell D, Movahedi N, Codrean C, Fiedler T (2019) Compressive properties of zinc syntactic foams at elevated temperatures. *Compos B Eng* 167:122–134
6. Zagho MM, Hussein EA, Elzatahry AA (2018) Recent overviews in functional polymer composites for biomedical applications. *Polymers* 10(7):739
7. Movahedi N, Linul E (2017) Quasi-static compressive behavior of the ex-situ aluminum-alloy foam-filled tubes under elevated temperature conditions. *Mater Lett* 206:182–184
8. Movahedi N, Linul E (2017) Quasi-static compressive behavior of the ex-situ aluminum-alloy foam-filled tubes under elevated temperature conditions. *Mater Lett* 206:182–184
9. Kozłowski R, Władyska-Przybylak M (2008) Flammability and fire resistance of composites reinforced by natural fibers. *Polym Adv Technol* 19(6):446–453
10. Biagiotti JMKJ, Puglia D, Kenny JM (2004) A review on natural fiber-based composites-part i: structure, processing and properties of vegetable fibers. *J Nat Fibers* 1(2):37–68
11. Karthi N, Kumaresan K, Sathish S, Gokulkumar S, Prabhu L, Vigneshkumar N (2020) An overview: natural fiber reinforced hybrid composites, chemical treatments and application areas. *Mater Today Proc* 27:2828–2834
12. Pickering KL, Efendy MA, Le TM (2016) A review of recent developments in natural fiber composites and their mechanical performance. *Compos A Appl Sci Manuf* 83:98–112
13. Arpitha GR, Sanjay MR, Yogesha B (2017) State-of-Art on hybridization of natural fiber reinforced polymer composites. *Colloid Surf Sci* 2(2):59–65
14. Chand N, Fahim M (2020) *Tribology of natural fiber polymer composites*. Woodhead Publishing
15. Venkateshwaran N, Elayaperumal A (2010) Banana fiber reinforced polymer composites-a review. *J Reinf Plast Compos* 29(15):2387–2396
16. Sangwan KS, Mittal VK (2015) A bibliometric analysis of green manufacturing and similar frameworks. *Manag Environ Qual* 26(4):566–587
17. Devaraju A (2015) Influence of fiber percentage on mechanical properties of hybrid composite materials. *J Mater Sci Mech Eng* 2(13):1–5
18. Athijayamani A, Thiruchitrambalam M, Manikandan V, Pazhanivel B (2010) Mechanical properties of natural fibers reinforced polyester hybrid composite. *Int J Plast Technol* 14(1):104–116
19. Gupta MK, Srivastava RK (2016) Mechanical properties of hybrid fibers-reinforced polymer composite: a review. *Polym-Plast Technol Eng* 55(6):626–642
20. Rajak DK, Pagar DD, Menezes PL, Linul E (2019) Fiber-reinforced polymer composites: manufacturing, properties, and applications. *Polymers* 11(10):1667
21. Shireesha Y, Nandipati G, Chandaka K (2019) Properties of hybrid composites and its applications: a brief review. *Int J Sci Technol Res* 8(08)
22. Yadav SKJ, Vedrtam A, Gunwant D (2020) Experimental and numerical study on mechanical behavior and resistance to natural weathering of sugarcane leave reinforced polymer composite. *Constr Build Mater* 262:120785
23. Ku H, Wang H, Pattarachaiyakooop N, Trada M (2011) A review on the tensile properties of natural fiber reinforced polymer composites. *Compos B Eng* 42(4):856–873
24. Agarwal J, Sahoo S, Mohanty S, Nayak SK (2020) Progress of novel techniques for lightweight automobile applications through innovative eco-friendly composite materials: a review. *J Thermoplast Compos Mater* 33(7):978–1013
25. Chandgude S, Salunkhe S (2021) In state of art: mechanical behavior of natural fiber-based hybrid polymeric composites for application of automobile components. *Polym Compos*
26. Hill K, Swiecki B, Cregger J (2012) The bio-based materials automotive value chain. *Cent Automot Res* 112



27. Schmiedel I, Barfuss GS, Nickel T, Pfeufer L (2014) Use of visible natural fibers in vehicle interiors. *ATZ Worldwide* 116(6):20–23
28. Bolcu D, Stănescu MM (2020) A study of the mechanical properties of composite materials with a dammar-based hybrid matrix and two types of flax fabric reinforcement. *Polymers* 12(8):1649
29. Singh JIP, Dhawan V, Singh S, Jangid K (2017) Study of effect of surface treatment on mechanical properties of natural fiber reinforced composites. *Mater Today Proc* 4(2):2793–2799
30. Sinha AK, Narang HK, Bhattacharya S (2017) Effect of alkali treatment on surface morphology of abaca fiber. *Mater Today Proc* 4(8):8993–8996
31. Yu Y, Jiang Z, Fei B, Wang G, Wang H (2011) An improved microtensile technique for mechanical characterization of short plant fibers: a case study on bamboo fibers. *J Mater Sci* 46(3):739–746
32. Giorcelli M, Khan A, Pugno NM, Rosso C, Tagliaferro A (2019) Biochar as a cheap and environmental friendly filler able to improve polymer mechanical properties. *Biomass Bioenergy* 120:219–223
33. Balasubramanian K, Rajeswari N, Vaidheeswaran K (2020) Analysis of mechanical properties of natural fiber composites by experimental with FEA. *Mater Today Proc* 28:1149–1153
34. Getu D, Nallamotheu RB, Masresha M, Nallamotheu SK, Nallamotheu AK (2021) Production and characterization of bamboo and sisal fiber reinforced hybrid composite for interior automotive body application. *Mater Today Proc* 38:2853–2860
35. Jothibasus S, Mohanamurugan S, Vijay R, Lenin Singaravelu D, Vinod A, Sanjay MR (2020) Investigation on the mechanical behavior of areca sheath fibers/jute fibers/glass fabrics reinforced hybrid composite for light weight applications. *J Ind Text* 49(8):1036–1060
36. Chegiani F, Takabi B, El Mansori M, Tai BL, Bukkapatnam ST (2020) Effect of flax fiber orientation on machining behavior and surface finish of natural fiber reinforced polymer composites. *J Manuf Process* 54:337–346
37. Zeeshan M, Ali M, Anjum AS, Nawab Y (2021) Optimization of mechanical/thermal properties of glass/flax/waste cotton hybrid composite. *J Ind Textiles* 51(5):768–787
38. Lokesh P, Kumari TS, Gopi R, Loganathan GB (2020) A study on mechanical properties of bamboo fiber reinforced polymer composite. *Mater Today: Proc* 22:897–990
39. Reddy MI, Varma UP, Kumar IA, Manikanth V, Raju PK (2018) Comparative evaluation on mechanical properties of jute, pineapple leaf fiber and glass fiber reinforced composites with polyester and epoxy resin matrices. *Mater Today Proc* 5(2):5649–5654
40. Premnath AA (2018) Impact of surface treatment on the mechanical properties of sisal and jute reinforced with epoxy resin natural fiber hybrid composites. *J Nat Fibers*
41. Olorunnishola AAG, Adubi EG (2018) A comparative analysis of a blend of natural jute and glass fibers with synthetic glass fibers composites as car bumper materials. *IOSR J Mech Civil Eng (IOSR-JMCE)* 15(3):67–71
42. Ali BA, Sapuan SM, Zainudin ES, Othman M (2015) Implementation of the expert decision system for environmental assessment in composite materials selection for automotive components. *J Clean Prod* 107:557–567
43. Agunsoye JO, Isaac TS, Samuel SO (2012) Study of mechanical behaviour of coconut shell reinforced polymer matrix composite. *J Miner Mater Charact Eng* 11(8):774–779
44. Rammath BV, Sharavanan R, Chandrasekaran M, Elanchezhian C, Sathyanarayanan R, Raja RN, Kokan SJ (2015) Experimental determination of mechanical properties of banana jute hybrid composite. *Fibers Polym* 16(1):164–172
45. Cinelli P, Chiellini E, Imam SH (2008) Hybrid composite based on poly (vinyl alcohol) and fillers from renewable resources. *J Appl Polym Sci* 109(3):1684–1691
46. Khandai S, Nayak RK, Kumar A, Das D, Kumar R (2019) Assessment of mechanical and tribological properties of flax/kenaf/glass/carbon fiber reinforced polymer composites. *Mater Today Proc* 18:3835–3841

# Issues and Challenges in Fabrication of Conductive Parts by Additive Manufacturing and Their Applications: A Study



Arpit Bajpai and Prashant K. Jain

**Abstract** This article shows the study of addition of conductive materials like carbon nanotubes, graphene and graphite powder to the base materials like ABS and PLA used for fused filament fabrication in additive manufacturing. The results showed the improved electrical conductivity of the specimen produced. The application of conductive parts lies in various devices like capacitors, LED and sensors. Additive manufacturing facilitates us with fabrication of customized parts as per the user requirement. Fabrication of conductive parts by additive manufacturing reduces the complexity of fabrication process. Some basic defects present in the structure of graphene and carbon nanotubes are discussed in the article. The effects of these defects on the properties of the specimen are also studied. A literature review on various methods and materials adopted have been done. The result discussion of different process adopted by the researchers is presented in this article.

**Keywords** Additive manufacturing (AM) · Carbon nanotubes (CNT) · Graphene · Electrical conductivity

## 1 Introduction

The extensive use of polymeric materials in almost all domains has created a feasible alternative to the conventionally used materials. Additive manufacturing (AM) technology has emerged as an optimum solution for manufacturing of these polymer composite parts. It is an economical process which provides adequate flexibility of production. The requirements of mould and heavy machine setup is completely removed while using AM process. Parts with specific requirements can be easily fabricated by choosing suitable Additive Manufacturing approach. Further the properties of these parts can be enhanced by addition of fillers to the base material. Materials like carbon nanotubes, graphene platelets, carbon fibres and metal powders can

---

A. Bajpai (✉) · P. K. Jain  
Fused Filament Fabrication Lab, Indian Institute of Information Technology Design and Manufacturing, Jabalpur, Madhya Pradesh, India  
e-mail: [1913602@iiitdmj.ac.in](mailto:1913602@iiitdmj.ac.in)

© The Author(s), under exclusive license to Springer Nature Singapore Pte Ltd. 2023  
R. P. Singh et al. (eds.), *Advances in Modelling and Optimization of Manufacturing and Industrial Systems*, Lecture Notes in Mechanical Engineering,  
[https://doi.org/10.1007/978-981-19-6107-6\\_47](https://doi.org/10.1007/978-981-19-6107-6_47)

661

be added as fillers to increase the electrical conductivity of the material. The use of 3D printed parts which exhibit electrical conductivity exists in various domains. 3D printed parts with electrical conductivity can be used in fabrication of printed circuit boards, portable antenna, display boards, fitness equipment and sensors. If the conductive printed parts are flexible in nature fabrication of certain crucial components like flexible circuit boards and sensors of neuro-prosthetic parts can also be done economically by adopting AM approach. The complex geometries of flexible electrically conductive parts can be achieved considering the specific requirements of the users by additive manufacturing approach.

Though the AM of electrically conductive parts shows promising results there are certain issues which needs to be considered during part fabrication. Selection of suitable additive and correct AM process is the most important parameter. The proportion of additive and base material, homogeneous mixing of additive, printing process parameters and feasibility of the produced parts are some important issues which needs to be taken into consideration.

The polymeric materials provides high strength in low weight making it more usable in construction industries, automobile sector, sports equipment, health monitoring devices, aviation sector and many more areas [1]. The parts made by these materials are comparatively low in cost when compared to metals. The addition of reinforcements in these polymers further enhances the properties of these polymers increasing its usability. The flexibility of using various types of fibres irrespective of its length and nature makes the AM process most suitable in composite manufacturing industry. Keeping control on certain parameters like compatibility of fibres with the base material, amount of reinforcement, orientation of printing and adoption of suitable method of printing, the desired samples of required properties can be fabricated.

Additive manufacturing process provides an advantage of rapid production of complicated geometries. Acrylonitrile-butadiene-styrene (ABS) and poly-lactic acid (PLA) are the most widely used materials [2]. When compared to conventional machining processes, ABS and PLA products are light in weight, cost effective, takes less manufacturing time and are environment friendly. In order to enhance specific properties of AM products, reinforcement has become a trending method. Additives are added in various proportions to the base material to build up properties like tensile strength, flexural strength and conductivity.

Producing conductive samples by additive manufacturing has always been a challenging task. In order to achieve the best conductive properties the most common materials added are carbon nanotubes and graphene [3]. Besides this, other materials like graphite powder [1], ZnO [4] and metal flakes can also be used to improve the thermal and electrical conductivity. Graphene and carbon nanotubes are most widely used allotropes of carbon nanomaterial. The addition of small amount of these to the base material changes the properties drastically. The selection of one amongst the two may depend on the requirement and properties of the base material. Carbon nanotubes are long tubular structures of carbon which shows enhanced tensile strength and superior thermal and electrical conductivity. The diameter of these tubes is in nanometres. Commercial carbon nanoplatelet powder is available nowadays and

can be effectively mixed with polymers to form composites with enhanced properties. Graphene is an allotrope of carbon which can be used as a substitute of carbon nanotubes. The superior mechanical property, high interfacial area and high dielectric permittivity makes it suitable for the use. It has high surface-to-volume ratio and has dispersible nature in organic solvents which makes it most suitable for fuel cell application [4].

In order to develop fibre reinforced composites methods like melt compounding, powder bed fusion, material extrusion and sheet lamination can be adopted [1]. Besides this, chemical mixing process can also be adopted for producing polymer composites. Selective laser sintering process is another method which can be used to mix material in powder form. Reinforcements compatible with the base material are melted and fused together with the help of power from laser. Material mixing in liquid phase can be done with the help of VAT polymerization using photo curable resin as base material. Fused filament fabrication is one of the most economical methods which can be adopted for 3D printing of composite material. Single or multiple nozzles can be adopted for this purpose. Though the use of long continuous fibres is not feasible in this process but short fibres can easily be used. Besides this, chemical mixing can be adopted for preparing polymers which can be extruded in form of filament and can be directly used in conventional FFF printers.

## 2 Fabrication of Conductive Parts

Additive manufacturing is one of the most suitable approach for prototyping and fabrication of complex geometries. Addition of certain additives in the base material enhances the properties of the fabricated parts. Properties like tensile and compressive strength, stiffness and toughness can be altered by this process. Thermal and electrical conductivity can be incorporated and increased by this process. Additives like CNT, Graphene, carbon fibres, metal powders, etc., can be added specifically in order to increase the electrical conductivity of the material. The most common amongst them is the use of Graphene and CNT. Single and multi-layer graphene nano-platelets are easily commercially available and can be used. The use of multi-walled CNT is more economical when compared to single walled CNT. The homogeneous dispersion of these additives in suitable amount in the base material and selection of the suitable additive on the basis of the base material is the most important parameter.

### 2.1 Use of Graphene and CNT as Conductive Additive

The widespread use of conductive polymers in the present day scenario is quite vital. Fabrication of conductive parts by additive manufacturing has come out as a recent trend. Various researchers have worked on the fabrication of conductive polymers. An investigation on the properties of ABS fabricated by fused deposition modelling

discussed the addition of two different nano composites (a) graphene nanoplatelets and (b) carbon nanotubes [5]. Two different methods of melt compounding and fused filament fabrication can be employed for the fabrication of samples. On variation of the weight percentage of graphene nanoplatelets and carbon nanotube, variation in the properties could be observed. A change in tensile strength, flexural strength and electrical conductivity could be observed as a result of addition. Due to weak covalent forces between graphene and material matrix the tensile and flexural strength of the specimen decreases but the conductivity increased in an appreciable manner. On the other hand, addition of carbon nanotubes increased both tensile and flexural strength of the material as well as the conductivity is also increased. Though the brittleness of the material also increases by addition of carbon nanotubes. The concentration of the carbon nanotubes and graphene nanoplatelets plays the significant role in conductivity. A minor rise in electrical conductivity is observed with addition in small amount but the actual increase in electrical conductivity is observed above 4% addition of carbon nanotubes and graphene nanoplatelets by weight percentage.

Ultrathin composite films of poly vinyl chloride can be fabricated by addition of both carbon nanotubes and graphene. As the cost of carbon nanotubes is high, graphene can be used as an economical substitute for the same. The marginal addition of graphene in the PVC enhances its mechanical and electrical properties abruptly. The fabrication of graphene nano flakes can also be done experimentally by graphite flakes [6]. The resulting graphene flakes are multilayer in nature. Addition of multilayer flakes in excess results in clogging of nozzle in fused filament fabrication.

Printing structures in different orientations by fused deposition modelling can affect the properties of the CNT mixed ABS samples [7]. The samples can be printed in horizontal, vertical and perpendicular building orientations. The additive percentage can be simultaneously varied along with the orientation to observe the variation in yield properties and electrical conductivity. The electrical resistivity of the material strongly decreased even after 1% addition of carbon nanotubes to ABS material.

Other than ABS and PVC, polylactic acid (PLA) can also be used as a base material for nanofiller addition. Addition of Graphene enhanced the mechanical, electrical and thermal usability of material [8]. Considering various orientations of printing the specimen, the upright or vertical orientation gives the maximum tensile and flexural strength on addition of graphene nanoplatelets in PLA base. No significant effect in electrical conductivity is observed in PLA on changing the orientation of printing.

Polybutylene terephthalate (PBT) can also be considered as a base polymer material for addition of CNT and graphene [9]. The printing of material can be attempted by commercially available desktop 3D printer. PBT can be considered as an alternative to ABS and PLA for 3D printing as no significant change in parameters are needed to attempt its printing.

The studies of Ghoshal [10] stated the increase of conductivity on addition of carbon nanotubes when compared to graphene nanoplatelets. CNT when compared to graphene provides better mechanical and electrical properties. The electrical conductivity, thermal conductivity, tensile, and flexural strength of the material are observed

to improve drastically. As the concentration of CNT is increased in the base material, after a certain point the problem of clogging of nozzle arises in fused filament fabrication process.

The use of conductive ABS to produce working prototypes of models has been considered as a complicated task. Mirzaee et al. [11] fabricated a prototype of flexible 3D printed bow tie antenna by additive manufacturing using flexible PLA and conductive ABS material. The frame of this antenna is made by flexible PLA material and the remaining part by the conductive ABS. The fabricated antenna is compact in size, light weight and mechanically flexible providing a suitable bandwidth range. The use of commercially available conductive ABS for the fabrication of electromechanical products and parts can be explored further.

Melt compounding is generally used for addition of nano fillers to the base material. The filament of the material produced is extruded which is used in commercially available 3D printers. On a different approach, combination of direct write method with additive manufacturing was attempted by Perez et al. [12]. The electronic components were embedded in the structure of components by additive manufacturing process. The use of conductive material in between the integrated electronic components may further increase the efficiency of the system by providing desired conductivity for passing of signals. The fabrication of electrically conductive parts by direct write method is difficult as the material needs to be in paste form with number of additives. As the part is fabricated these additives needs to be removed by different processes. Post curing of parts affects the accuracy and in many cases the high loss of electrical conductivity is observed post curing.

## ***2.2 Use of Other Additives to Improve Electrical Conductivity***

The multi-walled carbon nanotubes can also be used for enhancing the properties of 3D printed specimen [13]. Number of carbon nanotubes rolled over one another forms multiwalled CNT structure. They are allotropes of carbon with high aspect ratio. The addition of MWCNT in varying percentage increases the strength of the specimen. Addition of metal oxides like ZnO enhances the thermal conductivity of the ABS but no significant increase in electrical conductivity is observed [14]. Mechanical property like tensile strength increases first than decreases as the percentage concentration of ZnO increases.

The conductivity of ABS can also be increased by addition of carbon fibres. Small carbon fibre of length 0.2–0.4 mm can be embedded in the ABS matrix by FDM printing and compression moulding process. The maximum value of carbon fibres was 40% by weight after which the clogging of nozzle was observed by Tekinalp et al. [15] when fused filament fabrication process was used.

The use of carbon fibres between layers of ABS to improve strength was done by Nakagawa et al. [16]. The reinforcement was done by sandwiching the layers of carbon fibres between the layers of ABS. This was done by conventional fused filament fabrication printer in which layers of ABS was printed with bundles of

carbon fibres strands placed between these layers. An attempt to insert the bundles of strands of carbon fibres in the extruder head during the melting phase of ABS was also attempted in the process. Carbon fibres strands in the form of threads were fed to the extruder head along with the filament. In order to do so the input diameter of the nozzle head was increased to 2.7 mm which is 1.7 mm in conventional printers. The size of the nozzle is also increased to 0.9 mm from 0.4 mm to avoid the clogging of the nozzle during the extrusion. In many cases, the no mixing of carbon fibres with the ABS filament was observed. Instead of fibres entering the filament, the carbon fibres strands came adjacent to the filament separately. As the carbon fibres are not stretchable in nature the extrusion speed was different for the fibres and ABS from the same nozzle. To overcome this, the filament extrusion speed was reduced, but in this case, the ABS filament coming out of the nozzle started curling, and printing of parts was not possible in this case. Thus, the feeding of carbon fibres along with the filament was found unsuitable. Thus, the material was added in the form of sandwich layers to add bundles of carbon fibres between ABS layers.

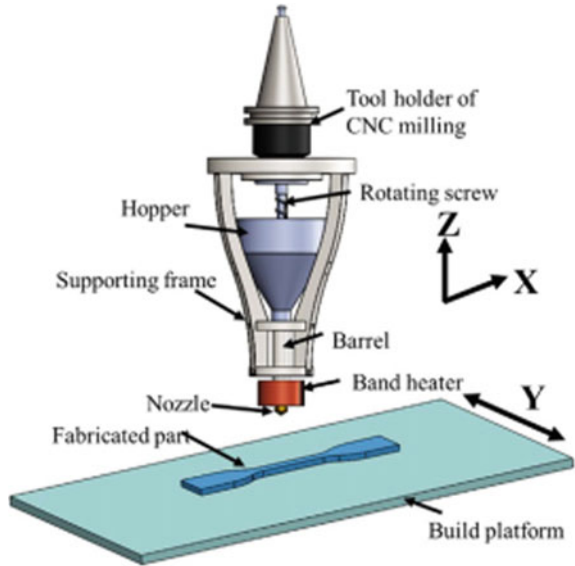
### ***2.3 Limitations of Using Graphene and CNT***

Two major types of defects are observed in case of graphene structure. These are point defects and line defects. The change of lattice structure of graphene due to missing atoms causes the point defects and combination of these point defects creating a boundary gives line defects. Missing of one atom from the hexagonal structure may result in formation of pentagon structures. Fusion of two layers of hexagon such that these layers combine with each other and two atoms from each structure is missing, results in formation of octagon structure. In certain cases of missing atoms dangling edges may also occur. These defects when present on large scale affect the chemical, electronic and mechanical properties. The missing atoms make the graphene structure chemically more reactive. The tensile strength and other mechanical properties may also decrease when these defects increases [17]. In case of CNT the presence of Schottky defect may occur. The missing atom from the structure affects the conductivity of the CNT. The breaking of CNT tubes to a very large extent may also affect the conductivity exhibited [18].

## **3 Fabrication of Flexible Electrically Conductive Parts Using AM**

Kumar et al. [19] worked on a novel approach of fabrication of flexible conductive parts using EVA material. Pellet-based extrusion process was used for the fabrication of flexible EVA material. A solution to problem of buckling of flexible filament in fused deposition was solved by development of in house CNC-assisted material

**Fig. 1** Material deposition tool for using EVA pellets developed by Kumar et al. [20]



deposition tool. The results showed the potential to use EVA material for additive manufacturing by fused deposition modelling (Fig. 1).

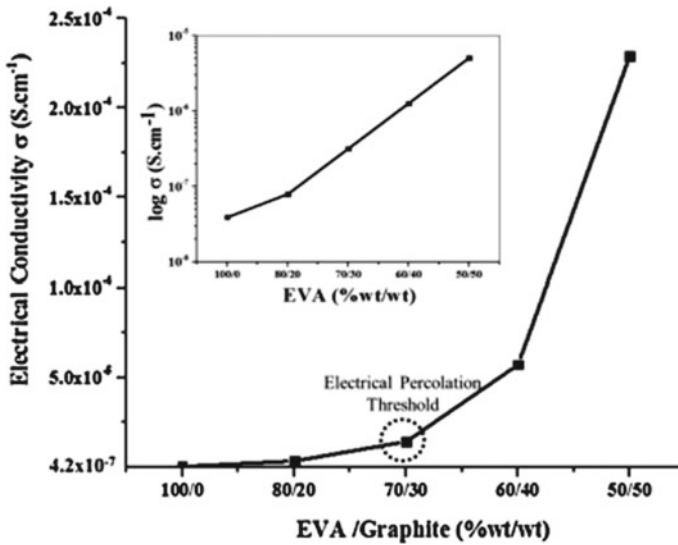
In order to enhance the conductive nature of the material, graphite powder was added to the EVA material. The pellets of EVA graphite composites were generated which were further used for printing parts. A CNC-assisted material deposition tool was made for material deposition. The EVA graphite composite pellets were directly fed to this tool, where the temperature was continuously monitored. Pellets of EVA material with graphite powder were fabricated and were used for printing the specimen [21] (Fig. 2).

### 3.1 Issues in 3D Printing of Flexible Part

For fabrication of flexible parts a CNC-assisted material deposition tool was in house developed by Kumar et al. [21]. Specific retro fitting of this material deposition tool was done on CNC milling machine and extrusion and printing of flexible parts using ethylene vinyl acetate as base material. Various issues observed during the process are hereby discussed.

**Screw speed**—The selection of optimum screw speed for extrusion of material from material deposition tool was one of the major requirement of the system. The minimum screw speed possible in CNC milling starts with 50 RPM. At 50 RPM, the flow of the material from the nozzle is not adequate affecting the material deposition rate during the part printing.





**Fig. 2** Electrical conductivity of Gr-filled EVA composites. Inset: log plot of electrical conductivity for Gr-filled EVA composites. Kumar et al. [21]

**Bed temperature**—The bonding of layers of the printed part gets affected by the bed temperature on which deposition of material takes place. The bed on which material is deposited needs to be heated to avoid the issue of warpage of parts. If the bed is not heated at adequate temperature the part may leave the bed in between the printing process. The temperature of bed maintained here in this case was between 40 and 55 °C.

**Gaps and voids**—During the printing of specimen the selection of nozzle size along with proper road width is essential to avoid the presence of gaps during part printing. The presence of voids and gaps between layers is present in certain cases when the size of the filament coming out is not suitable.

**Improper extrusion**—The selection of suitable nozzle temperature of efficient extrusion of material is essential along with the optimum screw speed. Failing in any of the parameters may result in improper extrusion of material. The material coming out of the nozzle is either less or more than the requirement. Less material extrusion results in void formation and more material extrusion results in overlapping of layers with distorted geometry.

**Over heating**—When the temperature of the nozzle is more than the required temperature the viscosity of the material starts reducing resulting in pouring of material rather than filament extrusion. The material extrusion rate increases rapidly and the printing of desired geometry becomes difficult.

**Under heating**—When the temperature of the nozzle is less than the desired temperature of the material the problem of under extrusion is observed. The tool moves at a comparatively faster rate leaving the distorted geometry of the printed part. Besides curly filament coming out of the nozzle is also observed when the material gets insufficient heat from the nozzle.

**Support material**—For 3D printing of parts through the material deposition tool proper G and M codes needs to be generated by the user before printing. In this case fabrication of parts which requires support material is quite difficult. The single nozzle of the extruder dispersing material at a constant rate makes the 3D printing of flat parts easy. Providing support structure is not possible when material deposition tool is used.

## 4 Application

In recent years the applications of 3D printed conductive filaments have increased drastically. The use of conductive polymers in various fields such as health monitoring devices, sensors and displays justifies the need of conductive polymers with suitable properties. Capacitors, light emitting diode, solar cells, field effective transistors, and biosensors are some major devices in which the use of conductive polymers is increasing in the current scenario [22].

Ates et al. [22] studied the nature of various conductive polymers along with its applications. Polythiophene, polyparaphenylene vinylene, polycarbazole, polyaniline and polypyrrole were the major conductive polymers of their study. The various applications of these materials are in super capacitors, light emitting diodes (LEDs), solar cells, field effect transistor (FET) and biosensors. Super capacitors have comparatively very high value of capacitance as compared to conventional capacitors. They are used in power supplies, cells and batteries. The use of super capacitor is also vital in computers. The use of LED is very common these days and can be observed all around us. It is used in lights and indicators in automobiles, remotes, television units, music systems and various domestic appliances. As we are living in the era of conservation of energy, solar cells have emerged as one of the cleanest source of energy. The solar cells convert the energy from the sunlight to electric energy by photovoltaic effect. The abundant use of solar cells, solar panels, solar power appliances like cooker, water heater, street light, etc., has gained acceptance globally. Field effective transistors are used in electrical circuits. Biosensors are used to convert signals of biological responses into electrical responses. A combination of thermoplastic polyurethane and multi-walled carbon nanotube was used for fabrication of sensors [23].

## 5 Conclusion

Fabrication of electrically conductive flexible components by extrusion based additive manufacturing process is an initial step of the development of a new concept. Suitable percentage of additives can be identified to improve the conductivity of the flexible component while keeping it suitable for 3D printing. The fabrication of components can be done in low cost taking into consideration the requirement of the product on the basis of its desired flexibility and conductivity. The fabrication of conductive parts by additive manufacturing can be a promising technique solving various requirements of future.

## References

1. Zindani D, Kumar K (2019) An insight into additive manufacturing of fiber reinforced polymer composite. *Int J Lightweight Mater Manuf* 2(4):267–278
2. Fitz-Gerald D, Boothe J (2016) Manufacturing and characterization of poly (Lactic Acid)/carbon black conductive composites for FDM feedstock: an exploratory study
3. Kumar N, Jain PK, Tandon P, Mohan Pandey P (2018) 3D printing of flexible parts using EVA material. *Mater Phys Mech* 37(2)
4. Punetha VD, Rana S, Yoo HJ, Chaurasia A, McLeskey JT Jr, Ramasamy MS, Sahoo NG, Cho JW (2017) Functionalization of carbon nanomaterials for advanced polymer nanocomposites: a comparison study between CNT and graphene. *Prog Polym Sci* 67:1–47
5. Vidakis N, Maniadi A, Petousis M, Vamvakaki M, Kenanakis G, Koudoumas E (2020) Mechanical and electrical properties investigation of 3D-printed acrylonitrile–butadiene–styrene graphene and carbon nanocomposites. *J Mater Eng Perform* 29(3):1909–1918
6. Vadukumpully S, Paul J, Mahanta N, Valiyaveetil S (2011) Flexible conductive graphene/poly (vinyl chloride) composite thin films with high mechanical strength and thermal stability. *Carbon* 49(1):198–205
7. Dorigato A, Moretti V, Dul S, Unterberger SH, Pegoretti A (2017) Electrically conductive nanocomposites for fused deposition modelling. *Synth Met* 226:7–14
8. Caminero MÁ, Chacón JM, García-Plaza E, Núñez PJ, Reverte JM, Becar JP (2019) Additive manufacturing of PLA-based composites using fused filament fabrication: effect of graphene nanoplatelet reinforcement on mechanical properties, dimensional accuracy and texture. *Polymers* 11(5):799
9. Gnanasekaran K, Heijmans T, Van Bennekom S, Woldhuis H, Wijnia S, De With G, Friedrich H (2017) 3D printing of CNT-and graphene-based conductive polymer nanocomposites by fused deposition modeling. *Appl Mater Today* 9:21–28
10. Ghoshal S (2017) Polymer/carbon nanotubes (CNT) nanocomposites processing using additive manufacturing (three-dimensional printing) technique: an overview. *Fibers* 5(4):40
11. Mirzaee M, Noghianian S, Wiest L, Chang I (2015) Developing flexible 3D printed antenna using conductive ABS materials. In: 2015 IEEE international symposium on antennas and propagation and USNC/URSI national radio science meeting. IEEE, pp 1308–1309
12. Perez KB, Williams CB (2013) Combining additive manufacturing and direct write for integrated electronics—a review. In: 24th International solid freeform fabrication symposium—an additive manufacturing conference, SFF, pp 962–979
13. Sezer HK, Eren O (2019) FDM 3D printing of MWCNT re-inforced ABS nano-composite parts with enhanced mechanical and electrical properties. *J Manuf Process* 37:339–347

14. Aw YY, Yeoh CK, Idris MA, Amali HK, Aqzna SS, Teh PL (2017) A study of tensile and thermal properties of 3D printed conductive ABS–ZnO composite. In: AIP conference proceedings, vol 1835, no 1. AIP Publishing LLC, p 020008
15. Tekinalp HL, Kunc V, Velez-Garcia GM, Duty CE, Love LJ, Naskar AK, Blue CA, Ozcan S (2014) Highly oriented carbon fiber–polymer composites via additive manufacturing. *Compos Sci Technol* 105:144–150
16. Nakagawa Y, Mori KI, Maeno T (2017) 3D printing of carbon fibre-reinforced plastic parts. *Int J Adv Manuf Technol* 91(5–8):2811–2817. <https://doi.org/10.1007/s00170-016-9891-7>
17. Liu L, Qing M, Wang Y, Chen S (2015) Defects in graphene: generation, healing, and their effects on the properties of graphene: a review. *J Mater Sci Technol* 31(6):599–606
18. Louie SG (2001) Electronic properties, junctions, and defects of carbon nanotubes. *Carbon Nanotubes* 113–145
19. Kumar N, Jain PK, Tandon P, Pandey PM (2018a) Extrusion-based additive manufacturing process for producing flexible parts. *J Braz Soc Mech Sci Eng* 40(3):1–12
20. Kumar N, Jain PK, Tandon P, Pandey PM (2018c) The effect of process parameters on tensile behavior of 3D printed flexible parts of ethylene vinyl acetate (EVA). *J Manuf Process* 35:317–326
21. Kumar N, Jain PK, Tandon P, Pandey PM (2018b) Additive manufacturing of flexible electrically conductive polymer composites via CNC-assisted fused layer modeling process. *J Braz Soc Mech Sci Eng* 40(4):1–13
22. Ates M, Karazehir T, Sezai Sarac A (2012) Conducting polymers and their applications. *Curr Phys Chem* 2(3):224–240
23. Christ JF, Aliheidari N, Ameli A, Pötschke P (2017) 3D printed highly elastic strain sensors of multiwalled carbon nanotube/thermoplastic polyurethane nanocomposites. *Mater Des* 131:394–401

# Agglomeration of the Various Industry 4.0 Perspectives in the Supply Chain Performance Systems



Ram Dayal Pandey, Mohit Tyagi, Narendra Kumar, and R. S. Walia

**Abstract** Manufacturing sector plays a cosmological function in growth and development of any industrialized country. In today's era the manufacturing industries are facing difficulties about numerous aspects such as, forecasting demands for products, delay in lead time, inventory control, increasing return on investment, and improving efficiency. Present study grounds the "Industry 4.0" perceptions which need to be embedded, for converting the traditional manufacturing practices to smart ones. Extending the principles of the industry 4.0 eases the operation feasibility and improves the performance of supply chain. In continuation to the same various barriers, hindering its adoption in the supply chain performance system are identified, underpinning the notions allied with manufacturing arena. Outcomes of the presented work, is favored to enact the manufacturing organizations and their supply chains, to adopt the various Industry 4.0 initiatives.

**Keywords** Industry 4.0 · Supply chain · Manufacturing systems

## 1 Introduction

The word "Industry 4.0" is frequently used to state the rising activity in the controlling of manufacturing and fetter production. Industry 4.0 also entitled as the 4th industrial revolt (4IR). In recent years, the rapid development of facts and messaging tools, blending in with the provision of morning purchases in Industry 4.0 [1, 2]. From the

---

R. D. Pandey · N. Kumar  
Department of Industrial and Production Engineering, Dr. B.R. Ambedkar National Institute of Technology, Jalandhar, Punjab, India

R. S. Walia  
Department of Production and Industrial Engineering, PEC University, Chandigarh, India

M. Tyagi (✉)  
MED, NIT, Kurukshetra, India  
e-mail: [mohitmied@gmail.com](mailto:mohitmied@gmail.com)

user opinion, there is an indication of the influence of “Industry 4.0” on both the technical, internal as well as communal sectors [3].

Organizations have seen it the importance of technological development and consider technology as a solid strategy a tool to ensure sustainable performance [4, 5]. In the recent scenario, numbers of corporations are using this approach to improve organizational performance [6, 7]. In particular, the steady growth of automation of business plans and the ability to work effectively and productively development encourages organizations to increase the performance of Industry 4.0 vision in other areas of the organization such as asset management (Schuh et al., 2013). Industry Ideas 4.0 assists in supply chain as decision-making which means reducing the price of goods, and improving group performance and product quality [8]. By doing literature review (LR) and logical planning, objective to discover the influence of developing new tools in line with industry 4.0 to improve procurement functioning [9–12]. These days’ customer demand is changing day by day, with the help of Industry 4.0 we can meet their needs more accurately. Still, the situation is supposed that Industry 4.0 and its empowering technology have the capability to influence all corners of plants and organizations and can carry substantial enhancements in governance sectors like, for example procurement management and supply chain management [13]. Avenues allied with the supply chain management can be secured by aligning its chores with the fundamentals of Industry 4.0 [14]. Effective and efficient mapping of the supply with the demand cycles in the supply chain performance system is possible by grounding Industry 4.0 perspectives.

Operational potencies of the supply chain can have yielded by extending the Industry 4.0 initiatives. Most firms are now changing their business model and continue to use e-business tools to measure their processes by creating process combinations (Chen et al. 2012; Weingarten et al. 2013; Srinivasan et al. 2015). A complex and flexible professional environment and consumer petition, as well as the need to adapt and respond to organizations turning on the lights advanced technology [15–17]. Industry 4.0 helps to analyze instantaneous records in many fields, for example Logistic 4.0, Automotive 4.0, and Education 4.0 [8]. The intention behind high awareness is that Industry 4.0 has the ability to change its assessment crafted and circulated, and how firm’s rivalry [18].

Industry 4.0, as a performance concept, has been conversed in particular the idea of manufacture in the latest books and industry documents. Still, it is supposed that Industry 4.0 and its empowering technology have the capability to influence all corners of plants and organizations and can carry substantial enhancements in governance sectors for example- procurement management and supply chain management (Blue 2014). It is multiplex and continuously changes the professional atmosphere as well consumer petition, and the requirement to adapt and respond to organizations turning on the lights advanced technology [15–17].

Aligning dynamics of supply chain with the walks of Industry 4.0, underpinning digital implementation of robust procedures [19]. Adoption of specific technologies (ex: advanced big data analytics techniques and information systems) are needed to achieve this alphanumeric revolution. On the other hand, the introduction of alphanumeric supply chains and highly developed marketing strategies

preventing high investment and significant challenges associated with the computerization method (Melville 2010; Ranganathan et al. 2011). Globalization has pressurized supply chains, for acquisition of technical advances, as well has responded positively to changes in administration rules as well client demand [20]. Confirmation has emerged that this can merely be obtain by sketching energy associated to e.g. sharpness, customization, reflectiveness and clearness (Zhong et al. 2017; Blome et al. 2013; Aslam et al. 2018), which is a major challenge in making a small amount of various yields (Park et al. 2020).

## 2 Literature Review and Background

Presented section outlays the insights clustered from the core of the research literature allied with the various developments in the field of Industry 4.0 and supply chain performance system.

### 2.1 *Outline of Industry 4.0*

Industry 4.0 focuses on the assimilation and growth of interaction as well as information technologies in corporate developments [1, 21]. The huge apparition of Industry 4.0 calls for agendas and or else or planning for joining bodily belongings and alphanumeric machineries in a cyber-physical system [22]. The part of Internet of Things (IoT) in fourth industrial revolution is very broad in manner [23, 24]. Not only IOT but also some other important tools like artificial intelligence (AI), computer-aided manufacturing (cam), computer-aided design (CAD), additive manufacturing, simulation, cloud computing, industrial robots, sensors/actuators, programmable logic controllers (PLCs), and intelligent enterprises resource planning (I-ERP), and other modern tools helps in supply chain 4.0 [1, 23]. The first three industrial revolts were activated by way of progresses in modernization, energy, and IT, the advent of advance machinery in to manufacturing adjacent has introduced nearly 4th industrial revolt (Industry 4.0) [25]. This industrial revolt introduced a new business module due to which people of the organizations, machines, and devices are connected through cyber-physical system (CPS) and internet [17]. Fourth Industrial revolution was oriented towards smooth method management and new theories development (Moeuf et al. 2017). With the help of information and communication tools inside the industry, Industry 4.0 has facilitated self-governing and vibrant fabricating [26, 27]. Concluded changing manipulate regularities in enterprise operation have appreciably stepped forward the spirit of facilities and goods supplied by

organization [18]. Industry 4.0 also helps in additive manufacturing. Flexible manufacturing system (FMS) and vastly adapted invention are provided by additive manufacturing, done with the help of alphanumeric 3D models [1]. As opposed to era, other pupils emphasis the crucial function of traditional, tactical and employee elements in accomplishing Industry 4.0 [23, 28, 29]. Some new techniques are also introduced for maximize automation those techniques are as follows: machine learning (ML), business analysis (BA), algorithms, optimization, artificial intelligence (AI), especially dynamic optimization (DM) [30]. Some technologies related to Industry 4.0 are illuminated given below.

**Big data:** It states to extensively large data that are problematic to handle via outdated method. It is used to improve the adeptness and yield of massive capacity of data [31].

**Internet of things:** It refers to the lots of virtual machines worldwide now connected to the internet. IOT is a control system that integrates various equipment and system. It enables real time tracking through extended analysis and decision-making [32].

**Smart factory:** It is a concept used to define the application of several grouping of recent tools to construct overexcited springy, self-customizable manufacturing capability. Smart factory automation provides specialized solutions combining various hardware, software, and machines [8].

**Cloud computing:** It is on call admittance, via Internet to computing sources programs, servers (physical and virtual), statics garage, improvement equipment, network abilities, and more. It makes resources available for a month to month subscription price or payment them in keeping with usage.

**Cyber-physical system:** It is the shrewd system that connect interaction and figuring competences with engineering and corporal structure and permit for relating the computer-generated and physical world across assisting an extreme level of connectivity amid hardware and software [33–35].

## ***2.2 Impact of Industry 4.0 on Supply Chains***

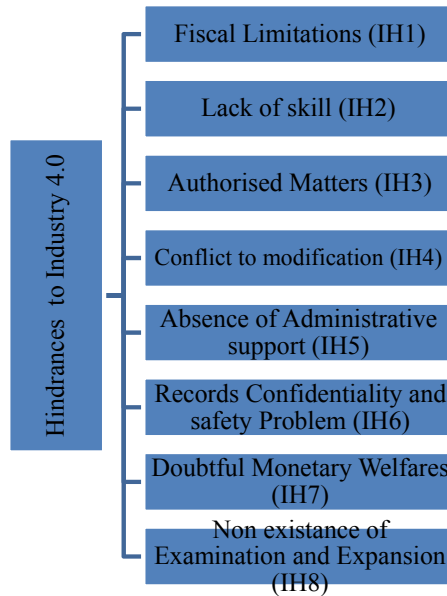
As discussed above, Industry 4.0 uses numerous innovative kits and machineries for helping to redefine conservative industrial method [3]. Impact of Industry 4.0 can be handled in extraordinary degrees of supply chains and additionally in supply chain management technologies; for example unique forecasting and making plans via included glide and accelerated traceability of products and materials, stepped forward dealer operation due to actual time statics allocating and harmonization with supplier and sensible warehousing and automobile direction-finding structures [23]. Effective SCM (supply chain management) requires evaluating and refining both



specific bodies' presentation and whole SCP (supply chain performance) [36]. This is called as universal methodology to supply chain management [37]. As discussed above, structures concept enables research of phenomenon from a approach called as holistic [38] by way of it allow for progressing from a solitary plant degree to the whole supply chain stage concerning numerous firms and methods in supply chain [39]. The larger assimilation amid subsystems can guide to the formation of an absoluteness and end to end supply chain (supra-structure), where there is an extreme indentation of evidence swap in the assessment making procedure [39]. Interference due to digitization weights firms to reconsideration the approach their supply chain network is considered. In particular, the Internet of Things (IoT) plays a key role in transforming supply chain by offering a variety of occasion for example—remote monitoring, actual period position and speed automotive, the condition of decay products with sensor temperature, condition and functioning of machinery, etc. [40]. Empowered by e-business stage push the antagonism in supply chains, there is clearness and stress-free way in to several preferences concerning where to go to the shops and when and what to buy [3, 41]. To accumulation the prerequisite and inclination toward driving alphanumeric revolution in supply chains, new obstructions and hazards were focused for occupational atmosphere. Certain of these problems contain absence of records, information safety hazard, nonexistence of proficient employees, etc. [6, 42] (BRICS Business council 2017).

### 3 Problem Formulation

For performing this investigation, a profound reading of various research papers allied to enlightening the various perspectives (Hindrances) of supply chains and analytics hierarchy process (AHP) methodology has been used. AHP is frequently used for project ranking and assortment. AHP seizure tactical goal as a set of weighted criteria that is used to score project. AHP technique has been used to find out the important ranking of the Hindrances based on the value of their critical weight. On the source of current literature review and views acquired as of domain professionals, eight hindrances have been selected which names are: Fiscal limitations (IH1), Lack of skill (IH2), Authorized matters (IH3), Conflict to modification (IH4), Absence of administrative support (IH5), Records confidentiality and safety problem (IH6), Doubtful monetary welfares (IH7), and Non-existence of examination and expansion (IH8). To accomplish the preferred objective of this study a model of hindrances of Industry 4.0 has been created given in Fig. 1.



**Fig. 1** Study model of hindrances of industry 4.0

## 4 Research Methodology

The objective of this investigation is to find out the ranking of the hindrances on the basis of their critical weight. The set of hindrances has been explored by designing a survey on semantic terms.

### 4.1 Analytic Hierarchy Process (AHP)

AHP is the highly popular approach which is used for multi-criteria decision-making (MCDM) and it is applied by way of a usual method for MCDM challenge since it is easy and tractable to actual world complications. The AHP was adapted by Thomas Saaty in 1980. It is an effective method for dealing with multifaceted assessment creation. This may allow the evaluator to fixed importance and sort the finest result. Through decreasing tough results to a sequence of pairwise evaluations, and then creating the outcomes. This method aids to seizure both subjective and objective features of a conclusion [43]. AHP combines a beneficial procedure for examine the consistency of the evaluators calculations, therefore decreasing the unfairness in the result building procedure. Assessment amid the standards has been prepared thru “Saaty’s” 1–9 scale of comparative concentration given in Table 1. Saaty’s proposed that if the value of consistency ratio (COR) is less than or equal to 0.1, then the

**Table 1** Scale of Saaty for intensity of comparative prominence

Clarification	Intensity of relative importance
Alike favored	1
Inadequately favored	3
Toughly favored	5
Very toughly more favored	7
Unconditionally more favored	9
Transitional position between two adjacent conclusions	2, 4, 6, 8

consistency occurs and the importance weights can be nominated for creation of the result. Steps of AHP technique is given below.

### 4.2 Executions of AHP

AHP can be executed in three steps:

- Calculating the vector of benchmarks weight.
- Calculating the matrix of decision score.
- Position the options.

Steps involved in calculations:

**S-1** Build a matched set of evaluation matrix for standards wasting 1–9 scales for comparative rank. If  $P$  standards are there in the comparison, then the evaluation of standards  $m$  with particular to standards  $n$  will outcome in a square matrix. The evaluation matrix for standards must fulfill the obeying norms.

$$a_{mn} = 1, \text{ When } m = n \text{ and } a_{mn} = \frac{1}{a_{nm}}$$

**S-2** Figure out the comparative standardized weight ( $w_{c_m}$ ) for every norm.

$$GM_m = \left( \prod_{m=1}^M a_{mn} \right)^{1/M}; \text{ and}$$

$$W_{c_m} = \frac{GM_m}{\sum_{m=1}^M GM_m}$$

**S-3** Constructed matrix  $B_3$  along with  $B_4$  where  $B_3 = B_1 \times B_2$  and  $B_4 = \frac{B_3}{B_2}$ ;

where,

$$B_2 = [W_1, W_2, W_3, \dots, W_i, W_n]^T$$

**S-4** Maximum Eigen value is calculated form mean of matrix  $B_4$ .

**S-5** Compute the Consistency Index (COI).

COI =  $(\lambda_{\max} - \text{Order of the matrix}) / (\text{order of the matrix} - 1)$ . Where  $\lambda_{\max}$  is maximum Eigen value. **Note**—Lesser the value of Consistency Index lesser the nonconformity from the uniformity.

**S-6** Compute the COR—Consistency ratio = Consistency index/Random index.

For a perfect evaluator value of consistency ratio must be zero but practically this is not possible. So, the lesser value of irregularity may be accepted, i.e.,

$$\text{Consistency ratio} \leq 0.1$$

## 5 Numerical Illustrations

AHP has been conducted to detect the importance weight of the standards as shown in above AHP methodology steps. For pairwise assessment among standards, professional’s views found as outcome of personally conversation and survey collaboration have been applied. The standards which have the maximum importance weights should be occupied at major importance for reflection. The standard values of random index with respect to size of the matrix are given in Table 2. Furthermore, the pairwise evaluation and their importance weights as achieved are provided in Tables 3 and 4.

Satty stated that if the consistency ratio for pair-wise comparison matrix is less than or equal to 0.1, then matrix has been acknowledged, if not then revise the pairwise comparison matrix. For above matched set evaluation matrix (Table 3), the illustrated amount of COR as stated in the formula for AHP approach is 0.093683 which matches Saaty’s standards for presence of uniformity hence, the matched set evaluation is reliable and the precedence weights are good enough to accept.

**Table 2** Table of Saaty for number of standard  $n$

Order of the matrix	1	2	3	4	5	6	7	8	9	10
Random Index (ROI)	0.00	0.00	0.58	0.90	1.12	1.24	1.32	1.41	1.45	1.49

**Table 3** Pairwise comparison matrix for hindrances

IH <sub>i</sub>	IH <sub>1</sub>	IH <sub>2</sub>	IH <sub>3</sub>	IH <sub>4</sub>	IH <sub>5</sub>	IH <sub>6</sub>	IH <sub>7</sub>	IH <sub>8</sub>	GM <sub>m</sub>	WC <sub>m</sub>	B <sub>3</sub>	B <sub>4</sub>
IH <sub>1</sub>	1	2	3	2	5	2	3	2	2.2759	0.2361	2.2065	9.3432
IH <sub>2</sub>	0.5	1	0.33	0.25	4	0.2	0.2	0.33	0.4648	0.0482	0.4766	9.8826
IH <sub>3</sub>	0.33	3	1	3	5	2	1	3	1.7528	0.1818	1.5836	8.7071
IH <sub>4</sub>	0.5	4	0.33	1	3	0.5	0.33	2	0.9482	0.0984	0.8497	8.6364
IH <sub>5</sub>	0.2	0.25	0.2	0.33	1	0.33	0.25	0.5	0.3286	0.0341	0.2938	8.6146
IH <sub>6</sub>	0.5	5	0.5	2	3	1	2	4	1.6682	0.1731	1.5177	8.7675
IH <sub>7</sub>	0.33	5	1	3	4	0.5	1	3	1.5279	0.1585	1.3863	8.7443
IH <sub>8</sub>	0.5	3	0.33	0.5	2	0.25	0.33	1	0.6705	0.0695	0.6053	8.7012

**Table 4** Summary of stability check for pairwise evaluation amid hindrances

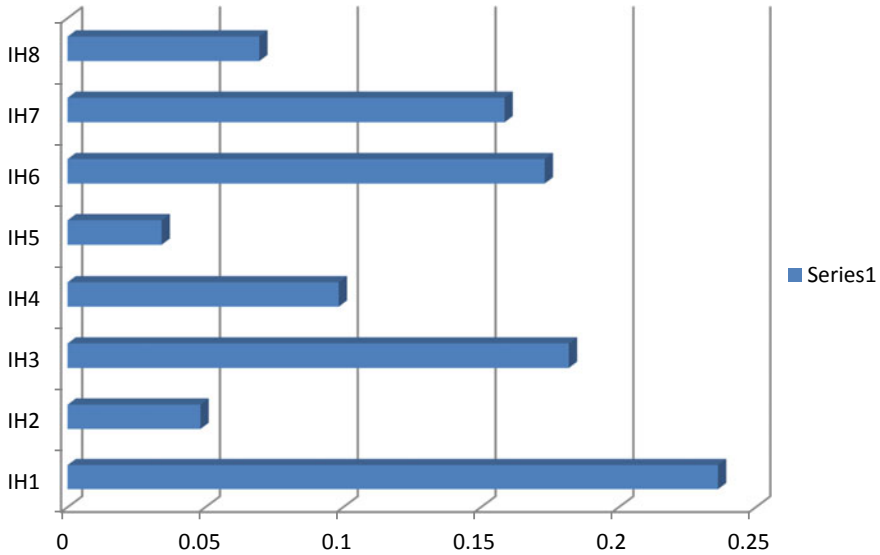
Factor	Calculated value
$\lambda_{max}$	8.9246
Consistency index	0.1321
Random index (from Table 2)	1.41
Consistency ratio	0.0937

## 6 Result and Discussion

In this investigation, an effort has been made to identify the more impactful hindrance which can cause difficulties to achieve our goal in supply chains. According to the above calculation Fiscal limitation that is hindrance no-1(IH<sub>1</sub>) is most dangerous and Absence of administrative support, i.e., hindrance no-5 (IH<sub>5</sub>) is very less harmful. That’s why (IH<sub>1</sub>) creates more problem in the supply chain and (IH<sub>5</sub>) will not create more obstruction. So, by considering above calculation hindrances should be identified on the basis of their weights. The hindrances which have more weight should remove first. By considering these things supply chain performance will increase. Ranking of hindrances has been decided based on their weight. Rating orders of hindrances are as follows

$$IH_1 > IH_3 > IH_6 > IH_7 > IH_4 > IH_8 > IH_2 > IH_5$$

Graphical representation of barriers based on their weight is shown in Fig. 2.



**Fig. 2** Bar chart representing hindrances weight

## 7 Conclusion

Comparing the hindrances of any organization is very useful for improvement of productivity as well as effectiveness. AHP approach is very simple as well as suitable for finalizing the ranking of the norms. For the investigation of this examination work AHP approach is anticipated. As we calculated above hindrance no1 which is fiscal limitation have maximum weight. So, we can say that this hindrance can cause difficulties in supply chain. Fiscal limitations are related to fiscal policy and other expenses. So, it is necessary to consider that fiscal limitations are most hazardous hindrance in the supply chain performance. In the present investigation, by the source of present literature review (L.R.), acknowledged information gaps and conversation with professionals, eight greatest dangerous hindrances have been identified. For finding precedence weights of the hindrances AHP methodology has been anticipated. With the assistance of this investigation work ranking on hindrances have been identified.

## References

1. Dalenogare LS, Benitez GB, Ayala NF, Frank AG (2018) The expected contribution of industry 4.0 technology for industrial performance. *Int J Prod Econ* 204:383–394
2. Frank AG, Dalenogare LS, Ayala NF (2019) Industry 4.0 technologies: implementation patterns in manufacturing companies. *Int J Prod Econ* 210:15–26

3. Ghadge A, Er Kara M, Moradlou H, Goswami M (2020) The impact of industry 4.0 implementation on supply chains. *J Manuf Technol Manag* 31(4):669–686
4. Chavarría-Barrientos D, Batres R, Wright PK, Molina A (2017) A methodology to create a sensing, smart and sustainable manufacturing enterprise. *Int J Prod Res* 56(1–2):584–603
5. Shrivastava P, Ivanaj S, Ivanaj V (2016) Strategic technological innovation for sustainable development. *Int J Technol Manage* 70(1):76–107
6. Barreto L, Amaral A, Pereira T (2017) Industry 4.0 implications in logistics: an overview. *Procedia Manuf* 13:245–1252
7. Rachinger M, Rauter R, Müller C, Vorraber W, Schirgi E (2018) Digitalization and its influence on business model innovation. *J Manuf Technol Manag* 30(8):1143–1160
8. Patil DA (2020) The study of industry 4.0 and its impact on supply chain management. *Int Res J Eng Technol* 07:2038
9. Bhagwat R, Sharma MK (2009) An application of the integrated AHP-PGP model for performance measurement of supply chain management. *Prod Planning Control* 20(8):678–690
10. Bititci US, Firat SUO, Garengo P (2012) How to compare performances of firms operating in different sectors? *Prod Planning Control* 24(12):1039–1042
11. Martinez V, Pavlov A, Bourne M (2010) Reviewing performance: an analysis of the structure and functions of performance management reviews. *Prod Planning Control* 21(1):70–83
12. Neely A (2005) The evolution of performance measurement research: developments in the last decade and a research agenda for the next. *Int J Oper Prod Manag* 25(12):1264–1277
13. Blau J (2014) Revolutionizing industry the German way. *Res Technol Manage* 57(6):2–3
14. Sharma J, Tyagi M, Bhardwaj A (2020) Parametric review of food supply chain performance implications under different aspects. *J Adv Manage Res* 17(3):421–453. <https://doi.org/10.1108/JAMR-10-2019-0193>
15. Genovese A, Koh LSC, Kumar N, Tripathi PK (2014) Exploring the challenges in implementing supplier environmental performance measurement models: a case study. *Prod Planning Control* 25(13–14):1198–1211
16. Lang M, Defflorin P, Dietl H, Lucas E (2014) The impact of complexity on knowledge transfer in manufacturing networks. *Prod Oper Manag* 23(11):1886–1898
17. Oberg C, Graham G (2016) How smart cities will change supply chain management: a technical viewpoint. *Prod Planning Control* 27(6):529–538
18. Porter ME, Heppelmann JE (2014) How smart, connected products are transforming competition. *Harv Bus Rev* 92(11):64–88
19. Sharma J, Tyagi M, Bhardwaj A (2021) Exploration of COVID-19 impact on the dimensions of food safety and security: a perspective of societal issues with relief measures. *J Agribusiness Developing Emerg Economies* 11(5):452–471. <https://doi.org/10.1108/JADEE-09-2020-0194>
20. Kusiak A (2021) Universal manufacturing: enablers, properties and models. *Int J Prod Res* 1–17
21. Wagire AA, Rathore APS, Jain R (2019) Analysis and synthesis of industry 4.0 research landscape: using latent semantic analysis approach. *J Manuf Technol Manag* 31(1):31–51
22. Sarvari PA, Ustundag A, Cevikcan E, Kaya I, Cebi S (2018) Technology roadmap for industry 4.0. In: Ustundag A, Cevikcan E (eds) *Industry 4.0: managing the digital transformation*. Springer, Cham, pp 95–103
23. Ghobakhloo M (2018) The future of manufacturing industry: a strategic roadmap toward industry 4.0. *J Manuf Technol Manag* 29(6):910–936
24. Haddud A, DeSouza A, Khare A, Lee H (2017) Examining potential benefits and challenges associated with the internet of things integration in supply chains. *J Manuf Technol Manag* 28(8):1055–1085
25. Wiengarten F, Longoni A (2015) A nuanced view on supply chain integration: a coordinative and collaborative approach to operational and sustainability performance improvement. *Supply Chain Manage Int J* 20(2):139–150
26. Fatorachian H, Kazemi H (2018) A critical investigation of industry 4.0 in manufacturing: theoretical operationalization framework. *Prod Planning Control* 29(8):633–644

27. Tortorella GL, Fettermann D (2017) Implementation of industry 4.0 and lean production in Brazilian manufacturing companies. *Int J Prod Res* 56(8):2975–2987
28. Schumacher A, Erol S, Sihm W (2016) A maturity model for assessing industry 4.0 readiness and maturity of manufacturing enterprises. *Procedia CIRP* 52:161–166
29. Telukdarie A, Buhulaiga E, Bag S et al (2018) Industry 4.0 implementation for multinationals. *Process Saf Environ Prot* 118:316–329
30. Abdirad M, Krishnan K (2021) Industry 4.0 in logistics and supply chain management: a systematic literature review. *Eng Manag J* 33(3):187–201
31. Wamba SF, Gunasekaran A, Akter S, Ren SJ, Dubey R, Childe SJ (2017) Big data analytics and firm performance: effects of dynamic capabilities. *J Bus Res* 70:356–365
32. Gunasekaran A, Subramanian N, Tiwari MK (2016) Information technology governance in internet of things supply chain networks. *Ind Manage Data Syst* 116(7)
33. Leitao P, Colombo AW, Karnouskos S (2016) Industrial automation based on cyber physical systems technologies: prototype implementations and challenges. *Comput Ind* 81:11–25
34. Poovendran R, Sampigethaya K, Gupta SKS, Lee I, Prasad KV, Corman D, Paunicka JL (2012) Special issue on cyber-physical systems. *Proc IEEE* 100(1):6–12
35. Stojmenovic I, Zhang F (2015) Inaugural issue of ‘cyber-physical systems.’ *Cyber Phys Syst* 1(1):1–4
36. Gorane SJ, Kant R (2015) Supply chain practices. *Int J Product Perform Manag* 64(5):657–685
37. Factorachian H, Kazemi H (2021) Impact of industry 4.0 on supply chain performance. *Prod Planning control* 32(1):63–81
38. Capra F (1997) *The web of life*. Doubleday-Anchor Book, New York
39. Mele C, Pels J, Polese F (2010) A brief overview of systems theories and their managerial implications. *Serv Sci* 2(1–2):126–135
40. Manavalan E, Jayakrishna K (2019) A review of internet of things (IOT) embedded sustainable supply chain for industry 4.0 requirements. *Comput Ind Eng* 127:925–953
41. Tyagi M, Kumar P, Kumar D (2014) A hybrid approach using AHP-TOPSIS for analyzing e-SCM performance. *Procedia Eng* 97:2195–2203
42. Deloitte (2017) *Industry 4.0 and cyber security: managing risk in an age of connected production*. Deloitte University Press. Available at: [https://www2.deloitte.com/content/dam/insights/us/articles/3749\\_Industry40\\_cybersecurity/DUP\\_Industry4-0\\_cybersecurity.pdf](https://www2.deloitte.com/content/dam/insights/us/articles/3749_Industry40_cybersecurity/DUP_Industry4-0_cybersecurity.pdf). (Accessed 5 Jan 2020)
43. Tyagi M, Kumar P, Kumar D (2015) Permutation of fuzzy AHP and AHP methods to prioritizing the alternatives of supply chain performance system. *Int J Ind Eng Theory Appl Pract* 22(6):729–752



# Exploration of Circular Economy Enablers Using Fuzzy DEMATEL Approach



Shivam Mishra, Mohit Tyagi, Anish Sachdeva, and Ravi Pratap Singh

**Abstract** Every year, massive amount of waste is generated from manufacturing companies and business organizations around the world, which has created anxiety in society due to its hazardous nature. From this waste various type of toxic emission releases including carbon dioxide, methane, sulphur dioxide, nitrogen dioxide, carbon monoxide, etc., affecting the environment and human health. In the recent years, circular supply chain management (CSCM) concept has been adopted by the manufacturing companies, that having the target to reduce the negative environmental impressions and social impact. Manufacturing companies are facing problems to take the profit from the waste due to lack of new evolving circular economy (CE) concept. This research aims to accelerate the CE practices in manufacturing firms by enlighten the important associated enablers for CE success. Further these identified CE enablers has been analyzed through fuzzy Decision-Making Trial and Evaluation Laboratory (fuzzy DEMATEL) approach in order to classify them based on their influencing nature along with designing a mutual relation between the enablers. Outcomes of the study would help the managers and policy makers to improve the current circular practices and focuses more on CE to improve the supply chain performance.

**Keywords** Circular economy · Supply chain performance · Circular supply chain · Circular economy enablers · Circular economy performance · Fuzzy DEMATEL approach

## 1 Introduction

Excessive waste generation is a problematic concern that the industrial managers and policy makers are facing in today's era. Due to such type of problem, a demand arises

---

S. Mishra · M. Tyagi (✉) · A. Sachdeva  
Department of Industrial and Production Engineering, Dr B R Ambedkar National Institute of Technology, Jalandhar, Punjab, India  
e-mail: [mohitmied@gmail.com](mailto:mohitmied@gmail.com)

M. Tyagi · R. P. Singh  
Department of Mechanical Engineering, National Institute of Technology, Kurukshetra, India

© The Author(s), under exclusive license to Springer Nature Singapore Pte Ltd. 2023  
R. P. Singh et al. (eds.), *Advances in Modelling and Optimization of Manufacturing and Industrial Systems*, Lecture Notes in Mechanical Engineering,  
[https://doi.org/10.1007/978-981-19-6107-6\\_49](https://doi.org/10.1007/978-981-19-6107-6_49)

685

to development of innovative ways for reduction and utilization of that waste for the useful purposes. By using the various available process that converted waste into the useful form, which again used into the various places, and also help to growth the economy [1]. If waste will not convert into the other forms, then it will be harmful for the environment and human health, also will not take any leverage from that waste. CE concept has been projected as a dominant route to enhancing the mode which use efficiently to balance among the social impact, economy and negative environment impact [16]. CE gives an efficient model which dominant to enhanced the linear economy model called as 'take, make and waste' [45].

The use of CE not only enhanced in manufacturing area but also enhances in academic area [13]. Still several studies of CE have been printed worldwide such as case studies, analyzes, scientific report etc. [69]. Generation of waste is most important concern in all over the world because from this waste various type of toxic gases generated such as carbon dioxide, carbon monoxide, and methane which polluted the environment, and occupy the land and also impact the human health. Some of the gases produces from the waste, which are very dangerous for ozone layer that fall on the ozone layer, due to degradation of ozone layer, some ultraviolet rays directly fall on the earth which enhancing the temperature of earth and also cause the cancer disease.

In CE, raw material and energy resources are used in closed loop throughout the various stages [71] and produce the final product. The CE concept joints the economy and environment, objective is to growth sustainability, effectively convert unsustainable material into the sustainable material [55]. The concept end-of-life (EOL) again pondered, as action of economy mainly attentive on how to material and product to reuse to ignoring the product or material become as the waste [28]. Further, turn the waste into usable form after fixed period of time, using the concept of end life, so that the product does not become like garbage. The concept of CE has been adopted by the manufacturing companies which mainly focus on applying the concept in the small size company rather than larger size sample of multi-national enterprises (MNE) organizing global supply network [32].

CE is not only crucial for manufacturing industry but also in the academic research area, the importance of CE has been enhanced in various areas, number of articles and journal on this topic has been researching and publishing rapidly during last some years [1], for example on circular economic topic in 2016 more than 100 articles published as compare to 2014 where 30 articles publish [13]. Companies enhanced the awareness of the chances provide by the CE and commence to perceive the circular economy value for ourselves and also for his stakeholders. Circular economy looks as untapped model probable to led extra sustainable progress and melodious society [14, 40, 42, 74]. The literature recognizes CE is one of the organization resources that face the challenge of the growing end-of-service resource [23]. Purpose of CE practices to disseminate present resources, waste production and create a more efficient and effective renewable energy model, empowering resource efficiency [19, 23, 39].

## 2 Literature Review

The field of industrial research has been focused mainly on two sector, that is, CE and industry 4.0 [29]. CE term first time had been introduced by Stahel and Reday in [60]. After some decades, CE concept has been used in various sectors. Work of CE has been based on close loop manufacturing system and used as to enhance the resource efficiency [30]. Present work focuses on identifying the issues that arises during the application of the CE model in the supply chain system, and the defines the ways towards transforming the circular supply chain to achieve a zero-waste economy. CE provide a recycling system based on the zero-waste philosophy, the idea that waste generated within a manufacturing industry has the likely to be used as an important asset by another manufacturing industry [31].

Some characteristics of the CE have been generated which focused on the industrial economy [60]. CE comprises various components which used in the manufacturing industry to produce the final product in a close loop [13]. Cradle-to-cradle design has been observed as one of the most important component of CE [7], industrial symbioses [9], product-service system [62], circular flow of materials [36], industrial ecosystems [24], blue economy [49] and eco-efficiency [20] etc.

Material reuse theory has been extensively used in cradle-to-cradle model which demonstrates that the industrial materials are categorised into technical and biological materials [30]. Technical material not having the toxic also not hazardous and it is used again and again after applying some process, biological materials is organic nutrients which decompose themselves without influencing the environment and the human health [29]. After the millions of years, these biological material converted into other form on which applying the various process to convert the usable form such as petrol, crude oil, and diesel.

For increasing the life of the material, manufacturing company has been used the concept of CE, CE required the sustainability of operation [26]. The sustainability of procedure can be determined by counting the amount of various type of emission such as carbon dioxide, sulfur dioxide, nitrogen dioxide, various type of waste like solid waste, e-waste, plastic waste, etc., and the use of harmful and contaminated substances [50]. Sustainability is ensured by execution of asset recession and other commodities fluctuation between the sale of goods and services [52, 57, 59]. Companies must be generated a method which assist to enhancing the efficiency of the resource, increase the quality of the manufacturing product and minimize the garbage that will help to sustain performance [15, 59].

If the manufacturing companies produced the product on the basis of green design, it reducing the consumption of energy as well as minimize the waste generation [11, 21], to preserve the environment these green products should be require the green material and rotten packaging material [3, 66]. Green supply chain management needs completely moving the plan of 'post-pollution treatment' again emphasizes the concept of 'reducing pollution in the source' prevention first, second treatment, that

is at the construction of product and purchase categories, will be fully considered in terms of their impact environment, thereby decreasing the cost of business treatment and improving the business environment performance and economic performance [2].

The circular CE has been introduced and authorized based on the 3R such as (reduction, reuse, and recycling) in supply chain management [48]. Reduce related to input method aims to decrease the raw material and energy inputs in the manufacturing and improve the utilization process (reuse is the process which aims to extend the durability and service life of the product while recycle refers to the process of returning the object or material to renewable resource so that they can be utilised again) [73]. However, as the topic has grown-up and it has developed to 6R which has also included Recover, Redesign, and Remanufacturing, showing good consequences for promoting reuse [18].

CE gives a unique assessment on the functioning and construction of used and waste management assets [30]. Their effectiveness and efficiency have been key factor in transforming the business model of the conference into an extra sustainable one [13, 16]. Based on policy-structure and planned, CE has been used to create effective shopper products through industry 4.0 [51]. Therefore, to reduce the wastage, improve the product sustainability, enhancing the quality of the product, reducing manufacturing cost, enhance the production, and improve the economy of the manufacturing companies and organization for all these factor amends to apply the concept of CE.

### 3 Problem Formulation

To perform this study paper, a deep study of previous research paper related to improving the supply chain performance (SCP) has been analyzed. Present work emphasized on CE enablers and thus through literature analysis, a total of eight prominent CE enablers has been recognized among the available one in the literature analysis. Table 1 presents the CE enablers identified from the literature analysis.

### 4 Research Methodology

The purpose of this study paper is to determine the significant level of those considered enablers to be approving CE in order to improve SCP. The fuzzy DEMATEL method was developed to find the significant enablers effect the SCP. Fuzzy DEMATEL method has been used to analyze the set of enablers. In order to obtain data for the fuzzy DEMATEL method, the questionnaire is structured according to the linguistic scale demonstrated in Table 2.

**Table 1** Classification of CE enablers

Enablers	Enabler of CE	Reference
CEE1	Long term strategy planning	De Mattos and de Albuquerque [10], Xue et al. [67], Razminiene [53], Bolger and Doyon [6]
CEE2	Energy recycling	Frank et al. [12], Li et al. [34], Kalmykova et al. [25], Yong [70], Kumar et al. [30]
CEE3	Digitalisation	Neligan [43], Saberi et al. [56], Antikainen et al. [4]
CEE4	Green procurement	Govindan and Hasanagic [18], Yaduvanshi et al. [68], Lopes de Sousa Jabbour et al. [37], Zhijun and Nailing [74]
CEE5	Waste recycling	Kalmykova et al. [25], Malinauskaite et al. [38], Nelles et al. [44]
CEE6	Society well-being toward CE	Murray et al. [41], Jaeger-Erben et al. [22], Schröder et al. [58]
CEE7	Organization environment	Wang [65], Kirchherr et al. [27], Gorane and Kant [17], Rizos et al. [54]
CEE8	Reduction in manufacturing cost	Ormazabal et al. [47], Lewandowski [33], Razminiene [53]

**Table 2** Conversion of linguistic variable in triangular fuzzy numbers [63]

Influence score	Linguistic variable	Triangular fuzzy numbers (TFN's)
0	No impact (NO)	(0, 0.1, 0.3)
1	Very less impact (VL)	(0.1, 0.3, 0.5)
2	Less impact (LI)	(0.3, 0.5, 0.7)
3	High impact (HI)	(0.5, 0.7, 0.9)
4	Very high impact (VH)	(0.7, 0.9, 1.0)

The questionnaire has been sent to various industrial and academic experts to obtain the relevant data. After obtaining the data, the data were then analyzed through fuzzy DEMATEL approach. The details of the steps of the fuzzy DEMATEL have been elaborated in the trailing section.

### 4.1 DEMATEL Method

DEMATEL approach was firstly introduced by Battle Memorial Institute of Geneva [46]. The chief leverage of DEMATEL method is that it assists in classifying the parameters in cause-and-effect group, along with this it also aids in identifying the most critical parameters through finding their prioritized ranks [64]. DEMATEL

method has been used in several applications, for example, selection of truck [5], sustainable management [61] etc.

DEMATEL method having the limitation, where it failed to capture the uncertainty present in the direct-relation matrix obtain from the judgement of decision-maker, so that to overcome this limitation fuzzy set theory has been used [46].

## ***4.2 Fuzzy Set Theory and Triangular Fuzzy Numbers***

In multi-criteria decision-making problem, the decisions are based on the opinions or judgements received from the field experts that often-incurred uncertainty or vagueness about the data. This made the problem solution very complex and uncertain results. Therefore, to remove the vagueness or uncertainty of the data, the fuzzy sets are involved in decision making employing linguistic terms instead of a crisp numeric value [31]. In this research work fuzzy DEMATEL approach has been conducted to minimize the uncertainty associated with the judgement obtain from of expert, fuzzy DEMATEL approach based on the questionnaire according to linguistic terms shown in Table 2, which designed by the researcher and send to the expert through the Google Doc and obtain their significant opinion regarding the questionnaire designed. Linguistic term has been used as to represent the linguistic variables. In this research work, linguistic terms used such as: very small, small, high, and very high. The opinion obtain from the decision maker in the term of linguistic terms are represent by triangular fuzzy number [63]. The uncertainty which is associated with human judgement reduce by fuzzy set theory, has been suggested by the [72]. Degree of belongings has been used in the fuzzy set, which belong among 0 and 1, whereas crisp set having the binary logic 0 and 1 [63]. So that the uncertainty which are associated with the crisp set, that can be be reduce through of fuzzy set.

## ***4.3 Fuzzy DEMATEL Approach***

The DEMATEL approach examine the mutual interaction between a set of complex criteria factor on the graph-based diagram [63] and divided into cause-and-effect group based on the behavior of enablers and make the referential relationship between existing criteria [8, 35].

- (a) DEMATEL approach having various significant importance's to analyze the enablers for the problem under consideration such as:
- (b) DEMATEL method convert the relation between cause and effect of criteria into the graph theory.
- (c) It may also be used as a means of dealing with an internal dependent within a set of conditions.

- (d) DEMATEL approach has been used in many fields to find out the cause and effect of complex set of criteria, the fields are hospital management for enhance the quality, selection of suppliers in the supply chain management etc.

**Steps of Fuzzy DEMATEL Approach**

- To make the fuzzy direct-relation matrix where the element present in the linguistic variable form which obtain from the decision maker shown in Table 2. After that, these linguistic variables converted into the TFN which taken from [63]. Then the fuzzy initial direct-relation matrix consists  $\tilde{W}_k$  triangular fuzzy number denoted as  $\tilde{W}_k = (\tilde{w}_{ijk})_{n \times n} = ((p_{ijk}, q_{ijk}, r_{ijk}))_{n \times n}$

where  $\tilde{w}_{ijk}$  is the judgement obtain from  $k$  decision maker on the degree of impact of element  $i$  on element  $j$  demonstrated in Eq. (1).

$$\tilde{W}_k = (\tilde{w}_k)_{n \times n} = \begin{bmatrix} 0 & \tilde{w}_{12k} & \cdots & \tilde{w}_{1nk} \\ \tilde{w}_{21k} & 0 & \cdots & \tilde{w}_{2nk} \\ \vdots & \vdots & \ddots & \vdots \\ \tilde{w}_{n1k} & \tilde{w}_{n2k} & \cdots & 0 \end{bmatrix} \tag{1}$$

- Determine the average direct relation matrix of obtain the judgement of  $k$  decision maker given in Eq. (2).

$$\tilde{W} = (\tilde{w})_{ij} = \left( \left( \frac{\tilde{w}_{ij1} + \tilde{w}_{ij2} + \cdots + \tilde{w}_{ijk}}{K} \right) \right)_{n \times n} \tag{2}$$

- Normalization of direct relation matrix  $N$  using Eq. (3):

$$N = (\tilde{y}_{ij})_{n \times n} = \begin{pmatrix} \tilde{y}_{11} & \tilde{y}_{12} & \cdots & \tilde{y}_{1n} \\ \tilde{y}_{21} & \tilde{y}_{22} & \cdots & \tilde{y}_{2n} \\ \vdots & \vdots & \ddots & \vdots \\ \tilde{y}_{n1} & \tilde{y}_{n2} & \cdots & \tilde{y}_{nn} \end{pmatrix} \tag{3}$$

where  $\tilde{y}_{ij} = \frac{\tilde{w}_{ij}}{s} = (\frac{p_{ij}}{s}, \frac{q_{ij}}{s}, \frac{r_{ij}}{s})$ ;  $s = \max_{1 \leq i \leq n} (\sum_{j=1}^n u_{ij})$ .

To convert the criteria scale into the corresponding scales, linear scale has used as formula mentioned in Eq. (4) in normalization.

$$\tilde{b}_{ij} = \sum_{j=1}^n \tilde{w}_{ij} = \left( \sum_{j=1}^n p_{ij}, \sum_{j=1}^n q_{ij}, \sum_{j=1}^n r_{ij} \right), s = \max_{1 \leq i \leq n} \left( \sum_{j=1}^n u_{ij} \right). \tag{4}$$

where  $\tilde{b}_{ij}$  is the TFN in each cell of  $\tilde{W}$  and  $s$  represent the maximum summation value in the entire row of each TFN shown in Eq. (4).

- Let  $\tilde{Y} = (\tilde{y}_{ij})_{ij} = (p'_{ij}, q'_{ij}, r'_{ij})$  and express  $N_p = (p'_{ij})_{n \times n}$ ,  $N_q = (q'_{ij})_{n \times n}$  and  $N_r = (r'_{ij})_{n \times n}$ . In this matrix all element extracted from  $\tilde{N}$  shown in Eq. (5):

$$\begin{aligned}
 N_p &= \begin{pmatrix} 0 & p'_{12} & \cdots & p'_{1n} \\ p'_{21} & 0 & \cdots & p'_{2n} \\ \vdots & \vdots & \ddots & \vdots \\ p'_{n1} & p'_{n2} & \cdots & 0 \end{pmatrix}; \\
 N_q &= \begin{pmatrix} 0 & q'_{12} & \cdots & q'_{n1} \\ q'_{21} & 0 & \cdots & q'_{n2} \\ \vdots & \vdots & \ddots & \vdots \\ q'_{n1} & q'_{n2} & \cdots & 0 \end{pmatrix}; \\
 N_r &= \begin{pmatrix} 0 & r'_{12} & \cdots & r'_{n1} \\ r'_{21} & 0 & \cdots & r'_{n2} \\ \vdots & \vdots & \ddots & \vdots \\ r'_{n1} & r'_{n2} & \cdots & 0 \end{pmatrix} \tag{5}
 \end{aligned}$$

- Using Eq. (6) to compute the total direct-relation matrix:

$$\tilde{T} = \lim_{k \rightarrow \infty} (\tilde{N}^1 + \tilde{N}^2 + \cdots + \tilde{N}^k) \tag{6}$$

where  $\tilde{T}$  matrix comprises TFNs

$$\tilde{T} = \begin{pmatrix} \tilde{t}_{11} & \tilde{t}_{12} & \cdots & \tilde{t}_{1n} \\ \tilde{t}_{21} & \tilde{t}_{22} & \cdots & \tilde{t}_{2n} \\ \vdots & \vdots & \ddots & \vdots \\ \tilde{t}_{n1} & \tilde{t}_{n2} & \cdots & \tilde{t}_{nn} \end{pmatrix}$$

$$\tilde{t}_{ij} = (p''_{ij}, q''_{ij}, r''_{ij}) \text{ and } [p''_{ij}] = N_p \times (I - N_p)^{-1},$$

$$[q''_{ij}] = N_q \times (I - N_q)^{-1}, [r''_{ij}] = N_r \times (I - N_r)^{-1} \tag{7}$$

- To find the value of  $D_1$  and  $R_1$  using the Eqs. (8) and (9) corresponding

$$\tilde{T} = [\tilde{t}_{ij}]_{m \times m} \text{ where } i, j = 1, 2, \dots, m \tag{8}$$



$$D_1 = \left[ \sum_{j=1}^m \tilde{t}_{ij} \right]_{m \times 1} = [\tilde{t}_i]_{m \times 1} \tag{9}$$

$$R_1 = \left[ \sum_{i=1}^m \tilde{t}_{ij} \right]_{1 \times m} = [\tilde{t}_j]_{1 \times m} \tag{10}$$

where  $D_1$  = is the sum of row, and  $R_1$  = is the sum of columns.

After that, calculate the value of Prominence ( $D_1+R_1$ ) and Relation ( $D_1-R_1$ ) by add the corresponding value of  $D_1$  and  $R_1$ .

- Formation of casual diagram of enablers on the basis of Prominence and Relation value:

The casual diagram is formed by mapping the ( $D_1+R_1$ ) and ( $D_1-R_1$ ) data, ( $D_1+R_1$ ) and ( $D_1-R_1$ ) data value marked horizontally and vertically corresponding. If ( $D_1-R_1$ ) value come negative then this enabler defined in effect group and if positive value then defined in cause group [64].

- Total relation matrix contains the defuzzify entries using Eq. (11). The non-fuzzy total relation matrix denoted as  $T = (t_{ij})_{n \times n}$  where

$$t_{ij} = \left( \frac{p''_{ij} + 4q''_{ij} + r''_{ij}}{6} \right) \tag{11}$$

## 5 Numerical Illustration

To derive the analysis for the ranking of enablers, a fuzzy linguistic scale-based questionnaire has been designed as demonstrated in Table 2, and send to the expert through Google Docs and obtain their importance’s regarding enablers. Then, linguistic table is arranged, and obtain matrix from the expert in linguistic term has been shown in Table3. Table 3 demonstrates the impact nature of consider enablers over each other. For example, CEE1 enabler has no impact on CEE2 enabler, very low impact on CEE6 enabler, low impact on CEE4 and CEE7 enabler, high impact on the CEE3 and CEE8 enabler, and very high impact on CEE5 enabler.

After that linguistic scale direct-relation matrix, has been converted into the TFN and then the aggregated matrix has been defuzzified. The defuzzification direct-relation matrix is shown Table 4.

According to the next step, average direct-relation matrix shown in Table 5.

where  $\sum_{ij}^n a_{ij} = [\sum_{i=1}^n \tilde{t}_{ij}]_{n \times 1}$ ,  $i, j = 1, 2, 3, \dots, n$

Thereafter, normalization of the average direct relation matrix has been obtained.

Normalization of average direct-relation matrix has been demonstrated in Table 6.

To find the value of  $D_1$  using the Eq. (9) and for  $R_1$  using the Eq. (10) is demonstrated in Table 7.

**Table 3** The linguistic scale direct-relation matrix by expert-1

	CEE1	CEE2	CEE3	CEE4	CEE5	CEE6	CEE7	CEE8
CEE1	0	NO	HI	LI	VH	VL	LI	HI
CEE2	LI	0	VH	VL	LI	HI	VL	LI
CEE3	NO	VL	0	LI	VH	LI	HI	NO
CEE4	HI	VH	NO	0	LI	VH	VL	VH
CEE5	VL	LI	HI	VH	0	LI	NO	HI
CEE6	HI	VL	LI	HI	VH	0	HI	VL
CEE7	LI	VH	HI	VL	LI	HI	0	LI
CEE8	VL	HI	VH	LI	HI	VL	VH	0

**Table 4** Defuzzification direct-relation matrix

	CEE1	CEE2	CEE3	CEE4	CEE5	CEE6	CEE7	CEE8
CEE1	0.0000	0.1167	0.7000	0.5000	0.8833	0.3000	0.5000	0.7000
CEE2	0.5000	0.0000	0.8833	0.3000	0.5000	0.7000	0.3000	0.5000
CEE3	0.1167	0.3000	0.0000	0.5000	0.8833	0.5000	0.7000	0.0000
CEE4	0.7000	0.8833	0.1167	0.0000	0.5000	0.8833	0.3000	0.8833
CEE5	0.3000	0.5000	0.7000	0.8833	0.0000	0.5000	0.0000	0.7000
CEE6	0.7000	0.3000	0.5000	0.7000	0.8833	0.0000	0.7000	0.3000
CEE7	0.5000	0.8833	0.7000	0.3000	0.5000	0.7000	0.0000	0.5000
CEE8	0.3000	0.7000	0.8833	0.5000	0.7000	0.3000	0.8833	0.0000

**Table 5** Average direct-relation matrix

	CEE1	CEE2	CEE3	CEE4	CEE5	CEE6	CEE7	CEE8	$\sum_{ij}^n a_{ij}$
CEE1	0.0000	0.2444	0.4333	0.6333	0.5000	0.9000	0.6944	0.6944	4.1000
CEE2	0.4389	0.0000	0.6944	0.3667	0.7556	0.7000	0.3667	0.4333	3.7556
CEE3	0.1889	0.6278	0.0000	0.3722	0.4944	0.3333	0.4000	0.2333	2.6500
CEE4	0.5000	0.6889	0.3722	0.0000	0.6333	0.5278	0.3000	0.8222	3.8444
CEE5	0.6278	0.5000	0.3722	0.7556	0.0000	0.6944	0.4611	0.4000	3.8111
CEE6	0.4000	0.5667	0.5000	0.6278	0.3944	0.0000	0.7000	0.3667	3.5556
CEE7	0.4333	0.5889	0.6278	0.5000	0.5000	0.5667	0.0000	0.5000	3.7167
CEE8	0.6278	0.6944	0.5611	0.4333	0.6333	0.3000	0.6278	0.0000	3.8778

After that, calculating the value of prominence ( $D_1 + R_1$ ) and Relation ( $D_1 - R_1$ ) shown in Table 7. If the enabler value in the ( $D_1 - R_1$ ) is positive then it come under the cause category and if value negative then it classified into the effect category [64].

**Table 6** Normalization of average direct-relation matrix

	CEE1	CEE2	CEE3	CEE4	CEE5	CEE6	CEE7	CEE8
CEE1	0.0000	0.0596	0.1057	0.1545	0.1220	0.2195	0.1694	0.1694
CEE2	0.1070	0.0000	0.1694	0.0894	0.1843	0.1707	0.0894	0.1057
CEE3	0.0461	0.1531	0.0000	0.0908	0.1206	0.0813	0.0976	0.0569
CEE4	0.1220	0.1680	0.0908	0.0000	0.1545	0.1287	0.0732	0.2005
CEE5	0.1531	0.1220	0.0908	0.1843	0.0000	0.1694	0.1125	0.0976
CEE6	0.0976	0.1382	0.1220	0.1531	0.0962	0.0000	0.1707	0.0894
CEE7	0.1057	0.1436	0.1531	0.1220	0.1220	0.1382	0.0000	0.1220
CEE8	0.1531	0.1694	0.1369	0.1057	0.1545	0.0732	0.1531	0.0000

**Table 7** Total relation matrix

	CEE1	CEE2	CEE3	CEE4	CEE5	CEE6	CEE7	CEE8	$D_1$
CEE1	0.9350	1.1774	1.1174	1.1940	1.2165	1.3204	1.1653	1.1341	<b>9.2601</b>
CEE2	0.9428	1.0124	1.0736	1.0450	1.1649	1.1805	1.0042	0.9847	<b>8.4082</b>
CEE3	0.6696	0.8800	0.6849	0.7885	0.8522	0.8374	0.7619	0.7114	<b>6.1859</b>
CEE4	1.0012	1.2060	1.0568	1.0052	1.1943	1.1963	1.0356	1.1091	<b>8.8045</b>
CEE5	1.0144	1.1587	1.0454	1.1567	1.0467	1.2221	1.0576	1.0237	<b>8.7252</b>
CEE6	0.9029	1.0977	1.0037	1.0550	1.0599	0.9941	1.0306	0.9451	<b>8.0889</b>
CEE7	0.9374	1.1349	1.0586	1.0624	1.1133	1.1486	0.9152	0.9969	<b>8.3672</b>
CEE8	1.0197	1.2021	1.0922	1.0982	1.1906	1.1537	1.0943	0.9349	<b>8.7858</b>
$R_1$	<b>7.4229</b>	<b>8.8693</b>	<b>8.1326</b>	<b>8.4049</b>	<b>8.8382</b>	<b>9.0531</b>	<b>8.0648</b>	<b>7.8399</b>	

Bold indicates the sum of columns scores of CE enablers relative to others and itself in total relation matrix

## 6 Results and Discussion

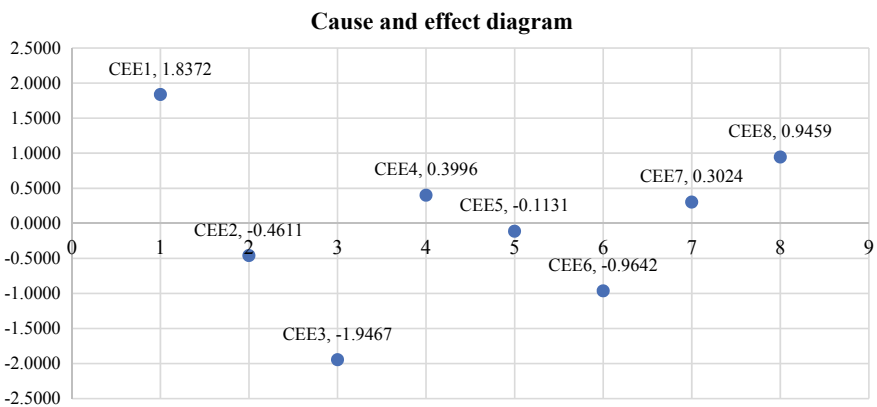
Product become as a waste material after completing their life cycle, and producing various type harmful gases which effect the environment and human health. So, in this paper, an effort has been made to identify important enabler on the basis of their ranking which improving the performance of supply chain and more important in term of reduce the negative environment influence and social impact. Determine the important ranking of all enablers based on the value of Prominence ( $D_1 + R_1$ ) shown in Table 8 and Fig. 2. In Table 8, CEE5 have greater important than the other enablers. The important rating order of all enablers comes as:  $CEE5 > CEE2 > CEE4 > CEE6 > CEE1 > CEE8 > CEE7 > CEE3$ . From the findings it can be said that the organizations should primarily focus on the waste recycling. And also analyzing the value of Relation ( $D_1 - R_1$ ), basis on the value of ( $D_1 - R_1$ ) enablers defined in the cause-and-effect group. The enablers such as Energy recycling (CEE2), digitalization (CEE3), waste recycling (CEE5) and social well-being toward CE (CEE6) have

‘negative’ ( $D_1 - R_1$ ) value and come under the category of effect group. While other enablers such as: long term strategy planning (CEE1), green procurement (CEE4), organization environment (CEE7) and reduction in manufacturing cost (CEE8) have the ‘Positive’ ( $D_1 + R_1$ ) value and define in the cause group. The impact of cause over the effect enablers has shown in Fig. 1.

The  $D_1 + R_1$  values in fuzzy DEMATEL method provide the information about the importance significance of considered parameters. Here, different CE enablers has attained different values of  $D_1 + R_1$ . Higher is the  $D_1 + R_1$  value for an enabler, higher is its importance rating. Figure 2 displays the attained important rating by each CE enablers.

**Table 8** Scores of prominences and relation of enablers

Enablers	$D_1$	$R_1$	$D_1 + R_1$	$D_1 - R_1$	Cause and effect	Rating
CEE1	9.2601	7.4229	16.6831	1.8372	Cause	5
CEE2	8.4082	8.8693	17.2775	-0.4611	Effect	2
CEE3	6.1859	8.1326	14.3185	-1.9467	Effect	8
CEE4	8.8045	8.4049	17.2094	0.3996	Cause	3
CEE5	8.7252	8.8382	17.5634	-0.1131	Effect	1
CEE6	8.0889	9.0531	17.1421	-0.9642	Effect	4
CEE7	8.3672	8.0648	16.4321	0.3024	Cause	7
CEE8	8.7858	7.8399	16.6257	0.9459	Cause	6



**Fig. 1** Cause-and-effect diagram of enablers



Fig. 2 Enabler’s rating diagram

## 7 Conclusion

In this research paper eight enablers have been considered and analyzed using the fuzzy DEMATEL approach. Identify the enablers rating and on the basis of rating obtain classified enablers into the most important and less important category. And also classified the enablers into the cause-and-effect category by using fuzzy DEMATEL method on the basis of Prominence ( $D_1 + R_1$ ) and Relation ( $D_1 - R_1$ ) value. The fuzzy DEMATEL method is an extension of simple DEMATEL method with the use of linguistic variables (shown in Table 2) and fuzzy aggregation method, in order to reduce the uncertainty associated with the human judgement.

In this research work, long-term strategy (CEE1) having the highest positive value due to which CEE1 enabler come into the cause group. Long-term strategy (CEE1) having the highest impact over all the enablers and organization environment (CEE7) having the least impact over all the enablers. It effected the energy recycling (CEE2), digitalization (CEE3), waste recycling (CEE5), and society well-being toward CE (CEE6). Waste recycling (CEE5) enabler having the highest negative value over all enablers, so that it is affected more as comparison to all other enablers. The effecting order of enablers found as: waste recycling (CEE5) > energy saving (CEE2) > society well-being (CEE6) > digitalization (CEE3). The ratings of all considered enablers have been found out of those the enabler name as: digitalization (CEE3) acquired the highest rating. So that the conclusion of this research paper is organization has been more focused on the waste recycling enabler because it having the more impact which affect the all-other enablers more as compare the other enablers of more impact and effect the all enablers high as compare another enabler.

## References

1. Agarwal S, Tyagi M, Garg RK (2021a) Conception of circular economy obstacles in context of supply chain: a case of rubber industry. *Int J Prod Perform Manage* Emerald Publishing Limited, ahead-of-print. Available at: <https://doi.org/10.1108/IJPPM-12-2020-0686>
2. Agarwal S, Tyagi M, Garg RK (2021b) Restorative measures to diminish the covid-19 pandemic effects through circular economy enablers for sustainable and resilient supply chain. *J Asia Bus Stud* Emerald Publishing Limited, ahead-of-print. Available at: <https://doi.org/10.1108/jabs-05-2021-0217>
3. Agarwal S, Tyagi M, Garg RK (2021) Prioritizing circular economy performance measures. In: *Operations management and data analytics modelling*. CRC Press, pp 107–123
4. Antikainen M, Uusitalo T, Kivikytö-Reponen P (2018) Digitalisation as an enabler of circular economy. *Procedia CIRP* 73:45–49
5. Baykasoglu A, Kaplanoglu V, Durmusoglu ZDU, Sahin C (2013) Integrating fuzzy DEMATEL and fuzzy hierarchical TOPSIS methods for truck selection. *Expert Syst Appl* 40(3):899–907
6. Bolger K, Doyon A (2019) Circular cities: exploring local government strategies to facilitate a circular economy. *Eur Plan Stud* 27(11):2184–2205
7. Braungart M, McDonough W, Bollinger A (2007) Cradle-to-cradle design: creating healthy emission—a strategy for eco-effective product and system design. *J Clean Prod* 15:1337–1348
8. Charan P, Shankar R, Baisya RK (2008) Analysis of interaction among the variable of supply chain performance measurement system implementation. *Bus Process Manag J* 14(4):512–529
9. Chertow M, Ehrenfeld J (2012) Organizing self-organizing system. *J Ind Ecol* 16:13–27
10. De Mattos CA, de Albuquerque TLM (2018) Enabling factors and strategies for the transition toward a circular economy. *Sustainability* 10(12):4628
11. Foo PY, Lee VH, Tan GWH, Ooi KB (2018) A gateway to realising sustainability performance via green supply chain management practices: A PLS\_ANN approach. *Expert Syst Appl* 107:1–14
12. Frank AG, Dalenogare LS, Ayala NF (2019) Industry 4.0 technologies: implementation patterns in manufacturing companies. *Int J Prod Econ* 210:15–26
13. Geissdoerfer M, Savaget P, Bocken NMP, Hultink EJ (2017) The circular economy—a new sustainability paradigm? *J Cleaner Prod* 143:757–768
14. Geng Y, Doberstein B (2008) Developing the circular economy in China: challenges and opportunities for achieving Leapfrog development. *Int J Sustain Dev Word Ecol* 15:231–239
15. Geng R, Mansouri SA, Aktas E (2017) The relationship between green supply chain management and performance: a meta-analysis of empirical evidences in Asian emerging economies. *Int J Prod Econ* 183:245–258
16. Ghisellini P, Cialani C, Ulgiati S (2016) A review on circular economy: the expected transition to a balanced interplay of environment and economy system. *J Clean Prod* 114:11–32
17. Gorane SJ, Kant R (2013) Modelling the SCM enablers: an integrated ISM-fuzzy MICMAC approach. *Asian Pac J Mark Logistics* 25(2):263–286
18. Govindan K, Hasanagic M (2018) A systematic review on driver, barrier, and practices towards circular economy: a supply perspective. *Int J Prod Res* 56(1–2):278–311
19. Guo B, Geng Y, Ren J, Zhu L et al (2017) Comparative assessment of circular economy development in China's four megacities: the case of Beijing, Chongqing, Shanghai, and Urumqi. *J Clean Prod* 162:234–246
20. Haas W, Krausmann F, Wiedenhofer D, Heinz M (2015) How circular is the global economy? An assessment of material flows, waste production, and recycling in the European Union and the world in 2005. *J Ind Ecol* 19:765–777
21. Jabbour CJC, Jabbour ABL (2016) Green human resource management and green supply chain management: linking two emerging agendas. *J Clean Prod* 112:1824–1833
22. Jaeger-Erben M, Jensen C, Hofmann F, Zwiers J (2021) There is no sustainable circular economy without a circular society. *Resour Conserv Recycl* 168:105476

23. Jakhar DT, Nain S, Jakhar N (2018) Effect of plant growth regulator on growth yield and quality of tomato (*Solanum lycopersicum*) cultivar "Shivaji" under Punjab condition. *Int J Curr Microbiol Appl Sci* 7:2630–2636
24. Jelinski LW, Graedel TE, Laudise RA, McCall DW, Patel CKN (1992) Industrial ecology: concepts and approaches. *Proc Nat Acad Sci* 89:793–797
25. Kalmykova Y, Sadagopan M, Rosado L (2018) Eco-innovation in the transition to circular economy: an analytical literature review. *J Clean Prod* 172:2999–3018
26. Kazancoglu Y, Kazancoglu L, Sagnak M (2018) A new holistic conceptual framework for green supply chain management performance based on circular economy. *J Clean Prod* 195:1282–1299
27. Kirchherr J, Reike D, Hekkert M (2017) Conceptualizing the circular economy: an analysis of 114 definitions. *Resour Conserv Recycl* 127:221–231
28. Kirchherr J, van Santen R (2019) Research on circular economy: a critique of the field. *Resour Conserv Recycl* 151:104480
29. Kumar P, Singh RK, Kumar V (2021) Managing supply chain for sustainability operations in the era of industry 4.0 and circular economy: analysis of barriers. *Resour Conserv Recycl* 164:105215
30. Kumar N, Tyagi M, Garg RK, Sachdeva A, Panchal D (2021) A framework development and assessment for cold supply chain performance system: a case of vaccines. *operations management and systems engineering. Lecture notes on multidisciplinary industrial engineering*. Springer, Singapore, pp 339–353. [https://doi.org/10.1007/978-981-15-6017-0\\_22](https://doi.org/10.1007/978-981-15-6017-0_22)
31. Kumar N, Tyagi M, Sachdeva A (2021) Depiction of possible solutions to improve the cold supply chain performance system. *J Adv Manage Res*. <https://doi.org/10.1108/JAMR-10-2020-0285>
32. Lahane S, Kant R, Shankar R (2020) Circular supply chain management: a state-of-art review and future opportunities. *J Cleaner Prod* 258:120859
33. Lewandowski M (2016) Designing the business model for circular economy—toward the conceptual framework. *Sustainability* 8:43
34. Li H, Bao W, Xiu C et al (2010) Energy conservation and circular economy in China's process industries. *Energy* 35(11):4273–4281
35. Li CW, Tzeng GH (2009) Identification of threshold value for the DEMATEL method using the maximum mean de-entropy algorithm to find critical services provided by a semiconductor intellectual property mall. *Expert Syst Appl* 8(1):9891–9898
36. Lieder M, Rashid A (2016) Toward circular economy implementation: a comprehensive review in context of manufacturing industry. *J Clean Prod* 115:36–51
37. Lopes de Sousa Jabbour AB, Rojas Luiz JV, Rojas O et al (2019) Circular economy business models and operations management. *J Cleaner Prod* 235:1525–1539
38. Malinauskaite J, Jouhara H, Czajczyńska D, Stanchev P, Katsou E et al (2017) Municipal solid waste management and waste-to-energy in the context of a circular economy and energy recycling in Europe. *Energy* 141:2013–2044
39. Mangla SK, Luthar S, Mishra N, Singh A, Rana NP et al (2018a) Barriers to effective circular economy supply chain management in a developing country context. *Prod Planning Control* 29:551–569
40. Mathews JA, Tan H (2011) Progress toward a circular economy in China. *J Ind Ecol* 15:435–457
41. Murray A, Skene K, Haynes K (2017) The circular economy: an interdisciplinary exploration of the concept and application in global context. *J Bus Ethics* 140(3):369–380
42. Naustdalid J (2014) Circular economy in China—the environment at dimension of the harmonious society. *Int J Sustain Dev Word Ecol* 21:303–313
43. Neligan A (2018) Digitalisation as enabler towards a sustainable circular economy in Germany. *Intereconomics* 53(2):101–106
44. Nelles M, Gruenes J, Morscheck G (2016) Waste management in Germany—development to a sustainable circular economy? *Procedia Environ Sci* 35:6–14
45. Ness D (2008) Sustainable urban infrastructure in china: toward a factor 10 improvement in the resource productivity through integrated infrastructure system. *Int J Sust Dev World* 15:288–301

46. Ocampo LA, Tan TAG, Sia LA (2018) Using fuzzy DEMATEL in modeling the casual relationship of the antecedents of organizational citizenship behavior (OCB) in the hospitality industry: a case study in the Philippines. *J Hospitality Tourism Manage* 34:11–29
47. Ormazabal M, Prieto-Sandoval V, Puga-Leal R, Jaca C (2018) Circular economy in Spanish SMEs: challenges and opportunities. *J Clean Prod* 185:157–167
48. Papadopoulos A, Giama E (2007) Environmental performance evaluation of thermal insulation material and its impact on the building. *Build Environ* 42:2178–2187
49. Pauli GA (2010) The blue economy. Available at: [https://www.jef.or.jp/journal/pdf/175th\\_cover04.pdf](https://www.jef.or.jp/journal/pdf/175th_cover04.pdf)
50. Paulraj A, Chen IJ, Blome C (2017) Motives and performance outcomes of sustainable supply chain management practices: a multi-theoretical perspective. *J Bus Ethics* 145:239–258
51. Pham TT, Kuo TC, Tseng ML, Tan RR et al (2019) Industry 4.0 to accelerate the circular economy: a case study of electric scooter sharing. *Sustainability* 11:1–16
52. Pourjavad E, Shahin A (2018) The application of Mamdani fuzzy inference system in evaluating green supply chain management performance. *Int J Fuzzy Syst* 20:901–912
53. Razminiene K (2019) Circular economy in cluster performance evaluation. *Equilibrium* 14(3):537–559
54. Rizos V, Behrens A, van der Gaast W, Hofman E et al (2016) Implementation of circular economy business models by small and medium-sized enterprises (SMEs): barrier and enablers. *Sustainability* 8(11):1212
55. Roy FO, Benson D, Monciardini D (2019) Going around in circles? Conceptual recycling patching and policy layering in the EU circular economy package. *Environ Polit* 29:983–1003
56. Saberi S, Kouhizadeh M, Sarkis J (2018) Blockchain technology and its relationship to sustainable supply chain management. *Int J Prod Res* 57(7):2117–2135
57. Sarkis J (2003) A strategic decision framework for green supply chain management. *J Cleaner Prod* 11:397–409
58. Schröder P, Lemille A, Desmond P (2020) Making the circular economy work for human development. *Resour Conserv Recycl* 156:104686
59. Shàrma VK, Chandna P, Bhardwaj A (2017) Green supply chain management related performance indicator in agro industry: a review. *J Clean Prod* 141:1194–1208
60. Stahel WR, Reday G (1976) The potential for the substituting manpower for energy report to the commission of the European communities, Brussels, no 76. Battelle, Geneva Research Centre, Geneva, Switzerland, pp 109–113
61. Tsai WH, Chou WC (2009) Selecting management systems for sustainable development in SMEs: a novel hybrid model based on DEMATEL, ANP, and ZOGP. *Expert Syst Appl* 36(2):1444–1458
62. Tukker A (2015) Product services for a resources-efficient and circular economy a review. *J Clean Prod* 97:76–91
63. Tyagi M, Kumar P, Kumar D (2014) Assessment of critical enablers for flexible supply chain performance measurement system using fuzzy DEMATEL approach. *Glob J Flex Syst Manag* 16(2):115–132
64. Tzeng GH, Chiang CH, Li CW (2007) Evaluating intertwined effect in e-learning program: a novel hybrid MCDM model based on factor analysis and DEMATEL. *Expert Syst Appl* 32(4):1028–1044
65. Wang JY (2014) The organization of SMEs innovation research based on circular economy. *Appl Mech Mater* 675–677:1846–1850
66. Wu KJ, Liao CJ, Tseng ML et al (2015) Exploring decisive factors in green supply chain practices under uncertainty. *Int J Prod Econ* 159:147–157
67. Xue J, Liu G, Casazza M, Ulgiati S (2018) Development of an urban FEW nexus online analyzer to support urban circular economy strategy planning. *Energy* 164:475–495
68. Yaduvanshi NR, Myana R, Krishnamurthy S (2016) Circular economy for sustainable development in India. *Indian J Sci Technol* 9(46):1–9
69. Yap NU (2005) Toward a circular economy: progress and challenge. *Green Manage Int* 50:11–24



70. Yong R (2007) The circular economy in China. *J Mater Cycles Waste Manage* 9(2):121–129
71. Yuan Z, Bi J, Moriguchi Y (2006) The circular economy: a new development strategy in China. *J Ind Ecol* 10:4–8
72. Zadeh LA (1965) Fuzzy set. *Inf Control* 8(3):338–353
73. Zhao Y, Zang L, Li Z, Qin J (2012) Discussion on the model of mining circular economy. *Energy Procedia* 16:438–443
74. Zhijun F, Nailong Y (2007) Putting a circular economy into practice in china. *Sustainability* 2:95–101

# Multi-criteria Assembly Line Design and Configuration Using Heuristics—An Automotive Case Study



Rajeev Singh Rawat, Anish Sachdeva, Mohit Tyagi, and Dilbagh Panchal

**Abstract** This paper is based on the case study of an automotive component production assembly line that was undertaken in order to design an efficient version of the assembly line against multiple user-defined criteria. Some of the criteria used in the design are investment cost, machine utilization, operator utilization, availability and annual production volume. The productivity of an assembly line is directly influenced by determining a company's position in the market. The production line's balance would undoubtedly aid personnel and facilities in increasing operational efficiency. The design of a manufacturing line is a difficult and complex problem to tackle. Computer simulation and modelling optimize and predict the layout of the production line, and it can shorten the R&D cycle. The method is evaluated and tested on this case study, inspired by a real automotive assembly line.

**Keywords** Line balancing · Heuristics · Simulation · Wheel assembly line

## 1 Introduction

An assembly line is a part of a manufacturing facility where a series of identical goods are constructed in a sequential order. A basic assembly line is made up of workstations that are linked together by material handling equipment. On an assembly line, a workstation is a location where a portion of the overall assembly job is completed. An assembly line's workstations are allocated distinct jobs or operations and are equipped with the essential supplies, machinery, workers, and even robotic arms. The part will be delivered to the subsequent station by material handling equipment once operation is done, and the next station will execute the assigned operation. These steps are continued until the desired outcome is obtained. Operation time is

---

R. S. Rawat · A. Sachdeva

Department of Industrial and Production Engineering, Dr. B.R. Ambedkar National Institute of Technology, Jalandhar, Punjab, India

M. Tyagi (✉) · D. Panchal

Mechanical Engineering Department, National Institute of Technology, Kurukshetra, India  
e-mail: [mohitmied@gmail.com](mailto:mohitmied@gmail.com)

taken to perform one operation at a workstation, whereas cycle time refers to time taken to complete all operations at the workstation.

## 2 Literature Review

The purpose of this section is to provide a brief review of available research work related to assembly line balancing. Bryton [5] was the first to propose the concept of line balance. However, Salveson [11] presented the first published work on the ALBP. In this, assembly line has a satisfactory precedence relationship and appropriate effectiveness measures are defined. Assembly line balancing was established with the purpose of ensuring that an assembly line has a satisfactory precedence relationship and appropriate effectiveness measures (e.g. line efficiency enhancement, productivity increment, reduction of idle time and balance delay minimization). Jamil and Razali [9] provide the improved production rate and efficiency in this study, and two assembly line improvement layouts were successfully proposed.

According to Pekin, to this study to manufacture a product in an assembly line, the total work must be divided into a set of elementary operations. Fleszar [6] presented a study on enumerative reduction and heuristic methods for the ALBP. For the type I assembly line balance problem, they presented a new reduction techniques and new heuristic algorithm. The aim of this reduction techniques to improve combine activities, precedence and speed up operations. A test on a well-known benchmark set of problem instances testifies to the combined algorithm's efficiency [1]. The goal of the project was to reduce the cost of the line that was being designed. As well as research on reduction approaches for a generalized ALBP, a heuristic-based guidance for the enumeration process required an efficient component for algorithm.

## 3 Classification of ALBP (Assembly Line Balancing Problems)

According to Baybars [2], in the ALBP, there are various problems. This is one of the possible classifications, in which he differentiates between two classical problems: the general (GALP) and simple (SALBP).

### 3.1 SALBP (*Simple Assembly Line Balancing Problem*)

Boysen et al. [3] and Scholl and Becker [12]: In this study the simple assembly line balancing problem is the basic optimization problem in assembly line balancing

research. A set of tasks with deterministic task times is given. The SALBP can be classified based on its objective.

*SALBP 1:* To attain a desired cycle time, reduce the number of workstations.

*SALBP 2:* To achieve the desired number of workstations, minimize the cycle time.

*SALBP E:* The line efficiency maximizes by minimizing the cycle time and number of workstations simultaneously.

*SALBP F:* To estimate the feasibility of balancing an assembly line for cycle time and given number of combination of workstations.

### 3.2 GALBP (*General Assembly Line Balancing Problem*)

*Bryan Pearce* [4]: GALPs are problems that are not addressed by SALBP. For example, when if there are parallel stations, process's time is variable and so on. There are four types of GALBP:

*MOALBP (multi-objective assembly line balancing problem):* In these problems, various objectives are considered at the same time, such as minimizing number of stations and the total cost, maximizing the line's efficiency and so on.

*RALBP (robotic assembly line balancing problem):* That problem appears when the allocation of a robot and task allocation to each workstation are evaluated in order to improve the efficiency of the tasks in assembly line.

*MALBP (mixed-model assembly line balancing problem):* This type of problem occurs when same product but consider various models, then have a set of basic operations that are followed on all models, independent of setup time.

*UALBP (U-line assembly line balancing problem):* The difference between a serial line and a UALBP is that which task predecessors have already been assigned a serial line can only assign them, whereas the UALBP can assign tasks whose successors or predecessors have already allocated. It means the stations can be assigned in such a way that they can manage two components at the same time in different positions of the line throughout the same cycle time.

## 4 Research Methods

### 4.1 Heuristic Methods

Fleszar [6] presented a study on enumerative reduction and heuristic methods for the ALBP. For the type I assembly line balance problem, they presented a new reduction

technique and a new heuristic algorithm. The new method is based on Hoffmann's heuristic and chooses the appropriate solution from each side of precedence network.

The heuristic method is defined as a problem-solving strategy in which the approach is simply to achieve rational solutions, and it can be used to solve line balance. The assembly line balance problem is based on a complex set of considerations and assumptions, because there is no absolute solution. However, researchers have used it in various case studies. Some heuristic procedures are selected for assembly line balancing.

#### 4.1.1 KWM (Kilbridge and Wester Method)

Kilbridge and Wester [10] proposed this heuristic method. The objective is to select tasks and distribute them to workstations based on their position in the precedence diagram. Tasks with identical precedence must be organized in columns in the prepared precedence diagram.

#### 4.1.2 RPW (Ranked Position Weight Technique)

Helgeson and Birnie [8] introduced this technique. RPW is a heuristic approach for assigning tasks to workstations based on their positional weightage. Positional weight is the sum of the task processing time and all of its successors' processing times.

## 5 Terms in Line Balancing Technique

**Cycle time** is total time to producing an item, and it can be said as the sum of all task time

$$CT = \sum_{i=0}^K TT_i \quad (1)$$

where  $TT_i$  = Task time of Task  $i$

$K$  = Total number of tasks.

**Range** is difference between the maximum and minimum task time

$$\text{Range} = TT_{\max} - TT_{\min} \quad (2)$$

where  $TT_{\max}$  = Maximum task or process time

$TT_{\min}$  = Minimum task or process time.

**Allowance** is described as any unavoidable additional delays that must be added to the operation’s basic time.

$$\text{Allowance} = \frac{CT_{\min} - \sum TT_{\min}}{\sum \text{Range}} \times \text{Range}_i \tag{3}$$

$$\text{Standard task or process time} = TT_{\min} + \text{Allowance} \tag{4}$$

$$\text{Standard workstation time} = \sum_{i=0}^k TT_i \tag{5}$$

where  $\text{Range}_i =$  Range of Task  $i$

$CT_{\min} =$  Minimum cycle time.

$k =$  Total number of workstation.

The **rate of production** is the rate at which products are produced.

$$\text{Rate of production} = \frac{\text{Total productivity per day}}{\text{Total running hour per day}} \tag{6}$$

The degree to which the assembly line’s resources, including capital resources and human, are utilized strategically and effectively is referred to as **line efficiency**.

$$\text{Line efficiency} = \frac{SCT}{SWT_{\max} \times k} \tag{7}$$

where  $SWT_{\max} =$  Maximum standard workstation time

$SCT =$  Standard cycle time.

The relative smoothness of the assembly line is measured by the **smoothness index**. A smoothness value of 0 indicates perfect equilibrium [7].

$$\text{Smoothness index} = \sqrt{\sum_{i=1}^k (SWT_{\max} - SWT_i)^2} \tag{8}$$

where  $SWT_i =$  Standard workstation time of Workstation,  $i$ .

## 6 Case Study

The wheel assembly process is divided into multiple workstations, each of which performs a number of processes, and each of which is assigned an alphabetical designation as indicated in Table 1.

A well-calibrated professional stopwatch was utilized to conduct the time study. Each step was timed accurately and without delay, and 40 samples were taken. The cycle time for each batch of samples was then calculated using Eq. 1. The minimum task duration for each process was established, and the range was calculated using Eq. 2. The allowance and standard time were calculated using Eqs. 3 and 4, respectively. The results of each computation are shown in Table 2.

According to the process analysis, the existing assembly line has eight workstations and each of which is operated by one well-trained and skilled operator. Table 3 depicts the responsibilities given to each operator at each workstation and standard workstation time of each workstation.

The standard task time derived from time study was allocated to each task in this model. The model was run for 28,800 s, which is the total time of the assembly line runs in a shift. Simulation shown in Fig. 1 results, assembly line is producing 1179 units in 8 h. However, Fig. 2 shows the process ideal, processing and idle time and Fig. 3 shows the details of operator utilization and idle data.

**Table 1** Process and descriptions

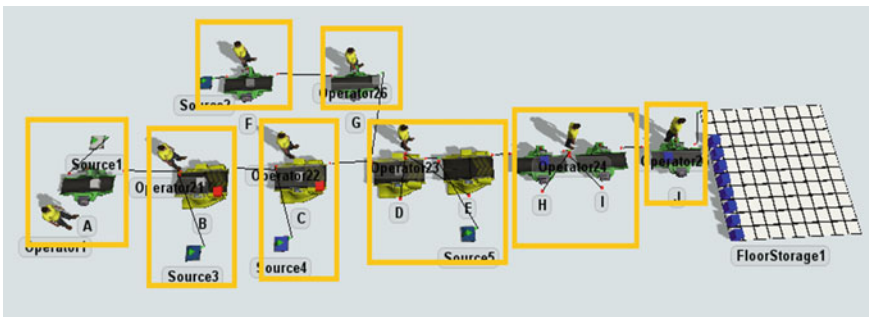
Notation	Process	Description
A	Unloading and inspection of alloy painted rim	Unload the painted rim from conveyor and check for paint and other defects on rim and then put on trolley
B	Seal press on rim	Rim set on hydraulic press and assemble seal on rim
C	Tyre mounting on rim	Rim clamp on tyre mounting and then tyre mount on rim
D	Fitting 'O' ring on rim	A black O shape rubber ring fit on rim
E	Tyre inspection and leakage checking	Inspect tyre visually and submerged tyre in water and check leakage on tyre
F	Apply vegetable soap on tyre	Apply vegetable soap on tyre for lubrication at the time of mounting
G	Air filling in tyre	Put wheel on spindle and fill air on tyre
H	Runout of wheel	Check radial and lateral runout on linear variable differential transformer (LVDT) machine
I	Pre-delivery inspection	It is final inspection of tyre before delivery
J	Tyre mounting on rim	Rim clamp on tyre mounting and then tyre mount on rim

**Table 2** Current assembly line standard time

Process	Tmin	Tmax	Range	Allowance	Standard process time
A	12.22	13.8	1.57	0.44	12.67
B	17.63	23.59	5.96	1.68	19.31
C	14.18	16.97	2.79	0.79	14.97
D	19.31	21.74	2.43	0.69	20
E	3.29	5.91	2.62	0.74	4.03
F	14.17	16.97	2.8	0.79	14.96
G	8.28	10.96	2.68	0.76	9.03
H	8.16	9.99	1.83	0.52	8.67
I	12.13	13.88	1.75	0.49	12.62
J	10.01	12.91	2.89	0.82	10.83
CT	119.38	146.72	27.33	7.7	Standard cycle time = 114.72

**Table 3** Workstations and operators involved in process

Workstations	Operator	Process	Standard workstation time (s)
1	O1	A	12.67
2	O2	B	19.31
3	O3	C	14.97
4	O4	D, E	24.03
5	O5	F	14.96
6	O6	G	9.03
7	O7	H, I	21.29
8	O8	J	10.83



**Fig. 1** Current assembly line workstation simulation model



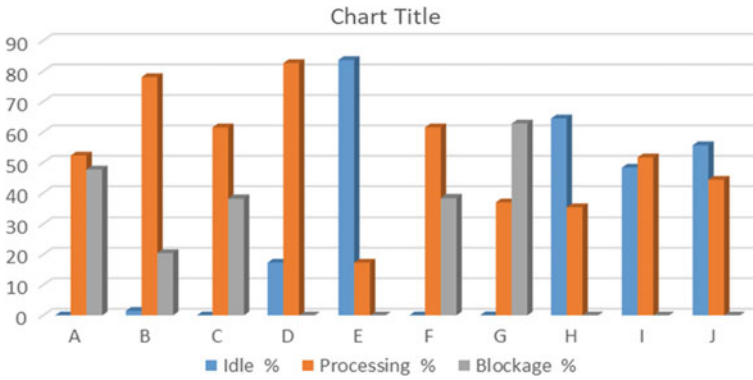


Fig. 2 Current assembly line process

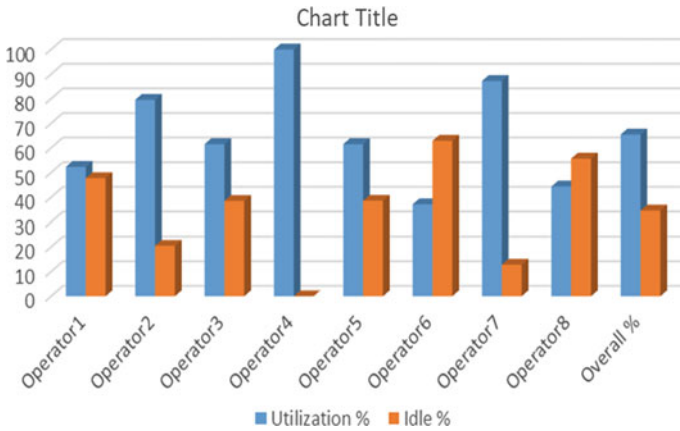


Fig. 3 Current assembly line operator

### 6.1 Root Cause Analysis

Analysing and examining the data from the present assembly line methodically in order to find the main cause. The overall percentage of blocking is 33.89%, the overall percentage of process idle is 22.56%, and the overall percentage of processing is 43.62%, according to the findings. The line efficiency is 44.07%, while the smoothness index is 26.87. The assembly line has been identified as having an uneven Workstation time and an asymmetrical workload result in a low line efficiency and a poor smoothness index. As a result, assembly line balancing is essential to reduce the workload and workstation time of the operators. Then, all factors of overall performance can be improved.

## 7 Assembly Line Balancing

Assembly line balance is a production technique that establishes a target rate of production in order to produce a specific product in a specific amount of time. The assembly line must be well-designed, with jobs allocated among employees, machines and workstations to ensure that all line segments in the production process are completed within the time frame.

### 7.1 KWM Assembly Line Balancing

Limit the precedence diagram so that nodes representing processes with comparable priority are arranged in columns vertically. This is demonstrated in Fig. 4. Then, tasks are assigned to workstations using the KWM approach as described in Table 4.

The KWM assembly line model was run for 28,800 s, which is the total time of the assembly line runs in a shift. Simulation shown Fig. 5 the result, assembly line is producing 1210 units in 8 h. Figure 6 shows process ideal, processing and idle time, and Fig. 7 shows the data of operator utilization and idle data.

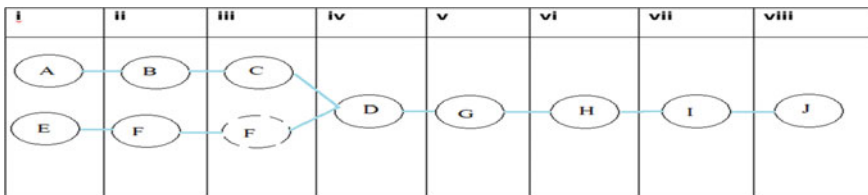


Fig. 4 KWM precedence diagram, process divided in column

Table 4 KWM process assigning to workstation

Workstation	Operator	Process	Standard workstation time (s)
W1	O1	A	12.67
W2	O2	B	19.31
W3	O3	C, G	24
W4	O4	F	14.96
W5	O5	D	20
W6	O6	E, H	12.7
W7	O7	I, J	23.45

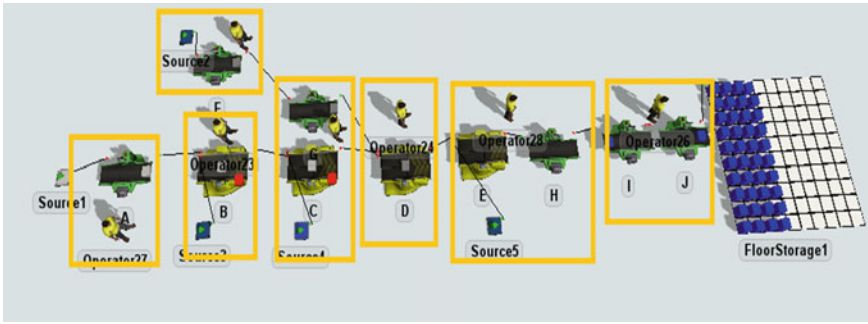


Fig. 5 KWM modified assembly line workstation simulation model

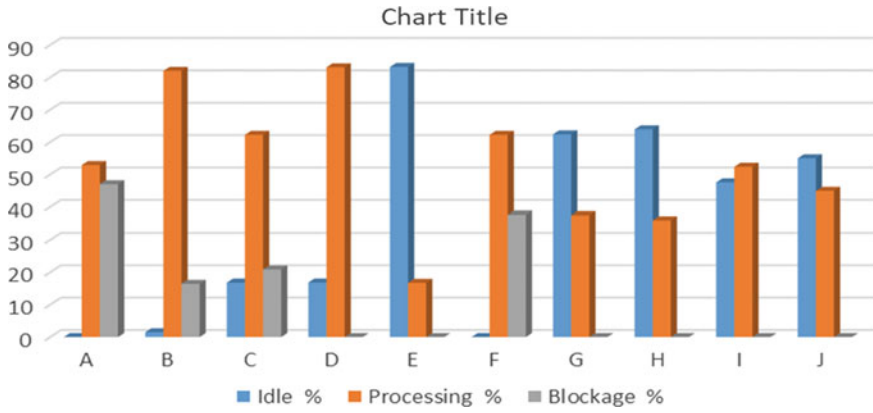


Fig. 6 Current assembly line process using KWM method

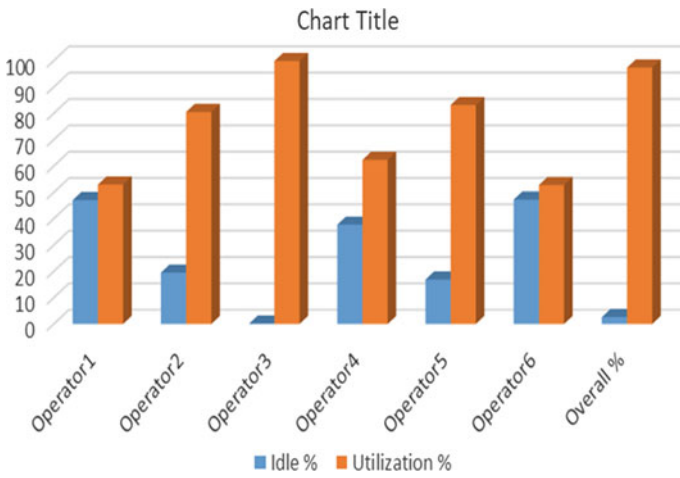
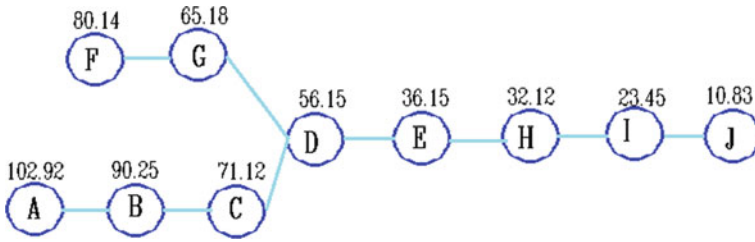


Fig. 7 Current assembly line operator using KWM Method



**Fig. 8** RPW assembly line precedence diagram with positional weight

**Table 5** RPW process assigning to workstation

Workstation	Operator	Process	Standard workstation time (s)
W1	O1	A, G	21.7
W2	O2	B, E	23.34
W3	O3	C	14.97
W4	O4	F, H	23.63
W5	O5	D	20
W6	O6	I, J	23.45

### 7.2 RPW Technique Assembly Line Balancing

On the present assembly line, the Ranked Position Weight (RPW) approach is used. Begin by drawing the precedence diagram as shown in Fig. 8.

Determine the weight of each task process’s location. It is the total amount of time spent on the network’s longest path from the start to the finish. The results of process assignment using the RPW approach are shown in Table 5.

The model was run for 28,800 s, which is the total time of the assembly line runs in a shift. Simulation shown Fig. 9 the result, assembly line is producing 1195 units in 10 h. Figure 10 shows the process ideal, processing and idle time, and Fig. 11 shows the data of operator utilization and idle data.

## 8 Results and Discussion

Table 6 summarizes the previous sections’ information on the present assembly line, as well as the RPW and KWN modified assembly lines. Based on the observation, the data of the two modified assembly line versions has been significantly improved.

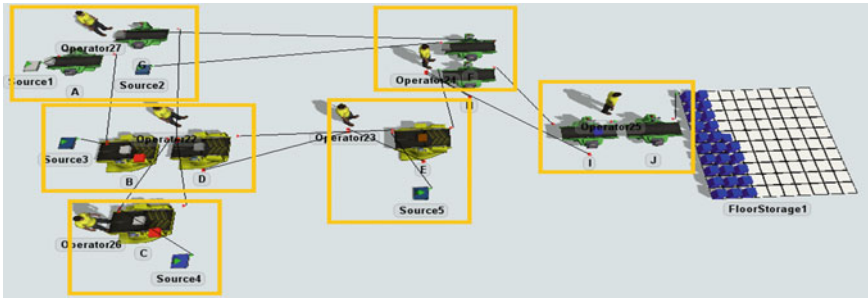


Fig. 9 RPW modified assembly line workstation simulation model

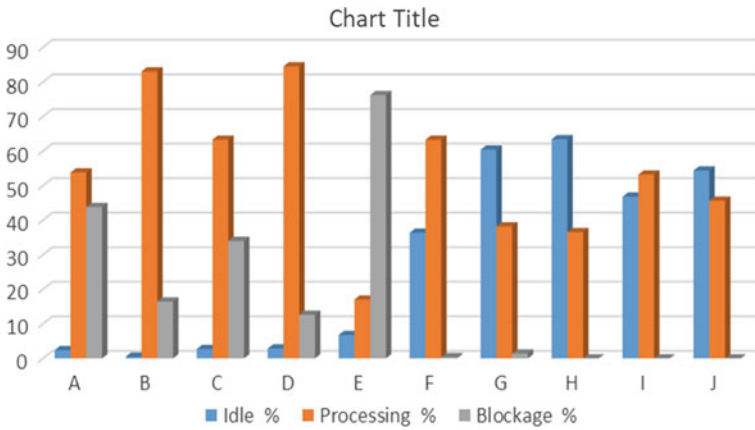


Fig. 10 Current assembly line process using RPW method

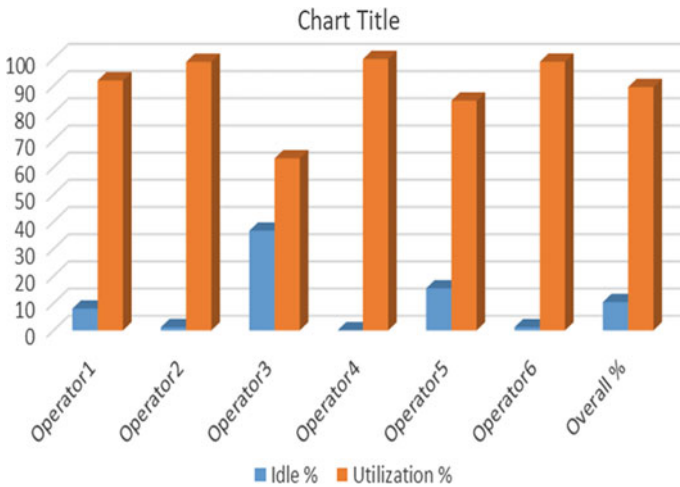


Fig. 11 Current assembly line operator using RPW Method

**Table 6** Data comparison table of modified versions and current of assembly line

	RPW	KWM	Current
Number of workstation	6	7	8
Number of operator	6	7	8
Line efficiency %	89.63	75.64	44.07
Smoothness index	9.59	19.39	26.87
Overall blockage %	21.11	21.01	33.89
Overall process idle %	34.11	34.9	22.61
Overall processing %	44.77	44.07	43.62
Overall operator utilization %	89.54	75.55	65.44
Overall operator idle %	10.43	24.44	34.56
Total production/shift	1210	1195	1179

## 9 Conclusion

The existing wheel assembly line was conducted to a root cause analysis. The assembly line showed an unequal allocation of workstation time among the workstations, as well as an unequal burden for the operators. Among all the variations, the Ranked Position Weight (RPW) upgraded version assembly line was chosen as the proposed assembly line. The planned assembly line has only six operators and workstations, compared to eight operators and workstations on the current production line. In addition, the assembly line's performance has been enhanced.

Furthermore, the manufacturing process is one of the most essential components in obtaining high production efficiency. While providing high-quality assembly and fabrication, a well-designed manufacturing process saves time, money and resources. As a result, a process optimization analysis is strongly advised. Finally, as technology progresses, assembly line technologies such as computer-integrated manufacturing, automated packing systems, robotic assembly arms and automated conveying systems are implemented to improve performance.

## References

1. Battaia O, Alexandre D (2012) Reduction approaches for a generalized line balancing problem. *Comput Oper Res* 39(10):2337–2345
2. Baybars I (1986) An efficient heuristic method for the simple assembly line balancing problem. *Int J Prod Res* 24(1):149–166
3. Boysen N, Flidner M, Scholl A (2007) A classification of assembly line balancing problems. *Eur J Oper Res* 183(2):674–693
4. Bryan Pearce (2015) A study on general assembly line balancing modeling methods and techniques. Diss. Clemson University
5. Bryton B (1954) Balancing of a continuous production line. M.S. Thesis, Northwestern University, Evanston, IL, USA

6. Fleszar MF (2003) Thermal effusivity as a non-destructive method to characterize thin films. Army armament research development and engineering center watervliet NY Benet Labs
7. Grzechca W, Foulds LR (2015) The assembly line balancing problem with task splitting: a case study. *IFAC-Papers OnLine* 48(3):2002–2008
8. Helgeson WB, Birnie DP (1961) Assembly line balancing using the ranked positional weight technique. *J Ind Eng* 12(6):394–398
9. Jamil M, Razali N (2016) Simulation of assembly line balancing in automotive component manufacturing. *IOP Conf Ser: Mater Sci Eng* 114:012049
10. Kilbridge MD, Wester L (1961) A heuristic method of assembly line balancing. *J Ind Eng* 12(4):292–298
11. Salveson ME (1955) The assembly-line balancing problem. *Trans Am Soc Mech Eng* 77(6):939–947
12. Scholl A, Becker C (2006) State-of-the-art exact and heuristic solution procedures for simple assembly line balancing. *Eur J Oper Res* 168(3):666–693

# A Postural Risk Assessment of Manual Dairy Farm Workers Using REBA Technique



Umesh Gurnani, Sanjay Kumar Singh, Manoj Kumar Sain,  
and M. L. Meena

**Abstract** Postural assessment plays a vital role to find out the causes of musculoskeletal fatigue endured by the human body due to awkward bending, kneeling, twisting and material handling during different manual activities. Various ergonomic tools like REBA, RULA, OWAS, NIOSH equation, OSHA, JSI and JSA have been used frequently to calculate the risk level faced by workers in different sectors where the workers are prone to uncomfortable movement of various body parts repeatedly. Unendurable level of stress, strain and over-exertion of load may lead to musculoskeletal disorders with serious injuries. Most of the dairy farms in India are still not modernized, and therefore, manual work with traditional hand tools and techniques is preferred. Manual work in awkward posture with traditional methods led to various musculoskeletal health issues among dairy farm workers. The aim of present investigation is to study and find the level of MSDs and risk score among manual dairy farm workers and suggest remedial measures for high risk factors. Rapid Entire Body Assessment technique is used to assess the posture of farm workers in dairy industry.

**Keywords** Dairy farming · Musculoskeletal disorders · Manual material handling · REBA technique

---

U. Gurnani (✉)

Department of Mechanical Engineering, University of Engineering and Management, Jaipur, India  
e-mail: [gurnani.123@gmail.com](mailto:gurnani.123@gmail.com)

U. Gurnani · S. K. Singh

Department of Electrical and Electronics Engineering, Amity University Rajasthan, Jaipur, India

M. K. Sain

Department of Mechanical Engineering, Swami Keshvanand Institute of Technology, Management and Gramothan, Jaipur, India

M. L. Meena

Department of Mechanical Engineering, Malaviya National Institute of Technology, Jaipur, India



## 1 Introduction

Different occupational activities performed by dairy farm workers lead to musculoskeletal risk and serious injuries caused by heavy load lifting and repetitive muscle movement in awkward postures. Since dairy industry in India has engrossed a value of 11 billion in 2020 and India is already having a milk production of about 20% of the total global output (IMARC report), it becomes necessary to improve the health of dairy farm workers and reduce unnecessary efforts. REBA, RULA, OWAS, NIOSH equation, OSHA, JSI and JSA are the common assessment tools used to calculate the risk level of workers in various industries. Application of Rapid Entire Body Assessment (REBA) technique helps to identify and quantify the fatigue developed in dairy farming tasks [15]. REBA investigates the risk factors developed in human body associated with postures of neck, trunk, legs, upper arm position, lower arm and wrist position. The standard chart of REBA helps to analyze the working posture of human body accounting pictures and video recordings and generate reports based on the bending, kneeling and lifting angles created by the body parts with respect to normal [16]. The scores can be evaluated for every worker which helps to identify the individuals whose working postures are more prone to musculoskeletal disorders and injuries. With results obtained by REBA, the tasks are to be further assessed and redesigned to improve the probability of MSDs developed in occupational activities [4]. From ergonomics point of view, the muscular pain might be bearable but over a span of time, it may result in serious injuries depending on the scale of exertion tolerated by an individual.

## 2 Research Background

The musculoskeletal health-related research work among manual dairy farm workers is very less reported. However, a sufficient amount of research has been done in other similar sectors. According to [10], occupational risk and injuries affect the work productivity and the cost of business around the world. They have assessed the demographic factors like gender, age, experience, education, height and weight on ergonomic risk and occupational injuries using REBA analysis and Quick Exposure Check (QEC). Jain et al. [5] studied the factors influencing MSDs using logistic regression on a data of 138 manual farm workers using Nordic equation and RULA score. The study reveals significant occurrence of MSDs in lower back (71.4%), fingers (62.1%) and shoulders (56.4%) associated with age, daily working duration, work experience in farms, fatigue developed and the hand muscle movements.

According to Jain et al. [5], an investigation on harvesting farmers of Rajasthan using RULA assessment technique shows the effect of increasing age, farming experience, hand tool design and body mass index on the occurrence of MSDs in human body. The results state that MSDs are prevalent in more than 50% of the farmers in one or more body parts.

Sain et al. [14] conducted a similar study in brick kiln industry using modified Nordic equation and logistic regression where the results showed 76.19% workers prone to MSDs who were involved in mold evacuating task. 62.35% workers reported wrist and lower back issues who were involved in spading task. Workers with more than five years of experience in kiln industry were also prone to neck muscular disorders. Enez and Nalbantoğlu [2] conducted a study for an auto parts manufacturer. The results confirmed that the information gathered from Data Envelopment Analysis is reliable with REBA and QEC, which focus on the role of education, experience and weight in reducing the ergonomic risks.

According to Zubar and Alamoudi [19], a number of operations in a bearing manufacturing industry like honing, laser cutting, face grinding, rib grinding, laser marking, roller filing, hard turning, slushing and visual inspection indulge ergonomic risk at various levels. Many workstations in a manufacturing industry may not be ergonomically designed. Authors insisted to add application of anthropometry in different occupational tasks in manufacturing industry to develop ergonomically designed tools and workplace. REBA scores were obtained for different activities, and the most stressful tasks were categorized to be resolved by better administrative controls like rest pauses and job rotation to reduce the stress level of employees and control ergonomic risks.

Reyes-zárate and Garcia-cavazos [13] used the application of Microsoft Kinect V2 hardware on database of workers and their posture images in wireframe model in a textile garment industry in Monterrey (Mexico). The Kinect movement sensor helped to capture the human body movements and represent them in X, Y, Z coordinates in 3D plane. RGB color, depth map, infrared image and graphical representation of skeleton through Kinect helped to gather the accurate data for REBA. After analyzing the REBA scores, remedial measures were taken on existing workstation by providing the workers with an inclined wooden support to help them improve the trunk and neck posture thereby reducing the REBA score from 7 to 2 and enhancing the efficiency of workers.

Haekal et al. [3] conducted a study on the workers who are involved in extreme load carrying, lifting, pick and place of freight, pulling and pushing of hand pallet and packaging activities in a pharmacy warehouse of Indonesia. The load lifting varied from 5 to 100 Kgs for an individual worker and for certain activities like lifting the carton from container causes the body to bend by  $102^\circ$  to generate support and results in uncomfortable posture for the workers. Using Nordic questionnaire, the posture data of workers was analyzed, and using REBA technique, scores were generated for workers engaged in completion of different activities. The scores of majority of workers were beyond 9, which enforced them to make improvements in existing workstation design by rearranging the packaging material according to sequence of activities, reducing load on pallet, use of portable ladder for objects to be placed at heights and goods delivery in slots to manage space constraint issues. Above all, the training and learning sessions were suggested for workers to improve their working capabilities and productivity of the organization and resolve health issues of workers.

Yu et al. [18] confirmed the use of JVEC (Joint-Level Vision-Based Ergonomic Assessment) tool in extraction of skeleton data from pictures and videos of construction workers using deep learning methods and the implementation of 2D and 3D pose estimation algorithms for obtaining the final results of musculoskeletal disorder cases among survey participants. Kulkarni and Devalkar [8] used the concept of REBA and RULA assessment techniques for construction industry workers who are repeatedly involved in load lifting and over-exertion and experience increased fatigue after a certain span of age. The authors aimed at calculation of risk level of workers and suggest corrective measures to resolve it.

The authors worked on development and improvement of hand tools to resolve work-related health problems in the field of agriculture. The researchers focused on product manufacturing and quality variables for improvement in hand tools along with consideration of variables, from the view of an operator and the particular task to be performed with that tool [6]. This even enhanced an increased scope of research in the field where traditional methods of working are being employed. Arendra et al. [1] assessed the ergonomic risks involved by salt evaporation field workers in Indonesia. The application of esMOCA sensor hardware helped them to record the muscle movements of upper limb thereby using the data for assessment through REBA and RULA techniques. The authors worked on redesigning of work tools for pick and place of rock salt which was the one resulting in heavy ergonomic risks according to their study. The workstation redesign and the work tool redesign help to control ergonomic risks up to a huge extent and reduce injuries developed due to MSDs [15].

Lowe et al. [9] studied on a web-based survey conducted for ergonomic practitioners over the importance and demands of work postures and through various tools and observational techniques including the strain index and stress in upper extremities using REBA and RULA techniques. The survey was mainly conducted in Canada, Great Britain, Australia and New Zealand with 1221 eligible participants to develop better ways of ergonomic assessment in future. Ramadhani et al. [12] made a study at Passenger Transportation Company General Djakarta which was randomly involved in installation of wheels in transportation services. The entire method involving installation was the one which could cause musculoskeletal disorders among workers and trigger health problems for an individual's future. The authors worked on a prevention note to avoid these health hazards using REBA assessment.

## **3 Research Methods**

### ***3.1 Work Details***

The experiment was carried out in a dairy farm in Jaipur city in state of Rajasthan in western India. For postural analysis, dairy farm expert workers with a good experience were chosen in consultation with dairy incharge. The sampling involved 50

participants completing their daily activities in farm, and their videos and pictures are recorded for a detailed study. The analysis was carried out on dairy farm tasks like fodder cutting, washing cattle, milking process, harvesting, material handling and cleaning the cattle shed area. All these activities involve repetitive working in awkward postures like bending, kneeling and twisting with strained muscles for prolonged durations resulting in serious injuries [7]. Nordic questionnaire was filled by all 50 dairy farm participants to reveal their age, experience, gender, working hours, rest pauses and the strained parts in human body and the muscular pain felt by them during performance of material handling activities.

### ***3.2 Data Collection***

Dairy farming is generally done throughout the year. So, data was collected in the month of April–May–June–July in different months for different set of workers for dairy tasks. The consent from workers and dairy managers/owners was also taken before pursuing the entire study.

The entire study was conducted keeping without any violation of the World Medical Association Declaration of Helsinki 41 (2001) and National Ethical Guidelines for Biomedical and Health Research (2016). All the steps in dairy farming process were observed carefully for 3 days, and it was observed the workers do bending, kneeling, squatting, load lifting, filling fodder in bags, scraping animal dung in ground and cleaning of ground and cattle shed area. Workers were randomly selected for study in various tasks, and all details like weight, height and experience of workers were saved for future reference. Videos and pictures were recorded for REBA analysis without disturbing the routine task of workers.

The usability of hand tools was assessed through the comfort questionnaire for hand tools (CQH). Anthropometric kit and weighing machine were also used to record the other data. A minimum value (+1) was assigned to the working posture for which risk is minimum and higher numbers were allocated to extreme postures in range of 20° and beyond that with extreme stretching of muscles. Varied scatter charts, bar graph, pie chart and tables were helpful in descriptive statistics.

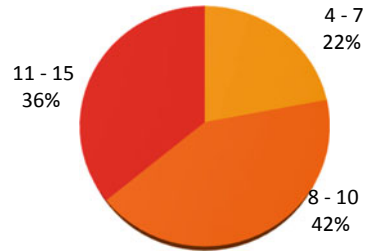
## **4 Case Study**

The experimentation process conducted on 50 participants with varying age, height and experience reveals the following analysis as shown below. The standard Ergo plus REBA calculator permits Risk Index of less than 4 as a safe zone for workers.

**Table 1** REBA standard risk index categories

REBA score	No of workers	Risk level	Action
1	0	Negligible	Not necessary
2-3	0	Low	May be necessary
4-7	11	Medium	Necessary
8-10	21	High	Necessary soon
11-15	18	Very high	Immediate action required

**Fig. 1** Percentage distribution of musculoskeletal disorders among dairy workers



### 4.1 Application of Research Methods

The risk score covered 5 categories varying from permissible limit to high risk zone as shown in Table 1. Those having Risk Index value 4 and above need necessary action for change in their work parameters to avoid MSDs and injury due to excessive exertion of muscles (Fig. 1).

Based on the survey conducted for 50 participants who were involved in different dairy farm activities, more than 3/4th of them were reported to have musculoskeletal disorders and developed risk scores beyond 8 which is usually believed to be the point where an individual needs attention on his daily occupational tasks (Figs. 2, 3, 4 and 5).

REBA scores were generated for all 50 participants using the actual data of their age, height and experience in dairy farm based on their body postures while doing their daily activities in dairy farms (Table 2).

The below mentioned graphs in Figs. 6, 7 and 8 show the relations or trends in risk levels of workers with respect to increasing age, experience and height.

## 5 Results and Discussion

The results obtained through REBA analysis show a general trend of almost 36% workers suffering from high level of musculoskeletal disorders which need immediate cure in their routine tasks. 42% workers are those who are under medium level of risk, but still need action to improve the work technique in their occupation. Less

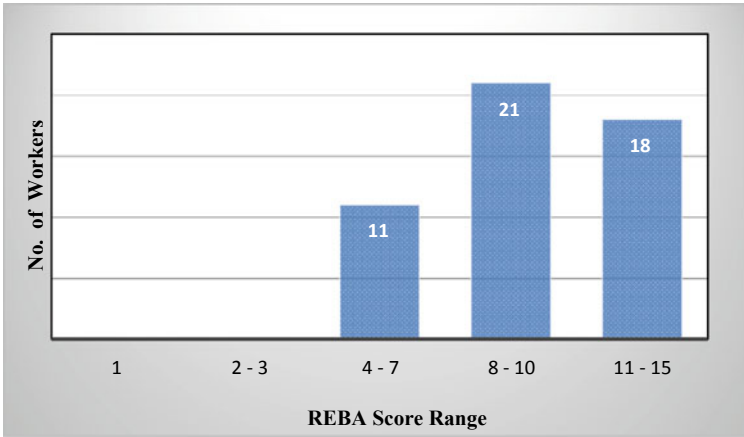


Fig. 2 REBA score frequency among 50 survey participants



Fig. 3 Case 1—REBA analysis while carrying load on shoulders and back

**Fig. 4** Case 2—REBA analysis while carrying load on head



than 1/4th of the survey participants are under secure who have a safety in occupational activities. The second trend shows an increasing wave of musculoskeletal disorders with increasing age in most of the cases. This may happen due to fatigue and fragility developed in the body after a certain age and the increased strain in muscles on lifting load and carrying out different dairy activities without utmost care.

The observation was also made with respect to experience of workers in dairy farms. The general trend says that workers who have worked more number of years in dairy farm have frequent issues related to MSDs and their bodies are more prone to injuries compared to those who have spent less years in dairy farm occupation. However, this trend of increasing MSDs or risk score of workers is general as it may not apply to 100% of workers but usually expected to be followed by majority of dairy workers. The REBA score tendency does not vary much with height as it shows that workers of all age groups may be prone to MSDs, irrespective of their heights. It depends more on the duration of working hours, the level of force exertion borne by the workers' body and the more of bending, kneeling and twisting activities done by muscles which go out of permissible zone of human body resulting in injuries sooner or later in neck, lower back, upper extremities and shoulders.

**Fig. 5** Case 3—REBA analysis while lifting the load to a certain height



## 6 Conclusion

The above results after comparison with the permissible limits show that MSDs are common among dairy farm workers and a majority of workers suffer from medium- or high-level disorders and need immediate cure to that problem. Apart from that, those who have spent more time in dairy farm activities are more likely to have severe injuries after a certain span of time with the increasing age. Few remedial measures could be taken to resolve these issues like proper training of workers, proper rest pauses between continuous occupational activities and pick and place of manure which is a heavy load frequently through a trolley system to avoid rigorous exercise and prevent time of dairy workers. Designing of workstation or tools used in daily activities such that if we are able to reduce the repeated bending and kneeling occupational tasks, the risk level of workers can be reduced to a much low score compared to that being now. A few modifications in workplace design and proper training and lifting techniques will reduce the fatigue experienced by the workers thereby creating a safe, secure and healthy work environment and thus also improve the productivity of the workers by a considerable level.



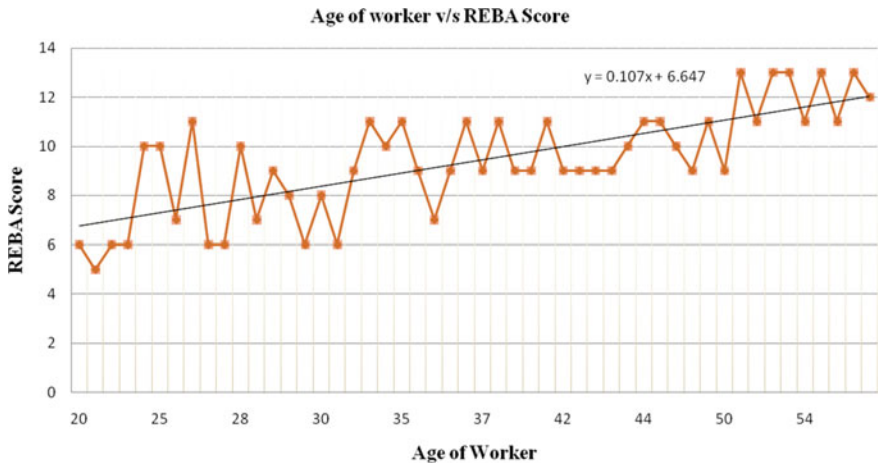
**Table 2** REBA scores for 50 participants using standard REBA calculator

Subject	Age	Height	Weight	Dairy work experience	Posture score in table A	Posture score in table B	Table C	REBA score
		(inches)	(inches)					
1	20	67	62	2	2	6	4	10
2	22	60	58	2	1	8	5	13
3	22	63	76	3	1	9	6	15
4	22	64	67	3	1	9	6	15
5	25	62	66	5	5	7	9	16
6	25	63	71	5	5	7	9	16
7	26	66	70	4	4	9	10	19
8	26	70	76	3	3	6	5	11
9	28	64	60	3	3	6	5	11
10	28	65	64	5	5	7	9	16
11	28	71	77	4	2	6	4	10
12	29	61	64	6	3	8	8	16
13	29	64	70	2	2	8	6	14
14	29	64	67	7	3	6	5	11
15	29	65	69	6	3	8	7	15
16	30	68	67	4	3	8	7	15
17	32	60	68	5	1	7	4	11
18	32	61	64	6	3	8	8	16
19	34	66	67	8	6	8	10	18
20	35	63	65	7	5	7	9	16
21	35	63	62	8	3	9	10	19
22	35	65	69	9	3	6	8	14
23	36	67	59	10	3	7	8	15
24	36	70	68	5	2	8	6	14
25	37	60	62	8	6	8	10	18
26	37	63	69	8	3	8	8	16
27	37	65	59	10	6	8	10	18
28	38	66	69	12	3	7	8	15
29	38	72	76	9	3	8	8	16
30	40	63	66	8	6	7	10	17
31	42	59	55	13	4	9	8	17
32	42	63	61	9	3	6	8	14
33	42	67	55	10	2	6	8	14
34	43	62	70	15	3	8	9	17
35	43	69	75	9	3	6	8	14

(continued)

**Table 2** (continued)

Subject	Age	Height	Weight	Dairy work experience	Posture score in table A	Posture score in table B	Table C	REBA score
		(inches)	(inches)					
36	44	72	81	13	6	8	10	18
37	45	65	64	13	6	8	10	18
38	45	66	68	14	3	8	9	17
39	48	64	68	10	3	7	8	15
40	48	66	61	16	6	8	10	18
41	50	62	56	14	3	7	8	15
42	50	67	75	25	3	9	10	19
43	50	68	81	22	6	9	12	21
44	52	63	71	19	6	9	12	21
45	53	65	62	18	6	9	12	21
46	54	66	61	8	3	9	10	19
47	55	62	56	24	6	9	12	21
48	58	68	76	30	5	6	10	16
49	62	62	71	32	6	8	11	19
50	62	65	78	25	4	8	12	20



**Fig. 6** Correlation between age of worker and REBA score

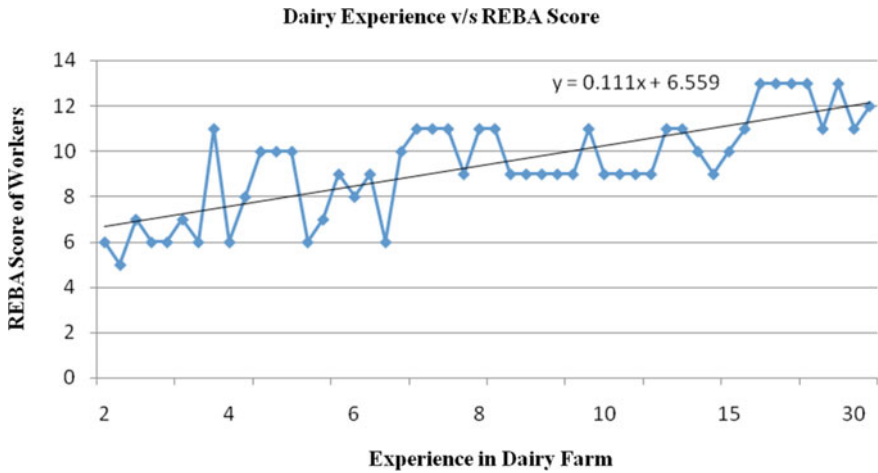


Fig. 7 Correlation between dairy experience of worker and REBA score

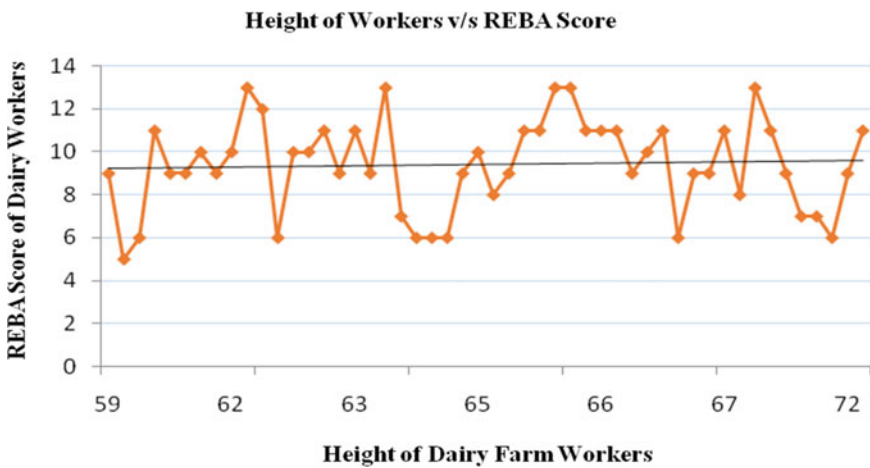


Fig. 8 Correlation between height of worker and REBA score

## References

1. Arendra A, Akhmad S, Mu' Alim Lumintu I (2020) Working tool redesign to reduce ergonomic risk of salt evaporation field workers based on RULA and REBA assessments using esMOCA Instrument. *J Phys Conf Ser* 1477. <https://doi.org/10.1088/1742-6596/1477/2/022034>
2. Enez K, Nalbantoğlu SS (2019) Comparison of ergonomic risk assessment outputs from OWAS and REBA in forestry timber harvesting. *Int J Ind Ergon* 70:51–57. <https://doi.org/10.1016/j.ergon.2019.01.009>
3. Haekal J, Hanum B, Prasetyo DE (2020) Analysis of operator body posture packaging using rapid entire body assessment (REBA) method: a case study of pharmaceutical company in

- Bogor, Indonesia. *Int J Eng Res Adv Technol* 06:27–36. <https://doi.org/10.31695/ijerat.2020.3620>
4. Hita-Gutiérrez M, Gómez-Galán M, Díaz-Pérez M, Callejón-Ferre AJ (2020) An overview of REBA method applications in the world. *Int J Environ Res Public Health* 17. <https://doi.org/10.3390/ijerph17082635>
  5. Jain R, Meena ML, Dangayach GS (2017) Factores de riesgo de trastornos musculoesqueléticos en agricultores de recolección manual de Rajasthan. *Ind Health* 56(7)
  6. Jain R, Sain MK, Meena ML, Dangayach GS, Bhardwaj AK (2018) Non-powered hand tool improvement research for prevention of work-related problems: a review. *Int J Occup Saf Ergon* 24:347–357. <https://doi.org/10.1080/10803548.2017.1296214>
  7. Joshi M, Deshpande V (2020) Investigative study and sensitivity analysis of rapid entire body assessment (REBA). *Int J Ind Ergon* 79:103004. <https://doi.org/10.1016/j.ergon.2020.103004>
  8. Kulkarni VS, Devalkar RV (2019) Postural analysis of building construction workers using ergonomics. *Int J Constr Manag* 19:464–471. <https://doi.org/10.1080/15623599.2018.1452096>
  9. Lowe BD, Dempsey PG, Jones EM (2019) Ergonomics assessment methods used by ergonomics professionals. *Appl Ergon* 81:102882. <https://doi.org/10.1016/j.apergo.2019.102882>
  10. Mahboobi M, Taghipour M, Azadeh MA (2020) Assessing ergonomic risk factors using combined data envelopment analysis and conventional methods for an auto parts manufacturer. *Work* 67:113–128. <https://doi.org/10.3233/WOR-203257>
  11. Mets JT (1980) Industrial health. *S Afr Med J* 57:433
  12. Ramadhani M, Rukman R, Prayogo D, Ayu D (2018) Assessment analysis of ergonomics work posture on wheel installation with Ovako work posture analysis system (OWAS) method and rapid entire body assessment (REBA) method preventing musculoskeletal disorders AT Perum PPD Jakarta. *IOSR J Humanit Soc Sci (IOSR-JHSS)* 23:1–11. <https://doi.org/10.9790/0837-2310030111>
  13. Reyes-zárate GG, Garcia-cavazos I (2020) REBA workplace ergonomics using kinect 17–18
  14. Sain MK, Meena ML (2018) Exploring the musculoskeletal problems and associated risk factors among brick kiln workers. *Int J of Workplace Health Manag* 11(6):395–410
  15. Schwartz AH, Albin TJ, Gerberich SG (2019) Intra-rater and inter-rater reliability of the rapid entire body assessment (REBA) tool. *Int J Ind Ergon* 71:111–116. <https://doi.org/10.1016/j.ergon.2019.02.010>
  16. Yadi YH, Kurniawidjaja LM, Susilowati IH (2018) Ergonomics intervention study of the RULA/REBA method in chemical industries for MSDs' risk assessment. *KnE Life Sci* 4:181. <https://doi.org/10.18502/kls.v4i5.2551>
  17. Yu Y, Li H, Yang X, Kong L, Luo X, Wong AYL (2019) An automatic and non-invasive physical fatigue assessment method for construction workers. *Autom Constr* 103:1–12. <https://doi.org/10.1016/j.autcon.2019.02.020>
  18. Yu Y, Yang X, Li H, Luo X, Guo H, Fang Q (2019) Joint-level vision-based ergonomic assessment tool for construction workers. *J Constr Eng Manag* 145:04019025. [https://doi.org/10.1061/\(asce\)co.1943-7862.0001647](https://doi.org/10.1061/(asce)co.1943-7862.0001647)
  19. Zubar HA, Alamoudi R (2019) Analysis of body postures of employees in manufacturing industry by using ergonomic tools. *J Sci Ind Res (India)* 78:144–147

# Feasibility Investigations on the Development of Hybrid Pellet-Based Extruder with Fused Filament Fabrication



Yash Soni, Narendra Kumar, Ravi Pratap Singh, and Prashant K. Jain

**Abstract** Quintessential additive manufacturing has established Fused Filament Fabrication (FFF) as the major technique due to ease in handling of the equipment. Despite limitations such as restricted material choices, usage of FFF has become de facto among 3D printing enthusiasts. Although several independent researchers, industry and academia have tried to use pellet-based extrusion as a prominent method for additive manufacturing, still the respective field has relatively less accessibility and requires more handling effort compared to traditional filament extrusion. The current research focuses on the validity of pellet-based extruder in a hybrid form factor to rectify its handling issues and, henceforth, its credibility when compared to a filament extruder. Thus, experiments are conducted using Acrylonitrile Butadiene Styrene (ABS) and Ethylene-Vinyl Acetate (EVA) in order to validate the developed system. The research is also validated by comparing the part quality with numerous diverse test parts for validation of pellet extruder in comparison with conventional filament extruder. The presented research also explores the printability among various materials and methods.

**Keywords** Additive manufacturing · 3D printing · Fused filament fabrication · Pellet · Extrusion · CAD

---

Y. Soni · P. K. Jain

Mechanical Engineering Department, PDPM Indian Institute of Information Technology, Design and Manufacturing Jabalpur, Jabalpur, India

N. Kumar (✉) · R. P. Singh

Industrial and Production Engineering Department, Dr. B R Ambedkar National Institute of Technology, Jalandhar, India

e-mail: [kumarn@nitj.ac.in](mailto:kumarn@nitj.ac.in)

R. P. Singh

Department of Mechanical Engineering, National Institute of Technology, Kurukshetra, India

# 1 Introduction

Additive manufacturing, once viewed as a breakthrough in manufacturing sector, has plateaued in recent years. Despite being applied in varied forms and processes, such as Fused Filament Fabrication (FFF), Laser Engineered Net Shaping (LENS), Selective Laser Sintering (SLS) and Selective Laser Melting (SLM), its application is still limited to prototyping and selective test cases in medical and aerospace sectors.

Among these methods, FFF is the most popular globally for the aforementioned purpose. Due to easy handling and relatively inexpensive factor, the prominence of FFF is widely justified among the masses. Largely employed for concept validation among researchers, it has so far provided enough support to shape blooming ideas but with years going by, the eligibility of FFF is gradually decreasing. This is attributed to factors such as limited application of materials in FFF processes, exhaustion of novel concepts/ideas regarding material combination and its application, along with that, stagnant growth in the FFF community. Furthermore, a shift in interests of scientific stakeholders due to earlier mentioned factors has also caused negligence in innovation [3].

Alternatively, some academicians have tried to opt for different techniques in order to widen the range of additive manufacturing. One of those techniques is pellet extrusion which involves layer-by-layer deposition of material present in pellet stock form instead of filament form [7]. This enables to incorporate mixtures and combinations of several materials in predefined proportion, without worrying about its mechanical properties due to imminent filament conversion from its initial raw form. Along with that, traditional injection moulding principles can be applied for simulating the workflow behaviour initially. Despite several advantages, its usage is still not prominent in the scientific community. The reasons can be credited towards the lack of professional equipment in the market dedicated towards pellet extrusion additive manufacturing [2].

The present study presents on one such pellet extrusion system developed in house with the ability to alternate between both traditional filament extrusion and pellet extrusion [4]. The details about the design and development of the pellet extruder are published elsewhere. The independent setup can be mounted and driven through the open-source software such as Ultimaker Cura with minor tweaks in settings [10]. The design was validated and optimized via various methodologies in order to calibrate the pellet extrusion hardware with commercial filament extrusion setup which is published elsewhere. Additionally, experimental analysis of fabricated parts also has been performed in order to validate its competence in comparison with conventional FFF technique. Its printability is also tested by throughput analysis of various material not compatible ordinarily with filament extrusion system. Along with that, throughput from different nozzle sizes is also explored [9].

Section 2 includes the discussion on the performed experiments with the apparatus, Sect. 3 is the analysis of results by the experimentation, Sect. 4 lists some issues inferred during the result analysis, and Sect. 5 concludes the presented research work.

## 2 Materials and Methods

The experimentation utilized diverse materials having different mechanical properties and behaviour such as toughness and elasticity. Figure 1 shows the material in pellet form which was used for the test patterns with ABS and EVA, respectively. A constant rate of pellet input was established beforehand in order to smoothen the material flow across the extrusion process resulting a consistent melting. ABS is tough and rigid, while EVA is an elastomer which cannot be used in filament form. Thus, the pellet extrusion system adds a new dimension of materials especially flexible materials which are strenuous to mould in filament form and also sometimes fails the printing process due to buckling in the extrusion's material feeding system [6]. The pellets utilized in the study size at an average under  $3 \times 3 \times 3$  mm.

### 2.1 Pilot Experimentation

Initially, the extruder had printed some elementary prints such as filament of different nozzle sizes and filaments with different print speeds, with varied temperature, with different materials, etc., to check the viability of the extruder. Some of these throughputs built using the pellet extruder are shown in the forthcoming section along with the throughput of extreme diameters. These filaments are necessary to understand the repeatability of the extruder and versatility using different types of materials [5].

These experiments were designed with optimum process parameters to get a clear idea of extruder's extruding ability and consistency along with its repeatability. The observation from the experiment establishes the foundation of the pellet-based extruder towards extruding full-fledged parts. The process utilizes the extruder at 250 °C of extrusion temperature, 25 mm/s of print speed, 25 mm/s of feed speed and 0.6 mm of standoff distance from the printing bed for ABS parts and, similarly, 100 °C of extrusion temperature, 25 mm/s of print speed, 25 mm/s of feed speed

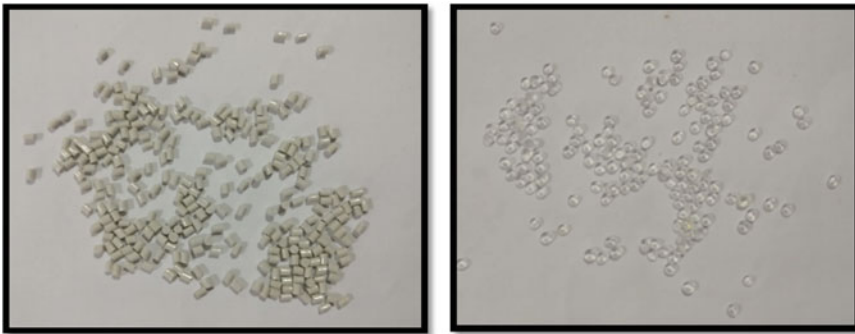


Fig. 1 ABS and EVA pellets

and 0.6 mm of standoff distance from the printing bed for EVA parts. The details on the parameter optimization for the respective pellet extruder and its calibration with filament extruder firmware and hardware via various Design of Experiments methods are published elsewhere.

## 2.2 Fabricated Parts

This section shows the printability of the pellet-based AM extruder with different nozzle size from 0.4 to 1.5 mm nozzles. Depending on the kind of application, either can be used. Here, the nozzle used to print different parts is 1.2 mm diameter in size due to its high flowability and low back pressure on the feeding auger.

This indicates that the parts printed via the pellet-based AM extruder have the accuracy and ability to print standard parts which can be controlled with an open-source slicing software like Ultimaker Cura. Figures 2 and 3 prove the aforementioned points and are discussed in detail in forthcoming section.

## 3 Results and Discussion

The various experimentation resulted in different learnings about the validity of the pellet extruder, and also, exploration is done in the area of the possible commercialized version of the hybrid extruder in current scenario. Some of the fabricated

**Fig. 2** Microscopic image of EVA throughput



**Fig. 3** Microscopic image of ABS throughput





parts are in direct connection with standard filament extrusion systems which also helps understand the merits and demerits of the system. Furthermore, the analysis of the different parts and throughput built from the pellet extrusion system enables to comprehend the further scope of design and parameter modification which can be improved in the setup.

### 3.1 Pilot Experiments

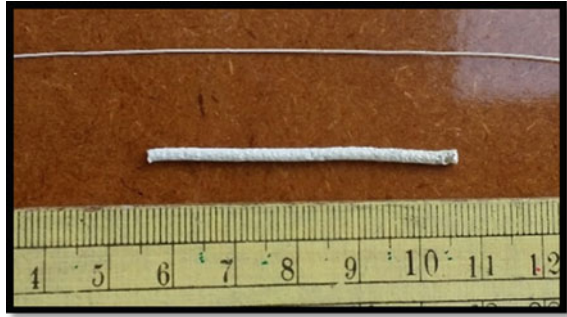
The results of the initial experiments depict that the extruder shows positive effect on changing the process parameters such as temperature and nozzle sizes. The microscopic image of the filament extruded shown in Figs. 2 and 3 displays no signs of under-extrusion or over-extrusion, thus negating the possibility of the filament stretch or accumulation. Additionally, it also verifies the printability of pellet extruder across various materials from recycled ABS to elastomer EVA, without any burrs. The throughput of the pellet extruder with different materials of extreme characteristics such as ABS and EVA shows the compatibility of the extruder with tough as well as flexible materials. Conventionally, the flexible materials are difficult to print with FFF extruders due to buckling issue and also provide fewer permutations of composite materials, which is not the case with the pellet extruder. The diameter variation is measured to check the repeatability and consistency of the pellet extruder. The following Table 1 presents the details of the deviation of diameter with different material.

Thus, the variation in diameter of the throughput is also found to be less than 0.1%, ascertaining the repeatability of the extruder’s accuracy. The image shown in Fig. 4 shows the versatility of the extruder setup with the ability to print via different nozzle sizes from 0.2 to 1.5 mm. Furthermore, the tensile specimens printed as shown in Fig. 5 involved different extrusion parameters such as variation of print speed and nozzle temperature [1].

**Table 1** Theoretical and actual throughput

Material			
ABS		EVA	
Nozzle size (mm)	Actual throughput diameter (mm)	Nozzle size (mm)	Actual throughput diameter (mm)
0.40	0.40	0.40	0.39
1.20	1.20	1.20	1.18

**Fig. 4** Throughput from nozzle of 0.4 and 1.5 mm diameter

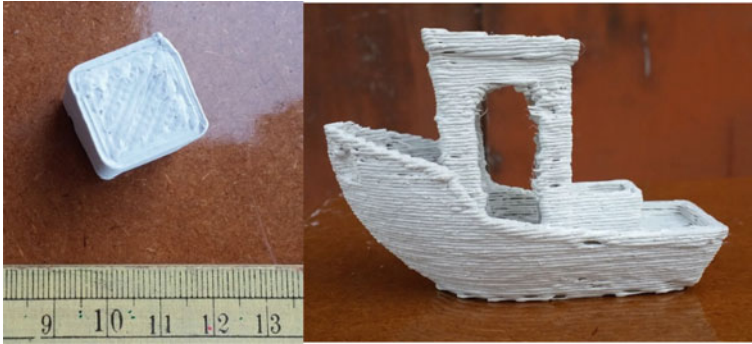


**Fig. 5** Tensile specimens printed with ABS

### 3.2 Fabricated Parts

Thus, the upgraded FFF printer possesses a hybrid printing feature which can print through both filament and pellet material. The pellet extruder enhances the printability of the 3D printer with its ability to print various materials unconventionally not available commercially in filament form. In addition to the hardware, the use of an open-source firmware and software to operate the pellet extruder and synchronize with software provides the ingenuity to add and modify observed changes in parameters, in order to fine-tune the extruder for user-defined operations on selective materials/parts.

Figure 6 shows a simple cube built using the pellet extruder and also the standard boat benchy part which is used for calibration of various filament-based systems and fine-tuning its output by tweaking its parameters [8]. It incorporates various complex features such as roundness and inclination to measure and analyse the accuracy of the printing system in unison.



**Fig. 6** Some more parts built using pellet extruder

## 4 Issues and Challenges

During the development, there are many factors which influence the printability of the pellet extruder. These factors are further classified as external and internal factors, which include heat transfer, cooling rate, design optimization, etc. To rectify these issues, changes must be accommodated and justified within the range of calculated operation parameters. The observed shortcomings of shrinkage and rough surface blobs are further rectified by using a nozzle of smaller size. The existing pellet extruder has the allowance to opt between nozzle sizes which is as convenient as changing nozzle in standard FFF printers. The fabricated parts such as tensile specimens and boat benchy further verify the printability of the pellet extruder among a variety of shapes and sizes.

Additionally, in future a gantry system can also be manufactured having an extruder storage tread head, providing the accessibility to choose from filament-based and pellet-based AM extruder on the same machine thus enabling large possibilities of hybrid printing for aerospace and automotive turbo-machinery sector. Furthermore, due to change in its input material form from filament to pellet, extensive use of flexible polymer can also be employed irrespective of its buckling strength, which is generally limited to printability in the filament-based printer.

## 5 Conclusion

The conducted research explained the possibility of a pellet-based extrusion system with a comprehensive analysis between standard parts built with either extruder. The development of pellet-based extruder was done in such a way that a commercial FFF printer can be modified and utilized as pellet-based system without any major modifications on printer's motion chassis. Along with the successful upgrade,

some throughputs extruded with different parameters and hardware have been investigated also, to establish the groundwork for justification of the developed setup. Additionally, different materials were also used to validate the increase in printer's applicability in comparison with traditional FFF printer.

The resulted output illustrates that the direct pellet fabricated parts are closely comparable with conventional FFF parts. The post-processing attributes such as shrinkage factor, overall strength and surface finish are similar to the standard systems. Furthermore, the manufacturing of complex parts such as boat benchy and standard tensile specimens widens the spectrum of the pellet-based extrusion system application. In future, several different material combinations can be tested for further research in the respective field. A gantry system for switching between pellet and filament extruder can be built to add an industrial perspective to the extrusion system.

## References

1. ASTM International (2013) F2792-12a—Standard terminology for additive manufacturing technologies. *Am Soc Test Mater* 10–12. <https://doi.org/10.1520/F2792-12A.2>
2. Childs THC (1994) Linear and geometric accuracies from layer manufacturing. *43(2)*:163–166
3. Jyothish Kumar L, Pandey PM, Wimpenny DI (2018) 3D printing and additive manufacturing technologies. *3D printing and additive manufacturing technologies*. Springer, Singapore. <https://doi.org/10.1007/978-981-13-0305-0>
4. Karunakaran KP, Suryakumar S, Pushpa V, Akula S (2009) Retrofitment of a CNC machine for hybrid layered manufacturing. *Int J Adv Manuf Technol* 45(7–8):690–703. <https://doi.org/10.1007/s00170-009-2002-2>
5. Kumar N, Jain PK, Tandon P, Pandey PM (2018a) 3D printing of flexible parts using EVA material. *Mater Phys Mech* 37(2):124–132. <https://doi.org/10.18720/MPM.3722018-3>
6. Kumar N, Jain PK, Tandon P, Pandey PM (2018) Extrusion-based additive manufacturing process for producing flexible parts. *J Braz Soc Mech Sci Eng* 40(3):143. <https://doi.org/10.1007/s40430-018-1068-x>
7. Kumar N, Jain PK, Tandon P, Pandey PM (2018) Investigation on the effects of process parameters in CNC assisted pellet based fused layer modeling process. *J Manuf Process* 35:428–436. <https://doi.org/10.1016/j.jmapro.2018.08.029>
8. Measure and calibrate. (n.d.). Retrieved from <http://www.3dbenchy.com/dimensions/>
9. Momenzadeh N, Berfield TA (2019) Polyvinylidene fluoride (PVDF) as a feedstock for material extrusion additive manufacturing, (June). <https://doi.org/10.1108/RPJ-08-2018-0203>
10. Ultimaker Cura. Retrieved Aug 20 2017, from <https://ultimaker.com/software/ultimaker-cura>

# Investigations on the Effect of Nanoclay Reinforced ABS/Nylon-Blended Copolymer Filament for Extrusion-Based 3D Printing



Vishal Francis, Narendra Kumar, Sonika Sahu, and Ravi Pratap Singh

**Abstract** Nylon is one of the widely used semi-crystalline thermoplastics for various engineering applications. However, the materials have limited impact strength and relatively low-dimensional stability. This limits its application especially for the extrusion-based 3D printing process. On the contrary, acrylonitrile butadiene styrene (ABS) has excellent printability and better toughness. ABS/nylon blend can be an effective alternative for extrusion-based 3D printing with excellent properties of both the polymers. However, these polymers are immiscible in nature. Nanoclay is an excellent additive for the polymer which can enhance the material properties of the polymer composite. Moreover, these nanoparticles can also provide a compatibilization effect along with reinforcement. The present paper investigates the effect of nanoclay addition on various blends of ABS/nylon blends for possible 3D printing applications. Filaments were prepared for 30/70, 50/50 and 70/30 wt% of ABS/nylon blends along with nanoclay as compatibilizer. Thermal analysis was performed to investigate the effect of various compositions using DSC analysis. The morphology of the polymer blends was investigated by SEM analysis. Moreover, mechanical testing was performed on the developed filaments.

**Keywords** 3D printing · Additive manufacturing · ABS/nylon · Nanoclay · Copolymer filament

---

V. Francis

School of Mechanical Engineering, Lovely Professional University, Phagwara, Punjab, India

N. Kumar (✉) · R. P. Singh

Department of Industrial and Production Engineering, Dr B R Ambedkar National Institute of Technology, Jalandhar, India

e-mail: [kumarn@nitj.ac.in](mailto:kumarn@nitj.ac.in)

S. Sahu

Department of Mechanical and Industrial Engineering, IIT Roorkee, Roorkee, India

R. P. Singh

Department of Mechanical Engineering, National Institute of Technology, Kurukshetra, India

© The Author(s), under exclusive license to Springer Nature Singapore Pte Ltd. 2023

739

R. P. Singh et al. (eds.), *Advances in Modelling and Optimization of Manufacturing and Industrial Systems*, Lecture Notes in Mechanical Engineering,

[https://doi.org/10.1007/978-981-19-6107-6\\_53](https://doi.org/10.1007/978-981-19-6107-6_53)

## 1 Introduction

Multi-phase copolymer systems provide numerous benefits by combining the attractive properties of each material or by reducing the deficiencies of a single component material. The use of polymer blends in order to improve the impact strength of semi-crystalline thermoplastics has attracted several special attentions and is a well-established process of providing toughness. Nylon 6 is semi-crystalline thermoplastic, with a strong chemical resistance. On the other hand, it also has disadvantages. Low impact strength, high absorption of moisture and poor dimensional stability are few of its major limitations. ABS is a thermoplastic of good impact strength at low temperatures [1–5]. It is also much less prone to the expansion of the notch and is economical compared to nylon. The blends of these two polymers are usually incompatible; therefore, it is important to add a compatibilizer to the blend in order to achieve the desired properties [6–9]. Nanoclay-based polymer nanocomposite materials have influenced both scientific and industrial interest due to ease of development of composites by melt intercalation techniques which requires established processes like extrusion and injection moulding. Moreover, the high aspect ratio and the interfacial area of this nanoparticles have been reported to improve compatibility of immiscible polymers along with providing the reinforcement effect [10]. Extrusion-based 3D printing utilizes thermoplastic polymeric filaments. The most widely used material is ABS, though nylon filaments are also used [11]. However, it is difficult to some extent to print with nylon filaments. The present paper investigates the effect of nanoclay addition on various blends of ABS/nylon blends for possible 3D printing applications. Filaments were prepared for 30/70, 50/50 and 70/30 wt% of ABS/nylon blends along with nanoclay as compatibilizer. Thermal analysis was performed to investigate the effect of various compositions using DSC analysis. The morphology of the polymer blends was investigated by SEM analysis.

## 2 Materials and Methods

The investigations were carried out by using ABS and nylon pellets. The pellets were extruded using the tailor-made setup. Nanoclay powder was added in the polymer blend and mechanically mixed before extrusion. The extruded filament was re-platted and extruded again to form a filament of diameter of 1.75 mm. The nanoclay content was kept as 1 wt% in the polymer blend. Filaments were prepared for 30/70, 50/50 and 70/30 wt% of ABS/nylon blends. The developed filament was characterized with SEM and DSC techniques. The extrusion was carried at 230 °C barrel temperature. The screw speed was kept at 50–60 rpm to provide proper mixing of the blend and residence time. The properties of the material used are illustrated below (Table 1).

**Table 1** Properties of the materials used for the study

1	ABS density	1.05 g/cm <sup>3</sup>
2	Nylon density	1.13 g/cm <sup>3</sup>
3	Organically modified montmorillonite (OMMT) cloisite 30B	Organic modifier: Methyl, tallow, bis-2-hydroxyethyl, quaternary ammonium
	Density	1.98 g/cm <sup>3</sup>
	d-spacing	18.5 Angstrom

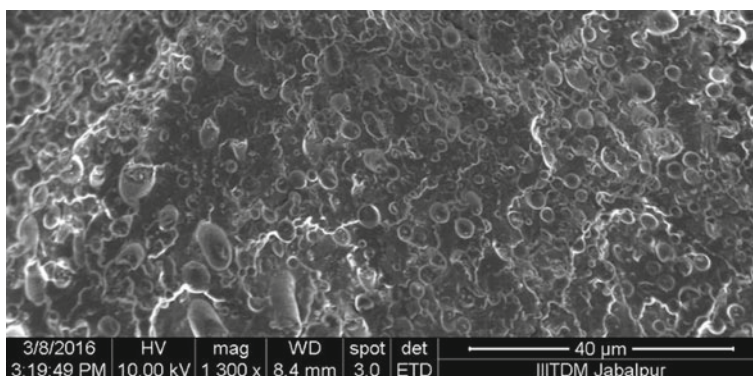
### 3 Filament Characterisation

The developed filament was characterised to investigate the dispersion of the polymers and the blending effect of nanoclay. SEM analysis was performed to observe the morphology of the fractured filaments. Figure 1 shows the SEM image of the 70/30 ABS/nylon blend with 1 wt% nanoclay. The ABS is in the dispersed phase, and smaller dispersed particles were formed.

The morphology of the second composition which consists of 50/50 wt% ABS/nylon blend with 1 wt% nanoclay as compatibilizer is shown in Fig. 2. The fractured specimen of the filament shows the nonspherical dispersed phase morphology.

Figure 3 shows the SEM image of the fractured filament which consists of 70/30 blend. ABS particles in the blend debonded and showed little plastic deformation. Moreover, larger dispersed particles could have been accumulated in the blend.

Further, the filaments were investigated to observe the effect of blending on thermal properties by DSC analysis. Figure 4 shows the DSC graph for 30/70 blend. The melting peak was observed at 221.43 °C. Figure 5 shows the DSC graph for 50/50/ blend. The peak was observed at 221.78 °C. Similarly, when the blend contains 70/30 ratio, the peak was observed at 220.17 °C (Fig. 6). It can be seen that processing temperatures of the polymer blend filament could be processed around 210–250 °C

**Fig. 1** SEM image of 30/70 blend

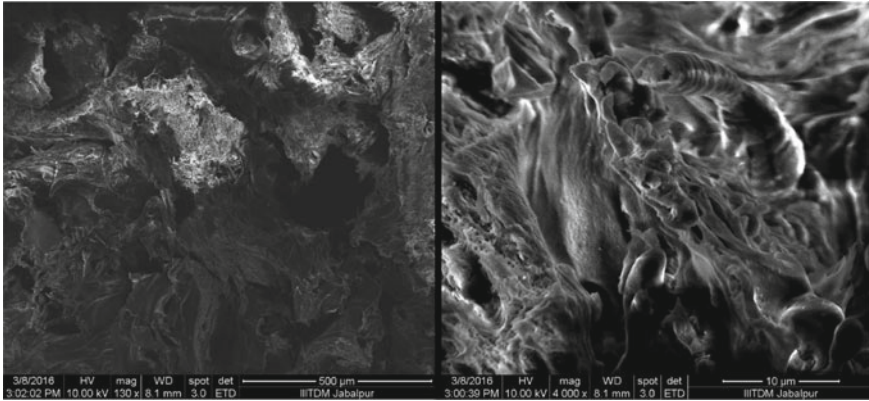


Fig. 2 SEM image of 50/50 blend

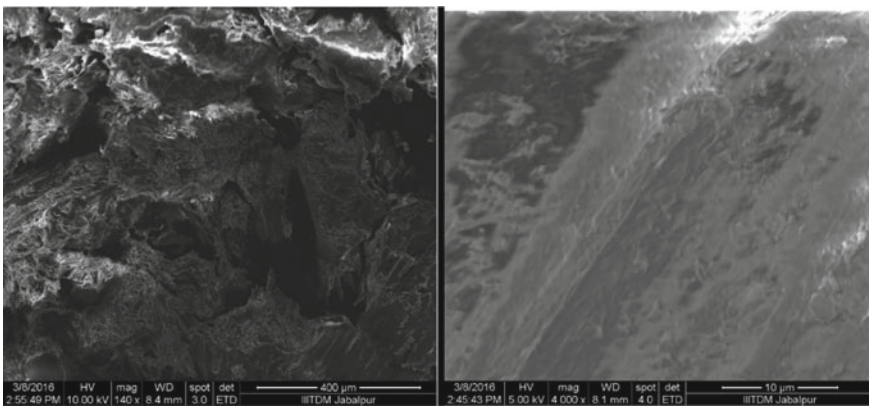


Fig. 3 SEM image of 70/30 blend

during 3D printing. However, determination of the appropriate extruder temperature needs further investigations. The study provides a preliminary data which can be utilized to conduct such experiments and selection of extruder temperature for extrusion-based 3D printing.

## 4 Conclusion

Extrusion-based 3D printing is widely used for fabrication of complex shapes with ease. However, the materials available for the technology are limited. In this regard, development of filaments with high performance will add value to the technology. ABS/nylon blends were prepared with 1 wt% nanoclay as compatibilizer. Filaments



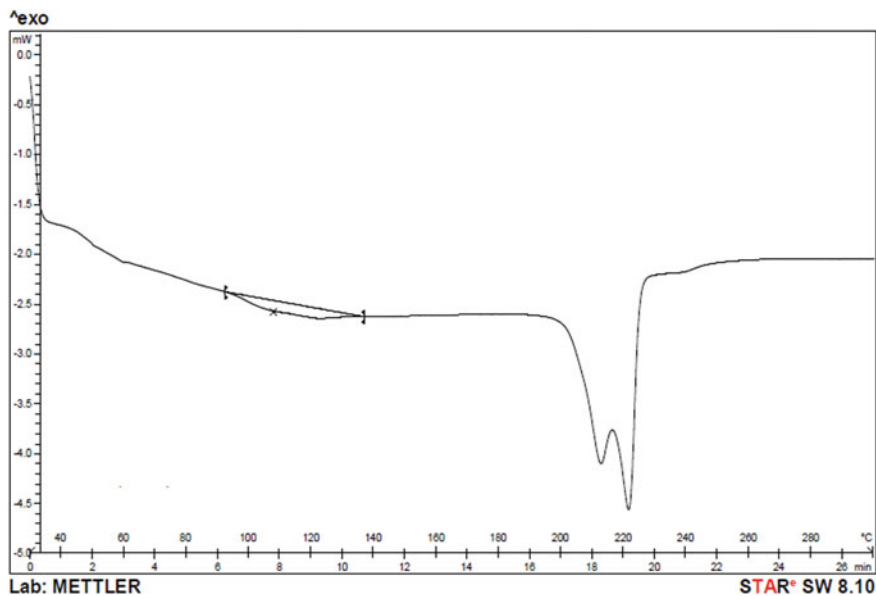


Fig. 4 DSC graph for 30/70 blend

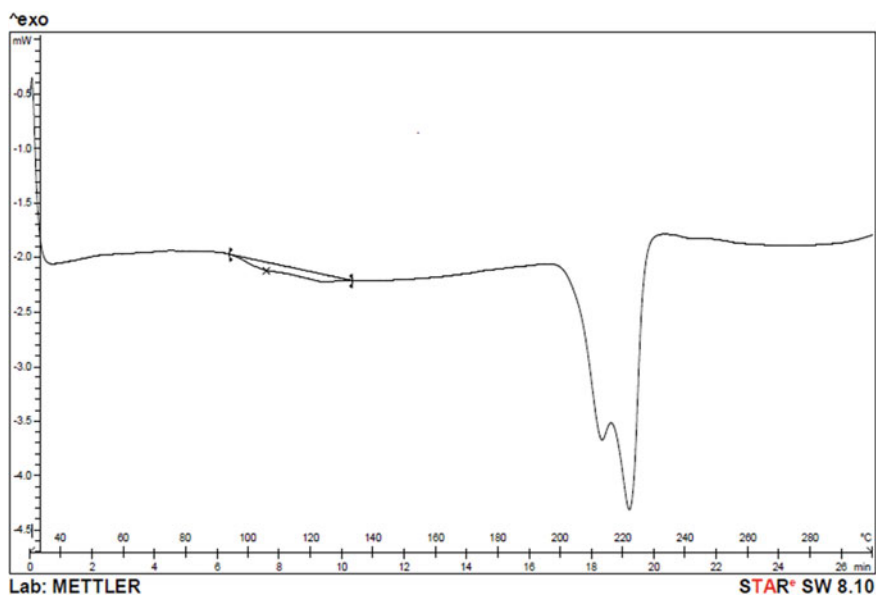
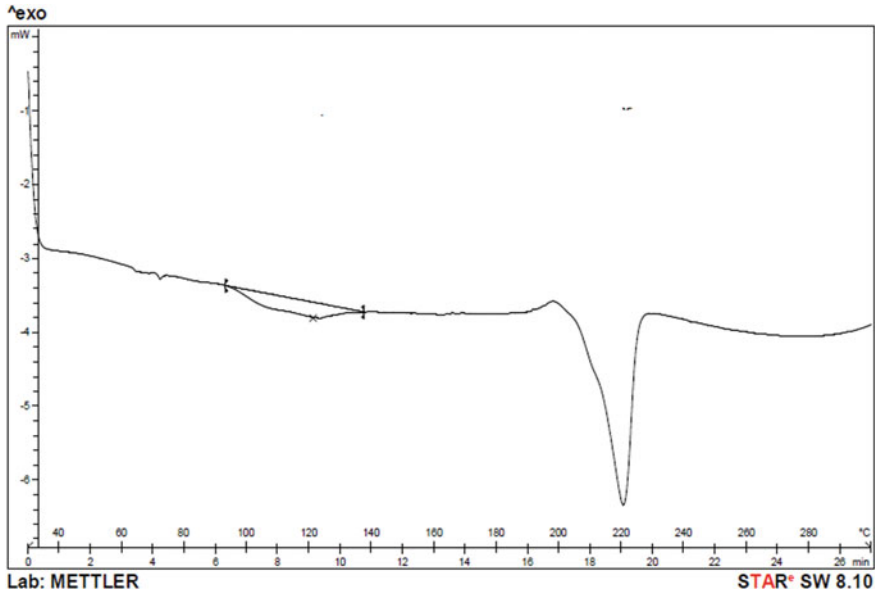


Fig. 5 DSC graph for 50/50 blend



**Fig. 6** DSC graph for 70/30 blend

were prepared for 30/70, 50/50 and 70/30 wt% of ABS/nylon blends along with nanoclay as compatibilizer. Thermal analysis was performed to investigate the effect of various compositions using DSC analysis. The morphology of the polymer blends was investigated by SEM analysis. It can be concluded that the ABS/polymer blend with nanoclay as compatibilizers can be utilized for 3D printing process; however, further studies need to be conducted.

## References

1. Vaia RA, Ishii H, Giannelis EP (1993) Synthesis and properties of two-dimensional nanostructures by direct intercalation of polymer melts in layered silicates. *Chem Mater* 5:1694
2. Vaia RA, Jandt KD, Kramer EJ, Giannelis EP (1995) Kinetics of polymer melt intercalation. *Macromolecules* 28:8080
3. Dennis HR, Hunter DL, Chang D, Kim S, White JL, Cho JW, Paul DR (2001) Effect of melt processing conditions on the extent of exfoliation in organoclay-based nanocomposites. *Polymer* 42:9513
4. Lertwimolnun W, Vergness B (2006) Effect of processing conditions on the formation of polypropylene/organoclay nanocomposites in a twin screw extruder. *Polym Eng Sci* 46:314
5. Lertwimolnun W, Vergness B (2005) Influence of compatibilizer and processing conditions on the dispersion of nanoclay in a polypropylene matrix. *Polymer* 46:3462
6. Li X, Park HM, Lee JO, Ha CS (2002) Effect of blending sequence on the microstructure and properties of PBT/EVA-g-MAH/organoclay ternary nanocomposites. *Polym Eng Sci* 42:2156

7. Quaedflieg M, Rijks L (2005). New developments in micro-compounding of nanocomposites. DSM Xplore Internet-Paper, pp 1–2. [www.xplore-together.com/data/xplore\\_internet\\_paper.pdf](http://www.xplore-together.com/data/xplore_internet_paper.pdf)
8. Tiesnitsch J (2005) New development in micro-scale compounding of polymeric materials. SPE ANTEC 6:9
9. Walia P, Barger M, Mc Kelvey M (2005) Quantitative mixing uniformity assessment in two laboratory scale devices. SPE ANTEC 1:252
10. Francis V, Jain PK (2015) Advances in nanocomposite materials for additive manufacturing. Int J Rapid Manuf 5:215–233
11. Francis V, Jain PK (2018) Investigation on the effect of surface modification of 3D printed parts by nanoclay and dimethyl ketone. Mater Manuf Processes 33(10):1080–1092